



**FACULTY OF MECHANICAL AND CIVIL ENGINEERING KRALJEVO  
UNIVERSITY OF KRAGUJEVAC  
KRALJEVO – SERBIA**

---

---

**THE NINTH INTERNATIONAL TRIENNIAL CONFERENCE**

# **HEAVY MACHINERY HM 2017**

**PROCEEDINGS**

**ORGANIZATION SUPPORTED BY:**

Ministry of Education, Science and Technological Development

Development Agency of Serbia

**Zlatibor, June 28 – July 1 2017**



**PUBLISHER:**

Faculty of Mechanical and Civil Engineering, Kraljevo

**EDITORS:**

Prof. dr Milomir Gašić, mech. eng.

**PRINTOUT:**

SaTCIP d.o.o. Vrnjacka Banja

**TECHNICAL COMMITTEE**

dr Vladimir Stojanović  
Jovana Bojković  
Goran Bošković  
Marina Bošković  
Vladimir Đorđević  
Vladan Grković  
Vladimir Mandić  
Saša Marinković  
Aleksandar Nikolić  
Marko Nikolić  
Nenad Stojić  
Slobodan Todosijević  
Jelena Tomić  
Slobodan Bukarica  
Bojan Beloica

No. of copies: 100

**REVIEWS:**

All papers have been reviewed by members of scientific committee



## CONFERENCE CHAIRMAN

Prof. dr Milomir Gašić, FMCE Kraljevo

## INTERNATIONAL SCIENTIFIC PROGRAM COMMITTEE

### CHAIRMAN

Prof. Dr Mile Savković, FMCE Kraljevo

### VICE-CHAIRMAN

Prof. Dr Milan Kolarević, FMCE Kraljevo, Serbia

### MEMBERS

1. Prof. Dr M. Alamoreanu, TU Bucharest, Romania
2. Prof. Dr S. Arsovski, FME Kragujevac, Serbia
3. Prof. Dr D. Atmadzhova, VTU “Todor Kableskov”, Sofia, Bulgaria
4. Prof. Dr M. Berg, Royal Institut of Tecnology-KTH, Sweden
5. Prof. Dr H. Bogdevicius, Technical University, Vilnius, Lithuania
6. Prof. Dr S. Bošnjak, FME Belgrade, Serbia
7. Prof. Dr A. Bruja, TU Bucharest, Romania
8. Prof. Dr Z. Bučevac, FME Belgrade, Serbia
9. Prof. Dr R. Bulatović, FMCE Kraljevo, Serbia
10. Prof. Dr A. Bukvić, FME East Sarajevo, Bosnia and Herzegovina
11. Prof. Dr S. Ćirić-Kostić, FMCE Kraljevo, Serbia
12. Prof. Dr M. Dedić, FMCE Kraljevo, Serbia
13. Prof. Dr R. Durković, FME Podgorica, Montenegro
14. Prof. Dr M. Đapić, FMCE Kraljevo, Serbia
15. Prof. Dr Z. Đinović, Integrated MicroSystem, Vienna, Austria
16. Prof. Dr K. Ehmann, Northwestern University, Chicago, USA
17. Prof Dr O. Erić, FMCE Kraljevo, Serbia
18. Prof. Dr A. Emeljanova, HGTUSA Harkov, Ukraine
19. Prof. Dr V. Filipović, FMCE Kraljevo, Serbia
20. Prof. Dr G. Minak, University of Bologna, Italy
21. Prof. Dr M. Gagl, Integrated MicroSystem, Vienna, Austria
22. Prof. Dr D. Golubović, FME East Sarajevo, Bosnia and Herzegovina
23. Prof. Dr V. Jovišević, FME Banja Luka, Bosnia and Herzegovina
24. Prof. Dr B. Jerman, FME Ljubljana, Slovenia
25. Prof. Dr Z. Jugović, Tehnical Faculty Čačak, Serbia
26. Prof. Dr V. Karamarković, FMCE Kraljevo, Serbia
27. Prof Dr R. Karamarković, FMCE Kraljevo, Serbia
28. Prof. Dr M. Karasahin, Demirel Univerity, Istanbul, Turkey
29. Prof. Dr I. Kiričenko, HNADU Kiev, Ukraine
30. Prof. Dr K. Kocman, Tecnical University of Brno, Czech Republic
31. Prof. Dr S. Kolaković, Faculty of Tehnical Sciences, Novi Sad, Serbia
32. Prof. Dr M. Kostic, Northern Illinois University, DeKalb, USA
33. Prof. Dr M. Králik, FME Bratislava, Slovakia



34. Prof. Dr E. Kudrjavcev, MGSU, Moscow, Russia
35. Prof. Dr Đ. Lađinović, Faculty of Tehnical Sciences, Novi Sad, Serbia
36. Prof. Dr LJ. Lukić, FMCE Kraljevo, Serbia
37. Prof. Dr Z. Marinković, FME Niš, Serbia
38. Prof. Dr N. Mešćerin, MGSU, Moscow, Russia
39. Prof. Dr N. Nedić, FMCE Kraljevo, Serbia
40. Prof. Dr N. Nenov, VTU “Todor Kableskov”, Sofia, Bulgaria
41. Prof. Dr V. Nikolić, FME Niš, Serbia
42. Prof. Dr E. Nikolov, Technical University, Sofia, Bulgaria
43. Prof. Dr M. Ognjanović, FME Belgrade, Serbia
44. Prof. Dr J. Peterka, FMS&T, Trnava, Slovakia
45. Prof. Dr D. Petrović, FMCE Kraljevo, Serbia
46. Prof. Dr J. Polajnar, BC University, Prince George, Canada
47. Prof. Dr D. Pršić, FMCE Kraljevo, Serbia
48. Prof. Dr V. Radonjanin, Faculty of Tehnical Sciences, Novi Sad, Serbia
49. Prof. Dr V. Raičević, FME Kosovska Mitrovica, Serbia
50. Prof. Dr M. Rajović, FMCE Kraljevo, Serbia
51. Prof. Dr M. Stefanović, FME Kragujevac, Serbia
52. Prof. Dr D. Sever, Maribor, Civil Engineering, Slovenia
53. Prof. Dr M. A. Stepanov, MGSU, Moscow, Russia
54. Prof. Dr I. S. Surovcev, VGSU, Voronezh, Russia
55. Prof. Dr S. Šalinić, FMCE Kraljevo, Serbia
56. Prof. Dr Z. Šoškić, FMCE Kraljevo, Serbia
57. Prof. Dr LJ. Tanović, FME Belgrade, Serbia
58. Prof. Dr S. Trifunović, FMCE Kraljevo, Serbia
59. Prof. Dr J. Vladić, Faculty of Tehnical Sciences, Novi Sad, Serbia
60. Prof. Dr M. Vukićević, FMCE Kraljevo, Serbia
61. Prof. Dr K. Weinert, University of Dortmund, Germany
62. Prof. Dr N. Zrnić, FME Belgrade, Serbia

## ORGANIZING COMMITTEE

### CHAIRMAN:

Prof. Dr Ljubomir Lukić, FMCE Kraljevo

### VICE-CHAIRMAN:

Prof. Dr Zlatan Šoškić, FMCE Kraljevo, Serbia

### MEMBERS:

Doc. Dr Lj. Dubonjić, FMCE Kraljevo, Serbia  
Doc. Dr M. Bižić, FMCE Kraljevo, Serbia  
Doc. Dr M. Bjelić, FMCE Kraljevo, Serbia  
Doc. Dr N. Bogojević, FMCE Kraljevo, Serbia  
Doc. Dr M. Ljujić, FMCE Kraljevo, Serbia  
Doc. Dr M. Marašević, FMCE Kraljevo, Serbia

Doc. Dr G. Marković, FMCE Kraljevo, Serbia  
M.A. N. Pavlović, FMCE Kraljevo, Serbia  
Doc. Dr A. Petrović, FMCE Kraljevo, Serbia  
Doc. Dr B. Radičević, FMCE Kraljevo, Serbia  
Doc. Dr N. Zdravković, FMCE Kraljevo, Serbia



## PREFACE

Ladies and gentlemen, dear colleagues,

Welcome to Zlatibor, to the International Scientific Conference Heavy Machinery 2017.

This year the International Conference Heavy Machinery is held by the University of Kragujevac, Faculty of Mechanical and Civil Engineering in Kraljevo from 28 of June to 1 of July 2017.

It has gained a unique recognizable form for exchange of information, ideas and new scientific researches. The Conference is held in the year when the Faculty of Mechanical and Civil Engineering in Kraljevo celebrates the 58<sup>th</sup> year of university teaching in mechanical engineering and sixth year of university teaching in civil engineering.

For 24 years of its existence it has acquired specific and recognizable form in domestic and foreign scientific circles thanks to its scientific and research results.

The goal of the Conference is to make the research from the fields covered at the Faculty of Mechanical and Civil Engineering in Kraljevo available and applicable both within domestic and foreign frames. Also, our scientific workers will have the opportunity to learn about results of research done by their colleagues from abroad in the fields of transport design in industry, energy control, production technologies, and civil engineering through the following thematic sessions:

- Earth moving and transportation machinery,
- Production technologies,
- Automatic control, robotics and fluid technique,
- Machine design and mechanics,
- Railway engineering,
- Thermal technique and environment protection,
- Civil engineering and materials.

High scientific rating of domestic and foreign participants as well as the number of papers provide guarantees that the Conference is going to be very successful.

I wish to emphasize that this year we have a large number of papers, especially from abroad. The program also contains 104 invited papers in the plenary session. The invited lectures reflect the wide spectrum of important topics of current interest in heavy machinery. The sponsorship by the Ministry of Education and Science of the Republic of Serbia is supportive of efforts to promote science and technology in the area of mechanical and civil engineering in Serbia. We would like to express our sincere thanks to all members of scientific and organizing committee, reviewers, as well as to all participants including invited speakers for coming to Zlatibor to present their papers.

Thank you and see you at the next conference.

Kraljevo – Zlatibor, June 2017

Conference Chairman,

  
Prof. Dr. Milomir Gašić, mech eng.



## PLENARY SESSION

<b>COMPUTER MODELLING OF A DIGGING ZONE OF A SINGLE-BUCKET EXCAVATOR</b> Evgeniy M. Kudryavtsev	1
<b>AN EXPERIMENTAL STUDY ON THE FATIGUE RESPONSE OF 15-5 PH STAINLESS STEEL BUILT BY DMLS</b> Dario Croccolo, Massimiliano De Agostinis, Stefano Fini, Giorgio Olmi, Aleksandar Vranic, Snezana Ciric-Kostic	9
<b>TRIBOLOGICAL PROPERTIES OF DETERGENTS AS ADDITIVES FOR MOTOR OILS</b> Anatoly Dotsenko, Vladimir Samusenko	17
<b>A SURVEY OF RESEARCHES IN THE FIELD OF ECODESIGN RELATED TO INTRALOGISTICS AT THE UNIVERSITY OF BELGRADE - FACULTY OF MECHANICAL ENGINEERING (2010-2017)</b> Nenad Zrnić	23
<b>DAMPING CHARACTERISTICS OF THE SEISMIC ISOLATION BEARINGS GROUP, IN MODULAR DESIGN, FOR BRIDGES AND VIADUCTS</b> Marian Dima, Catalin Francu	41

## SESSION A: EARTH-MOVING AND TRANSPORTATION MACHINERY

<b>DYNAMIC ANALYSIS OF TOWER CRANE MOVEMENT MECHANISM</b> Evgeniy Kudryavtsev	1
<b>THE DEFINITION OF BASIC PARAMETERS OF THE SET OF SMALL-SIZED EQUIPMENT FOR PREPARATION OF DRY MORTAR FOR VARIOUS APPLICATIONS</b> Inga Emelyanova, Vladimir Blazhko, S.I Karpenko	7
<b>SHAPELESS MANUFACTURE OF REINFORCED CONCRETE CYLINDRICAL AND SPHERICAL SHELLS WITH THE HELP OF NEW GENERATION HYDRAULIC EQUIPMENT OF NEW GENERATIONS</b> Inga Emelyanova, Ana Anishchenko, Sergey Guzenko, Denis Chayka	11
<b>RESEARCH OF STRESS-STRAIN STATE OF METAL CONSTRUCTIONS FOR STATIC AND DYNAMIC LOADS MACHINERY</b> Ivan Nazarenko, Oleg Dedov, Igor Zalisko	17
<b>RESEARCH OF ENERGY-SAVING VIBRATION MACHINES WITH ACCOUNT OF THE STRESS-STRAIN STATE OF TECHNOLOGICAL ENVIRONMENT</b> Ivan Nazarenko, Oleg Dedov, Anatoly Svidersky, Nicolay Ruchinsky	21
<b>APPLICATION OF NUMERICAL METHODS FOR ANALYSIS OF VERTICAL TRANSPORT SYSTEMS</b> Jovan Vladić, Radomir Đokić, Anto Gajić	25
<b>GEOMETRICAL IDENTIFICATION OF CYLINDRICAL CARRIER OF AXIAL BEARINGS WITH BIG DIAMETERS</b> Milomir Gašić, Mile Savković, Goran Marković, Nebojša Zdravković, Srđan Ribar	33

<b>DESIGN OPTIMIZATION OF THE RECTANGULAR BOX SECTION OF THE DOUBLE BEAM BRIDGE CRANE USING MATLAB OPTIMIZATION TOOLBOX</b>	<b>37</b>
Goran Pavlović, Mile Savković, Nebojša Zdravković, Vladimir Kvrđić, Stefan Mitrović	
<b>INTEGRITY OF BEAM BRACES AND THREADED SPINDLE FOR CONJOINT OPERATION OF TWO 5 MN BRIDGE CRANES</b>	<b>45</b>
Miodrag Arsić, Mladen Mladenović, Bojan Međo, Zoranka Malešević, Zoran Savić	
<b>ORGANIZATIONAL-TECHNOLOGICAL MODELS FOR THE FORMATION OF EFFECTIVE SETS OF MACHINES AND TECHNOLOGIES IN THE PERFORMANCE OF CONSTRUCTION WORKS</b>	<b>53</b>
Maxim Nazarenko, Ivan Pereginets, Viktor Leschinsky	
<b>RISK MANAGEMENT IN MECHANICAL ENGINEERING</b>	<b>57</b>
Vladimir Zorin	
<b>LABORATORY TEST RIG FOR NONDESTRUCTIVE INSPECTION OF STEEL CORD BELTS</b>	<b>61</b>
Miloš Đorđević, Nenad Zrnić, Srđan Bošnjak	
<b>ANALYSIS OF THE INFLUENCE OF BASIC PARAMETERS OF THE MAGNETIC SEPARATOR ECMS-500 FOR NON-FERROUS METALS ON THE SEPARATION FORCE INTENSITY</b>	<b>69</b>
Mile Savković, Milomir Gašić, Nebojša Zdravković, Goran Marković, Goran Pavlović	
<b>APPLICATION OF RELIABILITY CENTERED MAINTENANCE METHODOLOGY FOR MAINTENANCE OF AN SPECIAL MILITARY VEHICLE ENGINE</b>	<b>75</b>
Slavko Rakić, Uglješa Bugarić	
<b>THE APPLICATION OF VOITH HYDRODYNAMIC COUPLERS WHILE STARTING THE BELT CONVEYORS OF MINING</b>	<b>83</b>
Dragoljub Veličković, Svetislav Marković, Dragana Andjelić	
<b>SOME MODERN SOLUTIONS FOR DELIVERY OPERATION IN POSTAL TRAFFIC</b>	<b>87</b>
Aleksandar Čupić, Mladenka Blagojević, Goran Marković	
<b>MATERIAL HANDLING EQUIPMENT SELECTION USING AN INTEGRATED APPROACH F-MODIPROM: AN ADVANTAGE GAINED FROM USING FUZZY NUMBERS</b>	<b>95</b>
Goran Marković, Mile Savković, Nebojša Zdravković, Aleksandar Čupić, Marko Popović	
<b>DIGGING RESISTANCE MODEL SHOVEL MANIPULATOR OF HYDRAULIC EXCAVATOR</b>	<b>101</b>
Vesna Jovanović, Dragoslav Janošević, Jovan Pavlović, Goran Petrović	
<b>ANALYSIS OF THE INFLUENCE OF PARAMETERS OF HYDROSTATIC SYSTEM ON THE MANIPULATOR DRIVE OF THE MOBILE MACHINE</b>	<b>105</b>
Jovan Pavlović, Dragoslav Janošević, Vesna Jovanović, Nikola Petrović	
<b>RESEARCH AND CALCULATION OF RATIONAL MODES AND PARAMETERS OF AN ULTRASONIC CAVITATOR</b>	<b>109</b>
Irina Bernyk, Oleksandr Lugovskoy	

## **SESSION B: PRODUCTION TECHNOLOGIES**

<b>DETERMINATION OF EXPULSION COSTS IN RESISTANCE SPOT WELDING</b>	<b>1</b>
Miomir Vukićević, Mišo Bjelić, Marina Pljakić, Milan Tešević	



<b>NUMERICAL SIMULATION OF HARDNESS DISTRIBUTION AT THE HAZ OF P355GH STEEL</b>	<b>7</b>
Mišo Bjelić, Karel Kovanda, Ladislav Kolařík, Marie Kolaříková, Miomir Vukićević, Branko Radičević	
<b>APPLICATION OF MULTICRITERIA DECISION MAKING IN SELECTION OF OPTIMAL TOOLPATH</b>	<b>13</b>
Aleksandra Petrović, Slobodan Ivanović, Goran Miodragović, Vladan Grković	
<b>ELECTRODE INVESTIGATION AT PLASMA CUTTING</b>	<b>19</b>
Bogdan Nedić, Marko Jankovic, Peko Ivan	
<b>ANALYTICAL ANALYSIS OF DRILLING-ASSOCIATED DAMAGE IN COMPOSITES</b>	<b>23</b>
Navid Zarif Karimi, Giangiacomo Minak	
<b>THE SIMULATION PROCESS IN SMALL AND MEDIUM ENTERPRISES: DECISION-MAKING SUPPORT</b>	<b>29</b>
Miroslav Dragić, Miloš Sorak	
<b>THE INFLUENCE OF WORKING EXPERIENCE AND LEVEL OF EDUCATION ON THE MARKET ORIENTATION OF SMES IN TRANSITION</b>	<b>37</b>
Ljiljana Pecić, Milan Kolarević, Vladan Grković, Natasa Obradović	
<b>ESSENTIAL REQUIREMENTS FOR SUSTAINABILITY COMPLIANCE IN THE PROCESS OF EXPLOITATION MACHINES</b>	<b>45</b>
Miljan Cvetković, Žarko Janković, Dragan Cvetković	
<b>PARTNERSHIP FOR ENTREPRENEURIAL ENGINEERING EDUCATION</b>	<b>51</b>
Milica Gerasimović, Ugljesa Bugarić	
<b>ORAL PRESENTATIONS OF COMPANIES IN ESP CLASSES AS A MULTI-PURPOSE TASK</b>	<b>55</b>
Nataša Pavlović	
<b>MACHINING SIMULATION AND VERIFICATION OF TOOL PATH FOR CNC MACHINE TOOLS WITH SERIAL AND HYBRID KINEMATICS</b>	<b>63</b>
Saša Živanović, Slobodan Tabaković, Milan Zeljković, Cvijetin Mladenović, Aleksandar Košarac	
<b>3D ANIMATION OF WORKPIECE TRANSFORMATION DURING MILLING OPERATION</b>	<b>69</b>
Slobodan Ivanović, Aleksandra Petrović, Ljubomir Lukić, Marina Pljakić	
<b>OPTIMIZATION MODEL FOR MACHINING PROCESSES DESIGN IN FLEXIBLE MANUFACTURING SYSTEMS</b>	<b>75</b>
Ljubomir Lukic, Slobodan Ivanovic, Aleksandra Petrovic, Mirko Djapic	
<b>APPLICATION OF AXIOMATIC DESIGN THEORY AND BELIEF FUNCTION THEORU IN THE ASSEMBLY SYSTEM IMPROVEMENT</b>	<b>83</b>
Zvonko Petrović, Mirko Đapić, Ljubomir Lukić	
<b>THE APPLICATION OF DEMPSTER-SHAFER THEORY ON FAILURE ANALYSIS OF HYDRAULIC HAND PUMPS</b>	<b>89</b>
Violeta Đorđević, Mirko Đapić, Zvonko Petrović	

<b>REMOTE MONITORING AND CONTROL OF ASYNCHRONOUS DRIVES PERFORMANCE – LABORATORY STAND</b>	<b>97</b>
Vasil Dimitrov, Petko Kostadinov	
<b>SYNERGISTIC MODEL OF TRAFFIC FLOWS</b>	<b>103</b>
Galina Cherneva, Emiliya Dimitrova	
<b>DYNAMIC FAULT TREE. COMPUTATION OF PARAMETERS – PART I</b>	<b>109</b>
Emiliya Dimitrova, Plamen Atanasov	
<b>DYNAMIC FAULT TREE. COMPUTATION OF PARAMETERS – PART II</b>	<b>115</b>
Emiliya Dimitrova, Plamen Atanasov	
 <b>SESSION C: AUTOMATIC CONTROL, ROBOTICS AND FLUID TECHNIQUE</b>	
<b>ADAPTIVE INPUT DESIGN FOR ROBUST IDENTIFICATION OF OUTPUT-CONSTRAINED OE MODELS</b>	<b>1</b>
Vladimir Stojanović, Novak Nedić, Dragan Pršić	
<b>CONDITIONAL OPTIMIZATION OF COMPUTER AUTOMATIC CONTROL SYSTEM OF AN SELECTED PLANT AT ARBITRARY INITIAL CONDITIONS</b>	<b>7</b>
Vladimir R. Zarić, Zoran M. Bučevac, Radiša Ž. Jovanović	
<b>CONDITIONAL OPTIMIZATION OF TRANSIENT BEHAVIOUR OF PLANT CONTROLLED WITH PI CONTROLLER CONSIDERING INITIAL CONDITIONS</b>	<b>13</b>
Goran Petrović, Zoran Ribar , Radiša Jovanović	
<b>IDENTIFICATION OF MIMO HAMMERSTEIN MODELS IN THE PRESENCE OF PIECEWISE POLYNOMIAL DISTURBANCES USING KACZMARZ ALGORITHM</b>	<b>19</b>
Vojislav Filipović, Vladimir Djordjević	
<b>PHILOSOPHICAL INTERPRETATION OF CONNECTION OF ROBUST STATISTICS AND FUZZY LOGIC: THE ROBUST FUZZY CLUSTERING</b>	<b>25</b>
Vladimir Djordjević, Vojislav Filipović	
<b>SELF-TUNING PID CONTROLLER BASED ON TIME RESPONSE CHARACTERISTICS</b>	<b>31</b>
Novak N. Nedić, Saša Lj. Prodanović	
<b>DESIGN OF FIXED ORDER <math>H_{\infty}</math> CONTROLLERS WITH SPECIFIED SETTLING TIME USING D-DECOMPOSITION</b>	<b>37</b>
Ljubiša Dubonjić, Vojislav Filipović, Novak Nedić, Vladimir Đorđević	
<b>DATA CLASSIFICATION USING A SET OF NEURAL NETWORKS</b>	<b>43</b>
Srdjan Ribar	
<b>KINEMATIC AND DYNAMIC ANALYSIS OF THE PATH OF MOVEMENT OF THE ROBOT</b>	<b>49</b>
Ljiljana Pecić, Zvonko Petrović, Nikola Kostić	
<b>WATER DRAIN EMERGENCY SYSTEM</b>	<b>55</b>
Nikola Terzić, Dragan Pršić	

## SESSION D: MECHANICAL DESIGN AND MECHANICS

<b>DAMPING AND SEISMIC ISOLATION BEARINGS GROUP, IN MODULAR DESIGN, FOR BRIDGES AND VIADUCTS. CONSTRUCTION AND WORKING PRINCIPLE</b> Marian Dima, Catalin Francu	1
<b>DYNAMICS OF THE ROTATING CANTILEVER BEAM</b> Aleksandar Nikolić, Slaviša Šalinić	7
<b>EXPERIMENTAL INVESTIGATION OF TRIBOLOGICAL BEHAVIOR OF JOURNAL BEARING COATED BY BABBITT ALLOYS TEGOTENAX V840</b> Amir Alsammarraie, Dragan Milčić, Milan Banić, Goran Radenković, Miodrag Milčić	13
<b>SURFACE QUALITY OF MARAGING STEEL PARTS PRODUCED BY DMLS</b> Nebojša Bogojević, Aleksandar Vranić, Nusret Muharemović, Nenad Drvar	21
<b>MACHINING AND HEAT TREATMENT EFFECTS ON THE FATIGUE PROPERTIES OF MARAGING STEEL PRODUCED BY DMLS</b> Snežana Ćić-Kostić, Nebojša Bogojević, Aleksandar Vranić, Dario Croccolo, Massimiliano De Agostinis, Stefano Fini, Giorgio Olmi	27
<b>A HEURISTIC APPROACH TO THE ESTIMATION OF MASS OF THE WASTE POWDER DURING SELECTIVE LASER SINTERING OF POLYAMIDE PA2200</b> Zlatan Šoškić, Simona Montanari, Gian Luca Monti, Michele Monti	37
<b>PRACTICAL EXAMPLES OF REGENERATION OF THE DAMAGED HEAVY MACHINERY PARTS</b> Svetislav Marković, Vladimir Stepanović, Lazar Jovičić, Milijan Ćić, Ivan Stanišić, Miroslav Ćirić, Nemanja Petrović	45
<b>ANALYSIS OF FREE OSCILLATION OF SPATIAL FRAMES APPLYING THE METHOD OF CONSISTENT MASSES</b> Rade Vasiljevic	51
<b>NUMERICAL ANALYSIS OF TRIBOMECHANICAL SYSTEM BRAKE DISC-PAD FOR HEAVY DUTY VEHICLES</b> Nadica Stojanović, Jasna Glišović, Blaža Stojanović, Ivan Grujić	57
<b>ANALYTICAL, EXPERIMENTAL AND NUMERICAL STUDY OF SEMI-RIGID BEAM-TO-COLUMN CONNECTIONS IN THE STEEL STRUCTURE OF PALLET RACKS</b> Rodoljub Vujanac, Snezana Vulovic, Nenad Miloradovic, Aleksandar Disic	65

## SESSION E: RAILWAY ENGINEERING

<b>THE PURPOSE OF DIAGNOSTICS OF PANTOGRAPHS USED IN THE SERBIAN RAILWAYS</b> Branislav Gavrilović, Zoran Bundalo	1
<b>PROCESSES AND DEPENDENCIES RELATED TO NADAL'S FORMULA</b> Dobrinka Atmadzhova	7
<b>OSCILLATION OF RESERVOIR OF TANK-WAGON IN DYNAMIC LONGITUDINAL LOAD</b> Dragan Petrović, Milan Bižić	17

<b>RELIABILITY INDICATORS OF THE BRAKE DISTRIBUTORS KE 1 FOR ROLLING STOCK IN OPERATION</b> Vasko Nikolov	23
<b>THE IMPORTANCE OF THE RAILWAY INFRASTRUCTURE IN THE OPERATIONAL PROGRAM "TRANSPORT AND TRANSPORT INFRASTRUCTURE."</b> Mira Zafirova	27
<b>STUDY OF THE INTERACTION "WHEELSET-TRACK" OF THE ATTACKING WHEELSET OF TRAM BOGIE TYPE T81 IN EXPLOITATION IN SOFIA</b> Dobrinka Atmadzhova, Emil Mihaylov, Emil Iontchev	33
<b>OVERVIEW OF WHEEL-RAIL ROLLING CONTACT THEORIES</b> Milan Bižić, Dragan Petrović	41
<b>STUDY OF THE MOVEMENT OF THE ATTACKING TRAM WHEELSET ON TRACK WITH GAUGE 1009 MM</b> Emil Mihaylov, Emil Iontchev, Vladimir Zhekov, Zornitsa Evlogieva, Metodi Atanasov	49
<b>THE IMPACT OF THE CHARACTERISTICS OF TRAIN ON THE TRAIN BRAKING DISTANCE AT CRITICAL SECTIONS OF THE BELGRADE – BAR RAILWAY LINE</b> Dusan Vujović	57
<b>METHODS FOR CARRYING OUT TRACK MAINTENANCE AND OPTIMIZATION POSSIBILITIES</b> Metodi Atanasov	65
<b>MEASUREMENTS OF NOISE LEVELS OF FREIGHT TRAIN ON SERBIAN RAILWAYS</b> Jelena Tomić, Nebojša Bogojević	71

## **SESSION F: THERMAL TECHNIQUE AND ENVIRONMENT PROTECTION**

<b>MODELING OF TECHNOLOGICAL EQUIPMENT AND TECHNOLOGICAL TRANSPORTATION FLOWS OF THE INDUSTRIES BINDER USING MATHEMATICAL METHODS</b> Cristina Sescu-Gal	1
<b>ENSURING PHONIC COMFORT IN URBAN ENVIRONMENT</b> Vasile Bacria, Nicolae Herisanu	9
<b>OPTIMIZATION OF FLOW SCHEMES IN RADIANT RECUPERATORS</b> Rade Karamarković, Vladan Karamarković, Miloš Nikolić, Nenad Stojčić, Miljan Marašević	15
<b>ACOUSTIC PROPERTIES OF RECYCLED RUBBER AT NORMAL INCIDENCE</b> Milan Kolarević, Branko Radičević, Nicolae Herisanu, Miloje Rajović, Vladan Grković	23
<b>DESIGNING RECUPERATOR ON A ROTARY KILN SUPPLIED WITH ENRICHED AIR DURING THE CALCINATION OF DOLOMITE</b> Miljan Marasevic, Vladan Karamarković, Nenad Stojic, Milos Nikolic, Djordje Novčić	29
<b>ANALYSIS OF DYNAMIC PINCH</b> Aleksandar Vičovac, Rade Karamarković, Dragan Pršić	37

**SELECTION OF THE OPTIMAL ROUTE OF TRANSPORTATION – A CASE STUDY OF TRANSPORT OF MUNICIPAL WASTE IN THE MUNICIPALITY OF TRSTENIK** 45  
Nikola Kostic, Milomir Mijatovic, Sasa Babic, Branimir Milosavljevic, Zvonko Petrovic

**DESIGN IMPROVEMENT OF A SIDE WATER INTAKE ON A SMALL HYDROPOWER PLANT** Miloš 51  
Nikolić, Vladan Karamarković, Rade Karamarković, Miljan Marašević

**MEASUREMENT AND ANALYSIS OF CHANGES IN TOTAL QUANTITY OF INJECTION DEPENDING ON THE CHANGES IN VALUE OF PRESSURE IN COMMON RAIL SYSTEM** 57  
Nikola Kostic, Božidar Krstic, Milomir Mijatovic, Sasa Babic, Branimir Milosavljevic

**DETERMINATION OF TRANSFER FUNCTION OF PHOTOACOUSTIC SYSTEM BY ACQUISITION CARDS WITH UNSYNCHRONIZED SIGNAL INPUT AND OUTPUT** 69  
Slobodan Todosijević, Nenad Drvar, Zlatan Šoškić

**PROTOTYPE SYSTEM FOR GAS TANKS CLEANING** 74  
Zoran Petrović, Mirosljub Babić, Uglješa Bugarić, Dušan Petrović

## **SESSION G: CIVIL ENGINEERING AND MATERIALS**

**MACHINE FOR IMPACT TESTING OF PLASTIC PIPES - IMPACT 2000 DESIGN, DEVELOPMENT AND PROTOTYPING** 1  
Ivan Milićević, Miloš Božić, Vojislav Vujičić, Radomir Slavković

**MULTI-CRITERIA SELECTION OF OPTIMAL MECHANIZATION FOR ROAD CONSTRUCTION** 7  
Vladimir Mandić, Saša Marinković, Jovana Bojković

**PREDICTION OF ACOUSTICAL PROPERTIES OF POROUS BUILDING MATERIALS** 13  
Jovana Bojković, Branko radičević, Nedeljko Manojlović, Mišo Bjelić, Vladimir Mandić, Saša Marinković,

**FLOTATION TAILINGS FROM COPPER MINING AND SMELTING PLANT AS MINERAL ADDITIVES FOR SCC** 19  
Saša Marinković, Vladimir Mandić, Jovana Bojković, Stefan Mihajlović

**RESEARCH OF SHEAR STRENGTH AND COMPATIBILITY BY HEAT CONDITIONING OF SHEETS FOR WATERPROOFING USED IN CONCRETE BRIDGE DECKS** 27  
Nikolina Porozhanova

**WELDING OF THE RESERVOIRS FOR OIL DERIVATIVES STORAGE WITH SELF-SHIELDED CORED WIRE** 33  
Radomir Jovičić, Olivera Erić Cekić, Aleksandar Sedmak, Sanja Petronić, Vukić Lazić

**DETAILED GEOTECHNICAL INVESTIGATIONS OF THE LANDSLIDE BOCKE** 41  
Mitar Đogo, Milinko Vasić



# **PLENNARY SESSION**





# Computer Modelling of a Digging Zone of a Single-bucket Excavator

Kudryavtsev E.M.

The Moscow state building university (Russia)

The paper shows the technique, algorithm and computer programs in system Mathcad for definition of a working digging zone a single-bucket excavator with the working equipment a return shovel. The working zone of digging of a ground a single-bucket excavator includes several sites. The each site of a zone represents with computer program and graphically in system Mathcad. The offered algorithm of calculation and graphic representation of sites of a digging zone a single-bucket excavator with the working equipment the return shovel allows to reduce on order use time and labour input of such calculations, and also to make the corresponding researches connected about change of parameters of elements of the working equipment.

**Keywords:** Digging zone, Single-bucket excavator, Technique, Computer program

## 1. INTRODUCTION

One of the important characteristics a single-bucket excavator is the digging zone, which depends on equipment type, sites of the working equipment, the sizes of elements of the working equipment and corners of their turn. We will consider as an example modelling of a digging zone by excavator with working the equipment a backdigger fig. 1. This digging zone consists of following sites (arches): (0 - 1); (1 - 2); (2 - 3); (3 - 4); (4 - 5); (5 - 6); (6 - 7) (7 - 0). Each of arches of a digging zone has the radius, a turn angle and a center of arches.

Construction of a digging zone is difficult process. It can be executed graphically or analytically. On Fig. 1 the example of a digging zone of a single-bucket excavator with the image of elements of the working equipment is resulted.

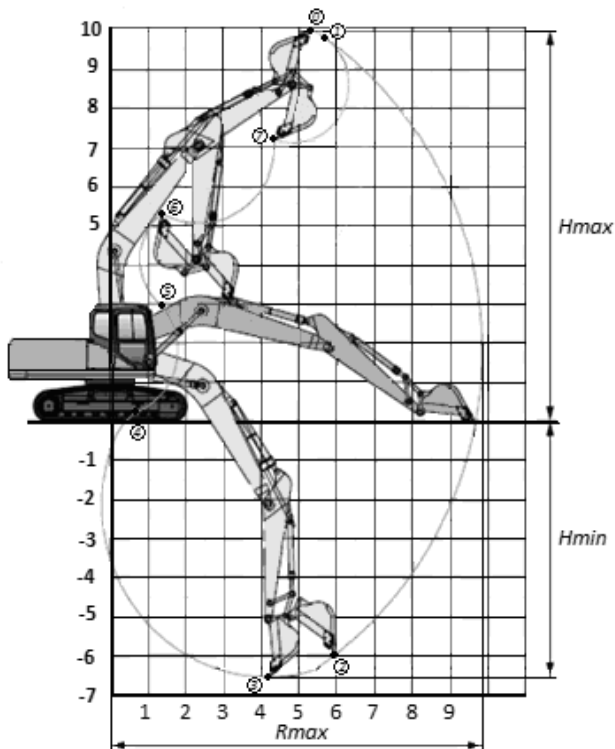


Fig. 1. An example of a digging zone by excavator with a backdigger

## 2. KINEMATIC ANALYSIS

The digging zone a single-bucket excavator represents certain sequence of the interconnected sites. For each of sites are known values of turning angles all elements of the working equipment (a boom, a bucket arm and a bucket). The digging zone a single-bucket excavator includes several sites:

- the first site (0 - 1) - is formed by turn only a bucket from the maximum turning angle ( $\alpha_{3max}$ ) when the end of a tooth of a bucket moves from a point 0, to a point 1 laying on a line a boom passing through an axis and an axis of turn of a bucket. Thus turning angles of boom ( $\alpha_{1max}$ ) and the bucket arm ( $\alpha_{2max}$ ) do not change;

- the second site (1 - 2) - is formed by turn only boom from the maximum turning angle ( $\alpha_{1max}$ ) to the minimum turning angle ( $\alpha_{1min}$ ) with the maximum start of a bucket. Thus turning angles of bucket arm and bucket do not change;

- the third site (2 - 3) - is formed by turn only a bucket from a point 2 to a point 3. The end of a tooth of a bucket moves from a point 2, to a point 3 laying on a line, a bucket arm passing through an axis and an axis of turn of a bucket. The turning angle a bucket will make - ( $\varphi$  fig. 4). Thus turning angles of boom and bucket arm do not change;

- the fourth site (3 - 4) - is formed by turn only bucket arm from the maximum turning angle ( $\alpha_{2max}$ ) to the minimum turning angle ( $\alpha_{2min}$ ) with the maximum start when the end of a tooth of bucket moves from a point 3, to a point 4. Thus turning angles of boom and bucket do not change;

- the fifth site (4 - 5) - is formed by turn only boom with change turning angle of a boom from the minimum ( $\alpha_{2min}$ ) to maximum possible ( $\alpha_{2max}$ ). The end of a tooth of a bucket moves from a point 4, to a point 5. Thus turning angles of a bucket arm and a bucket do not change;

- the sixth site (5 - 6) - is formed by turn only a bucket with change of a turning angle from former position to is minimum possible ( $\alpha_{3min}$ ). The end of a tooth of a bucket moves from a point 0, to a point 1. Thus turning angles of a boom and a bucket arm do not change;

- the seventh site (6 - 7) - is formed by turn only bucket arm from the maximum turning angle ( $\alpha_{2max}$ ) to is minimum possible ( $\alpha_{2min}$ ). The end of a tooth of a bucket

moves from a point 6, to a point 7. Thus turning angles of a boom and a bucket do not change;

- the eighth site (7 - 0) - is formed by turn only a bucket from its minimum possible ( $\alpha_{3min}$ ) to the maximum turning angle ( $\alpha_{3max}$ ). Thus turning angles of a boom and a bucket arm do not change.

As a rule, for simplification of the description of each element of the machinery and the mechanism it is spent in the local system of coordinates adhered to the projected or investigated element (a boom, a bucket arm and a bucket). However, for reception more product general characteristics the detailed description of the interconnected elements already in the basic system of coordinates is required.

### 3. MODELLING OF A DIGGING ZONE

Modelling of a digging zone of a ground includes:

- construction of a matrix of transition from local system of coordinates of a bucket to local system of a bucket arm;
- construction of a matrix of transition from local system of coordinates of a bucket arm to local system of a boom;
- construction of a matrix of transition from local system of coordinates of a boom to the basic system of coordinates of excavator;
- definition of values of angles of an inclination of a boom, a bucket arm and a bucket in the set ranges;
- consecutive calculation of coordinates of each of sites of a digging zone with use of the developed algorithm of calculation both corresponding programs and representation of results of calculation in a graphic kind

### 4. CONSTRUCTION OF A MATRIX OF TRANSITION FROM ONE CO-ORDINATES TO ANOTHER

The basic system of coordinates  $O_0X_0Y_0$  excavator - is the system combined with a basic surface (ground) and an axis of rotation of a rotary platform.

The working equipment of a single-bucket excavator has three degrees of freedom. Each element of working equipment (a boom, a bucket arm and a bucket) is defined by function of three angular coordinates:  $\alpha_1$  - a corner of turn of a boom,  $\alpha_2$  - a corner of turn of a bucket arm and  $\alpha_3$  - a corner of turn of a bucket. We will accept, that positive value of angular coordinates of turn of each subsequent system of coordinates corresponds to turn of axes of coordinates counter-clockwise.

Each element of the working equipment has the local system of coordinates: a boom -  $O_1X_1Y_1$ ; a bucket arm -  $O_2X_2Y_2$ ; a bucket -  $O_3X_3Y_3$ . The beginning of local system of coordinates choose in the basic or connecting hinge of the working equipment. Coordinates of each point of an element of the working equipment to define in the local system of coordinates much easier.

Let's consider in the beginning transformation of coordinates of a point from local system of coordinates on a boom in the basic system of coordinates of excavator.

On fig. 2 are presented the basic system of coordinates  $O_0X_0Y_0$  excavator and local system of coordinates of a boom  $O_1X_1Y_1$ .

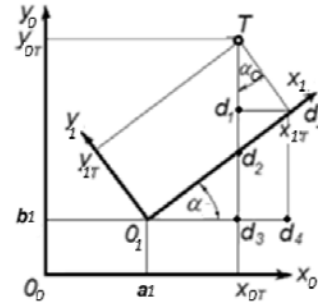


Fig. 2. Connection of two adjacent coordinates

Assume, that coordinates of point  $T(X_{1T}, Y_{1T})$  in local system of coordinates  $O_1X_1Y_1$  boom are known. It is required to define coordinates of this point in the basic system of coordinates  $O_0X_0Y_0$  - system of coordinates of excavator.

The coordinate of point  $T$  on axis  $X_1$  in system of coordinates  $O_0X_0Y_0$  can be defined, using rectangular triangles  $O_1d_4d_5$  and  $d_1d_5T$ ,

$$X_{0T} = O_1d_4 - d_3d_4 + a1 = O_1d_4 - d_1d_5 + a1, \quad (1)$$

where:  $O_1d_4$  - a side of a rectangular triangle  $O_1d_4d_5$ ;

$d_1d_5$  - a side of a rectangular triangle  $d_1d_5T$ ;

$a1$  - coordinate of the beginning of coordinates of system  $O_1X_1Y_1$  on axis  $X_0$  of system  $O_0X_0Y_0$ .

Knowing value of a turning angle  $\alpha_1$  of system  $O_1X_1Y_1$  concerning axis  $X_0$  of system  $O_0X_0Y_0$ , it is possible to find value of a side of a triangle  $O_1d_4$  from a triangle  $O_1d_4d_5$ .

$$O_1d_4 = X_{1T} \cdot \cos(\alpha_1). \quad (2)$$

It is possible to find value of a side of a triangle  $d_1d_5$  from a triangle  $d_1d_5T$

$$d_1d_5 = Y_{1T} \cdot \sin(\alpha_1). \quad (3)$$

Substituting expressions (2) and (3) in initial (1), we will receive expression  $X_{0T}$

$$X_{0T} = X_{1T} \cdot \cos(\alpha_1) - Y_{1T} \cdot \sin(\alpha_1) + a1. \quad (4)$$

The coordinate of point  $T$  on axis  $Y_0$  in coordinate system of  $O_0X_0Y_0$  can be defined, using sides of a triangle of rectangular triangles  $O_1d_4d_5$  and  $d_1d_5T$ ,

$$Y_{0T} = d_1d_3 + Td_1 + b1 = d_4d_5 + Td_1 + b1, \quad (5)$$

where:  $d_4d_5$  - a side of a rectangular triangle  $O_1d_4d_5$ ;

$Td_1$  - a side of a rectangular triangle  $d_1d_5T$ ;

$b1$  - coordinate of the beginning of coordinates of system  $O_1X_1Y_1$  on axis  $Y_0$  of system  $O_0X_0Y_0$ .

Knowing value of a turning angle  $\alpha_1$  it is possible to find value of a side of a triangle  $d_4d_5$  from a triangle  $O_1d_4d_5$ .

$$d_4d_5 = X_{1T} \cdot \sin(\alpha_1). \quad (6)$$

It is similarly possible to find value of side of a triangle  $Td_1$  from a triangle  $d_1d_5T$

$$Td_1 = Y_{1T} \cdot \cos(\alpha_1). \quad (7)$$

Substituting expressions (6) and (7) in initial (5), we will receive expression  $Y_{0T}$

$$Y_{0T} = X_{1T} \cdot \sin(\alpha_1) + Y_{1T} \cdot \cos(\alpha_1) + b1. \quad (8)$$

For modelling of movement of working body excavator - a bucket in space we will take advantage of a mathematical apparatus based on representation of entrance and target data in the form of vectors of columns and matrixes of transitions by dimension 4\*4. Then, above received expressions of transformation of coordinates of moving, it is possible to present in the form of such matrix expression

$$T = \begin{pmatrix} x_{0T} \\ y_{0T} \\ z_{0T} \\ 1 \end{pmatrix} = \begin{pmatrix} \cos(\alpha_1) & -\sin(\alpha_1) & 0 & a1 \\ \sin(\alpha_1) & +\cos(\alpha_1) & 0 & b1 \\ 0 & 0 & 1 & 0 \\ 0 & 0 & 0 & 1 \end{pmatrix} \begin{pmatrix} x_{1T} \\ y_{1T} \\ z_{1T} \\ 1 \end{pmatrix} = \begin{pmatrix} x_{1T} \cdot \cos(\alpha_1) - y_{1T} \cdot \sin(\alpha_1) + a1 \\ x_{1T} \cdot \sin(\alpha_1) + y_{1T} \cdot \cos(\alpha_1) + b1 \\ z_{1T} \\ 1 \end{pmatrix} \quad (9)$$

### 5. DETERMINATION OF A TURNING ANGLE OF A BUCKET

Further we will define a turning angle of a bucket on the first site of a digging zone - (0-1). On fig. 3 the scheme of position of elements of the working equipment of excavator for definition a turning angle of a bucket on the first a site of a digging zone (0-1) is presented. A bucket turn on the first site is made on a turning angle  $(\alpha_{3max} - \varphi)$  at boom position under a turning angle  $\alpha_{1max}$  and bucket arm under a turning angle  $\alpha_{2max}$  to a line which are passing through an axis of turn of a boom -  $O_1$  and an axis of turn of a bucket -  $O_3$ , providing the maximum start of a bucket.

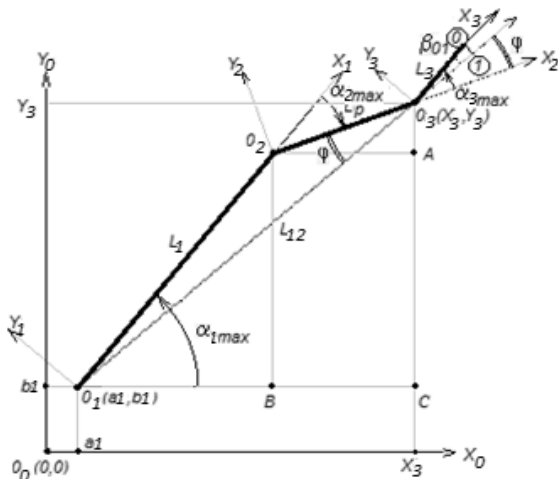


Fig. 3. The scheme of position of elements of the working equipment of excavator for definition of a turning angle of a bucket on the first site of a digging zone (0-1)

Using position of the working equipment with as much as possible lifted: a boom, a bucket arm and a bucket fig. 3, we will define:

- coordinates of the centre of turn of bucket  $O_3 (X_3, Y_3)$  in local system a boom  $O_1 X_1 Y_1$ :

$$X_3 = O_1 B + B X_3 = L_1 \cdot \cos(\alpha_{1max}) + L_2 \cdot \cos(\alpha_{1max} + \alpha_{2max}); \quad (9)$$

$$Y_3 = O_3 A + A X_3 = L_2 \cdot \sin(\alpha_{1max}) + L_2 \cdot \sin(\alpha_{1max} + \alpha_{2max}); \quad (10)$$

- coordinates of the centre of turn of bucket  $O_3(X_3, Y_3)$  in the basic system  $O_0 X_0 Y_0$ :

$$X1_3 = X_3 + a1; \quad (11)$$

$$Y1_3 = Y_3 + b1; \quad (12)$$

- Distance from an axis of a boom to an axis of bucket  $L_{12}$ , m

$$L_{12} = \sqrt{X_3^2 + Y_3^2}, \quad (13)$$

- The corner of turn of a bucket  $\beta_{01}$  on a site (0 - 1) will define from a triangle  $O_1 O_2 O_3$  fig. 3, using the theorem косинуса.

$$L_1^2 = L_2^2 + L_{12}^2 - 2 \cdot L_2 \cdot L_{12} \cdot \cos(\varphi); \quad (14)$$

$$\varphi = a \cos\left(\frac{L_2^2 + L_{12}^2 - L_1^2}{2 \cdot L_2 \cdot L_{12}}\right); \quad (15)$$

$$\beta_{01} = \alpha_{3max} - \varphi. \quad (16)$$

Further we will define a turn corner of a bucket on the first site of a digging zone of excavator - (2-3).

On fig. 4 the scheme of position of elements of the working equipment of excavator for construction of a site of a digging zone (2-3) by turning a bucket from a corner  $0$  to  $(-\varphi)$  is presented at boom position under a corner  $\alpha_{1min}$  and bucket arm under a corner  $\alpha_{2max}$ .

On fig. 4 the scheme of position of elements of the working equipment for definition of a turning anole of bucket on the third site of a digging zone (2-3) is presented. A bucket turns on the third site is made on a corner  $(-\varphi)$  at boom position under a corner  $\alpha_{1min}$  and bucket under a corner  $\alpha_{2max}$  to a line which are passing through an axis of turn of a bucket arm -  $O_2$  and an axis of turn of a bucket -  $O_3$ , providing the maximum start of a bucket on a following site (3-4) at bucket arm turn.

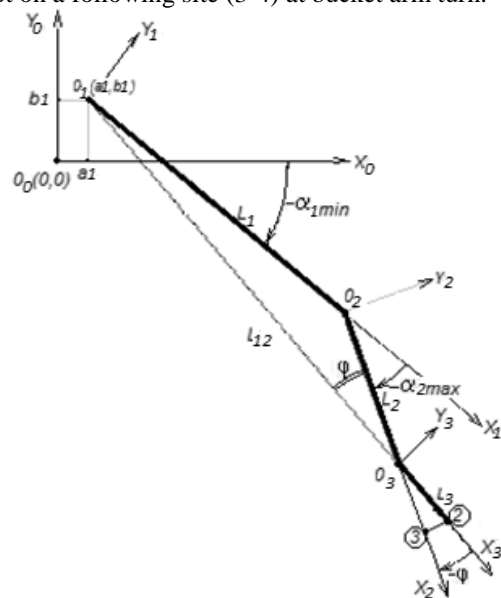


Fig. 4. The scheme of position of elements of the working equipment of excavator for definition of a corner of turn of a bucket on the third site of a digging zone of excavator (2-3)

## 6. COMPUTER MODELLING OF A DIGGING ZONE

The algorithm of computer modelling of a digging zone by excavator with the working equipment a return shovel in system Mathcad is presented below.

### Input data:

- max and min turning angles of boom in  $X_0Y_0$  plane, degree.  $\alpha_{1max} := 50deg$   $\alpha_{1min} := -60deg$
- distance between the axis of rotating platform and the axis of boom swing, m  $a1 := 0.2$
- distance between the natural surface of the ground and the axis of boom swing, m  $b1 := 2.0$
- max and min turning angles of bucket arm in  $X_1Y_1$  plane, degree.  $\alpha_{2max} := -20deg$   $\alpha_{2min} := -180deg$
- kinematic length of a boom, m  $L1 := 6.5$
- max and min turning angles of bucket arm in  $X_2Y_2$  plane, degree:  $\alpha_{3max} := 30deg$   $\alpha_{3min} := -120deg$
- kinematic length of a bucket arm, m  $L2 := 3.2$
- kinematic length of a bucket, m  $L3 := 1.64$
- vector of coordinates of a bucket tooth in local coordinates  $O_3X_3Y_3$  of a bucket, m

$$TZ := (L3 \ 0 \ 0 \ 1)^T$$

### Calculation procedure

1. Steps of change of angles of an inclination of boom  $\Delta \alpha_1$ , bucket arm  $\Delta \alpha_2$  and a bucket  $\Delta \alpha_3$ , radian

$$\Delta \alpha_1 := \frac{\alpha_{1max} - \alpha_{1min}}{N}$$

$$\Delta \alpha_2 := \frac{\alpha_{2max} - \alpha_{2min}}{N}$$

$$\Delta \alpha_3 := \frac{\alpha_{3max} - \alpha_{3min}}{N}$$

2. Calculation of the matrix  $M32(\alpha_3)$  of transfer from the co-ordinates of a bucket  $O_3, X_3, Y_3$  to the co-ordinates of a bucket arm  $O_2, X_2, Y_2$  and matrix  $M21(\alpha_2)$  transfer from the co-ordinates of a bucket arm  $O_2, X_2, Y_2$  to the co-ordinates of a boom  $O_1, X_1, Y_1$

$$M32(\alpha_3) := \begin{pmatrix} \cos(\alpha_3) & -\sin(\alpha_3) & 0 & L2 \\ \sin(\alpha_3) & \cos(\alpha_3) & 0 & 0 \\ 0 & 0 & 1 & 0 \\ 0 & 0 & 0 & 1 \end{pmatrix}$$

$$M21(\alpha_2) := \begin{pmatrix} \cos(\alpha_2) & -\sin(\alpha_2) & 0 & L1 \\ \sin(\alpha_2) & \cos(\alpha_2) & 0 & 0 \\ 0 & 0 & 1 & 0 \\ 0 & 0 & 0 & 1 \end{pmatrix}$$

3. Calculation of the matrix  $M10(\alpha_1)$  of transfer from the co-ordinates of a boom  $O_1, X_1, Y_1$  to the main co-ordinates of an excavator  $O_0, X_0, Y_0$

$$M10(\alpha_1) := \begin{pmatrix} \cos(\alpha_1) & -\sin(\alpha_1) & 0 & a1 \\ \sin(\alpha_1) & \cos(\alpha_1) & 0 & b1 \\ 0 & 0 & 1 & 0 \\ 0 & 0 & 0 & 1 \end{pmatrix}$$

4. Coordinates of the centre of turn of bucket  $O_3$  on a site (0-1)

$$X31 := L1 \cdot \cos(\alpha_{1max}) + L2 \cdot \cos(\alpha_{1max} + \alpha_{2max}) + a1 = 7.149$$

$$Y31 := L1 \cdot \sin(\alpha_{1max}) + L2 \cdot \sin(\alpha_{1max} + \alpha_{2max}) + b1 = 8.579$$

5. Distance from an axis of a boom to an axis bucket arm  $L12$ , m

$$L12 := \sqrt{(X31 - a1)^2 + (Y31 - b1)^2} = 9.57$$

6. Value of an angle of turn of a bucket on site (0-1), rad., using the cosine theorem

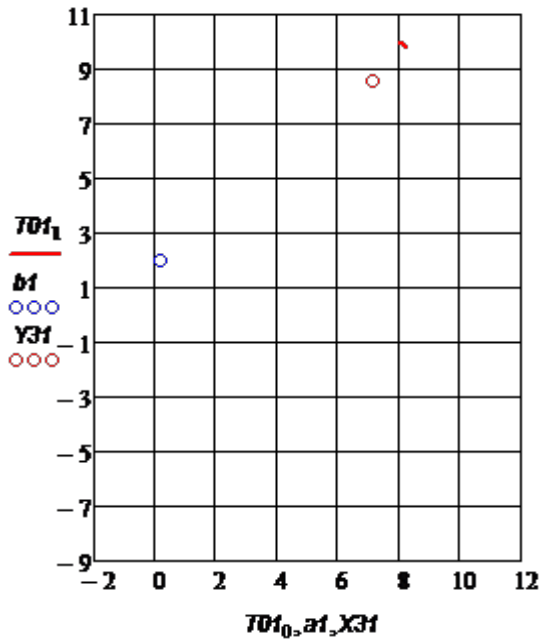
$$\varphi := \arccos\left(\frac{L2^2 + L12^2 - L1^2}{2 \cdot L2 \cdot L12}\right) = 0.234$$

$$\beta 01 := \alpha_{3max} - \varphi = 0.289$$

7. The program of calculation and the graph of a site (0-1) a working zone of an excavator: turn of a bucket from an angle  $\alpha_{3max}$  to an angle  $\beta 01$ ; a bucket arm under an angle  $\alpha_{2max}$ ; a boom under an angle  $\alpha_{1max}$ , radian

$$T01 := \begin{array}{l} \text{for } j \in 0..N \\ \alpha_{3j} \leftarrow \alpha_{3max} - j \cdot \Delta \alpha_3 \\ \alpha_{3j} \leftarrow \alpha_{3j} \text{ if } \alpha_{3j} > \beta 01 \\ \alpha_{3j} \leftarrow \beta 01 \text{ if } \alpha_{3j} < \beta 01 \\ T2 \leftarrow M32(\alpha_{3j}) \cdot TZ \\ T1 \leftarrow M21(\alpha_{2max}) \cdot T2 \\ T \leftarrow M10(\alpha_{1max}) \cdot T1 \\ X_j \leftarrow T_0 \\ Y_j \leftarrow T_1 \\ T01 \leftarrow \begin{pmatrix} X \\ Y \end{pmatrix} \end{array}$$

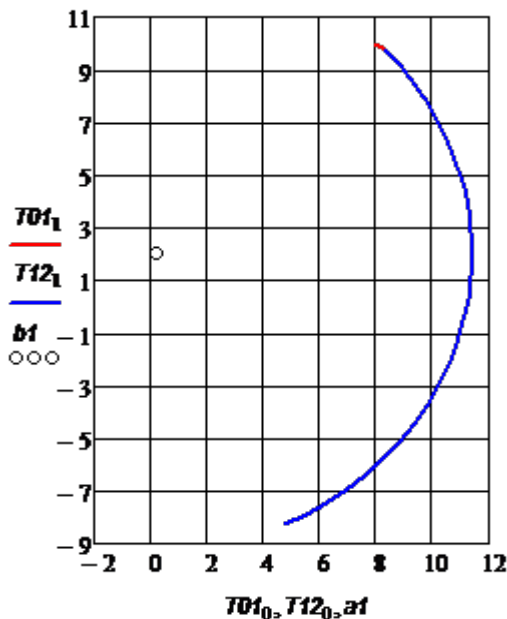
The graph of a site (0-1) working zones of an excavator



8. The program of calculation and the graph of a site (0-1-2) a working zone of an excavator: turn of a boom from angle  $\alpha 1max$  to  $\alpha 1min$ ; bucket arm under angle  $\alpha 2max$ ; a bucket under angle  $\beta 01$ , radian

$$T12 := \begin{cases} T2 \leftarrow M32(\beta 01) \cdot TZ \\ T1 \leftarrow M21(\alpha 2max) \cdot T2 \\ \text{for } j \in 0..N \\ \quad \alpha 1j \leftarrow \alpha 1max - j \cdot \Delta\alpha 1 \\ \quad T \leftarrow M10(\alpha 1j) \cdot T1 \\ \quad X_j \leftarrow T_0 \\ \quad Y_j \leftarrow T_1 \\ T12 \leftarrow \begin{pmatrix} X \\ Y \end{pmatrix} \end{cases}$$

The graph of a site (0-1-2) working zones of an excavator

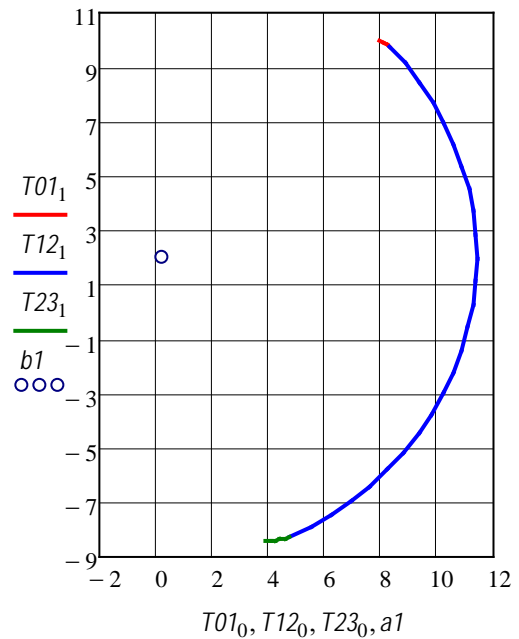


9. The program of calculation of a site (2-3) and the graph of a site (0-1-2-3) working zones of an excavator: turn of a bucket from an angle 0 to  $\beta 23$ ; a bucket arm under an angle  $\alpha 2max$ ; a boom under an angle  $\alpha 1min$ , radian

$$\beta 23 := -\varphi = -0.234$$

$$T23 := \begin{cases} \text{for } j \in 0..N \\ \quad \alpha 3j \leftarrow \beta 01 - j \cdot \Delta\alpha 3 \\ \quad \alpha 3j \leftarrow \alpha 3j \text{ if } \alpha 3j > \beta 23 \\ \quad \alpha 3j \leftarrow \beta 23 \text{ if } \alpha 3j < \beta 23 \\ \quad T2 \leftarrow M32(\alpha 3j) \cdot TZ \\ \quad T1 \leftarrow M21(\alpha 2max) \cdot T2 \\ \quad T \leftarrow M10(\alpha 1min) \cdot T1 \\ \quad X_j \leftarrow T_0 \\ \quad Y_j \leftarrow T_1 \\ T23 \leftarrow \begin{pmatrix} X \\ Y \end{pmatrix} \end{cases}$$

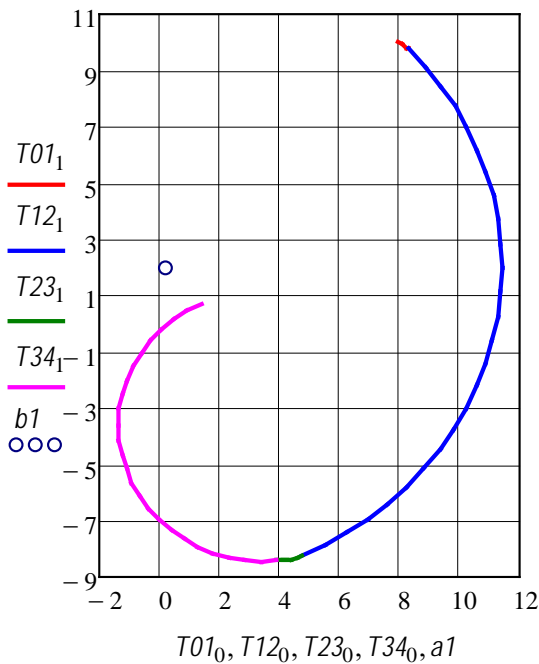
The graph of a site (0-1-2-3) working zones of an excavator



10. The program of calculation of a site (3-4) and the graph of a site (0-1-2-3-4) working zones of an excavator: a boom under an angle  $\alpha 1min$ ; turn of a bucket arm from an angle  $\alpha 2max$  to  $\alpha 2min$ ; a bucket under an angle 0

$$T34 := \begin{cases} \text{for } j \in 0..N \\ \alpha 2j \leftarrow \alpha 2max - j \cdot \Delta \alpha 2 \\ T2 \leftarrow M32(\beta 23) \cdot TZ \\ T1 \leftarrow M21(\alpha 2j) \cdot T2 \\ T \leftarrow M10(\alpha 1min) \cdot T1 \\ X_j \leftarrow T_0 \\ Y_j \leftarrow T_1 \\ T34 \leftarrow \begin{pmatrix} X \\ Y \end{pmatrix} \end{cases}$$

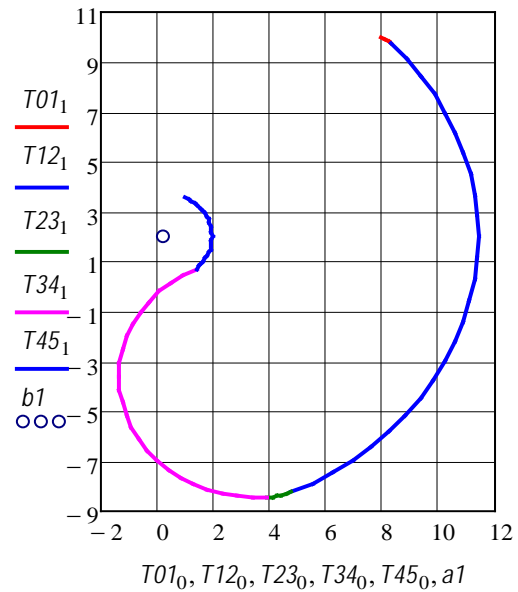
The graph of a site (0-1-2-3-4) working zones of an excavator



11. The program of calculation of a site (4-5) and the graph of a site (0-1-2-3-4-5) working zones of an excavator: turn of a boom from an angle  $\alpha 1min$  to  $\alpha 1max$ ; a bucket arm under a angle  $\alpha 2min$ ; a bucket under an angle 0

$$T45 := \begin{cases} \text{for } j \in 0..N \\ \alpha 1j \leftarrow \alpha 1min + j \cdot \Delta \alpha 1 \\ T2 \leftarrow M32(\beta 23) \cdot TZ \\ T1 \leftarrow M21(\alpha 2min) \cdot T2 \\ T \leftarrow M10(\alpha 1j) \cdot T1 \\ X_j \leftarrow T_0 \\ Y_j \leftarrow T_1 \\ T45 \leftarrow \begin{pmatrix} X \\ Y \end{pmatrix} \end{cases}$$

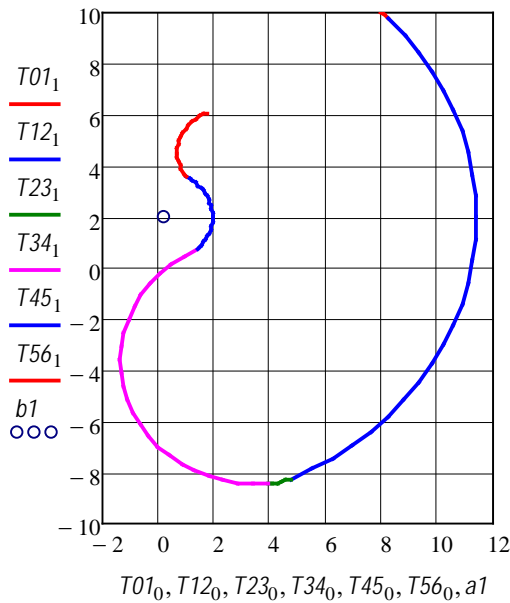
The graph of a site (0-1-2-3-4-5) working zones of an excavator



12. The program of calculation of a site (5-6) and the graph of a site (0-1-2-3-4-5-6) working zones of an excavator: a boom under an angle  $\alpha 1max$ ; a bucket arm under an angle  $\alpha 2min$ ; turn of a bucket from an angle 0 to  $\alpha 3min$ .

$$T56 := \begin{cases} \text{for } j \in 0..N \\ \alpha 3j \leftarrow \beta 23 - j \cdot \Delta \alpha 3 \\ \alpha 3j \leftarrow \alpha 3j \text{ if } \alpha 3j > \alpha 3min \\ \alpha 3j \leftarrow \alpha 3min \text{ if } \alpha 3j < \alpha 3min \\ T2 \leftarrow M32(\alpha 3j) \cdot TZ \\ T1 \leftarrow M21(\alpha 2min) \cdot T2 \\ T \leftarrow M10(\alpha 1max) \cdot T1 \\ X_j \leftarrow T_0 \\ Y_j \leftarrow T_1 \\ T56 \leftarrow \begin{pmatrix} X \\ Y \end{pmatrix} \end{cases}$$

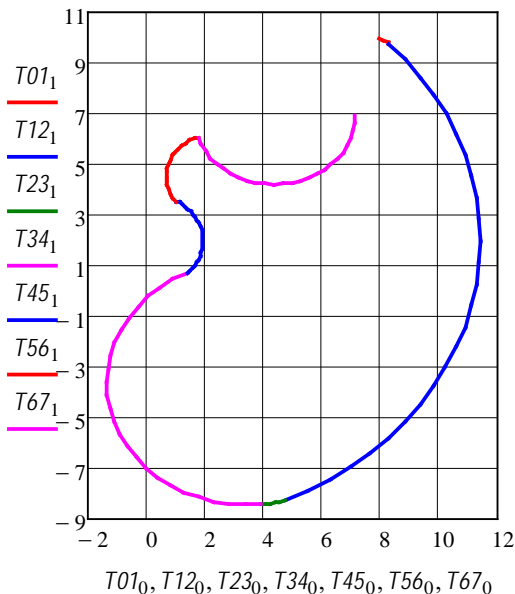
The graph of a site (0-1-2-3-4-5-6) working zones of an excavator



13. The program of calculation of a site (6-7) and the graph of a site (0-1-2-3-4-5-6-7) working zones of an excavator: a boom under an angle  $\alpha 1m a x$  ; turn of a bucket arm from an angle  $\alpha 2max$  to  $\alpha 2min$ ; a bucket under an angle  $\alpha 3min$

$$T67 := \begin{cases} T2 \leftarrow M32(\alpha 3min) \cdot TZ \\ \text{for } j \in 0..N \\ \quad \alpha 2j \leftarrow \alpha 2min + j \cdot \Delta \alpha 2 \\ \quad T1 \leftarrow M21(\alpha 2j) \cdot T2 \\ \quad T \leftarrow M10(\alpha 1max) \cdot T1 \\ \quad X_j \leftarrow T_0 \\ \quad Y_j \leftarrow T_1 \\ T67 \leftarrow \begin{pmatrix} X \\ Y \end{pmatrix} \end{cases}$$

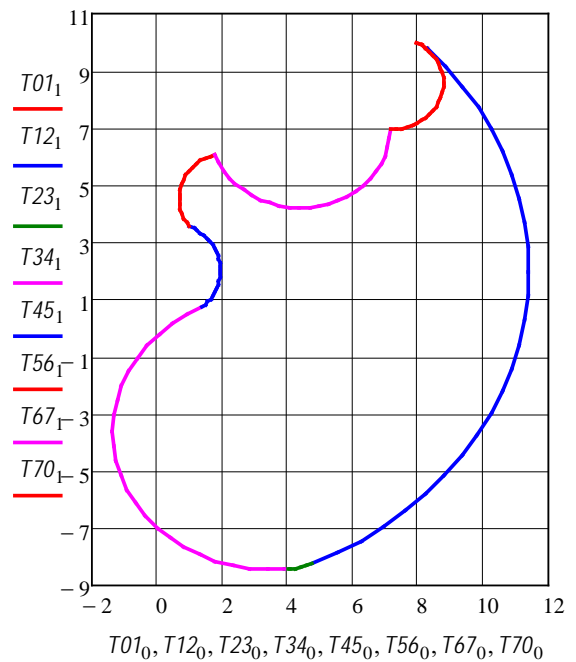
The graph of a site (0-1-2-3-4-5-6-7) working zones of an excavator



14. The program of calculation of a site (7-0) and the graph of a site (0-1-2-3-4-5-6-7-0) working zones of an excavator a boom under an angle  $\alpha 2m a x$  ; a bucket arm under an angle  $\alpha 2m a x$  ; turn of a bucket from an angle  $\alpha 3m in$  to  $\alpha 3m ax$

$$T70 := \begin{cases} \text{for } j \in 0..N \\ \quad \alpha 3j \leftarrow \alpha 3min + j \cdot \Delta \alpha 3 \\ \quad T2 \leftarrow M32(\alpha 3j) \cdot TZ \\ \quad T1 \leftarrow M21(\alpha 2max) \cdot T2 \\ \quad T \leftarrow M10(\alpha 1max) \cdot T1 \\ \quad X_j \leftarrow T_0 \\ \quad Y_j \leftarrow T_1 \\ T70 \leftarrow \begin{pmatrix} X \\ Y \end{pmatrix} \end{cases}$$

The graph of a site (0-1-2-3-4-5-6-7-0) working zones of an excavator



### 7. CONCLUSION

The offered algorithm of calculation and graphic representation of sites of a digging zone excavator with the working equipment the return shovel allows to reduce on order with system Mathcad use time and labour input of such calculations, and also to make the corresponding researches connected about change of parameters of elements of the working equipment.

## REFERENCES

- [1]. E.M. Kudryavtsev, "Building cars and the equipment" (with examples of calculations, including and on the computer): The Textbook. – M: Publishing house ASV, (Russia), (2012).
- [2]. E.M. Kudryavtsev, V.V.Stepanov," Execution of final qualifying work on the computer": the Manual for high schools. - M: the Publishing House "BASTET", (Russia), (2013).
- [3]. E.M. Kudryavtsev, "CAD systems of the machine and the equipment". The Textbook for high schools. M: Publishing house ASV, (Russia), (2013).
- [4]. E.M. Kudryavtsev, "The basis of the automated designing":The textbook for high schools. M: Publishing centre "Academy", p. 304 , 2011.
- [5]. E.M. Kudryavtsev," KOMPAS-3D V10. As much as possible full management". In 2 volumes. M: DMK Press. (Russia), (2018).
- [6]. E.M. Kudryavtsev, "Modeling, design and calculation of mechanical systems". M: DMK Press. p. 400, 2008.
- [7]. E.M. Kudryavtsev, "Practical work on KOMPAS-3D V8: Machine-building libraries". M.: DMK Press/ (Russia), (2007).
- [8]. E.M. Kudryavtsev, "Machine-building designing Mechanical Desktop". M.: DMK Press. (Russia), (2006).



# An Experimental Study on the Fatigue Response of 15-5 PH Stainless Steel Built by DMLS

D. Croccolo<sup>1</sup>, M. De Agostinis<sup>1</sup>, S. Fini<sup>1</sup>, G. Olmi<sup>1\*</sup>, A. Vranic<sup>2</sup>, S. Ciric-Kostic<sup>2</sup>

<sup>1</sup>Department of Industrial Engineering (DIN), University of Bologna, Bologna, Italy

<sup>2</sup>Faculty of Mechanical and Civil Engineering in Kraljevo, University of Kragujevac, Serbia

*The present study is focused on the fatigue strength of 15-5 PH stainless steel parts built by DMLS. Four sets of specimens were manufactured, mechanically and thermally treated, and tested under rotating bending fatigue. The samples of the first two sets were built with their longitudinal axis perpendicular or parallel to the vertical stacking direction. In both cases, a 1mm allowance was uniformly distributed. The samples of the third and the fourth sets were similarly generated, with the same orientations. The samples of the last two sets were built with cylindrical shape and with 3mm allowance at gage. The results, processed also by analysis of variance tools, indicate that, considering the first two sets, the fatigue limit, approximately 39% of the ultimate strength, is almost independent of the build orientation. Conversely, the samples with incremented allowance, which required significant machining at gage, exhibit a much higher fatigue limit, very close to the commonly accepted reference value of one-half of the ultimate strength. This is quite an interesting result, as machining seems to be able to remove the process-induced irregularities, thus making it possible to achieve comparable properties to those of wrought material.*

**Keywords: Fatigue strength, Stainless steel, Additive manufacturing, Direct Metal Laser Sintering, Build orientation, Machining**

## 1. INTRODUCTION

Nowadays, there is an increasing interest towards Additive Manufacturing (AM) techniques, as this technological process is potentially capable of producing even complexly shaped parts in a relatively short time [1]. In addition, the parts can be easily built, starting from a CAD model, which is automatically processed to determine the main manufacturing parameters and the required amount of material. The parts are built layer by layer in a similar manner to rapid prototyping of plastic materials: a high-power laser beam scans over a metallic powder bed and selectively melts the powder. The melted powder solidifies and forms a layer: upon the completion of each layer, powder is added, laser scanning is repeated and a subsequent layer is deposited [2-4]. The unused powder may be partly recycled for a further process. A possible drawback of AM techniques consists in the residual stresses that may be generated during part building. Therefore, suitably shaped supports are usually applied to safely attach the built part to a rigid base-plate, thus preventing its movements through the powder bed or distortions induced by the residual stress field [2]. Direct Metal Laser Sintering (DMLS) by EOS and Selective Laser Melting (SLM) by MTT Technologies Group can be mentioned among the most important AM processes for metals [4].

The aforementioned base-plate is usually placed on a horizontal plane, and the parts are generated along a vertical stacking direction. A number of studies, involving different materials and AM processes have been focused on the possible effect of the build direction on the mechanical static and fatigue responses of the manufactured parts. Some researchers investigated a possible influence of the angle between the main axis of inertia (namely, the longitudinal axis of the specimen) and the stacking direction on the part strength. Intensive

studies were performed on selective laser melted Ti6-Al-4V samples. The results indicated that the build orientation may significantly affect the fatigue response, in particular the endurance strength in the finite life domain. A higher life for the same load entity was retrieved for the build orientation where the layer plane is parallel to the loading axis [5]. A similar effect was also observed on fracture toughness [6]. The possible effect of the build direction on the fatigue response, considering both the fatigue limit and the fatigue strength in the finite life domain was also the topic of a previous study by the same authors. This research involved MS1 Maraging steel parts, built, considering three different orientations, with post-manufacture mechanical and heat treatments. An extended experimental campaign led to the result that the fatigue response is not significantly affected by the build direction, since, for Maraging steels, post-manufacture treatments have a great role at removing sources of anisotropy [7].

Further research in the literature was focused on the mechanical behaviour 15-5 PH stainless steel parts. This type of steel is commonly used in applications such as aircraft components, or for parts under high pressure or working in harsh corrosive environments, including valves, shafts, fasteners, fittings and gears [2, 8]. A lack of studies on the effect of the build direction on the fatigue properties of this steel can be pointed out. In particular, the research in [2] was focused on the build orientation effect on the static response only. Experimental results indicated that the response is enhanced, when the load direction acts along the layer plane, but the fatigue properties for different build directions were not investigated. Other studies are documented in [9-10], but are more oriented to the effects on technological issues like machinability, rather than to the outcomes on the fatigue strength.

\*Corresponding author: Giorgio Olmi, Department of Industrial Engineering (DIN), University of Bologna, Viale del Risorgimento 2, 40136 Bologna, Italy, e-mail: [giorgio.olmi@unibo.it](mailto:giorgio.olmi@unibo.it)

The subject of this paper consists in an experimental study on the fatigue response of 15-5 PH stainless steel parts fabricated by the *DMLS* process. Two factors were considered: the build direction and the fabrication procedure. In particular, two different build orientations were considered, with the main axis of inertia of the parts being aligned to the load direction or perpendicular to it. Regarding the fabrication procedure, the effect of allowance and subsequent machining was studied: in one case, a conventional 1mm allowance was considered, whereas, in the second one, a larger allowance was adopted with the consequent need of machining to the core of the part. Issues of novelty arise from the lack of studies dealing with fatigue on this steel. Furthermore, the general absence of investigations on the effect of allowance on the properties of *AM* processed parts of any material must be emphasized.

2. MATERIALS AND METHODS

The experimental campaign was performed under rotating bending, following the ISO1143 [11] Standard. Specimens were designed accordingly with reference to the cylindrical smooth geometry (with uniform cross section at gauge). The smallest dimension suggested by the standard, 6mm diameter at gauge was chosen as a good compromise between standard requirements and the need of reducing production costs. A drawing of the specimen is shown in Fig. 1, with indication of all its dimensions and tolerances. The chemical composition of 15-5 PH stainless steel (by EOS GmbH – Electro Optical Systems, Krailling/Munich, Germany) is provided in Table 1 [12].

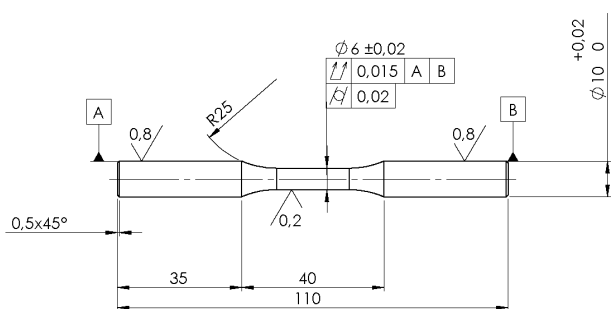


Figure 1: Specimen with 6 mm diameter at gauge in agreement with ISO 1143 Standard [11]

Table 1: Chemical composition of 15-5 PH Stainless Steel by EOS

Cr [%]	Ni [%]	Cu [%]	Mn [%]	Si [%]	Mo [%]	Nb [%]	C [%]	Fe [%]
14-15.5	3.5-5.5	2.5-4.5	≤ 1	≤ 1	≤ 0.5	0.15-0.45	≤ 0.07	Balance

The specimens were manufactured by EOSINT M280 system (EOS GmbH - Electro Optical Systems, Krailling/Munich, Germany), equipped with Ytterbium fibre laser with 200W power and emitting 0.2032mm thickness and 1064nm wavelength infrared light beam. The process takes place in an inert environment and the scanning speed may range up to 7000 mm/s. The layer thickness was set to 20 µm. A parallel scan strategy with alternating scan direction was adopted: for the subsequent layers the scanning direction was rotated to 70°, in order to prevent or reduce in-plane property variations. Some examples of the scanning patterns are shown in Fig. 2,

where arrows indicate the different scan directions at different stages of production and on different layers. A contour line was finally scanned, in order to complete the part shaping and to make its external surface as smoother as possible [13]. The machine features a working space with 250 × 250mm dimensions on the horizontal plane and a maximum height of 325mm.

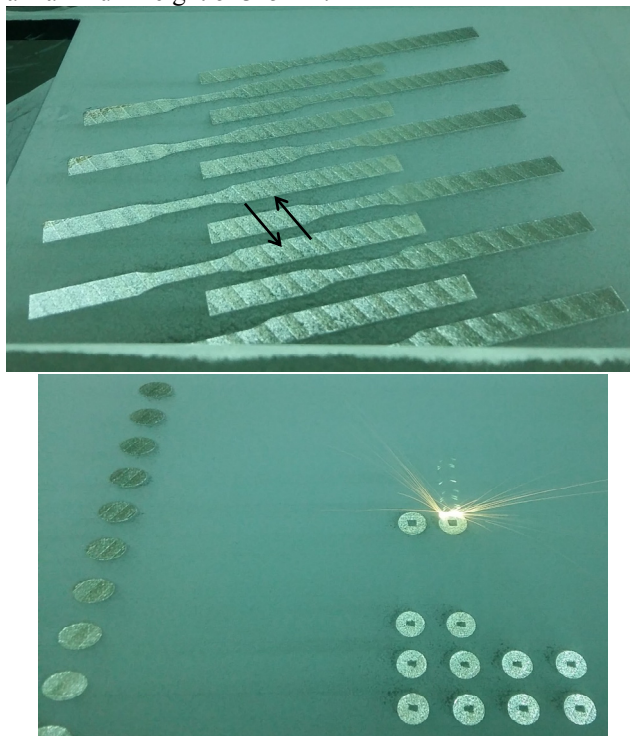


Figure 2: Some examples of the scanning patterns as the specimens are being built (arrows indicate the scan directions)

All the specimens underwent surface cleaning by micro-shot-peening: this treatment is usually performed in order to close the pores that may be induced by laser sintering. Afterwards, H900 heat treatment was performed [2, 12]: it consists in gradual heating in oven from room temperature to 482°C in 1 hour time, afterwards this temperature is kept constant for 2 hours. The parts are finally taken out of the oven and cooled in fresh air. This treatment, which is particularly effective at reducing the residual stresses, thus enhancing the fatigue response of the built parts, was performed maintaining the samples attached to their supports to prevent them from bending. Finally, the specimens underwent machining and refining by grinding with the aim of achieving the surface roughness requested by the ISO 1143 Standard [11] and of improving the fatigue performance.

Four specimen sets were manufactured: those of types #1 and #3 were built while lying horizontally on the base plate, therefore the angle between their longitudinal axis and the vertical stacking direction was 90°. Whereas, those of types #2 and #4 were built along the vertical direction: in this condition, the angle between their main axis of inertia and the stacking direction was 0°. The difference between the samples of sets #1 and #3 is that the first ones were produced with the same shape as shown in Fig. 1 with a 1mm allowance both at the gauge (diameter increased from 6 to 8 mm) and at the heads (diameter increased from 10 to 12 mm). The samples were then machined to meet the drawing specifications, regarding

dimensional and geometrical tolerances and roughness. Conversely, the samples of set #3 were built with a cylindrical shape with 12 mm diameter over their entire length. It means that the allowance was 1mm at the heads and 3mm at the specimen gage. These samples were also reworked to meet the same specifications of the drawing in Fig. 1. The same difference applies also to sets #2 (built with uniform allowance and reduced section at gage) and #4 (built with cylindrical layout). Each set was composed by 7 to 10 samples, considering that some samples were unfortunately damaged during manufacturing. Some stages of production, with reference to the aforementioned sample sets, are shown in Fig. 3.

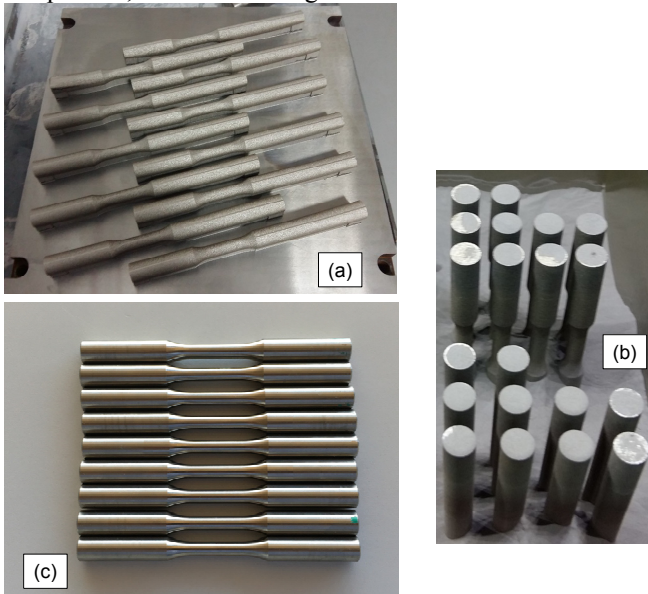


Figure 3: Some stages of sample production: (a) Set #1 samples just after DMLS manufacturing and before the heat treatment, (b) Sets #2 and #4 samples during residual powder removal with internal gage (top) and cylindrical shape (bottom), (c) Set #3 samples after machining and finishing, just before the beginning of the fatigue campaign

The fatigue campaign made it possible to obtain the *S-N* curves and the fatigue limits (*FLs*). A staircase method was applied to determine the *FL*: for this purpose, the series of failure and not-failure events was processed by the Dixon method [14-17]. A life duration of 107 cycles was set as run-out, based on the few available data on the fatigue response of sintered 15-5 PH stainless steel [2]. The Dixon method is an abbreviated staircase method that makes it possible to estimate *FL* even from a short series of nominal trials at staircase (four to six in this work). The estimation of the standard deviation makes also possible to provide an estimation of the uncertainty of the *FL* and to determine a confidence band to be applied to it. The data in the finite life domain were processed according to the Standard ISO 12107 [18]: the stress and life were linearly interpolated in logarithmic coordinates. The lower and upper limits of the *S-N* curve were been determined, based on the standard deviation of the logarithm of the fatigue life, and considering, respectively, probabilities of failure of 10% and 90% and a 90% confidence level.

### 3. EXPERIMENTAL PROCEDURE

All the samples were initially measured, in order to check the accomplishment of drawing requirements from the points of view of dimensions and roughness. For this purpose, a micrometre screw gauge, a digital calliper (both with the resolution of 0.01mm) and a portable surface roughness tester (with the resolution of 0.01  $\mu\text{m}$ , Handysurf E-30A; Carl Zeiss AG, Oberkochen, Germany) were used. The heads at both ends and the sample gauges were measured at 90° angled points with 4 replications. Similar measurements were performed at specimen gages with 6 replications. The averaged values are collected in Tables 2-5, referred to the left-side head of the four sample sets. Regarding roughness, it has also been measured, considering 90° angled points around full diameters at both specimen heads with 8 replications. Similar measurements were then carried out at the gages after sample breakage. The averaged values are included as well in the same Tables. All the yields are generally well consistent with the requirements in ISO 1143 [11] and with drawing specifications. The samples were also checked for hardness: *HRC* Rockwell hardness was determined on all the samples with three replications. The average values, ranging from 42 to 43.5 *HRC* confirm an Ultimate Tensile Strength (*UTS*) from 1325 to 1375 MPa, which is in the order of that indicated in [12, 19-20] of 1310 MPa.

Table 2: Measurement outcomes for the sample type #1

Specimen ID	Gauge diameter			Head diameter		
	Mean [mm]	St dev. [mm]	Roughness [ $\mu\text{m}$ ]	Mean [mm]	St dev. [mm]	Roughness [ $\mu\text{m}$ ]
1.1	6.01	0.064	0.190	10.04	0.014	0.44
1.2	5.89	0.106	0.200	9.93	0.055	0.52
1.3	6.09	0.064	0.296	10.06	0.005	0.27
1.4	6.06	0.022	X	10.06	0.010	0.39
1.5	6.05	0.029	0.289	10.03	0.012	0.59
1.6	6.07	0.031	0.128	10.04	0.021	0.60
1.7	6.00	0.039	0.178	9.99	0.020	0.17

Table 3: Measurement outcomes for the sample type #2

Specimen ID	Gauge diameter			Head diameter		
	Mean [mm]	St dev. [mm]	Roughness [ $\mu\text{m}$ ]	Mean [mm]	St dev. [mm]	Roughness [ $\mu\text{m}$ ]
2.1	6.03	0.035	0.400	10.01	0.005	0.38
2.2	6.01	0.029	0.323	10.01	0.002	0.30
2.3	6.02	0.036	0.413	10.01	0.004	0.31
2.4	5.98	0.044	0.246	10.01	0.005	0.41
2.5	6.02	0.027	0.425	10.01	0.003	0.35
2.6	6.00	0.026	0.338	10.00	0.002	0.35
2.7	6.01	0.035	X	10.01	0.002	0.37
2.8	6.02	0.036	0.340	10.00	0.003	0.35
2.9	6.01	0.025	0.370	10.00	0.003	0.36
2.10	6.00	0.038	0.308	10.00	0.010	0.44

Table 4: Measurement outcomes for the sample type #3

Specimen ID	Gauge diameter			Head diameter		
	Mean [mm]	St dev. [mm]	Roughness [ $\mu\text{m}$ ]	Mean [mm]	St dev. [mm]	Roughness [ $\mu\text{m}$ ]
3.1	6.01	0.014	0.270	10.02	0.002	0.64
3.2	6.01	0.016	0.340	10.02	0.005	0.48
3.3	6.01	0.011	X	10.01	0.003	0.71
3.4	6.00	0.009	0.260	10.02	0.009	0.65
3.5	6.01	0.010	X	10.02	0.003	0.50
3.6	6.00	0.014	0.440	10.02	0.005	0.59
3.7	6.01	0.008	0.250	10.02	0.003	0.63
3.8	6.01	0.009	0.400	10.02	0.003	0.64
3.9	6.00	0.012	0.350	10.02	0.004	0.63

Table 5: Measurement outcomes for the sample type #4

Specimen ID	Gauge diameter			Head diameter		
	Mean [mm]	St dev. [mm]	Roughness [ $\mu\text{m}$ ]	Mean [mm]	St dev. [mm]	Roughness [ $\mu\text{m}$ ]
4.1	6.03	0.041	0.300	10.00	0.002	0.22
4.2	6.00	0.019	0.369	10.00	0.003	0.28
4.3	6.00	0.028	X	10.00	0.003	0.23
4.4	6.01	0.040	0.363	10.00	0.003	0.30
4.5	6.00	0.036	X	10.00	0.002	0.32
4.6	6.01	0.040	0.398	10.00	0.003	0.31
4.7	6.01	0.026	X	10.00	0.003	0.25
4.8	6.02	0.032	0.328	10.00	0.003	0.27
4.9	6.00	0.019	0.478	10.00	0.003	0.24
4.10	6.00	0.018	0.280	10.00	0.002	0.23

The specimens were tested under rotating bending fatigue by a rotary bending testing machine, where the specimen is loaded in the four-point bending configuration, so that bending moment keeps constant over the entire sample length, and in particular at its gage [14]. The sample was pinched at its ends by a pressure of approximately 70 MPa [21-22]. All the tests were conducted under fully reversed bending load (stress ratio  $R = -1$ ) at the frequency  $f$  of 60 Hz. At the end of the experimental campaigns, some samples were cut and resin embedded. In particular, transverse sections of the gages and longitudinal sections of the heads were considered. Micrographic analyses were performed both at the gages and at the ends, following chemical attacks according to this recipe. 20 cc of Glycerol ( $\text{C}_3\text{H}_8\text{O}_3$ ) and 10 cc Nitric Acid ( $\text{HNO}_3$ ) were mixed together and the same was done with 20 cc of Chloridric Acid ( $\text{HCl}$ ) and 10 cc of Hydrogen peroxide ( $\text{H}_2\text{O}_2$ ). These two mixtures were finally 50%-50% mixed together.

#### 4. RESULTS

The results of the fatigue tests for type #1 specimens (horizontally built, with 1mm allowance) are collected in Table 6: in particular, sample identifier, the load level in terms of the applied force and of the nominal stress at gage, the observed life and the test outcome are reported.

Table 6: Data retrieved from the tests on the sample type #1

Specimen ID	Load [N]	Stress [MPa]	Life [N]	Failure
1.1	127.2	420	---	N
1.2	166.6	550	144,726	Y
1.3	158.8	524	167,829	Y
1.4	151.5	500	---	N
1.5	151.5	500	728,708	Y
1.6	143.9	475	8,423,284	Y
1.7	197.2	651	47,315	Y

Table 7: Data retrieved from the tests on the sample type #2

Specimen ID	Load [N]	Stress [MPa]	Life [N]	Failure
2.1	197.2	651	4,834,809	Y
2.2	215.4	711	1,871,476	Y
2.3	178.7	590	108,926	Y
2.4	178.7	590	68,686	Y
2.5	142.8	470	---	N
2.6	169.6	560	43,729	Y
2.7	160.6	530	---	N
2.8	169.6	560	2,807,208	Y
2.9	160.6	530	2,564,861	Y
2.10	151.5	500	5,047,111	Y

Table 8: Data retrieved from the tests on the sample type #3

Specimen ID	Load [N]	Stress [MPa]	Life [N]	Failure
3.1	206.0	680	---	N
3.2	215.4	711	3,274,162	Y
3.3	206.0	680	---	N
3.4	215.4	711	8,364,965	Y
3.5	206.0	680	---	N
3.6	242.4	800	183,582	Y
3.7	233.3	770	368,551	Y
3.8	224.2	740	297,241	Y
3.9	224.2	740	2,850,771	Y

Table 9: Data retrieved from the tests on the sample type #4

Specimen ID	Load [N]	Stress [MPa]	Life [N]	Failure
4.1	196.9	650	6,082,766	Y
4.2	215.4	711	7,366,205	Y
4.3	242.4	800	532,725	Y (NOT VALID)
4.4	178.7	590	---	N
4.5	187.8	620	1,256,019	Y (NOT VALID)
4.6	187.8	620	8,932,232	Y
4.7	178.7	590	---	N
4.8	187.8	620	6,397,216	Y
4.9	242.4	800	260,944	Y
4.10	233.3	770	503,334	Y

The results of sets #2 (vertically built, with uniform allowance), #3 (horizontally built, with greater allowance at gage) and #4 (vertically built, with greater allowance at gage) are respectively reported in Tables 7-9, where the same data are present. A not failure outcome indicates that the trial was stopped upon run-out without breakage occurrence. In the case of failure, it was of course checked that specimen separation had occurred at gage. Afterwards, the fracture surfaces were observed to make sure that a fatigue initiation and propagation mechanism was actually responsible of the observed failure. Most failures regularly occurred at gage, but in two cases, for the same sample set (Set #4), unusual and unexpected failures at specimen heads were observed. One of these failures is depicted in Fig. 4. It must be remarked that this outcome is not completely new, as it had also been observed (again in two cases) in the previous research regarding Maraging steels. In that study, an analysis by dye penetrants had indicated the presence of some spots of unconformable roughness, which were likely to have triggered the crack in combination with the clamping

pressure. In the present study, the roughness at sample ends was carefully checked by multiple measurements and was found to be consistent with specifications. The analysis was therefore deepened by micrographic analyses, as described in the previous Section.



Figure 4: Unexpected failure at sample head

The samples that were involved in the aforementioned outcome were of course discarded for further processing regarding the fatigue response. The final outcomes of these two trials are therefore tagged as NOT VALID in Table 9. The other results were anyway sufficient to determine both the sloping part of the S-N curve and the fatigue limit.

5. DISCUSSION

The results reported in the previous Section were initially processed, in order to determine the fatigue curves in the finite life domain. The S-N curves, retrieved as linear regressions in double logarithmic scale, are plotted in the graphs in Figs 6-9 for sets #1 to #4 respectively. The corresponding equations that yield the expected life as a function of the actual stress level are included in the figures. The related maximum likelihood bands at the 90% confidence level and the experimental data are also plotted in the same diagrams, following the recommendations of [18]. The experimental results can be generally well fitted along a straight line with a linear correlation coefficient ( $R^2$ ) up to 0.8.

The slopes of the interpolating lines were also determined during the regression procedure. The angle between the S-N line and the vertical axis is  $86^\circ$  for set #1,  $88^\circ$  for set #2,  $88^\circ$  for set #3 and  $85^\circ$  for set #4. The resulting inclination can be compared to those of the S-N curves determined for Maraging Steel MS1: considering Ref. [7] the angles of the determined curves were ranging between  $75^\circ$  and  $80^\circ$ . The generally higher angle retrieved for stainless steel indicates that its S-N curves have a less steep trend, where small variations of the state of load may correspond to huge variations of the fatigue life, from the order of  $10^5$  to almost  $10^7$  cycles. A great role seems to be due to the level of roughness: as documented by the data in Tables 2-5, related values were quite low in this study, ranging from  $0.2$  to  $0.3\mu\text{m}$  as an average. The experimentations reported in [19-20] were performed on samples of the same material and with comparable roughness and led to a nearly horizontal curve, with a similar slope. Conversely, the experimentations in [2], involving the same stainless steel produced by SLM, were performed on samples with a 10-time higher roughness and led to a much lower fatigue resistance with a particularly sharp drop of the curve for increasing life (corresponding to a much lower angle).

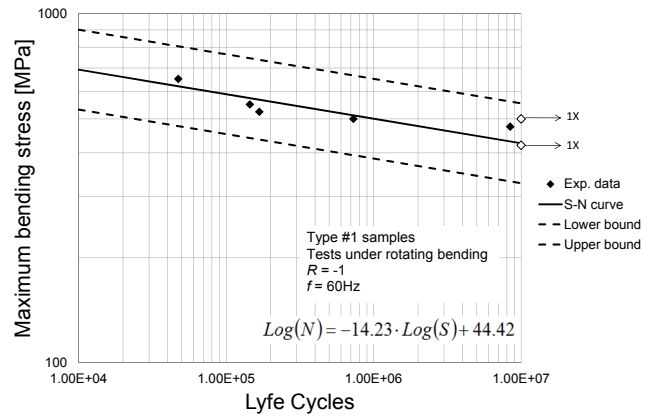


Figure 5: S-N curve for type #1 specimens (arrows indicate run-outs)

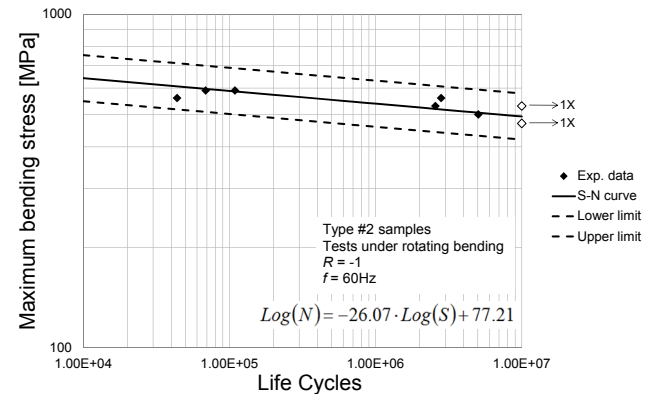


Figure 6: S-N curve for type #2 specimens (arrows indicate run-outs)

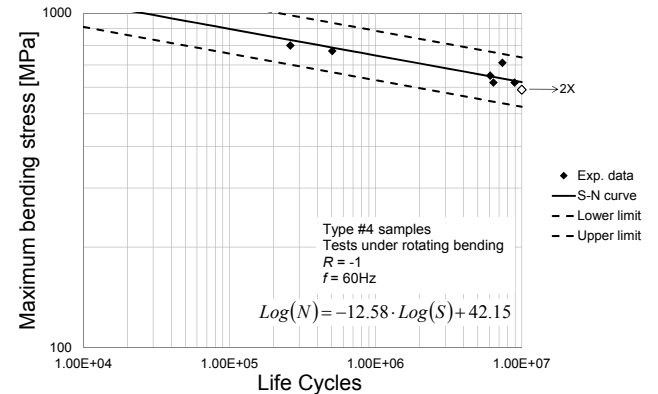


Figure 7: S-N curve for type #3 specimens (arrows indicate run-outs)

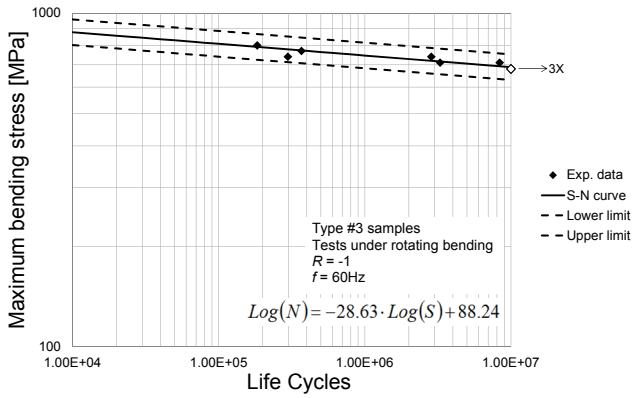


Figure 8: S-N curve for type #4 specimens (arrows indicate run-outs)

The results of the trials at staircase were processed by the Dixon method and led to the estimation of the *FLs* collected in the bar graph in Fig. 10, along with related confidence bands. The limit for the sample type #1 was estimated as 480 MPa, a well comparable value to that for type #2, 507 MPa. The other limits were conversely significantly higher: 701MPa for type #3 and 605MPa for the fourth sample set.

It is interesting to compare the determined *FLs* to the *UTS* strength of the material according to [12, 19-20], considering that a commonly accepted ratio (*FL/UTS*) is approximately 50% for metallic materials [23]. The *FLs* for horizontally and vertically built samples with 1mm allowance are quite close each other and correspond to 37% and 39% of the *UTS*. This isotropic behavior is consistent to that reported in [7] for Maraging steels. Moreover, the determined ratios to *UTS* are lower than 50%, but about ten points higher than the same ratio determined for Maraging steel. It indicates that, on one hand the *DMLS* processed parts have a lower fatigue limit than expected, but that this detrimental effect is less significant for 15-5 Stainless steel rather than for Maraging steel.

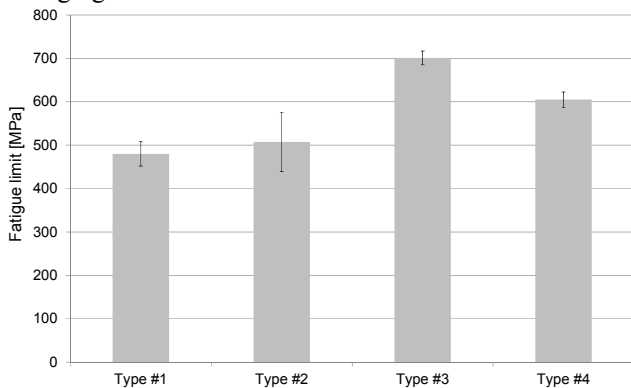


Figure 9: Bar graph summarizing the fatigue limits for the four sample types along with their confidence bands

Regarding the *FLs* for sets #3 and #4, ratios to *UTS* are respectively 54% and 46%. This outcome indicates that a post-manufacture machining up to the material core seems to have a beneficial effect on the fatigue response. In particular, the post-manufacture machining seems to be able to remove the irregularities at the surface layers, where, as remarked in the Materials and Methods Section, contour lines are scanned to complete the part shaping.

These irregularities may be able to trigger fatigue cracks and may therefore be responsible of the aforementioned lower fatigue response of *DMLS* (and generally *AM*) processed parts. As a consequence, the ratio to *UTS* is significantly increased up to the reference value of 50%. Moreover, the response is better, when the load direction acts on the layer plane, which is consistent to the results in [5-6] for Maraging steels and in [2] for the same steel under static load.

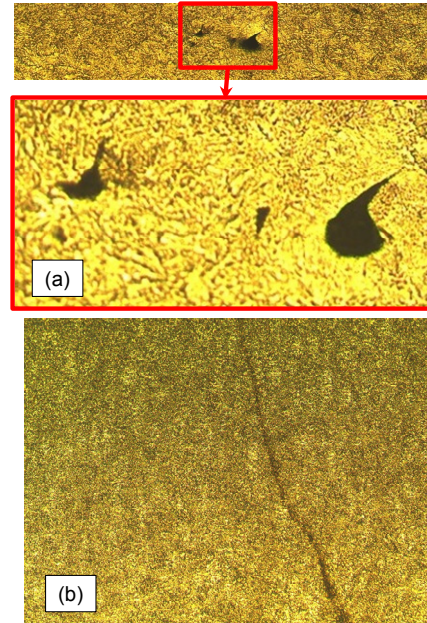


Figure 10: (a) Example of a void; (b) transverse crack detected at specimen head

Finally, some micrographic and fractographic analyses were performed on the samples, to check the material structure and to investigate the possible reasons for the unexpected failures at heads. It can be remarked that some voids were observed: an example is shown in Fig. 10 (a). These voids are likely to have triggered most of these irregular failures, acting in combination with the clamping pressure. In addition, it is interesting to observe that a transverse crack was observed at the head of a specimen of Set #4 that had regularly broken down at the gage. It may indicate that another crack was propagating at the head, but that separation at the gage occurred earlier.

The visual observation of the regular cracks at gage by stereo and optical microscopes indicated that pores with 30-40µm diameter just beneath the surface (at about 80µm depth) were responsible for the initiation of most cracks. An example is shown in Fig. 11.

Finally, some micrographies were devoted to the observation of the microstructure generated by the building process: the picture in Fig. 12 (a) was taken along the build plane: it can be observed that laser scans on contiguous planes are well visible and the related angle (highlighted) is consistent with the process setting. A micrography along a perpendicular plane (parallel to the vertical stacking direction) is finally depicted in Fig. 12 (b), where the build direction is also indicated. These outcomes indicate that the *AM* induced structure is still well visible, even after the recommended heat treatments.

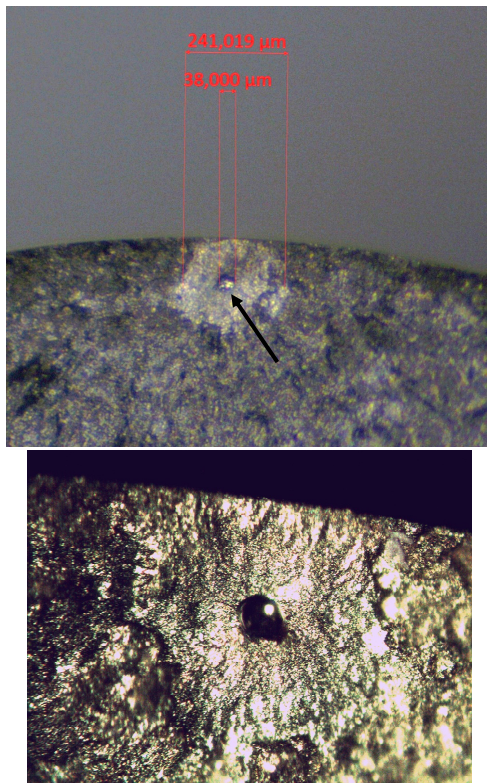


Figure 11: Example of a pore that triggered a crack

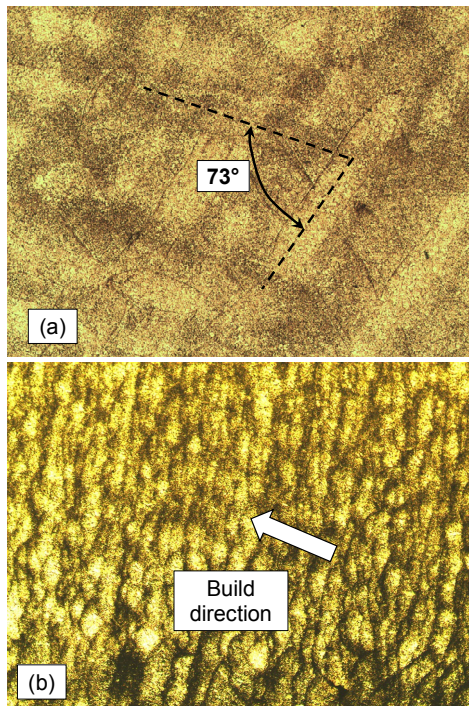


Figure 12: Micrographic analyses on unmachined horizontally built samples: (a) laser scans on the build plane (contiguous planes are visible, relative angle highlighted), (b) layers along the stacking direction

## 6. CONCLUSIONS

This study aims at defining the fatigue strength of 15-5 PH Stainless Steel manufactured by direct selective laser sintering (DMLS) machine. Literature survey indicated that Additive Manufacturing (AM) techniques, such as DMLS or Selective Laser Melting are highly effective at producing even complicated parts. Moreover, there is a lack of data concerning the fatigue response of

AM processed parts of the aforementioned stainless steel. Four sample sets were manufactured: horizontally and vertically built with uniform allowance and with an incremented allowance at specimen gage (manufactured as cylindrical parts). This experiment can therefore be regarded as a two-factor plan with two levels (2<sup>2</sup>). The results indicate that the fatigue curves have a high inclination with respect to the vertical axis and that the fatigue limits of horizontally and vertically built samples with uniform allowance are almost the same. The ratio of the fatigue limits to the ultimate tensile strength is approximately 38%. Conversely, when considering samples with higher allowance, which required the removal of a remarkable amount of material at gage, the fatigue limit is averagely one-half of the ultimate strength. Machining up to the material core seems to be able remove the additive process induced irregularities at the external layers that reduce the fatigue strength of AM processed parts. Moreover, the limit was higher for samples where the layer planes are parallel to the load direction. Afterwards, fractographic and micrographic analyses made it possible to provide explanations to the observed outcomes, and to check the microstructure resulting from the additive process.

## ACKNOWLEDGEMENTS

The research presented in this paper has received funding from the European Union's Horizon 2020 research and innovation programme under the Marie Skłodowska-Curie grant agreement No. 734455.

## REFERENCES

- [1] F. Abe, K. Osakada, M. Shiomi, K. Uematsu and M. Matsumoto, "The manufacturing of hard tools from metallic powders by selective laser melting", *Journal of Materials Processing Technology*, Vol. 111, pp. 210-213, (2001)
- [2] H.K. Rafi, T.L. Starr and B.E. Stucker, "A comparison of the tensile, fatigue, and fracture behaviour of Ti-6Al-4V and 15-5 PH stainless steel parts made by selective laser melting", *The International Journal of Advanced Manufacturing Technology*, Vol. 69, pp. 1299-1309 (2013)
- [3] E. Santos, S. Masanari, K. Osakada and T. Laoui, "Rapid manufacturing of metal components by laser forming", *International Journal of Machine Tools and Manufacture*, Vol. 46, pp. 1459-1468 (2006)
- [4] E. Herderick, "Additive Manufacturing of Metals: A Review", *Proceedings of "Materials Science and Technology (MS&T)"*, October 16-20, 2011, Columbus, Ohio, (2011)
- [5] P. Edwards and M. Ramulu, "Fatigue performance evaluation of selective laser melted Ti-6Al-4V", *Materials Science and Engineering A*, Vol. 598, pp. 327-337, (2014)
- [6] P. Edwards and M. Ramulu, "Effect of build direction on the fracture toughness and fatigue crack growth in selective laser melted Ti-6Al-4V", *Fatigue & Fracture of Engineering Materials & Structures*, Vol. 38, pp. 1228-1236 (2015)
- [7] D. Croccolo, M. De Agostinis, S. Fini, G. Olmi, A. Vranic and S. Ciric-Kostic, "Influence of the build

orientation on the fatigue strength of EOS maraging steel produced by additive metal machine", *Fatigue & Fracture of Engineering Materials & Structures*, Vol. 39, pp. 637-647, (2016)

[8] M. Abdelshehid, K. Mahmodieh, K. Mori, L. Chen, P. Stoyanov, D. Davlantes, J. Foyos, J. Ogren, R. Clark Jr. and O.S. Es-Said, "On the correlation between fracture toughness and precipitation hardening heat treatments in 15-5PH Stainless Steel", *Engineering Failure Analysis*, Vol. 14, pp. 626-631, (2007)

[9] K. Ozbaysal and O.T. Inal, "Age-hardening kinetics and microstructure of PH 15-5 stainless steel after laser melting and solution treating", *Journal of Materials Science*, Vol. 29, pp. 1471-1480, (1994)

[10] D. Palanisamy, P. Senthil and V. Senthilkumar, "The effect of aging on machinability of 15Cr-5Ni precipitation hardened stainless steel", *Archives of Civil and Mechanical Engineering*, Vol. 16, pp. 53-63, (2016)

[11] International Organization for Standardization ISO 1143:2010, "Standard - Metallic materials – Rotating bar bending fatigue testing", International Organization for Standardization (ISO), Geneva, Switzerland, (2010)

[12] <http://www.eos.info/material-m>

[13] D. Croccolo, M. De Agostinis and G. Olmi, "Experimental characterization and analytical modelling of the mechanical behaviour of fused deposition processed parts made of ABS-M30", *Computational Materials Science*, Vol. 79, pp. 506-518, (2013)

[14] G. Olmi and A. Freddi, "A new method for modelling the support effect under rotating bending fatigue: Application to Ti-6Al-4V alloy, with and without shot peening", *Fatigue and Fracture of Engineering Materials and Structures*, Vol. 36 (10), pp. 981-993, (2013)

[15] W.J. Dixon and F. Massey Jr., "Introduction to Statistical Analysis", McGraw-Hill, New York, United States, (1983)

[16] G. Olmi, M. Comandini and A. Freddi, "Fatigue on shot-peened gears: Experimentation, simulation and sensitivity analyses", *Strain*, Vol. 46 (4), pp. 382-395 (2010).

[17] B. Van Hooreweder, D. Moens, R. Boonen and P. Sas, "The critical distance theory for fatigue analysis of notched aluminium specimens subjected to repeated bending", *Fatigue and Fracture of Engineering Materials and Structures*, Vol. 35, pp. 878-884 (2012)

[18] International Organization for Standardization ISO 12107:2003, "Metallic Materials – Fatigue Testing – Statistical Planning and Analysis of Data", International Organization for Standardization (ISO), Geneva, Switzerland, (2003)

[19] ASM International, "ASM Handbook", Vol. 1, Materials Park, Ohio, (2016)

[20] ASM International, "ASM Handbook", Vol. 2, Materials Park, Ohio (2016)

[21] D. Croccolo, M. De Agostinis and G. Olmi, "Fatigue life characterisation of interference fitted joints", *Proceedings 2013 ASME International Mechanical Engineering Congress and Exposition*, in Proc. IMECE 2013, San Diego, CA, United States, Vol. 2B, V02BT02A015 (10 pages), (2013)

[22] D. Croccolo, M. De Agostinis, S. Fini, A. Morri and G. Olmi G, "Analysis of the Influence of Fretting on the Fatigue Life of Interference Fitted Joints", *Proceedings ASME - American Society of Mechanical Engineers*, Montreal, Canada, 14-20, November, 2014, Vol. 2B: Advanced Manufacturing, pp. 1-10, 2014.

[23] G. Niemann, H. Winter, B.R. Hohn, "Maschinenelemente", Springer-Verlag, Berlin, Germany (2005)



# Tribological Properties of Detergents as Additives for Motor Oils

A.I. Dotsenko, V. D. Samusenko<sup>1\*</sup>

<sup>1</sup> National Research Moscow State University of civil engineering

*Conducted research in a wide temperature range anti-friction properties of detergent – phenolate and calcium sulfonates of different levels of alkalinity as additives to polyalphaolefine oil. It is found that in the formation of a detergent of boundary lubricating layers main role belongs to the calcium carbonate.*

**Keywords: detergents, lubrication oil; two-stroke petrol engines; temperature; coefficients of friction**

## 1. INTRODUCTION

Detergent – it is a surface-active substance. It contains molecules that are able to stick round grease particles and rinse them from the surface.

The influence of surfactants as detergents is currently studied adequately. At the same time, the issues associated with the study of the tribological properties of the detergents, as additives for motor oils, is not yet sufficiently studied and are the subject of research in National Research Moscow State University of civil engineering [1].

Study of tribological properties of detergents was realized for two-stroke petrol engines.

Two-stroke petrol engines are used mainly where critical parameters of the choice are the high power density, lightweight and low price (for example, drones, scooters, chainsaws, construction equipment, outboard applications, etc). One of the main features of operation of two-stroke engines is absence of the lubrication system in them. Almost in all two-stroke engines the total-loss lubrication is applied. Oil does not circulate, and the recommended amount of motor oil is diluted in fuel, and through the carburetor this fuel and oil mixture gets to the engine. Mixture passes through the engine with a high speed, the part of oil in the form of a thin film settles on details, and it lubricate. The rest of oil burns down together with fuel in a combustion chamber. Simple engines, use the way of mixing which is that the corresponding oil quantity mixes up manually with petrol concerning from 1:20 to 1:100.

In this regard increased requirements are imposed to quality of oils for two-stroke petrol engines. Are the most important: prevention of intensive wear and scuffing; prevention of formation of deposits on details in a combustion chamber [2]. Also big importance was gained by ecological requirements.

During development oils for two-stroke petrol engines the different research equipment – translatory oscillation apparatus [3, 4], four-ball test machine [5] is applied to an initial assessment of lubricant property.

As the important characteristic of motor oils exerting considerable impact on lubricating property is their thermal stability at friction. In this work, were used a temperature method [5] for receiving temperature–friction characteristics of the chosen oils. So using this method the inverse correlation between critical temperatures of a

number of motor oils and wear of piston rings has been established in four-stroke internal combustion engines [6]. The preliminary estimate in consequence of the analysis of results the tribological tests of oils for two-stroke petrol engines by this method allows to evaluate lubricating properties of oils with the broad range of temperatures and the level of deposits on details.

## 2. THE OBJECT OF THE STUDY

The objects of a study of the lubricating properties of detergents were calcium sulfonates, which are one of the most widely used detergents in current motor oils. The used sulfonates differ in the value of the initial base number, which varied in the range of 15–400 mg KOH/g (Table 1).

To exclude the influence of the colloidal structure of detergents on their tribological characteristic, they were studied at a concentration of 1.0 vol %, which exceeds the concentration critical micelle formation of the studied compositions. The additives were introduced in poly alpha olefin oil PAO-4 in the above concentration ( $v_{100} \approx 4 \text{ mm}^2/\text{s}$ ). This oil has a high purity and was chosen due to the minimum influence of natural detergents on the behavior of the studied additives.

It is known that calcium sulfonate forms a micellar solution and is a colloidal dispersion of calcium carbonate ( $\text{CaCO}_3$ ) stabilized by neutral sulfonate [8]. In turn, the  $\text{CaCO}_3$  dispersion has an average particle size of <10 nm, a density of  $\sim 2200 \text{ kg/m}^3$  (versus  $1200\text{--}1700 \text{ kg/m}^3$  in neutral sulfonate), and is characterized by a quasi-stable (vaterite) form. On the whole, 60–70% of the alkali reserve of the additive is determined by the  $\text{CaCO}_3$  content; upon an

**Table 1.** Base numbers of the studied calcium sulfonates

Detergent	Base number, mg KOH/g
C1	15
C2	150
C3	175
C4	370
C5	400

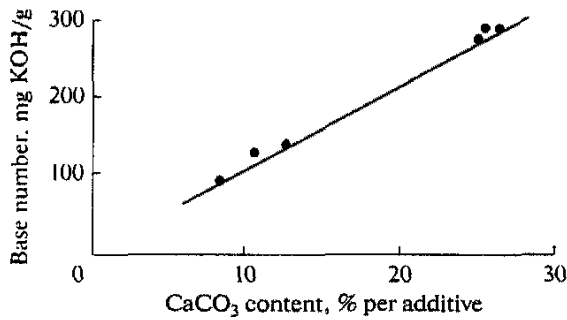


**Fig. 1.** Dependence of the base number of calcium sulfonates on the content of carbonates ( $\text{CaCO}_3$ ). Graph is developed according to [9].

increase in the carbonate concentration, the base number of the detergent increases (Fig. 1).

According to the structure and composition of detergents, they are not supposed to demonstrate high reactivity toward metals of a friction pair with the formation of chemically modified layers that have a noticeable influence on the friction and wear processes. Under these conditions, the influence of dispersions ( $\text{CaCO}_3$ ) in the composition of detergents, which determine their alkalinity, or other technological admixtures is mainly apparent.

The detergent (calcium sulfonate) can be considered to be a combination of three components, namely, neutral calcium sulfonate, calcium carbonate ( $\text{CaCO}_3$ ), and base oil. As mentioned above, the content of calcium carbonate mainly determines the alkalinity of the additive: under its increase, the base number increases. Neutral calcium sulfonate causes a slight additional alkalinity of the additive owing to  $\text{CaO}$  and  $\text{Ca}(\text{OH})_2$ . It is assumed that the used base oil does not noticeably influence the tribological characteristics of the studied detergents.

### 3. METHODS

The tests were performed using a KT-2 (GOST 23-221) four-ball friction machine [7], in which, in order to prevent noticeable friction heating, low sliding speed in the friction assembly is provided, and friction samples and the surrounding oil layer are heated using an external heat source. Samples were 100Cr6 steel balls with a diameter of 7.94 mm. The axial load was 107.8 N, the contact load on one ball was 44.2 N, and the pressure in the contact of the upper and each of the lower balls (Hertz) was about 2.1 GPa. The sliding speed on the contact surface was 0.24 mm/s (Fig. 2).

The study was performed in the temperature range of 30–300°C, which is close to the oil temperatures in internal combustion engines. The temperature of the friction assembly increased stepwise using an external heat source at a rate of 5°C/min. The coefficient of friction was evaluated every 10–20°C. The duration of the experiment at each temperature was 60 s. The estimated indicators were the dependences of the coefficient of friction  $f$  on the temperature  $T$ , i.e., the function  $f = F(T)$ . The

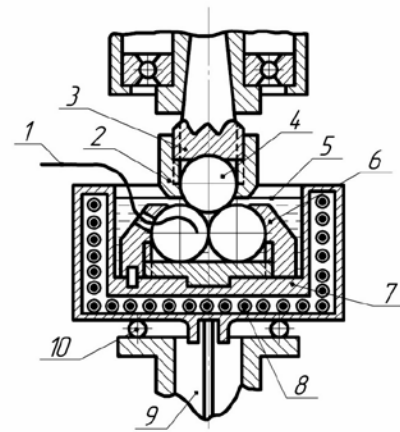


**Fig. 2.** The machine of friction: 1 – thermoelectrigrig; 2 – nut; 3 – tige; 4 – ball; 5 – oil; 6 – mounting; 7 – beaker for oil; 8 – worming up; 9, 10 – support

curves were developed using the average values of three tests.

The preference of this technique compared to other methods for evaluating the friction and wear lies in the fact that the change in  $f$  also helps to determine the energy of the formation and destruction of the boundary lubricating layers. The chemical composition of the surface layers contacting bodies was determined using a FEI Quanta 200 scanning microscope with an Apollo 40 device for elemental analysis by energy dispersive spectroscopy [10].

### 4. RESULTS AND DISCUSSION

The results of the experiments are shown in Fig. 3. It follows from the obtained data that the addition of detergents in base oil leads to a significant decrease in the coefficient of friction in all the temperature interval; note that, upon a increase in the base number of the detergent, its tribological characteristics improve.

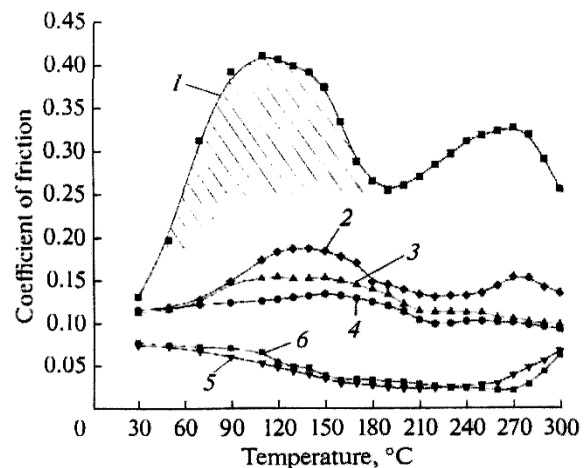


**Fig. 3.** Dependence of coefficient of friction of detergents with different alkalinities on the temperature: (1) PAO-4; (2) PAO-4 + 1% C1; (3) PAO-4 + 1% C2; (4) PAO-4 + 1% C3; (5) PAO-4 + 1% C4; (6) PAO-4 + 1% C5. Hatching denotes the zone of the sharp change in the coefficient of friction.

**Table 2.** Testing results of the studied lubricant compositions

Lubricant composition	$T_{i1}$ , °C	$T_{i2}$ , °C	$T_{i3}$ , °C	$f_{max}$	$f_{min}$	Average $d_w$ , $\mu\text{m}$
PAO-4	30	–	–	0.41	0.1315	234
PAO-4 + 1% C-1	70	210	250	0.1875	0.116	222
PAO-4 + 1% C-2	70	210	–	0.155	0.11	212
PAO-4 + 1% C-3	–	210	–	0.135	0.0935	206
PAO-4 + 1% C-4	–	160	260	0.0745	0.023	207
PAO-4 + 1% C-5	–	160	270	0.078	0.021	205

The curves of the dependence of the coefficient of friction on the temperature developed under preset conditions are similar to the curves obtained as a result of testing chemically active additives [8]. Denote the transitional temperatures through  $T_{i1}$ ,  $T_{i2}$ , and  $T_{i3}$ . Assume that  $T_{i1}$  is the boundary layer destruction temperature, which is caused by the sharp increase in the coefficient of friction;  $T_{i2}$  is the temperature at which a modified layer is formed of the friction surface, which manifests in a decrease in the coefficient of friction establishing it at a constant level in a certain temperature range;  $T_{i3}$  is the destruction temperature of the modified layer, which manifests in a sharp increase in the coefficient of friction. The values of the transitional temperatures and the coefficients of friction at typical temperatures are shown in Table 2.

In the case of PAO-4, the decrease in the coefficient of friction at temperatures exceeding  $T_{i1}$  is apparently caused by the fact that, in the temperature range of 50–160°C, the intense sharp change in the coefficient of friction occurs. After the completion of this period, the stabilization of the coefficient of friction follows, which is probably caused by the breaking-in of surfaces.

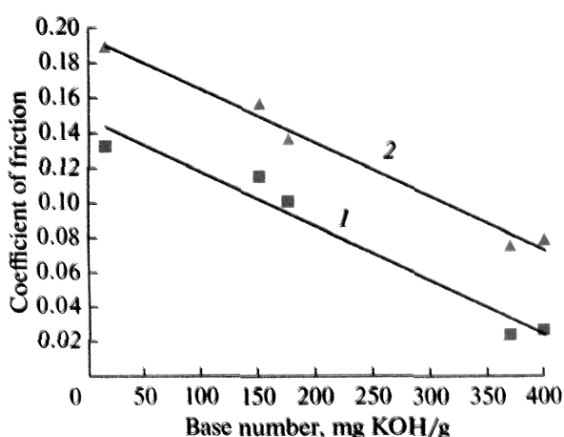


**Fig. 4.** Dependence of the coefficient of friction on the base number of calcium sulfonate. (1) stable; (2) maximum

For low alkaline calcium sulfonate C1 and middle alkaline C2, the presence of the intermediate temperature  $T_{i1}$ , which indicates the destruction of the adsorption boundary layer, is typical. In the case of detergent C3, an insignificant increase in the coefficient of friction is observed, which indicates the partial destruction of the

boundary layer. When testing highly alkaline calcium sulfonates, the coefficient of friction is initially lower and  $T_{i1}$  is not registered.

In addition, in a certain temperature range, the stabilization of the coefficient of friction at a certain level is typical for the studied detergents, i.e., the intermediate temperature  $T_{i2}$ , which indicates the formation of a modified layer on the friction surface. Upon an increase in alkalinity, the temperature range in which the boundary layers are stable also increases.

In the case of highly alkaline detergents C4 and C5, at  $T_{i3}$ , the destruction of the modified layers occurs at 300°C, and the coefficient of friction remains lower than the coefficients of friction of middle alkaline calcium sulfonates C2 and C3. For middle alkaline calcium sulfonates C2 and C3, the transition temperature  $T_{i3}$  is not registered in the studied temperature range.

In Fig. 4, the dependences of the coefficients of friction on the maximum and the stable (assumed equal to 220°C for all calcium sulfonates) base number of the detergent are shown. It can be seen that, upon an increase in alkalinity, the values of the coefficients of friction decrease almost linearly.

Samples of five commercial oils applied to lubricant of two-stroke petrol engines were tested also. The basic characteristics of these oils are shown in Table 3. Oils C, D and E of one manufacturer. Oils D and E, according to the categories JASO and ISO, are low-smoke oils, and oil E has to have the increased detergent effect. According to classifications of ISO, JASO and NMMA of distinction in lubricating ability between oils C, D and E are not established. In classification of API the distinct separation by lubricating ability of oils is not present, besides only the category TC is acting.

**Table 3.** The basic characteristics of oils.

Oil	Kinematic viscosity at 100 °C	Base stocks	Meeting the specification
A	11,8	Mineral	–
B	12	Mineral	API TB
C	9,7	Mineral	API TB, ISO-L-EGB, JASO FB, NMMA TC-W3

D	9,5	Semisynthetic	API TC, ISO-L-EGC, JASO FC, NMMA TC-W3
E	8	Synthetic	API TD, ISO-L-EGD, JASO FD, NMMA TC-W3

Because of detailed information about composition of the tested commercial oils for two-stroke petrol engines is not available to us, it is difficult to define precisely what influences on the thermal stability of oils at a certain temperature: structure of a package of additives or base oil.

Among the tested mineral oils (Fig. 5) the best thermal stability was shown by oil C. For this oil in the studied range of temperatures the critical temperature at which boundary layers collapse is not revealed. The friction coefficient is stable and makes about 0,1-0,12.

Oils A and B have approximately identical thermal stability, and their critical temperatures ~ 240 and ~ 230 °C respectively. Oil A shows equal or even the best lubricating ability. On the basis of what it is possible to assume that similar in composition packages of additives were used.

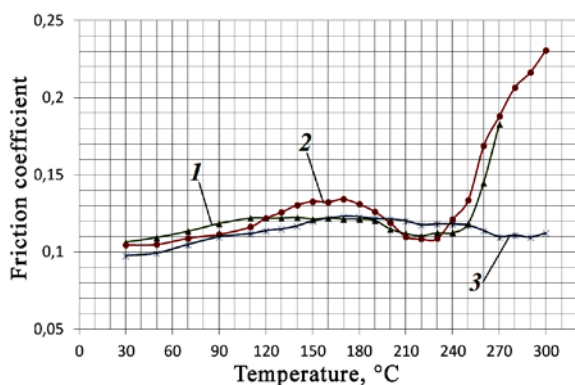


Fig. 5. Temperature-friction characteristics of mineral oil: 1 – oil A, 2 – oil B, 3 – oil C.

Among the compared oils of one manufacturer (fig. 7) thermal stability of mineral oil C the highest. Semisynthetic oil D takes an intermediate position.



Fig. 6. Photographs of a mandrel after testing of oils: a – oil C; b – oil D; c – oil E.

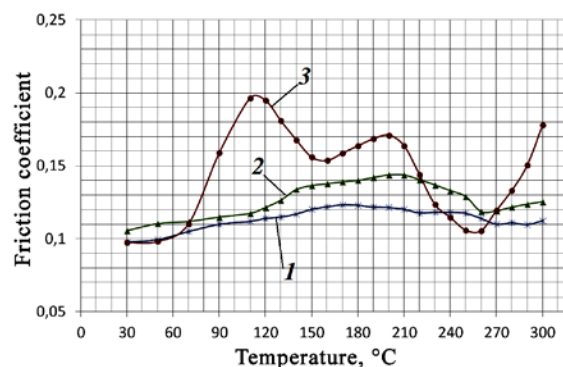


Fig. 7. Temperature-friction characteristics of oil from one manufacturer: 1 – oil C, 2 – oil D, 3 – oil E.

Synthetic oil E in the studied range of temperatures has shown the worst lubricating ability almost in all interval of the studied temperatures. Several peaks on graphics of temperature-friction characteristic of oil E demonstrate that its formulation contains not less than two chemically active additives forming chemically modified layers providing decrease in friction coefficient in the different ranges of temperatures on friction surfaces [8]. Destruction of the modified layers separating the rubbing surfaces is reflected in sharp raising of friction coefficient after 250 °C. Low lubricating ability of oil E (synthetic) in comparison with oils C (mineral) and D (semisynthetic), apparently, is explained by the fact that the synthetic oil which is an base stock is practically not oxidized at temperature increase in the studied interval while oils on mineral (and even on semisynthetic basis) are oxidized that increases lubricating ability of the studied lubricants. Deterioration in lubricating ability can be also connected with the fact that the manufacturer uses a smaller quantity of additives to reduce smoke and the amount of deposits in a combustion chamber. In fig. 6 shows the photographs of mandrels after tests of oils of one manufacturer. The difference between mandrels is visually well distinguishable. So the mandrel after testing of oil of mineral oil C has the greatest darkening, and in a case with synthetic oil E traces of influence of high temperatures are minimum. It is possible to range oils on their detergency thus  $C < D < E$ . The obtained data correspond to the characteristics of oils of their detergency declared in classifications of JASO and ISO.

## 5. CONCLUSION

Hence, the study of the tribological characteristic of detergents for motor oils in the case of calcium sulfonates of different alkalinities established the positive role of calcium carbonate in the composition of a micelle of the additive. This not only provides the required alkalinity of the additive, but also influences a decrease in the coefficient of friction.

Based on a chemical analysis of the sample surface, it can be assumed that, in addition to a temperature increase, friction is also necessary to form a protective film on the surface.

The performed study shows that the influence of detergent additives (at least, calcium sulfonate) on the lubricating properties of oils is rather significant and it should be considered in the development of lubricant compositions.

The possibility of differentiation of oils for two-stroke petrol engines based on lubricating ability, and also on the detergency by means of a temperature method of an assessment of lubricating ability of oils is established.

In the set conditions the best thermal stability was shown by oil C on a mineral basis. Oils on a mineral basis of A and B have shown close thermal stability that suggest similar additive packages. Oil E on a synthetic basis has shown the greatest friction coefficient almost in all range of temperatures.

The visual assessment of mandrels after testing allows to evaluate the detergency of oils. Least of all traces of temperature influence when using synthetic oil E that will be coordinated with classifications of JASO and ISO.

## REFERENCES

- [1] Dotsenko A.I., Buyanovskij I.A. Osnovy tribotekhniki. M: Infra-M, 2014. 335 s.
- [2] Meshcherin E.M., Ostrovskaya M.E. Oils for two-stroke petrol engines. Thematic review. – M.: TSNIITEHneftekhim, 1989. – 72 pp.
- [3] Igartua A., et al. Alternative eco-friendly lubes for clean two-stroke engines. *Tribology International* 44.6 (2011): 727–736.
- [4] Singh A. K. Castor oil-based lubricant reduces smoke emission in two-stroke engines. *Industrial crops and products* 33.2 (2011): 287–295.
- [5] Kumar G. S., Balamurugan A., et al. Tribological and emission studies on two stroke petrol engine lubricated with sunflower methyl ester. *J Sci Ind Res* 71 (2012): 562–565.
- [6] Matveevsky R.M., Lashkhi V.L., Buyanovsky I.A. et al. Lubricants. Antifrictional and antiwear properties. Test methods. – M.: Mashinostroenie, 1989. 192 pp.
- [7] ZHilko V.N., Buyanovsky I.A., Lisenkov Yu.G. About bond between temperature firmness of engine oils and their antiwear properties. *Friction and wear* T.4, № 4 (1983): 724–727.
- [8] Matveevsky R.M., Buyanovsky I.A., Karaulow A.K., et al. Transition temperatures and tribochemistry of the surfaces under boundary lubrication. *Wear* 136.1 (1990): 135–139.
- [9] Glavati O.L. Fiziko-khimiya dispergiruyushchikh prisadok k maslam. Kiev: Naukova Dumka, 1989.
- [10] Stachowiak G., Batchelor A.W. *Experimental Methods in Tribology*. Amsterdam, 2004.



# A Survey of Researches in the Field of Ecodesign Related to Intralogistics at the University of Belgrade - Faculty of Mechanical Engineering (2010-2017)

Nenad Zrnić<sup>1</sup>\*

<sup>1</sup> Faculty of Mechanical Engineering, Department of Material Handling Constructions and Logistics, University of Belgrade, Belgrade (Serbia)

Since its inception in the educational process at the Faculty of Mechanical Engineering (University of Belgrade) in 2008/2009 (Master and PhD studies), as the result of the Tempus project JEP 40069 "Design in Mechanical Engineering" (2006-2008), the field of ecodesign and sustainable logistics has a permanent growth both in tuition and research. That finally resulted in establishing Laboratory of ecodesign and logistics in 2014 and several researches conducted through the work in this Lab. Some of them have been done in the cooperation with some foreign academic institutions. The main stream of the mentioned researches was related to the assessment of environmental effects of intralogistics equipment, such as material handling (cargo handling equipment in ports such as are cranes and terminal tractors) and conveying (belt conveyors) equipment. Accordingly, the conducted researches and findings have been presented to a broader scientific community and published in international journals, books and presented at the international conferences. This paper gives a survey and compilation of those publications in the period 2010-2017.

**Keywords:** Ecodesign, sustainable logistics, life cycle assessment, cargo handling equipment, conveyors

## 1. INTRODUCTION: ECODESIGN AND LCA AS ITS CORE

From the environmental point of view, sustainability represents the system's capacity (in this case the Earth) to support anthropogenic activities' impact on the environment without putting the future of human race under risk. From the designer point of view, sustainable development is about designing objects that use limited resources; it is also about social responsibility and ethics [1], [2].

Growing interest in environmental condition and concept of sustainable development resulted in appearance of design disciplines with goal to develop solutions for decreasing the impact of human activities and industrial products on environment. Such discipline is well known as Ecodesign or Design for Environment. Based on fundamentals of ecodesign, all products and services must be designed to scope all of their life cycles stages. Processes needed for manufacturing, distributing and disposing of the product at the end, are considered to be one. Beside the design of product itself, this approach

designs product system, in a way that it defines all possible events in product life cycle [3].

In 2006 the European Environment Agency defines Ecodesign as "the integration of environmental aspects into the product development process, by balancing ecological and economic requirements. Ecodesign considers environmental aspects at all stages of the product development process, striving for products which make the lowest possible environmental impact throughout the product life cycle." Ecodesign integrates the idea of sustainability as well as environmental considerations into the product development. It considers the contribution of the product to environmental impact through all of its life cycle stages. Speaking of Ecodesign and environmental friendly product development it is important to bring together environmental requirements from stakeholders, as well as legal frameworks. For the purpose of product improvement, Ecodesign process integrates stakeholder and environmental point of view, see Figure 1 [4].

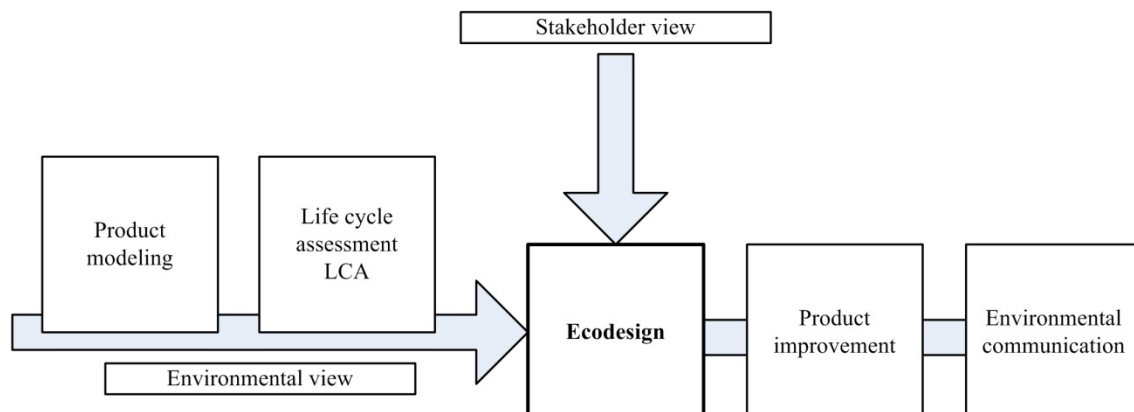


Figure 1: Inputs to the Ecodesign process [4]

Having this in mind, ecodesign as relatively new engineering discipline makes a radical discontinuity with traditional design process [5]. The purpose of this is to design product life cycles, in order to identify and efficiently combat environmental impacts. In other words, it is possible to create product and minimize the input of raw materials and energy, and the impact of all emissions and waste.

Before design of any new product life cycle, and before any improvement of existing product life cycles, it is of vital importance to estimate the present effects on environment. The only way to both quantitatively and qualitatively calculate the harm of all effects of products and human activities on environment is to conduct Life Cycle Assessment or LCA [6]. As the core of ecodesign LCA is quantitative tool for assessment of environmental impacts of products and services such as climate change, global warming, ozone depletion, (smog) creation, eutrophication, acidification, toxicological impact on humans and ecosystems, the depletion of resources, and others. It is systematic approach for analyzing the entire life cycle stages of products from material extraction through manufacturing, use and eventually disposal or

recycling preferably. Therefore it is often called a "cradle-to-grave" analysis [3].

LCA is an iterative technique. In accordance with EN ISO 14040: 2006, life cycle of a product consists of five consecutive and interlinked stages. Therefore life cycle includes:

1. Raw material stage,
2. Manufacturing stage (design and production),
3. Distribution stage (packaging and transportation),
4. Use stage, and
5. End of life stage (EoL).

In accordance with the same standard EN ISO 14040: 2006, the formal structure of an LCA contains four phases:

- Goal and scope definition,
- Life cycle inventory analysis (LCI),
- Life cycle impact analysis (LCIA),
- Life cycle interpretation.

These phases are consecutive and interlinked, as life cycle stages, see Figure 2 [7].

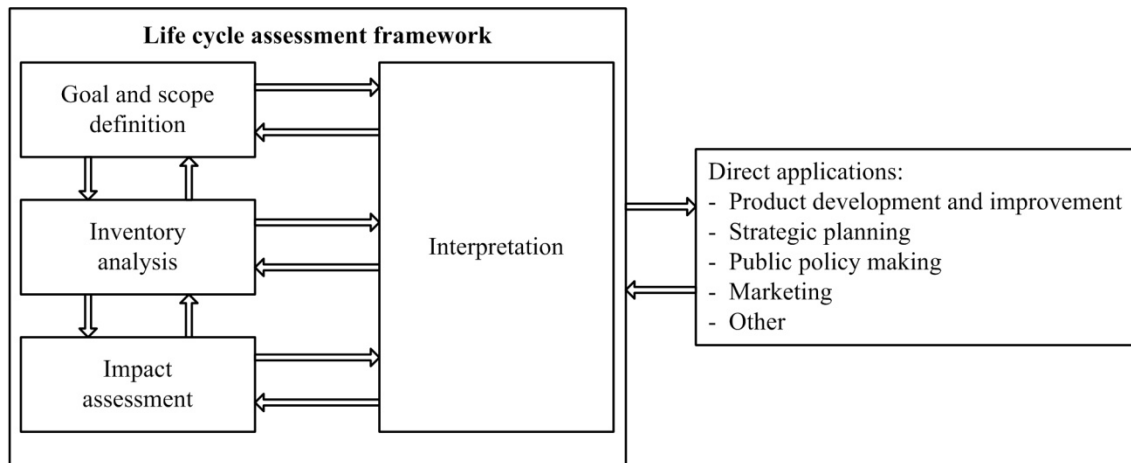


Figure 2: Phases of an LCA [7]

## 2. 2. CURRENT TRENDS IN GREEN (INTRA)LOGISTICS

The forum intralogistics at the association "Verband Deutscher Maschinen- und Anlagenbau" (VDMA) defines intralogistics as the organization, control, realization and optimization of in-plant goods and their material flow and logistics, of the streams of information as well as the movement of goods in industry, trade or public facilities [8].

Corresponding to the 20 mega-trends specified in [9] specific subject areas have been established as important future research focuses (Figure 3).

As it can be concluded from Fig. 3 of the 20 global megatrends one of the most significant trends for intralogistics as a part of logistics sector (energy consumption in intralogistics is estimated to about 25% of the whole logistics sector [10]) is climate change and environmental impact, while one of the main

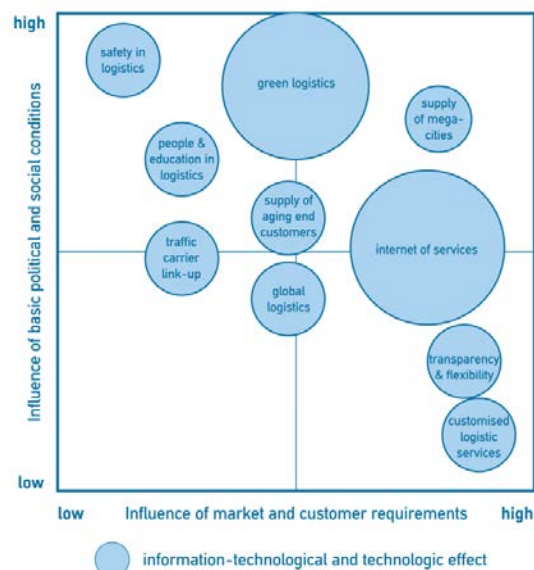


Figure 3: Tasks in intralogistics in the future [11]



research thrusts is "Green Logistics". Although the logistics greenhouse gas (GHG) footprint may appear relatively modest (estimated for around 5.5% of global emissions), transport sector has been increasing its output of these gases, while other sectors are reducing their footprint [12]. For this reason it is quite sure that in the next few decades a major challenge for the companies in logistics sector will be to implement practical and cost-effective carbon mitigation strategies to cut their GHG emissions in an effort to achieve very ambitious carbon reduction targets at national, EU and global levels by 2050 [13].

Companies can reduce carbon emissions from their logistics operations in many ways. According to [12] several ideas for decarbonization of logistics activities, focus is on five key freight transport parameters: reducing freight transport intensity, shifting freight to less carbon-intensive transport modes, increasing vehicle utilization, raising the energy efficiency of freight transport operations and finally reducing the carbon intensity of the energy source (i.e. the amount of CO<sub>2</sub> emitted per unit of energy consumed either directly by the vehicle or indirectly at the primary energy source for electrically-powered freight transport operations, what will be particularly considered later in this paper) used in logistics. Obviously, decarbonization must be followed by developing innovative technologies [14] in order to improve intermodal transport chains, logistics services and consequently environmental performances of logistics equipment.

### 3.3. ENVIRONMENTAL EFFECTS OF CARGO HANDLING EQUIPMENT (CHE) IN CONTAINER PORTS

With almost 90 percent of non-bulk cargo moved worldwide by containers, the container shipping and handling industries have immense economic footprint both

locally and globally. Ports play a huge role in the regional economies and the growth and the development is directly related to ports abilities to adapt to new challenges [15]. As according to Guerrero and Rodrigue [16], the five waves (phases or cycles) of containerization that essentially influenced development of port and terminals are presented in Fig. 4, 2014, [17]).

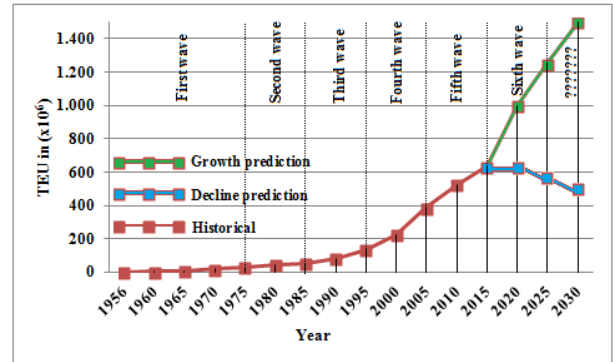


Figure 4: TEU number (1956-2015 with 2030 prediction) and waves of containerization according to Guerrero and Rodrigue [16],[17]

After summarizing the containerization development and having in mind the mentioned megatrends, the imposing conclusion is to seek challenges and changes in containerization not only within technological arena, but equally significant social and economical ground. Containerization has given revolutionary change for the transportation and shipping industry, leading to globalization. The technology could provide evolution for the containerization to maintain its important role, but it is strong belief that only the social and economical changes at global scale can make revolutionary change, Fig. 5 [17].

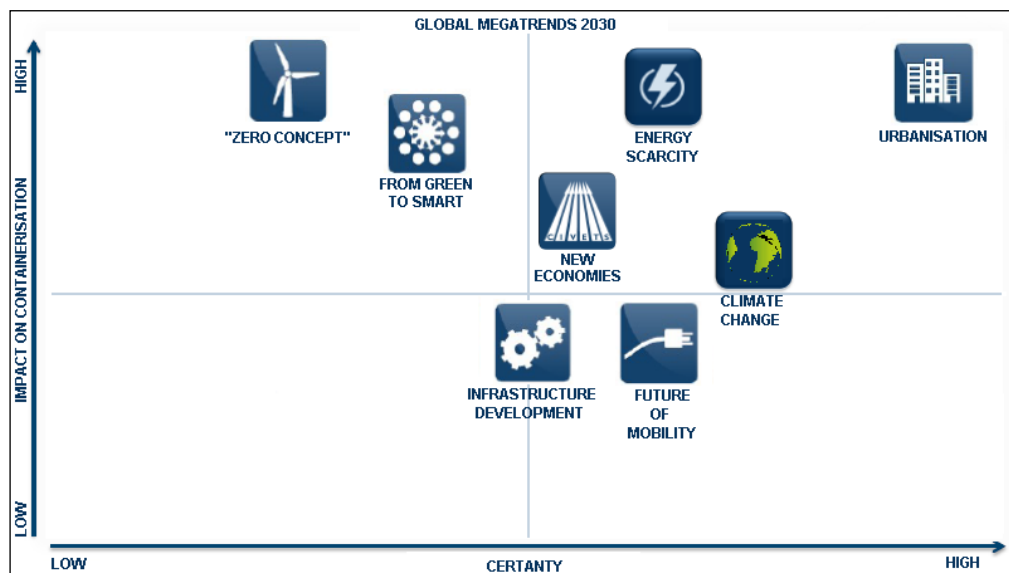


Figure 5: Impact of global megatrends on containerization [17]

It is also important to underline that the environmental footprint of the ports is rising to the top of the port authorities' agenda in the moment when economic downturn has already exerted container operations

struggling to hold on cost effective side. The new demands are pushing port related industries to offer "green" solutions for ports who seek to mitigate their environmental footprints. Emissions in ports come from

operations of three different sectors. The first sector is related to the arrival and berthing of vessels, the second involves activities within the port boundaries such as unloading of cargo from the ships and their transfer by Cargo-Handling-Equipment (CHE) and the third includes the transport (vehicles, trains and inland shipping) within or near the port and departure [15].

In port container terminals, cargo (in this paper only containers) are ferried around using special designed machines called CHE. These machines usually include various types of cranes and specially designed forklifts, tractors or trucks. The containers are lifted from a marine vessel by a crane at latter moved or picked by other crane, handler or forklift. In between each use of a crane or pick, the container is transported around the terminal using a yard truck.

Greatest in CHE fleet population are the yard trucks and forklifts, followed by handlers and gantry cranes. These machines are conventionally power with Internal-Combustion-Engine (ICE) which most often is a diesel. Due to the fact that handling container with as much as 40 tonnes of cargo is an energy-intensive function and the fact that CHE is powered with diesel burning engines it is often considered as one of the most significant sources of air pollution caused by terminal operations [15].

Fortunately, an answer to port "green" strategies, the CHE industry offered a wide range of solutions, from retrofits to brand new high efficiency models, such as hybrid and all-electric drives. Depending on solution and equipment type some technologies are advertised to reduce the CO<sub>2</sub> emissions up to 70 percent and NO<sub>x</sub> and SO<sub>2</sub> up to 90 percent (according to manufacturers). Most common pieces of CHE found in container terminals are [15]:

- Rubber Tired Gantry (RTG) cranes (RTGs)
- Utility tractor rigs (UTRs), which is also known as Yard Trucks or Terminal Tractors
- Straddle Carriers
- Container Forklifts
- Reach Stackers

Determining environmental footprint of container terminal or CHE is important and complex task. The environmental footprint of CHE activities at container terminals can be defined either by directly measuring emissions or estimating them using various models or methods [15]. Generally, CHE emissions at ports are estimated using either the off-road emission models or methods similar to those in the models [18]. In order to understand the environmental impact of container terminals, various models and tools that quantify the emissions of relating sources are used or developed. Each model can vary greatly in terms of complexity and accuracy on one side, and time and resources on the other. The non-modeling approach to create an emission inventory of CHE is to directly measure emissions or energy consumption. Although it could be considered as the most accurate way, it is also the most expensive and time demanding and can only be done as aftermath. Direct emissions measurement, thus disables early stage planning process and is more suitable for establishing the baseline inventory. The modeling is therefore more appropriate as preventive approach, as support for decision making. The complexity of modeling methodologies can also vary depending on intended use and users and can also be time

and resource consuming if detailed and validated model is wanted, according to [19]. Regardless of which modeling approach is chosen it enables prediction of emission of any source at port without actually ever visiting facility. That can be also used for comparison of different types of CHE. The drawback of modeling is that any uncertainty in baseline parameters can eventually lead to significant uncertainty in the final results of estimated CHE emissions. This is of great importance, particularly when comparison of any type of CHE is made, since even the slightest aberration in early modeling can result in favoring one piece of equipment over other [13].

On the significance of CHE emissions, also reveals the fact that many ports today are considered to be the largest sources of air pollution in coastal cities. For instance, according to the data collected in report [20] in 2007, the Port of Long Beach found that 81% of the CHE port wide was employed by its container terminals and that 8% of total NO<sub>x</sub> emissions were due to CHE; the Port of Houston found that 15% of its 2007 total NO<sub>x</sub> emissions came from CHE; New York/New Jersey found that 25% of their 2006 NO<sub>x</sub> emissions were due to CHE. To get better fuel economy and accordingly to reduce GHG emissions, ports around world are considering using either "low carbon" (hybrid) or "zero emissions" (electric) technologies that are currently deployed for port equipment such as cranes – Rubber Tired Gantry Cranes [21] and UTRs [22] and other vehicles.

In the presented research the concept was on the RTG cranes and UTRs, since they are the most common pieces of CHE found in container terminals accounting combined over 55% of all CHE [23]. RTGs are dependable on the support of UTRs for quick container transport across the terminal and combined evaluation of their environmental impact and operating costs is common approach in terminal planning, also recommended by Böse [24].

### 3.1. Examples of RTGs [25], [26]

In port container terminals, RTG cranes are used for movement of shipping containers, once they are placed on to the distribution channels from a vessel. The cranes are powered by a diesel generator set (genset), which consists of a diesel engine coupled with an alternator. An RTG crane is capable of moving containers weighing up to 50 tonnes at a rate of 20 moves per hour. Since it is one of the largest machines on tires in the world powered by large non-road diesel engine, turning it into the eco-friendly machine is a challenging task.

A conventional diesel genset provides electrical power for the hoist, trolley, and gantry electric motors, as well as for the routine demands of the crane. Utilizing this type of power system on a RTG allows the crane to move independently throughout the container terminal as is required by daily port operation. The freedom of movement and the high peak power demand for hoist motor consume a large amount of fuel and emit significant emissions of GHG.

Today, variety of technologies and systems are available to reduce fuel consumption and emissions and improve overall RTG efficiency. They include technologies such as, variable-speed generators, flywheel energy storage, hybrid RTGs with regenerative braking

and super or ultra capacitor technology and electrified "zero emission" cranes (E-RTGs). Most of them are available as retrofits for conventional cranes, but also as manufactured brand new RTG option.

An electrified RTG (E-RTG) crane in the past was often avoided due to complicated electric-power feeding via cable, narrowed movability and limited flexibility. Today E-RTG's disadvantages are overcome with the cable reel and latest with drive-in conductor bar solution with collector trolley that automatically engages and disengages. Although the main disadvantage remains – the need to adapt the terminal for electrification, the fact is that with the latest solutions, environmental advantages of E-RTG are in prime again. The 90% of operating time electrified RTG cranes uses solely electricity and 10% of time uses diesel engine, during block changes and maintenance. The manufacturers promise E-RTG staggering potential for CO<sub>2</sub> reduction.

Certain solutions for RTG cranes have advantages over others and certain terminal configurations and port authorities favor some of them, but from environmental point of view it is important to find out which solution is more eco friendly. Again, certain methodologies for assessment of environmental impact of products have advantages over others, but according to the author's opinion the most appropriate way is to carry out Life Cycle Assessment (LCA) of three most widespread implemented technologies of nowadays RTG cranes which include conventional solution and two emerging technologies (hybrid and electrified zero emission RTGs).

Thus, the objective of this research is twofold. The first objective is to evaluate environmental benefits of emerging technologies for RTG cranes over conventional and the second is to promote the use of (LCA) methodology for this purpose. In this way, comparison of RTG cranes will offer results which could be used in further research of CHE emerging technologies.

Once the environmental impact of manufacturing stage of a conventional type of RTG is obtained, these results could be used for evaluation of environmental performances of future CHE technologies. Essentially, RTG support structure and its corresponding manufacture process are basically unchanged since these machines have been introduced in operation. Majority novel solutions offered for brand new cranes are also available as upgrades for older models [25].

Since conventional model of RTG crane is set as basic model, other two models: the hybrid RTG and electrified E-RTG are in essence upgraded versions of the basic model which use same gantry structure. The difference between basic (conventional) model over hybrid and E-RTG is in add-ons over standard diesel generator set. This principle of modeling allows the authors to use the most of inventory base of the first RTG crane which is in accordance with real life, dockside experience where conventional cranes already in use are modernized by new state-of-the-art add-on features.

The system boundaries are defined according to ISO 14000 recommendations and responding to work principle of used LCA software. The assessment is divided in two parts. First is "cradle to gate", sometimes noted as "upstream", where iron ore extraction and depletion and materials processing is addressed, then parts production

and gantry assembly and finally distribution is evaluated. The second stage of this assessment "gate to grave" basically consist of "use" and "downstream" phase in one. It refers to operational life of crane at port and scrapping and disposal/recycling.

The manufacturing step has been modeled as common parameter for all the three RTG cranes and is chosen to be the same. This includes the raw materials, the manufacturing processes, the energy consumption and the transport by rail and truck of the manufactured car to the end-user deterrent only for conventional RTG. The components which are specific to the Hybrid and E-RTG technology are modeled separately and added over results of conventional crane. For example carbon super-caps energy storage for Hybrid crane and collector trolley for E-RTG.

The "cut-off" criteria in manufacturing phase is applied, leaving out components with weight of less than 5% of the total mass of crane, thus excluding parts which contribution to overall results of this phase is insignificant.

The Functional Unit (FU) defined in this assessment, although simplified, corresponds to the use of a RTG cranes in port operations during average 5,000 working hours per annum and 15 years of lifetime. The FU is 1 working hour of container manipulation which consists of 32 percent of hoisting operations, 16 percent of spreader movement and 52 percent of crane movement across the port yard.

The work environment of RTG cranes is in accordance with GaBi software inventory base. The power grid mix is chosen to be current EU-25 (ports at EU seas). Fuel used for diesel generator set is off-road petroleum diesel with high sulfur content. The end-of-life has been modeled with respect to the state-of-the art in EU recycling plants and according to GaBi software available data. The recycling process of large steel sheet gantry construction and consumption of resources during the recycling process have been included having in consideration the dominance of steel material over others.

The LCA of three RTG cranes is carried out using state-of-the-art software GaBi developed by PE International as the most represented LCA tool on the market. A full LCA was conducted, and the necessary input/output data were determined using immense GaBi data base. Since modeling the life cycle of such a complex machine as RTG crane, certain assumptions are done to simplify the assessment. These approaches are common in order to lower the costs of LCA and eliminate data uncertainties [27], especially due to fact that study is entirely independent. The goal of study is intended solely for scientific research and therefore critical review is not necessary.

The adopted conventional structure of RTG crane with lifting capacity of 40 tonnes is shown in Figure 6. Its self weight is ca. 115 tonnes, which consist of 80 tonnes steel box gantry structure, spreader and trolley with total weight of 25 tonnes and remain weight of diesel generator set, cables and other features. This support structure is adopted for evaluation of all three analyzed solutions of RTG cranes. Adopted drive system is on board diesel generator set. It has got 600 kVA AC/DC generator with 6 cylinders, 12 liter (732 cubic inches) diesel engine with power of over 300 kW [25].

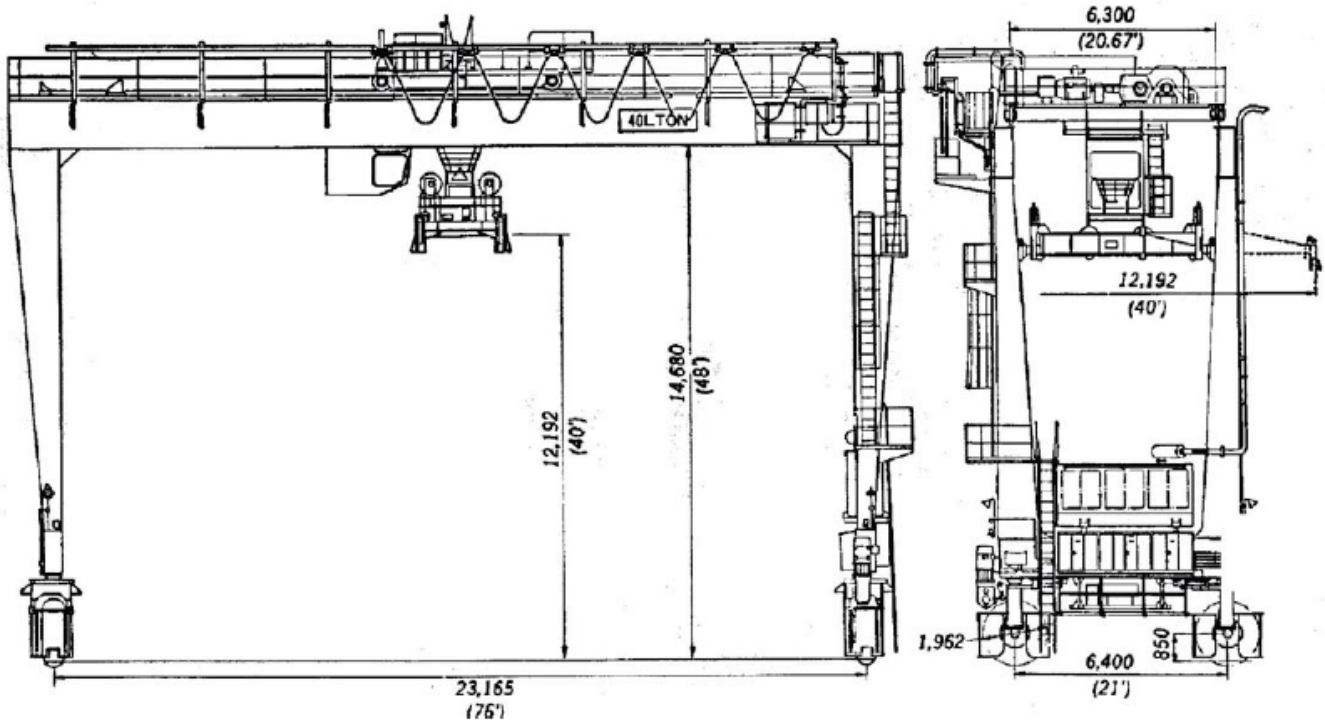


Figure 6: 40 tonnes RTG crane

The obtained results of the LCA of RTG cranes are presented in accordance to ISO 14040 principles with the highlight on two most representative impact assessment methods Dutch CML and US TRACI. The results are also divided according to system boundaries (Fig. 7): “Cradle-to-gate”, “Gate-to-grave” and finally as entire life-cycle-impact-assessment “Cradle-to-grave”. In this way, overview of footprints of “upstream” and “off-road” or operational part of life are clearly divided.

dominant one part of entire life cycle. The same applies RTG cranes. The operational life of RTG cranes spans from 15 to 30 years with engine overhauling which puts the use phase in focus since it contributes to overall results in great proportion. Environmental profile of RTG crane is given in Figure 7. Nevertheless it is important to conduct entire LCA in order to rule out significant issues that could appear in the production phase.

As for the most vehicles and long-life machineries (life cycle over 5 years) the use phase tends to be the most

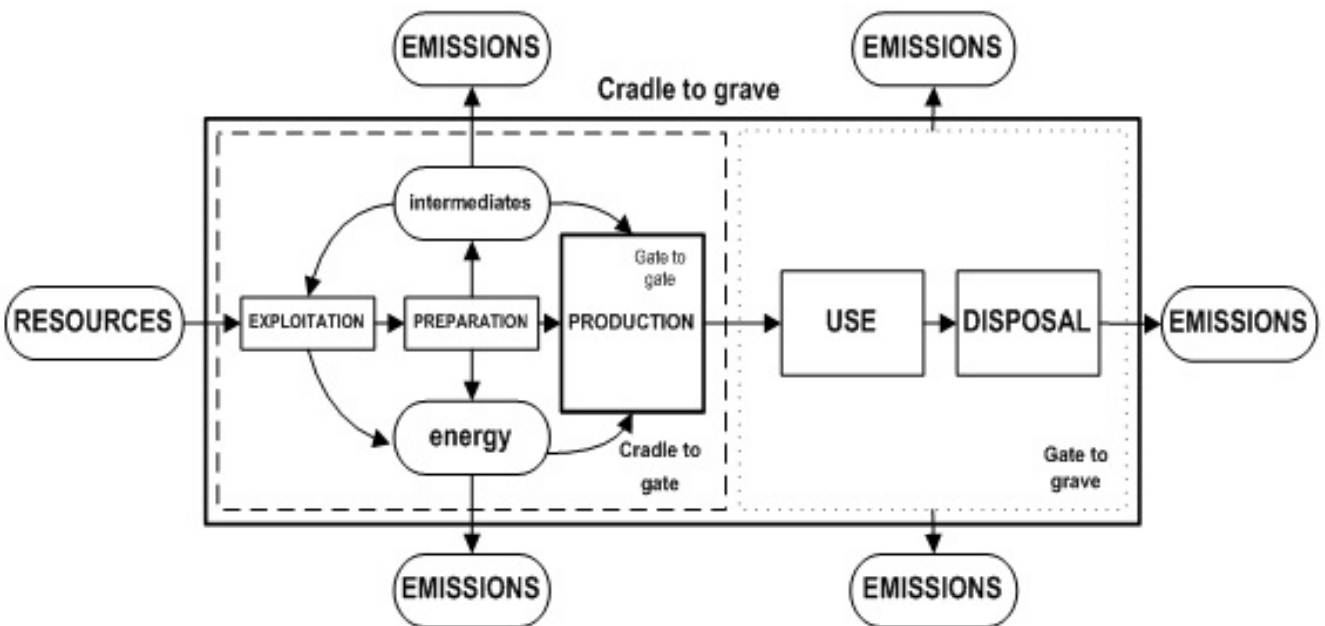


Figure 7: System boundaries [3]

Some obtained results are presented in Figures 8, 9, 10, 11 [25].

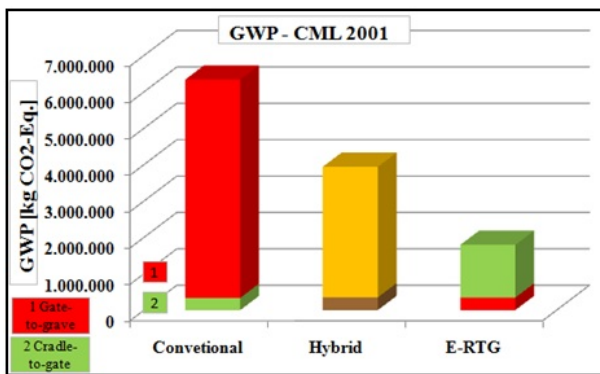


Figure 8: Global-warming-potential of RTG cranes

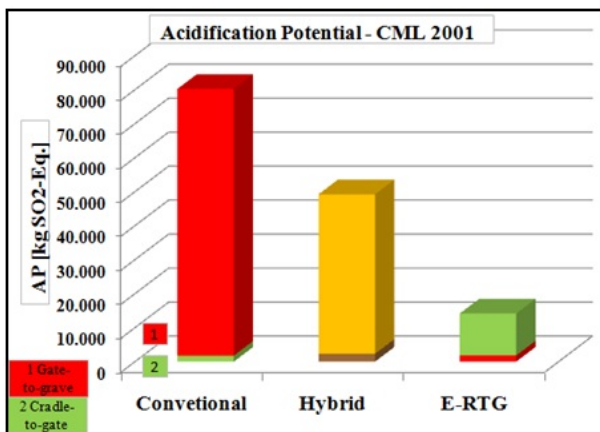


Figure 9: Acidification-potential of RTG cranes

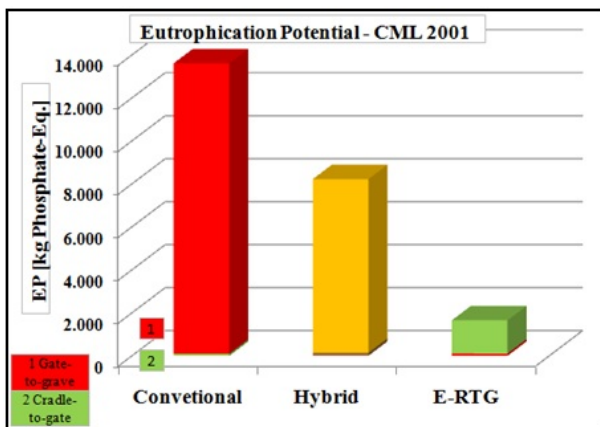


Figure 10: Eutrophication-potential of RTG cranes

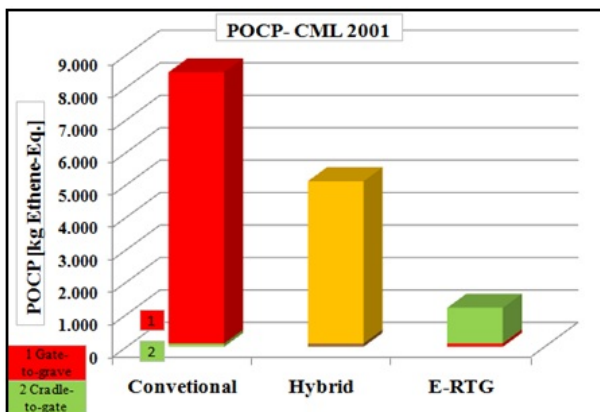


Figure 11: Photochemical-ozone-creation-potential of RTG cranes

After analyzing the results and comparison of conventional RTG with Hybrid and E-RTG, clear conclusion can be made. Today, when environmental concerns are part of almost every day discourse conventional RTG cranes are obsolete. The hybrid super-cap. systems and electrified solutions offered by CHE industry are desirable from both environmental and entrepreneurs perspective. The Hybrid and E-RTG have significant emission reduction and fuel saving potentials and their introduction in to the port operations has almost no environmental downside.

In this way emerging CHE technology for RTG cranes could settle environmental concerns of port authorities without jeopardizing everyday container handlings and at the same time lower operational and maintenance costs in long term.

### 3.2. Examples of UTRs [13]

The UTRs are heavy-duty off-road single cab vehicles designed for towing trailers with containers in terminals. They are by far the most common type of CHE used at container terminals, especially in North America and often cover over 50% of the total CHE population. In typical operations at container terminal UTRs support almost every CHE for swift ferrying of the containers across the terminal [13].

The duty cycle of UTR consist of long idling periods and stop and go movements with high or low load accelerations. This results in inefficient operation of diesel engine and significant air emission and noise pollution. Based on some annual port emission reports and available air emissions inventories, it is stated that UTRs contribute with half of entire terminal carbon and particulate matter (PM) emissions associated by CHE. This is due to the fact that currently, conventional UTRs are fitted internal combustion engine (ICE) with fuel consumption reaching average of up to 10 liters per hour [28].

Despite major advances in technologies improving vehicles environmental performance (especially in automotive industry), the application of diesel alternatives for off-road vehicles is still in "baby steps". Several solutions are being on and off recognized as top contenders for making mainstream application. From the alternative fuels to powertrain variations the corresponding industries forced by policy makers and environmentally concerned public are actively pursuing a pathway to mitigate emissions. Based on market success of hybrid passenger vehicles and re-emerging electric vehicles, the heavy duty off-road manufacturers are exploiting the potential of well understood technology that can be integrated with UTRs. The transition from ICE to broad use of zero (electric) and near zero emission (hybrid) is the most governed solution at present and seams as the most feasible.

The hybrid solutions for yard tracks exploit the random duty cycle in order to improve the overall efficiency of diesel engine. In a UTR equipped with a diesel hybrid drive system, the engine is shut down during idling periods and regenerative braking allows kinetic energy normally wasted during braking to be captured by the hybrid energy storage system, subsequently improving

fuel efficiency and lowering emissions. There are two hybrid systems available for UTRs, which differ only in concept of kinetic energy storage. The first is electric hybrid system which endorse battery storage solution, while second is based on hydraulic high pressure accumulator energy storage.

The diesel electric hybrid UTR uses basically the same hybrid technology proven in on-road hybrid vehicles. The battery pack (most common is lithium-ion) or ultra capacitor is used to store kinetic energy when decelerating or braking. Stored energy is later used for to assist ICE during acceleration, or for short distance zero emissions movement in battery mode. The latest evolution of electric hybrid UTRs is plug-in hybrid with additional option of battery recharging at grid. With this feature diesel generator set could be used as range-extender enabling downsizing of ICE.

The hydraulic hybrid UTR is alternative for electric hybrid truck often criticized for battery fallibility and hazards potential. The hydraulic hybrid system uses high accumulator and low pressure reservoir filled with hydraulic fluid and nitrogen (N<sub>2</sub>) to capture kinetic energy. During vehicle braking, the rotating energy of the wheels is used to pump fluid from the low pressure reservoir into the high pressure accumulator where nitrogen is compressed. Up to 70% of the kinetic energy stored can be reused for vehicle acceleration. The system can also be equipped with start-stop feature enabling engine shut down to eliminate idling.

One of the latest trends in CHE industry is fully electric UTR, advertised as zero-emission equipment since it has no "tail-pipe" emissions. This system uses electric motor and battery storage system (lead, nickel or lithium-ion battery packs). The electric UTR range is from 80 km to 150 km, depending on battery pack size which is up to 300 kWh. Overall autonomy is sufficient for two shift operations. The overall success of electric UTR concept in making mainstream is linked to outlook of battery development for electric vehicles.

In order to straightforward the LCA comparison having in concern its goal and scope and intended purpose, certain simplifications and assumptions are made. These are done relating to duty cycles of UTRs and dock side operation experience avoiding data uncertainties. Therefore conventional diesel model UTR is determined as base models, while other three: hydraulic hybrid, electric hybrid and full electric cover use over 98% of the same construction and components (chassis, wheels, diesel engine, cabin, interior features). Adopting this modeling principle most of inventory base of conventional diesel UTR can be used for creation of inventory base of hybrid and electric models.

The size of selected conventional UTR, set for a base model for LCA study is the same as for hybrids and electric, and the dimensions are presented in Fig. 12. The net weight is 7 tonnes and gross combined weight is 40 tonnes. The powertrain variations are shown in Table 1.

The Functional Unit (FU) is also defined according to the LCA practice. The FU for the UTR is defined as one operating hour at container terminal (yard work), where 40% of a time is spent in idling, 35% of time is related to lower load and 25% with high load. The annual operation time for UTRs in this LCA comparison is 2,500 working hours. The life cycle is 10 years. The fuel consumption of selected models is calculated based on LCA software inventory and checked with reports from [28].

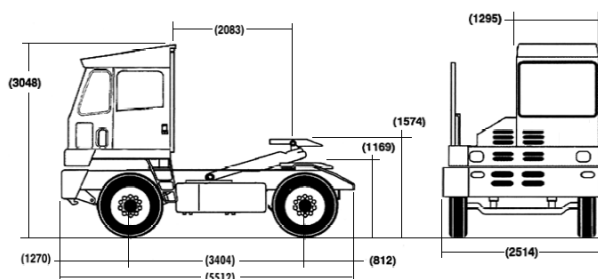


Figure 12: Base model of a UTR with dimensions in millimeters [13]

Table 1: Powertrain variations of compared UTR models [13]

Powertrain	Feature	Conventional diesel	Hydraulic hybrid	Electric hybrid	Full electric
Diesel engine	Size	6.7 l	6.7 l	6.7 l	-
	Power	150 kW	150 kW	150 kW	-
Battery	Capacity	-	-	5 kWh	150 kWh
Electric motor	Power	-	-	80 kW	140 kW
	Voltage	-	-	150 V	230 V
Hydraulic system	Pressure	-	400 bar	-	-
	Power	-	160 kW	-	-
Reservoir	Capacity	-	0.5 kWh	-	-

The results conducted assessment are classified and characterized in accordance with ISO 14040. For the comparative LCA the most significant impacts are evaluated and presented via life cycle impact assessment (LCIA) problem-orientated method developed by Institute of Environmental Sciences from Leiden (CML 2001) and damage orientated Swiss method Ecoinvent.

The "upstream" stage illustrates significant differences between UTRs equipped with diesel engine and electric motor. The environmental impact of lithium-ion battery pack production is much greater than of

conventional diesel engine. The global warming potential (GWP) of 150 kWh battery pack selected for electric UTR model is approx. 40,000 kg of CO<sub>2</sub> equivalent, which is twenty times larger than GWP of 6.7 liter diesel engine. This ratio is an "issue" that detracts the "upstream" stage.

The results of "use" stage reveal lesser environmental impact of electric UTR over other three models. This is due to selected EU-25 power grid mix with average of 0.539 kg of CO<sub>2</sub> eq. per kWh. Other power grid mix scenarios could influence results of electric UTR in

both directions. The two hybrids show certain reduction of environmental impact in range of 20% over conventional, but in small favor of hydraulic due to burden of electric hybrid's batteries impact.

The "end of life" stage is again influenced with lithium-ion batteries of electric UTR, while conventional

and hybrid versions share near the same results. The additional abbreviations used in Table 2 are: acidification potential (AP), eutrophication potential (EP), phosphate (Ph.) and radioactive waste (RW).

Table 2: LCIA of UTRs in kg (CML 2001- problem method)

UTR	Impact	Upstream	Use	End of life	Total
Conventional diesel	<b>GWP [CO<sub>2</sub> eq]</b>	35,850	499,152	247	<b>535,249</b>
	<b>AP [SO<sub>2</sub> eq]</b>	192	6,508	1	<b>6,701</b>
	<b>EP [Ph. eq]</b>	9	1.201	0,06	<b>1,210</b>
	<b>RW</b>	117	0	0.8	<b>118</b>
Hydraulic hybrid	<b>GWP [CO<sub>2</sub> eq]</b>	38,880	432,126	265	<b>471,271</b>
	<b>AP [SO<sub>2</sub> eq]</b>	210	5,647	1.00	<b>5,859</b>
	<b>EP [Ph. eq]</b>	9	973	0.06	<b>982</b>
	<b>RW</b>	135	0	0.9	<b>136</b>
Electric hybrid	<b>GWP [CO<sub>2</sub> eq]</b>	43,135	438,101	1,239	<b>482,475</b>
	<b>AP [SO<sub>2</sub> eq]</b>	278	5,725	1	<b>6,009</b>
	<b>EP [Ph. eq]</b>	14	986	1	<b>1,001</b>
	<b>RW</b>	140	0	0.33	<b>140</b>
Full electric	<b>GWP [CO<sub>2</sub> eq]</b>	68,025	269,500	4,950	<b>342,475</b>
	<b>AP [SO<sub>2</sub> eq]</b>	361	1,430	3	<b>1,817</b>
	<b>EP [Ph. eq]</b>	25	65	4	<b>94</b>
	<b>RW</b>	221	875	1	<b>1,097</b>

Table 3: LCIA of UTRs (Ecoinvent - damage method)

Life cycle impact [units]	Conventional diesel	Hydraulic hybrid	Electric hybrid	Full electric
Acidification [PDF*m <sup>2</sup> *a]	828,521.00	688,122.00	715,401.00	542,485.00
Ecotoxicity [PDF*m <sup>2</sup> *a]	1,173	963.38	990.59	698.44
Climate Change [DALY]	16.00	13.63	13.86	9.26
Respiratory (inorganic) [DALY]	0.95	0.97	1.27	2.00
Respiratory (organic) [DALY]	0.07	0.05	0.06	0.04

The comparative LCA of different UTR concepts reveals limitations of application of electric-diesel hybrid technology for off-road vehicles in terms of environmental benefits. On the other side, the results promote full electric UTR as cleaner solution if the right power grid mix is selected. However, the hydraulic-diesel hybrid could turn out as more simple near future alternative, if the battery technology goes to a standstill. The presented example illustrates importance of life cycle thinking for decision making and identifying the drawbacks of technologies promoted as solutions to mitigate environmental impacts.

#### 4. SIMPLIFIED LCA OF BELT CONVEYORS

Belt conveyors belong to the class of high performance machines (HPMs) and present also the backbone of surface mining and conveying systems [29]. Up to now several researches related to environmental effects, such as LCA studies [30] and energy efficiency issues have been conducted [31].

Previous researches in the Laboratory of ecodesign and logistics at the FME Belgrade were focused on investigation of environmental properties of belt conveyors on BWEs and similar types. It is based on simplified LCA of SRs 1201 BWE's belt conveyor and its components, which is a part of an ECS system. Each one of simplified LCAs, presented in scientific papers [32], [33], [34] and [35] was conducted with Ecodesign Assistant (EA) and Ecodesign PILOT (EP) software tools [36], [4]. In addition to the conducted simplified analysis

of the complete belt conveyor and its main components, three more simplified analyses were conducted in order to verify previously obtained results. These analyses included simplified LCA of ball bearing 6310 C3, belt conveyor gearbox BKF 320 and conveyor belting. Analysis of belting is conducted for the second time with more accurate data, obtained from the manufacturer. However, this analysis has shown the same result as the one previously obtained and published in [34].

Unlike formal LCA with energy values where absolute numbers are derived, the Ecodesign Assistant (EA) and Ecodesign PILOT (EP) only calculate relative environmental impacts by comparing the occurring impacts of the different life cycle stages of the product [4]. In that way EA and EP define basic type of a product which is determined with the most significant stage of its life cycle. Relative to life cycle stages, there are 5 basic types of the product:

- Basic type A - raw material intensive product,
- Basic type B - manufacture intensive product,
- Basic type C - transportation intensive product,
- Basic type D - use intensive product and
- Basic type E - disposal intensive product.

Analysis of the BWE's belt conveyor, which is 8.3 m long, with 1.6 m wide belting and throughput of 3,465 m<sup>3</sup>/h of brown coal was presented in [37].

In accordance with its throughput the functional unit of the belt conveyor is determined as: "Transportation

of 3,465 m<sup>3</sup>/h of brown coal". Functional unit is used for normalization of total energy, materials and emissions. In such way different conveyors with the same throughput of brown coal can be compared. Moreover, results of such comparison can lead to improvement of design of short conveyors from the environmental point of view or choosing adequate type of conveyor for required purpose (perhaps change in concept or some other changes).

Minimum service life of a belt conveyor is expected to be 5 years. It is calculated in accordance with 110 bearing service life. Actual life span of a belt conveyor is considerably longer and it equals 25 to 30 years. Therefore, ball bearings are to be replaced at least 5 to 6

times during the conveyor lifetime. Gearbox oil is changed on a yearly basis. Most of the data are taken from previous partial analyses and implemented into the analysis presented in [38].

For the purpose of the presented analysis, the belt conveyor is divided into five main groups of parts as presented in [38], see Figure 13 [37]:

1. Idlers/rollers,
2. Pulleys,
3. Belting,
4. Electric motor (EM),
5. Other.

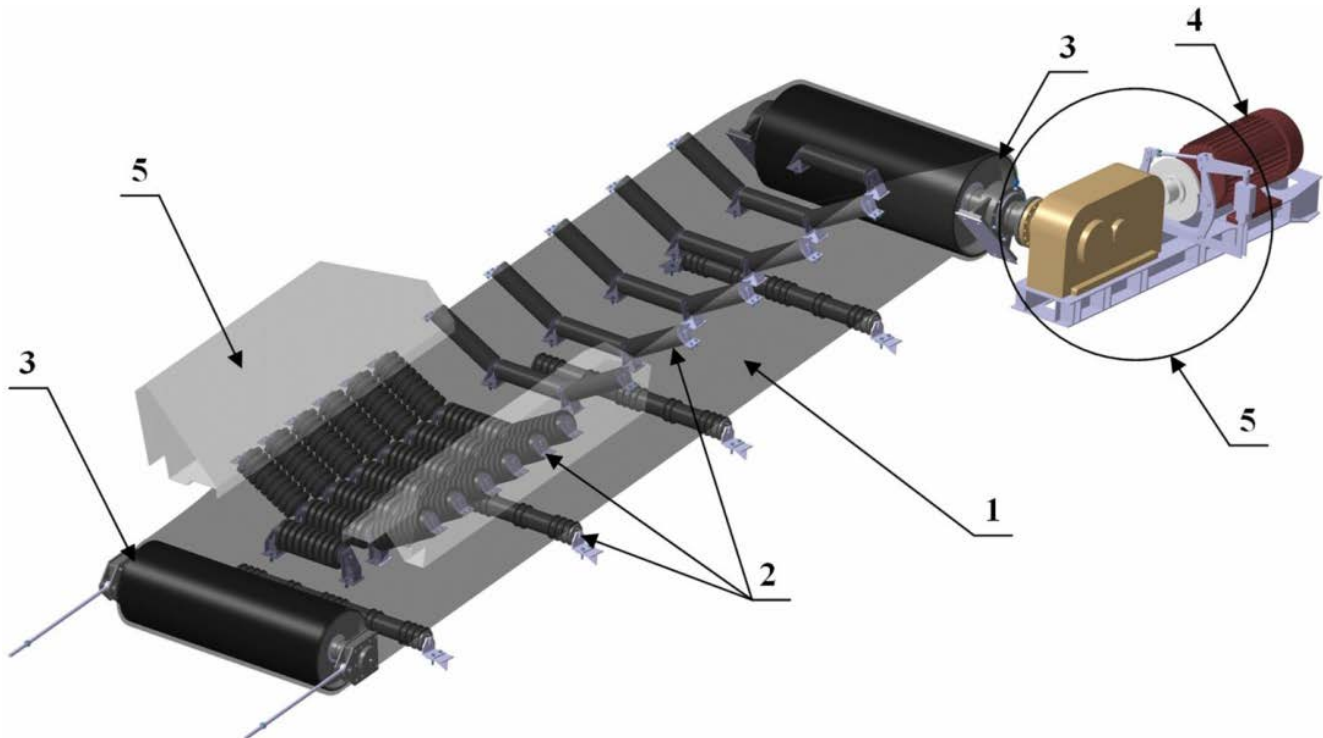


Figure 13: Main components of a conveyor: 1. belting, 2. idlers/rollers, 3. pulleys, 4. electric motor, 5. other

Group of parts named "other" consists of belt conveyor drive components (without EM), take up device and accessories. Drive components considered here are gearbox unit, coupling and drum brake, see Figure 14 [37]. Take-up device is not considered within the analysis because of the lack of data. Normally, take-up device could be considered as component that:

1. Consumes electric or other kind of energy,
2. Does not consume energy.

In case that take-up device consumes energy, the type and amount of consumed energy per use should be calculated and added to the total energy consumed by the belt conveyor in its use stage. In the second case, take-up device is considered a part predominantly made of steel which is produced by machining. Generated waste during the production stage of take-up device is assumed to be 10% of its mass. The second case will be used as a pattern for modelling parts and components predominantly made of single material and do not consume energy.

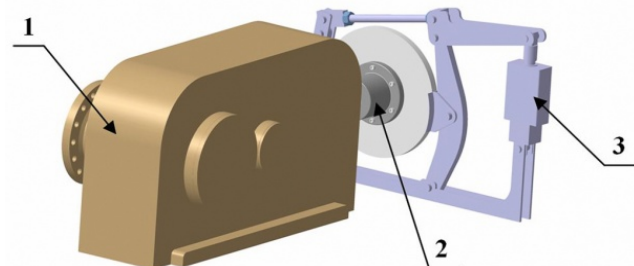


Figure 14: Belt conveyor drive components: 1. gearbox, 2. coupling, 3. drum brake

Parts and components which belong to the accessories are analyzed the same way as the take-up device. The only component from this group of parts considered here is chute. During the analysis, the belt conveyor is divided into 5 groups of parts. These 5 groups are further classified in accordance with their constituent materials. This classification is presented in Table 4 and summarized in Figure 15 [38].



Table 3: LCIA of UTRs (Ecoinvent - damage method)

Group of parts	Pieces	Weight/piece [kg]	Weight [kg]	Material	Class	Scrap [kg]
<b>1. Rollers</b>						
Steel parts	47 rollers	27.8	1,307.0	Steel	III	10% = 130.7
Rubber parts	31 rollers	6.2	192.0	Rubber	IV	10% = 19.2
Lubricating grease: considered in raw material stage considered in use stage			7.52 0.023 kg/use	Li-based oil	V V	
<b>2. Pulleys</b>						
Steel parts	1.5	1,252.0	1,878.0	Steel	III	10% = 187.8
Alloyed steel parts	1.5	751.3	1,127.0	Alloyed steel	VI	10% = 112.7
Rubber parts	1.5	157.37	236.0	Rubber	IV	10% = 23.6
Lubricating grease: considered in raw material stage considered in use stage			4.095 0.013 kg/use	Li-based oil	V V	
<b>3. Belting</b>						
Carcass	1	112.64	112.64	EP & PA	V	10% = 11.3
Covers	1	450.56	450.56	Rubber	IV	10% = 45.1
<b>4. Electric motor</b>						
Windings and bars	1	176.0	176.0	Copper	V	10% = 17.6
Housing	1	264.0	264.0	Cast iron	IV	10% = 26.4
Steel parts	1	440.0	440.0	Steel	III	10% = 44.0
<b>5. Other</b>						
<b>5.1 Gearbox</b>						
Casing	1	450.0	450.0	Cast iron	IV	10% = 45.0
Flange	1	74.0	74.0	Alloyed steel	VI	10% = 7.4
Steel parts	1	376.0	376.0	Steel	III	10% = 37.6
Lubricating oil: considered in raw material stage considered in use stage			50 l $\approx$ 45 kg 0.144 kg/use	Mineral oil	V V	
<b>5.2 Coupling</b>	1	20.0	20.0	Steel	III	$\approx$ 50% = 10.0
<b>5.3 Drum brake</b>	1	120.0	120.0	Steel	III	10% = 12.0
<b>5.4 Chute</b>	1	1,950.0	1,950.0	Steel sheet	IV	10% = 195.0

In accordance with the "cut-off" rule, parts with mass inclusion lower than 5% of total mass of the product have been neglected. In this case, since there were partial analyses conducted, "the product" stands for components of the belt conveyor presented in papers [32], [33], [34], [35] and summarized in paper [38]. "Cut-off" rule based on energy inclusion gives similar results.

Lubricants can be considered either within raw material stage or within use stage. Regardless of which of these two options are chosen, the result remains the same. Besides the belt conveyor parts, packaging and packaging material are taken into account as presented in [38]. Total energy input and generated waste during the manufacturing of the belt conveyor are obtained from [38] and shown in Figure 16. Data from the manufacturing

stage form for initial iteration are shown in Figure 16. The initial iteration presents the worst case scenario and basis for further optimization of environmental properties of the belt conveyor. The belt conveyor, as a part of BWE, is utilized at the open pit mine near Lazarevac. Most of the belt conveyor components are supplied from the manufacturer in the proximity to the open pit mine. Calculated hauling distance for transportation of external parts by truck was 1,865 km. In accordance with [37], this distance can be classified as "rather short". The drum brake is transported from the greatest distance (approximately 1,500 km) and it is considerably affecting total transportation distance [38].

# Assistant

Description

**Raw Material** ▶

Manufacture

Distribution

Product Use

End of Life

Result

Please indicate the parts and components of your product and its packaging.

If you need support in assigning the different materials to the appropriate class of materials, click the help-symbol next to the "Class" heading.

## 1. Product data

Product part	Mass [kg]	Material	Class <span>?</span>
Steel parts	4141	Steel	III ▼
Alloyed steel parts	1201	Alloyed steel	VI ▼
Rubber parts	879	Rubber	V ▼
Plastics parts	113	EP & PA	V ▼
Copper parts	176	Copper	V ▼
Cast iron parts	714	Cast iron	IV ▼
Sheet metal parts	1950	Steel sheet	IV ▼
FOR LPD 2 Lubricant	8,37	Lithium based	V ▼
Gearbox oil - Reduktol	45	Mineral based oil	V ▼
			▼
			▼
			▼
			▼
			▼
			▼

## 2. Product data

Part of packaging	Mass [kg]	Material	Class <span>?</span>
Euro Palletes	288	Wood	I ▼
Wooden Cases	380	Wood	I ▼
			▼
			▼
			▼

3. Does the Product contain parts that constitute a hazard to the environment at the end of life without expert disposal ("small quantities - great impact")?

unknown ▼

Figure 15: Raw material stage form with lubricants considered within it [38]

The use stage is determined with the number of operating hours per day and consumption of electricity and auxiliary material. The belt conveyor operates 20 hours per day 325 days a year. It is assumed that one use equals one working day. The belt conveyor consumes 2.64 MWh/use, but due to software limitations this value is set to 1.0 MWh/use. However, this fact does not affect the result. Besides the electricity consumption, the belt

conveyor needs lubrication for its proper operation. Lubrication could be considered either in this stage or in raw material stage. In case of lubricating the belt conveyor in use stage there is a need for 0.036 kg/use of FOR LPD 2 lubricating oil for ball bearings and 0.144 kg/use of Reduktol oil for gearbox unit. As previously stated, both options give the same result [38].



INTRODUCTION

PILOT
ASSISTANT

@ ▲ ◀ ▶ 🏠 📄 🖨

# Assistant

Description   Raw Material   **Manufacture** ▶   Distribution   Product Use   End of Life   Result

Please indicate data referring to the manufacture of your product.  
 Again, you will get support by clicking the help-symbol next to the "Class" heading.

**4. Energy input**

Electric energy  [kWh]   Overhead energy: Energy for heating, lighting, ... in addition to process energy  ▼

Thermal energy  [MJ]

**5. Waste per Unit**

Waste	Mass [kg]	Material	Class <span style="font-size: small;">?</span>
Scrap steel	422,1	Steel	III ▼
Scrap alloyed steel	120,1	Alloyed steel	VI ▼
Scrap steel sheet	195	Steel sheet	IV ▼
Scrap cast iron	71,4	Cast iron	IV ▼
Scrap copper	17,6	Copper	V ▼
Scrap rubber	87,8	Rubber	IV ▼
Scrap plastics	11,3	EP & PA	V ▼
			▼
			▼
			▼
Material	<input type="text" value="Unsorted to waste"/>		▼

6. Production volume (Units/Pieces per Year)  ▼

7. Input of environmentally hazardous auxiliary and process materials per unit produced  ▼

8. Percentage of external parts  ▼

9. Hauling distance for external parts per unit  ▼

*Figure 16: Manufacturing stage form for initial iteration [38]*

Spare parts and their consumption were not considered during the analysis presented in [38]. This fact will certainly affect the increasing consumption of auxiliary material in the use stage. However, this will not change the result since use stage already has the greatest impact to the environment in accordance with [38]. Spare parts and their consumption affect more the maintenance strategy and service intervals.

The first iteration assumed the worst case scenario for EoL options also. All of the belt conveyor components are disposed of in a landfill. When lubricants are considered as a parts in raw material stage, at the EoL stage there has to be chosen the way of their disposal.

Finally, it was concluded that the belt conveyor is a D-type product [37]. Initial iteration is conducted in a way that results in maximum environmental load. Result of initial iteration is initial result, and it serves as a basis for further environmental improvements of the belt conveyor, refer to Figure 17. Further optimizations of environmental properties of the belt conveyor are described in [38]. Regardless of variations in input parameter values through iterations the belt conveyor remained use intensive product. Strategy S13 remained the strategy with the highest priority (main), while strategies S10, S12 and S15 had been assigned to the strategies that are to be realized latter (more) and all other strategies disappeared from

recommendations due to proper optimization of input parameters that already involved their implementation.



Description Raw Material Manufacture Distribution Product Use End of Life **Result**

### Product

Name:  Functional Unit  
 Life Time:  years   
 Use:  times per year

### Classification

The analysed product seems to be a basic type D, the phase 'use' is significant here.

### Recommendations

We recommend the following improvement strategies. The listed strategies forward you to the checklists of the ECODESIGN PILOT.

#### (Main) Strategies with high priority:

- S12. [Ensuring environmental safety performance](#)
- S13. [Reducing consumption at use stage](#)

#### (More) Strategies to be realized later:

- S10. [Optimizing product functionality](#)
- S15. [Improving maintenance](#)

#### (Other) Additional, recommended strategies:

- S4. [Optimizing type and amount of process materials](#)
- S5. [Avoiding waste in the production process](#)
- S6. [Ecological procurement of external components](#)
- S19. [Recycling of materials](#)

Figure 17: The result of the first iteration - initial result [38]

In compliance with previously conducted researches and related published papers it can be said that:

- Since EM is a belt conveyor component that contributes most to electricity consumption, just increase in its energy efficiency delivers the greatest reduction of environmental impact,
- Adequate maintenance strategy and similar service intervals for different components of the belt conveyor ensure reduction of overhauling time,
- Reliability of the belt conveyor is largely dependent on selected maintenance strategy,

- Improving functional quality increases reliability, improves maintenance and reduces consumption,
- Replacement of process and auxiliary materials, especially lubricants, with renewables contributes to reduction of environmental impact of the product,
- Lubricants are marked as hazardous waste and they have to be treated in a proper manner at the EoL; possible improvements related to lubricant characteristics will be considered later,
- In-house recycling eliminates transportation needed in case of external recycling or disposal,
- Regionally available parts and materials reduce need for transportation,
- Production volume does not affect the result,
- Number of external components has greater impact than their hauling distance,
- Steel parts are recycled (this applies particularly to the rollers),
- Any EoL option for packaging does not affect the result, but it is likely that the euro pallets are reused and the wooden cases are disposed of in a landfill.

The listed issues with corresponding recommendations have been thoroughly further elaborated in [37].

## CONCLUSIONS

Among all other aspects intralogistics is related to material handling and conveying technologies and equipment. Consequently, investigations and research of potential improvements of environmental properties of intralogistics equipment, especially energy efficiency, has great impact on future trends in intralogistics. Development of innovative technologies is strategically focused on improving environmental performances and reducing emissions. Therefore, it would be recommendable to prove the real environmental benefits of newly established innovative technologies. The presented researches conducted in the recent years at the Faculty of Mechanical Engineering in Belgrade are related to cargo handling equipment and belt conveyors. The presented examples illustrate importance of life cycle thinking for decision making and identifying the drawbacks of technologies promoted as solutions to mitigate environmental impacts.

The efforts of CHE industry in providing ports and container terminals with environmentally more efficient technologies are becoming more visible than ever. Almost

every piece of CHE today is offered with some solution for reduction of emissions and energy consumption, from alternative fuels and hybrid technology, to promising "zero emission" concept. The "zero emission" concept applied on RTG crane and UTR as core of CHE is investigated in the presented researches using LCA methodology. The LCA proved itself as a valuable tool for comparison of even such complex products as the CHE. It offers systematic approach for sustainability evaluations of life cycles of conventional and novel technologies. However, in order to avoid any major data inventory uncertainties often pointed out by LCA critics, the random comparison of onsite measurements results with functional unit assumptions is recommended.

The entire life cycles of conventional diesel RTG crane and UTR were compared with electric ones in order to reveal any sustainability sensitivities that are common with energy source transitions. In this respect, the results of LCA present electrification of CHE as a feasible and sustainable solution aimed to mitigate environmental impact of ports. The transition from diesel to electric handling equipment is a step forward, although "zero emission" operations from LCA perspective are impossible to be achieved.

The fact that selection of power grid mix can, due to nature of LCA, provide completely different results, a short "what if" analysis was conducted in [26]. In order not to overextend the comparison of data, only GWP is taken into account. The calculation for replacement of lithium ion battery pack of electric UTR after 5 years is also shown in Figure 18 [26]. The assumptions made, for instance, for comparison of environmental impacts of UTRs are:

- Electric 1 refers to result from LCA, without battery change and EU-25 power grid mix with GWP of 0.539 kg of CO<sub>2</sub> eq. per kWh;
- Electric 2, same as above with battery replacement (disposal of old batteries and entire life cycle of new batteries);
- Electric 3 – For this UTR, the power grid mix is adopted to be the world average with GWP of 0.749 kg of CO<sub>2</sub> eq. per kWh; the battery replacement is also taken into account.
- Electric 4 – The power grid mix is an average GWP for coal power plant approximated to 1 kg of CO<sub>2</sub> eq. per kWh;
- Diesel – results from LCA study.

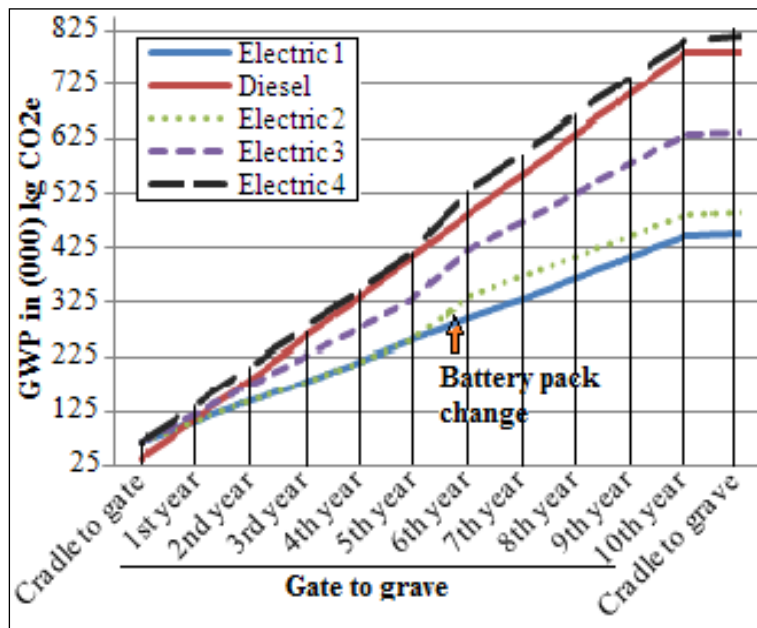


Figure 18: LCA of UTRs depending on power grid mix [26]

Analysis shows that electric over diesel UTR has lower GWP only up to the level of 0.9 kg of CO<sub>2</sub> eq. per kWh of electric energy. In the case of coal burning power plants, the emissions of conventional diesel UTR are only replaced with similar level of GWP of electric UTR. If the additional environmental impact of battery replacement is taken into account, as with case of presented electric UTR no. 4, the overall results are actually worse than conventional diesel burning UTR [26].

If we speak about the conducted simplified LCA analysis of a complete belt conveyor presented in [37], it shown that the most significant stage of a BWE belt conveyor life cycle is its use stage. Besides EM, consumption of the belt conveyor is determined with different kind of resistances to motion. Improving EM efficiency together with reduction of these resistances contributes to minimization of electricity consumption, reduction of wear of moving parts such as belting surface, prolonging of belt conveyor's life and consequently to sustainable development in general.

Further and deeper research should consider generalization which should include:

- most common types of idlers/rollers, normalized by their length and diameter;
- pulleys with different kinds of coatings, normalized by their length and diameter;
- steel cord beltings and beltings with textile reinforcing plies, normalized by their unit of length, belt width and reinforcing plies (in case of beltings with textile reinforcing plies, normalization should be done in accordance with number of reinforcing plies and in case of steel cord beltings, normalization should be done in accordance with steel cord diameter), establishment of relation between power and weight of EM and normalization of EM in accordance with its power.

The idea of this simplified LCA was to implement further the gained generalizations into formal LCA, which will be conducted with corresponding LCA software.

#### ACKNOWLEDGEMENTS

This paper is a contribution to the Ministry of Education, Science and Technological Development of Republic of Serbia funded project TR 35006.

#### REFERENCES

- [1] A. Bârsan and L. Bârsan, "Ecodesign for Sustainable Development, Volume 1: Fundamentals", Transylvania University of Brasov, ISBN: 978-973-598-104-4, Brasov (Romania), (2007)
- [2] N. Zrnić and M. Đorđević, "Ecodesign: Sustainable Product Development" ("Dizajn i ekologija - Održivi razvoj proizvoda"), book in Serbian, University of Belgrade, Faculty of Mechanical Engineering, ISBN: 978-86-7083-772-0, Belgrade (Serbia), (2012)
- [3] A. Vujičić and N. Zrnić, "State-of-the-art in life cycle assessment as a core of life cycle design", Proceedings of the 10<sup>th</sup> International Conference on Accomplishments in Electrical, Mechanical and Informational Engineering "DEMI 2011", University of Banja Luka, Banja Luka (Bosnia and Herzegovina), 26-28 May 2011, pp. 203-208 (2011).
- [4] W. Wimmer, "Ecodesign for Sustainable Development, Volume 4: Product Development", Transylvania University of Brasov, ISBN: 978-973-598-107-5, Brasov (Romania), (2007)
- [5] N. Zrnić, S. Bošnjak and M. Đorđević, "Design for modernization – A way for implementation of eco improvements of port's cranes", Machine Design, Faculty of Technical Sciences, Novi Sad, Vol. 2(1), pp. 07-13, (2010)
- [6] A. Azapagić and R. Clift, "The application of life cycle assessment to process optimisation", Computers and Chemical Engineering 23, Elsevier, pp. 1509–1526, (1999)

- [7] EN ISO 14040: 2006
- [8] Michael ten Hompel, "Volker Heidenblut: Taschenlexikon Logistik", Springer-Verlag, (2008)
- [9] G. Kartnig, B. Grösel and N. Zrnić, "Past, State-of-the-Art and Future of Intralogistics in Relation to Megatrends" FME Transactions, ISSN: 1451-2092, Vol. 40(4), pp. 193-200, (2012)
- [10] O. Altintas, C. Avsar and M. Klumpp, "Change to Green in Intralogistics", Proceedings of the 2010 European Simulation and Modeling Conference, Hasselt University, Oostende (ETI), pp. 373-377, (2010).
- [11] F. Straube, "Trendforschung in der Logistik – Logistikinnovationen 2015+", Berlin-Brandenburg Konferenz 2008, Berlin (Germany), 11-12 September 2008, (2008)
- [12] A. McKinnon, "Green logistics: The Carbon Agenda", Scientific Journal of Logistics, Vol. 6, Issue 3, No. 1, p. 9, (2010)
- [13] N. Zrnić, and A. Vujičić, "Life-Cycle Approach to Characterizing Environmental Impact of Logistics Equipment in Container Ports: An example of Yard Trucks", Lecture Notes in Logistics 2014, Efficiency and Innovation in Logistics, Dortmund: Springer, U. Clausen, M. ten Hompel and F. Meier (eds.), pp. 135-146, (2014)
- [14] E. Savelsberg, "Innovation in European Freight Transportation: Basics, Methodology and Case Studies for European Market", Springer, (2008).
- [15] A. Vujičić, N. Zrnić, and B. Jerman, "Ports sustainability: trends in CHE industry", Proceedings of The 20<sup>th</sup> International Conference of Material Handling, Constructions and Logistics "MHCL'12", FME Belgrade (Serbia), 3-5 October 2012, pp. 395-401, (2012)
- [16] D. Guerrero and J.P. Rodrigue, "The Waves of Containerization: Shifts in Global Maritime Transportation", Journal of Transport Geography, Vol. 34, pp. 151-164, (2014)
- [17] A. Vujičić, "Future of containerisation sustainability - Shifting from green to smart port", Proceedings of The 21<sup>th</sup> International Conference of Material Handling, Constructions and Logistics "MHCL'15", ISBN: 978-86-7083-863-5, Vienna: University of Technology, Vienna (Austria), 23-25 September 2015, pp. 395-401, (2015)
- [18] H. Geerlings and R. van Duin, "A New Method for Assessing CO<sub>2</sub>-emissions from Container Terminals: A Promising Approach Applied in Rotterdam", Journal of Cleaner Production, Vol. 19(6-7), pp. 657-666, (2011)
- [19] C.I. Liu, H. Jula and P.A. Ioannou, "Design, Simulation, Evaluation of Automated Container Terminals", IEEE Transactions on Intelligent Transportation Systems, Vol. 3(1), pp. 12-26, (2002)
- [20] National Cooperative Freight Research Program, "Report 4: Representing Freight in Air Quality and Greenhouse Gas Models" Transportation Research Board, Washington D.C. (USA), (2010)
- [21] N. Zrnić, and A. Vujičić, "Reduction of RTG Cranes Emission by Using Hybrid Technology", Proceedings of the International Conference REACT, Shaping Climate Friendly Transport in Europe: Key Findings & Future Directions, University of Belgrade, FTTE (Serbia), 16-17 May 2011, pp. 180-187, (2011)
- [22] J. Kim, M. Rahimi and J. Newell, "Life-Cycle Emissions from Port Electrification: A Case Study of Cargo Handling Tractors at the Port of Los Angeles", International Journal of Sustainable Transportation, Vol. 6(6), pp. 321-337, (2012)
- [23] Starcrest, "San Pedro Bay Ports: Emissions Forecasting Methodology and Results", Starcrest Consulting Group, Poulsbo, (2008)
- [24] J.W. Böse, "Handbook of Terminal Planning", Springer, New York (USA), (2011)
- [25] N. Zrnić and A. Vujičić, "Evaluation of environmental benefits of CHE emerging technologies by using LCA" Progress in Material Handling Research: 2012, A. Carrano, R. Koster, B. Montreuil, K. Gue, M. Ogle and J. Smith (eds.), Charlotte: Material Handling Industry of America, pp. 713-731, (2012)
- [26] A. Vujičić, N. Zrnić and B. Jerman, "Ports sustainability: A life cycle assessment of zero emission cargo handling equipment", Strojniški vestnik - Journal of Mechanical Engineering, Vol. 59(9), pp. 547-555, (2013)
- [27] H. Ostad-Ahmad-Ghorabi and D. Collado-Ruiz, "Tool for the environmental assessment of cranes based on parameterization", Int J Life Cycle Assess, Vol. 16, pp. 392-400, (2011).
- [28] Calstart, "Hybrid yard hostler demonstration and commercialization project report", The Port of Long Beach and Port of Los Angeles, (2011)
- [29] S. Bošnjak and N. Zrnić, "Dynamics, Failures, Redesigning and Environmentally Friendly Technologies in Surface Mining Systems", Archives of Civil and Mechanical Engineering, ISSN: 1644-9665, Vol. 12(3), (September 2012), pp. 348-359, (2012)
- [30] O.K. Awuah, D. Checkel and N. Askari, "Evaluation of belt conveyor and truck haulage systems in an open pit mine using life cycle assessment", CIM Bulletin, Vol. 4(5), pp. 1-6, (2009).
- [31] M. Langerholc, N. Zrnić, M. Đorđević and B. Jerman, "Conveyor Design Optimization as the Provision of Sustainability", Technical Gazette, ISSN: 1330-3651 (Print), ISSN: 1848-6339 (Online), Vol. 20(5), (October 2013), pp. 837-846, (2013)
- [32] M. Đorđević, N. Zrnić and M. Pantelić, "Simplified Life Cycle Assessment of a Return Belt Conveyor Idler", Proceedings of The 11<sup>th</sup> International Conference on Accomplishments in Electrical and Mechanical Engineering and Information Technology "DEMI 2013", ISBN: 978-99938-39-46-0, University of Banja Luka, Faculty of Mechanical Engineering, Banja Luka (BiH), 30<sup>th</sup> May - 1<sup>st</sup> June 2013, pp. 201-206, (2013)
- [33] M. Đorđević, N. Zrnić and B. Jerman, "Simplified Life Cycle Assessment of Belt Conveyor Drive Pulley", Proceedings of The 5<sup>th</sup> International Conference Transport and Logistics "TIL 2014", University of Niš, Faculty of Mechanical Engineering, Niš, ISBN: 978-86-6055-053-0, Niš (Serbia), 22-23 May 2014, pp. 55-58, (2014)

- [34] M. Đorđević, N. Zrnić and B. Jerman, "Simplified Life Cycle Assessment of a Conveyor Belting", Proceedings of The 8<sup>th</sup> International Conference Heavy Machinery "HM 2014", University of Kragujevac, Faculty of Mechanical and Civil Engineering in Kraljevo, ISBN: 978-86-82631-74-3, Zlatibor (Serbia), 24-26 June 2014, pp. A.165-A.170, (2014)
- [35] M. Đorđević, N. Zrnić and B. Jerman, "Simplified Life Cycle Assessment of a Belt Conveyor Electric Motor", Proceedings of The 14<sup>th</sup> International Conference "Research and Development in Mechanical Industry" "RaDMI 2014", SaTCIP, Vrnjačka Banja, ISBN: 978-86-6075-043-5, Topola (Serbia), 18-21 September 2014, pp. 671-678, (2014)
- [36] Austrian Ecodesign Platform, available at: [www.ecodesign.at](http://www.ecodesign.at), (2006)
- [37] M. Đorđević, N. Zrnić and S. Bošnjak, "LCA of a belt conveyor and its application", In: Next generation logistics: Technologies and Applications, Scientific monograph, edited by Jereb, B., SPH - Scientific Publishing Hub, ISBN 978-961-6948-07-4, pp. 175-197, (2017)
- [38] M. Đorđević, N. Zrnić and B. Jerman, "Simplified Life Cycle Assessment of a Belt Conveyor", Proceedings of The 21<sup>th</sup> International Conference of Material Handling, Constructions and Logistics "MHCL'15", ISBN: 978-86-7083-863-5, Vienna: University of Technology, Vienna (Austria), 23-25 September 2015, pp. 199-206, (2015)



# Damping Characteristics of the Seismic Isolation Bearings Group, in Modular Design, for Bridges and Viaducts

Marian Dima<sup>1</sup>, Cătălin Frâncu<sup>1\*</sup>

<sup>1</sup> Faculty of Technological Equipment, Technical University of Civil Engineering, Bucharest (Romania)

*In this paper we present the damping characteristic and how to determine it through modelling and numerical simulation of the seismic isolation bearings group in modular design for bridges and viaducts.*

**Keywords:** Damping characteristic, Seismic isolation, Bridges, Viaducts

## 1. INTRODUCTION

In the modular bridge and viaduct seismic grouping and seismic isolation group, Figure 1, analysed in the present paper, the component elements which have the role of damping the motion of the bridge superstructure by dissipating the kinetic energy are:

1. the elastomeric insulator, provides viscoelastic damping and has a viscous damping equivalent to the type of rubber used: soft  $G=0,4\text{N/mm}^2$ ,  $\xi=10\%$ , normal  $G=0,8\text{N/mm}^2$ ,  $\xi=10\%$  și hard  $G=1,4\text{N/mm}^2$ ,  $\xi=16\%$ ;
2. spherical bearing, provides dry friction damping  $\mu = 0,02$ ;
3. a system consisting of six hydraulic shock absorbers, arranged in a geometric configuration according to the cinematic scheme of the Stewart platforms, provides viscous damping, the viscous damping coefficient of each damper being adjustable by changing the passage hole area between the two chambers of the cylinder.

In conclusion, the only item that has a functionally adjustable parameter is the six hydraulic dampers system and the adjustable parameter is the viscous damping coefficient of each hydraulic damper.

## 2. DETERMINING THE DAMPING CHARACTERISTICS

The damping of the seismic isolation bearings group is assessed by the dissipated energy during a period of seismic motion that is given by the magnitude of the hysteresis area of the force-displacement diagram.

In order to obtain the force-displacement diagram, a virtual model was constructed and simulated the operation of the seismic isolation bearings group, in modular design, for bridges and viaducts. The simulation was done for various values of the viscous damping coefficient of the hydraulic dampers and also for the different directions of the seismic movement in relation to the bearing group; the representative directions being  $O_x$  and  $O_y$  respectively. In the simulation, a displacement of the upper plate was imposed relative to the lower plate and the force required to achieve the displacement considered as the sum of all dissipative forces in the direction of motion was measured. Characteristics of the components of the simulated group are:

1. Elastomeric insulator ALGA HDS300x96,  $G=0,4\text{N/mm}^2$ ,  $k=0,29\text{kN/mm}$ ;  $V_{\max}=500$ ;  $V_{\text{din}}=210\text{kN}$ ;  $s_{\max}=200\text{mm}$ ;
2. spherical bearing MAGEBA KA 1.0,  $\mu = 0.02$ ,  $V_{\max} = 1000$ ;  $V_{\text{din}} = 300\text{kN}$ ,  $p = 180\text{N/mm}^2$
3. Hydraulic dampers ACE, HB-70-100-EE-P, stroke 100 mm,  $F_{\max} = 50\text{kN}$

The results obtained are presented below.

### 2.1. Displacement by the $O_x$ axis

The large plate is considered fixed and the small plate translates along the  $O_x$  axis following the law  $x(t) = 100 * \sin(\pi \cdot t + \pi)$  mm. On top of the small plate acts a vertical force of 210 kN. The results for the force required for displacement, measured in N, for various values of the dampening coefficient  $c$  of the hydraulic dampers are shown in Figure 2 to 5.

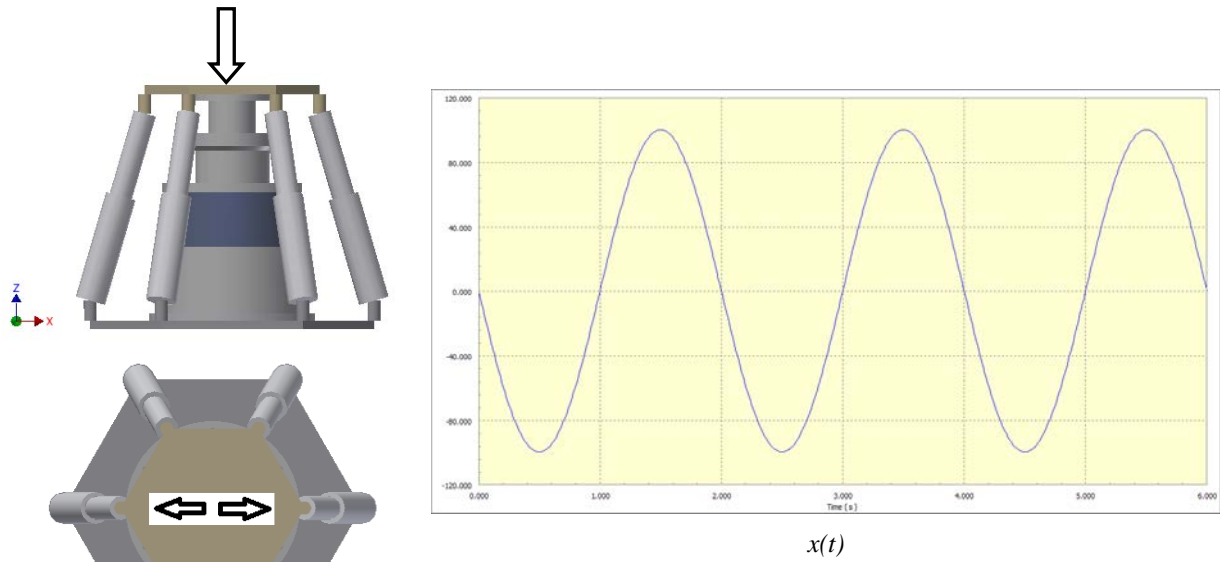


Figure 1. Displacement by the Ox axis and acting force on the upper plate.

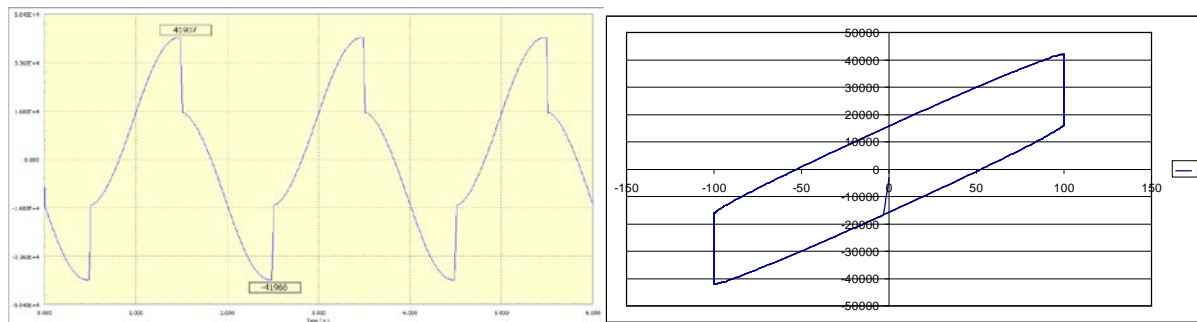


Figure 2.  $F_d(t)$  și  $F_d(x)$  for  $c = 0$  Ns/mm

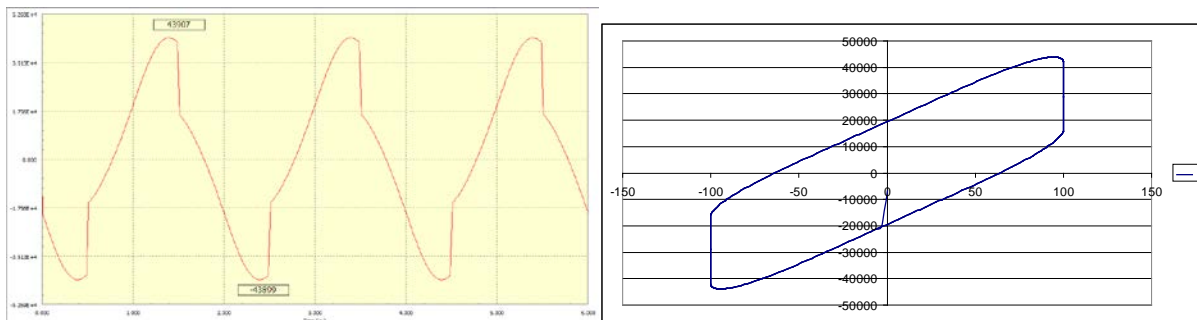


Figure 3.  $F_d(t)$  și  $F_d(x)$  for  $c = 50$  Ns/mm

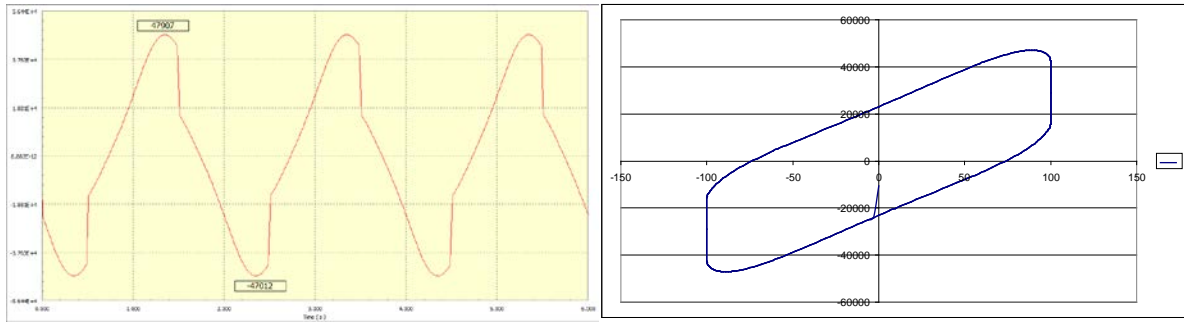


Figure 4.  $F_d(t)$  și  $F_d(x)$  for  $c = 100 \text{ Ns/mm}$

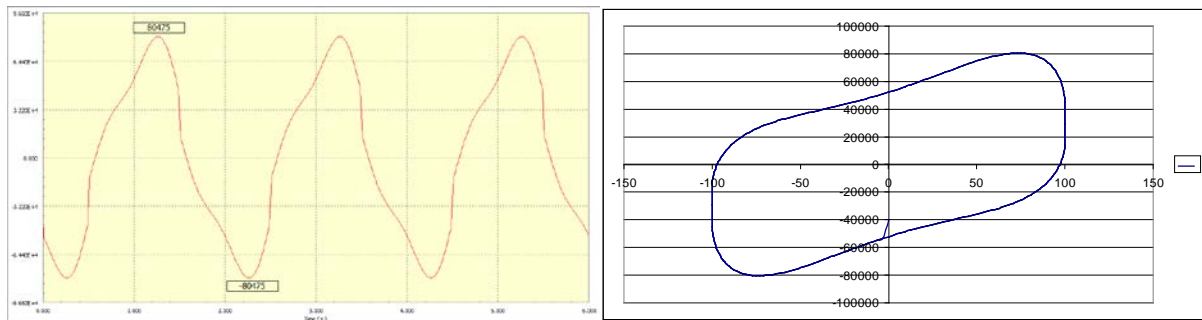


Figure 5.  $F_d(t)$  și  $F_d(x)$  for  $c = 500 \text{ Ns/mm}$

2.2. Displacement by the Oy axis

The large plate is considered fixed and the small plate translates along the Oy axis following the law  $y(t) = 100 * \sin(\pi \cdot t + \pi) \text{ mm}$ . On top of the small

plate acts a vertical force of 210 kN. The results for the force required for displacement, measured in N, for various values of the dampening coefficient  $c$  of the hydraulic dampers are shown in Figure 7 ... 10.

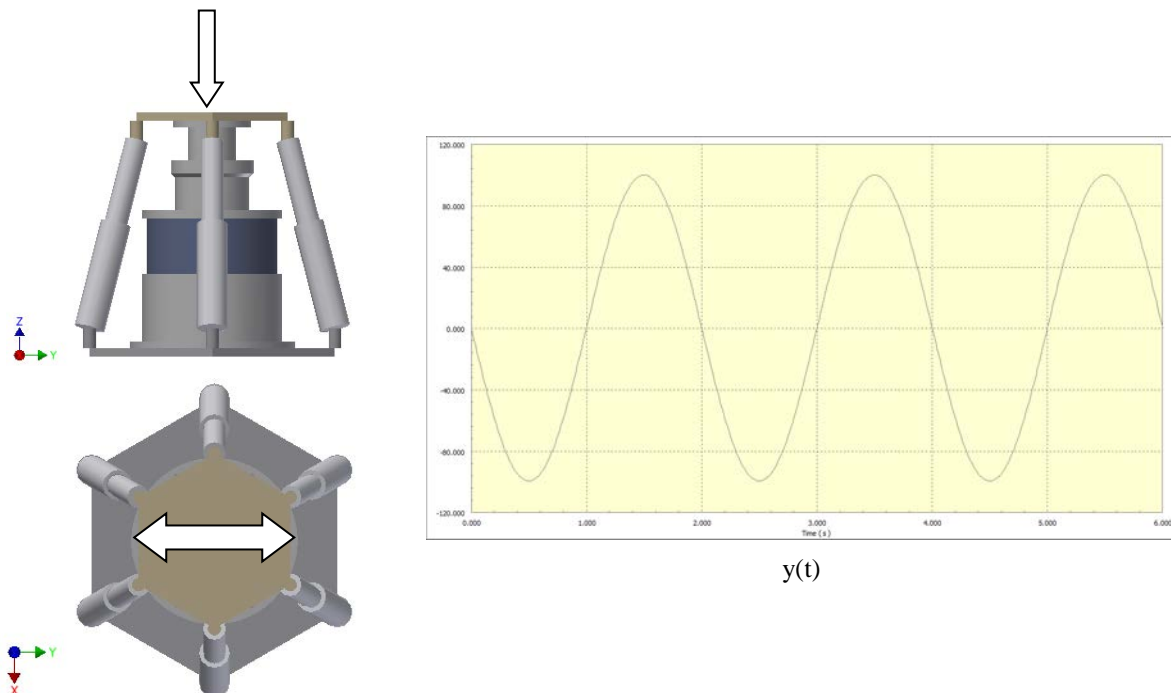


Figure 6. Displacement by the Oy axis and acting force on the upper plate.

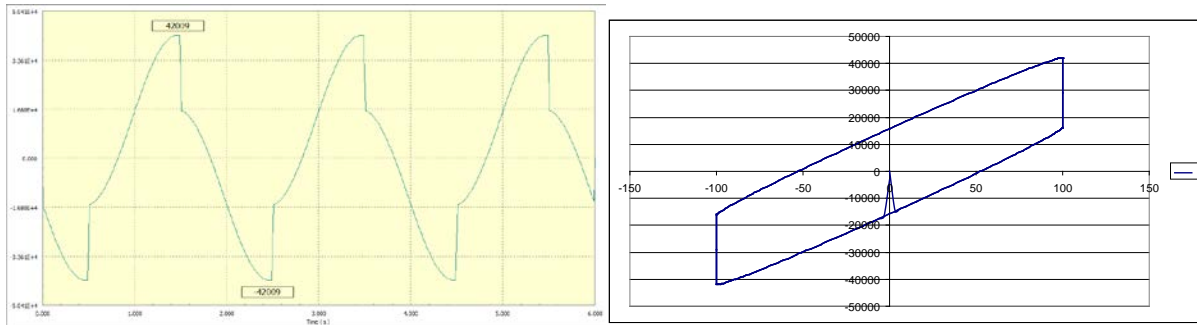


Figure 7.  $F_d(t)$  și  $F_d(y)$  pentru  $c = 0$  Ns/m

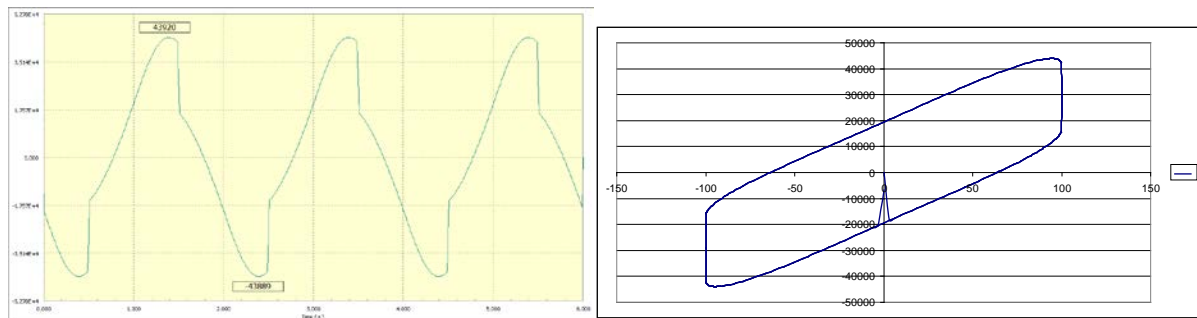


Figure 8.  $F_d(t)$  și  $F_d(y)$  pentru  $c = 50$  Ns/m

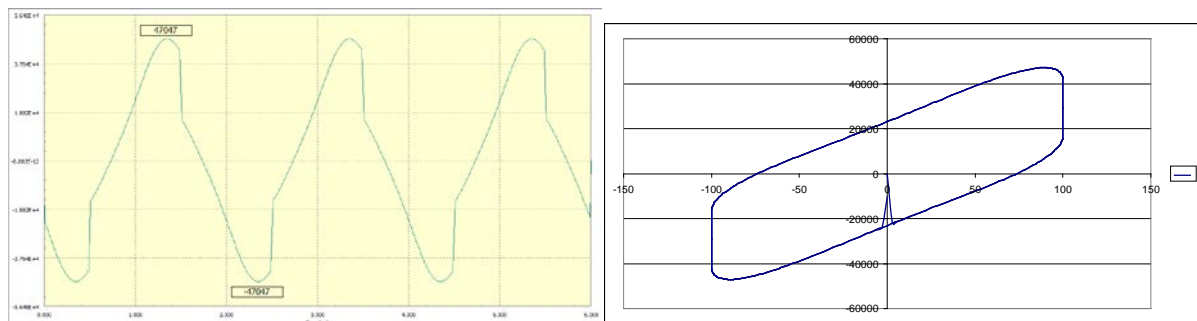


Figure 9.  $F_d(t)$  și  $F_d(y)$  pentru  $c = 100$  Ns/m

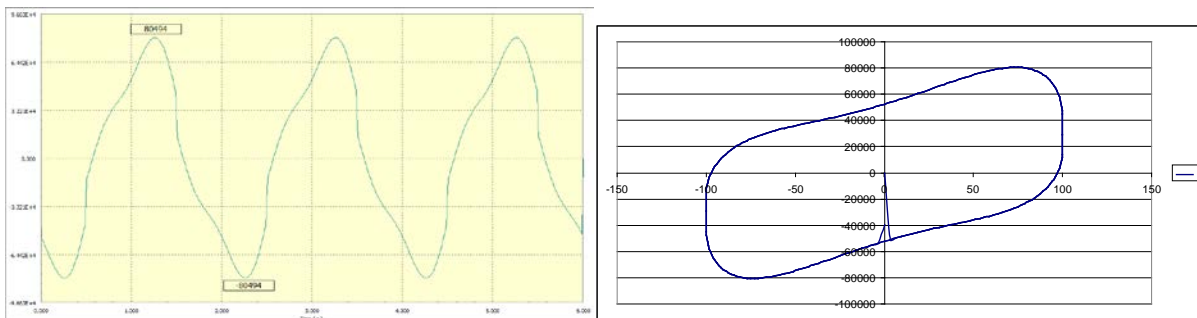


Figure 10.  $F_d(t)$  și  $F_d(y)$  pentru  $c = 500$  Ns/m

### 3. CONCLUSIONS

1. The behavior of the seismic isolation bearings group, in modular design, for bridges and viaducts in terms of dissipated energy does not depend on the direction of seismic motion.

2. The energy dissipated per cycle, fig. 11, practically varies linearly with the viscous damping coefficient of the hydraulic dampers.

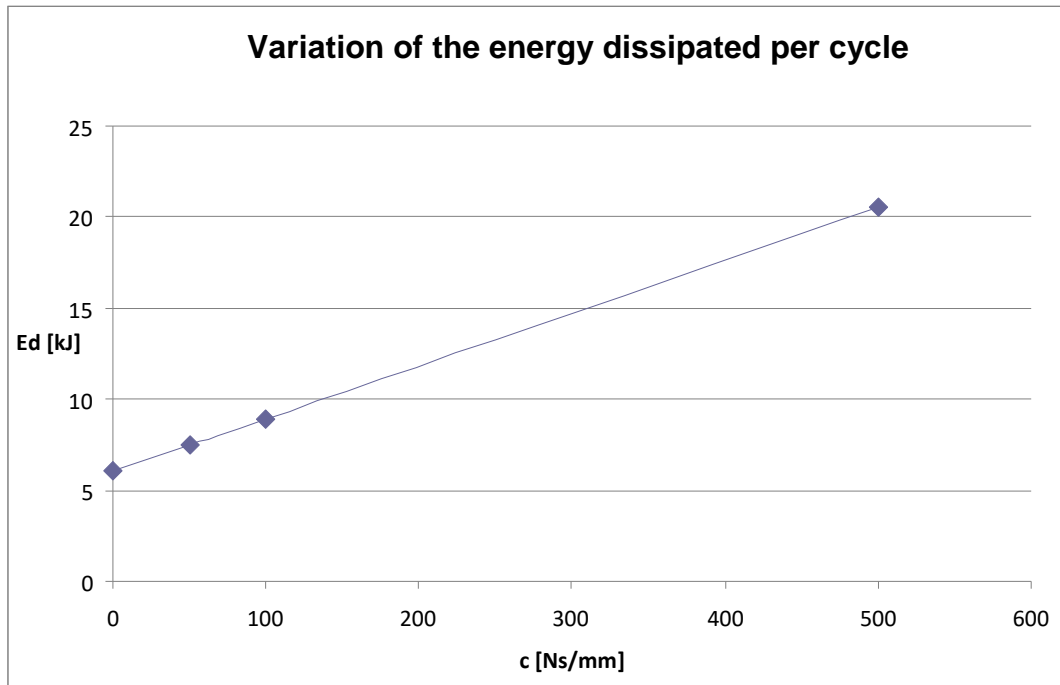


Figure. 11. Dissipated energy ( $c$ )

### REFERENCES

[1] Dima M., Frâncu C, ș.a. - Damping and Seismic Isolation Bearings Group, in Modular Design, for Bridges and Viaducts. Contract PNII- Partnerships nr. 235/2014.

[2] Bratu P., Dima M. – Damping and Seismic Isolation Bearings Group, in Modular Design, for Bridges and Viaducts. Patent nr. 130978A0, BOPI nr. 3/2016.

[3] Brochures ALGA

[4] Brochures SOMMA.

[5] Brochures MAGEBA

[6] Brochures SKF.

[7] Brochures ACE.



# **SESSION A**

## **EARTH-MOVING AND TRANSPORTATION MACHINERY**





# Dynamic Analysis of Tower Crane Movement Mechanism

Evgeniy M. Kudryavtsev <sup>1\*</sup>

<sup>1</sup> Moscow State University of Civil Engineering, Russia

*It is offered the new approach to complex dynamic analysis of mechanical systems with use of a certain set of modern computer systems. This approach provides high level of dynamic analysis of mechanical systems, including and presentation of received results. It is especially important at the earliest design stages of mechanical systems.*

**Keywords: Mechanism, modeling, dynamic analysis, crane**

## 1. INTRODUCTION

Considers method of the dynamic analysis of mechanical systems on an example of modeling movement mechanism crane in system Mathcad.

This method includes several stages.

On the first stage creates the marked state graph of rotating bodies.

On the second stage creates mathematical model - differential equations system, describing functioning movement mechanism of crane. Such approach provides presentation of interaction of adjacent bodies of the mechanism and significantly facilitates creation of corresponding mathematical model for the dynamic analysis of the mechanism.

On the third stage defines mass-inertial characteristics of the basic rotating elements of the mechanism and reduced value (input data).

On the fourth stage creates the computer model for execution of the computer experiments in Mathcad systems. Next carries out modeling process.

## 2. CREATION OF MARKED STATE GRAPH

*The first stage.* The movement mechanism of the crane represents in the form of consistently connected bodies of rotation. It can be represented in a graphic kind by means of the marked graph (Figure 1).

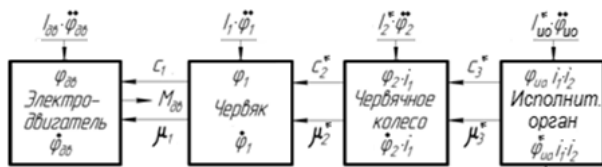


Figure 1: The marked state graph of rotating bodies movement mechanism of the crane

where are:

$M_{00}$  - the rotational moment of the engine;

$I_{00}$ ,  $I_1$ ,  $I_2^*$ ,  $I_{10}^*$  - moment of inertia of bodies: an engine rotor; a worm-shaft; a worm-wheel and an executive unit;

$c_1$ ,  $c_2^*$ ,  $c_3^*$  - coefficients of torsion rigidity bodies: the engine-worm; a worm-worm a wheel; a worm wheel-executive office;

$\mu_1$ ,  $\mu_2^*$ ,  $\mu_3^*$  - coefficients of dissipation bodies: the engine-worm shaft; a worm shaft-worm- wheel; a worm-wheel-executive unit;

$M_c^*$  - moment of resistance to movement and

$i_1$ ,  $i_2$  - gear-ratio of a worm reducer and open gear.

The rectangle of the count is driving (rotating or moving) a body of mechanical system. The arrows entering or leaving a rectangle, it is the operating moments for bodies of rotation and force for moving bodies. The arrows entering into a rectangle, define themselves jet, and the leaving active moments for bodies of rotation and corresponding forces for moving bodies.

On each body of rotation (moving) the jet moments (forces) can operate: the moments (forces) of inertia and the moments (forces) connected with диссипативными and elastic properties of a body.

The sizes connected with dissipative and elastic properties of a body, depend on properties of adjacent bodies with which the considered body cooperates.

## 3. MNEMONIC RULE FOR CREATION OF MATHEMATICAL MODEL

For creation of mathematical model - systems of the differential equations describing work of mechanical system, consisting of consistently connected bodies of rotation, the following mnemonic rule is offered:

- rotation of each  $i$ -th body of system is described by the differential equation of the second order;

- number of the differential equations of the second order to equally number of bodies of rotation of the mechanism;

- first member of the differential equation for each  $i$ -th body of rotation is equal  $I_i \cdot \ddot{\varphi}_i$ ;

- number of members in each  $i$ -th differential equation of system to equally number of the arrows entering or leaving the considered body of rotation, plus the first member;

- each member of the differential equation has the sign.

If the arrow is directed to an investigated body of system, the member undertakes with a sign plus if from a body with a sign a minus;

- the subsequent members of the differential equation are equal:

to multiply coefficient of rigidity adjacent body on a difference of turning angles of adjacent bodies  $c_j \cdot (\varphi_{j-1} - \varphi_j)$ ;

to multiply coefficient dissipation adjacent body on a difference of angular speeds of adjacent bodies  $\mu_j \cdot (\dot{\varphi}_{j-1} - \dot{\varphi}_j)$ ;

- it is necessary to consider gear-ratios also (see below).

#### 4. CREATION OF MATHEMATICAL MODEL

Using the marked state graph of rotating bodies of the mechanism and a mnemonic rule it is possible to write:

- first differential equation

$$I_{\partial\partial} \cdot \ddot{\varphi}_{\partial\partial} + c_1 \cdot (\varphi_{\partial\partial} - \varphi_1) + \mu_1 \cdot (\dot{\varphi}_{\partial\partial} - \dot{\varphi}_1) - M_{\partial\partial} = 0;$$

- second differential equation

$$I_1 \cdot \ddot{\varphi}_1 + c_2^* \cdot (\varphi_1 - \varphi_2 \cdot i_1) + \mu_2^* \cdot (\dot{\varphi}_1 - \dot{\varphi}_2 \cdot i_1) - c_1 \cdot (\varphi_{\partial\partial} - \varphi_1) - \mu_1 \cdot (\dot{\varphi}_{\partial\partial} - \dot{\varphi}_1) = 0.$$

The differential equations and for other bodies of rotation are similarly represented. Parameters with asterisks are the resulted parameters.

Final system of the differential equations describing work of the mechanism of movement of the crane will register so:

$$I_{\partial\partial} \cdot \ddot{\varphi}_{\partial\partial} + c_1 \cdot (\varphi_{\partial\partial} - \varphi_1) + \mu_1 \cdot (\dot{\varphi}_{\partial\partial} - \dot{\varphi}_1) - M_{\partial\partial} = 0;$$

$$I_1 \cdot \ddot{\varphi}_1 + c_2^* \cdot (\varphi_1 - \varphi_2 \cdot i_1) + \mu_2^* \cdot (\dot{\varphi}_1 - \dot{\varphi}_2 \cdot i_1) - c_1 \cdot (\varphi_{\partial\partial} - \varphi_1) - \mu_1 \cdot (\dot{\varphi}_{\partial\partial} - \dot{\varphi}_1) = 0;$$

$$I_2 \cdot \ddot{\varphi}_2 + c_3^* \cdot (\varphi_2 \cdot i_1 - \varphi_{\omega\omega} \cdot i_1 \cdot i_2) + \mu_3^* \cdot (\dot{\varphi}_2 \cdot i_1 - \dot{\varphi}_{\omega\omega} \cdot i_1 \cdot i_2) - c_2^* \cdot (\varphi_1 - \varphi_2 \cdot i_1) - \mu_2^* \cdot (\dot{\varphi}_1 - \dot{\varphi}_2 \cdot i_1) = 0;$$

$$I_{\omega\omega} \cdot \ddot{\varphi}_{\omega\omega} - c_3^* \cdot (\varphi_2 \cdot i_1 - \varphi_{\omega\omega} \cdot i_1 \cdot i_2) - \mu_3^* \cdot (\dot{\varphi}_2 \cdot i_1 - \dot{\varphi}_{\omega\omega} \cdot i_1 \cdot i_2) + \frac{M_c^*}{i_1 \cdot i_2} = 0.$$

This system of the differential equations describes work of elements of a drive at the appendix to a rotor of the engine of moment  $M_{\partial\partial}$ , and to executive (working) body of the moment resistance of movement  $M_c$ .

#### 5. CREATION OF COMPUTER MODEL

For the decision of system of the differential equations on the computer it is necessary to present it in the form of system of the differential equations of the first order:

$$d\varphi_{\partial\partial} / dt = \dot{\varphi}_{\partial\partial};$$

$$d\varphi_1 / dt = \dot{\varphi}_1;$$

$$d\varphi_2 / dt = \dot{\varphi}_2;$$

$$d\varphi_{\omega\omega} / dt = \dot{\varphi}_{\omega\omega};$$

$$\frac{d\dot{\varphi}_{\partial\partial}}{dt} = \frac{1}{I_{\partial\partial}} \cdot (M_{\partial\partial} - c_1 \cdot (\varphi_{\partial\partial} - \varphi_1) - \mu_1 \cdot (\dot{\varphi}_{\partial\partial} - \dot{\varphi}_1));$$

$$\frac{d\dot{\varphi}_1}{dt} = \frac{-1}{I_1} \cdot (c_2^* \cdot (\varphi_1 - \varphi_2 \cdot i_1) + \mu_2^* \cdot (\dot{\varphi}_1 - \dot{\varphi}_2 \cdot i_1) - c_1 \cdot (\varphi_{\partial\partial} - \varphi_1) - \mu_1 \cdot (\dot{\varphi}_{\partial\partial} - \dot{\varphi}_1));$$

$$\frac{d\dot{\varphi}_2}{dt} = \frac{-1}{I_2} \cdot (c_3^* \cdot (\varphi_2 \cdot i_1 - \varphi_{\omega\omega} \cdot i_1 \cdot i_2) + \mu_3^* \cdot (\dot{\varphi}_2 \cdot i_1 - \dot{\varphi}_{\omega\omega} \cdot i_1 \cdot i_2) - c_2^* \cdot (\varphi_1 - \varphi_2 \cdot i_1) - \mu_2^* \cdot (\dot{\varphi}_1 - \dot{\varphi}_2 \cdot i_1));$$

$$\frac{d\dot{\varphi}_{\omega\omega}}{dt} = \frac{-1}{I_{\omega\omega}} \cdot (c_3^* \cdot (\varphi_2 \cdot i_1 - \varphi_{\omega\omega} \cdot i_1 \cdot i_2) + \mu_3^* \cdot (\dot{\varphi}_2 \cdot i_1 - \dot{\varphi}_{\omega\omega} \cdot i_1 \cdot i_2) - \frac{M_c^*}{i_1 \cdot i_2}).$$

where are:

$I_{np}$  - the led moment of inertia to an engine shaft,  $\text{kgm}^2$  the mechanism of movement of the crane and the crane with the cargo, falling to one mechanism;

$I_{\partial\partial}$  - moment of inertia of a rotor of the engine with полумуфтой,  $\text{kgm}^2$ ;

$I_1$  - moment of inertia of an incorporated body the worm-shaft (half-coupling and a worm-shaft),  $\text{kgm}^2$ ;

$I_2$  - moment of inertia of an incorporated body the worm-wheel (a worm-wheel and a shaft a gear wheel),  $\text{kgm}^2$ ;

$\dot{\varphi}_{\partial\partial}$ ,  $\dot{\varphi}_1$ ,  $\dot{\varphi}_2$ ,  $\dot{\varphi}_{\omega\omega}$  - accordingly, angular speeds of bodies: engine, the worm-shaft, the worm-wheel, executive unit. (A running wheel),  $1/c$ ;

This system completely describes work of elements of a drive at the appendix to a rotor of the engine of the moment, and to a running wheel of the moment of resistance to movement  $M_c$ .

For simplification of the decision of the given system it is expedient to present it in the form of the system of the differential equations consisting not from four differential equations of the second order, and from eight differential equations of the first order.

#### 6. DETERMINATION OF INPUT DATA

Calculation of initial data includes calculation:

- the moments of inertia of all rotating elements of the mechanism of movement of the crane;

- factors rigidity of connections of adjacent elements of the mechanism;

- factors dissipation connections of adjacent elements of the mechanism.

In settlement dynamic schemes all real parameters of cars (the moments of inertia, weights, rigidity, external loadings, ...) are replaced with the resulted.

Reduction of the moving concentrated weights of bodies of the mechanism of movement of the crane we will make to a shaft of the engine on the basis of equality kinetic energy.

Kinetic energy at start-up of the mechanism of movement of the crane consisting of four rotating and one forward weights (the crane with cargo), resulted at an engine shaft, can be presented in such kind:

$$I_{np} \cdot \frac{\dot{\varphi}_{06}^2}{2} = I_{06} \cdot \frac{\dot{\varphi}_{06}^2}{2} + I_1 \cdot \frac{\dot{\varphi}_1^2}{2 \cdot \eta_1} + I_2 \cdot \frac{\dot{\varphi}_2^2}{2 \cdot \eta_1 \cdot \eta_2} + I_{uo} \cdot \frac{\dot{\varphi}_{uo}^2}{2 \cdot \eta_1 \cdot \eta_2 \cdot \eta_{uo}} + \frac{(m_{kp} + m_{cp})}{Z_M} \cdot \frac{v_{kp}^2}{2 \cdot \eta_1 \cdot \eta_2 \cdot \eta_{uo}},$$

where are:

$I_{uo}$  - moment of inertia of incorporated body (a cogwheel, a shaft and a running wheel),  $kgm^2$ ;

$\eta_1, \eta_2, \eta_{uo}$  - accordingly, coefficient of efficiency incorporated bodies: worm-shaft, worm-wheel, executive unit;

$m_{kr}$  - weight of the moved crane,  $kg$ ;

$m_{cp}$  - weight of moved cargo,  $kg$ ;

$V_{kp}$  - speed of movement of the crane,  $m/c$ ;

$Z_M$  - number of mechanisms of movement of the crane.

Having divided, the left and right parts of last expression on  $\dot{\varphi}_{06}^2$ , we will receive expression,  $kgm^2$ .

$$I_{np} = I_{06} + \frac{I_1}{\eta_1} + \frac{I_2}{i_1^2 \cdot \eta_1 \cdot \eta_2} + \frac{I_{uo}}{i_1^2 \cdot i_2^2 \cdot \eta_1 \cdot \eta_2 \cdot \eta_{uo}} + \frac{(m_{kp} + m_{cp})}{Z_M} \cdot \frac{(V_{kp} / \dot{\varphi}_{06})^2}{\eta_1 \cdot \eta_2 \cdot \eta_{uo}},$$

where are:  $i_1, i_2$  - accordingly gear-ratios of a worm reducer and an open tooth gearing.

But it is possible to present speed of movement of the crane in such kind

$$V_{kp} = \varphi_{xk} \cdot R_{xk} = \varphi_{06} \cdot R_{xk} / (i_1 \cdot i_2),$$

where is:  $R_{xk}$  - radius of a running wheel of the crane,  $m$ .

Definitively led moment of inertia to an engine shaft,  $kgm^2$  all moving bodies of one mechanism of movement of the crane and the crane with the cargo, falling to one mechanism, буде to look so

$$I_{np} = I_{06} + \frac{I_1}{\eta_1} + \frac{I_2}{i_1^2 \cdot \eta_1 \cdot \eta_2} + \frac{I_{uo}}{i_1^2 \cdot i_2^2 \cdot \eta_1 \cdot \eta_2 \cdot \eta_{uo}} + \frac{(m_{kp} + m_{cp})}{Z_M} \cdot \frac{R_{xk}^2}{i_1^2 \cdot i_2^2 \cdot \eta_1 \cdot \eta_2 \cdot \eta_{uo}},$$

### 7. CALCULATION OF THE MOMENTS OF INERTIA OF ROTATING BODIES AND THEIR RESULTED VALUES

The moments of inertia of rotating bodies can be defined calculation, using known formulas and drawings of corresponding details (knots), or, having created corresponding models of details (knots) in CAD in which they automatically pay off.

For example, the moment of inertia of a brake pulley can be defined, using the corresponding three-dimensional model constructed in system the KOMPAS 3D (Figure 2).

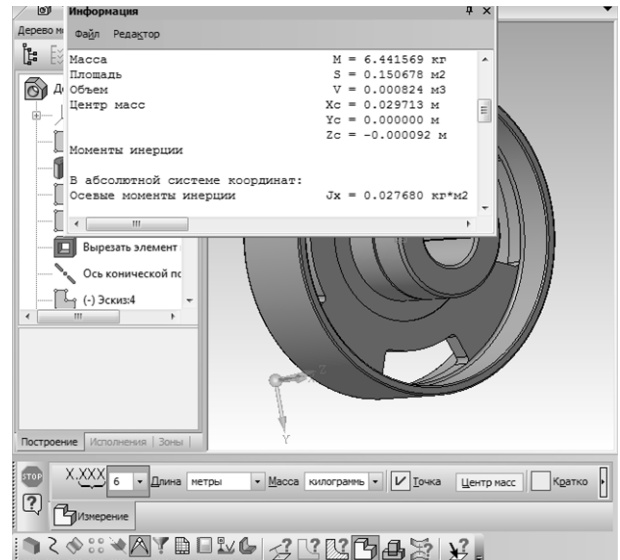


Figure 2: Result of definition of the moment of inertia of model the Brake pulley

The moment of inertia of a rotor of the engine is defined from engine technical characteristics.

$$I_{ром} = 0,065 \text{ kgm}^2.$$

The moment of inertia  $I_1$ ,  $kgm^2$  an incorporated body the worm (the cylindrical-shaft and the worm-shaft) it is possible to define and a settlement method with use of its sizes Figure. 3.

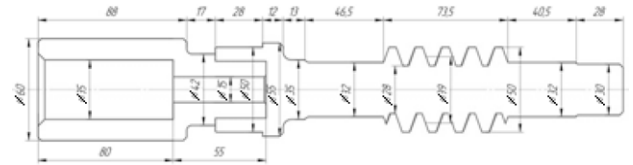


Figure 3: The sizes of an incorporated body the worm-shaft (the cylindrical shaft and the worm-shaft)

$$I_1 = \frac{\pi}{32} \cdot \rho \cdot \sum_{j=1}^{n1} (l_j \cdot d_j^4) = \frac{3,14}{32} \cdot 7826 \cdot (0,088 \cdot 0,06^4 - 0,08 \cdot 0,035^4 - 0,055 \cdot 0,015^4 + 0,017 \cdot 0,042^4 + 0,028 \cdot 0,05^4 + 0,012 \cdot 0,055^4 + 0,013 \cdot 0,035^4 + 0,0465 \cdot 0,032^4 + 0,0735 \cdot 0,039^4 + 0,0405 \cdot 0,032^4 + 0,028 \cdot 0,03^4) = 1,274 \cdot 10^{-3},$$

where are:

$\rho$  - material density of which the body is made,  $kg/m^3$ ;

$n_1$  - Number of steps on an incorporated body the worm-shaft;

$l_{ij}$  - Length  $j$  - oh steps of an incorporated body the worm-shaft,  $m$ ;

$d_{ij}$  - Diameter  $j$  - oh steps of an incorporated body the worm-shaft,  $m$ .

The moments of inertia and their resulted values under known formulas and for other bodies are similarly defined. Further factors of rigidity and disipation for each body under known formulas and their resulted values, and also parameters of the mechanical characteristic of the electric motor are defined.

### 8. CALCULATION OF PARAMETERS OF THE MECHANICAL CHARACTERISTIC IN SYSTEM MATHCAD

The dynamic analysis of the crane movement mechanism in system Mathcad.

**Initial data:**

- moment inertia of a join body an engine rotor, kgm<sup>2</sup>: I<sub>en</sub>= 0.093
- reduced moment of inertia of a join body the Worm, kgm<sup>2</sup>: I<sub>re</sub>= 0.001722
- reduced moment of inertia of a join body the: Worm heel, kgm<sup>2</sup>: I<sub>2re</sub>= 0.000167
- reduced moment of inertia of a join body the Execution unit, kgm<sup>2</sup>, I<sub>3re</sub>= 0.202
- rigidity coefficient of connections of a join body the Worm, Nm/radian: c<sub>1</sub> = 7754
- rigidity coefficient of connections of a join body the Worm heel, Nm/radian: c<sub>2</sub>= 4215
- rigidity coeff. of connections of a join body the Execution unit, Nm/radian:c<sub>3</sub>= 7122
- rigidity dissipation of connections of a join body the Worm, Nms/radian: p<sub>1</sub> = 0.731
- rigidity dissipation of connections of a join body the Worm heel, Nms/radian:p<sub>2</sub>= 0.336
- rigidity dissipation of con. of a join body the Execution unit, Nms/radian: p<sub>3</sub>= 1.373
- resulted moment of resistance of a crane movement mechanism, kgm<sup>2</sup>: M<sub>r</sub>= 103.161
- gear-ratio of the reductor: i<sub>1</sub> = 39
- gear-ratio of the open gear: i<sub>2</sub>= 2.52
- size of critical sliding S<sub>c</sub>= 0.551
- maximum (critical) moment of the engine in a static mode, Nm: M<sub>c</sub> = 165.066
- nominal moment of the engine, Nm: M<sub>n</sub>= 52.469
- angular velocity of rotation of the engine rotor, 1/s: r<sub>on</sub>= 95.295
- acceleration of gravity, m/s<sup>2</sup>: g= 9.81

**Required parameters:**

- angle of turn and angular velocity of the engine rotor with brake pulley: X<sub>0</sub>, X<sub>4</sub>
- angle of turn and angular velocity of the Worm: X<sub>1</sub>, X<sub>5</sub>
- angle of turn and angular velocity of the Worm heel: X<sub>2</sub>, X<sub>6</sub>
- angle of turn and angular velocity of the Execution unit (the running wheel): X<sub>3</sub>, X<sub>7</sub>

**Algorithm of calculation:**

1. Reduction of dimensions
 
$$I_{en}=I_{en} \cdot g$$

$$I_{1re}=I_{1r} \cdot e \cdot g$$

$$I_{2re}=I_{2r} \cdot g$$

$$I_{3r}e= I_{3re} \cdot g$$
2. Representation and the decision of system of the differential equations:
  - a vector-column of initial values required parameters
 
$$x := (0 \ 0 \ 0 \ 0 \ 0 \ 0 \ 0 \ 0)^T$$
  - a vector-column of the right part of system of the differential equations

$$D(t,x) := \begin{bmatrix} x_4 \\ x_5 \\ x_6 \\ x_7 \\ \frac{1}{I_{en}} \left[ \frac{2 \cdot M_c}{1 - \frac{x_4}{\omega t} + \frac{S_c}{Sc}} - \mu l \cdot (x_4 - x_5) - c l \cdot (x_0 - x_1) \right] \\ \frac{\mu l \cdot (x_4 - x_5) + c l \cdot (x_0 - x_1) - \mu_2 \cdot (x_5 - x_6 \cdot i l) - c_2 \cdot (x_1 - x_2 \cdot i l)}{I_{1re}} \\ \frac{\mu_2 \cdot (x_5 - x_6 \cdot i l) + c_2 \cdot (x_1 - x_2 \cdot i l) - \mu_3 \cdot (x_6 \cdot i l - x_7 \cdot i l \cdot i_2) - c_3 \cdot (x_2 \cdot i l - x_3 \cdot i l \cdot i_2)}{I_{2re}} \\ \frac{1}{I_{3re}} \left[ \mu_3 \cdot (x_6 \cdot i l - x_7 \cdot i l \cdot i_2) + c_3 \cdot (x_2 \cdot i l - x_3 \cdot i l \cdot i_2) - \frac{M_r}{i l \cdot i_2} \right] \end{bmatrix}$$

- modelling parameters:
- Initial time of modelling, s:t<sub>0</sub>= 0
- Final time of modelling, s:t= 2
- Number of steps of integration:N= 100

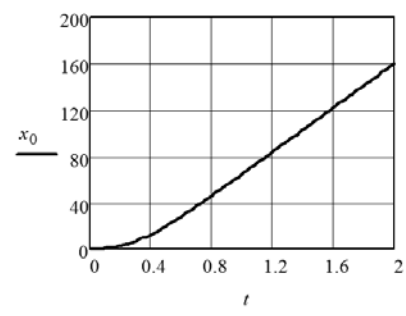
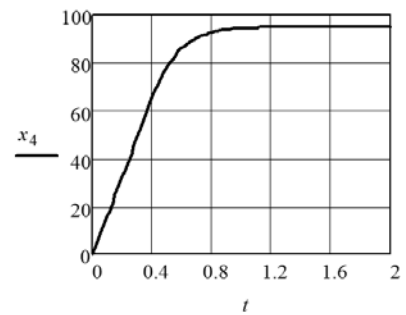
- decision of system of the differential equations by means of built in function Rkadapt (x, t<sub>0</sub>, t<sub>1</sub>,N,D)
- method Runge-Kutta with adaptive step. Z= Rkadapt (x, t<sub>0</sub>, t<sub>1</sub>,N,D)
- results of definition of required parameters:
 
$$t := Z^{(0)} \quad x_0 := Z^{(1)} \quad x_1 := Z^{(2)}$$

$$x_2 := Z^{(3)} \quad x_3 := Z^{(4)} \quad x_4 := Z^{(5)}$$

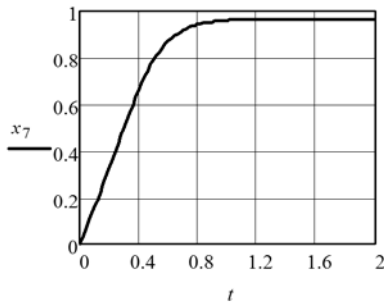
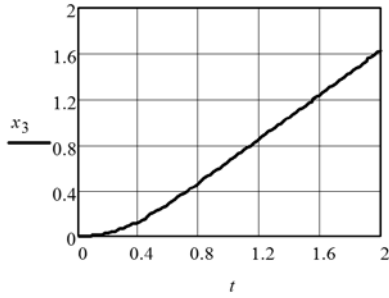
$$x_5 := Z^{(6)} \quad x_6 := Z^{(7)} \quad x_7 := Z^{(8)}$$

**3. Graphic representation of required parameters depending on time - t:**

- angular movings of bodies: an engine rotor (x<sub>0</sub>) and the running wheel (x<sub>3</sub>)



- angular speeds of bodies: an engine rotor ( $x_4$ ) and the running wheel ( $x_7$ ):



4. Comparison of results of calculation and simulation:

- settlement tabular values of angular speed of rotation of a rotor of the engine depending on time by results of modelling, radian/s

$x_4^T$	0	1	2	3	4	5	6	7
=	0	2.939	5.929	8.967	12.058	15.198	18.39	

- an error of modelling of angular speed of rotation of a rotor of the engine -  $\delta \omega n$ , %

$$(x_4)_N = 95.127 \quad \delta \omega n := \left| \frac{\omega n - (x_4)_N}{\omega n} \right| \cdot 100$$

$$\delta \omega n = 0.176$$

- settlement nominal angular speed of rotation of a running wheel, radian/s

$$\omega h := \frac{\omega n}{i1 \cdot i2} = 0.97$$

- settlement tabular values of angular speed of rotation of a running wheel depending on time by results of modelling, radian/s

$x_7^T$	0	1	2	3	4	5	6	7	8
=	0	0	0.031	0.062	0.093	0.125	0.157	0.19	0.223

- an error of modelling of angular speed of rotation of a running wheel. %

$$(x_7)_N = 0.968 \quad \delta \omega h := \left| \frac{\omega h - (x_7)_N}{\omega h} \right| \cdot 100$$

$$\delta \omega h = 0.176$$

5. The dynamic moment and factor of dynamism in the course of engine start-up:

- moment of inertia of weights of the crane movement mechanism, led to an engine shaft

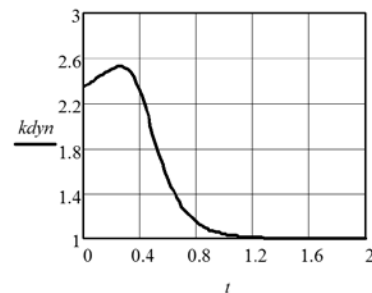
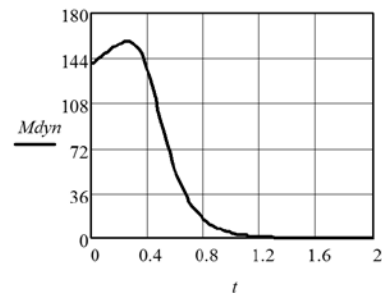
$$I_{re} = I_{en} + I_{ire} + I_{2re} + I_{3re} \quad I_{re} = 2.912$$

- angular acceleration of the engine rotor

$$a_{en} := \frac{1}{I_{re}} \left[ \frac{2 \cdot Mc}{1 - \frac{x_4}{\omega n}} - \mu l (x_4 - x_5) - c l \cdot (x_0 - x_1) \right] \cdot \frac{Sc}{1 - \frac{x_4}{\omega n}}$$

- dynamic moment, Nm and dynamism factor on an engine shaft under which action there is a dispersal of the crane movement mechanism

$$M_{dyn} = a_{en} \cdot I_{re} \quad k_{dyn} := \frac{M_{dyn} + Mr}{Mr}$$



- maximum dynamic moment, Nm and dynamism factor on an engine shaft

$$M_{dyni\ddot{a}o} = \max(M_{dyn}) \quad M_{dyni\ddot{a}o} = 157.556$$

$$k_{dynmax} = \max(k_{dyn}) \quad k_{dynmax} = 2.527$$

- condition check: the dynamic moment on a shaft of the engine in the course of dispersal should be less than the critical moment of the engine, Nm

$$M_{dyni\ddot{a}o} = 157.556 \text{ less } Mc = 165.066$$

The condition is carried out.

## 9. CONCLUSION

The proposed procedure of calculation of the dynamic analysis of work of mechanical drives using Mathcad software enables to decrease by an order of magnitude the time of labour inputs of such calculation, as well as pursue investigations related to changing parameters of attachment components.

## REFERENCES

- [1]. E.M. Kudryavtsev, M.A.Stepanov," Building cranes. A part 1. Tower cranes. Bases of the theory, a design and calculation": The Manual for high schools. - M: Publishing house ASV/ (Russia), (2016).
- [2]. E.M. Kudryavtsev, "Building cars and the equipment" (with examples of calculations, including and on the computer): The Textbook. – M: Publishing house ASV. (Russia), (2012).
- [3]. E.M. Kudryavtsev, V.V.Stepanov," Execution of final qualifying work on the computer": the Manual for high schools. - M: The Publ. House "BASTET". (Russia), (2013).
- [4]. E.M. Kudryavtsev, "CAD systems of the machine and the equipment". The Textbook for high schools. M: Publishing house ASV. (Russia), (2013).
- [5]. E.M. Kudryavtsev, "The basis of the automated designing":The textbook for high schools. M: Publishing centre "Academy". (Russia), (2011).
- [6]. E.M. Kudryavtsev," KOMPAS-3D V10. As much as possible full management". In 2 volumes. M: DMK Press. (Russia), (2008).
- [7]. E.M. Kudryavtsev, "Modeling, design and calculation of mechanical systems". M: DMK Press, 2008. - p. 400.
- [8]. E.M. Kudryavtsev, "Practical work on KOMPAS-3D V8: Machine-building libraries". M.: DMK Press. (Russia), (2007).
- [9]. E.M. Kudryavtsev, "Machine-building designing Mechanical Desktop". M.: DMK Press. (Russia), (2006).

# The Definition of Basic Parameters of the Set of Small-Sized Equipment for Preparation of Dry Mortar for Various Applications

I.A. Emelyanova<sup>1\*</sup>, V. Blazhko<sup>1</sup>, S. I. Karpenko<sup>1</sup>

<sup>1</sup> Kharkiv National University of Civil Engineering and Architecture

Department of Mechanization of Construction Processes, Kharkiv National University of Civil Engineering and Architecture, Kharkiv (Ukraine)

*Based on the conducted information retrieval and review of the scientific literature, unsolved issues have been identified in the process of preparation of dry construction mixtures in the conditions of a construction site.*

*The constructions of existing technological complexes for the production of dry construction mixtures are considered and their main drawbacks are identified in terms of application in the conditions of the construction site.*

*On the basis of the conducted research, the designs of technological sets of small-sized equipment for the preparation of dry construction mixtures in the construction site are proposed. It is found out that the basis for creating the proposed technological kits are new designs of concrete mixers operating in cascade mode.*

*A technique for calculating the main parameters of technological sets of equipment is proposed, depending on the use of the base machine of the kit.*

**Keywords:** Set of small-sized equipment, A dry construction mix, A concrete mixer, A cascade regime, The motion trajectory of the mixture particles.

## 1. INTRODUCTION

Modern dry building mixtures are complex compositions of components, different in their properties. Mixing these components together and creating a homogeneous mixture is a difficult task in a technical sense. Creation of effective equipment for these purposes is an urgent problem of modern construction. With its solution, special attention should be paid to the development of technological kits.

At present, in the process of preparation of dry construction mixtures, there is a number of unresolved issues: increased wear of the working bodies and mixer bodies, long time for the preparation of complex compositions, the presence of segregation during the mixture preparation and the complexity of preparing the mixtures directly at the construction site [1 - 4].

At present, technological complexes, which have the ability to produce mixtures of different types, are used for the preparation of dry construction mixtures [5 - 7].

The complexes are equipped with high-quality dosing devices and forced-action mixers with one or two shafts, on which various stirring devices are fixed [3, 9]. However, modern concrete mixers do not always allow to produce homogeneous mixtures with a small filling factor of the working volume of the machine. In addition, existing mixers do not allow to create a single organized work cycle in one place. From these positions, technological kits that allow to combine all operations in time are more attractive.

In addition, the variety of existing equipment, as well as technological lines and kits, is not aimed at solving the problem of making dry construction mixtures directly on the construction site.

Creation of effective small-sized equipment for the preparation of dry mixtures is an urgent task.

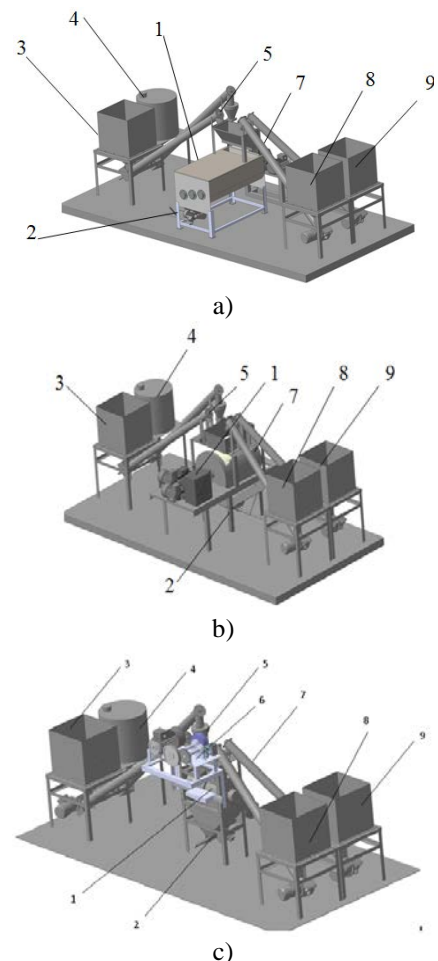


Figure 1: Technological sets of equipment for the preparation of dry building mixtures:  
 A) the base machine is a three-shaft mixer; B) the basic machine is a mixer of gravitational-forced action; C) basic machine - two-rotor turbulent mixer

The results of laboratory and industrial tests of new design mixers operating in a cascade mode, confirm their effectiveness in the preparation of dry building mixtures, which makes it possible to equip these machines with technological kits and complexes [8].

Main material and results. It is proposed to develop and introduce small-size sets of equipment for the preparation of dry construction mixtures on the basis of new mixers operating in a cascade mode in the production of small amounts of work (with individual low-rise construction, construction in the agricultural sector, repair and reconstruction of existing buildings). Technological equipment kits are shown in Figure 1. All equipment of these technological kits is based on a common base and is selected according to the performance of the base machine-mixer.

The technological set of equipment, presented in Figure 1, includes the following components: 1 - mixer (basic machine); 2 - filling machine 3 - sand bunker; 4 - silo of cement; 5 - weighing batcher; 6 - fiber cutter; 7 - auger feeder; 8 - bunker of granite grains; 9 - filler hopper

The basic machines of the technological set (Fig. 1) can be concrete mixers of a new constructive solution: a three-shaft concrete mixer, gravity-forced concrete mixer, a two-side turbulent mixer [5]. A feature of the work of these machines is the creation of a complex multi-path motion of the particles of the mixture in the body of the machine [9]. The adjacent equipment of the technological set is unified and has a traditional design solution.

The productivity of a technological equipment set is determined on the basis of the technical performance of the base machine used in the composition of the technological set. The productivity of the technological set with the use of a three-shaft concrete mixer is found according to the dependence [10]

$$\Pi_{mex} = 3600 \cdot \frac{\pi}{4} \cdot (D^2 - d^2) \cdot b \cdot n \cdot z_n \cdot \sin \alpha \cdot \kappa_s^{cp} \cdot \kappa_e^{II} \quad (1)$$

where are:

$D$  - is the diameter of the shaft along the end of the blade, m;

$d$  - is the diameter of the average shaft, m;

$b$  - blade width, m;

$z_n$  - number of blades of the middle shaft;

$\alpha$  - is the angle of installation of the blades, deg;

$K_{зсп}$  - load factor of the mixer relative to the average shaft,  $K_{зсп} = 0,75$ ;

$n$  - frequency of rotation of the shaft of the working element;

$\kappa_e^{II}$  - coefficient of return of the concrete mixture of the second zone.

Determination of the technical productivity of the equipment set, which includes a concrete mixer of gravitational-forced action, is defined as

$$\Pi_{mex} = V_{обм} \cdot Z_{II} = \frac{1}{2} [\pi \cdot L_k (R_k^2 \cdot k - r_0^2) - \pi \cdot r_n^2 \cdot l_n \cdot z_n - z_1 \cdot b_1 \cdot h_1 \cdot c_1 - z_2 \cdot b_2 \cdot h_2 \cdot c_2] \cdot Z_{II} \quad (2)$$

where are:

$V_{обм}$  - is the total volume of the mixture in the mixer, m<sup>3</sup>;

$Z_{II} = 3600/t_{II}$  - number of cycles of machine operation per hour ( $t_{II}$  - is the duration of one cycle, which consists of the sum of time for loading components  $t_1$ ,

mixing them  $t_2$  and unloading the finished mixture  $t_3$  ( $t_{II} = t_1 + t_2 + t_3$ ), c);

$L_k$  - length of the mixer body, m;

$R_k$  - is the radius of the mixer body, m;

$k$  - is a coefficient that takes into account the position of the mixture in the body;

$R_n, l_n, z_n, r_0$  - radius, length, number of legs of shaft blades and shaft radius, m;

$b_1, b_2, h_1, h_2, c_1, c_2$  - length, height and thickness of blades of the body and blades of the mixer shaft, m.

The productivity of the technological set when using a two-rotor turbulent mixer is found according to the dependence

$$\Pi_{mex} = V_{обм} \cdot Z_{II} \cdot k_M, \quad (3)$$

where are:

$V_{обм}$  - the total volume of the mixture in the mixer, m<sup>3</sup>;

$Z_{II} = 3600/t_{II}$  - number of cycles of machine operation per hour ( $t_{II}$  is the duration of one cycle, which consists of the sum of the time for loading components  $t_1$ , mixing them  $t_2$  and unloading the finished mixture  $t_3$  ( $t_{II} = t_1 + t_2 + t_3$ ), c);

$k_M$  is the machine utilization factor (0.85).

In this case, the feeding of the components of the concrete mixture into the mixer will be as follows:

$$M = \int_0^t (Q_{вх} - Q_{вых}) dt \quad (4)$$

where are:

$M$  - total mass of components;

$t$  - the time interval for loading all components;

$Q_{вх}$  - the flow of the components of the mixture upon leaving the storage bin;

$Q_{вых}$  - the flow of the components of the mixture as it leaves the feeder.

The ratio of the total mass of  $M$  components to the entire working volume of mixer  $V$  is as follows where:  $M$  - is the total mass of the components;  $t$  - is the time interval for loading all components;  $Q_{вх}$  - the flow of the components of the mixture as it exits the storage hopper;  $Q_{вых}$  - the flow of the components of the mixture when leaving the feeder.

The ratio of the total mass of  $M$  components to the entire working volume of mixer  $V$  is as follows:

$$\frac{M}{V} = \Delta x = \frac{Q}{V} \int_0^t (x_{вх} - x_{вых}) dt, \quad (5)$$

where are:  $x_{вых}$ ,  $x$  - respectively, the content of the components at the inlet, outlet and inside the mixer and  $Q$  - the capacity of the mixer under steady operating conditions.

Among the main performance indicators of a small-sized technological set of equipment for the preparation of a building mixture, it is worth mentioning the power costs. The power costs for the operation of a technological equipment set intended for the preparation of fiber-concrete mixtures consist of the sum of the power costs of the individual types of equipment that are included in the kit (Figure 1, c): the machine-tool of the fiber, the base machine (concrete mixer), feeders and dispensers.



Thus, the dependence for determining the power of the technological set of equipment has the form [7]

$$N_{TKO} = N_{\sigma.m} + N_p + N_{II} + N_o, \quad (6)$$

where are:

$N_{TKO}$  – Total costs of power for the operation of the technological set of equipment, kW;

$N_{\sigma.m}$  – power costs of the base machine, kW;

$N_p$  – power consumption of a fiber cutter, kW;

$N_{II}$  – power consumption of feeders, kW;

$N_o$  – power consumption of dispensers, kW.

Taking into account the design features of the base machine of the three-shaft concrete mixer (Figure 1), when working on dry building mixtures,  $N_{TKO}$  should be defined as for a three-shaft mixer  $N_{\sigma.m}$ , taking into account the operation of the machine on dry building mixtures

$$N_{\sigma.m} = \frac{N_1 + N_2 + N_3}{1000 \cdot \eta}, \quad (7)$$

where are:

$N_1$  – the power used to mix the components of the mixture with the upper shaft;

$N_2$  – the power used to mix the components of the concrete mix and transport it to the discharge port by the middle shaft;

$N_3$  – the power used to mix the components of the mixture by the lower shaft;

$\eta$  – the efficiency of the mixer drive.

$$N_1 = N_1' + N_1'', \quad (8)$$

where are:

$N_1'$  – the power expended on the mixing process in the first zone,

$N_1''$  – power costs for the mixing process in the second zone

$$N_1' = \omega \cdot F_n \cdot C_1 \cdot f \cdot (R^2 - r^2) \cdot Z_n^1 \cdot \kappa_3^e \cdot \rho_1, \quad (9)$$

where are:

$\omega$  – angular velocity of the shaft,  $s^{-1}$ ;

$F_n$  – Blade area,  $m^2$ ;

$C_1$  – coefficient of resistance to movement of particles of dry concrete mixture along the blades in the first zone,  $C_1 = 9$ ;

$f$  – coefficient of friction of the dry mixture over the surface of the blades,  $f = 0,4$ ;

$R$  – outer radius of rotation of the blade, m;

$r$  – internal radius of rotation of the blade, m;

$Z_n^1$  – number of blades on the upper shaft in the first zone;

$\kappa_{3\sigma}$  – load factor of the concrete mixer relative to the upper shaft;

$\rho_1$  – average density of dry mix,  $kg / m^3$ .

$$N_1'' = \omega \cdot F_n \cdot C_2 \cdot f' \cdot (R^2 - r^2) \cdot Z_n^{II} \cdot \kappa_3^e \cdot \rho_2, \quad (10)$$

where are:

$C_2$  – Coefficient of resistance to movement of particles of the dry mixture along the blades in the second zone,  $C_2 = 7$ ;

$f'$  – coefficient of friction of the mixture along the blade surface,  $f' = 0,1..0,2$ ;

$Z_n^{II}$  – number of blades on the upper shaft in the first zone.

After the transformations, the dependence for determining the power costs by the upper shaft of the mixer has the form

$$N_1 = \left[ (\omega \cdot F_n \cdot \rho \cdot (R^2 - r^2) \cdot \kappa_3) \right] \cdot C_1 \cdot f \cdot Z_n + C_2 \cdot f' \cdot Z_n' \quad (11)$$

The power expended on mixing the components of a concrete mix and its transportation to the discharge port by an average shaft

$$N_3 = N_2' + N_2'', \quad (12)$$

where are:  $N_2'$  – the power expended on the process of mixing the components of the dry construction mixture in the first zone on the process of mixing the components of the mixture and transporting it to the second zone;  $N_2''$  – power expended in the second zone of the mixer.

$$N_2' = m_c \cdot g \cdot W \cdot \omega \cdot R_w, \quad (13)$$

where are:  $m_c$  – mass of the components of the mixture in the auger zone, kg;  $W$  – Drag coefficient (when the body moves in hostile environments  $W = 4$ );  $\omega$  – Angular speed of rotation of the shaft, s;  $R_w$  – Radius of screw, m; and  $g$  – acceleration of gravity

$$N_2'' = \omega \cdot F_n \cdot C_2 \cdot f' \cdot (R^2 - r^2) \cdot Z_n^{II} \cdot \kappa_3^{ep} \cdot \rho_2, \quad (14)$$

where is:

$Z_n^{II}$  – number of blades on the middle shaft in the second zone.

The power required to mix the components of the mixture with the lower shaft

$$N_3 = N_3' + N_3'', \quad (15)$$

where are:

$N_3'$  – power expended on the process of mixing in the first zone;

$N_3''$  – the power expended on the mixing process in the second zone of the mixer;

$N_3'$  и  $N_3''$  – are determined by analogy with the upper shaft.

For a gravity-forced-action mixer [5]  $N_{\sigma.m}$ , spent on the process of preparing a dry construction mix, consists of the power required to rotate the mixer body and the power required to rotate the blade shaft

$$N_{\sigma.m} = N_K + N_B, \quad \kappa B m,$$

where is:  $N_K$  - power required to rotate the body of the mixer,

$$N_K = N_K^{(1)} + N_K^{(2)} = \frac{0,85 \cdot G_{cm} \cdot h \cdot Z \cdot \omega_{\kappa}}{\eta_{\kappa} \cdot 1000} + \frac{F_{mp,\kappa} \cdot V_{\sigma\sigma\kappa} \cdot z_1}{\eta_{\kappa} \cdot 1000}, \quad (16)$$

where are:

$G_{cm}$  – weight of the components of the mixture, H;

$h$  – vertical coordinate of mass mixture displacement in the body, m;

$Z$  – number of mixes circulating in the body of the machine;

$\omega_{\kappa}$  – angular speed of rotation of the mixer body,  $s^{-1}$ ;

$\eta_{\kappa}$  – efficiency of the housing drive;

$F_{mp,\kappa}$  – the frictional force arising when the particles of the mixture move along the surface of the blade of the mixer body, H;

$V_{\sigma\sigma\kappa}$  – absolute velocity of the mixture particles along the body blades, m / s .;

$z_2$  – number of blades on the inner surface of the body.

The power required to operate the paddle shaft during mixing of the components of the mixture,

$$N_B = N_B^{(1)} + N_B^{(2)} = \frac{\omega_B \cdot M_B}{\eta_B \cdot 1000} + \frac{F_{mp.B} \cdot V_{abs.B} \cdot z_2}{1000 \cdot \eta_B} \quad (17)$$

where are:  $\omega_B$  – angular speed of rotation of the mixer's blade shaft,  $s^{-1}$ ;  $M_B$  – torque of the blade shaft, H·m;  $\eta_B$  – efficiency of shaft drive;  $F_{mp.B}$  – the friction force that occurs when a particle of a concrete mix moves along the blade surface, H;  $V_{abs.B}$  – absolute velocity of the mixture particle along the shaft blade, m / s;  $z_2$  – number of blades on the shaft.

When installing a two-rotor turbulent mixer

$$N_{б.м} = \omega_{p.o} \cdot F_n \cdot q_{cm} \cdot f \cdot (R - r) \cdot \cos \beta \cdot Z_n \cdot \kappa_3 \cdot \rho_1, \quad (18)$$

where are:

$\omega_{p.o}$  – angular speed of rotation of the mixer's blade shaft,  $s^{-1}$ ;

$F_n$  – the area of the blade,  $m^2$ ;

$q_{cm}$  – pressure on the blade on the mixture side, Pa;

$f = 0,4$ ;

$R$  – outer radius of blade rotation, m;

$r$  – internal radius of blade rotation, m;

$Z_n$  – number of blades on the upper shaft in the first

zone;

$\kappa_3$  – load factor of the concrete mixer;

$\rho_1$  – average density of dry mix,  $kg / m^3$ ;

$\beta$  – blade angle.

Thus, the proposed technological kits of small-sized equipment can be successfully used to work directly on the construction site.

## 2. CONCLUSIONS

1. Technological sets of small-sized equipment of a new configuration and a new design solution are proposed to perform small volumes of work in the conditions of a construction site.

2. Dependencies are given allowing to determine the performance indicators of new technological equipment sets for the preparation of dry building mixtures in the construction site.

## REFERENCES

- [1] Емельянова И. А. Новый принцип создания бетоносмесителей принудительного действия работы / И. А. Емельянова, А. Н. Баранов, В. В. Блажко // Труды Международной научно-технической конференции «Интерстроймех-2005». – Тюмень, 2005. – Ч. 1. – С. 38 – 43.
- [2] Емельянова И. А. Особенности рабочего процесса принудительно-гравитационного

бетоносмесителя / И. А. Емельянова, В. В. Блажко, А. И. Анищенко // Науковий вісник будівництва. – Х. : ХДТУБА, ХОТВ АБУ, 2009. – Вип. 52. – С. 317 – 325.

- [3] Kudrolli A. Saze separation in vibrated granular matter / A. Kudrolli // Reports on progress in physics-2004. – Т.67(3). – С. 209 – 247.
- [4] Campbell C. S. Rapid granular flows / C. S. Campbell // Annual Revue of Fluid Mechanics. – 1990. – Т. 22. – Р. 57 – 92.
- [5] Особенности работы бетоносмесителей в каскадном режиме / И. А. Емельянова, В. В. Блажко, О. В. Доброходова, А. И. Анищенко // Материалы Международной научно-технической конференции «Интерстроймех-2009». – Бишкек, 2009. – С. 398 – 403.
- [6] Analysis of the operation of concrete mixer with gravitational and forced action / И. А. Емельянова, В. В. Блажко, А. И. Анищенко, О. В. Доброходова // Proceedings «HEAVY MACHINERY – HV 2011»: The seventh international triennial conference. – Kraljevo, Serbia, 2011. – Session B: S. 11 – 14.
- [7] General classification for small-sized technological sets for production of dry building mixtures / И. А. Емельянова, В. В. Блажко, А. И. Анищенко, О. В. Доброходова // Proceedings «HEAVY MACHINERY – HV 2014»: The seventh international triennial conference. – Kraljevo, Serbia, 2014. – Session B: S. 35 – 38.
- [8] Бетоносмесители, работающие в каскадном режиме: монография / И. А. Емельянова, А. И. Анищенко, С. М. Евель и др. – Х. : Тим Паблиш Груп, 2012. – 146 с.
- [9] Емельянова И. А. Определение рациональных режимов работы бетоносмесителя гравитационно-принудительного действия / И. А. Емельянова, А. И. Анищенко, Ф. А. Стоянов // Новые материалы и технологии в машиностроении: сборник научных трудов по итогам Международной научно-технической конференции. – Брянск: БГИТА, 2012. – Вып. 16. – С. 137 – 140.
- [10] Новые технологические комплекты оборудования для работы в условиях строительной площадки на фибробетонных смесях / И. А. Емельянова, В. В. Блажко, А. С. Непорожнев, В. Ю. Шевченко // Новые материалы и технологии в машиностроении: сборник научных трудов по итогам Международной научно-технической конференции. – Брянск: БГИТА, 2011. – Вып. 13. – С. 155 – 157.

# Shapeless Manufacture of Reinforced Concrete Cylindrical and Spherical Shells with the Help of New Generation Hydraulic Equipment

I. Emelyanova<sup>1\*</sup>, A. Anishchenko<sup>1</sup>, S. Guzenko<sup>1</sup>, D. Chaika<sup>1</sup>

<sup>1</sup> Department of Mechanization of Construction Processes, Kharkiv National University of Construction and Architecture, Kharkiv (Ukraine)

*For the manufacture of reinforced concrete shells, it is proposed to use a self-supporting skeleton consisting of a spatial curvilinear reinforcement skeleton and non-removable liners of hollow-core, made of polystyrene or mineral wool, which serve as a permanent formwork.*

*Schematic diagrams of a non-piston universal concrete pump and a truck mixer of gravitational-forced action with hydraulic control are presented. Technological schemes of work are given. The obtained dependences for the determination of the range and height of the concrete mixture supply by the hoseless piston-type concrete pumps are provided.*

**Keywords:** Reinforced concrete shell, Universal hose concrete pump, Three-shaft concrete mixer, Truck mixer, Wet shotcrete, Shotcrete nozzle

## 1. INTRODUCTION

As the experience of reusable use has shown at construction sites of different purposes, technological sets of small-sized universal equipment that include new machines patented in Ukraine operate effectively. These are, first of all, mortar-concrete pumps of various design solutions, concrete mixers operating in a cascade mode and shotcrete nozzles with annular nozzles [1, 2].

It is of interest to use such kits for formless concreting directly on the construction site. For the manufacture of reinforced concrete shells, it is proposed to use a self-supporting skeleton, including a spatial curvilinear reinforcing skeleton and non-extractable liner-void-formers made of polystyrene or mineral wool (inner non-removable formwork) that form the predetermined geometry of the structure and are a screen for spraying on both sides of the wet concrete spraying of concrete mixture with synthetic fibers [3]. Due to the use of the spatial design of the reinforcing cage, consisting of the outer shells and the system of flat ribs connecting them, the necessary stiffness and load-carrying capacity of the frame for applying the shotcrete-concrete coating is provided.

Manufacture of reinforced concrete shells (Figure 1) was performed in the landfill conditions using the following equipment set: mobile compressor unit → two-piston mortar pump with poppet valves → gravity concrete mixer → shot-nozzle with ring nozzle → rubber hoses  $d_1 = 50$  mm and  $d_2 = 32$  mm. Hose in diameter 32 mm was used to feed additional compressed air flow in the annular nozzle of gunning nozzle. Shells are made with the mobility of the mixture  $P = 6 \dots 8$  cm and the following consumption of constituents per 1 m<sup>3</sup> of concrete of class C30 ... C35: cement PC 500 – 300 t, crushed stone fraction

5 ... 10 mm – 250 kg, crushed stone fraction 2 ... 5 mm – 875 kg, sand – 875 kg, water – 150 kg, supplement "Adminol-Rapid" – 3 kg, basalt fiber with the length of the elements  $l_f = 12$  mm (F% – 0.1).

Concreting by the wet shotcrete was carried out with the following technological parameters: working pressure  $p = 0,6$  MPa, compressed air consumption for supply of concrete mix with a nozzle  $q_1 = 7$  m<sup>3</sup>/min, additional supply of compressed air through the ring nozzle  $q_2 = 2$  m<sup>3</sup>/min, spraying speed of fiber-reinforced concrete mixture on the shotcrete surface of the shell  $V_{abr} = 55 \dots 60$  m/s.

Subsequent tests showed that reinforced concrete casings of lightweight construction, whose weight is 40 ... 50 % less compared to solid structures, due to the use of non-extractable liners – polystyrene concrete hollow-outers, which have all the necessary characteristics of strength and rigidity of load-bearing elements of buildings and structures from monolithic reinforced concrete. Such reinforced concrete casings open up fundamentally new opportunities in the off-the-shelf monolithic construction with the use of new equipment and vibration less sealing of the mixture by the wet-shotcrete method [4].

Currently, in addition to proven equipment in the technology used, new machines have been developed that should improve the efficiency of the work performed. It is a universal non-piston hose concrete pump [5] (Figure 2) and a truck mixer of gravitational-forced action (Figure 3).

The universality of this concrete pump is ensured by the ability to work on hoses  $d_h = 32 \dots 75$  mm with a wide range of performance and smoothly changing operating conditions due to the use of a hydraulic drive. The technological scheme of the formless concreteless using a universal hose concrete pump with a three-shaft concrete mixer is shown in Figure 4.

\*Corresponding author: Sumska str. 40, Kharkov, 61002 Ukraine, KSTUCA, dep. MBP, emeljanova-inga@rambler.ru



Figure 1: The process of wet gunned shells with a working nozzle with a ring nozzle (a) and a finished reinforced concrete shell (b)

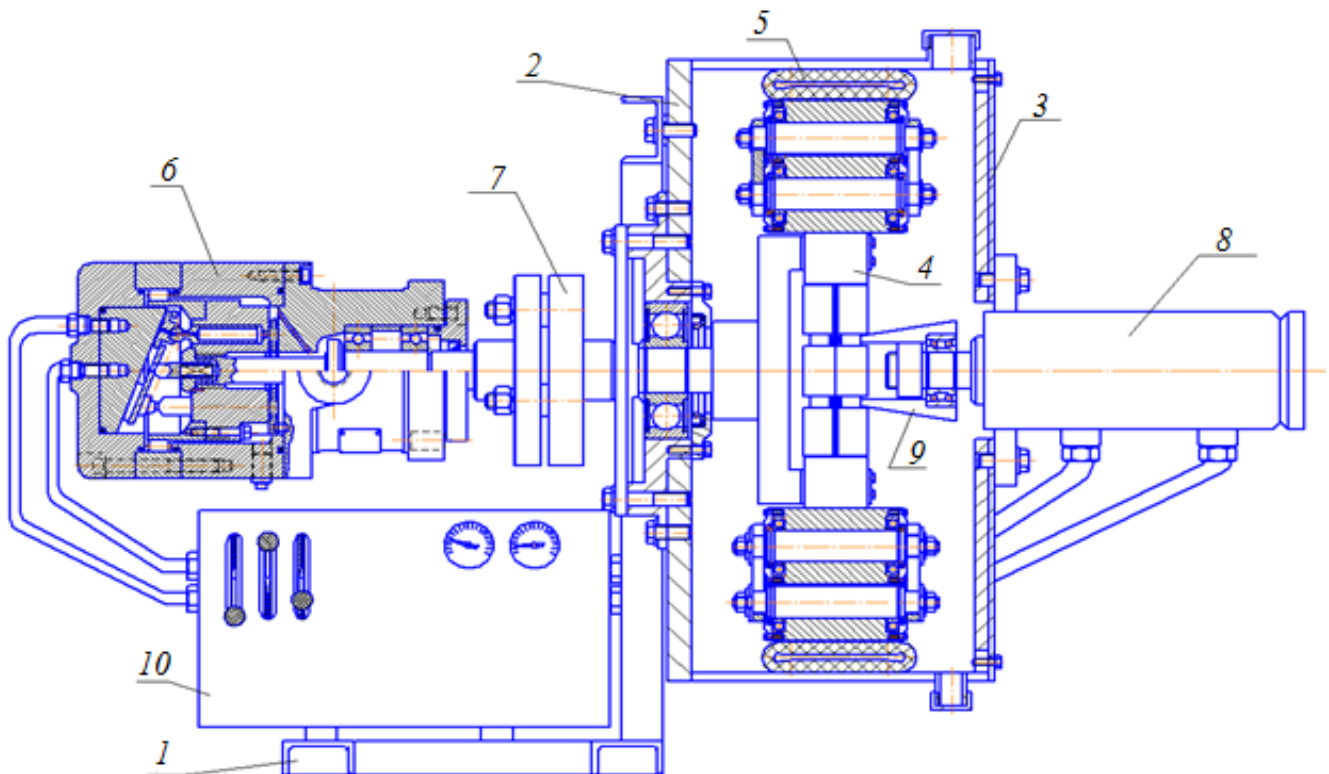


Figure 2: Scheme of a non-piston universal hose concrete pump of a new design with a hydraulic drive  
 1 – frame; 2 – pump housing; 3 – the cover of the case; 4 – rotor with rollers; 5 – flexible hose; 6 – the hydraulic motor;  
 7 – coupling; 8 – the hydrocylinder; 9 – conical tip, 10 – hydraulic distribution unit

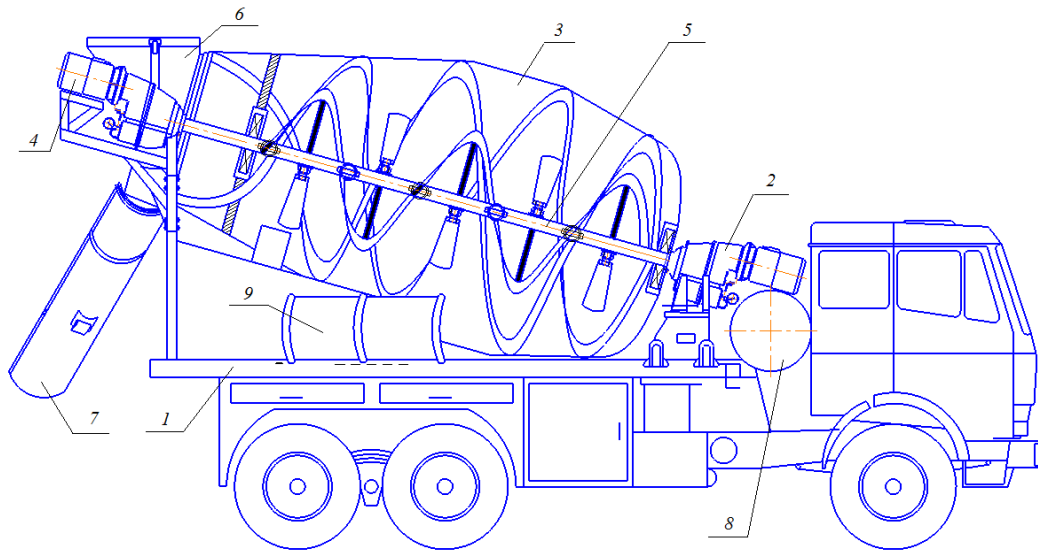


Figure 3: Scheme of a truck mixer with hydraulic drive

1 – self-propelled chassis; 2 – hydromotor-reducer, drive of the drum; 3 – the drum; 4 – hydromotor-reducer, shaft drive; 5 – mixing shaft; 6 – feed hopper; 7 – the discharge tray; 8 – a tank with water; 9 – additional section of the discharge tray

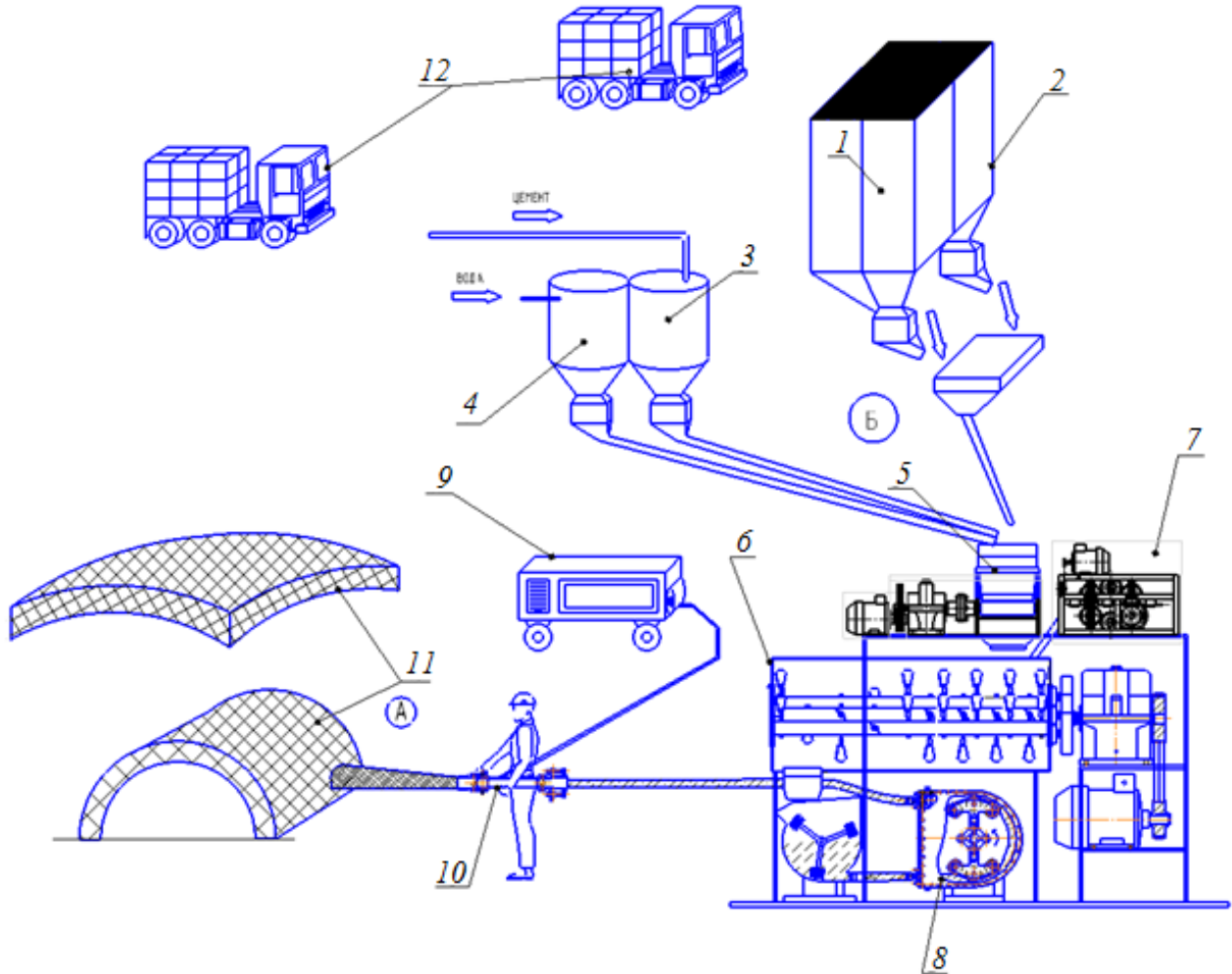


Figure 4: Technological scheme of works by the wet shotcrete method directly on the construction site

1 – bunker with sand; 2 – bunker with rubble; 3 – bunker with cement; 4 – water tank; 5 – belt feeder; 6 – three-shaft concrete mixer; 7 – a machine-cutter of a fiber; 8 – universal hose concrete pump; 9 – the compressor; 10 – shotcrete nozzle; 11 – shotcrete shells; 12 – truck for transportation of materials; A – the area of shotcrete works; B – concrete mixing unit

The delivery distance of the concrete mix when using the technological scheme with a universal hose concrete pump (Figure 4) is determined according to the dependencies:

– horizontally

The results of laboratory and industrial tests of new design mixers operating in a cascade mode, confirm their effectiveness in the preparation of dry building mixtures, which makes it possible to equip these machines with technological kits and complexes [8].

$$L = \frac{d_{TP} \cdot \Delta p}{\lambda \left( \rho_0 \frac{V_{cp}^2}{2} \right)}, \quad (1)$$

where are:

$d_{TP}$  – is the diameter of the pipeline through which the concrete mixture is transported;

$\Delta p$  – pressure drop at the ends of the pipeline;

$\lambda$  – coefficient of resistance to movement of the concrete mixture through the pipeline;

$\rho_0$  – the average density of the mixture that is transported through the pipeline;

$V_{cp}$  – average speed of transportation of a concrete mix through the pipeline;

– vertically

$$H = \frac{\Delta p \frac{8 \mu L_{TP}}{\pi R_{TP}^4} (\Pi_{tex} + \frac{\pi R_{TP}^3 \tau_0}{3 \mu})}{\rho_0 \cdot g}, \quad (2)$$

where are:

$\mu$  – is the dynamic viscosity of the concrete mixture;

$R_{TP}$  – radius of the pipeline;

$\Pi_{tex}$  – technical performance of a concrete pump;

$\tau_0$  – is the ultimate shear stress;

$g$  – acceleration of gravity.

Table 1 shows the relationship of the parameters of the concrete mix with the performance of the universal hose concrete pump and the pressure drop at the ends of the transport pipeline. Technological scheme of the formless concreting in the construction site using an auto concrete pump with a manipulator is shown in Figure 5.

The use of the truck mixer of gravity-forced action in the technological scheme with a universal hose auto concrete pump allows using the technological set for work, both mobile and inactive concrete mixes.

Thus, the availability of newly developed new machines in technological schemes extends the capabilities of technological kits and, in some cases, allows them to be used more efficiently than existing equipment. For the advantageous sides of the proposed new construction of the universal hose concrete pump, the working hose is smoothly loaded, which should ensure a longer working life of the new machine compared to the current ones. This will accordingly positively affect the operation of the entire set of equipment as a whole, which is confirmed by the calculation of the operating cycles of the existing and proposed hose concrete pump (Figure 2):

Table 1: Parameters for feeding concrete mix with universal hose concrete pump

L (m)	H (m)	$\Delta p$		
		$\Pi_{tex} = 5 \text{ m}^3/\text{h}$	$\Pi_{tex} = 10 \text{ m}^3/\text{h}$	$\Pi_{tex} = 15 \text{ m}^3/\text{h}$
5	2,75	$1 \times 10^4$	$6,4 \times 10^4$	$7,6 \times 10^4$
10	5,49	$8,764 \times 10^5$	$1,797 \times 10^6$	$2,676 \times 10^6$
15	8,25	$1,165 \times 10^6$	$2,375 \times 10^6$	$3,543 \times 10^6$
20	10,99	$1,31 \times 10^6$	$2,663 \times 10^6$	$3,976 \times 10^6$
25	13,75	$1,396 \times 10^6$	$2,837 \times 10^6$	$4,236 \times 10^6$
30	16,49	$1,454 \times 10^6$	$2,952 \times 10^6$	$4,409 \times 10^6$
35	19,24	$1,495 \times 10^6$	$3,035 \times 10^6$	$4,533 \times 10^6$
40	21,99	$1,526 \times 10^6$	$3,097 \times 10^6$	$4,626 \times 10^6$
45	24,74	$1,547 \times 10^6$	$3,145 \times 10^6$	$4,698 \times 10^6$
50	27,49	$1,57 \times 10^6$	$3,183 \times 10^6$	$4,756 \times 10^6$
55	30,24	$1,585 \times 10^6$	$3,215 \times 10^6$	$4,803 \times 10^6$
60	32,99	$1,599 \times 10^6$	$3,241 \times 10^6$	$4,843 \times 10^6$
65	35,74	$1,61 \times 10^6$	$3,263 \times 10^6$	$4,876 \times 10^6$
70	38,49	$1,619 \times 10^6$	$3,282 \times 10^6$	$4,905 \times 10^6$
75	41,24	$1,627 \times 10^6$	$3,299 \times 10^6$	$4,929 \times 10^6$
80	43,99	$1,635 \times 10^6$	$3,313 \times 10^6$	$4,951 \times 10^6$
85	46,73	$1,641 \times 10^6$	$3,326 \times 10^6$	$4,97 \times 10^6$
90	49,48	$1,647 \times 10^6$	$3,337 \times 10^6$	$4,987 \times 10^6$
95	52,23	$1,652 \times 10^6$	$3,348 \times 10^6$	$5,002 \times 10^6$
100	54,98	$1,656 \times 10^6$	$3,353 \times 10^6$	$5,016 \times 10^6$
110	60,48	–	–	$5,04 \times 10^6$
120	65,98	–	–	$5,059 \times 10^6$

$$Z_{ц} = \frac{3600 \cdot T \cdot K_{н}}{T_1 + T_2}, \quad (3)$$

where are:

$T$  – is the time of non-recyclable work of the hose concrete pump under consideration with hydraulic drive;

$K_{н}$  – factor of reliability of work of a hose concrete pump ( $K_{н1}$  – offered,  $K_{н2}$  – operating).

The service life of a new concrete pump is 25% higher than the life of a watch in modern hose concrete pumps.

## 2. CONCLUSIONS

1. The possibility of manufacturing ferro-concrete shells of cylindrical and spherical shape is shown in the conditions of a construction site with the help of equipment by the wet shotcrete method.

2. The basic schemes of the proposed hydraulic machines for use in technological kits are presented: the truck-concrete pump hose-free with the manipulator and the truck mixer of the gravitational-forced action.

3. Technological schemes of work with new machines are presented.

4. The obtained dependences for the determination of the delivery distance of a concrete mixture with the help of new technological sets of equipment are given.

5. Dependences have been found to determine the number of operating cycles of process equipment. The service life of the new concrete pump, and, consequently, of the whole kit, is 25% higher than that of the operating machines.

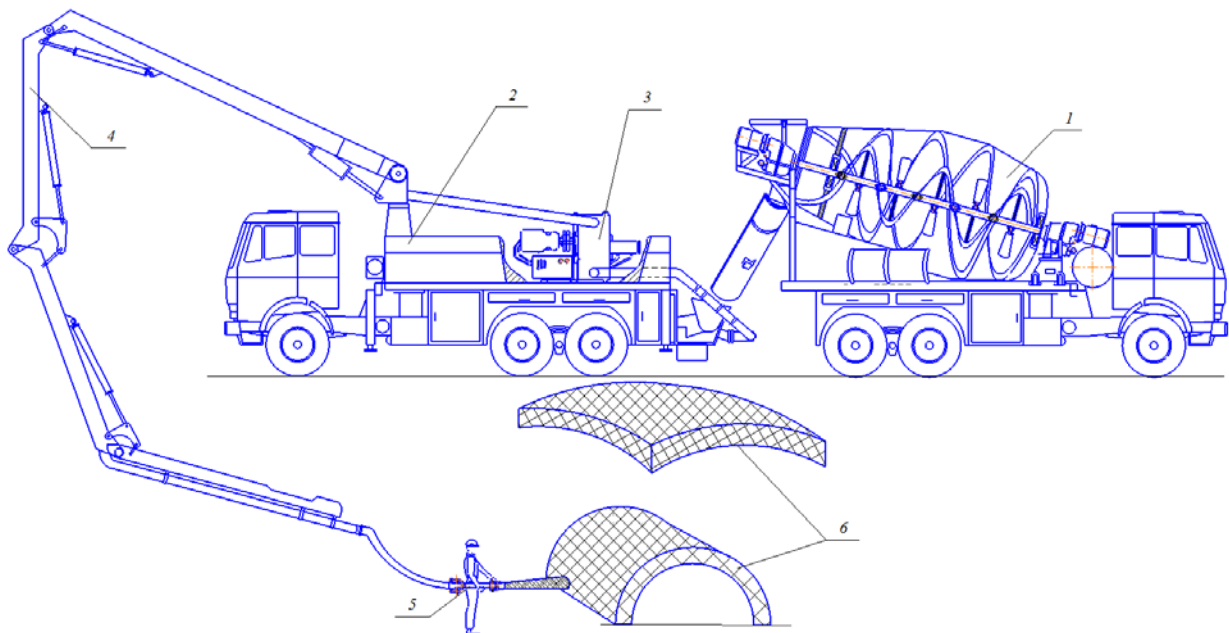


Figure 5: Technological scheme of carrying out works by the method of wet shotcrete using a manipulator  
 1 – truck mixer; 2 – autoconcrete pump; 3 – universal hose concrete pump; 4 – boom of a truck mixer; 5 – shotcrete nozzle; 6 – shotcrete casings

#### REFERENCES

- [1] Двухпоршневые растворобетонасосы для условий строительной площадки. Монография / И.А. Емельянова, А.А. Задорожный, С.А. Гузенко, Н.А. Меленцов – Харьков: Тимченко А.Н., 2011. – 196 с.: ил., табл.
- [2] Бетоносмесители, работающие в каскадном режиме. Монография / И.А. Емельянова, А.И. Анищенко, С.М. Евель, В.В. Блажко, О.В. Доброходова, Н.А. Меленцов. – Харьков: Тим Паблиш Групп, 2012. – 146 с. ил., табл.
- [3] Емельянова И.А. Оборудование для приготовления и уплотнения фибробетонных смесей. Монография / И.А. Емельянова, В.Ю. Шевченко, В. В. Асанов – Харьков: Тим Паблиш Групп, 2015. – 124 с.
- [4] Емельянова І.А. Технологічні особливості зведення будівель та споруд криволінійної форми по будівельній системі «Монофант» з використанням малогабаритного обладнання способом мокрого торкретування. / І.А. Емельянова, С.О. Гузенко, Д.О. Чайка та інші. // Колективна монографія – Харків: ХНУБА, 2017. – С. 323 – 330.
- [5] Пат. 112585 України МПК (2609.2016) F 04B 43/12 F 04B 15/02 Універсальний шланговий бетононасос / Емельянова І.А., Задорожний А.О., Клименко М.В., Чайка Д.О.





# Research of Stress-Strain State of Metal Constructions for Static and Dynamic Loads Machinery

I.I. Nazarenko <sup>1\*</sup>, O.P. Dedov <sup>1</sup>, I.I. Zalisko <sup>2</sup>

<sup>1</sup> Kyiv National University of Construction and Architecture, Kiev

<sup>2</sup> Drogobych crane factory, Drogobych

*The theoretical substantiation of the possibility of creating bulk molding Vibration Machines with highly effective parameters of energy intensity and material consumption for various conditions for the formation of concrete and reinforced concrete products is given in the paper. This is due to the creation and rational use of the regularities of changes in the internal (elastic-inertial and dissipative) properties of the "machine-environment" system in the regime, which is approximate to the mode of its free oscillations.*

*A theory is proposed for the interaction between the working parts of vibration machines and media to be processed, which, on the basis of an estimate of the stress state of the medium in the contact zone, makes it possible to determine the effect of the medium being processed on the dynamics of the machine working parts.*

*The principles of creation of volumetric forming machines with highly effective parameters for energy intensity and material consumption are proposed.*

**Keywords: Stress-strain state of metal constructions, Diagnostic systems, Vibration frequency, Vibration amplitude, Dynamic loading**

## 1. INTRODUCTION

The modern development of construction in Ukraine puts forward new requirements for equipment that would ensure high reliability, performance, and a range of economic and ergonomic requirements. To a large extent this applies to steel structures construction vehicles and equipment, demand for which is growing every year. The solution of this problem lies in the direction of improving the design, the identification of the potential of existing structures, improving their productivity and efficiency, the development of diagnostic systems.

Metal construction machines of various technological purpose in the operation accept both static and dynamic loads and tend to work in the mode of alternating load, the effectiveness of such cars due to software defined technology modes and parameters impact on the processed material, which can be realized by careful selection of mathematical calculation models that adequately reflect the actual motion of the system.

Modern machinery provides a solution to a number of issues that are caused by factors of a different nature. The main factor influencing the implementation of projects of construction of new machines are purpose requirements of today's market and directly to consumers of such technology.

Over time, the appearance of new construction materials and technologies for their manufacture and processing, the vector of development of engineering change its direction. Undoubtedly, the design requirements of modern machines and high stiff enough, but the fundamental concepts of what the machine has to be changed somewhat. That is, when it comes to modern technological machine, is to identify the main issues to be addressed [1, 2]: a low power consumption of the implementation process with a high quality;

low consumption of materials; high reliability; certain durability; low manufacturing cost.

In carrying out theoretical studies [1-3], as well as practical implementation [1-5], it began the scientific study of the problem: the development of the most effective and reliable construction machines for different loads, provided by the establishment and management of changes in domestic laws (elastic and dissipative) properties of the system "vehicle - environment".

In recent years, development and creation of construction machines of various technological purpose being to find ways of constructive solutions with a variable.

In operation of such machines is assumed maximum utilization of internal resources to the machine in turn makes it necessary to ensure durability and reliability with desired dynamic parameters. Production of such a problem is to determine the intensity of the structural elements of the machine and the assessment of their stress-strain state.

In the case of dynamic performance on metal structure as a linear elastic body, equation of motion has the form:

$$z_{ij,j} + F_i = \rho \cdot U_i, \quad (1)$$

where  $\rho$  - density material. Given the viscous properties then replace in (1) the operator:

$$\rho \cdot \frac{\partial^2}{\partial t^2} \Leftrightarrow \rho \left( \frac{\partial^2}{\partial t^2} \right) + k \frac{\partial}{\partial t}, \quad (2)$$

where is k- viscosity.

Equation (2) as such remains unchanged.

We introduce notation for the wave propagation velocity of the reference circle.

$$C_1^2 = \frac{1-\nu}{(1+\nu)(1-2\nu)} \cdot \frac{E}{\rho}; \quad C_2^2 = \frac{1}{2(1+\nu)} \cdot \frac{E}{\rho}, \quad (3)$$

For the case when the force  $F(t)$  is common and operates along the axis  $OX_1$  (at the beginning of the coordinate system)

$$U_1(x_1, x_2, x_3, t) = \frac{1}{4\pi\rho R} \cdot \left[ \frac{1}{c_1^2} \cdot \frac{x_1^2}{R^2} \cdot P\left(t - \frac{x_1}{c_1}\right) + \frac{1}{c_1^2} \cdot \left(1 - \frac{x_1^2}{R^2}\right) P\left(t - \frac{x_1}{c_1}\right) - \left(1 - 3 \frac{x_1^2}{R^2}\right) \cdot \int_{\frac{1}{c_1}}^{\frac{1}{c_2}} \lambda P(t - \lambda R) d\lambda \right]; \tag{4}$$

$$U_2(x_1, x_2, x_3, t) = \frac{x_1 x_2}{4\pi\rho R} \cdot \left[ \frac{1}{c_1^2} \cdot P\left(t - \frac{R}{c_1}\right) - \frac{1}{c_2^2} \cdot P\left(t - \frac{R}{c_2}\right) + 3 \int_{\frac{1}{c_1}}^{\frac{1}{c_2}} \lambda P(t - \lambda R) d\lambda \right]; \tag{5}$$

$$U_3(x_1, x_2, x_3, t) = \frac{x_1 x_3}{4\pi\rho R} \cdot \left[ \frac{1}{c_1^2} \cdot P\left(t - \frac{R}{c_1}\right) - \frac{1}{c_2^2} \cdot P\left(t - \frac{R}{c_2}\right) + 3 \int_{\frac{1}{c_1}}^{\frac{1}{c_2}} \lambda P(t - \lambda R) d\lambda \right]. \tag{6}$$

If the force acts along the axis  $OX_2$ , then you have to replace the index:

$$y(22) \Rightarrow \begin{cases} 1 \rightarrow 2; \\ 2 \rightarrow 3; \\ 3 \rightarrow 1. \end{cases}$$

If the force acts along the axis  $OX_3$ , then you have to replace the index:

$$y(22) \Rightarrow \begin{cases} 1 \rightarrow 3; \\ 2 \rightarrow 1; \\ 3 \rightarrow 2. \end{cases}$$

For the plane problem ( $x_3 = 0$ ); for one-dimensional problems: ( $x_1 \neq 0$ ;  $x_2 = x_3 = 0$ ).

So, as a result of dependencies are as follows: using Cauchy relations, Hooke's law and relations that bind Lamé elastic constants of Young's modulus, shear modulus and Poisson's ratio is decisive for calculating the stress-strain state of stresses in reference circle of application solutions in the form of third-rank tensor:

$$V_{ijk}(x_1, x_2, x_3) = \frac{1}{8\pi(1-\nu)} \frac{1}{R^3} \left[ (1-2\nu) \cdot (x_k \cdot \delta_{ij} - x_i \cdot \delta_{jk} - x_j \cdot \delta_{ki}) - 3 \frac{x_i x_j x_k}{R^2} \right],$$

$$V_{ijk}(x_1, x_2, x_3) = \frac{1}{8\pi(1-\nu)} \frac{1}{R^3} \left[ (1-2\nu)(x_k \cdot \delta_{ij} - x_i \cdot \delta_{jk} - x_j \cdot \delta_{ki}) - 3 \frac{x_i x_j x_k}{R^2} \right], \tag{i = 1, 2, 3}.$$

In this case, the right kind of movement will be:

$$U_i(x_1, x_2, x_3) = U_{ij}(x_1, x_2, x_3) * F_j(x_1, x_2, x_3), \tag{i = 1, 2, 3}.$$

Design model frame with outriggers shown in Figure 1a as well. Design model adopted in the form of construction consisting of rods rigidly interconnected the nodes. Units conventionally shown as small circles numbered in Arabic numerals. Serial number of the rod (item) affixed in a circle. Each rod section is now with geometrical characteristics. Design model building on a line connecting the centers of gravity of cross sections of rods.

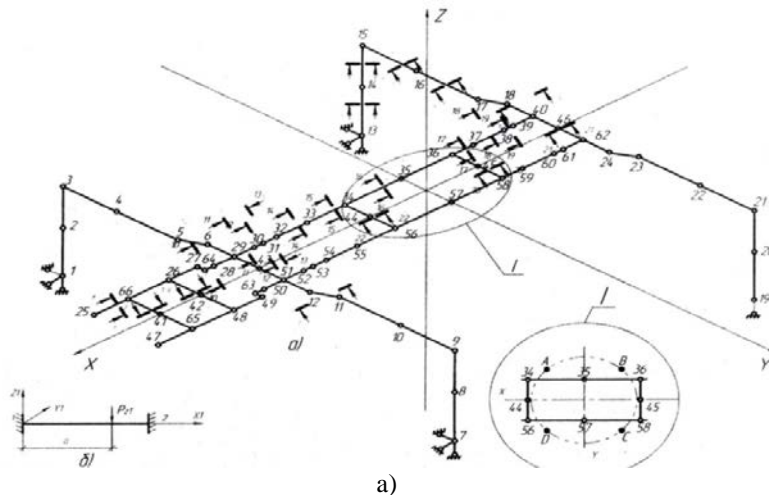
Design model is in rectangular coordinates  $X, Y, Z$  (general coordinate system). The result of the calculation of finite element of this design is shown in Figure 1 b.

The correctness of the results of mathematical modeling to a greater extent depends on the mechanical properties of structural materials and the study of complex work units bearing structural elements. Test procedures for mechanical characteristics of the static effect is to create a load on the test sample in order to create in it a certain kind of stress (tension, compression, shear). Thus a tensile test determined the basic mechanical characteristics not only of constructional materials, and their connection to each other (Figure 2a). Quite often undergo static tests not only the individual samples of the materials, but entire units (Figure 2b) future construction in order to study their stress-strain state and evaluation of stiffness.

Integral assessment of the metal structures of the finished product can be made on the basis of the dynamic tests. The idea of testing is to find the actual dynamic characteristics of the structure (natural vibration frequency, vibration amplitude, etc.) and then comparing these characteristics with the characteristics obtained by mathematical simulation of the system design. The mathematical model must be created so that adequately describes the real structure and its behavior under various loads and the ability to reflect the simulations of various kinds of defects associated with the manufacture and operation of the immediate appointment.

At the dynamic loads on structural elements inherent in most vehicles technological purpose, the main type of damage is the formation and development of cracks caused by the accumulation of stress fatigue.

Durability destruction determined long cycles of stresses on the supporting structure of the machine and its individual elements, resulting in a crack gradually develops and leads to destruction.



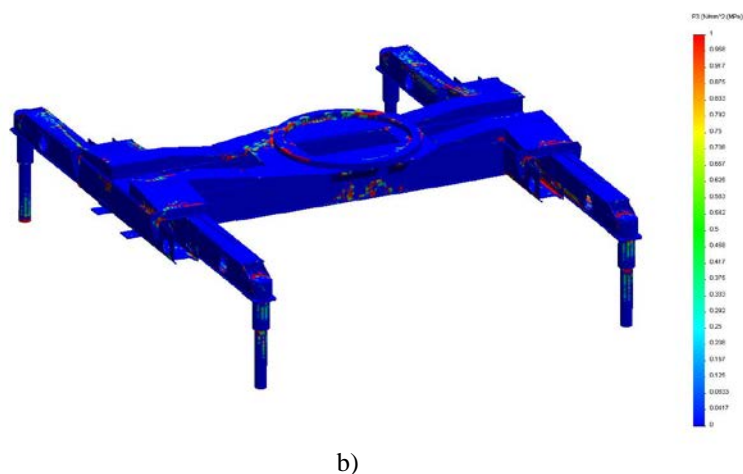


*Figure 1: Simulation of road construction cranes:  
a) - design scheme; b) - the result of the calculation.*

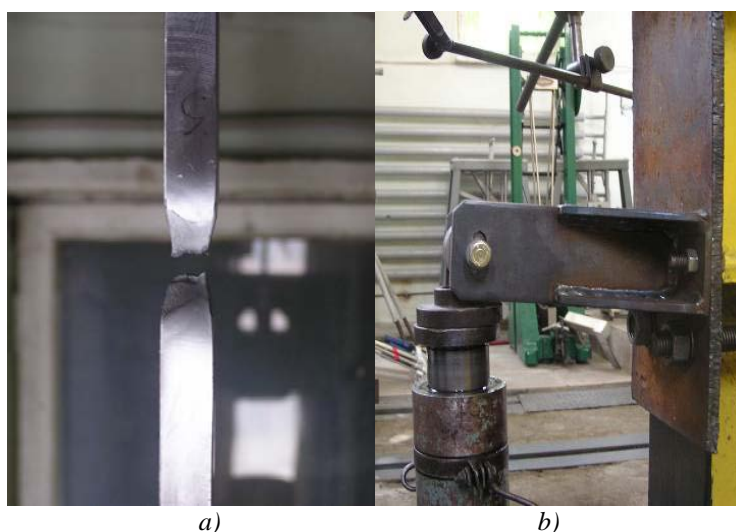


*Figure 2: Test the structural elements of steel structures:  
a) The welded joint in tension; b) Test bracket.*

Calculation and testing of individual elements of the design of the machine is not too difficult, although in some cases require a lot of material resources and time-consuming. When it comes to more complex parts and assembly units of the accuracy of the analytical calculation is subject to doubts in terms of the rational use of materials, resulting in an increase in material consumption structure, and further the energy intensity of the whole technological process, which performs such a design.

It is obvious that the solution of this problem lies in the integrated approach should combine analytical calculations, mathematical modeling and direct experimental studies.

To implement this approach assumes the following sequence of research work:

- analysis calculation of structural elements of the machine in terms of for all types of loads that were made in the design of the machine;
- the development of a computer model of the object of study (general or individual most loaded components, structural elements);
- determining a possible combination of loads acting on the elements;

- conduct additional simulations and calculations to determine the behavior of structural elements and the whole machine while the action of various loads (if necessary);

- verification of design decisions and the choice of the most efficient, by modeling teamwork loads on computer models, evaluation and analysis of stress-strain state, identify the most stressful elements of the structure;

- to develop a computer model of the matrix control points limits the integral characteristics of the state of design for future use in field trials;

- conducting full-scale and model (computer experiments) by applying certain loads on the real sample and its model;

- adjusting the computer model until the comparison is integral characteristics obtained by measurements at control points during the experiment and the simulation will differ among themselves within the allowable error (the thus obtained computational model is adequate actual design within the points adequate - integral control points characteristics).

To construct a mathematical model can be used general purpose computational systems, which are based on numerous calculations and the fundamental laws of the theory of elasticity, plasticity, and the like. Recently, such settlement systems have been widely used in various industries, including mechanical engineering. The results of analysis of structures by numerical methods (eg finite element method) is a movement (deformation), effort (stress) at the nodes of the mesh design of the structure. Depending on the need for rational calculation accuracy, the number of nodes and finite elements, respectively, can be measured in hundreds and thousands. On the one hand the processing of the results of such calculations is time-consuming, but allows at the design stage to obtain a general picture of the structural layout of the machine components and the improvement of its conduct in terms of the rational use of materials. In the case of upgrading an existing machine model of technological purpose, calculation model in this sector, will allow to analyze the technical level of the design and fulfill its forecasting reliability, and in conjunction with the implementation of the pilot studies to assess the current technical condition of the appearance of possible failures, and the like.

## 2. CONCLUSIONS

1. The analysis methods of modeling and machine indicates the need to consider the stress-strain state of the steel structures.

2. Proposed methodology and test methods for machines under static and dynamic loading, the way the software determines the load on the metal machine.

## REFERENCES

- [1] Nazarenko I.I. Applications of the theory of vibrating systems (second edition). K.: Publishing House "Word." 2010 – 440 p.
- [2] Nazarenko I.I. Fundamentals of design and construction of machinery and equipment of processing manufactures / I.I. Nazarenko, I.M. Bernik // - K.: LLC "Agrar Media Group», 2013. - 544 p.
- [3] Nazarenko I.I. Vibrating machines and processes of the construction industry: - K.: KNUCA, 2007. - 203 p.
- [4] Zalisko I.I. Study of influence of technology factors on durability of the support frame / I.I. Zalisko // Mountain, building, road, reclamation machines - K.: KNUCA, 2012. - №80. - P. 44 - 88.
- [5] Dedov O.P. Mathematical model and determination of parameters of movement compactors for soil compaction. O.P.Dedov, Mountain, building, road, reclamation machines .№ 66, Kiev, 2006, P.41-46.

# Research of Energy-Saving Vibration Machines with Account of the Stress-Strain State of Technological Environment

Ivan Nazarenko<sup>1\*</sup>, Oleg Dedov<sup>1</sup>, Anatoly Svidersky<sup>1</sup>, Nicolay Ruchinsky<sup>1</sup>

<sup>1</sup> Kyiv National University of Construction and Architecture, Kiev

*An analytical method for determining the influence of a process medium on the dynamics of the working bodies of vibrating machines is considered. The results of the research are presented, which made it possible to identify the zones of effective action of parameters and characteristics of the "machine - environment" system to ensure the high quality of the compaction process, which is based on the idea of purposeful use of the elastic characteristics of a common vibration system.*

*The scientific idea is put forward, which consists in the fact that during the study of a particular process the mathematical model of the vibration system "machine-environment" should be determined on the basis of taking into account the internal structure of these subsystems as a single one, despite their different physical nature and structure.*

*The theoretical substantiation of the possibility of creating bulk molding Vibration Machines with highly effective parameters of energy intensity and material consumption for various conditions for the formation of concrete and reinforced concrete products is given in the paper. This is due to the creation and rational use of the regularities of changes in the internal (elastic-inertial and dissipative) properties of the "machine-environment" system in the regime, which is approximate to the mode of its free oscillations*

**Keywords: Vibration system, Vibrator, Vibration frequency, Vibration amplitude, Dynamic loading, Efficiency of the vibrating machine**

## 1. INTRODUCTION

Vibrating machines are widely used in the construction industry to seal concrete mixtures and soil. The most effective of these are vibro-impact machines. This is due to the fact that during the impact of the impact in the working mixture there are large compressive stress (due to large accelerations), which cause deformation and, consequently, increase the density of the mixture. However, the degree of efficiency of these machines is largely determined by the magnitude of energy costs for the implementation of necessary workloads. Therefore, solving the problem of reducing energy consumption of vibration damping machines while preserving their high technological efficiency is an important scientific and practical task.

Vibrating machines are widely used in various branches of the national economy to perform a significant range of technological processes. A common characteristic feature of this class of machines is the vibrational effect on the material being processed, as a result of which the material changes its properties, thus ensuring the corresponding technological process.

Many studies devoted to the study of the vibration damaging systems are presented, which are the analysis and synthesis of mechanical vibration damaging systems. Concerning works devoted to the study of vibration damping machines for sealing concrete mixtures, it is possible to note that in these works the parameters of motion of such systems are determined, based on certain assumptions. The most general is the assumption of a "vibrating machine - processing environment" system in the form of a discrete model. The work of [1, 2] clarifies this model and proposes a method of transition from

discrete continuum systems (discrete - machine, continuum - environment) to purely discrete ones taking into account wave phenomena in a concrete mixture. This approach makes it possible to significantly simplify the calculation scheme. The principle of transition of the most realistic scheme to the calculated (discrete) is given in [1] (Fig. 1).

One of the main criteria of such systems is the impact energy in periodic motion, which determines the effectiveness of the regime.

The purpose of the article is to study and establish effective zones of stability and assessment of the energy characteristics of the "vibrating machine - processing environment" system for the development of new progressive machines, taking into account the stress-strain state of the environment.

Consider the existence condition of the stability of modes of the system with a separation from the elastic limiter of oscillations (Fig. 1, c) on the boundaries of linear sections in accordance with the work [2]:

$$\frac{\varepsilon^2}{|1-\varepsilon^2|} \cdot \frac{\sin \varphi + \sin(\tau_x + \varphi)}{2} \leq q \leq \frac{\varepsilon^2}{1-\varepsilon^2}; \quad (1)$$

where

$$\varepsilon^2 = \frac{c}{m\omega^2}; \varphi = \frac{\pi + \tau_x}{2}; \left( \varphi = \frac{3\pi + \tau_x}{2} \right)$$

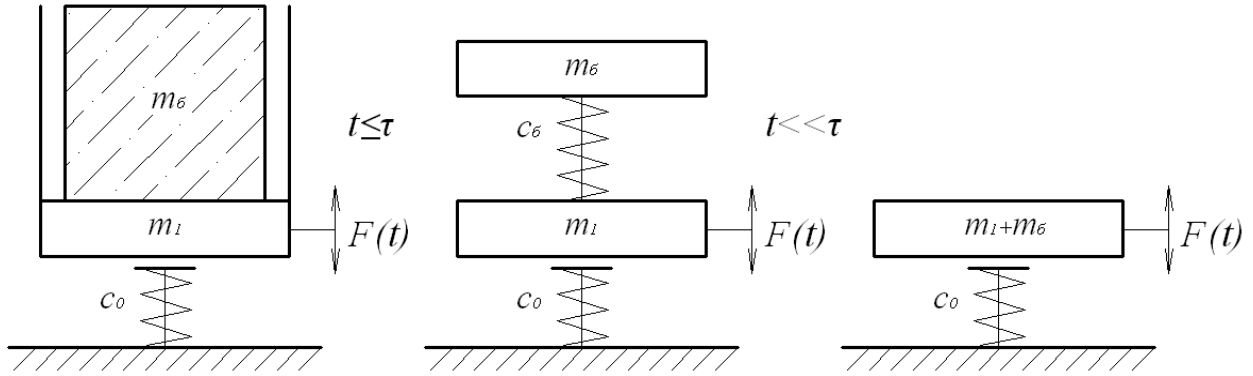


Figure 1: Calculation models of vibration systems :  
a – discrete-continuous, b – discrete (two mass), c – discrete (one mass)

In the dependencies (1) the following symbols are adopted:  $c$  - the stiffness of the restrictor;  $q = \frac{Q}{F_0}$  - the ratio

of the weight of the vibrating machine ( $Q = mg$ ) to the amplitude of the force  $F_0$  of perturbation;  $\omega$  - frequency of perturbation force;  $\tau_x$  - the duration of movement of the vibrator in contact with the elastic limiter of oscillations:

$\tau_x = \frac{\pi}{\varepsilon}$ ;  $\varphi$  - the phase angle, which in the calculations is assumed to provide a positive value at the boundaries  $c = \infty$  ( $\varepsilon = \infty, \tau_x = 0$ ), condition (1) gives the value:

$$q = 1 \quad (2)$$

From (2) it follows that the upper and lower boundaries of regions of stable modes are combined.

However, the stability of periodic regimes under absolutely rigid constraints of oscillations is determined by the ratio:

$$1 \leq q \leq \infty \quad (3)$$

When comparing relations (2) and (3), it follows that the existence of stable periodic modes of motion of systems with elastic constraints (with stiffness) at the limit value does not pass into the condition of stability under the motion of the corresponding systems with the rendering of absolutely strict constraints. To eliminate this disparity, the consideration of shock interaction is the replacement of the elasticity and dissipation of the constraints by the shock pair, taking into account the length of the play. Such an approach allows to take into account the shock interaction in the vibration system by the pulse theorem and the recovery rate of the impact velocity.

$$q_{onm} = \frac{1+R}{1-R} \cdot \frac{\sqrt{2(1+\cos\tau)}}{(2\pi \cdot i - \tau_x)^2} \left( 2\pi \cdot i - \tau_x + 2tg \frac{\tau_x}{2} \right) \quad (4)$$

Then the maximum impact velocity will be determined by the dependence:

$$\dot{y}_0 \max = q_{onm} \frac{2\pi \cdot i - \tau_x}{1+R} \quad (5)$$

Consider now the motion of the vibrator in the range  $0 \leq \tau \leq \tau_x$ .

In dimensionless variables we will have:

$$\ddot{y}_1 + 2n\dot{y}_1 + \varepsilon^2 y_1 = \cos(\tau + \varphi) + mg \quad (6)$$

where  $\varepsilon^2 = \frac{c_0}{m\omega^2}$ ;  $2n = \frac{n'}{m\omega}$ ,  $n'$  - dissipation rate.

$$y_1(0) = y(2\pi \cdot i) = 0; \quad \dot{y}_1(0) = \dot{y}(2\pi \cdot i) = \dot{y}_0 \quad (7)$$

$$y_1 = \dot{y}_0 a_1 + b_1 \sin \varphi + c_1 \cos \varphi + d_1 q, \quad (8)$$

$$\dot{y}_1 = \dot{y}_0 \dot{a}_1 + \dot{b}_1 \sin \varphi + \dot{c}_1 \cos \varphi + \dot{d}_1 q.$$

$$a_1 = e^{-n\tau} \varepsilon^{-1} \sin \varepsilon \tau; d_1 = (1 - \dot{a}_1 - na_1) \varepsilon^{-2}; \quad (9)$$

$$b_1 = [(a_1 - \sin \tau) \cos \psi + (\cos \tau - d_1 - na_1) \sin \psi] \cdot [(1 - \varepsilon^2)^2 + 4n^2]^{-\frac{1}{2}};$$

$$c_1 = [(\cos \tau - d_1 - na_1) \cos \psi - (a_1 - \sin \tau) \sin \psi] \cdot [(\varepsilon^2 - 1)^2 + 4n^2]^{-\frac{1}{2}};$$

$$\varepsilon_1 = \sqrt{\varepsilon^2 - n^2}; tg \psi = \frac{2n}{\varepsilon^2 - 1}.$$

$$y_1(\tau_x) = y(\tau_x) = 0; \quad \dot{y}_1(\tau_x) = \dot{y}(\tau_x) = -R\dot{y}_0 \quad (10)$$

By substituting the conditions (10) in equation (8), as well as the meaning  $\sin \varphi$  and  $\cos \varphi$  through  $q_{onm}$  and  $\dot{y}_0 \max$  in accordance with formulas (8) and (10), we obtain dependences for determining  $R$  and  $\tau_x$ :

$$R = \frac{\delta \left( \dot{c}_1 + \dot{b}_1 ctg \frac{\tau_x}{2} \right) + 2\lambda_1 (\dot{d}_1 + \delta \dot{a}_1)}{\delta \left( \dot{c}_1 + \dot{b}_1 ctg \frac{\tau_x}{2} \right) - 2\lambda_1 (\delta + \dot{d}_1)}, \quad (11)$$

$$2\lambda_1 \left[ \dot{d}_1 (d_1 - 1) - a_1 (\delta + \dot{d}_1) \right] + \left( c_1 + b_1 ctg \frac{\tau_x}{2} \right) \left[ 2\dot{d}_1 + \delta (1 + d_1) \right] - \left( \dot{c}_1 + b_1 ctg \frac{\tau_x}{2} \right) (2d_1 + \delta a_1) = 0$$

where  $\lambda_I = \frac{2}{\delta} + ctg \frac{\tau_x}{2}$ ;  $\delta = 2\pi \cdot i - \tau_x$ .

According to the work [1]:

$$\tau_x = \frac{\pi}{\sqrt{\varepsilon^2 - n^2}}; R = e^{-n\tau_x}. \quad (12)$$

Determine now the condition of existence and stability of periodic regimes. The scope of actual values is limited by the ratio:

$$q \leq \frac{\lambda \sqrt{\varepsilon_I^2 + \varepsilon_2^2}}{f_I}. \quad (13)$$

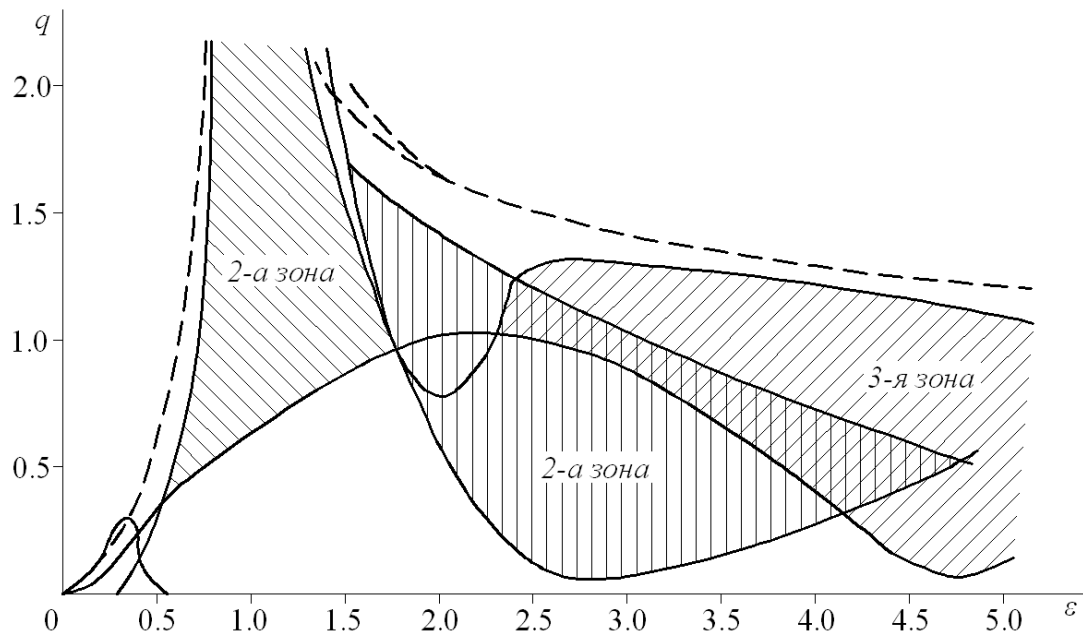


Figure 2: Stability map of vibro-impact machines

To study the intensity of dynamic influence in work, the method of dynamic loop hysteresis is used. Expressions for areas of a hysteresis loop with various load laws are obtained. In the non-symmetric law in the stationary mode we have:

$$\Delta W = \frac{\sigma_{cm}^2 \gamma \pi}{2E_0 (1 + \gamma^2)} \left[ 1 + \frac{(1 - K_\tau)}{K_\tau^2} \right], \quad (15)$$

Dependences (15) are given for the stationary (established) mode of motion, that is, the energy  $\Delta W$  going on the densification of the unit volume of the mixture is constant. To estimate the energy required to compaction the mixture from the initial value of density to the required technology, expression (15) is represented as:

$$E_n = \frac{t_n}{T} \Delta W_0 v \frac{K_s - 1}{K_s \ln K_s} \quad (16)$$

Where  $t_n$  - the length of the technological process;  $\Delta W_0$  - area of the hysteresis loop at the initial moment of

For the real occurrence of periodic regimes, it is necessary to provide certain restrictions of system parameters and perturbations determined by the stability conditions of these regimes. For a system (Fig. 1, c), the boundary of stability regions of periodic regimes is determined by the equation:

$$\pm y_0 (1 \pm R)^2 + (2\pi \cdot i - \tau_x) [q(1+R) + \cos(\tau_x + \varphi) + R \cos \varphi] = 0$$

Analysis of the results indicates the existence of several zones of stability (Fig. 2), which is important for determining the parameters of the vibration damaging system, which are known to be reduced to two mains [2]:

$$\varepsilon = \sqrt{\frac{c}{m\omega^2}} \quad q = \frac{mg}{F_0} \quad (14)$$

sealing the mixture;  $K_s$  - coefficient characterizing changes in the area of the loop of hysteresis in the process of oscillations.

On the basis of formulas (15) and (16) expressions for specific power and the coefficient of efficiency, which has the greatest value  $K_\tau = 1/\sqrt{2}$ . A generalizing criterion

for assessing the effectiveness of vibrational effects is presented, which, along with the contact stress and deformation velocity  $\sigma$ , takes into account the slope of the load wave profile:

$$\frac{\sigma_{cm} \cdot v_{\varepsilon_1} \cdot \Gamma\left(\frac{n_1+1}{2}\right)}{\Gamma\left(\frac{n_1+1}{2}\right)} = \frac{\sigma_{cm} \cdot v_{\varepsilon_2} \cdot \Gamma\left(\frac{n_1+1}{2}\right)}{\Gamma\left(\frac{n_2+1}{2}\right)} \quad (17)$$

Where  $\Gamma(x)$  - gamma function  $X$ ;  $v_{\varepsilon_1}$  - strain rate;  $n$  - coefficient characterizing the steepness of the front.

The system in which the score (17) will be higher will be more effective.

According to research results, the principles of the creation of new progressive vibrating machines for the building industry in the formation of multi-hollow slabs and foundation blocks have been developed.

## 2. CONCLUSIONS

1. A theory is proposed for the interaction between the working parts of vibration machines and media to be processed, which, on the basis of an estimate of the stress state of the medium in the contact zone, makes it possible to determine the effect of the medium being processed on the dynamics of the machine working parts.

2. The principles of creation of volumetric forming machines with highly effective parameters for energy intensity and material consumption are proposed.

3. The zones of effective operation of the parameters and characteristics of the machine-environment system are found to ensure the high quality of the sealing process, which is based on the idea of the purposeful use of elastic characteristics of the general vibration system,

which, under all the same conditions, also results in the reduction of energy costs for some machines up to 50%.

4. The analytical dependences are obtained for estimating the energy of considering the interaction of the working organ and the medium on the basis of the use of the method of dynamic hysteresis loops.

## REFERENCES

- [1] Nazarenko I.I. Applications of the theory of vibrating systems (second edition). K.: Publishing House "Word." 2010 – 440 p.
- [2] Nazarenko I.I. Vibrating machines and processes of the construction industry: - K.: KNUCA, 2007. - 203 p.
- [3] Nazarenko I.I. Fundamentals of design and construction of machinery and equipment of processing manufactures / I.I. Nazarenko, I.M. Bernik // - K.: LLC "Agrar Media Group», 2013. - 544 p.
- [4] Nazarenko I.I., Svidersky A.T., Ruchinsky N.N., Dedov O.P. Research and the creation of energy-efficient vibration machines based on the stress-strain state of metal and technological environments. Heavy Machinery HM 2014, B, Kraljevo-Serbia. 2014 pp. 85-89



# Application of numerical methods for analysis of vertical transport systems

Jovan Vladić<sup>1\*</sup>, Radomir Đokić<sup>1</sup> Anto Gajić<sup>2</sup>

<sup>1</sup>Faculty of Technical Sciences, University of Novi Sad, Serbia

<sup>2</sup>Mine and Thermal Power Plant, Ugljevik, Republic of Srpska

*Analysis of the vertical transport systems and machines means that we must form mathematical models with systems of differential and algebraic equations. During the exploitation one can encounter different types of vertical transport machines, from mining and contemporary passenger elevators with extreme heights and lifting velocities, to the classic elevators with relatively small parameter values which leads to the usage of different dynamic models and mathematical methods for their solving. The paper presents the issues with mechanical models of the vertical transport systems (elevators and the mining elevators) and numerical methods for formed mathematical models solving according to basic parameters of exploitation facilities in mines. Besides the features analyses and the convenience of applying certain mathematical methods, the paper also provides the overview of using specialized software for analysis of vertical transport machines.*

**Keywords:** Vertical transport systems, Elevators, Numerical methods

## 1. INTRODUCTION

The claims set upon by the economy and contemporary society have caused the development and application of the vertical transport machines of specific characteristics, referring to the elevators implementation (Fig. 1a) and exploitation facilities in mines (Fig. 1b) with great lifting heights and velocities in high constructions and mines with underground exploitation.

Today, we use plants with the velocity of 20 m/s, i.e. 72 km/h with the lifting heights up to 1000 m and the transport capacity of hundreds of tons in the domain of building construction and underground exploitation of the mineral resources. These devices have special emphasis in dynamic influences, which require selection to achieve the appropriate and reliable application.

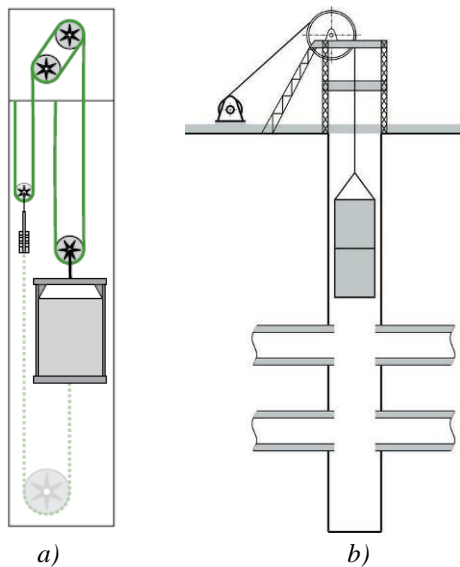


Figure 1: Scheme of the elevator (a) and exploitation facility in mines (b)

Particular interest regarding systems of vertical transport as well as vertical lifting and lowering of people and loads has been dedicated to exploitation facilities in mines or, so called, mining elevators.

## 2. MODELS OF VERTICAL TRANSPORT SYSTEMS

The proper dynamic model for describing dynamic behavior of the device with a driving pulley is shown in Fig. 2. The model represents a model of elevators and exploitation facility in mines with a "heavy" rope of a variable length.

For the elevators with big lifting heights (to 2000 m and more) and velocity movements (to 20 m/s), apart from the weight of the rope's free end, there is a significant change in the basic parameter of dynamic models – stiffness  $EA/L$ . Such model has to be applied with the modern elevators, and with the mining elevators in the analysis of dynamic behavior and the stability of the system's movements.

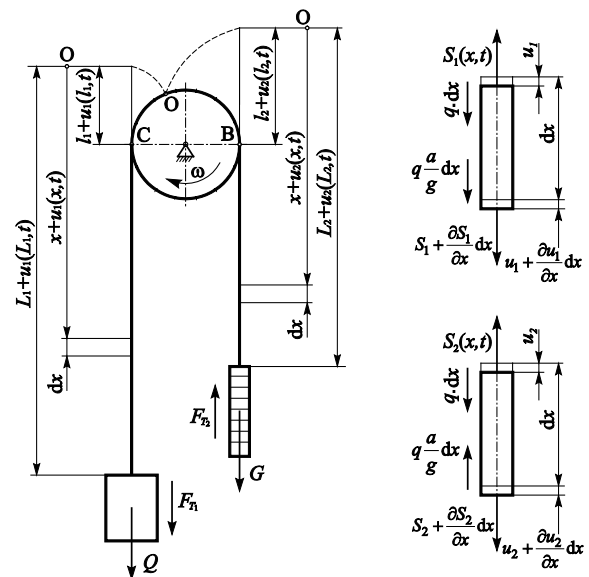


Figure 2: Dynamic model of vertical transport machines

The model takes into account the influence of the rope free length variations on both the incoming and outgoing pulley side. The variations in rope free length (shortening or lengthening) directly affect the rope stiffness, and therefore also the dynamic behavior of the

rope, which is of significant importance in the systems with high lifting velocities. The influence of elastic rope slipping over the driving pulley is considered through the adequate boundary conditions.

According to [5] and Fig. 2, on the basis of the equilibrium conditions for the elementary rope length and for the driving pulley, the following system of equations can be established:

$$\frac{q}{g} \cdot \frac{\partial^2 u_1(x,t)}{\partial t^2} = E \cdot A \cdot \frac{\partial^2}{\partial x^2} \left[ u_1(x,t) + b \cdot \frac{\partial u_1(x,t)}{\partial t} \right] + q \cdot \left( 1 \pm \frac{a}{g} \right) \quad (1)$$

$$\frac{q}{g} \cdot \frac{\partial^2 u_2(x,t)}{\partial t^2} = E \cdot A \cdot \frac{\partial^2}{\partial x^2} \left[ u_2(x,t) + b \cdot \frac{\partial u_2(x,t)}{\partial t} \right] + q \cdot \left( 1 \pm \frac{a}{g} \right) \quad (2)$$

$$M_m = \frac{R}{i \cdot \eta} \cdot E \cdot A \cdot \frac{\partial}{\partial x} \left\{ u_1(l_1,t) - u_2(l_2,t) + \frac{\partial}{\partial t} [u_1(l_1,t) - u_2(l_2,t)] - J_r \cdot \frac{a \cdot i}{\eta} \right\} \quad (3)$$

where:

$u_1, u_2$  - rope elastic deformations, m

$E$  - elasticity modulus, Pa

$b$  - damping parameter, Ns/m

$A$  - rope cross-section, m<sup>2</sup>

$a$  - driving mechanism acceleration, ms<sup>-2</sup>

$M_m$  - driving motor torque, Nm

$i$  - gear ratio,

$\eta$  - driving mechanism efficiency,

$J_r$  - moment of inertia of rotating masses, reduced to the pulley shaft, kgm<sup>2</sup>

$R$  - driving pulley radius, m

$q$  - rope weight pro meter, Nm<sup>-1</sup>

For solving the system of partial differential equations, (1) and (2), it is necessary to define the appropriate boundary conditions which depend on the previously mentioned parameters of the facility.

### 3. SUITABLE MODEL FOR THE DYNAMIC ANALYSIS OF VERTICAL TRANSPORT MACHINES

As it was mentioned before, the characteristic features of mine elevators are reflected in high lifting heights up to 2000 m and the velocity up to 20 m/s (max 19,2 m/s), [4]. This paper deals with Koepe system because the experiments were performed on a mine elevator in RTB Bor mine (Serbia). The basic dynamic model for this system is shown in Fig. 2. Nevertheless, if one looks at the regular operation of the facility, without the slipping of the steel rope in a driving pulley, and if as the driving characteristic is accepted rope velocity at the moment of rope upcoming the pulley (measuring the velocity of the pulley), the model of the mine elevator can be represented in the form shown in Fig. 3.

This model shows a system with longitudinal oscillations of a "heavy" steel rope with an infinite number of degrees of freedom (DOF), which is at one end wound onto a pulley at a velocity  $v(t)$ , while it is loaded with a concentrated mass on the other end. Forming a representative model for the analysis of dynamic behavior implies simplification of the model so as to exclude the small influences of the "higher" order and to keep only the most influential (representative) parameters [8]. In the process of vibration due to the varied length of the rope, joint stiffness, as a parameter of dynamic model, is changing which implies the occurrence of oscillations and resonances. These types of devices must have the occurrence of resonances prevented. This leads to defining the critical velocity of lifting which includes unstable

movements i.e. the increase of loads when the length of the rope is decreased, which this paper does not demonstrate.

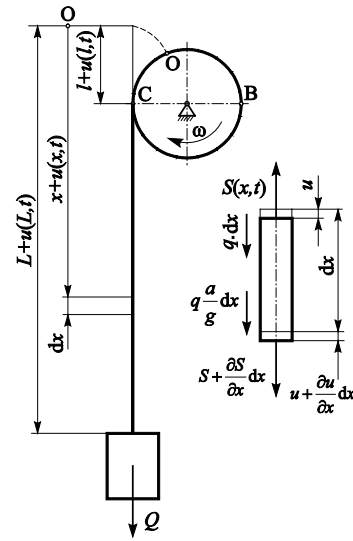


Figure 3: Oscillation of the constant length rope

#### 3.1. Reduction of the number of degrees of freedom

In accordance with previous considerations, deformation of the arbitrary cross section is represented as a function of position  $x$  and time  $t$ , i.e.:

$$u = f(x, t) \quad (4)$$

By observing the balance of the elementary part ( $dx$ ) it can be noted that:

$$\frac{q \cdot dx}{g} \cdot \frac{\partial^2 u(x,t)}{\partial t^2} = -S + S + \frac{\partial S}{\partial x} dx + q \cdot dx \pm \frac{q \cdot dx}{g} \cdot a \quad (5)$$

If the axial force  $S$  is described as a relative deformation function  $\varepsilon = \partial u / \partial x$ , for the case of damping oscillations:

$$S = E \cdot A \cdot \frac{\partial}{\partial x} \left[ 1 + b \cdot \frac{\partial}{\partial t} \right] \cdot \varepsilon \quad (6)$$

and if the (5) is divided with  $\frac{q \cdot dx}{g}$ , we get:

$$\frac{\partial^2 u(x,t)}{\partial t^2} = \frac{g \cdot E \cdot A}{q} \cdot \frac{\partial^2}{\partial x^2} \left( u(x,t) + b \cdot \frac{\partial u(x,t)}{\partial t} \right) + g - a \quad (7)$$

Boundary condition for rope incoming point on the pulley without slipping, Fig. 3 (point C), is given in the form:

$$u_1(l_1, t) = \int_0^t \frac{\partial u_1(l_1, t)}{\partial x} \left( \frac{dl_1}{dt} \right) \cdot dt \quad (8)$$

where:

$l_1$  - wound rope length, m

$dl_1/dt = v$  - winding velocity, ms<sup>-1</sup>

Boundary condition for the connection point of the rope with the elevator car or counterweight, when the friction forces between the sliding shoes and guiding rails are neglected, Fig. 3, is given as:

$$Q = E \cdot A \cdot \frac{\partial}{\partial x} \left( u_1(L_1, t) + b \cdot \frac{\partial u_1(L_1, t)}{\partial t} \right) + \left( \frac{Q}{g} \cdot \frac{\partial^2 u_1(L_1, t)}{\partial t^2} - a \right) \quad (9)$$

Partial differential equation (7) can be translated into the ordinary differential equations system by the variables separation method. Applying the method of particular integrals, e.g. [11], given as:

$$u(x,t) = X(x) \cdot T(t) \tag{10}$$

If we take  $\frac{g \cdot E \cdot A}{q} = c^2$ , where (c) is the propagation velocity of the elastic wave throughout the rope, the (10) is differentiated in time and place, and it is inserted in the simplified (9), so we perform the separation of the variables, and we get that:

$$\frac{\ddot{T}}{c^2(T + b \cdot \dot{T})} = \frac{X''}{X} = -k^2 \tag{11}$$

where (k) is the constant which is independent of time and position. That evolves into two common differential equations:

$$\begin{aligned} \ddot{T} + b \cdot k^2 \cdot c^2 \cdot \dot{T} + k^2 \cdot c^2 \cdot T &= 0 \\ X'' + k^2 \cdot X &= 0 \end{aligned} \tag{12}$$

A more detailed solving procedure of differential equations with boundary conditions is provided in [5]. The solution to the other equation defining the basic oscillation forms of specific harmonics is as follows:

$$X(x) = A_i \cdot \sin \beta_i \cdot \frac{x-l}{L-l} \tag{13}$$

where we get a frequency equation in the form of:

$$\beta_i \cdot \tan(\beta_i) = \alpha \tag{14}$$

where:

$$\begin{aligned} \beta_i &= k \cdot (L-l) \\ \alpha &= \frac{q \cdot (L-l)}{Q} \end{aligned}$$

- represents the weight ratio between the

rope's free length and the car.

For different ratios of the rope weight and the load it is possible to find the solutions for the transcendental equation (14) by using the calculation methods or graphically. It has an infinite number of roots, therefore the number of its own circular frequencies is indefinitely large.

The limiting values for  $\alpha$  (in the specific vertical transport system - mining elevator in RTB Bor mine) are given in Tab. 1. In the expression for  $\alpha$ , total length of wire ropes (L) is 540 m, when the cage at the lower level (horizon), i.e. 29 m when the cage at the upper level (on the ground). The value of (l) represents the wound length of hoisting ropes.

A small weight of the rope's free length in comparison to the concentrated mass greatly simplifies the analysis of the dynamic behavior of vertical transport machines.

Table 1: Boundary values for  $\alpha$

$\alpha$		Cage position	
		up	down
Cage state	empty	0.037	0.70
	loaded	0.022	0.41

Due to the fact that oscillation amplitudes of higher harmonics are rather small, their influence can be neglected, so the whole oscillation process, represented in (7) with an infinite number of DOF, whose collective oscillation form is shown in Fig. 4 as a broken line (d), can be satisfactorily accurate if replaced with a straight line (a), i.e. a system with one DOF with a constant dilatation ( $\epsilon$ ) down the free end of the rope.

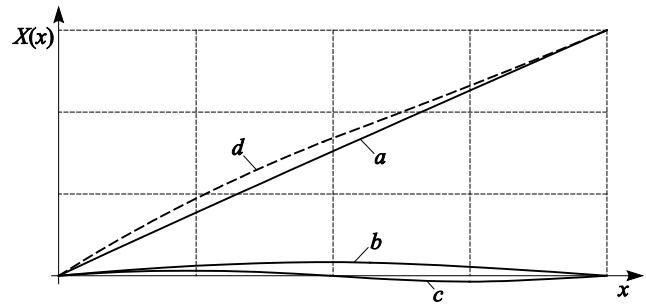


Figure 4: The oscillations forms of the first three harmonics (a, b, and c) and the collective oscillation form for  $\alpha=0.1$

The most numerical procedures have considerable limitations when it comes to solving realistic dynamic problems of vertical transport systems, especially since there is a need for transforming the partial into ordinary differential equations with nonholonomic boundary conditions. After analyzing the parameters for the mathematical model which describes longitudinal oscillations in the machines for vertical transport, it can be concluded that they are equations of a hyperbolic type, which leads to the rest of the paper focusing on the methods and manners of solving partial differential equations of the hyperbolic type.

### 3.2. Application of the finite difference method for solving of hyperbolic partial differential equations

Numerical solution is desirable even in the cases when there is a finite solution, but it's very complicated. We should bear in mind that the numerical solution of a differential equation is obtained in a quantitative form so that the analytical expression for the function remains unknown.

Numerical solving of a partial differential equation is generated in the form of a table of approximate values for the requested function  $u(x,y)$  for the equidistant values of independent variables. In order to explain it in the best way possible, we will show the numerical methods for solving the partial differential equations of the hyperbolic type, which are closely connected to the dynamic analyses of elevators and exploitation facilities, in mines especially.

#### ▪ Finite difference methods

The finite difference method for numerical solving of partial differential equations comprises:

- Discretization of the area (domain) of the independent variables,
- Approximation of partial derivatives with finite differences,
- Solving the resulting system of algebraic equations.

That means that the inside points of the area (mesh) satisfy the differential equation, and the points on the boundary of the area (domain) satisfy the boundary conditions.

The basic idea behind the finite difference method is in the replacement of derivatives of the considered function with their approximate values. In the realization of the idea we introduce points, i.e. mesh of nodes (hence the name – mesh method), where we look for the solution.

To consider the specific cases, such as elevators and exploitation facilities in mines, we are going to take a look at the one-dimensional partial differential equation of

the hyperbolic type of the second order, which corresponds to the problem described by (7):

$$\frac{\partial^2 u}{\partial t^2} - a(x,t) \frac{\partial^2 u}{\partial x^2} = f(x,t) \quad (15)$$

where  $a(x,t) > 0$  for every  $x$  and  $t > 0$ .

In the boundary area for the variable coordinate  $x$  (for instance a change in the length of the free rope end with the elevators where the total length is  $L$ ) we define the boundary conditions:

$$\begin{cases} u(0,t) = g_1(t) \\ u(L,t) = g_2(t) \end{cases} \quad \text{za } t > 0 \quad (16)$$

And also the initial conditions:

$$\begin{aligned} u(x,0) &= u_0(x), \quad x \in \{0,L\} \\ \left. \frac{\partial u}{\partial t} \right|_{(x,t=0)} &= v_0(x), \quad x \in \{0,L\} \end{aligned} \quad (17)$$

In which the second condition is known as the so-called Cauchy's condition.

If we introduce the  $a(x,t) = c^2$ , in which  $c$  represents the positive constant, then the general (analytical) solution for (15) is given in the form of:

$$u(x,t) = \frac{f(x+ct) + f(x-ct)}{2} + \frac{1}{2c} \int_{x-ct}^{x+ct} v_0(x) dx \quad (18)$$

For the sake of a more comprehensible explanation we will introduce signs  $N$  and  $K$ , representing the number of points in the spatial coordinate  $x$  and the number of points (divisions) per time coordinate  $t$ . For that reason the function  $u(x,t)$  changes into the form of  $u_n^k$ . By introducing the extra signs:

$$-\frac{1}{2} \lambda a_n^{k+1} u_{n-1}^{k+1} + (1 + \lambda a_n^{k+1}) u_n^{k+1} - \frac{1}{2} \lambda a_{n+1}^{k+1} u_{n+1}^{k+1} = \frac{1}{2} \Delta t^2 (f_n^{k+1} + f_n^{k-1}) + 2u_n^k - \left[ \frac{\lambda}{2} a_n^{k-1} u_{n-1}^{k-1} - (1 - \lambda a_n^{k-1}) u_n^{k-1} + \frac{\lambda}{2} a_n^{k-1} u_{n+1}^{k-1} \right] \quad (23)$$

According to (23), in order to reach the solution, we also have to know the field (values) in  $(k-1)$  points. This is enabled by the initial conditions (21). Using the development in Taylor's order per  $t$  we get:

$$u_n^k = u_n^{k-1} + \left. \frac{\partial u}{\partial t} \right|_{k-1} \Delta t + \frac{1}{2} \left. \frac{\partial^2 u}{\partial t^2} \right|_{k-1} \Delta t^2 \quad (24)$$

All that is needed is to determine the  $u_n^1$ , in which we write the following according to (15):

$$\begin{aligned} u_n^1 &= u_n^0 + v_n^0 \Delta t + \frac{1}{2} f_n^0 \Delta t^2 + \\ &+ \frac{1}{2} \lambda a_n^0 (u_{n+1}^0 - 2u_n^0 + u_{n-1}^0) \quad \text{za } (1 \leq n \leq N-1) \end{aligned} \quad (25)$$

By taking into consideration a special case (homogenous differential equation where  $f(x,t) = 0$  and

$$\begin{bmatrix} (1+\alpha) & -\frac{1}{2}\alpha & 0 & 0 \\ -\frac{1}{2}\alpha & (1+\alpha) & -\frac{1}{2}\alpha & 0 \\ 0 & -\frac{1}{2}\alpha & (1+\alpha) & -\frac{1}{2}\alpha \\ 0 & 0 & -\frac{1}{2}\alpha & (1+\alpha) \end{bmatrix} \cdot \begin{bmatrix} u_1^{k+1} \\ u_2^{k+1} \\ u_3^{k+1} \\ u_4^{k+1} \end{bmatrix} = \begin{bmatrix} 2u_1^k + \frac{1}{2}u_2^{k-1} - (1+\alpha)u_1^{k-1} \\ 2u_2^k + \frac{1}{2}u_3^{k-1} - (1+\alpha)u_2^{k-1} + \frac{1}{2}\alpha u_1^{k-1} \\ 2u_3^k + \frac{1}{2}u_4^{k-1} - (1+\alpha)u_3^{k-1} + \frac{1}{2}\alpha u_2^{k-1} \\ 2u_4^k + \frac{1}{2}u_3^{k-1} - (1+\alpha)u_4^{k-1} \end{bmatrix} + \begin{bmatrix} \frac{1}{2}\alpha(u_0^{k-1} + u_0^{k+1}) \\ 0 \\ 0 \\ \frac{1}{2}\alpha(u_5^{k-1} + u_5^{k+1}) \end{bmatrix} \quad (27)$$

$$x_n = n \cdot \frac{L}{N}, \quad t_k = k \cdot \frac{T}{K} \quad (19)$$

where:

$$0 \leq n \leq N, \quad 0 \leq k \leq K$$

$L$  - total spatial coordinate (length),

$T$  - total (final) integration time,

And then the boundary and initial conditions become:

$$\begin{cases} u_0^k = g_1(t_k) \\ u_N^k = g_2(t_k) \end{cases} \quad 0 \leq k \leq K \quad (20)$$

$$\begin{cases} u_n^0 = u_0(x_n) \\ \left. \frac{\partial u}{\partial t} \right|_{n,0} = v_0(x_n) \end{cases} \quad 0 \leq n \leq N \quad (21)$$

By using the central difference theory and by replacing the suitable derivatives in time and place coordinate  $x$ , it can be written that, [10]:

$$\begin{aligned} \frac{\partial^2 u}{\partial t^2} &= \frac{u_n^{k+1} - 2u_n^k + u_n^{k-1}}{\Delta t^2} \\ \frac{\partial^2 u}{\partial x^2} &= \frac{1}{2} \left( \frac{u_{n+1}^{k+1} - 2u_n^{k+1} + u_{n-1}^{k+1}}{\Delta x^2} + \frac{u_{n+1}^{k-1} - 2u_n^{k-1} + u_{n-1}^{k-1}}{\Delta x^2} \right) \end{aligned} \quad (22)$$

where:

$$\Delta t = T/K \quad \text{and} \quad \Delta x = L/N.$$

By introducing the sign (abbreviation)  $\lambda = \frac{\Delta t^2}{\Delta x^2}$ , we get

the system for  $(N-1)$  equations as a replacement for the partial differential equation in the area from  $(k+1)$  points per time. In order to solve the system, we have to know the field at the  $(k+1)$  point.

using the already mentioned positive constant  $a(x,t) = c^2$ , we get a simple system of algebra equations:

$$\begin{aligned} (1+\alpha)u_n^{k+1} - \frac{1}{2}\alpha u_{n+1}^{k+1} - \frac{1}{2}\alpha u_{n-1}^{k+1} &= \\ = 2u_n^k + \frac{1}{2}\alpha u_{n+1}^{k-1} - (1+\alpha)u_n^{k-1} + \frac{1}{2}\alpha u_{n-1}^{k-1} \end{aligned} \quad (26)$$

where:

$$\alpha = c^2 \frac{\Delta t^2}{\Delta x^2}$$

Equation (26) represents an excellent form and basis for solving such problems in a numerical way in contemporary software tools, such as MATLAB, Mathcad, Mathematica and so on.

Primarily, this can be concluded by conveying it to its matrix form. The example given is for  $N = 5$ :

Where boundary conditions have been set apart through the last vector column on the right side of the equivalence.

Matrix equation (27) presents a system which results in defining the vector  $(u_1^{k+1} u_2^{k+1} u_3^{k+1} u_4^{k+1})$ , and implies the understanding of vector given from the following equation  $k = 1$  :

$$u_n^1 = u_n^0 + v_n^0 \Delta t + \frac{1}{2} \alpha (u_{n+1}^0 - 2u_n^0 + u_{n-1}^0), \text{ for } (1 \leq n \leq N) \quad (28)$$

Graphic presentation of the solution of hyperbolic partial differential equation (wave equation in special forms) is in the Fig. 5.

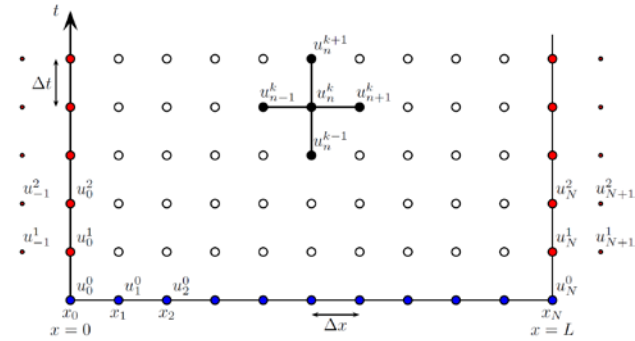


Figure 5: Description of the grid with the equation of hyperbolic type with boundary and initial conditions

Terminology (22), (23) and (26), as well as the matrix (27) present so called implicit method of the finite differences.

The simplistic method for using is the so called explicit method, according to which the finite differences (22) have the form:

$$\frac{\partial^2 u}{\partial t^2} = \frac{u_n^{k+1} - 2u_n^k + u_n^{k-1}}{\Delta t^2} \quad (29)$$

$$\frac{\partial^2 u}{\partial x^2} = \frac{u_{n+1}^k - 2u_n^k + u_{n-1}^k}{\Delta x^2}$$

Where the result of the equation (15), for  $f(x, t) = 0$ , is presented in explicit form as:

$$u_n^{k+1} = 2u_n^k - u_n^{k-1} + \alpha (u_{n+1}^k - 2u_n^k + u_{n-1}^k) \quad (30)$$

i.e.:

$$u_n^{k+1} = 2(1 - \alpha)u_n^k + \alpha (u_{n+1}^k + u_{n-1}^k) - 2u_n^{k-1} \quad (31)$$

where:

$\alpha = c^2 \frac{\Delta t^2}{\Delta x^2}$  - introduces abbreviation, as it is in the implicit method.

Punctuality, as well as stability of the calculating process and the criterion for stability in the explicit method, with numerical integration, depend on the size of time range in:

$$\sqrt{\alpha} = c \cdot \frac{\Delta t}{\Delta x} \leq 1 \quad (32)$$

known as Courant-Friedrichs-Lewy (CFL) condition.

In order to get high accuracy of the result (small range  $\Delta x$ ), it has been noted that a small time range  $\Delta t$  is essential to secure stability, which makes the explicit method ineffective.

In relation to the explicit method, the advantage of the implicit method is its absolute stability - no matter the size of the time range. However, the setback is that it is

more complex and therefore requires tridiagonal system of algebraic equations solving in any time range.

#### 4. APPLICATION OF THE FINITE DIFFERENCE METHOD ON MINING ELEVATORS

This chapter is providing the steps for solving the movement differential equations (oscillations) of the load with the hoisting element (rope) which is in a stick form (the "heavy" rope) of a constant length. It is possible to be approximately determined as oscillations with one degrees of freedom, with a "heavy" spring. However, the problem can be modelled even more accurately as a system with an infinite number of degrees of freedom (longitudinal stick oscillation) with the suitable boundary conditions.

When it comes to longitudinal oscillations of the great mass ropes, all the particles within the rope are moving parallel to the rope axis. The elongation is repeated one after the other with the time  $t$  and spatial coordinate  $x$ .

Fig. 6 shows the "heavy" rope with the load at its end. This model generally can be used as a representation of the exploitation facility in mines at the moment when the cage stops and it starts to oscillate freely (if we ignore the friction in guide rails).

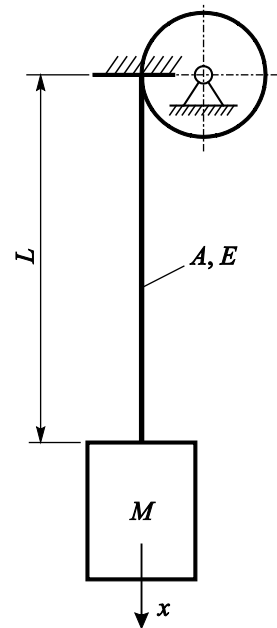


Figure 6: Model of the "heavy" rope with the load (cabin, cage) at its end

The starting parameters for the dynamic model analyses in Fig. 6 are:

$L = 500$  m - the total free length of the ropes at the moment of stopping the cage,

$M = 30$  t - reduced oscillation mass,

$A = 1700$  mm<sup>2</sup> - total metal cross-section area of ropes,

$E = 1,3 \cdot 10^5$  MPa - rope elasticity modulus for the chosen parameters.

The data (suggested parameters) are acquired for a specific mine elevator obtained through measurements and later determination of certain dynamic parameters.

A movement differential equation is a hyperbolic partial differential equation described in (15) for  $f(x, t) = 0$  and  $a(x, t) = c^2$ , which is expressed as:

$$\frac{\partial^2 u}{\partial t^2} - c^2 \frac{\partial^2 u}{\partial x^2} = 0 \quad (33)$$

With constant  $c$  being equal to:

$$c^2 = \sqrt{\frac{E}{\rho}}$$

And it stands for how fast the waves are spreading, whereas  $\rho = 7,86 \text{ t/m}^3$  is the thickness of the wire materials in the driving ropes.

Boundary conditions are defined for the rope's ends. At the upper end, if  $x=0$ , based on expression (16), the first boundary condition would be:

$$u(0, t) = 0 \quad (34)$$

The second boundary condition is gained for the lower part of the rope, where it is connected to the load. Based on the expressions in [11] and the applied method of separating the variables, it is confirmed that the second boundary condition is:

$$\frac{\partial u(L, t)}{\partial x} - \frac{M \cdot k^2}{A \cdot \rho \cdot c^2} u(L, t) = 0 \quad (35)$$

Where constant  $k$  in this case equals, [11]:

$$k = (2m-1) \frac{\pi}{2 \cdot L}, \quad (m=1, 2, 3, \dots)$$

The "heavy" rope is initially burdened with the load ( $M \cdot g$ ), so its end is stretched for [11]:

$$\Delta L = \frac{M \cdot g \cdot L}{E \cdot A}$$

And we observe the other parts in a linear manner:

$$u(x, 0) = \frac{\Delta L}{L} \cdot x = \frac{M \cdot g}{E \cdot A} \cdot x \quad (36)$$

This expression represents the first initial condition. The second initial condition is obtained with the assumption that the system was still at first, i.e. all the parts of the "heavy" rope had the zero velocity.

$$\frac{\partial u(x, 0)}{\partial t} = 0 \quad (37)$$

Solution for the movement differential equation (oscillation) of the "heavy" rope has been gained with the finite difference method in MATLAB software package, by using the explicit method for solving the equations of the hyperbolic type.

The results shown in Fig. 7 were obtained by using the mentioned boundary and initial conditions, with the second initial condition (37), taking that  $v_n^0 = 0$ .

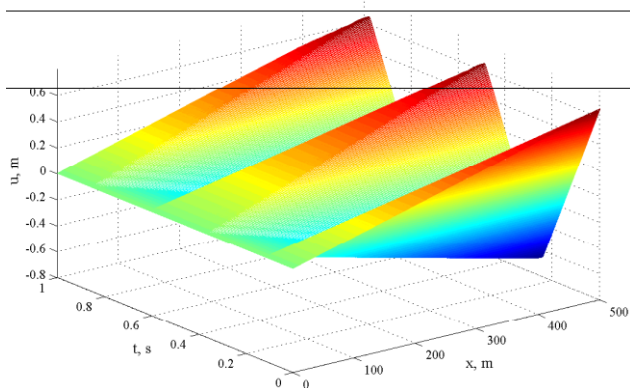


Figure 7: How elongation depends on the time ( $t$ ) and space coordinate ( $x$ )

#### 4.1. Application of specialized software systems for the vertical transport machines analysis

Owing to problems and restrictions in the software MATLAB application for differential equations solving systems with variable (nonholonomic) boundary conditions has its limits, the only solution lies in the application of specialized software systems for dynamic analysis. One of the software systems, which is especially suitable for the analysis of system's dynamic behavior in the mechanism form, is the software MSC ADAMS.

Complete separation analysis of the dynamic behavior for the cage side as well as for the counterweight side can be executed if the regular cases of the vertical transport device have been observed. Those devices do not contain any rope sliding at a driving pulley (the modification of the hoisting velocity is defined). Further text will demonstrate the analysis of the dynamic behavior of the elements for the cage.

The conception of the dynamical model accepted represents the model of the wire rope as the hoisting element with the damping spring (Calvin's model), which is, on one end, joined to the beam of specific stiffness which presents the upper beam of the cabin (cage), and on the other end, it is joined to the solid component that is driven by the electric motor, Fig. 8a.

The cabin frame can be modelled using concentrated weights which represent the weights of the certain upper beam of the cabin frame, connected with beams (Massless Beam), Fig. 8b.

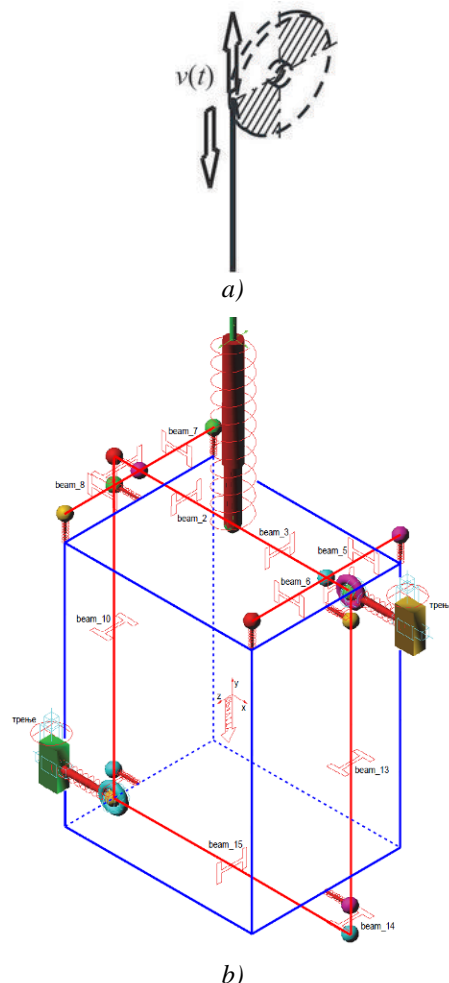


Figure 8: Computer model of elevators

The drive characteristic is represented through setting the velocity, i.e. changing the number of rotations in a driving pulley. In this paper, the velocity is set in the form of „spline“ (Fig. 9), which is unambiguous when it comes to describing the changes in the rotations number in a driving electric motor which is reduced to the circumferential velocity on the drum, i.e. driving pulley, obtained through an incremental encoder during the measurements performed on a mining elevator.

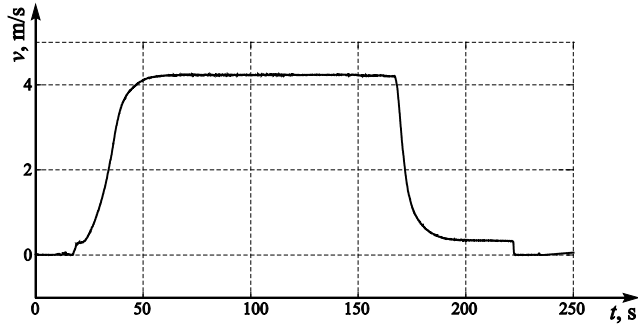


Figure 9: Changing of velocity as a driving characteristic on the pulley

As an illustration of the possibilities of dynamic analysis, the following figures show the diagrams for changes in certain values, done in MSC ADAMS software, while using the real experimental data.

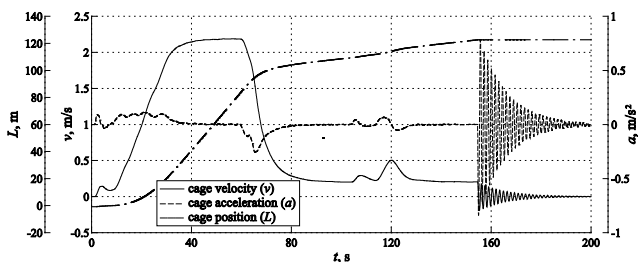


Figure 10: Diagrams of the change in cage position, velocity and acceleration

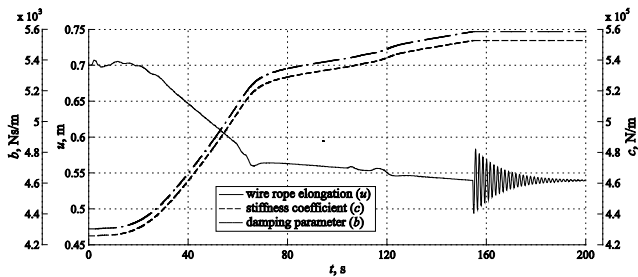


Figure 11: Diagrams of the change in hoisting ropes elongation, stiffness coefficient and damping parameter

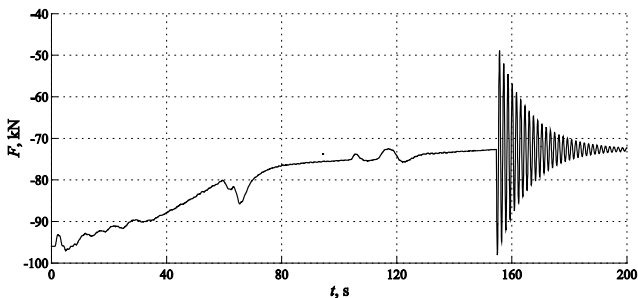


Figure 12: Diagram of the force in ropes changing

The given part of the research points and analysis results out the possibilities to analyze the impact of variable stiffness ( $EA/L$ ) and movement velocity

(nonholonomic boundary condition at the point where rope comes to the pulley) on vertical transport systems at great lifting velocities, which was not possible to do using the mentioned numerical methods.

### 5. CONCLUSION

By analyzing the parameters of a concrete exploitation facility it is possible to simplify a dynamic model to a great extent if we omit the small values of the higher order and gain the suitable model for a dynamic analysis.

For driving mechanisms used for vertical load lifting (elevators and cranes), it is necessary to provide adequate conditions for the correct dynamic analysis of their parts' behavior and especially for the rope as the basic element, already in the design phase. Due to a significant influence of rope free length changes, due to its slipping over the driving pulley and for the reason of its mechanical characteristics, it is impossible to apply a classical dynamic model of longitudinal oscillations for homogenous stick of a constant length, especially by the elevators with large velocities and large lifting heights (express and mine elevators).

The system of partial differential equations of the hyperbolic type is possible to be solved by using the numerical methods (MATLAB), but only in the cases after stopping (braking) the driving mechanism. In that case we trust the stiffness suits the current values of the rope's free length as a constant size with the suitable boundary conditions. In order to do the analysis of the dynamic behavior of the system during the movement (variable stiffness and nonholonomic boundary conditions) it is necessary to apply the specialized software packages with specifically defined (adjusted) parameters of dynamic models that can be obtained through measuring at vertical transport real systems.

### REFERENCES

- [1] J. Bao, P. Zhang, C. Zhu, "Computing Simulation and Dynamics Modeling of Flexible Hoisting Rope with Time-varying Length", Journal of Computational Information Systems, Vol. 8(10), pp. 4177–4184, (2012)
- [2] R. Đokić, J. Vladić, D. Živanić, "Standard dynamic models of machines for vertical transport and its modeling"; IMK-14 – Research and development in Heavy Machinery, Vol. 22, No. 3, Institut IMK "14. oktobar", Kruševac, pp. EN75-80, (2016)
- [3] M. Pakdemirli and A.G. Ulsoy, "Stability analysis of an axially accelerating string", Journal of Sound and Vibration 203, 5, pp 815-832, (1997)
- [4] J. Vladić, M. Jovanović, R. Đokić, M. Kljajin, M. Karakašić, "Theoretical and experimental analysis of elevator dynamic characteristics", Tehnički vjesnik/Technical Gazette, Vol. 22, No. 4, July – August 2015, pp. 1011-1020, (2015)
- [5] J. Vladić, P. Malešev, R. Šostakov, N. Brkljač, "Dynamic analysis of the load lifting mechanisms", Strojniški Vestnik/Journal of Mechanical Engineering, Vol. 54, No. 10, pp. 655-661, (2008)

- [6] R. Đokić, J. Vladić, A. Gajić, D. Živanić, "Numerical analysis of elevator ropes vibration with time varying length", The Eighth International Conference HEAVY MACHINERY-HM 2014, Zlatibor, Serbia, 25-28 June 2014., pp. A.119-124, (2014)
- [7] M. Bertolino, "Diferencijalne jednačine", Naučna knjiga Beograd, (1980), (In Serbian)
- [8] Z. Li, Z. Qiao, T. Tang, "Numerical solution of partial differential equations – an introduction to finite difference and finite element methods", Center for research and scientific comput. & Department of mathematics, North Carolina State University, (2011)
- [9] A. Goroshko, G. Savin, "Vvedenie v mehaniku deformirujemych tel peremennoj dliny", Naukova dumka, Kiev, (1971), (In Russian)
- [10] A.R. Mitchell, D.F. Griffiths, "The Finite Difference Method in Partial Differential Equations", John Wiley & Sons, Inc. Chichester, (1980)
- [11] B. Vujanović, "Teorija oscilacija", Univerzitet u Novom Sadu, (1995), (In Serbian)
- [12] R. Đokić, "Dynamics researching and development of vertical transport machines using numerical-experimental procedures", PhD Thesis, University of Novi Sad, (2016)
- [13] A. Xavier, "Study in finite difference methods III: wave equation by the implicit method", Technical Educational Note #03, (2014)



# Geometrical Identification of Cylindrical Carrier of Axial Bearings with Big Diameters

Milomir Gašić<sup>1\*</sup>, Mile Savković<sup>1</sup>, Goran Marković<sup>1</sup>, Nebojša Zdravković<sup>1</sup>, Srđan Ribar<sup>2</sup>

<sup>1</sup>Faculty of Mechanical and Civil Engineering in Kraljevo, University of Kragujevac, Kraljevo (Serbia)

<sup>2</sup> Faculty of Mechanical Engineering, University of Belgrade, Belgrade (Serbia)

*The paper deals with the analysis of deformation of cross section of cylindrical carrier of axial bearings with big diameters at portal cranes. Fundamental theory on calculating plates and shells with restrictions about proper function of these bearings, helps to define relations for determining required height of cylindrical carrier with the following conditions being met: first, the change of cylindricality of upper part has to be as small as possible; second, movements of supporting points of support surface for connecting axial bearing must not exceed the allowed value. Finally, the expressions for determining height of cylindrical carriers are presented and they can be used by construction engineers when designing optimal connection between rotating platform and carrying structure of portal cranes through axial bearings having big diameters.*

**Keywords:** Cylindrical carrier, Axial bearing, Deformation, Allowed movement, Carrier height

## 1. INTRODUCTION

Application of axial bearings with big diameters is widely used in means of transport mechanization, especially in portal cranes (Figure 1). The bearing (3) (Figure 2) connects the rotating platform (2) with the cylindrical carrier (4) of the carrying structure (5) in the portal crane. Platform is rotated by planetary reducer (1).



Figure 1: Portal crane with axial bearing

Structural designs of portal carrying structures with stiff cylindrical carrier and flexible upper and lower

portal elements offer an opportunity to partially eliminate the influence of roughness of tracks on elimination of deviation from horizontal supporting areas of cylindrical carrier to which axial bearing is screwed. When external loads, in the form of moment  $M$ , axial forces  $F_a$  and radial forces  $F_r$ , are conveyed primarily in the boom plane, there is angular turning of the segments of supporting areas of cylindrical carrier.

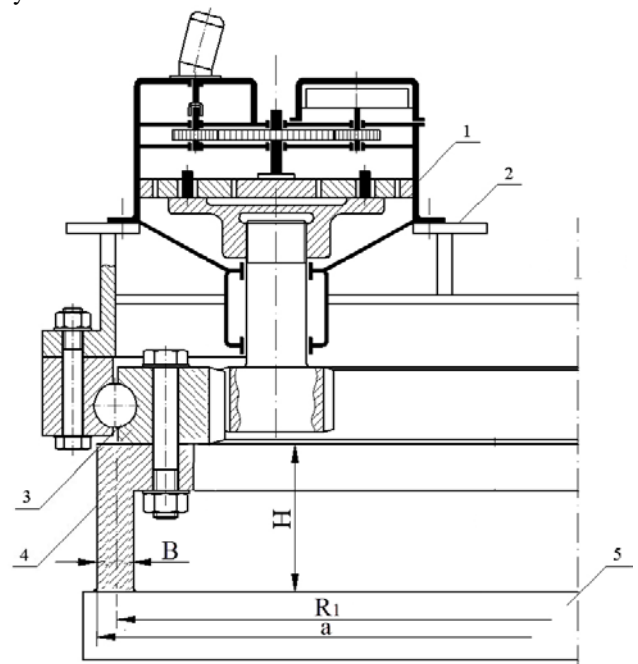


Figure 2: Axial bearing with cylindrical carrier

The angular turning of cross section of cylindrical support has to be within the limits in order to provide safe and reliable operation of the axial bearing.

## 2. THEORETICAL FUNDAMENTALS ON CALCULATING CYLINDRICAL CARRIERS

If theoretical fundamentals on plates and shells are applied [1], we can define with great accuracy the

height of cylindrical carrier  $H$  (Figure 2) which results in considerable decrease of deformation of supporting area of cylindrical carrier over which the axial bearing lies. Cylindricity is not changed [2] if the dependence is defined:

$$\beta \cdot H \geq 3 \quad (1)$$

The parameter  $\beta$  is calculated from the following relation:

$$\beta = \sqrt[4]{\frac{3(1-\nu^2)}{B^2 \cdot R_1^2}}$$

where:

$H$  – height of cylindrical carrier,  
 $\nu$  – Poisson quotient ( $\nu = 0.3$  for steel),  
 $R_1$  – curve radius of cylindrical carrier,  
 $B$  – thickness of cylindrical carrier.

Expression (1) gives the smallest height  $H$  at which the change of carrier cylindricity is not practically conveyed from the lower part to the upper part:

$$H \geq \frac{3\sqrt{R_1 \cdot B}}{\sqrt[4]{(1-\nu^2)}} \quad (2)$$

After substituting values of  $\nu$ , we get [1]

$$H \geq 2,5\sqrt{R_1 \cdot B} \quad (3)$$

The analysis of derived constructions, for the relation between radius and thickness of cylindrical carrier  $R_1 / B = 20 \div 30$ , results in

$$H \geq (0,45 \div 0,56)R_1 \quad (4)$$

The external loads  $M$ ,  $F_a$  and  $F_r$ , which are transferred to the cylindrical carrier through the axial bearing, have various influences on turning of the cross section on the cylindrical carrier (Figure 3).

Due to small dimensions of axial bearing sections, their stiffness can be ignored in further analysis.

As Figure 3a shows, the axial force  $F_a$  is equally transferred along the periphery of cylindrical carrier. At portals with four legs the quarter of the value  $F_a$  loads the cylindrical carrier causing the turning of its cross section which is defined by turning angle  $\varphi$ :

$$\varphi_{F_a} = \frac{F_a(a-R_1) \cdot R_1^2}{8\pi R_1 EI_x} = \frac{F_a(a-R_1) \cdot R_1}{8\pi EI_x} \quad (5)$$

Load caused by the moment  $M$  (Figure 3b) can be replaced with the couple  $2F_M R_1$ , so the moment force being transferred through the cylindrical carrier causes turning of its cross section for the angle  $\varphi_M$ :

$$\varphi_M = \frac{M(a-R_1) \cdot R_1^2}{4R_1^2 \pi EI_x} = \frac{M(a-R_1)}{4\pi EI_x} \quad (6)$$

Total angular turning of the cross section of the cylindrical carrier is:

$$\varphi = \varphi_{F_a} + \varphi_M = \frac{F_a(a-R_1) \cdot R_1}{8\pi EI_x} + \frac{M(a-R_1)}{4\pi EI_x} \quad (7)$$

$$\varphi = \frac{(a-R_1)}{4\pi EI_x} \left[ \frac{F_a R_1}{2} + M \right]$$

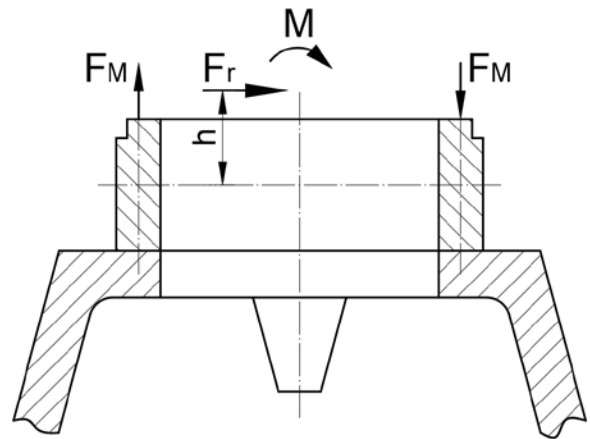
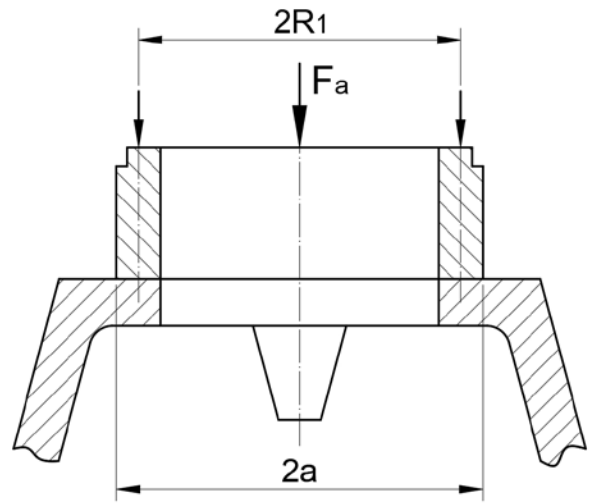


Figure 3: Loads transferred from the axial bearing to the cylindrical carrier

The radial force  $F_r$  (Figure 2b) acts on the small arm  $h$ , so its influence on the turning of the cylindrical carrier section is negligible.

Movements of supporting points of the cylindrical carrier in the vertical direction  $\Delta$  can be defined through the turning angle of the cross section:

$$\Delta = a \cdot \varphi \quad (8)$$

but the movement has to be smaller or equal to maximally allowed movement  $\Delta_{max}$  whose value for the axial bearing with big diameters is as follows [4]:

$$\Delta_{max} = 0,1mm \text{ for the diameter of } 1m \quad (9)$$

Defined relation (9) provides proper function and long lifetime.

After substituting (7) into (8) and having in mind the restriction (9), it follows:

$$\frac{(a-R_1)}{4\pi EI_x} \left[ \frac{F_a R_1}{2} + M \right] \leq \frac{\Delta_{max}}{a} \quad (10)$$

The moment of inertia for the right-angled cross section of the cylindrical carrier is defined by the following expression:

$$I_x = \frac{BH^3}{12} \quad (11)$$

When expression (11) is taken into expression (10) and when respective figures are reduced and rounded, we get the formula for calculating the height of the cylindrical carrier:

$$H \geq \sqrt[3]{\frac{a(a-R_1) \left[ \frac{F_a R_1}{2} + M \right]}{\Delta_{\max} \cdot E \cdot B}} \quad (12)$$

For a portal crane having:

$$F_a = 16000 \text{ kN}, \text{ and}$$

$$M = 575000 \text{ kNcm}$$

the adopted axial bearing has the following basic parameters (Figure 4) [3]:

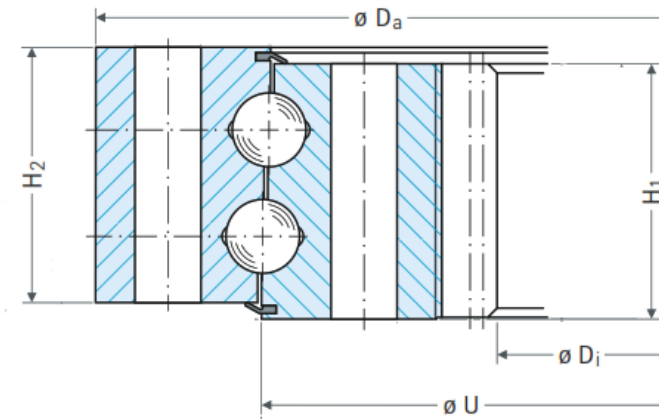


Figure 4: Axial bearing

External diameter of supporting ring  $U = 2915 \text{ mm}$ ,

Internal diameter of supporting ring  $D_i = 2715 \text{ mm}$ ,

Height of internal ring  $H_1 = 117 \text{ mm}$ ,

Height of external ring  $H_2 = 150 \text{ mm}$

These parameters are used to define the radii of the cylindrical carrier and its thickness:

$$a = 1500 \text{ mm},$$

$$R_1 = 1470 \text{ mm},$$

$$B = 60 \text{ mm}.$$

Now we can determine the height of the cylindrical carrier by expression (12):

$$H \geq \sqrt[3]{\frac{a(a-R_1) \left[ \frac{F_a R_1}{2} + M \right]}{\Delta_{\max} \cdot E \cdot B}}$$

$$H \geq \sqrt[3]{\frac{150(150-147) \left[ \frac{16000 \cdot 147}{2} + 575000 \right]}{2,915 \cdot 0,01 \cdot 2,1 \cdot 10^4 \cdot 6}}$$

$$H \geq 47,44 \text{ cm} \sim 50 \text{ cm}$$

Cylindrical carriers of axial bearings with big diameters (more than 3m) are made of thinner plates in the form of box-like cross section.

If the thicknesses of horizontal and vertical steel plates of which the cylindrical carrier is made are equal, i.e. if  $\delta_1 = \delta_2 = \delta$ , then the moment of inertia of the cross section (Figure 5) is defined by the following expression:

$$I_x = \frac{\delta(H+\delta)^3}{6} + \frac{(B-\delta)\delta H^2}{2} \quad (13)$$

where:

H – height of the cylindrical carrier,

B – width of the cylindrical carrier,

$\delta$  – thickness of the plates.

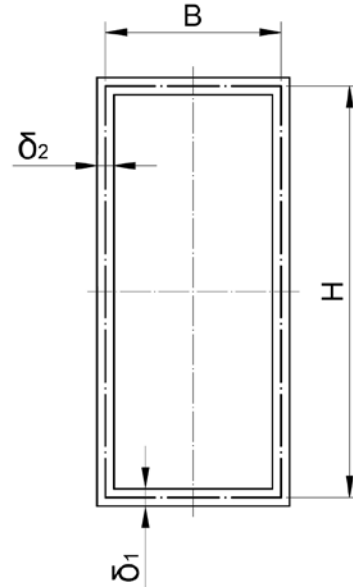


Figure 5: Cross section of the box-like cylindrical carrier

If the elements with the multipliers  $\delta^3$  and  $\delta^4$  are neglected, the expression (13) leads to the simplified expression for the moment of inertia of the box-like cross section, which is more acceptable in engineering practice:

$$I_x = \frac{\delta H^3}{6} + \frac{\delta H^2 B}{2} = \frac{\delta H^2}{2} \left( \frac{H}{3} + B \right) \quad (14)$$

To define loads of the mentioned portal crane ( $F_a$  and  $M$ ) and geometrical parameters of axial bearing  $a$  and  $R_1$ , the moments of inertia are connected through expressions (10) and (14) so it follows:

$$I_x \geq \frac{a(a-R_1)(F_a R_1 + 2M)}{8\pi E \Delta_{\max}} = \frac{\delta H^2}{2} \left( \frac{H}{3} + B \right) \quad (15)$$

If the relation between the width and height of the cross section of box-like carrier is  $B = H/5$ , the minimum height of cylindrical carrier can be defined by the expression (15):

$$H \geq \sqrt[3]{\frac{a(a-R_1)(F_a R_1 + 2M)}{2\pi E \Delta_{\max} \delta}} \quad (16)$$

In the concrete case, after replacing the values into expression (16) and if  $\delta = 1.0 \text{ cm}$ , it follows that  $H \geq 75 \text{ cm}$ .

### 3. CONCLUSION

The selection of axial bearing with big diameter which connects the rotating platform and carrying structure of portal cranes, enables us to calculate the needed height of the cylindrical carriers of the bearings.

The constructed analysis leads to the conclusion that in geometrical identification of cylindrical carrier its height should have the value which does not change the cylindricality of carrier and deviations of supporting points of the area for bearing connection should not exceed allowed values. If the carrier height is calculated this way, lifetime of the bearing is significantly increased.

### ACKNOWLEDGEMENTS

This paper is the result of the project number TR35038, financed by the Ministry of Education, Science and Technological Development of the Republic of Serbia.

### REFERENCES

- [1] С.В. Бояршинов: Основы строительной механики машин, МАШИНОСТРОЕНИЕ, Москва, 1973.
- [2] Milomir Gašić, Mile Savković, Goran Marković, Nebojša Zdravković: Research and Development of Carrying Structure of Radial-axial Bearing of Construction and Transport Machines, The Sixth International Symposium about forming and design in mechanical engineering KOD2010, 29-30 September 2010, Palić, Serbia
- [3] Rothe Erde GmbH, bearings catalogue
- [4] П.З. Петухов., Г.П. Ксюнин, Л.Г. Серлин: Специальные краны, МАШИНОСТРОЕНИЕ, Москва, 1985.

# Design Optimization of the Rectangular Box Section of the Double Beam Bridge Crane Using Matlab Optimization Toolbox

Goran Pavlović<sup>1\*</sup>, Mile Savković<sup>2</sup>, Nebojša Zdravković<sup>2</sup>, Vladimir Kvrđić<sup>1</sup>, Stefan Mitrović<sup>1</sup>

<sup>1</sup>Institute Lola, Belgrade (Serbia)

<sup>2</sup>Faculty of Mechanical and Civil Engineering Kraljevo, University of Kragujevac, Kraljevo (Serbia)

*The paper considers the problem of optimization of the rectangular box section of the double beam bridge crane. Reduction of the girder mass is set as the objective function. The constrained optimization applied in Matlab Optimization Toolbox was used as the methodology for determination of optimal geometrical parameters of the rectangular box section. The criteria of permissible stresses, local buckling of plates, static deflection, permissible period of oscillation, minimum plate thickness and production feasibility were applied as the constraint functions. Verification of the used methodology was carried out through numerical examples and the comparison with some existing solutions of cranes was made. Numerical result shown that the mathematical model of optimization was exact and the algorithm effective.*

**Keywords:** Double beam bridge crane, Eurocodes, Matlab Optimization Toolbox, Optimization, Rectangular box section

## 1. INTRODUCTION

Double beam bridge cranes are very much present in industry plants, and all of which are intended for lifting and transportation of large loads and for larger spans. The mass of the girders has the largest share in the total mass of the double beam bridge crane, and that is the reason why it is very important to reduce it in order to obtain a lighter structure, which also reduces the market price of the crane.

There are a large number of papers which deal with the problem of analysis of stresses of main girders of cranes as well as with their optimization. Most papers treat the problem of optimization or stress analysis of the main girder of the bridge crane.

Most authors set permissible stress or permissible stress and permissible deflection as the constraint functions. The criteria of lateral stability, local buckling of plates and permissible period of oscillation have lately been increasingly applied as the constraint functions.

Matlab software is a very effective tool in the optimization procedures, particularly in engineering practice, as is the case with the main girders of the bridge cranes. Application of Matlab software in optimization of the main girder of the single-girder bridge crane is shown in [01]. The single-girder crane is loaded with two loaded trolleys. The performed optimization showed there can be savings in the mass of the main girder, using Matlab Graphical User Interface (GUI). Optimization of geometric parameters of different types of cross-sectional shapes of the main girders of the double beam bridge cranes is shown in [02], using the multi-criteria optimization process in Matlab software. Application of Matlab Optimization Toolbox in optimization of the section of the prestressed steel-concrete composite box girder is shown in [03]. The price of the girder is significantly reduced for a concrete example.

In most cases, the optimization of the girders is performed by FEA. In the paper [04], manual and FEA report for plates buckling is presented to reduce overall weight and cost of the main girder of the bridge cranes. Results obtained from FEM, manual calculations and experimental analysis.

The paper [5] carried out the analysis of local buckling of plates and rigidity of the bridge cranes by using Polish standards, which were later compared with the results of analysis performed according to European standards, using Ms Excel software and FEM. The paper [6] performed topology optimization of the main girder of the double beam crane using by Optistruct solver tool in HyperWorks software, according to the criteria of strength, stiffness and lateral stability. 3D model was made in Pro/E software. The mass of the girder is reduced by 21.16%. Similarly to previous, the paper [07] carried out optimization of the geometrical characteristics (thickness, height and width) of the box girders of the bridge crane using by Patran/Nastran software, and based on these results the secondary optimization is fulfilled with MMA programme (The Method of Moving Asymptotes algorithm).

In [8], optimization of the main girder of the double beam bridge crane using by SolidWorks software, according to the criteria of strength, stiffness and local stability of plates is presented. Similarly to previous, the paper [09] performed optimization of the main girder of the bridge crane using by Ansys software, according to the criteria of strength and stiffness, where the total volume of girder is decreased by about 21.8%.

Besides the above mentioned softwares for FEM, in [10], by using LIAfem software, indicated that the size of the finite element affects the accuracy of the results, where the double beam bridge crane is analyzed.

Application of Abaqus software in the analysis of strength and stiffness of the girder of the double beam bridge crane is shown in [11]. The observed example of the crane is modeled in Inventor software. The authors also analyzed the natural frequencies with a modal analysis of the girder with and without load. On the importance of dynamic effects in the analysis and optimization by FEM, show us the following papers. In [12], the analysis was carried out by Ansys software, and the conclusion of the study was that double beam bridge cranes have had less dynamic effects under the same loads as single-girder bridge cranes so they proved to be working faster.

\*Corresponding author: Kneza Višeslava 70A, 11030 Belgrade, Serbia, goran.pavlovic@li.rs

The paper [13] carried out the analysis of the effects that have inertial forces on the stresses and deflections, by FEM, where the derived certain conclusions for the optimization of these types of girders.

In addition to FEM application, is increasingly being applied various analytical and numerical methods for optimization process. Multi-criteria optimization was conducted in the paper [14] for the purpose of reducing the crane mass using Ms Excel software, and the solution was verified using Ansys software. The mass of the girder was reduced about 10%.

In the paper [15], problem of reducing the weight of the box girder of the bridge crane, at the same time increasing the productivity and to improve quality of product as required by the Indian standard, is tackled by preparing programme in Visual Basic 6.0. Optimal dimensions of the box girder of the bridge crane are affected by choice of standards, as shown in the paper [16], where the results obtained by Serbian standard and European standard, and compared, on examples of existing solutions of single-girder bridge cranes. GRG2 algorithm in Ms Excel software was used for the optimization process.

Application of the centered differential evolution (CDE) algorithm in the process of optimization of the box girder of the bridge crane is shown in [17], where as opposed to the previously mentioned papers, the cross-section of the box girder is variable along the span. In this way, the mass of the girder is decreased by about 23.50%.

Application of Mathcad software in optimization of the box girder of the bridge crane is shown in [18], where is graphically presented the dependence of the cross-sectional area in relation of capacities of the cranes, for characteristic spans. Similarly to previous, in [19] is graphically presented the dependence of the cross-sectional area in relation of the spans, for characteristic capacities of the cranes. In [20] is also applied Mathcad for multi-criteria optimization and comparison of the results for the welded box girder, for the cases when the objective function is the cross-sectional area and the cost of the girder manufacturing.

The mentioned papers point to the importance of optimization of the main girder of the bridge crane and creation of the model which can allow a more real description of the crane behaviour in operation. As it can be seen in the mentioned papers, there are different constraint functions so that it can be concluded that a better objective

$$[X, fval, exitflag, output, lambda, grad, hessian] = fmincon(fun, X0, A, b, Aeq, beq, lb, ub, nonlcon, options) \quad (7)$$

where:

*fval* - objective function value at solution (returned as a real number)

*exitflag* - shows reason for stop of *fmincon* function

*fun* - the target function

*fmincon* - function which find minimum of constrained nonlinear multi-variable function

*output* - function which outputs optimization information

*nonlcon* - function which calculates nonlinear inequality constraint  $C(X) \leq 0$  through the accepted vector  $X$  and the equality constraint  $Ceq(X) = 0$  is used by estimated  $C$  and  $Ceq$  at the poison of  $X$  though the appointed function handle *lambda* - the multiplier of Lagrange (it embodies which constraint is valid)

function, i.e. smaller girder mass is obtained for a larger number of constraints.

Taking into account the above mentioned results and conclusions, the aim of this paper is to define optimum values of parameters of the geometry of cross-sectional area of the rectangular box girder of the double beam bridge crane that will lead to the reduction of its mass.

## 2. MATHEMATICAL FORMULATION OF THE OPTIMIZATION PROBLEM

The task of optimization is to define geometrical parameters of the rectangular box section of the girder which result is its minimum mass.

Matlab Optimization Toolbox can be used to solve the problems of linear programming, non-linear programming and multi-target programming.

The optimization algorithm of the parameters of the cross-sectional area of steel rectangular box girder is to utilizing the *fmincon* function in the Optimization Toolbox to realize the minimization of the cross-sectional area of the rectangular box girder, i.e. constrained minimization problem.

The optimization problem can be defined by the following mathematical formulation, [21]:

$$\min f(X) \quad (1)$$

subject to:

$$C(X) \leq 0 \quad (2)$$

$$Ceq(X) = 0 \quad (3)$$

$$A \cdot X \leq b \quad (4)$$

$$Aeq \cdot X = beq \quad (5)$$

$$lb \leq X \leq ub \quad (6)$$

where:

$X, b, beq, lb, ub$  - vectors

$A, Aeq$  - matrices

$C(X), Ceq(X)$  - functions that return to vectors

$f(X)$  - the target function (the objective function)

Functions  $f(X), C(X)$  and  $Ceq(X)$  can be nonlinear functions.

In Matlab Optimization Toolbox, the constrained nonlinear optimization problem is realized by *fmincon* function. The specific forms are as followings:

*grad* - shows the gradient of the target function at  $X$

*hessian* - shows Hessiab value of the target function at  $X$

$X0$  - the initial value

$A$  and  $b$  meet the requirements of the inequality constraint  $A \cdot X \leq b$ , if there is no such constraint, then  $A=[ ]$  and  $b=[ ]$ .

$Aeq$  and  $beq$  meet the requirements of the equality constraint  $Aeq \cdot X = beq$ , if there is no such constraint, then  $Aeq=[ ]$  and  $beq=[ ]$ .

$lb$  and  $ub$  meet the requirements  $lb \leq X \leq ub$  if there is no scope, suppose  $lb=[ ]$  and  $ub=[ ]$ .

In the process of optimization, *fmincon* function adopts gradient projection method. Gradient projection method is a method to directly deal with the nonlinear programming constraint.

It made a projection matrix according to the initial points and boundary face where the initial points stand. Repeat this procedure frequently so as to obtain the best solution.

### 3. OBJECTIVE AND CONSTRAINT FUNCTIONS

#### 3.1. Objective function

The objective function is represented by the area of the cross section of the rectangular box girder (Figure 1). The paper treats five optimization parameters ( $h, b_1, t_1, t_2, y$ ), where:

- $h$  - web height
- $b_1$  - distance between webs
- $t_1$  - flange thickness
- $t_2$  - web thickness
- $y$  - value, according to recommendations

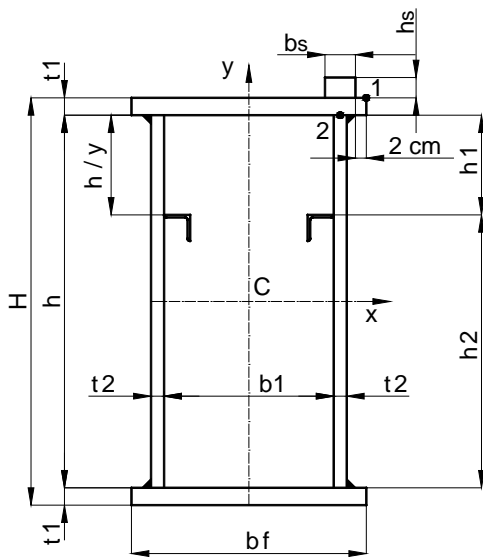


Figure 1: The rectangular box section of the main girder of the bridge crane

The vector of the given parameters is:

$$\vec{x} = (Q, L, m_k, b_k, k_a, f_y, b_s, h_s, D_t \dots) \quad (8)$$

where:

- $Q$  - the carrying capacity of the crane
- $L$  - the span of the crane
- $m_k$  - the mass of the trolley
- $b_k$  - the distance between the wheels of the trolley
- $k_a$  - the dynamic coefficient of crane load in the horizontal plane, [22]
- $f_y$  - the minimum yield stress of the plate material
- $b_s$  - rail width
- $h_s$  - rail height
- $D_t$  - the diameter of the trolley wheel

The area of the cross section (Figure 1), i.e. the objective function, is:

$$A_g = 2 \cdot (b_f \cdot t_1 + h \cdot t_2) \quad (9)$$

or

$$A_g = A_g(X) = 2 \cdot (x_1 + x_4 + b_s + 4) \cdot x_3 + 2 \cdot x_2 \cdot x_4 \text{ cm}^2 \quad (10)$$

where:

$A_g$  - the area of the cross section of the rectangular box girder (the objective function)

$X$  - the design vector made of five design variables

$$X = [x_1, x_2, x_3, x_4, x_5]^T = [b_1, h, t_1, t_2, y]^T \quad (11)$$

Other important relations can be written in the following way:

$$b_f = b_f(X) = b_1 + t_2 + b_s + 4 = x_1 + x_4 + b_s + 4 \text{ cm} \quad (12)$$

$$H = H(X) = h + 2 \cdot t_1 = x_2 + 2 \cdot x_3 \quad (13)$$

where:

$H$  - height of the girder

$b_f$  - flange width

The geometrical properties in the specific points of the rectangular box section (Figure 1) shall be determined by well-known expressions ( $I_x, W_{x1}, W_{y1}, W_{x2}, W_{y2}, S_{x2}$ ).

where:

$I_x$  - moment of inertia about x axis

$W_{x1}, W_{y1}$  - section moduli for point 1

$W_{x2}, W_{y2}$  - section moduli for point 2

$S_{x2}$  - static moment of area for point 2

#### 3.2. Constraint functions

##### 3.2.1. The criterion of permissible stresses

The maximum equivalent stresses in specific points of the rectangular box section (Figure 1) have to be lower than permissible stresses.

The values of the bending moments in the corresponding planes and the value of the transverse force are calculated in the following way (Figure 2):

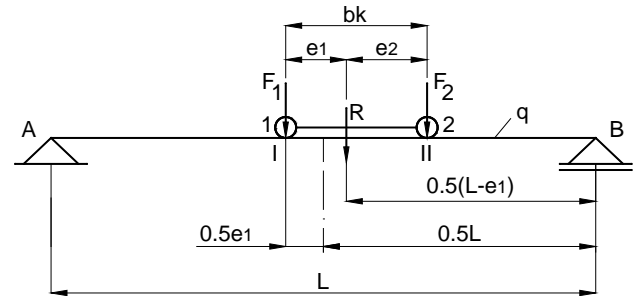


Figure 2: Model of the main girder of the bridge crane

$$M_{v1} = \frac{R}{4 \cdot L} \cdot (L - e_1)^2 + \gamma \cdot \frac{q \cdot L^2}{8} \quad (14)$$

$$e_1 = \frac{b_k}{2} \quad (15)$$

$$q = 1.1 \cdot \rho \cdot g \cdot A \quad (16)$$

$$M_{H1} = \gamma \cdot \left[ \frac{R_h}{4 \cdot L} \cdot (L - e_1)^2 + \frac{q \cdot L^2}{8} \cdot k_a \right] \quad (17)$$

$$F_t = \frac{R}{2 \cdot L} \cdot (L - e_1) + \frac{\gamma \cdot q \cdot L}{2} \quad (18)$$

while the values of the corresponding forces are:

$$F_1 = F_2 = \gamma \cdot \frac{\psi \cdot Q + m_k}{4} \cdot g \quad (19)$$

$$R = F_1 + F_2 \quad (20)$$

$$F_{1,st} = F_{2,st} = \frac{Q + m_k}{4} \cdot g = F_{st} \quad (21)$$

$$F_{1,h} = F_{2,h} = F_{st} \cdot k_a \quad (22)$$

$$R_h = F_{1,h} + F_{2,h} \quad (23)$$

where:

$\gamma$  - the coefficient which depends on the classification class, [22]

$\psi$  - the dynamic coefficient of the influence of load oscillation in the vertical plane, [22]

$F_1, F_2$  - forces acting upon girder beneath the trolley wheel 1 and trolley wheel 2, respectively

$R$  - resulting force in the vertical plane

$\rho = 7850 \frac{kg}{m^3}$  - density of material of the girder

$q$  - specifically weight per unit of length of the girder (increased by the weight of the diaphragms and the longitudinal stiffeners)

$M_{V1}, M_{H1}$  - the bending moments in the vertical and the horizontal planes, respectively

$F_{1,st}$  - static force acting upon girder beneath the trolley wheel

$R_h$  - resulting force in the horizontal plane

$F_t$  - maximum shear force

The value of the equivalent stress at point 1:

$$\sigma_{1,u} = \sigma_{zV1} + \sigma_{zH1} = \frac{M_{V1}}{W_{x1}} + \frac{M_{H1}}{W_{y1}} \leq f_{d,1} \quad (24)$$

$$f_{d,1} = \frac{f_y}{\gamma_m \cdot \nu_1} \quad (25)$$

where:

$\sigma_{1,u}$  - maximum equivalent stress at point 1

$f_{d,1}$  - permissible stress

$\gamma_m = 1.1$  - general resistance factor, [23]

$\nu_1 = 1.5$  - the factored load coefficient for load case 1

The value of the normal stress in the  $x$  direction at point 2:

$$\sigma_{z2} = \sigma_{zV2} + \sigma_{zH2} = \frac{M_{V1}}{W_{x2}} + \frac{M_{H1}}{W_{y2}} \leq f_{d,1} \quad (26)$$

The value of the normal stress in the  $y$  direction due to the action of wheel pressure on the web plate (Figure 3):

$$\sigma_y = \frac{F_1}{t_2 \cdot l_r} \leq f_{d,1} \quad (27)$$

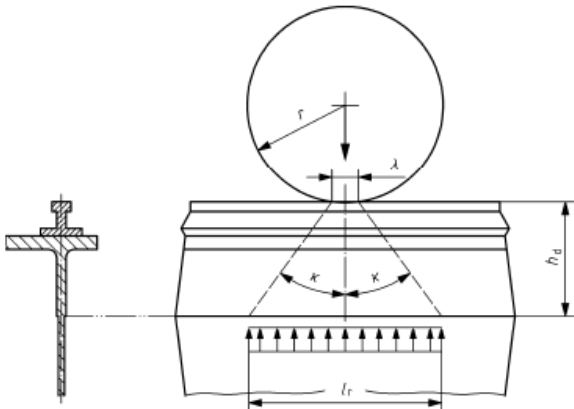


Figure 3: Effective distribution length under concentrated load

where:

$\sigma_{z2}, \sigma_y$  - the normal stresses in the  $x$  and  $y$  directions at point 2, respectively

$l_r$  - the effective distribution length (given in Annex C.4, [23])

$$l_r = l_{1r} = 2 \cdot h_d \cdot \text{tg} \kappa + 0.2 \cdot r = 2 \cdot h_{d1} \cdot \text{tg} \kappa + 0.1 \cdot D_t \quad (28)$$

$$h_d = h_{d1} = h_s + t_1 \quad (29)$$

where:

$h_d$  - the distance between the section under consideration and contact level of acting load (Figure 3)

$\kappa \leq 45^\circ$  - the dispersion angle, [23]

$r$  - the radius of the trolley wheel ( $D_t / 2$ )

The value of the tangential stress at point 2:

$$\tau_2 = \frac{F_t \cdot S_{x2}}{2 \cdot t_2 \cdot I_x} \leq \frac{f_{d,1}}{\sqrt{3}} \quad (30)$$

The value of the equivalent stress at point 2 (maximum equivalent stress at point 2):

$$\sigma_{2,u} = \sqrt{\sigma_{z2}^2 + \sigma_y^2 - \sigma_{z2} \cdot \sigma_y + 3 \cdot \tau_2^2} \leq f_{d,1} \quad (31)$$

### 3.2.2. The criterion of local buckling of plates

Testing of the box girder stability was carried out in accordance with the European standard, [23]. According to this standard, it is necessary to check the buckling of the flange plate with the width  $b_1$  and the thickness  $t_1$  (Figure 4 and Figure 5), the buckling of the web plate above the longitudinal stiffener (length  $a$ , height  $h_1$  and thickness  $t_2$  – Figure 4 and Figure 6) as well as the buckling of the web plate under the longitudinal stiffener (length  $a$ , height  $h_2$  and thickness  $t_2$  – Figure 4 and Figure 6). Length  $a$  is distance between the diaphragms (Figure 4).

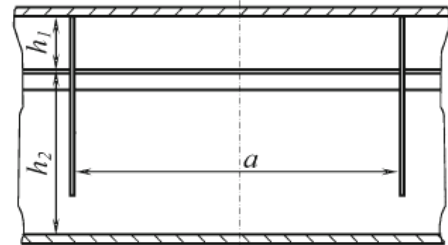


Figure 4: Stiffeners of the box girder

The criterion of local buckling of top flange plate of the box girder

Testing of the stability of the flange plate segment (Figure 5) subjected to the action of normal compressive stress in the  $x$  direction was carried out in compliance with [23]. This criterion is fulfilled if the following condition is satisfied:

$$|\sigma_{Sx}| = \nu_1 \cdot (\sigma_{zV1} + \sigma_{zH2}) \leq f_{b,Rx} \quad (32)$$

$$f_{b,Rx} = \kappa_x \cdot f_d \quad (33)$$

$$f_d = \frac{f_y}{\gamma_m} \quad (34)$$

where:

$|\sigma_{Sx}|$  - design value of the compressive stress in the  $x$  direction

$f_{b,Rx}$  - critical stress



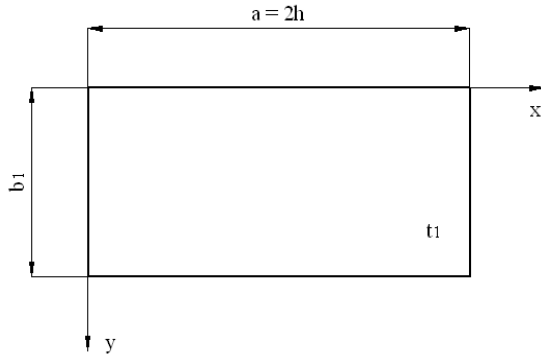


Figure 5: Top flange

$\kappa_x$  - a reduction factor, [23]

$$\kappa_x = c_e \cdot \left( \frac{1}{\lambda_x} - \frac{0.22}{\lambda_x^2} \right) \leq 1 \text{ for } \lambda_x > 0.673 \quad (35)$$

or

$$\kappa_x = 1 \text{ for } \lambda_x \leq 0.673 \quad (36)$$

where:

$\lambda_x$  - non-dimensional plate slenderness, [23]

$$\lambda_x = \sqrt{\frac{f_y}{K\sigma \cdot \sigma_e}} \quad (37)$$

$$c_e = 1.25 - 0.12 \cdot \psi_e, \quad c_e \leq 1.25 \quad (38)$$

where:

$K\sigma$  - a buckling factor (given in Table 15, [23])

$\sigma_e$  - a reference stress, [23]

$\psi_e$  - the edge stress ratio of the plate, relative to the maximum compressive stress

$$K\sigma = \frac{8.2}{\psi_e + 1.05} \quad (39)$$

$$\psi_e = \frac{\sigma_2}{\sigma_1} = \frac{\sigma_{zV1} - \sigma_{zH2}}{\sigma_{zV1} + \sigma_{zH2}} \quad (40)$$

$$\sigma_e = \frac{\pi^2 \cdot E}{12 \cdot (1 - \nu^2)} \cdot \left( \frac{t_1}{b_1} \right)^2 \quad (41)$$

where:

$\nu = 0.3$  - the Poisson's ratio of the plate

$E = 21000 \frac{kN}{cm^2}$  - the elastic modulus of the plate

The criterion of local buckling of web plate of the box girder

Testing of the stability of the web plate segment (Figure 6) subjected to the action of normal stresses in the  $x$  and  $y$  directions was carried out in compliance with [23].

The case when, in addition to vertical stiffeners at midspan, a row of horizontal stiffeners is also placed, the horizontal stiffeners being placed at the distance of  $h/y$  was considered (Figure 1).

The criterion of stability of the web plate in zone 1 is fulfilled if the following condition is satisfied:

$$\left( \frac{|\sigma_{S1x}|}{f_{b,R1x}} \right)^{e_{1x}} + \left( \frac{|\sigma_{S1y}|}{f_{b,R1y}} \right)^{e_{1y}} - (\kappa_x \kappa_y)^6 \left( \frac{|\sigma_{S1x} \sigma_{S1y}|}{f_{b,R1x} f_{b,R1y}} \right) \leq 1 \quad (42)$$

$$|\sigma_{S1x}| = \nu_1 \cdot (\sigma_{zV2} + \sigma_{zH2}) \quad (43)$$

$$|\sigma_{S1y}| = \frac{\nu_1 \cdot F_1}{t_2 \cdot l_r} \quad (44)$$

$$f_{b,R1x} = \kappa_{1x} \cdot f_d \quad (45)$$

$$f_{b,R1y} = \kappa_{1y} \cdot f_d \quad (46)$$

$$e_{1x} = 1 + \kappa_{1x}^4, \quad e_{1y} = 1 + \kappa_{1y}^4 \quad (47)$$

$$h_1 = \frac{h}{y} \quad (48)$$

where:

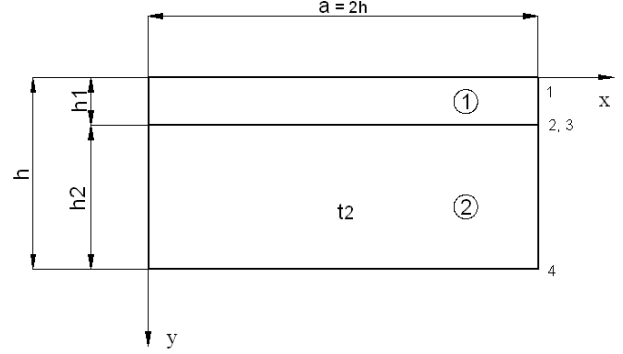


Figure 6: Web plate

$|\sigma_{S1x}|, |\sigma_{S1y}|$  - design values of the compressive stresses in zone 1 in the  $x$  and  $y$  directions, respectively

$f_{b,R1x}, f_{b,R1y}$  - critical stresses

$\kappa_{1x}, \kappa_{1y}$  - reduction factors for zone 1 in the  $x$  and  $y$  directions, respectively, [23]

$$\kappa_{1x} = c_{1e} \cdot \left( \frac{1}{\lambda_{1x}} - \frac{0.22}{\lambda_{1x}^2} \right) \leq 1 \text{ for } \lambda_{1x} > 0.673 \quad (49)$$

or

$$\kappa_{1x} = 1 \text{ for } \lambda_{1x} \leq 0.673 \quad (50)$$

where:

$\lambda_{1x}$  - non-dimensional plate slenderness, [23]

$$\lambda_{1x} = \sqrt{\frac{f_y}{K\sigma_1 \cdot \sigma_{1e}}} \quad (51)$$

$$c_{1e} = 1.25 - 0.12 \cdot \psi_{1e}, \quad c_{1e} \leq 1.25 \quad (52)$$

$$K\sigma_1 = \frac{8.2}{\psi_{1e} + 1.05} \quad (53)$$

$$\psi_{1e} = \frac{(y-2) \cdot \sigma_{zV1} + y \cdot \sigma_{zH2}}{y \cdot (\sigma_{zV1} + \sigma_{zH2})} \quad (54)$$

$$\sigma_{1e} = \frac{\pi^2 \cdot E}{12 \cdot (1 - \nu^2)} \cdot \left( \frac{t_2}{h_1} \right)^2 \quad (55)$$

$$\kappa_{1y} = 1.13 \cdot \left( \frac{1}{\lambda_{1y}} - \frac{0.22}{\lambda_{1y}^2} \right) \leq 1 \text{ for } \lambda_{1y} > 0.831 \quad (56)$$

or

$$\kappa_{1y} = 1 \text{ for } \lambda_{1y} \leq 0.831 \quad (57)$$

where:

$\lambda_{1y}$  - non-dimensional plate slenderness, [23]

$$\lambda_{1y} = \sqrt{\frac{f_y}{K\sigma_{1y} \cdot \sigma_{1e} \cdot \frac{a}{c_{1r}}}} \quad (58)$$

where:

$K\sigma_{1y}$  - a buckling factor for zone 1 (determined using Figure 11, [23])

$c_{1r}$  - the width over which the transverse load is distributed (equivalent to  $l_{1r}$ )

The criterion of stability of the web plate in zone 2 is fulfilled if the following condition is satisfied:

$$\left(\frac{|\sigma_{S2x}|}{f_{b,R2x}}\right)^{e_{2x}} + \left(\frac{|\sigma_{S2y}|}{f_{b,R2y}}\right)^{e_{2y}} - (\kappa_{2x}\kappa_{2y})^6 \left(\frac{|\sigma_{S2x}\sigma_{S2y}|}{f_{b,R2x}f_{b,R2y}}\right) \leq 1 \quad (59)$$

$$|\sigma_{S2x}| = v_1 \cdot \left( \sigma_{zV1} \cdot \frac{h/2 - h_2}{h/2} + \sigma_{zH2} \right) \quad (60)$$

$$|\sigma_{S2y}| = \frac{v_1 \cdot F_1}{t_2 \cdot l_{2r}} \quad (61)$$

$$l_{2r} = 2 \cdot h_{d2} \cdot \text{tg} \kappa + 0.2 \cdot r = 2 \cdot h_{d2} \cdot \text{tg} \kappa + 0.1 \cdot D_t \quad (62)$$

$$h_{d2} = h_s + t_1 + h_1 \quad (63)$$

$$f_{b,R2x} = \kappa_{2x} \cdot f_d \quad (64)$$

$$f_{b,R2y} = \kappa_{2y} \cdot f_d \quad (65)$$

$$e_{2x} = 1 + \kappa_{2x}^4, \quad e_{2y} = 1 + \kappa_{2y}^4 \quad (66)$$

$$h_2 = \frac{h \cdot (y-1)}{y} \quad (67)$$

where:

$|\sigma_{S2x}|, |\sigma_{S2y}|$  - design values of the compressive stresses in zone 2 in the  $x$  and  $y$  directions, respectively

$f_{b,R2x}, f_{b,R2y}$  - critical stresses

$\kappa_{2x}, \kappa_{2y}$  - reduction factors for zone 2 in the  $x$  and  $y$  directions, respectively, [23]

$$\kappa_{2x} = c_{2e} \cdot \left( \frac{1}{\lambda_{2x}} - \frac{0.22}{\lambda_{2x}^2} \right) \leq 1 \quad \text{for } \lambda_{2x} > 0.673 \quad (68)$$

or

$$\kappa_{2x} = 1 \quad \text{for } \lambda_{2x} \leq 0.673 \quad (69)$$

where:

$\lambda_{2x}$  - non-dimensional plate slenderness, [23]

$$\lambda_{2x} = \sqrt{\frac{f_y}{K\sigma_2 \cdot \sigma_{2e}}} \quad (70)$$

$$c_{2e} = 1.25 - 0.12 \cdot \psi_{2e}, \quad c_{2e} \leq 1.25 \quad (71)$$

$$K\sigma_2 = 7.81 + 6.29 \cdot \psi_{2e} + 9.78 \cdot \psi_{2e}^2 \quad (72)$$

$$\psi_{2e} = \frac{(y-2) \cdot \sigma_{zV1} + y \cdot \sigma_{zH2}}{y \cdot (\sigma_{zH2} - \sigma_{zV1})} \quad (73)$$

$$\sigma_{2e} = \frac{\pi^2 \cdot E}{12 \cdot (1-\nu^2)} \cdot \left( \frac{t_2}{h_2} \right)^2 \quad (74)$$

$$\kappa_{2y} = 1.13 \cdot \left( \frac{1}{\lambda_{2y}} - \frac{0.22}{\lambda_{2y}^2} \right) \leq 1 \quad \text{for } \lambda_{2y} > 0.831 \quad (75)$$

or

$$\kappa_{2y} = 1 \quad \text{for } \lambda_{2y} \leq 0.831 \quad (76)$$

where:

$\lambda_{2y}$  - non-dimensional plate slenderness, [23]

$$\lambda_{2y} = \sqrt{\frac{f_y}{K\sigma_{2y} \cdot \sigma_{2e} \cdot \frac{a}{c_{2r}}}} \quad (77)$$

where:

$K\sigma_{2y}$  - a buckling factor for zone 2 (determined using Figure 11, [23])

$c_{2r}$  - the width over which the transverse load is distributed (equivalent to  $l_{2r}$ )

### 3.2.3. The criterion of static deflection

In order to satisfy this criterion, it is necessary that static deflection in the vertical plane has the value smaller than the permissible one.

$$f_{st} = \frac{F_{1,st} \cdot L^3}{48 \cdot E \cdot I_x} \cdot [1 + \alpha \cdot (1 - 6 \cdot \beta^2)] \leq f_{dop} \quad (78)$$

$$\alpha = \frac{F_{2,st}}{F_{1,st}} = 1 \quad (79)$$

$$\beta = \frac{b_k}{L} \quad (80)$$

$$f_{dop} = k \cdot L \quad (81)$$

where:

$f_{st}$  - static deflection in the vertical plane,

$f_{dop}$  - the permissible deflection in the vertical plane, [22]

$\alpha, \beta$  - the coefficients, [22]

$k$  - the coefficient which depends on the purpose of the crane and control condition of the crane, [22]

### 3.2.4. The criterion of permissible period of oscillation

To determine the time of damping of oscillation, it is necessary to analyse the vertical oscillation of the main girder with the payload. The analysis procedure was performed in compliance with [22] and [24].

The mass  $m_l$  is determined according to the expression, [24]:

$$m_l = \frac{Q + m_k}{2} + \frac{35 \cdot m_m}{72} \quad (82)$$

where:

$\frac{35 \cdot m_m}{72}$  - the reduced continual mass of the girder at

midspan for the assumed function of displacement of the elastic line of the adopted discrete dynamic model for the simple girder, [24]

The time of damping of oscillation is determined from the expression, [22]:

$$T = \frac{6 \cdot \pi \cdot \sqrt{\delta_{11} \cdot m_l}}{\gamma_d} \leq T_d \quad (83)$$

$$m_m = 1.1 \cdot \rho \cdot A \cdot L \quad (84)$$

$$\delta_{11} = \frac{1.0 \cdot L^3}{48 \cdot E \cdot I_x} \quad (85)$$

where:

$m_m$  - the mass of the girder (increased by the mass of the diaphragms and the longitudinal stiffeners)

$\delta_{11}$  - the deflection of the girder caused by the action of the unit force

$T_d$  - the permissible time of damping of oscillation (permissible period of oscillation), which depends on the purpose of the crane, [22]

$\gamma_d$  - the logarithmic decrement which shows the rate of damping of oscillation, which depends on the ratio between the height of the girder  $H$  and the span  $L$ , [22]

#### 4. NUMERICAL REPRESENTATION OF THE RESULTS OBTAINED

The optimization process is done by Optimization Toolbox module of Matlab software.

Existing solutions of the double beam bridge cranes that were used as examples for the optimization process are in classification class 2m/M5, so that certain input parameters necessary for the optimization process are

adopted for mentioned classification class. Other input data are shown in Table 1.

As initial conditions (vector  $X_0$ ) in the optimization process are taken the dimensions of the rectangular box section of existing solutions of the double beam bridge cranes (shown in Table 1).

As additional criteria for the optimization process are taken production feasibility (distance between the webs) and the recommended minimum thicknesses of the plates.

Minimum thickness of the web plates is adopted to be 5 mm and minimum thickness of the bottom and top flange is adopted to be 6 mm, which are also the constraint functions. In addition, as one more constraint function, minimum distance between the web plates is taken to be: 20 cm, 25 cm and 30 cm. These values are shown by the minimum values (lower boundaries) of the optimization parameters (vector  $lb$ ).

The boundaries for the optimization parameter  $y$  are taken as recommended values ( $y = 3 \div 5$ ).

Table 1: Characteristics of existing solutions of the double beam bridge cranes

No.	Manufacturer	Q (t)	L (m)	$m_k$ (kg)	$D_t$ (mm)	Material	$b_k$ (mm)	$t_1$ (mm)	$t_2$ (mm)	h (cm)	$b_l$ (cm)	$b_r$ (cm)	$A_g$ (cm <sup>2</sup> )
1	Colpart	15	20.69	780	170	S355	1000	10	6	98	31	41	199.6
2	Colpart	10	23.3	690	140	S355	1000	10	6	98	30	40	185.6
3	Colpart	2x25	22.5	2x2920	230	S355	1350	12	8	147.6	41.8	52	360.96
4	Montavar Lola	20	18.95	860	170	S235	1000	10	8	98	31	41	238.8

Table 2: The values of optimum parameters and Savings

No.	$t_1$ (mm)	$t_2$ (mm)	h (cm)	$b_l$ (cm)	$b_r$ (cm)	$y$	$A_{opt}$ (cm <sup>2</sup> )	Saving (%)
1	7	6	113.74	20	29.6	4.07	177.93	10.86
1	7	6	113.74	25.04	34.64	4.06	184.98	7.32
<b>1</b>	6	5	111.15	30	39.5	3.96	158.55	<b>20.57</b>
<b>2</b>	6	5	120.91	20	29.5	3.76	156.31	<b>15.78</b>
2	6	5	117.4	25	34.5	3.73	158.8	14.44
3	8	6	136.1	50	60.6	3.84	260.28	27.89
<b>3</b>	8	6	132.28	52.78	63.38	4.02	260.14	<b>27.93</b>
<b>4</b>	6	5	107.26	45.23	55.73	3.89	174.14	<b>27.08</b>

Table 2 shows the results of the optimization for four existing solutions of the double beam bridge cranes, according to euro codes and material saving at different initial conditions (the minimum value of  $b_l$ ). It can be seen that in some cases of existing solutions of the double beam bridge cranes the optimization process gives different results. The plate thickness values are rounded to whole numbers. The values with the greatest savings of some examples are bolded.

#### 5. CONCLUSION

Based on the optimization theory and the procedure for calculation of steel box girder of the bridge cranes, this paper combines the optimum design philosophy and the design of the rectangular box girder. The cross-sectional area is optimized making full use of the optimization function in the Matlab Optimization Toolbox. The result shows that the Matlab Optimization Toolbox is reliable, convenient and rapid. Therefore, it can be widely utilized in the optimization of the cross-sectional area of steel box girders for similar constructions.

Application of Matlab Optimizaiton Toolbox on sections of the rectangular box girders of the bridge cranes allows designers to concentrate their attention on the

optimization rather than the realization of the specific calculation. The results of optimization (the main parameters of the cross-sectional area of the rectangular box girder) represent the starting point for designers while designing box girders. The justification of application of Optimization Toolbox module of Matlab software was checked on four solutions of the double beam bridge cranes which are in operation. The optimization task – minimization of the cross-sectional area was successfully realized, which is seen in the comparison of the obtained results with the solutions made in practice. The application of this method resulted in significant savings in the material, within the range of 15.78 ÷ 27.93%. Similar procedure can be carried out for the situation with two rows of longitudinal stiffeners, which is the case for greater spans and load capacities.

The conclusion is that further research should be directed toward a multi-criteria analysis where it is necessary to include additional constraint functions, such as: influence of manufacturing technology, types of material, conditions of crane control and operation, material fatigue and economy. Previously mentioned is the basis for further research in order to save material, and

also to minimize the cost of the girder manufacturing, [20]. The obtained results can be of great importance both for crane designers and for the researchers dealing with similar optimization problems.

#### ACKNOWLEDGEMENTS

A part of this work is a contribution to the Ministry of Science and Technological Development of Serbia funded Project TR 35038.

#### REFERENCES

- [1] P.F. Liu, L.J. Xing, Y. L. Liu and J.Y. Zheng, "Strength Analysis and Optimal Design for Main Girder of Double-Trolley Overhead Traveling Crane Using Finite Element Method", *J Fail. Anal. and Preven.*, Vol. 14, pp. 76-86, (2014)
- [2] Q. Wang, X. Zhang and C. Sun, "Lightweight Design and Research of Box Girder for Double Girder Bridge Crane", *Applied Mechanics and Materials*, Vols. 229-231, pp. 478-481, (2012)
- [3] J. Wang, W. Jan and X. Gui, "Application of Matlab Optimization Tool Box on Sections of Prestressed Steel-concrete Composite Box Girder", *Advanced Materials Research*, Vol. 366, pp. 177-180, (2011)
- [4] A. Kumar and R.R. Arakerimath, "Numerical and experimental buckling analysis of crane girder", *IJRET: International Journal of Research in Engineering and Technology*, Vol. 6, pp. 199-197, (2016)
- [5] D. Gaška and C. Pypno, "Strength and elastic stability of cranes in aspect of new and old design standards", *Mechanika*, Vol. 17, No. 3, pp. 226-231, (2011)
- [6] T. Yifei, T. Zhaohui, Y. Wei and Y. Zhen, "Research on Energy-saving Optimization Design of Bridge Crane", *Eksploatacja i Niezawodność – Maintenance and Reliability*, Vol. 15, pp. 449-457, (2013)
- [7] D. Qin, Y. Wang, Q. Zhu, J. Chen and Z. Liu, "Research and Practice for Structural Optimization Design of Large-Scale Continuum", 9th World Congress on Structural and Multidisciplinary Optimization "WCSMO-9", Shizuoka (Japan), 13-17 June 2011, (2011)
- [8] J. Gailius "Tiltinio krano konstrukcijos mases racionalizavimas", Proceedings of the 17th Conference for Junior Researchers "Science – Future of Lithuania" TRANSPORT ENGINEERING AND MANAGEMENT, Vilnius (Lithuania), 8 May 2014, pp. 243-2461, (2014)
- [9] Z. Ning, "Structural Optimization Research on Girder of 200t Bridge Crane Based on Ansys", *Advanced Materials Research*, Vols. 430-432, pp. 1708-1711, (2012)
- [10] И.А. Лагереv, "Влияние размера конечного элемента на точность статического расчета несущей металлоконструкции мостового крана", *Наука и современность – 2014*, pp. 36-40, (2014)
- [11] T. Haniszewski, "Strength analysis of overhead traveling crane with use fem", *Transport problems*, Vol. 9, pp. 19-26, (2014)
- [12] Ş. Yildirim and E. Esim, "A New Approach for Dynamic Analysis of Overhead Crane Systems Under Moving Loads", Proceedings of the 12th Portuguese Conference on Automatic Control "CONTROLO 2016", Guimarães (Portugal), 14-16 September 2016, pp. 471-481, (2016)
- [13] Y. He, Y. Zhang, B. Yang, S. Liu and D. Chen, "Finite element analysis in dynamic conditions of bridge crane beam", *Applied Mechanics and Materials*, Vol. 331, pp. 70-73, (2013)
- [14] L.B. Gayatrimani and A.D. Lagad, "Design of optimum cross section for EOT Crane Girder", *International Engineering Research Journal (IERJ)*, Special Issue 2, pp. 4233-4237, (2015)
- [15] A.M. Gohil and Y.D. Vora, "Bridge Girder Design of an EOT Crane Structure-A Cad Approach", National conference on current trends in technology "NUCONE 2007", Ahmedabad (Gujarat, India), 29 November-1 December 2007, pp. 256-259, (2007)
- [16] G. Pavlović, V. Kvrđić, S. Mitrović, M. Savković and N. Zdravković, "Optimization of the box section of the single-girder bridge crane by GRG algorithm according to domestic standards and eurocodes", 7th International Scientific Conference On Defensive Technologies "OTEH 2016", Belgrade (Serbia), 6-7 October 2016, pp. 211-217, (2016)
- [17] G.N. Xu, X.F. Wang, J.K. Zhang and W.J. Qin, "Optimization of the Multi-Sectioned Box Girder of the Bridge Cranes", Proceedings of the 2015 International Conference on Energy and Mechanical Engineering, Wuhan, Hubei (China), 17-18 October 2015, pp. 927-935, (2015)
- [18] V. Antsev, A. Tolokonnikov and P. Kalabin, "Optimization of bridge type hoisting machines' metal structure", *Известия ТулГУ. Технические науки*, Vol. 4, (2009)
- [19] A. Tolokonnikov and P. Kalabin, "Optimization of geometrical parameters of main beams of bridge cranes with belts of a different thickness", *Известия ТулГУ. Технические науки*, Vol. 2, pp. 53-57, (2009)
- [20] J. Farkas and K. Jármai, "Optimum Design of Steel Structures", Springer, Heidelberg (Germany), (2003)
- [21] T.F. Coleman and Y. Zhang, "Optimization Toolbox for use with Matlab - User's Guide", The MathWorks, Natick (Massachusetts, USA), (2005)
- [22] D. Ostrić and S. Tošić, "Dizalice", Institute for Mechanization of the Faculty of Mechanical Engineering of the University in Belgrade, Belgrade (Serbia), (2005)
- [23] prEN 13001-3-1, "Cranes - General Design - Part 3-1: Limit States and proof competence of steel structure", (2010)
- [24] D. Ostrić, "Dinamika mosnih dizalica", Faculty of Mechanical Engineering of the University in Belgrade, Belgrade (Serbia), (1998)

# Integrity of Beam Braces and Threaded Spindle for Conjoint Operation of Two 5 MN Bridge Cranes

Miodrag Arsić<sup>1\*</sup>, Mladen Mladenović<sup>1</sup>, Bojan Međo<sup>2</sup>, Zoranka Malešević<sup>3</sup>, Zoran Savić<sup>1</sup>

<sup>1</sup>Institute for Materials Testing IMS, Belgrade (Serbia)

<sup>2</sup>Faculty of Technology and Metallurgy, University of Belgrade, Belgrade (Serbia)

<sup>3</sup>High Technical School of Professional Studies, Aradlovac (Serbia)

**Abstract:** *Vital components of the beam that enable conjoint operation of two bridge cranes are braces and the threaded spindle. The beam connects two bridge cranes with the overall lifting capacity of 500 t (2x250 t) and enables their simultaneous conjoint operation during the rehabilitation or major overhaul of hydroelectric generating set equipment at the hydro power plant "Djerdap 2". Two braces are being installed instead of two hooks when that situation occurs. Threaded spindle is loaded with 500 t (5 MN), while braces are loaded with 250 t (2.5 MN) each.*

*Integrity of structures is a relatively new scientific and engineering discipline which in a broader sense comprises condition analysis, behaviour diagnostics, service life evaluation and rehabilitation of structures, which means that, beside the usual situation in which it is necessary to evaluate the integrity of structure when a flaw is detected by means of non-destructive tests, this discipline also comprises stress condition analysis for the structure without cracks, most often through the use of the finite element method. That's the way to obtain the precise and detailed distribution of displacements, deformations and stresses, which enables determination of weak spots at the structure, even before the initiation of the crack.*

*Non-destructive tests were performed in order to analyze the current condition of braces and of the threaded spindle. On the basis of performed analytical calculations it was determined that their integrity is not threatened, although some internal non-homogeneities were detected by ultrasonic testing.*

**Keywords:** Cranes, Ultrasonic Testing, Braces, Threaded Spindle, Integrity of Structures

## 1. INTRODUCTION

Inspection, condition analysis and testing of beam components for simultaneous conjoint operation of 2 bridge cranes with overall lifting capacity of 500 t (5 MN) are being performed as a preparation for work during rehabilitation or major overhaul of hydroelectric generating set equipment at hydro power plant 'Djerdap 2', because they are subjected to regulations for load lifting devices.

Therefore it's necessary:

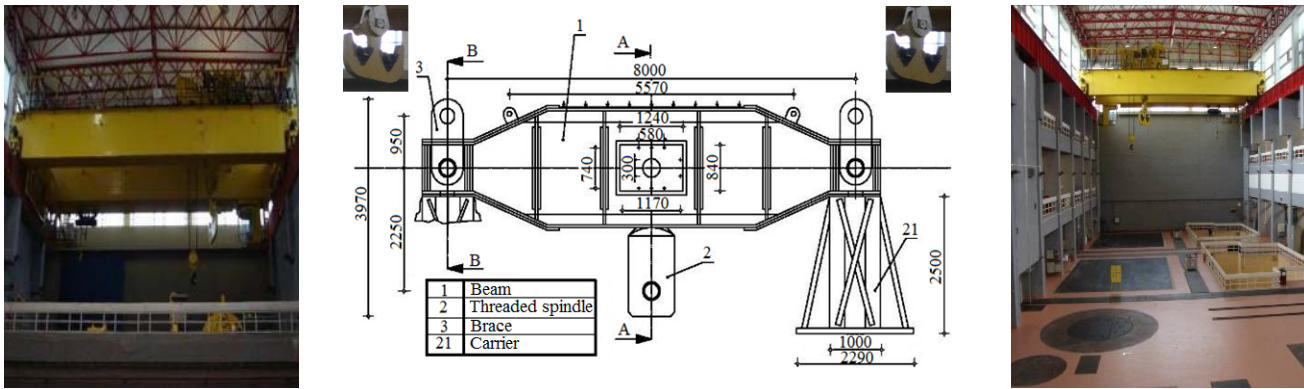
- to carry out condition analysis, check the load carrying capacity and integrity of material of which the vital components of the beam for simultaneous conjoint operation of bridge cranes at hydro power plant 'Djerdap 2' on the basis of results of non-destructive tests,
- to make a proposition regarding the repair of vital components if they become unusable in case when the check of load carrying capacity or integrity evaluation proves that degradation of material of particular components of the beam for the simultaneous conjoint operation of bridge cranes causes the reduction of load carrying capacity or threatens the integrity of the structure.

The beam connects two bridge cranes and enables their simultaneous conjoint operation, figure 1. It's being used during the rehabilitation or major overhaul of hydroelectric generating set equipment at the hydro power plant 'Djerdap 2'. Threaded spindle (marked 2 in figure 1b) is loaded with 500 t, while braces (marked 3 at figure 1b), which are being installed instead of hooks during the simultaneous conjoint operation of cranes, are loaded with 250 t each. Drawing of the device for simultaneous conjoint operation of bridge cranes is presented in figure 2.

According to design documentation [1], braces and threaded spindle were made by forging of steel with guaranteed chemical composition OLC 35 (romanian designation). Chemical composition is presented in table 1, while mechanical properties are given in tables 2 and 3.

## 1. NON-DESTRUCTIVE TESTING OF BEAM BRACES AND THREADED SPINDLE

In order to perform analysis of the current state, check the lifting capacity and evaluate the integrity of vital components (braces, threaded spindle) of the beam for simultaneous conjoint operation of bridge cranes visual testing (VT), magnetic particle testing (MT) and ultrasonic testing (UT) were carried out.



a) First bridge crane      b) Beam for simultaneous conjoint operation of bridge cranes      c) Second bridge crane

Figure 1: Appearance of the beam for simultaneous conjoint operation of 2 bridge cranes

Table 1: Chemical composition, values in [%]

Steel	C	Si	Mn	Cr	Ni	Mo	S	P
OLC 35	0.32-0.39	max 0.4	0.5 - 0.8	max 0.4	max 0.4	max 0.1	max 0.045	max 0.045

Table 2: Mechanical properties of steel OLC 35 for the thickness of brace forging  $t = 220$  mm

Steel	Yield strength, YS [N/mm <sup>2</sup> ]	Tensile strength, TS [N/mm <sup>2</sup> ]	Elongation, A5 [%]
OLC 35	245	500	min 15

Table 3: Mechanical properties of steel OLC 35 for the thickness of threaded spindle forging  $t = 900$  mm

Steel	Yield strength, YS [N/mm <sup>2</sup> ]	Tensile strength, TS [N/mm <sup>2</sup> ]	Elongation, A5 [%]
OLC 35	210	470	min 15

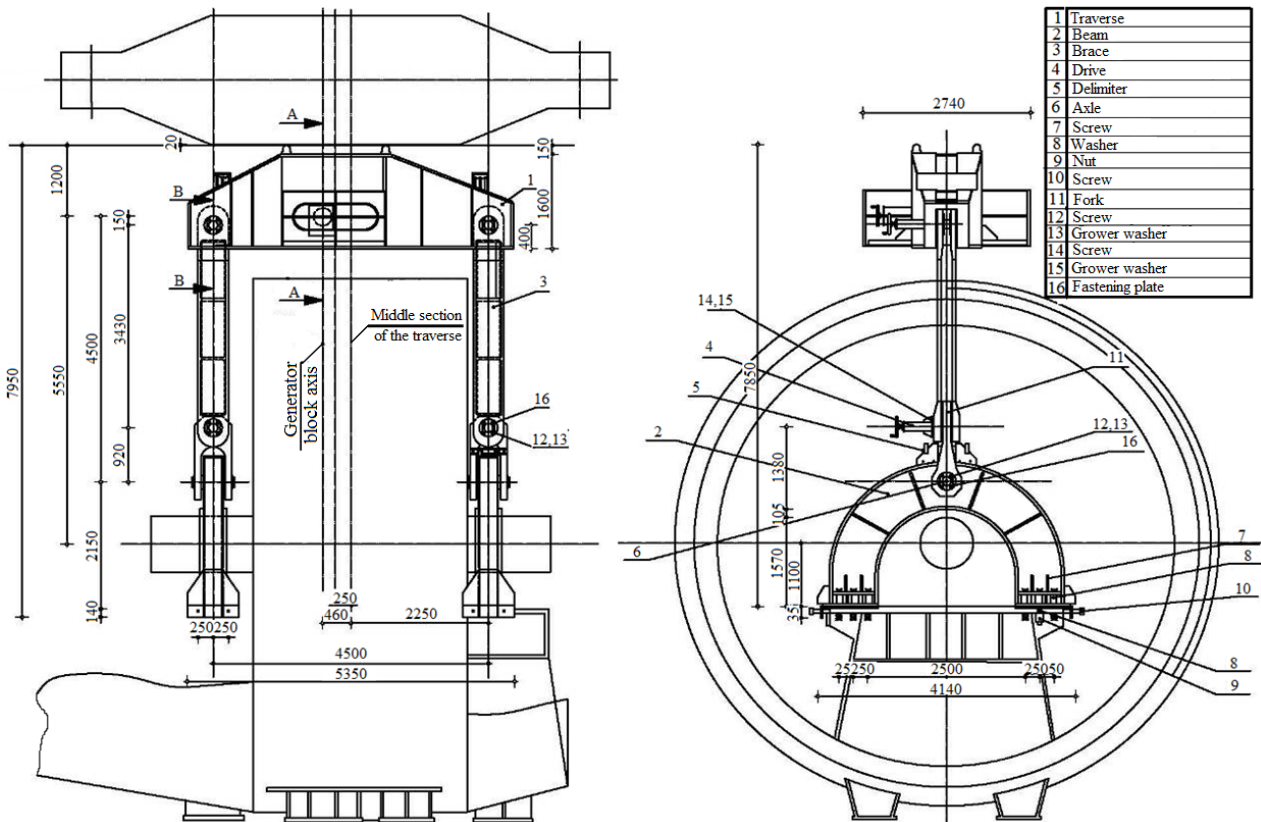


Figure 2: Assembly drawing of the device for simultaneous conjoint operation of 2 bridge cranes

1.1. Results of visual testing

Visual testing of all components of beam equipment confirmed the existence of corrosion products, as well as the existence of insignificant mechanical damages. Mechanical damages were repaired by fine grinding, and afterwards all components were subjected to sandblasting and application of anti-corrosive protection.

1.2. Magnetic particle testing

No surface defects were detected during the magnetic particle testing performed on braces and threaded spindle.

1.3. Ultrasonic testing

In figures 3-6, results of tests carried out on the right brace of the beam (at which internal non-homogeneities were detected), as well as on the threaded spindle, are shown. Findings, marked with red and yellow colour, refer to areas at which the testing was carried out.

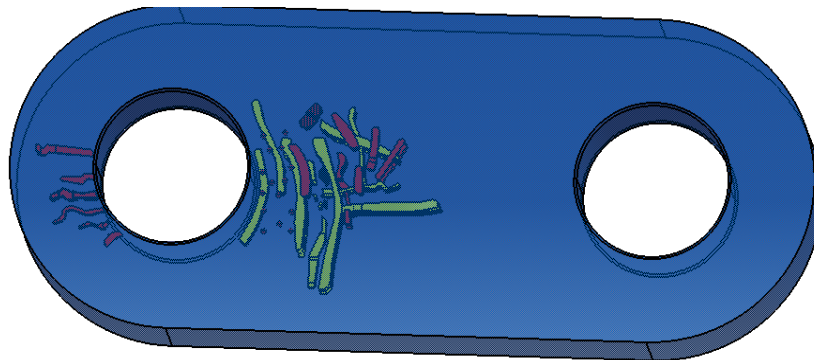


Figure 3: Results of ultrasonic testing performed on the right brace of the beam (upper view)

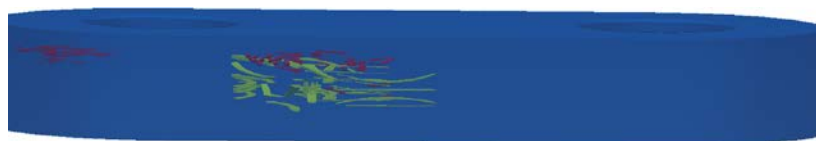


Figure 4: Results of ultrasonic testing performed on the right brace of the beam (side view)

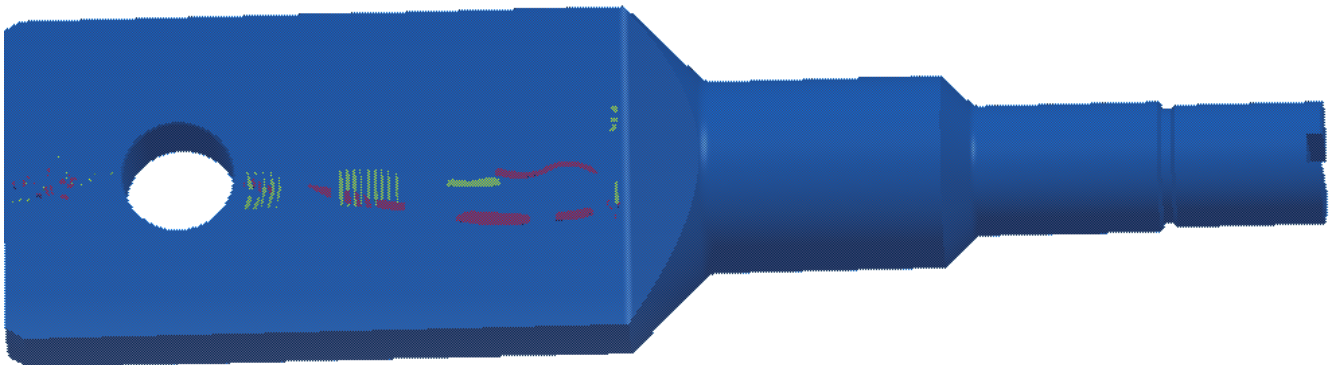


Figure 5: Results of ultrasonic testing performed on the threaded spindle of the beam (upper view)

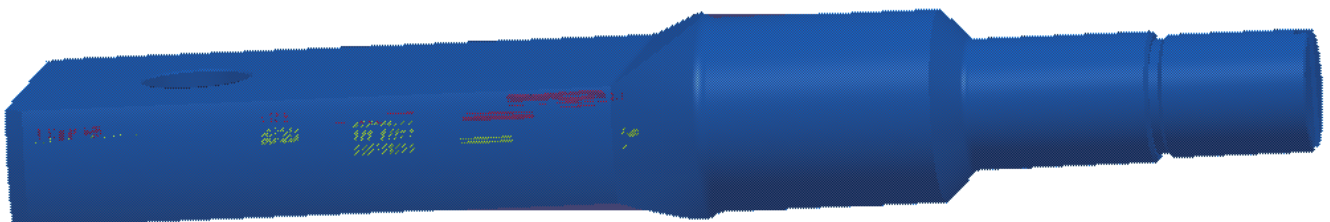


Figure 6: Results of ultrasonic testing performed on the threaded spindle of the beam (side view)

On the basis of results of ultrasonic testing performed on the right brace and on the threaded spindle, shown in figures 3 - 6, it can be concluded that detected non-homogeneities are discontinuous impurities of lamellar shape, grouped around the central area that originated during the process of forging, which is a relatively common occurrence during the manufacture of large forgings.

## 2. CALCULATION OF BRACES AND OF THE THREADED SPINDLE DURING THE SIMULTANEOUS CONJOINT OPERATION OF BRIDGE CRANES

In order to perform reliable check of load carrying capacity of braces (B) and of the threaded spindle (TS) of the beam during the simultaneous conjoint operation of 2 bridge cranes the analytical calculation and numerical calculation were carried out. Calculation was performed for brace loads  $Q_B = 250 \text{ t}$  (2.5 MN), as well as for the load at the threaded spindle  $Q_{TS} = 500 \text{ t}$  (5.0 MN).

### 2.1. Analytical calculation of stresses in critical cross-sections of braces

Beam braces are subjected to tension, each with 250 t (2.5 MN). Nevertheless, their analytical calculation was carried out for the load of 500 t (5 MN), in order to achieve safety in case when one of the braces fails. Dimensions and critical cross-sections used for the analytical calculation of beam braces are shown in figures 7 and 8.

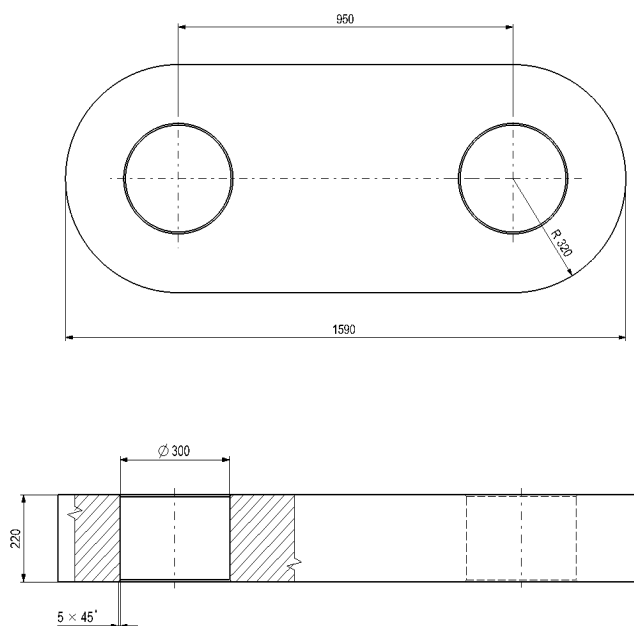


Figure 7: Basic dimensions of a beam brace

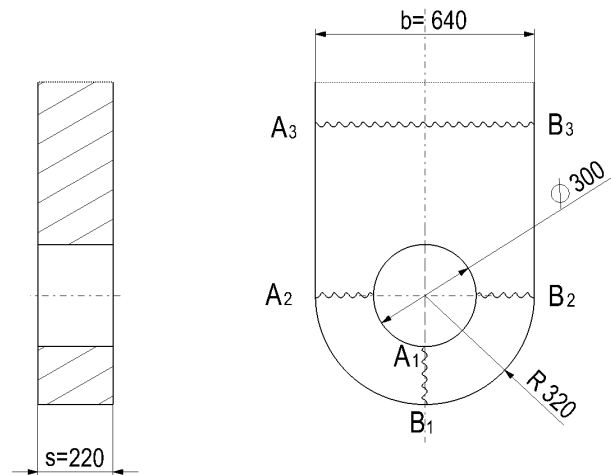


Figure 8: Detail around the opening at the brace with marked characteristic cross-sections

According to manufacturers' documentation, braces were made of steel OLC 35 [1]. Taking into account the fact that the calculation was carried out for the allowable stress  $S_{all} = 120 \text{ MPa}$ , it can be concluded that the safety factor with respect to yield strength (table 2) is:

$$S_{BM} = \frac{YS_{0.2}}{S_{all}} = \frac{245}{120} = 2.00 \quad (1)$$

By analytical calculation carried out for beam braces it was determined that the safety factor is equal or larger than 2 in all critical cross-sections, shown in figure 8 [2].

### 2.2. Analytical calculation of stresses in critical cross-sections of the threaded spindle

Analytical calculation was performed for all characteristic cross-sections of the threaded spindle, which served as a basis for determination of the minimum necessary diameter of the threaded segment. Dimensions and critical cross-sections are shown in figures 9 and 10.

Taking into account yield strength of material OLC 35 (table 3) and allowable stress  $\sigma_{all} = 120 \text{ MPa}$ , factor of safety of the threaded spindle is:

$$S_{mts} = \frac{YS_{0.2}}{\sigma_{all}} = \frac{210}{120} = 1.75 \quad (2)$$

By analytical calculation of the threaded spindle in critical cross-sections, shown in figure 10, it was determined that the lowest value of the factor of safety is 1.67 [2].



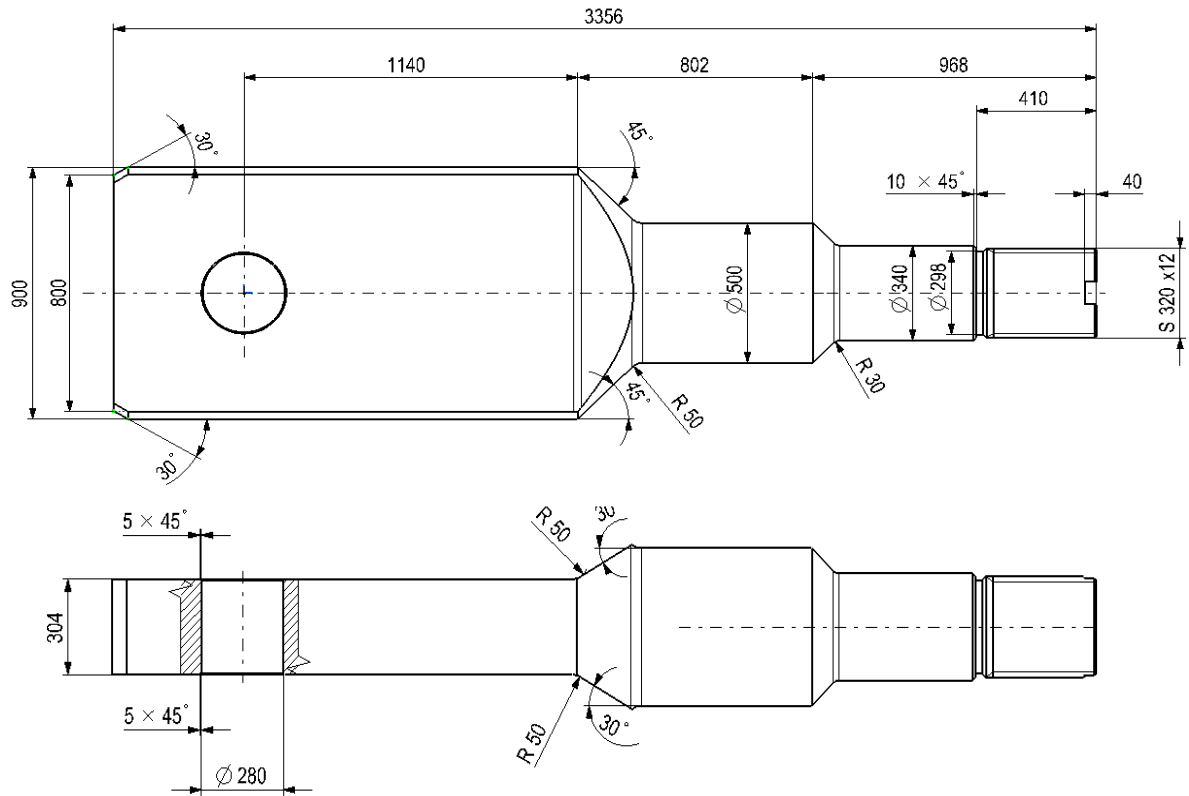


Figure 9: Basic dimensions of the threaded spindle

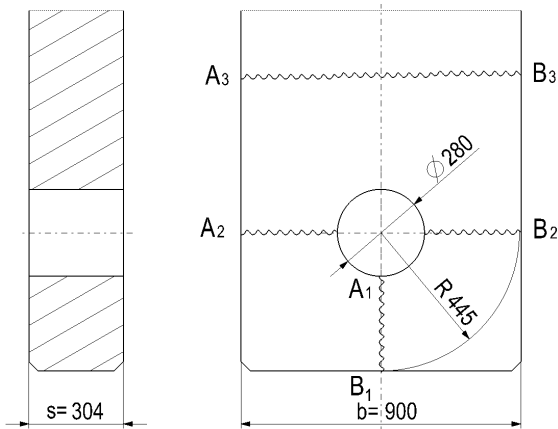


Figure 10: Detail around the eye opening at a threaded spindle with marked characteristic cross-sections

2.3. Numerical calculation of stresses in critical cross-sections of braces

Numerical calculation of braces, performed through the use of finite element method [3], was carried out for the load of 500 t (5.0 MN). Calculation was performed taking into account the fact that braces are subjected to tension. It was also taken into account that value of elasticity modul is  $E = 210 \text{ GPa}$ , value of Poisson's coefficient is  $\nu = 0.3$ , while value of yield stress is  $YS = 245 \text{ MPa}$ .

3D model of the brace is shown in figure 11a, while the finite element mesh is presented in figure 11b.

Results of numerical calculation of tensile stress to which the brace is subjected for load of 5 MN that includes the use of von Mises equations is presented in figure 12.

2.4. Numerical calculation of stresses in critical cross-sections of the threaded spindle

Finite element model has been formed by using two planes of symmetry and adequate boundary conditions, taking into account the geometry of the threaded spindle, figure 13. Load has been introduced by using the contact with a rigid body (shaft), which is presented in the same figure. Linear elastic model of material behaviour has been used. Calculation was performed taking into account the fact that braces are subjected to tension. It was also taken into account that value of elasticity modul is  $E = 210 \text{ GPa}$ , value of Poisson's coefficient is  $\nu = 0.3$ , while value of yield stress is  $YS = 210 \text{ MPa}$ .

The mesh consists of tetrahedral finite elements, with square interpolation functions. Load that acts on the model of 1,250,000 N presents 25% of the service load. Load acts on the shaft and is being transferred by contact on the spindle. Connection of the spindle with a crane (through threaded coupling) has been simplified through modelling - displacement of the surface which responds to the threaded segment of the spindle has been constrained.

Distribution of von Mises stresses is presented in figure 14, which also contains magnified detail at the threaded spindle, in close proximity of the opening. In figures 14 and 15, the shaft is not shown in order for the complete distribution of stresses to be presented.

It's clear that highest values of stress are significantly lower than 210 MPa, which is the value of yield stress.

Two paths (A-B and C-D) along which the variation of stress values has been monitored are shown in figure 14, in order to determine the stress state in close proximity of the opening as precisely as possible.

Distribution of stresses in longitudinal direction (axial stress) around the opening, with negative values of this component due to the contact with the shaft (i.e. to the

transfer of load across the contact surface) is shown in figure 16.

Variations of stress along the paths A-B and C-D are presented in figures 16 and 17. Equivalent Von Mises stress has higher values along the first path, due to the evident negative stress in the longitudinal direction.

In cross-section C-D, values of von Mises stress and of the stress in the longitudinal direction are almost equal, with the highest value at the very opening (point C) of approximately 90 MPa.



a) 3D model of the brace

b) Finite element mesh

Figure 11: 3D model and finite element mesh for one of the braces

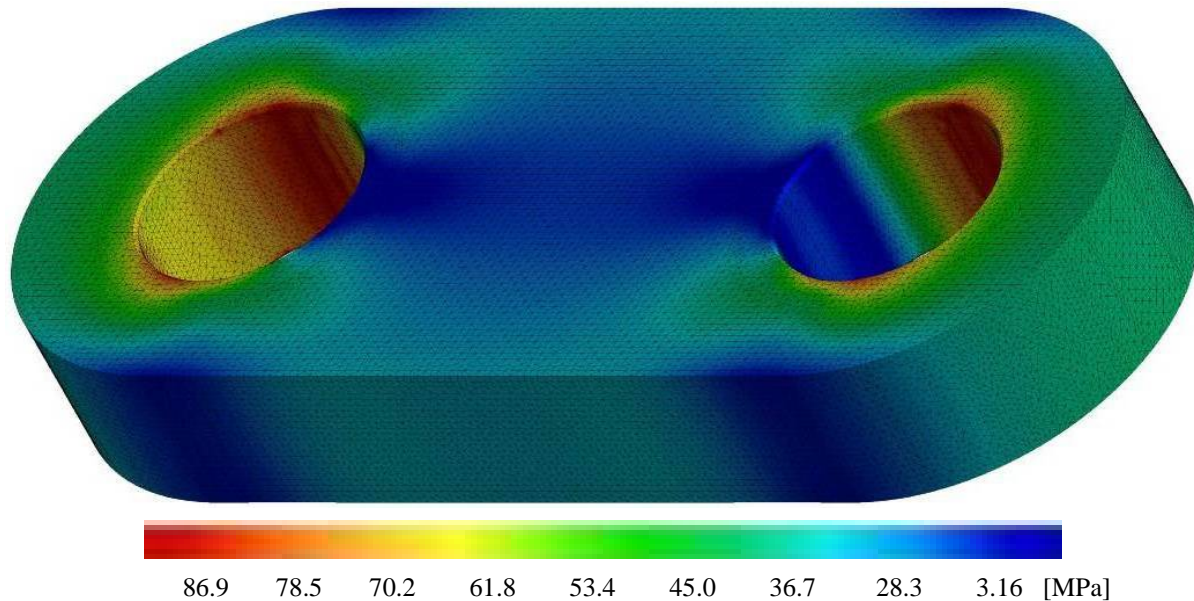


Figure 12: Results of numerical calculation and values of von Mises tensile stresses

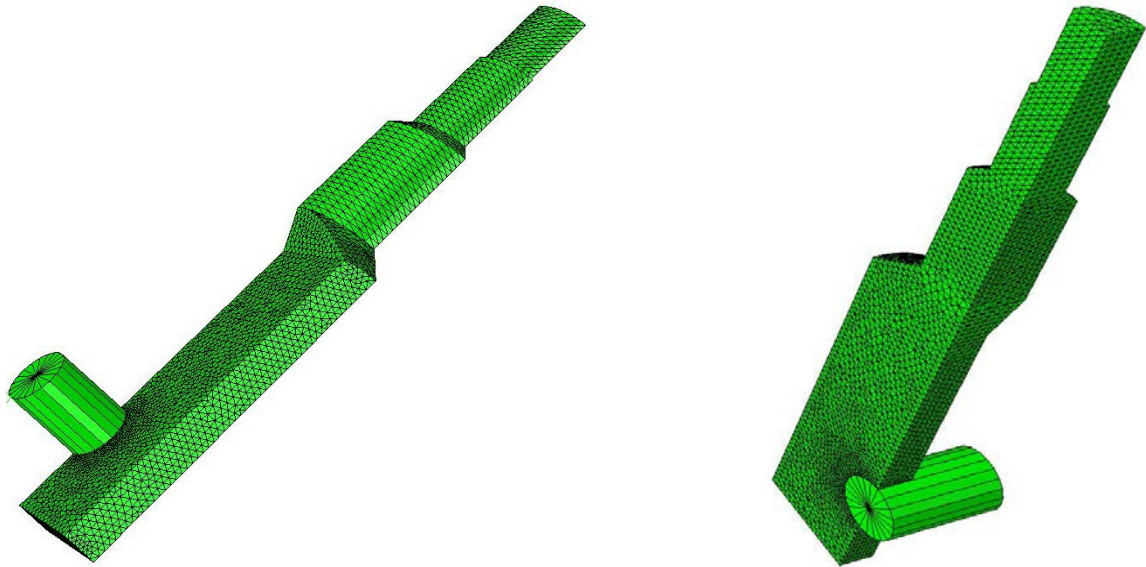


Figure 13: Finite element mesh of the threaded spindle

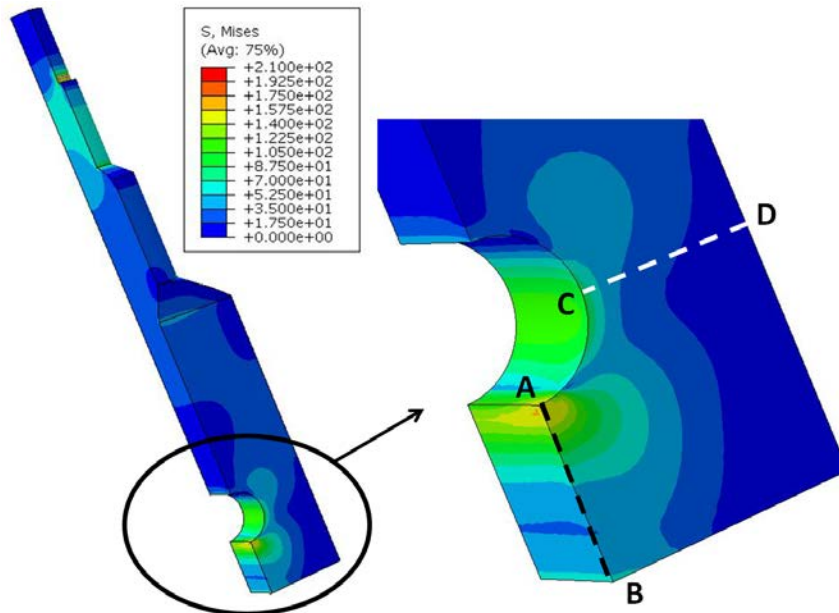


Figure 14: Distribution of equivalent von Mises stress

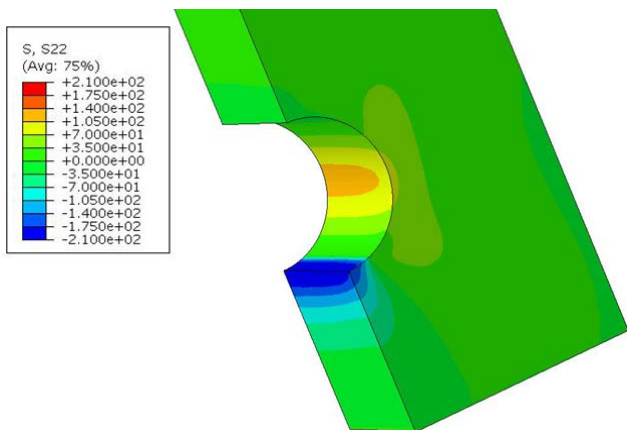


Figure 15: Distribution of stress in the longitudinal direction, area of the opening

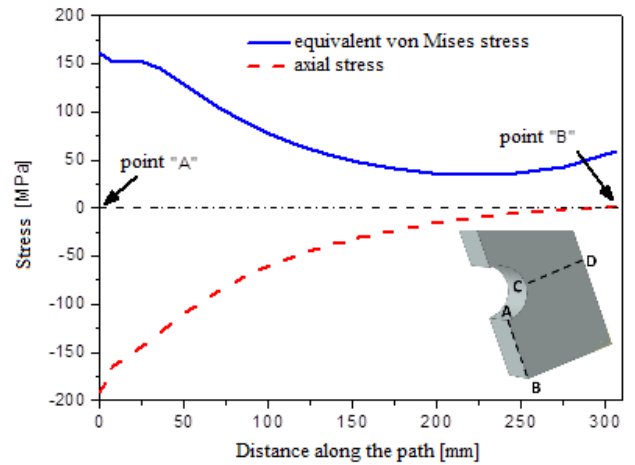


Figure 16: Variation of stress value along the path A-B

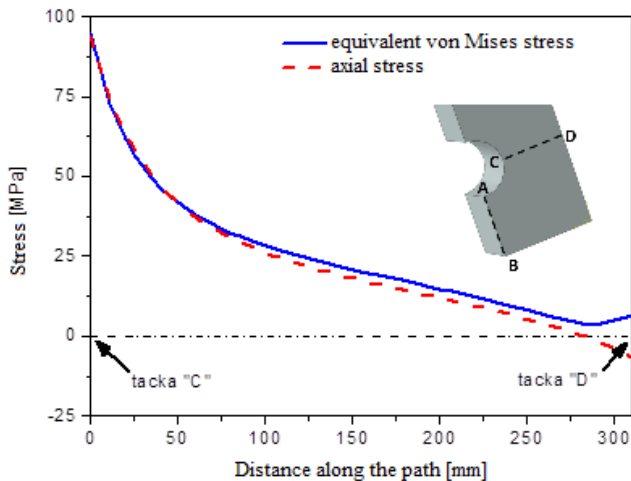


Figure 17: Variation of stress value along the path C-D

### 3. ANALYSIS OF RESULTS OBTAINED BY TESTING AND CALCULATION

Based on results of non-destructive tests and calculation of stress condition of the right brace and of the threaded spindle as parts of the beam for simultaneous conjoint operation of bridge cranes during rehabilitation or major overhaul of equipment of the hydroelectric generating set at HPP 'Djerdap 2', the following can be concluded:

- According to design documentation [1], braces and threaded spindle were made of steel with guaranteed chemical composition OLC 35 (romanian designation) by forging.
- Visual testing of all components of beam equipment confirmed the existence of corrosion products, as well as the existence of insignificant mechanical damages. Mechanical damages were repaired by fine grinding, and afterwards all components were submitted to sandblasting and application of anti-corrosive protection.
- No surface defects were detected during the magnetic particle testing of braces and threaded spindle for the simultaneous conjoint operation of bridge cranes.
- On the basis of reports OZPTT-ZA-01/013 UT for the right brace of the beam [4] and OZPTT-VR-01/013 UT for the threaded spindle [5], shown in 3D in figures 3 - 6, impurities of lamellar shape that occurred during the process of forging were detected locally. These impurities were grouped close to the central area, which is a relatively common occurrence during the process of manufacturing large forgings.
- Analytical calculations for braces and the threaded spindle were carried out taking into account values of allowable stress  $\sigma_{all} = 120$  MPa, yield stress  $YS = 240$  MPa (for thickness  $t = 220$  mm), yield stress  $YS = 210$  MPa (for thickness  $t = 900$  mm), as well as values of the factor of safety  $S_{mb} = 2.00$  and  $S_{mts} = 1.75$ . For

calculated stress states of braces and of the threaded spindle, in areas where non-allowable defects were detected, calculated values of the factor of safety were from  $S = 2.94$  to  $S = 11.48$  [2].

- Numerical calculations of stress in critical cross-sections and in areas where non-allowable defects were detected proved that the integrity of braces and of the threaded spindle is not threatened, especially taking into account that bridge cranes are being used for simultaneous conjoint operation solely during rehabilitation or major overhaul of the hydroelectric generating set, therefore they are subjected to negligible dynamic loading.

### 4. CONCLUSION

It can generally be concluded that non-allowable indications detected at the right brace and at the threaded spindle by ultrasonic testing do not influence the load carrying capacity of the equipment for simultaneous conjoint operation of bridge cranes 2500/500/50 KN, because analytical and numerical calculations proved that almost one third of characteristic cross-sections of the right brace and of the threaded spindle can carry the predicted load during rehabilitation or major overhaul of hydroelectric generating set equipment at HPP 'Djerdap 2'.

On the basis of performed tests, the use of vital components of beam equipment (right brace and threaded spindle) during rehabilitation or major overhaul of hydroelectric generating set equipment at HPP 'Djerdap 2' was allowed.

### ACKNOWLEDGEMENTS

Authors wish to thank the Ministry of Education, Science and Technological Development for the support in realization of project TR 35002.

### REFERENCES

- [1] Design documentation, 'CCSITMRTU', Timișoara (Romania)
- [2] M. Arsić, "Study on Integrity Assessment of Vital Parts of the Beam for Operation Two Bridge Cranes During Rehabilitation or Major Overhaul at Hydro Power Plant Djerdap 2", Institute for Materials Testing, Belgrade (Serbia), (2015)
- [3] Abaqus software package, www.simulia.com.
- [4] OZPTT-ZA-01/013 UT, Report on ultrasonic testing of braces, HPP 'Djerdap 2', Negotin (Serbia), (2013)
- [5] OZPTT-VR-01/013 UT, Report on ultrasonic testing of the threaded spindle, HPP 'Djerdap 2', Negotin (Serbia), (2013)

# Organizational-Technological Models for the Formation of Effective Sets of Machines and Technologies in the Performance of Construction Works

Maksim Nazarenko<sup>1\*</sup>, Ivan Pereginets<sup>1</sup>, Viktor Leschinsky<sup>2</sup>

<sup>1</sup>Kyiv National University of Construction and Architecture, Kiev

<sup>2</sup>Kyiv Academy of Construction of Ukraine, Kiev

*The criteria used to evaluate the optimization of decision making on the basis of the theory of praxeology have been applied in this work. The algorithm of supply of machines for construction works is made. The cluster approach for the organization of construction work technology, which is based on the theory of systems, criteria of decision-making and synergetic, is used. Its content essence has made it possible to create an optimized set of necessary, according to the relevant technology, method of organization of construction work in a single system. The results of the research include: raising the level of awareness and preparing potential participants for the creation of clusters. Development of criteria for evaluating the optimization of making managerial decisions in order to increase the efficiency of an optimized set of machines for a construction company.*

**Keywords:** *evaluation criteria, optimization, supply of machines, cluster approach*

## 1. FORMULATION THE PROBLEM

Transformation processes in the modern economy place the building complex in front of the requirement to stay in the market, which requires a lot of effort and carefully thought out solutions. The strategy of management, whose main goal is not so much profit making today, is becoming more widespread, as the increase in the investment value of equity capital provides the future of the economic condition of the construction company. The problem with construction equipment kits is that they have an increased degree of physical wear and tear, and low technological productivity leads to the use of a large amount of equipment.

The solution lies in finding new organizational and technological models for forming sets of machines in accordance with the program of the construction project, modern requirements and market needs. One such method is the application of the cluster approach, which is widely used in various fields and is based on the theory of systems [1], decision making criteria [2] and synergetic [3]. Its essence is due to the ability to create in a single system an optimized set of necessary, significant technology, methods of manufacturing any product of the highest quality, and the availability of adapted control to ensure minimum energy costs and the maximum productivity of the implementation of the final project.

## 2. STATEMENT OF THE MATERIAL

The criteria for the effectiveness of action are, to a certain extent, the criteria that evaluate the effectiveness of the universal and synthesized values, and are phraseological (practical) estimates [4]. Praxeology is a

general theory of the effectiveness of actions, which aims to achieve the broadest generalizations of a technological nature [8] (and it is about the technology of effective work, the recommendations and warnings that are important for each action and ultimately aimed at maximum efficiency), and mainly deals with the effectiveness of action and functioning.

Efficiency is identified with expediency, because productive actions or methods of action are those that ultimately lead to the desired result, called goal [4]. Marking the goal M, the result P, the main result - O and the cost - B, we can write the following phraseological indicators of universal efficiency [4,5].

The quality of the result

$$K_p = P/M, \quad (1)$$

is the relation of the result to the goal of action.

The quality of the main result

$$K_o = O/M \quad (2)$$

is the relation of the main result to the goal of action.

Inconsistency of the result

$$\bar{P} = P - M \quad (3)$$

is the difference between the result and the purpose of action.

Inconsistency of the main result

$$\bar{O} = O - M \quad (4)$$

is the difference between the main result and the purpose of action.

The benefit of the result

$$\chi = P - B \tag{5}$$

is the difference between the result and the cost of implementing the action.

Economy of the result:

$$\eta = P/B \tag{6}$$

represents the ratio of the result to the cost of the implementation of the action.

The quality of the main result  $K_0$  is the inverse of the degree of value of the goal, which is defined [3] as a "relation involves values that the goals (amounts of values of purpose) to the value of the real effect (the sum of values of real effects) of the action aimed at achieving this goal (goals) of action.

Using the resulted criteria (1-6) was a prerequisite for the development of a scheme for the formalization of supply of machines (Figure 1).

The cluster concept focuses on ties and interdependencies between companies integrated into the network structure for product manufacturing, service and innovation.

Clusters are different from other forms of cooperation of companies by the fact that the participating companies in it form a production and trading network.

The cluster concept goes beyond simple horizontal ties, in which firms operating on the general market of finished products belong to the same industrial group, cooperate in such areas of activity as research and development, demonstration programs, joint marketing or procurement activity.

Clusters in large part act as network structures of combined areas, staffed with heterogeneous and complementary firms specializing in the creation of any material or specific innovative product.

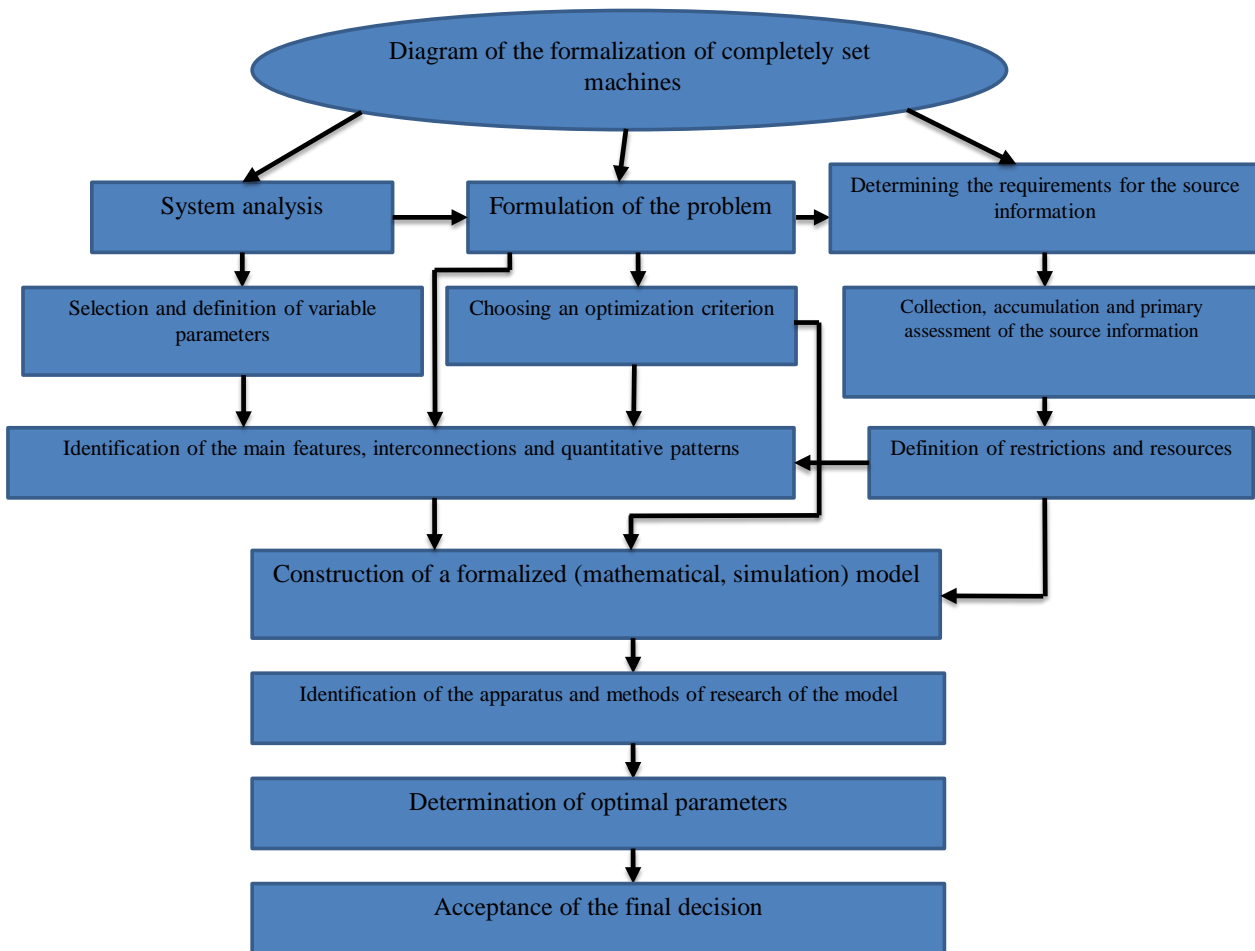


Figure 1: The algorithm of the reasonable choice and calculation of the set of machines

Within the framework of the implementation of this algorithm (Figure 1), appropriate research has been carried out in the development and implementation of the cluster approach.

When establishing strict boundaries for sectors and industries, the traditional research approach does not take into account the importance of establishing interconnections and sharing knowledge within a network structure.

The cluster concept serves as an alternative to the traditional sectoral approach in economic market research (Table 1).

Table 1: Differences between cluster and sectoral approaches

No	Cluster approach	Traditional sectoral approach
1	Strategic groups with heterogeneous, complementary firms in network structures	Groups of companies with similar network structures
2	Include suppliers, consumers, manufacturers of goods and services, specialized institutes	Focus on manufacturers of finished products
3	Combine a number of interconnected industries that use common technologies, education, information, resources, channels and clientele.	Focus on direct and indirect competitors
4	Most participants are not direct competitors, they have common problems and challenges	Doubtfulness in the organization of cooperation with competitors
5	Widespread improvements in the field of general interest that improve productivity and enhance competition.	Narrow-band approach
6	Forums for more constructive and effective dialogue between the government and the business community	The dialogue with the government is usually aimed at receiving subsidies, protectionism and limiting competition
7	Search for the synergy of new unions and associations	Search in the direction of efforts to diversify corporations under existing conditions

Output positions of the benefits of a cluster approach (Figure 2):

- firms rarely introduce innovations in isolation. It is much more intense in network science and production systems. Many participants are involved in a significant area of innovation activity, and its success is determined by their complementarity, the availability of their specialized knowledge;
- the effect of synergy that stems from the combination of knowledge of different firms and organizations that complement each other and the need for firms to combat the growing dependence on environmental conditions is a driving factor in the formation of clusters and the conclusion of agreements by firms on joint innovation activities;
- the initial theoretical position is concluded in the interaction-based theory of innovation systems, in which innovation is defined as an interactive learning process based on the exchange of knowledge and the joint activities of various participants and production network structures;
- significant innovations are born from new combinations of complementarity, diverse knowledge and competence;
- different types of network structures and markets require different styles of innovation;

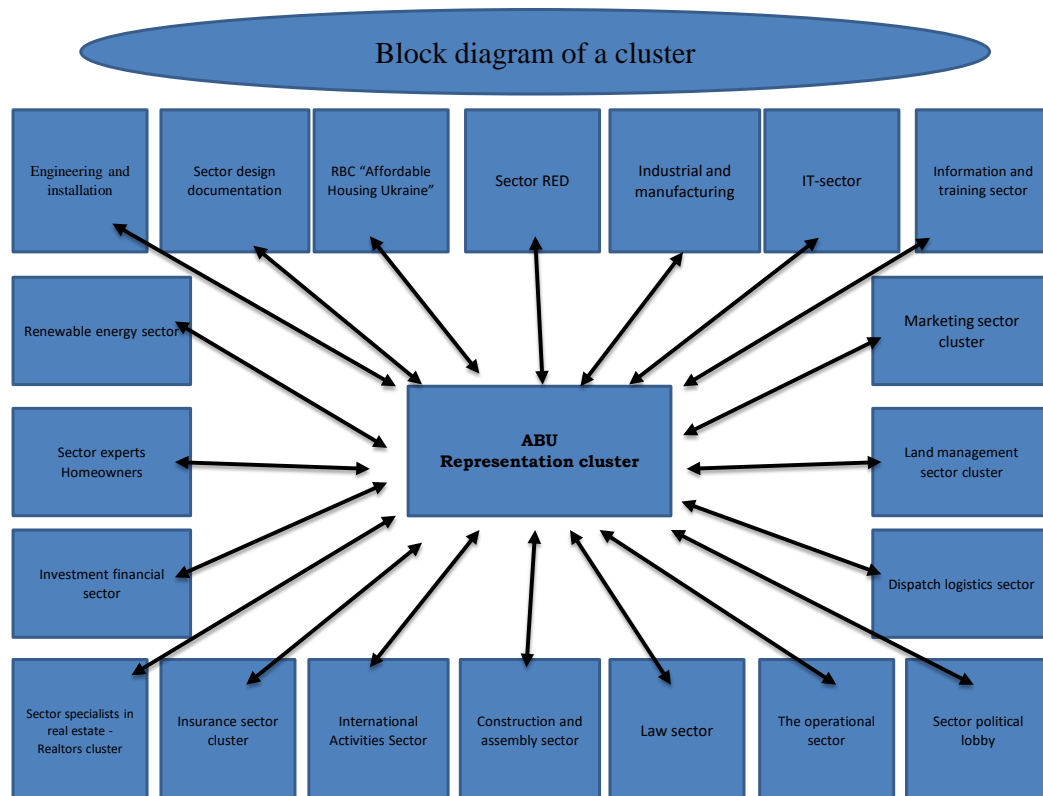


Figure 2: Innovative synergistic cluster

The economic efficiency of the enterprise (Figure 3) on the basis of the use of the cluster reduces up to 40% of the nominal structural cost of production, including: DC - the sum of direct costs: the cost of raw materials, direct wages, the work of machines and mechanisms, energy (the range of structural cost 40-50%); FC is the sum of constant general economic, general, administrative and social costs (decreasing the structural cost by 10-20%); LMA - transport logistics, cost of activities of outside organizations, marketing and advertising activity aimed at bringing and maintaining goods (services) in the market (range of structural cost 0-10%); Increase in sales volume; Enhancing company status as a cluster member.

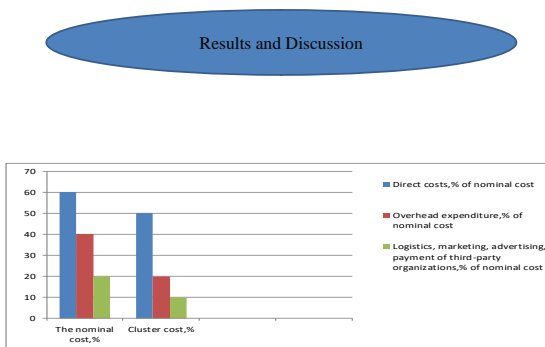


Figure 3: Economic efficiency of the enterprise based on the use of the cluster

### 3. CONCLUSIONS

1. The proposed criteria determine the rational set of machines for a construction company, their choice to compare different options in an explicit and synthesized form.

2. It is established that in modern conditions of control of the process of choosing a construction company a set of

machines based on the use of a cluster, which is based on the theory of systems, criteria of decision making and synergetic.

3. The application of the cluster method has the ability to create, in a single system, an optimized set of necessary, according to the relevant technology, methods of manufacturing any product of the highest quality and the availability of adapted control to ensure minimum energy costs and maximum productivity of the implementation of the final project.

### REFERENCES

- [1] Sokolenko S. I.: "Production systems of globalization", Logos, p. 645, (2002)
- [2] Nazarenko I.I.: "System analysis of technical objects", I. I. Nazarenko, V. N. Harnets, A. T. Svidersky and oth. // K.: KNUBA, p. 156, (2007)
- [3] Nazarenko I. I.: "Design and construction of machines and equipment for processing industries", / I. I. Nazarenko, I. M. Bernyk// K.: 'Publishing House 'Slovo', p. 495, (2014)
- [4] Gasparsky V.: "Praxeological analysis of design and engineering developments [Tran. from Polish by Chvanov Y.A.] / V. Gasparsky, M.: Mir, p. 172, (1978)
- [5] Nazarenko M.I. "Functional-cost analysis as a method for assessing the efficiency of using a park of construction machinery" / M. I. Nazarenko // Collection of scientific works "Ways to increase the efficiency of construction in conditions of formation of market relations". – K.: KNUBA, Issue 23, p. 231 – 237, (2010).



# Risk Management in Mechanical Engineering

Vladimir A. Zorin<sup>1\*</sup>

<sup>1</sup>Moscow State University of Automobile and Road Engineering, (Russia)

*In this article, the possibilities of risk management at design, production and repair of heavy machines taking into account of their operation conditions are considered. It is shown how on a basis of risk based thinking it is possible to prevent risks and to increase the level of safety of heavy machines. Methods of the analysis and assessment of risks in mechanical engineering are considered.*

**Keywords:** Heavy machinery, Mechanical engineering, Risk management, Risk based Thinking

## 1. RELEVANCE OF THIS PROBLEM

Until recently assessment of risks was not considered as compulsory procedure at design and production of the machine and many enterprises were limited to the analysis of level of their reliability. From the moment of adoption in the Russian Federation of technical regulations "About safety of machines and the equipment" TR CU 010/2011[1] which according to article 4 obliges to machinery out risk assessment at development stages (design) of machines and the equipment many organizations which are engaged in production and operation of such machines and the equipment faced need to conduct continuous work on assessment of possible risks and development of ways of their elimination. Unfortunately, it was quite difficult task. The reasons it is possible to bring quite a lot, but nevertheless it is possible to call the main: lack of wide circulation of risk evaluating. Despite existence of quite broad quantity of methods of risk assessment (according to ISO 31010-2010 [2] their application B 31) enough often such technique needs to be developed especially for a concrete case, the machine, the mechanism. Absence of experts and experience in machinerying out similar works introduces the amendments on the way of full application of technical regulations. Development of risks assessment methods at operation of machines is of great interest to the operational organizations and the enterprises which are engaged in guarantee maintenance of this production.

## 2. PROCESS OF RISK MANAGEMENT AND THE EXISTING METHODS OF RISKS ASSESSMENT

In a general view life cycle of the machine consists of four main stages: Design, Production, Operation and Utilization (Figure 1). Apparently from the drawing process the risk management at best is present only at the first two stages: design and productions, process of operation it is them not captured. Real data on operational properties begin to arrive only after the beginning of product operation. In most cases it means that in a link there is one more participant - the consumer who also as well as the producer, in case of detection of defects will incur additional expenses.

Therefore, existence of an opportunity previously to estimate the risks connected with product operation to launch in mass production for the producer or before acquisition for the consumer is the major task.

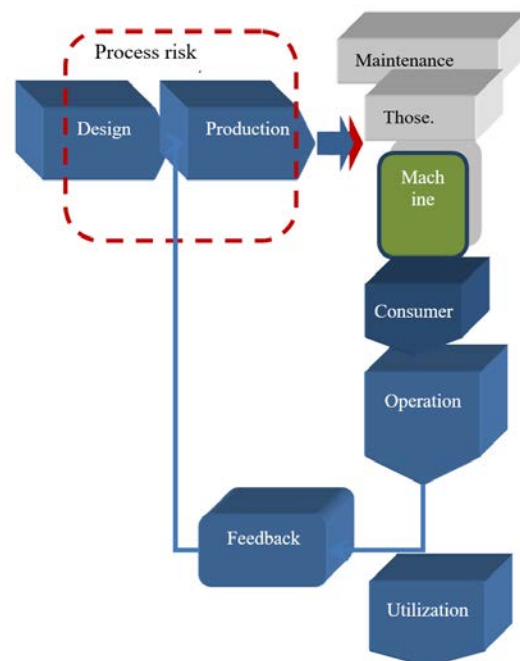


Figure 1: Simplified scheme of life cycle of the machine

The existing methods of risk assessment can conditionally be divided into 4 main groups [3]:

1. **Phenomenological** methods are based on identification of a possibility of development of emergency processes by results of the conducted tests and pilot researches. It is possible to refer high reliability of results to advantages of methods, but only in case it is possible with sufficient reliability to estimate current state of the studied system elements. Methods well are suitable for the comparative analysis of various models of the machine, but - are of little use for the analysis of difficult multipurpose objects.

\*Corresponding author: Leningradsky prospect 64, Moscow, Russia, madi-dm@list.ru

2. **The determined methods** assume machinerying out the analysis of the sequence of succession of events, beginning from an initial event and to a final condition of system, through a number of estimated intermediate stages and states. Development of processes is predicted by means of methods of mathematical modeling, imitations and difficult calculations.

The determined methods provide presentation of the received results and provide a possibility of identification of the major factors influencing process of change of a condition of system.

Need of development of difficult mathematical models and conducting difficult and expensive pilot studies belongs to shortcomings of this group of methods.

3. **Probabilistic methods** lean on assessment of probability of emergency and calculations of probabilities of events succession. The analysis of possible chains of events is for this purpose machinery out and the total probability of emergence of failure of the machine is estimated. Advantage of a method is the possibility of drawing up simplified, in comparison with the determined method, mathematical models. However, simplification of models leads to decrease in accuracy of estimates. To the main shortcomings of methods dependence on quality and volume of information on a condition of system is.

4. **The inductive method** allows to identify dangerous situations and events, probability of their emergence, and also size of possible damage at early stages. Application of this method allows to correct a system design at a design stage. Need to consider a set of various internal, external and random factors in calculations belongs to shortcomings of this method. For studying of difficult systems and obtaining the most exact results of assessment of risks it is necessary to use a combination of several methods. It allows to increase quality of the received results and to partially compensate shortage of statistical information.

### 3. CHOICE OF A METHOD OF RISK ASSESSMENT AND SEQUENCE OF ACTIONS

Risk assessment is a number of the logical steps allowing to apply system approach to consideration of factors of danger [3].

Basis for risks assessment  $R$  within technical regulation are the functionality of  $F$  connecting probability  $P$  emergence of an adverse event and population mean of damage of  $U$  from this adverse event

$$R = F_R \{U, P\} = \sum_i [F_R(U_i, P_i)] = \int C(U)P(U)dU = \int C(P)U(P)dP$$

where:  $i$  – types of adverse events,  $C$  – the weight functions considering interference of risks.

The offered technique to be under construction on the analysis of the possible failures of the machine revealed by results of preliminary researches. Main stages:

1. Formation of the list of possible dangers. At this stage, it is necessary to collect and analyses information on the possible dangers connected with operation of the machine. And also, to study available statistical information.

2. The choice of possible sources of threats, identification of the key knots which are sources of danger and to define their character.
3. Elimination of dangers which are impossible or improbable at operation of the studied machine. This action is necessary for reduction of volume of necessary works, simplification of estimated actions and improvement of quality of the received results.
4. Risks Assessment. Determination of probabilities of emergence of emergency situations, and also assessment of potential damage from their emergence.
5. Development of measures for elimination of threats. After determination of probability of emergence of an emergency situation and possible damage, the decision on expediency and ways of elimination of threats is made.

The most difficult is the calculation stage. For obtaining exact data on probability of approach of an event it is necessary to create the sufficient volume of statistical data that is quite difficult task as not all organizations have an opportunity to accumulate and analyze such information. In this situation method of expert evaluations can be also used. After risks assessment, it is necessary to obtain data on possible damages from these emergences.

Damage assessment as a result of realization of risk can be machinery out by means of insurance companies, the repair organizations or method of expert evaluations.

The conducted researches allow to create lists of risks and the related material inputs. Then on each point the decision on the risk level acceptability has to be passed. If value of risk appears beyond admissible limits, it is necessary to make the decision on development of measures for decrease in risk. In case decrease in risk is not possible, it is necessary to machinery out a package of measures for its prevention (exception). One of the main articles of expenses of any machinery producer make costs of guarantee maintenance. The term of guarantee maintenance is a strong argument at the choice of a make of the machine by the end user. Long since producers try to find optimum values of guarantee periods which will allow to attract consumers without essential losses on implementation of guarantee certificates. The main contribution on the way of achievement of this purpose is made by the level of technologies of the producer, "nou-Hau" which allow to distinguish it from a competitive environment. A lot of things depend also on quality of materials, level of production of the completing main suppliers of components, etc. All these factors in total exert the impact on reliability of the making units and knots of the machine, and eventually on the total level of reliability of the machine. Reliability of the machine is one of the main components of safety of its operation. Quite often high standards on production, and also high quality of constructional materials are not an absolute guarantee of low costs of ensuring reliability of the machine in operation as there is a set of factors which cannot be considered by production and design:

- human factor at control of machine;
- climatic features;
- modes of operation and frequency of technical service;

- quality and condition of a paving;
- quality of operational materials and spare parts;
- level of technological equipment of the service enterprises;
- skill level of the personnel making maintenance and repairs of the machine.

All these factors introduce serious amendments, changing a curve of costs of guarantee maintenance towards increase.

There are practically no tools allowing to predict precisely the size of expenses taking into account multiple-factor influence of service conditions on technical condition and requirement of the machine under repair. For this reason, the majority of decisions is made or directly by the dealer, on the basis of own experience and an intuition, or leans on a mathematical apparatus (mathematical modeling or elements of probability theory), but without features of operation. As an object of a research the machine, the most popular segment in Russia is chosen. (For maintaining confidentiality, the producer and a make of the machine do not reveal). On the basis of data on operation the schedule of distribution of the made replacements of details on systems of the machine (Figure 2) is constructed.

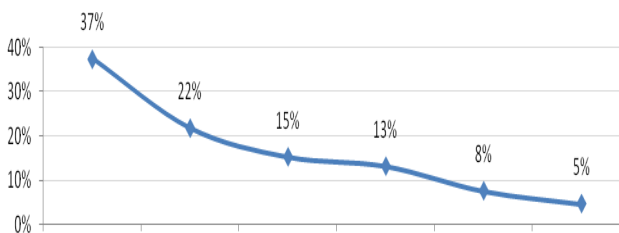


Figure 2: The schedule of distribution of replacements of details on systems of the machine: 1- System of steering; 2- Electronic equipment; 3- Transmission; 4- Glazing; 5- Fuel equipment; 6- Suspension bracket

From the point of view of safety of the machine the system of steering is the most important. The following list of the most often replaced details during the guarantee period (Table 1) is characteristic of steering i.e. on these positions the producer incurs the raised losses during the guarantee period.

In Figure 3 the example of quality standard of risk is given. Figures specified the possible analyzed risks. Let's allow at number 1 it is risk of failure of the pump of the power steering (GUR). This risk was the most critical. Respectively it is necessary to develop a number of the measures designed to reduce this risk. Replacement of GURA by the electro power steering can be one of such options.

Knowing distribution of refusals on spare parts, we machinery out the analysis of dangers and actually risks assessment. At the exit depending on the purpose of machinerying out risk analysis we receive high-quality or quantitative expression of risk.

In Figure 3 the example of quality standard of risk is given. Figures specified the possible analyzed risks.

Respectively it is necessary to develop a number of the measures designed to reduce this risk. Replacement of the hydraulic pump by the electro power steering can be one of such options.

Table 1. The most often replaced details during the guarantee period

Name of a detail	% of replacements
System of steering	54%
Hose of high pressure of GUR	16%
Steering rack	13%
Driveshaft	8%
Pump GUR	3%
Tube of system of steering	2%
The column is steering	1%
Air valve	1%
Lath emphasis arm	1%

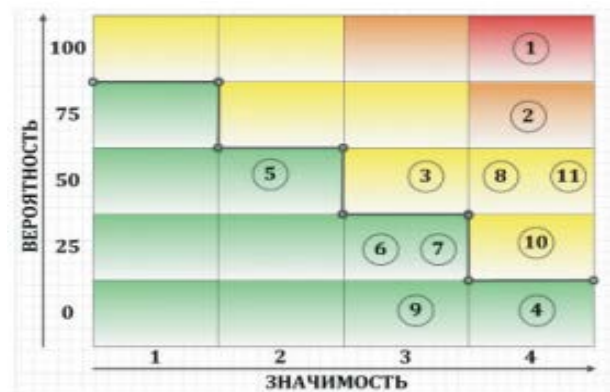


Figure 3: Results of quality standard of risk

For a solution of the problem of influence of regional features of operation on reliability it is offered to use two-stage approach to assessment of risks of the machine (Figure 4).

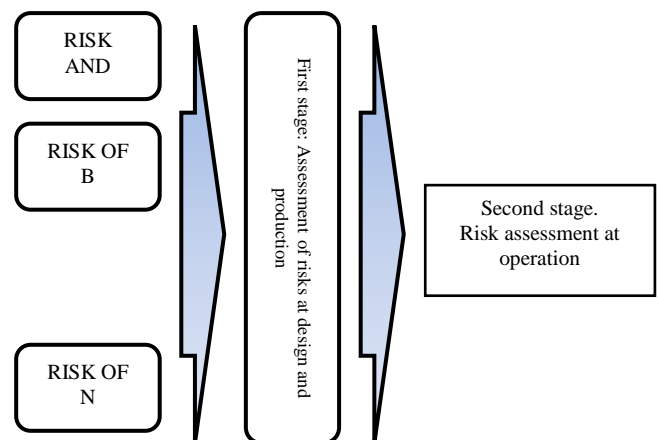


Figure 4: Two-stage approach to the generalized risk assessment at operation of the machine

Stage first: allocation of group of risks, the most critical for this machine.

Ranging of the chosen risks on the level of danger and cost of elimination of consequences.

*Stage second:* calculation of the general risk assessment taking into account service conditions.

It is necessary for obtaining preliminary data for further decision-making, concerning delivery of new model of the machine without any essential changes in a design or conditions of a guarantee provision. In this regard, it is offered to adapt a technique of risks assessment to operation realities in the conditions of the concrete region, in our case of the Russian Federation. On the basis of skilled observations, it was revealed that guarantee expenses are influenced by the following factors (Figure 5):

1. Level of reliability of the machine
2. Regional features of machine operation
3. Modes of use of the machine
4. Cost of spare parts, operational materials and works

For simplification of calculations we accepted some restrictions:

- in the course of development of the machine there are risks which are characterized by probability of emergence of refusals and malfunctions of its main knots, the systems influencing safe operation (without risk of refusals of electronic control systems).

- the mode of operation is defined by a manner of driving of the machine which depends on character of the driver and operation conditions. As it is not possible to predict a driving manner, we accepted assessment scale depending on age of the owner who is indirectly influencing the mode of operation of the machine. The age of the owner is specified upon purchase of a machine.

Assessment scales for each of types of risk are presented in Table 2.

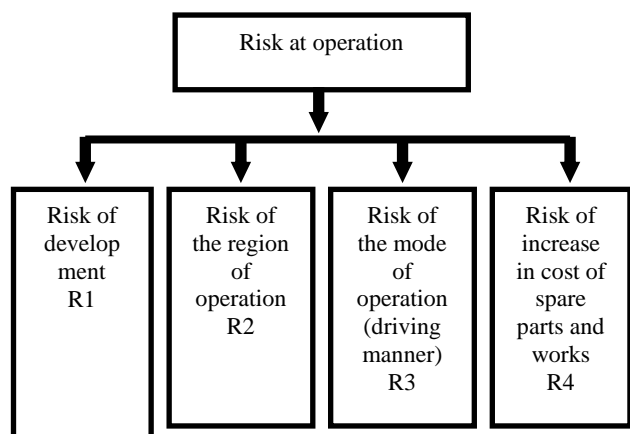


Figure 5: Types of manifestation of risk at operation.

For receiving uniform of risk assessment, it is offered to use linear model of the weighed sum of factors of a look:

$$R_{ob} = A_1X_1 + A_2X_2 + A_3X_3 + \dots + A_nX_n$$

For obtaining value from 0% to 100 % is normalized the total value of risk on a formula:

$$Y = 100\% * (R_{ob} - Min) / (Max - Min)$$

Table 2: A risk assessment scale at operation of the machine

Risk	Point	Assessment	Description
1	2	3	4
Risk developments	1	Low	elements of an exterior, body interior
	2	Average	Systems of passive safety, DVS, transmission, suspension bracket
	3	High	Steering, systems of active safety
	4	Critical	Brake system
Risk region of operation	1	Low	Moscow and Northwest region
	2	Average	Central and Southern regions
	3	High	Far East
	4	Critical	Siberia
Risk operation mode	1	Low	over 45 years
	2	Average	30-45 years
	3	High	23-30 years
	4	Critical	up to 23 years
Risk of increase in cost of spare parts and works	1	Low	The model is local and the main spare parts are made in the territory of the Russian Federation
	2	Average	The majority of spare parts are imported. There is an opportunity to arrange local production
	3	High	100% import and impossibility to arrange local production in view of lack of technologies
	4	Critical	The producer abandons the market of the Russian Federation

The table of interpretation of rated risk assessment can be adapted under the concrete organization taking into account its policy and standards. Use of the offered approach during the planning of deliveries of new models of machines and justification of warranty periods of their operation provides a possibility of planning of the operating technical influences for the purpose of safety of use of the machine taking into account regional operation features.

REFERENCES

[1] Technical regulations of the Russian Federation TR CU 010/2011 "About safety of machines and the equipment"  
 [2] State standard specification P ISO/MEK 31010-2011 Management of risk. Risk assessment methods  
 [3] Zorin, V. A. Reliability of mechanical systems M: INFRA-M publishing house, 2015. – 380 pages.

# Laboratory Test Rig for Nondestructive Inspection of Steel Cord Belts

Miloš Đorđević<sup>1\*</sup>, Nenad Zrnić<sup>1</sup>, Srđan Bošnjak<sup>1</sup>

<sup>1</sup>Faculty of Mechanical Engineering, Department of Material Handling Constructions and Logistics, University of Belgrade, Belgrade (Serbia)

*The paper gives a survey of NDT of steel cord belts. For the purpose of NDT of steel cord belts a laboratory test rig is developed at the Faculty of Mechanical Engineering, University of Belgrade. Its intended use is nondestructive inspection of steel cord belts with Introcon S 2000 instrument. Axial distance between the drums of transporter is only 1500 mm and it can work with belt widths up to 400 mm. Due to its small dimensions and intended work with steel cord belts, in configuration with instrument for non-destructive testing, it represents a unique laboratory facility.*

**Keywords:** Laboratory belt conveyor, nondestructive testing, steel cord belts

## 1. INTRODUCTION

Belt conveyor systems and other subsequent systems usually have a serial structure. This means that a failure of a belt conveyor, brings all other machinery and equipment to a stall. Therefore, the problem of ensuring an adequate level of availability of a continuous transport system is extremely important [1]. To maintain optimal working conditions and avoid unexpected halts and shutdowns different inspection and monitoring methods of belt conveyor equipment can be applied. Those inspections and testing can be both destructive and nondestructive.

The belt conveyor consists of 5 main components, as described in [2]. Despite the fact that failure of any of these components could lead to the shutdown of the system, this paper focuses on nondestructive testing (NDT) of conveyor belts, as the most important component of the belt conveyor, particularly on the NDT of steel cord belts.

Expected steel cord belt service life is 3-6 years. With proper maintenance and care it could be prolonged to more than 10 years. Therefore, steel cord belts are tested for:

- steel cord state (number of broken cords)
- belt splices stability (consistency of longitudinal gap between adjacent cords)
- rubber covers (or structural) state [3].

Similarly, according to ContiTech [4], [5] steel cord belts are inspected in order to perform:

- belt rip detection
- cord condition monitoring
- splice elongation measurement
- belt thickness measurement
- belt surface inspection

For belt rip detection ContiTech uses RFID chips and closed circuit loops and magnetic method for cord condition and splice monitoring, while the surface is inspected for defects using line LASER technology. In accordance with [6] rip detection methods include:

- sensor loops
- LASER rip detection - triangulation
- wire under belt.

Although all of the aforementioned factors have a significant impact on the steel cord belt service life, one

should have in mind that durability of the belts is defined mainly by steel cord condition. Steel cords can be broken or corroded. Besides, rope splice damage is possible. Majority of steel cord defects is not visible because of their location inside rubber. Magnetic method of NDT is usual to detect the steel rope brakes inside the belts [7]. Besides that, magnetic devices can also be used for diagnostics of steel cord belts condition regarding their resistance to puncture as described in [8].

## 2. HISTORICAL REVIEW OF NDT

Harrison stated in [9] that "the science of NDT was born in Australia in 1979 with the patenting of a system that came to be known as the "CBM" or conveyor belt monitoring." This new technology permitted testing of conveyor belt damage and degradation and for the first time steel cord belts were tested for corrosion. Paper discussed safety factor analysis and dynamic safety factor analysis. Splices are considered potentially weak link in a steel cord belt. At the time the paper was written available sensors for testing steel-reinforced belting included magnetic, eddy-current, electromagnetic, X-ray and vibration sensor systems [9]. Further, Harrison explains magnetic NDT method that detects corrosion and breaks using variable magnetic reluctance transducer in [10] and magnetic NDT method with ferrite-cored coil array and external field of an axially magnetised cord in [11].

## 3. REVIEW OF NDT METHODS

Among the most common NDT methods analysed by Kumar and Mahto in a very comprehensive review presented in [12] are NDT methods listed below:

1. Visual & Optical
2. Ultrasonic
3. Electromagnetic (EMG)
4. Thermographic
5. Radiographic
6. Liquid Penetrant
7. Magnetic Particle
8. Acoustic Emission
9. Magnetic Resonance Imaging
10. Optical Microscope
11. Near-Infrared Spectroscopy

P. Cawley [13] highlights the "Big Five" among listed methods (methods marked with 2, 3, 5, 6 and 7 in previous list). Another systematization of NDT methods available online at [6] divides them into:

- Visual inspection
- Transmitter-receiver system
- Leakage field measurement
- Magnetic resistance
- Opto-electronic imaging
- Portable camera
- X-ray - portable camera
- X-ray - stationary, continuous

Speaking of X-ray testing, Li et al in [14] described the MRB (Modified Regular Bands) method which deals with X-ray images, has a higher precision so it can detect fine faults, is simple and fast enough for real-time online fault detection. Although X-ray systems, both portable and stationary continuous, have superior characteristics in comparison with all other NDT methods, they are not that much in use due to their possible hazardous effect on the human health. Therefore, the most common methods in use are EMG and magnetic methods.

#### 4. METHODS AND EQUIPMENT FOR NDT OF STEEL CORD BELTS

In general, steel cord belts are mostly tested with EMG or magnetic NDT methods. There is a vast variety of such methods and equipment available on the market. Some of them will be presented below alongside with the review of NDT equipment conducted by Blazej [15]. That review included:

- Beltscan Pty Ltd (Australia) - Belt Guard™ system - magnetic, high resolution system
- CBM Conveyor Belt Monitoring (Australia) - Magnetic Flux Leakage (MFL) system
- CBT Conveyor Belt Technology (USA) - C.A.T. MDR™ system - magnetic, high resolution system, where C.A.T. stands for Cable Anomaly Tomography and MDR for Magnetostatic Differential Reluctance measurement technique [16]
- Conveyor Technologies (CT Colorado & CT Pty. NSW Australia)
- TCK (China) - TCK Steel Cord Conveyor Belt Online Automatic Inspection System - weak magnetic field system
- Veyance Technologies (Goodyear) Cord Guard™ system - high resolution magnetic pictures, and
- Introcon system - Intron (Russia) - eddy-current system

DIAGBELT system is used for NDT of belt splices. It consists of 7 modules with magnetic coils, 2 permanent magnet bars, magnetic encoder (for measurement of conveyor velocity) and measuring head. Diagbelt uses Belt Guard™ (Australian) system's measuring head and data acquisition module [17].

Fenner Dunlop's EagleEye™ system is based on PLC and uses Magnetic Flux Leakage (MFL) panels or Conductive Loops or both for rip detection, plus provides continuous monitoring via Virtual Private Network (VPN) [18], [19]. G.S. Park et al explained Magnetic Flux Leakage method (MFL) in [20] in which the defect signals are mainly dependant on the change of the magnetic flux

leakage in the region of a defect. MFL technique is also explained in [7].

Metal Magnetic Memory (MMM) NDT technique for testing of steel cord belts is presented by Xuwei in [21]. It has high sensitivity, small lift-off effect and high reliability.

EyeQ is magnetic method of automatic detection. It provides real time monitoring and statistical analysis. Applied principle of measuring changes in magnetic field is coupled with vision module (for continuous inspection: linear DALSA camera with IMAQ vision software and LabView environment) [22]. A group of members of the Machinery Systems Division (MSD) in the Institute of Mining Engineering at Wroclaw University of Technology (WUT) worked with enhanced EyeQ system in combination with Computer Assisted Belt Card (belt management system). They also applied 2 magnetic scanners: HRDS (modified EyeQ system developed in MSD at WTU) and the LRM scanner (developed by servicing firm laboratory of Roman Martyna [23] - NDT system based on Magnetic Flux Leakage and permanent magnets) to establish steel cord condition of belt loops in working environment. This group also developed ABCDE tool - Automatic Belt Condition Diagnostic Equipment, consisted of 5 modules: A - vision (digital video recording + mechatronic sensor), B - magnetic, C - preventive, D - forecasting, E - safety factor [24], [25].

Embedded Conductive Detection system (ECD) stands for intelligent monitoring of belt conveyor systems, which is based on magnet matrix embedded in belt carcass in combination with outside sensors [26].

More advanced solutions may also include Artificial Intelligence (AI) systems. Kwasniewski presented in [3] state-of-the-art solutions for continuous monitoring of steel cord belts working conditions based on AI. "Major applications of AI include:

- Fuzzy logic technologies – widely used in diagnostics;
- Expert systems – in simple terms they include a "computer adviser", simulating the work of an expert in diagnostics that in certain situations is able to replace or advise the expert;
- Neural networks – commonly used in fault detection in diagnostics."

In accordance with the presented system, steel cord belt attributes of emergency conditions that are subjected to the continuous monitoring are:

- Broken cords over the entire belt width (in the belt cross-section)
- Longitudinal separation of layers along the rubber matrix (bad adhesion)
- Elongated connections (inconsistency of belt splices) [3].

At the end of this survey eddy current NDT method will be presented.

"Javier Garcia Martin et al [27] gives an overview of the fundamentals and main variables of eddy current testing. It also describes the state-of-the-art sensors and modern techniques such as multi-frequency and pulsed systems. Recent advances in complex models towards solving crack-sensor interaction, developments in instrumentation due to advances in electronic devices, and the evolution of data processing suggest that eddy current

testing systems will be increasingly used in the future." [12]. "Eddy current testing is one of the most extensively used nondestructive techniques for inspecting electrically conductive materials at very high speeds that does not require any contact between the test piece and the sensor." [12].

Finally, it should be mentioned that there is one more method that works on eddy current principle. It is pulsed eddy current (PEC) method, an effective electromagnetic NDT technique. PEC is explained in [28].

### 5. LABORATORY TEST RIG

Laboratory test rig for NDT of steel cord belts (Figure 1, 2 and 3), installed at the Laboratory for Logistics and Ecodesign at the Faculty of Mechanical Engineering - University of Belgrade (Department of Material Handling, Constructions and Logistics), consists of the belt conveyor (Figure 4) and its components, mobile carrier frame (Figure 5), NDT instrument (in further text scanner) Introcon S 2000 (Fig. 24, 25 and 26) and its girder (Figure 6).



Figure 3: Produced belt conveyor, mounted on mobile carrier frame with scanner girder attached to its frame

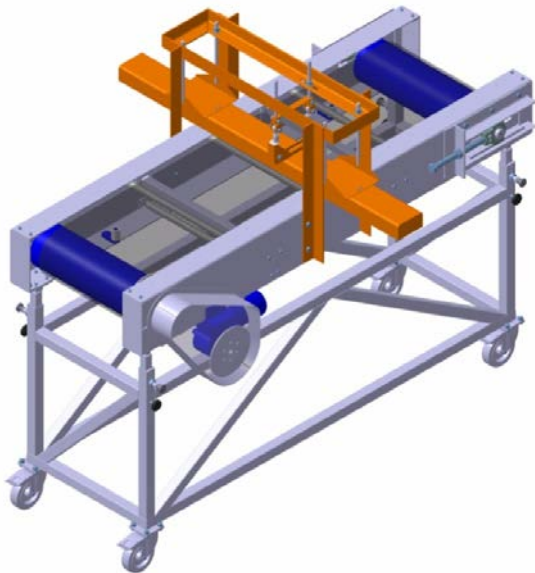


Figure 1: The 3D model of the test rig for NDT of steel cord belts

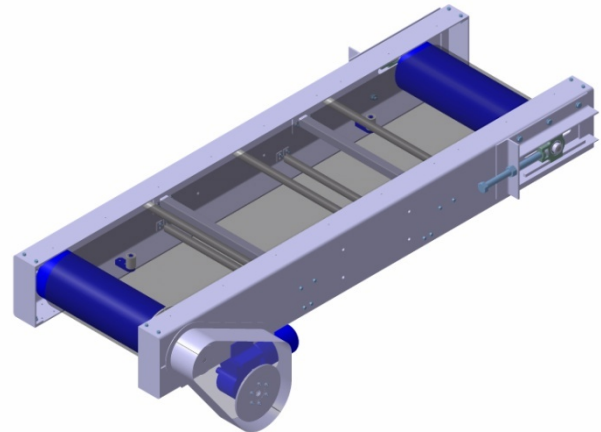


Figure 4: The belt conveyor



Figure 2: The 3D model of the test rig for NDT of steel cord belts

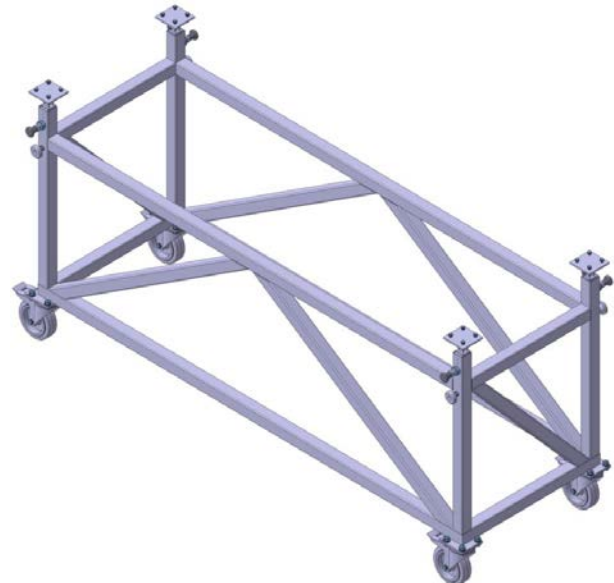


Figure 5: The belt conveyor mobile carrier frame



Figure 6: Scanner girder: 3D model (left) and produced construction (right)

The Laboratory acquired 2 steel cord belts for testing by the courtesy of Kolubara Univerzal d.o.o. (member of Continental corporation).

One steel cord belt is made by reworking of a worn-out steel cord belt intended for refurbishment. Both rubber covers are almost entirely stripped of. Therefore, belt surface is textured with shallow longitudinal grooves obtained by stripping of covers, see Figure 7. Overall belt thickness is 13 mm in average. Belt is made to be 400 mm in width and 3500 mm in length with vulcanised splice, see Figure 8 and 9. Steel cord filaments of the belt are 5.3 mm in diameter.



Figure 7: Textured surface of the worn-out steel cord belt

The other belt is specially made for the purpose of laboratory testing. Belt width and length are the same as of the first belt, see Fig. 8 and 9. Overall thickness is 9 mm in average. Steel cord filaments of the belt are made of breaker layer wires, which are 1.15 mm in diameter. This belt has intentional manufacture built-in defects made for the purpose of laboratory investigations. Exact position and type of defects are marked on map of the belt.



Figure 8: Steel cord belts for laboratory testing: worn-out belt (up) and specially made belt (down)

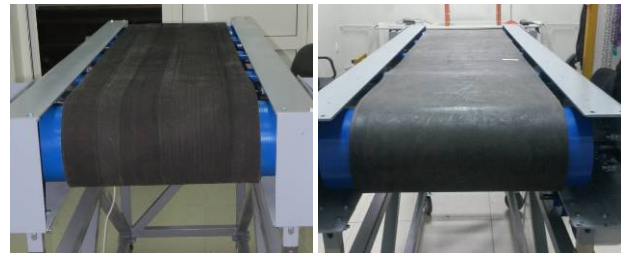


Figure 9: Steel cord belts mounted on the conveyor: worn-out belt (left) and specially made belt (right)

### 5.1. Belt conveyor and its components

The belt conveyor is 1800 mm long and 760 mm wide and it is consisted of the frame, 5 rollers, 2 pulleys, take-up device and drive, Figure 10.

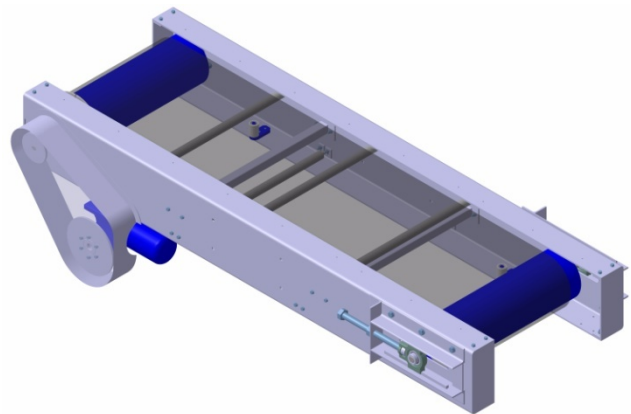


Figure 10: The belt conveyor with its components

The belt conveyor frame is made of 2 c-shaped sides of 5 mm thick steel sheet (Figure 11) connected with 2 supports made of 30x30x1.5 mm steel square tubes 590 mm in length, See Figure 12. Frame sides are on both ends closed with covers, see Figure 13.

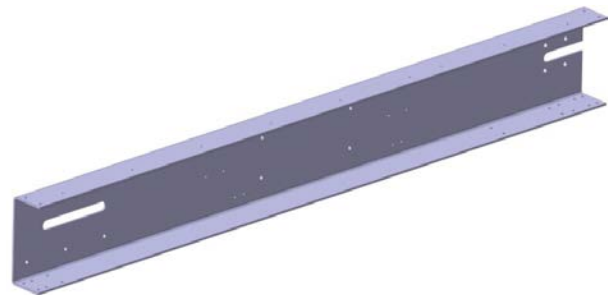


Figure 11: The belt conveyor frame side

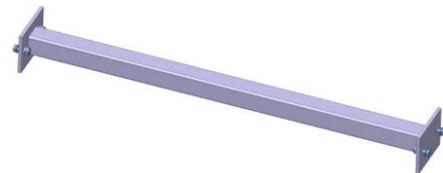


Figure 12: The belt conveyor frame support

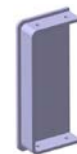


Figure 13: The belt conveyor frame cover



Rollers are made of  $\varnothing 28$  mm and 4 mm thick steel tubes, 560 mm in length with  $\varnothing 16$  mm shafts and a pair of 609 ZZ ball bearings each, see Figure 14 and 15.



Figure 14. The belt conveyor roller



Figure 15. The belt conveyor roller's end

Both pulleys are 500 mm long and 159 mm in diameter with  $\varnothing 20$  mm shafts, see Figure 16.



Figure 16. The belt conveyor pulley

Axial distance between conveyor pulleys is nominally 1500 mm. The take-up device is made of M20 threaded rod with travelling distance of 200 mm. The drive pulley is embedded in conveyor frame using two UCF 204 ball bearing units, see Figure 17.

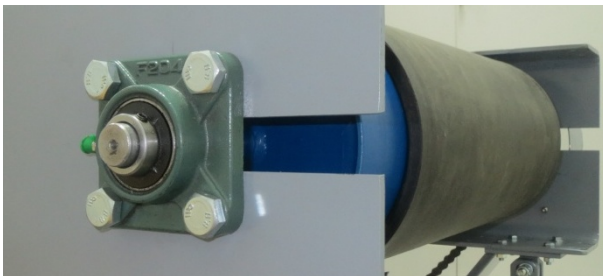


Figure 17: The drive pulley ball bearing unit UCF 204

The tensioning pulley shaft ends with UCT 204 ball bearing unit on both sides. These units are connected with threaded rods of tensioning mechanism and they slide between a pair of  $\square 10 \times 10 \times 250$  square steel rods. Together with the steel frame made of L50x50x5 and couple of M20 nuts they form the take-up device, see Figure 18.



Figure 18: The take-up device

Since steel cord belts are not intended for use in such short belt conveyors, misaligning of the belt occurs as an issue. Side belt training rollers (4 of them) are installed to

correct belt aligning. They are installed inside the belt conveyor frame, equally spaced from the front and the back end of the conveyor, at the distance of 400 mm from the belt conveyor frame covers, see Figure 19 and 20. Since they are mounted using slotted holes, they permit adjusting of the clearance between them and the edge of the belt.



Figure 19: The training roller placed on the inner side of the belt conveyor frame



Figure 20: Training rollers in their working position adjusted for belt width of 400 mm

However, additional belt tracking is needed. Since crowned pulleys are not intended for use with steel cord belts, another solution is needed. Flanges attached to the drums should solve this problem.

Power is transmitted from the 1.1 kW AC electric motor over the worm gear and a pair of replaceable chain sprockets, see Figure 21. Three sets of chain sprockets have been made. Combinations of sprockets provide 3 different belt speeds: 0.2 m/s, 0.4 m/s and 0.6 m/s.

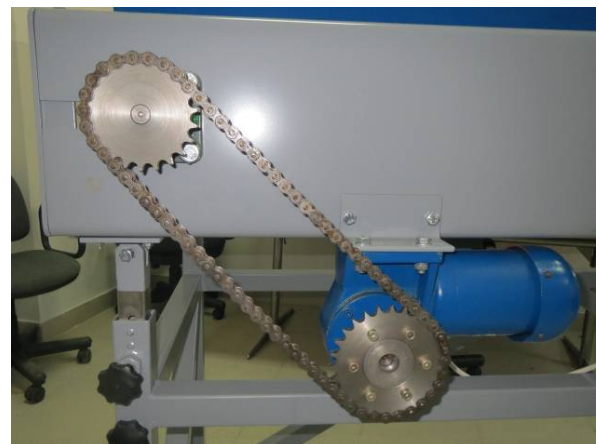


Figure 21: Belt conveyor drive

## 5.2. Belt conveyor mobile carrier frame

The belt conveyor mobile carrier frame is a welded construction made of  $\square 40 \times 40 \times 1.8$  mm square steel tubes with 4 telescopic pylons made of  $\square 30 \times 30 \times 1.5$  mm square tubes that are made of stainless steel.

Telescoping of tubes provides height adjustment ability which permits forming an inclined conveyor with incline up to 18°, see Figure 22. Height can be adjusted using levers shown in Figure 23. Whole frame is mounted on 4 wheels with brakes, 125 mm in diameter.



Figure 22: Inclined conveyor



Figure 23: Levers for conveyor height and incline adjustment

### 5.3. Description of the scanner and its working principle

The Laboratory is equipped with explosion-proof version of Introcon S 2000 scanner and it is suitable for NDT of steel cord belts in width up to 2000 mm. It works with belt speeds up to 7 m/s. The device is capable of detecting broken cords, as well as corroded areas and splice monitoring. Scanner's working principle is based on eddy currents. "Coil of the eddy current transducer induces eddy currents in steel cord ropes. The currents depend on rope condition: integrity and cross section area particularly. Sensing coil of the transducer gets a signal like a voltage pulse when break of the rope enters into the transducer's sensing area. The transducer covers 10-12 ropes if they are distanced (17-20) mm each other." [7].

Five transducers are united in a module. Our model of the scanner - Introcon S 2000 has 2 modules, each consisting of 5 transducers, see Figure 24.



Figure 24: One scanner module consisted of 5 transducers

Since the scanner is a portable device it can be disassembled, for storage and transport, see Figure 25.



Figure 25: Disassembled modules of the Introcon S 2000 scanner (Courtesy of Intron)

When the scanner is prepared for operation modules are interconnected one to another with cable and mechanically fastened with bolts, see Figure 26.



Figure 26: Assembled scanner with both modules fastened to each other with bolts and connected with cable

Each one of modules is connected to the separate basic unit (Figure 27, left), that provides the connection with the output of each of the transducers. The basic unit supplies the exciting coils of the transducers by alternating current, collects analog data from the transducers and gets pulses from distance counter [7]. The distance counter is attached to the one of the modules, Figure 27, right. It provides determination of the exact location of the defects within the belt, as well as measuring of the belt's speed. "There are 8 input channels for not more than 8 transducers. The data are transformed into digital form, processed by microprocessor, stored and displayed on LED display.

After downloading of the data to a computer they can be processed by the special software WINTROCON to analyse the test result and to print the final test report. The transducer works in one of two modes: local fault (LF), like rope break, and loss of metallic area (LMA), like rope corrosion. It is necessary to pass the belt through the scanner twice, if one wants to get the LF and LMA data both." [7].



Figure 27: Basic unit (left) and distance counter (right)

5.4. Installation of the scanner

Scanner's girder is mounted directly on belt conveyor frame, fastened with bolts, see Figure 1, 2 and 3. Since conveyor is built for inspection of belts in width up to 400 mm, the girder is designed to support only one module of the scanner. The girder provides adjustable clearance between the belt and the scanner. Prisms for adjusting exact clearance of 10 mm, 15 mm and 20 mm are provided alongside with the scanner from the supplier, see Figure 28 and 29.

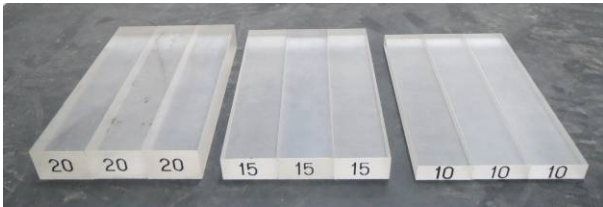


Figure 28: Prisms for adjusting the clearance between the belt and the scanner

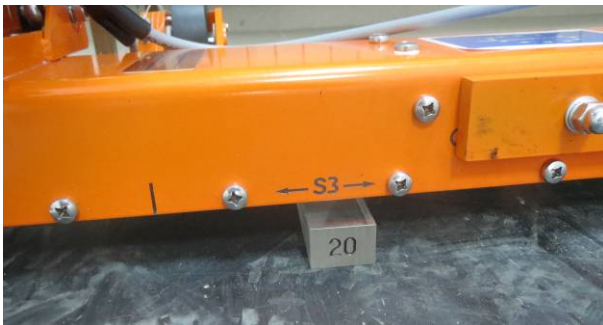


Figure 29: Actual use of prisms for adjusting the clearance

Module of the scanner with distance counter is attached to the girder over specially designed supports that are mounted on the hand lever's places on the instrument, see Figure 30, 31 and 32.



Figure 30: Hand lever for carrying the scanner



Figure 31: Specially designed support for the scanner

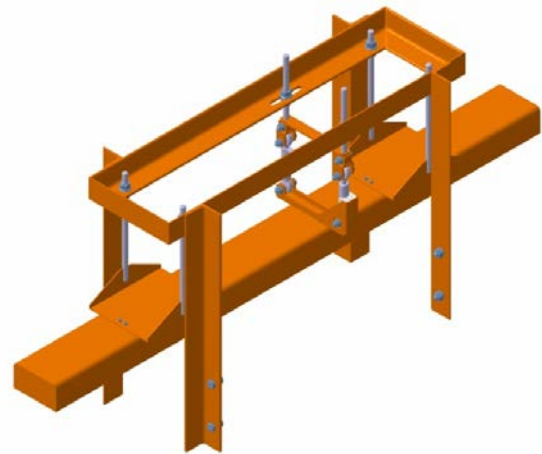


Figure 32: Module of the scanner mounted on the girder

6. CONCLUSION

Non-destructive testing of belt conveyors is one of the most important issues in maintaining proper operation of conveying machines, particularly for steel cord belts. However, the most of currently existing devices are merely used for field inspection. For the aforementioned fact it is necessary to create a laboratory test rig which can be used both for educational and research purposes. For such purposes a laboratory test rig is developed and installed in the Laboratory for Logistics and Ecodesign at the University of Belgrade - Faculty of Mechanical Engineering (Department of Material Handling, Constructions and Logistics). It is a unique test rig in the HEIs in the area of SEE and WB countries. Its characteristics, thoroughly presented in the paper, ensure the boost of educational and research potential of the institution and give a substantial opportunity for further development in linking intralogistics equipment and environmentally related issues.

ACKNOWLEDGEMENTS

This work is a contribution to the Ministry of Education, Science and Technological Development of Republic of Serbia funded project TR 35006.

REFERENCES

[1] D. Mazurkiewicz, "Computer-aided maintenance and reliability management systems for conveyor belts", *Eksploatacja i Niezawodność – Maintenance and Reliability*, Vol. 16(3), pp. 377–382, (2014)

- [2] M. Đorđević, N. Zrnić and B. Jerman, "Simplified Life Cycle Assessment of a Belt Conveyor", Proceedings of XXI International Conference on "Material Handling, Constructions and Logistics", Vienna (Austria), 23-25 September 2015, pp. 199-206, (2015)
- [3] J. Kwasniewski, "The use of monitoring to improve the reliability and endurance of continuous coal handling systems", Arch. Min. Sci., Vol. 56(4), pp. 651-664, (2011)
- [4] Continental AG, ContiTech AG, "Conti<sup>®</sup> Protect - Conti<sup>®</sup> Inspect. High-Performance Belt Monitoring Systems for ContiTech Conveyor Belts", brochure, (2014)
- [5] Continental AG, ContiTech AG, "Conveyor Belt. Conti TotalProtect Belt Monitoring", brochure, (2015)
- [6] <http://www.conveyorbeltguide.com>
- [7] V. Sukhorukov, "Steel-cord conveyor belt NDT", The 8<sup>th</sup> International Conference of the Slovenian Society for Non-Destructive Testing. "Application of Contemporary Non-Destructive Testing in Engineering", Portorož (Slovenia), 1-3 September 2005, pp. 237-244, (2005)
- [8] M. Bajda, R. Blazej and L. Jurdziak, "A new tool in belts resistance to puncture research", Mining Science, ISSN 2300-9586, Vol. 23, pp. 173-182, (2016)
- [9] A. Harrison, "15 Years of Conveyor Belt Nondestructive Evaluation", Bulk Solids Handling, Vol. 16(1), pp. 13-19, (1996)
- [10] A. Harrison, "A magnetic transducer for testing steel-cord deterioration in high-tensile strength conveyor belts", NDT International, Vol. 18(3), pp. 133-138, (1985)
- [11] A. Harrison and S. Ghys, "Evaluation of the inverse problem for NDT of magnetised steel cord belt splices", Proceedings of 12<sup>th</sup> World Conference of Non-Destructive Testing, Elsevier Science Publishers B.V., Amsterdam (The Netherlands), pp. 330-335, (1989)
- [12] S. Kumar and D. Mahto, "Recent trends in industrial and other engineering applications of nondestructive testing: A review", IJSER, ISSN 2229-5518, Vol. 4(9), pp. 183-195, (2013)
- [13] P. Cawley, "Nondestructive testing - current capabilities and future directions", Journal of Materials: Design and Applications, Vol. 215, pp. 213-223, (2001)
- [14] X.-G. Li, C.-Y. Miao, W. Wang and Y. Zhang, "Fault Automatic Detection Method for Steel Cord Conveyor Belt Based on the Regularity Analysis", International Journal of Digital Content Technology and its Applications (JDCTA), Vol.6(1), pp. 226-234. (2012)
- [15] R. Blazej, "Review of the newest NDT equipment for conveyor belt diagnostics", Diagnostyka - Applied Structural Health, Usage and Condition Monitoring, Tom Nr 4(64), pp. 21-24, (2012)
- [16] D.W. Blum, "Scanning steel cord conveyor belts with the "Belt C.A.T. " MDR system", Journal of Bulk Solids Handling, Vol. 16(3), p. 437, (1996)
- [17] R. Blazej, L. Jurdziak, A. Kirjanow and T. Kozłowski, "Evaluation of the quality of steel cord belt splices based on belt condition examination using magnetic techniques", Diagnostyka, Vol. 16(3), pp. 59-64, (2015)
- [18] Fenner Dunlop Conveyor Belting Australia, "Steel Cord Belt", Brochure
- [19] Fenner Dunlop Conveyor Diagnostics, "Fenner Dunlop Scanning Services", Brochure
- [20] G.S. Park, P.W. Jang and Y.W. Rho, "Optimum Design of a Non Destructive Testing System to Maximize Magnetic Flux Leakage", Journal of Magnetics, Vol. 6(1), pp. 31-35, (2001)
- [21] T.Q. Xuwei, "A study of steel cord belt magnetic memory testing system", International Colloquium on Computing, Communication, Control, and Management (ISECS), pp. 564-566, (2009)
- [22] R. Blazej, A. Kirjanow and T. Kozłowski, "A high resolution system for automatic diagnosing the condition of the core of conveyor belts with steel cords", Diagnostyka, Vol. 15(4), pp. 41-45, (2014)
- [23] Laboratory LRM<sup>®</sup> dr eng. Roman Martyna, LRM NDE, brochure
- [24] R. Blazej, L. Jurdziak and W. Kawalec, "Condition monitoring of conveyor belts as a tool for proper selection of their replacement time" Springer, Advances in Condition Monitoring of Machinery in Non-Stationary Operations. Proceedings of the 4<sup>th</sup> International Conference on Condition Monitoring of Machinery in Non-Stationary Operations (CMMNO'2014), Lyon (France), 15-17 December 2015, pp. 483-494, (2015)
- [25] R. Blazej, L. Jurdziak, R. Zimroz, M. Hardygora and W. Kawalec, "Investigations of conveyor belts condition in the institute of mining engineering at Wrocław University of Technology", 23<sup>rd</sup> World Mining Congress, Montreal (Canada), Canadian Inst. of Mining, Metallurgy and Petroleum, 11-15 August 2013, pp. 1-9, (2013)
- [26] Pang Y. and Lodewijks G. "A novel embedded conductive detection system for intelligent conveyor belt monitoring", IEEE International Conference on Service Operations and Logistics, and Informatics, 2006 (SOLI '06), Shanghai (China), 21-23 Jun 2006, pp. 803-808, (2006)
- [27] Javier García-Martín, Jaime Gómez-Gil and Ernesto Vázquez-Sánchez; "Nondestructive Techniques Based on Eddy Current Testing", Sensors, Vol. 11(3), pp. 2525-2565, (2011)
- [28] Y. He, F. Luo, M. Pan, X. Hu, J. Gao and B. Liu, "Defect classification based on rectangular pulsed eddy current sensor in different directions", Sensors and Actuators A: Physical, Vol. 157(1), pp. 26-31, (2010)

# Analysis of the influence of basic parameters of the magnetic separator EcMS-500 for non-ferrous metals on the separation force intensity

Mile Savković<sup>1\*</sup>, Milomir Gašić<sup>1</sup>, Nebojša Zdravković<sup>1</sup>, Goran Marković<sup>1</sup>, Goran Pavlović<sup>2</sup>

<sup>1</sup>Faculty of Mechanical and Civil Engineering in Kraljevo of the University of Kragujevac, Kraljevo, Serbia

<sup>2</sup>Lola Institute, Kneza Višeslava 70a, 11030 Belgrade, Serbia

*Eddy-current magnetic separator EcMS-500 for non-ferrous metals is primarily designed to separate aluminium cans from other waste, but it can separate other non-ferrous metals such as brass and copper. During operation, the magnetic roller of separator creates eddy current field. These currents interact with metallic waste and generate attractive forces and interact with non-ferrous metals (aluminium, brass, copper) generating repulsive forces. Consequently, due to the effects of eddy currents, aluminium cans and other waste of non-ferrous metals are separated by ejecting from the magnetic separator belt, while passing over the roller. The paper presents the different types of solutions of magnetic separators. A special review is given to the design of the magnetic separator EcMS-500. The influences of the magnetic roller speed (revolutions per minute) and the conveyor belt speed on the ejection distance of cans are analysed. Also, the effect of cans shape on the separation forces intensity is considered. For defined diameter of the belt guide roller, the analysis has identified the optimum revolutions per minute that provides sufficient force of separation for non-ferrous metals with minimal force that burdens the connection of the magnet and the rotor.*

**Keywords:** Eddy-current separator, Recycling, Metallic waste, Aluminium cans

## 1. INTRODUCTION

Application of eddy-current separators began in the early nineties. Increasing concerns about the preservation of the environment and the adoption of various directives on waste disposal increase the development of eddy-current separators. So, there are many manufacturers in almost all countries in the world today. At the same time, there has been published many papers about this subject. Nijhof G.H., [1] described one of the first principle of the separation of recycled aluminium and the significance of this separation. The paper describes the working principle of used equipment in the recycling process as well as the whole system of recycling. Rem P.C. et al., [2] are among the first who described the operation of the magnetic field on the particles separation. They showed the effects of particle size, shape and conductivity on the particle trajectory. Simulation results were compared with experimental data in order to optimize the design of the separator as well as its working parameters. Zhang S. et al., [3] investigated the influence of installation of two-drum eddy-current separators. The simulation results showed high compliance with the experimental results and it was the most significant for processing of small particles. ECSIM software was used for the simulation. Zhang S. et al., [4] explored the justification of applying of eddy-current separators. It is shown that the use of this separator can provide a high percentage of separation of aluminium waste.

Kohnlechner R. et al., [5] showed a new type of separator that takes the influence of variable magnetic forces and translation of particles. Lungu M., [6] presented the operation of a new type of separator which separates metallic particles in two stages: firstly, the high conducting particles are separated on the upper part of the drum, and then the remaining low conducting particles are separated at the lower part of the magnetic drum. Lungu M. and Schlett Z., [7] gave the solution for a new vertical

drum eddy-current separator for separation of small particles with the size of 2-8 mm. Permanent magnets are placed vertically. Comparative analysis has proved that it was successfully applied and the costs of the equipment is lower than that of the horizontal drum eddy-current separator.

Cui J. and Forssberg E., [8] gave an overview of the significance of mechanical recycling of electronic waste as a review of the directives for governing in this area. The paper by Fengjie Y. et al., [9] showed that forces in the particles of waste and the separation effect directly affect the flying distance of separated waste. In the paper, simulation of the process is carried out by the finite element analysis of the magnetic roller based on COMSOL software, and the flying distance was got by the joint simulation of COMSOL software and MATLAB software. Ruan J. et al., [10] considered the eddy-current separator parameters that should be set to increase the separation effect of small crushed particles of aluminium waste. The critical speed of separation and the detachment angles of crushed aluminium particles are defined.

The paper by Li J. et al., [11] shown an innovative method for separation of printed circuit board from unsorted waste. A model trajectories of particles was performed by computer simulation and optimal speed of feeding belt and rotating speeds of magnetic roller are determined. Fenercioglu A. and Barutcu H., [12] analysed the force for aluminium waste separation using by FEM, taking into consideration drum speed, air gap between the material and the magnet pole, dimensions and conductivity of the material and magnet height. The same authors Fenercioglu A. and Barutcu H., [13] analysed the separation of crushed aluminium and copper cables. Analysis was performed using by FEM. Optimal conveyor feeding belt and rotating speeds of the magnetic drum are defined.

## 2. DESCRIPTION OF THE SEPARATOR EcMS-500

Eddy-current separator is an important component in the recycling chain. This machine is used for separation

of non-ferrous metals, preferably aluminium, brass and copper, from unsorted or partially-sorted waste.

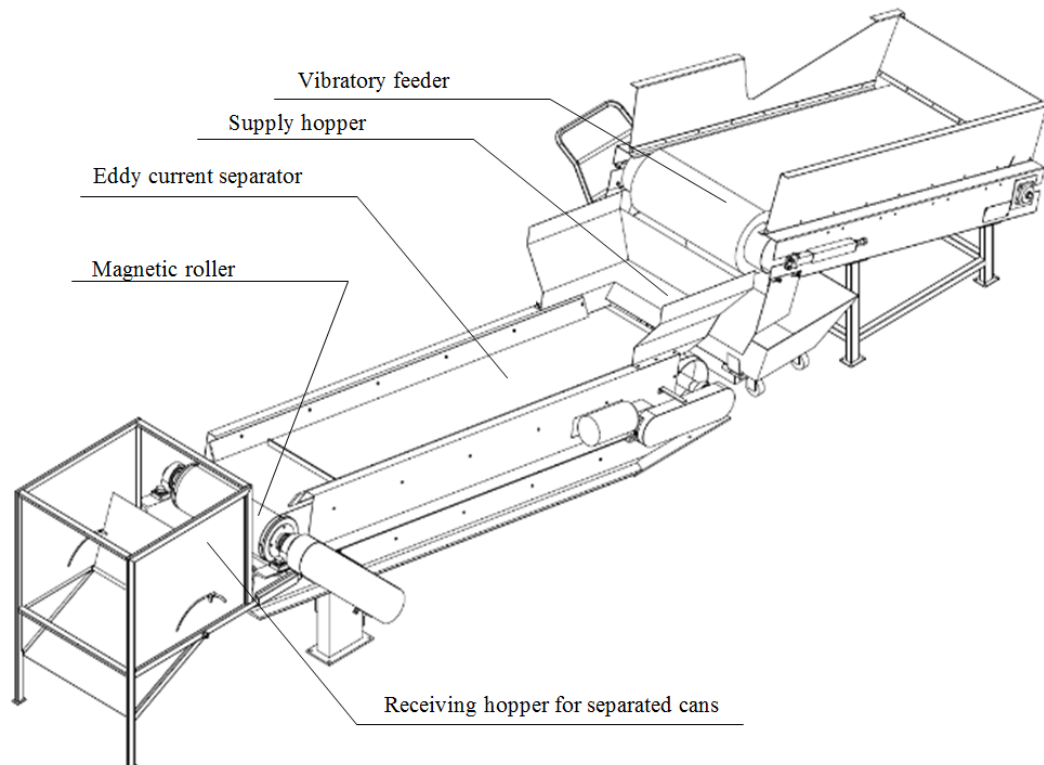


Figure 1: Position of eddy-current separator in the recycling process

In the recycling chain, bigger pieces are usually separated first (cardboard packaging, PET, etc.), then the metallic waste (separator of ferrous metallic waste) and finally, eddy-current separator that separates non-ferrous metals: aluminium, copper and brass of other non-metal waste. Vibrating feeder is often placed in front of eddy-current separator, distracting complete waste over conveyor belt to allow easier separation of non-ferrous metals (Figure 1).

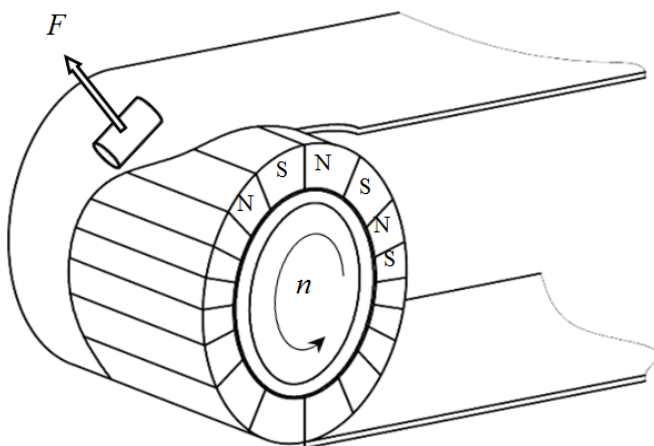


Figure 2: Sketch of magnetic roller and conveyor belt

The main segments of eddy-current separator at place of separation of waste are: conveyor belt, separator's magnetic roller shaft, magnetic and non-magnetic roller, supply hopper, electro-motor for magnetic roller shaft and conveyor belt drive.

Magnetic roller is a key component of eddy-current separator that is formed by alternately positioned permanent magnets in the S-N-S direction (Figure 2).

Magnetic roller, which is attached to the drive shaft, rotates at high speed. Non-magnetic roller, which is also connected to the drive shaft, rotates at considerably lower speed, in conjunction with the belt which is bended over it (Figure 3). Magnetic rotor is consisted from the shaft and permanent magnets, which are alternately positioned in the S-N-S pattern. Rotation of the magnetic roller creates an eddy magnetic field. When non-ferrous metal waste passes over the non-magnetic roller (cans, in this case), a magnetic field is created with an opposite polarity relative to the magnetic roller, which leads to the repulsive force in the non-ferrous metal. The intensity of the separation force is influenced by many parameters, including the speed of the magnetic roller, conveyor belt speed, the material characteristics (conductivity and density of the waste material are dominant). The higher conductivity and lower density of material creates higher force of separation. Size and shape of the material also affect to the intensity of the force of separation.

The materials being sorted are different in shape, size, density, etc., and it is difficult to issue conclusions about the intensity of the force without laboratory testing.

The direction of the force  $F_r$  acting on the metallic waste is shown in Figure 3. In the initial phase, the force of gravity is greater than the repulsive forces  $F_r$ , so the material stays in contact with the belt. When the value of the vertical projection of the force  $F_r$  exceeds the value of the force of gravity, waste separation occurs. Non-magnetic material

continues to move on the conveyor belt, passing over the roller and the centrifugal force acts on it. Receiving hopper

has, in its middle part, a splitter that separates non-metallic waste and non-ferrous metals.

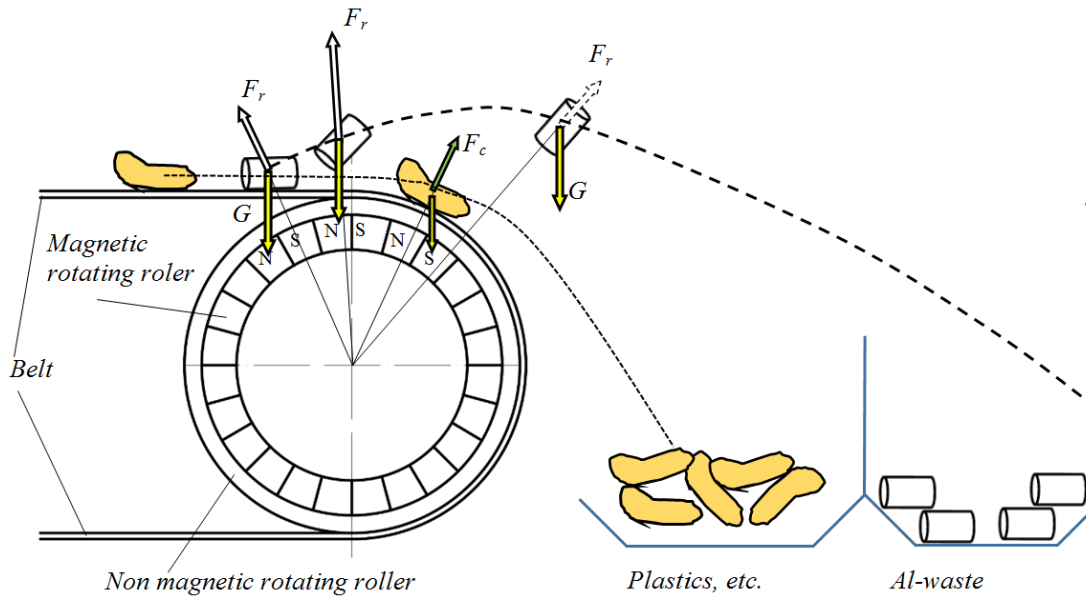


Figure 3: The principle of separation of aluminium cans

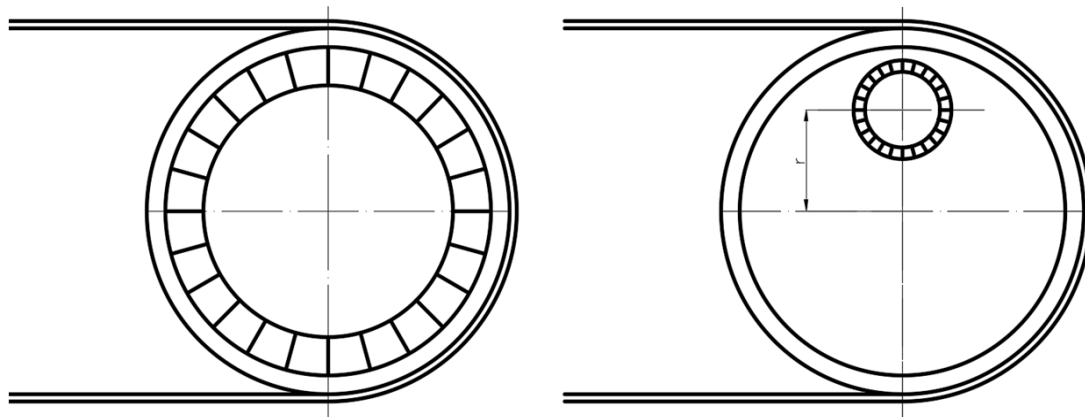


Figure 4: Basic functioning principle of eddy-current separator

As shown in Figure 3, the material is ejected and its movement represents the projectile motion, and the initial speed is important for the ejection distance of the object.

The characteristics which are significant for the separation of non-ferrous metals are the shape and the size of the pieces, density and conductivity of pieces, and also humidity of the metal pieces, adhesion, a fibrous properties of the material, etc. Besides this, the separation process may be affected by design parameters of eddy-current separator such as belt speed, rotor speed, way of delivery of unsorted waste, rotor design which directly determines the magnetic flux and magnetic frequency, type of magnet, etc.

According to the solution of the magnetic roller, there are two major type of eddy-current separator: with a centrally mounted axes of non-magnetic and magnetic rotor (Figure 4a) and with an eccentrically mounted axes of non-magnetic and magnetic rotor (Figure 4b).

Eccentrically mounted rotor is technically complicated to perform and produce. In this separator, magnetic field bandwidth is smaller, so that the non-ferrous

metal is in a shorter time period exposed to the effects of magnetic force. Separator EcMS-500 is constructed in a way where the axis of the magnetic and non-magnetic rotor are mounted centrally. This concept was chosen because it does not require installation of any electronic equipment, it is easy for maintenance and does not require a clean and dry working conditions. Also, the selection of the solution type is affected by the fact that it is known that cans are the dominant type of non-metal waste.

### 3. TESTING OF SEPARATOR EcMS-500

In order to define the basic performance of the magnetic separator EcMS-500, depending on the user requirements, it is not always necessary to measure the force on magnetic roller. Since the primary function of the separator EcMS-500 is separation of cans from the unsorted waste, it is assumed that it is enough to measure the horizontal distance where the cans fall into the receiving hopper, having in mind that the paper [11] shows that the

horizontal distance is directly dependent on the size of the magnetic force.

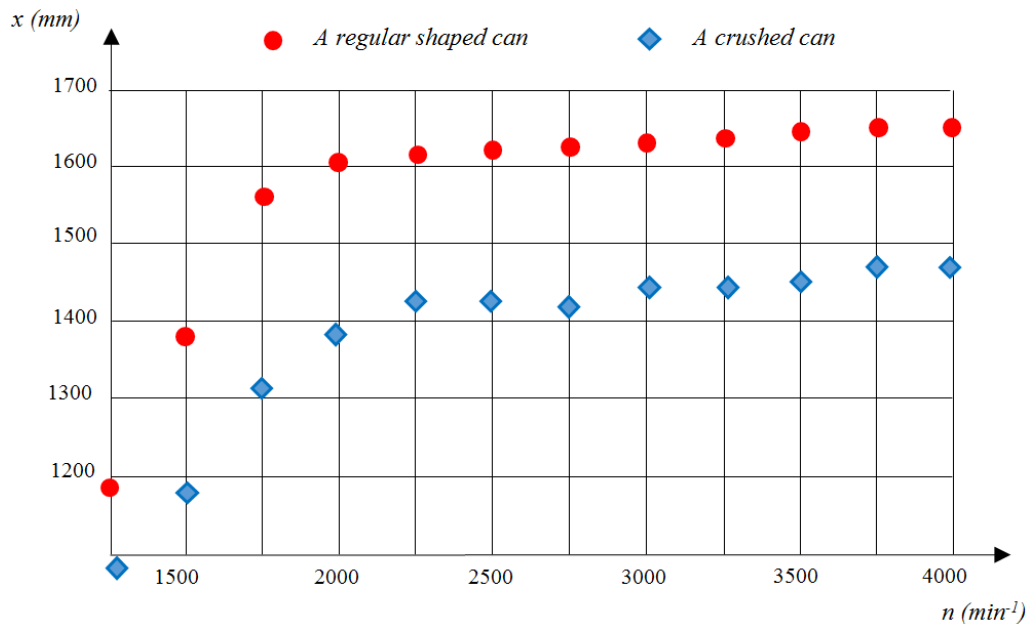


Figure 5: The effect of changes of number of revolution of magnetic head to the length  $x$

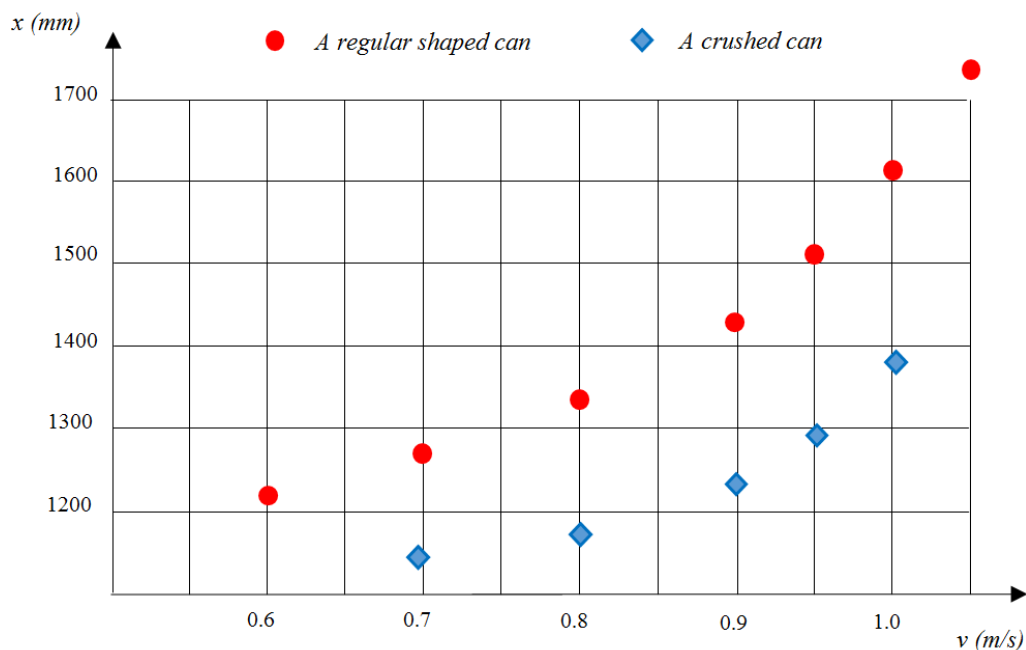


Figure 6: The effect of changes of belt speed to the length  $x$

Measurements were performed on existing solution design of EcMS-500 separator.

The ejection distance of cans depends on various parameters, but in this paper an influence of the number of revolution of the magnetic roller (Figure 5) and the effect of changing of the belt speed of the belt conveyor (Figure 6) are analysed. In both cases, during the examination, there were used two types of cans: cans of regular shape, i.e. those that are not crushed and totally crushed cans that have a minimum volume of form.

The main technical characteristics of the conveyor are: the height of the upper edge of the roller from the floor is 880 mm, the angle of the conveyor of the magnetic separator to the horizontal is  $10^\circ$ , and the width of the conveyor is 500 mm. While varying the number of revolution of the magnetic roller, the conveyor belt speed

was  $v = 1$  m/s. While varying the speed of the conveyor belt, the speed of the magnetic roller was  $n = 2000$  min<sup>-1</sup>.

It should be noted that the measurement was carried out so that the conveyor contained only aluminium cans without other waste. In this way, the obtained values of the horizontal distance where the cans fall is certainly greater than in the exploitation conditions. However, this does not reduce the significance of the results obtained, because the investigated parameters are the speed of rotation of the magnetic rotor and the speed of the conveyor belt. The test results showed that with increase of the number of revolution per minute (Figure 5) over  $2000$  min<sup>-1</sup>, the increase of the distance where the cans fall is very small. This applies to both types of cans, while the distance is shorter in case of totally crushed cans. Influence of the speed of the conveyor belt can be seen in Figure 6. When



the belt speed increases above 1 m/s, the distance ( $x$ ) is growing rapidly. The results shown in Figure 5 and Figure 6 were obtained by averaging the values of large number of repetitions. Also, for retesting with the changed parameters, the same set of cans was used and with the same order of placing on the conveyor belt. Changing the speed of the magnetic and non-magnetic roller was performed via frequency converters. Design of the magnetic separator EcMS-500 is shown in Figure 7.



a)



b)

Figure 7: Layout of solution for the magnetic separator EcMS-500

#### 4. CONCLUSION

This paper presented the basic technical characteristics of eddy-current separator EcMS-500, where the axis of the magnetic and non-magnetic rotor are mounted centrally.

Dependence of the horizontal length of the trajectory of the ejected cans on the number of revolutions of the magnetic roller is defined. It was noticed that the increase of the number of revolutions per minute of the magnetic roller over 2000  $\text{min}^{-1}$  leads to slight increase in the horizontal length of the trajectory. Since the horizontal length of the trajectory directly depends on the magnetic force, it is concluded that higher speed of the magnetic roller (more than 2000  $\text{min}^{-1}$ ) leads to slight increase of the magnetic force. This conclusion is important for the construction of eddy-current separators, because the increase of the number of revolutions per minute increases the centrifugal force of the magnets, which burdens their connection with the shaft of the magnetic roller.

Dependence of the horizontal length of the trajectory of the ejected cans to the conveyor belt speed is defined. It was observed that as the belt speed increases significantly, the intensity of separation force increases rapidly. This especially refers to the belt speed above 1 m/s. Increasing the speed also dictates the layout and content of the machine in the sorting line.

For both cases, it is shown that the shape and condition of cans affect the intensity of separation force. Nevertheless, the existing solution of the magnetic roller induces a separation force with sufficiently high intensity for any form of cans.

#### ACKNOWLEDGEMENTS

This paper is the result of the project number TR35038 financed by the Ministry of Education, Science and Technological Development of the Republic of Serbia.

#### REFERENCES

- [1] G.H. Nijhof, "Aluminium separation out of household waste using the Eddy Current technique and re-use of the metal fraction", *Resources, Conservation and Recycling*, Vol.10, pp. 161-169, (1994)
- [2] P.C. Rem, P.A. Leest and A.J. Akker, "A model for eddy current separation", *International Journal Mineral Processing*, Vol. 49, pp. 193-200, (1997)
- [3] S. Zhang, C.P. Rem and E. Forssberg, "Particle trajectory simulation of two-drum eddy current separators", *Resources, Conservation and Recycling*, Vol. 26, pp. 71-90, (1999)
- [4] S. Zhang, E. Forssberg, B. Arvidson and W. Moss, "Aluminum recovery from electronic scrap by High-Force eddy-current separators", *Resources, Conservation and Recycling*, Vol. 23, pp. 225-241, (1998)
- [5] R. Kohnlechner, Z. Schlett, M. Lungu and C. Caizer, "New wet Eddy-current separator", *Resources, Conservation and Recycling*, Vol. 37, pp. 55-60, (2002)
- [6] M. Lungu, "Separation of small nonferrous particles using a two successive steps eddy-current separator with permanent magnets", *International Journal Mineral Processing*, Vol. 93, pp. 172-178, (2009)

- [7] M. Lungu and Z. Schlett, "Vertical drum eddy-current separator with permanent magnets", *International Journal Mineral Processing*, Vol. 63, pp. 207–216, (2001)
- [8] J. Cui and E. Forssberg, "Mechanical recycling of waste electric and electronic equipment: a review", *Journal of Hazardous Materials*, Vol. B99, pp. 243–263, (2003)
- [9] Y. Fengjie, C. Weifang and Z. Dehao, "The research of simulation on eddy current separation process based on MATLAB and COMSOL", *Procedia CIRP*, Vol. 56, pp. 520–523, (2016)
- [10] J. Ruan, L. Dong, J. Zheng, T. Zhang, M. Huang and Z. Xu, "Key factors of eddy current separation for recovering aluminum from crushed e-waste", *Waste Management*, Vol. 60, pp. 84–90, (2017)
- [11] J. Li, Y. Jiang and Z. Xu, "Eddy current separation technology for recycling printed circuit boards from crushed cell phones", *Journal of Cleaner Production*, Vol. 141, pp. 1316-1323, (2017)
- [12] A. Fenercioglu and H. Barutcu, "Finite Element Analysis of Separation Force on Non-ferrous Metals Induced by Eddy Current Separator", *PIERS Proceedings, Prague, Czech Republic, 6-9 July 2015*, pp. 434-438, (2015)
- [13] A. Fenercioglu and H. Barutcu, "Separation of Granule Non-Ferrous Metals in Shredded Cable Waste with Eddy Current Separator", *Proceedings of the World Congress on Mechanical, Chemical and Material Engineering–MCM 2015, Barcelona (Spain), 20-21 July 2015, Paper No. 250*, pp. 250-1 – 250-5, (2015)

# Application of Reliability Centered Maintenance Methodology for Maintenance of an Special Vehicle Engine

Slavko Rakic<sup>1\*</sup>, Ugljesa Bugaric<sup>2</sup>

<sup>1</sup> Sector for Material Resources, Ministry of Defence of Republic of Serbia, Belgrade, Serbia,

<sup>2</sup> Department of Industrial Engineering, Faculty of Mechanical Engineering Belgrade, University of Belgrade, Serbia

*The paper analyses the possibility of revising the existing maintenance program of special vehicle engine by applying RCM methodology. The main objective in considering the application of the new maintenance methodology was to improve the effectiveness and efficiency of the maintenance of the internal combustion engine, retaining the required reliability of the engine. Analysis was carried out on the fuel supply engine subsystem, which is the most critical engine subsystem from the standpoint of the number of failures in the observed period during its exploitation. As a result of these systematic analyses, the maintenance concept of the critical parts and assemblies of the fuel supply subsystem were selected and the intervals of realization proposed maintenance activities in accordance with a predefined request that the reliability of the fuel supply engine subsystem is not less than 0.985. Based on the results, the conclusion is that the application of RCM for special vehicle engine would be justified since it would contribute to improving the effectiveness and efficiency of maintaining the engines.*

**Keywords:** Reliability Centered Maintenance, Engine, Failure, Special vehicle

## 1. INTRODUCTION

Special vehicles engine has an important role in achieving of one of the three key characteristics of special vehicles – the mobility. Maintainability, cost effectiveness of maintenance, reliability and readiness are very important factors of special vehicles engines.

This paper aims to analyse revision possibility of the existing maintenance program of a special vehicle engine by applying Reliability Centered Maintenance (RCM) methodology. RCM is one of the best known and most used tools to preserve the operational efficiency and reliability of large and complex systems (marine, aircraft, etc.), so the consideration of its application possibility on special vehicles is a real challenge. Expectations of this methodology application are to improve the readiness and availability of technical systems, which is very important for special vehicle.

RCM applies a systematic approach to determine the maintenance requirements of system in its operating context. It is often used to optimize preventive maintenance (PM) strategies.

## 2. RELIABILITY-CENTERED MAINTENANCE METHODOLOGY

Reliability-centered maintenance (RCM) is the best mix of reactive, time or interval-based, condition-based, and proactive maintenance practices. These principal maintenance strategies, rather than being applied independently, are integrated to take advantage of their respective strengths in order to maximize facility and equipment reliability while minimizing life-cycle costs [5].

The components of RCM program are shown in Figure 1. This figure shows that RCM program consists of (reactive maintenance, preventive maintenance, condition based maintenance, and proactive maintenance) and its patterns.

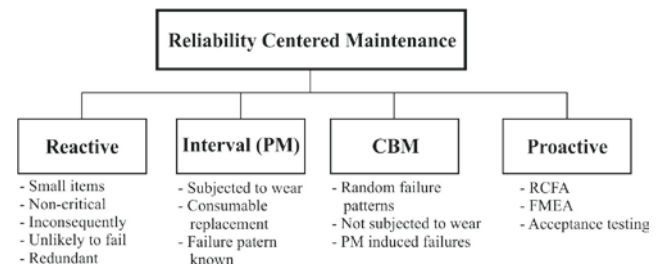


Figure 1: Components of RCM program

As shown in Figure 2, the RCM steps are presented. The steps describe the systematic approach used to implement the preserves the system function, identifies failure mode, priorities failure used to implement the preserves the system function, identifies failure mode, priorities failure modes and performs PM tasks.

## 3. ANALYSIS OF THE POSSIBILITIES OF APPLICATION OF RCM METHODOLOGY FOR MAINTENANCE OF THE SPECIAL VEHICLE ENGINE

Special vehicles engine subsystems that had defined maintenance and in accordance with the Pareto principle are found in 20-30% of engine subsystems which had 70-80% of the recorded engine failures in the observed period, will be subject to revision of current maintenance. At the end, there will be made selection of appropriate maintenance concept for assemblies and parts of the most critical engine subsystem.

In this regard, there will be carried out failure analysis for individual subsystems of the special vehicle engine in the observed period of exploitation. The engine subsystem that shows critical from the standpoint of reliability will be subject to consideration of the possibility to apply RCM methodology in the context of the revision of the existing maintenance program engine. Access to maintenance revision of the most critical engine subsystem would be further applied to other engine subsystems.

Additionally, should be done rationalization of maintenance activities intervals.

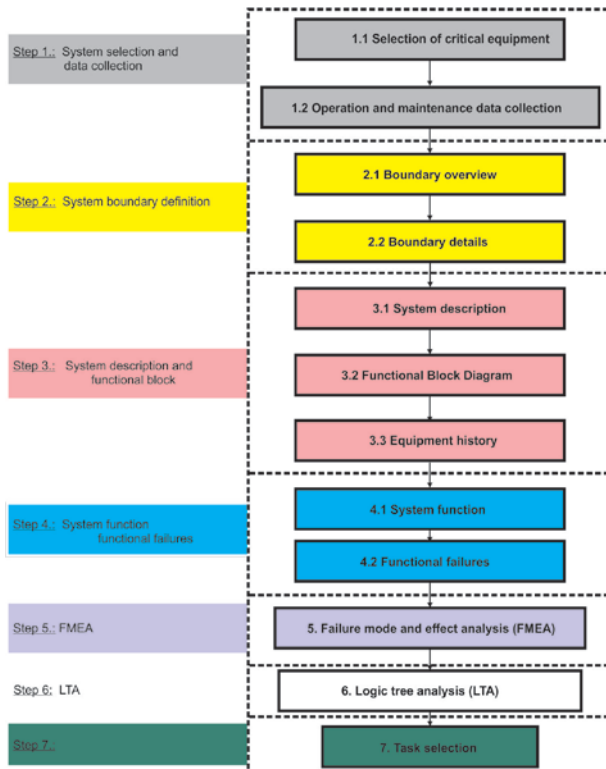


Figure 2: Main steps of the RCM

The main objective was to create conditions using some engineering methods and analysis for the Condition Based Maintenance (CBM) algorithm selection in order to systematically, in addition to previously preventive and corrective maintenance, consider the options for the application and other suitable concept maintenance with priority of maintenance according to the condition.

Revision of preventive maintenance and selection of concepts in the new maintenance algorithm should primarily achieve engine reliability improvement with the possibility of the maintenance cost reduction.

Also, as imperative is given the task to analyze a lack of preventive maintenance activities in existing maintenance, which could be the cause of the unexpected failures with possible safety or major systematic effects.

### 3.1. Determining the Probability and Cumulative Density Function of engine operating time to failure

Calculating an adequate mathematical model that can represent a principle of special vehicle engine performance during its exploitation, in terms of the appearance of failure, is one of the first steps to be undertaken. Based on the calculated results, there can be done an analysis of existing maintenance programs and if necessary, their revision in order to primarily optimize the engine maintenance in terms of improving its reliability.

For the purposes of this paper, the efficiency of the existing maintenance program has been carried out on twelve-cylinders diesel engine with 735 [kW] which is built-in in special vehicle.

There has been conducted a data collection of the engine operating times to the failure expressed in engine operating hours (EOH), which were obtained by observing

the vehicle exploitation and are shown in Table 1. Data were recorded only for engines that had failure. There are shown 105 records of times to engine failure, which is more than sufficient statistical collection in relation with the optimal plan of short tests for assessing the reliability (with the approved variation coefficient of 0.5, a priori relative error of assessment of the reliability of work of 0.05 and an initial number of necessary records of 40) [1]. The procedure for determining the Cumulative Density Function of engine operation time to failure, on the basis of empirical data, is executed in three steps. There have been estimated indicators of reliability in the first step. In the second step, based of the values obtained in the first step, are determined the theoretical models of the distribution for the approximation of the empirical distribution. Afterwards, in the third step is determined the confirmation approval of adopted theoretical model of the distribution with empirical distribution [1].

Table 1: Data of the engine operating times to the failure

Ordinal number of failure	Operating time to failure [EOH]	Ordinal number of failure	Operating time to failure [EOH]	Ordinal number of failure	Operating time to failure [EOH]	Ordinal number of failure	Operating time to failure [EOH]	Ordinal number of failure	Operating time to failure [EOH]
1	135	22	345	43	392	64	448	85	523
2	166	23	355	44	397	65	448	86	523
3	221	24	355	45	400	66	449	87	526
4	221	25	360	46	404	67	459	88	526
5	229	26	360	47	404	68	464	89	532
6	248	27	363	48	406	69	466	90	536
7	251	28	367	49	406	70	473	91	546
8	260	29	371	50	407	71	473	92	561
9	263	30	372	51	409	72	474	93	561
10	272	31	379	52	415	73	474	94	569
11	294	32	379	53	415	74	480	95	572
12	294	33	380	54	415	75	480	96	572
13	307	34	382	55	415	76	486	97	581
14	317	35	382	56	416	77	488	98	581
15	317	36	382	57	419	78	495	99	586
16	320	37	384	58	436	79	496	100	605
17	320	38	391	59	436	80	496	101	605
18	322	39	391	60	438	81	498	102	609
19	331	40	391	61	444	82	498	103	615
20	332	41	391	62	447	83	498	104	634
21	345	42	391	63	447	84	521	105	643

#### 3.1.1. The assessment of the reliability indicators

Based on the records from Table 1 the law of reliability distribution can be calculated.

From Table 1, it can be seen that:

- the total number of data (sample size):  $n=105$ ,
- minimum operating time to failure:  $t_{\min}= 135$  [EOH],
- maximum operating time to failure:  $t_{\max}= 643$  [EOH].

From the data presented in Table 1 statistical measures are calculated:

- mean operating time to failure:  $t_{\text{mot}}= 423.5619$  [EOH],
- the standard deviation of operating time to failure:  $SD= 105.24$  [EOH],
- median operating time to failure: median = 415 [EOH],
- rang (range) operating time to failure: rang= 508 [EOH].

Based on the calculated statistical measures, the coefficient of variation is calculated as follows:

$$CV=SD/t_{mot}=0.25.$$

Since the calculated value of the coefficient of variation is less than approved (CV=5), it can be started with determining of Probability Density Function of engine operating time to failure.

The number of intervals of operating time to failure is determined by the formula [2]:

$$z=1+3.3 \cdot \log_{10}(n) = 7.67, \text{ so it adopts a number of intervals: } z = 8.$$

Table 2: The estimated value of reliability indicators

i	n <sub>i</sub>	sv <sub>int</sub>	cn <sub>is</sub>	f	F	R	h
1	2	166.75	1	0.000287	0.008772	0.991228	0.000289
2	6	230.25	4	0.00086	0.035088	0.964912	0.000891
3	10	293.75	9	0.001433	0.078947	0.921053	0.001556
4	19	357.25	18.5	0.002723	0.162281	0.837719	0.003251
5	29	420.75	33	0.004157	0.289474	0.710526	0.00585
6	17	484.25	41.5	0.002437	0.364035	0.635965	0.003831
7	13	547.75	48	0.001863	0.421053	0.578947	0.003218
8	9	611.25	52.5	0.00129	0.460526	0.539474	0.002391

Symbols used in Table 2 have the following meaning:

- i - ordinal number of the interval,
- n<sub>i</sub> - number of failures in the interval,
- sv<sub>int</sub> - the mean value of the interval [EOH],
- cn<sub>is</sub> - the estimated value of the number of failures in the middle of the interval (calculated as the arithmetic mean of the number of failures at the beginning and the end of the interval);

f [EOH<sup>-1</sup>] = n<sub>i</sub>/(n·Δt) - Probability Density Function, n = 105 sample size, Δt = rang/z,

F [-] = cn<sub>is</sub>/n - Cumulative Density Function

R [-] = (n-cn<sub>is</sub>)/n = 1-F - Reliability Function,

λ [EOH<sup>-1</sup>] = f/R - Failure Intensity Function.

Figures 3. and 4. give a graphical representation of the estimated indicators of reliability.

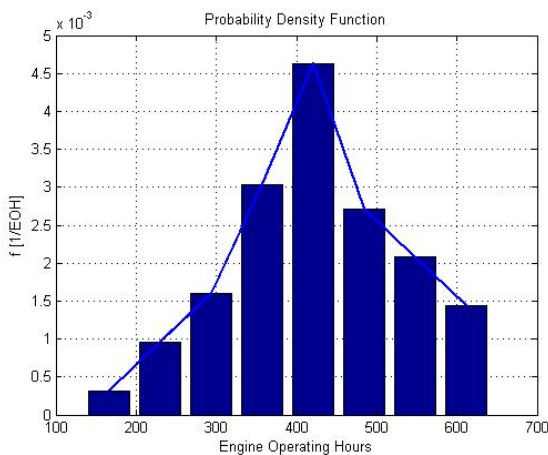


Figure 3: Estimated value of failure state density graph

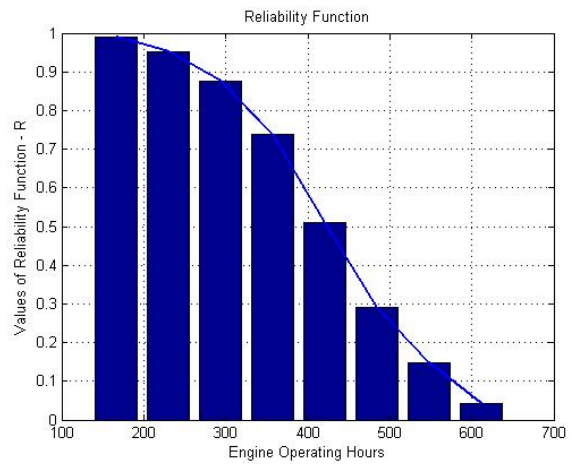


Figure 4: Estimated value of reliability function graph

### 3.1.2. Determination of the distribution model and parameters with the evaluation of the compliance

In order to determine the theoretical distribution model which could be used to approximate the empirical distribution, there was used an approximation of the empirical distribution with theoretical Weibull (Weibull), exponential, Rayleigh (Rayleigh) and normal distribution. Rating of compliance of the empirical and theoretical distributions was conducted by using the Kolmogorov-Smirnov test and Pearson test of Romanovski.

For the statistical analysis of data was used the Statistics Toolbox for use with MATLAB [3].

As quantitative deviation indicators (D<sub>n</sub> and χ<sup>2</sup>) for two of the three applied tests, are the far smallest for Weibull distribution, Figure 5., for the approximate model of the special vehicle engine reliability has been adopted the two-parameter Weibull distribution with Scale parameter η<sub>w</sub>=463.6393 and Shape parameter β<sub>w</sub>=4.5746, so the formula for reliability function of engine is:

$$R(t) = e^{-\left(\frac{t}{\eta_w}\right)^{\beta_w}} = e^{-\left(\frac{t}{463.6393}\right)^{4.5746}} \quad (1)$$

When calculating the reliability function according to the preceding equation, the variable t is expressed in the EOH.

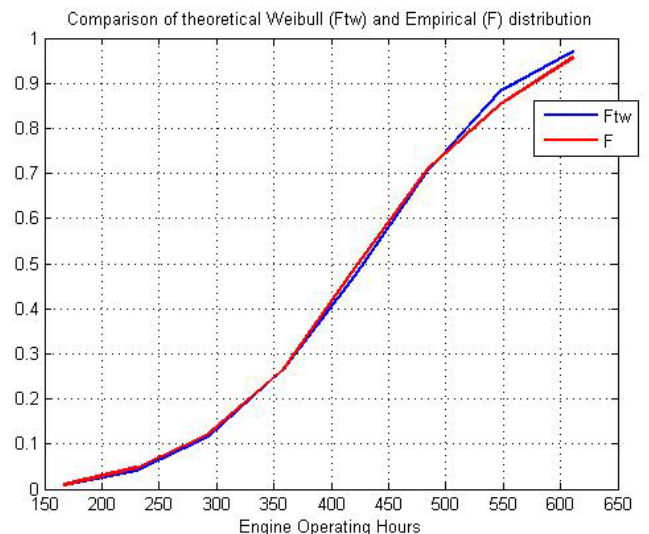


Figure 5: Graphic display of Weibull approximate distribution from the empirical distribution deviations

### 3.2. Selection of the critical engine subsystem

For further consideration of the engine maintenance program revision, on the basis of collected data on engine failure and calculating the engine reliability function, from the standpoint of number of failures of its components and subsystems in the observed period, it is chosen the most critical engine system of special vehicle - Fuel supply subsystem.

Namely, out of a total of 105 analyzed failures, 74 of them referred to the failures of devices, subsystems and components of the Fuel supply subsystem, which according to the Pareto principle contribute with 80% in the cost of engine maintenance, Figure 6.

Fuel supply subsystem is designed for storage, purifying and supply of the necessary quantities of fuel into the engine cylinders. The system also provides the fuel needed to operate the engine preheating system, engine cold start system, smoke screen forming system, as well as the overflow of the excess fuel from High Pressure Pump (HPP), injectors and heating system for the engine. Fuel supply subsystem comprise: the fuel tank, fuel distribution valves, electric pump for fuel supply, low-pressure pump, double-purifier tank, HPP, injectors, one-way valve for the fuel overflow, vent, pipes, hoses and electric fuel pump switches.

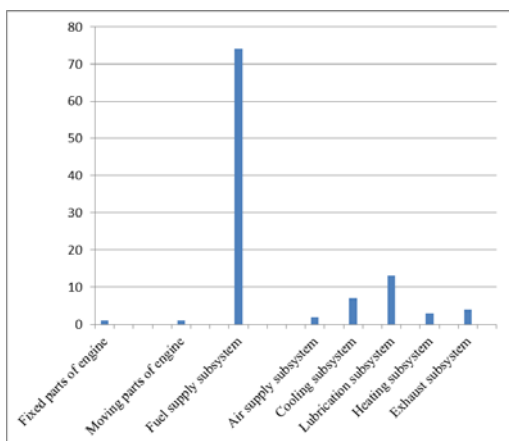


Figure 6: Number of failures by individual subsystems of the engine in the observed period

### 3.3. Identification of the maintenance activities

When identifying maintenance activities from the previous maintenance program, all planned activities of preventive maintenance for systems and subsystems of the engines were analyzed with the special emphasize to the analysis of the activities of maintenance programs that were related to the maintenance of the fuel supply engine subsystem. Preventive maintenance of subjected engine consists of Basic Maintenance (prior, during and after exploitation check), Periodic Maintenance (which is performed at least 2 times per month), 1st Technical Inspection (after 180 EOH) and 2nd Technical Inspection (after 350 EOH). Technical Inspection is performed by people from the technical workshop with the participation of the vehicle crew, who primarily perform basic work like washing, cleaning, lubricating, and other works entrusted by the specialists who perform supervision and checking of executed works.

During the analysis of the preventive maintenance activities it was concluded that provided technical guidelines do not plan activities on preventive maintenance of critical components and elements of the fuel supply engine subsystem of the vehicle, except checking the seals and tension of fuel tank caps, draining the fuel tanks with discharging of sludge from the tank, washing the vent with a float opening and washing of coarse fuel filter.

### 3.4. Failure modes and effects analysis

Failure modes and effects analysis (FMEA) is a tool that examines the potential system or process failures and helps to determine the specific activities in the field of maintenance in order to avoid the consequences of identified failures. Table format allows easy and simple overview of the analysis. FMEA helps to identify ways of creating functional failures. Table 4. represents the FMEA for the most critical fuel supply engine subsystem. It was performed FMEA at the local level, then at the level of the engine, and finally the analysis of the final effect of the failure to the entire special vehicle's mission, from the standpoint of whether it is a hidden failure, failure danger to the security of the system or the environment, failure with consequences for the system's functioning or failure without consequences for the system's functioning.

#### 3.4.1. Failures risk analysis

Consequences of failures can be categorized in various ways. The risk analysis of the fuel supply engine subsystem failures was performed, with analysis how the consequences of failure affect on availability and security as two key parameters essential for consideration of appropriate maintenance procedures of this engine subsystem. Also, the risk analysis takes into account the values of the particular engine systems. The performed failures risk analysis should serve for the ranking of the individual parts and assemblies of the fuel supply subsystem regarding prioritization of their maintenance work, reliability and availability improvement, maintenance cost reduction and others.

The effects of failure regarding safety were taken with a weight factor of 30%, the effects on availability of 40% and the effects related to the costs of 30%. It has been carried out risk failures categorization into 4 categories of A, B, C and D, depending on the criticality of the index, as shown in Table 3.

Table 3: Groups of the risk index

Group	The risk index
A	3-2.5
B	2.5-2
C	2-1.5
D	1.5-1

Due to the volume of work for risk analysis for a complete engine, it was performed the failures risk analysis for the fuel system as it is the most critical engine's system. In Table 4 are given indices which belong to the risk group of individual parts and components of the fuel subsystem.

Table 4: FMEA and groups of risk

Elements and assemblies of fuel supply subsystem	The mode and effect of failure	The cause of failure	A group risk
High-pressure pump (HPP) with commands	Decreased power of engine.	Elements of HPP not work (Worn out of element is the main cause of failure)	B
		HPP Regulator not work properly (Worn out of regulator or cracking of the spring regulator).	B
		No well-setting of HPP commands.	B
		No well-tuned fuel injection angle.	B
	The engine achieves high revs (may cause large damage)	High pressure pump Rack and Pinion Mechanism is blocked (engine develops speed higher than the maximum)	A
Injectors	Decreased power of engine. Engine smokes and not develop full power. Engine noises.	The defective injectors (uncontrolled leakage of fuel through a nozzle needle spray hole, nozzle needle is blocked or not close well, fracture of the return spring)	B
Low-pressure pump	Engine cannot start or starts but after the first revs stops.	Low pressure pump not deliver fuel to HPP.	C
Fuel filters	Engine cannot start.	Dirty filters or fuel pipelines closed.	B
Pipelines fuel assemblies	Engine noises. Engine cannot start. Engine after the first revs stops.	Air in the fuel supply subsystem.	C

At this step is achieved a key activity preparation for the determining of the maintenance on the basis of the result of failure concept, and not for maintenance due to failure occurrence. In other words, it is attempted to have the maintenance that manages the failures and not the failures that manage the maintenance.

3.5. Decision algorithm

Decision algorithm (DA), shown in Figure 7, is used to decide whether to use the corresponding optimal maintenance concept. The figure shows that making decisions, takes into account three key parameters: 1) security 2) availability 3) costs. After the completion of certain engineering methods mentioned in the previous section as well as performing the analysis of th repairs level, every possible failure mode is introduced into the algorithm by answering the typical questions through DA, so depending on the response and algorithm branch direction it is come to the final guidelines and proposals for the selection of optimal maintenance concept for that type of failure. For each maintenance activity is analyzed the technical feasibility and effectiveness, as already described. It is not ruled out and the selection of corrective maintenance for failure modes extracted from preventive maintenance, because it could be determined that some maintenance actions were previously identified on false assumptions. As for failure modes extracted from the earlier corrective maintenance, the assumption is that the majority of them will be again within the corrective maintenance after the application of the DA.

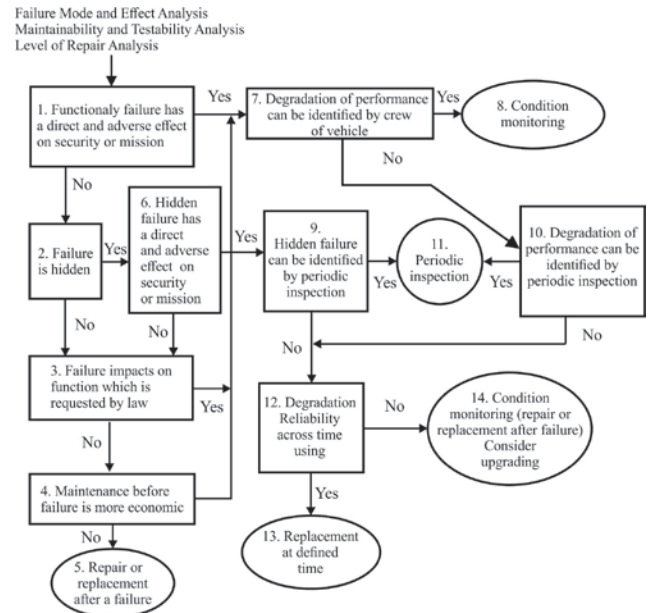


Figure 7: RCM decision algorithm

3.6. Selection of the optimal maintenance concept

After performing the above given analysis, it starts the selecting of optimum condition based maintenance by single engine subsystems, where for this particular case this will be presented only for the fuel supply subsystem.

One of the major advantages of using RCM methodology for maintenance is a mode that enables easy, precise and easily understandable criteria for deciding which (if any) of the preventive tasks is technically feasible in any context, and if so to decide how often they should be done and who should do it.

When considering the possibility of determining the concept of maintenance by the individual elements and engine fueling system assemblies, the main condition was that the reliability of the engine is less than 0,985.

Concepts of maintenance that were considered in the selection of the fuel supply subsystem maintenance concept were: run to failure (RTF) or corrective maintenance, maintenance on the basis of time resources (TD) and condition based maintenance (CD). The selected maintaining concepts by individual assemblies and

elements of the fuel supply engine subsystem with the intervals of their implementation are illustrated in the Table 5.

### 3.6.1. Rationalization of maintenance intervals

When the selection of maintenance concept is completed, as the result is obtained a set of maintenance actions within different time intervals, which is, from the viewpoint of efficiency, necessary to group into a certain maintenance programs or to incorporate into existing ones. One of the reasons may be that some maintenance actions are performed by crew and some require the capacity and resources of the repair facility, like engine test benches and stands or other specialist's equipment.

Table 5: Selection of the optimal maintenance concept and maintenance intervals

Elements and assemblies of fuel supply engine subsystem	Ordinal number	The concept (task) of maintenance	Description of maintenance activities	Frequency [EOH]
High-pressure pump (HPP) with commands	1	TD	Checking of setting commands of HPP and, if necessary, adjust it. Crew of vehicle is not carried out the setting of the commands. A mechanic performs the mentioned activities.	100
	2	CD	Dismantling and testing of HPP on bench. The engine is not removed from the vehicle. The activities are carried out by expert team from Overhaul Institute.	200
	3	CD	Disassembly and overhaul of HPP depending on condition of HPP. Then, assembly and setting of HPP on the bench. Checking of injection angle setting and, if necessary, adjust it. The activities are carried out by expert team from Overhaul Institute.	400
Injectors	4	TD	Dismantling and test of injectors on bench. Depending on of the test results, injector shall be replaced or repaired. The activities are carried out by expert team from Overhaul Institute.	200
Low-pressure pump (LPP)	5	RTF	In the previous period, the LPP was extremely reliable the assembly without failure. The proposal is that the LPP runs to failure without taking action on preventive maintenance.	
Fuel filters	6	CD	It is necessary to carry out a visual inspection of the fine filter cartridge. If during the inspection of filters, filter cartridges do not meet the declared characteristics, it should be replaced.	100
Pipelines fuel assemblies	7	TD	The emergence of air in the fuel supply subsystem is the result of the leakage of fuel, cracking pipes, bad hermetic of filter fuel. Checking of the subsystem is carried out on each of 100 [EOH], by a mechanic.	100

For example, two or more maintenance activities require repair capacity, and should be performed in a different, close time interval. In this case, from the standpoint of cost effectiveness and overall readiness is better to perform them in one interval.

If the maintenance activity which is determined by the interval, is faced with shortening the interval, the higher maintenance costs will occur. This is obvious because the maintenance activities are more frequent.



On the other hand, if the maintenance interval is extended, the maintenance costs will decrease, but increases the risk of failure. Here the problem of rationalizing interval will not be considered in detail, so only the basic remarks are given, bearing in mind that the optimal maintenance intervals of other engine's systems and other components of the vehicle systems are not known.

In this specific case of the fueling system, the maintenance intervals of the single assemblies and subsystems are determined so that the following interval is obtained by multiplying the basic one. In addition, the proposal is that interval of 1st Technical Inspection of an special vehicle engine, shifts from the existing (180 EOH) to 200 [EOH] with additional maintenance activities, which are given in Table 5. (except the activity at the ordinal number 3.), and the current interval of the 2nd Technical Inspection (350 EOH) is to be performed at 400 [EOH], after expanding the content of maintenance activities according to Table 5. (except the activity in the ordinal number 2.), by removing the engine from the vehicle, and performing a complete test and diagnostics at the test table. Depending on the condition of the engine, the further activities would be undertaken in order to bring it to functionally correct state.

#### 4. CONCLUSION

The paper analyses the possibility of revising the existing maintenance program of special vehicle engine by applying RCM methodology. Analysis was carried out for the fuel supply engine subsystem, which was showed as the most critical subsystem from the standpoint of the number of failures in the observed period during its exploitation. As the result of these systematic analyses, the maintenance concepts of the critical parts and assemblies of the fuel supply subsystem were selected and the intervals of realization proposed maintenance activities in accordance with a predefined request that the reliability of the fuel supply engine subsystem is not less than 0.985.

Compared to the existing program of the fuel supply subsystem preventive maintenance, a new program proposes additional maintenance activities as a condition based maintenance and maintenance on the basis of time resources of critical assemblies and elements of engine subsystems that are not covered by the current program of preventive maintenance. In order to optimize the maintenance interval, the recommendation is that proposed additional maintenance activities should be included during the first and second Technical Inspection with a slight extension of their maintenance interval.

Keeping in mind overall contents of the carried out analysis, which preceded the selection of maintenance concept of critical assemblies and elements of the fuel supply subsystem, the conclusion is that the application of the basic principles of the RCM methodology during the choice of optimal maintenance concepts and for other engine subsystems and by optimizing the interval of their execution would create conditions to significantly improve the effectiveness and efficiency of maintenance and thus the reliability and availability of these types of engines.

#### REFERENCES

- [1] D. Catic, The development and application of reliability theory, Faculty of Mechanical Engineering, Kragujevac, 2005.
- [2] G. Ivanovic, D. Stanivukovic, Reliability - Analysis and Design, Technical Directorate, Federal Secretariat of National Defense, 1988.
- [3] „Statistics Toolbox For Use With MATLAB“, The MathWorks, R2008a.
- [4] Islam H. Afefy, Reliability-Centered Maintenance Methodology and Application: A Case Study, Industrial Engineering Department, Faculty of Engineering, Fayoum University, Al Fayyum, Egypt, Engineering, 2, 863-873, 2010.
- [5] Stanley, N. F. Heap H. F.: "Reliability-Centered Maintenance". Washington DC: Defense Documentation Center, AD-A066-579. 1979.
- [6] M. Aleksic, Maintenance Strategies Selection Methodology for Complex Ship Systems, PhD Dissertation, Academy, Belgrade, 2006.



# The Application of Voith Hydrodynamic Couplers while Starting the Belt Conveyors of Mining

Dragoljub Veličković<sup>1</sup>, Svetislav Lj. Marković<sup>2\*</sup>, Dragana Andjelić<sup>3</sup>

<sup>1</sup> RB „Kolubara“, Lazarevac, Serbia, e-mail: dragoljub.velickovic451@gmail.com

<sup>2</sup> Technical College, 32000 Čačak, Svetog Save 65, Serbia, e-mail: svetom@mts.rs

<sup>3</sup> Srednja škola “Dragačevo”, Guča, e-mail: dragana.andjelic11@gmail.com

*The analysis of the possibility of applying hydrodynamic couplers between the drive electromotor and the gear reducer was carried out in the biggest Serbian mine in order to improve and modernize the operation of belt conveyors. This paper contains the basic parameters of these couplers manufactured by Voith, as well as the critical comment on their eventual application.*

**Keywords:** hydrodynamic coupler, conveyor

## 1. INTRODUCTION

The hydrodynamic coupler consists of the two working circuits: the pump circuit (P) - the entrance, connected to the drive engine shaft and the turbine circuit

(T) – the exit, which is connected to the working machine shaft. Both circuits are placed in the common housing filled with oil [1].

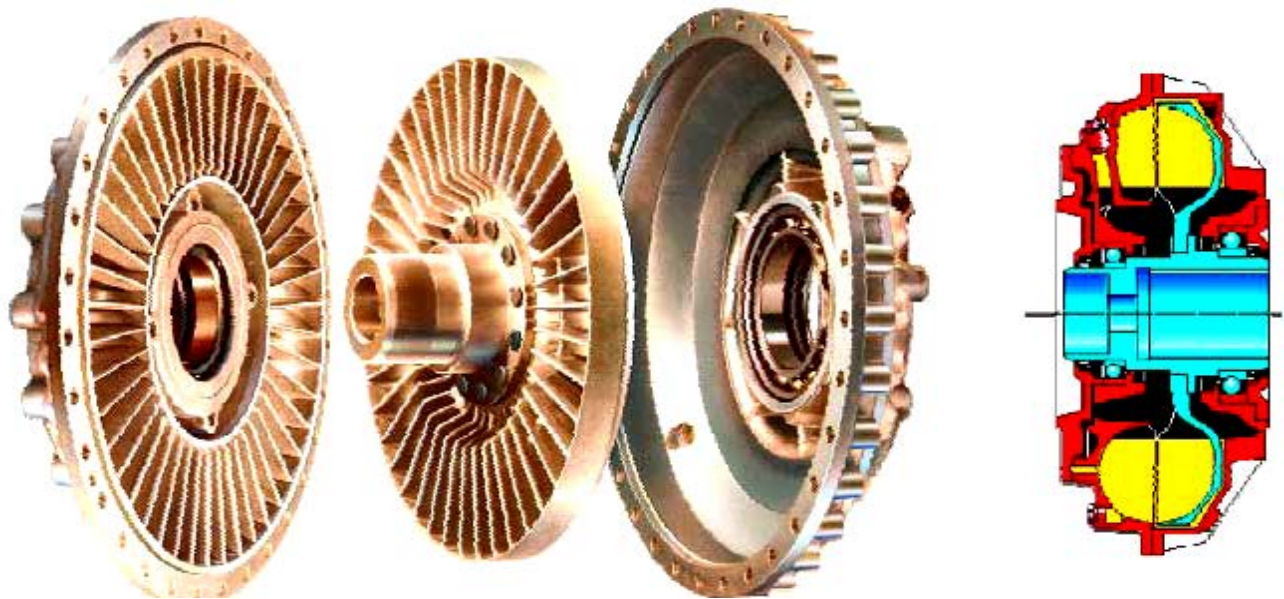


*Figure 1: The mechanisms of the hydrodynamic coupler: the pump working circuit (on the left), the turbine working circuit (in the middle) and the outer covering (on the right); the cross-section of the coupler*

The rotation of the pump circuit speeds up the working fluid which enters the working space of the turbine circuit with the increased kinetic energy which is further transferred to the working machine.

Namely, the oil as a working fluid flows at a great speed exposed to the low pressure in the closed circulation circle formed by the blades of the working circuits. When the speed of the working oil movement is increased, the mechanical energy of the engine is

transformed into the kinetic energy of the oil in the channels of the pump circuit. The reverse process takes place in the channels between the blades of the turbine circuit.

The oil is slowed down there, i.e. its kinetic energy is transformed again into the mechanical energy of the turbine circuit.

In this manner, the energy transfer from the pump circuit to the turbine circuit is performed hydraulically [1].

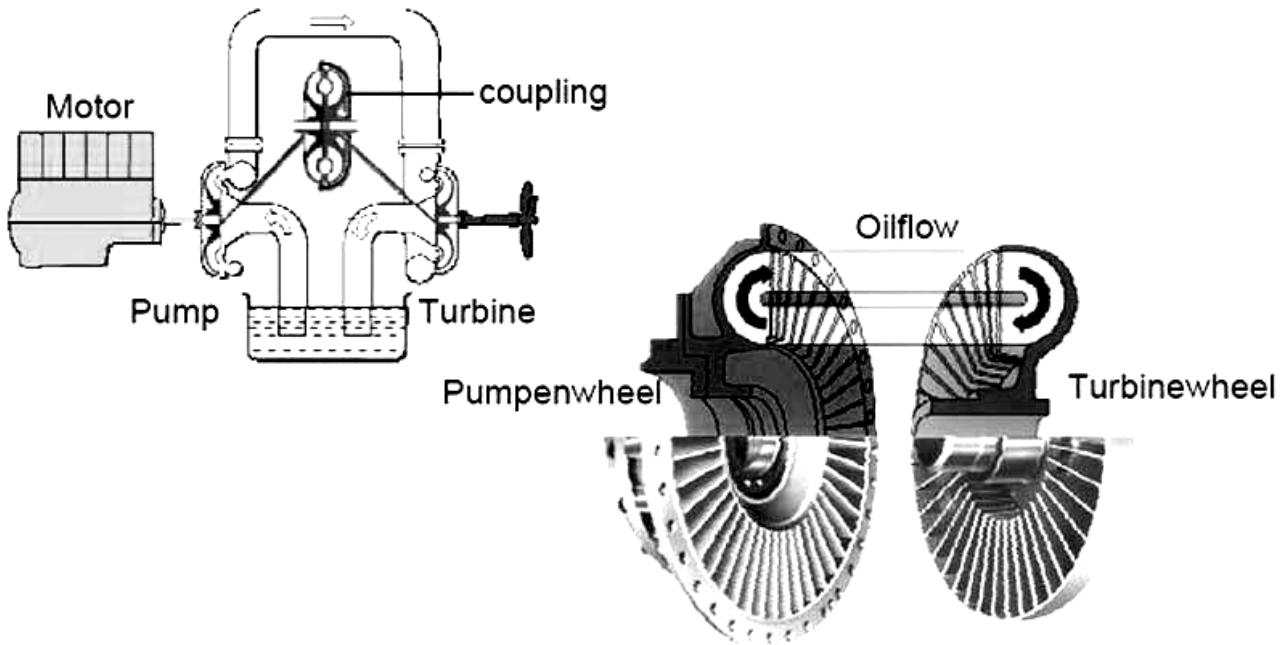


Figure 2: The scheme of the principle of operation of the hydrodynamic coupler

2. THE ANALYSIS OF THE POSSIBILITY OF INSTALLING THE VOITH TURBOCOUPLER TVVS ON THE BELT CONVEYOR

The Voith couplers are specially designed to adjust to working with different working fluids [2]:

- Oil-standard use,
- Water-especially in underground exploitation (TVV couplers), EP
- fluid (Environment Pollution-free Fluid) – biodegradable,
- Hi-fluid (High flash point fluid) - does not contain chlorinated hydrocarbon or phosphoric ester. The fluid density is smaller than water density.

- When there is too little oil:
  - It takes more time to start the machine,
  - The machine cannot be started at all,
  - The machine operates with the increased slippage.

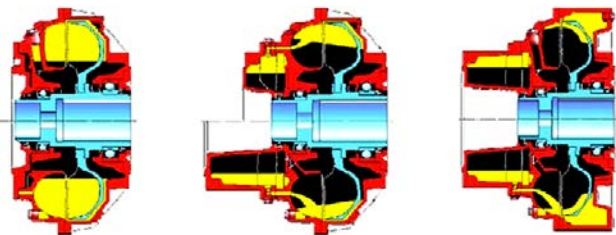


Figure 3: The basic types of the couplers with the constant quantity of oil: T (on the left), TV/TVV (in the middle) and TVVS (on the right)

The consequences of irregular pouring of oil may be the following [2]:

- When there is too much oil:
  - It takes more time to start the engine,
  - The engine cannot be started at all,
  - The engine cannot reach its nominal speed.



Figure 4: The hydrodynamic coupler Voith 750 TVVS

Table 1: The differences between the drive through the inner and the outer working circuit [3]

	Drive through the outer working circuit	Drive through the inner working circuit
The weight of the coupler	Affects the reducer shaft	Affects the engine shaft
Inertia	Less inertia on the reducer side (fewer blows in the event of a sudden blockage)	Greater inertia on the reducer side
Pouring of the fluids and the amount control	Easy - the coupler housing turns around even if the brake is closed	The entire machine must be started in order to perform inspection
Starting	Always acts the same at starting	Emptying of the slowdown chamber depends on the characteristics of starting – the starting can be problematic during the blockage of the belt conveyor
Cooling	Always the best possible	Less-especially during the starting and blockage
Starting characteristics	The Voith turbo couplers are optimal for starting the belt conveyors through the outer working circuit (the mixed profile in the inner working circuit)	
Slippage	Less	Greater
Brake installation	The construction with a shaft / additional brake flange necessary	The lower price for the brake installed on the elastic coupler

The special properties of TVVS coupler in comparison to the other types are [2]:

- the lengthened slowdown chamber and the additional rim chamber,
- this type has thermal capacity increased by 15% which allows the coupler to be started more often,
- the heat removal is faster by 10% providing faster cooling and shortening the period between two consecutive starts.

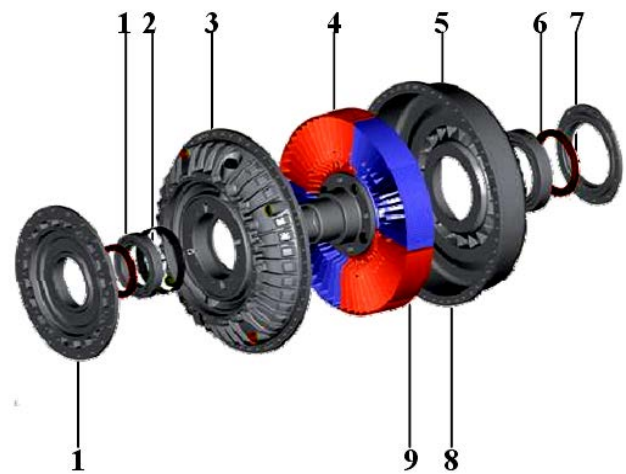


Figure 5: The coupler parts: 1 - the radial sealing ring, 2 - the ball bearing, 3 - the outer working circuit, 4 - the inner working circuit, 5 - the coupler housing, 6 - the ball bearing, 7 - the radial sealing ring, 8 - the counterweight, 9 - the frictional covering, 10 - the lid

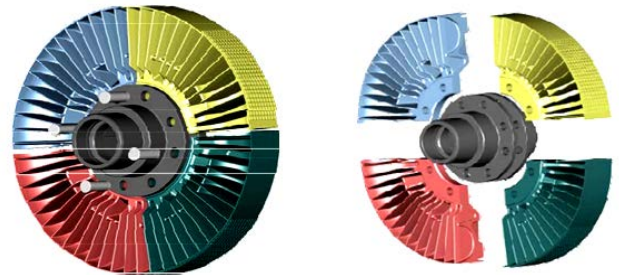
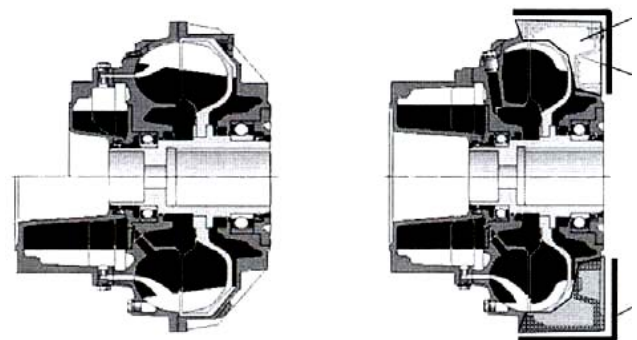


Figure 6: The inner working circuit has freely movable separate segments



TypeTV / TW

TypeTVS

Figure 7: The comparison of the different types of turbo couplers

### 3. CONCLUSION

Due to the characteristics of the hydrodynamic couplers, there exists the possibility of their application in belt conveyors in coal mines on condition of removing certain flaws which even this highly sophisticated equipment is not immune to.

Generally speaking, the turbo couplers have many advantages and therefore should be included in exploitation as soon as possible.

#### REFERENCES

- [1] Krsmanović Lj., Gajić A.: Turbomašine, hidrodinamički prenosnici snage, Mašinski fakultet, Beograd (1998).
- [2] Voith Turbo GmbH & Co. KG: katalozi, prilozi, aplikacioni programi, crteži, slike i ostalo.
- [3] Marković S., Erić D., Veličković D.: Analysis of testing the hydrodynamic coupler on the belt conveyor used for open-pit mining in the coal mine, 12<sup>th</sup> International scientific conference „Mechanical Engineering 2008“, Proceedings, Bratislava, Slovakia, 13÷14. November 2008 (2008).

## Some Modern Solutions for Delivery Operation in Postal Traffic

Aleksandar Čupić<sup>1,\*</sup>, Mladenka Blagojević<sup>1</sup>, Goran Marković<sup>2</sup>

<sup>1</sup>Faculty of Transport and Traffic Engineering, University of Belgrade, Belgrade (Serbia)

<sup>2</sup>Faculty of Mechanical and Civil Engineering in Kraljevo, University of Kragujevac, Kraljevo (Serbia)

*Drones, autonomous, ie. robotic vehicles that perform delivery operations to the final destination is topical subject of this paper. This paper provides a brief overview of the most important research in this area as well as a critical review of the results achieved and the potential for further experiments. Also there is overview of the experience of mostly involved postal companies in testing the possible use of drones and robots to the postal service. At the end some attempts with combined delivery by courier and drones together and prediction of consequences of automated delivery introduction has been presented.*

**Keywords: Automated delivery, Postal traffic.**

### 1. INTRODUCTION

Companies that dealing with transferring of items are faced with increasing customer requirements in terms of delivery deadlines and the total number of items, as well as specific requirements relating to the handling of goods. Automation of a broader spectrum of entrepreneurship, with optimization of network for items transport, has become a major tool in the struggle with competition [1,2]. Manipulating industrial robots have found their wide application in handling shipments. In the postal centres where is a large concentration of letters and parcels, introduction of manipulative robots increases the efficiency of processing by increasing the velocity and capacity. Also, costs of manipulation are reduced while quality, ie. reliability of processing, is improved [3,4,5]. This potential has been recognized long time ago and robots are a standard part of all modern sorting centers around the world.

After the introduction of automatic machines for processing of items by almost all major market participants, automation of other parts of the delivery chain has been started. The problem with that intent represents lower concentration of items outside the major processing centers. In such circumstances, the use of robots and automated machine is less profitable. At this moment around the world conducts a number of pilot projects related to the implementation of robots and drones mainly as solutions for automated delivery and/or collection of items.

This paper provides a brief overview of the most important research in this area as well as a critical review of the results achieved and the potential for further experiments.

### 2. HOMING DELIVERY ROBOTS AND VEHICLES

Homing delivery robots and vehicles represent a technology that was introduced in the postal traffic in the last few years. The idea is to replace couriers by robots in the future or at least to assist them in the delivery of items. This technology is in the early stages of testing in the UK, Switzerland and Germany. The robots use existing technologies developed in mobile communications, IT

industry, standard sensors, processors, microphones, cameras and speakers so that their price is not a limiting factor in the eventual use. Robots of Starship Technologies company (Fig. 1) used in these experiments have the ability to record all relevant events in their environment: using the built-in microphone operator can hear sounds from the environment, have a built-in camera in order to be guided and speakers which serve to client to hear the operator's instructions. Compared to the drones, which will be discussed below, this robot has a much higher capacity and longer battery life. Speed is, on the other hand, limited to the speed of pedestrians and the average is 5 km/h with expected delivery time of 30min.



Figure 1: Homing delivery robots

The client has the ability to communicate with the robot via a PC application or telephone so that, in addition to monitoring the current location of the robot by the customer, delivery is possible to the desired address and the location of the user's phone. Developed robot is rational in terms of resource use, has low maintenance, so that use does not depend on the techno-economic indicators. Possible problems might occur because of traffic safety and unclear legal regulation of technology that is still in its infancy [6].

## 2.1 Homing delivery vehicles

The idea of autonomous, ie. robotic vehicles that perform all operations from the start to the final destination is not new but still self-guiding delivery vehicles exist only as prototypes whose testing is still done on the streets in the cities. Techniques used by autonomous vehicles for moving in their own environment are based on technologies such as radar, GPS, LiDAR (Light Detection and Ranging), 3D mapping, odometry, etc. (Fig. 2). Advanced guidance and control systems perform the collection and processing of information obtained from the sensor to decide of the next action which vehicle should make. In other words autonomous vehicles learn and adapt to the surroundings of their environment.

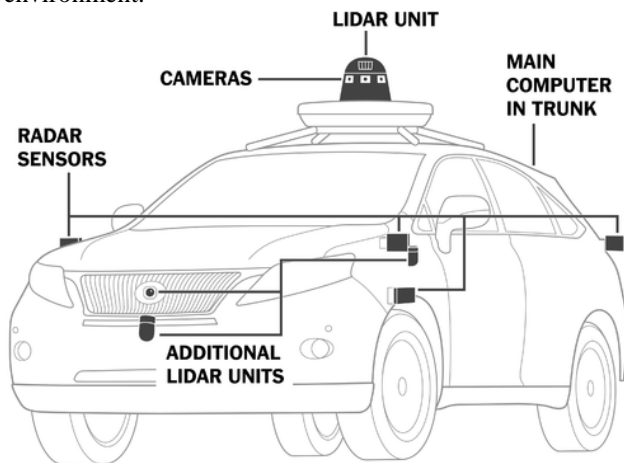


Figure 2: Homing vehicle [7]

The first homing car appeared in the 80s of the last century at Carnegie Mellon University and since then numerous companies and research centers have experimented with this type of transport mean. There are several reasons for resistance in this area regardless of the poor results achieved in the implementation of these systems. Introducing of homing vehicles in widespread use should bring:

- Reducing the number of traffic accidents and thereby reducing the number of injured and killed, reducing damage and insurance costs.
- Increase of production capacity of roads leading to a decrease in the density of traffic.
- Reduction of man's obligations while driving (increasing vacation time, less fuel consumption, less air pollution, reducing parking area, etc.).
- Improvement of existing and creation of new business models of transport services such as car sharing, e-hailing, real-time ridesharing and other

services called "divisible" economy, aimed at reducing the number of private cars.

The main problem and reason because self-guiding vehicles, despite the clear benefits, are not flourished in traffic is the time required for transformation from not autonomous to autonomous. Besides, people from different reasons (lack of trust, fear, driving pleasure, job losses in the transport industry, etc.) in a large number do not want to give up control of their vehicles.

By development of this technology companies engaged in the transfer of items and their clients should have significant benefits. That it is not just about some toys from science fiction films evidence the first delivery by the autonomous truck that took place 25th October, 2016 between Fort Collins and Colorado Springs (about 190 km). That day the truck equipped with hardware and software of start up company Otto (Fig. 3) made delivery of 50,000 units of beer from the factory to the distribution center. The driver turned on the autopilot immediately after entering the highway and took command during the descent of the highway. According to SAE standard autonomous cars are divided into six groups (0-5), regarding the levels of autonomy. Mentioned truck is the fourth level and is capable of fully autonomous driving at highway speed of 90km/h (without complicated tasks as leak pedestrians, intersections and other restrictions on driving through the urban environment). The company Uber is immediately prior to previously mentioned delivery bought the Otto company for 680 million dollars, which clearly shows that the technology of autonomous vehicles, especially in truck transport, is on the step of introducing the large-scale use.



a)



b)

Figure 3: Homing delivery vehicles: a) OTTO truck; b) equipment for guidance;

It should be expected that the autonomous transport first introduces in the transport of goods by trucks because, for example, in USA 70% of transported cargo (10.5



billion tons) is transported by trucks and they simply do not have enough drivers (deficit currently stands at 48,000, but until 2024 could reach 175,000 drivers) [8]. Drivers will continue to remain an important part in the transport, but it is not difficult to imagine how their role changes in a role similar to role of port pilots. They, in overseas traffic, have the task to "only" import and export the ship to/from the port. In road transport drivers should take trucks on/off the highway along which transport of goods should take a place in a kind of virtual compositions of trucks like wagons whose "rails" would be software.

The first company of the postal sector which has one of its research arm devoted to this particular field is DHL. They plan to implement robotisation of logistics operations completely and leave them to the autonomous delivery robots. Perhaps for this step is still early in Serbia, but if in the world some pizzerias introduce prototypes in the delivery, why it would be impossible for the Post of Serbia or any of the courier company?

Despite the obvious benefits of self-guiding robots and delivery vehicles, there are many restrictions in their use, especially in the so-called "last mile" delivery.

## 2.2 Robots that are already in use in the postal sector

Robots in the postal sector, as already mentioned, are no exception and they are widely applied. Except delivery robots, far wider application found different variations of industrial robots, particularly in the sorting process.

There is a lot of examples, but at this point will be emphasized three concepts. The first is the increasingly frequent use of robots for sorting. They are placed along the conveyor (the left edge) and serve to direct items to destination routes. The advantage of this method of sorting compared to conventional machines for the processing of items is that the robot can perform divert of items to a far greater number of different directions in relation to the executive mechanism (which has following rule: one device - one or two destinations). Another, no less important, advantage is reflected in the fact that robots placed along the sorting line have option of accepting and packaging the sorted package on the palets or other means of consolidation.

Besides, great application robots are found in the merging of packages where they are used as sophisticated solutions for packaging and palletizing of processed and unprocessed packages.

Following the trend of more intensive introduction of an AGV (Automated Guided Vehicle) system in logistics, appeared systems for items sorting which function is to set items on the individual robots (mini AGV). Each robot has a rotating mechanism by which, when it is placed next to aperture for the acceptance of packages to a particular delivery route, renders the package to a corresponding aperture. Apertures are, as opposed to the slides in the continuous processing systems, arranged in two directions. Parcels are coming by continuous conveyor and after that they are taken and placed on robots. Based on the code of items, robots can transport items to the field with the destination ports extending along the conveyor, but also normally to its

direction. Sorting capacity of such systems is flexible and determined by the number of robots that are included in the process. Despite the large number of robots, destination directions (apertures) and the capacity, the sorting system works perfectly.

## 3. DRONES

Aircrafts without crew are called drones (pilotless radio-controlled aircraft). International Civil Aviation Organization groups the aircrafts into two categories according to the mode of handling: the aircraft which is operated by remote controls and autonomous aircrafts. In autonomous aircrafts trajectory, altitude, speed and other flight characteristics are entered into a computer that is located at the drone before the journey begins, then drone execute orders independently.

It is important to distinguish modern drones of nowadays from aircraft used for military purposes, which are a kind of forerunner. The aircrafts used for military purposes are simple but they are generally complex robotic machines, airplanes and helicopters. The drones were originally designed for military purposes. The idea about drones dates from the 19th century and the Austrian balloon with gunpowder for bombing of Venice. Modern drones for the first time, then, secretly, were used in II World War by the US military. The technology was later largely evolved in the direction of development guided and homing rockets. In the following decades drones arrived in the armies of other countries. With the advent of new technologies, such as digital camera, satellite navigation and microprocessors, the possibilities of unmanned aircraft are improved. Some countries, such as China, Israel and Iran have companies for the production of military drones. The second group of drones could be classified as all the others, which are used in other areas of life and business. Drone technology is now available to everyone.

### 3.1 Drones classification

Currently, the European Union does not regulate civilian use of drones whose mass is less than 150 kilograms. These drones are regulated by national rules adopted by the EU member states. Drones over 150 kilograms falling within the competence of the European Aviation Safety Agency (EASA). In relation to the mass drones are divided into three classes:

- Class I: up to 5 kilograms,
- Class II: 5 to 25 kilograms,
- Class III: 25 to 150 kilograms.

In relation to the level of construction, population density and the presence of people, drone's flying area is divided into 4 classes:

- Class I: an area where is no elevated structures or facilities and where are no people, except staff necessary to fly and operate dron.
- Class II: an area in which are additional commercial facilities or buildings that are not intended for people, except staff necessary to fly and operate dron. There are allowed only occasional people passing through the area (cyclists, pedestrians, etc.) but without retention.
- Class III: an area in which are buildings and facilities primarily intended for residential,

business or recreation (residential buildings, residential houses, schools, sports fields, parks, etc.).

- Class IV: area of narrow urban areas (inner cities, towns, and cities).

In our country, the Civil Aviation Directorate deals with regulation of this area. According to the rules on the unmanned aircraft from the 2016, Directorate divided drones into 4 groups [7]:

- a mass up to 0.5 kilograms, a maximum flight altitude of 50 meters, a maximum speed of 30 m/s and the maximum range of 100 meters,
- a mass of 0.5 to 5 kilograms, a maximum flight altitude of 150 meters, a maximum speed of 30 m/s and the maximum range of 2500 meters,
- a mass of 5 to 20 kilograms, a maximum flight altitude of 500 meters, a maximum speed of 55 m/s and the maximum range of 2500 meters,
- a mass of 20 to 150 kilograms, without height, speed and range restrictions.

To be able to use drone, ie. be able to fly, it is necessary comply with strict rules and have the required documentation for flying. First of all, the drone must be registered in the records of the aircraft, which leads the Civil Aviation Directorate. Since safety is always at the first place, there are rules that must be followed when using a drone. It can fly only during the day and whoever manages drone must perform all the checks before the start of the flight. In other words, the drone must be technically correcting for flight. It is prohibited to operate with more than two drones at a time, as well as manage the drone from a moving vehicle. Also, it is forbidden to operate drone under the influence of alcohol and psychoactive substances. Must fly at least 30 meters away from people, objects, vehicles, roads, boats and power lines. Above the group of people distance should be minimum 150 meters. Dron can not fly close to the airports, the minimum distance from the airport must be 3 kilometers. In the world there are even special devices that prevent drones from flying in areas where they could be harmful by operating at frequencies on which they are managed, taking control over them and land or return them to the starting point.

### 3.2 Drones components

There are a number of different drones, but the base components of each of them are (Fig. 4):

- RC transmitter and receiver,
- Frame,
- engines, propellers and speed controller,
- flight controller (autopilot),
- battery and charger.

Frame is a platform for building a drone. The most common frames are with four engines uniformly distributed on the diagonals. However, if it carries a greater burden, it is necessary to use multi-engine drone, with six or eight engines. In addition to the frame, engines and propellers are a very important part because they allow the drone to fly.

The flight controller is the brain of each aircraft which allows the stabilization. There are also advanced controllers with pre-set computer path which includes the operations of take off and landing. The selection of the autopilot usually depends on the purpose for which the drone is used and how big is the budget. Lithium - ion batteries are almost always used because they have a high power and they are easily accessible. When choosing batteries, two most important factors are the capacity and voltage. The voltage depends on the number of cells (usually 3 or 4) cells. The battery capacity is usually 3000 mAh. Generally speaking, greater capacity allows for longer flight time.

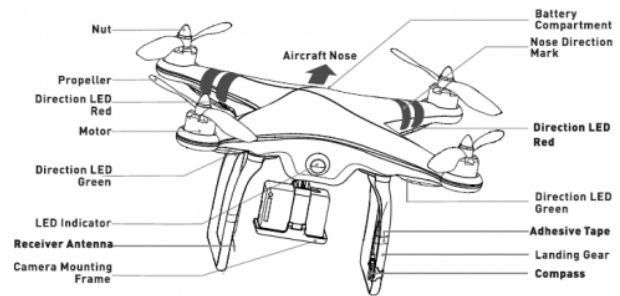


Figure 4: Quadcopter drone parts [9]

RC receiver and transmitter are also very important because they are an essential part of drones which are manually controlled from the ground. There are a number of different transmitters on the market. Higher number of channels are better solution because that allows to control multiple functions and services. The transmitter usually transmits signals at a frequency of 2.4 GHz. This range was chosen because it is very reliable and resistant to interference. In addition to the main parts, the drone may contain accessories such as: camera, parachute, GPS, navigation systems, telemetry, wireless video, etc.

### 3.3 The use of drones in the postal traffic

The drones are used for different purposes, however, these devices have become popular only in recent years and their applications in various fields rapidly increasing. The drones are used for police purposes like robots for surveillance of various rallies and campaigns. FBI uses drones to patrol the border of the United States. In the UK, drones are used to search for missing persons and monitoring of traffic accidents. The drones are also used for scientific and research purposes. They allow easier access to investigated places (glaciers, volcanoes, archaeological sites). They are also used in nuclear accidents to measure contamination. Drones have many applications in agriculture. In the United States drones are used to monitor the fields and record crops. They are also used in the art, for movies, music videos and concerts. Drones are also used in construction, medicine, emergency situations, rescue services and even in some special tasks, such as, for example, disperse the fog (China) or drone hunter (USA). The drones are also used for entertainment purposes, but there are also drone races, as well as competition in acrobatics. Also, drones are used for the delivery of food and medicine in emergencies, as well as delivery of shipments.

Postal administrations around the world, in order to remain competitive and maintain a leading role in its sector of business, must provide to their customers the best services and promote them on a daily basis. Delivery of shipments by drones or other services based on their use had not yet officially appeared in any of the post offices. So far postal operators have done experiments and set plans for further development and testing of this technology. Here is a brief overview of the experience of mostly involved postal companies in testing the possible use of drones to the postal service.

**Deutsche Post** – in collaboration with DHL ("Deutsche Post DHL") is the first company in the postal sector which is engaged in the development of this service. In Bonn 2013th the first time was tested drone that could be used for the urgent necessary goods delivery to difficult reach areas. The aircraft is named Paketkopter. Dron was going from the post office, which is located on the left side of the Rhine river, to deliver the drugs to pharmacy which is located about 800 meters away on the opposite side of the river. The experiment was successfully carried out which encouraged people employed on this project for the further development of service. The next experiment was in 2014, when was performed delivery of package with drugs on the island of Juist located about 11 kilometers from mainland. Tests have been carried out less than a month and have done several deliveries. The biggest change at this stage was the transition from a manual to an autonomous control system. Drones have worked as autopilots and flight is scheduled to last about 30 minutes. The third, and so far, last, phase of a research was conducted at the beginning of 2016th. It was conducted the delivery of urgently needed goods from Ulm station to the Bavarian village Rit im Winkl. During the test, which lasted three months, was used third generation Paketkopter, called York. In the test participated villagers themselves by applying transfer of items also in the opposite direction, from the village to other places. For three months they carried 130 autonomous loading and unloading. The most important task was to overcome the height difference and often temperature fluctuation in testing. The distance of package transmission was 8 miles and drone took about 10 minutes to cross the road.

The next steps in the development of this service are increasing of drone's possibilities and finding new locations for testing. The next test should be package delivery in urban areas. Also, efforts will be made to the fact that in the future drones are in contact with the ground crew. It is planned to equip aircraft with communication module. The main objective of Deutsche Post is to provide a new service to customers which essence is rapid dispatch and delivery of shipments.

**Swiss Post**, in cooperation with the largest logistics center in the country "Swiss WorldCargo" and company for the production of drones "Mattern", in 2015 began testing drones for the parcel delivery. The first objective of the survey was abilities of drone technology and testing the profitability of these business ideas. At the end of 2015 Swiss Post made the first experiment in Switzerland with dron called Maternet One. It is specifically designed for this test. It was autonomous, designed to carry small packages and very simple to operate. Maternet One had capability to transport items up to 1 kg at a distance less

than 10 kilometers. The first test was considered as successful and the biggest problem was weak battery, which could not allow longer retention in the air.

For now, Swiss Post has not introduced this service to its range. This service was used selectively as a supplement, for the experimental purpose. The aim is to ensure safe and fast delivery regardless of geographical circumstances. The plan is to use drones in those areas where it makes economic sense and of course where it is technically feasible. The focus is primarily on the use of drones in exceptional cases (if some location is cut off from the outside world due to weather and other natural disasters). Another focus is on an emergency transport of items of the highest priority, such as, for example, laboratory samples. It is believed that this service, if it flourishes, will be introduced in 2020 in official use.

**Finland Post** "Posti" in cooperation with their largest e-commerce retailer "Verkkokauppa.com" started to develop delivery by drones in 2016. Finland is regarded as the first country that is doing experiments in urban areas. The test last for 4 days, from 2 to 5 September 2016. Dron was transporting packages, not heavier than 3 kilograms, from Helsinki to Somenlina island, which is located 5 kilometers from the capital of Finland. In the first delivery drone carried out task, with the landing of the location not far from planned. The reason was a strong wind durin the test. The test is considered successful. For those 4 days they done several transmissions because the plan was to move all the lighter packages by drone (letters and hevier parcels as before by boat).

The goal of Finland Post is to increase transmission speed and to improve access to rural areas. They believe that new technologies will enable faster and easier shopping and delivery for both the sender and the recipient. It is expected that this service will be officially in use in 2020.

**"Australia Post"** was started in 2016 on the development of this service. One of the main reasons is that there are a large number of customers in remote areas who purchase a services three times more than those who live in the cities, but postal operator make delivery for them at most once a week. The first experiments were done around Melbourne. They done several test flights at a distance from 10 to 15 kilometers. They were used most sophisticated drones equipped with parachutes, lights and sirens to warn people if they are too close to the drone (Fig. 5). The tests have lasted for 2 weeks and characterized as successful.



Figure 5: Australia Post dron

The plans are to perform testing in 2017 as often as possible, up to twice a week. Testing will be conducted at different locations, with up to 50 deliveries per test. Civil Aviation Directorate of Australia approved the commercial use of drones in rural and less populated areas, while for the densely populated areas license does not exist yet. In accordance with that, if tests give good results, operator plans to begin delivery by drone in rural areas in 2019.

"La Poste" in cooperation with the manufacturer of drones company "Atechsys", was during 2016 carried out the first test of shipment transfer by drone. Dron was able to make autonomous delivery at a distance of 8.7 kilometers carrying a weight of 1.5 kilograms.

Currently plan is to test new drones that can carry loads of up to 3 kilograms, at a distance of up to 20 kilometers and at speeds up to 30 km/h. The main objective of La Poste in the future is better connectivity to rural areas and faster item transfer.

The **USPS** in cooperation with Amazon did a couple of tests. Amazon already has in its range this service and occasionally delivers packages by drones. However, USPS still considering the introduction of this service because they previously conducted a survey among citizens on the subject of what they think about drones in the post. Opinions were divided so everything is still questionable.

In addition to these posts, which have the best results, there are several others that have shown interest in this service. China Post had done the first tests in November 2016 in several locations in the country. Posts of Singapore, Denmark and the United Kingdom are next that will start the process of research and development of this service in their countries.

#### 4. COMBINED DELIVERY

From above text, it is clear that each technology has its advantages and disadvantages. The main disadvantage of automated product delivery by robots, self-guiding vehicles and drones is reflected in the so called last mile delivery. At this stage, it is necessary to make individual delivery to each recipient. In rural areas, this means high mileage per each item and, in this case, delivery by robots or drones can easily compete with the classic courier delivery. This can be seen also from the directions in which experiments were conducted, mentioned in the previous section. However, in urban areas, where the density of delivery is expressed, couriers have a great advantage because they can perform a large number of deliveries at a small delivery area and reduce the unit price per delivery. Robots and drones described in this paper are provided for a single delivery of items which greatly reduces their effectiveness in this part of the delivery, in particular if a package has been taken over in one of the units of postal network.

With this in mind, the increasingly frequent are attempts with combined delivery by courier and drones together, ie. robots that take over items in delivery vehicle. This reduces the path and time that these devices should overcome, the vehicle becomes a kind of outward-incoming platform and courier gets the role of the operator who sets the items on robots/drones, performe their journeys and collection after delivery and organizes the

whole process. Thereby robots and drones become courier "helpers" thereby increasing the range and speed of delivery.

UPS has successfully tested a drone designed to launch from the top of one of its delivery trucks (Fig. 6). The test, performed in Lithia, Florida, with Workhorse Group, an Ohio-based electric truck and drone developer, successfully sent the drone first on an autonomous package delivery and then back to the truck while it was out making a separate delivery. This test is different than anything they've done with drones so far. It has implications for future deliveries, especially in rural locations where their package cars often have to travel miles to make a single delivery. Sending a drone from a package car to make just one of those deliveries can reduce costly miles driven. This is a big step toward bolstering efficiency in network and reducing emissions at the same time.



Figure 6: Combined delivery by UPS

However, as TechCrunch reports, it wasn't all smooth flying. During a second test, some type of interference caused the drone to abort its launch the aircraft tried to land on top of the UPS truck, fell to the side and was nearly crushed by the still-closing lid of the vehicle. With ORION, UPS's On-Road Integrated Optimization Navigation routing software, a reduction of just one mile per driver per day over one year can save the company up to \$50 million. UPS has about 66,000 delivery drivers on the road each day. Rural delivery routes are the most expensive to serve due to the time and vehicle expenses required to complete each delivery. In this test, the drone made one delivery while the driver continued down the road to make another. This is a possible role UPS envisions for drones in the future [10].

These efforts follow a boom in electronic commerce, which has forced logistics companies to find new faster ways to deliver packages to customers. The key is to make integrating smart technology, such as a small computer, so that the van can collect and process data on the vehicle's location, load, and delivery route and then send that information to the distribution manager. The vans should be electric – a critical feature as cities pass stricter emissions laws for its busiest urban centers, and should be equipped with an automated cargo space and delivery robots and/or drones.



Figure 7: Mercedes concept Robovan

The van driver can deploy the autonomous vehicles to deliver multiple lighter packages to customers by road/air, while he or she walks to another customer's home carries a heavier parcel. Cloud-based software could communicate with a main distribution center or calculate ideal delivery routes for the package deliverer.

These vans (Fig. 7) would be equipped with a racking system that would enable 400 packages to be delivered every 9-hour shift, compared to 180 packages using previously available methods [11].

#### 5. CONSEQUENCES OF INTRODUCTION OF AUTOMATED DELIVERY

Automated delivery will bring many benefits for investors, owners of delivery companies and their clients. But the implications of automated delivery will likely have a profound effect on the postal workers around the world. Only some, not all, workers will be able to upskill, because the challenge now is that robots will always learn faster than humans, as they are networked and can process faster and work at an accelerated pace. The postal industry will need solutions to unemployment and they must prepare for changes in society and their economy. While universities actively try to teach students coding, technology is quickly advancing that robots will be able in a close future to self-code. This means that understanding how to manage systems of robots towards solving problems will be key. How will postal industry respond to automation? We see a few options:

- 1) Resist automation. The companies may seek to stay in this level of automation, keeping their workers intact. The risk is that their competitors could move ahead in productivity by deploying robots.
- 2) Embrace automation, as it lifts companies' productivity. The management might welcome automation, embracing the productivity benefits it brings to company performance. The risk is that displaced workers who are unable to upskill will be left in the cold.
- 3) Upskill workers with STEAM (learning that uses Science, Technology, Engineering, the Arts and Mathematics) education. All workers whose positions are threatened by automation could benefit from provided or low-cost education that enables them to upskill so they can manage or support automation rather than

be displaced. Some have found that robots actually increase the number of jobs in some scenarios.

- 4) They could wait for administration to embrace universal basic income (the experiments are happening in Finland, Oakland and more). In a less likely scenario, administration embracing universal basic income, which would be a social program to provide all citizens with a living wage (food, clothing, shelter, and education) regardless of employment status or age. The funds would be derived from taxes on the companies that are deploying automation. The hope is that automation increases total productivity, generating more food, goods, and services than ever before, thereby creating a surplus for humanity [12].

It is likely that every employer and every country will find its measure in the introduction of automation, which also applies to automated delivery. One thing is certain, the pressure of a competitive environment in the transfer of items will bring, sooner or later, more efficient and productive solutions based on automation in areas where it has not been.

#### 6. CONCLUSIONS

About robots, autonomous delivery vehicles and drones as possible solutions for specific segments of the delivery in the Post of Serbia has not yet been discussed. Currently it is not realistic to expect any activity in this direction due to the fact that technologically advanced postal operators in the world perform only testing of this technology. However, the period of time between testing and deployment with any new technology it's shorter and shorter. The chances are that the introduction of automated delivery robots, autonomous delivery vehicles, drones or some even more sophisticated means will not wait as the introduction of automation in the processing of postal items. This would be not only unjustified but also harmful and irresponsible due to the fact that from the committed errors and omissions must learn.

#### ACKNOWLEDGEMENTS

This research was supported by Serbian Ministry of Education, Science and Technological Development with project TR36022 and TR36002.

#### REFERENCES

- [1] A. Čupić, D. Teodorović, "Lociranje habova za ekspres pošiljke primenom genetskih algoritama", XXXVI Simpozijum o operacionim istraživanjima "SIM-OP-IS", Beograd (Srbija), 22-25 Septembar 2009, pp. 651-654, (2009)
- [2] A. Čupić, "Višekriterijumski pristup projektovanju mreže za prenos ekspres pošiljaka primenom genetskih algoritama", XLI Simpozijum o operacionim istraživanjima "SIM-OP-IS", Divčibare (Srbija), 16-19 Septembar 2014, pp. 741-747, (2014)

- [3] B. Stanivuković, A. Čupić, "Nove perspektive primene postojećih sistema automatizacije prerade poštanskih pošiljaka", XXVI Simpozijum o novim tehnologijama u poštanskom i telekomunikacionom saobraćaju "POSTEL 2008", Beograd (Srbija), 16-17 Decembar 2008, pp. 167-176, (2008)
- [4] M. Bukumirović, A. Čupić, "Tehnologija mehanizovane prerade poštanskih pošiljaka", Saobraćajni fakultet, Beograd, (2012)
- [5] M. Bukumirović, "Automatizacija procesa rada u poštanskim sistemima ", Saobraćajni fakultet, Beograd, (1999)
- [6] <http://mashable.com/2016/07/06/robot-delivery-uk/#nuPRomk2gOqW>
- [7] [http://cad.gov.rs/upload/regulativa/Pravilnik%20o%20bespilotnim%20vazduhoplovima%20\(SI%20glasnik%20RS,%20broj%20108-15\).pdf](http://cad.gov.rs/upload/regulativa/Pravilnik%20o%20bespilotnim%20vazduhoplovima%20(SI%20glasnik%20RS,%20broj%20108-15).pdf)
- [8] <http://www.vired.com/2016/10/ubers-self-driving-truck-mades-first-delivwery-50000-beers/>
- [9] <https://3dprinting.com/how-to/3d-print-drone/>
- [10] <http://www.equipmentworld.com/ups-launches-drone-from-truck-to-make-first-unmanned-residential-delivery-video/>
- [11] <http://fortune.com/2016/09/07/mercedes-vans-drones-matternet/>
- [12] <http://www.web-strategist.com/blog/category/autonomous-world/>

# Material Handling Equipment Selection Using an Integrated Approach F-MODIPROM: An Advantage Gained from Using Fuzzy Numbers

Goran Marković<sup>1\*</sup>, Mile Savković<sup>1</sup>, Nebojša Zdravković<sup>1</sup>, Aleksandar Čupić<sup>2</sup>, Marko Popović<sup>3</sup>

<sup>1</sup>Faculty of Mechanical and Civil Engineering in Kraljevo, University of Kragujevac, Kraljevo (Serbia)

<sup>2</sup> Faculty of Transport and Traffic Engineering, University of Belgrade, Belgrade (Serbia)

<sup>3</sup> Faculty of Technical Science, University of Kragujevac, Čačak (Serbia)

*Combining the methods for determining the relative importance of criteria and alternatives ranking methods, the optimal decision is made about certain multicriteria problem regardless the nature of parameters describing it. The appropriate material handling equipment (MHE) selection is a vital task for improving the productivity of an organization. Hence, the problem of selecting the right type of MHE for a given task can be solved using multi-criteria decision-making (MCDM) approach capable of dealing with a combination of crisp and fuzzy data. This paper tries to quantify the level of benefit provided by employing the fuzzy numbers in the MCDM models. In the paper, by increasing the fuzziness level steadily in the fuzzy numbers, the obtained rankings by F-MODIPROM approach are compared with the ranking obtained with the crisp values. The statistical significance of the differences between the ranks is calculated using Spearman's rank-correlation coefficient. The purpose of this paper is to give systematic review and adequate support for decision-making in the selection procedure and find appropriate situations when using crisp or fuzzy numbers will be more adequate.*

**Keywords:** MCDM, stochastic test, crisp, fuzzy, F-MODIPROM

## 1. INTRODUCTION

Generally, while considering any selection problem in the domain of logistics and logistics systems there is a great number of technically feasible alternatives, and the task of designer is to choose from the set of possible solutions the one that best meets the technical and economic conditions defined by the terms of reference [9]. As a process, material handling incorporates a wide range of equipment and systems that support logistics and make the logistics system work. The determinations of proper material handling system is important for reduced costs, increased profits and efficiency of labor force. For example, material movements accounts for about 30 to 40% of the cost of final product [11]. It is observed that there are about 50 different types of MHEs and they are characterized by about 30 different attributes [4].

The proper type of MHE must be chosen taking into consideration all the relevant parameters and functions. For MHE selection, most of the influencing attributes are expressed linguistically and use of fuzzy set theory comes as an aid for obtaining the final solution. The problem of selecting the right type of MHE for a given task can be solved using MCDM approach capable of dealing with a combination of crisp and fuzzy data.

In the existing literature, fuzzy MCDM models, in which fuzzy numbers are used instead of crisp values, are proposed to deal with the vagueness and imprecision. Also, there are numerous examples where various outranking methods and their modifications are used in the selection of final decisions in solving various multicriteria problems [9]. Therefore, a small number of available studies in the literature propose approaches to measure the benefit generated by incorporating fuzziness in their selection models [17].

Generally, an integrated approach (F-MODIPROM [10]) is used to obtain final ranking of alternatives of considered problem and to compare ranking obtaining with crisp and fuzzy data. The proposed approach minimizes the influence of experience and subjective evaluation of the decision-maker.

In this study, by increasing the fuzziness level steadily in the fuzzy numbers, the obtained MHE rankings are compared with the ranking obtained with the crisp values. The purpose of this paper was to give systematic review and adequate support for decision-making in the selection procedure and find appropriate situations when using crisp or fuzzy numbers will be more adequate. A study comparing usage of the fuzzy and crisp numbers or one that provides recommendations about when one is preferred over the other. The statistical significance of the differences between the ranks is calculated using Spearman's rank-correlation coefficient. When the statistical significance of the difference is above a pre-defined value, it is recommended to use the fuzzy numbers instead of crisp ones.

## 2. METHODOLOGY

### 2.1 An integrated approach F-MODIPROM

An integrated approach F-MODIPROM (Fuzzy-MODified PROMethee Method) [10] is a combination and expansion of some formulated models for ranking alternatives of the considered problem and also for a sensitivity analysis of the final order of alternatives due to changes in criteria relative weights. The proposed algorithm of integrated approach, with all the above elements, is shown in Figure 1.

The developed method for decision-making is carried out in several stages, for multiple criteria scenario and with the possibility of taking into account the linguistic expressions of the importance of criteria.

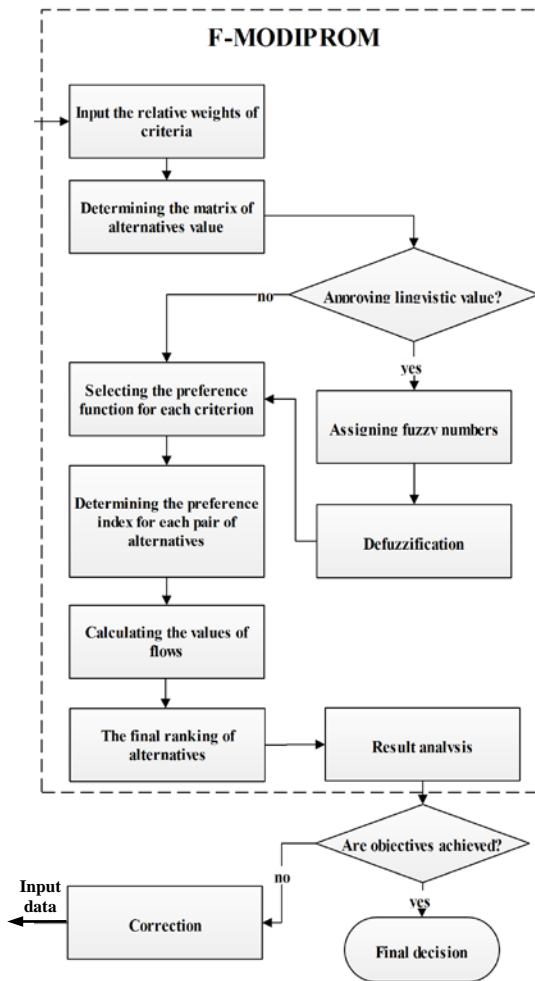


Figure 1: The integrated approach F-MODIPROM

The MODIPROM method (MODified PROMethee Method) [9], which is combined with fuzzy set theory, is based on the improvement of a group of methods for multicriteria ranking, as follows:

- change of the existing generalized criteria and introduction of the new ones,
- procedure of selection of generalized criteria within one criterion function,
- analysis of effects of change of weight coefficients, transformation of the mean values of the outranking flow for the purpose of solving complex criterion functions and
- the possibility of taking into account the linguistic expressions of the importance of criteria.

Changes of generalized criteria refer to retaining generalized criteria type I (Usual criterion), type II (U-shape criterion), type IV (Level criterion) and type VI (Gaussian criterion).

Criterion type III (V-shape criterion) and type V (V-shape with indifference criterion) is replaced with the linear criterion whose parameters are calculated through linear regression.

The square and cube criteria whose parameters are calculated by regression analysis are introduced (Figure 2) [9]. The final order of alternative solutions depends on the applied technique of multi-criteria decision-making and, especially, on the procedure of defining the evaluation criteria, transformation (normalization) of criteria and determination of their relative importance.

TYPE OF GENERALIZED CRITERION			Parameters	$P_j(x)$
Type	Name	Shape		
III	Criterion with linear preference		$q, p, b_0, b_1$	$P_j(x) = \begin{cases} 0, & d < q \\ b_0 + b_1x, & q \leq d < p \\ 1, & d \geq p \end{cases}$
V	Square criterion		$q, p, b_0, b_1, b_2$	$P_j(x) = \begin{cases} 0, & d < q \\ b_0 + b_1x + b_2x^2, & q \leq d < p \\ 1, & d \geq p \end{cases}$
VI	Cube criterion		$q, p, b_0, b_1, b_2, b_3$	$P_j(x) = \begin{cases} 0, & d < q \\ b_0 + b_1x + b_2x^2 + b_3x^3, & q \leq d < p \\ 1, & d \geq p \end{cases}$

Figure 2: Changes of generalized criteria

( $q$  – the threshold or indifference,  $p$  – the threshold of strict preference,  $\sigma$  – the standard deviation of Normal distribution and  $b_0, b_1, b_2, b_3$  – the coefficients of the regression line)

## 2.2. Spearman’s rank correlation test

To analyse the statistically significant differences between the ranks with fuzzy and crisp data Spearman's rank-correlation test is used. Spearman's rank correlation test, which is a special form of correlation test, is used when the actual values of paired data are substituted with the ranks which the values occupy in the respective samples [8]. In this study, Spearman's rank correlation test evaluates the similarity of the outcomes (rankings a set of MHE alternatives). To test the null hypothesis in Spearman's correlation test, test statistic  $Z$  is calculated using Eqs. (1) and (2) and compared with a pre-determined level of significance  $\alpha$  value. In Eqs. (1) and (2),  $d_j$  represents the ranking difference between  $j$  results,  $K$  is the number of alternatives to be compared and  $r_s$  represents the Spearman's rank correlation coefficient.

$$r_s = 1 - \left[ \frac{6 \cdot \sum_{j=1}^K (d_j)^2}{K(K^2 - 1)} \right] \tag{1}$$

$$Z = r_s \sqrt{K - 1} \tag{2}$$



2.3. Fuzzy set theory

Fuzzy sets theory is a convenient mathematical tool for modeling various processes dominated by uncertainty, ambiguity, subjectivity, uncertainty. The fuzzy data can be linguistics terms, fuzzy sets or fuzzy numbers. In the following few lines, in order to apply the proposed method, are given some terms related to the theory of fuzzy sets.

Fuzzy set theory states that, in a universe of discourse  $X$ , a fuzzy subset  $\tilde{A}$  of  $X$  is defined by a membership function  $\mu_{\tilde{A}}(x)$ , which maps each element  $x$  in  $X$  to a real number  $R$  in unit interval of  $[0,1]$ . The function value  $\mu_{\tilde{A}}(x)$  represents the grade of membership of  $x$  in  $\tilde{A}$ . The larger the value of  $\mu_{\tilde{A}}(x)$ , the stronger is the grade of membership for  $x$  in  $\tilde{A}$  [4].

Fuzzy set theory is used to convert imprecise linguistic terms, such as “high” and “moderate” into numerical values using triangular fuzzy numbers (TFNs) or trapezoidal fuzzy numbers (TrFNs). Similarly, when a quantitative property is stated vaguely or imprecisely, it is also expressed by TFN or TrFN according to fuzzy set theory.

For example, if it is stated that the distance travelled by an MHE is approximately equal to 200 units, it becomes difficult for the DM to ascertain the exactness of the data for further processing. Therefore, this imprecise value is represented by a TrFN as (180, 200, 200, 220), taking into consideration 10% fuzziness. On the other hand, another MHE property with a value “approximately between 360 and 400” can be denoted by a TrFN as (324, 360, 400, 440) with 10% fuzziness [4]. Figure 3 exhibits a triangular and trapezoidal fuzzy membership function.

A fuzzy number is a convex normalized fuzzy set with continuous membership function that characterized confidence interval  $[m, n]$  and level of security  $\alpha$  ( $\alpha \in [0,1]$ ). The TFN can be denoted as  $\tilde{A} = (a, m, n)$ , where  $m$  – left spread,  $a$  – central value and  $n$ – right spread (Figure 3).

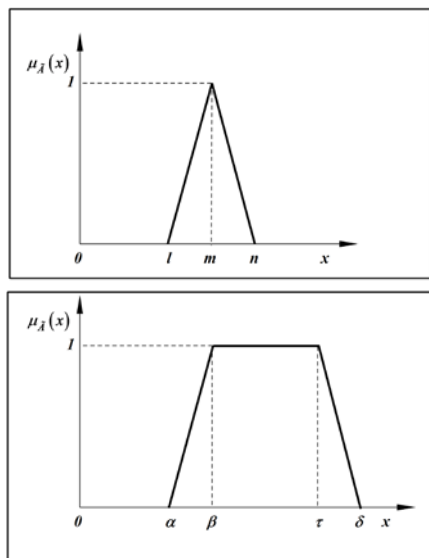


Figure 3: Membership function of TFN and TrFN

A fuzzy number  $\tilde{A} = (\alpha, \beta, \tau, \delta)$  is a TrFN if its membership function is expressed as follows:

$$\mu_{\tilde{A}}(x) = \begin{cases} (x-\alpha)/(\beta-\alpha), & \alpha \leq x \leq \beta \\ 1, & \beta \leq x \leq \tau \\ (x-\delta)/(\tau-\delta), & \tau \leq x \leq \delta \\ 0, & \text{otherwise} \end{cases} \quad (3)$$

Each fuzzy number is defuzzified using Eq. 4. For a trapezoidal fuzzy number  $\tilde{A} = (\alpha, \beta, \tau, \delta)$  its defuzzied value is defined to be

$$A = \frac{\alpha + \beta + \tau + \delta}{4} \quad (4)$$

Based on Yager’s centroid index, the geometric center of fuzzy number  $\tilde{x}$  on the horizontal axis is calculated as follows:

$$x_0 = \frac{\int_0^1 g(x)\mu_x dx}{\int_0^1 \mu_x dx} \quad (5)$$

where  $g(x)$  can be considered as a weight function of  $x$  values. Usually,  $g(x)$  is assumed equal to  $x$ ,  $\tilde{x}$  is the membership degree of  $x$  values, and the denominator is considered as a normalizing factor equal to the total area under the membership degree function in Figure 3 [18].

3. ANALYSIS OF THE LEVEL OF FUZZINESS

F-MODIPROM approach requires the weights of criteria and MHE alternative values at the criteria as inputs. For numerical illustration of correlational test in further works it will be considered a selection of three wheel electro forklift unit for warehouse operation [7, 8].

An organization was in need of purchasing forklift for its warehouse facility. It is a MCDM problem and for ranking a set of alternatives of forklifts that satisfy in advance required parameters, the initial set of 9 characteristics was observed (Table 1) as a initial set of selection criteria.

Starting sample that is considered consists of 10 forklifts of different manufacturers. Their initial values are collected from appropriate catalogs. Only criteria weights are required to be fuzzy numbers, since MHE characteristics values at criteria are crisp values.

In this study, five cases (B-F) are developed by varying the lower and upper values of fuzzy numbers while keeping their centres constant at their crisp values (case A). The level of fuzziness is determined with the spread (the number of units that lower and upper values apart in TFN and TrFN and takes 0,1,2,...,4).

For each case, the criteria weights are readjusted by equaling the number of units upper and lower values are apart with the spread value given for that case.

Table 1: Forklifts characteristic values for 9 criteria

Model	Capacity (kg)	Max. lift height (mm)	Travel speed with the load (km/h)	Lift speed with the load (m/s)	Turning radius (mm)	Level of noise (dB)	Engine power (kW)	Wheel-base (mm)	Total width (mm)
7FBEST15	1500	3310	12	0.3	1450	62.4	7.5	1200	990
2ET2500	1300	3000	16	0.48	1440	66	11.5	1249	1060
2ETC3000	1600	3000	16	0.49	1548	66	11.5	1357	1060
J30XNT	1361	3032	15.7	0.39	1481	69	4.8	1290	1050
J35XNT	1588	3032	15.7	0.36	1577	69	4.8	1386	1050
TX30N	1350	3300	14.5	0.34	1525	61	10.7	1300	1105
TX35N	1600	3300	14.5	0.31	1525	61	10.7	1300	1105
ERP15VC	1500	3320	12	0.3	1452	59	6	1222	996
ERP15VT	1500	3320	16	0.43	1476	65	12	1290	1050
ERP16VT	1600	3320	16	0.43	1476	65	12	1290	1050

Table 2: Criteria weights for six cases A-F

Criteria	Criteria weights for six cases (A-F)					
	(A) Crisp, Spread 0	(B) TFN, Spread 1	(C) TFN, Spread 2	(D) TrFN, Spread 3	(E) TrFN, Spread 4	(F) TrFN, Spread 5
Capacity (kg)	9	8,9,9	8,9,10	7,8,9,10	6,8,9,10	5,7,9,10
Max. lift height (mm)	8	7,8,8	7,8,9	6,7,8,9	5,7,8,9	5,6,9,10
Travel speed with the load (km/h)	6	5,6,6	5,6,7	5,6,7,8	4,6,7,8	3,4,7,8
Turning radius (mm)	4	3,4,4	3,4,5	3,4,5,6	2,4,5,6	2,3,4,7
Level of noise (dB)	3	2,3,3	2,3,4	2,3,4,5	1,3,4,5	1,2,3,6
Engine power (kW)	2	1,2,2	1,2,3	1,2,3,4	1,2,3,5	1,2,3,6
Lift speed with the load (m/s)	5	4,5,5	4,5,6	4,5,6,7	3,5,6,7	4,5,7,9
Wheelbase (mm)	1	0,1,1	0,1,2	0,1,2,3	0,1,2,4	0,1,2,5
Total width (mm)	7	6,7,7	6,7,8	6,7,8,9	5,7,8,9	5,7,8,10

For each case, the ranking scores are obtained by F-MODIPROM approach and provided in Table 3.

Table 3: Ranks of forklift alternatives obtained by combined approach

Alternatives	Ranking score					
	A	B	C	D	E	F
7FBEST15	1	1	1	1	1	1
2ET2500	3	3	3	5	6	6
2ETC3000	7	7	7	8	7	7
J30XNT	2	2	2	3	3	3
J35XNT	4	4	4	2	2	2
TX30N	9	9	9	10	10	10
TX35N	10	10	10	9	9	8
ERP15VC	5	5	5	4	4	4
ERP15VT	8	8	8	7	8	9
ERP16VT	6	6	6	6	5	5

### 3.1. Analysis of statistical significances

In order to analyze statistical significances of the differences and to compare the results of ranking for each case are developed the program tools in the environment of Microsoft Excel, that uses a special type of correlation test - Spearman's rank correlation test (Figure 4). Developed tool, it's possible for a given level of significance to compare the results of ranking and compare outputs the ranking obtained using by combined approach. Testing the null hypothesis  $H_0$ , i.e. the Spearman's test statistic Z value is determined by using the expression (1) and (2) and compares it with a value that corresponds to a given significance level  $\alpha$ .

Correlation is a bivariate analysis that measures the strengths of association between two variables and the direction of the relationship. In terms of the strength of relationship, the value of the correlation coefficient varies between +1 and -1. When the value of the correlation coefficient lies around  $\pm 1$ , then it is said to be a perfect degree of association between the two variables. As the correlation coefficient value goes towards 0, the relationship between the two variables will be weaker. The direction of the relationship is simply the + (indicating a positive relationship between the variables) or - (indicating a negative relationship between the variables) sign of the correlation. In this study,  $Z = 1.645$  is selected as the critical value at the level of significance  $\alpha = 0.05$ . If we set  $\alpha = 0.05$ , achieving a statistically significant Spearman rank-order correlation means that we can be sure that there is less than a 5% chance that the strength of the relationship we found happened by chance if the null hypothesis were true.

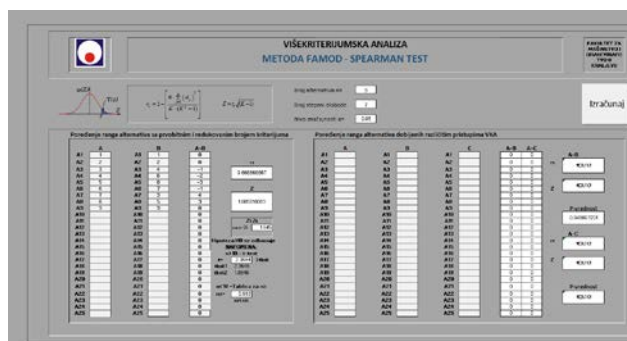


Figure 4: Spearman's rank correlation test program tool

If the calculated value of Z obtained by test exceeds the critical value, the null hypothesis is rejected and it is concluded that there is evidence of a positive relationship - agreement between the two sets of rankings.

The Spearman's correlation test results (Table 4) indicate that the differences between rankings are not statistically significant (Z values are above the critical value of 1.645).

Table 7: The differences and correlation values

Alternatives	Analysis of differences using Spearman's rank correlation test				
	A-B	A-C	A-D	A-E	A-F
7FBEST15	0	0	0	0	0
2ET2500	0	0	-2	-3	-3
2ETC3000	0	0	-1	0	0
J30XNT	0	0	-1	-1	-1
J35XNT	0	0	2	2	2
TX30N	0	0	-1	-1	-1
TX35N	0	0	1	1	2
ERP15VC	0	0	1	1	1
ERP15VT	0	0	1	0	-1
ERP16VT	0	0	0	1	1
Spearman's correlation coefficient $r_s$	1	1	0,9515	0,8909	0,8666
Statistical significance value Z	3	3	2,745	2,672	2,6

As the outcome of the test, can be observed that as the level of fuzziness increases, the similarity of the rankings decreases. The all Z-values even the lowest value indicates that using fuzzy numbers instead of crisp values does not provide any differences in the ranking. Confirmation of above mention fact is provided in Table 7. Cases B and C provided the exact ranking with Case A. The highest rank difference is 3 for cases E and F when the spread is increased to 4 and 5. Generally, the rank difference increases when the spread is increased. The advantages gained from changing the spread without changing the center of the fuzzy number is statistically insignificant. In that case the user can use crisp values as the criteria weights.

#### 4. CONCLUSION

This paper tries to quantify the level of benefit provided by employing the fuzzy numbers in the MCDM models. The increasing of fuzziness level steadily in the fuzzy numbers, the obtained rankings by F-MODIPROM approach are compared with the ranking obtained with the crisp values. There are developed the various cases by increasing the spread while keeping the centre of the fuzzy numbers constant. The Spearman's correlation test results indicate that the differences between rankings are not statistically significant in some cases.

As the outcome of the test, can be observed that as the level of fuzziness increases, the similarity of the rankings decreases. The Z-values indicates that using fuzzy numbers instead of crisp values does not provide any differences in the ranking. In the proposed cases, it is assumed that the mean values are known with certainty but the users are not sure about the spreads. However, the average values may be unknown along the spread of the fuzzy number which implies increased uncertainties and imprecision.

Definition of new cases i.e. comparasions of Z-values obtained for shifted the average and spread value together, are direction for feature research and justifying the usage of fuzzy numbers instead of the crisp ones. The purpose of this paper was to give systematic review and adequate support for decision-making in the selection procedure and find appropriate situations when using crisp or fuzzy numbers will be more adequate.

#### REFERENCES

- [1] Chu, H. K., Egbelu, P. J., Wu, C. T.: "ADVISIOR: A computer-aided material handling equipment selection system", Int. J. Prod. Res., 33 (12): 3311-3329, (1995)
- [2] Dagdeviren, M.: "Decision Making in equipment selection: an integrated approach with AHP and PROMETHEE", Journal of Intelligent Manufacturing, 19, pp. 397-406, (2008)
- [3] Fisher, E.L., Farber, J. B., Kay, M. G.: "MATEHS: An expert system for material handling equipment selection", Engineering Costs and Production Economics, 14, pp. 297-310, (1998)
- [4] Khandekar A.V., Chakraborty, S.: "Material Handling Equipment Selection using Fuzzy Axiomatic Design Principles", 5<sup>th</sup> International & 26<sup>th</sup> All India Manufacturing Technology, Design and Research Conference (AIMTDR 2014), IIT Guwahati, Assam, India, pp. 21-1-21-7, (2014)
- [5] Kim, K. S., Eom, J. K.: "An expert system for selection of material handling and storage systems", Int. J. Ind. Eng., 4(2), pp. 81-89, (1997)
- [6] Kulak, O., Satoglu, S. I., Durmusoglu, M. B. "Multi-attribute material handling equipment selection using information axiom", Proceeding of ICAD2004, The Third International Conference on Axiomatic Design, Seoul, pp. 1-9, (2004)
- [7] Marković, G., Gašić, M., Savković, M., Marinković, Z., Tomić, V.: "Criteria system defining in multicriteria decision making problem at transport-storage system elements choice", 5th International conference – Transport and logistics, pp.177-184, Niš, (2014)
- [8] Marković G., Bogićević Z., Savković M., Marinković Z., Tomić V.: "Application of correlation test to criteria selection for multi criteria decision making problems in domain of logistics systems ", The Eighth International Conference Heavy Machinery HM 2014, p.p. G31-36, (2014)

- [9] Marković, G., Gašić, M., Kolarević, M., Savković, M., Marinković, Z.: "Application of the MODIPROM method to the final solution of logistics centre location", *Transport* 28(4), pp. 341-351, (2013)
- [10] Marković, G.: "Model of regional logistics with transport systems", PhD thesis, pp.183, (2014)
- [11] Onut, S., Kara, S.S, Mert, S.: "Selecting the suitable material handling equipment in the presence of vagueness", *International Journal of Advanced Manufacturing Technology*, Vol. 44, pp. 818-828, (2009)
- [12] Park. Y.: ICMESE: "Intelligent consultant system for material handling equipment selection and evaluation", *Journal of Manufacturing Systems*, 15(5), pp. 325-333, (1996)
- [13] Sabzi, H. Z., King, J. P., Gard, C., Abudu, S.: "Statistical and analytical comparison of multi-criteria decision-making techniques under fuzzy environment", *Operation Research Perspectives*, 3 (2016), pp. 92-117, (2016)
- [14] Tabucanon, M. T., Batanov, D. N., Verma, D.K.: "Intelligent decision support system (DSS) for the selection process of alternative machines for flexible manufacturing systems (FMS)", *Computers in Industry*, 25, pp. 131-143, (1994)
- [15] Taha, Z., Rostam, S.: "A hybrid AHP-PROMETHEE decision support system for machine tool selection in flexible manufacturing cell", *J. Intell. Manuf.* 23 (2012), pp.2137-2149, (2012)
- [16] Yurdakul, M., Tansel, I. Y.: "Application of correlation test to criteria selection for multi criteria decision making (MCDM) models", *International Advanced Manufacturing Technology* 40 (2009), pp. 403-412, (2009)
- [17] Yurdakul, M., Tansel, I. Y.: "Analysis of the benefit generated by using fuzzy numbers in a TOPSIS model developed for machine tool selection problems", *Journal of Material Processing Technology*, 209, pp. 310-317, (2009)
- [18] Yager, R. R.: "A procedure for ordering fuzzy subsets of the unit interval", *Information Sciences*, 24, 143-161, 1981
- [19] <http://www.toyota-forklifts.eu/en/Products/electric-counterbalanced-trucks/toyota-traigo-24/Pages/Default.aspx>
- [20] [http://www.cat-lift.com/\\_cat/index.cfm/north-america/english/products/lift-trucks/class-i-electric-counterbalanced/2500-4000-lb-capacity-3-wheel-pneumatic-tire](http://www.cat-lift.com/_cat/index.cfm/north-america/english/products/lift-trucks/class-i-electric-counterbalanced/2500-4000-lb-capacity-3-wheel-pneumatic-tire)
- [21] <http://www.hyster.com/north-america/en-us/products/3-wheel-electric-trucks/>
- [22] <http://nissanforklift.com/forklifts/TX-3Wheel-AC-ElectricRider.htm>
- [23] <http://www.yale.com/emea/en-gb/our-products/product-overview/3-wheel-electric-trucks/electric-fork-lift-truck-rear-wheel-drive-1250-1500kg/>
- [24] [http://www.jungheinrich-lift.com/\\_jh/index.cfm/products/forklifts-and-lift-trucks/electric-counterbalanced-forklifts/efg-110k-115-electric-3-wheel-counterbalanced-forklift](http://www.jungheinrich-lift.com/_jh/index.cfm/products/forklifts-and-lift-trucks/electric-counterbalanced-forklifts/efg-110k-115-electric-3-wheel-counterbalanced-forklift)

# Digging Resistance Model Shovel Manipulator of Hydraulic Excavator

Vesna Jovanović<sup>1\*</sup>, Dragoslav Janošević<sup>1</sup>, Jovan Pavlović<sup>1</sup>, Goran Patrović<sup>1</sup>  
<sup>1</sup>Faculty of Mechanical Engineering, University of Niš, Niš (Serbia)

The paper defines a mathematical model of resistance digging of hydraulic excavators with shovel manipulator. Mathematical model of resistance digging covered are: motion parameters of bucket in digging operation, the geometry of the slice of material, geometry of the bucket and the captured material characteristics. The developed mathematical model of resistance digging can be used for numerical dynamic simulation of excavator operation. As an example, are determined components of resistance digging for shovel bucket capacity of 4.4 and 6,5m<sup>3</sup> for model of crawler hydraulic excavator, weighing approximately 100000kg.

**Keywords:** Hydraulic excavators, resistance digging

## 1. INTRODUCTION

For optimal design and efficiency work rating of hydraulic excavator it is necessary detailed analysis of digging force in a whole working range.

For such analyses, previous studies were focused on the analytical determination of changes digging forces during digging operations. Whereby the developed mathematical models that define the digging resistance depending on the geometry of the tool-bucket, geometry and physical properties of materials steak-land and the operation time of digging. In this paper is developed a procedure for determining the components of digging force (resistance).

## 2. MATHEMATICAL MODEL

Mathematical model of resistance digging is developed based on a physical model of the excavator with manipulator shovel bucket (fig.1). The configuration of the kinematic chain of the excavator is composed on: the support and movement mechanism  $L_1$ , rotating platform  $L_2$  and a four-member planar manipulator with: boom  $L_3$ ,

stick  $L_4$ , bucket plates  $L_5$  and bucket jaw  $L_6$ . Members of the manipulator moved by drive mechanisms with hydrostatic actuators - hydraulic cylinder: boom  $c_3$ , stick  $c_4$  bucket  $c_5$  and jaw  $c_6$ .

Dynamic numerical simulation of the excavator is defined on the basis of general mathematical model of the excavator and model simulation conditions. Mathematical model of the excavator consists of a mathematical model of the kinematic chain and a mathematical model of the driving mechanisms of the excavator. Models of simulation conditions include parameters excavator working conditions and working technology models - models manipulative task of excavator. Mathematical model of excavator is considered in the absolute coordinate system  $OXYZ$  while members of the excavator kinematic chain are defined in the local coordinate system  $O_i x_i y_i z_i$ . In the simulation, is adopted in a general excavator manipulative task comprising the operations of: digging - horizontal loading materials (fig.2), capturing - filling buckets material, transfer of material in the unloading plane, and unloading of material back onto a new plane - digging a new position [1].

Excavator with loading manipulator, loading materials, with a reduced digging resistance,

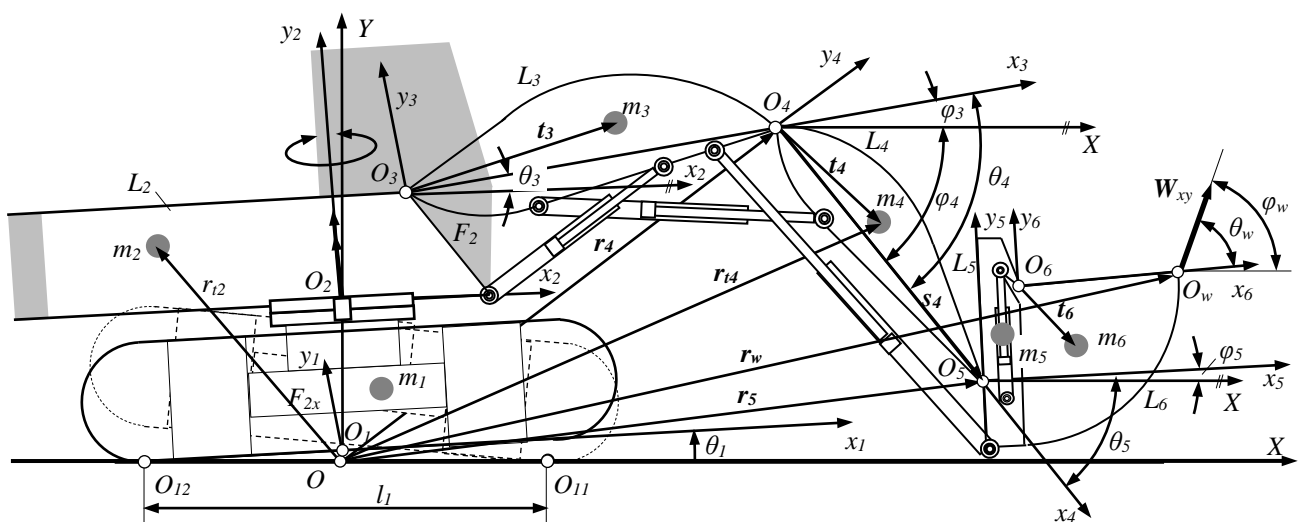


Figure 1: Mathematical model excavator with loading manipulator

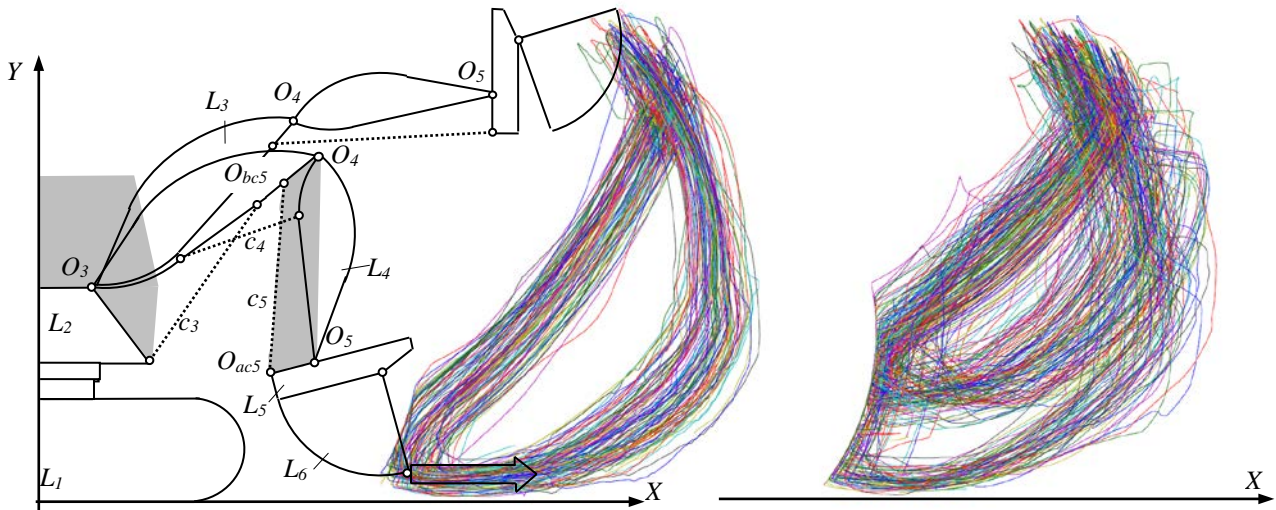


Figure 2: Trajectories bucket teeth during manipulative task of excavator with loading manipulator

is achieved with horizontal path of bucket teeth maintain constant optimum cutting angle bucket. Horizontal capturing enables the cranked quadrilateral driving mechanism buckets, facilitated operating, only by starting hydrocylinder of the boom  $c_3$  (fig.2), and stick  $c_4$  [2].

During the operations of digging and loading materials occurs the outer (technological) load of kinematic chain excavator in the form of vector force digging resistance  $W$  determined in the absolute coordinate system of the excavator by the equation:

$$W = W_x \mathbf{i} + W_y \mathbf{j} + W_z \mathbf{k} \quad (1)$$

where:  $W_x, W_y$  - digging resistance force components along the axes that are building the resultant:

$$W_{xy} = (W_x^2 + W_y^2)^{0.5} \quad (2)$$

oriented normal to the cutting edge of the bucket,  $W_z$  - lateral resistance digging collinear with the cutting edge of the bucket. The general model of the resistant digging force has been developed with the following assumptions: a) a components of digging resistance force normal to the to cutting edge of bucket are unevenly distributed along the cutting edges (fig. 3) with the resultant

$W_{xy}$  shifted with respect to the center of the cutting edges of bucket  $O_w$  for coordinate  $z_w$ , b) the direction of digging resistance force perpendicular to the cutting edge of the bucket is defined with angle of resistance digging  $\theta_w$  in the local coordinate system of the jaw bucket, c) the lateral components digging resistance forces  $W_{z1}$  and  $W_{z2}$  are different in size but opposite directions with resultant  $W_z = W_{z1} - W_{z2}$  acting in the direction of the cutting edge of the bucket.

The intensity of the components digging resistance force perpendicular to the the bucket cutting edge is determined depending on the geometry of the slice, the physical and mechanical characteristics of the captured materials and the method to control the movement bucket, by the equation [3][4]:

$$W_{xy} = k_k \cdot b_5 \cdot h_k \cdot \zeta_u \cdot \zeta_k \quad (3)$$

where:  $k_k$  - specific digging resistance of material,  $b_5$  - width slice of land,  $h$  - height slice of land,  $\zeta_k$  - specific resistance digging factor,  $\zeta_u$  - factor of method to control the movement bucket in digging operation.

Kinematics of digging is carried out by the horizontal capturing and arch filling bucket, in the plane digging  $OXY$  of the absolute coordinate system, wherein the slice

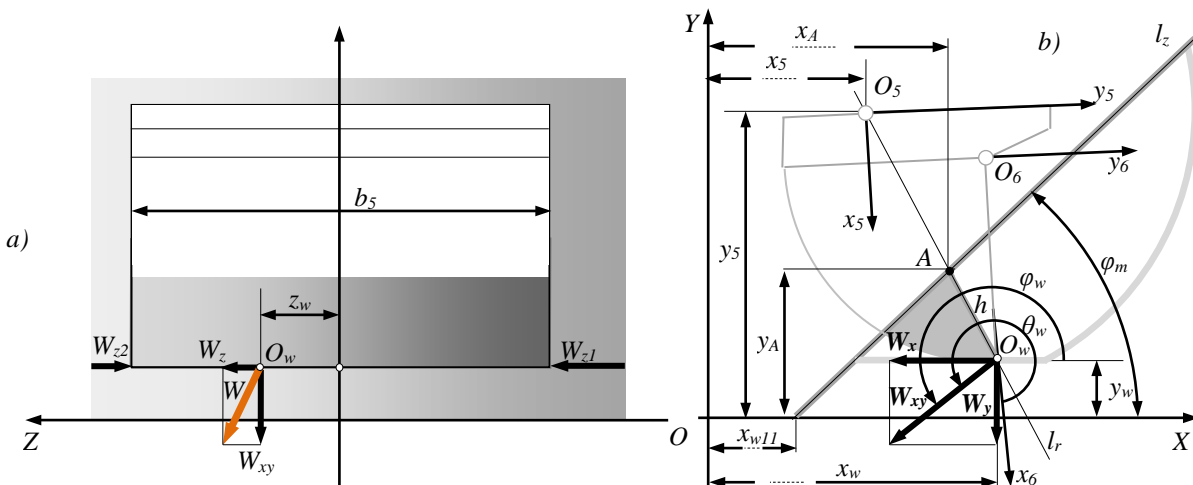


Figure 3: Models of resistance digging: a) unequal distribution of digging resistance along the cutting edge of the bucket, b) height slice

of captured material has a constant width, equal to the the width of the bucket and a variable height  $h$  along a cutting radius, determined by the equation (fig. 3):

$$h = \sqrt{(x_w - x_A)^2 + (y_w - y_A)^2} \quad (4)$$

where:  $x_w, y_w$  - coordinates of the center cutting edge of the bucket,  $x_A, y_A$  - coordinates of the point A which is in the intersection of the line  $l_r$  placed along the radius of the cutting lines and  $l_z$  placed along the slope of the excavation materials of the massif determined equations:

$$l_r: y = y_5 + \frac{y_w - y_5}{x_w - x_5}(x - x_5) \quad (5)$$

$$l_z: y = tg \varphi_m (x - x_{w11}) \quad (6)$$

Because occurrence inhomogeneity of the material excavation on digging trajectory there is a need to the intermittent movement of bucket whose influence on changing character of resistance digging, take into account the factor method of control  $\xi_u$  determined by the equation:

$$\xi_u = (1 + 3f_u) + f_u \sin\left(\frac{\pi t}{4 t_5}\right) \cdot \sin\left(n_u \pi \frac{t}{t_5}\right), \forall t \leq t_5 \quad (7)$$

where:  $f_u$  - coefficient change amplitude of resistance digging,  $n_u$  - coefficient change period of amplitude of resistance digging,  $t$  - current time digging operation,  $t_5$  - end time digging operation.

Changing the specific resistance digging, resulting from the difference in the physical characteristics of captured material in the operation start of the loading - when separating the material from massifs in the natural state, and at the end of the charging bucket - when includes the very loosely by the material, taking into account the factor the specific resistance digging  $\xi_k$  is determined equation:

$$\xi_k = \left[ 1 - \left( \frac{t}{t_5} \right)^2 \right]^{0.5} \quad \forall t \leq t_5 \quad (8)$$

In the simulation excavator, changing the direction of action the normal component of resistance digging  $W_{xy}$  is defined in the local coordinate system and in the

absolute coordinate system of closed bucket by changing the angle of resistance digging (fig.3):

$$\theta_w = \theta_{wp} + \frac{t}{t_{524}} (\theta_{wk} - \theta_{wp}) ;$$

$$\varphi_w = \theta_w + \sum_{i=3}^6 \theta_i \quad (9)$$

where:  $\theta_{wp}, \theta_{wk}$  - the start and end angles of the direction of action the components of the normal digging resistance, which correspond to the natural directions of actions digging resistance for digging technology of a loading manipulator excavator.

Component of the resistance digging force  $W_z$  collinear with the cutting edge of the bucket is determined, depending on the moment of resistance of rotation the caterpillar of the support and movement mechanism in relation to the substrate and action horizontal resistance components digging, by equation [3]:

$$W_z = \left( \mu_o \frac{mg \cdot l_1}{4} \frac{h}{h_{max}} + W_x \cdot z_w \right) \frac{1}{x_w} \quad (10)$$

where:  $\mu_o$  - coefficient of rotation the caterpillar of the support and movement mechanism  $m$  - total mass of excavator,  $l_1$  - length of reliance of the support and movement mechanism,  $h_{max}$  - maximum height the slice excavation material,  $z_w$  - coordinate positioning of resistance digging in relation to the center of the cutting edge of the bucket.

### 3. EXAMPLE

On the basis of the developed mathematical model, a detailed analysis of the components of resistance digging force which loading kinematic chain crawler excavator mass of about 100000 kg with loading manipulator. The analyzed two possible variants A and B separated kinematic chain excavator model (Table T1). Both variants of the kinematic chain excavator, for comparative analysis, simulated model are the same technology i.e. the same manipulative work task with the given external coordinates. During manipulative task is simulated:

Table 1: Material characteristics of the excavation and method of movement bucket

Characteristics	Parameters		Variants of excavator	
	Mark	Dimension	A	B
Excavator mass	$m$	kg	100000	90000
Bucket volume	$V$	$m^3$	6,5	4,4
Bucket width	$b_5$	mm	3150	2300
Category of excavation material			II	IV
Specific resistance digging	$k_k$	kN/m <sup>2</sup>	165	320
Material density		kg/m <sup>3</sup>	1650	2200
Coefficient change amplitude of resistance digging	$f_u$	-	0,03	0,08
Coefficient change period of amplitude of resistance digging	$n_u$	-	2	3
The initial angle of direction of resistance digging	$\theta_{wp}$	°	220	220
The end angle of direction of resistance digging	$\theta_{wk}$	°	270	270
Coefficient of rotation the caterpillar of the support and movement mechanism	$\mu_o$	-	0,6	0,6
Coordinate of positioning resistance digging	$z_w$	mm	1050	750

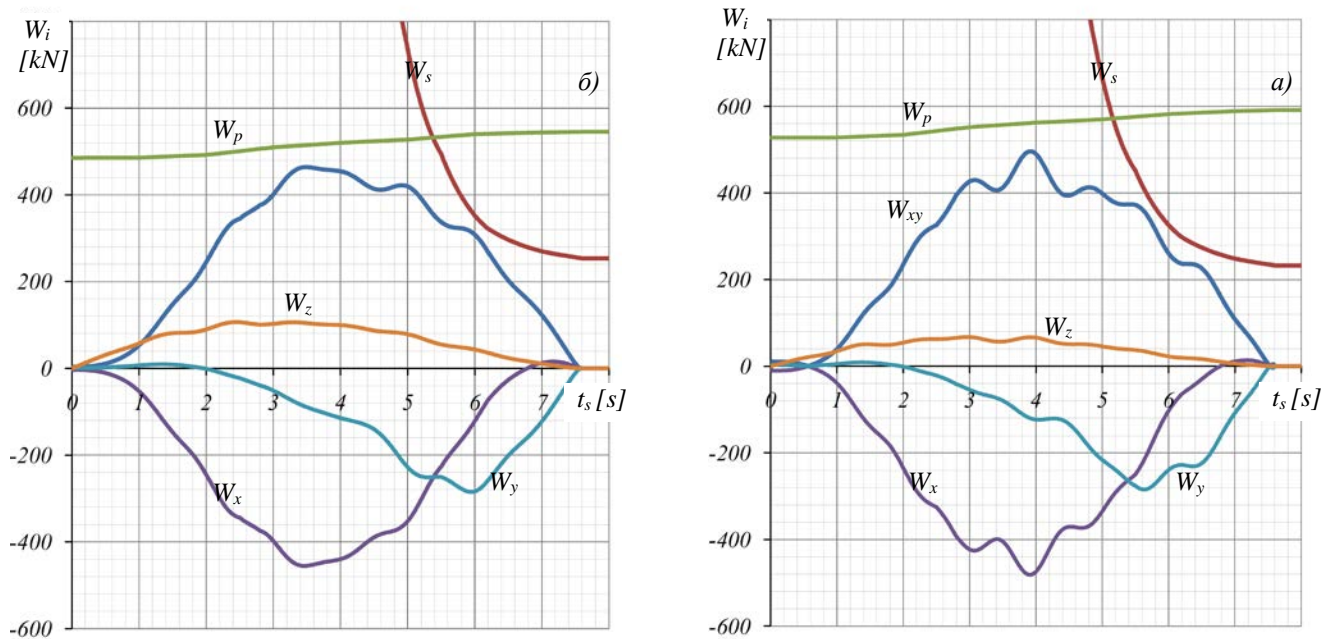


Figure 4: Components of resistance digging: a) variant A, b) variant B - normal  $W_x$ ,  $W_y$ ,  $W_{xy}$  and collinear  $W_z$  in relation to the cutting edge of the bucket and which allows the stability of the excavator  $W_s$ ,  $W_p$

a) stable operation of excavator - without moving the support and movement mechanism; b) trapezoidal cycloidal model character changes of the angular velocities of member's kinematic chain excavator with accelerated, slow-motion and constant phase.

For excavator models A and B the components of resistance digging force, normal  $W_{xy}$  (Figure 4, b) and  $W_z$  collinear with respect to the cutting edge of the bucket are determined for different characteristics of the material and methods to control the movement bucket in digging operation (Table T1). Since the model excavator A with a larger capacity bucket intended for the excavation of softer material category II, in determining the resistance digging are adopted less values of the amplitude coefficients and the period of the change resistance digging, assuming the loading of a softer homogeneous material occurs need for a smaller number of interruptions movement of bucket in loading material.

At excavator model B with a smaller capacity bucket are adopted higher values of the amplitude coefficients and the period of the change resistance digging assuming the loading of a harder material IV categories appears need for a greater number of interruptions movement of the of bucket due to inhomogeneous structure of the material.

Other characteristics of the material and geometry slice of materials are chosen and defined in such a way that the normal component of resistance digging the less than intensity boundary resistance digging force from a stability condition  $W_s$  (Figure 4, b) and the conditions non slipping  $W_p$  of excavator, thus fulfilling the requirement of a stable operation of excavator at the digging operation.

#### 4. CONCLUSION

Changes in component of resistance digging of the bucket loading manipulator of hydraulic excavators, obtained based on developed mathematical model,

shows that the largest intensity has the horizontal component, which occurs approximately half the duration of the operation digging. Vertical component of resistance digging force is bit smaller, with increased intensity in the end of the digging operation when there is a higher filling bucket with material. The minimum intensity has a lateral component digging resistance force acting in the direction of the cutting edge of the bucket.

#### ACKNOWLEDGEMENTS

Acknowledgment: This manuscript is a part of the project no. 035049 funded by the Ministry of Education and Science of the Republic of Serbia.

#### REFERENCES

- [1] D. Janošević, P. Milić, D. Marković, V. Nikolić, "Optimization of Kinematic Chain Parameters in Hydraulic Excavators", Journal of Institute IMK "14. oktobar" Krusevac, IMK-14 Research & Development, Vol.18, No.2, pp. EN 43-47, (2012)
- [2] D. Janošević, "Optimal Synthesis of Drive Mechanisms in Hydraulic Excavators", doctoral dissertation, Faculty of Mechanical Engineering, University of Niš, (1997)
- [3] D. Janošević, "Projektovanje mobilnih mašina", Univerzitet u Nišu Mašinski fakultet, Niš, (2006).
- [4] Д.П. Волков, В.Я. Крикун, П.Е. Тоголин, К.С. Гаевская, П.Н. Никулин: "Машины для земляных работ", Машиностроение, Москва, (1992)
- [5] F.Geu Flores, A. Kecskemethy, A. Pottker, "Workspace Analysis and Maximum Force Calculation of a Face-Shovel Excavator using Kinematical Transformers", 12th IFToMM World Congress, Besancon, June 18-21, (2007)
- [6] A. Dudczak: "Kryteria doboru parametrow mechanizmow napadowych osprzetu koparki hydraulicznej", Instytut mechanizacji budownictwa, Warszawa (1977)



# Analysis of the Influence of Manipulator Mechanisms Parameters of Mobile Machines on their Performance

Jovan Pavlović<sup>1\*</sup>, Dragoslav Janošević<sup>1</sup>, Vesna Jovanović<sup>1</sup>, Nikola Petrović<sup>1</sup>

<sup>1</sup>Faculty of Mechanical Engineering/Department for Material Handling Systems and Logistics, University of Niš, Niš (Serbia)

The paper present analysis of parameters of drive mechanisms and hydrostatic system of four-bar linkage manipulators of drive mechanisms in mobile machines with hydro-cylinders for actuators. General transformation and transfer functions of drive mechanisms are defined. Also is developed a mathematical model for determination of the duration of operations of manipulation task depending on: scope of the movement of manipulator member that performs an operation, the parameters of the drive mechanism and a pressure and flow of the hydrostatic drive system. As an example, results of the analysis of parameters influence on loader performance are given, for drive mechanism of the manipulator and of the hydrostatic system.

**Keywords: Loaders, Drive mechanisms, Manipulators**

## 1. INTRODUCTION

Mobile machine manipulators represent a transfer part of a kinematic chain that connects a supportive member with an executive member - a machine tool. The basic function of the manipulator is to enable the active operation of the tool on the subject of work in a particular working area of the machine. Depending on the shape of the work area, the kinematic chains of the machine manipulators have a certain number of members that build the kinematic pairs of fifth class - rotary or sliding joints with one degree of freedom (Fig.1). The drive mechanisms of mobile machine manipulators for the actuators have hydro-cylinders that are powered by hydrostatic systems with hydropumpes of constant and variable specific flow [1].

The paper analyzes the influence of the parameters of the drive mechanisms of the manipulator and the parameters of the hydrostatic system on the duration of the manipulation task of mobile machines.



Figure 1: Manipulators of mobile machines

## 2. TIME OPERATIONS

The duration of the manipulation task is one of the basic parameters of the performance of mobile machines. This is also indicated by the equation that defines the technical performance of the machine:

$$U_t = \frac{3600}{t_c} V \quad (1)$$

where:  $U_t$  - performance of mobile machine [ $m^3/h$ ],  $V$  - volumen (capacity) of tool [ $m^3$ ],  $t_c$  - duration of time operation of manipulative task [ $s$ ].

According to the given equation, for the same tool capacity, the machine will achieve the maximum performance for the minimum cycle time.

In order to set the observed time criterion as a criterion for evaluating the efficiency of the machine drive mechanisms, the analysis of the influence of the parameters of the manipulator driving mechanisms on the duration of the machine's manipulation task was first performed.

The duration of the machine's manipulation task equals the sum of the duration of each operation:

$$t_c = \sum_{j=1}^{n_o} t_j \quad (2)$$

where:  $n_o$  - number of manipulation task operations,  $t_j$  - duration of time operation.

Duration of time operation is determined by equation [2]:

$$t_j = \int_{\theta_{ij1}}^{\theta_{ij4}} \frac{d\theta_i}{\dot{\theta}_{ij}} = \int_{\theta_{ij1}}^{\theta_{ij4}} \frac{d\theta_i}{Q i_n^Q i_{ci}^{\dot{\theta}}} \quad (3)$$

where:  $\theta_{ij1}, \theta_{ij4}$  - The initial and final generalized (inner) coordinates of the member  $i$  of the kinematic chain of the machine which is the operator of the operation  $j$ ,  $\dot{\theta}_{ij}$  - angular velocity of the member of the kinematic chain of the machine

during the operation  $j$ ,  $i_{ii}^Q$  - the transformation function of the flow of the member of drive mechanism which is the carrier of the operation  $j$ ,  $i_{ci}^{\dot{\theta}}$  - the kinematic transformation function of the member of drive mechanism which is the carrier of the operation  $j$ ,  $Q$  - the flow of actuators of the drive mechanism during the operation.

The transformation function of the flow and the kinematic transformation function of the drive mechanism are known for a particular position of the executive member of the mechanism that is performing the operation. However, in order to determine, according to equation (3), the operation time of the manipulation task of the machine, it is necessary to define the change in the flow in the actuator (hydro-cylinder) of the mechanism during the operation.

The flow and pressure of the actuator of the drive mechanism are the parameters of the power of the hydrostatic system of the machine. Hydrostatic drive systems of mobile machines have been developed and further they are developing, in the direction of optimally utilizing the energy of the drive engine under different operating conditions of the machine, with the possibility of simultaneously unfolding at least two operations of the manipulation task. These requirements are achieved by hydropumps of the hydrostatic system with regulation of power parameters. Regulation of hydropumps is volumetric. The signal of regulation is a change in the pressure in the actuators or a change in the speed of the drive motor, resulting from a change in movement resistance during the operation [3] [4].

### 3. ANALYSIS

An analysis of the influence of the parameters of the manipulator driving mechanisms during the duration of the manipulation task is given for the drive system of the excavator with the following parameters and characteristics (fig. 2):

- the hydrostatic power  $N_h$  of the drive system of the excavator is known,
- the excavator drive system has a double piston-axial hydropump of a variable specific flow with collective regulation according to the criterion of *constant hydraulic power* ( $N_h = \text{const}$ ) (Fig. 2b).

For the adopted regulation of the hydrostatic power parameters, the dependence of the flow rate on the hydropump pressure is determined by the equation (Fig. 2):

$$Q = \begin{cases} Q_{min} = \frac{N_h}{p_k} & \forall p = p_i \geq p_k \\ Q = \frac{N_h}{p_i} & \forall p_p \leq p = p_i \leq p_k \\ Q_{max} = \frac{N_h}{p_p} & \forall 0 \leq p = p_i \leq p_p \end{cases} \quad (4)$$

Where:  $p_p, p_k$  - the pressure of the start and end of hydropump regulation,  $p_i, p_j$  - pressure in the actuators ( $i, j$ ) of the drive mechanisms with which the operation of the manipulation task is performed simultaneously.

By changing the equation (4) into equation (3), the duration of the operation, among other things, depends on the pressures in the actuators of the drive mechanisms. In this way, the digging resistance that occurs during the operation, through the drive mechanisms, affect on the flow regulation, respectively the duration of the operation.

As an example of an analysis of the influence of the parameters of the drive mechanisms on the duration of the manipulation task of the excavator it is given for the operation of the material transport at arm lifting of the shovel excavator manipulator.

The time of arm lifting  $t_3$ , at transferring of the affected material from a certain loading position  $\theta_{3p}$  to a certain unloading position  $\theta_{3k}$ , has the value (Fig. 2) [5] according to the equation (3):

$$t_3 = \int_{\theta_{3p}}^{\theta_{3k}} \frac{d\theta_3}{\dot{\theta}_{31}} = \int_{\theta_{3p}}^{\theta_{3k}} \frac{d\theta_3}{Q \cdot i_{t_{31}}^Q \cdot i_{c_3}^{\dot{\theta}}} \quad (5)$$

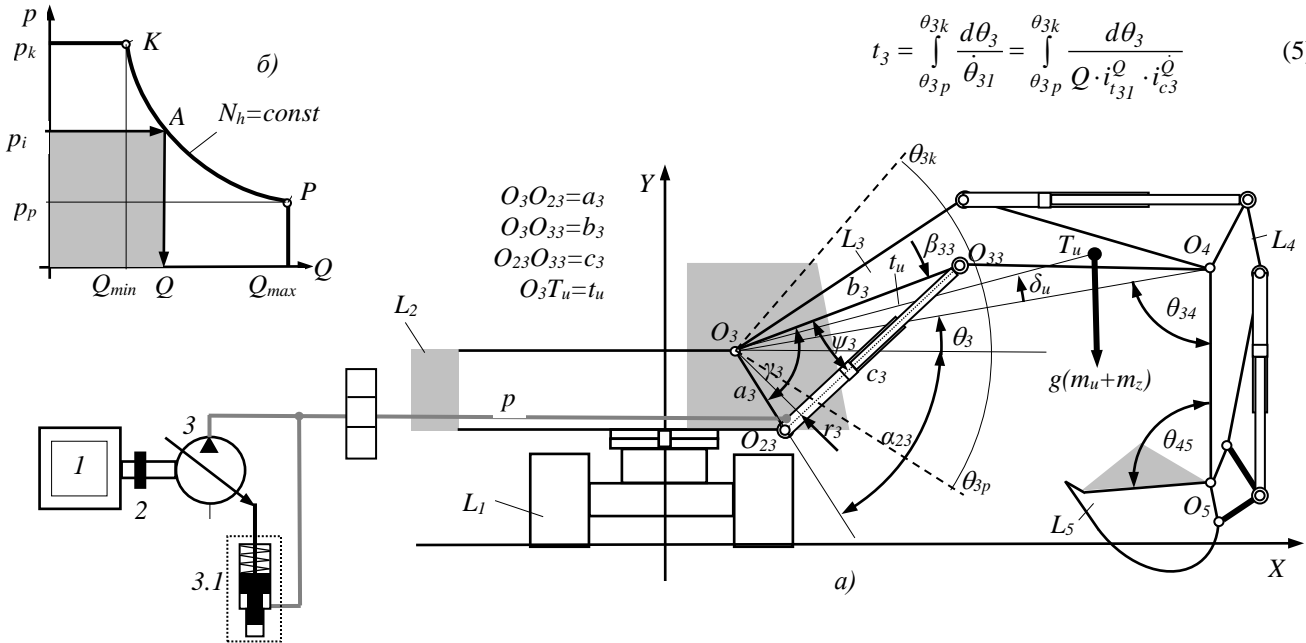


Figure 2: Hydraulic excavators: a) drive system and kinematic chain of manipulator: 1 - diesel engine, 2 - elastic coupling, 3-hydropump,  $L_1$  - motion mechanism,  $L_2$ -platform,  $L_3$ -arm,  $L_4$  - stick ,  $L_5$  - bucket , a) diagram of regulation of hydropump [5]

For the excavator drive system with hydropump of the variable specific flow with collective regulation according to the *constant hydraulic power criterion*, the time of arm lifting  $t_3$  will be minimal if the condition (fig. 2b) is fulfilled:

$$t_3 \rightarrow \min \quad \forall \quad Q_{max} \Rightarrow p \leq p_p \quad (6)$$

The dependence of the pressure  $p$  in hydro-cylinder of arm on parameters of arm drive mechanism can be determined, for the most frequent relative position of the members of the kinematic chain of the manipulator, in the transfer of loaded material, determined by the angles  $\theta_{34}$  and  $\theta_{45}$ , from the equilibrium conditions for the joint  $O_3$  of manipulator expressed by equation in terms of equality [6]:

$$M_{o3g} = M_{p31} \quad (7)$$

respectively:

$$g(m_u + m_z) \cdot t_u \cdot \cos(\theta_3 + \delta_u) = p \cdot i_{i31}^p \cdot i_{c3}^M \quad (8)$$

where:  $M_{o3g}$ ,  $M_{p31}$  - the moment of loading and the drive moment of arm mechanism,  $m_u, m_z$  - the total mass of the members of the manipulator and the mass of the affected material,  $t_u, \delta_u$  - the coordinates of the center of the mass of the manipulator in the position of material transfer determined by the angles  $\theta_{34}$  and  $\theta_{45}$ ,  $p$  - pressure in the hydro-cylinder of the arm,  $i_{i31}^p$  - the transformation function of the pressure of arm drive mechanism,  $i_{c3}^M$  - the transformation function of the moment of the arm drive mechanism [2].

For the position of the arm  $\theta_3 = -\delta_u$ , the time  $t_3$  will be minimal if the condition is satisfied:

$$g(m_m + m_z) \cdot t_u = p_p \cdot i_{i31}^p \cdot i_{c3max}^M \quad (9)$$

where:  $p_p$  - pressure of start of the hydropump regulation,  $i_{c3max}^M = a_3$  - maximum value of the transfer function of the moment of the arm drive mechanism.

By replacing equation (8) with equation (9), equality is obtained:

$$p = p_p \frac{i_{c3max}^M \cdot \cos(\theta_3 + \delta_u)}{i_{c3}^M} = p_p \frac{a_3}{b_3} \cdot \frac{\cos(\theta_3 + \delta_u)}{\sin \gamma_3} \quad (10)$$

Which according to relations (Fig. 2a):

$$\frac{a_3}{\sin \psi_3} = \frac{c_3}{\sin \gamma_3} \quad (11)$$

$$c_3 = \sqrt{a_3^2 + b_3^2 - 2a_3b_3 \cos \gamma_3}$$

Can be expressed depending on the parameters of the arm drive mechanism:

$$p = p_p \frac{\cos(\theta_3 + \delta_u) \sqrt{1 + k_3^2 - 2k_3 \cos \gamma_3}}{\sin \gamma_3} \quad (12)$$

where:  $k_3 = a_3^2 / b_3^2$  - the ratio of the connection lengths of the arm drive mechanism to which the coordinates of the joints of the hydraulic cylinder on the platform and on the arm are determined,  $\gamma_3 = \theta_3 + \beta_{33} - \alpha_{32}$  - the angle between the

connecting lengths of the hydro-cylinder.

According to equation (12), the time  $t_3$  of the transfer operation of the material is going to be minimal, if the condition is fulfilled:

$$\frac{p}{p_p} = \frac{(\cos \theta_3 + \delta_u) \sqrt{1 + k_3^2 - 2k_3 \cos \gamma_3}}{\sin \gamma_3} \leq 1 \quad (13)$$

when the hydropump, according to equation (4), gives a maximum flow  $Q_{max}$ .

The pressure  $p$  in the hydro-cylinder of arm depends on the ratio of the torque load  $M_{o3g}$  and the drive moment of  $M_{p31}$  expressed in function from the angle of the arm position  $\theta_3$ .

#### 4. EXAMPLE

A numerical analysis of the influence of the parameters of the manipulator drive mechanisms and the parameters of the hydrostatic system during the duration of the manipulation task is given for a hydraulic excavator, weighting 17000 kg, equipped with a shovel bucket, volmen of 0,6 m<sup>3</sup>.

The operation of the lifting of the manipulator with a full bucket was considered, from the starting angle  $\theta_{3p} = -10^\circ$  to the final angle  $\theta_{3p} = 30^\circ$  of the arm lifting. The manipulator was lifted by pulling out two hydro-cylinders of arm, a piston/piston rod diameter of 115/80 mm, powered by a piston-axial hydropump of a variable specific flow with collective regulation of constant hydraulic power ( $N_h = const$ ). The pressure and flow rate of the hydropump at the start of the regulation is:  $p_p = 12 \text{ MPa}$ ,  $Q = 120 \text{ l/min}$ .

At the lifting operation, the drive moment of the  $M_{o3g}$  of drive mechanism was determined based on the measured values of the condition of the excavator's operation in exploitation conditions [2]. The moment intensity has an extremely variable character (Fig. 3).

Two variants I and II of arm drive mechanisms are observed with the same sizes of hydro-cylinders and various transmission functions (Fig. 4a) apropos different coordinates of joints in which hydrocylinders are connected to members of the kinematics pair of arm mechanism.

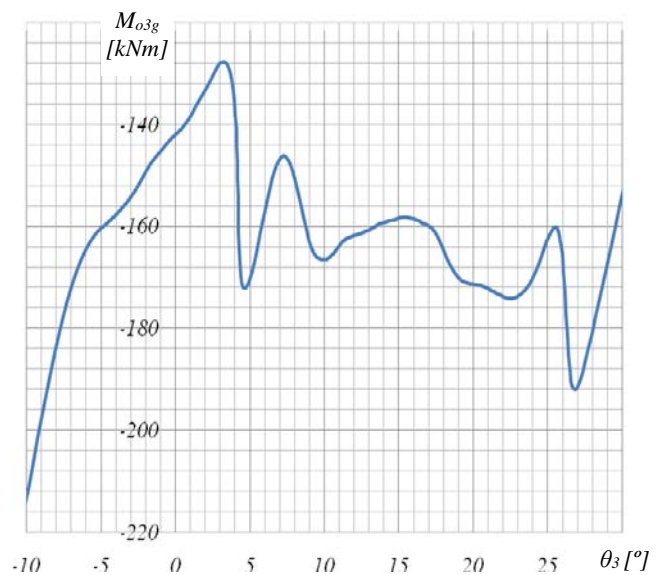


Figure 3: Change of drive moment of the drive mechanism of the hydraulic excavator's arm

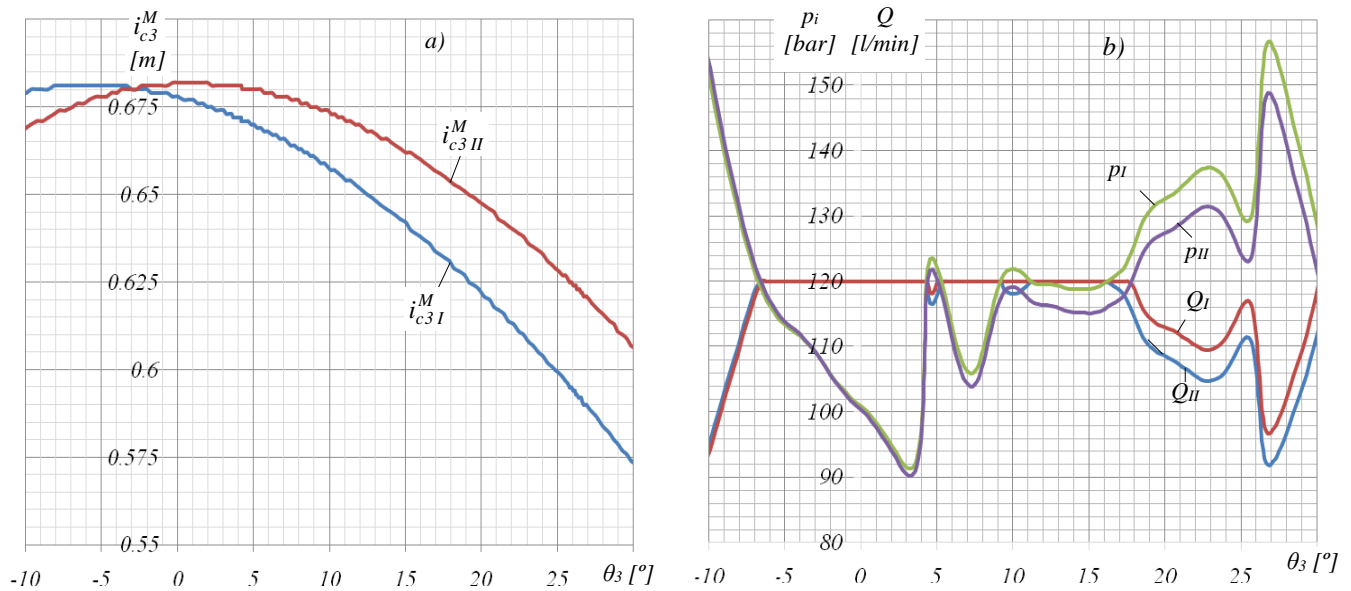


Figure 4: Parameters of arm drive mechanism: a) transformation function, b) pressure and flow in the hydraulic cylinders of the drive mechanism depending on the change in the angle of the lifting angle

The obtained results show that the pressure and the flow of the hydrocylinders of the mechanism are different for the same change in the drive moment for variants I and II of the arm drive mechanism (Figure 4b). The differential pressure, apropos flow of the hydrocylinder occurs due to the different transmission functions of the selected variant solutions I and II of the arm drive mechanism.

The duration time (fig. 5) of the lifting operation of the excavator manipulator for the same range of arm movements is different for the variant solutions I and II of drive mechanisms due to the difference in the transmission functions of the mechanisms.

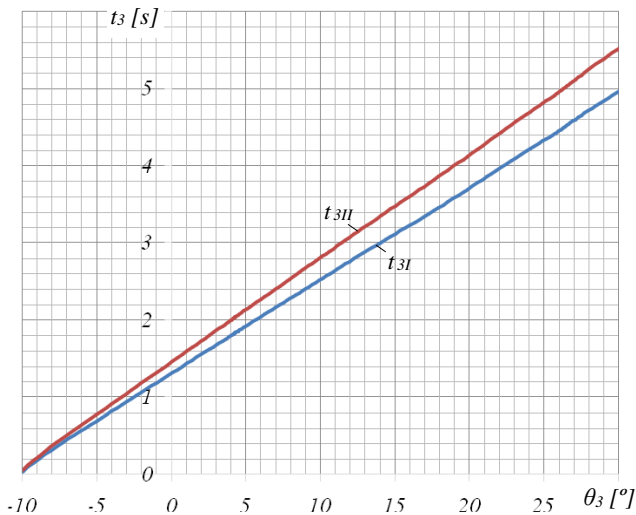


Figure 5: Time change of arm lifting

## 5. CONCLUSION

Based on the performed analysis and the presented results, it can be concluded that during the duration of the operations of manipulation tasks, apropos performance of mobile machines, the transmission functions of the drive mechanisms of the manipulator and

the character of the regulation of the hydrostatic parameters of the hydropump powered by the actuators of the mechanisms is important.

The defined duration of mobile machine operations can be used as a criterion for the optimal synthesis of drive mechanisms of machine manipulators.

## ACKNOWLEDGEMENTS

This paper is result of technological project No. TR35049, supported by Ministry of Education, Science and Technological Development of the Republic of Serbia

## REFERENCES

- [1] D. Janošević, "Projektovanje mobilnih mašina," Faculty of Mechanical Engineering University of Niš, (2006)
- [2] D. Janošević, Optimalna sinteza pogonskih mehanizama hidrauličkih bagera, Ph. D. thesis, Faculty of Mechanical Engineering University of Niš, (1997)
- [3] Mobile 2000, International Mobile Hydraulics Conference, Ulm, Brueninghaus Hydromatik GmbH, Elchingen, (2000)
- [4] Mobile 2003, International Mobile Hydraulics Conference, Ulm, Bosch Rexroth AG, Mobile hydraulics, Elchingen, (2003)
- [5] D. Janošević, V., Jovanović, Sinteza pogonskih mehanizama hidrauličkih bagera, Monographia, Faculty of Mechanical Engineering University of Niš, (2015)
- [6] В. А. Башкиров, Выбор оптимальных параметров стрелоподъемного механизма с гидропроводом, СДМ, Брой 4, Москва, (1982)

# Research and Calculation of Rational Modes and Parameters of an Ultrasonic Cavitator

Iryna Bernyk<sup>1\*</sup>, Oleksandr Luhovski<sup>1</sup>

<sup>1</sup> National Technical University of Ukraine "Igor Sikorsky Kyiv Polytechnic Institute"

*In the executed researches it is accepted that the highest efficiency of transformation of electric energy into energy of acoustic vibrations and radiation in the work environment is subject to the approval of the resistance of the medium and the use of force apparatus. Implementation of the proposed approach is implemented reflect the changes in the rheological properties of the technological environment, by choosing the physical model and its mathematical description. Presented in the mathematical form of the stages of the cavitation process. The key parameters of cavitation bubbles in an acoustic field. The estimation of the cavitation process on the coefficient of the cavitation index and absorption coefficient in cavitating medium. The absorption coefficient is a measure of the efficiency of cavitation effect, the connection of this parameter with power density of shock waves.*

**Keywords:** disperse medium, ultrasound, cavitation, rheology, intensity, impedance, absorption coefficient.

## 1. FORMULATION THE PROBLEM

Ultrasonic cavitation technology allows to intensify the technological processes, to increase the utilization of raw materials, to modify the original properties of the material, to create new substances and the environment to ensure environmental cleanliness and safety of production [1–11]. The process of turning electric energy into acoustic waves and its radiation in the working environment shall be carried out with the greatest efficiency, subject to the approval of the resistance of the medium and the use of force apparatus. Therefore, research aimed at improving the efficiency of cavitation technologies for the realization of different kinds of technological processes is the task urgent.

## 2. FORMULATION OF THE TASK

The aim of this work is to study the process of cavitation treatment of technological environments, the setting of parameters of influence and assess its effectiveness.

## 3. STATEMENT OF THE MATERIAL

Implementation of the proposed approach requires determining the change in rheological properties of the technological environment, which is the viscosity, plasticity and elasticity [2]. The procedure for accounting of these properties lies in the choice of the physical model with further mathematical description and assessment of the impact in the calculation of dependencies. From a physical point of view, the choice of model predefined the main characteristics of the deformation and stresses that occur during the technological influence and form the so-called stress-strain state.

The main properties of the processed media are the basis of any material. There are three idealized models of materials: the ideal elastic body (Hooke); ideally viscous liquid (Newtonian); a perfectly plastic body (Saint-Venant) [3]. In real-world environments, which have a complex structure, can occur for all three rheological properties. To build the model they are interconnected in series or in parallel (tab. 1). Such models belong to the basic elastic-plastic body Saint-Venant, the viscoelastic body of the Kelvin-Voigt and Maxwell visco-plastic body Shvedov-Bingham and others, the use of which is determined by other properties.

The next step envisaged in the mathematical form of the stages of the process of cavitation: the formation of bubbles, their oscillation, the development and collapse. This process is accompanied by complex mass and heat transfer in the formed cavitation region.

The key parameter in the evolution of the gas and air bubbles in the acoustic field is the energy, the components of which are the pressure, time and speed of flow of the process of cavitation [5, 6]. Under the action of ultrasonic harmonic oscillation on environments, the amplitude of the sound pressure is determined in accordance with dependencies:

$$P_m = \rho_k c_k \omega A, \quad (1)$$

where:  $\rho_k$  and  $c_k$  – the density and speed of sound in cavitating medium;  $\omega$  – the circular frequency of the sound wave;  $k = \frac{\omega}{c}$  – wave number;  $A$  – the vibration amplitude of the radiator;  $\rho_k c_k$  – the impedance of the medium, which determines the speed of oscillations for a given acoustic pressure.

\*Corresponding author: Prospect Peremogu, 37, Kyiv, Ukraine, iryna\_bernyk@i.ua

The propagation of ultrasonic waves associated with the transfer of energy. The energy density of sound waves, which falls per unit volume of the medium, can be expressed as:

$$E_s = p v^2 / 2 = 2\pi^2 p f^2 A^2 \quad (2)$$

The energy of ultrasonic waves that pass through unit area per unit time, it is customary to characterize the intensity of ultrasonic vibrations. When the plane wave is perpendicular to the surface, ultrasound intensity is associated with the amplitude of the sound pressure dependence:

$$I = 2\pi^2 p c f^2 A^2 = P_M^2 / (2 p c) \quad (3)$$

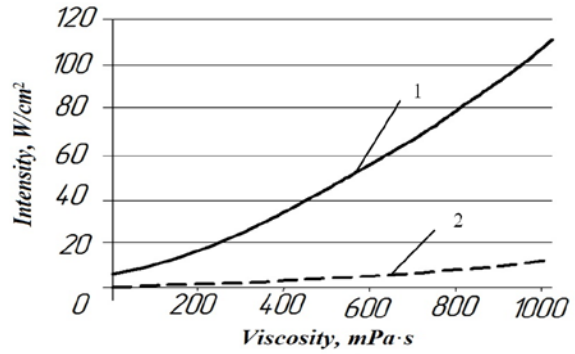


Figure 1: The change in the intensity of the cavitation processing of disperse media, depending on their viscosity: 1 – maximum intensity, 2 – min intensity

Table 1: Rheological models of simple and complex dispersed technological environments

In practice, an estimation of the cavitation process


using the ratio of the index of cavitation K, which equals the time average volumetric concentration of bubbles:

$$K = \frac{\sum_i V_i}{V_p + \sum_i V_i} \quad (4)$$

The change in the intensity of the viscosity (Figure 1) proves the necessity of taking into account dissipation in the determination of the parameters of the cavitation process.

where:  $V_p$  – the volume of fluid without bubbles,  $V_i$  – the average volume of cavitation bubble,  $i = 1, N$ ,  $N$  – the number of bubbles.

Then the wave resistance of cavitation medium can be represented as:

$$\rho_k c_k = \rho_0 c_0 \left[ \frac{1}{1 + \frac{K\beta_n}{\beta_0}} \right]^{1/2}, \quad (5)$$

where:  $\rho_0 c_0$  – the wave resistance of the medium;  $\frac{\beta_n}{\beta_0}$  – the ratio of compressibility of gas-vapor mixture in the bubbles to the compressibility of the fluid.

The dependence of the wave resistance of the medium from the cavitation index (Figure 2) shows that when the cavitation index of only 0.2% impedance and hence the amplitude of the current bubble sound pressure is reduced almost five times.

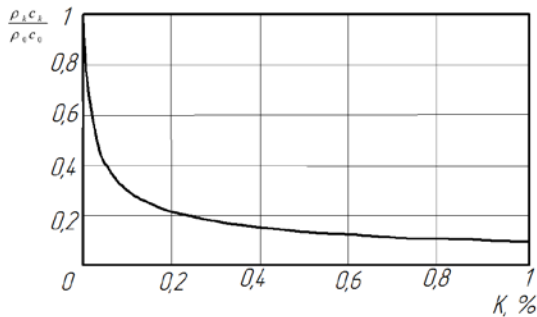


Figure 2: The dependence of the impedance changes of the medium from the cavitation index.

The bubbles, having a high compressibility, assume the external force in the sound wave, the same reducing the bulk modulus of elasticity of the medium of the  $E_c$  and the speed of sound:

$$c_k = \sqrt{\frac{E_c}{\rho_k}}. \quad (6)$$

An important parameter in the evaluation of process efficiency is the ratio of the velocities at the initial speed the process of cavitation  $c_c$ , which varies from the origin of cavitation bubbles, their collapse  $c_k$ :

$$k_c = c_c / c_k \quad (7)$$

The next process parameter is the absorption coefficient in cavitating medium  $K_\bullet$ . This parameter depends on the complex amplitude of acoustic pressure in the cavitation medium and the complex amplitude of the volumetric content of cavitation bubbles.

$$K_\bullet = -\frac{\omega}{c_0} \ln \frac{\rho_0 c_0 \bar{V}_1}{\bar{P}_1}, \quad (8)$$

where:  $\rho_0$  – the equilibrium density of the medium,  $\text{kg/m}^3$ ;  $p$  – the instantaneous pressure,  $\text{PA}$ ;  $c_0$  – the speed of sound in the liquid phase,  $\text{m/s}$ ,  $\bar{V}$  – instantaneous volume content of bubbles. Analysis of the dependence (8) shows that the absorption rate corresponds to the maximum efficiency of the cavitation process. In Fig. 3 shows the dependence of the absorption coefficient in cavitating liquids on the intensity effects for different viscosity ratios.

The absorption coefficient can be a measure of the effectiveness of the cavitation effect. Evidence of this conclusion to serve the relationship of the absorption coefficient with the specific power of the shock waves on the basis of consideration of local area processing medium volume  $\Delta S \Delta x$ . So, using the law of conservation of energy, we find that the power density of the shock waves to be determined according to the expression:

$$P_{num} = \frac{\Delta S l}{\Delta x \Delta S} = \frac{\Delta S (I - I e^{-k \Delta x})}{\Delta x \Delta S} = \quad (9)$$

$$\frac{(I - I e^{-k \Delta x})}{\Delta x} = k \frac{I (1 - e^{-k \Delta x})}{k \Delta x} \approx k I,$$

where:  $\Delta I$  – the change in the intensity of this wave as a result of absorption,  $\text{W/m}^2$ .

The expression for the work of the cavitator in contact area has the form [6]:

$$A_k = \pi m_c A_0^2 \omega^2 \mu \quad (10)$$

where:  $m_c$  – mass technological environment;  $A_0$  – the amplitude of the contact zone;  $\mu$  – wave coefficient, which takes into account the influence of the environment on the movement of the cavitator.

Average power cavitator  $P_{cp}$ :

$$P_{cp} = 0,5 m_c A_0^2 \omega^3 \mu \quad (11)$$

Expressions (10) and (11) are the values of the unknown parameters of the work and power of the cavitator, which are implemented in the contact zone of the cavitator and technological environment. The difference of the dependence (11) from the existing ones lies in the fact that in the known dependence [4, 8, 9] used the concept of added mass, which is supposedly attached to the surface of the cavitator. In fact, the mass of the environment is variable [6] and depends on acoustic parameters in (11) takes into account the wave factor  $\mu$ . Under the conditions of pulsed energy transfer cavitator to the notion of vibration amplitude loses its definition, because the regime is not harmonic, but nonlinear.

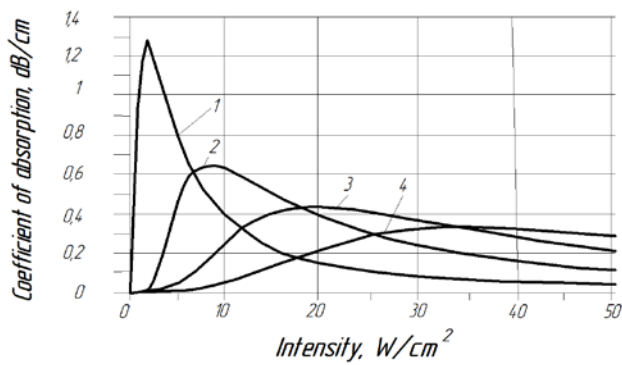


Figure 3: The dependence of the absorption coefficient in cavitating liquids on the intensity effects for different viscosity ratios: 1 - 1 MPa·s; 2 - 200 MPa·s; 3 - 400 MPa·s; 4 - 600 MPa·s

With this kind of movement is determined by the movement in the relevant time periods:  $t_{II} = t_1 + t_2$  where  $t_1$  – part of the period in a single move  $A_1$ , and  $t_2$  – in  $A_2$ . Denoting  $\alpha = t_1 / t_2$  и  $\omega_{cp} = 2\pi / t_{II}$  – the average frequency of;  $F_1, F_2$  – the amplitude of forces in the respective periods of oscillation of the contact zone.

Under these conditions, the expression of specific energy, per unit volume of the cavitation medium has the form:

$$\bar{E} = \frac{\Delta E}{V} = \frac{F \Delta x t_1}{\rho S \Delta x t_1} = \frac{F t_1 \omega_{cp}}{2\pi \rho S \alpha} \quad (12)$$

In the formula (12) contains all the components of parameters of the dynamic action of the cavitation device and the characteristics of the technological environment. Given formula (1 – 12) are initial information for development of algorithm of calculation of the cavitation device, which implements a harmonious and non-linear law of actions on the technological environment. And the absorption coefficient is a measure of the efficiency of ultrasonic cavitation, because of (9) follows: the specific energy of shock waves generated per unit time, is equal to the product of the absorption coefficient and the intensity of the primary ultrasound waves. Therefore, the absorption coefficient defines the ratio of useful energy created in the form of shock waves are necessary for the realization of cavitation process energy.

#### 4. CONCLUSIONS

1. An accurate description of cavitation processing technology of dispersed media depends on the choice of the model. The key parameter in the evolution of bubbles in an acoustic field is the energy, the components of which are the pressure coefficient of energy absorption, the time and speed of flow of the process.

2. We found that the characteristics of manufacturing environments, which can serve to define a rational model of technological process are: the load on the emitter, rheological properties and conditions influence the emitter.

3. The absorption coefficient is a measure of the efficiency of ultrasonic cavitation, i.e., determines the ratio of useful energy created in the form of shock waves are necessary for the realization of cavitation process energy.

#### REFERENCES

- [1] R. J. Wood, J. Lee, M. J. Bussemake, A parametric review of sonochemistry: Control and augmentation of sonochemical activity in aqueous solutions, *Ultrasonics Sonochemistry*, 38 (2017), 351-370.
- [2] Kenneth S. Suslick, *Sonoluminescence and Sonochemistry*, Encyclopedia of Physical Science and Technology, 3rd Ed., R. A. Meyers (ed.); Academic Press, Inc.: San Diego, 2001, 22.
- [3] Reiner M. Rheology / per. from English. [Text] / M. Rayner. - M.: Nauka, 1965. - 224 p.
- [4] Stepnowski S. V. a Generalized rheological model cavitating condensed matter / Stepnowski S. V. // *Applied mechanics and technical physics*. - 2001. - T. 42. - №3. - P. 116-129.
- [5] Luhovskyi O. F. The physical model of ultrasonic cavitation exception of pectin from recycled plant material / Luhovskyi O. F., I. N. Beryk // *Bulletin of national technical University of Ukraine "Kyiv Polytechnic Institute"*, series "Chemical engineering, ecology and resource saving". - 2010. - №1 (5) - P. 25-30.
- [6] Beryk, I. N. Establishment of basic parameters of technological environment influence on the working process of ultrasonic cavitation treatment / I. N. Beryk, O. F. Luhovskyi // *Vibrations in technics and technologies*. - 2014. - № 3 (75). - P. 121-126.
- [7] Beryk I. Research parameters of ultrasound processing equipment dispersed in technological environment / I. Beryk // *MOTROL. Commission of Motorization and Energetics in Agriculture*. - 2016. - Vol. 18. - № 3. - P. 3 - 13.
- [8] Margulis M. A., Dynamics of bubbles ensemble in cavitating liquid [Text] / M. A. Margulis, I. M. Margulis in *Journal of physical chemistry*. - 2007. - T. 81. - No. 12. - P. 2290-2295.
- [9] Shestakov S. Multibubble acoustic cavitation: a mathematical model and physical similarity [Text] / S. D. Shestakov // *Electronic journal "Technical acoustics"*. - 2010. - №14. - 16 c.
- [10] Kenneth S. Suslick, *The Chemical Consequences of Cavitation, SONOLUMINESCENCE*. [http://icacommission.org-Proceedings/ICA2001Rome/2\\_04.pdf](http://icacommission.org-Proceedings/ICA2001Rome/2_04.pdf). 12.04.2017.
- [11] Aganin A. A. Dynamics of a gas bubble excited by pulses of compression and rarefaction in the liquid / A. A. Aganin, M. A. Ilgamov, *DOKL.* - 2002. - T. 382. - No. 2. - P. 176-180.



**SESSION B**

**PRODUCTION TECHNOLOGIES**



# Determination of Expulsion Costs in Resistance Spot Welding

Miomir Vukićević<sup>1\*</sup>, Mišo Bjelić<sup>2</sup>, Marina Pljakić<sup>1</sup>, Milan Tešević<sup>2</sup>

<sup>1</sup>Faculty of Mechanical and Civil Engineering, University of Kragujevac, Kraljevo (Serbia)

*This article deals with calculation of the expulsion costs during resistance spot welding. It identifies significance of this phenomenon in the overall technology and also indicates the possible directions for action to tackle or eliminate this phenomenon.*

**Keywords: Welding, Resistance spot welding, Expulsion, Costs**

## 1. INTRODUCTION

Transformation of the electric energy into the heat i.e. the heating of the conductor during the time is described by Dzul's law:

$$Q = \int_{t_1}^{t_2} \rho \cdot j^2 \cdot \ell \cdot S \cdot dt \quad (1)$$

Q – generated heat, W

$\rho$  – specific electrical resistance,  $\rho = R \cdot S / \ell$ ,  $\Omega \cdot m$

j – current density,  $j = I / S$ , A/m<sup>2</sup>

$\ell$  – length of conductor, m

S – area of cross-section, m<sup>2</sup>

V – volume, m<sup>3</sup>,  $V = \ell \cdot S$

Resistance spot welding is performed by placing welded sheets in an overlapping position between the electrodes, Fig. 1. Electrical current is conducted through the electrodes into the sheets. In the area of sheets contact, the temperature rapidly increasing to a value above melting point. RSW is terminated by reduction of current to zero and by the electrodes opening.

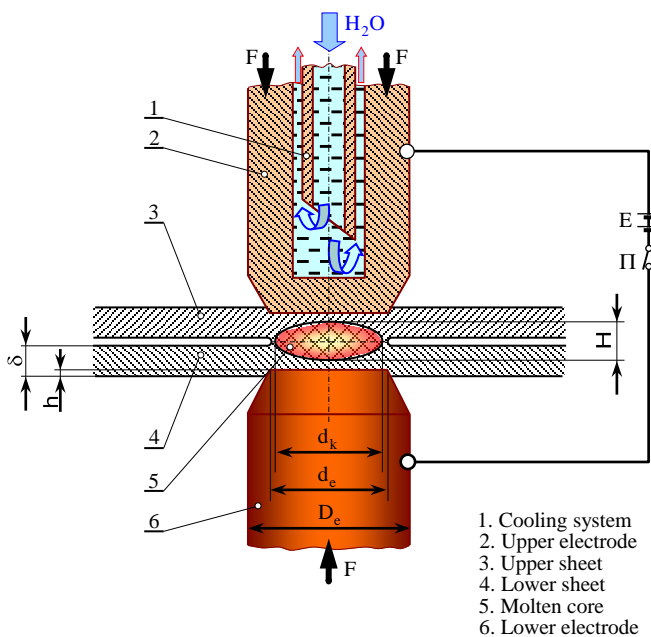


Figure 1: Resistance spot welding [1]

Formation of connection between welded sheets can be divided into three phases, fig 2.

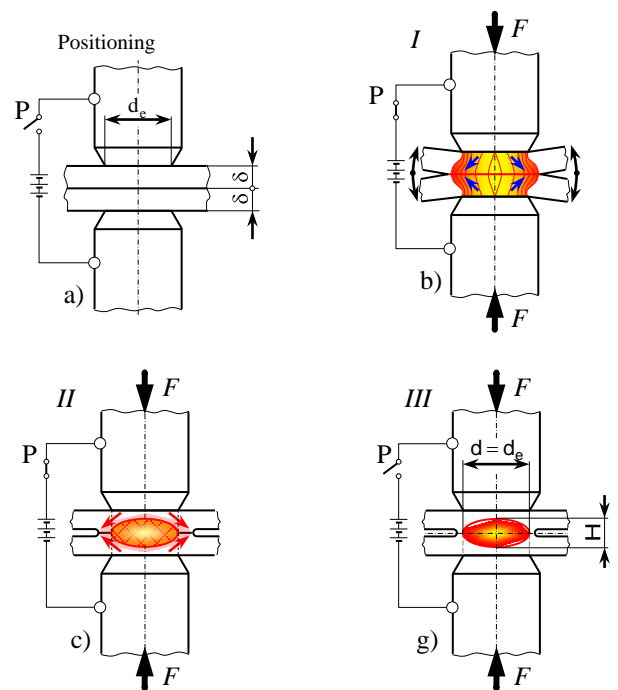


Figure 2: Phases of RSW [1]

The first phase starts immediately with the flow of electrical current. There is an intense heating and stirring of the metal.

The second phase begins at the moment when solidus temperature is reached. Highest temperatures occur on contact surfaces between two sheets.

The third phase includes the cooling and crystallization of the molten core. Molten core is a part of the welded sheets with variable volume formed by the melting of welded sheets.

Shape of molten core as well as final shape and its dimensions depend on welding parameters, fig 3. If we use mild regimes during welding, the isotherms will have the shape of an ellipse so the core and the welded point will have the shape of an ellipsoid. Welding with sharp regimes will produce a much more complex shape of the isotherm and the welded points, too. Peaks of the isotherms will have the tendency to break through to the surface of the welded sheets in the contact zone between the electrode

and the sheet. Or they will tend to break the coronary zone towards the gap between the welded sheets. Such a tendency is created by the combined influence of the so-called skin effect and contact resistance. In extreme conditions, liquid metal manages to break through to the surface of the sheets, which is called expulsion in that area. In order to avoid expulsion, the welding times are radically shortened, the force increases in order to increase the resistance of the coronary zone and the amount of coolant is increased.

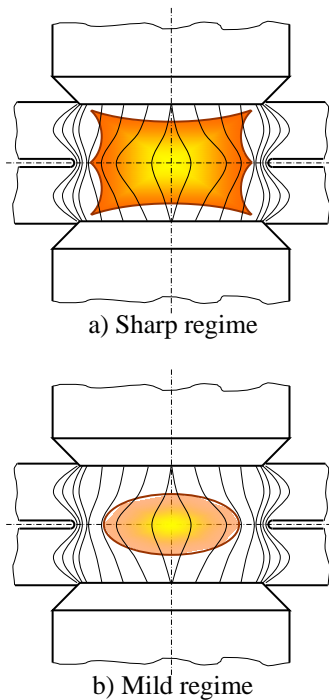


Figure 3: Influence of welding regimes on dimensions and shape of welded spot [1]

## 2. KINETIC OF ELECTRICAL RESISTANCE

The change in total electrical resistance during the RSW is obtained by experimental measurements and has the structure and appearance as in fig 4.

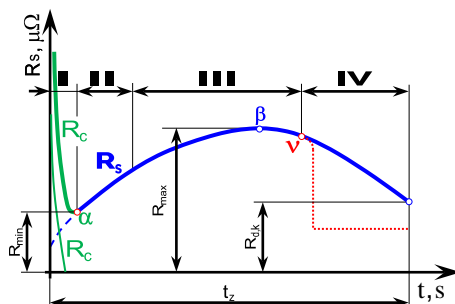


Figure 4: Kinetic of RSW [1]

Dickinson [1] has defined minimum of electrical resistance and denoted it by  $\alpha$ . This is the point where the value of the contact resistance drops to the zero value. From this point onwards, the welding process takes place on the basis of changes in its own electrical resistivity. The point of maximum resistance  $\beta$  [1] represents the maximum amount of energy involved in the process, while the

point  $v$  [1] indicates a moment of material displacement. Kinematics of electrical resistance consists of four zones.

### I – Establishing physical and electrical contact.

Under the influence of the welding force and the temperature rise, deformation of contact micro relief accelerates rapidly, the surface of the local contact increases and contact resistance drops. Increase of electrical resistance is result of heating caused by the high initial value of the contact resistance.

II – Initiation of the melting process in the area of contact surfaces of welded sheets. Given the great mutual proximity of the  $\alpha$ -peak and inflection points, the beginning of the formation and the process of growth of the melted core are related to the minimum resistance ( $\alpha$ ,  $R_c = 0$ ), so there is no difference between them, that is, the zones I and II are considered as one.

### III – It is characterized by three processes:

- the temperature rise in the volume layers of welded sheets has as a consequence increase of electrical resistance which causes release of larger amount of heat by which
- increases the volume of molten metal core, ie affects on
- increases the diameter of the coronary zone, which surrounds the core.

Temperatures in coronary zone are lower in comparison to the temperatures in molten core and of course value of electrical resistance is lower, due to which the electrical current tends to flow precisely through that part of the conductive material. The incidence of the described cyclical changes has a tendency to be reduced during the welding, so there is temperature stabilization in the vicinity of the  $\beta$ -peak.

IV – The continuation of the decrease in electrical resistance due to the growth of the melted core and the growth of plastic deformations. It is carried out on the basis of inertia of characteristic processes, ie latent heat. At some point, such a thermal state of the surrounding ring is established, and mechanical properties that prevent the further growth of the core reach. This is the moment when the pressure of the liquid metal increased so much that it is greater than the tensile strength of the coronary zone and when there is a high likelihood of expulsion. If the expulsion is reached, the liquid metal breaks into the gap between the welded sheets and further into the surrounding space, that is, the liquid metal pierces the surface of the welded sheets around the contact area between sheets and electrodes.

## 3. WHAT IS EXPULSION

The influence of the basic process parameters, as well as the influence of the type of welded material on the kinetics of electrical resistance is advantageous to be shown through the area of definition of the welding process, fig 5. It is obtained by experimental measurements in which the welding time and current vary at certain values of the welding force. Two sets of points are characteristic:

- beginning of the metal melting,  $\alpha$ -peaks, and
- start of metal expulsion,  $v$ -peaks.

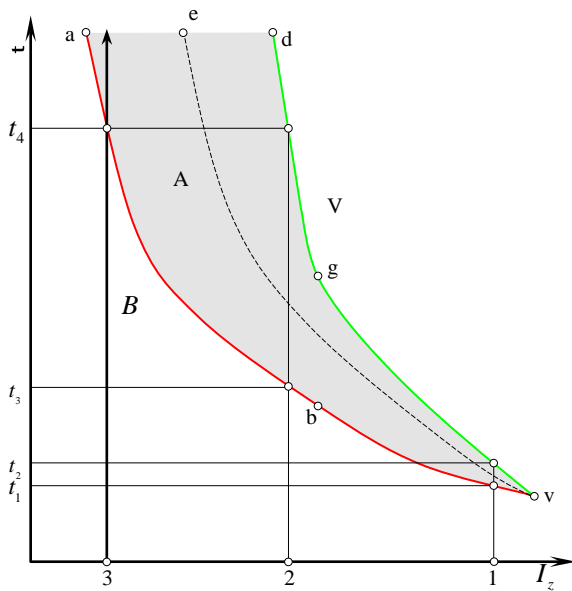


Figure 5: The domain of existence for RSW[1,4,5]

As can be seen, the  $\beta$ -peak is not important for this procedure, ie appropriate set of points does not set the boundary of the process. When a number of dots corresponding to  $\alpha$ -vertices, ie the origin of the melted core (curve a-b-v) and the set of dots that correspond to the occurrence of the expulsion or a series of v-peaks (curves v-g-d) are obtained a three-part process space is obtained.

The middle segment A, defined by the curve  $\alpha$  and  $\pi$ -peaks, with a cross-section v, represents the space of the existence of a RSW process for a given welding force and base material. The boundary curves of this segment are derived from the fact that the set of a-peaks corresponds to the minimum dimensions of the molten core, that is the beginning of base material melting and the set of n-peaks corresponds to the largest possible dimensions of the welded point. It is evident therefore that only the process whose value of electrical current and time of welding determine the point located in the area between boundary curves that is in the area of the existence of welding (A) is considered successful. Marked zones are characterized by the following characteristics.

A - The zone of the existence of the process. It also includes optimal technology parameters. By comparing ordinates 1 and 2, it is noted that the process realized with parameters closer to ordinate 1 corresponds to sharp regimes, while the mild regimes correspond to the ordinate 2. For the selected welding current, the diameter of the point will be even greater if the time of welding is close to the value  $t_2$  and vice versa if  $T_z \leq t_1$  point will not be formed, because the process will be terminated. In contrast, the welding technology should be designed so that the point of the state is in the considered zone A, but close to the boundary v curve.

The welding technology with value of electric current which correspond to ordinate 2 has a much wider interval of time regulation ( $\Delta t_z = t_4 - t_3$ ).

The welding technology realized at time  $t_z = t_4$ , but with a current smaller than the value which correspond to the ordinate 2, allows obtaining points with smaller diameter as the current approaches to the value which correspond to the ordinate 3. Increase of time of welding at this par-

ticular value of electric current point allows growth of point dimensions but in a way that expulsion can not happen.

B - Unachievable to hard-to-achieve welding technology. This zone is on the right side determined by the curve of the  $\alpha$ -peaks.

V - The zone where expulsion will happen for sure. The welding time and current are inversely proportional, that is, this is the limit of sharp regimes. Namely, if longer time of welding is applied expulsion will occur at the moment when the value of welding current which correspond to the ordinate 2 is reached. During this period of time, all phases of the welded point development will be carried out, fig. 2. It is especially important that a coronary zone with good mechanical characteristic is formed which reduces the likelihood of leakage of liquid metal from the welding zone. With increased value of electric current while simultaneously shortening time of welding all phases of point development will be also shortened. In such conditions, the coronary zone can not be fully formed and, in particular, it can not achieve the necessary resistance in order to prevent the pouring of liquid metal into the surrounding area.

#### 4. RSW COSTS

In the automotive industry large production series are realized. RSW is used to produce a large number of welded points. Therefore it is justified to use highly automated equipment. The structure of the welding costs consists of the six elements, fig 6.

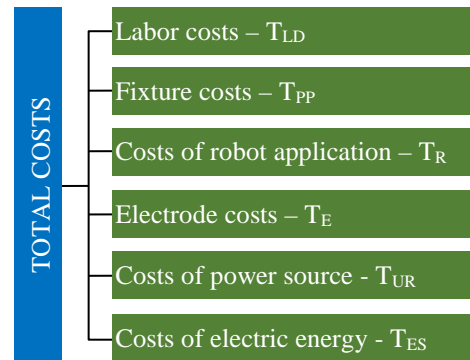


Figure 6: Total costs for RSW[1,4,5]

Total welding costs for car bodywork [2], fig. 6 can be calculated as:

$$T_U = T_{ES} + T_{UR} + T_E + T_R + T_{PP} + T_{LD}$$

$$T_U = 409.20 + 473.66 + 402.44 + 506.26 + 205.01 + 583.36 = 2579.93 \text{ RSD}$$

Costs of material expulsion can be calculated as:

$$T_{IS} = m_{IS} \cdot C_{OM} + C_S \cdot P \cdot t_{IS}$$

$T_{IS}$  – costs of material expulsion, RSD  
 $m_{IS}$  – mass of expelled material, kg  
 $m_{IS} = p_{is} \cdot m_{IM}$   
 $p_{is}$  – portion of expelled material, %  
 $m_{IM}$  – mass of molten core, kg  
 $C_{OM}$  – costs of base material, RSD,  
 $C_S$  – costs of electric energy, RSD/kWh,  
 $P$  – power of welding machine, kW/point,

$$P = \frac{U \cdot I_z}{1000 \cdot \eta_s} \cdot \varepsilon + P_o \cdot (1 - \varepsilon)$$

$U$  - voltage, V

$I_z$  - current, A

$\eta_s$  – efficiency of power source,

$\varepsilon$  - duty cycle of welding machine,

$P_o$  – idle power, kW/point,

$t_{IS}$  – time of expulsion, hours

$$t_{IS} = t_z \cdot \frac{m_{IS}}{m_{IM}}$$

$t_z$  – time of welding, hours

The car body consists of several different parts (floor, side panels, roof, door, door of luggage, hoods and side wings, figure 7) of various sheet thicknesses, and therefore it is necessary to calculate the extrusion costs for each part of the body, especially. Structure of expulsion costs can be described by:

- mass of expelled material,
- the energy of the expelled material,
- the kinetic energy of the expelled material,
- light energy,
- sound energy ...

Of these impacts, this article includes the first two.

The mass of the expelled material is expressed by the percentage of the expelled amount of material,  $p$ .

Table 1 shows the following values:  $p = 2, 4, 6, 8, 10\%$ .

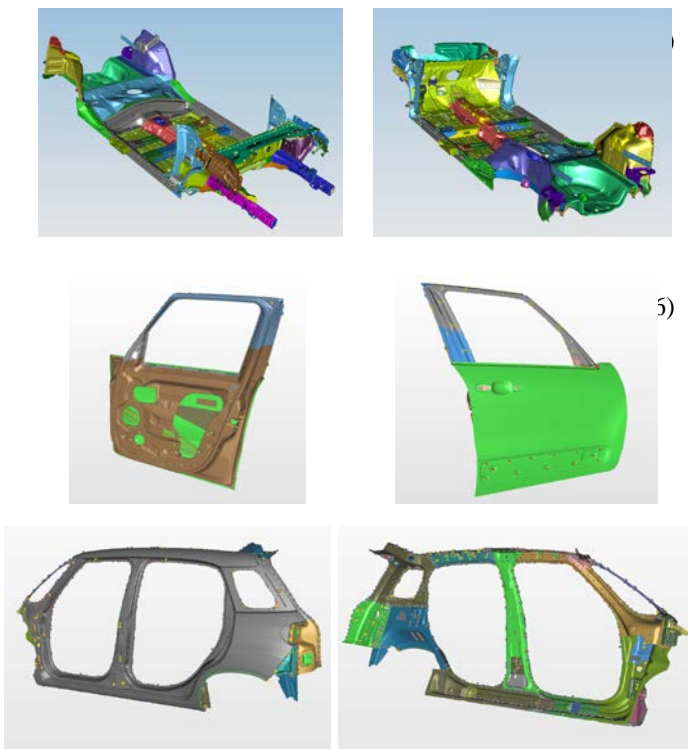


Figure 7: Parts of car body

In accordance with the achieved mass amount of expulsion and the methodology of the calculation, the cost of expulsion is calculated and shown in the table 1 and in fig 8.

Table 1. Costs of expulsion during the year

Body parts	Costs of expulsion, RSD				
	Amount of expulsion, $p$ , %				
	2	4	6	8	10
Floor	13.14	26.28	39.42	52.56	65.70
Side panels	4.21	8.42	12.63	16.84	21.05
Roof	0.51	1.02	1.53	2.04	2.55
Four doors	5.91	11.82	17.73	23.64	29.55
Doors of lugage department	1.48	2.96	4.44	5.92	7.40
Hood	0.26	0.52	0.78	1.04	1.30
Side wings	1.03	2.06	3.09	4.12	5.15
Cost of expulsion for one car body, RSD					
Total costs, RSD/car	26.54	53.08	79.62	106.16	132.70
Costs of expulsion per year (for 90000 cars), RSD					
TOTAL COSTS, RSD/year	2388600	4777200	7165800	9554400	11943000

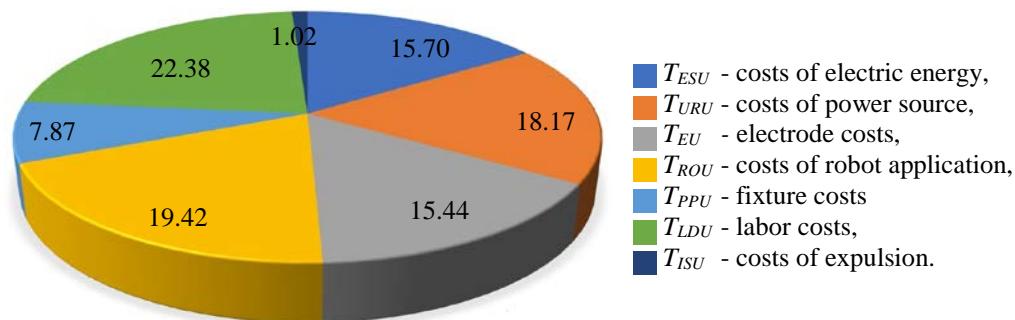


Figure 8: Percentage participation of individual costs

The costs of extrusion costs are relatively low and ranges from TIS = 0.26 din / point on the motor cover (so-called hood) at the amount expelled material of 2%, to TIS = 65.7 din / point on the car floor and at the amount of expelled material from a welded point of 10%. The significance of this phenomenon, in a cost-effective sense, is illustrated [2] by the number of cars and apartments that would be "saved" if the expulsion was eliminated. At  $p = 2\%$ , it would be saved for example 1.85 FIAT 500L cars or one-bedroom apartment at prices that are present in Kragujevac. For the most pronounced displacement,  $p = 10\%$ , the corresponding cost is for example 9.25 FIAT 500L cars, which is the equivalent of five one-bedroom apartments, again in Kragujevac. It is obvious that this type of cost should be included in the total cost of the process, figure 6. Compared to the total number of 90000 cars per year these costs are not high.

It is therefore concluded that the phenomenon of expulsion is inadmissible and it is a sign of the imperfection of technology and that it is necessary to take measures to avoid expulsion. Such attitudes would certainly be more convincing when changes in mechanical properties of the welded joints due to the expulsion and therefore the resistance of the welded points would be analyzed.

This paper has the task of pointing out or suggesting at least one direction that can suppress or reduce the expulsion of the material.

### 5. POSSIBILITIES OF AVOIDING EXPULSION

It has already been pointed out that for the area of the defined process technology, the value and position of the  $\beta$ -peak point (the maximum value of electrical resistance) are not of crucial importance. However, in the process of determination of optimum values of the welding parameters the set of this peak positions is important which is shown as a dotted line at fig 5.

Domains of welding technology parameters definition are determined for particular values of force and particular sheet material. Variation of force value gives us whole set of domains of defined technology for particular sheet material. By their superposition a three-dimensional space which define possible welding parameters is formed, fig. 9. It is characterized by two planes.

The first represents a set of  $\alpha$ -vertices i.e. it is obtained by superposition of the boundary curves of the starting formation of welded point. The second characteristic plane represents a set of  $v$ -points which correspond to the beginning of expulsion. Space which is covered by these planes is basically a domain of welding parameters definition for RSW. Since each point of this space is determined by the values of all three basic parameters of the welding technology every change of their value directly creates new position of the correspondent point.

Therefore one of the basic values of this representation is the our ability to predict consequences of any parameter value variation. On the other hand this representation can have significant application in the domain of process design in welding technology and also in the management, optimization and other simulation methods.

The third value is connected to the choice of logistics which can be applied in order to reduce the occurrence

of expulsion ie in order to totally eliminate possibility of expulsion.

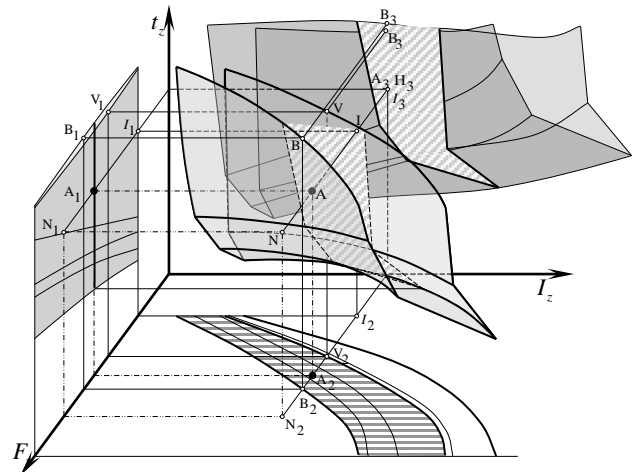


Figure 9: Domain of process parameters definition for RSW

Representation of domain of process parameters definition is directly related to the changes in the value of two characteristic electric resistances; At the contact between the welded sheets ( $\rho_{ad}$ ) and the volume or thermogenic resistance of the sheet material ( $\rho_d$ ). The shape and position of the curve and the plain of process starting position ( $\alpha$ -peaks) are determined by the values of the contact electrode resistance or by the heat induced in the contact zone of welded sheets.

Reduction of contact resistance leads to shifting of boundary curve and plane into the domain of larger welding currents. And vice versa if contact resistance increases, boundary curve and plane are shifted into the domain of higher current values. The shape and position of the boundary curve and expulsion plane ( $v$ -points) is determined by the values welded sheets resistance ie by the quantity of induced heat. Bigger value of electrical resistance narrows the domain of process parameter definition and vice versa.

### 6. CONCLUSIONS

The phenomenon of expulsion occurs at the end of the process of forming a welded point. The expulsion must be suppressed or reduced because it represents a qualitative evaluation of the resistance spot welding process. Expulsion costs should be included in calculation of total costs of the process especially in large series production.

The methods of expulsion preventing described in this article are reduced to the optimization of the basic parameters through logistics built on the basis of the domain of process existence.

### ACKNOWLEDGEMENTS

The authors wish to express their gratitude to the Ministry of Education and Science of the Republic of Serbia (project TR37020).

## REFERENCES

- [1] M Vukićević, "Joining technologies. Welding 2.", Faculty of Mechanical and Civil Engineering,, Kraljevo, 2017
- [2] M. Tešević, "Estimation of expulsion costs in case of resistance spot welding", Master thesis, University of Kragujevac, Faculty of Mechanical and Civil Engineering, Kraljevo 2017
- [3] M Vukićević, "Process Design in Welding Technology – Part 2: Methodology", Faculty of Mechanical and Civil Engineering, Kraljevo, 2014
- [4] H. Sung, K. Mun, C. Dong, "Expulsion Reduction in Resistance Spot Welding by Controlling of welding Current Waveform", International conference on the mechanical behavior of materials, Procedia Engineering 10 (2011) 2775–2781, 2011
- [5] J. Senkara, H. Zhang, S. Hu, "Expulsion Prediction in Resistance Spot Welding", Welding Research, 123-132, 2004



# Numerical Simulation of Hardness Distribution at the HAZ of P355GH Steel

Mišo Bjelić<sup>1\*</sup>, Karel Kovanda<sup>2</sup>, Ladislav Kolařík<sup>2</sup>, Marie Kolaříková<sup>2</sup>, Miomir Vukičević<sup>1</sup>, Branko Radičević<sup>1</sup>

<sup>1</sup>Faculty of Mechanical and Civil Engineering, University of Kragujevac, Kraljevo (Serbia)

<sup>2</sup>Faculty of Mechanical Engineering, Czech Technical University, Prague (Czech Republic)

*Microstructure of the weld seam and the HAZ has an essential impact on different mechanical properties of welded joint. This article presents a methodology for prediction of Vickers hardness in HAZ of welded plates. In order to achieve this goal we have used 3D model of heat transfer during welding, coupled with Kirkaldy's model of austenite decomposition. This coupling have made possible prediction of the volume fractions of ferrite, pearlite and bainite and also prediction of Vickers hardness distribution. Results of simulation run were found to be in reasonable good accordance with experimental ones.*

**Keywords:** Welding, Numerical modeling, Simulation, Microstructure, Hardness

## 1. INTRODUCTION

Simulation models of welding processes give us an insight into the influence of welding parameters on temperature field in welded parts and by means of temperature fields and the influence to geometry and microstructure of welded joints. Microstructure of welded seam and HAZ has critical impact on mechanical properties of welded joint. Since the first analytical models of Rosenthal [1] and Rykalin [2], complexity of simulation models has grown rapidly [3,4]. But this complexity makes these models unreachable in realistic conditions due to the long time to run the simulation.

Despite good weldability of P355GH steel, it is very important to predict microstructural changes during its welding having in mind that this type of steel is widely used for elevated temperature purposes. Hardness of HAZ which mainly depends on martensite content, has great influence on cracking resistance [5]. Bearing in mind the need to reduce the simulation time, in this article we have coupled an analytical, three-dimensional, quasi-stationary model of heat transfer during GMA welding [6] with Kirkaldy's model [7] of austenite decomposition during cooling stage of welding process. Coupling of these models made us possible to estimate the value of Vickers hardness in the cross section of the welded joint.

## 2. MODEL OF HEAT TRANSFER

Welding heat source acts in a narrow localized area where a molten pool is formed. Regardless of difficulties, modeling the heat transfer during welding gives us informations about the influence of different process parameters on the heat transfer process itself and also nformations about the influence to the output results that include seam geometry, welded microstructure, deformation, etc.

Quasy-stationary partial differential equation which describes 3-D heat conduction during welding [6] in moving coordinate system, fig. 1 is given by (1):

$$-v_z \left( 1 + \frac{L}{c_p} \frac{\partial f_{liq}}{\partial T} \right) \frac{\partial T}{\partial \xi} = \frac{\lambda}{\rho c_p} \left( \frac{\partial^2 T}{\partial \xi^2} + \frac{\partial^2 T}{\partial y^2} + \frac{\partial^2 T}{\partial z^2} \right) + q_l \quad (1)$$

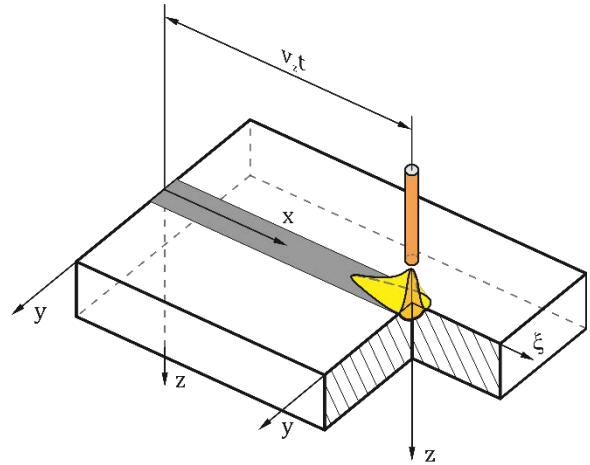


Figure 1: Moving coordinate system

Proportion of the liquid phase can be represented by (2):

$$f_{liq} = \begin{cases} 0 & \text{for } T \leq T_{sol} \\ \frac{T - T_{sol}}{T_{liq} - T_{sol}} & \text{for } T_{sol} < T < T_{liq} \\ 1 & \text{for } T \geq T_{liq} \end{cases} \quad (2)$$

As a heat source model, we have used Goldak's double elliptic model [8]. The feature of this model is that the front half of the model is a part of an ellipsoidal source, while the last half is a part of the second ellipsoidal source. Within the front half of the model, heat density distribution is carried out by (3):

$$q_{lf}(x, y, z) = \frac{6\sqrt{3}f_f Q}{a_{hf} b_h c_h \pi \sqrt{\pi}} e^{-\frac{3x^2}{a_{hf}^2}} e^{-\frac{3y^2}{b_h^2}} e^{-\frac{3z^2}{c_h^2}} \quad (3)$$

The heat density distribution within the last half of the heat source model is described by (4):

$$q_{lb}(x, y, z) = \frac{6\sqrt{3}f_b Q}{a_{hb}b_h c_h \pi \sqrt{\pi}} e^{-\frac{3x^2}{a_{hb}^2}} e^{-\frac{3y^2}{b_h^2}} e^{-\frac{3z^2}{c_h^2}} \quad (4)$$

It is necessary that the following condition be fulfilled (5):

$$f_f + f_b = 2 \quad (5)$$

On the basis of (1) it may be seen that the calculation of temperatures in welded plates requires knowledge of the values of selected thermo-physical parameters: density, specific heat capacity and thermal conductivity. It is possible to adopt that the values of these parameters are constant, but in real terms this is not the case. In order to calculate temperature distribution in welded plates more accurately, it is necessary to use values of the given parameters as a function of temperature.

### 3. THERMOPHYSICAL PROPERTIES

In the experimental part of this article we have used P355GH steel with chemical composition shown in Table 1 as a base material and OK Autrod 12.50 wire with chemical composition shown in Table 2 as a filler material. Since it was not possible to find literature data about the density, specific heat capacity and thermal conductivity as a function of temperature, we have used methodology presented in [6,9].

Table 1. Chemical composition of base material

C %	Si %	Mn %	Nb %	P %	S %
0.20	0.19	1.45	0.014	0.016	0.062

Table 2. Chemical composition of filler material

C %	Si %	Mn %	P %	S %
0.08	0.58	1.06	0.009	0.01

Results of density modeling using mentioned methodology can be seen on fig. 2.

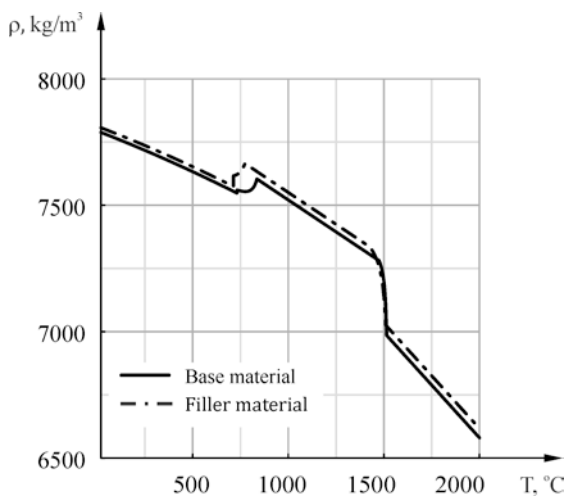


Figure 2: Density of base and filler material vs. temperature

Thermal conductivity and effective heat capacity for base and filler material as a functions of temperature are shown in fig 3 and fig. 4.

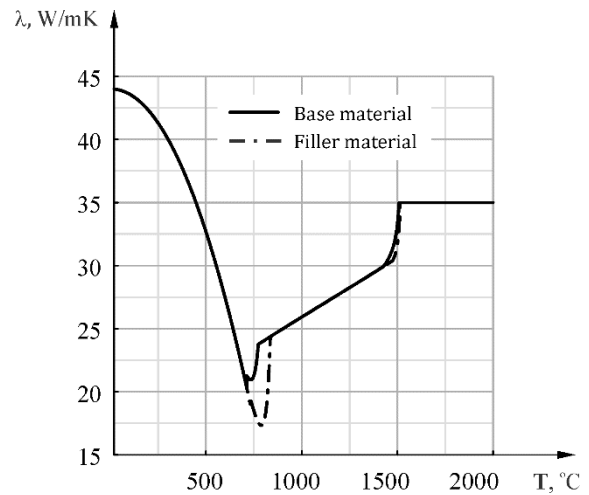


Figure 3: Thermal conductivity of base and filler material vs. temperature

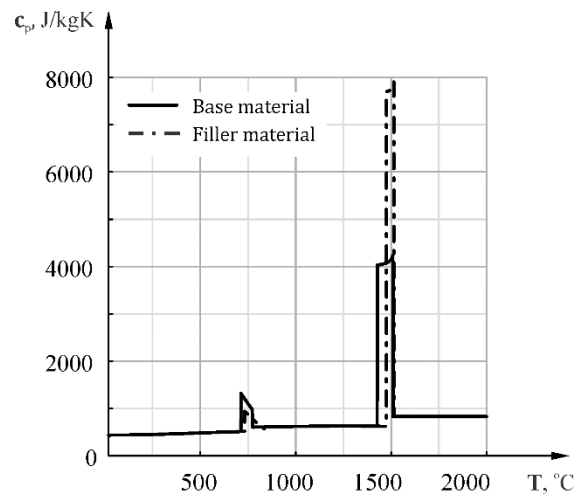


Figure 4: Effective heat capacity of base and filler material vs. temperature

### 4. MICROSTRUCTURAL MODEL

The microstructure of the welded joint, that is, microstructure of the weld seam and the HAZ, has a crucial effect on the mechanical properties of the welded joint. Description of steel microstructure in practice is most commonly made using austenite isothermal transformation diagrams and the continuous cooling diagrams in welding. For specific steel, these diagrams are obtained by experimental testing. However, in the absence of experimental diagrams for the steel of a particular chemical composition, models which describe austenitic isothermal transformation process can be used. Based on the research [10,11], Kirkaldy [7] proposed a series of equations which describe kinetics of austenitic isothermal transformation.

For the reaction of the austenite transformation into ferrite under isothermal conditions, the time required for the particular amount  $X_F$  of ferrite to be formed can be described as (6):

$$\tau_F = R_F \int_0^{X_F} \frac{dX_F}{X_F^{\frac{2(1-X_F)}{3}} (1-X_F)^{\frac{2X_F}{3}}} \quad (6)$$

Simillary, for the reaction of the austenite trasformation into pearlite, Kirkaldy proposed (7):

$$\tau_p = R_p \int_0^X \frac{dX_p}{X_p^{\frac{2(1-X_p)}{3}} (1-X_p)^{\frac{2X_p}{3}}} \quad (7)$$

And for the reaction of the austenite trasformation into bainite (8):

$$\tau_B = R_B \int_0^X \frac{dX_B}{X_B^{\frac{2(1-X_B)}{3}} (1-X_B)^{\frac{2X_B}{3}}} \quad (8)$$

Coefficients  $R_F$ ,  $R_P$ ,  $R_B$  are described by (9-11):

$$R_F = \frac{59.6Mn + 1.45Ni + 67.7Cr + 244Mo}{2^{\frac{(G-1)}{2}} (Ae_3 - T)^3 \cdot e^{\left(\frac{-23500}{RT}\right)}} \quad (9)$$

$$R_P = \frac{1.79 + 5.42(Cr + Mo + 4Mo \cdot Ni)}{2^{\frac{(G-1)}{2}} (Ae_1 - T)^3 \cdot D_p} \quad (10)$$

$$R_B = \frac{(2.34 + 10.1C + 3.8Cr + 19Mo)10^{-4} Z}{2^{\frac{(G-1)}{2}} (B_s - T)^3 \cdot e^{\left(\frac{-27500}{RT}\right)}} \quad (11)$$

While coefficients  $Z$  and  $D_p$  can be calculated as (12-13):

$$\frac{1}{D_p} = \frac{1}{e^{\left(\frac{-27500}{RT}\right)}} + \frac{0.01Cr + 0.052Mo}{e^{\left(\frac{-37000}{RT}\right)}} \quad (12)$$

$$Z = e^{\left[X_B^2(1.9C + 2.5Mn + 0.9Ni + 1.7Cr + 4Mo - 2.6)\right]} \quad (13)$$

Or if following condition (14) is satisfied then value of the coefficient  $Z$  is equal to 1.

$$(1.9C + 2.5Mn + 0.9Ni + 1.7Cr + 4Mo - 2.6) < 0 \quad (14)$$

Based on Kirkaldy's model, we have calculated TTT diagrams for the base material, fig. 5, as well as for filler material, fig. 6, using MATLAB.

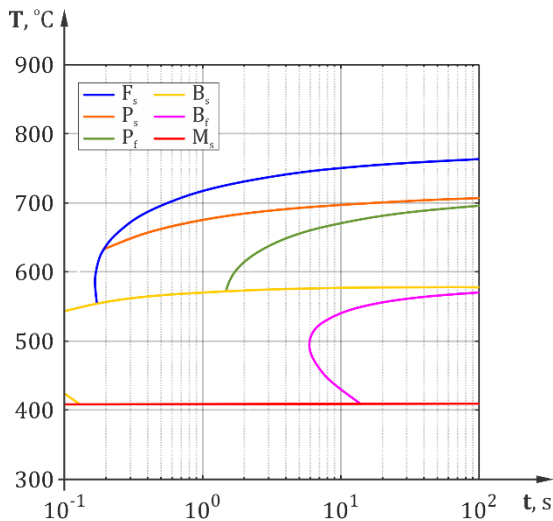


Figure 5: TTT diagram for base material

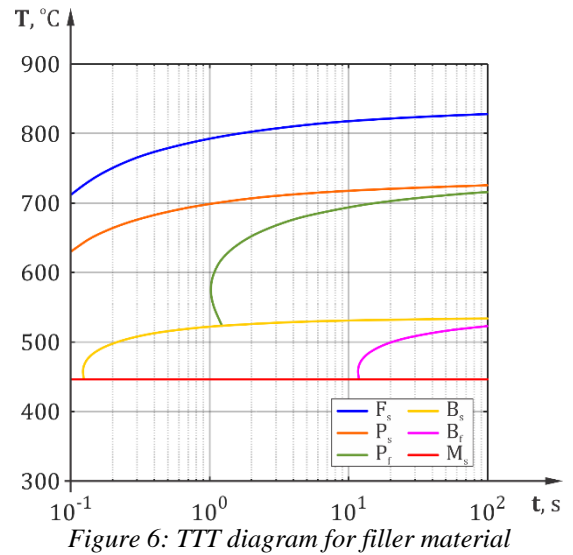


Figure 6: TTT diagram for filler material

### 5. HARDNESS

Hardness at any point in HAZ depends on the fraction ammount of individual phases: ferrite,  $X_F$ , pearlite,  $X_P$ , bainite,  $X_B$  and martensite,  $X_M$ . If we know fraction ammount of each of these phases at a certain point, the hardness can be computed [12] using the equation (15):

$$HV = HV_F \cdot X_F + HV_P \cdot X_P + HV_B \cdot X_B + HV_M \cdot X_M \quad (15)$$

Hardness of the individual phases depends on the chemical composition of the steel and on the cooling rate at 700 °C [13]. Hardness of ferrite and pearlite can be calculated as (16):

$$H_{FP} = 42 + 223C + 53Si + 30Mn + 12.6Ni + 7Cr + 19Mo + (10 - 19Si + 4Ni + 8Cr + 130V) \log(V_r) \quad (16)$$

For the bainite and martensite hardness is calculated based on (17-18):

$$H_B = -323 + 185C + 330Si + 153Mn + 65Ni + 144Cr + 191Mo + (89 + 53C - 55Si - 22Mn - 10Ni - 20Cr - 33Mo) \log(V_r) \quad (17)$$

$$H_M = 127 + 949C + 27Si + 11Mn + 8Ni + 16Cr + 21 \log(V_r) \quad (18)$$

Cooling rate at 700°C is described by (19):

$$V_r = 3600 \left( \frac{800^\circ - 500^\circ}{\Delta t_{8/5}} \right) \quad (19)$$

During the time, grain size increases while the level of increase depends on temperature, activation energy and time [12,14] and can be described by (20):

$$\frac{dg}{dt} = \frac{k}{2g} \cdot e^{\left(\frac{Q}{RT}\right)} \quad (20)$$

Direct application of Kirkaldy's model in case of welding is not possible because the welding processes take place with variable heating and cooling rates. According to Scheil's additivity rule [15], fig 7, during continous cooling, austenite decomposition starts when the following condition is fulfilled (21):

$$\sum_{j=1}^m \frac{\Delta t_j}{\tau_j} = 1 \quad (21)$$

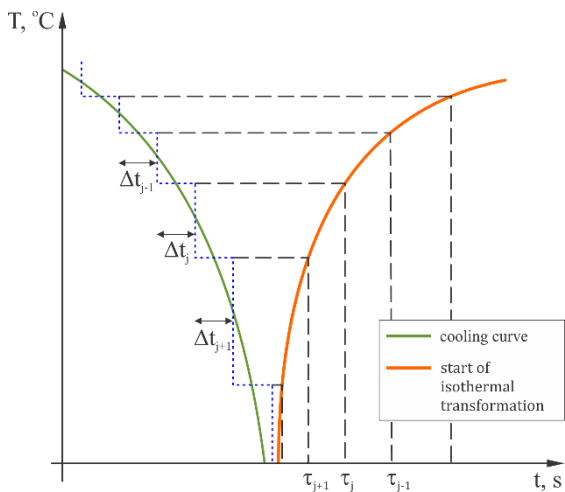


Figure 7: Scheil's additivity rule

### 6. SIMULATION

The simulation was conducted with following welding parameters: welding current  $I = 221.1$  A, arc voltage  $U = 21.9$  V, welding speed  $v_w = 0.008$  m/s, temperature of plate  $T_p = 22^\circ\text{C}$ , and atmosphere temperature,  $T_a = 20.5^\circ\text{C}$ .

Results of simulation are shown of figs.8 - 12.

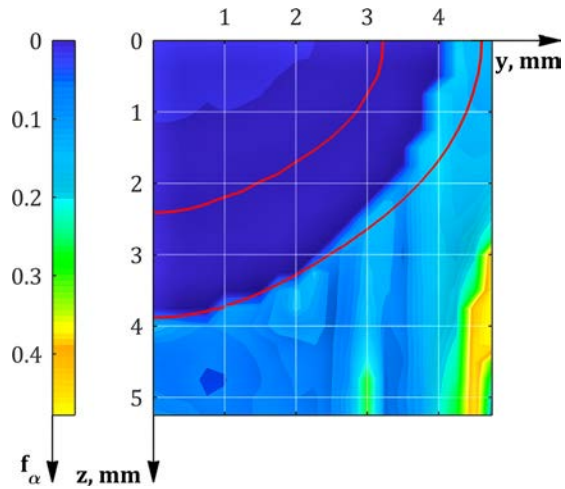


Figure 8: Simulation of ferrite volume fraction

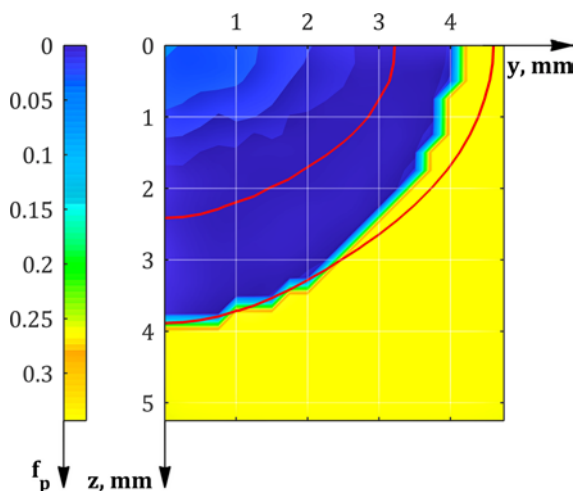


Figure 9: Simulation of pearlite volume fraction

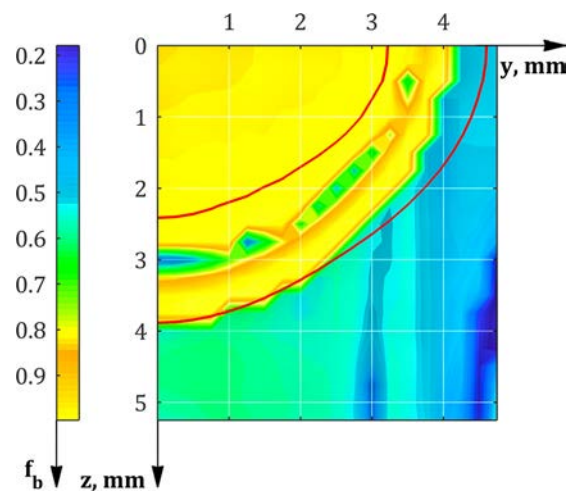


Figure 10: Simulation of bainite volume fraction

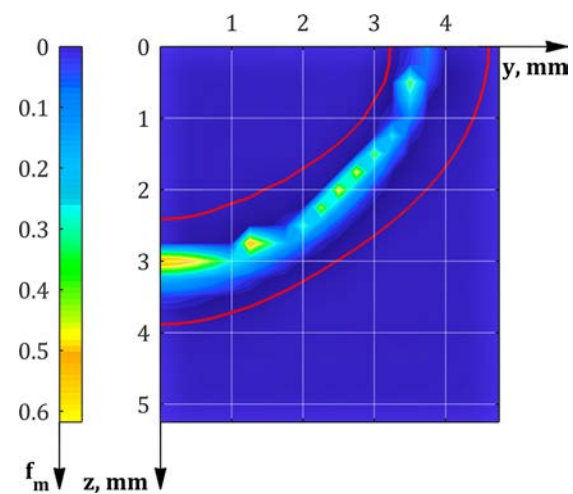


Figure 11: Simulation of martensite volume fraction

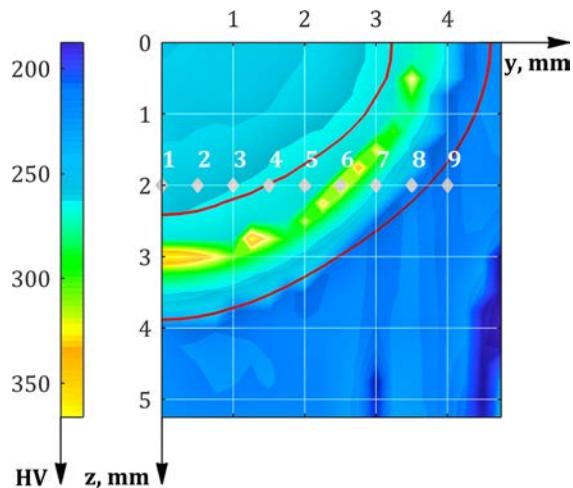


Figure 12: Simulation of Vicker's hardness in weld cross section

### 7. EXPERIMENT

Dimensions of the P355GH welded steel sample were  $300 \times 150 \times 5$  mm, fig 13. Filler material used was OK Autrod 12.50 wire, with 1.0 mm diameter. As a shielding gas, we have used Arcal 5 (82%Ar + 18%CO<sub>2</sub>). Values of welding parameters were the same as in case of simulation.

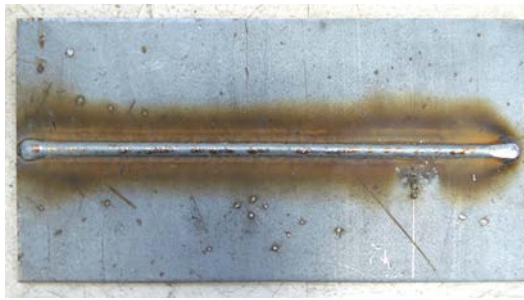


Figure 13: Welded sample

Fig. 14 shows comparison between simulated and experimental weld bead geometry while values of absolute and relative geometry of weld bead width – B, weld penetration – H, weld shape penetration factor –  $\psi$  are shown in table 3.

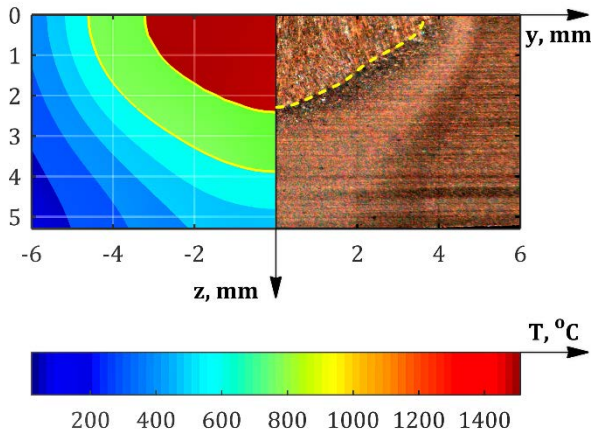


Figure 14: Comparison of simulated and experimental weld bead geometry

Table 3. Absolute and relative error of simulated weld bead geometry

Parameter	Unit of measurement	Absolute error	Relative error [%]
B	mm	0.83	11.4%
H	mm	0.09	4.1%
$\psi = B/H$		0.47	14.9%

Measurements of hardness were performed using Vickers method. Due to the small dimensions of the welded joint, the measurements were performed using a load of 9.81N. Hardness was measured in a series of points at a distance of 2 mm from the upper surface of the samples. The distance between the measuring points was 0.5 mm, fig 8.

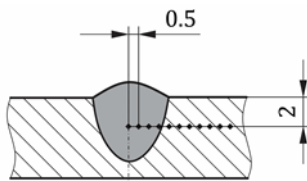


Figure 15: Location of indentations

We have made comparison of simulated and experimental values of hardness at indentations which is shown at fig.16.

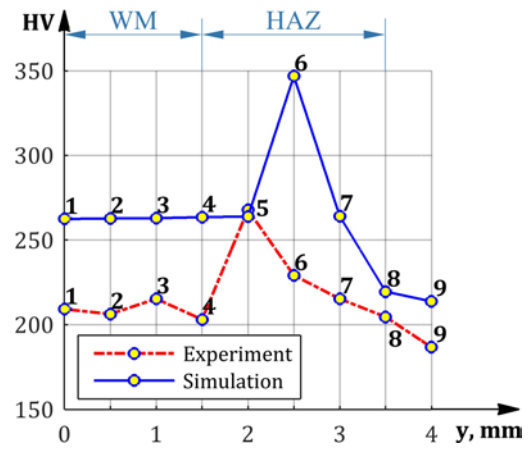


Figure 16: Comparison of simulated and experimental hardness at indentation points

Relative error of hardness simulation at indentations is shown on fig. 17.

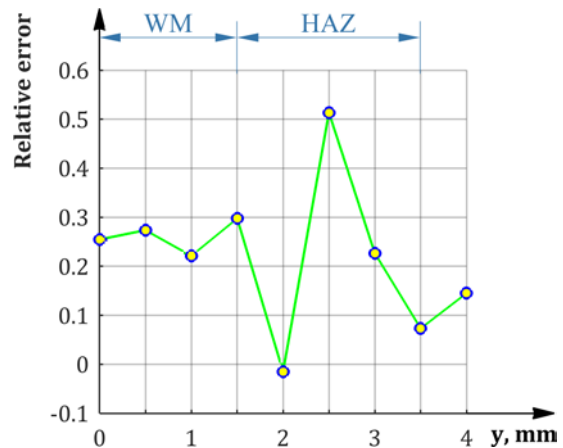


Figure 17: Relative error of simulation

## 8. SUMMARY AND CONCLUSIONS

In order to simulate hardness distribution at HAZ we have combined three dimensional model of heat transfer during welding with Kirkaldy's model of austenite decomposition. Results obtained by simulation are compared with experimental ones. In case of weld bead geometry results of simulation were in very good agreement with experimental results. Something larger deviations that occurred in case of hardness can be explained as a result of direct application of the metallurgical model without calibration. The calibration of the model could not be performed due to the lack of an experimentally obtained isothermal transformation diagram for the P355GH steel which could be used to adjust the parameters of the microstructural model. Presented method represents a good starting position for simulation of microstructure volume fractions and hardness in HAZ.

## ACKNOWLEDGEMENTS

The authors wish to express their gratitude to National CEEPUS Office of Czech Republic (project CIII-HR-0108-07-1314) and to the Ministry of Education and Science of the Republic of Serbia (project TR37020).

## NOMENCLATURE

$Ae_1$	– lower equilibrium austenite formation temperature, [°C]
$Ae_3$	– upper equilibrium austenite formation temperature, [°C]
$a_{hf}$	– semiaxis of front half-ellipse in x - direction, [m]
$a_{hb}$	– semiaxis of rear half-ellipse in x - direction, [m]
$B_s$	– bainite start temperature, [°C]
$b_h$	– semiaxis of front half-ellipse in y - direction, [m]
$c_p$	– specific heat, [J·kg <sup>-1</sup> ·K <sup>-1</sup> ]
$c_h$	– semiaxis of front and rear half-ellipse in z - direction, [m]
$f_b$	– bainite volume fraction
$f_p$	– pearlite volume fraction
$f_m$	– martensite volume fraction
$f_\alpha$	– ferrite volume fraction
$g$	– grain size, [m]
$H$	– depth of penetration, [m]
$HV$	– Vicker's hardness
$HV_B$	– Vicker's hardness of bainite
$HV_{FP}$	– Vicker's hardness of ferrite and pearlite
$HV_M$	– Vicker's hardness of martensite
$I$	– welding current, [A]
$k$	– grain growth constant, [mm <sup>2</sup> /min]
$L$	– latent heat, [Jkg <sup>-1</sup> ]
$M_s$	– martensite start temperature, [°C]
$q_{1f}$	– power density in front quadrant, [Wm <sup>-3</sup> ]
$q_{1b}$	– power density in rear quadrant, [Wm <sup>-3</sup> ]
$R$	– universal gas constant, [J·mol <sup>-1</sup> ·K <sup>-1</sup> ]
$T$	– temperature, [°C]
$T_a$	– ambience temperature, [°C]
$T_{liq}$	– liquidus temperature, [°C]
$T_{sol}$	– solidus temperature, [°C]
$U$	– arc voltage, [V]
$V_r$	– cooling speed at 700°C, [°C·s <sup>-1</sup> ]
$v_z$	– welding speed, [m·s <sup>-1</sup> ]
$X_F$	– normalized volume fraction of ferrite, [%]
$X_P$	– normalized volume fraction of pearlite, [%]
$X_B$	– normalized volume fraction of bainite, [%]
$\Delta t_{8/5}$	– cooling time from 800 – 500°C
$\lambda$	– thermal conductivity, W·m <sup>-1</sup> ·K <sup>-1</sup>
$\tau$	– time, [s]
$\tau_B$	– time to isotherm. transf. of austenite fraction to bainite, [s]
$\tau_F$	– time to isotherm. transf. of austenite fraction to ferrite, [s]
$\tau_P$	– time to isotherm. transf. of austenite fraction to pearlite, [s]
$\psi$	– weld bead width to depth ratio

## REFERENCES

- [1] D. Rosenthal, "Mathematical theory of heat distribution during welding and cutting", *Welding Journal*. 20 (1941) 220s–234s.
- [2] N.N. Rykalin, "Calculations of thermal processes in welding", 1951.
- [3] G. Xu, J. Hu, H.L. Tsai, "Three-dimensional modeling of arc plasma and metal transfer in gas metal arc welding", *International Journal of Heat and Mass Transfer*. 52 (2009) 1709–1724.
- [4] M. Schnick, U. Fuessel, M. Hertel, M. Haessler, A. Spille-Kohoff, A.B. Murphy, "Modelling of gas-metal arc welding taking into account metal vapour", *Journal of Physics D: Applied Physics*. 43 (2010) 434008.
- [5] Ø. Grong, "Metallurgical modelling of welding", Institute of Materials, London, 1997.
- [6] M. Bjelić, "Characterization of weld geometry and microstructure based on heat-transfer and metallurgical model of the GMAW process as a basis for prediction of the technological parameters", University of Kragujevac, 2016.
- [7] J. Kirkaldy, D. Venugopalan, "Prediction of microstructure and hardenability in low-alloy steels, in: International Conference on Phase Transformations in Ferrous Alloys", 1983: pp. 125–148.
- [8] J. Goldak, A. Chakravarti, M. Bibby, "A new finite element model for welding heat sources", *Metallurgical Transactions B*. 15 (1984) 299–305.
- [9] M. Bjelić, K. Kovanda, L. Kolařík, M. Vukićević, B. Radičević, "Numerical modeling of two-dimensional heat-transfer and temperature-based calibration using simulated annealing optimization method: Application to gas metal arc welding", *Thermal Science*. 20 (2016) 655–665.
- [10] C. Zener, "Kinetics of the decomposition of austenite", in: *Trans. AIME*, 1946: pp. 550–595.
- [11] M. Hillert, "The role of interfacial energy during solid state phase transformations", *Jernkontorets Annaler*. 141 (1957) 757–789.
- [12] J.A. Goldak, M. Akhlaghi, "Computational welding mechanics", Springer, New York, 2005.
- [13] P. Maynier, B. Jungmann, J. Dollet, "Creusot-Loire System for the Prediction of the Mechanical Properties of Low Alloy Steel Products", *Trans. AIME*, 1977: pp. 518–545.
- [14] M.F. Ashby, K.E. Easterling, "A first report on diagrams for grain growth in welds", *Acta Metallurgica*. 30 (1982) 1969–1978.
- [15] C.H. Gür, C. Şimşir, "Simulation of Quenching", in: *Handbook of Thermal Process Modeling of Steels*, CRC Press, Boca Raton - Florida, 2009.

# Application of Multicriteria Decision Making in Selection of Optimal Toolpath

Aleksandra Petrović<sup>1\*</sup>, Slobodan Ivanović<sup>2</sup>, Goran Miodragović<sup>2</sup>, Vladan Grković<sup>1</sup>

<sup>1</sup>Faculty of Mechanical and Civil Engineering in Kraljevo, University of Kragujevac (Serbia)

<sup>2</sup>High Technical Mechanical School Trstenik (Serbia)

*Peripheral pocket or contour milling using flat end milling tool can be performed using different tool paths. Tool path determines radial and axial depth of cut, engagement angle, feed and feed rate profile. Each possible tool path will result with different machining characteristics: cutting force, tool life, process stability, machining time etc. Some of milling process characteristics are conflicting each other which makes difficult for technology designers to choose optimal tool path.*

*This paper presents using multicriteria decision making in selection of optimal tool path. The program for calculating machining elements along the toolpath is developed and applied on one example of pocket machining for 10 different tool paths. Based on obtained machining parameters 10 criteria for selecting optimal tool path are formed. Using basic version of ELECTRE method for choosing optimal tool path, application of multicriteria decision making is shown.*

**Keywords:** Multicriteria decision making, tool path, milling

## 1. INTRODUCTION

Most of mechanical parts consist of faces parallel or normal to a single plane and free form objects which require a 2.5D rough milling operation of the raw work piece [1]. In practice, classical methods of machining in one direction, in both directions and contour parallel milling are still commonly used. Recently, CAM programs developed applications that support HSM machining in terms of application spiral, trochoidal and D tool paths in order to meet high speed machining demands. Using CAM programs for creating tool path, technology designers face some choices which determine the final shape of tool path. They use their experience, knowledge and intuition to choose some of offered options, so that generated tool path still largely depend of individual judgement [2]. Figure 1. shows an example of different tool paths generated with the same CAM program for pocket machining.

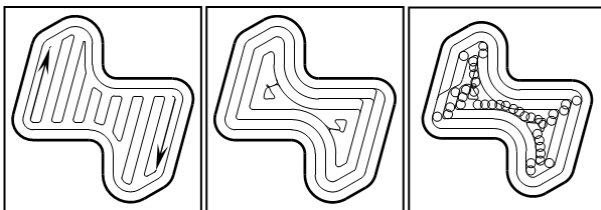


Figure 1. Examples of typical tool paths generated by CAM program

This paper presents approach to choose one of offered tool paths using multicriteria decision making based on calculated elements of machining process.

For given pocket contour, using two CAM programs, 9 toolpaths and corresponding NC programs are generated, and one NC program is manually written. Radial and axial depth of cut along the tool path, feed rate profile, cutting force profile, machining time and tool path length are calculated using developed module for cutting elements monitoring. Based on obtained machining parameters 10 criteria for optimal tool path selection are

established. ELECTRE multicriteria decision making method is used for selection of the best tool path among 10 available tool paths.

## 2. OPTIMIZATION PROBLEM

Tool path is generally generated based on the shape of contour (pocket or island), tool diameter and given stepover so that the workpiece is completely machined. It is usually generated by contour offsetting inward or outward. Tool path determines cutting directions, path curvature, changes in cutting directions and nominal values of axial and radial cutting depth.

Actual radial cutting depth changes along the tool path during cutting direction changes, especially at sharp corners. Engagement angle variations are similar to radial cutting depth, except it depends on shape of machining surface: linear, concave or convex.

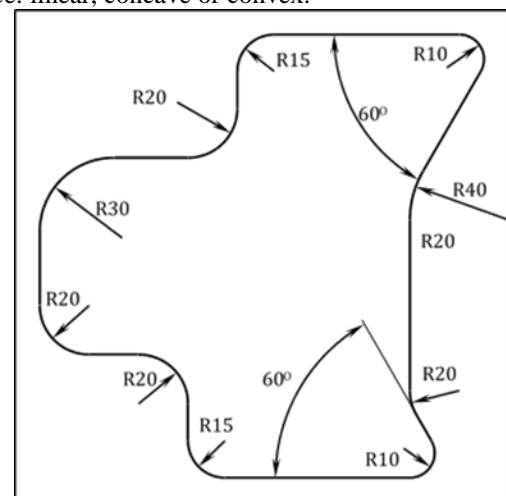


Figure 2. Pocket contour example

It is clear that, as the tool is moving along the tool path, cutter engagement can drastically change, which causes the changes in the cutting loads too.

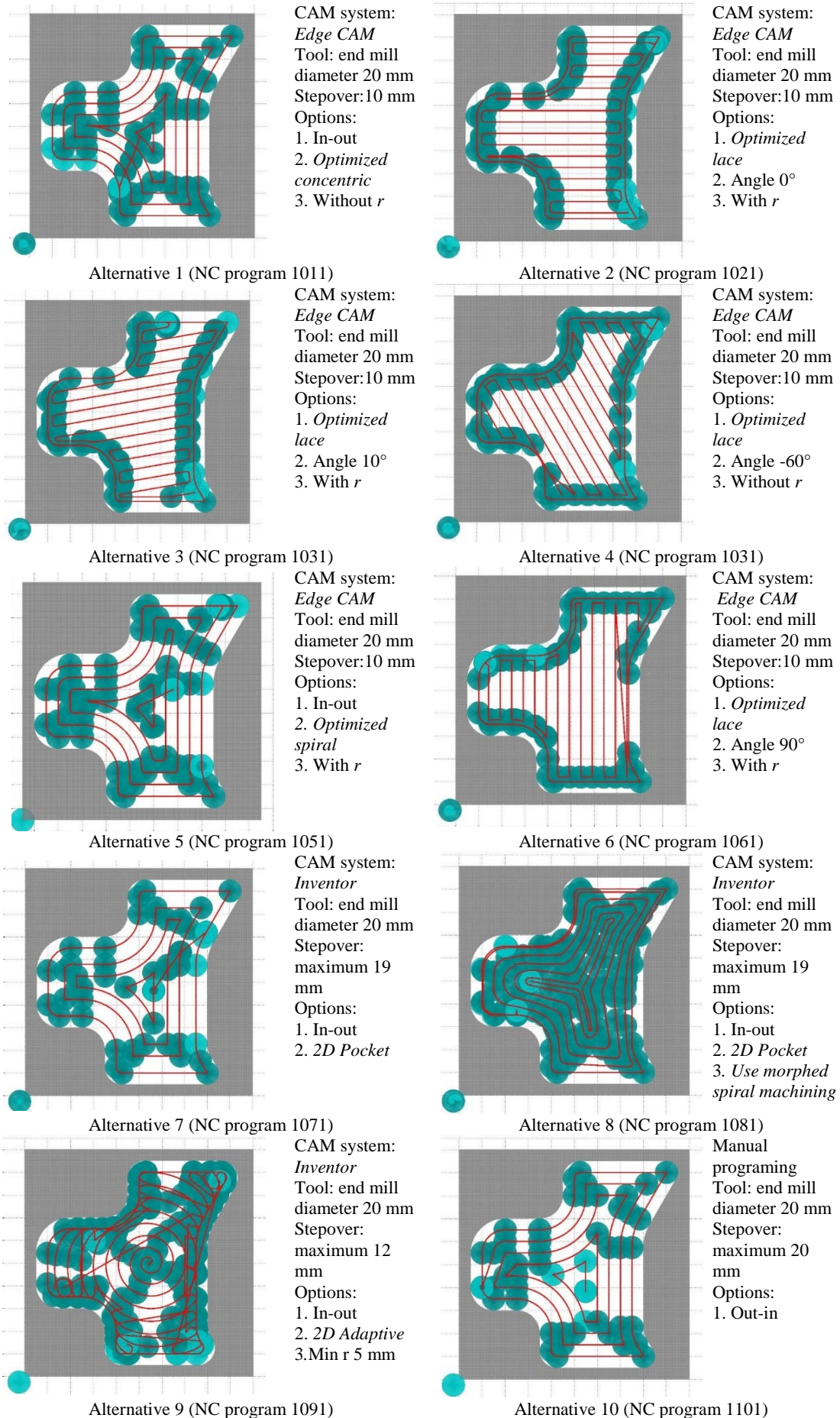


Figure3. 10 alternatives for pocket machining of given contour



A sudden increase in cutter engagement may result in dynamic instability, reduced tool life and even in tool breakage [3]. Therefore approaches to adapt or modify the tool path for achieving a constant load were studied recently ([4],[5],[6]).

Tool path shape determines its total length, too. Axial depth of cut can be changed by tool path when workpiece isn't prismatic or has some holes.

At each change of direction, the velocity has to be lowered to allow for the smooth change of the motion direction of the tool. How much lower, that depends on the angle between the two successive path segments ([7],[8]).

Accordingly, tool path determines axial and radial depth of cut, engagement angle, feed and feed rate profile. Knowledge of the above machining elements along the tool path gives us insight into the adequacy of the generated tool path from different aspects.

For a given pocket contour (Figure 2), we want to choose optimal tool path for milling operation. Using two CAM programs and different options which they offer, 9 tool paths and corresponding NC programs are generated. One program for pocket machining is written using manual programming. Tool paths and options used are presented in Figure 3.

NC code data for each tool path is imported into a database and processed. For each path segment the coordinates of start and end point, interpolation parameters, cutting conditions and geometric characteristics of the tool are obtained. Detailed description of used procedure is given in [9].

For evaluation of toolpaths it is necessary to determine radial and axial depth of cut along the tool path, feed rate profile, cutting force profile, machining time and tool path length.

Required elements of the cutting process can be calculated if, in addition to data contained in generated NC programs, geometric characteristics of blank and geometric and technological characteristics of the tool are defined.

Blank workpiece is imported in Matlab as a bitmap image representing view of blank from above, where each colour corresponds to an appropriate height of the blank, detailed description is given in [10].

Geometrical description of the tool is based on ASCII database in which diameter and shape of tool are

written. Based on tool diameter  $d_t$  and radius  $r_t$ , as well as millimetre net division  $w_{mp}$  matrix of points on cylindrical tool net are calculated [11].

Then, according to the processed data from the NC program, tool path and the cutter location relative to the workpiece are generated at appropriate spatial intervals along a path.

Based on the cross-section of the cutting tool volume and the blank net, it is determined which section of the volume of the tool is in contact with the blank. In order to determine the angle of engagement and cutting depth in selected points of the tool path it is required to monitor section of the cutter half volume in the direction of the tool velocity in a bottom plane of tool, as well as at the axial depth of cut level. It is also necessary to subtract previously removed material from the blank before computation of these elements. Figure 3 shows tool positions at points in which it is changing motion direction.

Based on cross-section of cutting tool and blank network, values of radial depth of cut and cutting engagement angle are calculated at selected points of the tool path and diagrams of their variation along the tool path are generated.

Based on tool motion direction in junction points of tool path, optimal feed rate is determined using model described in [8]. Then the feedrate profile is determined according to model given in [7].

Applying of the linear model of cutting forces [2] and engagement angle and axial depth of cut, the value of the cutting force and its change along the tool path are determined.

Using module for milling parameters determination developed in [12], briefly described above, radial and axial depth of cut, feed rate profile, cutting force, milling type, machining time and tool path length are determined for all 10 tool paths. Obtained data is sorted in Tables 1-4 for purpose of tool path evaluating.

### 3. OPTIMIZATION CRITERIA

Tool path affects multiple characteristics of machining process. Criteria for tool path rating are developed based on: depth of cut, milling type, total tool path length and machining time and cutting force.

Table 1: Distribution of radial depth of cut in percentage

NC program	Radial depth of cut intervals [mm]																			
	0-1	1-2	2-3	3-4	4-5	5-6	6-7	7-8	8-9	9-10	10-11	11-12	12-13	13-14	14-15	15-16	16-17	17-18	18-19	19-20
1011	4.64	1.03	0.73	0.6	0.96	0.58	0.41	0.49	12.01	42.11	5.37	2.86	3.46	2.12	2.84	1.69	1.69	2.24	2.09	12.08
1021	3.99	0.71	1.89	7.95	9.91	2.67	1.45	0.71	0.73	47.79	2.98	1.63	1.45	1.1	0.82	0.81	0.92	1.76	2.67	8.06
1031	1.97	0.17	0.98	8.66	5.46	3.55	3.43	2.3	1.55	26.53	24.92	2.19	1.38	1.13	1.09	1.02	1.38	1.48	1.8	9.01
1041	3.66	0.78	1.26	12.36	6.32	3.06	1.4	1.5	1.24	21.39	28.13	1.44	1.3	1.3	1.34	1.2	1.26	1.36	1.68	8.04
1051	1.1	0.38	0.16	0.41	0.38	0.63	0.52	0.45	14.7	41.36	6.53	3.33	4.01	2.27	2.63	2.93	2.03	2.14	2.81	11.23
1061	2.91	5.09	2.55	8.86	6.47	2.44	2.13	2.68	3.59	2	45.08	1.36	1.12	0.85	0.91	0.7	0.59	0.82	0.96	8.89
1071	4.49	1.01	0.81	0.71	0.66	0.74	1.14	1.04	0.91	10.6	10.93	6.22	3.86	8.88	17.83	3.48	4.31	2.66	3.27	16.44
1081	4.68	3.83	7.05	3.71	6	15.02	15.44	10.53	7.2	4.67	2.2	2.51	2.83	2.69	1.65	1.23	1.05	0.88	0.82	6.01
1091	41.85	1.72	1.17	1.15	1.03	0.92	2.07	1.13	1.03	1.19	1.03	6.75	37.78	0.73	0.31	0.01	0	0.01	0.01	0.11
1101	10.31	2.16	1.72	1.65	1.36	1.94	1.56	1.72	2.61	20.12	14.97	8.93	0.13	0.16	0.11	0.16	0.18	0.18	0.45	29.61

### 3.1. Depth of cut

Radial and axial depth of cut along with spindle speed determine stability lobe diagrams. In selected example, axial depth of cut and spindle speed are constant, therefore process stability estimation is based only on radial depth of cut. For given combination of workpiece and tool it is checked on stability lobe diagram which radial depths of cut ensure stable milling process.

For given example it is assumed: based on stability lobe diagrams it is determined that the process is stable for radial depth of cut below 18 mm; tool life is increasingly shorten for radial depth of cut smaller than 2 mm; preferable radial depth of cut is between 9 and 11 mm.

Criteria based on radial depth of cut are (Table 1):

- K1: Minimum contribution of radial depth of cut  $a < 2$  mm,
- K2: Maximum contribution of radial depth of cut  $9 < a < 11$  mm,
- K3: Minimum contribution of radial depth of cut  $a > 18$  mm.

### 3.2. Type of milling

In down milling (or climb milling) the cutting chips are carried downward by the tool. Rough machining can be performed faster because cutting forces are lighter and the thick-to-thin chip profile carries the heat away on the chip. Tool wear in down milling is less compare to the up milling, due to the cutter rotate with the feed and therefore tool life is longer. The cutting chips fall down behind the tool which gives better surface finish.

Following criteria based on milling type are adopted (Table 2):

- K4: Minimum contribution of combined milling,
- K5: Minimum contribution of up milling,
- K6: Minimum contribution of idle time.

In high speed machining, too small radial depth of cut causes excessive heating in shearing zone shortening the tool life. Also, small part of tool diameter engaged in machining process leads to tool deflection.

It is preferable that radial depth of cut corresponds to the given stepover which is previously determined as optimal value for given combination of workpiece and tool.

Table 2: Contribution of milling type in total tool path in percentage

NC program	Up milling	Down milling	Combined milling	Idle time
1011	0	61.78	37.28	0.94
1021	27.6	48.76	22.83	0.81
1031	15.16	37.8	46.08	0.96
1041	13.13	37.35	48.64	0.88
1051	0.02	58.87	40.62	0.49
1061	7.36	30.58	61.85	0.21
1071	0	19.99	78.72	1.29
1081	0	76.54	22.4	1.06
1091	0	17.73	47.15	35.12
1101	1.11	31.72	61.57	5.59

### 3.3. Total tool path length and machining time

For a long time total tool path length is used as basis criterion for tool path evaluation. With high speed machining development and inclusion of machining dynamics, total machining time become more significant indicator of machining process speed.

Based on tool path length and machining time (Table 3), the following criteria are adopted:

- K7: Minimum total tool path length and
- K8: Minimum total machining time.

Table 3: Tool path and machining time

NC program	Total		Rapid		With feed rate		Machining	
	Tool path length [mm]	Time [min]	Tool path length [mm]	Time [min]	Tool path length [mm]	Time [min]	Tool path length [mm]	Time [min]
1011	2024.32	3.143	148.77	0.00297	1875.54	3.140	1858.54	3.110
1021	2341.74	3.628	168.32	0.00336	2173.41	3.624	2156.41	3.595
1031	2257.13	3.491	167.32	0.00334	2089.80	3.488	2070.71	3.455
1041	2279.22	3.662	94.86	0.00189	2184.36	3.660	2167.36	3.631
1051	2016.93	3.019	209.86	0.00419	1807.07	3.014	1798.21	2.998
1061	2555.01	3.848	258.74	0.00517	2296.26	3.843	2292.06	3.835
1071	1752.79	2.665	161.08	0.00322	1591.71	2.662	1572.27	2.629
1081	2837.97	4.518	132.05	0.00264	2705.92	4.516	2677.77	4.467
1091	3550.25	4.782	244.66	0.00489	3305.58	4.777	2101.67	3.506
1101	1904.48	3.026	96.6	0.00193	1807.88	3.024	1708.61	2.851

### 3.4. Cutting force

With increase of cutting force, tool wear is increasing and tool life is shortening. Cutting force variations affect stability of milling process as well. The goal is to reduce mean value of cutting force as well as cutting force deviation.

Based on cutting force (Table 4), the following criteria are adopted:

- K9: Minimum cutting force for when feed rate is used,
  - K10: Minimum deviation of cutting force
- Using multicriteria decision making the optimal tool path can be selected for defined criteria.

Table 4: Mean value of cutting force  $F_{sr}$  and mean absolute deviation of cutting force  $F_{od}$

NC program	$F_{sr}$ (with feed rate) [N]	$F_{od}$ (with feed rate) [N]	$F_{sr}$ (machining) [N]	$F_{od}$ (machining) [N]
1011	591.047	83.713	596.659	75.31
1021	425.71	169.519	429.168	168.19
1031	443.644	166.811	447.937	164.796
1041	431.934	168.354	435.767	166.76
1051	605.364	61.183	608.341	56.751
1061	432.163	154.262	433.069	153.901
1071	597.825	86.212	605.66	73.391
1081	369.46	182.693	373.371	180.805
1091	355.526	287.178	547.516	149.488
1101	511.285	188.942	541.218	155.999

4. MULTICRITERIA DECISION MAKING

Multiple-criteria decision-making (MCDM) is a procedure that combines the performance of decision alternatives across several, contradicting, qualitative and/or quantitative criteria and results in a compromise solution [13]. A typical MCDM problem can be defined as a ranking aid to arrange a finite number of decision alternatives, each of which is clearly described in terms of different characteristics. These characteristics are also often called attributes or decision criteria [14].

In this paper ELECTRE I method is used for selecting optimal tool path, since it is found to be best suited for selection problems.

4.1. ELECTRE method

The ELECTRE (Elimination and Choice Translating algorithm) family was introduced by Benayoun, Roy and Sussman in 1968. The method was later developed by Bernard Roy. This family includes ELECTRE I, II, III, IV, IS and TRI methods [14].

The basic concept of the ELECTRE method is to deal with "outranking relations" by using pairwise comparisons among alternatives under each one of the criteria separately. The organization of the ELECTRE method is best illustrated in the following steps [15]:

- *Normalizing the Decision Matrix:* This procedure transforms various units in the decision matrix into dimensionless comparable units.
- *Weighting the Normalized Decision Matrix:* The column of the matrix is then multiplied by its associated weights which were assigned to the criteria by the decision maker.
- *Determine the Concordance and Discordance Sets:* The concordance set of two alternatives is defined as the set of all criteria for which one alternative is preferred to other. The complementary subset is called the discordance set.
- *Construct the Concordance and Discordance Matrices:* The relative value of the elements in the concordance matrix is calculated by means of the concordance index. The concordance index is the sum of the weights associated with the criteria contained in the concordance set. The concordance index indicates the relative importance of one alternative with respect to other alternative.
- *Determine the Concordance and Discordance Dominance Matrices:* The concordance dominance matrix is constructed by means of a threshold value for the concordance index.
- *Determine the Aggregate Dominance Matrix.*
- *Eliminate the Less Favorable Alternatives.*

4.2. Application of ELECTRE I method in selecting optimal tool path

Based on criteria defined in section 3 decision matrix is formed (Figure 4).

According to steps briefly described in previous subsection (detailed description of steps given in [15]), program for ELECTRE application is created [12].

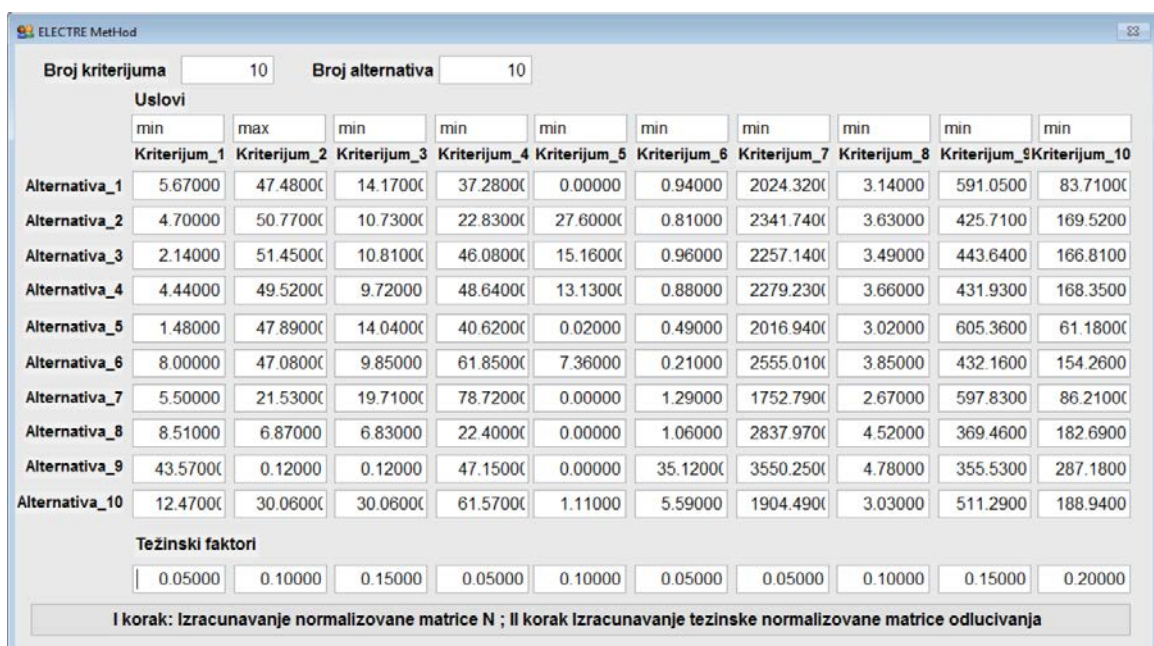


Figure 4. Decision matrix

Final result is that Alternative 5 (NC program 1051) absolutely dominates over other alternatives.

Using individually criteria following results are obtained:

- According to criteria K1- alternative 5,
- According to criteria K2- alternative 2,
- According to criteria K3- alternative 9,
- According to criteria K4- alternative 8,
- According to criteria K5- alternatives 1, 7, 8 and 9,
- According to criteria K6- alternative 6,
- According to criteria K7- alternative 7,
- According to criteria K8- alternative 7,
- According to criteria K9- alternative 9 and
- According to criteria K10- alternative 5.

It is clear that for solving problem of selecting optimal tool path, using multicriteria decision making gives more comprehensive solution.

## 5. CONCLUSION

In this paper, application of multicriteria decision making is presented on example of selecting optimal tool path for pocket milling.

CAM software offer multiple options for generation of tool path, in addition using same options in different software will result with different tool paths. Therefore, final decision depends largely on technology designer's experience.

Using module for milling parameters determination developed in [12], data necessary for tool path evaluating is obtained for 10 different tool paths for pocket milling of given contour. Several criteria for tool path rating are established. ELECTRE multicriteria decision making method is implemented, which result in selection of Alternative 5 as optimal tool path.

Presented approach helps technology designers in choosing options for NC program generation.

Some other criteria are to be added in future work, such as maximum productivity and its minimum variation along the tool path.

## ACKNOWLEDGEMENTS

The authors would like to express their gratitude to the Ministry of Education and Science of the Republic of Serbia for their support to this research through the project TR37020.

## REFERENCES

- [1] Sandeep DHANIK, "NC Tool Path Evaluator and Generator for High Speed Milling," vol. 4533. ÉCOLE POLYTECHNIQUE FÉDÉRALE DE LAUSANNE, Lausanne, Switzerland, p. 201, 2009.
- [2] A. Petrović, S. Ivanović, and L. Lukić, "NC Tool Path and Its Influence on Cutting Force in Peripheral Milling Analyses," *IMK -14-- Res. Dev. Heavy Mach.*, vol. 21, pp. 41–46, 2015.
- [3] S. K. Gupta, S. K. Saini, B. W. Spranklin, and Z. Yao, "Geometric algorithms for computing cutter engagement functions in 2.5D milling operations," *Comput. Des.*, vol. 37, no. 14, pp. 1469–1480, Dec. 2005.
- [4] M. S. Uddin, S. Ibaraki, A. Matsubara, S. Nishida, and Y. Kakino, "A Tool Path Modification Approach to Cutting Engagement Regulation for the Improvement of Machining Accuracy in 2D Milling With a Straight End Mill," *J. Manuf. Sci. Eng.*, vol. 129, no. 6, p. 1069, Dec. 2007.
- [5] H. Wang, P. Jang, and J. A. Stori, "A Metric-Based Approach to Two-Dimensional (2D) Tool-Path Optimization for High-Speed Machining," *J. Manuf. Sci. Eng.*, vol. 127, no. 1, p. 33, Feb. 2005.
- [6] J. . Stori and P. . Wright, "Constant engagement tool path generation for convex geometries," *J. Manuf. Syst.*, vol. 19, no. 3, pp. 172–184, Jan. 2000.
- [7] N. Nestic, "Modeling and Simulation of Energy Efficient Milling Process Plans for Prismatic Parts," ÉCOLE POLYTECHNIQUE FÉDÉRALE DE LAUSANNE, 2012.
- [8] B. H. Kim and B. K. Choi, "Machining efficiency comparison direction-parallel tool path with contour-parallel tool path," *Comput. Des.*, vol. 34, no. 2, pp. 89–95, Feb. 2002.
- [9] A. Petrović, S. Ivanović, and L. Lukić, "Generating Parametres from the NC Code Needed for Defining the Optimal Tool Path," in *MMA 2015 - FLEXIBLE TECHNOLOGIES*, 2015, pp. 157–160.
- [10] S. Ivanović, A. Petrović, and L. Lukić, "Matrix blank description as part of module for machining parameters generation along the tool path for peripheral milling," *IMK-14 – Res. Dev. Heavy Mach.*, vol. 21, no. 4, pp. EN119–124, 2015.
- [11] Petrovic A, Lukic Lj, Ivanovic S, Pavlovic A, „Optimisation of tool path for wood machining on CNC machines“, Proceedings of the Institution of Mechanical Engineers, Part C: Journal of Mechanical Engineering Science, (2016)
- [12] A. Petrović, "Optimizacija putanje glodala pri konturnoj obradi velikim brzinama rezanja", PhD Thesis, University of Kragujevac, Serbia, 2016.
- [13] A. Dadda, I. Ouhbi, "A decision support system for renewable energy plant projects", In Proceedings of the 2014 Fifth International Conference on Next Generation Networks and Services (NGNS), Casablanca, Morocco, 28–30 May 2014.
- [14] Mary, S. and Suganya, G. (2016) Multi-Criteria Decision Making Using ELECTRE. *Circuits and Systems*, 7, 1008-1020.
- [15] E. Triantaphyllou, B. Shu, S. Nieto Sanchez, and T. Ray, "Multi-Criteria Decision Making: An Operations Research Approach" Encyclopedia of Electrical and Electronics Engineering, John Wiley & Sons, New York, NY, Vol. 15, pp. 175-186, (1998).

# Electrode Investigation at Plasma Cutting

Bogdan Nedić<sup>1\*</sup>, Marko Janković<sup>2</sup>, Ivan Peko<sup>3</sup>

<sup>1</sup>Faculty of engineering University of Kragujevac, Kragujevac (Serbia)

<sup>2</sup>Yugoimort SDPR, Belgrade (Serbia)

<sup>3</sup> University of Split, Faculty of Electrical Engineering, Mechanical Engineering and Naval Architecture, Split (Croatia)

*This paper analyzes electrode at plasma cutting. Importance of the electrodes at plasma process is showed. Analyzed influence factor of electrode wear. In the second part of the document is presented experimental research. Samples of 15 mm thickness steel plate were cutting with different levels of electrode wear and with different traverse rate. The levels of electrode wear, was defined with the number of piercing and cutting length. Visually analysis of samples showed that surface quality, obtained using the worn electrode, can not improve by changing the traverse rates. The quality can be the same or the worst.*

**Keywords:** electrode, plasma torch, consumable elements, number of pierces, cut duration, surface quality

## 1. INTRODUCTION

Plasma jet cutting process was developed at the end of 1950s [1]. Plasma can be defined as the fourth state of substance which is obtained by supplying a tremendous amount of energy to gas or when a gas is subjected to a high electric field. In this process an electric arc is generated between the electrode and the workpiece. An electrode acts as an anode and the workpiece as a cathode. The plasma gas expands with the high velocity through the nozzle at the same time an electric current passes through the gas with the help of a tungsten electrode due to which a high intensity plasma jet is generated. This jet is able to melt or vaporize the plate surface that should be cut and to blow the molten metal away from the cut. The most commonly used gases for this process are compressed air, nitrogen, argon-hydrogen, oxygen and their combinations. They can be used both as a plasma and shield gases.

Main components of plasma jet cutting system are power supply unit, an arc starting circuit and a torch. In order to obtain good quality at plasma cutting, it is very important to well know each of these components.

In this paper will be analyzed electrode, which is the part of plasma torch. Theoretical consideration will be presented. In the second part of paper is presented experiment. The aim of the experiment was to exam the influence of piercing and cutting length on the electrode. Also aim is try to reduce negative effects of worn electrodes on surface quality by changing the cutting speed.

## 2. ELECTRODE

The first torches were squared-off, clunky hunks of plastic [2]. These torches did the trick, but as plasma cutting and gouging evolved, it became clear torches needed to evolve as well to withstand harsher conditions and meet a wider variety of needs. After all, the torch that cuts perfect parts on a CNC table is not necessarily the torch that works well in a 3-D cutting application. For hand cutting, a torch used to cut a flat piece of steel does not necessarily work for someone trying to gouge out a weld on the pipeline.

Engineers quickly realized the solution was to remove the starting mechanism from the torch and build it into the electrode. It was not easy, but after much work, engineers figured out a way to get rid of the plunger inside the torch body and replace it with a blowback spring on the back end of the electrode. This technology opened up all sorts of possibilities for torch design as engineers were no longer limited to a certain size or shape.

As a result, many different torch styles are available today: short, long, angled, straight. They are made for both hand-held and mechanized cutting and gouging, as well as robotic cutting.

Plasma cutting torches operate at extremely high temperatures, and various parts of the torch must be considered to be consumable.

Electrodes for high power plasma cutting systems are highly engineered consumable parts, similar in design, material, and function to an automotive spark plug. Electrodes emit high voltage electricity in a very hot environment, and they are the hardest working part in the system.



Fig. 1 Torch Hypertherm 260A [3]

It is important to establish correlation between the electrode and influencing factors on the electrode wear. In this area there are manufacturers recommendations of plasma torch which is mainly confined to the time period of replacing electrode as well as advice how to extend the life of electrode.

In a properly functioning system and quality cut plasma cutting, three key factors affect on electrode life [4, 5]:

\*Prof. dr Bogdan Nedic, Faculty of engineering University of Kragujevac, nedic@kg.ac.rs

1. **Number of pierces** – Stresses to the electrode during arc initiation and termination cause hafnium erosion.

2. **Cut duration** – Heat stress developed during long cuts erodes the hafnium.

3. **Material thickness** – Thick materials require higher output current, which causes more rapid hafnium erosion. In addition, thick materials take longer to pierce, causing increased nozzle and electrode wear.

Over the years plasma cutting technology has introduced numerous advances to mitigate these wear factors. Manufacturers improved and controlled many of the processes and parameters during plasma cutting, but electrode wear could not be avoided, but it is reduced and more controlled.

So in try to extend the life of the electrode and to improve surface quality by the concrete problems, thickness of the material can not be change, so the solution must be sought in number of pierces and cut thickness.

Researchers [6] published that the consumption of electrodes depends more strongly on the number of arc starts than on arc-on time. That mens that on pierces should be given more attention and analysis

### 3. EXPERIMENTAL EXAMINATION AND DISCUSSION

Based on theory it is clear that the electrode wear affects on the surface quality, which also can be seen from previously conducted experiments. In this experiment, were used electrodes with different wear levels. The levels of electrode wear, was defined with the number of piercing and cutting length.

Table 1 Levels of electrode wear

Level of electrode wear	Number of pierces	Cutting length (mm)
The first - I	110	24 000
The second - II	215	48000
Thr third - III	320	74000

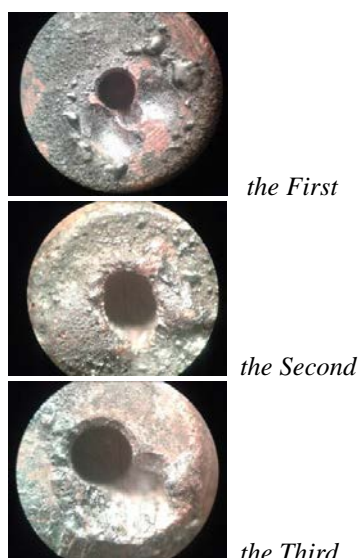


Fig. 2 Level of electrode wear

Visually cen see that electrode with second and third level of electrode wear are more damaged from the

electrode with the first level of wear, which is logical since they have a larger number of piercing as well as cutting length.

The cuts were performed on CNC machine STEELTAILOR, used 15 mm thickness steel plate material for creating 9 cuts. Parameters plasma cut process: nozzle diameter 1.2 mm, gas pressure 6 bar, cutting height 5 mm.

Traverse rate was chosen taking in account the tablet values for cutting operations of this kind that can be found in the technical literature and 20% bigger and 20 % less. Other process parameters such as gas flow, distance from the work piece were constant for the observer level of electrode wear. Used current was 60 A. The quality of samples will be visually analyzed.

Table 2 Parameters of samples for analysis

Sample number	Level of electrode wear	Traverse rate mm/min
1	I	530
2	I	425
3	I	635
4	II	530
5	II	425
6	II	636
7	III	530
8	III	425
9	III	635



Fig. 3 Cutting with the First level of electrode wear and 530 mm/min (sample 1)



Fig. 4 Cutting with the First level of electrode wear and 425 mm/min (sample 2)

Surface quality of sample 1 can be described as very bad. The cut has unacceptable deviation from the predicted geometry and there are deposits of waste material at the bottom of the plate. So the First level of electrode wear and tablet traverse rate value can not be used for pieces less tolerance of  $\pm 5$ mm. With reducing

traverse rate by 20% the surface quality is even worse, while increase by 20% does not change the surface quality.



Fig. 5 Cutting with the First level of electrode wear and 635 mm/min (sample 3)



Fig. 6 Cutting with the Second level of electrode wear and 530 mm/min (sample 4)



Fig. 7 Cutting with the Second level of electrode wear and 425 mm/min (sample 5)



Fig. 8 Cutting with the Second level of electrode wear and 635 mm/min (sample 6)

Surface quality of sample 4 can be described as worse than then cutting with the First level of electrode wear. The cut has unacceptable deviation from the predicted geometry and there are deposits of waste material at the bottom of the plate. The upper side of the cut is larger than anticipated, and the lower is narrower. Axis from the upper and lower sides of the cut do not match. Reducing trvaverse rate by 20% does not change

the surface quality. With increase traverse rate by 20% the surface quality is even worse.



Fig. 9 Cutting with the Third level of electrode wear and 530 mm/min (sample 7)

Surface quality of sample 7 can be described as amazing good. There is a small amount of waste material from the bottom side and one side of the cut have a small tilting. Cause of such good result can be considered by presence of influence factors, unaffected by the operator, and some of them are variations of current, variations of air quality, variations in air pressure, etc... These factors may have an impact improvements, as well as the deterioration of the surface quality. These effects are never able to completely avoid, but it is possible to reduce them on minimal level. This can be done with the maximum quality of compressed air, pneumatic and electrical installations.



Fig. 10 Cutting with the Third level of electrode wear and 425 mm/min (sample 8)



Fig. 11 Cutting with the Third level of electrode wear and 635 mm/min (sample 9)

Reducing traverse rate by 20% does not change the surface quality. Increase traverse rate by 20% (sample 9) the surface quality is very very bad. The geometry and the direction of the cut are unacceptable, and this combination was not even able to get through the entire length of the cut material. When using the Third level of

electrode wear, the quality is unstable and these electrode should not be used

#### 4. CONCLUSION

This document analyzes the electrodes, as well as its impact on the surface quality. Has been shown that the number of pierces and cutting length affect on electrodes condition and therefore affect on surface quality.

As a conclusion of considered analysis, can said that all electrode with more than 110 pierces and 24000 mm section are not adequate for cutting 15 mm thickness steel plate. Surface quality, obtained by using the worn electrode, can not improve by changing the cutting speed. The quality can be the same or the worst.

Therefore, on electrode should be paid great attention.

#### ACKNOWLEDGEMENTS

This paper is part of project TR35034 The research of modern non-conventional technologies application in manufacturing companies with the aim of increase efficiency of use, product quality, reduce of costs and save energy and materials, funded by the Ministry of Education, Science and Technological Development of Republic of Serbia.

#### REFERENCES

- [1] Peko I., Nedić B, Đorđević A, Džunić D, Janković M., Veža I. (2016). Modeling of Surface Roughness in Plasma Jet Cutting Process of Thick Structural Steel. *Tribology in Industry*, Vol. 38, no. 4, p. 522-529.
- [2] MIichelle Avlia. Plasma cutting torches: the long and short of it from, <http://www.thefabricator.com/article/plasmacutting/plasma-cutting-torches-the-long-and-short-of-it>, accessed on 04.03.2017.
- [3] Ljubisa Popovic (2013). Plasma process of cutting material. Final work at Faculty of Engineering University of Kragujevac, Serbia.
- [4] Nedić B., Janković M, Radovanović M., Globočki G. (2013). An investigation of quality in plasma cutting. *11TH International conference on accomplishments in electrical and mechanical engineering and information technology DEMI 2013*, p. 275-282.
- [5] Optimizing consumable life in mechanized plasma cutting from, <http://www.thefabricator.com/article/plasmacutting/optimizing-consumable-life-in-mechanized-plasma-cutting>, accessed on 15.03.2017.
- [6] Y. Yamaguchi, K. Yoshida, Y. Uesugi, Y. Tanaka, S. Morimoto, M. Minonishi, K. Saio (2012) Experimental study of consumption of hafnium electrode in oxygen plasma arc cutting. *Welding in the world- Springer Science+Business Media*, p. 72-81.



# Analytical Analysis of Drilling-Associated Damage in Composites

Navid Zarif Karimi<sup>1</sup>, Giangiacomo Minak<sup>1\*</sup>

<sup>1</sup>DIN, Alma Mater Studiorum – Università di Bologna, Forlì (Italy)

*Drilling of composite materials is a very common and an important process used in industry to perform the assembly of automotive composite structures. However, during the drilling of composite materials many problems arise, among which delamination is considered as the most prevalent life limiting damage growth mode. Drilling-induced delamination is directly related to the component of cutting force along the drill axis which greatly depends on the feed rate. In this paper, analytical models were developed to predict critical axial load and feed rate necessary to propagate the delamination. The analysis conducted is based on linear elastic fracture mechanics, classical plate bending theory and mechanics of oblique cutting. The models can be used to maximize productivity in free-delamination drilling.*

**Keywords:** Composite laminates, Drilling, Analytical modeling, Delamination, Thrust force, Feed rate

## 1. INTRODUCTION

The importance of composite materials has been growing over the last thirty years. These materials have a variety of unique properties, including light weight, high value of stiffness, excellent corrosion resistance and high specific strength. Due to these distinctive properties, they have been widely used in many different applications, such as automobile, and sport goods. With the growing usage of composites in different industrial applications, there is a strong need to understand the issues associated with the manufacture of composite components. The existing manufacturing technique of fabricating to near-net shape is incomplete unless the component is subjected to secondary machining operations like trimming, finish grinding, and drilling holes based on the requirement [1, 2].

Hole making operations like drilling are frequently needed in composite structures, as the use of bolts, rivets or screws is required to join the parts. But, drilling is quite difficult and challenging due to high tendency of composite laminates to delamination [3]. Delamination is the most common damage mechanisms in laminated composites. This type of damage is caused by the low interlaminar strength of the composite plate and high transverse cutting forces. Two important mechanisms of delamination were 'Peel-up' at the drill entry and 'push-down' at the exit side of the laminate, as shown in Figure 1. Peel-up happens as the drill bit enters the composite plate. After the cutting edge of the drill comes into contact with the laminate, the cutting force acting in the peripheral direction is the driving force for delamination. It produces a peeling force in the axial direction through the slope of the drill flute resulting in separation of the layers from each other at the top, forming a delamination zone. The peeling force varies with tool geometry and friction between the tool and the workpiece. Push-out is the delamination mechanism happening as the drill bit reaches the back side, exit side, of the plate, where the uncut thickness is smaller and resistance to flexural deformation decreases. At some point, the load goes beyond the interlaminar bond strength and delamination happens. A different drill geometry and cutting conditions can prevent delamination propagation by means of reducing the cutting forces. In practice, it has been

shown that the delamination associated with push-out is more severe than that associated with peel-up [4-7].

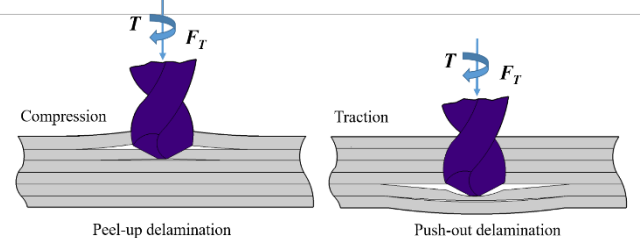


Figure 1: Two mechanisms of delamination in drilling process.

It has been shown that delamination at the hole exit, push-out, is directly related to the component of cutting force along the drill axis known as thrust force [8-10]. The study of thrust force is thus interesting in order to reduce delamination. Several authors have developed models in order to predict the critical thrust force for delamination propagation. The first analytical model was formulated by Hocheng and Dharan [11] based on linear elastic fracture mechanics. The isotropic behavior and pure bending of the laminate are assumed in their model. Single circular delamination located at the mid-plane is assumed in their model as shown schematically in Figure 2.

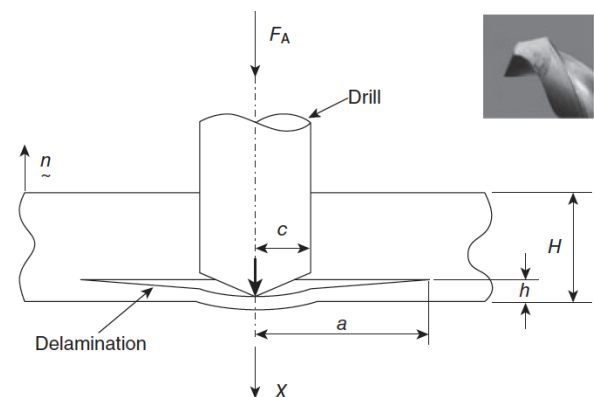


Figure 2: Circular plate model for delamination analysis (twist drill) [1].

\* Giangiacomo Minak: via Fontanelle 40, 47121 Forlì, Italy; email: giangiacomo.minak@unibo.it

**Nomenclature**

$\varepsilon$	drill point angle	$F_h$	projection of force on drill axis
$i$	inclination angle	$F_{hu}$	horizontal force
$\psi$	helix angle	$F_{vu}$	vertical force
$\varphi$	chisel edge angle	$T$	total thrust force
$\gamma$	rake angle	$T_L$	thrust force on cutting lips
$\gamma_s$	static portion of rake angle	$T_C$	thrust force on chisel edge
$\gamma_d$	dynamic portion of rake angle	$T_{exp}$	Experimental thrust force
$\gamma_m$	average rake angle	$a$	crack radius
$\gamma_c$	chisel edge rake angle	$w$	deflection of plate
$r_c$	chisel edge radius	$A$	delamination area
$R$	drill radius	$D$	flexural rigidity
$\rho$	normalized radius	$D'$	equivalent flexural rigidity
$t_c$	half the thickness of the chisel edge	$U_d$	Strain energy absorbed by crack growth
$t$	cutting depth	$U$	stored strain energy
$f$	feed rate	$W$	work done
$G$	Geometrical parameter	$G_{IC}$	critical strain energy release rate in mode I
$K_n$	specific energy for vertical force		
$K_{n,chisel}$	specific energy at chisel edge		

Based on these assumptions, they determined the threshold load known as critical thrust force  $F_{cr}$  leading to the onset of delamination as follows:

$$F_{cr} = \pi \sqrt{32G_{IC}M} \quad (1)$$

$$= \pi \sqrt{\frac{8G_{IC}Eh^3}{3(1-\nu^2)}}$$

Where  $M = \frac{Eh}{12(1-\nu^2)}$  is the stiffness per unit width of the fiber reinforced material,  $E$  is Young's Modulus and  $\nu$  is Poisson's ratio for the material. To avoid drilling-induced delamination, the applied thrust force should not exceed this threshold value, which is a function of the material properties and the uncut thickness.

Jain and Yang [12, 13] developed this model, considering the anisotropy of the material and hypothesizing that the cracks are elliptical. In their model, the drilling thrust force is simplified by a representative single concentrated central load. Lachaud *et al.* [14] determined critical axial force for two cases, concentrated and uniformly distributed, considering an embedded small-diameter circular plate and non-propagated cracks. Hocheng and Tsao [15, 16] extended this model, taking into consideration a series of loading types for various drill types.

The main parameter which influences the value of the thrust force in drilling is feed rate [14, 17, 18]. Several analytical models were developed to relate the drilling thrust force with feed rate based on mechanics of orthogonal and oblique cutting. Relating thrust force with feed rate is important because feed rate can be directly controlled. One of the most accurate published cutting force prediction models for drilling composite is presented by Langella *et al.* [19]. They used the orthogonal cutting model suggested by Caprino *et al.* [20, 21] as a basis by observing that during a drilling process the prerequisites for orthogonal cutting are met for an infinitesimal instant.

In the present study, an orthotropic analytical model is developed to predict the critical thrust force based on linear elastic fracture mechanics, classical plate bending

theory and energy conservation. Furthermore, this critical force is used in the cutting force model presented by Langella to determine the critical feed rate at the onset of delamination.

## 2. MECHANICS OF OBLIQUE CUTTING

Most of the studies on drilling composites have adopted the empirical approach which is very useful in observing the effect of process parameters. However, theoretical studies are needed to understand the physics of composite drilling. From an analytical point of view, the different machining processes may be classified into two categories, namely orthogonal cutting processes and oblique cutting processes. In the orthogonal cutting, the tool approaches the workpiece with its cutting edge parallel to the uncut surface and at right angles to the direction of cutting. Thus, tool approach angle and cutting edge inclination are zero. This type of cutting is also known as two-dimensional cutting. In many cases, orthogonal cutting is assumed for simplifications reasons. Caprino *et al.* [20, 21] conducted a series of experiments on orthogonal cutting of fiberglass composites to find an analytical model for cutting forces as shown below:

$$F_{hu} = 4.29 + 257.804 \times 10^{-0.019\gamma} t \quad (1.a)$$

$$F_{vu} = 95.3 \times 10^{-0.02\gamma} t^{0.5} \quad (1.b)$$

Where  $F_{hu}$  and  $F_{vu}$  are, respectively, the horizontal and vertical forces per unit of width of the tool,  $\gamma$  is the rake angle and  $t$  is the cutting depth, as shown in Figure 3.

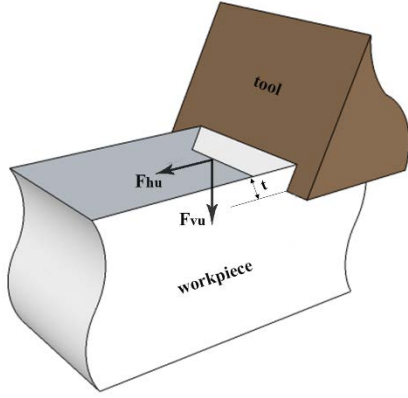


Figure 3: Cutting forces in orthogonal cutting process.

Caprino's model is only valid for orthogonal cutting which limits its application for the drilling process, which is three-dimensional and oblique. In the oblique cutting, the cutting edge of the tool is inclined at an acute angle with the direction of tool feed, the chip begins disposed of at a certain angle. This type of cutting is called three-dimensional cutting. Oblique cutting is more difficult to analyze and few attempts have been made to understand the mechanics of oblique cutting. Even so, as reported in [19], it is possible to extend the scope of this model as follows:

$$F_{hu} = A + B \times 10^{-0.019\gamma} t \quad (2.a)$$

$$F_{vu} = B \times 10^{-0.02\gamma} t^{0.5} \quad (2.b)$$

Where  $A$ ,  $B$ ,  $a$ , and  $b$  are the constant coefficients depending on the drilling conditions. Langella [19] showed that if the value of the rake angle is in radian, then  $a = b = 1.089$ .

To use these formulas for the drilling process, the cutting depth  $t$  which is a function of feed rate  $f$  and drill point angle  $\varepsilon$  should be calculated. Owing to the fact that the drill point angle  $\varepsilon$  and inclination angle  $i$  change along the cutting lips of the drill, an integration along the whole length of the cutting lips is needed to obtain the total cutting forces.

Figure 4 shows a schematic of a standard twist drill geometry. In this figure,  $R$  is the drill radius,  $r_c$  is the chisel edge radius,  $t_c$  is the half the thickness of the chisel edge,  $\psi$  is the helix angle and  $\varepsilon$  is the drill point angle. The elementary area  $dA$  is equal to the product  $dx(f/2)$ , where  $f$  is the feed rate and  $f/2$  is the cutting depth as there are two cutting lips. From geometry, one can derive:

$$dx = dr \cos i(\rho) = R d\rho \cos i(\rho) \quad (3)$$

where  $\rho$  is the normalized radius ( $\rho = r/R$ ) and  $i$  is inclination angle that varies depending on the radius along the cutting lip of the drill ( $\rho$ ).

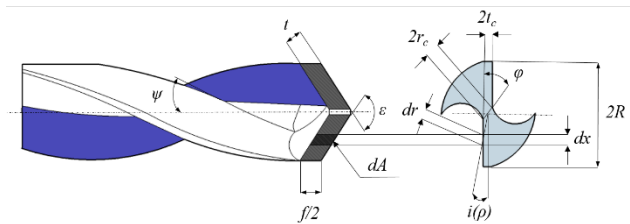


Figure 4: The nomenclature of the standard twist drill features.

Based on drill geometry;

$$t_c = \frac{r}{\sin(\frac{\varepsilon}{2})} \sin i(\rho) \quad (4)$$

$$i(\rho) = \sin^{-1} \left( \frac{t_c}{\rho} \sin(\varepsilon/2) \right) \quad (5)$$

To calculate  $\cos i(\rho)$  approximately,

$$\begin{aligned} \cos i(\rho) &= \sqrt{1 - \sin^2 i(\rho)} = \sqrt{1 - \frac{t_c^2 \sin^2(\varepsilon/2)}{\rho^2 R^2}} \approx \quad (6) \\ &\approx 1 - \frac{t_c^2 \sin^2(\varepsilon/2)}{2\rho^2 R^2} \end{aligned}$$

and, therefore:

$$dx = \left( 1 - \frac{t_c^2 \sin^2(\varepsilon/2)}{2\rho^2 R^2} \right) R d\rho \quad (7)$$

In order to calculate the total thrust force applied on cutting lips, ignoring the chisel edge section, the projection of force  $F_h$  on drill axis is integrated along the cutting lips. By substituting the values of  $t$  and  $dx$  shown in Figure 3, we can derive:

$$T_L = 2 \int_{\tau}^1 \dots \quad (8)$$

$$B \times 10^{-10.089\gamma} \left( \frac{f}{2} \right)^{\frac{1}{2}} \left( 1 - \frac{t_c^2 \sin^2(\frac{\varepsilon}{2})}{2\rho^2 R^2} \right) R \sin \left( \frac{\varepsilon}{2} \right) d\rho$$

Where the limits of integration are:

$$\text{lower: } \tau = \frac{r_c}{R} = \frac{t_c / \sin \varphi}{R} \quad (9)$$

$$\text{upper: } \frac{R}{R} = 1 \quad (10)$$

Where  $\varphi$  is the chisel edge angle. In Eq. (8) the rake angle  $\gamma$  is the sum of static  $\gamma_s$  and dynamic  $\gamma_d$  sections which vary depending on the radius ( $\rho$ ).

$$\gamma = \gamma_s + \gamma_d = \quad (11)$$

$$= \tan^{-1} \left( \frac{\rho \tan \psi}{\sin(\varepsilon/2)} \right)$$

To simplify integration, an average value of the rake angle  $\gamma_m$  is defined as below:

$$\gamma_m = \frac{\int_{\tau}^1 (\tan^{-1}(\frac{\rho \tan \psi}{\sin(\varepsilon/2)}) + \tan^{-1}(\frac{f}{2\rho R})) d\rho}{\int_{\tau}^1 d\rho} \quad (12)$$

Finally, after simplification, the resulting adjusted thrust force exerted on the cutting lips will be:

$$T_L = 2B \times 10^{-1.089\gamma_m} \left( \frac{f}{2} \right)^{0.5} G \quad (13)$$

Where geometrical parameter  $G$  is defined as follows:

$$\begin{aligned} G &= \int_{\tau}^1 \left( 1 - \frac{t_c^2 \sin^2(\varepsilon/2)}{2\rho^2 R^2} \right) R \sin \left( \frac{\varepsilon}{2} \right) d\rho \quad (14) \\ &= \frac{\sin(\frac{\varepsilon}{2}) \left( 1 - \frac{r_c}{R} \right)}{2r_c} (2r_c R - t_c^2) \sin \left( \frac{\varepsilon}{2} \right) \end{aligned}$$

Where  $r_c$  is the chisel edge radius defined as below:

$$r_c = \frac{t_c}{\sin \phi} = \tau R \quad (15)$$

And unknown parameter  $B$  is determined as follows:

$$B \times 10^{-10.089\gamma_m} = K_n \quad (16)$$

Where  $K_n$  is the specific energy for the vertical force which can be determined by means of a single test as described in [19].

The same approach is used to calculate the total thrust force exerted on the chisel edge, considering the fact that the rake angle of the chisel edge  $\gamma_c$  is assumed to be constant.

$$T_c = 2C \times 10^{-1.089\gamma_c} (f)^{0.5} t_c \quad (17)$$

Where the chisel edge rake angle is obtained as follows:

$$\gamma_c = -\tan^{-1}(\tan(\varepsilon/2) \cos \phi) \quad (18)$$

In order to determine unknown constant  $C$ , the specific energy at the chisel edge  $K_{n,chisel}$  is used:

$$C \times 10^{-10.089\gamma_c} = K_{n,chisel} \quad (19)$$

The specific energies can be determined by a single drilling test. In this method, a drilling sample with a pilot hole is prepared. The diameter of the pilot hole is equal to the length of chisel edge and its depth is equal to the half thickness of the specimen. This sample is drilled and the experimental thrust forces in each section are measured. The values of the specific energies are determined as follows:

$$K_n = \frac{T_{exp}}{2(f/2)^{0.5} G} \quad (20)$$

$$K_{n,chisel} = \frac{T_{exp}^{chisel}}{2t_c f^{0.5}} \quad (21)$$

The total thrust force will be the sum of the part values generated by cutting lips and the chisel edge.

#### Analytical approach

In drilling composite laminates, when the drill bit approaches the exit side, the uncut plies withstanding the axial force become more susceptible to deformation owing to decrease of its thickness. Eventually, the force applied to the uncut plies exceeds the interlaminar bond strength and delamination occurs. This happens before the laminate is completely penetrated by the drill.

The present analytical analysis is based on a number of assumptions. Propagation of delamination is assumed to be due to the pressure of the drill tool on the last layers and it is directly related to the axial load. Besides, the effect of drill rotation is neglected; hence, mode III delamination caused by tool rotation is regarded as having secondary significance in the analysis. Therefore, the kinetic energy of propagation applied within the scope of a mode I linear elastic fracture mechanism can be used to predict the initiation of delamination.

The energy balance equation at the onset of delamination propagation gives:

$$dU_d = dU - dW \quad (22)$$

Where  $dU$  is the infinitesimal stored strain energy,  $dW$  is the infinitesimal work done by the thrust force and deflection of plate.  $dU_d$  is the infinitesimal strain energy absorbed by crack growth which is as follows:

$$dU_d = G_{IC} dA \quad (23)$$

Where  $dA$  is the change in the delamination area and  $G_{IC}$  is the critical strain energy release rate in mode I, which

is assumed to be constant according to Saghizadeh and Dharan [22]. Assuming the crack to be circular:

$$dA = 2\pi a da \quad (24)$$

To calculate the work and stored strain energy, the deflection of the plate has to be calculated. According to the classical plate bending theory applied to axisymmetrical circular plates loaded transversely with small deformations, and taking into account a shear force of intensity  $q$ , the equation of equilibrium of the plate is given by [23, 24]:

$$\nabla^4 w = \frac{1}{r} \frac{d}{dr} \left( r \frac{d}{dr} \left[ \frac{1}{r} \frac{d}{dr} \left( r \frac{dw}{dr} \right) \right] \right) = \frac{q}{D} \quad (25)$$

Where bending stiffness for orthotropic material is:

$$D = \frac{3D_{11} + 2D_{12} + 4D_{66} + 3D_{22}}{8} \quad (26)$$

Figure 4. shows the schematic of delamination in the last uncut laminae of the workpiece. In this figure,  $T$  is the total thrust force exerted by a twist drill which is assumed to be distributed uniformly over the entire length of the drill bit, and  $a$  is the radius of crack. For a circular orthotropic plate clamped at the edges and subjected to a uniformly distributed load ( $q$ ) over the central circular area of radius  $R$ , the amount of deflection is expressed as:

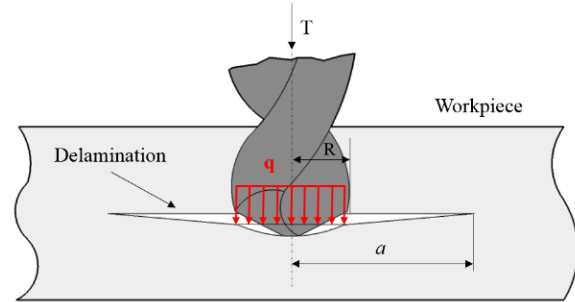


Figure 4: Delamination propagation model.

(i) for  $0 < r < R$

$$w_1(r) = \frac{T}{64\pi D} \left[ \left( 4a^2 - 3R^2 + 4R^2 \ln \left( \frac{R}{a} \right) \right) - \left( -2r^2 \left( \frac{R^2}{a^2} - 4 \ln \left( \frac{R}{a} \right) \right) + \frac{r^4}{R^2} \right) \right] \quad (27.a)$$

(ii) for  $R < r < a$

$$w_2(r) = \frac{T}{32\pi D} \left[ \left( 2a^2 + R^2 - r^2 \left( 2 + \frac{R^2}{a^2} \right) + \left( +2R^2 \ln \left( \frac{r}{a} \right) + 4r^2 \ln \left( \frac{r}{a} \right) \right) \right) \right] \quad (27.b)$$

Where the total thrust force  $T$  is the sum of force applied on the cutting lips and chisel edge expressed as below in the form of exponential:

$$T = T_L + T_c = \frac{K_L}{e^{\alpha_L \gamma_m}} \sqrt{f} + \frac{K_C}{e^{\alpha_C \gamma_C}} \sqrt{f} \quad (28)$$

Where the constants  $K_L$ ,  $K_C$ ,  $\alpha_L$  and  $\alpha_C$  are calculated based on the following equations:

$$K_L = \sqrt{2} BG \quad (29.a)$$

$$K_C = 2C t_c \quad (29.b)$$

$$\alpha_L = \alpha_C = 1.089 \ln(10) \quad (29.c)$$

The work done is:

$$W = \int dw = \int_0^r \int_0^{2\pi} q w_1(r) r dr d\theta \quad (30)$$

$$\begin{aligned}
 &= \frac{T}{\pi R^2} \int_0^r \int_0^{2\pi} w_1(r) r dr d\theta \\
 &= \frac{T^2}{64\pi D} \left[ 4a^2 - \frac{8R^2}{3} + 4R^2 \ln\left(\frac{R}{a}\right) - \frac{R^4}{a^2} + \right. \\
 &\quad \left. + 4R^2 \ln\left(\frac{R}{a}\right) + \frac{R^2}{3} \right]
 \end{aligned}$$

And the total stored strain energy is the sum of the part values generated by the inner and outer portion:

(i) for  $0 < r < R$

$$U_1 = \frac{T^2}{64\pi D} \left[ \frac{2R^2}{3} - \frac{R^4}{a^2} + \frac{R^6}{2a^4} - \frac{4R^4}{a^2} \ln\left(\frac{R}{a}\right) + \right. \quad (31.a) \\
 \left. + 4R^2 \ln\left(\frac{R}{a}\right) + 8R^2 \left(\ln\left(\frac{R}{a}\right)\right)^2 \right]$$

(ii) for  $R < r < a$

$$U_2 = \frac{T^2}{64\pi D} \left[ 2a^2 - 2R^2 + \frac{R^4}{2a^2} - \frac{R^6}{2a^4} - \right. \quad (31.b) \\
 \left. - 8R^2 \left(\ln\left(\frac{R}{a}\right)\right)^2 + \frac{4R^4}{a^2} \ln\left(\frac{R}{a}\right) \right]$$

After calculation of the work done and stored strain energy, resolving the energy balance equation gives the expression of the resulting critical thrust force:

$$T_{critical} = \frac{\pi\sqrt{32G_1CD}}{1-1/2s^2} \quad (32)$$

Finally, by replacing the total force with its value as a function of feed rate  $f$ , as expressed in Eq. (9), the critical feed rate will be:

$$f_{critical} = \frac{32\pi^2 G_1 C D}{\chi^2 (1-1/2s^2)^2} \quad (33)$$

Where  $s = R/a$ , and the constant  $\chi$  is calculated as below:

$$\chi = \frac{K_L}{e^{\alpha_L \gamma_m}} + \frac{K_C}{e^{\alpha_C \gamma_C}} \quad (34)$$

To avoid drilling-induced delamination, the applied thrust force and adjusted feed rate should not exceed these critical values.

### 3. DISCUSSION AND CONCLUSIONS

In this paper, analytical models to predict critical thrust force and feed rate at the onset of delamination are proposed. To achieve this aim, the oblique cutting model proposed by Langella was employed to determine an analytical relation between feed rate and thrust force. The force exerted by the rotating twist drill to the laminate is assumed to be distributed uniformly over the entire length of the drill bit. Then, elastic fracture mechanics and classical plate bending theory were used to determine the critical thrust force above which delamination is initiated. Finally, the critical feed rate for the onset of delamination was modeled by combining the resulting equations for the oblique cutting model and critical thrust force. The results of the proposed analytical models can be investigated from different points of view. For example, the effects of each drill geometrical parameters, such as point angle, helix angle or rake angle, on the critical feed rate can be studied. However, it is not possible to discuss all these findings and investigations in this article. In brief, proposed model provides the possibility of using optimal feed rate directly to avoid delamination. Detailed results of the proposed models including experimental data will be published in future articles.

### REFERENCES

1. Hocheng, H., *Machining technology for composite materials: principles and practice*. 2011: Elsevier.
2. Krishnaraj, V., R. Zitoun, and J.P. Davim, *Drilling of polymer-matrix composites*. 2013: Springer.
3. Liu, D., Y. Tang, and W.L. Cong, *A review of mechanical drilling for composite laminates*. *Composite Structures*, 2012. 94(4): p. 1265-1279.
4. Zarif Karimi, N., et al., *Experimental analysis of GFRP laminates subjected to compression after drilling*. *Composite Structures*.
5. Zarif Karimi, N., G. Minak, and P. Kianfar, *Analysis of damage mechanisms in drilling of composite materials by acoustic emission*. *Composite Structures*, 2015. 131(0): p. 107-114.
6. Karimia, N.Z., et al., *The effect of support plate on drilling-induced delamination*. *Acta Polytechnica CTU Proceedings*, 2016. 3.
7. Zarif Karimi, N., et al., *Effect of the drilling process on the compression behavior of glass/epoxy laminates*. *Composite Structures*, 2013. 98(0): p. 59-68.
8. Abrão, A.M., et al., *Drilling of fiber reinforced plastics: A review*. *Journal of Materials Processing Technology*, 2007. 186(1-3): p. 1-7.
9. Gaitonde, V.N., S.R. Karnik, and J. Paulo Davim, *Taguchi multiple-performance characteristics optimization in drilling of medium density fibreboard (MDF) to minimize delamination using utility concept*. *Journal of Materials Processing Technology*, 2008. 196(1-3): p. 73-78.
10. Pinho, L., D. Carou, and J. Davim, *Comparative study of the performance of diamond-coated drills on the delamination in drilling of carbon fiber reinforced plastics: assessing the influence of the temperature of the drill*. *Journal of Composite Materials*, 2016. 50(2): p. 179-189.
11. Hocheng, H. and C.K.H. Dharan, *Delamination During Drilling in Composite Laminates*. *Journal of Manufacturing Science and Engineering*, 1990. 112(3): p. 236-239.
12. Jain, S. and D.C.H. Yang, *Effects of Feedrate and Chisel Edge on Delamination in Composites Drilling*. *Journal of Manufacturing Science and Engineering*, 1993. 115(4): p. 398-405.
13. Jain, S. and D.C.H. Yang, *Delamination-Free Drilling of Composite Laminates*. *Journal of Manufacturing Science and Engineering*, 1994. 116(4): p. 475-481.
14. Lachaud, F., et al., *Drilling of composite structures*. *Composite Structures*, 2001. 52(3-4): p. 511-516.
15. Hocheng, H. and C.C. Tsao, *Comprehensive analysis of delamination in drilling of composite materials with various drill bits*. *Journal of Materials Processing Technology*, 2003. 140(1-3): p. 335-339.
16. Tsao, C. and H. Hocheng, *Effects of exit back-up on delamination in drilling composite materials*

- using a saw drill and a core drill.* International Journal of Machine Tools and Manufacture, 2005. 45(11): p. 1261-1270.
17. Zarif Karimi, N., H. Heidary, and M. Ahmadi, *Residual tensile strength monitoring of drilled composite materials by acoustic emission.* Materials & Design, 2012. 40(0): p. 229-236.
  18. Chen, W.-C., *Some experimental investigations in the drilling of carbon fiber-reinforced plastic (CFRP) composite laminates.* International Journal of Machine Tools and Manufacture, 1997. 37(8): p. 1097-1108.
  19. Langella, A., L. Nele, and A. Maio, *A torque and thrust prediction model for drilling of composite materials.* Composites Part A: Applied Science and Manufacturing, 2005. 36(1): p. 83-93.
  20. Caprino, G. and L. Nele, *Cutting Forces in Orthogonal Cutting of Unidirectional GFRP Composites.* Journal of Engineering Materials and Technology, 1996. 118(3): p. 419-425.
  21. Caprino, G., L. Santo, and L. Nele, *On the origin of cutting forces in machining unidirectional composite materials.* ASME International. Reprinted from: PD, 1996. 75: p. 83-89.
  22. Saghizadeh, H. and C.K.H. Dharan, *Delamination Fracture Toughness of Graphite and Aramid Epoxy Composites.* Journal of Engineering Materials and Technology, 1986. 108(4): p. 290-295.
  23. Timoshenko, S. and S. Woinowsky-Krieger, *Theory of plates and shells.* 1959: McGraw-Hill.
  24. Reddy, J.N., *Theory and analysis of elastic plates and shells.* 2006: CRC press.

# The Simulation Process in Small and Medium Enterprises: Decision-making Support

Miroslav Dragić<sup>1\*</sup>, Miloš Sorak<sup>1</sup>

<sup>1</sup>Faculty of technology, University of Banja Luka, Banja Luka (Bosnia and Herzegovina)

*This paper examines possibility the use of the simulation process in small and medium enterprises in order to support the decision-making process. Namely, the success of small and medium enterprises to adapt to constant changes in the environment largely depends on the different strategies and management decisions taken by managers at the operational level. The applied model recognizes the specificities of SMEs, such as a large range of products, the use of a wide variety of materials, production in small batches and requests for reduction of lead time. The effects of applying the model to increase the efficiency and effectiveness of the simulated systems will be monitored through performance measures, i.e. by monitoring performance measures depending on the process of simulated values of the model parameters. Through a series of experiments the effects of changes in inventory management policies, the availability and size of the lot were simulated. Performance measures which are monitored are performance for the delivery, capacity utilization, inventory turnover, and others. The results of experiments showed that the variation of the model parameters should be oriented simultaneously towards several of the aforementioned directions.*

**Keywords:** decision-making, performance measures, simulation, SMEs

## 1. INTRODUCTION

World markets at which many of nowadays small and medium enterprises operate are characterized by fast changing needs and expectations of customers. Only companies which have learnt how to adapt quickly and efficiently and which are fast learners will survive [1,2]. Consequently, the success of small and medium enterprises to adapt to constant changes in the environment largely depends on the different strategies and management decisions taken by managers from top to bottom level [2,3,4].

Small businesses are more flexible, compared to big ones, and have the ability to quickly adapt to constant change, but their main problem is the lack of resources (financial resources, lack of modern equipment, knowledge and the like). Consequently, SMEs are trying to achieve the synergistic effect of a whole and be as efficient and effective as possible. That synergistic effect depends heavily on both chosen strategy and managerial decisions made by the managers at the all level during adjustment of work processes. Research has shown that managers, in most cases, make decisions that are most advantageous for a business entity in their charge. Of course, such decision-making is influenced by the objectives and politics of the organizational unit in their charge.

The reasons why managers, in most cases, make decisions closely tailored to the business entity in their charge, should be sought in the fact that, without a quality software solution and a quality training encompassing problems of the influence of partial (individual) managerial decisions on the overall optimum of the system, they are unable to perform their activities [2,4].

Any decision making process has several steps (phases) but should always flow from a thorough analysis of the given situation to a good understanding of options and alternatives, and reliable forecasting. It's often seeking

a compromise between costs and benefits in order to achieve optimal outcome. Therefore, Decision makers faced with complex problems which often have multiple, conflicting objectives for its solution. To be acceptable, a solution must reconcile these conflicting goals.

A variety of analytical techniques have been developed to help decision makers to solve problems with multiple criteria. Consequently, decision makers have turned to analysts and analytical modelling techniques to enhance their decision making capabilities. Since real processes in small and medium-sized enterprises comprise a very large number of interrelated variables, their modelling requires a lot of experience and use of mathematical tools. Modern research in the field of computer modelling and simulation are in constant search for new and better approaches to the specification and implementation of simulation models in manufacturing systems. Thus, the development of computers has opened a new perspective in this regard and created the conditions for a wider use of modelling and simulation techniques [4,5,6,7].

Taking the above mentioned problem into account, this paper is searching for a solution on how chosen strategies and managerial decisions made by the managers may affect the overall performance of the enterprise as a whole. The model for simulation processes used in this research is built by using system dynamics method. The effects of applying the model to increase the efficiency and effectiveness of the simulated systems will be monitored through performance measures, i.e. by monitoring performance measures depending on the process of simulated values of the model parameters. Process performances which have to be monitored are performance for the delivery, capacity utilization, inventory turnover, and others.

## 2. DEVELOPMENT OF MODEL FOR SIMULATION

### 2.1. Models, modelling and simulation

The creative process of creating the model is called modelling. The model represents the real system with a description of those features that are relevant for a given study. The models are always abstractions of the real system, and retain only those features originals that are relevant to the purpose of his study. The level of abstraction in the modelling process affects the validity of the model and the performance of the model representation of the real system. The creative process of creating the model is called modelling [1,7,8].

The simulation process involves a number of activities related to the experimental determination of the effects that occur in the system, process or model which imitates them. In addition, the simulation involves analysing the results based on the developed criteria: test (verification) and validity (validation) of the model [4,9]. Experimenting on the simulation model, as experimenting with real objects, for various reasons it is not always possible, leads to information about the behaviour of the elements of the real system [7,10,11,12]. Simulation on models, industrial systems can explore and improve their condition through appropriate methods and techniques, primarily by monitoring the time course of the effects of changes in the system.

In this paper we propose a modular system dynamics model of integrated business processes. System Dynamics is an academic discipline emerged during the 1960s at the Massachusetts Institute of Technology (MIT), led by Professor Jay Forrester [10]. It's a method for continuous system simulation with feedback, i.e. system in which individual elements can affect itself through a chain of cause and effect. The general process of simulation, which is accepted in this work, basically involves the process of building simulation models, planning and execution of simulation experiments and analyses the results and draws conclusions [2, 4, 14, 15].

### 2.2. Development of a model for the simulation

Constant changes of environmental conditions and disturbances in the business processes of small and medium enterprises require the development of a flexible simulation model of production process flows. In front of this model there are specific requirements that are reflected in:

- the necessity to follow different trends in demand of finished products,
- the simulation procedures of planning and adjustment of work processes,
- requirements for continuous monitoring of materials, work in process and finished products and
- The need for continuous harmonization of the distribution of finished products according to customers' requirements [2].

On this occasion, it is necessary to satisfy the specificity of small and medium-sized enterprises, the manufacturing sector, which is reflected in:

- large range of products,
- using a number of different materials,

- preparation and execution of the production process usually in small batches,
- need for the development of technical documentation in most cases for the modified products, and in many cases necessary to start modifying technical documents and
- repeated requests to reduce the time of receipt of customer request to bidding and manufacturing [2, 4,15].

The general process of simulation, which is accepted in this work, basically involves the process of building simulation models, planning and execution of simulation experiments and analyses the results and draws conclusions.

For the need of the simulation process flows in small and medium-sized enterprises a modular approach is preferred to construction, building simulation models. This approach involves building a model of discrete units (modules), each unit has its own objective, decision rules and performance measures. The advantages of this approach to simulation modelling are reflected in:

- facilitated definition of the purpose of each module,
- simplified verbal, mathematical and logical description of the model,
- adjust the level of details of modules needs simulation process,
- possibilities to improve certain modules without the need for changes in other modules,
- ability to engage the appropriate professional staff in the individual modules,
- easier debugging model,
- easy monitoring of processes and simulation results and
- the possibility of a modular approach to building simulation program [2,4,16].

The model for simulation processes used in this research is built by using system dynamics method. The logic of the built model is shown in figure 1.

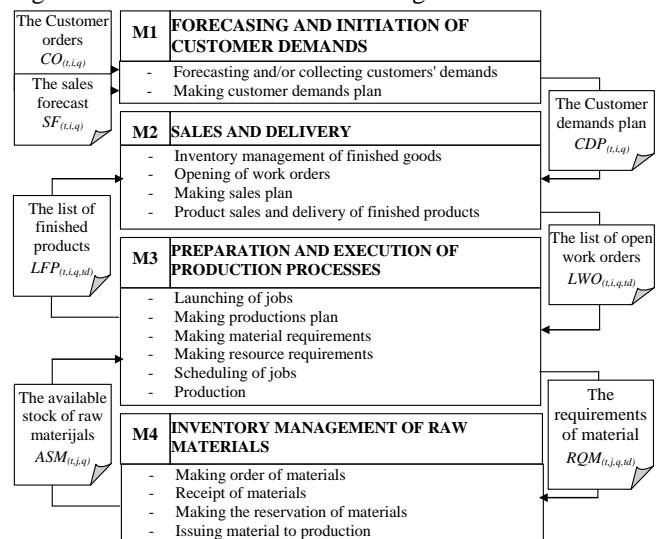


Figure 1: Integrated simulation model

### 2.3. Model description

The chosen modular approach involves building a model of discrete units (modules), where each unit has its own objective, decision rules and performance measures.



By performing simulations under different conditions (changing model parameters) performance measures can be monitored depending on the process of simulated values of the model parameters. As the performance of the process to be followed have been adopted for the delivery performance, capacity utilization and inventory turnover (Table I, II and III) [2, 4, 9, 15,17]. Detailed mathematics description of the simulation model is given in our previous works [2,4,16], so only the basic logic of the developed system dynamics simulation model is described below.

2.3.1. M1-Forecasting and initiation of customer demands

As a basis for defining the parameters of this module sales data in the previous period, sales forecast contracts and plans can be used. Based on these data, for the period covered by simulation, this module simulates the arrival of customer demands (The Customer Demands Plan CDP). It is expressed as a function of the order time (t), type of product (i) and the order quantity (q). The module supports a variety of different types of flow of customer demands arrival, as well as variations in these flows (Figure 2).

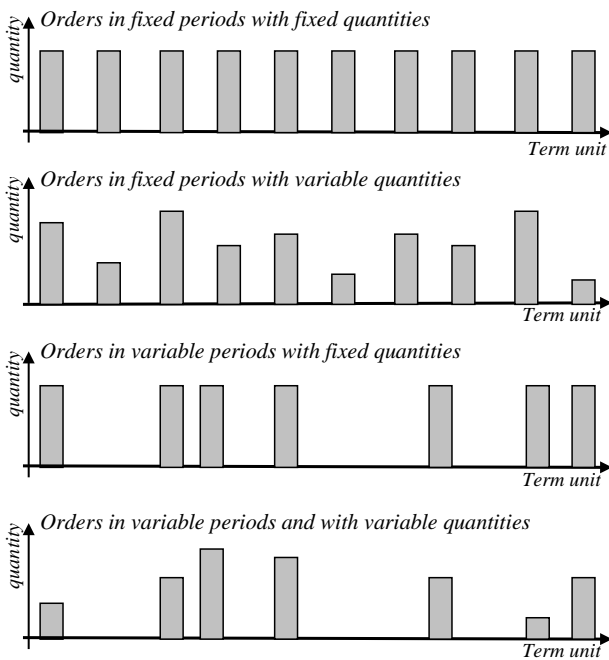


Figure 2: The variety of different types of flow of customer demands

2.3.2. M2-Sales and delivery

This module monitors the reception and processing of customer requirements. Module supports two basic options for meeting the orders: Make-to-Stock (MTS) and Make-to-Order (MTO).

In the first case the products are delivered directly from the warehouse of finished products. If there is not sufficient quantity in stock, the request is recorded as unrealized customer order. Adjustment of stocks of finished products is carried out using defined safety and maximum quantities. In the second case, the request shall be recorded in the list of unimplemented demands, and then a work order is opened. Opening a work order is not possible until the development of the necessary technical documentation is finished. The time required for

preparation of technical documentation varies from case to case.

Assuming that the requirements are arriving according to the rules defined in the previous module, the goal is to find a model to satisfy the demands of customers with a minimum level of stocks of finished products (Table 1).

Table 1: Performance and management objectives

Goal	Name	Definition
↑	<b>Fulfilment of orders from existing stocks</b>	Percentage of the amount of goods that customers request and that can be met with existing supplies
↑	<b>Timeliness of delivery</b>	The percentage of orders that are met before or as scheduled / promised delivery date.
↑	<b>The value of executed orders</b>	The total value of orders received in the relevant period.
↓	<b>The average level of finished goods supply</b>	The average value of finished goods supply over time

2.3.3. M3-Preparation and execution of work processes

The module follows the course from the opening of the task to delivery of finished goods to the warehouse. Production process is organized as a process focused and that a batch method is used (each batch goes through one stage of the production process before moving onto next stage). The module M3 is associated with the module M2 through the list of open work orders, and through the materials requisitions with module M4 simulation model. From the list of open work orders (module M2) the works are taken over and their launch is carried out into the production process. At the same time, the module is forming material requisitions based on the norms of material and batch size.

For each launched work order definitions are provided for the start and end of each operation. They shall contain the dates of the production plan. The data on operations (list of operations) and data on available resources are used as a basis for the development of term production plan. The ultimate goal is to increase capacity utilization while reducing the level of unfinished production, so the performance regarding capacity utilization and the level of unfinished production are imposed as optimization criteria for simulated processes (Table 2).

Table 2: Performance and management objectives

Goal	Performance	Definition
↑	<b>Capacity utilization</b>	The relationship between the required and available capacity
↓	<b>The flow coefficient</b>	Dimensionless number that shows the actual production cycle is greater than the theoretical production cycle in ordinal way switch series from one operation the other operation
↓	<b>The average level of work in progress</b>	The average value of work in progress

2.3.4. M4- Inventory management of raw materials

This module monitors the processes related to providing materials necessary for the smooth running of the production process. Thereby it includes procedures such as inventory control, purchasing and receiving

materials. Inventory control method can be implemented via Fixed Size Ordering System (Q-system) or Fixed Period Ordering System (P-system).

In the Fixed Size Ordering System, the maximum and minimum of standard inventory quantities are defined in advance, and the quantity of inventory gradually decreases, and when the number reaches ROP (Reorder Point Quantity), an order of EOQ (Economic Order Quantity) is placed. The Fixed Period Ordering System is an inventory control method where orders are periodically placed, but the order quantity is different every time and it depends of inventory quantity, released orders quantity and fluctuation in demand.

The material requirements are defined in the previous module. It is assumed that the purchase lead time is known and there are always sufficient quantities of material. Also, we assumed that the materials required for the process of production are exempted once in the total amount when the production process starts. There is a tendency to maintain lower inventory levels while fulfilling the demand of the production process (Table 3).

Table 3: Performance and management objectives

Goal	Performance	Definition
↓	The average level of stocks of materials	The average value of finished goods over a period
↑	Inventory turnover	The ratio of total material consumption in a certain period and intermediate levels of inventories in the same time interval

#### 2.4. The possibility of applying developed model

The production process in SMEs is characterized by delays in production, lines in front of workplaces, lack of materials, and the like. In most cases, the above problems have significant impact on most of the process because there is no clear knowledge of their impact on the overall performance of the enterprises. The reasons are usually as follows:

There is no standardized methodology for planning and testing various options and / or

Not enough time to explore different options.

It is for these reasons that the developed model allows consideration of different options when choosing the optimal solution for a given situation. By performing simulations for a certain period of time and under certain conditions (adjusting process parameters) the future behaviour of the process can be predicted shown through the expected performance of the process (Table 1, 2 and 3). These performances are compared to planned performances, and if necessary, corrective actions are initiated (by changing the parameters of the process). The experiment needs to show how such changes affect other measures of business performance.

In this research, we have used our own software in the Visual Basic environment to complete the model simulation and analysis. The software was primarily developed for previous research [16] and for the purposes of this research it has been upgraded [4]. This software fully supports the developed system dynamics simulation model, and allows us to perform simulations through a series of discrete events. The user interface allows the defining of system elements (production program, demand

and demand forecast, list and quantity of raw materials, normative of raw materials, required and installed capacities, initial conditions, etc.) and elements of the simulation experiment (period of the simulation, simulation step, batch size, inventory management policy etc.). ODBC (Open Database Connectivity) interface enables data exchange with MS Access, MS SQL Server and PostgreSQL databases. This provides partial integration of model with existing information systems of the enterprise. The software automatically calculates the defined performance and results displayed through tables and graphics.

### 3. CASE AND SIMULATION ANALYSIS

This paper describes a case study concerning the application of simulation in a small company with a lot of experience in the manufacture and trade of metal products and accessories for different purposes. Production plants that cover 3000m<sup>2</sup> are equipped with modern machines for processing sheet metals of various thicknesses and there is a paint shop for electrostatic coating-plasticization. In order to simplify the process of analysis, the product range, number of raw materials and recourses were reduced. So we have 5 kinds of products (with two order fulfilment options: Make-to-Order and Make-to-Stock), 30 kinds of raw material (Fixed Size Ordering System and Fixed Period Ordering System), 9 kinds of recourses (13 units in total) and 9 phases of production. The basic data is shown in Tables 4 to 7.

Table 4: Reduced product range with the demand model parameters

PRODUCT	Price (€)	Order fulfilment options	Initial stock (Units)	Safety stock (Units)	Batch size (Units)	Product develop. period (WH)	Demand lead-time (WH)	Average demands (units/WH)	Deviation of demand (units/WH)	Order lead-time (WH)
400000	120	MTS	40	50	100	0	8	6	2	0
410000	45	MTS	320	100	200	0	8	16	4	0
420000	400	MTO	0	0	-	40	8	4	2	120
440000	120	MTO	0	0	-	16	8	12	4	64
490000	16	MTS	140	100	200	0	2	6	3	0

Table 5: Reduced list of material with the corresponding parameters of the model (reduced list)

MATERIAL	Price (€)	Initial stock (Units)	Reorder point quantity (Units)	Maximum quantity of material (units)	Ordering cycle (WH)	Procurement lead time (WH)
WH – the working hour						
<i>j</i> ID						
1 200005	10	220	200	400	0	18
2 200011	16	120	100	300	0	18
3 200080	4	1100	400	2800	0	8
...	...	...	...	...	...	...
32 201196	28	0	1	10	0	8

Table 6: Normative of raw materials (reduced list)

		j	1	2	...	31	32
Material ID		200005	200011	...	200990	201196	
i	Product ID	...					
1	400000	0.85	0.43	...			0.01
2	410000		0.40	...			0.01
3	420000	3.67	0.17	...	8.00		
4	440000		3.50	...			
5	490000		0.12	...			

Table 7: Capacity required per product unit

r	Resource	Operation No.	Setup time (min)	Run time (min)				
				400000	410000	420000	440000	490000
1,2	HMZ	10	15	3.33	1.50	10.83	10.00	1.60
3	EUR	20	20	2.83	1.50	0.72	10.00	1.50
4	MHP	30	20	4.00	2.50	7.00		
5	APP	40	15	7.50	3.50	18.00	14.00	1.60
6	CO2	50	15	4.00	6.00	20.00	8.00	3.00
7,8	BRU	60	10	4.00	2.00	3.00	8.00	
9	LAK	70	30	4.00	3.00	10.00	18.00	0.25
10,11	MONT	80	20	10.00	5.00	10.00		
12,13	MONE	90	30	8.00		150.00		

In first stage we must define time parameters of the experiment. The period of one working hour (1 WH) is adopted as the basic time unit (step of the simulation). The period of the simulation execution corresponds to the second half of the fiscal year 2016. If we assume that the enterprise operates five days a week, in this period there are 130 working days (with 8 WH), the total time will be 1040 WH.

3.1. Basic variant of the experiment

The first experiment was conducted using the model parameters adopted from the real data of the simulated system (Table 4 to 7). The behaviour of the simulated system can be represented by series of graphics, including changes in the level of finished goods (Fig. 3), raw materials (Fig.4.) and the occupancy rate (Table 8) or even by monitoring performance measures (Table 9).

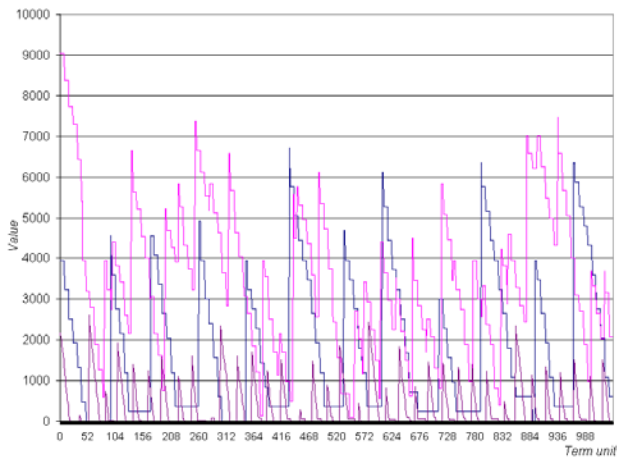


Figure 3: The level of finished goods

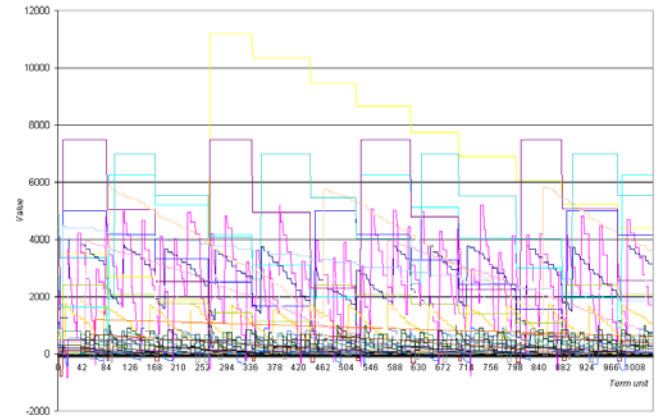


Figure 4: The level of raw materials

Table 8: Term production plan (part)

Term unit	51	52	53	54	55	Utilization %
1 HMZ	22/10	22/10	22/10	22/10	22/10	51.38 %
2 HMZ	23/10					29.92 %
3 EUR	17/20	17/20				52.18 %
4 MHP	6/30	23/20	17/30			45.95 %
5 APP		6/40	6/40	17/40	17/40	73.73 %
6 CO2	15/50	15/50	8/50	8/50	8/50	77.92 %
7 BRU				5/60	5/60	73.55 %
8 BRU	12/50	12/50	12/50	12/50	12/60	52.09 %
9 LAK	1/70		15/60	15/60	23/50	63.94 %
10 MONT		1/80	1/80			69.28 %
11 MONT						43.01 %
12 MONTE	22/10 – Work orders No./ Operation No.					54.76 %
13 MONTE						55.03 %

Table 9: Overview of the experiment results

Business performance measure		Value
↑	Fulfilment of orders from existing stock	49.01 %
↑	Timeliness of delivery	63.12 %
↑	The value of realized orders	388 325 €
↓	The average level of finished goods inventory	1 411 €
↑	Capacity utilization	61.55
↓	The flow coefficient	1.28
↓	The average level of work in progress	16 520 €
↓	The average level of materials in stock	24 428 €
↑	Inventory turnover	9.62

New variants of the experiment can be obtained by changing (to more or to less) the model parameters, all in order to improve of one or more processes performance measures.

3.2. Defining problem and possible solutions

Customer satisfaction is the key to continuing success of the enterprise, so below, we shall look into the effects of the three different decisions in order to find the best solution. The proposed solutions with the plan of model parameter variations are given in Table 10. The simulation experiments needs to show how such changes affect performance measures, especially on the fulfilment

of orders from existing stock and timeliness of delivery (see Table 9).

Table 10: The solution plan

<b>S 1</b>	<p><u>Increased available capacity</u> The introduction of new machines is primarily aimed at affecting reduction of the production cycle and the level of work in process, so consequently we expect a number of positive effects on customer satisfaction. We shall increase groups which have the highest capacity utilization like as APP, CO2 and LAK (see Table 8).</p>
<b>S 2</b>	<p><u>Increased level of finished products in stock</u> By analysing the obtained results of basic experiment, it is possible to expect that the increase in stock level of products leads to an increase in the level of customer services especially the fulfilment of orders from existing stock and timeliness of delivery. Hence, we shall increase the safety stock level (see Table 4).</p>
<b>S 3</b>	<p><u>Decreased batch size</u> Decreasing the batch size aims to decrease the level of unfinished goods and consequently to increase the level of customer service. The batch size of product will be decreased from 200 to 50 units.</p>

### 3.3. The solution evaluation

The ultimate value of the solution should be defined by the improvement of the processes performance measures, without negative effects if possible. A comparative overview of the experiment results are shown in the table 11.

Table 11: A comparative overview of the experiment results

Performance	Basic	S1	S2	S3
Fulfilment of orders from existing stock (%)	49.01	52.01	82.13	85.81
Timeliness of delivery (%)	63.12	65.64	88.06	91.37
The value of realized orders	388325	400217	426395	439576
The average level of finished goods (€)	1411	1356	3030	5175
Capacity utilization (%)	61.55	50.41	65.90	77.02
The flow coefficient	1.28	1.27	1.27	1.72
The average level of work in progress (€)	16520	16509	22785	11908
The average level of materials in stock (€)	24428	24123	24912	24472
Inventory turnover	9.62	9.63	10.08	10.45

Increase in available production capacity (S1) decreases their utilization with no significant (positive) effects on other performance measures.

By analysing the obtained results of experiment S2, it is possible to conclude that the increase in stock level of products leads to an increase in the level of customer services especially the fulfilment of orders from existing stock and timeliness of delivery. An undesirable increase in the level of work in process and the average level of finished goods was expected.

Decreasing batch size in production (S3) entails a number of positive effects on performance measures (better customer service, better capacity utilization, lower level of work in progress and a better inventory turnover),

along with somewhat poorer flow coefficient and increasing level of finished goods inventory.

### 3.4. Decision making

A comparative overview of the experiment results show that it is not possible to find a set of model parameters that will improve all the performances without any negative effects. In this regard we propose solution S4 with a reduced size of series. This has proved to be the best solution because this solution achieved the best improvement in the level of service, capacity utilization levels and unfinished products. However the average level of finished product inventories increased by 366 %, which in practice requires an additional storage capacity (Figure 5).

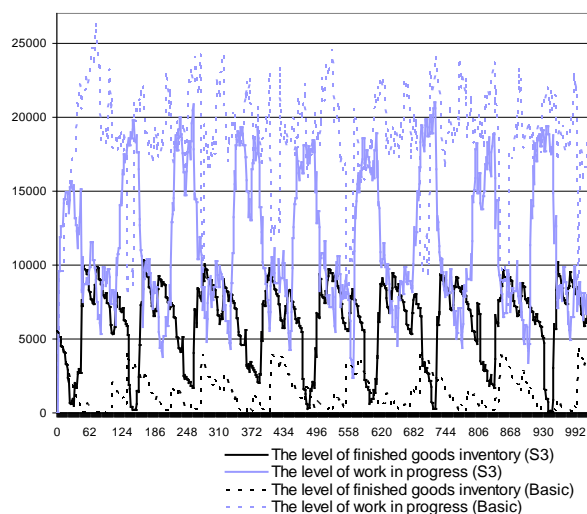


Figure 5: A comparative overview of the level finished and unfinished goods

## 4. CONCLUSION

Results of experiments showed that it is difficult for the managers of SMEs to make decisions that will lead to improvement without any negative effects on the other processes. Therefore, coordination of management actions made by managers at various levels is imposed as a key issue in the business practices of SMEs. The paper has demonstrated that a dynamic simulation tools can significantly improve the coordination process. Thus, by performing simulations of the model one can predict the effects of running various actions.

The model can be used for finding solutions for wide range of problems related to process management, starting with determining the type of production processing organization (long-term decision) up to observing the effects of changes in the work schedule in production (current decision).

## ACKNOWLEDGEMENTS

This research was supported by Ministry of Science and Technology of the Republic of Srpska under Grant No. 19/6-020/961-34/15.

## REFERENCES

- [1] K. Burnard and R. Bhamra, "Organisational resilience: development of a conceptual framework for organisational

- responses", *International Journal of Production Research*, Vol. 49 (18), pp. 5581-5599, (2011)
- [2] M. Sorak and M. Dragic, "Supply Chain Management of Small and Medium-Sized Enterprises", In: Katalinic, B., Tekic, Z. (Eds.), *DAAAM International Scientific Book 2013*, DAAAM International, Vienna, pp. 951-968, (2013)
- [3] H. Andreas, "Enabling Successful Supply Chain Management: Coordination, Collaboration, and Integration for Competitive Advantage", PhD Thesis, University of Mannheim, (2006)
- [4] M. Dragic and M. Sorak, "Simulation for Improving the Performance of Small and Medium Sized Enterprises", *International Journal of Simulation Modelling*, Vol. 15 (4), pp. 597-610, (2016)
- [5] M. Özbayrak, T.C. Papadopoulou and M. Akgun, "Systems dynamics modelling of a manufacturing supply chain system", *Simulation Modelling Practice & Theory*, Vol. 15 (10), pp.1338-1355, (2007)
- [6] J. S. B. Hall, "Corporate Cartooning: The Art, Science and Craft of Computer Business Simulation Design", Hall Marketing, London (England), (2010), from <http://www.simulations.co.uk>, accessed 25-07-2016
- [7] A.A. Tako, and S. Robinson, "The application of discrete event simulation and system dynamics in the logistics and supply chain context", *Decision Support Systems*, Vol. 52 (4), pp.802–815, (2012)
- [8] M.J. Radzicki, and R.A. Taylor, "Origin of System Dynamics: Jay W. Forrester and the history of system dynamics", In: U.S. Department of Energy's Introduction to System Dynamics, (2008), from <http://www.systemdynamics.org/DL-IntroSysDyn/>, accessed 26-08-2016
- [9] R.G. Coyle, "System dynamics modelling: a practical approach", Chapman and Hall/CRC, Boca Raton, Florida US, (1996)
- [10] J.W. Forrester, "Industrial Dynamics", MIT Press, Cambridge, Massachusetts, (1961)
- [11] J.S.B. Jeremy, "Corporate Cartooning: The Art, Science and Craft of Computer Business Simulation Design", (2010) from <http://www.simulations.co.uk>
- [12] R. Špicar, "System Dynamics Archetypes in Capacity Planning", *Procedia Engineering: 24th DAAAM International Symposium on Intelligent Manufacturing and Automation*, Vol. 69, pp.1350-1355, (2014)
- [13] Y. Feng, S. D'Amours, and R. Beauregard, "Simulation and performance evaluation of partially and fully integrated sales and operations planning", *International Journal of Production Research*, Vol. 48 (19), pp. 5859-5883, (2010)
- [14] S. Cheraghi, M.M. Thirtha and K.K. Krishnan, "An optimization-based system for adaptive planning in a discrete part manufacturing environment", *International Journal Of Computer Integrated Manufacturing*, Vol. 19 (2), pp. 125-135, (2006)
- [15] J. Vlajić, J., M. Vidović and M. Miljuš, "Lanci snabdijevanja - definisanje i performance", *Transport i logistika*, Vol. 2005(9), pp. 85-112, (2005)
- [16] M. Dragić, "Optimizacija lanaca snabdijevanja proizvodnih sistema primjenom metoda simulacije", Master Thesis, Mašinski fakultet, Banja Luka, (2010)
- [17] H. Min and G. Zhou, "Supply chain modelling: past, present and future", *Computers & Industrial Engineering*, Vol. 43, pp. 231-249, (2002)



# The Influence of Working Experience and Level of Education on the Market Orientation of SMEs in Transition

Ljiljana Pecić<sup>1\*</sup>, Milan Kolarević<sup>2</sup>, Vladan Grković<sup>2</sup>, Nataša Obradović<sup>2</sup>

<sup>1</sup> College for Applied Mechanical Studies, Trstenik (Serbia)

<sup>2</sup> Faculty of Mechanical and Civil Engineering in Kraljevo, University of Kragujevac, Kraljevo (Serbia)

*Depending on the fundamental strategy of running business, most companies follow an organizational culture orientation that matches one of the following categories: product-oriented, sales-oriented and market oriented. The purpose of this paper is to determine the influence of years of working experience (YWE) and the level of education (LE) on the level of market orientation of organizational culture. This research included 20 companies from Serbian metal industry. The conducted analysis showed that the influence of investigated factors is non-linear and that the influence of LE has the effect which is opposite to the effect of influence of YWE on the market orientation in the investigated range. The inherent way of thinking and the inadequate influence of the Government significantly slow down the development of SMEs in transition and they do not succeed in implementing market orientation in their organizational structures and behaviours.*

**Keywords:** Market orientation, Organizational culture, SMEs, Transition

## 1. INTRODUCTION

Today's business is not about selling or providing services to customers. In facing rapid evolution of the global market place, having a set of common rules is critical to facilitating trade. It is well-known that business excellence in companies is realized through implementation of the concept of total quality management (TQM). ISO officially defines TQM as a way of managing an organization which aims at continuous participation and co-operation of all its members in the improvement of quality in order to achieve customer's satisfaction, long-term profitability of the organization and benefit of its members, in accordance with requirements of the society. TQM is seen as a description of a culture, attitude and organization of a company that aims to provide products and services that meet customers' needs. Culture requires quality in all aspects of organizational operations, with things being done the right way instantaneously, with defects and waste being simultaneously eradicated from its operations. TQM is a culture in an organization committed to total customer satisfaction through continuous improvement. That is why resources in such cultures are totally utilized [1,2]. Benefit comes in all segments of business: fewer defects, reduced rework and lead times, lower inventory levels, cost reduction, and a higher level of customer satisfaction [3,4].

On the other hand, the world's most successful business leaders agree that corporate culture, if correctly aligned with the external environment, is the glue that ensures long-term organizational success. The former IBM CEO Lou Gerstner, who led its spectacular transformation from a products company to a service organization, says: "I came to see, in my time at IBM, that culture isn't just one aspect of the game-it is a game" [5].

The organizational culture or what is known as the "organization values and personality" was not given the natural interest before the second half of the twentieth century. The 1970s era witnessed an increasing interest in

this concern, which culminated in the 1990s [6]. Even then, it was totally clear that there are differences among national cultures and among companies within the same national culture. Also, it is known that the company's organizational culture directly depends on several different factors: size, tradition, communication among its employees [7].

Nowadays, when the world has become a global village connected by modern communication methods, achieving business excellence and good business parameters becomes impossible for any country and any company staying in isolation from changes [8].

The observations of Gerstner, Welch and Oreck support the importance of culture as a driver of competitive advantage and business performance. They also illustrate that all business leaders need to see their central job as proactively leading their firm's culture for superior performance [8].

Implementing TQM means changes, and for all changes organizational culture is a key. Altering the way people perceive changes and react to them plays an important role in such efforts [9,10,11].

Slater [12] expresses this notion explicitly when stating "A market orientation is the aspect of business culture that motivates employees throughout the organization to place the highest priority on the profitable creation and maintenance of superior customer value. As such, it establishes norms for behavior regarding the organization-wide development of and responsiveness to information about customers and competitors, both current and potential." Slater distinguishes between the traditional and new approaches to market orientation. "Market oriented businesses have traditionally focused on understanding the expressed needs of the customers in their served markets and on developing products and services that satisfy those needs" [13]. In this way, market orientation is focusing on current products and services, incremental rather than breakthrough learning and the

short term. Slater [12] continues by stating that the, "Second generation market-oriented businesses are committed to understanding both the expressed and unexpressed needs of their customers, and the capabilities and plans of their competitors through the processes of acquiring and evaluating market information in a systematic and anticipatory manner." Now, the focus is more on the long-term and on breakthrough learning. Again, we see the concept of market orientation relates to the values of any organisation: its culture [14]. In their meta-analysis of many articles investigating the relationship between market orientation and business performance, Rodriguez Cano, Carillat and Jaramillo conclude that this relationship is positive and consistent worldwide [15].

A lot of companies in the world did not succeed on the road to achieving business excellence and TQM. Now, if we assume that a company's culture influences everything the company does, it is clear that if you want to achieve TQM business excellence in the era of globalization, you have to be marketing oriented. In their visions companies all around the world have defined that they want this, but everything is different in the field.

## 2. RESEARCH

The following paragraphs deal with evaluating the state of marketing orientation of organizational culture in 20 companies within Serbian mechanical industry: all companies are nowadays independent entities, whereas in the recent past they have used to be a part of the giant IHP Prva Petoletka in Trstenik (PPT – the field of hydraulics and pneumatics, which gives to almost all of them the prefix PPT). Nineteen companies are currently undergoing the process of restructuring.

### 2.1. Data collection and processing

In order to identify the present level of organizational culture in terms of marketing orientation of in those 20 companies it was first necessary to make an appropriate questionnaire, which would provide the answer to the key question: what is the direction of our business. The questionnaire was based on MARK – PLAN questionnaire [16]. This poll list was used to conduct the research in companies, in terms of determining management orientation, i.e. whether it is *production, sales or market*.

The questionnaire was structured in such a way that the answers to the previously mentioned issues led to the conclusion about the state of organizational culture in terms of marketing orientation. The questionnaire was compiled from 15 questions with the options given in a way that would prevent routine answering. The data collected from anonymous respondents in the interview were: degree of professional education, years of working experience and their occupation.

For scoring the survey, the points scale was adopted where a response is scored 0 points for indicating production orientation, 5 points for indicating technological orientation, and 10 points for indicating marketing orientation. In the context of the survey results, the marketing orientation of a company can be described as:

- advanced (121-150 points),
- barely satisfactory (91-120 points),
- conservative (61-90 points),
- bad (31-60 points), and
- hopeless (0-30 points).

The starting point of the research was to collect data using surveys on the representative sample of employees in every company. The survey was conducted in the period from the beginning of December 2010 to the end of March 2011. The number of interviewed workers was 2729 from the total of 4343 employed in those companies i.e. 62.84% (Table 1). The workers took questionnaires home, and the following day they left them in the boxes, kept by delegated people.

Table 1. Overview of the enterprises surveyed, the number of employees and the number of respondents

Name of the company	Number of employees	Number of respondents
Armature	391	236
Cilindri	258	180
Energetika	103	73
FUD Brus	305	225
Hidraulika	537	244
Holding	12	10
Industrijska pneumatika	262	200
Inženjering	53	49
Ishrana	56	24
Kočna tehnika	586	328
Namenska	690	383
NIC	4	4
Obezbeđenje	52	49
PPT Delovi Novi Pazar	56	53
Petoletka Promet	119	118
Remont & Energetika	101	100
Servoupravljači	235	172
TMO	178	176
Transport	25	12
Zaptivke	320	93
<b>SUM:</b>	<b>4343</b>	<b>2729</b>

The average number of achieved points per question and per company and the summary and average values per company are shown in Table 2. The average score per question is  $\bar{X}=4.887$ , the average standard deviation is  $\bar{\sigma}=4.172$ , and the total average score for all questions is  $\bar{R}=73.283$ . So, all companies can be classified as conservative and they have hardly satisfied the level of market orientation.

### 2.2. Results and Discussion

Software Design Expert is used for building an empirical model to determine how the level of market orientation depends on the level of education (LE) and the years of working experience (YWE). The names and levels of the two chosen process factors to study are shown in the table 3.



Table 2. Average number of points per question and per company, the summary and average values per company

Name of the company	Question															SUM	Mean
	1	2	3	4	5	6	7	8	9	10	11	12	13	14	15		
Armature	4.936	4.237	4.746	4.068	4.915	6.780	5.699	5.932	6.335	3.877	3.983	4.004	5.191	2.034	4.513	71.250	4.750
Cilindri	4.806	4.694	5.333	5.111	6.000	5.083	6.222	4.417	6.306	2.944	6.083	6.722	6.000	3.806	5.139	78.667	5.244
Energetika	3.288	3.493	3.630	1.986	4.726	7.740	5.068	4.863	5.068	5.274	2.945	3.699	3.836	0.548	4.658	60.822	4.055
FUD brus	5.267	5.067	6.200	4.533	6.600	5.333	6.733	3.200	6.267	3.733	4.533	6.133	6.333	3.467	4.000	77.400	5.160
Hidraulika	5.143	5.205	3.709	4.918	4.836	6.680	4.344	3.709	4.898	3.197	5.123	4.488	5.820	3.176	3.094	68.340	4.556
Holding	6.000	4.000	1.000	2.000	7.000	4.500	3.000	1.500	7.500	3.500	2.500	2.500	8.500	4.500	3.000	61.000	4.067
Industrijska pneumatika	6.400	4.525	4.900	4.700	4.975	6.725	5.775	5.600	6.600	2.550	6.650	4.700	7.075	2.150	2.800	76.125	5.075
Inženjering	5.510	3.163	5.510	5.000	5.102	6.122	5.612	5.612	7.449	1.327	6.327	4.082	7.755	2.551	3.061	74.184	4.946
Ishrana	5.833	3.542	5.208	3.750	6.875	3.125	7.708	8.542	4.792	3.958	2.083	4.792	6.667	2.917	5.000	74.792	4.986
Kočna tehnika	4.939	4.421	5.061	4.909	6.037	4.573	5.473	4.726	5.244	3.369	5.213	5.366	5.991	2.942	4.390	72.652	4.843
Namenska	4.452	4.413	4.478	3.629	4.987	6.841	5.274	5.039	5.836	3.930	3.773	3.747	5.157	1.971	4.256	67.781	4.519
NIC	6.250	2.500	6.250	2.500	2.500	6.250	3.750	1.250	6.250	1.250	2.500	3.750	5.000	2.500	1.250	53.750	3.583
Obezbedjenje	7.653	7.449	5.000	5.204	6.122	6.429	7.041	5.918	4.592	3.163	4.082	5.612	6.735	1.837	3.878	80.714	5.381
PPT Delovi Novi Pazar	6.604	3.396	5.189	5.094	5.472	4.717	5.189	3.679	5.189	3.113	5.755	6.132	5.283	4.340	4.623	73.774	4.918
Prva petoletka promet	5.381	4.195	5.890	3.983	6.780	5.339	6.059	2.712	5.551	3.305	4.110	6.229	5.847	3.220	3.856	78.458	4.831
Remont i energetika	7.200	3.800	6.750	6.650	4.600	6.400	6.150	5.600	6.800	3.100	5.750	6.050	6.500	2.700	3.650	81.700	5.447
Servoupravljači	6.919	3.808	4.331	4.157	6.541	7.384	6.483	6.948	6.541	2.965	6.250	5.494	6.977	4.302	2.035	81.134	5.409
TMO	5.483	4.119	4.489	3.778	5.313	5.795	5.710	3.920	6.506	2.614	6.023	3.892	6.278	3.267	3.523	70.710	4.714
Transport	8.333	6.667	7.917	7.500	5.833	5.417	5.000	3.333	4.583	2.917	4.167	5.000	6.667	1.250	2.581	78.333	5.222
Zaptivke	6.828	4.247	5.538	4.892	4.624	6.774	6.667	5.699	5.323	4.462	5.753	5.215	7.473	2.312	2.581	78.387	5.226
<b>Mean</b>	<b>5.416</b>	<b>4.441</b>	<b>4.934</b>	<b>4.447</b>	<b>5.511</b>	<b>6.097</b>	<b>5.729</b>	<b>4.798</b>	<b>5.905</b>	<b>3.375</b>	<b>5.015</b>	<b>4.949</b>	<b>6.032</b>	<b>2.812</b>	<b>3.822</b>	<b>73.283</b>	<b>4.887</b>

Table 3. Factors for response surface study

Factor	Units	Low Level (-1)	High Level (+1)
A -LE	level -number	1	8
B-YWE	year	1	40

The response, marked by letter "R" is the total number of points per respondent based on all 15 questions, i.e. it presents the level of market orientation of organizational culture. Independent variables are: Level of Education (LE), marked as "A" and Years of Working Experience (YWE), marked as "B".

The levels of educational classification (LE) in the examined sample in Serbia is set in compliance with *The International Standard Classification of Education*

(ISCED) [17] and *The European Qualifications Framework (EQF)* [18].

2.2.1. Analysis of the results

The regression model of the lowest order, which meets the requirement of adequacy, based on the conducted ANOVA analysis [19-21] is a second-order polynomial, i.e. Quadratic model:

$$R = \beta_0 + \beta_1 A + \beta_2 B + \beta_{12} AB + \beta_{11} A^2 + \beta_{22} B^2 \quad (1)$$

In this model, **R** is the dependent variable, **A** and **B** are independent variables,  $\beta_0, \beta_1, \beta_2, \beta_{12}, \beta_{11},$  and  $\beta_{22}$  are the model term, i.e. regression coefficients.

The Model F-value of 4.83 (Table 4) implies that the model is significant. There is only a 0.02% chance that the Model is not significant.

Table 4. ANOVA for Response Surface Quadratic Model

Source	Sum of Squares	df	Mean Square	F Value	p-value Prob > F	
Model	8921.08	5	1784.22	4.83	0.0002	significant
A-LE	1624.17	1	1624.17	4.39	0.0361	
B-YWE	1821.31	1	1821.31	4.93	0.0265	
AB	721.35	1	721.35	1.95	0.1625	
A^2	965.73	1	965.73	2.61	0.1061	
B^2	6144.60	1	6144.60	16.623	< 0.0001	
Residual	1006310.97	2723	369.56			
Cor Total	1015232.05	2728				

The values of "Prob > F" less than 0.0500 indicate that the model terms are significant. In this case A, B, and B2 are significant model terms. The values greater than 0.1000 indicate that the model terms are not significant.

2.2.2. Diagnosis of Statistical Properties of the Predicted Model

The normal probability plot of the residuals (Figure 1) indicates non-normality in the error term, which may be corrected by a transformation.

The Box-Cox diagnostics [21, 22] recommends the "Square-root" transformation for variance stabilization.

2.2.3. Transformation of the Predicted Model

The new, transformed model is presented in this form:

$$\text{Sqrt}(R) = \beta_0 + \beta_1 A + \beta_2 B + \beta_{12} AB + \beta_{11} A^2 + \beta_{22} B^2 \quad (2)$$

The repeated analysis for *Square-root* model transformation confirms the significance of the Quadratic Model (Table 5).

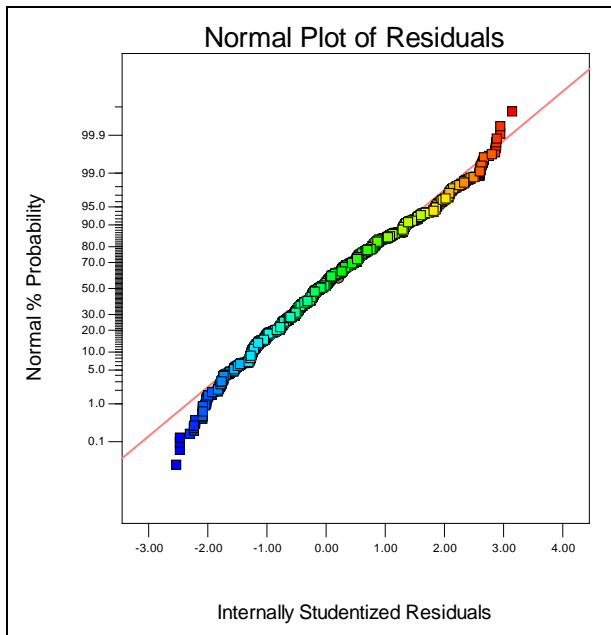


Figure 1. Normal probability plot of Internally Studentized Residuals

The Model F-value of 4.51 implies that the model is significant. There is only a 0.04% chance that the model is not significant. The values of "Prob > F" less than 0.0500 indicates that the model terms: A, B, A<sup>2</sup> and B<sup>2</sup> are significant model terms. The values greater than 0.1000 indicate that the model terms AB are not significant.

The new improved model is presented in this form:

$$\text{Sqrt}(R) = \beta_0 + \beta_1A + \beta_2B + \beta_{11}A^2 + \beta_{22}B^2 \quad (3)$$

The ANOVA in this case confirms the adequacy of the Reduced Quadratic Model (Table 6).

The Model F-value of 5.17 implies that the model is significant. In this case, all the model terms are significant.

Individual regression coefficients, Standard error, 95% confidence interval and Variance inflation factor (VIF) for the regression coefficient are shown in Table 7.

Table 5. ANOVA for Response Surface Quadratic Model

Response	I	R				
Transform:	Square Root	Constant:	0			
ANOVA for Response Surface Quadratic Model						
Analysis of variance table [Partial sum of squares - Type III]						
Source	Sum of Squares	df	Mean Square	F Value	p-value Prob > F	
Model	28.62	5	5.72	4.51	0.0004	significant
A-LE	6.77	1	6.77	5.34	0.0210	
B-YWE	4.93	1	4.93	3.89	0.0488	
AB	2.334	1	2.34	1.84	0.1749	
A <sup>2</sup>	4.84	1	4.84	3.81	0.0509	
B <sup>2</sup>	18.26	1	18.26	14.39	0.0002	
Residual	3456.43	2723	1.27			
Cor Total	3485.05	2728				

Table 6. ANOVA for Response Surface Reduced Quadratic Model

Response	I	R				
Transform:	Square Root	Constant:	0			
ANOVA for Response Surface Reduced Quadratic Model						
Analysis of variance table [Partial sum of squares - Type III]						
Source	Sum of Squares	df	Mean Square	F Value	p-value Prob > F	
Model	26.28	4	6.57	5.17	0.0004	significant
A-LE	6.95	1	6.95	5.47	0.0194	
B-YWE	6.99	1	6.99	5.50	0.0191	
A <sup>2</sup>	5.11	1	5.11	4.02	0.0450	
B <sup>2</sup>	18.29	1	18.29	14.41	0.0002	
Residual	3458.77	2724	1.27			
Cor Total	3485.05	2728				

Table 7. Coefficients for the Reduced Quadratic Model

Factor	Coeff.	df	Stand. Error	95% CI		VIF
				Low	High	
Intercept	8.549	1	0.0348	8.481	8.618	
A-LE	-0.207	1	0.0887	-0.381	-0.034	1.825
B-YWE	-0.122	1	0.0521	-0.224	-0.020	1.178
A <sup>2</sup>	0.344	1	0.1717	0.008	0.681	1.837
B <sup>2</sup>	-0.399	1	0.1052	-0.606	-0.193	1.172

The Final Equation of the predictive model in Terms of Coded Factors is:

$$\text{Sqrt}(R) = 8.549442362 - 0.207492094*A - 0.12219104*B + 0.344239483*A^2 - 0.399341225*B^2 \quad (4)$$

The Final Equation of the predictive model in Terms of Actual Factors is:

$$\text{Sqrt}(R) = 8.824 - 0.224*LE + 0.034*YWE + 0.022*LE^2 - 0.001*YWE^2 \quad (5)$$

2.2.4. Diagnosis of Statistical Properties of the Reduced Quadratic Model

After transformation of the model, the response variance is stabilized, the distribution of the response variable is closer to the normal distribution, and the fit of the model to the data is improved. None of the plots: a) a normal probability plot of studentized residuals, b) a plot of studentized residuals versus the predicted values, and c) a plot of studentized residuals versus run order, reveals any model inadequacy.

After the applied Box-Cox procedure, the optimum value of λ is 0.47 and the 95% confidence interval for λ contains the value 0.47, so the use of a Square root transformation is indicated (Figure 2).

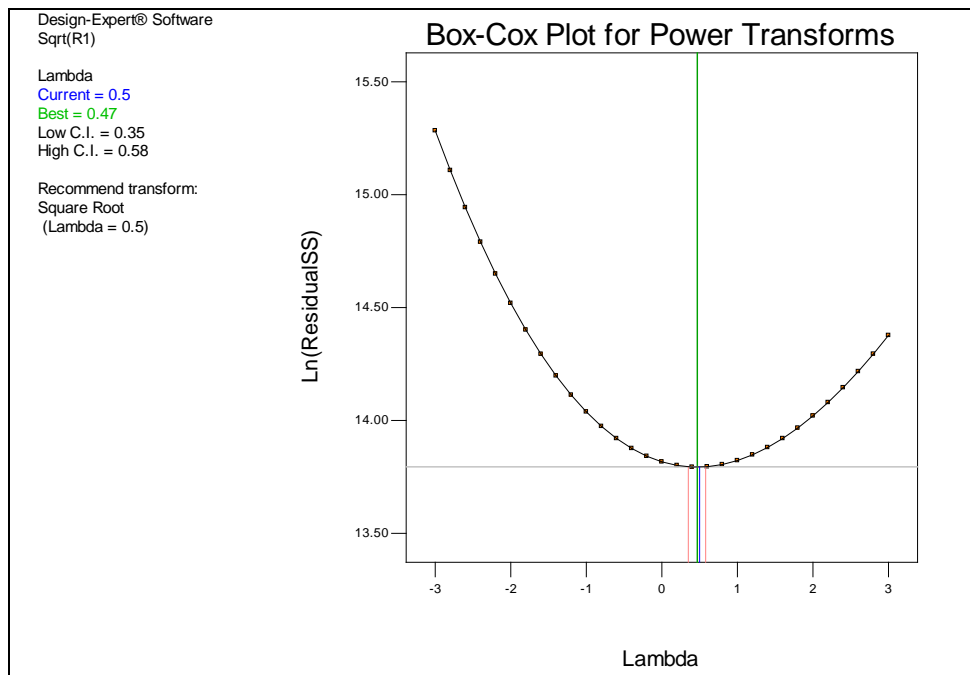


Figure 2. Box-Cox plot for power transformations

2.2.5. Model Graph Examination

The plots of the conversion response surface and contour plot, respectively, for the fitted model are shown in Figures 3 and 4. It can be seen that the level of market orientation is in non-linear dependence from the LE and YWE. The response surface plot indicates that the maximum level of marketing orientation is at the point where A= 1 and B=17.

The Perturbation plot (Figure 5) shows how the response changes when each factor moves from the chosen reference point, with other factors held constant at the reference value. This diagram clearly shows the opposite effects of analysed factors.

As ANOVA analysis showed that there is no interaction between the analysed factors A and B, they can be analysed individually.

Figure 6a shows the influence of variable A for B=20. The dotted line on the same diagram shows the 95% interval of confidence in which the theoretical line is R=f(A)<sub>B=20</sub>.

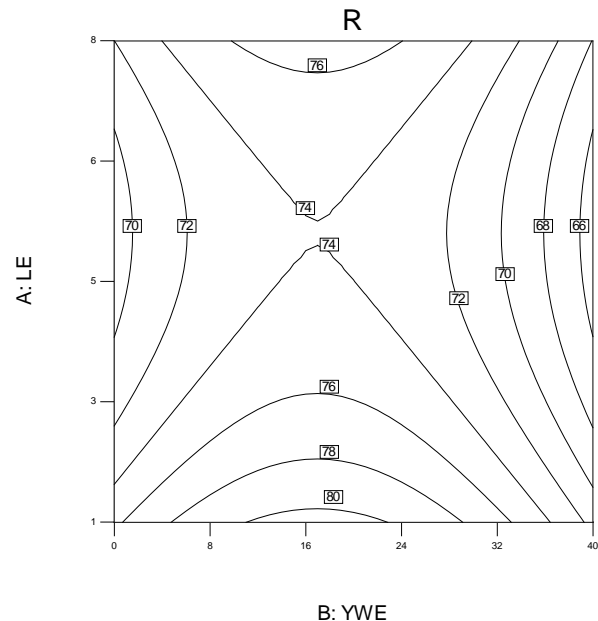


Figure 3. Response surface contour plot

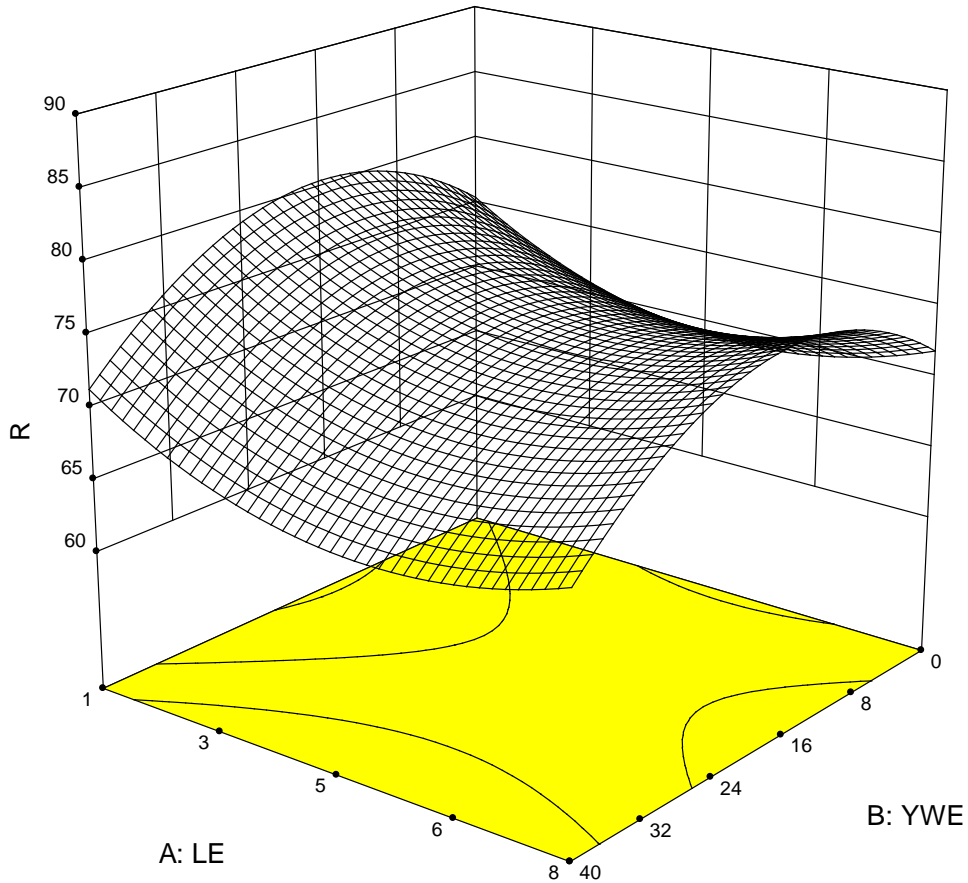


Figure 4. 3D response surface plot

The highest level of awareness about market orientation can be found at the lowest LE ( $R=80$  for  $A=1$ ) and highest LE ( $R=77$  for  $A=8$ ). The lowest level of awareness can be found among the employees with the middle level of education ( $R=74$  for  $A=4$ ), and they present the main part of the examined employees. This means that something should be changed in the system of education so that the way of thinking and organizational culture could be changed and lead to the market way of thinking.

Figure 6b shows the influence of factor B (YWE) for  $A=4$ . The dotted line in the same diagram shows the 95% interval of confidence for function  $R=f(B)_{A=4}$ . It can be seen that the employees with the highest number of years of experience ( $R=65$  for  $B=40$ ) have the lowest level of awareness about market orientation, while the highest level of awareness is shared by the employees with 20 years of experience ( $R=75$ ). The good fact is that the employees with the fewest years of experience ( $B=0$ ) have a higher level of awareness of the need to be market-oriented than the oldest employees ( $R=70$ ). Young workers are probably still not aware of the importance to be market-oriented, while older workers, who are at the end of their careers are under the influence of long-term contractual economy. In any case, it is positive that the employees with working experience between 10 and 30 years are aware of the changes which should be done.

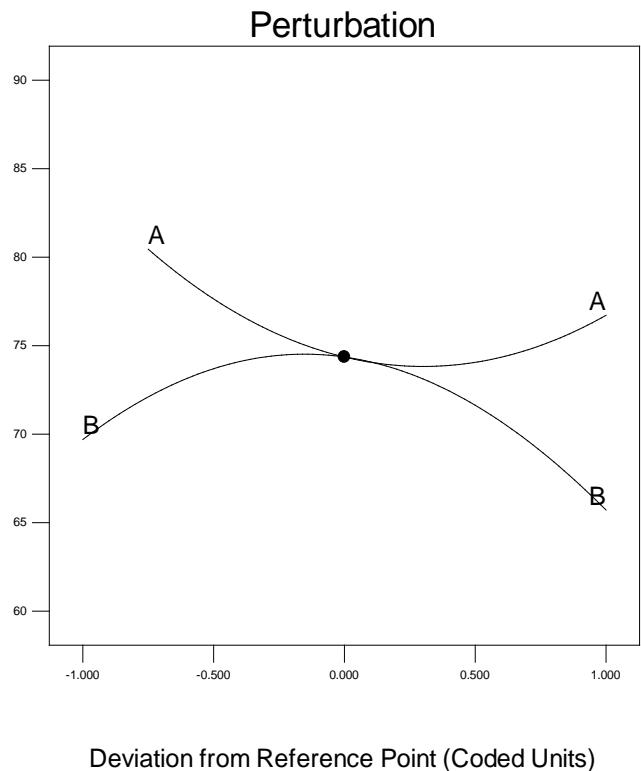


Figure 5. Perturbation plot

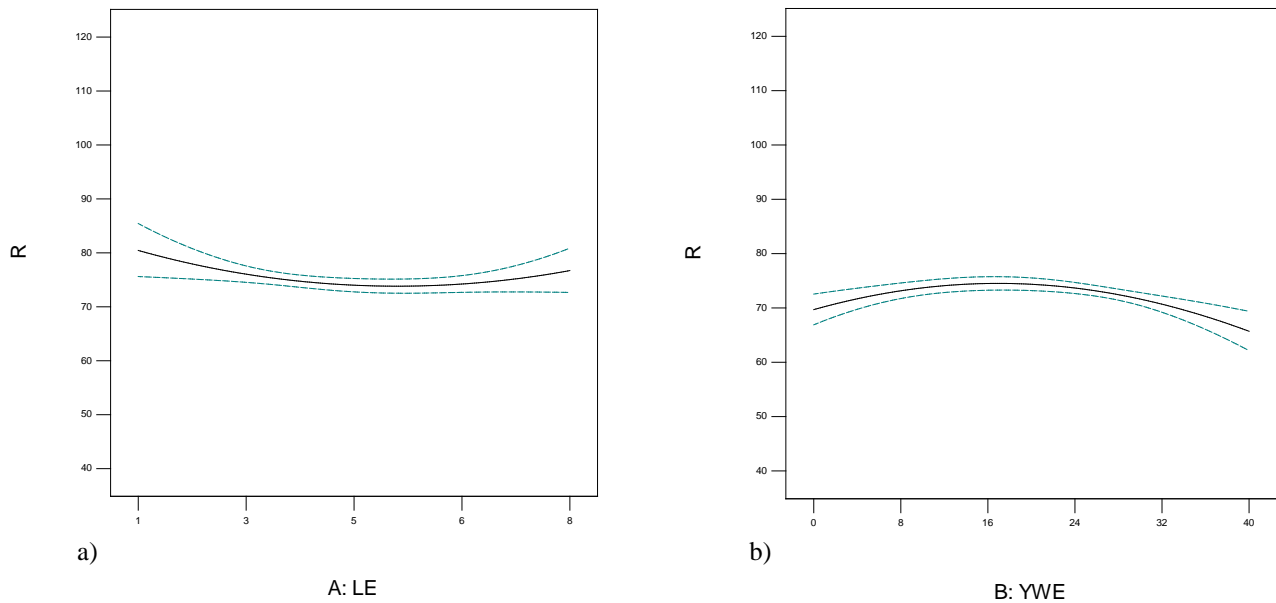


Figure 6. a) Influence of the level of education, b) Influence of the years of working experience

### 3. CONCLUSIONS AND FUTURE RESEARCH

The conducted study has showed that the level of market orientation in Serbian SMEs is unsatisfactory. Deeper analysis and the history overview have confirmed that the principles of contractual economy are still deep in the thoughts of all employees. What is especially worrisome is the fact that top management also have such opinions. Besides that, the political influence and the influence of the Government on setting up top management in companies in reconstruction deeply slow down strategic decisions which should be based on scientific opinion. Despite the fact that all companies included in this research have implemented QMSs, they did not succeed in implementing market principles in their structures and behaviour, i.e. market management in their business, which is a prerequisite for TQM implementation.

The conducted research should be expanded to all companies in the Serbian metal complex as well as to companies from other branches. The results will for sure give a much clearer picture about the organizational culture in Serbia. Also, in further research, some new variables should be included, such as: type of business, size of the company, occupation, type and kind (state or private), etc. We believe that this kind of research should be conducted beyond the Serbian borders, in all countries in transition and in a wider region.

For businesses in underdeveloped economies, and for economies in transition, which are numerous, this is very important. They have to find a way how to get to the market, but, simply, problems related to their successful business operations are much more complex. Problems in developing world economies have mainly a multidimensional character [16]:

- lack of quality marketing practices,
- lack of adequate technological equipment,
- lack of adequate financial means,
- lack of satisfactory management behaviour,
- presence of political and economic instability, etc.

If the research gives such results that they indicate a low level of market orientation, then the company reengineering should be launched (all processes, management), which would give a basis for developing a totally new management methodology-company reengineering. This methodology will primarily be important for countries in transition and all specificities of national cultures should be considered. Also, the new methodology must take into consideration the need to have long-term management and a balanced and integrated approach to the business structure of the business subject.

Therefore, identification of the level of market orientation in the companies in transition should be the starting point for defining a methodology for solving problems in the companies which are striving to achieve TQM.

### REFERENCES

- [1] A. Gunasekaran, "Enablers of total quality management implementation in manufacturing: a case study", *Total Quality Management*, Vol. 10(7), pp. 987-996, (1999). doi:10.1080/0954412997172
- [2] M. A. Youssef, "The impact of total quality management on firms' responsiveness: an empirical analysis", *Total Quality Management*, Vol. 7(1), pp. 127-144, (1996). doi:10.1080/09544129650035098
- [3] G. Salegna and F. Fazel, "Obstacles to implementing quality", *Quality Progress*, Vol. 33(7), pp. 53-57, (2000)
- [4] A. M. R. Mosadegh, "The impact of organizational culture on the successful implementation of total quality management", *The TQM Magazine*, Vol. 18(6), pp. 606 – 625, (2006). doi:10.1108/09544780610707101
- [5] L. V. Gerstner, "Who says elephants can't dance? Inside IBM's historic turnaround", New York: HarperCollins, (2002).

- [6] F. A. Al-Bourini, G. M. Al-Abdallah and A.A. Abou-Moghli, "Organizational culture and total quality management", *International Journal of Business and Management*, Vol. 8(24), pp. 95-106, (2013). doi:10.5539/ijbm.v8n24p95
- [7] N. Jančićević, "Organizaciona kultura: kolektivni um preduzeća". Ulixes, Novi Sad (Srbija), (1998).
- [8] S. Gallagher, C. Brown, L. Brown, "A strong market culture drives organizational performance and success", *Employment Relations Today*, Vol. 35(1), pp. 25- 31, (2008). doi:10.1002/ert.20185
- [9] V. Grover, S.R. Jeong, W.J. Kettinger and J.T.C. Teng, "The implementation of business process reengineering", *Journal of Management Information Systems*, Vol. 12(1), pp. 109-144, (1995).
- [10] D. Marchand and M. Stanford, "Business process redesign: a framework for harmonizing people, information and technology, *Business Process Change: Concepts, Methods and Technologies*". Ideas Publishing. Harrisburg (United States), (1995)
- [11] M.G. Wells, "Business process re-engineering implementations using Internet technology", *Business Process Management Journal*, Vol. 6(2), pp. 164-184, (2000). doi: 10.1108/14637150010321303
- [12] S. F. Slater, "Market orientation at the beginning of a new millennium", *Managing Service Quality: An International Journal*, Vol. 11(4), pp. 230-233, (2001). doi:10.1108/EUM0000000005609
- [13] S. F. Slater and J. C. Narver, "Market Orientation and the Learning Organization", *Journal of Marketing*, Vol. 59(3), pp. 63-74, (1995). doi:10.2307/1252120
- [14] S. F. Slater and F. Stanley, "Market orientation at the beginning of a new millennium", *Managing Service Quality*, Vol. 11(4), pp. 230-232, (2001).
- [15] C. R. Cano, F.A. Carrillat and F. Jaramillo, "A meta-analysis of the relationship between market orientation and business performance: evidence from five continents", *International Journal of Research in Marketing*, Vol. 21(2), pp. 179-200, (2004). doi: 10.1016/j.ijresmar.2003.07.001
- [16] Lj. Pecić, M. Klarin, D. Trifunović and P. Dašić, "Marketing-oriented organizational culture and implementation of total quality management: The case study of Prva petoletka", *Metalurgia International*, Vol. 18(6), pp. 121-126, (2013).
- [17] UNESCO, *International Standard Classification of Education ICED 2011*, UNESCO Institute for Statistics, Montreal, 2012. <http://www.uis.unesco.org/Education/Documents/isced-2011-en.pdf>
- [18] European Commission, *Referencing National Qualifications Levels to the EQF*, ISBN 978-92-79-26563-1, Belgium, 2013. <http://ec.europa.eu/ploteus/sites/eac-eqf/files/EQF%20131119-web.pdf>
- [19] D. Montgomery, "Design and Analysis of Experiments, 5th edition", New York: John Wiley&Sons, Inc, (2001).
- [20] N. Draper, and H. Smith, "Applied Regression Analysis, 3rd edition", New York: John Wiley&Sons, Inc., (1998).
- [21] R. H. Myers, D. Montgomery and C. Anderson-Cook, "Response Surface Methodology: Process and Product Optimization Using Designed Experiments, 3rd edition", New Jersey: John Wiley & Sons, Inc., (2009).
- [22] G. Box and N. Draper, "Response Surface, Mixtures, and Ridge Analyses, 2nd edition", New Jersey: John Wiley & Sons, Inc., (2007).

# Essential Requirements for Sustainability Compliance in the Process of Exploitation Machines

Miljan D. Cvetković, Žarko Janković, Dragan S. Cvetković<sup>1</sup>

<sup>1</sup>Faculty of Occupational Safety in Nis, University of Nis, Paper is the result of research within the project TR 37020

**Abstract:** *The nature of the free market imposed certain mechanisms in the form of mandatory requirements. Among these mechanisms important place occupied by the so-called New Approach (New approach) to determine the essential technical requirements for products and the Global Approach (Global approach) to determine compliance. This paper attempts to answer the following questions: What happens to the product when it passes into the phase of exploitation? How long process owner can count on the projected level of acceptable risk, as well as the validity of the CE mark of conformity?*

*The remaining risk is considered to be the risk that accompanies the product after compliance with current directives of the new approach and harmonized standards. Problem residual risk requires an analytical approach to the dominant processes that require specific engineering knowledge, based on risk management, with the aim to highlight and emphasize the character of engineering, which corresponds to the concept of integrated safety needs of processes and preserving the health of the employee.*

**Keywords:** compliance; residual risk, risk management g

## 1. INTRODUCTION

Each process owner has the overriding aim is to develop and improve the operations and competitiveness on the market. From the aspect of the process as an element on which rests quality management, we see that security has the same indivisible character to the owner of the process, and for the community. Industrial production of the production system as an embodiment of the process of transformation of input values (inputs) at the designed value of the output (output) also necessarily entails the same safety and sustainability. The authors' intention is that the work of analysing the risk management process, based on the elements of safety equipment in the process of exploitation. The concept of risk is associated with the context of the system of "safety and" health "(Occupational Safety and Health), the current model of the system of safety at work. Safety, as well as the system has been developed in the organizational form in legal entities (Protection du travail, Occupational Safety, Arbeitsschutz, Ohrana bezopasnosti truda) as well as organized social function, resulting in the time of an objective reality of social development in the process of replacement of manufacturing, industry and the introduction of machines in production processes.

Machine as a product and as a part of the process by definition, the assembly is provided and designed for fitting a drive system which is not used directly to human or animal power and which is composed of interconnected parts or components for specific purposes, of which at least one is driven by [1]. From the aspect of safety, the machine as the product passes through three logical "life" phases: production, placing on the market and exploitation. The last phase, the owner of the process requires that the safety of the products used machines - held management tools, based on risk. The meaning of proper maintenance has not achieved security value in the process of creating a product, be sustainable throughout its

lifetime. Only such an approach will justify the efforts being made in the creation of the product and its safety value for the market.

The interest of the authors in this paper is to analytically examine the dominant processes that require specific engineering knowledge, based essentially on the basis of risk management, point out and emphasize the character of engineering engagement which corresponds to the concept of integrated and needs in the field of controlled safety, as a result of residual risk.

## 2. TERM RESIDUAL RISK

What is meant by the term "residual risk"? The remaining risk is considered to be the risk that accompanies the product after compliance with current directives of the new approach and harmonized standards. On the other hand, the remaining risk is a collection of factors that its presence in the "process" can endanger the health of entities that process realized, if we follow the procedures laid down and which are a function of "process control" over the operations in which the real hazards exist within the limits allowable value.

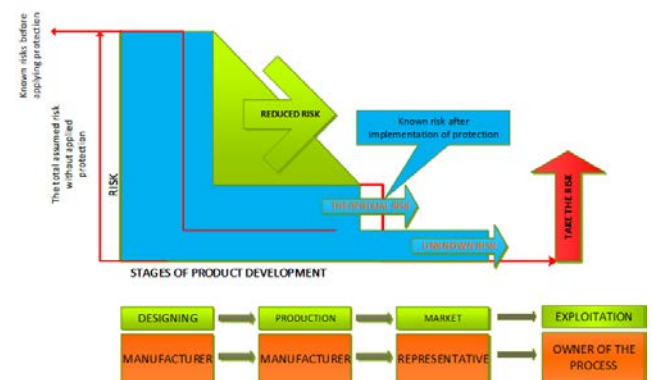


Figure 1.01 Procedure control over risk

Safety equipment such products intended for the market, involves conceptual omission unacceptable risk or damage, establishing the most appropriate relationship between a number of factors, including non-technical as well as human behaviour, and to reduce the risk to people and property to an acceptable level. Safe product - essentially any product which, under normal or reasonably foreseeable conditions of use, including installation, commissioning, operation, and requirements in terms of maintenance, does not present any risk or presents minimal risk to the appropriate use of the product and considered to be acceptable and matched with a high level of safety and health protection. This stance, articulated in the documents of the new approach raises the question. How and why the residual risk is defined as the reason for his record?

The answer is in chronological facts; that is to ensure the free flow of goods on the market, the European Union has developed certain mechanisms in the form of mandatory requirements. Among these mechanisms important place occupied by the so-called New Approach for determining the essential technical requirements for products and global approach to determine compliance. These two approaches complement each other.

**New approach:** The new approach means the set of legislative tools (directives) that prescribe the essential requirements to be met by each product. The process of fulfilling the essential requirements are most easily implemented through the use of the harmonized standard, which is a European standard published in "Official Journal of the European Union". For the preparation and publication of these standards are in charge of European standardization organizations:

CEN - European Committee for Standardization, in charge of general standards and standards that are not within the jurisdiction of the other two organizations listed below;

CENELEC - European Committee for Electrotechnical Standardization, in charge of electrical standards; and

ETSI - European Telecommunications Standards Institute, in the field of telecommunications standards.

Harmonized standards by its concept includes the basic technical requirements for products to which the new approach directives. Each product, which is designed, engineered and manufactured to meet the demands of the applied harmonized standards, it is expected realized with an excess degree of probability that the product complies with the essential requirements of new approach applied. When it comes to machine safety, there are different types of harmonized standards:

**STANDARDS TYPE - A** - European standards which define the basic requirements for all types of machines, and regulating the basic concepts and principles of design of machinery. Conceived as a form in which to interpret the requirements of the Directive and the Regulations on the safety of machinery.

**STANDARDS TYPE - B** - European safety standards. Essentially discuss aspects of security and the protection of designs, which can be applied to a large

number of machines. Within this category, there are two sub-categories of standards:

Standardization of the type - B1 - defining specific aspects of safety (e.g., distance, noise, temperature)

Standardization of the type - B2 - which describe devices that are related to the types of protection (eg. the command, the fence, locking devices)

**STANDARDS TYPE - C** - European standards regarding security for specific machine types. Contain detailed requirements for safety and specific sources of risk. With respect to a specific character, as a rule, have an advantage in the application, in relation to the standards of type A and B.

The current European regulations unequivocally insists on considering the phenomenon of risk on the machines as a means of work, based on the principle of prevention. Harmonized standard that gives guidelines for the implementation of risk analysis is EN ISO 12100 Safety of machinery - General principles for design - Risk assessment and risk reduction. This standard specifies general terminology, principles and methods for achieving safety in the design of machinery. Standard describes the procedure and for the identification of risk and risk assessment, during certain stages in the life cycle of the machine, as well as to remove the threat or risk of remaining. The document on risk analysis shall be accompanied by the technical file and machinery, which is delivered to the user, and may be available to search for and market surveillance. Technical file is saved to make it available to market surveillance for at least 10 years from the last date of manufacture of the machine type. Any avoidance of dealing with the technical file and intolerance control at their request, constitutes grounds for doubting the conformity of machinery with the essential requirements of the Directive or the Rules on security.

Global approach, establishing the institutional environment for checking compliance with the essential requirements of the directive, the implementation of conformity assessment procedures. Methods of conformity assessment are grouped into eight modules, designated by letters A to H. Evaluation procedure is a process which comprises the step of the product design, the manufacturing stage of the product and one or and the second phase. Manufacturer in accordance with the technical characteristics of the product, as well as the risk that the product is worn in use, selects the appropriate method of conformity assessment for each of the applicable directive.

Conformity assessment procedures implemented by the producer or the notified body. Conformity assessment is carried out in relation to the module from A to H, with the exception of the Directive on construction products, for which do not apply global access.

When it comes to modules of conformity assessment, Directive/Ordinance gives the possibility to the manufacturer that I set the appropriate conformity mark (CE mark or Serbian conformity mark), if the machine is made in compliance with all harmonized, and Serbian



standards that apply to it and covering all aspects of health and safety.

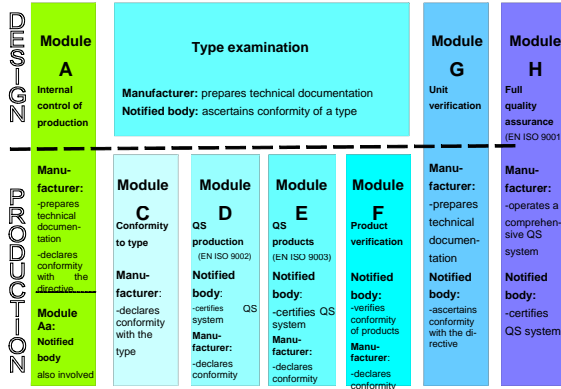


Figure 1.02 Conformity assessment procedures of the new approach the modules

Conformity assessment is carried out according to defined procedure depending on the nature of the product and the level of applied binding documents.

In cases where the machine is not listed in the list of machines in Annex 4 of the Directive - Ordinance applies to internal production control, as well as conformity assessment module.

If a machine listed in Annex marked and manufactured in accordance with harmonized standards that cover all essential requirements applied to one of the modules of conformity assessment:

- the internal production control<sup>1</sup>
- (EC) type examination<sup>2</sup>
- Full quality assurance<sup>3</sup>

<sup>1</sup> Procedure of internal production control, the manufacturer guarantees that the machine meets all the essential requirements of the Directive / Regulation. It is understood that the manufacturer for each machine type produces technical documentation, and that during the process of manufacture provides a machine made compliance to specifications [5].

<sup>2</sup> Examination is the procedure whereby notified (in the EU) or appointed (in Serbia) confirms that the body is a machine made in accordance with the Directive / Regulation. Manufacturer constitutes the technical documentation for each machine type, then the manufacturer or his ovlašćenizastupnik submitted to the notified (notified) body requirements of (EC) type examination. The notified (called) the body shall review the technical documentation, controls, perform measurements and tests. If the type complies with the requirements of Directive / Regulations, is notified to the (known) of a certificate issued by the body (EC) type examination. Thereafter, any change in the type of equipment must be reported to the notified (notified) body. Every five years is necessary to make an extension of the certificate, otherwise the machine can not be placed on the market. Certificates and documents relating to the type examination are kept for 15 years. [5].

<sup>3</sup> This procedure notified (appointed) body approved quality system manufacturers of machines and monitor its implementation. The manufacturer or his authorized

With regard to the machines listed in Annex 4 of the Directive - Rules, and not in accordance with harmonized standards, or are partially applied harmonized European standards, and Serbian standards, which do not cover all the essential requirements, or where there are harmonized and Serbian standards applied to one of the following modules for conformity assessment:

- (EC) an overview of the type + Internal production control
- Full quality assurance

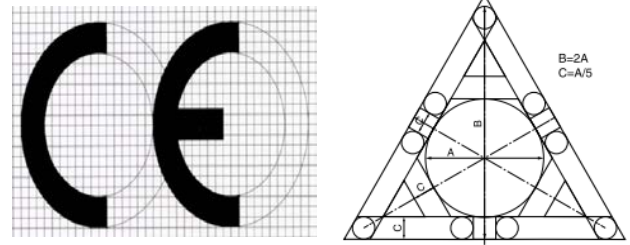


Figure 1.03 European and Serbian conformity mark

After carrying out the procedures of conformity assessment; EC - Declaration of conformity of machines, the manufacturer declares that his product is in compliance with applicable directives - regulations. The declaration of conformity with the product on the market, and keeps the manufacturer or his authorized representative, at least 10 years from the last date of manufacture of the machine type. The declaration must be in Serbian (if it is a product which is produced in Serbia), English, and, optionally, the language of the target market.

Finally, following the procedure of labelling products with CE mark, and is set after making the EC declaration of conformity and is not a mark of quality but a proof that the product meets all the requirements given in the Directives relating to the product and that it is carried out conformity assessment procedures. By placing CE marking on a product, the manufacturer ensures that the product is designed, manufactured and complies with the essential requirements of the New Approach Directives applicable to the product. The manufacturer is the one who is responsible for the final product, regardless of component parts used and integrated components. It is certain that partner's component parts suppliers must obtain the necessary certificates, approvals, CE mark or test results

representative shall submit an application for assessment of the quality system the notified (notified) body. The notified (appointed) body assesses the quality system (does not have to be certified, but the certificate ISO 9001 facilitates the process). What checks and controls plant manufacturers (through review of documentation and insight into the functioning of the quality system). The manufacturer shall apply an approved quality system for design, manufacture, final inspection and testing machines. The quality system must include procedures and measures for ensuring quality. Followed by checks for a year, a reassessment of the quality system for three years. However, as well as some unannounced visits. After approval of the quality system, any changes must be reported. They are kept for 10 years. [5].

from accredited laboratories for the goods delivered. In this way, the doctrine combines quality management.

CE is designed for market surveillance, also represents an unusually important assistance to the customer and a kind of "quasi-passport" to enter the EU market

### 3. RISK MANAGEMENT

Harmonized and marked Multiplies formally and actually has a guarantee that the estimated residual risk may be on the market, products ready to enter the exploitation phase and becomes an integral part of the creation of new value. At the same time, it must be stressed that the harmonized product itself does not represent an absolutely safe product even though they are administered expert risk assessment procedures and implemented all the directives that apply to it. Modules for conformity assessment and freedoms that allowed the manufacturer to put himself CE conformity mark, hypothetically make it possible to "tune" Multiplies be defective and unsafe in operation with a higher degree of risk than the estimated residual risk.

Institutional tool to prevent such cases activation of residual risk is the Directive on general product safety, on whose principles established RAPEX rapid alert system, which applies to non-food dangerous products between Member States. The essence of the mechanism is developed to achieve rapid response alert system to ensure rapid notification of relevant bodies of dangerous products. The information in the RAPEX rapid alert system can be exchanged with non-EU countries. In the case of serious risks associated with the health and safety of consumers, in accordance with the Directive on general product safety provides for the possibility for the Commission to make interim decisions on the measures to be applied throughout the Union, the so-called "emergency measures". Under certain conditions, the Commission may decide to restrict or prohibit the placing on the market of products which pose a serious risk to the health and safety of consumers. Regulation (EC) No. 765/2008 impact of the directive is extended to all harmonized industrial products irrespective of who the end user, as well as products that pose a risk to other protected interests other than health and safety, such as risks to the environment.

Consequences that leaves acceptable - residual risk, contained far back as defective product. What is actually defective product or defective products? The answer to this issue then do not give positive legislation.

The legislature, the product is not correct if we take into account all the circumstances of the case, in particular the way the product is presented, the purposes for which the reasonable expectation of the product can be used as a time when the product was put into circulation, but does not provide the safety which is of such a product has a reasonable expectation. Security products that are reasonably expected from products is the main criterion that produce parts to safe and unsafe. In practice, such a method is characterized as a "consumer expectations test".

Parallel to this conclusion, the question of who is responsible for the damage? The legislation does not explicitly define entities that are passive and not actively legitimate. Endangered no knowledge of the amount of

damages, as well as the rule for determining the same. Another is a dilemma relating to the time frame in which realizes this responsibility?

Therefore, the right to wonder whether the manufacturer complies machines and marked automatically liable for the damage that they are causing in the exploitation phase. Based on current attitudes of European legislation that follows the "new approach" is NOT the answer. The injured person, regardless of whether the buyer or user of the defective - unsafe products, must "seek" redress to enforce his right. The injured party will determine the compensation only if he proves that he has suffered damage, the product was defective and that the damage caused by the product used. However, if it is determined that the injured party contributed to the damage, the responsibility of the producer may be reduced or even completely shut down. The injured party need not prove that the producer was negligent, because the Directive on product liability is based on the principle of "liability without fault". Therefore, the manufacturer will not be acquitted, even in cases where it is proved that he was not negligent, if considered caused by an act or omission contributing to a third party, if the applied positive norms or if his product has been tested.

Ten years after placing the product on the market, the manufacturer's liability cases, unless the court proceedings began. In this context, the injured party must initiate proceedings within three years since the damage, malfunction, or the identity of the manufacturer.

The manufacturer is required to identify the risks arising from their machines and to design a machine with integrated security to the same harmonized with the New Approach to designate a product CE label and market the same places, taking responsibility for all the situations that have been analysed in the paper. In accordance with the directives of the new approach, the manufacturer must identify hazards and assess risks associated with using the product. Risk assessment is an integral part of the process whereby the manufacturer ensures that the product does not endanger the health and safety of people,

The question then arises, which is of particular importance for the structure of this work, to evaluate responsibility for consequences resulting from activation of residual risk.

What happens to a product that the market moves to the phase of exploitation? How long process owner can count on the projected level of acceptable risk, as well as the validity of the CE mark of conformity?

The answer can be sought through processes that are integrated into the management. The owner of the process in the exploitation of the product can analyse the risks that are covered by harmonized standards. This means that it takes just bought the baton of responsibility for process safety and risk in the process introduces harmonized product. Hypothetically request the equipment supplier - Product is an acceptable risk to be within projected, to liability for damage could be attributed to the manufacturer.

How to respond to this request? Owner harmonized products, if it wants to secure the process is required to elements of the technical file which takes over from the manufacturer maintains at least as far as the obligation of the manufacturer to keep the data, and it is 10 years old. The question is whether the owner of the process of the current legislation obliges some deadlines. Serbian legislation that treats the phenomena of the risks expressly obliged only estimates. However, management processes almost do not recognize. Therefore, the question is how to prove that it is in the process of exploitation the owner maintained the level of residual risk? Does the process owner has valid maintenance records compliant machines or installations? Does the same owner has the obligation to using a fast algorithm for inspection and testing, check the level of compliance after a period of exploitation? The practice of this model obviously does not recognize. Liabilities arising from current national normative acts of inspection and testing equipment for operation are totally anachronistic in relation to the European regulations New and Global Approach.

Therefore, logically imposes a need to create a quick algorithm to control the security state machine based on the regulations of obtaining harmonized and labelled products. Only under such conditions we can speak about meeting customer expectations machines.

#### 4. CONCLUSION

The legislation, which regulates the elements of safety at work or those of health and safety at work, involves the principle of prevention and the development of services that employers use in the course of acceptable risk of any measures that ensure the suitability and safety of the process, and thus the safety of the operator, the environment and other material values.

In the case of equipment which is part of the process, which is marked with "CE" - mark, i.e. compliant means that in all satisfy the principle of prevention, then the engineering practice leaves the jurisdiction of that software downloaded from the manufacturer and that carries a certain level of residual risk, maintain functional and security attributes. The employer is obliged to implement procedures to ensure control over the condition of the equipment.

This fact is sufficient that the concept of risk and specific engineering knowledge to be managed risk classified elements of security processes in the highest level of proactive management model.

The function of such interest develops in the process model management set of tools based on the risk that corresponding with the concept of proactive management.

Only maintenance management, risk-based approach can serve as a basis for the design of management health and

safety, which are supported by engineering diagnostic methods, the concept of risk to convert into a powerful management tool and define the responsibility of each element in the process of exploitation, such as product conformity regulate the obligations of producers.

#### REFERENCES

- [1] Official Journal of the European Union. European Commission "Blue Guide" on the implementation of EU rules on products 2016.
- [2] European Commission: Guide to the implementation of directives based on the New Approach and the Global Approach, Luxembourg: Office for Official Publications of the European Communities, 2000
- [3] Arsovski S.: The project of establishing a QMS. in the way of establishing QMS, Kragujevac, 2001
- [4] Popovic P.: Accreditation and Conformity Assessment, University Singidunum, Belgrade, 2010
- [5] Serbian Chamber of Commerce, GUIDE FOR MACHINE SAFETY "How to get the CE mark and the Serbian conformity mark"? ISBN 978-86-80420-06-6)
- [6] Cvetković D., Cvetković M.: ENGINEERING PROFILE INTEGRATED SYSTEM OF SAFETY AT WORK, Proceedings of the 12th National Conference with international participation Improving the system of safety at work, Tara 2015
- [7] Cvetković D, Blagojević D.: RISK AS A TOOL prevention engineering, Proceedings of the XI. International Conference "risk and safety engineering" Kopaonik 2016, pp 552 – 561
- [8] Cvetković D.: VALIDITY OF ACTS OF THE RISK ASSESSMENT BASED ON OHS- system and the process of the forensic expertise, the world of work, journal issues of health and safety at work, occupational medicine and protection of musical environment for South Eastern Europe ISSN 1451-7841, Vol. 11 no. 2/2014, pp 255 - 264, 2014
- [9] Cvetković D; Cvetković M.: OCCUPATIONAL SAFETY AND HEALTH - THE SYSTEM WITH A PROACTIVE STRUCTURE Scientific Journal FACTA UNIVERSITATIS Series: Working and Living Environmental Protection, 2013; Vol. 10, No. 1, p. 69 – 78
- [10] Cvetković D.: Risk Assessment WORK process of executing medical expertise; 2012 JOURNAL OF SCIENTIFIC - PROFESSIONAL CONFERENCE Forensic expertise of non-pecuniary damage in occupational medicine, Vrnjačka Banja, the Council of Labour ISSN 1451-7841



## Partnership for Entrepreneurial Engineering Education

Milica Gerasimovic, PhD, Advisor/Coordinator<sup>1\*</sup>, Ugljesa Bugaric, PhD, Professor<sup>2</sup>

<sup>1</sup> Institute for Improvement of Education Belgrade Serbia

<sup>2</sup> University of Belgrade Faculty of Mechanical Engineering Serbia

Entrepreneurship is identified as important development goal for the future of the modern industry. New technologies require greater entrepreneurial activity in order to further strengthen its economic position. Reformed technical and engineering education system in Serbia is directed to strengthening vocational knowledge and acquiring of key skills necessary to join the world of work and the whole society. The new concept of curriculum has been introduced which, among the others, contains teaching subject entrepreneurship as a novelty. Within this subject students acquire: skills of planning, organizing, analyzing, communicating, realizing and evaluating; abilities for team work; abilities for proactive behaviour and positive reacting to changes; abilities for risk overtaking; positive attitude toward changes and innovation. This paper presents needs for model based on two-way communication and dialogue between learning and business environment. Main objectives of this partnership are: organization and joint efforts with the purpose of gaining wider public, making benefit of the enterprises of entrepreneurial education and development and improvement of the program of entrepreneurial education.

**Keywords: Entrepreneurial education, Enterprises, Partnership**

### 1. INTRODUCTION

The great scientific, economic and technical progress is typical for modern times, and refers specifically to the globalization and the revolution in information and communication technologies. Life-long entrepreneurial education should be a vital aspect of the educational process. The main objective of modern education system is development of competent students and future citizens, professionals and entrepreneurs. Vision of the knowledge society is a vision of society competent people whose ideas, innovation and knowledge are the main driver of development. The documents of European institutions define entrepreneurship as one of the eight key competencies in modern education: „Key competences represent transferable, multifunctional package of knowledge and abilities necessary for the individual to achieve personal fulfillment, development, professional mobility and employment. An individual acquire key competences at the end of vocational education and training and they represent the basis for individual's lifelong learning.”<sup>1</sup> This conceptualization of entrepreneurship as a key competence has since been further developed by the European Commission Thematic Working Group on Entrepreneurship Education: „Entrepreneurship education is about learners developing the skills and mind-set to be able to turn creative ideas into entrepreneurial action. This is a key competence for all learners, supporting personal development, active citizenship, social inclusion and employability. It is relevant across the lifelong learning process, in all disciplines of learning and to all forms of education and training (formal, non-formal and informal) which contribute to an

entrepreneurial spirit or behaviour, with or without a commercial objective.”<sup>2</sup>

The entrepreneurial and innovative spirit are defined by European key competencies framework as well as willingness to accept change, support and adaptation according to external conditions, to take responsibility for their own actions, developing strategic vision, setting and achieving objectives.

Has entrepreneurship been identified as important development goal for the future of the modern industry? The new industry comparative advantage lies in knowledge-based activities. Therefore, actions are needed that will boost growth through the creation of knowledge, innovation and business dynamism. As part of this process, new technologies require greater entrepreneurial activity in order to further strengthen its economic position.

The most economics agree that entrepreneurs are central to the functioning of the economy. According to Shook, Priem and McGee “the enterprising individual is a critical component of venture creation” [1]. Educational background and related industry experience of the entrepreneurs have well-established direct effects on the sales and company employment growth [2]. The same authors emphasize different capabilities required of the entrepreneur and employees depending on the companies growth strategy: creativities and technological capabilities requires in the case of external growth and innovation in the case of internal growth. Bush [3] lists three major entrepreneurial skill capabilities: visioning, bootstrapping and social skills. Markman and Baron [4] point out that the chances of entrepreneurial success grow in the presence of personal characteristics and skills such as self-efficacy, ability to recognize opportunities, personal perseverance, human and social capital and superior social skills.

<sup>1</sup> Recommendation of the European Parliament and of the Council of 18 December 2006 on key competences for lifelong learning. OJ L 394.

<sup>2</sup> Agreed on in Geneva on 18 January 2012 by a working group that included representatives from ETF, GIZ, ILO, UNESCO and UNEVOC.

## 2. ENTREPRENEURIAL LEARNING ENVIRONMENT

Modernization and development of the technical and engineering education system in Serbia is based on principals of social partnership, decentralization, accessibility, openness, program and organizational variety, professionalization of the teachers' and associates' work, as of outcome orientation [5]. Teaching contents have modular organization whereas modules, specific segments of learning, lead to achievement of clearly defined learning outcomes i.e. to acquirement of vocational competences (knowledge, skills and attitudes). Reformed technical and engineering education system is directed to strengthening vocational knowledge and acquiring of key skills necessary to join the world of work and the whole society. Strategy of technical and engineering education system development in Serbia [6] foresees possibility to acquire business and entrepreneurial skills and knowledge through education. Education Development Strategy in Serbia 2016-2020 [7] supports the concept of "entrepreneurial university" as nuclei of the creation of new industries based on knowledge. Strategy provides that all institutions of higher education should enable students to develop innovation and entrepreneurship.

### 2.1. Entrepreneurial Engineering Education

Growing businesses need to adapt to environmental and technological changes. This major will prepare students for the challenges of establishing and growing a business in today's dynamic climate. This major communicates the skills and techniques behind entrepreneurial thought and action, imparting expertise which enables managers and entrepreneurs to make crucial decisions and compete successfully. Business creation and business development competences are keys to the global business arena of the future. Furthermore, it is a requisite for a range of organisations, from large private and public companies to small and medium-sized companies, start-up companies, as well as public service and knowledge-based organisations.

It is no longer enough to come out of school with a purely technical education; engineers need to be entrepreneurial in order to understand and contribute in the context of market and business pressures. For engineers who start companies soon after graduation, entrepreneurship education gives them solid experience in product design and development, prototyping, technology trends, and market analysis [8]. These skills are just as relevant for success in established enterprises as they are in start-up's; students with entrepreneurial training who join established firms are better prepared to become effective team members and managers and can better support their employers as innovators. Entrepreneurship education teaches engineering students in all disciplines the knowledge, tools, and attitudes that are required to identify opportunities and bring them to life. Students who take part in entrepreneurship programs as undergraduates gain insights not available from traditional engineering education, such as understanding and designing for end users ("empathy"), working in and managing interdisciplinary teams, communicating effectively, thinking critically, understanding business basics, and solving open-ended problems [9], [10].

First models of dual university education in Serbia occurred at the areas of computing, i.e. software development and information technology. This model is

related to formal university education and informal acquisition of applicable professional knowledge and skills students work on practical problems in companies. Students are trained to acquire competences required employers. Students who are educated in this way, easier get a better job, but also get the opportunity to study free of charge and scholarship. According to the dual concept is expected that the average student spends 40 hours a week at the university. Half of the time the student participates in class (lectures and exercises), a half-time in the company where implemented continuous professional training during their studies. Company in this way ensure its future engineers educated in accordance with their needs. They are ready to provide them with employment after graduation, free studies and scholarships during their studies.

According these strategies the new concept of curriculum has been introduced which, among the others, contains teaching subject entrepreneurship as a novelty. Within this subject students acquire: skills of planning, organizing, analyzing, communicating, realizing and evaluating; abilities for team work; abilities for proactive behaviour and positive reacting to changes; abilities for risk overtaking; positive attitude toward changes and innovation.

Entrepreneurship as a subject represents consistent part of curricula of all educational profiles in technical education, secondary education level and elective course in engineering education level. The objectives of the subject are set as follows [7]:

- development of business and entrepreneurial knowledge, skills and behaviour;
- development of entrepreneurial values and abilities to recognize entrepreneurial opportunities in the local market and to act accordingly;
- development of business and entrepreneurial way of thinking;
- development of consciousness of own knowledge and abilities in further professional orientation;
- development of ability for active job seeking (employment and self-employment);
- development of ability to make a simple business plan for a small firm.

The program of the entrepreneurship subject is organized thematically and based on learning outcomes. Up on the end of defined themes, the student has acquired the outcomes of entrepreneurial knowledge and skills e.g. he/she will be able to:

- explain the significance of motivational factors in entrepreneurship;
- develop marketing strategy for his/her business idea and to present his/her marketing plan;
- collect information needed to lead a successful business;
- compose financial reports in the most simple form (balance-sheet, cash-flow of the enterprises);
- make a simple business plan according to adopted business idea.

Serbian education system define the concept of entrepreneurial learning as a entrepreneurial learning environment in which students acquire a wide range of competencies that may have broader individual, social and

economic benefits. Entrepreneurial competence can be applied in every aspect of life and throughout life.

## 2.2. National model of dual and entrepreneurship education

Elements of dual education have long existed in our educational system. It is assumed that the unsustainability of such a dual system in the past was the result of a separate and independent attending theoretical and practical classes. As research has shown, this model was an inadequate way for profiling students for comprehensive integration into modern trends based on innovative and dynamic systems of social processes. Such an approach makes it impossible to adequately involving students, future professionals, in a very demanding processes dictated by modern technology and the labour market. Serbia has created a dual national model of entrepreneurship education and support with respect to the experiences of Switzerland, Germany and Austria. The starting point in the objectives of this model consists of the needs of the economy and, in its formation equally involved the Ministry of Education, Science and Technological Development and the Serbian Chamber of Commerce. A significant step in advancing our secondary vocational education is signing of the contract by the school and parents with companies that will pay compensation to the student's work certainly represents. Benefit of this model, among others, presents opportunities for students that during formal education acquire functional knowledge in a real working environment. It also create the possibility that students after graduation employment. In this way will decrease the unemployment rate of young people up to 25 years. The role of companies in the framework of the active participation of young people in the production process is reflected in the significant reduction of the cost of the country which has so far invested heavily in equipment and raw materials classrooms-workshops in order to implement the students' practice. The introduction of dual education solves the problem of qualified workforce who would be through the formal process of dual education to enable active participation in the production process immediately after training and thus ensure the quality of company operations. New methodology for planning enrolment in secondary vocational schools has been developed and includes representatives of businesses, local governments, National Employment Service, school directors and representatives of the Ministry of Education.

Serbia is now possible to carry two models of dual access to education. One is **Dual-curricular education** that would be done since elementary school and would include all children in the education system. Another model is **Dual education aimed at the practice that takes place in businesses**.

The dual system is necessary to ensure the aspect of encouraging creative and conceptual approaches that give meaning and made a synthesis between the acquired theory and practice, and that students directed towards the creative pooling their knowledge, but also the directing of their knowledge and experience in a freely chosen areas of interest. National model of dual education allows students to develop an active approach to acquiring and linking different knowledge (theory) and experience (practice) and, in this way they were able to follow their educational evolution and define their identity, and to learn to value and preserve their work. Connecting representatives of

businesses and schools is an important activity in the framework of this model, which allows the permanent development of knowledge and skills of young people and gain experience and networking through different areas in accordance with the needs of the economy.

## 3. ENTREPRENEURIAL BUSINESS ENVIRONMENT

There is a close and continuous interaction between the business and its environment. This interaction helps in strengthening the business firm and using its resources more effectively. The term business environment refers to the aggregate of all forces, factors and institutions which are internally affecting the business through management structure and policies as well as which are external to and beyond the control of individual business enterprises.

All businesses have a common objective of earning profit, they differ from each other with respect to their size, nature, volume of transaction, management and ownership, etc. Thus, structurally they are different. Broadly business may be classified on basis of size, functions and ownership.

The category of micro, small and medium-sized enterprises (SMEs) is made up of enterprises which employ fewer than 250 persons and which have an annual turnover not exceeding EUR 50 million, and/or an annual balance sheet total not exceeding EUR 43 million. SMEs are the engine of the European economy. They drive job creation and economic growth and ensure social stability. In 2013, over 21 million SMEs provided 88.8 million jobs throughout the EU. Nine out of every 10 enterprises is an SME, and SMEs generate two out of every three jobs. SMEs also stimulate an entrepreneurial spirit and innovation throughout the EU and are thus crucial for fostering competitiveness and employment. SMEs come in many different shapes and sizes; however, in today's complex business environment they may have close financial, operational or governance relationships with other enterprises. These relationships often make it difficult to precisely draw the line between an SME and a larger enterprise. Small and medium-sized enterprises (SMEs) are key players in the transformation of the European knowledge economy. Their ability to apply, adapt and spread new technologies, as well as to create and develop them, is unique. Realising the full potential of SMEs is an essential part of the European Union's strategy for maintaining prosperity and high-quality employment. They are a major source of entrepreneurial skills, innovation and employment.

### 3.1. The engagement of SMEs with education

Employer engagement with education is a fairly common activity. However, there is a relationship between the size of businesses and their tendency to engage with education. Smaller businesses are being less likely to engage in education than larger companies. This trend continues within the overarching SME category as there is a positive association between SME size and level of engagement with education; as company size increases, so does the frequency, range of activities and formality of engagement with education. The most common ways for STEM-related (e.g. science, technology, engineering and mathematics, aerospace, electronics, mechanical, metals, automotive areas) SMEs to be involved with education include:

- links with universities and colleges;
- offering work experience placements;

- involvement in specific schemes and projects.

Other ways for SMEs to be involved with education include: subject talks and practical demonstrations; post-16 and post-18 apprenticeships; careers fairs, careers talks and mock interviews; company visits and tours; input to curriculum and course design; providing equipment, sponsorship and donations; and engaging with parents. There is evidence to suggest that size and sector may influence the nature of SMEs' engagement with education. For instance, company visits and tours, and apprenticeship schemes, appear to be less popular activities amongst smaller SMEs in comparison to their larger counterparts. Furthermore, there is some variation in the nature of SMEs' engagement with education depending on their sector. SMEs from advanced manufacturing and manufacturing sectors are most likely to participate in a broader range of activities with education, including apprenticeship schemes.

The literature and interviews [11] suggest a wide range of benefits for employers of engaging with education; benefits are both actually experienced by those that engage with education and perceived by those that do not. Predominantly these benefits include:

- professional development of staff;
- promoting a positive image of the company/sector;
- capitalising on young people's ideas, skills and productivity;
- direct recruitment to the company;
- personal satisfaction, enjoyment and motivation of staff.

SMEs also commonly identify the altruistic nature of their involvement with education and the benefits realised by young people as a result of them being provided with opportunities to engage with businesses and industry. This type of benefit is seen by SMEs as an opportunity to 'give something back' by passing on knowledge and experience. Young people gain experience of different practical skills, the real-world applications of STEM subjects, and advice, insights and inspiration for STEM careers, as well as more general employability skills, which they may otherwise not

have access to, or be able to develop, in school. Opinions vary regarding the extent to which this form of benefit for young people is also coupled with benefits for the company or sector. The smaller SMEs (with fewer than 100 employees) are more likely to identify engagement with education in altruistic terms than the larger SMEs.

The literature indicate [11] that many of the challenges in employer engagement in education are generic – they are common for most organisations but are often amplified within small organisations. The main challenges tend to relate to:

- time, capacity and financial constraints;
- low awareness and understanding of schemes and how to link with education;
- lack of commitment and interest of schools and pupils to engaging with industry;
- health and safety constraints and bureaucracy;
- lack of staff confidence and skills;
- low awareness of benefits;
- lack of skilled young people to engage with;
- issues in relating the business activities to the curriculum and making a relevant partnership;
- time constraints for schools.

#### 4. PARTNERSHIP MODEL

Cooperation between technical schools, technical faculties and enterprises represents one of the ways for development of social partnership. As it is the one of the strategic areas of technical and engineering education reform in Serbia, it needs to be improved. This improvement could be done only if the improvement happens in the two-way communications and dialogue between Learning Environment and Business Environment (Figure 1). Learning Environment consists of Ministry of Education, Science and Technological Development (MoESTD), Technical Faculties (Uni) and Technical Schools. Business Environment is formed of National Employment Service (NES), Small and Medium Enterprises (SME) and Chamber of Commerce and Industry (CCI).



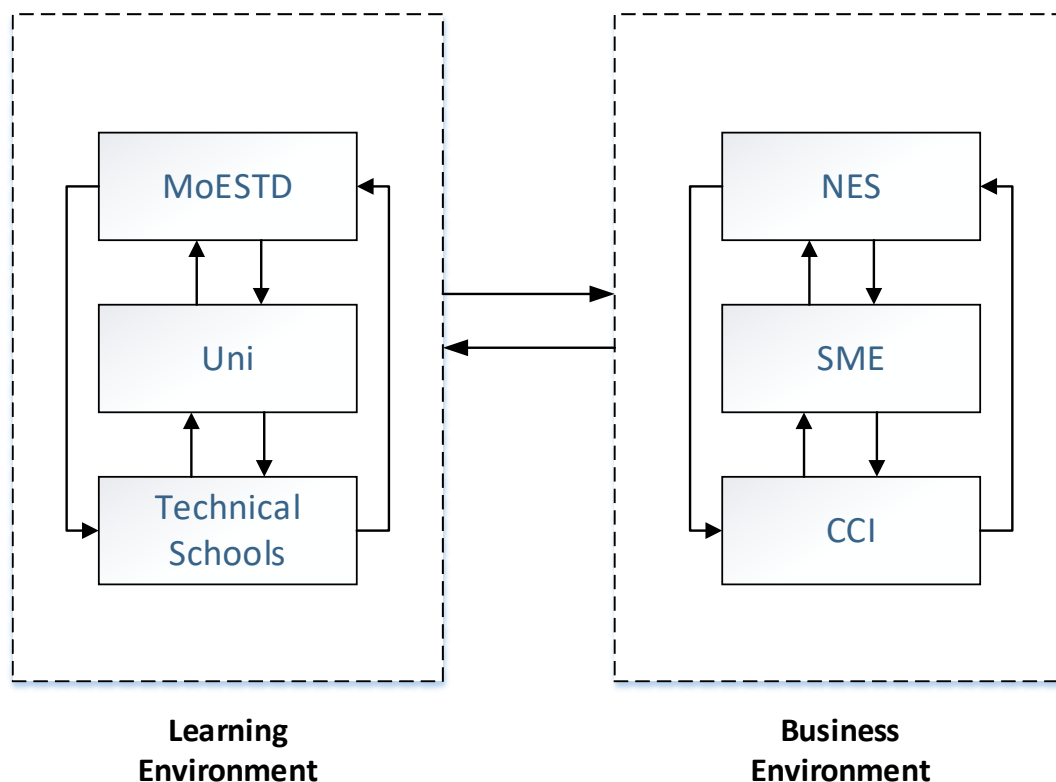


Figure 1: Partnership model

The purpose of this cooperation is the benefit of the enterprises of entrepreneurial education. In the same time, this should become the first issue on the list of the technical school and faculty priorities.

Necessity of the two-way communications and dialogue represents the essential need with the tendency to become long-term sustainable model. Few of the objectives of the partnership defined in this way are:

- organization and joint efforts with the purpose of gaining wider public;
- development and improvement of the program of entrepreneurial education.

## 5. CONCLUSION

Strengthened role of entrepreneurs, as a social partners in educational system and their active involvement in the creation of the entrepreneurial education program, will contribute to harmonization of the needs and demands in the employment system. Contemporary teaching methods based on the case studies' analysis, simulation of economy surrounding, establishment of social partnership with the entrepreneurs, but also based on their active involvement in the practical teaching of students in secondary vocational schools, undoubtedly will contribute to more qualitative entrepreneurial education and its implementation in practice. There may be a need to raise awareness of the support available, the opportunities for engagement with education and the benefits for SMEs of engaging with education. As the size of business appears to be a factor in engaging with education, SMEs, and particularly smaller SMEs, may need greater support and encouragement to engage with education than their larger counterparts. As smaller companies tend to

engage with education on a more ad hoc and infrequent basis, and with a narrower range of activities, some SMEs may have a limited view of what type of activity constitutes engagement with education and there may be scope to engage SMEs with education and schools in ways in which they had not previously conceived.

## REFERENCES

- [1] C. L. Shook, R. L. Priem and J. E. McGee, "Venture creation and the Enterprising Individual: A Review and Synthesis," *Journal of Management*, Vol. 29 (3), pp. 379-399, (2003)
- [2] B. A. Gilbert, P. P. McDougall and D. B. Audretsch, "New venture growth: a review and extension," *Journal of Management*, Vol. 32 (6), pp. 926-950, (2006)
- [3] C. Bush, "Pioneering strategies for entrepreneurial success," *Business Horizons*, Vol. 51 (1), pp. 21-27, (2008)
- [4] G. D. Markman and R. A. Baron, "Person – entrepreneurship fit: why some people are more successful as entrepreneurs than others," *Human Resource Management Review*, Vol. 13, pp. 281-301, (2003)
- [5] M. Gerasimović, Lj. Stanojević, A. Veljović and N. Cvijović, "Application of geographic information systems technology in entrepreneurship education," *Annals of Faculty Engineering Hunedoara – International Journal of Engineering*, Vol. 8 (2), pp. 197-200, (2010)
- [6] Official Gazzete RS – Educational Gazzete 9/2007.
- [7] Official Gazzete RS – Educational Gazzete 107/2012.
- [8] A.J. Nelson, T. Byers, "Challenges in University Technology Transfer and the Promising Role of

Entrepreneurship Education," Kauffman: Emerging Scholars Initiatives, (2010)

[9] ABET [Accreditation Board for Engineering and Technology], "The Vision for Change: A Summary Report of the ABET/NSF/Industry Workshops," Baltimore MD, (1995)

[10] NAE [National Academy of Engineering], "The Engineer of 2020: Visions of Engineering in the New Century," Washington: National Academies Press, (2004)

[11] J.Harland, S.Straw, E.Stevens and A.Dawson, "Exploring the engagement of STEM SMEs with education: Key Findings Research Summary, " National Foundation for Educational Research, Berkshire (England), (2012)

# Oral Presentations of Companies in ESP Classes as a Multi-Purpose Task

Nataša Pavlović<sup>1,\*</sup>

<sup>1</sup>University of Kragujevac, Faculty of Mechanical and Civil Engineering, Kraljevo, Serbia

*This paper presents a well-established activity with ESP students at the Faculty of Mechanical and Civil Engineering in Kraljevo – oral presentation of a company in English, which was designed in order to direct students toward the real world outside the classroom. The skills and self-confidence gained during preparation and delivery of presentations will benefit both the ESP students and their future employers. This activity in which ESP students blend their professional knowledge with language skills is enriched with non-linguistic features, and the lessons learnt can be applied within other courses requiring similar tasks.*

**Keywords: English for Specific Purposes, oral presentations, mechanical engineering students**

## 1. INTRODUCTION

Presentations are increasingly used as a classroom activity at all levels of education. They might become less effective if their purposes are neglected.

The author of this paper, working as an English Language teacher at the Faculty of Mechanical and Civil Engineering in Kraljevo, has gained an impression that presentations are not exploited sufficiently and adequately enough. Students are given different types of assignments, but a lot of them are not faced with the challenge of speaking in front of the audience until the presentation of their final paper as the last step before earning the bachelor's degree. On the other hand, through the cooperation with numerous companies for many years, the author has recognized their need to have employees who would be capable of presenting their production programme in English at any time. Such a task, sometimes ad hoc, is usually entrusted with those who are extroverts, fairly talkative, communicative, explicit. Since most employers take it for granted that the students who have learnt English for some 15 years should have sufficient knowledge of that language to present their company, the students should, for their part, assume that one day they may be chosen for such a task.

The idea of the teacher was to bring her mechanical engineering students closer to their future job by helping them to develop presentation skills and build the awareness of their importance.

## 2. PRESENTATIONS IN AN ESP CONTEXT

“What distinguishes ESP from General English is not the *existence* of a need as such but rather an *awareness* of the need. If learners, sponsors and teachers know why the learners need English, that awareness will have an influence on what will be acceptable or reasonable content in the language course and, on the positive side, what potential can be exploited”. [1]

The knowledge of English language gained in the previous stages of education should now be synthesized and redirected toward new strategies that would be of direct use in future jobs. In order to strengthen the already acquired language skills, deepen and extend the knowledge and self-confidence of ESP students, ESP

teachers should include new learning techniques to make the classes more effective. Introduction of real-life situations should add to the feeling of logical and natural continuity of the previous learning. [2]

The goal of ESP at the tertiary level is to provide students with sufficient knowledge for successful use of the foreign language during their studies, but also during their future professional career or any form of further specialization. New genres should be applied in the teaching practice with interactive forms of communication in class. Presentations as a form of oral communication should occupy more and more space in the university environment. In addition to a lot of benefits of this activity which will be described in further text, they can also be observed within the so-called transfer of learning, i.e. the relation between ESP and some other subjects taught at the faculty. The term “transfer of learning” refers to the influence of the lessons already learnt on some new activities or situations in which new knowledge should be gained. One of the key factors in the transfer of learning is surely the similarity between tasks. [3] If presentations are considered to be such a link between different courses at the faculty, then the idea of the teacher to use them in ESP classes certainly exceed the initial aims thus showing their importance in the context of education which prepares students for networking of various type.

Presentation skills cover both verbal and non-verbal forms of communication. They may be learnt during ESP classes, but in the future career students will be exposed to different contexts in which they will be able to use them. Although their speech will always be adjusted to a new topic, the basics of presentation skills they acquire during ESP classes should remain a stable foundation for building up their knowledge and experiences. Those who learn how to deliver a presentation in English or any other foreign language will certainly have an advantage over those who are trained how to do it only in their mother tongue. The former ones kill two birds with one stone.

Presentations can be taken as an overall activity because students as presenters practise all the four systems of language (vocabulary, grammar, discourse and phonology) as well as all the four language skills (speaking, reading, writing and listening).

According to the literature, oral presentations can be divided into four categories: 1) memorized speech (speech learnt by heart), 2) manuscript speech (speech delivered by reading the written text), 3) extemporaneous speech (speech delivered by using notes), and 4) impromptu speech (spontaneous, without preparation and, therefore, most demanding). As there are a lot of engineering students whose English is not at a high level and whose self-confidence is at a rather low level, the most suitable and suggested category is the third one, i.e. extemporaneous speech. Learning by heart or reading texts from slides are neither interesting to the audience nor useful for presenters. They are just a waste of their time understood as a burden necessary to earn a grade. [3]

A successful presentation must have a well-structured organization, with the three standard wholes: introduction (in this case, greeting the audience, introducing himself/herself, introducing the company that will be the subject of the presentation), central part (main details about the company with the emphasis on the leading edge products and competitive advantages) and conclusion (final and most persuasive part which should make the audience wish to cooperate with the company, inviting questions). Skillful presenters are, as a rule, better communicators, since they are able to structure their ideas well and express them clearly. The presenter should develop good techniques of attracting attention in the introductory part and leaving a good impression in the final part of the speech. Besides language elements, an important characteristic of oral presentations is the use of non-linguistic forms of communication, such as visual means and elements of nonverbal communication, like posture, gestures, eye-contact, etc. [3]

Oral presentations should fit into an ESP course. They should rely on the previous topics and lessons and aim at a point in the future when they might be of use in the world of work.

Normally, presentations will come towards the end of a series of lessons as a type of freer practice. This is because the students need to feel relatively confident about what they are doing before they stand up and do it in front of other people. A very important issue here is to talk openly to the students about their possible stagefright and appearance in front of a wider group. "In order to help students effectively cope with their fear of oral presentations, it is essential for them to acknowledge that speech fright or speech anxiety is perfectly normal. Having an open discussion of speech anxiety and the treatments will make students feel that they are not alone." [4]

### 3. PRESENTATIONS AS THE FINALIZATION AND HIGHLIGHT OF AN ESP COURSE

Oral presentations of companies were introduced as part of an ESP course for the first Bologna generation at the Faculty of Mechanical and Civil Engineering in Kraljevo (at that time the Faculty of Mechanical Engineering in Kraljevo). This activity was tried with a group of master students who had completed their English courses at an intermediate level, or B1-B2 according to the Common European Framework of Reference for Languages, during their bachelor studies. The B1-B2 level is quite sufficient for performing the activity of oral

presentation. As it was successfully done, the teacher decided to make it an integral part of the course.

The fourth-year students at the module Production Engineering and the module Energetics and Environmental Protection have English for Engineers 1 as an elective course, and the first-year master students attending the module named Automatic Control, Robotics and Fluid Technique have English for Engineers 2 as a compulsory course. They are now those who have oral presentations in English as an obligatory assignment by which they can earn the maximum of 25 points. Anyway, both groups consist of the students who are aware of the need to enhance their language skills. Their expectations regarding the English course they attend may be slightly different, but all agree that communication skills that will make them more open to interaction in future professional surroundings are of greatest importance to them. It is up to the teacher to respond to those expectations and even adjust the classes to a certain degree if necessary.

Oral presentations cannot be successfully delivered in large groups because it would take a lot of time for everyone to present individually. In such groups, they would be only a means to complete a part of obligatory activities, and not at all a memorable and fruitful activity. The abovementioned groups have never consisted of more than 15 students, which means that the delivery of presentations have rarely lasted for more than a couple of hours. Every student is given 10 minutes for presentation at the end of which questions are invited.

The structure of the entire course is such that oral presentations are the culmination of all the activities and topics covered before. The main units of the course are dedicated to jobs and responsibilities in a company, touring a company, organigrams, production processes, graphs and charts, product descriptions, gadgets and innovations, technical problems and solutions, different industrial sectors, case studies, etc. During the course, the teacher slowly introduces main elements of presentation skills with adequate examples and exercises. To finalize the course, the teacher leaves students' presentations for the last class in the semester. At the beginning of the course, students are informed of all course requirements and are well aware of their task to prepare presentations for the end of a series of ESP lessons. The knowledge they gain from week to week enables them to be ready for that event.

"Every professional is involved in some aspects of communication which usually involve gathering, analyzing, and distributing scientific and/or technical information efficiently and accurately for specific audiences." [5] So, the first task for the students is to gather available data about the company they want to present and select the information that could be interesting to the audience. The easiest and simplest way to do it is to copy the information from the website of the company and paste them onto slides. The copy-paste technique is neither allowed nor creative. The students should combine various information collected from different sources, not only from the official site of the company. It is clear that they cannot invent any new details about a company, but it is up to them to structure the descriptions already known into a presentation which will incite further interest of the audience.

#### 4. MULTI-PURPOSE ACTIVITY

There are a lot of purposes of oral presentations of companies in English. Some visible ones, which are included in the task set by the teacher, are as follows:

- 1) To present a company in an interesting way that may draw attention of possible clients or partners;
- 2) To produce a text which is correctly written, freed from excess terms and details, and without grammatical mistakes;
- 3) To pronounce the words properly;
- 4) To avoid reading from slides;
- 5) To be prepared to answer the anticipated questions from the audience;
- 6) To learn the adequate body language.

However, there are also some purposes which may be understood as intangible. They make a deeper layer of goals hidden below the abovementioned ones and can be formulated in the following way:

- 1) To make students gain self-confidence by presenting in English in front of the public;
- 2) If students are already employed with the subject companies, to let them feel more strongly linked to such companies, more committed to their jobs, more proud of deserving the chance to act on behalf of their colleagues or superiors;
- 3) If they choose a company in which they would like to work, to encourage or strengthen their motivation to strive toward getting employed there or at least in a company dealing with similar business;
- 4) To impose a lively discussion and healthy rivalry among the students who will do their best to leave as good impression as possible and thus prepare them for the real world full of competition;
- 5) To make them open to making and answering questions in English and thus let them forget the initial fear of making mistakes or exposing their colleagues-presenters to an unpleasant situation if they cannot provide an appropriate answer;
- 6) To provide them with the opportunity to see and hear different visions and ideas, anticipate the behaviour of their friends in their future professional careers as well as foster stronger connections among them as future associates or business partners;
- 7) To enable them to become more aware of the weak points in their language skills, no matter whether they are weaknesses in their knowledge of grammar, vocabulary, pronunciation, conversation or just the lack of courage to face the challenge of expressing themselves in English; if they feel the need to correct their mistakes after the presentation day or improve their skills in any way, it is for sure one of the "profits" of the whole activity

#### 5. FRAMEWORK AND CONTENT

##### 5.1. Organization of the presentation day

The day which completes the work done throughout the semester is planned as a relaxing event for all participants – both the teacher and the students. The atmosphere is friendly, and even coffee and tea are ordered for the successful start and elimination of possible stagefright. The teacher talks to those who are shy or nervous trying to cheer them up. The necessary equipment

for Power Point presentations is installed and ready for use.

There is no special order in which presentations are delivered. Every group has its volunteers, whose knowledge and self-confidence are at a significant level, but it does not mean that their presentations are always the best ones. Such persons may be too fast and impossible to follow, which results in the loss of interest in the body of their presentation. The teacher may determine the order of delivery if there are no more volunteers.

The teacher acts both as the instructor and the mediator, particularly at the end of presentations when questions are invited. The questions are usually posed by those who are more communicative, but the others also join. If the level of their English knowledge is not high, the teacher should interfere with certain prompts. Peer feedback, either in the form of questions or as a friendly comment on good and bad points of presentations, are one way to get students listening and learning from the presentations of their colleagues and avoid boredom in class. The quality of the peer feedback seems even more important to the presenters than the feedback provided by the teacher.

The rule for the question time is clear: those who pose questions do not gain extra points for that, and the presenters do not get minus points if they cannot give appropriate answers. It is allowed not to know everything. It is also allowed to enter a dialogue with the one who is posing the question or start a conversation with more participants if the topic arouses their interest. The flaming conversation of that type, full of information and witty questions and answers, is the most rewarding part for the teacher. That is the moment when the teacher realizes that the students have become professionally mature and prepared for sustainable development of their potentials.

##### 5.2. Memorable examples of presentations

In the past several years, students have been showing increasing inventiveness and devotion to the mentioned assignment.

Some of them did not hide their wish to differ from the others in the group by enriching their presentation with uncommon contents. There were occasions when the content was really tangible, e.g. in the form of sweets when a student treated the audience with the products of a well-known chocolate and candy factory, which was the subject of his presentation, and thus made the whole event more enjoyable. It can be said that his presentation hit the target by having effects on all senses.

Another memorable presentation was delivered by a student who, at that time, was interested in drones. Those gadgets were entering the market and he was fascinated by them. He brought a real drone to the classroom and, delivering the required presentation, used the occasion to show all its capabilities. The audience was absolutely impressed and those interested had the chance to control the drone by themselves. His English language was not excellent, but his communication skills and a persuasive element in his nature prevailed, which was also a very good example for those who are shy, less eloquent and scared of using any foreign language. One of the aims of ESP is certainly to eliminate language mistakes of any kind, but maybe an even more important aim should be to

help students build their attitudes, confidence or bravery and eliminate the hindering elements in these fields. An engineering student may be excellent at grammar, but no employer will ask him to do grammatical exercises at work. Communication skills, quick response to any task which requires the knowledge of English and willingness to expand the existing knowledge are the characteristics which will enable our students to excel in the professional world. It is worth saying that the student who showed the drone now owns a small business which deals with recording video clips and ads by using drones. He is often hired by reputable companies to prepare official presentations of their business in the form of short clips.

Perhaps the most memorable example of students' presentations was the one delivered by a student who had never learnt English before. He had learnt another foreign language, but, due to some inevitable circumstances, in his later study years he had to enrol in the module that included learning English within the compulsory course. The student regularly attended classes, but was very reluctant - he would never utter a word in English. It seemed that it would be impossible for him to accomplish the necessary number of points to pass the exam. What was the turning point in his attitude toward the English language was the task to elaborate a presentation. The whole group, including the teacher, feared his performance. The first surprise was to see him among the volunteers. When he started his speech, the audience remained breathless. His performance was smooth, his pronunciation excellent, his eye contact with the audience and his whole body language were relaxed and he really acted as an expert. He did have a piece of paper in his hands just in case, but he did not use it. The other students and the teacher wondered if he had earlier pretended that he could not speak English. He was even able to answer some simple questions regarding the subject company. At the end, he explained to the astonished audience that a friend had helped him with the preparation of the whole presentation, with pronunciation, rehearsal and anticipation of possible questions. His preparatory activities for the presentation day were both demanding and challenging. His effort and success were rewarded with a sufficient number of points to pass the exam. The student's target may have been reached in that way, but one of the teacher's targets was reached, too – a presentation task inspired someone to overcome his initial reluctance, start learning English and bravely appear in front of the audience.

### 5.3. Most recent experience

The last presentation day was in January 2017. Although it was planned as an ordinary activity, it exceeded all expectations.

The presenters were the first-year master students who attended the module Automatic Control, Robotics and Fluid Technique. What was uncommon for that group of students was that out of 7 of them, 5 were already employed. The companies where they worked and which were the subjects of their presentations differed to a large extent, either by their ownership or by the type of business operations. The students' language skills were different, as well. Nevertheless, so many initial differences resulted in a

medley of positive energy, enthusiasm and creative exchange of knowledge and experiences.

#### 5.3.1. Initial situation and expected outcome

Let us show the initial situation, i.e. the task force for that specific presentation day:

Student 1 is employed with one of the largest and most successful energy companies in Europe. Its principal activities are exploration, production and refining, sales and distribution of a broad range of petroleum products, as well as the implementation of energy projects. His English is at an intermediate level, with a lot of weaknesses concerning grammar.

Student 2 is older than the others, with a lot of experience at a managing position of the local public utility company dealing with the production and distribution of water, waste water treatment, design, investments and implementation of legislation regulating this field. His knowledge of English is at a very high level, with minor weak points.

Student 3 has just got employed as a promising engineer. The company where she works is a prospective private-owned company specializing in designing, producing, and installing advertising units. The close cooperation between its mechanical engineers and graphic designers is the competitive advantage which makes it unique in its sector. Her English is excellent.

Student 4 has been granted an award at a competition for young people with business ideas. He and his friends have devised an application for mobile phones for simultaneous recording with both front and rear cameras, i.e. capturing double photos and sharing them on social networks. As a follow-up, they have established their own start-up company, which now employs several young entrepreneurs from different fields. They implement the abovementioned invention through the cooperation with various companies, some of them being famous world-wide. Student 4 speaks excellent English and is very self-confident.

Student 5 is employed in marketing business. His job is to be the leader of a group of young workers engaged in promoting activities of a lot of brands. His English is rather poor, but he expresses his strong wish to expand his knowledge in order to get a better position in his further career.

Student 6 is not employed. She is the best student in the generation, but what she misses is the knowledge of English. Her shyness and low self-confidence, obviously resulting from the lack of language skills, are real obstacles despite her perfect reception of everything taught in class. The private company she wants to present has its seat in her hometown. It deals with the development and production of various types of programmable pneumatic machines for pressing, punching, drilling, etc. Being one of the leading manufacturers in that region, it is no wonder why it has been chosen by an excellent student for her presentation.

Student 7 is the other student without employment. The subject of his presentation is one of the best-known companies in the world which primarily deals with the production of electronic devices. He speaks very good

English and is able to correct the weaknesses very easily and quickly.

The expected outcome of the whole activity is to complete the whole semester by interesting and carefully elaborated presentations followed by the teacher's remarks and two questions per presentation at the end of their delivery and probably some useful comments or questions posed by the audience, as usual.

### 5.3.2. Actual outcome

Beyond all expectations, the actual outcome was extraordinary. The students with a lower level of English knowledge amazed the audience by their presentation skills and the relaxed delivery of their presentations. The mistakes they made were less heard than the content of their speech or seemed less important than the communication they imposed. Shyness was hidden by good posture, smile and determination to be equal to the task.

Student 7 had some technical problems with his presentation but it did not prevent him from being ready to give his contribution to the event.

Student 6 presented her topic with perfect pronunciation, her slides were effective and her behaviour did not reveal any weaknesses in language skills. She understood all the questions and answered concisely. If anyone from the subject company had been in the audience, the presentation would have been a good recommendation for employing the presenter.

Student 5 showed his willingness to participate and the aptness to use his positive attitude in order to compensate for weak points in his English.

The presentation of Student 4 was particularly interesting for the young audience because of the novelty applicable in their everyday life. It inspired numerous questions and, for the first time during a presentation day, we could listen to very professional answers given by a young engineer who was at the same time one of the inventors of a product and one of the owners of the company presented. The student provided a lot of information on how the idea for the application had been born, who the users were, what the prospects for developing his company were, etc.

Student 3 showed her abilities to present the production programme of her company briefly, persuasively and very professionally. Her presentation skills and excellent English were a significant plus hopefully recognized by her employer. A multitude of specialized words connected with a wide range of products she described made a valuable part of her vocabulary. The audience could feel her enthusiasm, commitment to the company and readiness to contribute to its success.

Student 1 and 2 exceeded the time limit for presentations, but with the tacit agreement of the whole audience. Student 1 did something absolutely unexpected. Namely, during his presentation of exploration of oil, some slides could not be shown due to some technical problems. In most similar cases, inexperienced young presenters would apologize and quickly finish their speech. However, this time the lack of excellent English remained unnoticed because of the abundant professional knowledge, good presentation skills and an outstanding response to the challenging situation. He immediately took

a piece of chalk and started to draw the missing slides on the blackboard. At the same time, he skillfully juggled a large number of narrowly specialized terms which he could describe to a detail. The audience was astonished by his professionalism, communication skills and capability to answer any question, despite some obvious weaknesses in his English.

Student 2 occupied more time than the other presenters because the combination of his excellent English and engineering knowledge already applied in the water supply company easily attracted the attention of the audience. His highly informative and well-structured presentation turned out to be just an introduction to the discussion that followed. Almost all students participated in posing questions to him thus creating an atmosphere of professional exchange of ideas and experiences. They learnt interesting details about the water supply network, plans for its modernization, remote control and supervision of water supply, IPA funding, etc.

The exchange of ideas and fruitful discussion turned the individual presentations into a form of team work and created a powerful synergy worth mentioning to the other students, teachers and, whenever possible, employers.

## 6. CONCLUSION

The benefits of oral presentations of companies within an ESP course justify the idea to introduce that activity as a powerful tool for preparing students to operate effectively in the professional setting. This multi-purpose task is a logical finalization of the whole course and a smooth transition to the world of work outside the classroom.

Being personally involved in a real-life situation, ESP students become more aware of the importance of acquiring presentation skills.

Further ideas are directed toward opening the ESP classroom for the teaching staff, industrial people and other students who may be interested in oral presentations of companies in English. The audience composed of various stakeholders could produce an even more creative exchange of ideas and experiences.

## REFERENCES

- [1] T. Hutchinson and A. Waters, "English for Specific Purposes: A learning-centred approach", Cambridge University Press, Cambridge (UK), (1987)
- [2] S. Blagojević, "Novi akcenti u nastavi engleskog jezika za akademske potrebe na masterskim studijama", Tematski zbornik radova "Aktuelne teme engleskog jezika nauke i struke u Srbiji", Centar za izdavačku delatnost Ekonomskog fakulteta Univerziteta u Beogradu, pp. 247-258, (2013)
- [3] LJ. Knežević, "Efekti razvijanja veštine usmenog izlaganja u okviru nastave engleskog jezika struke", Tematski zbornik radova "Aktuelne teme engleskog jezika nauke i struke u Srbiji", Centar za izdavačku delatnost Ekonomskog fakulteta Univerziteta u Beogradu, pp. 201-212, (2013)
- [4] J. King, "Preparing EFL learners for oral presentations, Dong Hwa Journal of Humanistic Studies, No. 4, pp. 401-418, (2002)

[5] S. Živković, "The Importance of Oral Presentations for University Students", *Mediterranean Journal of Social*

*Sciences* MCSER Publishing, Rome-Italy, Vol. 5 (19), pp. 468-475, (2014)



# Machining Simulation and Verification of Tool Path for CNC Machine Tools with Serial and Hybrid Kinematics

Sasa Zivanovic<sup>1</sup>, Slobodan Tabakovic<sup>2\*</sup>, Milan Zeljkovic<sup>2</sup>, Cvjetin Mladjenovic<sup>2</sup>  
Aleksandar Košarac<sup>3</sup>

<sup>1</sup>Faculty of Mechanical Engineering/Production Engineering Department, University of Belgrade, (Serbia)

<sup>2</sup>Faculty of Technical Sciences, / Department of Production Engineering, University of Novi Sad (Serbia)

<sup>3</sup>Faculty of Mechanical Engineering, Faculty of Mechanical Engineering, University of East Sarajevo (B&H)

Development of modern machine tools basically is directed on improvement of kinematic structures and exploitation characteristics. As a result of this in last two decades industry more and more uses machine tools based on parallel and hybrid kinematics with significant increasing of speed of main and movement and feedrate. In order to provide more efficient exploitations of these machines, reduce of the preparation time of production, increase of the safety of users and machines is necessary application of software for simulation and verification programs.

This paper presents the concept of modern technological preparing of manufacturing in the case of the definition of virtual machine tools based on conventional - serial and hybrid kinematics, simulation of machining and verification of programs for machining of characteristic workpiece.

**Keywords:** *Virtual machine tool, machining simulation, verification of tool path, CAD/CAM, CLF, NC program*

## 1. INTRODUCTION

Development of industrial production with a view to further development of the society in the twenty-first century is largely based on the development of production capacities and resources that enable their effective exploitation. In the area of discrete mechanical production this primarily involves significant innovation in the field of machine tools. Their development in a contemporary environment entails further development of: exploitation characteristics (that is primarily to increase processing regime up to several times) and kinematic structure.

These trends in production engineering have necessitated the use of an appropriate software the objectives of which include reducing the time for production preparation, increasing processed surface quality and the elimination of waste.

The machining simulations and verification programs before executing which includes of virtual machine prototype when it works according to the running program is broad topic and includes the complete models of machining process, structure of machine, actuators, kinematic subsystem, etc [1]. All of these models can be integrated into a some software systems, which allows a part of the virtual production [2-4].

For the purpose of the simulation and verification tool path, i.e., the NC program, different tools such as CNC editors, CNC simulators, CAD / CAM systems and CAM systems can be used, Fig.1. Common to most of these software, except CNC editor, is the possibility of verify the NC program by simulation of the processing that includes a complete virtual model of the machine tools.

CNC editors are used when instructions for machines are generated in manual programming. Their main advantages are: the visualization of the programmed tool path and the possibility of simulating the movement of the tool during removal of the material [5], Fig. 2, for both new and previously made CNC programs. Drawback

of such a program is impossibility of simulation cutting processing which includes model of machines tools.



Figure 1: Machining simulation for verify NC programs

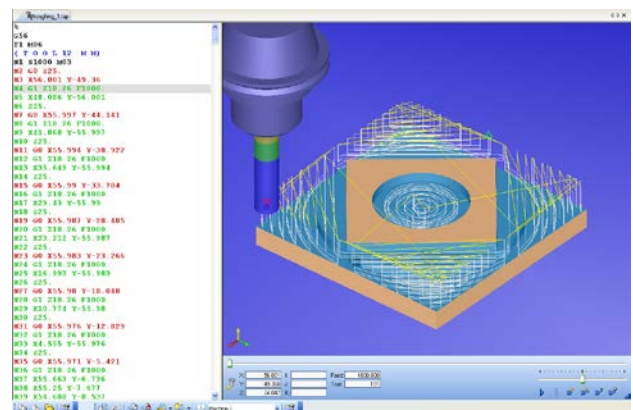


Figure 2: Cimco CNC editor

CNC simulators allow loading and verification programs as well as training in using different types of control units.

There are also a lot of CNC Simulation Software for programming training, such as CNC Swansoft simulator [6] - Fig. 3, CNC simulator Pro [7], and others.

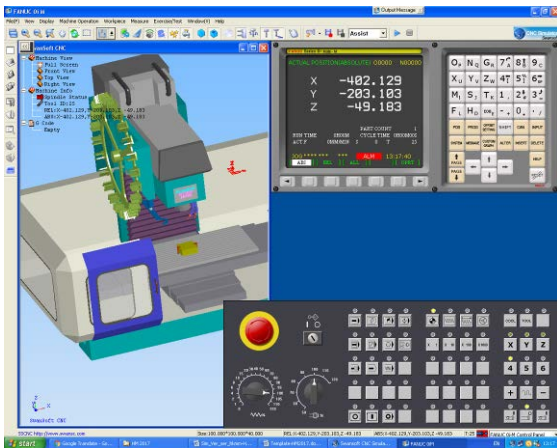


Figure 3: Swansoft CNC simulator

These simulators in addition to the emulation of different control units, offering the possibility to work with virtual machine tools in the software environment which includes both handling and simulation cutting process. These software are developed for the milling and turning processes.

For verification and optimization of CNC programs, including cutting process on virtual machine tool, there are commercial software such as VeriCUT [8], NC Simul [9], NC Brain [10], CAMWorks [11] etc.

Figure 4 shows verification of NC program by simulation of material removing that includes a complete virtual model of a 5-axis machine tool [12] in the software VeriCUT.

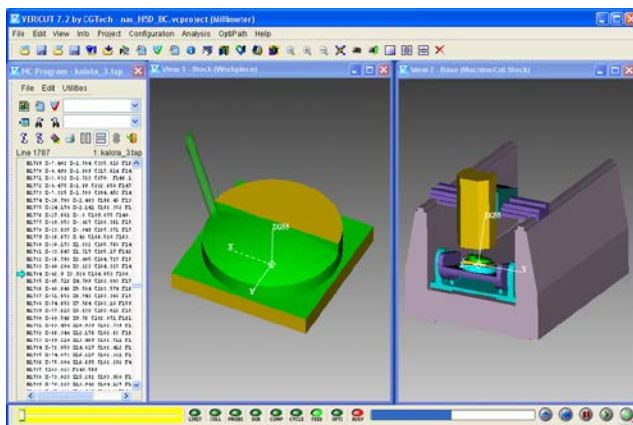


Figure 4: VeriCUT machining simulation [12]

Modern CAD/CAM systems such as the PTC Creo [13], Catia [14], NX, [15] SolidCAM [16], MasterCAM [17], GibbsCAM [18] Inventor-HSM [19], CIMATRON [20], and others, have modules for cutting process simulation using virtual machine tools.

Configure of the virtual machines with serial kinematics is a relatively simple task, which cannot be said for machines with parallel and / or hybrid kinematics.

The paper shows the simulation cutting process that includes configuring the machines in CAD/CAM system PTC Creo 2.0 in case of an existing machine with a serial and a machine with hybrid kinematics.

## 2. CONCEPTIONS OF CNC MACHINE TOOLS WITH SERIAL AND HYBRID KINEMATICS

Demands for improvement of exploitation characteristics of machine tools in the last twenty years, apart significantly improved characteristics of existing components and subsystems, require also the use of different kinematic structure concepts. Thus, apart to conventional serial kinematic, increasingly in the application are parallel and hybrid kinematics which, in certain conditions, significantly improve characteristics of machine tools.

The main difference in the process of analysis of the paths, simulation and verification CNC programs in numerically controlled machine tools with different kinematic structure is a problem of defining the position of the elements of the machine in relation to the tool, i.e. its trajectory. In machine tools whose kinematic structure is based on parallel or hybrid mechanisms, procedures for solving of this kinematic problem is significantly different compared to solving of serial kinematics mechanisms problems.

The paper uses two different machine tools for the analysis of this problem: horizontal machining center Heidenreich & Harback FM38 (H&H FM38) with serial kinematic structure and the experimental machine tool based on a hybrid O-X mechanism.

### 2.1. Horizontal machining center

Horizontal Machining Center H&H FM38 belongs to a group of numerically controlled machine tools conventional kinematic structure, with 3 numerically controlled linear axis and the index programming CNC rotary table i.e. rotational axis (B axis), Fig. 5.



Figure 5: CNC Horizontal Center H&H FM38

The machine is equipped with automatic tool changer with drum style magazine containing 15 tools for milling and drilling and a mechanism for automatic tool

change and handling. Control unit is Siemens Sinumerik 840D.

In the context of conducted research, H&H FM38 horizontal milling center, due to its structure and accessibility on the Faculty of Technical Science Novi Sad was used for analysis the possibility of forming the virtual machine tool and accuracy in the simulation tool path processing.

2.2. O-X glide hybrid kinematics milling machine

The second part of the research is analyzing possibilities for application of advanced software for simulating operation of machine tools with hybrid kinematic structures, which include a combination of parallel and serial mechanisms.

Machine tool based on the original O-X glide mechanism with hybrid kinematics was taken as a basis for this analysis. This type of machine tool is created by combining planar parallel mechanism and the machine structure which allows its translational movement. Plane parallel mechanism is designed so that the tool can reach the biggest part of work space in two configuration of mechanism which behaves as dual two parallel mechanisms with different characteristics in terms of: the dimension of the working space, stiffness, speed etc. Figure 6 shows the initial concept machine with hybrid kinematics in two positions: extended (O) and cross (X) O-X structure [21, 22].

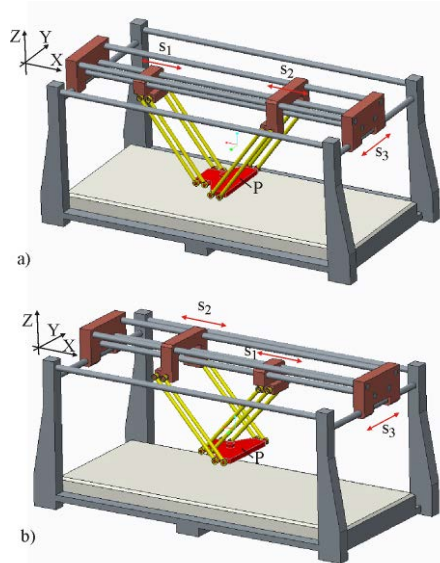


Figure 6: CAD model of the O-X glide mechanism

Plane parallel mechanism consists of the mobile platform, connected via spherical joints to the rods of constant length. On the second end rods are connected to sliders via revolute pair (with one degree of freedom), each of them moves on its own guide rails. In order to increase the autonomy of sliders, they are positioned at different distances in the vertical direction, which enables their passing in the plane, and the movement mechanism in an extended position (O) and cross (X) position.

In the first phase of O-X glide mechanism prototype development based on previously acquired

dimension of parallel mechanism, first physical prototype is made using the rapid prototyping technology, Figure 7a.

On the example of this prototype, verification of working space O-X glide mechanism is performed by moving the slider and following the center of gravity of the mobile platform. Thus it is confirmed that workspace of prototype mechanism corresponds to mathematically obtained workspace. Characteristic positions of prototype O-X glide mechanism, in which center of gravity of mobile platform is observed, are shown on Fig. 7b for extended shape and on Fig. 7c for cross shape of mechanism [24].

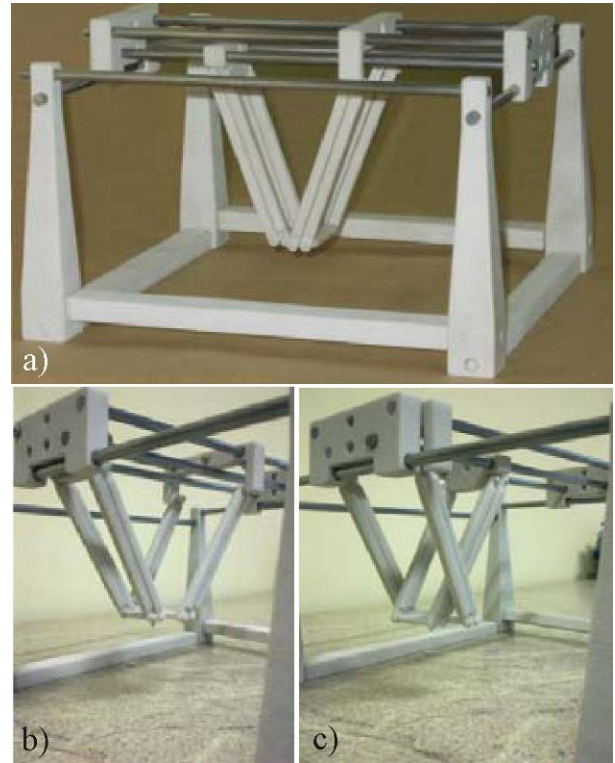


Figure 7: 3D printed real model of the O-X glide mechanism [24]

This paper shows the simulation kinematics machine based on the O-X glide mechanism on the virtual prototype.

3. MACHINING SIMULATION IN THE CAD/CAM ENVIRONMENT

The configured virtual CAD models of CNC machine tools with serial and hybrid kinematics is used for the verification of tool path using machining simulation in CAD/CAM environment. This machining simulation based on generated tool path, which also includes machine simulation. This machining simulation is very important in order to: (i) configure the off-line programming environment, (ii) verify program before machining, (iii) detect collision during program execution.

3.1. Machine virtual models for simulation

Machining simulation by running the program is possible thanks to the applied modelling of machine virtual model for simulation with all kinematic connections between the components, which allows the motion of a virtual model as a system of rigid bodies.

Figures 8 and 10 shows a detailed virtual model of machine tool for machining simulation. Those machine models, configured in CAD/CAM system PTC Creo 2, with all kinematic relationships. Examples of such simulations can also be found in the previous papers [12, 21-23]. Virtual machine models discussed in this paper, are configured including appropriate kinematic connections. For CNC H&H FM38, Fig.8, which has all three translational axes are used only kinematic connection type *Slider*.

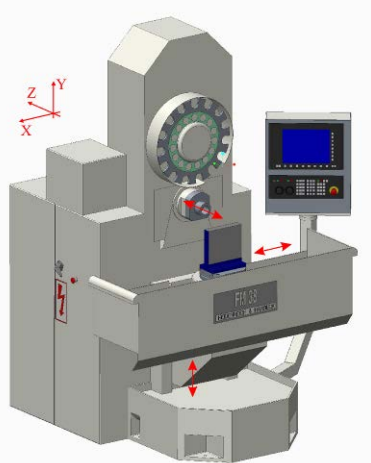


Figure 8: CAD model of the CNC Horizontal Machining Center H&H FM38

An example of defining translational axis (Y) for the horizontal machining center H&H FM38 is presented on Fig. 9.

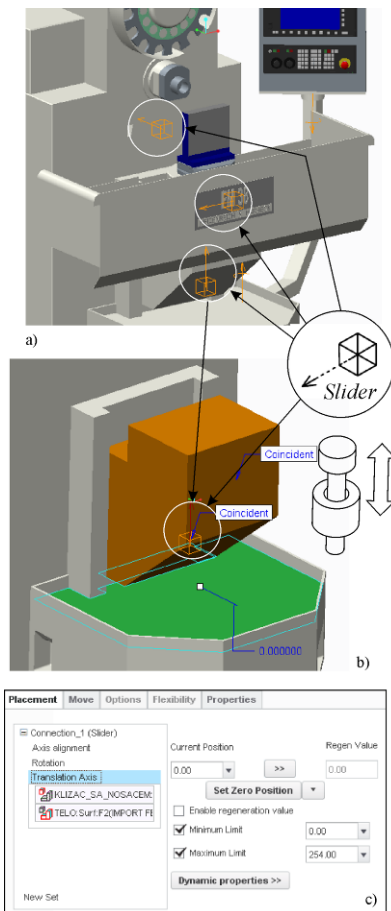


Figure 9: An example of defining the kinematic connection type *Slider*

During designing of the machine model in PTC Creo, movable elements are connected by kinematic relationship. According to Fig. 9 all movement are translations. It's necessary: (i) match all translation axis, (ii) match surfaces or planes of translation, (iii) define referent point of translation axis and travel length. Virtual machine model designed in such way can be included in the cutting process simulation.

In case of machines with a hybrid kinematics, for both variants shown on Fig. 10, except translational axis, rotary joint were used to link the support plate on the slider to platform using 4 pair of coupling, corresponding to joints type *Pin*.

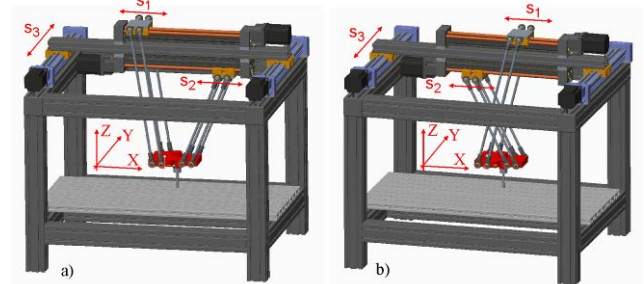


Figure 10: Virtual prototype of a) extended and b) crossed form of the O-X glide hybrid kinematic milling machine

Figure 11 shows the detail of machines used kinematic joints type *Slider* and *Pin*.

An example of defining the kinematic connection type *Pin*, which represents the rotary joint on the machine is shown on Fig. 11b.

The procedure defining pin joint connection includes: (i) align axis of rotation, (ii) match surfaces or planes to align the rotating components along the rotation axis (iii) define current position of rotary axis and minimum and maximum of rotation limits.

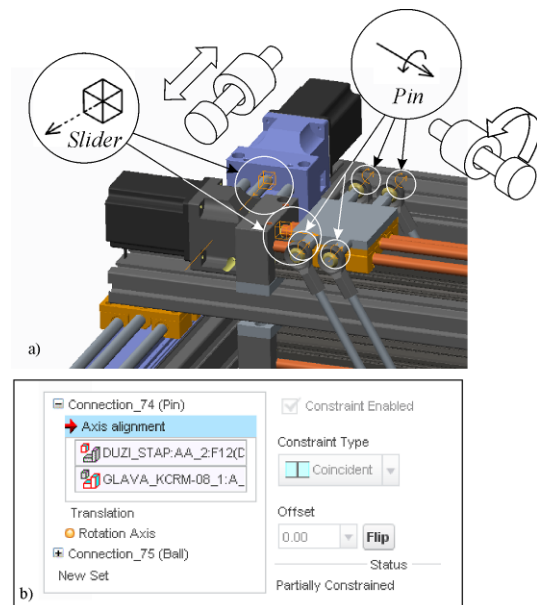


Figure 11: An example of defining the kinematic connection type *slider* and *pin* for the machine with hybrid kinematics

On the base of defined kinematic joints on designed virtual machine model, it is possible to include a complete

virtual model of the machine during simulation of the tool path.

### 3.2. Machining simulation

Simulation of the machining using a virtual prototype is the safest and most economical way of program verification.

This type of simulation is particularly important in the development phase of new machines because it allows the identification of possible deficiency, which is especially interesting in the case of second discussed machines with hybrid kinematics whose development is in progress. System for programming using CAD/CAM system PTC Creo 2.0 [13] is designed so that include a simulation of discussed virtual machine model, thus performing a verification of the obtained programs. Fig.12 shows the programming environment applicable to both considered machines.

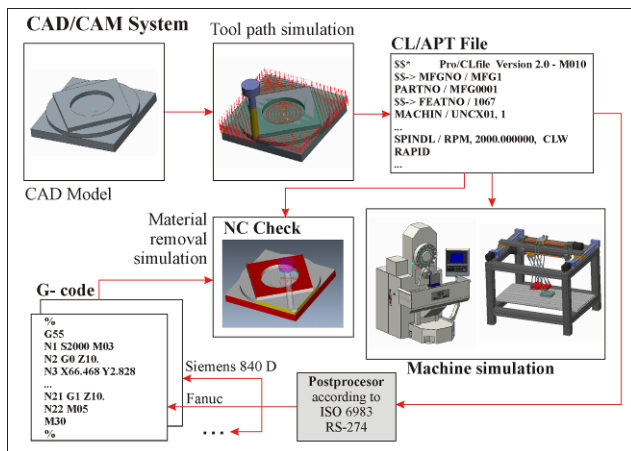


Figure 12: The structure of programming system based on CAD/CAM system

As an example, variant of modified workpiece for testing the accuracy of machine tools was used for the simulation. After generating the tool path (CLF - Cutter Location File), it is possible to verify these paths by simulation of material removal and machining of the entire virtual machine model. For configured virtual machine models, simulation of the machining processing using the entire virtual machine is starting by Machine play. This simulation is realized in the running mod using defined program.

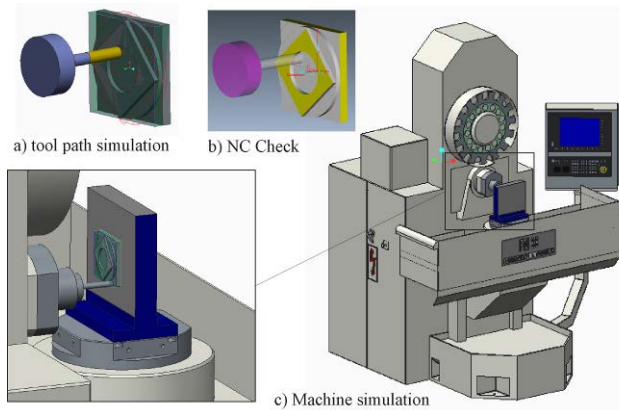


Figure 13: Simulation and verification of tool path for CNC Horizontal Center H&H FM38

Examples of simulation for both machines in the system for programming PTC Creo 2 environment, are shown in Figs. 13 and 14.

For machines with hybrid kinematics particularly important possibility is checking the positioning of the workpiece in the machine workspace, since machine does not have the regular shape of workspace geometry [21]. Corresponding post-processor for NC program generating according to ISO 6983 is configured in the CAD/CAM system, for both machines and for Siemens Fanuc CNC systems, Fig.12.

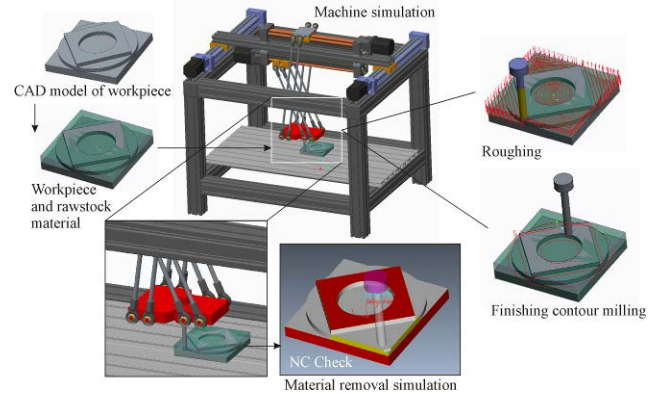


Figure 14: Simulation and verification of tool path for O-X glide hybrid kinematic milling machine

## 4. MACHINING TEST

Cutting process testing for modified workpiece used for testing the accuracy of machine tools is implemented on machining centre H&H FM38.

Dimensions of workpiece used for testing are the same like dimensions of model used in simulation. Also, identical CNC program was used for both, testing and simulation. Figure 15 shows the workpiece obtained during testing.

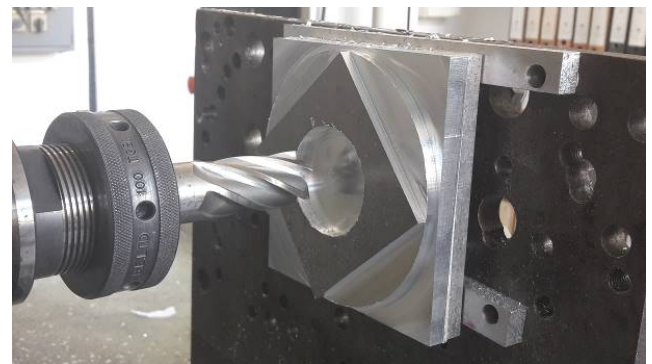


Figure 15: Test workpiece after machining test

Control of geometric shapes and dimensions of the workpiece after testing shows that result obtained by simulation based on generated CNC program fully meet workpiece dimensions.

## 5. CONCLUSION

Machining simulation plays an important role in modern manufacturing. There are many benefits to machining simulation, and one of the most important is testing program for machine, without pressure. Crashing machine on the computer screen is not a big problem. The process of setting up machine simulations is very similar

to setting up a real machine. The part must be placed in the machine in the correct position and orientation.

Analysing generally accepted simulation processes and verification of CNC program for CNC machine tools on the example of machine tools with different kinematic structures, advantage of their use can be seen: (i) Significantly shorter period of time for the preparation and verification of the program for the CNC machine tools; (ii) the machining simulation enabled prior identification of possible collisions between the machine elements during program execution and verification; (iii) ability to simulate removal of material and analyses of virtually produced workpiece; (iv) significant reduction in the percentage of waste on the produced parts.

However in order to simulate the cutting process on the virtual machine, it is necessary to configure it according to the procedure that is different in particular software environments. This paper shows how this can be done using CAD / CAM system: PTC Creo 2.0 in the case of one machine with the serial and one with hybrid kinematics.

On the first machine, horizontal machining center H&H FM38 process verification was done by producing modified workpieces for testing the accuracy of machine tools.

Based on the above it can be concluded that in modern production application of appropriate software systems for simulation and verification of CNC program is necessary. This becomes more important when preparing complex workpieces in individual production where waste occurrence are extremely expensive and obtaining optimal tool path during production by adjusting existing programs is not possible.

#### ACKNOWLEDGEMENTS

In this paper are presented some results of the projects: "Development of a new generation of domestic manufacturing systems" (TR 35022) and "Contemporary approaches to the development of special solutions related to bearing supports in mechanical engineering and medical prosthetics" (TR 35025), supported by the Ministry of Education, Science and Technological Development of Republic of Serbia.

#### REFERENCES

- [1] Y. Altintas, C. Brecher, M. Weck, S. Witt, "Virtual machine tool, " CIRP Annals - manufacturing technology, Vol.54(2), pp. 115-138, (2005)
- [2] A. Fortunato, A. Ascari, "The virtual design of machining centers for HSM: Towards new integrated tools," Mechatronics, Vol.23(3), pp.264-278, (2013)
- [3] J.H. Ko, W.S. Yun, S.J. Kang, D.W. Cho, K.G. Ahn, S.H. Yun, "Development of a Virtual Machine Tool - Part 2: Dynamic Cutting Force Model, Thermal Behavior Model, Feed Drive System Model, and Comprehensive Software Environment," International Journal of the KSPE, Vol. 4(3), pp. 42-47, (2003)
- [4] A.A. Kadir, X. Xu, E. Hämmerle, "Virtual machine tools and virtual machining - A technological review," Robotics and Computer - Integrated Manufacturing, Vol. 27, pp.494-508, (2011)
- [5] <http://www.cimco.com/>
- [6] <http://swansoftcncsimulator.com/>
- [7] <http://cncsimulator.info/>
- [8] <http://www.cgtech.com/>
- [9] <https://www.ncsimul.com/>
- [10] <http://www.tenmillion.co.th/website/PRODUCTS/NCBrain/tabid/46/Default.aspx>
- [11] <http://www.camworks.com/modules/camworks-virtual-machine/>
- [12] S. Zivanovic, B. Kokotovic, "Configuring a virtual desktop 5-axis machine tool for machine simulation", Proceedings of the 12th International Conference on Accomplishments in Electrical and Mechanical Engineering and Information Technology "DEMI 2015", Banja Luka, B&H, Republic of Srpska, 29-30 May, 2015, pp 255-262, (2015)
- [13] <http://www.ptc.com/cad/creo>
- [14] <http://www.techniatranscat.com/solutions/dassault-systemes-software/catia>
- [15] [https://www.plm.automation.siemens.com/en\\_us/products/nx/for-manufacturing/](https://www.plm.automation.siemens.com/en_us/products/nx/for-manufacturing/)
- [16] <https://www.solidcam.com/>
- [17] <http://www.mastercam.com/en-us/>
- [18] <https://www.gibbscam.com/>
- [19] <http://www.autodesk.com/products/hsm/overview>
- [20] <http://www.cimatron.com/>
- [21] S. Živanović, S. Tabakovic, M. Zeljkovic, Z. Milojevic, "Configuring a machine tool based on hybrid O-X glide mechanism," Machine Design, Vol.8(4), pp. 141-148, (2016)
- [22] S. Tabaković, S. Živanović, "Simulation of kinematic of virtual prototype of a machine tool based on hybrid O-X mechanism", Proceedings of 3rd International Scientific Conference on Mechanical Engineering Technologies and Applications "COMETa 2016", Jahorina, B&H, Republic of Srpska, 7-9. December 2016, pp.199-206 (2016)
- [23] S. Živanović, N. Slavković, B. Kokotović, D. Milutinović, "Machine simulation of virtual reconfigurable 5 axis machine tool when machine working according to the running program", Proceedings of 3rd International Scientific Conference on Mechanical Engineering Technologies and Applications "COMETa 2016", Jahorina, B&H, Republic of Srpska, 7-9 December 2016, pp. 207-214, (2016)
- [24] C.Mladenović, S.Tabaković, M.Zeljkić, Workspace of the hybrid mechanism, Proceedings of XII International Scientific – Professional Symposium INFOTEH-JAHORINA 2013, Vol. 12, pp.526-529 (2013)

## 3D Animation of Workpiece Transformation during Milling Operation

Slobodan Ivanović<sup>1\*</sup>, Aleksandra Petrović<sup>2</sup>, Ljubomir Lukić<sup>2</sup>, Marina Pljakić<sup>2</sup>

<sup>1</sup> High Technical Mechanical School Trstenik, Serbia

<sup>2</sup> Faculty of Mechanical and Civil Engineering in Kraljevo, University of Kragujevac, Serbia

*Engagement zone is determined as instant intersection of workpiece and tool which is changing during milling operation. Engagement zone is identified as key parameter whose variations throughout the milling process causes the variations of cutting force. Knowledge of changes in engagement zone along the tool path is necessary for simulation and monitoring of the cutting force during the machining process.*

*In milling process workpiece geometry is changing from blank shape to finished product. For determination of engagement zone geometry it is necessary to have accurate instant workpiece geometry and tool position. This paper presents geometrical representation of blank, tool and tool path used for animation of current workpiece geometry and tool position. Calculation and animation of engagement zone geometry is also shown.*

**Keywords: Animation, Milling operation, Workpiece geometry**

### 1. INTRODUCTION

Cutter engagement or engagement zone in milling operation is described in literature [1] as measurement of portion of the cutter which is actually involved in machining at a given instant of time. Geometry of engagement zone is determined by radial and axial depth of cut and engagement angle [2].

Accurate cutter/workpiece engagement calculation is a key requirement for process modelling [3], and therefore engagement zone is identified as key parameter which variations during the process causes the variations of cutting force in milling operations [2]. Simulation of engagement zone elements can be used for determination of cutting force and cutting force variation during machining.

In general, there are two groups of approaches to model the cutting engagement:

- exact methods, using vector analytical geometry and Boolean operations to calculate exact positions and magnitudes of contact points, lines or surfaces in volumetric space [4],[5];
- discretized methods, based on bitmap image analysis in 2D (pixel-based methods) or finite-element methods in 3D [6], [7], [8], [9].

Approach used in this paper is combination of those two approaches.

For calculation of engagement zone elements it is necessary to determine tool position and current workpiece shape in each point of tool path.

Required elements of the cutting process can be calculated if, in addition to data contained in the generated NC programs, geometric characteristics of blank and geometric and technological characteristics of the tool are defined.

To calculate geometrical parameters, first of all, NC code data generated by some of the CAM packages have to be imported into a database and processed. For each path segment the coordinates of start and end point, interpolation parameters, cutting conditions and geometric characteristics of the tool are obtained [10].

This paper presents animation of tool position, tool movement direction, workpiece current shape and contact lines generated in intersection of tool and workpiece during machining.

### 2. GEOMETRICAL DESCRIPTION OF BLANK

Blank workpiece is imported in Matlab as a bitmap image representing view of blank from above, where each colour corresponds to an appropriate height of the blank (Figure1), detailed description is given in [11].

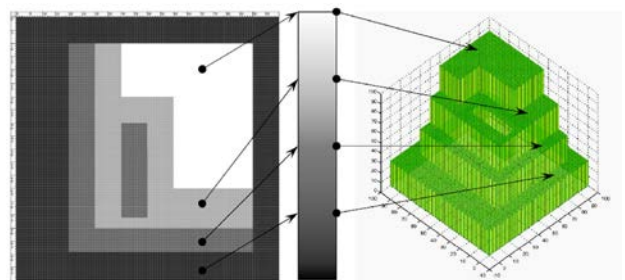


Figure 1: Transformation of bitmap image into blank network

Dimensions of rastered basis of the blank, the coordinates (position) and colour of each pixel are read from a bitmap file (Figure2). Blank matrix  $Wc$  containing the colours of all the pixels in the  $XY$  coordinate plane, is created (Equation 1).

Matrix  $Wc$  contains colours of each pixel in coordinate plane  $XY$ .

$$Wc(b_l + 1 - j, i) = B_c(j, i) \quad j: \begin{matrix} 1 \\ -1 \\ b_l \end{matrix} \quad i: \begin{matrix} b_w \\ 1 \end{matrix} \quad (1)$$

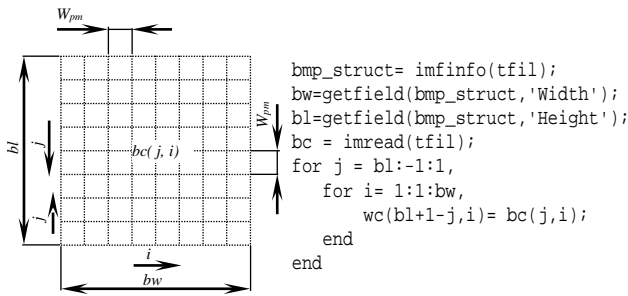


Figure 2. Bitmap data reading

Based on matrix  $Wc$ , given maximum blank height  $w_{zmax}$  and given length of pixel in millimetres  $w_{pm}$  matrices of point coordinates at blank net are calculated:

$$\begin{aligned}
 W_x(j, i) &= (i-1) \cdot w_{pm} \\
 W_y(j, i) &= (j-1) \cdot w_{pm} \\
 W_z(j, i) &= \begin{cases} NaN, W_c(j, i) = 0 \\ w_{zmax} \cdot \frac{W_c(j, i)}{255}, 0 < W_c(j, i) \leq 255 \end{cases}
 \end{aligned}
 \quad j: \begin{cases} b_l \\ i \\ 1 \end{cases} \quad i: \begin{cases} b_w \\ 1 \end{cases} \quad (2)$$

Blank boundary in  $XY$  plane is rectangular shape with length  $b_l$  and width  $b_w$ , and value of each pixel inside that boundary is determined by reading its colour from bitmap data.

On the basis of the matrix  $W_c$ , given maximum height of blank  $w_{zmax}$  and length of pixels in millimeters  $w_{pm}$ , matrix of points coordinates on the blank net are calculated.

If pixel colour is 0 (black), in that point there is no material in the workpiece (hole), otherwise, height of point at blank net  $W_z(j, i)$  corresponds to value of pixel colour.

Corresponding matrix of blank in Matlab is formed. Blank don't have to be prismatic, it can have vertical holes and grooves, but may not have the horizontal holes.

### 3. GEOMETRICAL DESCRIPTION OF TOOL

Geometrical description of the tool is based on ASCII database in which diameter and shape of tool are written. Based on tool diameter  $d_t$  and radius  $r_t$ , as well as millimetre net division  $w_{mp}$  matrix of points on cylindrical tool net are calculated. Program is developed for three different shapes of tool: cylindrical (flat endmill), conical (tapered endmill) and spherical (ball endmill),

Tool net  $U$  is described by matrix  $U_x, U_y$  and  $U_z$ :

$$U = (U_x, U_y, U_z) \quad (3)$$

and  $U_x, U_y$  and  $U_z$  matrix dimensions are:

$$u_j = u_d, \quad u_i = u_d \quad (4)$$

Matrix of tool points coordinates are written in ASCII files together with other tool data. Along with tool net  $U$ , based on tool radius  $r_t$ , maximum tool height  $t_{zmax}$ , and millimetre net discretization  $w_{mp}$  coordinates of points on tool generatrix are generated (Figure 3).

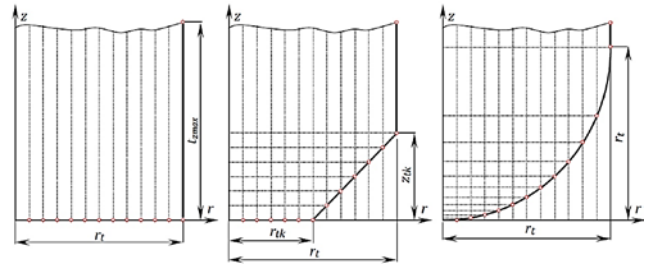


Figure 3: Matrices of points on tool generatrix coordinates for three types of tool: cylindrical, conical and spherical mill

The result of previous tool description are tool nets for cylindrical, conical and spherical mill (Figure 4) in Matlab program.

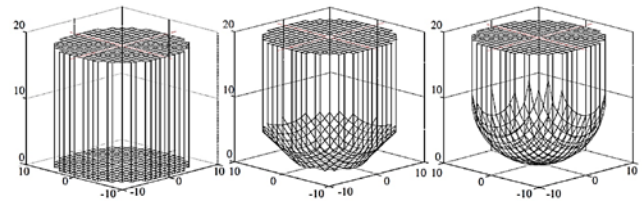


Figure 4: Tool nets for cylindrical, conical and spherical mill

### 4. GEOMETRICAL DESCRIPTION OF TOOL PATH

Geometrical description of tool path is obtained by transformation of NC program into ASCII file.

According to database, for each program sentence, tool path segment is reproduced (Figure 5). Tool path segments which corresponds to machining are presented with solid lines, and those that refer to positioning and rapid movement of tool are shown as dashed lines.

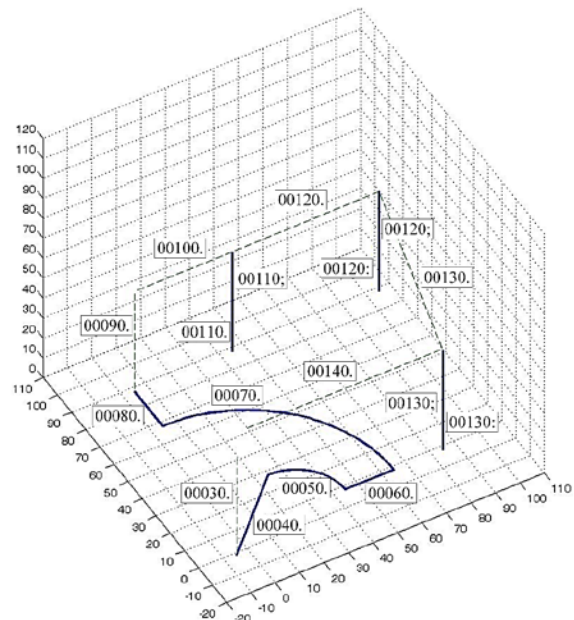


Figure 5: Tool path segments corresponding to ASCII file

Tool path defined by ASCII file is segmenting to elementary tool path segments  $P(m)$  corresponding to each data row (Figure 6). To each tool path segment  $P(m)$  following data are assigned: interpolation type -  $Pg(m)$ , feed rate-  $Pf(m)=s$ , spindle speed  $Ps(m)=n$ , start point



coordinates -  $x_1, y_1, z_1$ , end point coordinates -  $x_2, y_2, z_2$ , circular interpolation centre point-  $x_c, y_c, z_c$ , circular interpolation radius  $r$ , circular interpolation start angle-  $\alpha_0$  and circular interpolation angle-  $\alpha$ .

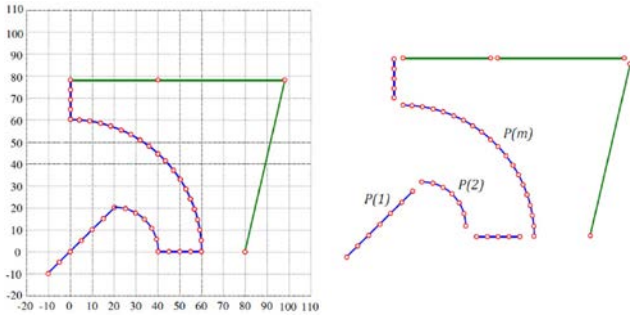


Figure 6: Tool path segmentation

For each tool path segment, length of segment  $P_l(m)$ , number of points on segment  $p_n$ , matrices of points coordinates at tool path  $P_x(n), P_y(n), P_z(n)$  and angles of tool path in that points  $P_a(n)$  are calculated. In each of these points, tool - workpiece intersection will be determined.

### 5. WORKPIECE TRANSFORMATION

For determination of tool - workpiece intersection, blank net is defined as line  $W_p$  which consists of parallel lines at part of blank net  $W$  at current tool position, and tool circumference is defined as polygon  $O_p$  in  $XY$  plane.

Polygon  $P_1$  is defined by matrices of vertices coordinates in  $XY$  plane  $P_1 = (px1, py1)$ . Line  $P_2$  is defined by matrices of line end points coordinates in  $XY$  plane which contains members  $NaN$  (Not A Number) as  $P_2 = (px2, py2)$ . Members  $NaN$  divide line  $P_2$  on segments. Result of line and polygon intersection  $P_i = P_1 \cap P_2$  are matrices of intersection points coordinates  $P_i = (pxi, pyi)$ . Dimension of matrices  $pxi$  and  $pyi$  are mutually equal and determine the number of intersection points.

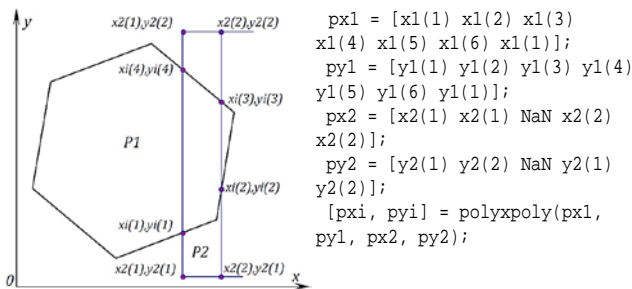


Figure 7: Definition of polygon  $W_p$  as line consisting of parallel lines

Connecting horizontal and vertical segmented lines gives  $W_p$  consisting of parallel segments and determined by matrices of points coordinates  $W_{px}$  and  $W_{py}$  on part of blank matrix  $W$ .

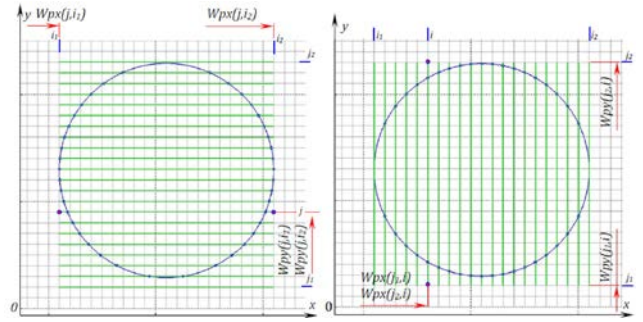


Figure 8: Lines consisting of horizontal and vertical segments of  $W_p$

Intersection of polygon  $O_p$  and line  $W_p$  results in matrices of coordinates  $O_x(k)$  and  $O_y(k)$ :

$$[O_x \ O_y] = O_p \cap W_p. \quad (5)$$

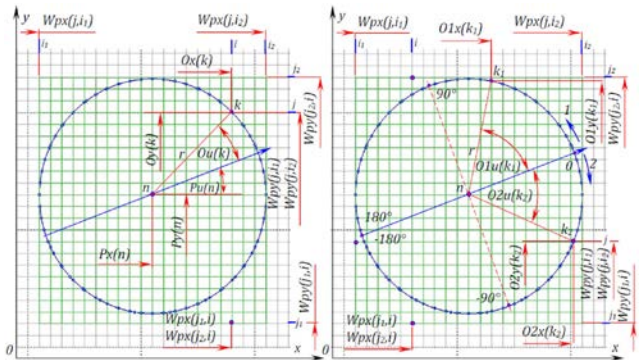


Figure 9: Intersection of polygon  $O_p$  and line  $W_p$

#### 5.1. Contact points determination

Points of contact between blank and tool circumference are determined based on matrices of coordinates on blank net  $W_x, W_y, W_z, W_{2x}, W_{2y}$  and  $W_{2z}$  and matrices of points coordinates in which tool circumference intersects workpiece net  $O_{1x}, O_{1y}, O_{1z}, O_{2x}, O_{2y}, O_{2z}$ . For each pair of adjacent points on tool circumference (Figure 10) with coordinates  $O_{1x}(k), O_{1y}(k)$  and  $O_{1x}(k+1), O_{1y}(k+1)$  elementary unit of workpiece net intersect by tool is determined by coordinates  $W_x(j, i)$  and  $W_y(j, i)$  and point position  $(j, i)$  in coordinate matrices  $W_x, W_y$  и  $W_z$ .

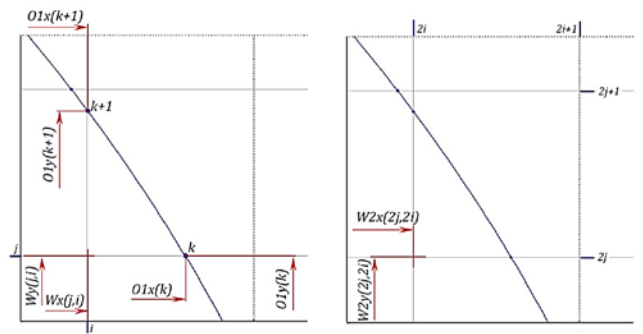


Figure 10: Two adjacent points on tool circumference: coordinates  $W_x(j, i)$  and  $W_y(j, i)$  and point position  $(j, i)$

Ratio of coordinates  $W_{2z}(2;j,2\cdot i)$  and  $O_{1z}(k)$  defines if intersection point on tool circumference is in contact with workpiece (Figure 11). For  $O_{1z}(k) \geq W_{2z}(2;j,2\cdot i)$  (Figure 11a), there is no contact between tool and workpiece. For  $O_{1z}(k) < W_{2z}(2;j,2\cdot i)$  (Figure 11b), contact point  $z$  coordinate is  $W_{2z}(2;j,2\cdot i)$ . For  $O_{1z}(k) <$

$W2z(2-j,2-i)$  and  $O1z(k) < w_{z0}$  (Figure 11c), contact point  $z$  coordinate is  $w_{z0}$ .

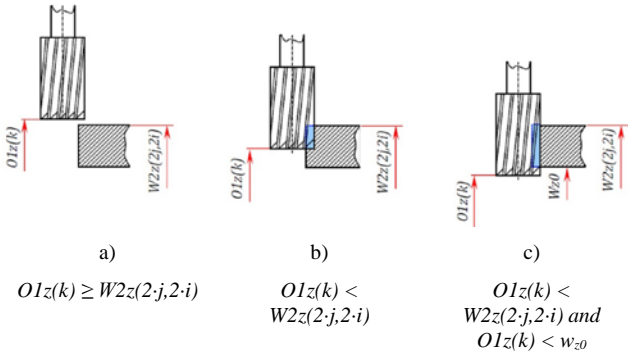


Figure 11: Checking for contact in intersection point of tool circumference and workpiece for different tool positions relative to workpiece in  $z$  direction

For contact point matrices of coordinates for bottom contact points  $K1x, K1y, K1z, K2x, K2y, K2z$ , matrices of central angles  $K1u, K2u$ , matrices of differences between angles  $K1i, K2i$  and matrices of projections of distances between points on tool path direction normal  $K1a, K2a$  (Figure 12), are formed.

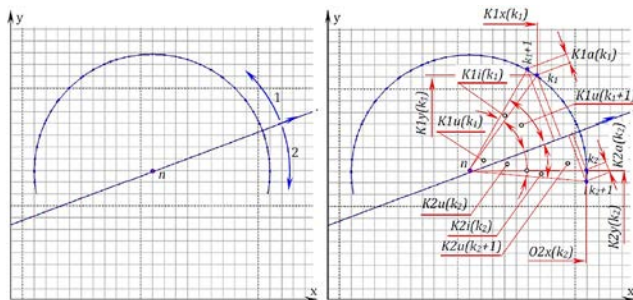


Figure 12: Tool-workpiece intersection: contact line and contact points from both sides of tool movement direction and respective geometrical elements

Besides coordinates of bottom contact points  $K1z, K2z$ , respective coordinates of upper contact points are calculated  $K1w, K2w$ . They depend on maximum tool height  $t_{zmax}$  (Figure 13).

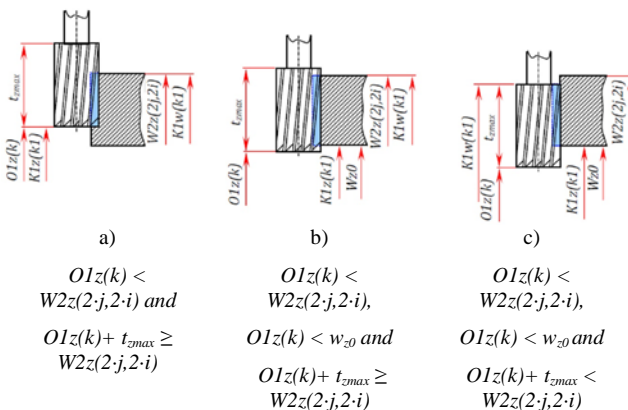


Figure 13: Coordinates of upper contact points  $K1w$  for different tool positions relative to workpiece in  $z$  direction

For cases a) and b) in Figure 13,  $K1w$  is equal to  $W2z(2-j,2-i)$  and for case c) in Figure 13,  $K1w$  is equal to  $O1z(k) + t_{zmax}$ .

Bottom contact points, obtained by presented procedure in each tool position at elementary segment of

tool path, are shown in Figure 14, left. Bottom contact points and corresponding upper contact points are shown in Figure 14, right.

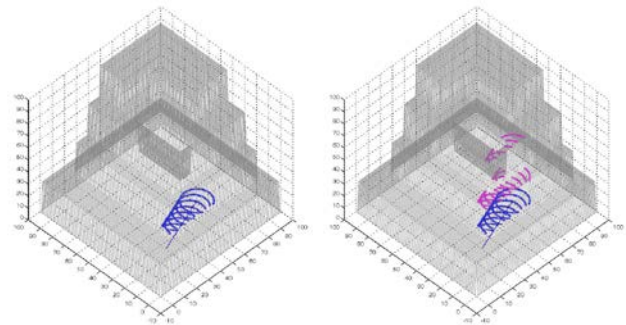


Figure 14: Bottom and upper contact points on elementary segment of tool path

Figure 15 shows contact points in two different points at elementary segment of tool path.

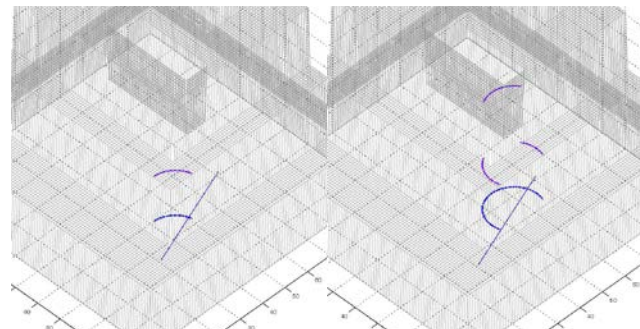


Figure 15: Contact points in two different points at elementary segment of tool path.

Figure 15, left, is an example for constant axial depth of cut, and Figure 15, right, shows case with two different axial depths of cut in single tool rotation.

### 5.2. Example of workpiece transformation using 3D animation

Process of workpiece transformation is illustrated by animation steps explained above (Figures 16-22).

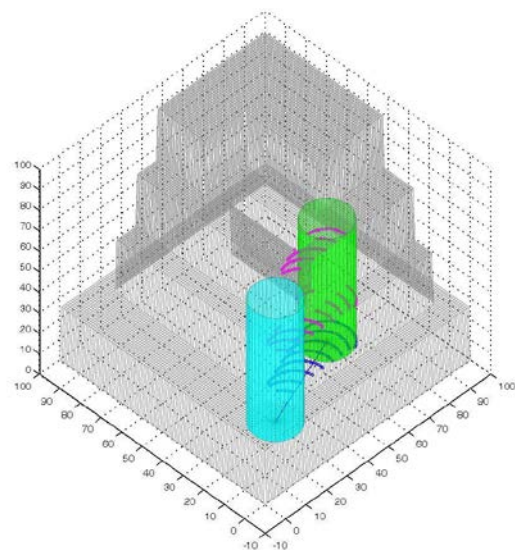


Figure 16: Bottom and top contact lines and tool positions at the start and the end of the first tool path segment

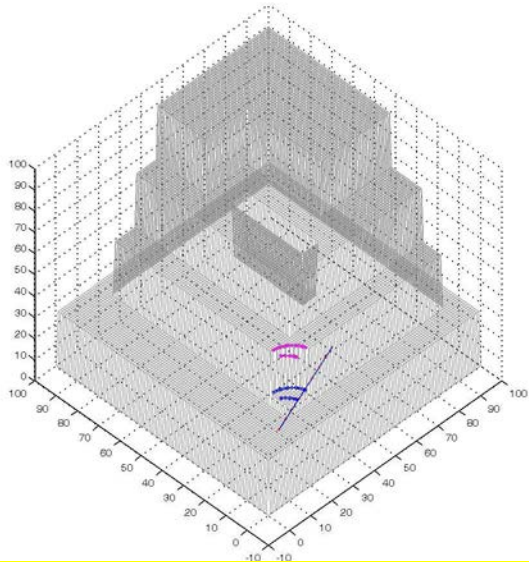


Figure 17: Bottom and top contact lines formed in two consequent tool rotations at the beginning of tool path segment

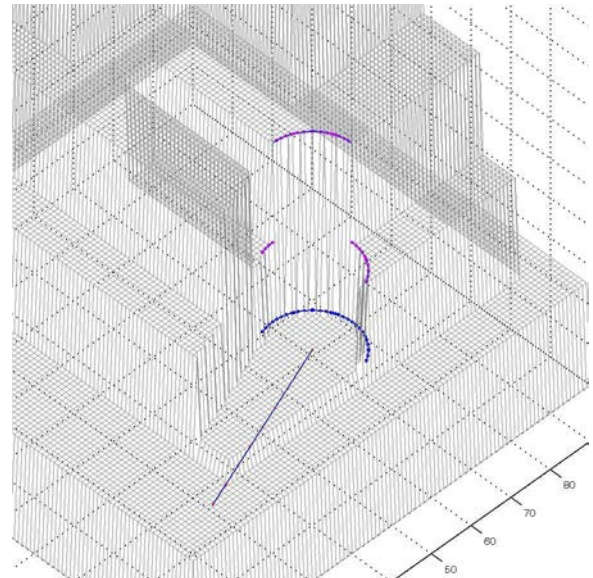


Figure 20: Enlarged view of bottom and top contact lines at the end of the first tool path segment

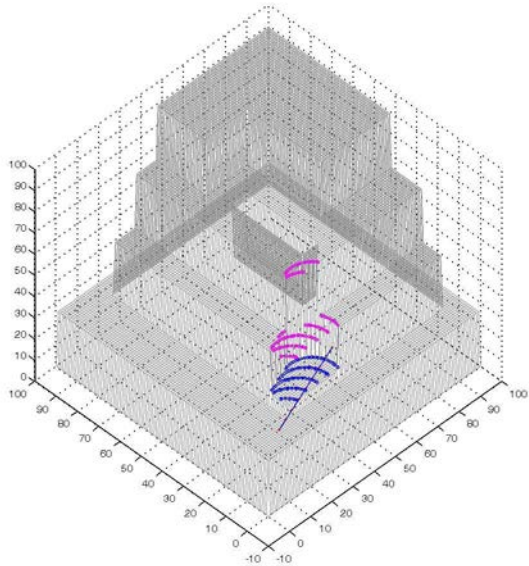


Figure 18: Bottom and top contact lines formed in consequent tool rotations at the first tool path segment

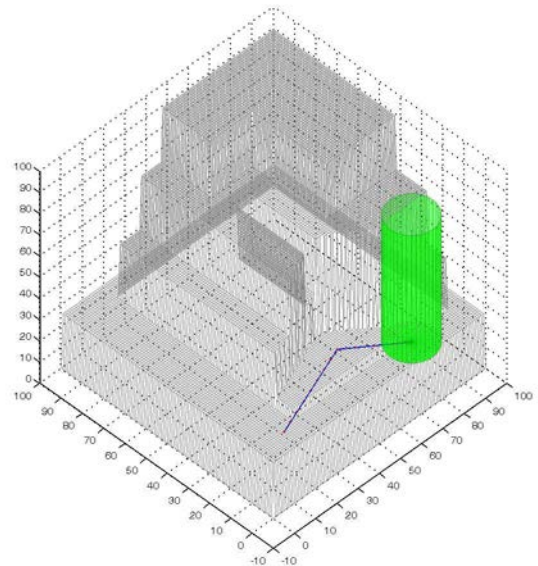


Figure 21: Tool position and transformed workpiece shape at the end of the second tool path segment

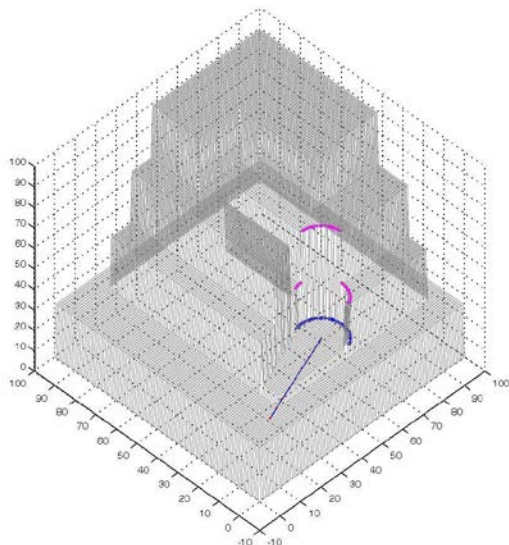


Figure 19: Bottom and top contact lines at the end of the first tool path segment

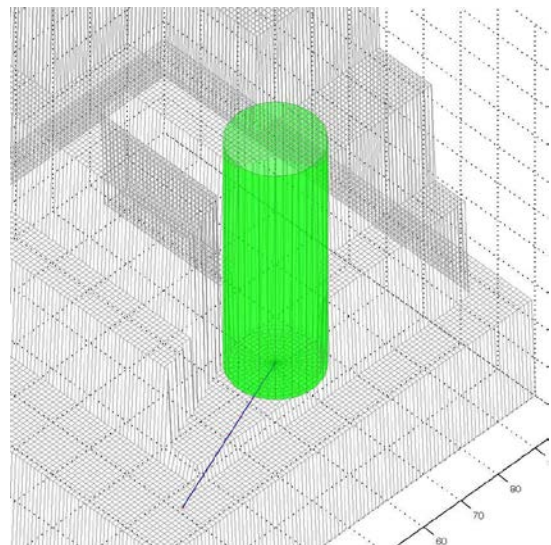


Figure 22: Tool position and transformed workpiece shape at the end of the first tool path segment

Figures show process of determination of bottom and top contact lines between tool and workpiece, tool positions and transformed workpiece at one segment of tool path. Presented animation of milling process and workpiece transformation is used for calculation of engagement zone elements and visual machining error detection on machined workpiece.

## 6. CONCLUSION

In this paper animation of engagement zone and workpiece current shape during milling operation is presented. Engagement zone is changing during the peripheral milling of pockets or islands. Variation of engagement zone causes variation of other milling factors such as cutting force or productivity. Knowledge of engagement zone elements along the tool path is therefore necessary for calculations of cutting force and other characteristics of milling process.

Presented methodology is part of program developed for optimal tool path selection based on different criteria such as minimum cutting force, minimum cutting force variation, type of milling (up or down), total tool path length etc.

## ACKNOWLEDGEMENTS

The authors would like to express their gratitude to the Ministry of Education and Science of the Republic of Serbia for their support to this research through the project TR37020.

## REFERENCES

- [1] S. K. Gupta, S. K. Saini, B. W. Spranklin, and Z. Yao, "Geometric algorithms for computing cutter engagement functions in 2.5D milling operations," *Comput. Des.*, vol. 37, no. 14, pp. 1469–1480, Dec. 2005.
- [2] Petrovic A, Lukic Lj, Ivanovic S, Pavlovic A, „Optimisation of tool path for wood machining on CNC machines“, *Proceedings of the Institution of Mechanical Engineers, Part C: Journal of Mechanical Engineering Science*, 2016.
- [3] D. Yip-Hoi and X. Huang, "Cutter/Workpiece Engagement Feature Extraction from Solid Models for End Milling," *J. Manuf. Sci. Eng.*, vol. 128, no. 1, p. 249, Feb. 2006.
- [4] B. K. Fussell, R. B. Jerard, and J. G. Hemmett, "Robust Feedrate Selection for 3-Axis NC Machining Using Discrete Models," *J. Manuf. Sci. Eng.*, vol. 123, no. 2, p. 214, May 2001.
- [5] J. Kloypayan and Y.-S. Lee, "Material engagement analysis of different endmills for adaptive feedrate control in milling processes," *Comput. Ind.*, vol. 47, no. 1, pp. 55–76, Jan. 2002.
- [6] B. K. Choi and B. H. Kim, "Die-cavity pocketing via cutting simulation," *Comput. Des.*, vol. 29, no. 12, pp. 837–846, Dec. 1997.
- [7] D. Roth, F. Ismail, and S. Bedi, "Mechanistic modelling of the milling process using an adaptive depth buffer," *Comput. Des.*, vol. 35, no. 14, pp. 1287–1303, Dec. 2003.
- [8] H. Wang, P. Jang, and J. A. Stori, "A Metric-Based Approach to Two-Dimensional (2D) Tool-Path Optimization for High-Speed Machining," *J. Manuf. Sci. Eng.*, vol. 127, no. 1, p. 33, Feb. 2005.
- [9] H.-C. Kim, "Tool path modification for optimized pocket milling," *Int. J. Prod. Res.*, vol. 45, no. 24, pp. 5715–5729, Dec. 2007.
- [10] A. Petrović, S. Ivanović, and L. Lukić, "Generating Parametres from the NC Code Needed for Defining the Optimal Tool Path," in *MMA 2015 - FLEXIBLE TECHNOLOGIES*, 2015, pp. 157–160.
- [11] S. Ivanović, A. Petrović, and L. Lukić, "Matrix blank description as part of module for machining parameters generation along the tool path for peripheral milling," *IMK-14 – Res. Dev. Heavy Mach.*, vol. 21, no. 4, pp. EN119–124, 2015.
- [12] A. Petrovic, Lj.Lukic, M. Bjelic, M. Pljakic, "Optimal tool path modeling in contour milling process," 36th International Conference on Production Engineering, Kopaonik, 2013, pp 263-270
- [13] A. Petrović, S. Ivanović, and L. Lukić, "NC Tool Path and Its Influence on Cutting Force in Peripheral Milling Analyses," *IMK -14-- Res. Dev. Heavy Mach.*, vol. 21, pp. 41–46, 2015.

# Optimization Model for Machining Processes Design in Flexible Manufacturing Systems

Ljubomir Lukic<sup>1\*</sup>, Slobodan Ivanovic<sup>2</sup>, Aleksandra Petrovic<sup>1</sup>, Mirko Djapic<sup>1</sup>

<sup>1</sup>Faculty of Mechanical and Civil Engineering Kraljevo, University of Kragujevac, Serbia

<sup>2</sup>High Technical Mechanical School, Trstenik, Serbia

*Engineering machining processes realized in flexible machining systems (FMS) is a highly complex engineering task, especially since it encompasses complex optimization procedures apart from engineering. For a broad array of different workpieces produced in different series it is very difficult to engineer a manufacturing process for attaining maximum processing productivity with minimal production costs. The paper presents a developed post-processor model enabling automatic generating of the NC code for all NC programs executed simultaneously in the production process on a greater number of machining centers. The model engrosses the different variants of tools in a machining center magazine, a different combination of elements of the machining mode, possibility of the most favorable layout of workpieces on palettes, compliance with the technological requirements in terms of simultaneous tool changes in machining center magazines, the required total processing time and minimal production costs. To that aim has been developed the post-processor generator, as a program and software system, enabling all NC programs to be automatically updated based on the set up optimization strategy from tool changes, changes in cutting mode elements and technological operations. Such updated NC programs contain optimal technological parameters and provide minimal costs of production while at the same time the maximum utilization of tools during manufacture at an exactly specified time.*

**Keywords:** NC program, optimization of machining processes, post-processor generator, FMS

## 1. INTRODUCTION

The optimal manufacturing process in a classical production system arises as a result of optimal performing of individual technological operations when developing each workpiece according to multifunctional dependencies between the machine tool, workpiece material, tools and elements of the machining mode [1]. In FMS technological processes this isn't the case, because procedural dependencies are very important in processing alongside the functional. Optimizing the technological process in FMS is based on a much more complex model, because production in FMS has a series of production specifics in a classic production system [2]:

- The workpieces for processing in FMS are geometrically and technologically of similar characteristics,
- Simultaneous – simultaneous processing of multiple same and/or different workpieces in FMS,
- Processing same and/or different workpieces is performed simultaneously on multiple different or same manufacture centers,
- The workpieces are processed usually in different series (whereby each workpiece type has its own specific series in which it should be manufactured),
- On one machining center are performed several machining operations with different tools,
- On one palette can be several same or different workpieces,
- Tool change is done automatically in two levels – change from the main spindle and tool magazine on the machining center and change of all tools from the machining center magazine,
- Simultaneous tool change from the machining center magazine conditions for one of the goal functions during optimization to be an even level of blade wear

on all tools, and for each tool to have durability approximately equal to its cutting time,

- Changing workpiece palettes is done automatically,
- Moving workpieces in a technological process is performed via an automatic transport system,
- Storing workpieces between individual technological phases in the manufacture process is performed on buffers – special palette storages,
- The preparation places for secondary and gripping requisites, tools and workpieces are specially organized and are set on palettes available to automatic transport systems,
- The delivery of preparation pieces is especially regulated (castings, forgings, welded blanks) to the FMS line and delivery of processed parts.

The technological task for processing a group of parts ( $A_1, A_2, A_3, \dots, A_n$ ) in FMS is set for the defined and pre-known FMS configuration. Besides, for designing an optimal technological process in FMS we need to have as input data the series that should be produced for every workpiece from the assortment ( $SA_1, SA_2, SA_3, \dots, SA_n$ , whereby in the general case is  $SA_1 \# SA_2 \# SA_3 \# \dots \# SA_n$ ), the total time for processing the entire assortment of parts in a given series ( $T_z$ ) and the grade ( $e$ ) of utilization over time of the machining centers (Fig. 1).

Part groups that are simultaneously processed in FMS can be comprised of a smaller or lesser number of different parts ( $A_1, A_2, A_3, \dots, A_n$ ), while its series can also be very different. Some workpieces can be made in a smaller number of pieces, while others can be in larger series. All workpieces in a group don't have to be of the same material. All this indicates that the production process in FMS is quite flexible from several aspects and that the engineering procedure and machining optimization in FMS is quite complex.

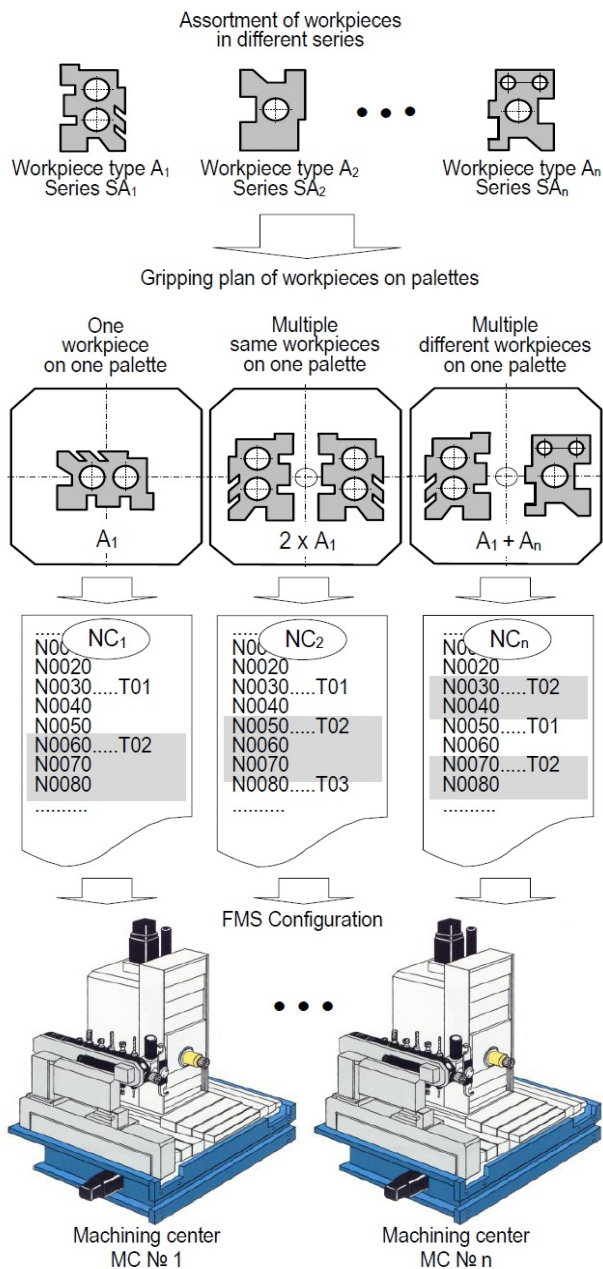


Figure 1: Procedure of engineering and optimizing the production process in FMS

## 2. OPTIMIZING FLEXIBLE MACHINING

The optimization of technology [3] starts in a phase when the NC programs for all grippings for a workpiece group that is simultaneously processed in FMS have been done. By analyzing each generated NC program, there are a couple of resulting parameters as statistic indicators of the quality of engineering the machining process (Fig.2):

- The total number of technological operations
- The duration of each operation,
- The total indexing number,
- A list of tool sets by each NC program and a list of elements for each individual set (main holder, extension piece, reducing piece, requisites, cutting tools),
- The total number of tool changes and number of all tools participating in executing the NC program,

- No-traverse period – the period the tools move without cutting the material,
- Cutting time– the period of time in which the tool blades mesh the workpiece material (working traverse rate),
- Total indexing period,
- Total time for tool change and
- Total time of executing the NC program on the machining center.

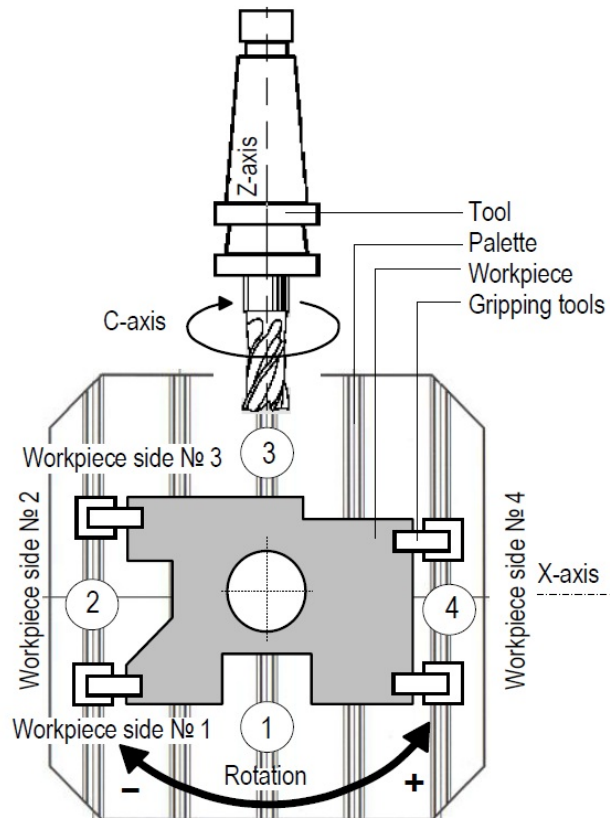


Figure 2: Position of the workpiece on the palette in relation to the tool

By analyzing, adding and comparing the values of output parameters, the parameterization of all NC programs whose execution is planned within the scope of one technological process is performed. In that manner we get to a general evaluation of the engineered technology for FMS, based on which we enter the optimization procedure.

The technological task defines a certain group of workpieces ( $A_1, A_2, A_3, \dots, A_n$ ) that is being processed, the series to be produced for every workpiece from the group ( $SA_1, SA_2, SA_3, \dots, SA_n$ ), the total time for processing a group of workpieces in a given series ( $T_{ij}$ ) and the rate of processing center utilization over time ( $e$ ). If we apply the convention that one NC program matches one gripping, then the number of NC programs ( $k$ ) must be higher than the number of different workpieces in the group ( $n$ ), because it is practically impossible for all workpieces to be processed in one gripping. Every workpiece type in the group ( $A_1, A_2, A_3, \dots, A_n$ ) is processed in one or more grips. The sum of the number of necessary grips for all workpiece types ( $S$ ) is equal to the total number of NC programs ( $N$ ),

$$S_1 + S_2 + S_3 + \dots + S_n = \sum_{i=1}^n S_i = S = N.$$

To determine the total processing time ( $TA_i$ ) of one specific type from a group of workpieces, the times of execution of the NC programs ( $T_{NCi}$ ) referring to a specific type are added and the palette change time is added ( $T_P$ ) increased as many times as the workpiece has grips ( $S_i$ ),

$$TA_i = \sum_{i=1}^{S_i} T_{NCi} + T_P \cdot S_i.$$

The total processing time ( $TSA_i$ ) of one type of workpiece in a given series is defined as

$$TSA_i = TA_i \cdot SA_i.$$

The total effective processing time ( $TSA$ ) of all workpiece types in a given series can be determined by adding the processing time

$$TSA = TA_1 \cdot SA_1 + TA_2 \cdot SA_2 + TA_3 \cdot SA_3 + \dots + TA_n \cdot SA_n$$

$$TSA = \sum_{i=1}^n TA_i \cdot SA_i.$$

Since it is impossible for a predetermined FMS configuration to organize the production process so that all manufacture centers are maximally utilized, the total effective time for processing a group of parts ( $TSA$ ) should be corrected according to the rate of utilization of machining centers ( $e$ ) and thus get the real required time ( $TSA_R$ ) for processing a group of parts in a given series. If the rate of utilization is expressed so that it is ( $e < 1.00$ ), we'll get the real time of processing by increasing the effective time ( $TSA$ ),

$$TSA_R = TSA \cdot 1/e.$$

The total time of palette changes ( $T_{IP}$ ) during the FMS process, is gotten by multiplying the palette change time ( $T_P$ ) as a functional feature of the manufacture center and number of all grips– or the number of all NC programs,

$$T_{IP} = T_P \cdot S = T_P \cdot N.$$

When the total real time ( $TSA_R$ ) for processing a group of parts in given series, arising as a result of executing all NC programs in FMS, is compared to the given total processing time ( $T_Z$ ) it is practically impossible for it to be  $TSA_R = T_Z$ , which would mean that the technological task was resolved in the first "passage" of NC programming. It can be expected that  $TSA_R > T_Z$  or  $TSA_R < T_Z$ , based on which is determined the optimization strategy (Fig. 3). The optimization strategy [4] is conducted by changing the elements in NC programs that are engineered in the first "passage" of NC programming, so that in the end result the real time for processing would be approximate to the given time. The optimization procedure is conducted firstly in the domain of cutting tools, then the cutting mode and finally in the manufacturing operation domain.

In the case of  $TSA_R > T_Z$ , we apply the optimization strategy for increasing the productivity of the machining process that will partially raise costs for a specific production cycle. Elements in NC programs must be changed to shorten the time of their execution. We need to choose tools of better cutting features and of better tool materials than in the first "passage" of NC programming, in all the machining operations where possible (Fig. 4).

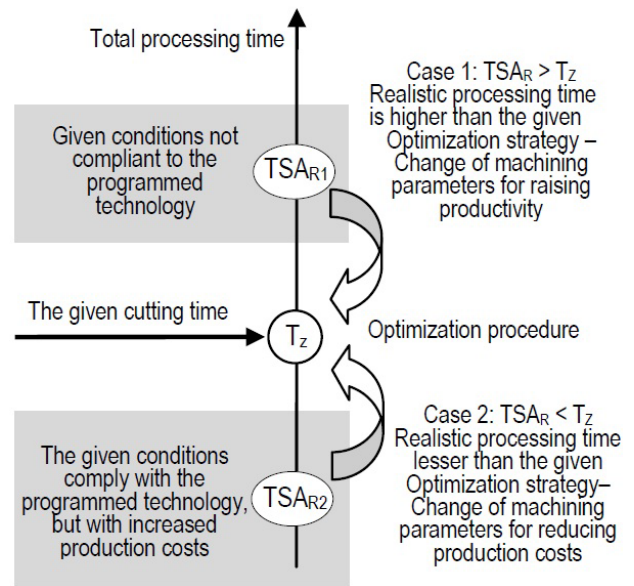


Figure 3: Strategy when optimizing manufacture processes in FMS

In case of  $TSA_R < T_Z$  we apply the optimization strategy for reducing the costs of the machining process. In this case by changing the elements in NC programs we increase the times of their execution. Cheaper tools of lower cutting quality are chosen than in the first "passage" of NC programming, in all the technological operations where this is possible. The cutting speeds decrease and the speeds of secondary movements in operations where the technological requirements allow it, while the alternative technological operations are determined that will enable longer processing time by reducing costs.

If through the optimization procedure we don't attain the desired result in the first stage ( $TSA_R \approx T_Z$ ), we go on to the second or third. Given that NC programs can contain a high level of manufacturing operations, and that the difference between  $TSA_R$  and  $T_Z$  doesn't always have to be great, the optimization procedure can be successfully completed in one step, but to be conducted only in certain NC programs.

The procedure for optimizing the manufacturing processes unfolding in FMS greatly differs from the optimization of conventional manufacture processes. The optimal technology for FMS isn't the sum of optimal individual manufacturing operations, but global optimization is carried out at the level of all operations that are performed on machining centers, by respecting the other aspects of the technological process besides the correlations of cutting parameters. It is very important to design the processing mode parameters for each tool participating in the execution of an NC program, so that the wear intensity is adapted to the projected durability for a group of tools participating in making a defined assortment of workpieces. This means that it is important to bear in mind the duration of certain operations in relation to the durability of the tool performing the operation.

The optimization of the technological process entails for the maximum rate of time utilization of machining centers, washing machine, measuring center, transport

system and all preparatory places. Depending on the manufacturing task, a higher or lesser degree of FMS resource utilization can be realized which is why when optimizing the production process in FMS, we must count on the available buffers for storing palettes between individual technological operations.

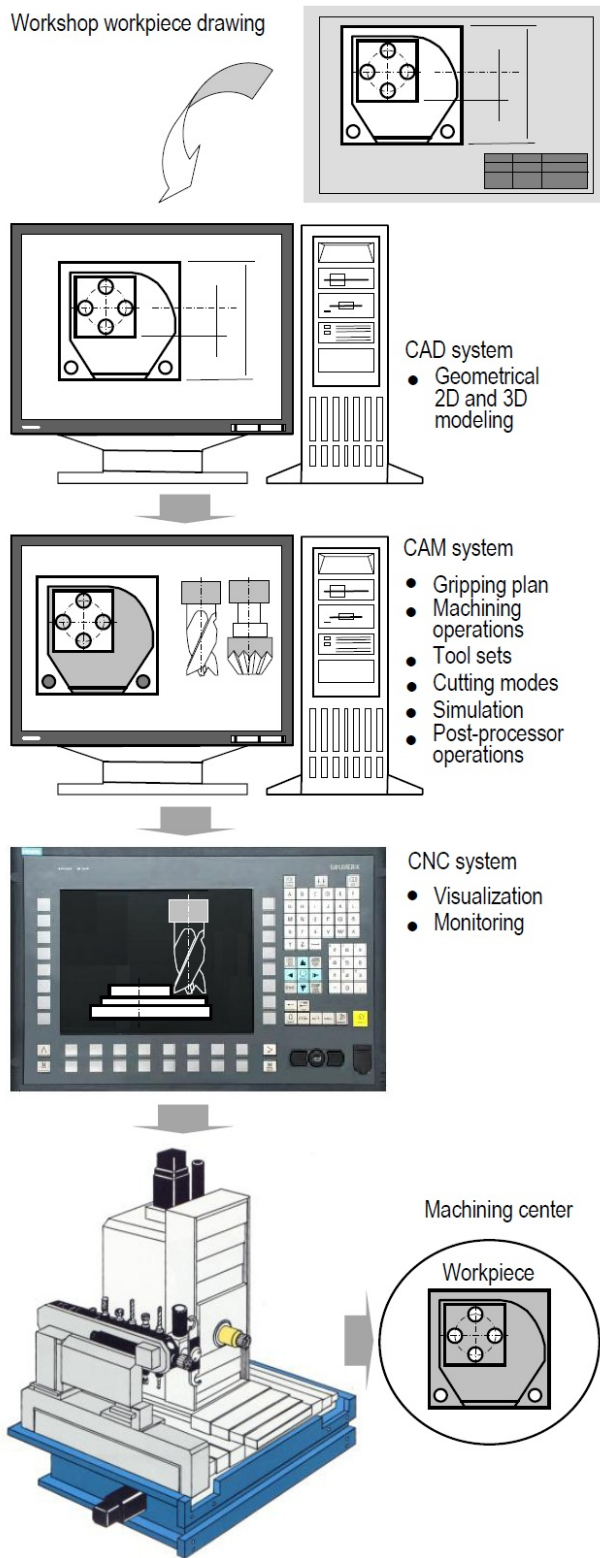


Figure 4: Methodology of FMS engineering technologies

The optimization of flexible technologies is quite a multi-parameter procedure and is done by applying

software packages integrated with CAM software systems that have the possibility of automatic regeneration of the NC code. During the first "passage" of NC programming, when defining the technological attributes are established the logical relations with the knowledge database and database of technological data. Optional manufacturing attributes that are later automatically loaded as inputs of algorithms of the optimization procedure are separately saved on the blackboard. The software systems for optimizing flexible machining are developed as expert systems, neural networks or multi-agent systems, and are based on artificial intelligence elements while additionally enabling for FMS to belong to a category of intelligent technological systems representing the highest level of informatics integration of production systems.

3. PROBLEM OF ENGINEERING AND OPTIMIZING MANUFACTURE PROCESSES IN FMS

The problem of engineering and optimizing technologies in FMS is comprised of a large number of selection possibilities:

- The cutting tool system (type, material and geometry of the blade, dimensions, ...) [5],
- The combination for the assembly of tool sets in the machining center magazine,
- The gripping modes and assembly of workpieces on palettes – palette sequences processed on the machining center and
- The cutting mode (cutting speed, speed of auxiliary movement, depth of the contact, tool durability...).

The same technological operation can be performed with different tools (Fig. 5), so that the optimal engineering of flexible machining entails for an optimal set in the tool magazine that can contain up to 40 tools. The optimal set is determined with a goal to change all the tools simultaneously while having roughly the same intensity of wear, or that their durability is completely used in the cutting process.

For every machining operation is chosen a certain cutting tool that can perform a technological operation in a different work regime, at a different intensity of wear, which directly impacts the productivity, economy of production and quality of the processed surface.

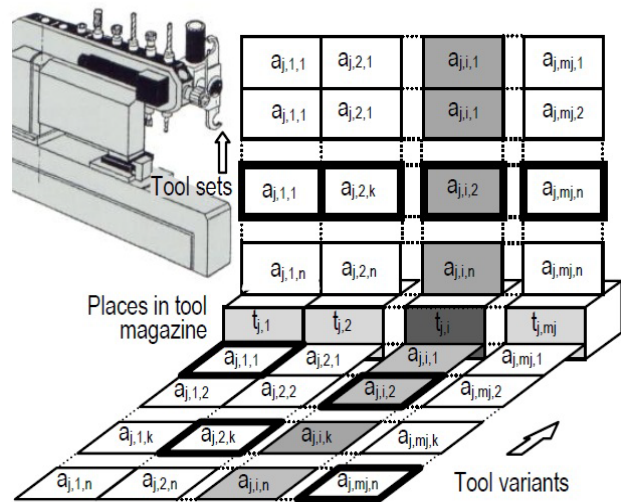


Figure 5: Potential variants of different tools in a manufacture center storage kit



Every technological operation has defined quality features that must be attained during processing, so that one and the same tool can perform an operation in a different processing mode (Fig. 6), but with a strictly defined interval, with the minimal and maximal values of cutting speeds and speed of the auxiliary movement for a defined contact depth.

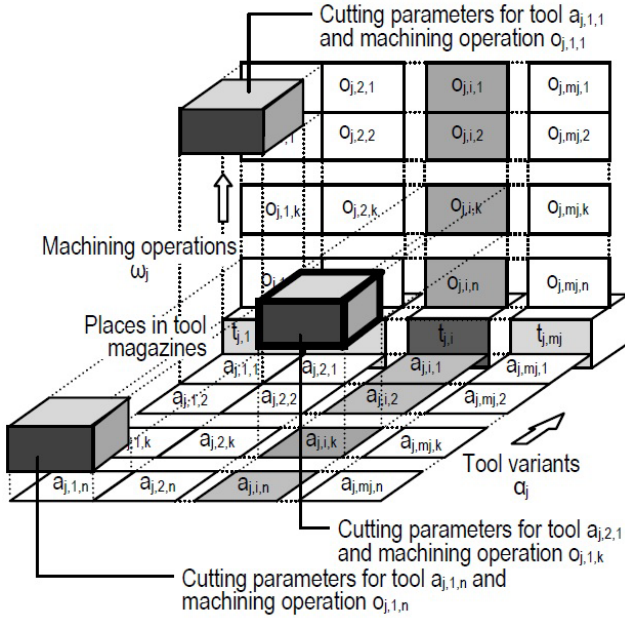


Figure 6: Alternative selection of processing mode elements

The technology engineer's task is to determine the optimally arranged pair of elements of the processing mode (cutting speed and auxiliary movement speed), that will be the most adequate selection from the viewpoint of a manufacturing requirement. The number of possible processing modes for one tool and one machining operation is equal to the number of possible combinations of speeds of the auxiliary and main movement for an operation (Fig. 7).

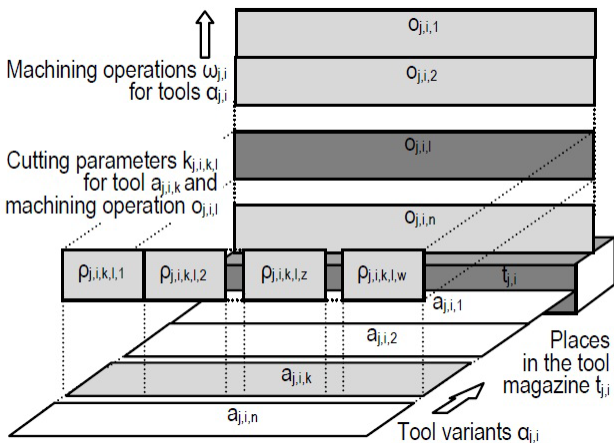


Figure 7: Possibility of choosing the processing mode for one tool and one operation

The engineer in the first passage of forming a program sheet chooses the processing mode according to functional dependencies, while at the same time the program system of the NC postprocessor generator memorizes all the

potential remaining options of the processing mode that could have been selected. These alternative options will be used in the optimization procedure.

The processing plan in FMS [6] entails that the optimal order for processing different palettes is defined with the assembled and set up workpieces (palette sequence), so that we get the maximum efficiency in balancing out the duration of technological operations and durability of the tools that perform the operations. Each machining center in the configuration of FMS has a certain number of palette sequences that are planned for processing in a given timeframe. As part of its given durability, the tool must realize a complete path within one or more machining operations. By engineering the production processes in FMS we determine the content and order of the palette sequences and the content of the tool storage for processing each palette sequence. Every palette has an NC program processing one or more workpieces placed by one grip on the palette.

Processing a family of parts in FMS can be optimized from different aspects [7], like for instance: the shortest processing time, lowest processing costs or shortest possible time at the lowest possible cost, whereby can be established the price or time criteria in an optimization algorithm (Fig. 8).

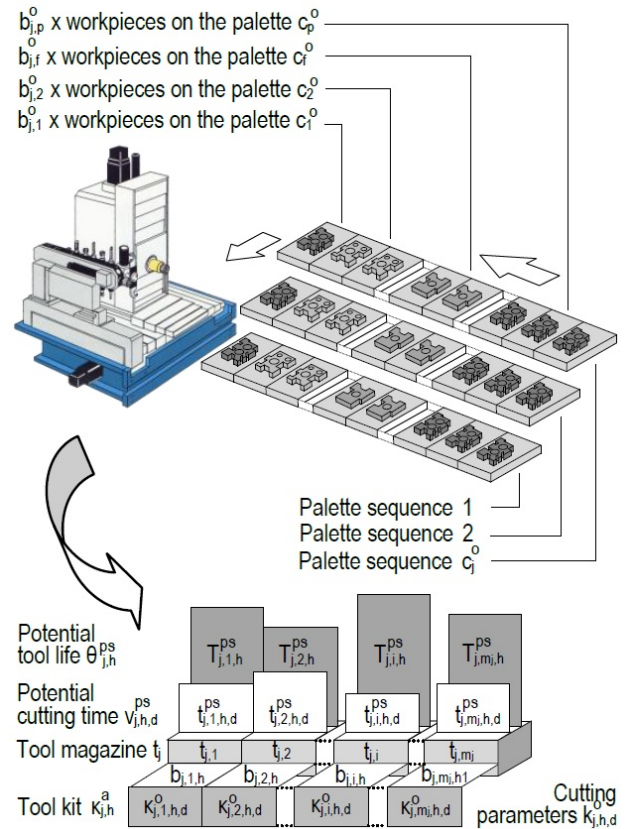


Figure 8: Dependency between processing time, tool durability and content of palette sequences

Bearing in mind the fact that the processing time depends on the elements of the processing mode that can move within a broader value interval, the goal is to determine the processing mode that allows for maximum tool utilization and minimal processing price within the necessary duration of a machining operation (Fig. 9). Also

we should take into consideration that as part of FMS is integrated a large number of machining centers, where each can process any palette sequence and to perform any kind of machining operation.

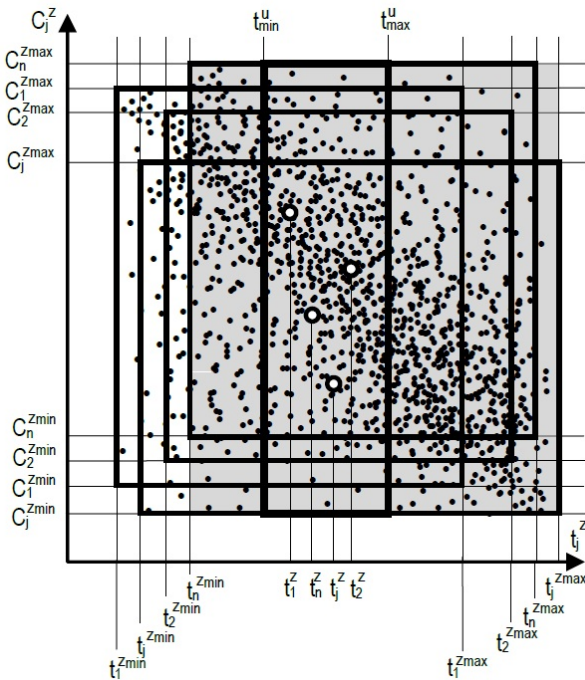


Figure 9: Time –cost diagram according to FMS time criteria

Via a combination of processing modes it is possible to realize the processing time for each palette sequence in an interval of minimal and maximum time ( $t_{jzmin}$ ,  $t_{jzmax}$ ), and also in an interval of different cost values ( $C_{jzmin}$ ,  $C_{jzmax}$ ).

Time values (Figure 9) for processing an assortment of workpieces with the chosen tool configurations on any process center are between the given bordering values:

$$t_{min}^u \leq t_j^z \leq t_{max}^u, j = 1, 2, \dots, n$$

While the total time required for processing a given assortment of workpieces for a flexible technology system is:

$$t^u = \max \{t_1^z, t_2^z, \dots, t_j^z, \dots, t_n^z\} = \max_{1 \leq j \leq n} (t_j^z)$$

$$t_{min}^u \leq t_j^z \leq t_{max}^u$$

where:

$t^u$  is the total time required for processing a given assortment of workpieces for a flexible technological system,

$t_j^z$  is the processing time of a given number of palette sequences with the selected tool configuration on a  $j$  process center.

Setting the “time” or “price” criteria or a combination of both enables the selection of a configuration of tools and according to an additional, third criteria – the tool wear coefficient in the process center storage. According to these criteria the choice should be the tool configuration with the largest coefficient for tool storage wear among

the configurations that are already marked with the previous time and price criteria.

Setting the “time” or “price” criteria or a combination of both enables the selection of a configuration of tools and according to an additional, third criteria – the tool wear coefficient in the process center storage. According to these criteria the choice should be the tool configuration with the largest coefficient for tool storage wear among the configurations that are already marked with the previous time and price criteria.

#### 4. NC PROCESSOR GENERATOR

A certain number of database tables are formed based on initial NC programs through the transformation of NC program blocks into appropriate data records, by transferring program block parameters (G-functions, M-functions, coordinate values, process mode values, tool markings, etc) into the record fields of NC blocks. Then, based on the values of those fields are calculated the kinematic and technological parameters (tool in rapid traverse speed, tool in working path, speed of main and auxiliary traverse and tool types) and stored into the appropriate fields with the same records. In the following step the values of these parameters are added for each operation and for every tool participating in one NC program [8].

A realized postprocessor (Fig. 10) automatically generates the content of tool storage of each of the process centers in a flexible technological system, based on calling a certain tool in the storage in all NC programs being executed on that machining center. To each place in the storage is assigned one or more tools with which we can perform the generated operations. Alternative tools for one position differ between them according to the material and number of blades, durability and price index, but are of equal diameters. The alternative tools from the technological database can be selected interactively or automatically. For each of the alternative tools are defined the bordering values of the processing mode, interactively or automatically according to the parameters from the machining database [9].

According to the selection of alternative tools, the postprocessor generates combinations of tools and forms possible tool kits for the machining center storage. This procedure is carried out by presenting the alternative tools by implementing strings and string operations. On the other hand, according to the borderline values of the process mode defined for alternative tool operations, the postprocessor generates possible combinations of the process mode for individual tools by forming variations of the processing mode for tool kits. This procedure is carried out by presenting arranged pairs of processing modes via strings and operations over those strings. The result is a series of possible tool configurations in a machining center storage, or a string of possible content of tool storage with assigned arranged pairs of processing modes for operations in which are used tools from the machining center storage. Tool configurations for storages of all machining centers, as well as the kinematic and technological parameters (path of the tools in rapid and traverse speed, tool diameters, tool durability, and tool prices), are entered into database tables.

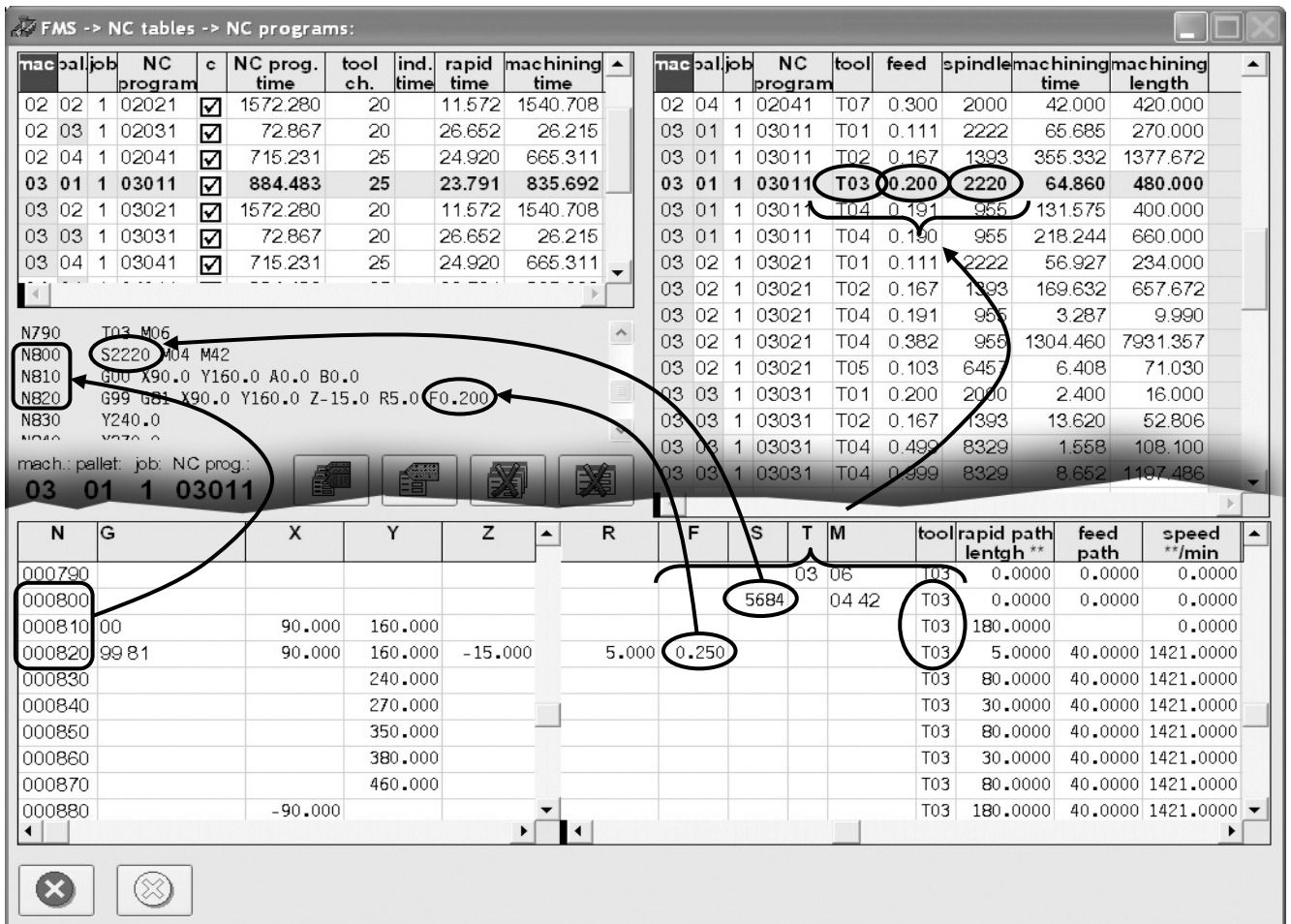


Figure 10: Application software modules of an NC program postprocessors generator for production technologies

The postprocessor for every tool configuration and for each workpiece is placed on the palette and calculates the total processing time representing a sum of the processing time for all operations from one kit. Given the number of tool changes and indexing number, all the rapid traverse and working rate are calculated, the auxiliary times and the total times of execution of the NC program. At the same time the index of the price of all tool configurations are made according to the price indexes of individual tools in those configurations. The process of forming tool configurations for machining center storages and calculating the processing time and index of the process price for workpieces on palettes is performed only once, before stating the total series being processed.

For the given number of workpieces that should be processed, the postprocessor calculates the number of required tool storage configurations, the time required for processing and tool costs. First, for every tool configuration is calculated the processing time of one palette sequence, and according to tool durability and work load time, the number of palette sequences is calculated which can be processed with this tool configuration. In that way, for a defined number of palette sequences for processing, we get the total time for processing and the number of tool kits required for one machining center. Based on the cutting time, by adding the time required for tool change in storage, we get the total required processing time for an assortment of workpieces.

Based on the number of tool kits and price indices of individual tools we get the costs for tools for processing an entire workpiece assortment.

For the goal of optimal tool configurations (tool sets and process modes), besides calculating the process time and tool costs, the postprocessor calculates the coefficient of general wear of tools in storage. When changing the tools from the storage of one machining center, the most favorable case is when all the tools in that storage are of approximate wear intensity.

Engineering and optimizing technological processes can refer to changing the number of machining centers in a flexible machining system, changing the number of workpieces in series from the workpiece assortment, changing the total processing time or changing tool costs. The selection of optimal parameters for a technological process is performed according to three criteria: the time required for processing a given assortment of workpieces, the tool price index used for processing a given assortment of workpieces and the coefficient of tool wear in storage. During selection, one of the three criteria represents the basic, while the other two - secondary criteria. The selection can be made interactively, from a group of tool configurations fulfilling the specified technological requirements or automatically, by selecting the most favorably evaluated tool configuration by the postprocessor for every individual machining center.

The postprocessor automatically updates NC programs by entering new values in the records of initially formed tables, according to the markings of tools in storage, into the fields for process modes, without changes to the other fields passed from blocks of the NC program (G-functions, M-function, coordinate values, cutting speed, auxiliary traverse rate). In the next step, the postprocessor, based on the number of program blocks performs changes of program words with the values of the process mode.

The process of defining palette sequences, calculations of the processing time, calculation of tool costs and coefficient of the tool wear configuration, selection of optimal parameters of the technological process and updating the NC program can be repeated unlimitedly, without reformulating the tool configuration or determining the processing parameters for machining operations.

## 5. CONCLUSIONS

The developed NC postprocessor generator model can be applied on all types of configurations of flexible technological systems with machining centers of same or different type, with an equal or different number of places in tool storage. Palette sequences for machining centers can be different, and the composition of workpieces on palettes can be completely random.

The possibilities of the developed software package are limited only in the characteristics of the systems for managing the database and system software parameters. The optimal number of simultaneously opened database tables and index numbers are application-wise, only theoretical limitations. These limitations can be overcome by distributing the database in a computer network, as well as with software solutions for coding records in tables.

The designed and realized postprocessor generator of an NC program has been tested on multiple practical examples from production practice. It can be applied in production systems that are not by definition flexible machining systems, but are configured from machine tools with CNC control.

## REFERENCES

- [1] Lj.Lukić, D. Polajnar and V. Šolaja, „A Yugoslav Approach to Decision Support for Optimization of FMS Technologies”, *Annals of the CIRP*, Vol.40/1, pp. 99-102, (1991)
- [2] Lj.Lukić, “Flexible technological systems”, University of Kragujevac, Faculty of Machine Engineering, Kraljevo (2008)
- [3] V.Šolaja, M.Dimitrić and Lj. Lukić, “On the Two Cases of Yugoslav Attempts in Adaptive Control”, *Robotics & Computer Integrated Machining* №4 Vol.1/2, pp. 241-244, (1988)
- [4] D.Polajnar, Lj.Lukić and V. Šolaja, “An Interactive Simulation Model for Multiparameter Optimization of Cutting Processes in FMS”, *Preprints 6th Symposium on Information Control problems in Machining technology (INCOM '89)*, Vol. I, pp.251-256, Madrid, (1989)

[5] J.J.S.Perez, R.A.O.Rios, R.J.R. Troncoso, E.C. Yopez and R.G.G. Gonzalez, “Feedrate optimization by polynomial interpolation for CNC machines based on a reconfigurable FPGA controller”, *Journal of Scientific & Industrial Research (JSIR)*, Vol.69, pp. 342-349, (2010)

[6] N.Selveraj, “Simulation modeling and analysis of single line multi stage manufacturing system”, *Journal of Scientific & Industrial Research (JSIR)*, Vol.67, pp. 277-281, (2008)

[7] S.Ivanović, Lj.Lukić and Z.Petrović, “Reconfiguring the database of a flexible production system based on parameters from the NC program”, *Expert and scientific magazine IMK-14 research and Development, Institute IMK 14*. October, Krusevac, year XIV, №(28-29) 1-2, pp.79- 84, (2008)

[8] S.Ivanović and Lj.Lukić, “Database Design from Technological and Kinematic Parameters of NC Program for Production in Flexible Machining Systems”, *Proceedings The Sixth Triennial International Conference "Heavy Machinery HM 2008"*, pp. G.7-G.12, 24-29 June, Kraljevo (2008)

[9] S.Ivanović, “CNC postprocessor generator model in flexible production systems”, *Dissertation, University in Kragujevac, Faculty of Machine Engineering Kraljevo*, (2009)

# Application of Axiomatic Design Theory and Belief Function Theory in the Assembly Improvement

Zvonko Petrović<sup>1\*</sup>, Mirko Đapić<sup>2</sup>, Ljubomir Lukić<sup>2</sup>

<sup>1</sup>College of Applied Professional Mechanical Studies/ University of Kragujevac, Trstenik (Serbia)

<sup>2</sup>The Faculty of Mechanical and Civil Engineering in Kraljevo, University of Kragujevac, Kraljevo (Serbia)

*Cost of the assembly (assembly systems) of metal products manufacturing industry significantly affect the total cost of production and therefore their profits. That is one of the reasons why it is necessary to perform improvement and in some cases re-engineering of the assembly process. One of design theory that allows the management of this process and decision-making in it is axiomatic design theory (ADT). ADT provides a theoretical basis for logical and rational thinking process and decision-making in the process of improving existing and creating new manufacturing assembly systems.*

*Significantly improved ability of designers is achieved if the results of the application of the ADT present as evidence networks that is developed on the base of Dempster-Shafer theory of belief functions. In the continuation of this the paper describes using of ADT in the development and improvement of the assembly system of hand pumps product and their modeling by belief functions of Dempster-Shafer theory.*

**Keywords:** Axiomatic design theory (ADT), Dempster-Shafer theory of belief functions.

## 1. INTRODUCTION

Product and processes (manufacturing technology) designing and the production, experienced a strong development, especially in the field of application of new technologies. Only in sector of assembly using of new technology has not yet taken adequate place. The main reasons for rationalization of the assembly sector of are:

- Large assembly time and thus cost,
- Large expenditure of human labor in all activities related to assembling,
- A relatively large number of activities that are not directly related to the assembling,

Potential areas where it is possible rationalization of assembly are:

- Design products, which must be oriented to the assembly,
- Automation operations and sequences of assembly,
- Organization of information flow,
- Structuring and physical appearance (layout) of the assembling systems.

Based on the analysis conducted in the assembly sector of 355 German companies from the manufacturing industry points out the fact that the main potential for assembly improvement lies in the rationalization of product design, which have to be oriented to the assembly, and automation of the assembly operations [1].

Continue to previously in this paper is presented the idea and initial results relating to the application of new theories (ADT and Dempster-Shafer theory of belief functions) to boost of improvement of the real assembly system from the Serbian industrial environments.

## 2. THE AXIOMATIC DESIGN THEORY (ADT)

Axiomatic design theory (ADT) is defined by Professor Nam P. Suh, who worked at the Massachusetts Institute of Technology (MIT) [2]. Suh started from the assumption that there is a set of fundamental principles that define a good business practice in the design of

products, processes, systems, software and organizational structures.

The goal of ADT is to establish a scientific basis for the designing process and to improve the activity of the designer by offering:

- Theoretical basis for a logical and rational thinking process and making decisions and
- Tools that allow it.

Key concepts that make up this theory are:

- Domain,
- Hierarchy of design,
- "Zig-Zag" mapping and
- Two axioms of design.

In the domains are grouped design process tasks. It is possible in the ADT to identify four groups of domains:

- Domain customer requirements (CNs),
- Domain functional requirements (FRs),
- Domain design parameters (DPs) i
- Domain process variables (PVs).

The design process proceeds through solving respective tasks on the one domain and the move from one domain to another.

The ADT design process begins at the initial level of abstraction (starting hierarchical level) by the defined functional requirements and then try to find appropriate design solution (design parameters) which fulfill the functional requirement in the design parameters domains. After that moves on to solving problems on the first lower hierarchical level, thus achieving the decomposition of the design concept and the transition from abstract to detailed design solution.

Decomposing is defined as the process of defining a set of subordinate functional requirements (sub-FRs) for a given pair of superior functional requirements (FRs), design parameters (DPs), as well as all other activities that are necessary to move from higher to first lower hierarchical level.

\*Corresponding author: Radoja Krstića 19, 37240 Trstenik, Serbia

Creating a hierarchical structure is realized by switching from one domain to another and from one hierarchical level to the next one lower. This process is called zig-zag mapping (Figure 1). It is performed by clearly established rules to the level of detail of the design solution which is sufficient to physical implementation.

For each design solution it is possible to define the design equation:

$$\left\{ \begin{matrix} FR_{x,1} \\ \cdot \\ \cdot \\ \cdot \\ FR_{x,n} \end{matrix} \right\} = [A \cdot x] \left\{ \begin{matrix} DP_{x,1} \\ \cdot \\ \cdot \\ \cdot \\ DP_{x,n} \end{matrix} \right\} \quad (1)$$

$[A_x]$ - design matrix which connects the functional requirements and design parameters.

Suh also defined two design axioms that are the basis for decision making:

- Is it a design solution is good or not and
- To select the best design solution from a set of satisfactory solutions.

On the basis of the first axiom acceptable design solution is one in which the mapping between functional requirements (FRs) and design parameters (DPs) such that the functional requirements (FR) is satisfied with a single design parameter (DP) without affecting other functional requirements.

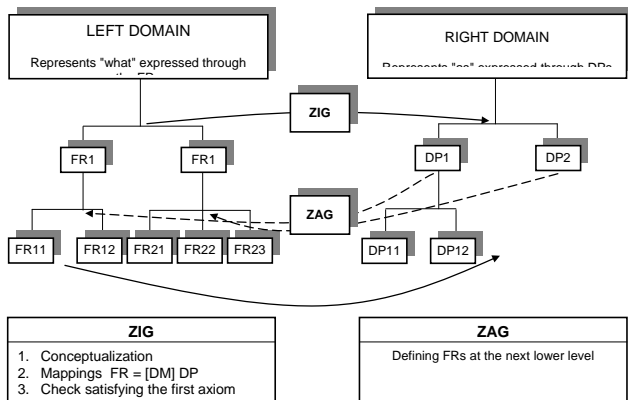


Figure 1: Zig-zag mapping

### 3. THEORY OF BELIEF FUNCTIONS

#### 3.1. The basic concepts of Belief functions

Model of the belief function consists of variables, their values and the evidence, which supports the value of variables. Variables represent specific questions regarding the aspect of the problem under consideration. Given questions are answered using data originating from various sources, i.e., from context of published papers, from measurement data, from expert opinions, etc. Fully integrated support to the sought answer is called evidence.

Evidence can be represented by belief functions, which are defined as follows:

Definition1 [5, 1]. Let  $\Theta$  be a finite nonempty set called the frame of discernment, or simply the frame. Mapping  $Bel: 2^\Theta \rightarrow [0,1]$  is called the (unnormalized) belief function

if and only if a basic belief assignment (bba)  $m: 2^\Theta \rightarrow [0,1]$  exists, such that:

$$\sum_{A \subset \Theta} m(A) = 1 \quad (2)$$

$$Bel(A) = \sum_{B \subset A, B \neq \emptyset} m(B) \quad (3)$$

$$Bel(\emptyset) = 0 \quad (4)$$

Expression  $m(A)$  can be viewed as the measure of belief which corresponds to subset  $A$  and takes values from this set.

Condition (2) means that one's entire belief, supported by evidence, can take the maximum value 1, and condition (4) refers to the fact that one's belief, corresponding to an empty set, must be equal to 0.

Value  $Bel(A)$  represents the overall belief corresponding to the set  $A$  and all of its subsets. Each subset  $A$  such that  $m(A) > 0$  is called a focal element.

The empty belief function is the function which satisfies  $m(\Theta) = 1$ , and  $m(A) = 0$  for all subsets of  $A \neq \Theta$ . This function represents total ignorance about the problem under consideration.

#### 3.2. Dempster rule of combining belief functions

Let the several independent belief function be given on the same recognition frame but with different bodies of evidence. The Dempster's combination rule (Figure 2) (Equ. 5, 6) produces new belief function which represents effect resulting from the connection of the different bodies of evidence.

Let us assume that the belief functions  $Bel_1$  and  $Bel_2$  are created on  $\Theta$  frame. Let  $A_1, \dots, A_k, k < 2^{|\Theta|}$  be the focal elements of function  $Bel_1$  with corresponding  $m$ -values  $m_1(A_i)$  for  $i=1, \dots, k$ ; and let  $B_1, \dots, B_j, j < 2^{|\Theta|}$  be focal elements of function  $Bel_2$  with corresponding  $m$ -values  $m_2(B_i)$  for  $i=1, \dots, j$  [5]

Combination of these two functions is denoted as  $Bel_1 \oplus Bel_2$  and its focal elements are  $C_1, \dots, C_m$  with corresponding  $m$ -values  $m_3(C_k)$  for  $k=1, \dots, m$ , created in the following way:

$$m_3(C_k) = K \left[ \sum_{\substack{i,j \\ A_i \cap B_j = C_k}} m_1(A_i) m_2(B_j) \right] \quad (5)$$

where  $K$  represents a normalization factor

$$K = \left[ 1 - \sum_{\substack{i,j \\ A_i \cap B_j = \emptyset}} m_1(A_i) m_2(B_j) \right]^{-1} \quad (6)$$

The normalization factor  $K$  is greater than 1 whenever  $Bel_1$  and  $Bel_2$  contain a part of mass of some belief that correspond to the subjective probability for the decoupled (contradictory) subsets of  $\Theta$ . In fact,  $K$  represents the conflict measure of the two belief functions. Whenever two or more functions are combined, the combination rule is associative and commutative. In general,  $Bel \oplus Bel = Bel$ . Combination of a certain number of belief functions  $Bel_1 \oplus \dots \oplus Bel_n$  is denoted as  $\oplus \{Bel_1, \dots, Bel_n\}$ .

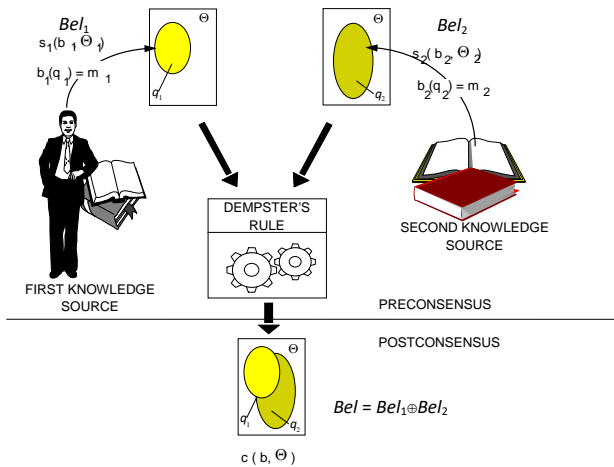


Figure 2. Graphics illustration using Dempster's rule of belief function combining [1]

3.3. What are the evidential systems

Valuation Based Systems - VBS is an abstract framework proposed by Shenoy for representing and reasoning on the basis of uncertainty. It allows representation of uncertain knowledge in various domains, including Bayes' probability theory, Dempster-Shafer's theory of evidence which is based on belief functions and Zadeh-Dubais-Prad theory of possibility. Graphically presented VBS is called valuation network [6].

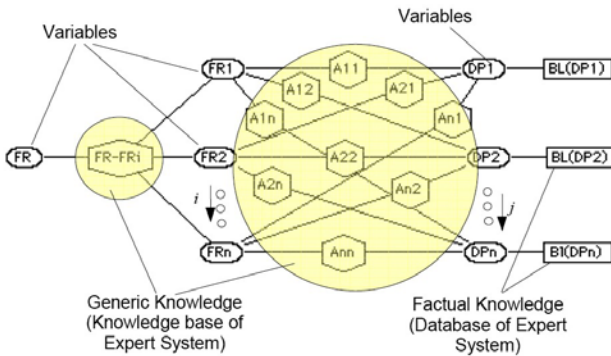


Figure 3. The concept of evidential networks

VBS consists of set of variables and set of valuations that are defined on the subsets of these variables. Set of all variables is denoted by U and represents a space covered with problem which is under consideration. Each variable represents a relevant aspect of a problem. For each variable  $X_i$  will be used  $\Theta X_i$  to denote the set of possible values of variables called the frame of  $X_i$ . For a subset A ( $|A| > 1$ ) of U, set of valuations that are defined over  $\Theta A$  represents the relationship between variables in A. Frame  $\Theta A$  is a direct (Cartesian) product of all  $\Theta X_i$  for  $X_i$  in A. The elements  $\Theta A$  are called configurations of A.

Knowledge presented in this type of valuations is called generic or general knowledge (figure 3), which can be represented as a knowledge base in expert systems.

The VBS also defines valuations on individual variables, which represents so-called factual knowledge, and it constitutes database in expert systems (figure 3). For a problem, general-generic knowledge defines an expert.

During reasoning process that knowledge won't be modified. Factual knowledge will vary in accordance with condition of a problem currently being under consideration. The VBS treats on the same way these two kinds of knowledge.

The VBS systems suited for processing uncertain knowledge described by functions of belief function theory are called Evidential Reasoning Systems or Evidential Systems, and valuation networks are now called evidential networks (EN) (figure 3).

The objective of reasoning based on the evidence is an assessment of a hypothesis, in case when the actual evidence are given (the facts). This can be accomplished by evaluating valuation networks in two steps:

- Combining all belief functions in evidential network, resulting in a so-called global belief function
- Marginalization of global belief functions in the framework of each individual variable or subsets of variables produces marginalized values for each variable or subset of variables.

Easily way of understanding the reasoning process and its graphical interpretation is the condition on which depends whether and how fast these systems will be applied in solving everyday problems. As a software support to the VBS systems application, several software tools have been developed. For evidential systems the very known are:

- McEvidence,
- Pulcinella and
- DELIEF.

4. APPLICATION ADT-A AND DEMPSTER-SHAFER THEORY IN THE IMPROVEMEN MANUFACTURING ASSEMBLY SYSTEMS

The application of the axiomatic design is presented in the manufacturing assembly system improvement of the hand pumps to lift the cabs of the Kamaz truck. It is a product of PPT from Trstenik, and it is produced a series of 4 to 5 thousand units of product per month which makes it a product with the highest monthly series in the company.

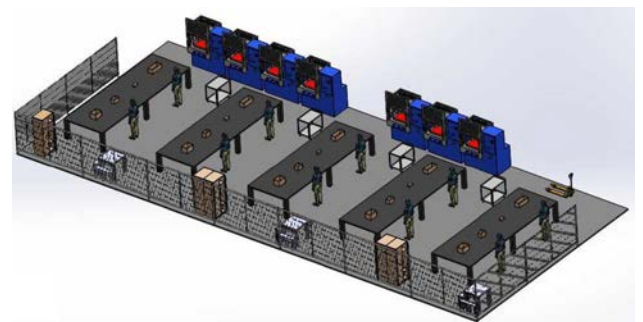


Figure 4. The technological assembly system

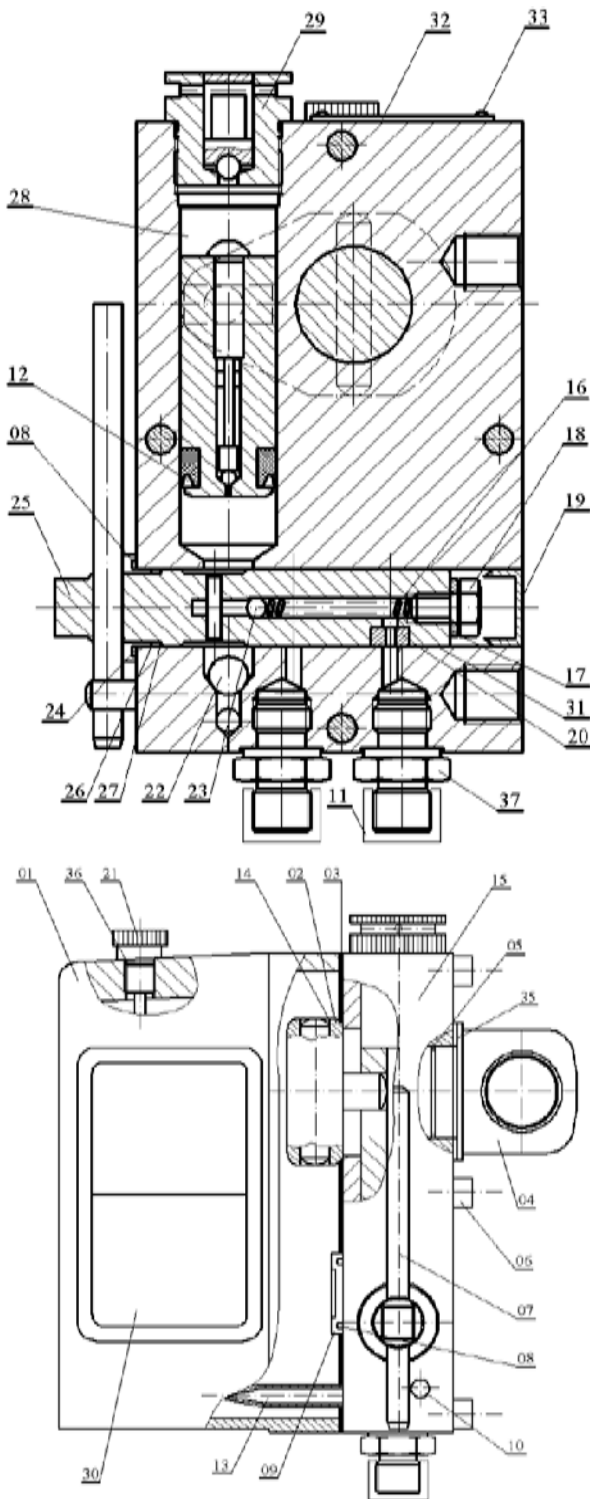


Figure 4. Assembly drawing of the hand pumps

The process of assembly is restricted from construction, technological, production and quality reasons [3]. In the improvement of manufacturing assembling systems have to be considered: plan of the assembly process, the possibility of applying robotic applications, the choice of the transportation system and attention have to be focused also on the economic aspect of automation of assembling processes.

Basic functional requirement on the beginning of hand pumps assembly system improvement is *maximize long-term return on investment*, which is realized through the design parameter: *redesign the hand pumps assembly*

line.

Processes of assembly line improvement continue in according with ADT principles creating design structure from abstraction to more detail structure creating system architecture.

#### 4.1. Presentation of system architecture

The system architecture is a tool for decision making and design process documentation in the axiomatic design. It includes requirements, components and their relationships. Under the requirements is presented functional requirements (FRs) and constraints (Cs), with the components presents design parameters (DPs) and under mutual relations involve the design matrix (DMs) and design hierarchy. This information may be presented in different ways, using: the design tree hierarchy, design matrix, design flow diagrams and structural diagrams of connecting modules [2].

Functional requirements and design parameters for hand pumps assembly system improvement are shown in table 1 and 2 and the design hierarchy for the second level of the developed structure in Figure 5.

The system architecture can be presented by the belief functions on the base it is possible to create appropriate evidence network which can be used as a tool for decision making in the process of assembly system improvements.

Table 1. Functional requirements

	Functional requirements
FR	Maximize long-term return on investment
FR <sub>1</sub>	Minimized hand pumps assembly costs
FR <sub>2</sub>	Minimized investment in hand pumps assembly line
FR <sub>11</sub>	Decreasing idle time of the hand pumps assembly line
FR <sub>12</sub>	Elimination of defective production of hand pumps
FR <sub>13</sub>	Facilitating value stream flow on the hand pumps assembly
FR <sub>14</sub>	Diminishing Work-in progress on the hand pumps assembly

Table 2. The design parameters

	Design parameters
DP	Redesign the hand pumps assembly line
DP <sub>1</sub>	Eliminating all types of wastes
DP <sub>2</sub>	Investment based on long – term strategy
DP <sub>11</sub>	Eliminating incidental stops on the hand pumps assembly
DP <sub>12</sub>	Enhancing the quality of assembly of hand pumps
DP <sub>13</sub>	Eliminating non-value adding operations on the hand pumps assembly
DP <sub>14</sub>	Create hand pumps assembly pull system



In the case of the hand pumps assembly process the set of variables for the first hierarchical level is:

$$U = \{FR, FR_1, FR_2, DP, DP_1, DP_2\} \quad (7)$$

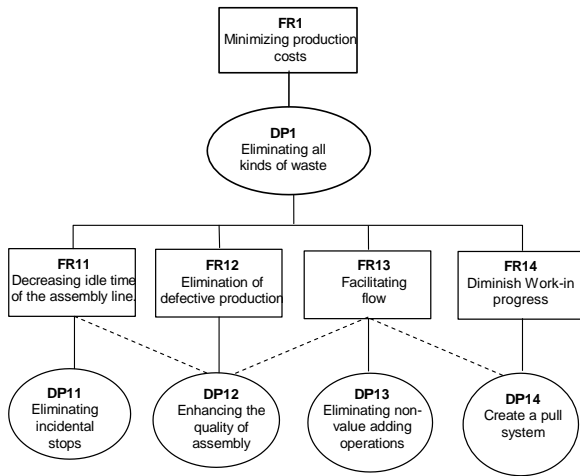


Figure 5. Second Level of the Developed Structure (Adapted on the base of [7])

For the second level of the development structure corresponding design equation is presented on the Equation 8 and same equation presented through belief functions (Equ. 9):

$$\begin{bmatrix} FR_{11} \\ FR_{12} \\ FR_{13} \\ FR_{14} \end{bmatrix} = \begin{bmatrix} A_{11} & A_{12} & 0 & 0 \\ 0 & A_{22} & 0 & 0 \\ 0 & A_{32} & A_{33} & A_{34} \\ 0 & 0 & 0 & A_{44} \end{bmatrix} \begin{bmatrix} DP_{11} \\ DP_{12} \\ DP_{13} \\ DP_{14} \end{bmatrix} \quad (8)$$

$$\begin{bmatrix} Bel(FR_{11}) \\ Bel(FR_{12}) \\ Bel(FR_{13}) \\ Bel(FR_{14}) \end{bmatrix} = \begin{bmatrix} Bel(A_{11}) & Bel(A_{12}) & 0 & 0 \\ 0 & Bel(A_{22}) & 0 & 0 \\ 0 & Bel(A_{32}) & Bel(A_{33}) & Bel(A_{34}) \\ 0 & 0 & 0 & Bel(A_{44}) \end{bmatrix} \begin{bmatrix} Bel(DP_{11}) \\ Bel(DP_{12}) \\ Bel(DP_{13}) \\ Bel(DP_{14}) \end{bmatrix} \quad (9)$$

All belief function from above design equation has corresponding frame of possible values or frame of discernment  $\Theta X_i$ .

For example  $FR_{11}$  can take values

$$\Theta FR_{11} = \{(SDI), (MDI), (HDI)\} \quad (10)$$

Where are: SDI – Small Decrease Idle time,  
MDI – Moderate Decrease Idle time,  
HDI – High Decrease Idle time

$DP_{11}$ :

$$\Theta DP_{11} = \{(SEI), (MEI), (HEI)\} \quad (11)$$

Where are: SEI – Small Eliminate Incidental stop,  
MEI – Moderate Eliminate Incidental stop,  
HEI – High Eliminate Incidental stop.

Belief functions elements of design matrix  $A_{ij}$  represent joint variables and its frame is defined as a direct product of the frames of individual variables which form it. For example the frame of  $A_{11}$  variable ( $\Theta A_{11}$ ) is formed as direct product of the frames of variables  $FR_{11} \times DP_{11}$ .

The frame of this joint variable is:

$$\Theta A_{11} = \Theta FR_{11} \times \Theta DP_{11} \quad (12)$$

$$\Theta A_{11} = \left\{ \begin{matrix} (SDI, SEI) & (SDI, MEI) & (SDI, HEI) \\ (MDI, SEI) & (MDI, MEI) & (MDI, HEI) \\ (HDI, SEI) & (HDI, MEI) & (HDI, HEI) \end{matrix} \right\} \quad (13)$$

On this way is possible to define the frames for all other joint and ordinary belief function from the Equation 9.

Now on the base of our knowledge about the variables we can recognized some of its frame subsets and allocate on it portion of our belief. Through this process we create belief functions but strictly taking rules given in the equations 2, 3 and 4. As an example of the above described process is presented creation of belief function  $Bel(A_{11})$  which is recognized on the subsets  $\Theta A_{11}$ :

$$Bel(A_{11}): \quad (14)$$

$$m\{(SDI, SEI) (MDI, MEI) (HDI, HEI)\} = 0.6 \quad (15)$$

$$m\{(SDI, MEI) (MDI, HEI)\} = 0.3 \quad (16)$$

$$m\{\Theta A_{11}\} = 0.1 \quad (17)$$

On this way we construct all other belief functions from the equation 9. Thus defined design equation can be presented as an evidence network, which can be used for the analysis and selection of appropriate design parameters of the hand pumps assembly system which will be the subject of our further research work.

## 5. CONCLUSION

This paper presents an example of the hand pumps assembly system improvement by the using axiomatic design theory and Dempster-Shafer theory of belief functions. Axiomatic design theory allows designers additional options in the management of the design process using axioms, theorems and consequences of design theorems.

In the paper is presented a way how to the functional requirements, design parameters and their relationship presented in the form of a design equation described by the appropriate belief functions of Dempster-Shafer theory. In this way it is possible that a system architecture that is generated during the design process using ADT can be presented as an evidential network which will present a continuation of this research work.

## REFERENCES

- [1] Djapic, M. Evidential Systems in Product and Process Development, Intelligent Manufacturing Series of Monographs No. 9, LOLA Institute, Belgrade, 2005 (In Serbian).
- [2] Suh, N., Principles of Design, Oxford University Press, 1990.
- [3] Ćosić, I., Montažni sistemi, IP Nauka, Beograd, 1991, ISBN: 86-7621-045-4.
- [4] Boothroyd, G. 1983. Design for Assembly Handbook, Design project, Dep. Of Mechanical Eng., University of Massachusetts, Amherst, Massachusetts, USA.
- [5] Shafer, G., A Mathematical Theory of Evidence, Princeton University Press, 1976.
- [6] Shenoy, P.P. Valuation-Based Systems: A framework for managing uncertainty in expert systems John Wiley & Sons, New York, 1992.

[7] Houshmand, M., Jamshidnezhad, B., A Lean Manufacturing Roadmap for an Automotive Body Assembly Line with in Axiomatic Design Framework,

IJE Transactions A: Basics, Vol. 17, No. 1, February 2004 -51.

# Application of the Dempster-Shafer Theory in Fault Tree Analysis of Hydraulic Hand Pump

Violeta Đorđević<sup>1\*</sup>, Mirko Đapić<sup>2</sup>, Zvonko Petrović<sup>1</sup>

<sup>1</sup>College of Applied Professional Mechanical Studies/ University of Kragujevac, Trstenik (Serbia)

<sup>2</sup>The Faculty of Mechanical and Civil Engineering in Kraljevo, University of Kragujevac, Kraljevo (Serbia)

*The modern business of each organization relies on information. However, there are often inaccurate and unspecified information and there is a need to find a way to present such information. For this purpose, the theory of the functions of conviction can be used to express the uncertain decisions of the experts and to help with the decision making process. Dempster-Shafer's theory of the function of conviction allows a mathematical representation of subjective uncertainty, and rely on the ability to define ignorance. The paper presents the FTA analysis of the hydraulic hand pump for tilting the cab on motor vehicles, and then applied the Dempster-Shafer theory of the confidence function tofor failure analysis.*

**Keywords: Dempster-Shafer Theory, evidence, uncertainty, Fault Tree Analysis, hydraulic hand pump**

## 1. INTRODUCTION

During the lifetime of the product errors may occur at any stage of formation and use of the product. Faults that occur during use of the product can have a very negative impact on the company's market position and initiate the finally effect: withdrawal from the market much earlier then funds invested in the development are returned and cause loss of customer trust in products, what can have disastrous consequences for the company.

One of the basic and most commonly used method for analysis of safety and reliability of the technical systems is the Fault Tree Analysis . Reliability is a characteristic of the system to operate without failure under certain conditions, in a certain period of time. Reliability theory deals with the study of the cancellation of technical systems and their constituent elements.

Real situations are full of imperfect information, which usually occur in the form of imprecision and uncertainty. Systems for representing and reasoning, based on uncertainty are evidence systems, and their graphical presentations are called evidential network [1].

Making conclusions (reasoning) about certain situation from the real world often takes place in difficult circumstances with insufficient knowledge and have not clearly defined criteria. Uncertainty is when there is not enough information about the status of an event, or when there is no assurance that such information is correct. A choice between the possible options then must makebe taken. The only one completely developed way of presenting imperfect information is probability theory. Because of its limitations other methods for presenting this information are developed recently. For uncertainty is introduced theory of belief functions [1].

Dempster-Shafer theory was developed by Arthur P. Dempster, in the middle of the 1960s, and about ten years later, this work was extended by Glenn Shafer, as a "Mathematical Theory of Evidence". He rebuilt the mathematical theory around Dempster concept and introduced degrees of belief instead of lower probabilities [2, 3].

In a finite discrete space, Dempster-Shafer theory can be interpreted as a generalization of probability theory where probabilities are assigned to *sets* as opposed to mutually exclusive singletons. In traditional probability theory, evidence is associated with only one possible event. In Dempster-Shafer theory, evidence can be associated with multiple possible events, e.g., sets of events [4].

## 2. THEORY OF BELIEF FUNCTION

### 2.1. The basic concepts of belief functions

Information about evidence can come from different resources: based on a person's experience, from signals recorded by appropriate sensors, from the contents of published papers and so on. Such evidence is rarely clearly delimited; it is often incomplete, subjective and full of flaws. Dempster-Shafer belief function theory provides powerful tools for mathematical presentation of the subjective (opposite of what probability theory is based on) uncertainty while it relies mainly on the possibility of explicit definition of ignorance [1, 8].

The reliability-oriented approach to Dempster-Shafer theory, as presented here, is based on a scenario that contains the system with all its hypotheses in a frame of discernment, the pieces of evidence and the data sources.

The *hypotheses* represent all the possible states (e.g. faults) of the system considered. It is required that all hypotheses are elements (singletons) of the frame of discernment.

*Frame of discernment* is given by the finite universal set  $\Omega$ . The set of all subsets of  $\Omega$  is its power set  $2^\Omega$ . A subset of those  $2^\Omega$  sets may consist of a single hypothesis or of a conjunction of hypotheses. Moreover, it is required that all hypotheses are unique, not overlapping and mutually exclusive.

If the frame of discernment is represented by the set  $\Omega$  with:

$$\Omega = \{A_1, A_2, \dots, A_N\} \quad (1)$$

then  $\Omega$  is a finite non-empty set of mutually N exhaustive and exclusive hypotheses related to a problem domain.

The corresponding power set of  $\Omega$  is:

$$2^\Omega = \{\emptyset, \{A_1\}, \{A_2\}, \dots, \{A_N\}, \{A_1 \cup A_2\}, \{A_1 \cup A_3\}, \dots, \Omega\} \quad (2)$$

The set  $\Omega$  has probability 1, the set  $\emptyset$  has probability 0, and probability of all other elements is between 0 and 1.

In this context *pieces of evidence* are symptoms or events (e.g. failures) that occurred or may occur within a system. One piece of evidence is related to a single hypothesis or a set of hypotheses; however, different pieces of evidence may not be assigned to the same hypothesis or set of hypotheses by the same data source.

The qualitative relation between a piece of evidence and a hypothesis corresponds to a cause-consequence chain: A piece of evidence implies a hypothesis or a set of hypotheses. The strength of an evidence-hypothesis assignment, and thereby the strength of this implication, is quantified by a statement of a data source.

Data sources are persons, organizations, or any other entities that provide information for a scenario. In safety and reliability engineering, data sources are usually the results of empirical studies or they are experts, who give subjective quantifiable statements.

From an objective point of view, exactly one single hypothesis is true; from a subjective point of data source view, it might be uncertain which hypothesis fits best to reality. The Dempster-Shafer theory describes the subjective viewpoint as an assessment for an unknown objective fact.

Evidence can be represented by belief functions. There are three important functions in Dempster-Shafer theory: basic belief assignment – bba or  $m$ , Belief -  $Bel$  and Plausibility –  $Pl$ .

Basic belief assignment is the key point of Dempster-Shafer evidence theory. Using a data source, mapping:

$$m : 2^\Omega \rightarrow [0,1] \quad (3)$$

assigns an evidential weight to a set  $A \subseteq \Omega$ , which contains a single hypothesis or a set of hypotheses.

The function  $m$  is called a basic assignment and fulfils:

$$\sum_{A \subseteq \Omega} m(A) = 1 \quad (4)$$

$$m(\emptyset) = 0 \quad (5)$$

Expression  $m(A)$  can be viewed as the measurement of belief which corresponds to subset  $A$  and takes values from this set.

The first condition means that one's entire belief, supported by evidence, can take the maximum value 1, and the second condition refers to the fact that one's belief, corresponding to an empty set, must be equal to 0.

Each  $A$  that holds  $m(A) > 0$  is called a focal element.

Applying the basic assignment function, several evidential functions can be created. A belief measure is given by the function  $bel: 2^\Omega \rightarrow [0, 1]$ . There is

$$Bel(A) = \sum_{B \subseteq A, B \neq \emptyset} m(B) \quad (6)$$

Value  $Bel(A)$  represents the overall belief corresponding to the set  $A$  and all of its subsets.

The empty belief function is the function which satisfies  $m(\Omega)=1$  and  $m(A)=0$  for all subsets of  $A \neq \Omega$ . This function represents total ignorance about the problem under consideration.

$$Bel(\emptyset) = 0 \quad (7)$$

There is a clear distinction between probabilities and basic belief assignments: probability distribution functions are defined on set  $\Omega$  and basic assignment functions on the power set  $2^\Omega$ . Probability gives information about support of hypothesis and simultaneously gives information about the negation (compliment) also. However, in Dempster-Shafer theory, the „uncertainty“ or „not knowing“ is also modelled.

The figure below shows the difference between the two concepts of Probability versus of the Dempster-Shafer concept.

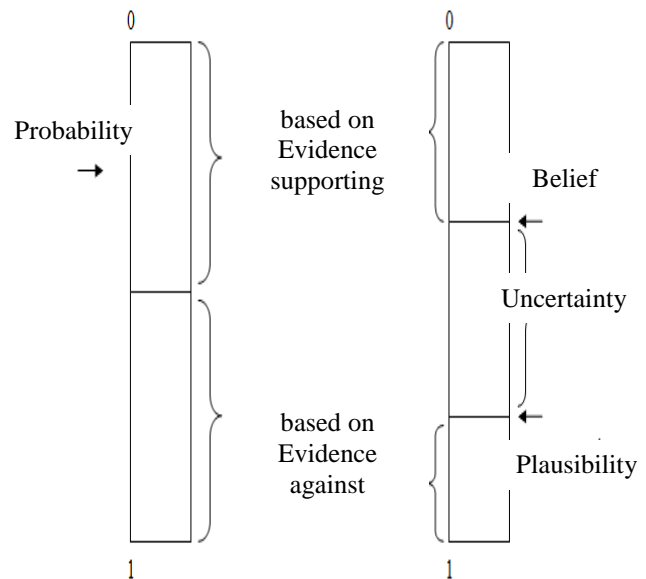


Figure 1: The difference between two concepts

For basic assignment for belief upper and lower limits of the interval can be defined. These limits are called Belief (lower) and Plausibility (upper).

The counterpart of  $bel$  is the plausibility measure  $pl: 2^\Omega \rightarrow [0, 1]$  with:

$$Pl(A) = \sum_{B \cap A \neq \emptyset} m(B) \quad (8)$$

$$Pl(\emptyset) = 0 \quad (9)$$

In fact,  $Bel(A)$  shows necessary (minimal) support for  $A$  and could be interpreted as a global measure of a belief that hypothesis  $A$  is true. Belief of  $A$  can be defined as sum of all the belief masses allocated to hypothesis  $B$ . But,  $Pl(A)$  gives potential (maximal) support for  $A$  and is sum of the parts of belief which are allocated to hypothesis  $B$  and compatible with  $A$ .

Figure 2 shows a graphical representation of the above-defined measures belief and plausibility. The difference  $pl(A) - bel(A)$  describes the evidential interval range, which represents the uncertainty concerning the set  $A$  and it is shaded grey. The measure  $pl(A)$  shall not be understood as the complement of  $bel(A)$ . Only:

$$\langle A \subseteq \Omega | m(A) > 0 \rangle \neq \emptyset \rightarrow Bel(A) \leq Pl(A) \quad (10)$$

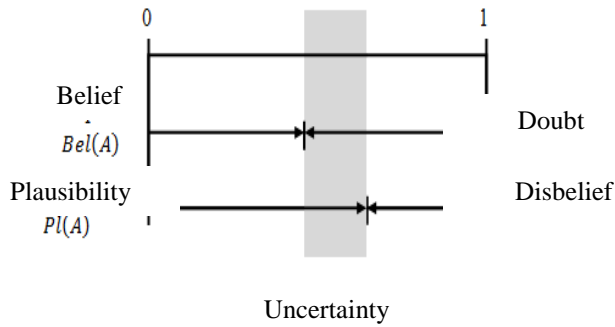


Figure 2: Measures of belief and plausibility complements for a given  $bel(A) < pl$

The complements to the measures of belief and plausibility are doubt and disbelief, respectively. The difference  $pl(A) - bel(A)$  describes the uncertainty concerning the hypothesis A represented by the evidential interval  $[Bel(A), Pl(A)]$ . The greater difference between belief and plausibility, the greater uncertainty (or ignorance).

### 2.2. Dempster-Shafer rule of combination

When the function of the basic belief obtained from a variety of independent sources, may arise a need for a combination. Dempster suggested a rule of combination which allows that the basic assignments are combined. For data fusion, multiple sources of information is combined to give us „better“ judgment of situation.

Let the several independent belief functions be given on the same recognition frame but with different bodies of evidence. The Dempster's combination rule produces new belief function which represents effect resulting from the connection of the different bodies of evidence.

Let us assume that there are two sources of information and let  $m_1$  and  $m_2$  are basic belief assignment function. Evidence can be combined by calculating orthogonal sum using Dempster's rule of combination, in which evidence A and evidence B are used for calculating a new belief function for a focal element C as:

$$m_{1,2}(C) = (m_1 \oplus m_2)(C) = K \left[ \sum_{A \cap B = C} m_1(A) \cdot m_2(B) \right] \quad (11)$$

with  $A, B, C \subseteq \Omega$ , and K represents a normalization factor:

$$K = \left[ 1 - \sum_{A \cap B \neq \emptyset} m_1(A) \cdot m_2(B) \right]^{-1} \quad (12)$$

The normalization factor K represents the conflict measure of the two belief functions. With increasing K, the sources have more conflict and their combinations become less relevant.

It is assumed, also:

$$m_{1,2}(\emptyset) = 0 \quad (13)$$

### 3. FAULT TREE ANALYSIS

Fault tree analysis is usually applied in the design phase of products and used to predict the most likely causes of product failure. Unwanted effects of the FTA (Fault Tree Analysis) called peak events. The aim of

constructing fault tree is modelling the conditions that result in the emergence of peak, unwanted cancellation.

Analysis begins with the qualitative definition of an unwanted event, and then to find failures of elements of the system and the procedural errors that may lead to an unwanted event.

A fault tree graphically shows the relationship between the specific event and the order of these events could cause an unwanted peak previously characterized in the event. Fault tree has an unwanted event in the top part of the diagram, a sequence of events that can cause this event, make the branches of the tree. Roads cancellation relating to the sequence of events that lead to unwanted events. Analyst establish any logical sequence of events, proving the origin through the chain case and recording the events that caused the event is already on the diagram. All sequences are starting with unwanted peak event.

Methodology of Fault Tree Analysis includes [16]:

- determination of peak events,
- the way of operation of a system to be analysed,
- the structure of the fault tree,
- adoption of the fault tree,
- assessment of fault tree and
- provision of recommendations and alternatives for making decisions on the necessary corrective measures..

Analysed system - hydraulic hand pump series 40-506.900 is pump for tilting the cab of the vehicle from production program of PPT Hydraulics AD.

Hydraulic pump for tilting the cab on vehicles series 40-506.900 is a hand pump a piston type, with high pressure and small dimensions. It guarantees functional lifting and lowering the cabin. It is designed to work in the hydraulic system with one-way or two-way cylinder. Clips in the pump are completely protected from the effects of dirt and weather conditions. They have a built-in filter to protect sensitive throttle opening and valve from dirt. This ensures high reliability in operation. Pump parts are made of high quality materials with appropriate heat treatment and galvanic protection. They are manufactured in serial production with the examination of all pumps after assembling. They are installed on trucks KAMAZ - Russia's largest manufacturer of commercial vehicles.



Figure 3: Hydraulic hand pump series 40-506.900 [13]

The principle of operation of this pump is as follows [14]:

Rotating the distribution shaft by the lever, is achieved communication for suppression the working fluid in line A or line B.

Alternating axial movement is achieved using the movement of the lever of the piston, and provides the suction or the suppression of the working fluid.

Lifting the lever in the above part provides the piston raising, thereby creating an empty space below the piston, due to which the pellet raises the intake valve and the working fluid from the chamber of the tank via the suction sieve filled chamber below the piston.

Moving the lever to the down and the piston moves downward and pushes the working fluid through the discharge valve into the chamber A. During this time the working fluid out of the chamber B, through the distribution shaft and a damper non-return valve, is returned to the tank.

The mode of operation of the hand pump is shown in the following figure.

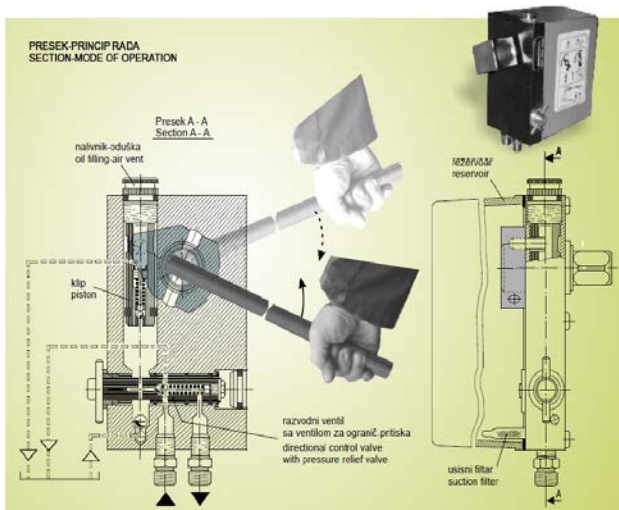


Figure 4: Section-mode of operation of the hand pump [13]

Hand pump for lifting and lowering the cabin should be installed in the vehicle at the access site. It needs to handle and lever is easily accessible and to facilitate their installation in positions that allow the raising and lowering of the vehicle cab.

Constructional structure of the hand pumps 40-506900-K1 consists of five sub-assemblies:

- plate 40-506.902,
- body 40-506.905,
- meter 40-506.920,
- piston 40-506.924 and
- vent 40-510.530.

The functions of these subassemblies in the device are as follows [15]:

- plate 40-506.902– guarantees transmission of torque from the crank to the working piston,
- body 40-506.905 – accepts seal between the body and the reservoir within the function without leaks
- meter 40-506.920 – to check the oil level in the tank for proper operation of the device
- piston 40-506.924 – to convert mechanical force into hydraulic and

- vent 40-510.530 – allows air flow into and out of the tank.

### 3.1. Fault tree of the hydraulic hand pump

Possible malfunctions that may occur during the usage of the hydraulic pump 40-506.900-K1 are:

- no lifting cab,
- raising of the cabin is insufficient and
- external leakage.

A fault tree graphically shows the relationship between the specific event and the order of these events could cause an unwanted peak previously characterized in the event. In this case, with the hydraulic hand pump, an unwanted peak event is the malfunction of the pump. Then entries possible faults, like the branches of a tree.

Fault tree of the hydraulic hand pump 40-506.900-K1 is shown in the figure 5.

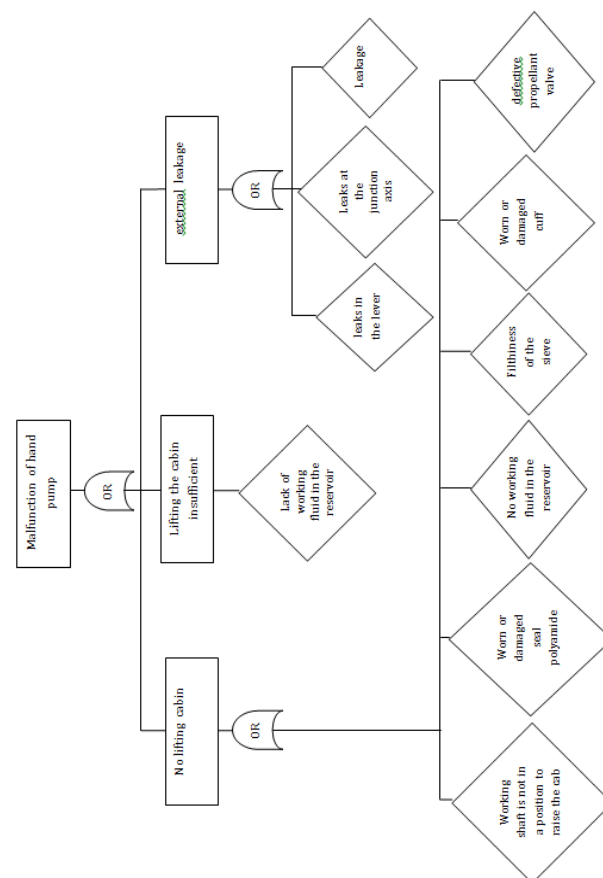


Figure 5: Fault tree of the pump 40-506.900-K1

## 4. APPLICATION OF DEMPSTER-SHAFER THEORY IN FTA

In this paper, Dempster-Shafer theory was applied in the analysis of the fault tree of the hydraulic hand pump. It was assumed that there was two sources of data and the entire process is presented in several steps. Dempster-Shafer approach is used to support decision making.

Step 1:

The scenario consists of a hydraulic pump (the system considered), two operators (data sources, denoted by the index 1), the failures detected (pieces of evidence), and the system fault states (set of hypotheses). As described above, the pieces of evidence correspond to

failures or causes and the hypotheses to faults or consequences.

The faults can be determined to at most three precisely defined hypotheses, represented by the set  $\Omega$  with:

$$\Omega = \{h_1, h_2, h_3\} \quad (14)$$

$(h_1)$ -no lifting cab,  $(h_2)$ -cab lifting insufficient and  $(h_3)$ -external leakage.

With that, the frame of discernment of this context is given. It should be noted that  $\Omega$  is postulated by the operators based on their subjective points of view, assuming that  $\Omega$  is complete. The corresponding power set of  $\Omega$  is:

$$2^\Omega = \{\emptyset, \{h_1\}, \{h_2\}, \{h_3\}, \{h_1, h_2\}, \{h_1, h_3\}, \{h_2, h_3\}, \Omega\} \quad (15)$$

The faults can be caused by five possible failures: defective propellant valve ( $ev_1$ ), a lack of fluids in the reservoir ( $ev_2$ ), worn or damaged rings ( $ev_3$ ), sieves ( $ev_4$ ) and dirt worn or damaged seals ( $ev_5$ ).

The first operator states that the failure ( $ev_1$ ) occurred and might have resulted in the consequence ( $h_1$ ), failure ( $ev_2$ ) occurred and might have resulted in the consequence ( $h_2$ ), the failure ( $ev_3$ ) occurred and might have resulted in the consequence ( $h_3$ ), the failure ( $ev_4$ ) occurred and might have resulted in the consequence ( $h_1$ ) or ( $h_2$ ), and the failure ( $ev_5$ ) occurred and might have resulted in the consequence ( $h_1$ ) or ( $h_3$ ).

The first operator states that the faults h1 or h2 are the main consequences for the problems. The assignments of the second operator are slightly different. Here, focus is on the faults h1 or h2. Both operators give their statements to the five pieces of evidence found. The complete survey of the qualitative failure-fault(s) assignments is given in Table 1.

Table 1: Qualitative failure-fault(s) assignments

	Failure	Fault(s)
Operator 1st	$ev_1$	$h_1$
	$ev_2$	$h_2$
	$ev_3$	$h_3$
	$ev_4$	$h_1, h_2$
	$ev_5$	$h_1, h_3$
Operator 2nd	$ev_1$	$h_1$
	$ev_2$	$h_2$
	$ev_3$	$h_2, h_3$
	$ev_4$	$h_1, h_2$
	$ev_5$	$h_1, h_2, h_3$

Note that contrary to the Fault Tree Analysis (FTA), Dempster-Shafer theory does not allow that more than one failure lead to the same fault (hypothesis). However, different failures may have different set of consequences, which may contain the same hypotheses as elements, e.g.  $ev_1, ev_3$ , and  $ev_4$  lead to hypotheses, which all contain h1 as a fault. Again, Dempster-Shafer theory allows modelling several

- single-failure-single-fault relations and
- single-failure-multi-fault relations

as an uncertain assessment of a system, which can take exactly one state at a time.

Exactly one hypothesis of  $\{h_1, h_2, h_3\}$  is true for the given scenario and situation if the system would be observed from an objective point of view. Subjectively, the operators are not sure, in which state the system actually is.

Step 2:

At this step, both operators quantify their statements as given in Table 2. The set of hypotheses A is assigned to the first operator, B to the second operator.

The subjective quantifications of the operators are based on their system experiences and mostly on their "engineering feelings". Certainly, these quantifications are imprecise. Non-specified statements are assigned by 0 and are not focal elements.

Table 2: Quantitative statements given by the operators involved

1st operator	$2^\Omega$	2 <sup>nd</sup> operator
$m(A_1) = 0.2$	$\{h_1\}$	$m(B_1) = 0.2$
$m(A_2) = 0.1$	$\{h_2\}$	$m(B_2) = 0.1$
$m(A_3) = 0.3$	$\{h_3\}$	$m(B_3) = 0$
$m(A_4) = 0.1$	$\{h_1 \cup h_2\}$	$m(B_4) = 0.2$
$m(A_5) = 0.3$	$\{h_1 \cup h_3\}$	$m(B_5) = 0$
$m(A_6) = 0$	$\{h_1 \cup h_3\}$	$m(B_6) = 0.1$
$m(A_7) = 0$	$\{h_1 \cup h_2 \cup h_3\}$	$m(B_7) = 0.4$

Based on the basic assignments, given by the operators, the belief and doubt, plausibility and disbelief measures can be calculated. The belief of hypotheses is the sum of its own basic assignment with those of all of its subsets. The plausibility includes basic assignments of all statements which have got at least one hypothesis with those of the discussed statement in common.

For example, the belief in the set of hypotheses  $\{h_1 \cup h_2\}$  is the sum of its own basic assignment with those of all of its subsets:

$$\{h_1\}, \{h_2\}, \{h_1 \cup h_2\} \subseteq \{h_1 \cup h_2\} \quad (16)$$

and

$$bel(A_4) = m(A_1) + m(A_2) + m(A_4) = 0.4 \quad (17)$$

with the corresponding doubt measure:

$$1 - bel(A_4) = 1 - 0.4 = 0.6 \quad (18)$$

The plausibility includes basic assignments of all statements which have got at least one hypothesis with those of the discussed statement in common.

For the same statement of the first operator (source);

$$\{h_1\}, \{h_2\}, \{h_1 \cup h_2\}, \{h_1 \cup h_3\}, \{h_2 \cup h_3\}, \{h_1 \cup h_2 \cup h_3\} \cap \{h_1 \cup h_2\} \neq \emptyset \quad (19)$$

which results in the plausibility and disbelief:

$$pl(A_4) = m(A_1) + m(A_2) + m(A_4) + m(A_5) + m(A_6) + m(A_7) \quad (20)$$

$$pl(A_4) = 0.2 + 0.1 + 0.1 + 0.3 + 0 + 0 = 0.7 \quad (20)$$

$$1 - pl(A_4) = 1 - 0.7 = 0.3 \quad (21)$$

Table 3 shows the results for belief and plausibility of all statements ( $k = 1, \dots, 7$ ).

Table 3: The values of basic assignments, belief and plausibility

$m(A_k)$	$bel(A_k)$	$pl(A_k)$	$2^\alpha$	$m(B_k)$	$bel(B_k)$	$pl(B_k)$
0.2	0.2	0.6	$\{h_1\}$	0.2	0.2	0.8
0.1	0.1	0.2	$\{h_2\}$	0.1	0.1	0.8
0.3	0.3	0.6	$\{h_3\}$	0	0	0.5
0.1	0.4	0.7	$\{h_1 \cup h_2\}$	0.2	0.5	1
0.3	0.8	0.9	$\{h_1 \cup h_3\}$	0	0.2	0.9
0	0.4	0.8	$\{h_1 \cup h_3\}$	0.1	0.2	0.8
0	1	1	$\{h_1 \cup h_2 \cup h_3\}$	0.4	1	1

Step 3:

The third step combines each hypothesis or set of hypotheses, from one data source with one from the other source and builds the cut set of both, see Table 4. Depending on quantifications given at Step 2, some of the cut sets may not be focal elements. Actually, this step was fit in for illustrative purpose and can be combined with the next step.

Table 4: The Combination Table

$\cap$	$A_1$	$A_2$	$A_3$	$A_4$	$A_5$	$A_6$	$A_7$
$B_1$	$h_1$	$\phi$	$\phi$	$h_1$	$h_1$	$\phi$	$h_1$
$B_2$	$\phi$	$h_2$	$\phi$	$h_2$	$\phi$	$h_2$	$h_2$
$B_3$	$\phi$	$\phi$	$h_3$	$\phi$	$h_3$	$h_3$	$h_3$
$B_4$	$h_1$	$h_2$	$\phi$	$h_1 \cup h_2$	$h_1$	$h_2$	$h_1 \cup h_2$
$B_5$	$h_1$	$\phi$	$h_3$	$h_1$	$h_1 \cup h_3$	$h_3$	$h_1 \cup h_3$
$B_6$	$\phi$	$h_2$	$h_3$	$h_2$	$h_3$	$h_2 \cup h_3$	$h_2 \cup h_3$
$B_7$	$h_1$	$h_2$	$h_3$	$h_1 \cup h_2$	$h_1 \cup h_3$	$h_2 \cup h_3$	$h_1 \cup h_2 \cup h_3$

Step 4:

At this step, those columns and rows of the Combination Table were dropped, which are related to non-focal elements (non-specified statements with  $m(A_k)=0$  and  $m(B_k)=0$ ). In this context, columns  $A_6, A_7$  and rows  $B_3, B_5$  are not applicable. Table 5 shows the reduced plot containing the combinations of focal elements exclusively.

Table 5: The reduced Combination Table

$\cap$	$A_1$	$A_2$	$A_3$	$A_4$	$A_5$
$B_1$	$h_1$	$\phi$	$\phi$	$h_1$	$h_1$
$B_2$	$\phi$	$h_2$	$\phi$	$h_2$	$\phi$
$B_4$	$h_1$	$h_2$	$\phi$	$h_1 \cup h_2$	$h_1$
$B_6$	$\phi$	$h_2$	$h_3$	$h_2$	$h_3$
$B_7$	$h_1$	$h_2$	$h_3$	$h_1 \cup h_2$	$h_1 \cup h_3$

Step 5:

At this step, products of the related basic assignments are calculated from the non-empty sets. Products of basic assignments corresponding to the same cut set have to be added.

For example, for the hypothesis  $\{h_1\}$ :

$$Z_1 = A_1 \cap B_1 = \{h_1\} \tag{22}$$

$$m(Z_1) = m(A_1) \cdot m(B_1) = 0.2 \cdot 0.2 = 0.04 \tag{23}$$

$$Z_2 = A_1 \cap B_4 = \{h_1\} \tag{24}$$

$$m(Z_2) = m(A_1) \cdot m(B_4) = 0.2 \cdot 0.2 = 0.04 \tag{25}$$

$$Z_3 = A_1 \cap B_7 = \{h_1\} \tag{26}$$

$$m(Z_3) = m(A_1) \cdot m(B_7) = 0.2 \cdot 0.4 = 0.08 \tag{27}$$

$$Z_4 = A_4 \cap B_1 = \{h_1\} \tag{28}$$

$$m(Z_4) = m(A_4) \cdot m(B_1) = 0.1 \cdot 0.2 = 0.02 \tag{29}$$

$$Z_5 = A_5 \cap B_1 = \{h_1\} \tag{30}$$

$$m(Z_5) = m(A_5) \cdot m(B_1) = 0.3 \cdot 0.2 = 0.06 \tag{31}$$

$$Z_6 = A_5 \cap B_4 = \{h_1\} \tag{32}$$

$$m(Z_6) = m(A_5) \cdot m(B_4) = 0.3 \cdot 0.2 = 0.06 \tag{33}$$

with the sum:

$$\sum_{k=1}^6 m(Z_k) = 0.3 \tag{34}$$

The results are given in Table 6, and they illustrate the whole procedure, where x means non-focal elements.

Table 6: The products of basic assignments

	$A_1$	$A_2$	$A_3$	$A_4$	$A_5$
$B_1$	0.04	x	x	0.02	0.06
$B_2$	x	0.01	x	0.01	x
$B_4$	0.04	0.02	x	0.02	0.06
$B_6$	x	0.01	0.03	0.01	0.03
$B_7$	0.08	0.04	0.12	0.04	0.12

Step 6:

The sum of all combinations calculated in previous step:

$$\sum_{k=1}^{18} m(Z_k) = 0.76 \tag{35}$$

With that, the basic assignment of every hypothesis can be calculated.

For the hypothesis  $\{h_1\}$ , there is:

$$m(\{h_1\}) = \frac{\sum_{k=1}^6 m(Z_k)}{\sum_{k=1}^{18} m(Z_k)} = \frac{0.3}{0.76} = 0.3947 \tag{36}$$

For the hypothesis  $\{h_2\}$ , there is:

$$m(\{h_2\}) = \frac{\sum_{k=7}^{12} m(Z_k)}{\sum_{k=1}^{18} m(Z_k)} = \frac{0.1}{0.76} = 0.1316 \tag{37}$$

For the hypothesis  $\{h_3\}$ , there is:

$$m(\{h_3\}) = \frac{\sum_{k=13}^{15} m(Z_k)}{\sum_{k=1}^{18} m(Z_k)} = \frac{0.18}{0.76} = 0.2368 \tag{38}$$

For the set of hypotheses  $\{h_1 \cup h_2\}$ , there is:

$$m(\{h_1 \cup h_2\}) = \frac{\sum_{k=16}^{17} m(Z_k)}{\sum_{k=1}^{18} m(Z_k)} = \frac{0.06}{0.76} = 0.0789 \tag{39}$$

For the set of hypotheses  $\{h_1 \cup h_3\}$ , there is:



$$m(\{h_1 \cup h_3\}) = \frac{m(Z_{18})}{\sum_{k=1}^{18} m(Z_k)} = \frac{0.12}{0.76} = 0.1579 \quad (40)$$

Step 7:

At this step, the evidence measures of combined hypotheses are calculated according to step 2. The basic assignments and the resulting evidence measures belief, commonality, and plausibility are given in the table 7. The sets  $h_2 \cup h_3$  and  $h_1 \cup h_2 \cup h_3$  does not occur because it vanished in Table 5. Hypotheses are ranked by their belief measures.

Belief measures:

$$bel(\{h_1\}) = m(\{h_1\}) = 0.3947 \quad (41)$$

$$bel(\{h_2\}) = m(\{h_2\}) = 0.1316 \quad (42)$$

$$bel(\{h_3\}) = m(\{h_3\}) = 0.2368 \quad (43)$$

$$bel(\{h_1 \cup h_2\}) = m(\{h_1\}) + m(\{h_2\}) + m(\{h_1 \cup h_2\}) = 0.6052 \quad (44)$$

$$bel(\{h_1 \cup h_3\}) = m(\{h_1\}) + m(\{h_3\}) + m(\{h_1 \cup h_3\}) = 0.7894 \quad (45)$$

Plausibility measures:

$$pl(\{h_1\}) = m(\{h_1\}) + m(\{h_1 \cup h_2\}) + m(\{h_1 \cup h_3\}) = 0.6315 \quad (46)$$

$$pl(\{h_2\}) = m(\{h_2\}) + m(\{h_1 \cup h_2\}) = 0.2105 \quad (47)$$

$$pl(\{h_3\}) = m(\{h_3\}) + m(\{h_1 \cup h_3\}) = 0.3947 \quad (48)$$

$$pl(\{h_1 \cup h_2\}) = m(\{h_1\}) + m(\{h_2\}) + m(\{h_1 \cup h_2\}) + m(\{h_1 \cup h_3\})$$

$$pl(\{h_1 \cup h_2\}) = 0.7631 \quad (49)$$

$$pl(\{h_1 \cup h_3\}) = m(\{h_1\}) + m(\{h_3\}) + m(\{h_1 \cup h_2\}) + m(\{h_1 \cup h_3\})$$

$$pl(\{h_1 \cup h_3\}) = 0.8683 \quad (50)$$

Table 7: The basic assignments and the resulting evidence measures belief and plausibility

$Z^{\omega}$	m	bel	pl
$\{h_1 \cup h_3\}$	0.1579	0.7894	0.8683
$\{h_1 \cup h_2\}$	0.0789	0.6052	0.7631
$\{h_1\}$	0.3947	0.3947	0.6315
$\{h_3\}$	0.2368	0.2368	0.3947
$\{h_2\}$	0.1316	0.1316	0.2105

Step 8:

This step is the last step in this procedure.

Uncertainty is defined by the evidential interval  $[Bel, Pl]$ , and it is the difference between belief and plausibility.

Uncertainty = Plausibility – Belief

So, the evidential interval for every hypothesis and set of hypothesis is:

$$\{h_1 \cup h_3\} \Rightarrow pl(\{h_1 \cup h_3\}) - bel(\{h_1 \cup h_3\}) = 0.0789 \quad (51)$$

$$\{h_1 \cup h_2\} \Rightarrow pl(\{h_1 \cup h_2\}) - bel(\{h_1 \cup h_2\}) = 0.1579 \quad (52)$$

$$\{h_1\} \Rightarrow pl(\{h_1\}) - bel(\{h_1\}) = 0.2368 \quad (53)$$

$$\{h_3\} \Rightarrow pl(\{h_3\}) - bel(\{h_3\}) = 0.1579 \quad (54)$$

$$\{h_2\} \Rightarrow pl(\{h_2\}) - bel(\{h_2\}) = 0.0789 \quad (55)$$

The greater difference between belief and plausibility, the greater uncertainty (or ignorance) is.

The hypothesis  $h_2$  should not be considered further due to the low values of belief and plausibility. With value about 0.24, the single hypothesis  $h_1$  is assigned with a wide range of uncertainty. The hypothesis  $h_3$  and the combination of  $h_1$  and  $h_2$ , covers a smaller range (0.16). The smaller value has the combination of  $h_1$  i  $h_3$  (0.08),

and it has a higher plausibility. Finally, the hypothesis  $h_2$  shows the smallest range of uncertainty (0.08), but it should not be considered further.

Dempster-Shafer approach, in this example, is indicating first hypothesis  $h_1$  and gives a hint to the hypothesis  $h_3$ , i.e. a combination of the hypothesis  $h_1$  and  $h_3$  is designated as the most serious and most common fault occurring in a hydraulic hand pump for tilting the vehicle cab.

The conclusion is that a combination of  $h_1$  i  $h_3$  may be responsible for the serious changes of the system properties.

## 5. CONCLUSION

The aim of any organization is to offer a quality product to the market, at a reasonable price, which will ensure the survival of the organization and its development in the future. For this reason applying, methods that can provide a relatively quick and easy, and safe way to discover hidden defects of products or methods to ensure the safety and reliability of products are used.

Modern business of every organization relies on information. However, all information is not fully defined and precise. There are often uncertain and imprecise information and need to find a way to present such information and reasoning system based on such information. For this purpose there is a theory of belief functions.

Theory of belief function or Dempster-Shafer theory is known for its usefulness for expressing uncertain decisions of experts and to assist in decision making. Human experts often have a difference of opinion, and even conflicting views and that this theory can be of great importance. When you apply a rule of combining function you will get better results than to observe each function separately, as combining multiple sources of information provides a better assessment of the situation.

This paper shows how this calculation can be applied to the fault tree analysis of the hydraulic hand pump for tilting the cab of the vehicle and assess which is the most serious failure of the device and what is most responsible for serious changes in the operation of the pump, or termination of its work.

Dempster-Shafer theory was carried through eight steps, all the belief functions have been calculated and applied rule of combination and finally got results that leads to two hypothesis, i.e. combination of hypothesis, as a major cause of failure of the hydraulic hand pump. Note that a probabilistic approach would have blamed only one hypothesis for being responsible. This result clearly shows the differences between both theories, and that the Dempster-Shafer theory has advantages compared to the classical theory of probability. Also, the results show that this method can increase the accuracy and reliability of the product when applied to the fault tree analysis.

## REFERENCES

[1] M. Đapić, "Evidencioni sistemi u razvoju proizvoda i procesa", Inteligentni tehnološki sistemi serija monografija br. 9, LOLA institut, Beograd, (2005)

- [2] U. K. Rakowsky, "Fundamentals of the Dempster-Shafer theory and its applications to reliability modeling", *International Journal of Reliability, Quality and Safety Engineering* Vol. 14, No. 6 (2007) 579–601
- [3] U. K. Rakowsky, "Fundamentals of the Dempster-Shafer theory and its applications to system safety and reliability modeling", University of Wuppertal, Germany and Vossloh Kiepe, Düsseldorf, Germany, (2007)
- [4] K. Sentz, S. Ferson, "Combination of Evidence in Dempster-Shafer Theory", *Systems Science and Industrial Engineering Department Thomas J. Watson, School of Engineering and Applied Science, Binghamton University, Applied Biomathematics, New York*, (2002)
- [5] M. Shahab, "Fault Diagnosis: a Dempster-Shafer Theory Approach", King Fahd University of Petroleum and Minerals EE 562 – Digital Signal Processing Course Project, (2009)
- [6] B. Yang, K. Jin Kim, "Application of Dempster-Shafer theory in fault diagnosis of induction motors using vibration and current signals", *School of Mechanical Engineering, Pukyong National University, San 100, Yongdang-dong, Nam-gu, Busan 608-739, Republic of Korea, Mechanical Systems and Signal Processing* 20 (2006) 403-420
- [7] S. Parsons, "Some qualitative approaches to applying the Dempster-Shafer theory", *Advanced Computation Laboratory Imperial Cancer Research Fund, Lincoln's Inn Fields, London*
- [8] M. Đapić, Lj. Lukić, "Application of Dempster-Shafer theory in conceptual design of the machining centres", ISSN 1330-3651 (Print), ISSN 1848-6339 (Online) UDC/UDK 621.9.06:004.891, *Tehnički vjesnik* 20, 1(2013), 65-71
- [9] K.-C. Ng, B. Abramson, "Uncertainty Management in Expert System", *Tools and Techniques, University of Southern California*, (1990)
- [10] P. Limbourg, R. Savić, J. Petersen, H.-D. Kochs, "Fault tree analysis in an early design stage using the Dempster-Shafer theory of evidence, Risk, Reliability and Societal Safety" – Aven & Vinnem (eds), Taylor & Francis Group, London, ISBN 978-0-415-44786-7, (2007)
- [11] X. Xiaobin, L. Ping, S. Yanbo, W. Chenglin, "Fault diagnosis based on the updating strategy of interval-valued belief structures", *Chinese Journal of Electronics*, Vol. 23, No. 4, (2014)
- [12] R. Gholamshahi, J. Poshtan, M. Poshtan, "Improving stator winding fault diagnosis in induction motor using Dempster-Shafer theory", *Electrical and Electronics Engineering: An International Journal (ELELIJ)* Vol 3, No 2, (2014) DOI: 10.14810/elelij.2014.3213 161
- [13] Katalog – ručne pumpe, PPT Hidraulika
- [14] Uputstvo za eksploataciju i održavanje – ručna pumpa 40.506.900, PPT Hidraulika
- [15] Blok šema uređaja ručna pumpa 40-506.900-K1 - FH.R.P2.73.01, PPT Hidraulika
- [16] V. Vulanović, D. Stanivuković, B. Kamberović, N. Radaković, R. Maksimović, V. Radlovački, M. Šilobad, "Metode i tehnike unapređenja procesa rada", *Fakultet tehničkih nauka, Univerzitet u Novom Sadu, Novi Sad*, (2012)
- [17] Uputstvo za eksploataciju i održavanje – ručna pumpa 40.506.900, PPT Hidraulika
- [18] J. Weisberg, "Dempster-Shafer Theory", *University of Toronto, Northern Institute of Philosophy*, (2010)
- [19] L. Troiano, L. Rodriguez-Muniz, I. Diaz, "Discovering user preferences using Dempster-Shafer theory", *Fuzzy Sets and Systems* 278 (2015) 98-117
- [20] B. Yang, K. Kim, "Application of Dempster-Shafer theory in fault diagnosis of induction motors using vibration and current signals", *Mechanical Systems and Signal Processing* 20 (2006) 403-420
- [21] D. Zengshou, Z. Xujiang, "Modified D-S evidential theory in hydraulic system fault diagnosis", *Procedia Environmental Sciences* 11 (2011) 98 – 102
- [22] S. Parsons, "Qualitative methods for reasoning under uncertainty", *The MIT Press, Cambridge, Massachusetts Institute of Technology*, (2001)
- [23] [https://wikipedia.org/wiki/Dempster-Shafer\\_theory](https://wikipedia.org/wiki/Dempster-Shafer_theory)
- [24] [https://en.wikipedia.org/wiki/Fault\\_tree\\_analysis](https://en.wikipedia.org/wiki/Fault_tree_analysis)

# Remote Monitoring and Control of Asynchronous Drives Performance – Laboratory Stand

Vasil Dimitrov<sup>1\*</sup>, Petko Kostadinov<sup>1</sup>

<sup>1</sup> Faculty of Telecommunications and Electrical Equipment in Transport / Department of Power Engineering and Electrical Equipment in Transport, Todor Kableshkov University of Transport – Sofia (Bulgaria)

*Soft starters are widely used in industry for control on asynchronous drives when the speed regulation is not a mandatory requirement. They are cheaper than inverters and frequency converters and allow temporal reduction of the torque and current surge during start-up, as well as smooth deceleration.*

*A laboratory stand has been designed and built. An asynchronous motor is controlled by a Soft starter. Remote control on the drive has been implemented using a PLC S7-200 and Touch Panel TP177micro, Siemens. The performance of the drive is monitored by an intelligent energy meter SentronPAC3200, Siemens. Remote monitoring has been involved – this device has been connected to the Ethernet network.*

*This laboratory stand offers various possibilities of implementation into practice many laboratory exercises, for example: examination of an asynchronous motor at a constant speed and variable load; study of the influence of the start-up and ramp-down time on the drive performance; training the programming skills for setting-up the soft starters, PLCs and touch screens, contemporary measuring devices and their communication through the Ethernet networks, etc.*

**Keywords:** Soft starter, PLC, remote monitoring and control, intelligent energy meter

## 1. INTRODUCTION

The speed regulation of the asynchronous motors in many fields of industry is not necessary. Many drives need to be started and stopped smoothly but its speed has to be constant through the operating modes:

- Conveyors and Conveyor belts;
- Pumps;
- Fans;
- Compressors;
- Automatic doors;
- Small cranes;
- Belt-drive machines, etc.

Intelligent devices called “Soft starters” can be used in those cases. Using soft starter enhances the starting performance of asynchronous motors by allowing the motor to start gradually and smoothly in a controlled manner [1-4]. This can also prevent mechanical shocks, which lead to wear and tear maintenance work and production downtime. Therefore, the study and examination of the soft starters is very important. A laboratory stand has been designed and built and remote monitoring and control has been provided.

## 2. PRINCIPLE OF OPERATION OF SOFT STARTERS

A soft starter is a device used with AC induction motors to temporarily reduce the torque and current surge during start-up and stop-down. This reduces the mechanical stress on the motor and shaft, as well as the electrodynamic stresses on the electrical distribution network, extending the lifespan of the system [7]. Electrical soft starters reduce the torque by temporal reduction of the voltage or current input. Typically, the voltage is controlled by reverse-parallel-connected thyristors. They can be connected in series with the line voltage applied to the star-connected motor, or can be connected inside the delta ( $\Delta$ ) loop of a delta-connected motor, controlling the voltage applied to each winding.

The thyristors can be bypassed by a relay or a contactor in steady-state operation (Fig. 1).

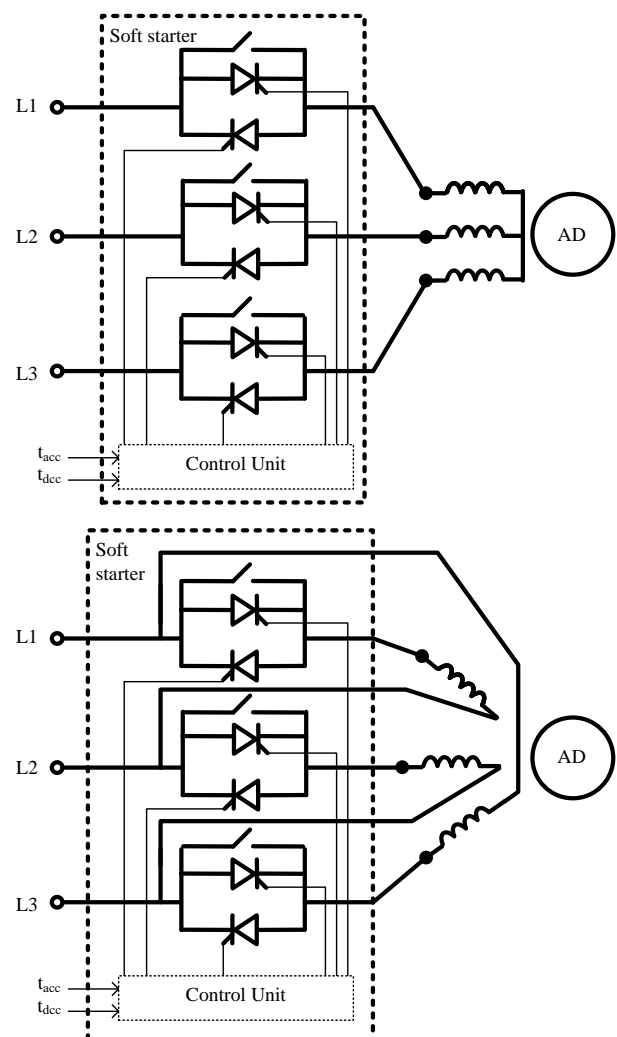


Figure 1: Star- and Delta-connection of Soft starters

Soft starters can be set up to the requirements of the individual application and the motor is adjusted to the machine's load behavior. In pump applications, a soft start can avoid pressure surges. Conveyor belt systems can be smoothly started, avoiding jerk and stress on drive components. Fans or other systems with belt drives can be started slowly to avoid belt slipping. Soft starts are also seen in electrical R/C helicopters, and allow the rotor blades to spool-up in a smooth, controlled manner rather than a sudden surge. In all systems, a soft start limits the inrush current and so improves stability of the power supply and reduces transient voltage drops that may affect other loads [4 - 7].

3. LABORATORY STAND

The laboratory stand for asynchronous drive examinations is shown in Fig. 2. The used motor is made in Bulgaria; its power is 3 kW. A load of the motor can be changed by an electromagnetic brake (EMB), which has to

be powered by an additional DC voltage source. The possibility of reverse is provided by two circuit breakers – F (forward) and R (reverse). The necessary locks and protection are also assured – 3 poles thermal magnetic motor circuit breaker *MCB GV2-ME14* (rated current 10A and thermal protection adjustment range 6...10 A), as well as three fast acting fuses *F* (rated current 10 A) [8].

The motor is controlled by an appropriate soft starter. Altistart 01 soft start / soft stop units ATS01N2 developed by Schneider Electric Company is used [5-7].

The Altistart 01 starters enhance the starting performance of asynchronous motors by allowing them to start gradually, smoothly, and in a controlled manner. It helps to prevent mechanical shocks, which cause wear and tear, and subsequent maintenance work and production downtime. The series includes several devices offering various features. Some of them operate only as a torque limiter on starting, but others can be used as a soft start/soft stop unit for asynchronous motors.

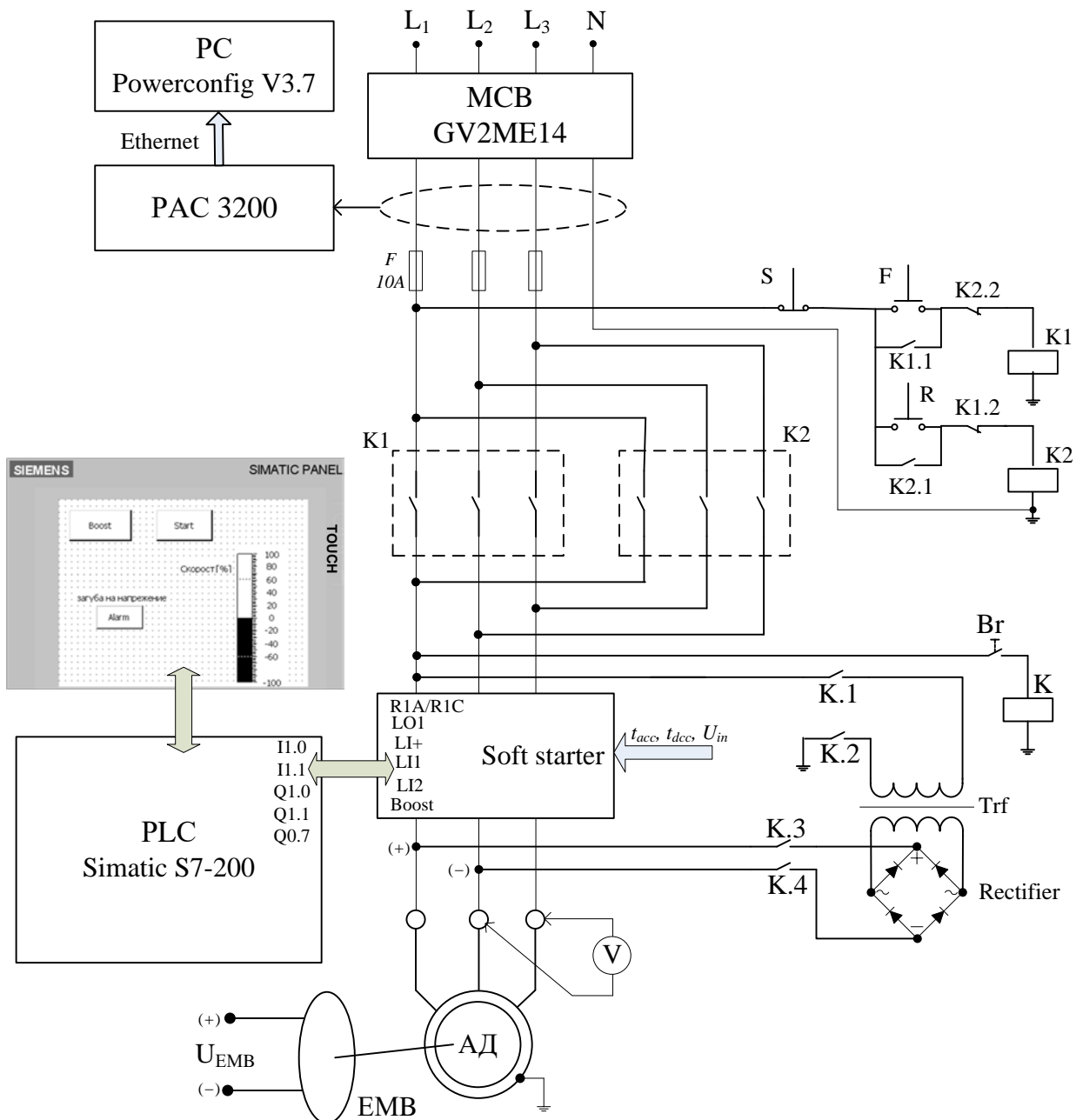


Figure 2: Laboratory stand for remote monitoring and control of asynchronous drive with soft starter

The Altistart 01 ATS01N2 soft start/soft stop units control the motor power supply to limit the starting current and for deceleration. They also feature an internal bypass relay. These devices are equipped with 3 potentiometers for setting the starting and deceleration time and for adjusting the starting voltage threshold according to the motor load. Two logic inputs provide Run/Stop commands and a logic input can be used for the Boost function (+24V positive logic). One logic output indicates the end of starting and one relay output indicates that the voltage is switched off at the end of the deceleration stage. A green LED indicates that the unit is powered up and a yellow LED indicates that the motor is powered at nominal voltage.

The appropriate model is selected according to the technical data of the asynchronous motor. Altistart ATS01N2\*\*QN is available for voltage 380V (380V -15% to 415V +10%). The model ATS01N209QN for nominal current 9A is appropriate for motors with power of 3-4 kW (the main technical parameters are given in table. 1).

The logical inputs and outputs are connected to the PLC Simatic S7-200 [9]. TP177micro Touch Panel is configured for Start / Stop and Boost commands that are transmitted through the PLC to the soft starter [10]. 2-wire control is realized – the run and stop commands are controlled by a single logic input. State "1" of logic input LI2 controls the run process and state "0" controls the stop process. A switch is configured on the Touch Panel and performs these functions. Another switch is configured for the Voltage Boost function via third logic input of the soft starter – activating this input enables the function for supplying a starting overtorque capable of overcoming any mechanical friction. When the input is at state "1", the function is active and the starter supplies the rated voltage to the motor for a limited time (200 ms) before starting.

Digital inputs of the PLC are used for receiving the information about drive condition. The logic output LO1 of the soft starter indicates the end of starting when the bypass relay has been switched on and the motor has reached nominal speed. A bar is configured on the Touch Panel and shows the motor speed. The Fault relay (built into the soft starter) opens when a fault is detected: the relay contact R1A-R1C closes with the Run command and opens when the motor voltage is around 0 with a decelerated stop or stop immediately on a fault. An alarm is configured on the Touch Panel and will indicate a fault.

Table 1: Main technical parameters of the soft starter ATS01N209QN

Power supply	342...456 V; 47,5...63 Hz
Current	9 A rated operating current 30A starting current at nominal load
Power dissipated	4 W (at full load at end of starting) 94 W (in transient state)
Starting time (acceleration time)	Adjustable 1 ... 10 s Maximum number of cycles per hour: 1 s / 100 cycles per 1 h. 5 s / 20 cycles per 1 h. 10 s / 10 cycles per 1 h.
Deceleration time	Adjustable 1 ... 10 s
Initial Voltage	$U_{in} = 30 - 80 \% U_n$
Starting torque	30...80% of starting torque of motor connected directly on the line supply

Measuring equipment with high accuracy is also provided. The power monitoring device Sentron PAC3200 developed by Siemens offers an analysis of the electrical system's current consumption and power flows [11-14]. It is connected direct in the voltage system. For measuring current, three 50/5 A current transformers are used.

It precisely and reliably detects the power values of electrical consumers and provides important measured values for assessing the system state and power quality. This device has a range of useful monitoring, diagnostics and service functions, a two-tariff active energy and reactive energy counter (imported and exported energy), a universal counter, and a working hours counter for monitoring the running time of connected loads.

All the relevant system parameters can be shown on the large graphical LC display that permits reading even from a distance [15]:

- Voltage (Phase-neutral –  $U_{1-n} / U_{2-n} / U_{3-n}$  and Phase-phase  $U_{1-2} / U_{2-3} / U_{3-1}$ );
- Currents (per phase –  $I_1 / I_2 / I_3$ );
- Active power (per phase –  $\pm P_1 / \pm P_2 / \pm P_3$  and total  $\pm P_{total}$ );
- Reactive power (per phase –  $\pm Q_1 / \pm Q_2 / \pm Q_3$  and total  $\pm Q_{total}$ );
- Apparent power (per phase –  $S_1 / S_2 / S_3$  and total  $S_{total}$ );
- Power factor (per phase –  $|PF_1| / |PF_2| / |PF_3|$  and total  $|PF_{total}|$ );
- Frequency f;
- Total harmonic distortion (THD) for voltage and current (per phase –  $THD-U_1 / THD-U_2 / THD-U_3 / THD-I_1 / THD-I_2 / THD-I_3$ );
- Phase unbalance (Voltage);
- Min. / max. values (Voltage / Current / Power / Power factor / THD / Frequency / Three phase average voltage and current / Three phase average rating for active and reactive power), a possibility of reset is provided.

The backlighting can be adjusted in steps for optimal readability even under poor lighting conditions. The combination of four function keys with the multi-language plaintext displays makes intuitive user prompting possible. The experienced operator can also use direct navigation for quicker selection of the desired display menu.

The integral Ethernet interface is provided for easy integration into any local or remote monitoring system. In the stand, it is used for communication between the device and a computer (PC). Modbus TCP Ethernet protocol is used (10 Mbps) and the relevant software product Powerconfig V3.7 has been installed on the PC. The Sentron PAC3200 transmits measured values to the supervisory systems, where the data can be further processed for display and control (there is a opportunity of exporting to Excel tables). Simple configuration of the parameters can be done either directly from the front display or through the communication interface using the PC.

In addition, the Sentron PAC3200 has a multifunctional digital input and digital output (simple logic functions for alarming can be set up).

#### 4. TESTING AND EXAMINATIONS

The laboratory stand offers various possibilities of research and implementation into practice many laboratory exercises, for example:

- Examination of an asynchronous motor at a constant speed and variable load;
- Study of the influence of the start-up and ramp-down time on the drive performance.

The laboratory stand gives possibilities of student's practical training in many terms of reference, for example:

- Training the programming skills for setting-up the soft starters, intelligent measuring devices, PLCs and touch screens, as well as the communication between these devices and PC – knowledge of the relevant software products is necessary;
- Analyzing the electrical system's current consumption and power flows;
- Synthesis of algorithms for optimal control on the drive systems;
- Evaluation of the PLC's possibilities of its using in the drive systems for the efficiency optimization.

The existence of a PLC with touch panel and a PC connected to the Sentron PAC3200 allows for simultaneous drive control, monitoring and parameters tracing and capturing. Methods for some laboratory examinations and tests by instrumentation with high accuracy are developed:

- Determination of the static mechanical and electromechanical characteristics of the asynchronous drive:

$$\omega = f(M), \omega = f(I) \quad (1)$$

- Determination of the characteristics that show the change of energetic parameters of the drive (power factor, efficiency, THD, etc.) at the different settings of the soft starter [5]:

$$\cos\varphi = f(M), \eta = f(M), THD_I = f(M), THD_U = f(M) \quad (2)$$

- Capturing the dynamic characteristics with starting, stopping and changing the load:

$$I = f(t), P = f(t), Q = f(t), U = f(t) \quad (3)$$

$$\cos\varphi = f(t), THD_I = f(t), THD_U = f(t) \quad (4)$$

##### 4.1. Configuring and Setting-up the PLC and Touch Panel

The PLC and the touch panel could be configured to realize 3-wire control on the soft starter – the run and stop commands will be controlled by different logic inputs. The logic inputs LI1 and LI2 have to be connected to two logic outputs of the PLC (for ex. Q1.0 and Q1.1). The relevant buttons have to be configured on the touch panel – a normally closed button for Stop command (associated to the Q1.0 and LI1) and a normally open button for Run command (associated to the Q1.1 and LI2). The switch for the Voltage Boost function, the speed bar and the alarm have to be also configured (Fig. 3). Knowledge of the software products Step 7-Micro/Win and WinCC flexible is necessary.

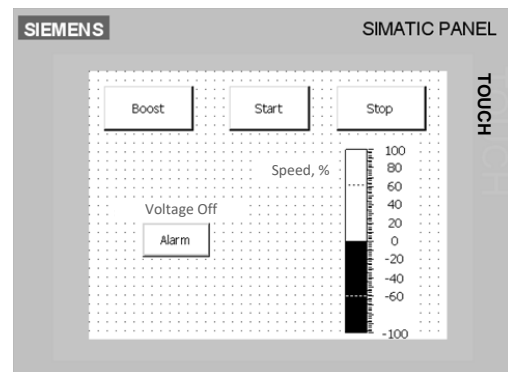


Figure 3: Touch panel view at 3-wire control

##### 4.2. Analyzing the electrical system's parameters

The device Sentron PAC3200 has to be connected to the PC and the software Powerconfig V3.7 has to be started. This software package is a combined service and commissioning tool for communication-capable measuring devices from the Sentron family. The parameters of the drive can be displayed on the PC monitor (Fig. 4).

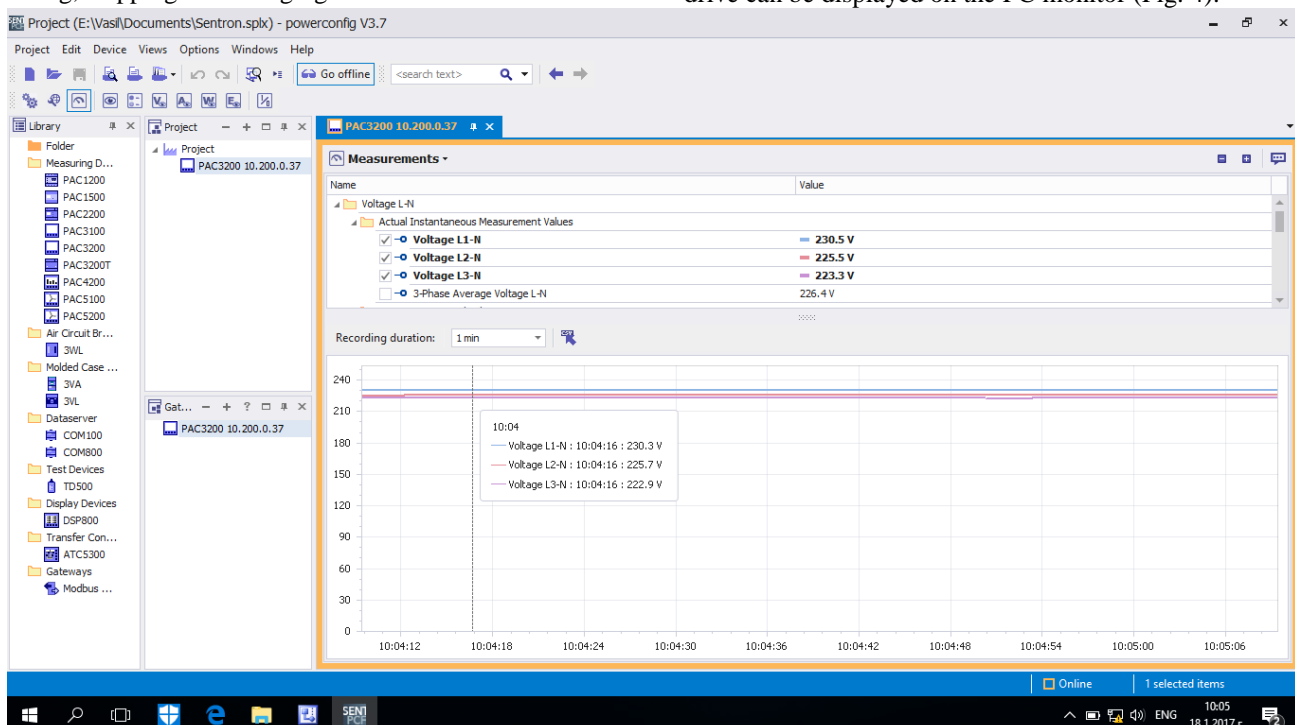


Figure 4: Software Powerconfig V3.7 – voltage monitoring

The measured values can be watched in real time in numerical and graphic type in standardized views. Three-phase voltage is monitored in the Fig. 4 – the date, time and value of each phase voltage are displayed in real time. The unbalance is clearly visible – the coefficient of the phase unbalance, as well as the average three-phase voltage can also be shown. The refresh time could be changed (minimum value is 330 ms) and the differences could be watched. Any other parameters can be monitored (selecting by the menu). The moment values are written and graphics can be plotted. Read-out and saving of message lists, load profiles, and histories is also possible.

The variation of the motor currents during different regimes is shown in the Fig. 5. The big values of the

starting currents are clearly visible. The currents are constant during the steady-state operation and decrease slowly after the Stop command.

The variation of the motor power during different regimes is shown in the Fig. 6. Three tests were made at different acceleration times. The active, reactive and apparent power was monitored. The big values of the starting power are clearly visible again, but these values can be decreased by increasing the acceleration time. The active power is very low during the steady-state operation because the drive is running without any load. The power is independent of the soft starter settings during the steady-state operation and decreases slowly after the Stop command.

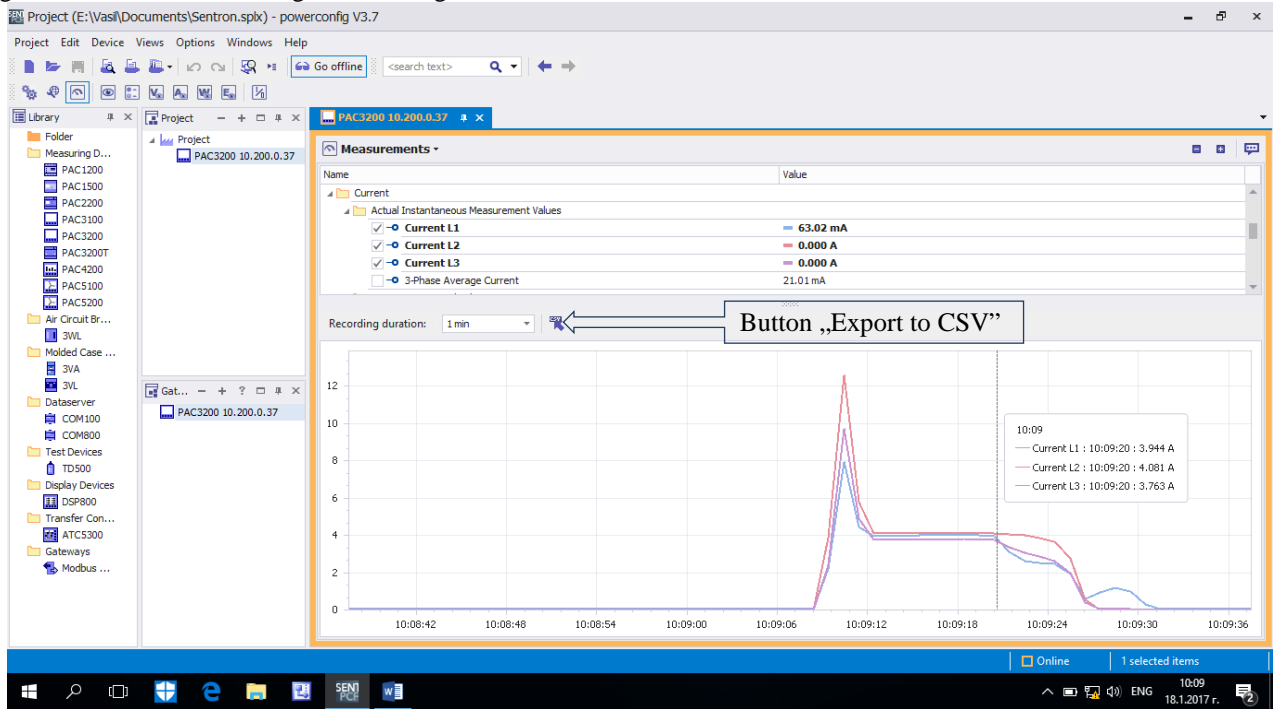


Figure 5: Laboratory Software Powerconfig V3.7 – current monitoring

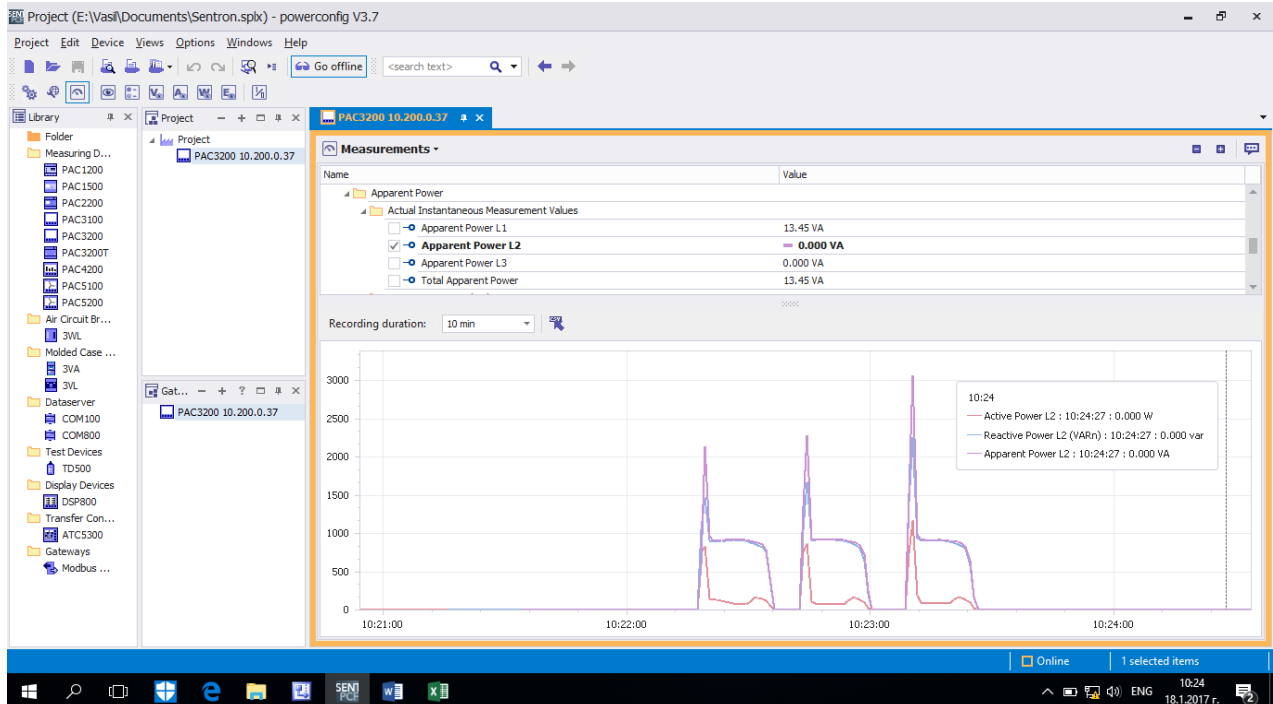


Figure 6: Laboratory Software Powerconfig V3.7 – power monitoring

The software Powerconfig V3.7 offers opportunity of exporting data to Excel tables using the button "Export to CSV" (see Fig. 5). The Recording duration have to be defined in advance. Data can be processed in Excel and many graphics can be plotted and analyzed.

## 5. CONCLUSION

Soft starters are widely used in industry for control on asynchronous drives when the speed regulation is not a mandatory requirement. They are cheaper than inverters and frequency converters and allow temporal reduction of the torque and current surge during start-up, as well as smooth deceleration. Therefore they can be also used in electric vehicles for control on auxiliary machines (pumps, air coolers, compressors, etc.).

PLCs are often implemented as primary components in small and medium control system configurations. The PLCs Simatic series offer maximum automation at minimum dimensions – it is compact, fast and highly powerful, feature great communications capabilities and it is based on very user-friendly software and hardware. They can be used for complex automation tasks and finds application in many branches of industry, power engineering and transport.

These advantages cause to teaching the students how to use and program soft starters and PLCs. The developed stand offers various possibilities of research and implementation into practice many laboratory exercises, for example:

- Examination of an asynchronous motor at a constant speed and variable load;
- Study of the influence of the start-up and ramp-down time on the drive performance;
- Selecting the right scheme of the drive depending on specific application;
- Training the programming skills for setting-up contemporary measuring and control devices and their communication through the networks, as well as their using in the control systems for monitoring and analyzing the electrical system's parameters;
- Synthesis of algorithms for optimal control on the drive systems depending on the load torque, as well as evaluation of possibilities of efficiency optimization.

## REFERENCES

- [1] U.A.Bakshi,M.V.Bakshi, "Electrical Drives and Control", Technical Publications Pune, India, (2009)
- [2] I. Boldea, S. A. Nasar, Electrical Drives, CRC/Taylor & Francis Group, NY, (2006)
- [3] N. K. De, P. K. Sen, "Electric Drives", Prentice Hall of India, (2006)
- [4] The essential guide of Automation & Control, Schneider Electric, (2012)
- [5] Soft Starts for Single-Phase and Three-Phase Asynchronous Motors, Catalog, Schneider Electric, (2011)
- [6] Soft starters Altistart 01 for asynchronous motors, Catalog, Schneider Electric, (2014)
- [7] ATS01N209QN Soft Starter for Asynchronous Motors, Product data sheet, Schneider Electric, (2011)
- [8] TeSys GV2-Circuit breaker-thermal-magnetic - 6...10 A, Product data sheet, Schneider Electric, (2016)
- [9] SIMATIC S7-200 - Programmable Controller, System Manual, Siemens, (2008)
- [10] SIMATIC HMI device TP 177micro (WinCC flexible), Operating Instructions, Siemens, (2005)
- [11] E.A.Dimitrova, "Building automation and control systems", Academic journal "Mechanics, Transport, Communications", ISSN 1312-3823, Vol. 14, 3/2, paper ID 1395, pp. X-26 – X-31, (2016)
- [12] SENTRON PAC Power Monitoring Devices, Siemens, (2009)
- [13] SENTRON PAC3200, Technical specification, Siemens, (2011)
- [14] SENTRON PAC3200, Manual, Siemens, (2008)
- [15] <http://w3.siemens.com/powerdistribution/global/en/lv/portfolio/pages/powerconfig.aspx>



## Synergistic Model of Traffic Flows

Galina Cherneva<sup>1</sup>, Emiliya Dimitrova<sup>2\*</sup>

<sup>1</sup> Faculty of Telecommunications and Electrical Equipment in Transport / Department of Electrical Engineering and Physics, Todor Kableshkov University of Transport – Sofia (Bulgaria)

<sup>1</sup> Faculty of Telecommunications and Electrical Equipment in Transport / Department of Telecommunications and Signaling, Todor Kableshkov University of Transport – Sofia (Bulgaria)

*Many different models are used for traffic flows examination - macroscopic, microscopic, kinetic, stochastic, timed, etc. models.*

*The traffic flow can also be examined as an open dynamic system that is subjected to the complex influence of different types of disturbances. This why the traffic flows can be modeled and analyzed using the methods of non-linear dynamics.*

*In view of the general laws of the traffic flow as a dynamic system, a traffic flows model based on the Lorenz system is proposed in the paper. The model has been simulated in Mathcad environment and has been tested at changing its parameters.*

**Keywords: Traffic flows, Transport systems, Synergy, Self-organization, Non-Linear dynamic system, Lorenz system**

### 1. INTRODUCTION TO THE PROBLEM

Traffic flows, regardless of their type and composition, are complex systems consisting of discrete units that move on a given channel (track) in the transport network. They can be a combination of technical means, transported goods, groups of people, etc., to which, however, a number of subsystems - infrastructure, organizational structure, rules, regulations, etc. are also referred (Fig. 1).

The traffic flows are characterized by certain parameters and are dependent on many factors – determined and random. Their study aims, on the one hand, to analyze the existing situation and, on the other hand, to predict, with sufficient precision, their future development.

There are a number of models of transport flows depending on the type of variables, the degree of detail, the way in which physical processes are presented, etc. [1, 2, 3].

Some of them are based on the relationships between the basic flow parameters and the theory of hydrodynamics – macroscopic models [1]. The transport flow is treated as a fluid stream.

Other models examine the movement of separate elements (individuals or vehicles) – microscopic models [2]. In them, the traffic is examined in detail, taking into account impacts on each vehicle.

Third kind of models report the dynamics of a group of vehicles – mesoscopic models [3]. They are a combination of macro and microscopic models.

Variables that characterize the traffic flows are continuous or discrete time functions [4].

The description of processes in transport systems can be determined [5] if it is based on precise dependencies and random disturbances and impacts on them are not taken into account. But these models are not real.

Stochastic models [6], which take into account random variables influencing the behavior of the system, are used for greater credibility.

In the literature, there are many results of traffic flow analysis based on the mentioned models [1] – [6]. Less research is based on the general theory of systems [7] and its basic concepts – organization, order, self-organization [8, 9].

From the positions of synergy [8, 9], a science that studies the common ideas and organization laws of systems, the traffic flow is a complex non-linear dynamic system. Its state is uniquely defined by a set of variables and the law describing the variation (evolution) of the initial state in time is known.

As it is explained in [9], phenomena arising from the joint action of various factors, each of which does not itself have the same effect, occur in complex systems. Any change in system parameters causes processes that build or break down its structures (synergies). Thus, it is gradually getting to self-organizing and complicating the structure of the system in order to perform new functions.

From synergic positions [8, 9], the macroscopic behavior of the system is described by one or more control parameters and row parameters. The mechanism of interaction between these parameters and the processes in the system determines its evolution.

The traffic flow considered in a synergic aspect is a self-organizing system in which order and chaos parallelly exist. It is subjected to a number of internal and external disturbances (Fig.1) caused by random factors. They lead to fluctuations that can bring it from one state to another.

According to the conventional classification of dynamic systems [7], the traffic flow can be defined as an open dissipative system because the number of elements in it is not constant. Furthermore, there is a continuous exchange of information and/or energy with the external environment as it is shown in Fig. 1.

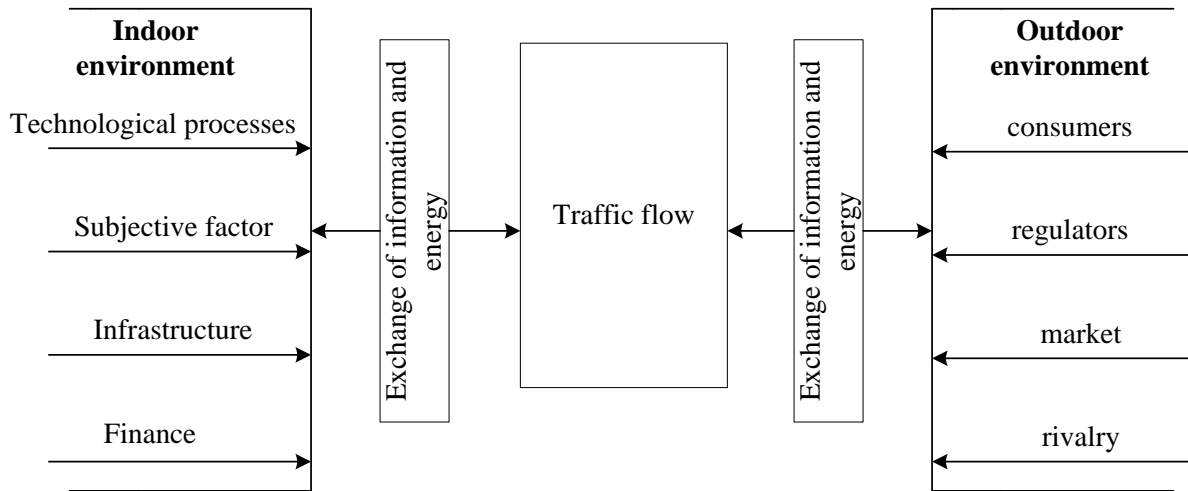


Figure 1: Traffic flow as an open dissipative system

The pentagram, shown in Fig. 2, can be given as an illustration of the prerequisites for application of the synergic approach in the analysis of the processes in the traffic flow.

The properties of coherence and reflexivity in this case refer to the consistency and reporting of implicit prerequisites and the logic of the development of the traffic flow processes.

In order to analyze the traffic flow through the main constructions of synergy – order, chaos, self-organization, an adequate mathematical model is needed to study the processes of self-organization and evolution.

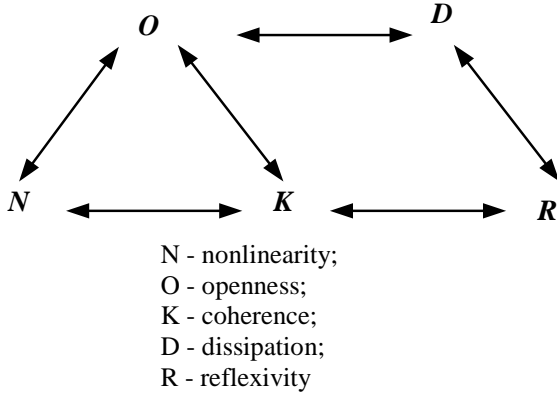


Figure 2: Pentagram of the synergic characteristics of the traffic flow

The purpose of the present work is to propose a model of a traffic flow in the form of a non-linear dynamic system. The model is based on the classic example of complex dynamic systems – the Lorenz equations. Through Mathcad's simulation, the dynamics of the processes in the model when changing its parameters has been studied.

## 2. MODEL OF A TRAFFIC FLOW THROUGH THE LORENZ SYSTEM

As it is known [8, 9], the Lorenz system is the simplest continuous non-linear dynamic system of third order, of the type:

$$\frac{\partial X_i}{\partial t} = F_i \left[ \left( X_1, \dots, X_n, x^j, t \right), \lambda_k \right], \quad (1)$$

where:

$X_i(x^j, t), j = 1 \div 3$ , is the set of variables in function of spatial coordinates  $x^j$  and the time  $t$ ;

$F_i$  - Non-linear functions;

$\lambda_k$  - control parameters;

$i = 1, 2, 3$  - number of degrees of freedom

It consists of three differential equations::

$$\begin{cases} \dot{x} = \sigma(y - x) \\ \dot{y} = \rho x - y - xz \\ \dot{z} = xy - \beta z \end{cases} \quad (2)$$

where  $\sigma, \rho$  and  $\beta$  are parameters,  $x(t), y(t), z(t)$  – variables.

The choice of Lorenz system for modeling of a traffic flow is also based on the fact that Eq. (2) can be written by dissipative members inversely proportional to the times of relaxation of the variables [10]. Thus the Lorenz system can also be used to analyze the self-organization phenomenon.

Given that each flow is characterized by the basic parameters:

- Intensity of movement
- Rate of change
- Density,

the following correspondence is introduced for the variables of Eq. (2).

It is accepted:

- $x(t)$  corresponds to the intensity of the traffic flow;
- $y(t)$  corresponds to traffic flow speed;
- $z(t)$  corresponds to the density of the traffic flow.

The parameter  $\sigma$ , which in this case reflects the intensity of the fluctuations from external disturbances, is accepted as a control parameter in Eq. (2).

The model described has been simulated in Mathcad. The value  $\sigma = 10$  has been initially set to the control parameter. A process whose phase portrait is shown in Fig. 3 has been realized.

The process's phase portrait changes with a small change in the control parameter  $\sigma$ .

The phase portrait of the model at  $\sigma = 12$  is shown in Fig. 4 and at  $\sigma = 15$  – in Fig. 5.

The classical attractor of Lorenz, shown in Fig. 6, is obtained at  $\sigma = 17$ .

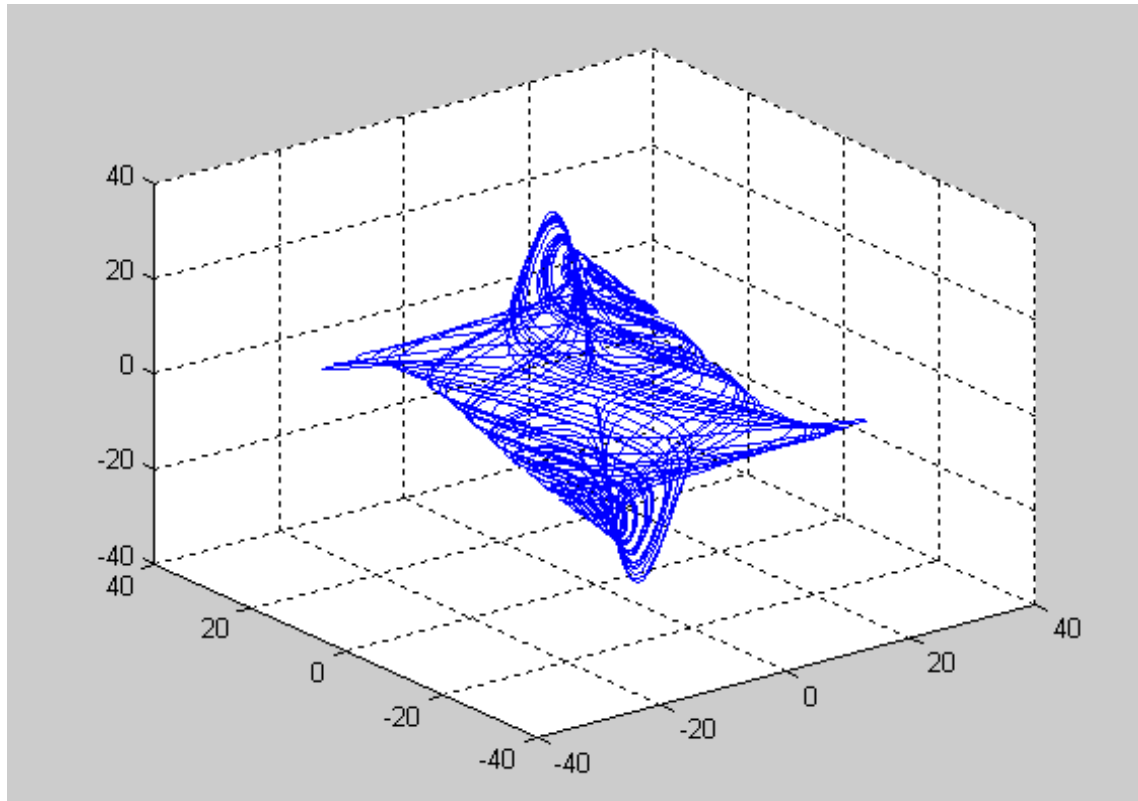


Figure 3: Phase portrait of the model at  $\sigma = 10$

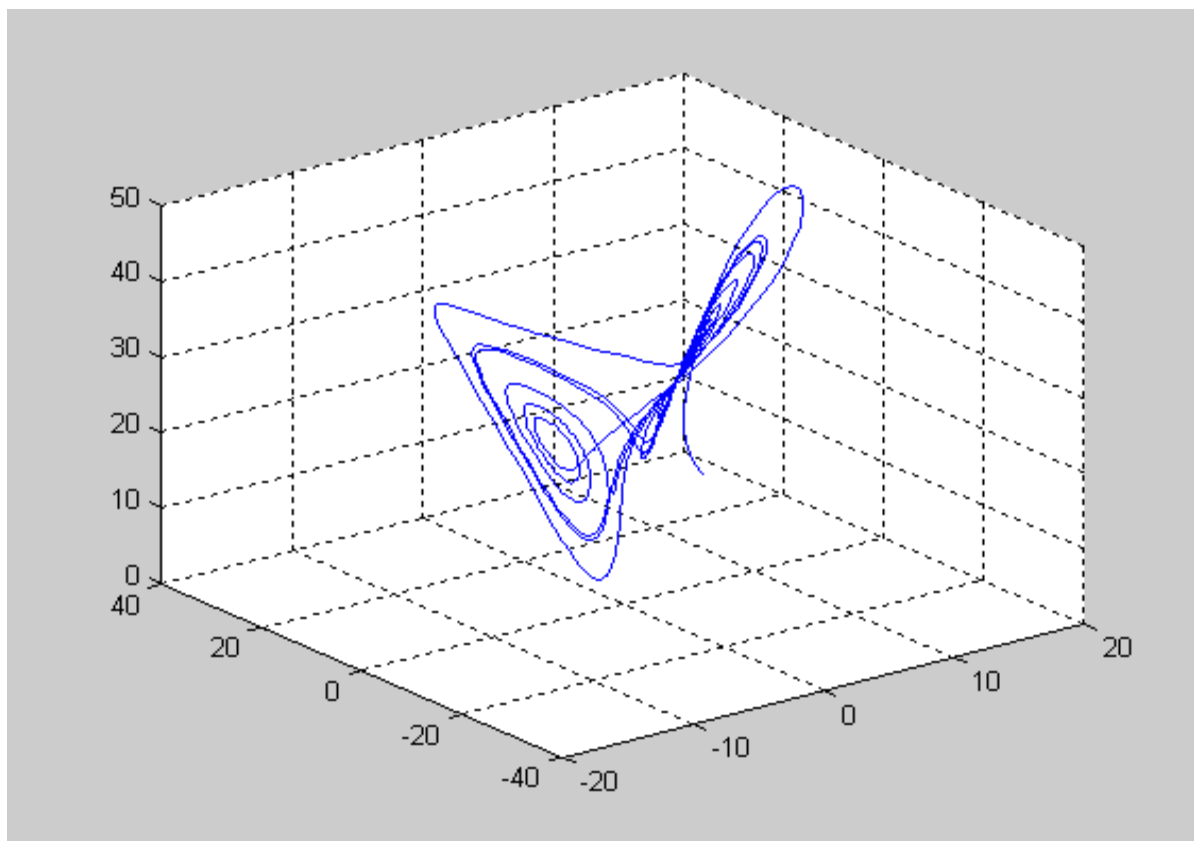


Figure 4: Phase portrait of the model at  $\sigma = 12$

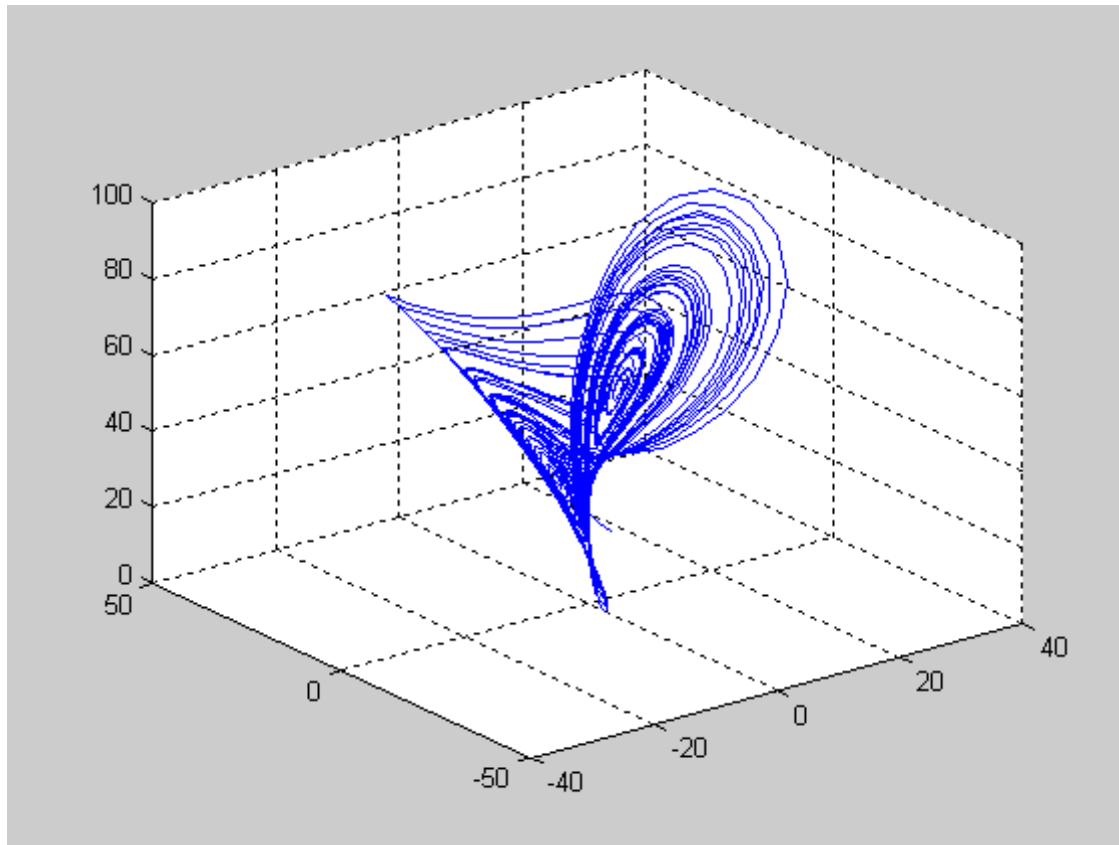


Figure 5: Phase portrait of the model at  $\sigma = 15$

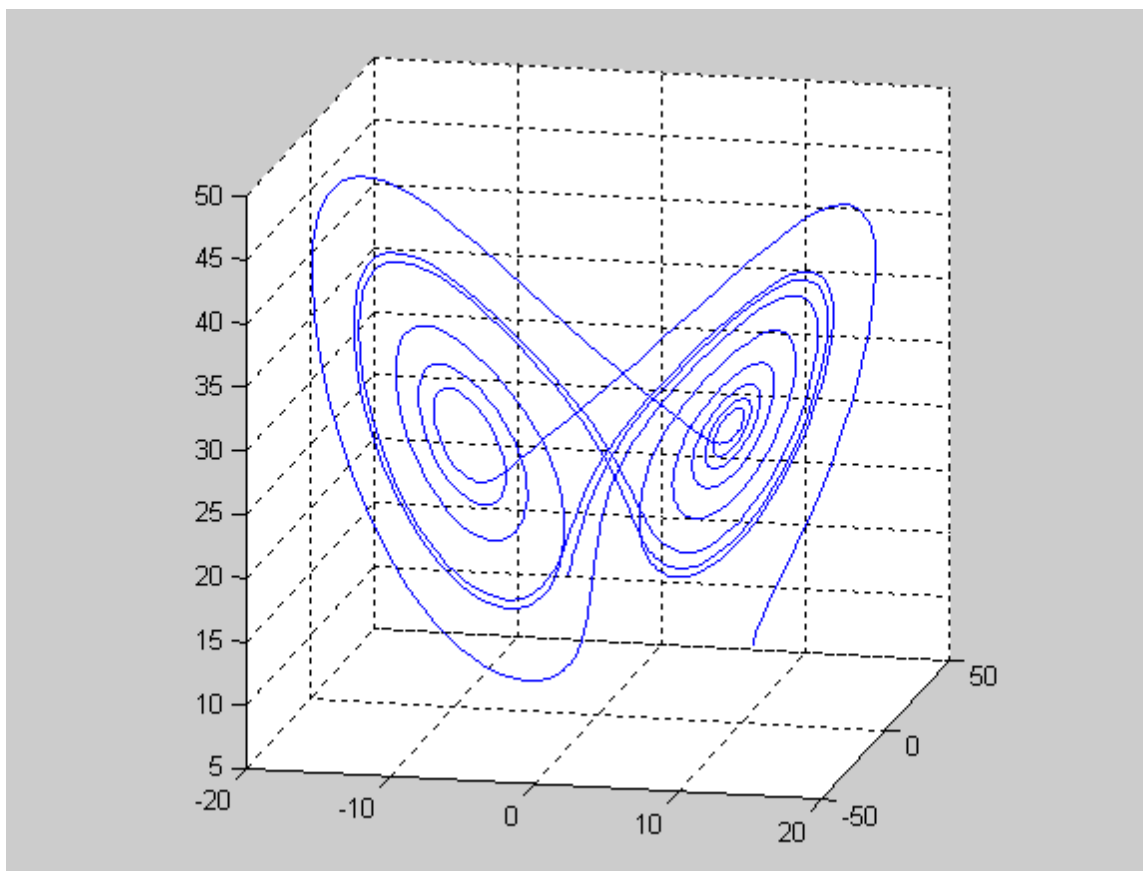


Figure 6: Chaotic Mode at  $\sigma = 17$

### 3. EVALUATION OF THE IMPACT OF EXTERNAL DISTURBANCES ON THE TRAFFIC FLOW

The proposed traffic flow model based on the Lorenz system can also be used to assess the impact of external disturbances on the flow intensity. For this purpose, the theory outlined in [10, 11, and 12] on the influence of noise on synergic systems is used.

$$\begin{cases} \dot{x} = -\frac{x}{\tau_x} + y \\ \dot{y} = -\frac{y_0 - y}{\tau_y} - g_y xz + g_x \sigma \xi(t) \\ \dot{z} = g_z xy - \frac{z}{\tau_z} \end{cases} \quad (3)$$

where  $g_x$ ,  $g_y$  and  $g_z$  are coefficients reflecting feedback in the system;

$y_0$  is the stationary value to which the function  $y(t)$  reaches for the time of relaxation.

External impact is presented as a source of multiplicative stochastic disturbances  $\xi(t)$  [13-18].

The simplest case of white noise disturbances has been considered. Then  $g_x = \sqrt{2}$  [10].

After converting the system Eq. (3), we obtain a differential equation for the variable  $x(t)$ :

$$\frac{dx(t)}{dt} = -x(t) \left[ 1 - \frac{1}{1+x^2(t)} y_0 \right] + \sigma \frac{x(t)\sqrt{2}}{1+x^2(t)} \xi(t) = f(x) \quad (4)$$

where:

$$f(x) = \frac{\partial V(x)}{\partial x} \quad (5)$$

$$V(x) = \frac{1}{2} \left[ x^2 - y_0 \ln(1+x^2) \right] \quad (6)$$

Thus, the system Eq. (3) is reduced to a one-parametric stochastic equation of the type Eq. (4), which takes into account the effect of external random disturbances on the intensity of the traffic flow.

According to [10, 11], the decisions of Eq. (4) are determined by the Focker-Plank equation [15] regarding the density of probability for a transition in a Markov process:

$$\frac{\partial p(x,t)}{\partial t} = -\nabla J(x,t) \quad (7)$$

where  $\nabla \equiv \frac{\partial}{\partial x}$

and the variable

$$J(x,t) = f(x)p(x,t) + \frac{\sigma^2}{2} \nabla \left[ g_x^2 p(x,t) \right] \quad (8)$$

is a probability flow.

In [15], a fixed solution of the Foker-Plank equation at probability

$$p_{st}(x) = \lim_{t \rightarrow \infty} p(x,t) \quad (9)$$

and probability flow

$$J(x) = f(x)p_{st}(x) + \frac{\sigma^2}{2} \nabla \left[ g_x^2 p_{st}(x) \right] = const \quad (10)$$

is exposed.

The stationary decision determines the limits of the sustainable area of variation of the traffic flow intensity depending on external disturbances for the model under consideration.

### 4. CONCLUSION

Transport flows, viewed as a complex dynamic system, obey the general laws and the synergy between chaos and order in their development. This allows modelling through the theory of nonlinear dynamics. The proposed traffic flow model, based on the Lorenz system, enables the flow dynamics to be studied according to its basic parameters. It can also offers opportunity to analyze the impact of disturbances caused by random factors on the intensity or other characteristics of the traffic flow.

### REFERENCES

- [1] Helbing D., "Improved fluid-dynamic model for vehicular traffic". Phys. Rev.E. Vol.51/95, pp.3163-3169 (1995)
- [2] Prigogine I., R. Herman, "Kinetic theory of vehicular traffic". American Elsevier, N.Y. (1971)
- [3] Paveri-Fontana S.L., "On Boltzmann-like treatments for traffic flow: A critical review of the basic model and an alternative proposal for dilute traffic analysis". Transportation Research. 1975. V. 9. № 4, pp. 225-235. (1975)
- [4] Adewumi A., J. Kagamba, A. Alochukwu, "Application of Chaos Theory in the Prediction of Motorised Traffic Flows on Urban Networks". Mathematical Problems in Engineering.V.2016, Article ID 5656734, pp. 15-31 (2016)
- [5] Shu-Zhi Zhao, Tong-He Ni, Yang Wang, Janice P.Li, "Train station passenger flow study". Proceedings of the Winter Simulation Conference. 2000, pp. 1173-1177 (2000)
- [6] Xiang-Tao Gao. "A new approach to the prediction of passenger flow in a transit system". Computers and Mathematics with Applications 61/2011, pp. 1968-1974 (2011)
- [7] Jackson E.A. "Perspectives of Nonlinear Dinamics". Vol. I, II, Cambridge Univ. Press, Cambridge, (1990)
- [8] Haken H. "The Science of Structure: Synergetics". Van Nostrand Reinhold, (1981)
- [9] Haken H., "Synergetics. Introduction and Advanced Topics". Springer-Verlag Berlin Heidelberg, (2004)
- [10] Olemskoi A., "Theory of stochastic systems with singular multiplicative noise". UFN, 1998, Volume 168, Number 3, pp. 287-321 (1998).
- [11] Olemskoi A. "In Physics Reviews". Ed. IM Khalatnikov. 18 Part/11, (1996).
- [12] Zinn-Justin J., "Quantum Field Theory and Critical Phenomena". NewYork: Oxford Science, (1990).

- [13] Horsthemke W., Lefever R. "Noise Induced Transitions". Springer-Verlag, Berlin, Heidelberg, New York, Tokyo p.395. (1984)
- [14] Dimitrov V., Indirect Identification of the Disturbances by Programmable Logic Controller Simatic S7-200, XLVI International Scientific Conference on Information, Communication and Energy Systems and Technologies ICEST 2011, Serbia, Niš, June 29 - July 1, 2011, Proceedings of Papers, Vol. 3, ISBN: 978-86-6125-033-0, pp. 1018 – 1021 (2011)
- [15] Risken H. The Fokker - Planck Equation. Berlin: Springer-Verlag, (1989).
- [16] Dimitrov V., Study of sensors specific to contemporary electric vehicles, Scientific Journal "Mechanics, Transport, Communications", ISSN 1312-3823, issue 12, 1, ID № 0933, (2014)
- [17] Helbing D. Traffic and related self-driven many particparticle systems // Reviews of modern physics. Vol. 73. № 4, pp. 1067-1141. (2001).
- [18] Kolesnichenko A. Self-organizing of Synchronized Traffic Flows under Influence of Noise-induced Transitions. IPM №57/2013, pp.19-39. (2013)

# Dynamic Fault Trees. Computation of Parameters – Part I

Emilia Dimitrova<sup>1\*</sup>, Plamen Atanasov<sup>2</sup>

<sup>1</sup>Department of Telecommunications and Safety Equipment and Systems, Todor Kableshkov Higher School of Transport, Sofia (Bulgaria)

<sup>2</sup>Department of Telecommunications and Safety Equipment and Systems, Todor Kableshkov Higher School of Transport, Sofia (Bulgaria)

*Risk analysis is an important activity to ensure that critical assets, like medical devices and nuclear power plants, operate in a safe and reliable way. Fault Tree analysis (FTA) is one of the most prominent techniques, used by a wide range of industries. Fault Trees (FTs) are a graphical method that model how failures propagate through the system, that is, how component failures lead to system failures. FTA investigates whether the system design is dependable enough. It provides methods and tools to compute a wide range of properties and measures. FTs can roughly be described as directed acyclic graphs, whose leaves model component failures and whose gates - failure propagation. Dynamic Fault Trees (DFTs) are the best known extensions to Static Fault Trees (SFTs). DFTs are capable of expressing features that are not expressible in SFTs, like spare management, different operational modes, dependent events. These properties of DFTs make them suitable for many situations, where SFTs cannot be applied. This paper will discuss the main methods for computation of some of the parameters of a DFT.*

**Keywords: Risk analysis, Fault tree, simulation, computation, dynamic**

## 1. INTRODUCTION

Risk analysis is a key feature in reliability engineering: in order to design and build transport systems, smart grids, and internet shops that meet the required dependability standards, we need to assess how dependable these systems are, and take appropriate measures if they are not dependable enough. This analysis is most useful when carried out at design time. Then important reliability decisions are made concerning the system architecture, the level of redundancy and spare management.

One method for risk analysis is a type of graph - more precisely, directed acyclic graph - the Fault Tree. Fault Trees were introduced in the 1960s at Bell Labs for the analysis of a ballistic missile. Fault Tree Analysis (FTA) identifies, models and evaluates the unique interrelationship of events leading to: Failure, Undesired Events / States, Unintended Events / States. Nowadays FTA plays an important role in product certification, and to show conformance to legal requirements. In the European Union, legislature mandates that employers assess and mitigate the risks that workers face [1]. FTA can be applied in this context, for example to determine the conditions under which a particular machine is dangerous to workers [1].

The better-known Static Fault Tree cannot model the dependability behavior of systems in which the consistency of origins of failures is crucial. Dynamic Fault Trees (DFTs) extend Standard (or Static) Fault Trees with a number of intuitive gates. These gates facilitate the modelling of often recurring concepts in reliability engineering: spare management, functional dependencies, and order-dependent behaviour. Three methods for analysis of DFTs will be presented in the next sections.

## 2. TYPES OF FAULT TREES

### 2.1. General notes

There are two important types: Discrete-time FTs equip each BE with a probability  $p$ , representing the probability that the component fails within a certain discrete time interval. In continuous-time FTs, each BE is equipped with a probability distribution  $f$  showing how the failure behaviour evolves over time, i.e.  $F(t)$  represents the probability that the BE is still running at time point  $t$ . The root of the tree, called the top-level event (TE), represents a system failure. FTA typically computes for a given FT the system reliability, i.e. the probability that the system has not failed within a given mission time  $T$ , the mean time to failure (MTTF), i.e. the expected time of a failure to occur, and the availability, i.e. the time that the system is up in the long run.

### 2.2. Static Fault Trees

A Static fault tree consists of two types of nodes: events and gates. An event is an occurrence within the system, typically the failure of a subsystem down to an individual component. Events can be divided into basic events (BEs), which occur spontaneously, and intermediate events, which are caused by one or more other events. The event at the top of the tree, called the top event (TE), is the event being analyzed, modeling the failure of the (sub)system under consideration.

In addition to basic events depicted by circles, Figure 1 shows other symbols for events. An intermediate event is depicted by a rectangle. If an FT is too large to fit on one page, triangles are used to transfer events between multiple FTs to act as one large FT. Finally, sometimes subsystems are not really BEs, but insufficient information is available or the event is not believed to be of sufficient importance to develop the subsystem into a subtree. Such an undeveloped event is denoted by a diamond.

\*Corresponding author: 158 Geo Milev str., Sofia, Bulgaria and edimitrova@bitex.bg

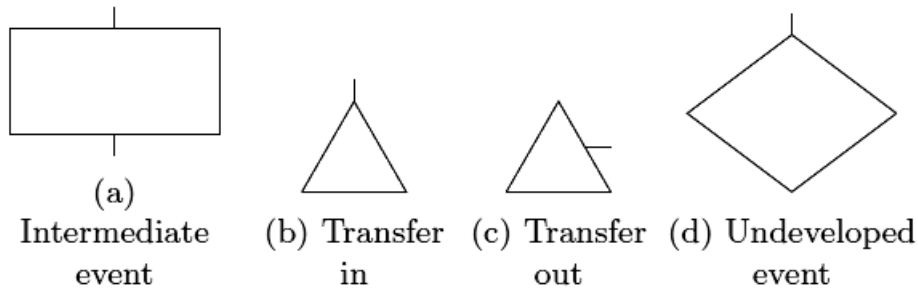


Figure 1: Images of non-basic events in fault trees

Gates represent how failures propagate through the system, that is, how failures in subsystems can combine to cause a system failure. Each gate has one output and one

or more inputs. The following gates are commonly used in fault trees. Images of the gates are shown in Figure 2.

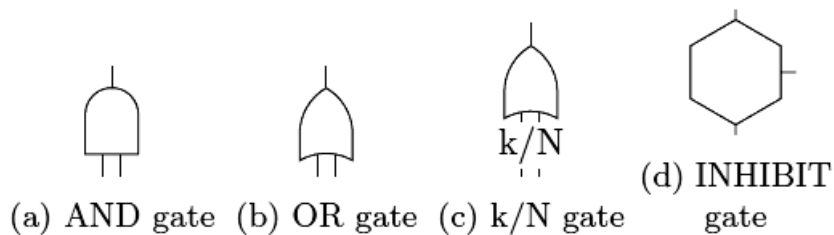


Figure 2: Images of the gates types in a fault tree

- AND - Output event occurs if all of the input events occur.
- OR - Output event occurs if any of the input events occur.
- k/N - Also known as VOTING, has N inputs. Output event occurs if at least k input events occur. This gate can be replaced by the OR of all sets of k inputs, but using one k/N gate is much clearer.
- INHIBIT - Output event occurs if the input event occurs while the conditioning event drawn to the right of the gate also occurs. This gate behaves identically to an AND gate with two inputs, and is therefore not treated in the rest of this paper. It is sometimes used to clarify the system behaviour to readers.

2.3. Dynamic Fault Trees

Traditional FTs can only model systems in which a combination of failed components results in a system failure, regardless of when each of those component failures occurred. In reality, many systems can survive certain failure sequences, while failing if the same components fail in a different order. For example, if a system contains a switch to alternate between a component

and its spare, the failure of this switch after it has already activated the spare does not cause a failure.

The most widely used way of including temporal sequence information in FT is the dynamic fault tree or DFT [1]. Since a DFT considers temporal behaviour, the methods used for the analysis of static FT cannot be directly used to analyze DFT.

The structure of a DFT is very similar to an FT, with the addition of several gate types shown in Figure 3. The new gates are:

- PAND (Priority AND) - Output event occurs if all inputs occur from left to right.
- FDEP (Function DEpendency) - Output is a dummy and never occurs, but when the trigger event on the left occurs, all the other input events also occur.
- SPARE - Represents a component that can be replaced by one or more spares. When the primary unit fails, the first spare is activated. When this spare fails, the next is activated, and so on until no more spares are available. Each spare can be connected to multiple Spare gates, but once activated by one it cannot be used by another. By convention, spares components are ordered from left to right.

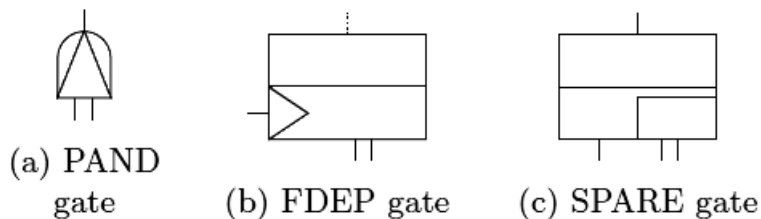


Figure 3: Images of the new gates types in a DFT



BEs can have an additional parameter  $\alpha$  called the dormancy factor. This parameter is a value between 0 and 1, and reduces the failure rate of the BE to that fraction of its normal failure rate if the BE is an inactive input to a SPARE gate [1]. For example, a spare tire will not wear out as fast as one that is in operation. For BEs that are not inputs to a SPARE gate,  $\alpha$  has no effect. The introduction of the PAND gate means that a DFT is not generally coherent: An increase in the failure rate of the right input to a PAND can increase the reliability of the gate. Since the inputs to PAND gates are commonly also inputs to other subtrees, non-coherence is often indicative of a modeling error or suboptimal system design. In non-repairable DFTs the FDEP gate can be removed by replacing its children by an OR gate of the child and the FDEP trigger. In repairable DFT the applicability of this approach depends on the definition of the FDEP gate: If failures triggered by the FDEP require separate repairs, the transformation is not correct. If repair of the FDEP trigger also restores the triggered components to operation, the transformation does preserve the behaviour. Since the output of the FDEP gate is a dummy output and not relevant to the behaviour of the FT, it is often useful to use a pruned input function which does not include FDEP inputs [1]. Some types of DFT have additional gates, which are:

- Hot Spare - Special case of SPARE gate, where the dormance factor of the spares is 1, i.e. the spare failure rate is the same as the normal failure rate [1].

- Cold Spare - Special case of SPARE, with a dormance factor of 0, i.e. spares cannot fail before activated [1].

- Priority OR - Fails when the leftmost input fails before the others [1]. Can be replaced by a PAND and an FDEP.

- Sequence enforcing - Prohibits failures of inputs until all inputs to the left have failed [1]. Can be replaced by (cold) SPARE provided the inputs are not shared with other gates.

Most of the values that can be computed for classic FT can still be used in the analysis of DFT: the reliability, availability, and MTTF are still of interest.

#### 2.4. Fault Trees with dependent events

Classic FT assume that the BE are all statistically independent. This is often not true in practice, as events can have common causes, or the failure of one component can accelerate the failure of another.

For models with particularly complex interdependencies, Bouissou [4] offers a formalism called Boolean logic Driven Markov Processes (BDMP) as an extension to fault trees. In this formalism, events are described by Markov Processes with designated failure states. Then, events in the FT can cause these events to switch to different processes, for example to increase the failure rate if another component fails.

### 3. ANALYSIS OF DYNAMIC FAULT TREES - METHODS

#### 3.1. Analysis by Markov Chains

The first method proposed to analyze DFT was by Dugan et al. [1], and computes the unreliability of the system during a time window  $[0; t]$ . This method converts

the DFT into a Markov Chain, in which the states represent the history of the DFT in terms of what components have failed and, where needed, in what order. Since the number of failed subsets grows exponentially in the number of BEs, this method is not practical for very complex systems.

#### 3.2. Modular analysis of a DFT

Boudali et al. [1] use a different method to calculate the reliability of a DFT, which reduces the combinatorial explosion in many common cases. They provide a compositional semantics for DFT, i.e. each DFT element is interpreted as an Interactive Markov Chain [1] and the semantics of the DFT is the parallel composition of the elements. The papers provide several reduction techniques to minimize the resulting Markov Chain. In addition, it allows DFT to be extended with repairable components and mutually exclusive events. The analysis is performed by converting a DFT into an Input/Output Interactive Markov Chain for analysis. This model is constructed by computing the parallel composition of the I/O IMCs for parts of the tree, down to individual gates and events. Since intermediate models can be analyzed to remove unnecessary states, the total I/O IMC can be much smaller than the Markov Chain produced by earlier methods, and the combinatorial explosion is reduced.

Input/Output Interactive Markov chains (I/O-IMCs) extend interactive Markov chains (IMCs) [1] by integrating features from input/output automata. An I/O-IMC consists of a number of states which are connected via transitions. As in interactive Markov chains, transitions are classified as either Markovian transitions or interactive transitions. Markovian transitions represent a system delay. They are labeled with rates  $\lambda$  indicating that the transition can be taken after an exponentially distributed delay with parameter  $\lambda$ .

On the other hand, interactive transitions are executed instantly. They are labeled with different kinds of actions:

- (a) Input actions (denoted  $a?$ ) can only be taken, if another I/O-IMC executes an output action  $a!$ ; we say that  $a?$  requires synchronization on  $a!$ . The action is thus possibly subject to delays.

- (b) Output actions (denoted  $a!$ ) cannot be delayed and have to be taken immediately. They emit the output signal  $a!$  on which corresponding input actions can synchronize.

- (c) Internal actions (denoted  $a;$ ) cannot be delayed, quite like output actions. However, they are not visible to other I/O-IMCs, i.e. they do not require synchronization.

I/O IMCs are input-enabled, meaning that all states in an I/O-IMC can respond to all input signals from any other I/O-IMC in the considered system.

One of the key properties of I/O-IMCs is that they are compositional. Complex models consisting of various interacting I/O-IMCs can be aggregated in a stepwise, hierarchical manner to obtain one I/O-IMC representation of the whole system.

In [1] it is stated that no synchronisation over Markovian transitions is done. This behaviour is justified by the memoryless property of exponential distributions: if two Markovian transitions with rate  $\lambda$  and  $\mu$  competing for execution, then the remaining delay of the  $\mu$ -transition

after taking the  $\lambda$ -transition is exponentially distributed with rate  $\mu$ .

After the parallel composition of two I/O-IMCs we can hide those actions which are no longer subject to further synchronisation.

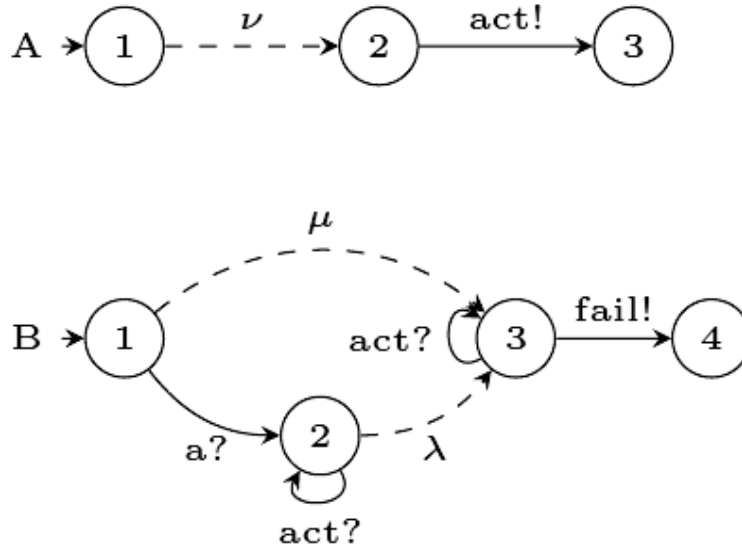


Figure 4: Two examples of I/O IMCs

Let us consider the two I/O-IMCs A and B in Figure 4, where A describes an activation after a delay given by rate  $\nu$  and B describes a dormant BE with dormant failure rate  $\mu$  and active failure rate  $\lambda$ . States are depicted by circles, initial states by an incoming arrow, Markovian transitions by dashed lines, and interacting transitions by solid lines. While A has only one possible path from the initial to the final state, B can either directly reach state 3 by a Markovian transition, or move via state 2. The path taken is determined by a race condition: If the

delay generated by the Markovian transition is shorter than the delay caused by the synchronization on action a, then B executes the transition from state 1 to state 3. When composing A and B (Figure 5) we synchronize on action act. Since B has act as input, it has to wait for A's output action act!. All Markovian transitions and non-synchronising signals are essentially interleaved during composition. All synchronising signals are transformed into internal actions and thereby hidden.

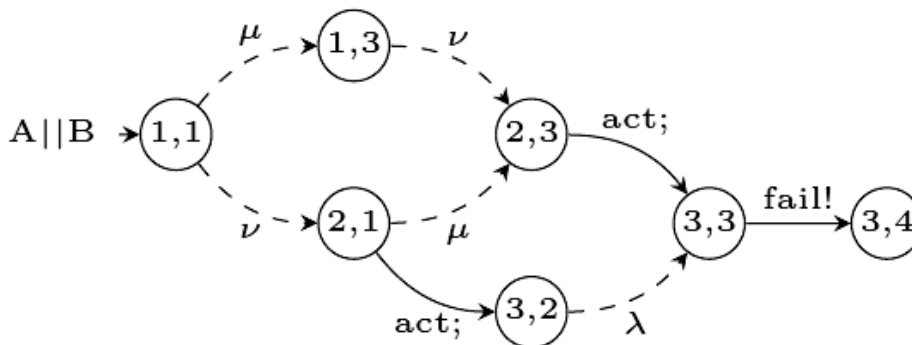


Figure 5: Parallel composition of A and B, hiding signal act

Unlike traditional Markov Chains, I/O IMC are capable of modeling non-determinism between actions.

In earlier development of the DFT modeling formalism, the semantics (i.e. the model interpretation) of some DFT configurations, where FDEP gates are used, remains unclear. For instance, in Figure 6, the FDEP gate triggers the failures of two basic events ( $E_2$  and  $E_3$ ). Does this mean that the dependent events fail simultaneously and if so which spare gate gets the shared spare  $E_4$  (in configuration b)? In [7], it is mentioned that these special cases are dealt with by systematically removing the non-determinism by transforming it into a probabilistic (or deterministic) choice. Moreover, if the non-determinism was not intended, then its detection indicates that an error

occurred during the model specification. Non-determinism could also be an inherent characteristic of the system being analyzed, and should therefore be explicitly modeled. An example of such a system would be a repairman following a first failed first repaired policy and being in charge of two components. Now, if both components fail at the same time, then we might decide to model the choice of which one to pick first for repair to be a non-deterministic choice made by the repairman.

In the I/O-IMC formalism, the DFT configuration depicted in Figure 6 will be interpreted as follows: Whenever the dependent events failure has been triggered, then the trigger event (the cause) happened first and was then immediately (with no time elapsing) followed by the

failure of the dependent events (the effect). This adheres to the classical notion of causality. Moreover, the dependent events fail in a non-deterministic order (i.e. essentially consider all combinations of ordering). In this case, the final I/O IMC model is not a Continuous-Time Markov

chain (CTMC) but rather a Continuous-Time Markov decision process (CTMDP), which can be analysed by computing bounds of the performance measure of interest ([8] gives an efficient algorithm on analysing CTMDP).

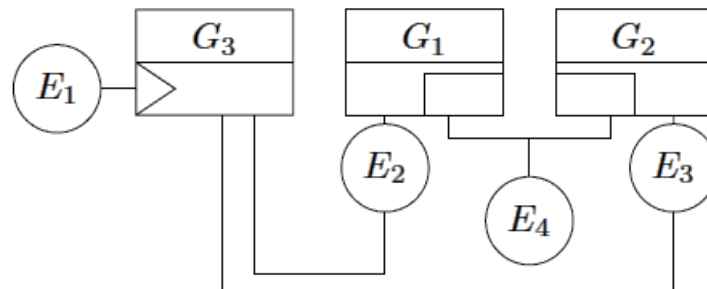


Figure 6: The occurrence of non-determinism

### 3.3. Monte Carlo Simulation

Monte Carlo methods can also be used to compute the system reliability. Most techniques are designed for continuous-time models [1] or qualitative analysis [1], but adaptation to discrete-time models is straightforward. Each component is randomly assigned a failure state based on its failure probability. The FT is then evaluated to determine whether the TE has failed. Given enough simulations, the fraction of simulations that does not result in failure is approximately the reliability.

Quantitative Monte Carlo analysis can be performed using the method by Durga Rao et al. [1], which can also be applied if the components are individually independently repairable.

Boudali et al. [1] developed a program to analyze DFT using Monte Carlo simulation. It allows BE failure distributions to change over time, and even based on different clocks for different BE, resulting in non-Markovian models. This is useful when, for example, a system takes time to warm up and this affects the failure rates.

If very high performance is required, it is possible to construct a hardware circuit to perform Monte Carlo Simulations much faster than normal computer simulation. Such an approach is described by Aliee and Zarandi [1].

## 4. TYPES OF PARAMETERS OF A DFT

### 4.1. Reliability

The reliability of a continuous-time FT  $F$  is the probability that it operates for a certain amount of time without failing.

In continuous-time systems, the reliability in a certain time period can be calculated by conversion into a discrete-time system, taking BE probabilities as the probability of failure within the specified timeframe.

### 4.2. Availability

The availability of a system is the probability that the system is functioning at a given time. Availability can also be calculated over an interval, where it denotes the fraction of that interval in which the system is operational. Availability is particularly relevant for repairable systems,

as it includes the fact that the system can become functional again after failure. For nonrepairable systems, the availability in a given duration may still be useful. The long-run availability always tends to 0 for nontrivial non-repairable systems, as eventually some cut set will fail and remain nonfunctional.

As the availability at a specific time is a simple probability, it is possible to treat the FT as a discrete-time FT, by replacing the BE failure distribution with the probability of being in a failed state at the desired time. The discrete-time reliability of the resulting FT is then the availability of the original. Failure probabilities of the BE are usually easy to calculate, also for repairable systems. Long-term availability of a system can be calculated the same way, provided the limiting availability of each BE exists. This is the case for most systems. Availability over an interval cannot be calculated so easily. Since this availability is defined as an integral over an arbitrary expression, no closed-form expression exists in the general case. Numerical integration techniques can be used should this availability be needed.

### 4.3. Mean Time To Failure (MTTF)

The Mean Time To Failure (MTTF) describes the expected time from the moment the system becomes operational, to the moment the system subsequently fails.

In repairable systems the time to failure depends on the system state when it becomes operational. The first time, all components are operational, but when the system becomes operational due to a repair, some components may still be nonfunctioning. This difference is made explicit by distinguishing between Mean Time To First Failure (MTTFF) and MTTF.

While MTTF and availability are often correlated in practise, only the MTTF can distinguish between frequent, short failures and rare, long failures.

### 4.4. Mean Time Between Failures (MTBF)

For repairable systems, the Mean Time Between Failures (MTBF) denotes the mean time between two successive failures. It consists of the MTTF and the Mean Time To Repair (MTTR). In general, it holds that

$$MTBF = MTTR + MTTF \tag{1}$$

The MTBF is useful in systems where failures are particularly costly or dangerous, unlike availability which focuses more on total downtime. For example, if a railroad switch failure causes a train to derail, the fact that an accident occurs is much more important than the duration of the subsequent downtime. The MTTR is often less useful, but may be of interest if the system is used in some time-critical process. For example, even frequent failures of a power supply may not be very important if a battery backup can take over long enough for the repair, while infrequent failures that outlast the battery backup are more important.

## 5. CONCLUSION

Three major quantitative methods for analysis of DFT were presented. The first one - with Markov chains (CTMC) is only preferable for smaller and less complex systems, because the CTMC becomes too large (its size grows exponentially with the number of BEs). The other two methods are more promising for complex systems. The analysis with I/O IMC is harder to implement and apply, yet it allows the creation of smaller models compared to the method with CTMC. The I/O IMC method also allows computation of parameters of DFTs with non-determinism. The Monte Carlo method has many applications and advantages, but in order to compute parameters of a DFT, the hardware, on which this simulation is realised, has to be with enough memory and processing power in order to benefit from the full potential of this method.

## REFERENCES

- [1] E. Ruijters, M.I.A. Stoelinga, "Fault tree analysis: A survey of the state-of-the-art in modeling, analysis and tools", *Computer Science Review* 15-16 (2015), pp. 29-62, (2015)
- [2] F. Arnold, A.F.E. Belinfante, F.I. Van der Berg, D. Guck, M.I.A. Stoelinga, "DFTCalc: A Tool for Efficient Fault Tree Analysis", 32nd International Conference on Computer Safety, Reliability and Security (SAFECOMP'13). LNCS. Springer, (2013)
- [3] G. Merle, "Algebraic modelling of Dynamic Fault Trees, contribution to qualitative and quantitative analysis", Ph.D. thesis, École normale supérieure de Cachan - ENS Cachan, (2010)
- [4] M. Bouissou, "BDMP (Boolean logic Driven Markov Processes) as an alternative to Event Trees", in: Proc. European Safety and Reliability Conf. (ESREL), (2008)
- [5] <http://www.fmt.ewi.utwente.nl/puptol/dftcalc/>
- [6] <https://sourceforge.net/projects/visualfigaro/files/>
- [7] H. Boudali, P. Crouzen, M. I. A. Stoelinga, "Dynamic fault tree analysis using Input/Output interactive Markov chains", In DSN, pp. 708-717, (2007)
- [8] C. Baier, H. Hermanns, J.-P. Katoen, B. R. Haverkort, "Efficient computation of time-bounded reachability probabilities in uniform continuous-time Markov decision processes", *Theor. Comput. Sci.*, 345(1):2-26, (2005)

## Dynamic Fault Trees. Computation of Parameters – Part II

Plamen Atanasov<sup>1</sup>, Emilia Dimitrova<sup>1\*</sup>

<sup>1</sup>Department of Telecommunications and Safety Equipment and Systems, Todor Kableshkov Higher School of Transport, Sofia (Bulgaria)

*Risk analysis is a crucial activity to ensure that critical assets, like medical devices and nuclear power plants, operate in a safe and reliable way. Fault Tree analysis (FTA) is one of the most prominent techniques, used by a wide range of industries. Fault Trees (FTs) are a graphical method that model how failures propagate through the system, that is, how component failures lead to system failures. FTA investigates whether the system design is dependable enough. It provides methods and tools to compute a wide range of properties and measures. FTs can roughly be described as directed acyclic graphs, whose leaves model component failures and whose gates - failure propagation. Dynamic Fault Trees (DFTs) are the best known extensions to Static Fault Trees (SFTs). DFTs are capable of expressing features that are not expressible in SFTs, like spare management, different operational modes, dependent events. These properties of DFTs make them suitable for many situations, where SFTs cannot be applied. It is therefore wise to be aware of the existing software for quantitative analysis of DFTs, as many types of systems can be described using this kind of FTs. This paper will examine the computation of failure probabilities and the characteristics of DFTs with two software products - DFTCalc, a tool for Input/Output Interactive Markov chain analysis of DFTs and YAMS, a tool for Monte Carlo simulation of DFTs.*

**Keywords: Risk analysis, Fault tree, simulation, computation, dynamic**

### 1. INTRODUCTION

Risk analysis is an important feature in reliability engineering: in order to design and build transport systems, smart grids, and internet shops that meet the required dependability standards, we need to assess how dependable these systems are, and take appropriate measures if they are not dependable enough. This analysis is most useful when carried out at design time. Then important reliability decisions are made concerning the system architecture, the level of redundancy and spare management. One method for risk analysis is a type of graph - the Fault Tree.

The known Static Fault Tree cannot model the dependability behavior of systems in which the consistency of origins of failures is crucial. Dynamic Fault Trees (DFTs) extend Static Fault Trees with a number of intuitive gates. These gates facilitate the modelling of often recurring concepts in reliability engineering: spare management, functional dependencies, and order-dependent behaviour. There are three major methods for analysis of DFTs (others also exist) - with Continuous-Time Markov Chains, with Input/Output Interactive Markov Chains and with Monte Carlo Simulation. Each method has its advantages and disadvantages. Two software products for computation of the parameters of a DFT will be presented - DFTCalc and YAMS. DFTCalc uses the second method and YAMS uses the third method.

### 2. COMPUTATION WITH DFTCALC

DFTCalc can compute a number of different reliability metrics. This includes properties such as:

- (1) Timed-Reliability: the probability that the system fails until a given time point  $T$  or in a given interval  $[T; T']$ ;
- (2) Mean Time To Failure: the expected time to a system failure;
- (3) Reliability: the probability that the system fails in the long-run.

In case of nondeterminism, DFTCalc calculates the minimum and maximum values for the above metrics. Each of these properties can either be evaluated from the initial state (i.e. the system is fully functional), or by setting evidence (i.e. certain components have failed already).

Whereas traditional FTA methods translate a DFT into a large and monolithic Continuous-Time Markov Chains (CTMC), DFTCalc does this in a stepwise fashion: First, DFTCalc translates each element (i.e., gate or BE) into an I/O IMC (and thus computation of non-deterministic). Then, DFTCalc obtains the underlying CTMC by composing all I/O-IMCs. DFTCalc composes these I/O-IMCs one-by-one, and employs aggressive state space compression technique in each step, to keep the state space minimal.

DFTCalc combines dedicated code and the state-of-the-art model checkers CADP, MRMC and IMCA (Fig. 1):

- CADP supports construction, minimisation and analysis of IMCs. It compiles and generates the state space from a LotosNT [1] specification. The compositional verification engine of CADP can compose a network of communicating IMCs. The tool set also enables minimisation modulo strong and branching bisimulation.
- MRMC is a model checker for discrete-time and continuous-time Markov reward models.

(select example)

DFT:

```

toplevel "A";
"A" or "A1" "A2";
"A1" and "P" "B";
"P" lambda=0.0001 dorm=0;
"B" lambda=0.0001 dorm=0;
"A2" pand "S" "P";
"S" lambda=0.001 dorm=0;

```

Compute unreliability in interval  $[0,T]$ ,  
 for mission times  $T$  ( $T > 0$ ), given as

list of values   
 range, from:  to:  step:

Model checker:  MRMC  IMCA

Compute unreliability in interval  $[T_1, T_2]$   
 T1:  T2:

Compute MTTF  
 (for plot: to:  step:  )

Evidence:

---

Error bound: Prob:  Time:  DFT:

---

Version:  Verboisity: 
 Coloured output  No pointmarks

---

Data set name:

---

Figure 1: View of the web interface of DFTCalc

- IMCA is a tool for the quantitative analysis of IMCs. In particular, it supports the verification of IMCs against unbounded reachability, time- and interval-bounded reachability, expected-time objectives, and long-run average objectives.

DFTCalc can be used by downloading a stand-alone version, and via a web interface. Both are accessible at <http://fmt.cs.utwente.nl/tools/dftcalc/>. DFTCalc is open source, but requires a license for CADP, which is free for academic institutions. The web interface (Figure 1) is realised with the use of PUPTOL and extends the downloadable version with a GUI as well as the plot function. It allows the user to (1) input DFT models via a text screen; (2) select the dependability metrics. This can be (a) the reliability for one or more mission times  $x$ , or (b) the probability on a system failure during an interval  $[T1; T2]$ , or (c) the mean time to failure; (3) set various

options: which model checker to use; the error bound, the level of verbosity, and whether to color output. The results can be given either by numbers, via the button show result, or as a plot, via the button plot result. The input and configuration of the web interface can be saved via the button permalink.

### 3. COMPUTATION WITH YAMS

#### 3.1. KB3

In order to compute the parameters of a DFT with YAMS, it has first to be drawn in KB3, part of the project Visual Figaro [6], which includes YAMS. The model also has to be exported from KB3 to FIGARO0 text file. Figure 2 shows one such tree. Of the new dynamic gates KB3 has only PAND, yet [3] shows equivalent transformations for other dynamic gates using the static ones and PAND.

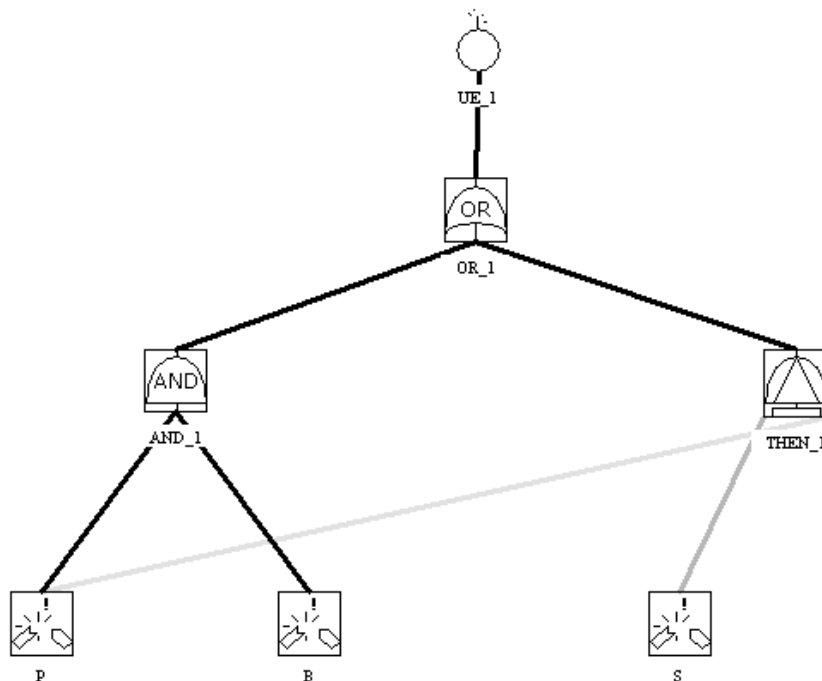


Figure 2: A DFT, drawn in KB3

#### 3.2. Simulation Settings Tab

Figure 3 gives a view of the main window of YAMS with the Simulation Settings Tab active.

The threshold settings allow to limit the search for sequences.

Certain settings are compulsory because they are railings intended to prevent the program from remaining blocked in an infinite loop (number of turns in the interaction rules and number of fixed time firings), the others can be inhibited by using the adjacent checkbox (ticking the compartment consists in activating the setting). The setting "max turns in interaction rules" limits the number of runs of the interaction rules of a stage; if the stabilization of the system is not obtained at the end of this number of turns, the sequence is stopped and is not taken into account for the calculation of the indicators.

The parameter "max fixed time firings" limits the number of successive instant states; if this number is exceeded, the sequence is stopped and is not taken into account for the calculation of the indicators.

The setting "max branches" limits the number of branches of a sequence (a branch allows to pass from a state to the other one); if this number is exceeded, the sequence is stopped and is not taken into account for the calculation of the indicators.

The setting "max histories simulated" limits the number of histories (of sequences) simulated; if this number is reached, the simulation is stopped.

The setting "max real time (mn)" limits the duration of the simulation (user time in minutes); if this time is reached, the simulation is stopped.

At least one of the two latter parameters must be active so that the simulation can be launched (existence of a stop criterion).

The instants can be described under two forms:

- Instant: absolute time from the 0 instant which is the beginning of any sequence,
- Interval: series of instants distributed in an interval defined by its time of beginning ( $T0 \geq 0$ ), its time of ending ( $T1 \geq T0$ ) and the number of stages of sampling ( $N > 0$ ).

Example : with  $T_0 = 0$ ,  $T_1 = 10$ ,  $N = 5$ , the defined instants are : 0, 2, 4, 6, 8, 10.

“Add Instant”, “Add Interval” and “Delete” buttons allow to manage the contents of the list.

The settings must be modified directly in the list.

The instants are always added at the head of the list and the intervals at the bottom, but the order of definition of the instants and of the intervals has no influence on the results of simulation.

- Seed of the pseudo random generator

The pseudo random generator is a Markovian process: every firing is deduced from the precedent.

By fixing the seed of the generator, we can define in a fixed way the successive firings done by the generator and thus exactly replay a simulation.

On the other hand, it is possible to have the seed pseudo randomly fired (by basing one’s argument on the current indication of the clock of the machine). This feature is obtained by not ticking the adjacent checkbox.

- Selected groups

The displayed groups constitute all the groups available in the FIGARO0 model.

The group ALL (or TOUT for a french FIGARO0 model) is added to facilitate the acquisition. It groups together all the groups of the model.

The group WITHOUT\_NAME (or SANS\_NOM for a french FIGARO0 model) is not explicitly described in the FIGARO0 model but it groups together all the rules which are not explicitly associated to a group.

The selection of the groups is made by using the adjacent checkboxes (the group is selected if its compartment is ticked).

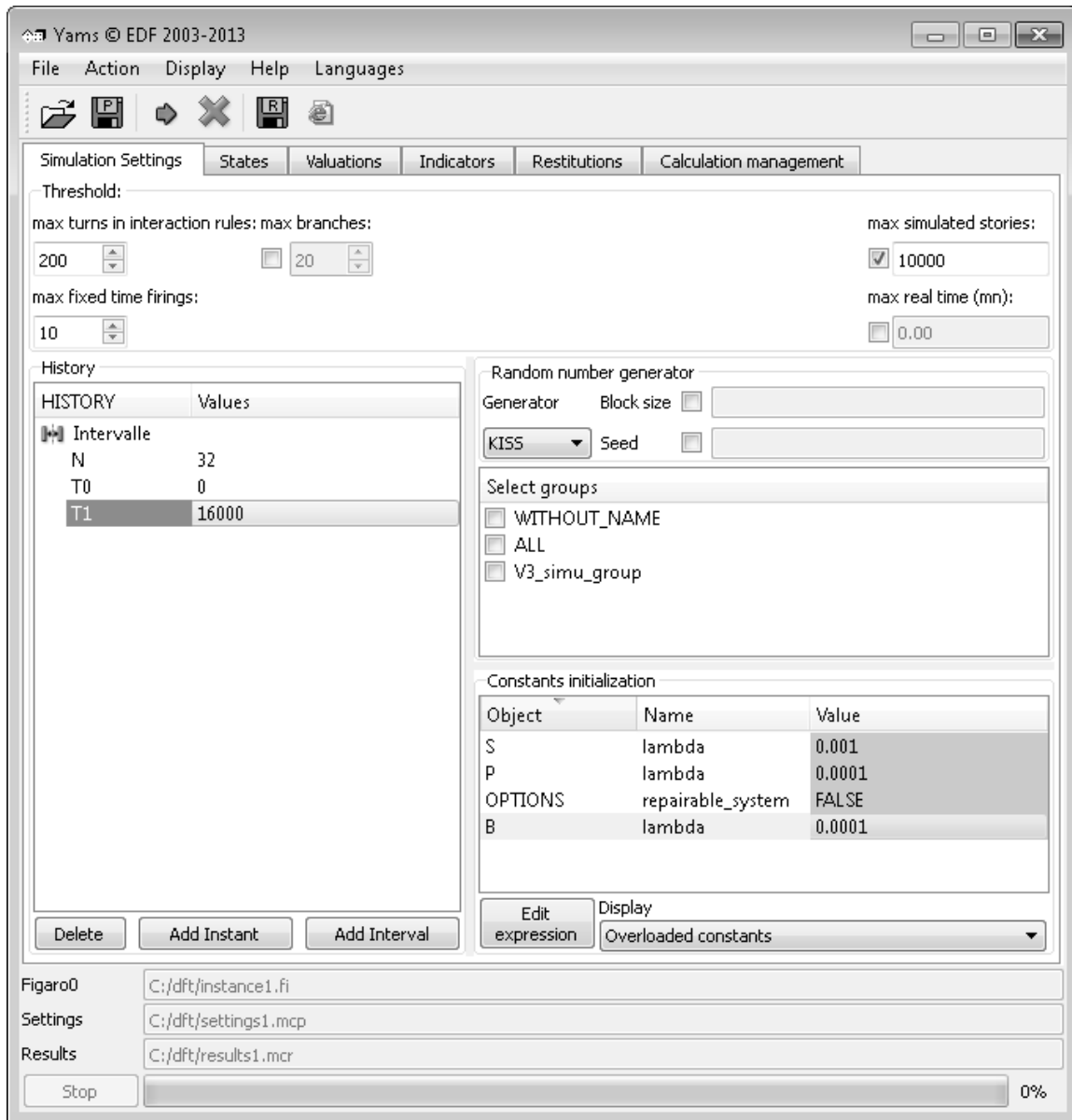


Figure 3: View of the simulation settings in YAMS

### 3.3. Indicators Tab

Indicators constitute the data, the calculation of which constitutes the purpose of a Monte Carlo simulation. Figure 4 shows this tab and its settings. The data can be directly defined by a FIGARO0 expression

(this expression is converted if necessary into a real expression) or by using one or several pre-definitions of expression in the form of “State” or of “Valuation”.

The functions represent the results to be restored from the valuations of the expression of the indicator on



the whole of the simulated histories. The informal definitions of these functions are:

- MEAN: estimates the mean of the indicator which is calculated as the average of the indicator values valued on the whole of the simulated histories.
- VARIANCE: estimates the variance of the indicator which is calculated as the variance of the indicator values valued on the whole of the simulated histories.
- STANDARD\_DEV: estimates the standard deviation of the indicator which is calculated as the standard deviation of the indicator values valued on the whole of the simulated histories.
- CONFIDENCE\_INT: half width of the confidence interval at 95% around the estimated mean of the indicator.

- MIN %: upper bound the indicator values valued on X% of the simulated histories. X is the value typed in the associated field.

- MAX %: lower bound the indicator values valued on X% of the simulated histories. X is the value typed in the associated field.

- ALL\_VALUES: it is not a calculation of a function of the indicator, but it is a command of restitution of the exhaustive list of the values obtained by the indicator during the simulated histories.

The kind of the indicator allows distinguishing:

- GLOBAL which characterizes the indicators which are estimated only for the highest date mentioned in the acquisition field HISTORY,

- LOCAL which characterizes the indicators which are estimated for all the dates of the history.

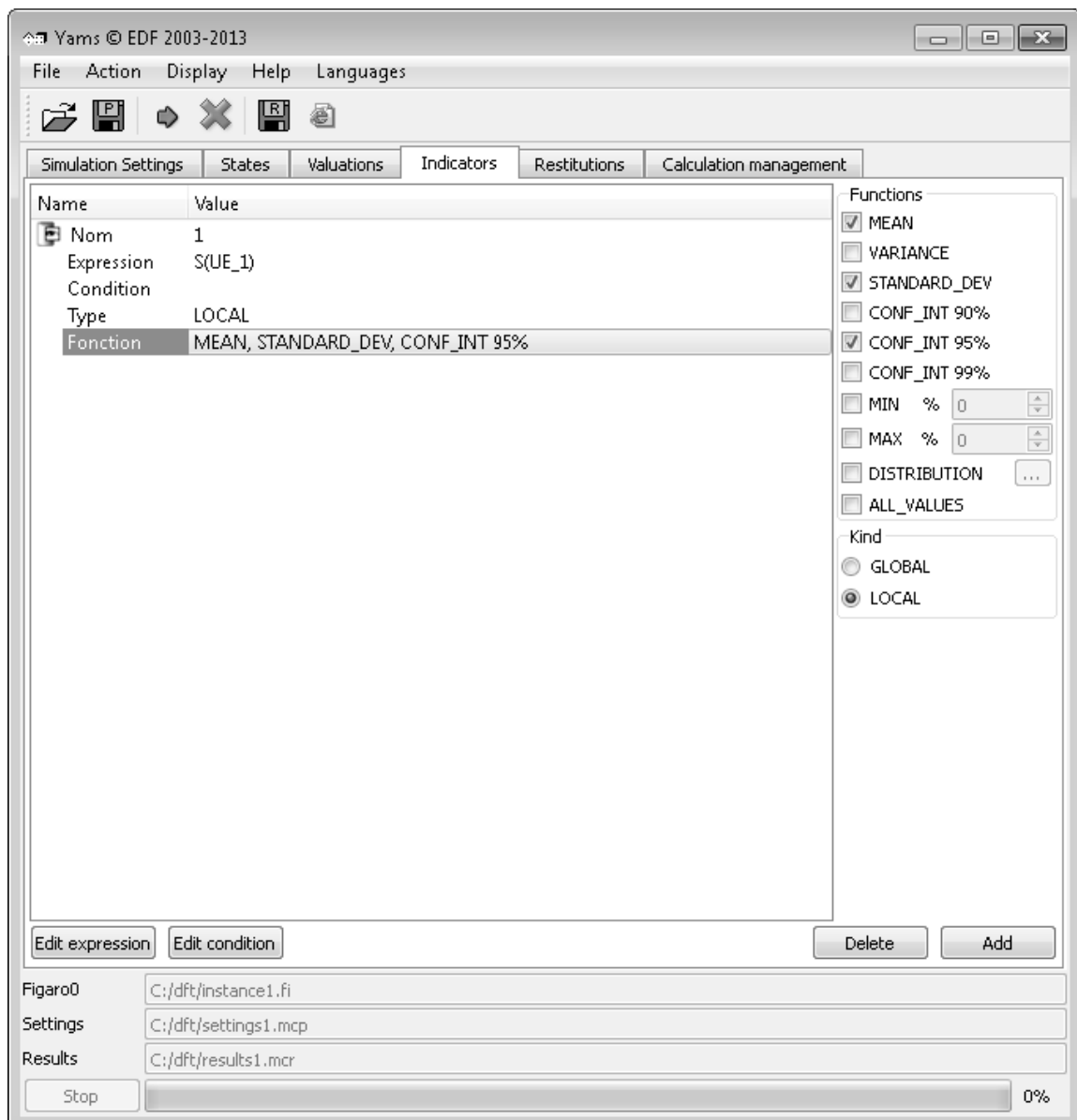


Figure 4: View of the Indicators tab in YAMS

### 3.4. States Tab

A "State" is defined as a boolean FIGARO0 expression which operates the variables of the system. The expression must be written in the FIGARO language of the same language (English or French) as the one of the model to be processed.

A "State" can be qualified as TARGET or as ANALYSIS.

In the case of a TARGET state, the simulation of a sequence is stopped at the first state in which the boolean expression of at least one of the TARGET states has the value TRUE (or VRAI in case of a french FIGARO0

model). The state reached thus is considered as an absorbing state, so indicators estimated at subsequent instants to this stop instant are calculated on this target state.

The main use of TARGET states aims at sparing time of calculation by avoiding simulating the evolution of the system after the first entry in a group of states when you are only interested in the distribution of the date of this entry: it is notably the case when you want to make a calculation of reliability, without being interested in the availability of the modelled system.

TARGET states and ANALYSIS states can be used in the indicators as booleans.

### 3.5. Valuations Tab

A "Valuation" is a FIGARO expression which operates the variables of the studied system and which can be expressed on a group of objects of the model. The expression must be written in the FIGARO language of the same language (English or French) as the one of the model to be processed.

The group of objects is defined by one or several patterns of search on the name of the FIGARO objects.

Patterns are placed in the field Objects of the list and must be separated by commas ','.

### 3.6. Restrictions Tab

The checkbox "transitions frequency" allows asking for the restitutions of the firing frequency of each of the transitions of the FIGARO0 model. The frequency is restituted in terms of average number of firings by sequence; this number can be above 1 (for example for the number of failings of a repairable component).

The tool can also reconstitute fired sequences by distinguishing between the three following kinds of sequences:

- wrong sequences: sequences stopped because of errors of various kinds,
- truncated sequences: sequences stopped because of reaching of stop criteria other than the reaching of a target state; these criteria are those specified in the tab of Simulation Settings,
- used sequences: sequences used in the calculation of the indicators.

When it is asked by the user, the restitution of the sequences in the result file is made in two groups: a first group presents the sequences that are not wrong (of the last two kinds described above) and a second group presents the wrong sequences (of the first kind described).

Sequences are stored by kind in the order of firing and can thus be memorized several times if several firings form identical sequences.

These options are to be used with caution, by specifying a reasonable maximal number of histories, otherwise the files of generated results will be very large and their opening will take a lot of time.

### 3.7. Calculation management Tab

This tab groups together the parameters which have no influence (or little influence) on the simulation results, and for that reason this tab will not be discussed in this paper.

## 4. COMPUTATION OF PARAMETERS OF AN EXAMPLE DFT

### 4.1. Computation with DFTCalc

Figure 5 shows the example tree. The system fails if both the primary (P) and backup (B) fail, or if the primary fails when the switch (S) to enable the backup has already failed.

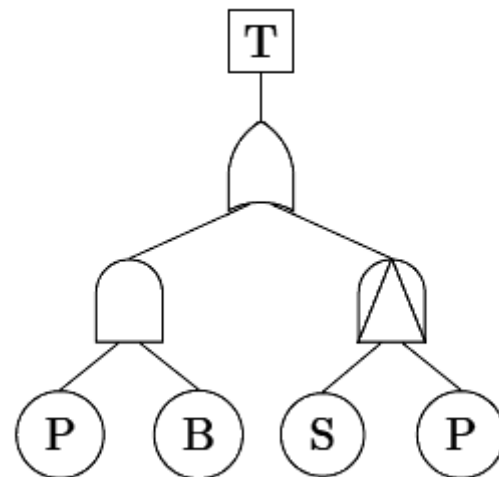


Figure 5: An example of a DFT

The MTTF is computed and this is also done for unreliability. Figure 6 shows a plot of these parameters, made with DFTCalc. The settings are: Compute MTTF to 16000, step 500. The values for  $\lambda$  for P, B and S are respectively 0.0001, 0.0001 and 0.001. MTTF is approximately 10833.3 hours.

### 4.2. Computation with YAMS

Below is the table with the computed unreliability of the example DFT with the following settings:

- Maximum number of branches per sequence : No limit
- Maximum number of successive instantaneous occurrences : 10
- Maximum number of turn in interaction rules before stabilization of the state : 200
- Maximum number of histories 10000
- repairable\_system FALSE
- $\lambda$ , respectively for P, B and S 0.0001, 0.0001 and 0.001

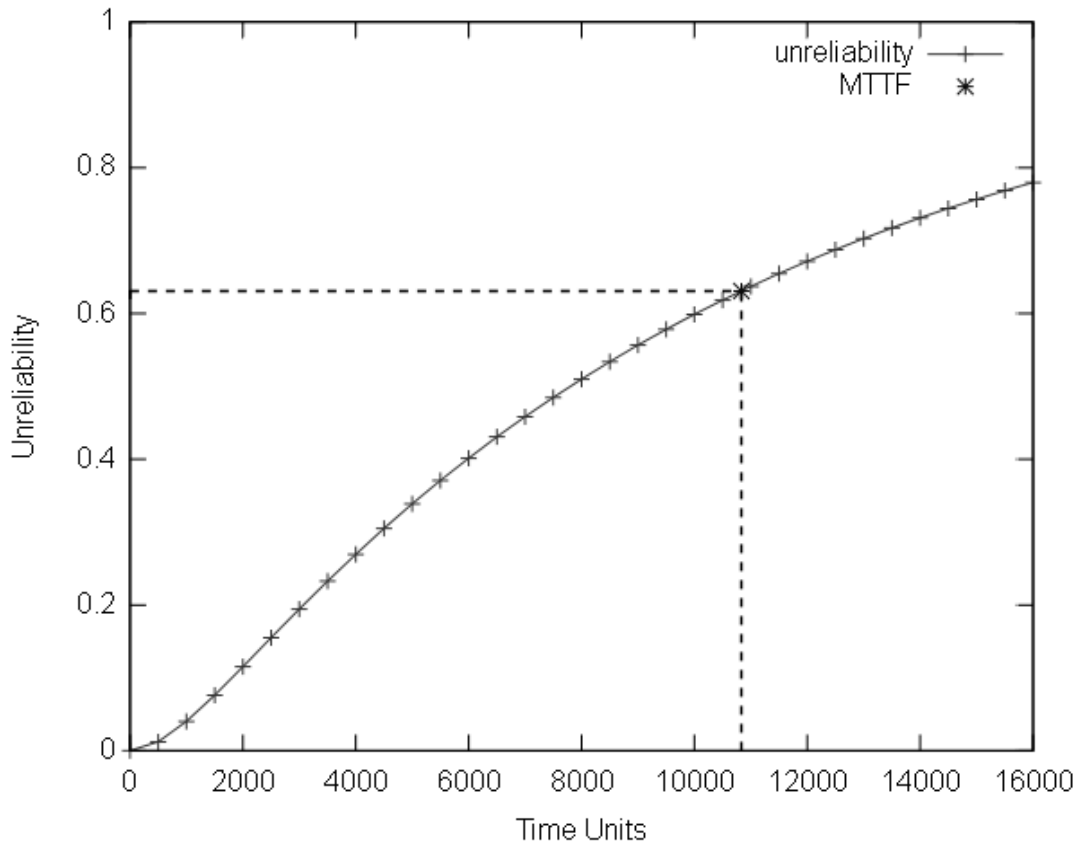


Figure 6: Plot of the unreliability and hours of operation

Table 1: Results of the Monte Carlo simulation with YAMS

Instant (Hours)	Unreliability
0	0
500	0.0125
1000	0.0394
1500	0.0747
2000	0.1134
2500	0.154
3000	0.192
3500	0.2317
4000	0.2689
4500	0.3053
5000	0.3394
5500	0.3737
6000	0.4037
6500	0.4316
7000	0.4613
7500	0.4872
8000	0.5106
8500	0.5365
9000	0.5601
9500	0.5833
10000	0.6005
10500	0.6182
11000	0.6375
11500	0.6555
12000	0.6728
12500	0.6891
13000	0.7023
13500	0.7162
14000	0.7292
14500	0.7418
15000	0.7539
15500	0.7656
16000	0.7774

It can be noticed that the results for unreliability, computed by the two programs, are almost the same.

### 6. CONCLUSION

Two software products for simulation of DFTs were presented. The advantage of DFTCalc is that it can plot the results and computes directly the MTTF. Its disadvantages are that it does not have a graphical utility for drawing of trees and it cannot compute parameters of a DFT with repairable components. YAMS on the other hand is not so user-friendly, it cannot plot the results, does not compute the MTTF and computation of non-deterministic DFTs (which DFTCalc does) is not clearly mentioned [6]. KB3 can draw DFTs relatively easy and these trees are used as an input for YAMS, which can compute parameters of a repairable DFT. Given the forementioned properties of the two products, there is a possibility to add new functions if a combination of these and other programs is used.

### REFERENCES

- [1] E. Ruijters, M.I.A. Stoelinga, "Fault tree analysis: A survey of the state-of-the-art in modeling, analysis and tools", Computer Science Review 15-16 (2015), pp. 29-62, (2015)
- [2] F. Arnold, A.F.E. Belinfante, F.I. Van der Berg, D. Guck, M.I.A. Stoelinga, "DFTCalc: A Tool for Efficient Fault Tree Analysis", 32nd International Conference on Computer Safety, Reliability and Security (SAFECOMP'13). LNCS. Springer, (2013)

- [3] G. Merle, "Algebraic modelling of Dynamic Fault Trees, contribution to qualitative and quantitative analysis", Ph.D. thesis, École normale supérieure de Cachan - ENS Cachan, (2010)
- [4] Dimkina E., Dimitrov V., Cherneva G., Examination of Synchronization of Communication Chaotic Systems by Simulink Simulation, 5th International Conference on Experiments/Process/System Modeling/ Simulation/ Optimization IC-EpsMsO, Athens, Greece, 3-6 July, 2013, Proceedings, Vol. I, SET: 978-618-80527-0-3, ISBN: 978-618-80527-1-0, pp. 218 – 221, (2013)
- [5] M. Bouissou, "BDMP (Boolean logic Driven Markov Processes) as an alternative to Event Trees", in: Proc. European Safety and Reliability Conf. (ESREL), (2008)
- [6] <http://www.fmt.ewi.utwente.nl/puptol/dftcalc/>
- [7] <https://sourceforge.net/projects/visualfigaro/files/>
- [8] H. Boudali, P. Crouzen, M. I. A. Stoelinga, "Dynamic fault tree analysis using Input/Output interactive Markov chains", In DSN, pp. 708-717, (2007)
- [9] C. Baier, H. Hermanns, J.-P. Katoen, B. R. Haverkort, "Efficient computation of time-bounded reachability probabilities in uniform continuous-time Markov decision processes", Theor. Comput. Sci., 345(1):2–26, (2005)

# **SESSION C**

**AUTOMATIC CONTROL, ROBOTICS  
AND FLUID TECHNIQUE**



# Adaptive Input Design for Robust Identification of Output-constrained OE Models

Vladimir Stojanovic<sup>1\*</sup>, Novak Nedic<sup>1</sup>, Dragan Prsic<sup>1</sup>

<sup>1</sup>Faculty of Mechanical and Civil Engineering in Kraljevo, Department of Automatic Control, Robotics and Fluid Technique, University of Kragujevac (Serbia)

*A robust identification of output error (OE) models with optimal input design for a case of constrained output variance is considered in this paper. In a case when observations have Gaussian mixture distributions, it is shown that the proposed robust algorithm for identification of OE models with constrained output, which is based on Huber's function, will give more accurate results in relation to the classical linear algorithm. In a form of the theorem, it is shown that an optimal input signal can be achieved by a minimum variance controller whose reference is a white noise. The essential problem is that the optimal input depends on the system parameters to be identified. In order to overcome this problem, a two-stage adaptive procedure is proposed, where iterations are alternately carried out between parameter estimation and experiment design using the current parameter estimates. It is shown that such obtained excitation signals result in a significant increasing in a convergence rate. Theoretical results are illustrated by simulations.*

**Keywords:** input design, output error model, constrained output, robust identification algorithm

## 1. INTRODUCTION

The area, which deals with obtaining the mathematical model of the process, remains vibrant, as shown by recent research [1,2]. The main task of the theory of identification is the extraction of maximum information from the measurements that are available. This requirement is realized by optimal experiment design [3]. The basic approach consists in minimizing the scalar function of the Fisher information matrix [4].

The key problem in the optimal input design is that the optimal input depends on the unknown system properties, which need to be identified. Namely, the Fisher information matrix typically depends on system parameters. There are two basic approaches to overcome this problem. The first approach is based on robust optimal experiment design. In this case, the procedure is slightly sensitive to the uncertainty of a priori information about the system [5]. The basic a priori knowledge of the system can be obtained using a nonparametric frequency method [6]. The new results in this area cover the case of a finite number of model parameters and a very large number of measurements. The second approach is based on adaptation. One such, two-stage procedure has been proposed in [7]. In the first stage, in a short time interval, the data are collected using PRBS input. Based on these data, a system model is identified, and that is an initial model for optimal input design. In the second stage, the obtained input signal, by using a minimum variance controller and a stochastic reference, is used to generate a new data set. Adaptive input design for the ARX models has been discussed in [4].

In many practical cases, constraints on the fluctuation of input and/or output signals are very important [8]. For example, in the industrial production, product quality must be within certain limits (constraints on the fluctuation of the output signal).

If the constraint is related to the variance of the output signal, it is shown that the experiment design is D-

optimal and that the input signal is generated using a minimum variance controller together with an external stochastic signal [8].

This paper considers the optimal experiment design for output error (OE) models. There is a constraint on the output power. When the corresponding noise is modelled as the Gaussian stochastic process, it is demonstrated in [9] that the presence of feedback is very important. Here, those results, using the Fisher information matrix, are extended on the case when the measurement noise is non-Gaussian. Justification of this approach was confirmed in practice [10]. Namely, in measurements there are rare, inconsistent observations with the largest part of population of observations (outliers). The presence of outliers can considerably degrade the performance of linearly recursive algorithms based on the assumptions that measurements have a Gaussian distribution. Therefore, synthesis of robust algorithms is of primary interest. The synthesis is based on Huber's theory of robust statistics [10]. Simulation results have shown that the proposed robust output error (OE) parameter estimation algorithm, based on the minimization of a robust criterion, will give more accurate results in relation to the conventional linear estimation algorithm, based on the recursive least squares (RLS) method.

It is shown that the optimal input signal can be obtained by a minimum variance controller whose reference is a white noise sequence with known variance. In order to be able to implement the algorithm, adaptive approach is applied. A direct adaptive minimum variance controller is used. The algorithm has two stages. In the first stage, the process parameters are estimated. In the second stage, based on thus obtained parameters, it is formed the minimum variance controller that generates the input signal of the process by which the identification is made. Because the reference signal is in the form of white noise, parameter estimation is consistent. The paper's results are supported by simulations.

\*Corresponding author: Dositejeva 19, Kraljevo (Serbia), stojanovic.v@mfkv.kg.ac.rs

## 2. ROBUST IDENTIFICATION ALGORITHM FOR OE MODELS

The general form of the OE model is

$$y(k) = \frac{B(q^{-1})}{A(q^{-1})}u(k) + e(k) \quad (1)$$

where  $u(k)$ ,  $y(k)$  and  $e(k)$  are input, output and stochastic noise, respectively. Polynomials  $A(q^{-1})$  and  $B(q^{-1})$  have the form:

$$\begin{aligned} A(q^{-1}) &= 1 + a_1q^{-1} + \dots + a_nq^{-n} \\ B(q^{-1}) &= b_1q^{-1} + \dots + b_mq^{-m} \end{aligned} \quad (2)$$

where  $q^{-i}$ ,  $i \in N$  denotes the backward shift operator i.e.  $q^{-i}x(k) = x(k-i)$ , while  $b_i (i=1, \dots, m)$  and  $a_i (i=1, \dots, n)$  are unknown parameters.

Practical and theoretical studies have shown that in a stochastic model of the system there are some observations that are inconsistent with the largest part of the population (outliers) [10], and that is why the disturbance (measurement noise)  $e(k)$  in the model (1) is a non-Gaussian. Hence, the probability density function of the disturbance belongs to approximately normal distribution class:

$$\mathcal{P}_\varepsilon = \{p(e) : p(e) = (1-\varepsilon)p_1(e) + \varepsilon p_2(e)\} \quad (3)$$

in which

$$p_1(e) \sim \mathcal{N}(0, \sigma_1^2), \quad p_2(e) \sim \mathcal{N}(0, \sigma_2^2), \quad \sigma_2^2 \gg \sigma_1^2.$$

In other words, the probability density function  $p(e)$  represents a mixture of normal (Gaussian) distributions where  $\sigma_1^2$  and  $\sigma_2^2$  denote variances. The parameter  $0 \leq \varepsilon < 1$  is called the degree of contamination.

Let us introduce an auxiliary model

$$y_M(k) = \frac{B(q^{-1})}{A(q^{-1})}u(k), \quad (4)$$

or in the following form:

$$\begin{aligned} y_M(k) &= -a_1y_M(k-1) - \dots - a_ny_M(k-n) + \\ &+ b_1u(k-1) + \dots + b_mu(k-m) \end{aligned} \quad (5)$$

Since true values of parameters  $a_i (i=1, \dots, n)$  and  $b_i (i=1, \dots, m)$  are unknown, the output of the auxiliary model is calculated using estimates of parameters:

$$\begin{aligned} \hat{y}_M(k) &= -\hat{a}_1\hat{y}_M(k-1) - \dots - \hat{a}_n\hat{y}_M(k-n) + \\ &+ \hat{b}_1u(k-1) + \dots + \hat{b}_mu(k-m) \end{aligned} \quad (6)$$

Let  $\hat{\theta}(k)$  be the estimated vector of parameters, and  $\varphi(k)$  be the observation vector at the moment  $k$ :

$$\begin{aligned} \hat{\theta} &= [\hat{a}_1, \dots, \hat{a}_n, \hat{b}_1, \dots, \hat{b}_m]^T, \\ \varphi(k) &= [-\hat{y}_M(k-1) \dots -\hat{y}_M(k-n), u(k-1) \dots u(k-m)]^T \end{aligned} \quad (7)$$

At the moment  $k$ , before the estimate  $\hat{\theta}(k)$  is known, the prediction of the model is:

$$\hat{y}_M(k) = \hat{\theta}^T(k-1)\varphi(k). \quad (8)$$

The problem of identification of the system described by (1) can be considered as the task of finding the vector  $\hat{\theta}$ , such that the mean square criterion:

$$J(\hat{\theta}) = E\{\varepsilon^2(k)\}, \quad \varepsilon(k) = y(k) - \hat{y}_M(k) \quad (9)$$

is minimized, where  $E\{\cdot\}$  represents the mathematical expectation operator and  $\varepsilon(k)$  is the prediction error.

Since the identification criterion (9) gives same weights to all residuals, these sporadic large observations (outliers) will have a significant influence on resulting parameter estimates. To achieve robustness we will consider the robust M-estimation criterion [10]:

$$J_{\mathcal{R}}(\theta) = E\{\Phi[\varepsilon(k, \theta)]\} \quad (10)$$

in which  $\Phi$  represents a robust loss function:

$$\Phi(\cdot) = -\log p^*(\cdot). \quad (11)$$

By using Huber's min-max approach, it is possible to find the least favorable probability density function  $p^*(\cdot)$  on a class of approximately normal distributions (3):

$$p^*(e(k)) = \begin{cases} \frac{1-\varepsilon}{2\pi\sigma_1} \exp\left\{-\frac{e^2(k)}{2\sigma_1^2}\right\} & |e(k)| \leq k_\varepsilon \\ \frac{1-\varepsilon}{2\pi\sigma_1} \exp\left\{-\frac{k_\varepsilon}{\sigma_1^2} \left(|e(k)| - \frac{k_\varepsilon}{2}\right)\right\} & |e(k)| > k_\varepsilon \end{cases} \quad (12)$$

where  $k_\varepsilon$  is the Huber function parameter.

The empirical robust criterion on the observed interval, obtained from the relation for sufficiently large  $k$ , has the form:

$$J_k(\theta) = \frac{1}{k} \sum_{i=1}^k \{\Phi(\varepsilon(i))\}. \quad (13)$$

Expanding  $J_k(\theta)$  in the vicinity of the preceding estimate  $\hat{\theta}(k-1)$  in Taylor series, one obtains:

$$\begin{aligned} J_k(\theta) &= J_k(\hat{\theta}(k-1)) + \nabla_{\theta} J_k(\hat{\theta}(k-1)) [\theta - \hat{\theta}(k-1)] + \\ &+ O\left(\|\theta - \hat{\theta}(k-1)\|^2\right) \end{aligned} \quad (14)$$

where

$$\lim_{\|x\| \rightarrow \infty} \frac{O(\|x\|)}{\|x\|} = 0. \quad (15)$$

By minimizing the expression (14), it is obtained:

$$\begin{aligned} \hat{\theta}(k) &= \hat{\theta}(k-1) - \left[ k \nabla_{\theta}^2 J_k(\hat{\theta}(k-1)) \right]^{-1} \left[ k \nabla_{\theta} J_k(\hat{\theta}(k-1)) \right] + \\ &+ O\left(\|\theta - \hat{\theta}(k-1)\|\right) \end{aligned} \quad (16)$$



A recursive form of the robust criterion (13) can be obtained as  $\theta = \hat{\theta}(k-1)$

$$kJ_k(\theta) = (k-1)J_{k-1}(\theta) + \Phi(\varepsilon(k)). \quad (17)$$

By differentiating the last relation twice one can obtain:

$$k\nabla_{\theta}^2 J_k(\theta) = (k-1)\nabla_{\theta}^2 J_{k-1}(\theta) + \Psi'(\varepsilon(k))\varphi(k)\varphi^T(k) \quad (18)$$

where  $\Psi(\cdot) = \Phi'(\cdot)$ ,  $\Psi(\cdot): R^1 \rightarrow R^1$ .

Furthermore, the following assumptions will be used:

- The estimate  $\hat{\theta}(k)$  is in the vicinity of the estimate  $\hat{\theta}(k-1)$
- The estimate  $\hat{\theta}(k-1)$  is optimal at the instant  $k-1$ .

After replacing  $\theta$  with  $\hat{\theta}(k-1)$  in the relation (18), one can obtain:

$$k\nabla_{\theta}^2 J_k(\hat{\theta}(k-1)) = (k-1)\nabla_{\theta}^2 J_{k-1}(\hat{\theta}(k-1)) + \Psi'(\varepsilon(k))\varphi(k)\varphi^T(k) \quad (19)$$

From the assumption a) it follows

$$\nabla_{\theta}^2 J_k(\hat{\theta}(k)) \cong \nabla_{\theta}^2 J_k(\hat{\theta}(k-1)) \quad (20)$$

Based on this, the relation (19) takes the form

$$k\nabla_{\theta}^2 J_k(\hat{\theta}(k-1)) = (k-1)\nabla_{\theta}^2 J_{k-1}(\hat{\theta}(k-2)) + \Psi'(\varepsilon(k))\varphi(k)\varphi^T(k) \quad (21)$$

Based on the assumption a) it also follows

$$O(\|\hat{\theta}(k) - \hat{\theta}(k-1)\|) = 0 \quad (22)$$

By introducing the notation  $\bar{R}(k) = k\nabla_{\theta}^2 J_k(\hat{\theta}(k-1))$  from relations (16) and (21) one can obtain:

$$\hat{\theta}(k) = \hat{\theta}(k-1) - \bar{R}^{-1}(k) \left[ k\nabla_{\theta} J_k(\hat{\theta}(k-1)) \right] \quad (23)$$

$$\bar{R}(k) = \bar{R}(k-1) + \Psi'(\varepsilon(k))\varphi(k)\varphi^T(k) \quad (24)$$

From the assumption b) it follows  $\nabla_{\theta} J_{k-1}(\hat{\theta}(k-1)) = 0$ .

Based on this condition, and if  $\theta = \hat{\theta}(k-1)$  is put in the relation (25), one obtains:

$$k\nabla_{\theta} J_k(\hat{\theta}(k-1)) = -\Psi(\varepsilon(k))\varphi(k) \quad (25)$$

Finally, based on relations (23) - (25), using the notation  $P(k) = \bar{R}^{-1}(k)$  and applying the matrix inversion lemma, one can obtain the definitive form of a recursive algorithm:

$$\hat{\theta}(k) = \hat{\theta}(k-1) + P(k)\varphi(k)\Psi(\varepsilon(k)) \quad (26)$$

$$P(k) = P(k-1) - \frac{P(k-1)\varphi(k)\varphi^T(k)P(k-1)}{\left[ \Psi'(\varepsilon(k)) \right]^{-1} + \varphi^T(k)P(k-1)\varphi(k)} \quad (27)$$

$$\varepsilon(k) = y(k) - \hat{\theta}^T(k-1)\varphi(k) \quad (28)$$

$$\Psi(x) = \min \{ |x|, k_{\varepsilon} \} \operatorname{sgn}(x) \quad (29)$$

$$\Psi'(x) = \begin{cases} 1 & |x| < k_{\varepsilon} \\ 0 & \text{otherwise} \end{cases} \quad (30)$$

The function defined by the relation (29) is the Huber function [10]. It is derived for a class of distributions (3). It is shown on Figure 1.

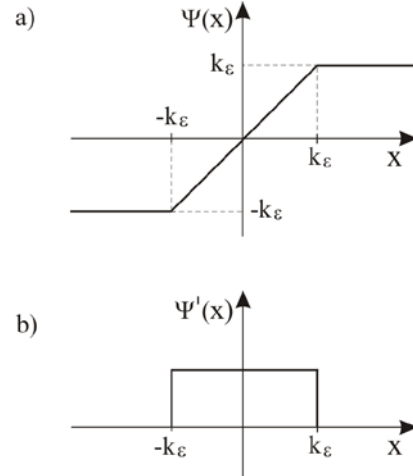


Figure 1: Nonlinear function of residuals

a) Huber's function

b) Derivative of Huber's function

### 3. OPTIMAL INPUT DESIGN FOR OE MODELS

Further, we will consider a special case of the model (1):

$$y(k) = \frac{b_1 q^{-1}}{A(q^{-1})} u(k) + e(k) = \frac{b_1}{A(q^{-1})} u(k-1) + e(k). \quad (31)$$

In this case the parameters  $b_1$  and  $a_i (i=1, \dots, n)$  are estimated.

The Fisher information matrix can be defined as [4]:

$$M = E_{Y|\beta} \left\{ \left( \frac{\partial \log p(Y|\beta)}{\partial \beta} \right)^T \left( \frac{\partial \log p(Y|\beta)}{\partial \beta} \right) \right\} \quad (32)$$

Based on  $N$  measurements, the vector of outputs is  $Y = [y(1) \dots y(N)]^T$ . Parameter vector  $\beta$  has the form:

$$\beta = \left[ \theta^T \quad \sigma_e^2 \right]^T \quad (33)$$

where  $\sigma_e^2$  represents the variance of the noise  $e(k)$ , and

$$\theta^T = \left[ a^T \quad b_1 \right] \text{ in which } a^T = [a_1 \dots a_n].$$

Since  $N$  is large, it is more convenient to work with the average value of the Fisher information matrix:

$$\bar{M} = \lim_{N \rightarrow \infty} \frac{1}{N} M \quad (34)$$

We shall principally use the determinant of the average information matrix as the design criterion leading to the following form of D-optimal criterion:

$$J = -\log \det \overline{M}. \tag{35}$$

Minimization of the scalar cost function (35) relies upon the calculation of the matrix  $\overline{M}$ .

**Lemma 1.** [[11], pp. 232] Let  $(\Omega, \mathcal{F}, P)$  be a probability space. Suppose also that there is a subalgebra  $\mathcal{F}_1 (\mathcal{F}_1 \subseteq \mathcal{F})$ . Then

$$E \left\{ E_{\mathcal{F}_1} \{ \xi \} \right\} = E \{ \xi \} \blacksquare \tag{36}$$

**Lemma 2.** [[8], pp. 244] Let  $\overline{M}$  be a positive definite matrix with unit diagonal elements  $\overline{M}_{ii} = 1, i = 1, \dots, n$ ,

then  $\det \overline{M}$  achieves its maximum value for  $\overline{M} = I$   $\blacksquare$

We will now formulate the optimal input in the form of the theorem.

**Theorem 1.** Suppose that for OE model (31), the following conditions are fulfilled:

1° Stochastic noise  $e(k)$  represents a zero mean Gaussian mixture with variance  $\sigma_e^2$ ,

2° A constraint on the output is  $E \{ y^2(k) \} \leq W$ ,  $W \in (0, \infty)$ .

Then the criterion  $-\log \det \overline{M}$  achieves its minimum value if the system input  $u(k)$  is generated by the

$$\overline{M} = \frac{1}{\sigma_e^2} E \left[ \begin{array}{ccc|cc} y_M(k-1)^2 & \dots & y_M(k-1) \cdot y_M(k-n) & -u(k-1)y_M(k-1) & 0 \\ \vdots & \ddots & \vdots & \vdots & \vdots \\ y_M(k-n) \cdot y_M(k-1) & \dots & y_M(k-n)^2 & -u(k-1)y_M(k-n) & 0 \\ \hline -u(k-1)y_M(k-1) & \dots & -u(k-1)y_M(k-n) & u(k-1)^2 & 0 \\ \hline 0 & \dots & 0 & 0 & 1/2\sigma_e^2 \end{array} \right] \tag{41}$$

where the sub-matrices correspond to the partitioning of the parameter vector  $\beta$  into  $[a^T \mid b_1 \mid \sigma_e^2]^T$ , in which  $\sigma_e^2$  represents the variance of Gaussian mixture noise.

The relation (41) can be written in a form that is more compact:

$$\overline{M} = \frac{1}{\sigma_e^2} \left[ \begin{array}{c|c|c} A & B & 0 \\ \hline B^T & C & 0 \\ \hline 0 & 0 & 1/2\sigma_e^2 \end{array} \right] \tag{42}$$

The following task is to determine elements of the matrix  $\overline{M}$  in the relation (42).

**Step 1** (Determining the matrix  $A$ )

Let us define

$$E \{ y_M(k-i)y_M(k-j) \} \triangleq \rho_{|i-j|} \tag{43}$$

minimum variance controller which reference is a zero mean white noise sequence  $\{\eta(k)\}$  with probability density function

$$p(\eta) = \frac{b_1}{\sqrt{2\pi W}} e^{-\frac{(\eta b_1)^2}{2W}} \blacksquare \tag{37}$$

**Proof:** Let us define the residual sequence as:

$$\varepsilon(k) = y(k) + a_1 y_M(k-1) + \dots + a_n y_M(k-n) - b_1 u(k-1) \tag{38}$$

Since we consider  $N$  observations, the likelihood function would be:

$$p(Y|\beta) = \prod_{k=1}^N \left( (1-\varepsilon) p_1(y(k)) + \varepsilon p_2(y(k)) \right). \tag{39}$$

After some calculations, according to **Lemma 1**, the mean value of the Fisher information matrix can be expressed as:

$$\overline{M} = \frac{1-\varepsilon}{\sigma_1^2} E \left\{ \left( \frac{\partial \varepsilon(k)}{\partial \beta} \right)^T \left( \frac{\partial \varepsilon(k)}{\partial \beta} \right) + \frac{1}{2\sigma_1^4} \left( \frac{\partial \sigma_1^2}{\partial \beta} \right)^T \left( \frac{\partial \sigma_1^2}{\partial \beta} \right) \right\} + \frac{\varepsilon}{\sigma_2^2} E \left\{ \left( \frac{\partial \varepsilon(k)}{\partial \beta} \right)^T \left( \frac{\partial \varepsilon(k)}{\partial \beta} \right) + \frac{1}{2\sigma_2^4} \left( \frac{\partial \sigma_2^2}{\partial \beta} \right)^T \left( \frac{\partial \sigma_2^2}{\partial \beta} \right) \right\} \tag{40}$$

From relations (33), (38), and (40) one can obtain

Based on the relation (43) the matrix  $A$  can be presented in the following form:

$$A = \begin{bmatrix} \rho_0 & \rho_1 & \dots & \rho_{n-1} \\ \rho_1 & \rho_0 & \dots & \rho_{n-2} \\ \vdots & \vdots & \ddots & \vdots \\ \rho_{n-1} & \rho_{n-2} & \dots & \rho_0 \end{bmatrix} \tag{44}$$

From relations (4) and (31) it follows:

$$y(k) = -a_1 y_M(k-1) - \dots - a_n y_M(k-n) + b_1 u(k-1) + e(k) \tag{45}$$

After multiplying the relation (45) with  $y_M(k-i), i = 1, \dots, n$  and applying the mathematical expectation operator to the obtained system of  $n$  equations, one can obtain:

$$V = -Af + Bb_1 \tag{46}$$

where  $a^T = [a_1 \dots a_n]$ ,  $V = [\rho_1 \ \rho_2 \ \dots \ \rho_n]^T$ .

Finally, it follows from the relation (46) that:

$$B = \frac{1}{b_1}(Af + V) \quad (47)$$

$$u(k-1) = \frac{1}{b_1}[y_M(k) + a_1 y_M(k-1) + \dots + a_n y_M(k-n)] \quad (48)$$

### Step 3 (Determining the scalar $C$ )

Scalar  $C$  is defined as:

From the relation (4) one can get the input signal  $u(\cdot)$ :

$$\begin{aligned} C = E\{u(k-1)^2\} &= \frac{1}{b_1^2} E\left[y_M(k)^2 + a_1 y_M(k-1)y_M(k) + \dots + a_n y_M(k-n)y_M(k) + \right. \\ &+ a_1 y_M(k)y_M(k-1) + a_1^2 y_M(k-1)^2 + \dots + a_1 a_n y_M(k-1)y_M(k-n) + \\ &\vdots \\ &\left. + a_n y_M(k-n)y_M(k) + a_n a_1 y_M(k-1)y_M(k-n) + \dots + a_n^2 y_M(k-n)^2\right] \end{aligned} \quad (49)$$

After arranging individual terms of (49), the finally expression for the scalar  $C$  is given by:

$$C = E\{u(k-1)^2\} = \frac{1}{b_1^2} (\rho_0 + 2aV^T + a^T Aa) \quad (50)$$

Since, all elements of the matrix  $\bar{M}$  (relation (42)) are now known, one can obtain:

$$\det \bar{M} = \frac{1}{2\sigma_e^2} \det A \cdot \det(C - B^T A^{-1} B) \quad (51)$$

Now, it can be shown that:

$$\begin{aligned} -\log \det \bar{M} &= \\ \log 2\sigma_e^2 - \log(\det A) - \log(\rho_0 - V^T A^{-1} V) + \log b_1^2. \end{aligned} \quad (52)$$

In accordance with the condition 2° of the **Theorem 1**, we have  $\rho_0 = W$ , so the diagonal elements of the matrix  $A$  are fixed. Based on **Lemma 2** it follows that  $-\log(\det A)$  has a minimum value when  $A$  is the diagonal matrix. This means that  $\rho_i = 0$ ,  $i > 0$ , which further gives  $V = 0$ . Because of this, the third term of the equation (52) has a minimum value  $-\log(W)$ . We finally get

$$\min\{-\log \det \bar{M}\} = \log \frac{2\sigma_e^2 b_1^2}{W^{n+1}} \quad (53)$$

It is necessary to note that  $\rho_i = 0$ ,  $i > 0$  is achieved when  $\{y(k)\}$  is an uncorrelated sequence. This condition is fulfilled if the input signal is chosen in the following form:

$$u(k) = \frac{1}{b_1}[a_1 y_M(k) + \dots + a_n y_M(k-n+1)] + \eta(k) \quad (54)$$

where  $\eta(k)$  is a reference signal that represents white noise with variance  $W/b_1^2$ . The relation (54) represents the minimum variance controller for the model (31). This theorem is proved. ■

This result also shows that the optimal input design requires knowledge of the true system parameters. In practical conditions, however, such a requirement is contradictory because the optimal input design is performed in order to speed up the identification process.

In other words, it is impossible that unknown system parameters are known a priori. In a real application this fact must be handled. In order to overcome this problem a two-stage adaptive procedure is proposed:

- A) By using PRBS signal as input, through  $N_{init}$  iterations, the initial model of the process is determined,
- B) After that, through  $N_{opt}$  iterations, adaptation is applied for the controller defined in **Theorem 1**.

In the section devoted to simulations, the proposed two-stage algorithm will be compared with the open loop system identification algorithm with the PRBS input signal.

## 4. SIMULATION RESULTS

The proposed two-stage identification algorithm is tested on the following OE model:

$$y(k) = \frac{0.5q^{-1}}{1 - 0.7q^{-1} + 0.5q^{-2}} u(k) + e(k) \quad (55)$$

The system identification example, is based on measured 1000 input-output data points obtained during the simulations. The measurement noise  $e(k)$  has non-Gaussian distribution defined by:

$$\mathcal{P}_e = \{p(e) : p(e) = (1-0.1)\mathcal{N}(0,0.1) + 0.1\mathcal{N}(0,10)\} \quad (56)$$

Figure 2 shows system input and corresponding system output when the robust two-stage identification algorithm is used. First 200 iterations, the system works in an open loop, with PRBS as the input signal. Then it switches feedback in the range of iterations 200-1000.

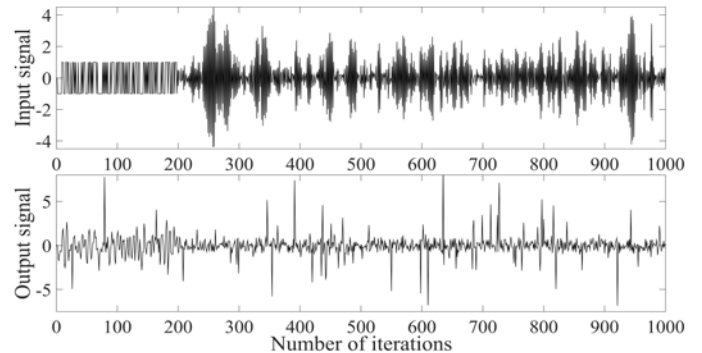


Figure 2: Adaptive input and corresponding output

Simulation results have illustrated significant increasing of accuracy in parameter estimates of OE model by using the robust identification algorithm in relation to the linear identification algorithm with PRBS [-1,1] as an input signal. Furthermore, it can be seen that the convergence rate of the robust algorithm is further increased by using the optimal input design, which further increases the practical value of proposed robust procedure.

Figures 3 and 4 show parameter estimates in the case where the output variance cannot be greater than  $W = 0.5$ .

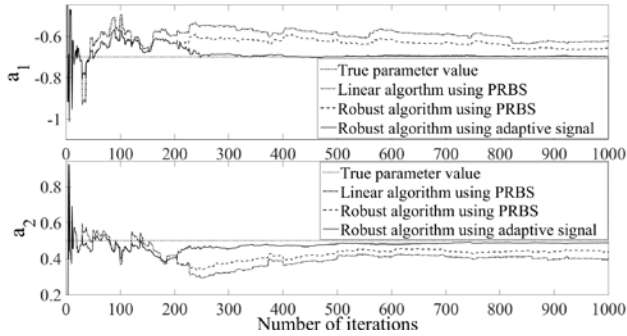


Figure 3: Estimates of parameters  $a_1$  and  $a_2$

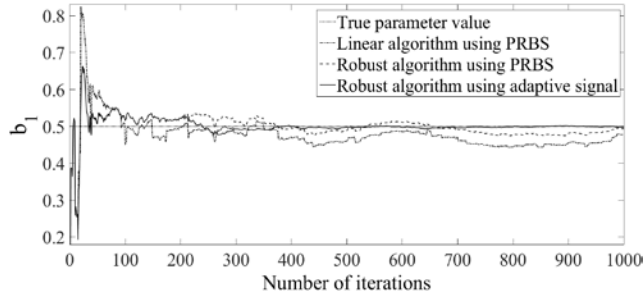


Figure 4: Estimate of parameter  $b_1$

The simulation results are compared in terms of mean square errors (see Figure 5), defined by

$$MSE = \ln \left( E \left\| \hat{\theta}(k) - \theta(k) \right\|^2 \right) \quad (57)$$

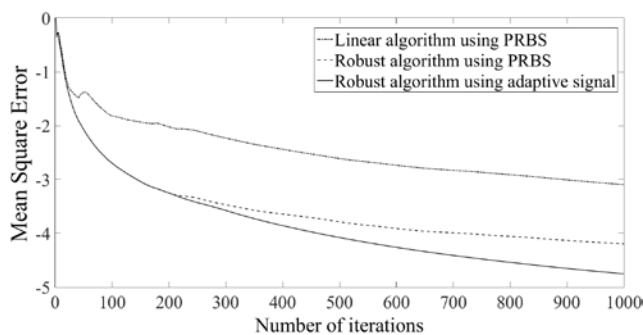


Figure 5: Mean square errors

Based on these figures, it can be concluded that experiment design increases the convergence speed of parameters to true values, keeping the given output variance  $W$ .

## 5. CONCLUSION

In this paper the optimal input design for robust identification of a special case of OE models, in the case of constrained output variance, has been considered.

Simulation results have shown that the proposed robust OE parameter estimation algorithm, produces more efficient parameter estimates in relation to the conventional linear algorithm.

Also, it is shown, that the optimal input is obtained by using the minimum variance controller and the stochastic reference signal. The adaptive two-stage procedure for generating the input signal is proposed. The initial model of the process is firstly obtained using PRBS input signal. In the second stage, the optimal input signal is generated by the minimum variance controller together with the stochastic reference. Simulation results have shown the superiority of the robust identification algorithm using proposed adaptive methodology for generating the optimal input signal.

## ACKNOWLEDGEMENTS

The authors would like to express their gratitude to the Serbian Ministry of Education, Science and Technological Development for supporting this paper through projects TR33026 and TR33027.

## REFERENCES

- [1] E.Zhang, R. Pintelon, "Identification of multivariable dynamic errors-in-variables system with arbitrary inputs", *Automatica*, Vol. 82, pp. 69-78, (2017)
- [2] A. Janot, P.-O. Vandanjon, M. Gautier, "A revised Durbin-Wu-Hausman test for industrial robot identification", *Control Engineering Practice*, Vol.48, pp.52-62, (2016)
- [3] M. Zarrop, "Optimal experiment design for dynamic system identification", Springer, Berlin, (1979).
- [4] G.C. Goodwin, R.L. Payne, "Dynamic system identification: Experiment design and data analysis", Academic Press, NY, (1977).
- [5] C.R. Rojas, J.C. Agüero, J.S. Welsh, G.C. Goodwin, A. Feruer, "Robustness in experiment design", *IEEE Transactions on Automatic Control*, Vol. 57(4), pp. 860-874, (2012).
- [6] J.S. Welsh, G.C. Goodwin, "Finite sample properties of indirect nonparametric closed-loop identification", *IEEE Transactions on Automatic Control*, Vol. 47(8), pp.1277-1292, (2002).
- [7] M. Barenthin, H. Jansson, H. Hjalmarsson, "Applications of mixed  $H_2$  and  $H_\infty$  input design in identification", *Proceedings of the 16th IFAC World Congress, Prague, July 3-8 2005*, pp. 458-463, (2005).
- [8] T.S. Ng, G.C. Goodwin, T. Söderström, "Optimal experiment design for linear systems with input-output constraints", *Automatica*, Vol. 13(6), pp.571- 577, (1977).
- [9] V. Stojanovic, V. Filipovic, "Adaptive input design for identification of output error model with constrained output", *Circuits, Systems, and Signal Processing*, Vol.33(1), pp.97-113, (2014)
- [10] P.J. Huber, "Robust Statistics", Wiley, NY, (1981).
- [11] A.N. Shirayayev, "Probability", Nauka, Moscow, (1989).

# Conditional Optimization of Computer Automatic Control System of an Selected Plant at Arbitrary Initial Conditions

Vladimir R. Zarić<sup>1\*</sup>, Zoran M. Bučevac<sup>1</sup>, Radiša Ž. Jovanović<sup>1</sup>

<sup>1</sup>Faculty of Mechanical Engineering/Control Engineering, University of Belgrade, Belgrade (Serbia)

*The aim of this paper is to present effect of initial conditions on choice of optimal parameters in computer automatic control system of an selected actual plant. Considering is made in a parameter plane wherein the area of formerly guaranteed relative damping coefficient of all closed-loop poles is separated. A performance index is chosen to be sum of error squared (SSE), taking into account of arbitrary initial conditions.*

*Experimental results obtained on coupled-tanks plant are provided.*

**Keywords:** conditional optimization, performance index, computer control system

## 1. INTRODUCTION

Over 95 % of coexisting practical industrial applications use PID (or PI as a special case) control algorithms and thus the suitable PID control design is still very actual, especially for systems under some nonlinearities, perturbations, or time-variant behaviour. Without any doubts, the ultimately primary and fundamental requirement of all applications is the stability of closed control loop, [1].

For the continuous-time PID controllers, in many works collected in [2], the stability regions in the space of the gains of the PID controllers are determined. A nice and simple procedure is also given in [3] that requires less numerical computations. One procedure is presented in [4], where the result of the parameter space approach [5] is used to derive the stability domain of PID controllers.

Nevertheless, PID controllers are very often implemented digitally using microprocessors [6]. Research on the stability of digital control system goes back to early 1960's, when stability of such system was investigated. In [7, 8] the results of [2] are generalized to the case of digital PID controllers.

The aim of this work is to show that integral criterion has different value when we take into account non-zero initial conditions from value of the same integral criterion at zero initial conditions. At the same time, and more important, optimal controller gains can have drastically different values when we take into account nonzero initial conditions from values that we get at zero initial conditions.

In many papers, as in [9, 10, 11], are assumed zero initial conditions for calculation of actual system output. The past and the present of a dynamic system are contained in a initial conditions. That same initial conditions together with the external input fully determine the output of the system. Initial conditions cannot be chosen and they are, usually, totally unpredictable. Complete analysis of continuous linear time invariant systems with nonzero initial conditions is presented in [12].

## 2. EXPERIMENTAL SETUP

The Coupled Tanks plant is a "Two-Tank" module made up of a pump with a water basin and two tanks. The

two tanks are built in the front panel such that flow from the first (i.e. upper) tank can flow, through an outlet orifice located at the bottom of the tank, into the second (i.e. lower) tank. Flow from the second tank flows into the main water basin. To name a few, practical industrial applications of such Coupled-Tank structure can be found in the processing system of petro-chemical, paper making, and/or water treatment plants, [13].

Two experiments will be performed. Goal in the first experiment will be to manage the level of water in the second tank whereby the optimal controller parameters  $K_p$  and  $K_I$  will be derived at zero initial conditions. In a second experiment our aim is also to maintain a level of water in the second tank, only in that case the optimum parameters of the controller  $K_p$  and  $K_I$  will be obtained at nonzero initial conditions. While the optimal parameters  $K_p$  and  $K_I$  will be different in first and second experiment, both experiments will be conducted with the same nonzero initial conditions.

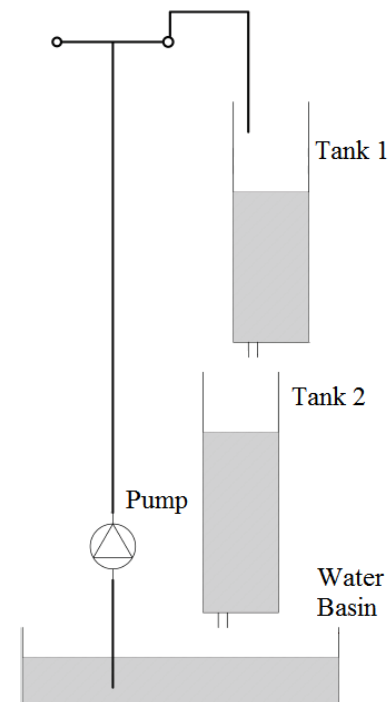


Figure 1: The Coupled Tanks plant

### 3. MATHEMATICAL MODELING

In order to obtain the mathematical model of Coupled-Tank system it is necessary to bring to mind that the pump feeds into tank 1 and that tank 2 is not considered. Thus, the input to the process is the voltage to the pump  $V_p$  and its output is the water level in tank 1,  $H_1$  (i.e. top tank). The purpose of the present modelling stage is to assure us with the system's open-loop transfer function  $W_1(z)$  and  $W_2(z)$  which in turn will be used to design an appropriate level controller. In obtaining the tank 1 equation of motion the mass balance principle can be applied to the water level in tank 1, i.e.

$$A_{t1} \frac{dH_1}{dt} = Q_{i1} - Q_{o1}, \quad (1)$$

where  $A_{t1}$  is the area of tank 1 while  $Q_{i1}$  and  $Q_{o1}$  are the inflow rate and outflow rate, respectively. The volumetric inflow rate to tank 1 is supposed to be directly proportional to the applied pump voltage, such that

$$Q_{i1} = KV_p. \quad (2)$$

Applying Bernoulli's equation for small orifices, the outflow velocity from tank 1,  $V_{o1}$ , can be expressed by the succeeding relationship

$$V_{o1} = \sqrt{2gH_1}. \quad (3)$$

In order to design and implement a linear level controller for the tank 1 system, the open-loop Laplace transfer function should be obtained. Nevertheless, by definition, such a transfer function can only express the system's dynamics from a linear differential equation. Because of that, the nonlinear equation of motion of tank 1 should be linearized around a nominal point of operation. By definition, static equilibrium at a nominal operating point  $(V_{pnom}, H_{1nom})$  is presented by the tank 1 level being at a constant position  $H_{1nom}$  due to a constant water flow generated by constant pump voltage  $V_{pnom}$ . In the case of the water level in tank 1, the operating range corresponds to small deviations heights,  $h_1$ , and small deviations voltages,  $v_p$ , from the desired nominal point  $(V_{pnom}, H_{1nom})$ . Therefore,  $h_1$  and  $v_p$  can be expressed as shown below

$$v_p = V_p - V_{pnom}, \quad (4)$$

$$h_1 = H_1 - H_{1nom}. \quad (5)$$

The derived linearized equation of motion should be a function of the system's small deviations about its nominal point  $(V_{pnom}, H_{1nom})$ . After linearization we get

$$W_1(s) = \frac{H_1(s)}{V_p(s)} = \frac{K_{dc1}}{\tau_1 s + 1}, \quad (6)$$

where  $K_{dc1}$  and  $\tau_1$  are tank 1's gain and time constant, respectively. Expression (6) represents tank 1's voltage-to-level 1 transfer function.

The water level equation of motion in tank 2 still needs to be obtained. The input to the tank 2 process is the water level,  $H_1$ , in tank 1 (generating the outflow feeding tank 2) and its output variable is the water level,  $H_2$ , in tank 2 (i.e. bottom tank). The obtained equation of motion

should be a function of the system's input and output, as previously defined.

By implementing a similar procedure by which we obtain tank 1's transfer function, now we get

$$W_2(s) = \frac{H_2(s)}{H_1(s)} = \frac{K_{dc2}}{\tau_2 s + 1}, \quad (7)$$

where  $K_{dc2}$  and  $\tau_2$  are tank 2's gain and time constant, respectively. Expression (7) represents tank 2's level 1-to-level 2 transfer function.

Discretization of continuous time system is showed on figure 2.

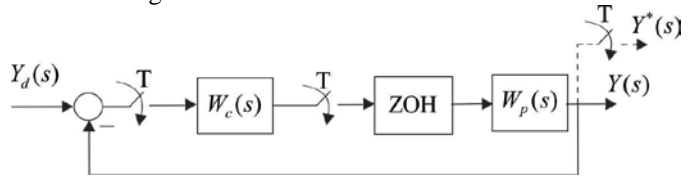


Figure 2: s-block diagram of discrete system

Zero-order hold assumes the control inputs are piecewise constant over the sampling period  $T$ . Applying zero-order hold method for finding z-transform of plant's s-transfer function we get following results

$$W_1(z) = \frac{c_2}{z - c_1}, \quad (8)$$

and

$$W_2(z) = \frac{c_4}{z - c_3}, \quad (9)$$

where  $c_1$ ,  $c_2$ ,  $c_3$  and  $c_4$  are corresponding real constants. Model verification of first tank discrete model is showed on figure 3.

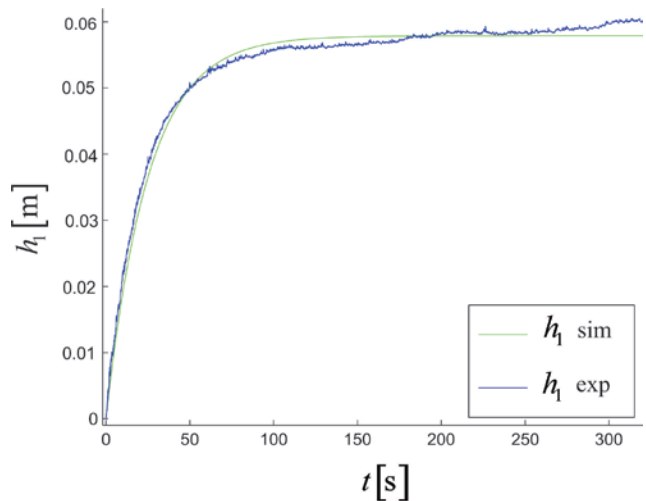


Figure 3: Verification of first tank discrete model

The transfer function of whole process is obtained by following relationship

$$W_p(z) = W_1(z)W_2(z). \quad (10)$$

Verification of whole plant's discrete transfer function model is showed on figure 4.

Transfer function of discrete PI controller is obtained by using trapezoid rule

$$W_c(z) = \frac{(2K_p + K_I T)z + K_I T - 2K_p}{2z - 2}, \quad (11)$$

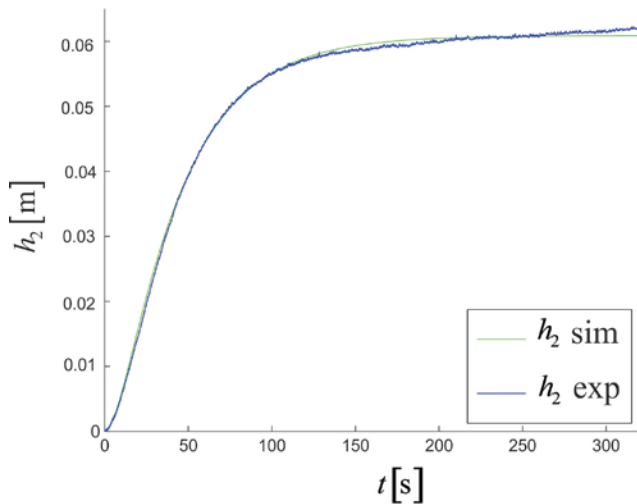


Figure 4: Verification of coupled tanks discrete model

where  $K_p$  and  $K_I$  are constants of proportional and integral gain, while  $T$  is the sampling period. Now we have z-block diagram of the same system.

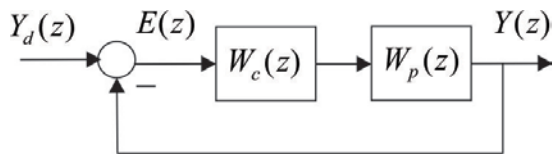


Figure 5: z-block diagram of discrete system

Transfer function of system showed on figure 5 is equal to

$$W(z) = \frac{W_c(z)W_p(z)}{1+W_c(z)W_p(z)}, \quad (12)$$

and this transfer function is used from now on.

#### 4. RELATIVE STABILITY

In the design of sampled-data control system the characteristic polynomial have parameter dependent coefficients, and it is essential to determine the ranges of parameter values which ensure the system relative stability. Sampled-data control systems can be analyzed in both the  $s$  and  $z$  planes. Siljak [14] proposed the following procedure for the determination of the parameters  $\alpha$  and  $\beta$  which are actually in our case  $K_p$  and  $K_I$ , respectively.

If the analysis is to be carried out in the  $s$  plane, the characteristic equation is given as

$$f(e^{sT}) = \sum_{k=0}^n a_k e^{ksT} = 0, \quad (13)$$

where  $a_k$  ( $k=0,1,\dots,n$ ) are real coefficients. In order to discuss sampled-data systems in the  $z$  plane, it is essential to introduce the substitution

$$z = e^{sT}, \quad (14)$$

and rewrite (13) as

$$f(z) = \sum_{k=0}^n a_k z^k = 0. \quad (15)$$

By substituting

$$z = \zeta_z \omega_z + j\omega_z \sqrt{1-\zeta_z^2}, \quad (16)$$

into (15), (15) can be rewritten as following two equations

$$\sum_{k=0}^n a_k \omega_z^k T_k(\zeta_z) = 0, \quad (17)$$

$$\sum_{k=0}^n a_k \omega_z^k U_k(\zeta_z) = 0, \quad (18)$$

where  $T_k(\zeta_z)$  and  $U_k(\zeta_z)$  are the Chebyshev functions of the first and the second kinds, respectively. The argument of these functions is denoted by  $\zeta_z$  ( $0 \leq \zeta_z \leq 1$ ). By using the relation

$$T_k(\zeta_z) = \zeta_z U_k(\zeta_z) - U_{k-1}(\zeta_z), \quad (19)$$

(17) and (18) can be further rewritten as

$$\sum_{k=0}^n -a_k \omega_z^k U_{k-1}(\zeta_z) = 0, \quad (20)$$

$$\sum_{k=0}^n a_k \omega_z^k U_k(\zeta_z) = 0. \quad (21)$$

Equations (20), (21) have an advantage over equations (17), (18) in that they use only one kind of the Chebyshev functions and the design procedure is much easier.

Now, we consider the case when the coefficients  $a_k$  ( $k=0,1,\dots,n$ ) are linear functions of system parameters  $\alpha$  and  $\beta$

$$a_k = b_k \alpha + c_k \beta + d_k. \quad (22)$$

Equations (20), (21) may be written in the form

$$\alpha B_1(\omega_z, \zeta_z) + \beta C_1(\omega_z, \zeta_z) + D_1(\omega_z, \zeta_z) = 0, \quad (23)$$

$$\alpha B_2(\omega_z, \zeta_z) + \beta C_2(\omega_z, \zeta_z) + D_2(\omega_z, \zeta_z) = 0, \quad (24)$$

where

$$B_1 = \sum_{k=0}^n -b_k \omega_z^k U_{k-1}(\zeta_z), \quad (25)$$

$$B_2 = \sum_{k=0}^n b_k \omega_z^k U_k(\zeta_z), \quad (26)$$

$$C_1 = \sum_{k=0}^n -c_k \omega_z^k U_{k-1}(\zeta_z), \quad (27)$$

$$C_2 = \sum_{k=0}^n c_k \omega_z^k U_k(\zeta_z), \quad (28)$$

$$D_1 = \sum_{k=0}^n -d_k \omega_z^k U_{k-1}(\zeta_z), \quad (29)$$

$$D_2 = \sum_{k=0}^n d_k \omega_z^k U_k(\zeta_z). \quad (30)$$

Equations (23), (24) may be solved for unknowns  $\alpha$  and  $\beta$  which gives us following expressions for parameters  $\alpha$  and  $\beta$

$$\alpha = \frac{C_1 D_2 - C_2 D_1}{B_1 C_2 - B_2 C_1}, \quad (31)$$

$$\beta = \frac{B_2 D_1 - B_1 D_2}{B_1 C_2 - B_2 C_1}. \quad (32)$$

Because attention is primary focused on the relative damping coefficient  $\zeta$ , or the undamped (natural) frequency  $\omega_n$ , it is important to replace the complex variable  $s$  in (13) with following expression

$$s = -\zeta \omega_n + j \omega_n \sqrt{1-\zeta^2}. \quad (33)$$

Then from (14), (15), (16) and (33)  $\omega_z$  and  $\zeta_z$  may be expressed as follows

$$\omega_z = e^{-\zeta\omega_n T}, \quad (34)$$

$$\zeta_z = \cos \omega_n T \sqrt{1 - \zeta^2}. \quad (35)$$

Substituting (34), (35) into (25)-(30), gives us following expressions

$$B_1 = \sum_{k=0}^n -b_k e^{-kT\omega_n \zeta} U_{k-1} \left( \cos \omega_n T \sqrt{1 - \zeta^2} \right), \quad (36)$$

$$B_2 = \sum_{k=0}^n b_k e^{-kT\omega_n \zeta} U_k \left( \cos \omega_n T \sqrt{1 - \zeta^2} \right), \quad (37)$$

$$C_1 = \sum_{k=0}^n -c_k e^{-kT\omega_n \zeta} U_{k-1} \left( \cos \omega_n T \sqrt{1 - \zeta^2} \right), \quad (38)$$

$$C_2 = \sum_{k=0}^n c_k e^{-kT\omega_n \zeta} U_k \left( \cos \omega_n T \sqrt{1 - \zeta^2} \right), \quad (39)$$

$$D_1 = \sum_{k=0}^n -d_k e^{-kT\omega_n \zeta} U_{k-1} \left( \cos \omega_n T \sqrt{1 - \zeta^2} \right), \quad (40)$$

$$D_2 = \sum_{k=0}^n d_k e^{-kT\omega_n \zeta} U_k \left( \cos \omega_n T \sqrt{1 - \zeta^2} \right). \quad (41)$$

If these equations are used in (31), (32)  $\alpha$  and  $\beta$  are expressed as functions of  $\omega_n$  and  $\zeta$ . Thus, (31) and (32) may represent in the parameter plane the loci of points corresponding to the roots with constant damping coefficient ( $\zeta$  curve), with constant undamped (natural) frequency ( $\omega_n$  curve), or with constant settling time ( $\omega_z$  curve), depending on which variable among  $\zeta$ ,  $\omega_n$  and  $\omega_z$  is considered constant. The loci of points corresponding to constant real roots, which represent the real-root boundaries in the parameter plane, are derived from the characteristic equation. If the  $z$  plane is considered, the substitution

$$z = \sigma_z, \quad (42)$$

in (13) yields the real-root boundary as

$$\alpha \sum_{k=0}^n b_k \sigma_z^k + \beta \sum_{k=0}^n c_k \sigma_z^k + \sum_{k=0}^n d_k \sigma_z^k = 0. \quad (43)$$

For a given  $\sigma_z$  this equation represents a straight line in the  $\alpha\beta$  plane which will be called  $\sigma_z$  line. A linear sampled-data control system is stable if there are no roots of the characteristic equation (13) outside the unit circle. To investigate the absolute stability in the parameter plane, it is necessary to map the unit circle onto the  $\alpha\beta$  plane by using (31), (32) and (43).

If we take into consideration  $\sigma_z = 1$ , that means that we wish all roots of characteristic equation to lie in unit circle. In that case radius is equal to one. When the radius is chosen small enough, the roots of characteristic equation are located close to the origin of the  $z$ -plane and in that case the control system behaves like a dead-beat control system, whose transient response settles down fast, [15].

Applying all previous analysis we get region in parameter plane where system have damping coefficient  $\zeta = 0.7$  or bigger, which is showed on figure 6. Denotation  $\Gamma_{0.7}(3,0)$  means that all three roots of characteristic equation (15) lie within unit circle in  $z$  plane.

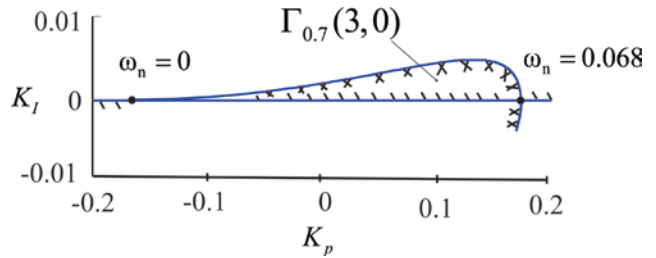


Figure 6: Region of relative stability

## 5. SYSTEM OPTIMIZATION

In general, the idea behind time domain optimization methods is to choose the PID controller parameters to minimize an integral cost functional, [16].

A design is performed on the basis of conditional optimization. The goal is to find a position of working point which assure minimum value of performance index and at the same time, relative stability to be satisfied. A position of working point in parameter plane determines relative stability and also minimal value of performance index in these cases.

In general, it is requested for a system output change  $y(kT)$  to vary as little as possible from the change of the wanted output  $y_d(kT)$  during a time interval. Integral square error may be expressed as function of the  $z$ -transform of quantity  $e(kT) = y_d(kT) - y(kT)$  depending on the means by which system is investigated

$$I = \sum_{k=0}^{\infty} e^2(kT) = \sum_{k=0}^{\infty} e(kT)e(kT). \quad (44)$$

As we know, inverse  $z$ -transform may be found using following expression

$$e(kT) = \mathcal{Z}^{-1}\{E(z)\} = \frac{1}{2\pi j} \oint_C E(z) z^{k-1} dz, \quad (45)$$

where  $C$  is circle in  $z$ -plane. So, expression (44) becomes

$$I = \sum_{k=0}^{\infty} e(kT) \frac{1}{2\pi j} \oint_C E(z) z^{k-1} dz, \quad (46)$$

$$I = \frac{1}{2\pi j} \oint_C E(z) \sum_{k=0}^{\infty} e(kT) z^{k-1} dz, \quad (47)$$

$$I = \frac{1}{2\pi j} \oint_C E(z) \sum_{k=0}^{\infty} e(kT) z^{-(1-k)} dz, \quad (48)$$

$$I = \frac{1}{2\pi j} \oint_C E(z) \sum_{k=0}^{\infty} e(kT) z^{-1} z^{-(-k)} dz, \quad (49)$$

By definition of  $z$ -transform we have

$$E(z) = \sum_{k=0}^{\infty} e(kT) z^{-k}. \quad (50)$$

In order to minimize integral cost functions (49), Parseval's theorem can be invoked to express the time functions in terms of their  $z$ -transforms, [17].

$$I = \frac{1}{2\pi j} \oint_C E(z) E(z^{-1}) z^{-1} dz. \quad (51)$$

Taking into account Cauchy residue theorem a value of the preceding expression is determined by sum of integrand residues for its poles enclosed by the contour  $C$ . As parameters  $\alpha$  and  $\beta$  are determined so that all poles of  $W(z)$  and  $E(z)$  lie in the unit circle of the plane  $z$ , it



means that no one pole of  $E(z^{-1})$  is encircled by contour  $C$ , and then performance index can be calculated as follows

$$I = \sum_{r=1}^n \text{Res} \left[ E(z)E(z^{-1})z^{-1} \right]_{z=z_r^*}, \quad (52)$$

where  $z_r^*$  is root from  $z^{-1}E(z)$ . It means calculation of integral along the contour  $C$  is substituted to calculation of integrand residue in its poles enclosed by this contour. Residues in complex poles of some rational function with real coefficients appear in conjugate-complex pairs. After summation of these residues their imaginary parts annul and real parts only remain. It is physically clear as sum of residues represents SSE, that performance index  $I$  must be positive real quantity.

After shading decomposition curve  $\Gamma_{0.7}$  and calculating performance index  $I$  for span of  $\omega_n \in ]0, 0.068[$  we find optimal values  $K_p = 0.1576$ ,  $K_I = 0.005121$  for zero initial conditions  $h_1(0) = 0$ ,  $h_2(0) = 0$ .

When we want to take into account nonzero initial conditions  $h_1(0) = -0.003$ ,  $h_2(0) = -0.005$  then we do z-transform of system difference equation by using following well known formula

$$\mathcal{Z} \{x(k+n)\} = z^n X(z) - z^n \sum_{k=0}^{n-1} x(k)z^{-k}. \quad (53)$$

Now we find new  $E(z)$  in which exists nonzero initial conditions. Using this new  $E(z)$ , and calculating performance index  $I$  using (52) new optimal controller gain values are  $K_p = 0.1476$ ,  $K_I = 0.004921$ .

Figure 7 shows the experimental results obtained for the two sets of parameters  $K_p$  and  $K_I$  at the zero and nonzero initial conditions.

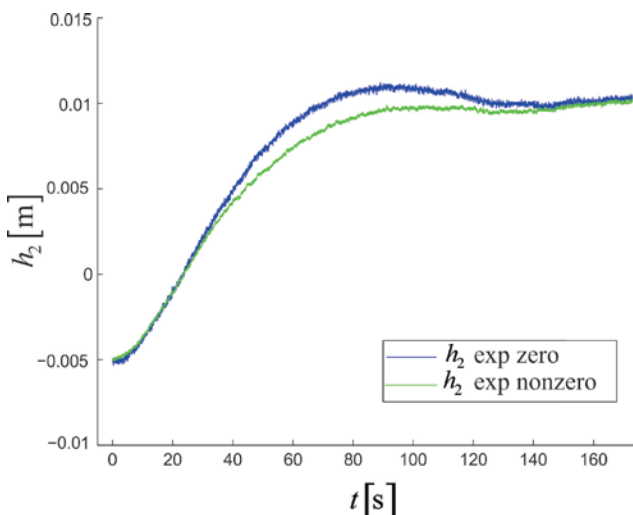


Figure 7: Experimental results

## 6. CONCLUSION

In many papers choice of optimal controller gains was carried out only on the basis of effect of inputs on behaviour of dynamic system, while the effect of initial conditions were neglected.

Effect of initial conditions on behaviour of every dynamic system must be taken into account in the process of finding optimal values for controller gains.

This paper presented methods for design of standard discrete PI controller with two adjustable parameters  $K_p$  and  $K_I$  taking into account of arbitrary initial conditions. Values of controller gains  $K_p$  and  $K_I$  which guarantee damping ratio of all closed loop poles to be greater or equal to 0.7 have been extracted.

Experimental results obtained on coupled tanks plant clearly shows that when initial conditions of plant are not zero, controller parameters derived taking into consideration initial conditions will provide optimal behaviour of system which is not guaranteed with controller parameters obtained at the zero initial conditions.

## REFERENCES

- [1] R. Matušů, "Calculation of all stabilizing PI and PID controllers", International Journal of Mathematics and Computers in Simulation, Vol. 5(3), pp. 224-231, (2011)
- [2] A. Datta, M.T. Ho, S.P. Bhattacharyya, "Structure and Synthesis of PID Controllers", Springer-Verlag, London, (United Kingdom), (2000)
- [3] M. T. Söylemez, N. Munro, H. Baki, "Fast calculation of stabilizing PID controllers", Automatica, Vol. 39(1), pp. 121-126, (2003)
- [4] J. Ackermann, D. Kaesbauer, "Design of robust PID controllers", European Control Conference, pp. 522-527, (2001)
- [5] J. Ackermann, "Robust Control: The Parameter Space Approach", Springer-Verlag, London, (United Kingdom), (2002)
- [6] K. Astrom, T. Hagglund, "PID Controllers: Theory, Design, and Tuning", Instrum. Soc. America, Research Triangle Park, (North Carolina), (1995)
- [7] H. Xu, A. Datta, S.P. Bhattacharyya, "Computation of all stabilizing PID gains for digital control systems", IEEE Trans. Automatic Control, Vol.46 (No.4), pp. 647-652, (2001)
- [8] L.H. Keel, J.I. Rego, S.P. Bhattacharyya, "A new approach to digital PID controller design", IEEE Trans. Automatic Control, Vol. 48 (No.4), pp. 687-692, (2003)
- [9] W. K. Ho, C. C. Hang, L. S. Cao, "Tuning of PID controllers based on gain and phase margin specifications", Automatica, Vol. 31(3), pp. 497-502, (1995)
- [10] F. Padula, A. Visioli, "Tuning rules for optimal PID and fractional-order PID controllers", Journal of process control Vol. 21(1), pp. 69-81, (2011)
- [11] S. Das, I. Pan, A. Gupta, "A novel fractional order fuzzy PID controller and its optimal time domain tuning based on integral performance indices", Engineering Applications of Artificial Intelligence, Vol. 25 (2), pp. 430-442, (2012)

- [12] L. T. Gruyitch, "Advances in the Linear Dynamic Systems Theory", Llumina Press, Plantation, (Florida), (2013)
- [13] Quanser inc., "Coupled Tanks - Workbook", Markham, Ontario, (Canada), (2013)
- [14] D. D. Šiljak, "Analysis and Synthesis of Feedback Control Systems in the Parameter Plane, Part II-Sampled Data Systems", IEEE Transactions on Applications and Industry, Vol. 83, pp. 449-458, (1964)
- [15] K. Ogata, "Discrete-time Control Systems", Prentice-Hall, Englewood Cliffs, (New Jersey), (1995)
- [16] S. P. Bhattacharyya, A. Datta, L. H. Keel, "Linear Control Theory – Structure, Robustness and Optimization", CRC Press, Boca Raton, (Florida), (2009)
- [17] Lj. T. Grujić, "Possibilities of Linear System Design on the Basis of Conditional Optimization in Parameter Plane, Part II-Linear Sampled-Data Systems with Constant Parameters", Automatika, pp. 61-71, (1966)
- [18] Lj. T. Grujić, "Possibilities of Linear System Design on the Basis of Conditional Optimization in Parameter Plane, Part I-Linear Continual Systems with Constant Parameters", Automatika, pp. 49-60, (1966)

# Conditional Optimization of Transient Behaviour of Plant Controlled with PI Controller Considering Initial Conditions

Goran Petrović<sup>1\*</sup>, Zoran Ribar<sup>1</sup>, Radiša Jovanović<sup>1</sup>

<sup>1</sup>Faculty of Mechanical Engineering/Control Group, University of Belgrade

*The aim of this paper is to present effect of initial conditions on choice of optimal parameters of standard PI controller and PI controller with set-point weight (two-degrees of freedom PI controller). Analysis is based on conditional optimization in the sense of formerly guaranteed relative damping ratio of all closed-loop poles and, in second case, formerly guaranteed phase margin, where additional optimization is carried away in the sense of integral criterions – integral of error squared (ISE) and integral of time absolute error (ITAE), taking into consideration initial conditions. Experimental results obtained on coupled-tanks plant are provided.*

**Keywords:** Conditional optimization, Initial conditions, PI controller, Two-degree of freedom PI controller

## 1. INTRODUCTION

PID controllers are one of the most common and most widely used tools for control, especially in industrial processes. In process control, more than 95 percent of the control loops are PID type; most of them are PI. They are based on the concept of negative feedback, which is intuitive, they have simple structure and their working principle is easy to understand, [1].

Performance of the control loop depends on the choice of PID gains. Many formulas for PID-type control design are developed after the publication of the straightforward Ziegler - Nichols tuning rule in 1942. These design methods differ in complexity, flexibility and in the amount of process knowledge used, [2, 3].

Characteristic polynomial of the single-control loop with plant and PI controller will, normally, have two adjustable parameters, which are proportional and integral gain.

The set of controllers of a given structure that stabilizes the closed loop is of fundamental importance, since every design must belong to this set and any performance specifications and any performance specifications that are imposed must be achieved over this set, [4].

Hurwitz conditions can provide us with a set of non-equalities that must hold in order for adjustable gains in order for closed-loop to be stable. Those non-equalities can be highly nonlinear. Neimark's D-decomposition is graphical technique for determining a set of all stabilizing values of two adjustable parameters. Today, one can find a number of significant results on PID stabilization, which are suitable for computer calculations, [5, 6, 7].

In order to perform conditional optimization, one focuses on specific subset of all stabilizing controller gains which provides certain closed-loop quality, not only stability. With control theory development, many papers have been also concerned with finding regions of PID controller parameters which guarantee not only stability, but robust performance, as in [8], where parametric approach was used to design PID controller satisfying  $H_\infty$  constraints, or to design PID satisfying phase and gain margin, thus demanding relative stabilization, [9].

If analytical expressions cannot be obtained for specific subsets, using computer, we can even perform brute force optimization search. Nevertheless, the fact that we are confined to the search in the stabilizing region makes the problem orders of magnitude easier, [4].

Design specifications imposed for PI controlled plant are usually concerned with disturbance rejection and good transient response to set-point changes, [1]. Measure for how good is transient response to set-point changes is often given as a cost function of the form of an integral of error, [10].

PI controller gains obtained by optimization based on the integral of error will probably result in low robustness of closed-loop control system, and/or bad disturbance rejection. Using two-degree-of-freedom (2DoF) controller, both objectives can be met, since set-point weight provides additional flexibility to the control system design, [11].

One graphical method that gives analytical expressions for determining a set of all PI controller parameters which guarantee that closed-loop poles will have relative damping ratio greater or equal to prescribed is described in, [12].

Analytical solutions that Siljak produced describe procedure for plotting the locus in the plane of adjustable parameters, in the parameter plane, as he called it, which guarantee relative damping coefficient of all transfer function poles to be greater or equal than some prescribed value.

Following mainstream of the system and control theories, many papers, as [13, 14, 15] assumed zero initial conditions for calculation of actual system output.

The past and the present of a dynamic system influences its future behaviour. If the system is without memory and without time delay, then the initial conditions express and transfer in the very condensed form, the permanent influence of the system past on its future behaviour. Evidently, the past is untouchable; the initial conditions cannot be chosen, even they are most often unpredictable. The influence of the system past is unavoidable; the initial conditions are imposed by the system history regardless of forms and intensities of current actions of the input variables.

When we wish to study the real system behaviour then we may not avoid to consider the influence of the initial conditions, [16]. It is, normally, expected that integral criterion has different value when we take into account non-zero initial conditions of input and output variables. More important, optimal controller gains, optimal in the sense of particular integral criterion, when we take into account non-zero initial conditions, can be completely different than optimal controller gains obtained when we take into account zero initial conditions.

This paper, thus, presents ideas for synthesis of standard PI controller and PI controller with two degrees of freedom using conditional optimization and taking into account initial conditions. Experimental results obtained on coupled tanks system are presented.

1.1. Notation

- $h_1(t)$  – deviation of water level in tank 1 from its nominal value,
- $h_2(t)$  – deviation of water level in tank 2 from its nominal value,
- $u(t)$  – deviation of control value from its nominal value,
- $K_p$  – PI controller proportional gain,
- $K_I$  – PI controller integral gain,
- $b$  – PI controller set-point weighting coefficient,
- $y(t)$  – deviation of system output value from its nominal value,
- $y_d(t)$  – desired value of the deviation of system output value,
- $e(t)$  – error signal,  $e = y_d(t) - y(t)$ .

2. EXPERIMENTAL SETUP

The plant used for experiment is Quanser Coupled-Tank Experiment, and sketch is given in Figure 1. The system consists of a water basin (number 1), water pump (number 2) and two tanks, namely, tank 1 (number 3) and tank 2 (number 4).

Linear equations for the coupled tanks system in vicinity of nominal point can be written as:

$$\begin{aligned} \frac{dh_1(t)}{dt} &= k_{11}h_1(t) + k_{pp}u(t), \\ \frac{dh_2(t)}{dt} &= k_{22}h_2(t) + k_{12}h_1(t). \end{aligned} \tag{1}$$

Experimentally obtained values for parameters, based on step response in the vicinity of nominal point are:  $k_{pp} = 0.00245$ ,  $k_{11} = -0.05$ ,  $k_{12} = 0.0475$ ,  $k_{22} = -0.05$ .

Arguing that linear model of nonlinear plant describes dynamic behaviour of a plant only in the vicinity of a nominal point and that it is always needed to first reach the vicinity of a nominal point in order for carried out analysis to be valid, controller always starts working when working point is in the vicinity of the nominal point.

It is not necessary and maybe not achievable that all initial conditions are equal zero in the moment when controller starts working. In order to present illustrative example, controller will start working when water level in tank 2 is 2cm less than nominal value. Until the moment when water level in tank 2 reaches value that is 2cm less

than nominal value, control signal will be nominal. Controller will be given command to raise level 2cm above nominal.

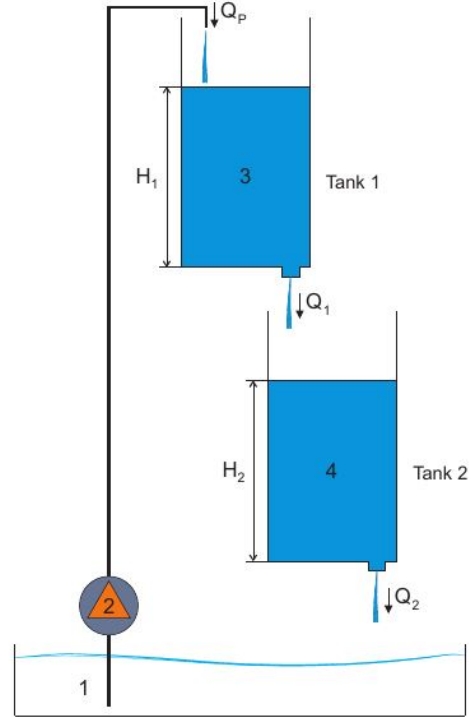


Figure 1: Experimental setup

3. SYNTHESIS OF STANDARD PI CONTROLLER

At first, the system that consists of plant and textbook PI controller is considered:

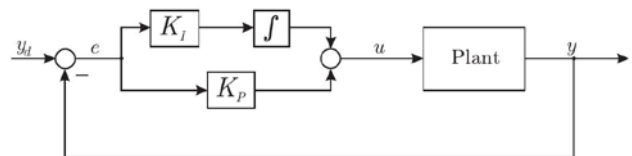


Figure 2: Plant and standard PI controller

Textbook PI controller equation is given by:

$$u(t) = K_p e(t) + K_I \int_0^t e(\tau) d\tau. \tag{2}$$

Based on (1), plant transfer function becomes:

$$W_p(s) = \frac{k_{pp}k_{12}}{(s - k_{11})(s - k_{22})} = \frac{N(s)}{D(s)}. \tag{3}$$

System characteristic polynomial becomes:

$$f(s) = sD(s) + (K_p s + K_I)N(s). \tag{4}$$

Starting from the methods of conditional optimization proposed in [17], idea of conditional optimization using Siljak's generalized parameter plane method is used to establish connection with initial conditions. Using algorithm presented in [12] analytical parametric expressions for controller gains, which guarantee damping ratio of all closed-loop poles to be

greater or equal to 0.7, with achievable undamped frequency as a parameter, can be obtained as:

$$\begin{aligned} K_p(\omega) &= -21.4823 + 1,203.01\omega - 8,249.19\omega^2, \\ K_I(\omega) &= 859.291\omega^2 - 12,030.1\omega^3. \end{aligned} \quad (5)$$

Parametric equations (5) are used to draw locus in the parameter plane and determine span of achievable undamped frequency.

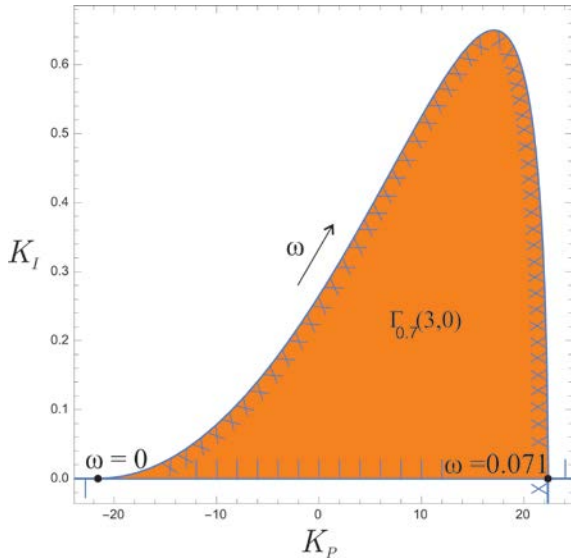


Figure 3: Parametric plane locus for  $\zeta = 0.7$

After shading, as described in [12], we deduce that span of  $\omega$  which guarantees prescribed degree of stability is  $\omega \in ]0, 0.0714286[$ .

For every achievable undamped frequency  $\omega$  in the determined range, there exists a pair  $(K_p(\omega), K_I(\omega))$  which guarantees that relative damping ratio of all closed-loop poles is greater or equal to prescribed and this knowledge gives us rough idea about transient response to set-point change, but there is no knowledge of the value of the cost function.

Since it is known that value of  $K_I$  is explicit measure of low-frequency disturbance rejection [1],  $\omega$  can be chosen so that  $K_I$  is maximum in order to have the best disturbance rejection.

Alternatively, if in addition to achieved relative damping ratio of all closed-loop poles, it is wanted to choose optimal controller gains in the sense of integral criterion value, we could choose  $\omega$  so that integral criterion, i.e., the cost function, has the smallest value. It is already pointed out that in the mainstream of this kind of optimization only zero initial conditions were used.

By fixing initial value of the integrator to zero and by having fixed  $h_2(0) = -0,02m$ , we can visually present how integral criterion value depends on  $\omega$  and  $h_1(0)$ . Value of  $h_1(0)$  is known only approximately by means of simulation and visual inspection in the moment when regulator starts working and because of that controller gains must be determined in the moment when regulator starts working.

In the following two Figures are presented values of ISE and ITAE as a function of  $h_1(0)$  and  $\omega$  for fixed  $h_2(0) = -0.02m$ , which is the only value we can rely on.

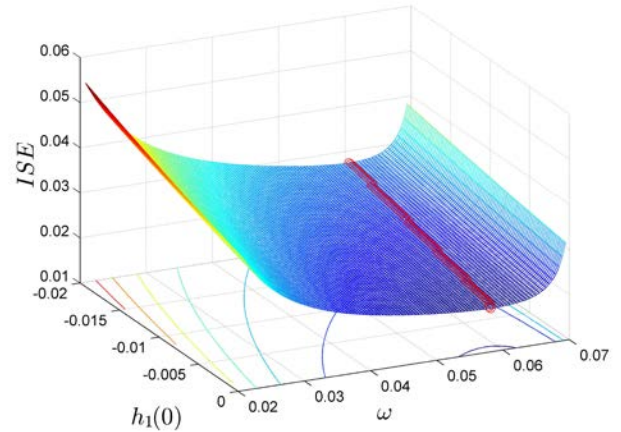


Figure 4: ISE as a function of  $\omega$  and  $h_1(0)$  in the case of plant controlled by standard PI controller

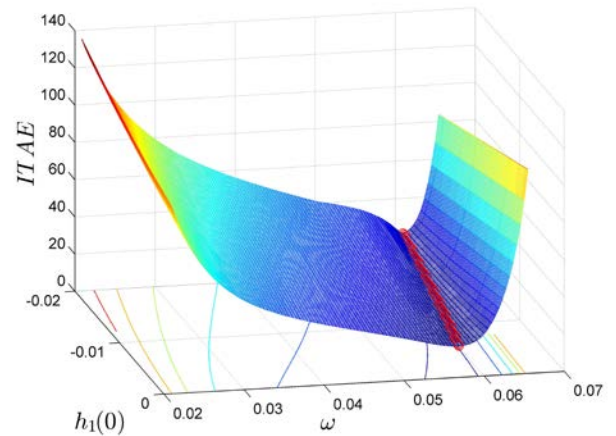


Figure 5: ITAE as a function of  $\omega$  and  $h_1(0)$  in the case of plant controlled by standard PI controller

Looking at Figures 4 and 5, it can be deduced that initial conditions influence choice of optimal value of  $\omega$  and that they cannot be ignored, which is more obvious in the case when ITAE criterion is used. ITAE criterion here also shows property of selectability, [10].

For example, optimal values of controller gains for  $h_1(0) = 0m$  and  $h_2(0) = -0.02m$  in the sense of ITAE are  $K_p = 20.2613$  and  $K_I = 0.5659$ , which are not same as optimal values for zero initial conditions,  $K_p = 18.5938$  and  $K_I = 0.6359$ . Also, for example, optimal values of controller gains for  $h_1(0) = -0.01m$  and  $h_2(0) = -0.02m$  in the sense of ITAE are  $K_p = 20.9147$  and  $K_I = 0.5055$ .

An idea for calculation of optimal values of controller gains is that look-up table is used, or that dependency of optimal  $\omega$  on  $h_1(0)$  is given as some analytical expression. Then, in the moment when regulator starts working, optimal value of  $\omega$  is calculated and corresponding values for  $K_p$  and  $K_I$  are determined.

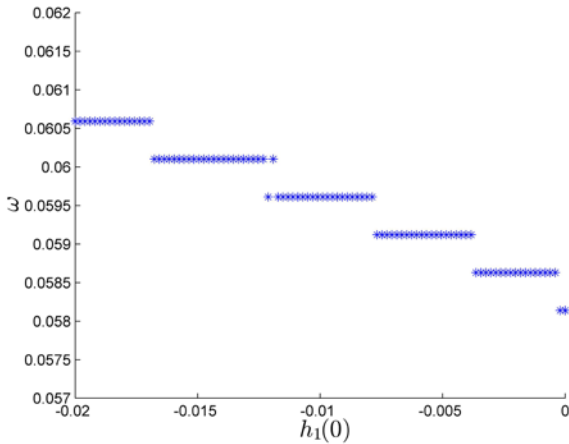


Figure 6: Optimal values of  $\omega$  as a function  $h_1(0)$  in the sense of ISE in the case of plant controlled by standard PI controller

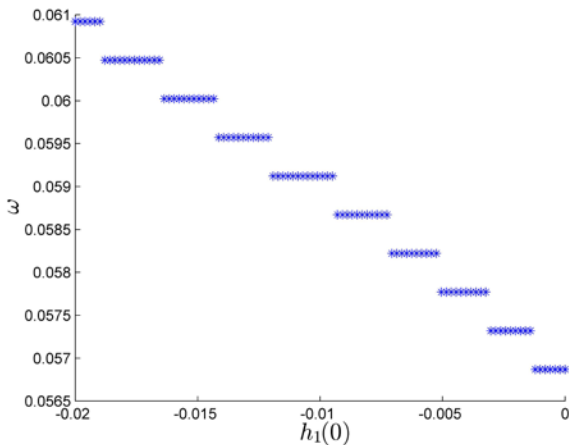


Figure 7: Optimal values of  $\omega$  as a function  $h_1(0)$  in the sense of ITAE in the case of plant controlled by standard PI controller

Distribution of optimal values of  $\omega$  is shown in Figures 6 and 7 and from these figures one can decide whether look-up table will be used or polynomial approximation.

4. SYNTHESIS OF 2DOF PI CONTROLLER

In order to decouple problems of choosing system parameters so that good disturbance rejection and good transient response to set-point change are achieved, two-degree-of-freedom (2DoF) PI controller is introduced.

Block diagram of the system that consists of the plant and 2DoF PI controller is given in the Figure 8.

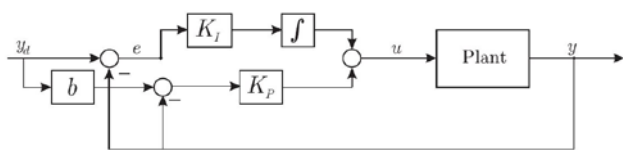


Figure 8: Plant and 2DoF PI controller

First step in the synthesis of the 2DoF controller can be choice of the proportional and integral gain so that certain value of phase margin is achieved for maximum value of  $K_I$ . By performing this kind of analysis, certain

level of relative stability is achieved and disturbance rejection is the best possible in that case. Using algorithm presented in [1] or [4] this problem can be easily solved using computer.

Optimal values of the controller gains obtained in this way are  $K_p = 22.5574$  and  $K_I = 0.5401$ , for phase margin value of  $60^\circ$ .

Similar analysis can be performed by focusing on choice of the controller gains so that magnitude of the sensitivity function has a value which is less than some prescribed and that this is achieved for values of controller gains so that the best possible disturbance and/or noise rejection is achieved. Maximum value of the sensitivity function determines minimum phase margin, [18].

After choosing controller gains using previously described or some other procedures, problem of conditional optimization can be reduced to choice of weight  $b$  so that integral cost has the smallest value.

From Figures 9 and 10, it can be seen that value of  $b$  depends on  $h_1(0)$  in the case of ITAE, but doesn't, or very little depend on  $h_1(0)$  in the case of ISE.

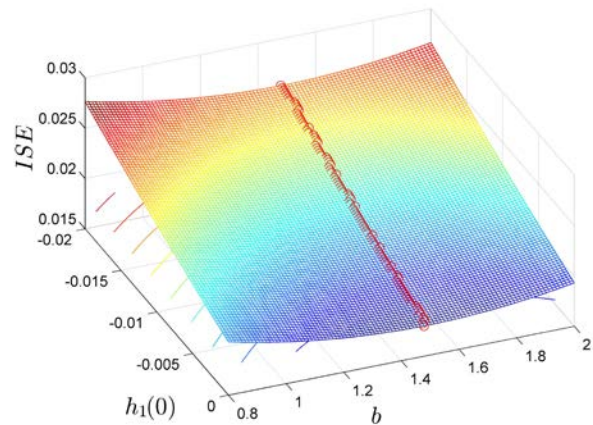


Figure 9: ISE as a function of  $\omega$  and  $h_1(0)$  in the case of plant controlled by 2DoF PI controller

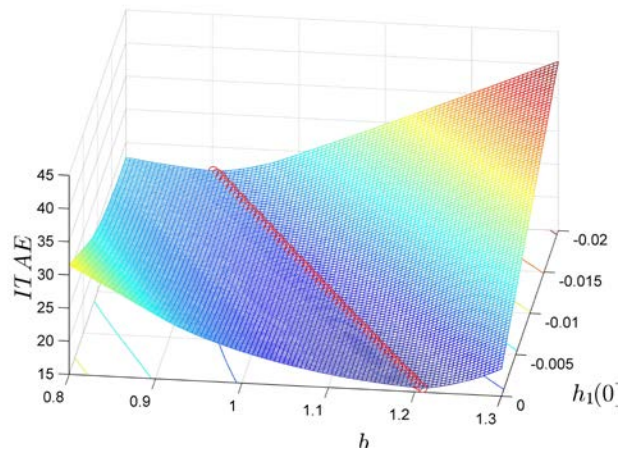


Figure 10: ITAE as a function of  $\omega$  and  $h_1(0)$  in the case of plant controlled by 2DoF PI controller

Now, one can proceed to observation of dependence of  $b$  on  $h_1(0)$ . This is shown in Figures 11 and 12.

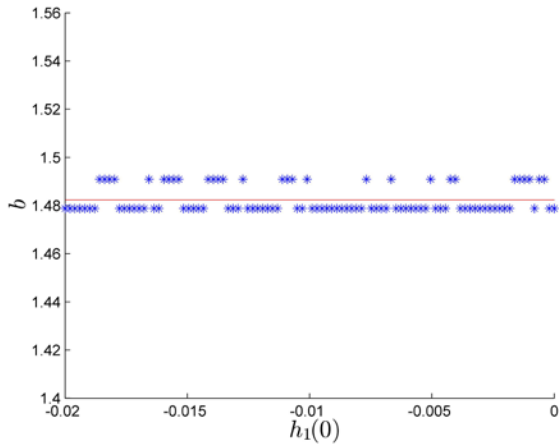


Figure 11: Optimal values of  $b$  as a function  $h_1(0)$  in the sense of ISE in the case of plant controlled by 2DoF PI controller

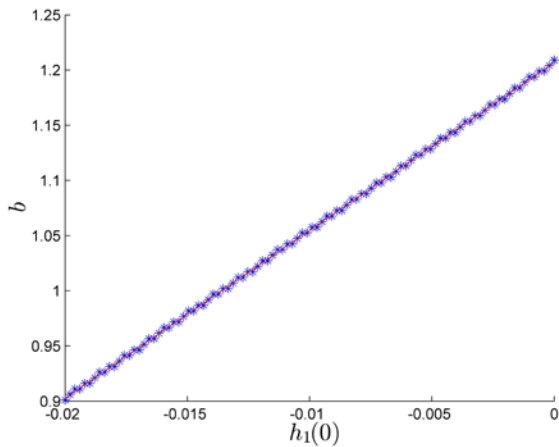


Figure 12: Optimal values of  $b$  as a function  $h_1(0)$  in the sense of ITAE in the case of plant controlled by 2DoF PI controller

It is interesting to observe in Figure 12 that optimal value of  $b$  in the sense of ITAE almost linearly depends on  $h_1(0)$  and this relation can be used in some more complicated control algorithm.

Nevertheless, since this linear relation is easier to implement in the controller and since it is weight coefficient in the two-degree of freedom PI controller recommended value to change in order to affect transient behaviour, experimental results that will be presented are acquired in the case of 2DoF PI controller for different values of weight coefficient  $b$ .

Two strategies for choice of  $b$  have been used. Firstly, relation obtained by using least squares method is:

$$b = 1.2015 + 15.0376h_1(0). \quad (6)$$

In the moment when controller starts working, value for  $b$  is determined using (6). It is again mentioned that controller starts working in the moment when  $h_2(0) = -0.02\text{m}$ .

Secondly, fixed value of  $b = 1.414$  is used, and this is a value that is optimal in the sense of ITAE for all zero initial conditions.

## 5. EXPERIMENTAL RESULTS

Plant step response in the vicinity of nominal point has been used for determination of linear system coefficients and is presented in the Figure 13.

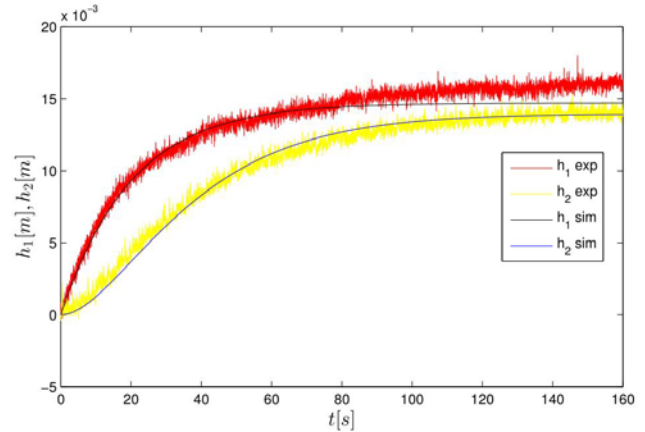


Figure 13: Plant step response in the vicinity of nominal point

Finally, main figure with experimental results is Figure 14. Two transient responses shown match different values of weight coefficient  $b$ , as mentioned. Transient response shown in blue colour is obtained for  $b = 1.0737$  and transient response in green colour is obtained for  $b = 1.414$ .

## 6. CONCLUSION

In the mainstream of control theory, only effect of inputs on behaviour of dynamic system has been considered when it comes to choice of optimal controller gains which minimize value of integral criterion related to transient response.

Effect of initial conditions on behaviour of every dynamic system cannot be neglected, so they have to be accounted in the process of controller design. This paper presented methods for design of standard PI controller with two adjustable parameters and two-degree of freedom PI controller with three adjustable parameters, taking into consideration initial conditions.

In case of standard PI controller, values of gains which guarantee damping ratio of all closed-loop poles to be greater or equal to 0.7 have been extracted. Three-dimensional plots showing which pair of gains minimizes ISE and ITAE, taking into consideration initial conditions, were shown.

Gains of two-degree of freedom PI controller were chosen so that phase margin is  $60^\circ$ . Three-dimensional plots showing which value of weight coefficient minimizes ISE and ITAE, taking into consideration initial conditions, were shown.

All above mentioned ideas were illustrated on the example of real hydraulic system which consists of two coupled tanks. Experimental results clearly show that when initial conditions are not zero, only controller parameters chosen taking into consideration initial conditions will provide optimal behaviour of system, as opposite to parameters chosen for zero initial conditions.

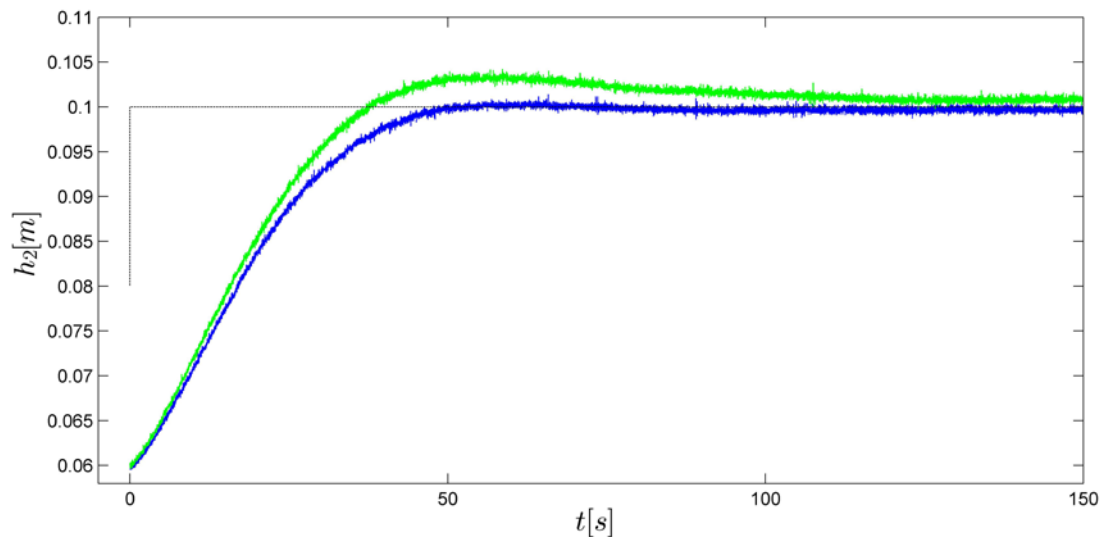


Figure 14: Transient response for two different values of weight coefficient  $b$

## REFERENCES

- [1] K. J. Åström and T. Hägglund, "Advanced PID control", ISA-The Instrumentation, Systems and Automation Society, (2006)
- [2] J. G. Ziegler and N. B. Nichols. "Optimum settings for automatic controllers", *trans. ASME* 64.11, (1942)
- [3] Y. Li, S. Andong and W. Yuangang, "Synthesis of PID-type controllers without parametric models: A graphical approach", *Energy Conversion and Management* 49.8, pp. 2392-2402, (2008)
- [4] S. P. Bhattacharyya, A. Datta and L. H. Keel., "Linear control theory: structure, robustness, and optimization", Vol. 33. CRC press, (2009)
- [5] Y. I. Neimark, "Stability of linearized systems", LKVVIA, Leningrad (1949)
- [6] A. Datta, M. T. Ho and S. P. Bhattacharyya, "Structure and synthesis of PID controllers", Springer Science & Business Media, (2013)
- [7] M. T. Söylemez, N. Munro and H. Baki, "Fast calculation of stabilizing PID controllers", *Automatica* 39.1, pp. 121-126 (2003)
- [8] M. T. Ho, "Synthesis of  $H_\infty$  PID controllers: A parametric approach", *Automatica* 39.6, pp. 1069-1075, (2003)
- [9] N. Tan, I. Kaya, C. Yeroglu and D. P. Atherton, "Computation of stabilizing PI and PID controllers using the stability boundary locus", *Energy Conversion and Management* 47.18, pp. 3045-3058, (2006)
- [10] D. Graham and R. C. Lathrop, "The synthesis of optimum transient response: Criteria and standard forms", *Transactions of the American Institute of Electrical Engineers, Part II: Applications and Industry* 72.5, pp. 273-288, (1953)
- [11] V. M. Alfaro and R. Vilanova, "Set-point weight selection for robustly tuned PI/PID regulators for over damped processes", In *Emerging Technologies & Factory Automation (ETFA)*, 2012 IEEE 17th Conference on (pp. 1-7). IEEE., (2012)
- [12] D. Siljak, "Generalization of the parameter plane method", *IEEE Transactions on Automatic Control* 11.1, pp. 63-70, (1966)
- [13] W. K. Ho, C. C. Hang and L. S. Cao, "Tuning of PID controllers based on gain and phase margin specifications", *Automatica*, 31(3), pp. 497-502, (1995)
- [14] F. Padula and A. Visioli, "Tuning rules for optimal PID and fractional-order PID controllers", *Journal of process control* 21.1, pp. 69-81, (2011)
- [15] S. Das, I. Pan, S. Das and A. Gupta, "A novel fractional order fuzzy PID controller and its optimal time domain tuning based on integral performance indices", *Engineering Applications of Artificial Intelligence* 25.2, pp. 430-442, (2012)
- [16] L. T. Gruyitch, "Advances in the Linear Dynamic Systems Theory", Aeon Publishing Incorporated, (2013)
- [17] D. Siljak, "Square Error Optimization with a Relative Stability Constraint (in Yugoslavian)", PhD Thesis, University of Belgrade, Yugoslavia, (1963)
- [18] S. Skogestad and I. Postlethwaite, "Multivariable feedback control: analysis and design (Vol. 2)", New York: Wiley, (2007)



# Identification of MIMO Hammerstein Models in the Presence of Piecewise Polynomial Disturbances using Kaczmarz Algorithm

Vojislav Filipovic<sup>1\*</sup>, Vladimir Djordjevic<sup>1</sup>

<sup>1</sup>Department for Automatic Control, Robotics and Fluid Technique, Faculty of Mechanical and Civil Engineering, University of Kragujevac, Kraljevo (Serbia)

*The Kaczmarz algorithm, originally, is an iterative projection algorithm for solving a linear system of equations. After the publications of the result, it was observed that it is possible to design simple recursive algorithm for parameters estimation. Because of its simplicity algorithm found different applications including tomography, distributed computation, computer vision and medicine (scanners) to name a few. In this paper, we try to expand the area of applications. Namely, we consider the problem of Hammerstein model identification. It is supposed that system has MIMO (multi-input multi-output) structure. The nonlinear part of Hammerstein model has general structure and disturbance has piecewise polynomial form. The algorithm is novel and the key ingredient of the algorithm is the Shannon – Kulebakin operator.*

**Keywords: MIMO Hammerstein models, Piecewise polynomial disturbance, Shannon-Kulebakin operator, Kaczmarz algorithm**

## 1. INTRODUCTION

Multivariable systems represent an important class of systems in practice. Special attention is devoted to their identification [1]. In this paper, we consider identification of nonlinear multiple-input multiple-output (MIMO) systems. A wide class of nonlinear systems is modeled as a linear model cascading with a static nonlinear function. In this paper, we consider the situation when the static function is prior to the linear subsystem. Such kind of models is known as a Hammerstein models and are relevant for engineering systems, social systems, biological systems, machine learning, pattern recognition and others. The Hammerstein models belong to the block-oriented models [2]. Here the static nonlinear block is given in the general polynomial form while the linear model is an output error (OE) model.

Special attention is given to modeling disturbances. The common assumption is that disturbance has Gaussian distribution [3]. In references [4]-[5] it is assumed that the stochastic disturbance is non-Gaussian. This assumption is confirmed in practice [6] where is shown that in a population of observations there are rare large observations (outliers). Owing to that fact the great effort has been invested in creating algorithms which have a low sensitivity to changes in the stochastic disturbance distribution. That part of identification theory is based on robust statistics [7].

In this paper, we consider a different mode to modeling the disturbance. In classical control theory, disturbances are described as steps, ramps, and sinusoids. Here we model disturbances with signals which share properties both with deterministic signals generated by difference equations and with stochastic processes [8]. It is proved that a wide class of continuous function can be represented in the form of solutions of homogeneous differential equations [9]. That is the consequence of investigations of differential analyzers. Similar results are given by Kulebakin for electrical driver [10]. From those results, it is possible to construct Shannon-Kulebakin

operator which can be very useful for the design of invariant control systems [11]. That operator is compensation matrix and has, as will be seen, a great influence on system identification [12].

Estimation of the unknown parameters is performed by Kaczmarz algorithm [13]. That is very simple and important algorithm in different areas: tomography, computer vision, synchronization in sensor networks, learning and adaptive control to name a few. In this paper, we extend the application of the algorithm to the identification of process models. The algorithm is new. As far as authors know that is the first application to the identification of MIMO models. The main feature of the algorithm is simplicity and version of the algorithm for SISO systems is applied to scanners.

## 2. MATHEMATICAL MODELS OF MIMO HAMMERSTEIN SYSTEM

Suppose that MIMO Hammerstein model has next structure

$$\mathbf{y}_k = \mathbf{F}^{-1}(q^{-1})\mathbf{B}(q^{-1})\mathbf{f}(\mathbf{u}_k) + \mathbf{d}_k \quad (1)$$

where  $\mathbf{B}(q^{-1})$  and  $\mathbf{F}(q^{-1})$  are matrix polynomial and  $q^{-1}$  denotes the shift-back operator ( $q^{-1}\mathbf{x}_k = \mathbf{x}_{k-1}$ ). Orders of polynomials  $\mathbf{B}(q^{-1})$  and  $\mathbf{F}(q^{-1})$  are  $m$  and  $n$  respectively

$$\mathbf{B}(q^{-1}) = \mathbf{B}_1 q^{-1} + \dots + \mathbf{B}_m q^{-m} \quad (2)$$

$$\mathbf{F}(q^{-1}) = \mathbf{I} + \mathbf{F}_1 q^{-1} + \dots + \mathbf{F}_n q^{-n} \quad (3)$$

where  $\mathbf{B}_i$  ( $i=1,2,\dots,m$ ) are  $r \times r$  matrices and  $\mathbf{F}_i$  ( $i=1,2,\dots,n$ ) are  $r \times r$  matrices. The disturbance  $\mathbf{d}_k$  is piecewise polynomial disturbances. The Hammerstein model is given in the Figure 1.

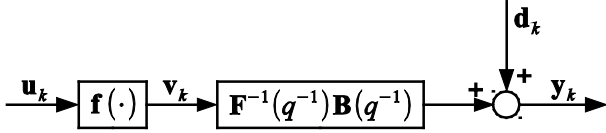


Figure 1: MIMO Hammerstein model

The function  $\mathbf{f}(\mathbf{u}_k)$  is a nonlinear vector function

$$\mathbf{f}(\mathbf{u}_k) = [f_1(u_k^1), f_2(u_k^2), \dots, f_r(u_k^r)]^T, \quad \mathbf{f}(\mathbf{u}_k) \in R^r \quad (4)$$

where  $f_i(u_k^i)$  ( $i=1,2,\dots,r$ ) is a nonlinear function of a known basis  $(\gamma_1, \gamma_2, \dots, \gamma_r)$

$$f_i(u_k^i) = d_1^i \gamma_1(u_k^i) + d_2^i \gamma_2(u_k^i) + \dots + d_{n_j}^i \gamma_{n_j}(u_k^i) \quad (5)$$

where  $d_j^i$  ( $i=1,2,\dots,r; j=1,2,\dots,n_j$ ) are unknown parameters.

Let us introduced

$$s = \max_j \{n_j\} \quad (6)$$

For nonlinear vector function  $\mathbf{f}(\mathbf{u}_k)$  from relations (5) and (6), it follows that

$$\begin{aligned} \mathbf{f}(\mathbf{u}_k) &= \begin{bmatrix} f_1(u_k^1) \\ f_2(u_k^2) \\ \vdots \\ f_r(u_k^r) \end{bmatrix} = \\ &= \begin{bmatrix} d_1^1 \gamma_1(u_k^1) + d_2^1 \gamma_2(u_k^1) + \dots + d_s^1 \gamma_s(u_k^1) \\ d_1^2 \gamma_1(u_k^2) + d_2^2 \gamma_2(u_k^2) + \dots + d_s^2 \gamma_s(u_k^2) \\ \vdots \\ d_1^r \gamma_1(u_k^r) + d_2^r \gamma_2(u_k^r) + \dots + d_s^r \gamma_s(u_k^r) \end{bmatrix} \end{aligned} \quad (7)$$

where some matrix elements, according to relation (6), are equal to zero.

Let us define

$$\mathbf{D}_i = \begin{bmatrix} d_i^1 & & \mathbf{0} \\ & d_i^2 & \\ & & \ddots \\ \mathbf{0} & & & d_i^r \end{bmatrix}, \quad i=1,2,\dots,s \quad (8)$$

$$\Gamma_i(u_k) = \begin{bmatrix} \gamma_1(u_k^1) \\ \gamma_2(u_k^1) \\ \vdots \\ \gamma_s(u_k^1) \end{bmatrix}, \quad i=1,2,\dots,s \quad (9)$$

Using relation (8) and (9) one can get

$$\mathbf{D}_i \Gamma_i(u_k) = \begin{bmatrix} d_i^1 \gamma_1(u_k^1) \\ d_i^2 \gamma_2(u_k^2) \\ \vdots \\ d_i^r \gamma_s(u_k^r) \end{bmatrix}, \quad i=1,2,\dots,s \quad (10)$$

From (7) and (10) it follows that

$$\mathbf{f}(\mathbf{u}_k) = \sum_{i=1}^s \mathbf{D}_i \Gamma_i(u_k) \quad (11)$$

**Remark 1:** The nonlinear function in relation (11) has general form and the first time in the literature is proposed in [14].

In what follows we will shortly describe disturbance  $\mathbf{d}_k^T = [d_k^1, d_k^2, \dots, d_k^r]$ . The piecewise polynomial disturbances have next analytical form [8]

$$d_k^i = \begin{cases} d_k^{0,i} = d_0^i + d_0^i k + \dots + (d_0^i)^{m_0} k^{m_0}, & 0 \leq k < n_0 \\ d_k^{1,i} = d_1^i + d_1^i k + \dots + (d_1^i)^{m_1} k^{m_1}, & n_0 \leq k < n_1 \\ \vdots & \vdots \\ d_k^{r,i} = d_r^i + d_r^i k + \dots + (d_r^i)^{m_r} k^{m_r}, & n_{r-1} \leq k < n_r \end{cases} \quad (12)$$

where  $d_k^i$  is the  $i$ -th component of disturbance  $\mathbf{d}_k$ .

It is possible to distinguish two class of piecewise polynomial disturbances. The first one is the continuous disturbances (Figure 2).

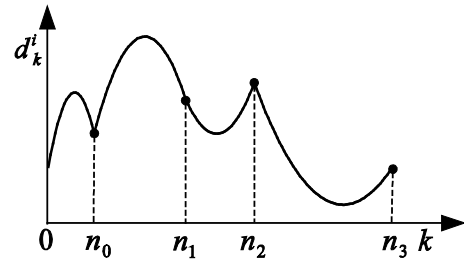


Figure 2: Piecewise polynomial disturbance (continuous case)

The second class of disturbance is discontinuous disturbances (Figure 3).

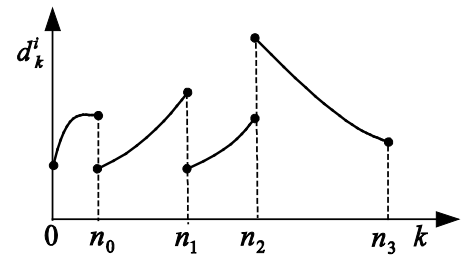


Figure 3: Piecewise polynomial disturbance (discontinuous case)

### 3. FUNDAMENTAL ASPECTS OF KACZMARZ ALGORITHM

The Kaczmarz method is an iterative projection algorithm for solving a linear system of equations [15]. Comprehensive treatment of algorithm and some generalization is presented in reference [16]. Due to its simplicity, the Kaczmarz algorithm has found numerous applications. The Kaczmarz algorithm is independently rediscovered in the field of image reconstruction under the name ART (algebraic reconstruction technique) [17].

Let  $\mathbf{A} \in \mathbb{R}^{m \times n}$  and  $\mathbf{b} \in \mathbb{R}^m$ . The Kaczmarz method operates as follows: Initially, it starts with an arbitrary vector  $\mathbf{x}^{(0)} \in \mathbb{R}^n$ . In each iteration, the Kaczmarz method runs through the rows of  $\mathbf{A}$  in a cyclic manner and for each selected row, say the  $i$ -th row  $\mathbf{A}^{(i)}$ , it orthogonally projects the current estimate vector onto the affine hyperplane defined by the constraint of  $\mathbf{A}\mathbf{x} = \mathbf{b}$ , i.e.  $(\mathbf{x} | \langle \mathbf{A}^{(i)}, \mathbf{x} \rangle = \mathbf{b}_i)$ , where  $\langle \cdot, \cdot \rangle$  Euclidian inner product. To be more specific assuming that the  $i_k$ -th row has been selected at the  $k$ -th iteration, than the  $(k+1)$ -th estimate vector  $\mathbf{x}^{(k+1)}$  is obtained as

$$\mathbf{x}^{(k+1)} = \mathbf{x}^{(k)} + \lambda_k \frac{\mathbf{b}_{i_k} - \langle \mathbf{A}^{(i_k)}, \mathbf{x}^{(k)} \rangle}{\|\mathbf{A}^{(i_k)}\|^2} \quad (13)$$

where  $\lambda_k \in \mathbb{R}^1$  is the relaxation parameter and  $\|\cdot\|$  denotes Euclidean norm. The original Kaczmarz method corresponds to  $\lambda_k = 1$  for  $k \geq 0$  and all other setting of the  $\lambda_k$  are referred to as the relaxed Kaczmarz method [18].

The geometrical interpretation is given in the next figure.

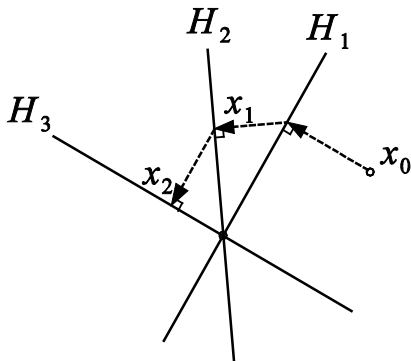


Figure 4: Geometrical interpretation of Kaczmarz algorithm

The hyperplane  $H_i$  is defined as

$$H_i = \{ \mathbf{x} | \mathbf{a}_i^T \mathbf{x} = b_i \} \quad (14)$$

where the  $i$ -th row of matrix  $\mathbf{A}$  is denoted with  $\mathbf{a}_i^T$  and  $i$ -th element of  $\mathbf{b}$  as  $b_i$ . The main task is to find solution of equation

$$\mathbf{A}\mathbf{x} = \mathbf{b} \quad (15)$$

where  $\mathbf{A} \in \mathbb{R}^{m \times n}$ ,  $m \geq n$ , is of full column rank and  $\mathbf{b} \in \mathbb{R}^m$ . Geometrically, the solution of (15) can be thought as the intersection of all hyperplanes  $\{H_i\}_{i=1}^m$ .

### 4. RECURSIVE FORM OF KACZMARZ ALGORITHM FOR IDENTIFICATION OF MIMO HAMMERSTEIN MODELS

Generally, identification procedure depends on the disturbance. The disturbance can, however, be rejected to eliminate their effect on the system identification. Such case will be considered in this paper.

Let us suppose that disturbance satisfies a difference equation

$$\mathbf{d}_k = \mathbf{D}(q^{-1})\mathbf{d}_{k-1} \quad (16)$$

where  $\mathbf{D}(q^{-1})$  is a  $(r \times r)$  matrix with elements in form of polynomials. The equation (16) is the equation of extrapolation or prediction and the matrix  $\mathbf{D}(q^{-1})$  is a prediction matrix.

We can introduce Shannon-Kulebakin operator

$$\mathbf{T}(q^{-1}) = 1 - q^{-(t+1)}\mathbf{D}(q^{-1}) \quad (17)$$

From (16) and (17) it follows that

$$\mathbf{T}(q^{-1})\mathbf{d}_k = 0 \quad (18)$$

The Shannon-Kulebakin operator we will call compensation operator or compensation matrix. In the presence of sufficiently complete information on disturbance a matrix  $\mathbf{T}(q^{-1})$  is quite easily determined.

The form of matrix  $\mathbf{T}(q^{-1})$  is

$$\mathbf{T}(q^{-1}) = \begin{bmatrix} t_1(q^{-1}) & & \mathbf{0} \\ & \ddots & \\ \mathbf{0} & & t_p(q^{-1}) \end{bmatrix} \quad (19)$$

where  $t_i(q^{-1})$  are polynomials. For sake of simplicity we suppose that

$$t_1(q^{-1}) = \dots = t_p(q^{-1}) = t(q^{-1}) \quad (20)$$

From (1) and (18) it follows that

$$\begin{aligned} \mathbf{T}(q^{-1})\mathbf{y}_k &= \mathbf{T}(q^{-1})\mathbf{F}^{-1}(q^{-1})\mathbf{B}(q^{-1})\mathbf{f}(\mathbf{u}_k) + \\ &+ \mathbf{T}(q^{-1})\mathbf{d}_k = \mathbf{T}(q^{-1})\mathbf{F}^{-1}(q^{-1})\mathbf{B}(q^{-1})\mathbf{f}(\mathbf{u}_k) \end{aligned} \quad (21)$$

From relation (20) and (21) we have

$$\mathbf{T}(q^{-1})\mathbf{y}_k = \mathbf{F}^{-1}(q^{-1})\mathbf{B}(q^{-1})\mathbf{T}(q^{-1})\mathbf{f}(\mathbf{u}_k) \quad (22)$$

and finally

$$\mathbf{F}(q^{-1})\mathbf{T}(q^{-1})\mathbf{y}_k = \mathbf{B}(q^{-1})\mathbf{T}(q^{-1})\mathbf{f}(\mathbf{u}_k) \quad (23)$$

Using last relation we can define filtered output and input

$$\mathbf{y}_k^f = \mathbf{T}(q^{-1})\mathbf{y}_k \quad (24)$$

$$\mathbf{f}^f(\mathbf{u}_k) = \mathbf{T}(q^{-1})\mathbf{f}(\mathbf{u}_k) \quad (25)$$

Now equation (23) becomes

$$\mathbf{F}(q^{-1})\mathbf{y}_k^f = \mathbf{B}(q^{-1})\mathbf{f}(\mathbf{u}_k) \quad (26)$$

The identification problem is to estimation matrix polynomials  $\mathbf{F}(q^{-1})$  and  $\mathbf{B}(q^{-1})$ . One can see that, through filtration, the influence of disturbance is removed.

$$\begin{aligned} \mathbf{B}(q^{-1})\mathbf{f}^f(\mathbf{u}_k) &= (\mathbf{B}_1q^{-1} + \mathbf{B}_2q^{-2} + \dots + \mathbf{B}_mq^{-m})\mathbf{f}^f(\mathbf{u}_k) = \mathbf{B}_1\mathbf{f}^f(\mathbf{u}_{k-1}) + \mathbf{B}_2\mathbf{f}^f(\mathbf{u}_{k-2}) + \dots + \mathbf{B}_m\mathbf{f}^f(\mathbf{u}_{k-m}) = \\ &= \mathbf{B}_1[\mathbf{T}(q^{-1})\mathbf{D}_1\Gamma_1(\mathbf{u}_{k-1}) + \mathbf{T}(q^{-1})\mathbf{D}_2\Gamma_2(\mathbf{u}_{k-1}) + \dots + \mathbf{T}(q^{-1})\mathbf{D}_s\Gamma_s(\mathbf{u}_{k-1})] + \\ &+ \mathbf{B}_2[\mathbf{T}(q^{-1})\mathbf{D}_1\Gamma_1(\mathbf{u}_{k-2}) + \mathbf{T}(q^{-1})\mathbf{D}_2\Gamma_2(\mathbf{u}_{k-2}) + \dots + \mathbf{T}(q^{-1})\mathbf{D}_s\Gamma_s(\mathbf{u}_{k-2})] + \\ &\vdots \\ &\mathbf{B}_m[\mathbf{T}(q^{-1})\mathbf{D}_1\Gamma_1(\mathbf{u}_{k-m}) + \mathbf{T}(q^{-1})\mathbf{D}_2\Gamma_2(\mathbf{u}_{k-m}) + \dots + \mathbf{T}(q^{-1})\mathbf{D}_s\Gamma_s(\mathbf{u}_{k-m})] = \\ &= [\mathbf{B}_1\mathbf{T}(q^{-1})\mathbf{D}_1\Gamma_1(\mathbf{u}_{k-1}) + \mathbf{B}_2\mathbf{T}(q^{-1})\mathbf{D}_1\Gamma_1(\mathbf{u}_{k-2}) + \dots + \mathbf{B}_m\mathbf{T}(q^{-1})\mathbf{D}_1\Gamma_1(\mathbf{u}_{k-m})] + \\ &+ [\mathbf{B}_1\mathbf{T}(q^{-1})\mathbf{D}_2\Gamma_2(\mathbf{u}_{k-1}) + \mathbf{B}_2\mathbf{T}(q^{-1})\mathbf{D}_2\Gamma_2(\mathbf{u}_{k-2}) + \dots + \mathbf{B}_m\mathbf{T}(q^{-1})\mathbf{D}_2\Gamma_2(\mathbf{u}_{k-m})] + \\ &\vdots \\ &+ [\mathbf{B}_1\mathbf{T}(q^{-1})\mathbf{D}_s\Gamma_s(\mathbf{u}_{k-1}) + \mathbf{B}_2\mathbf{T}(q^{-1})\mathbf{D}_s\Gamma_s(\mathbf{u}_{k-2}) + \dots + \mathbf{B}_m\mathbf{T}(q^{-1})\mathbf{D}_s\Gamma_s(\mathbf{u}_{k-m})] \end{aligned} \quad (28)$$

We also have

$$\mathbf{F}(q^{-1})\mathbf{y}_k^f = \mathbf{y}_k^f + \mathbf{F}_1\mathbf{y}_{k-1}^f + \dots + \mathbf{F}_n\mathbf{y}_{k-n}^f \quad (29)$$

Let us notice that

$$\begin{aligned} \mathbf{T}(q^{-1})\mathbf{D}_i\Gamma_i(\mathbf{u}_{k-i}) &= \mathbf{D}_i(\mathbf{T}(q^{-1})\Gamma_i(\mathbf{u}_{k-i})) = \\ &= \mathbf{D}_i\Gamma_i^f(\mathbf{u}_{k-i}) \end{aligned} \quad (30)$$

Let us introduce the vector

$$\begin{aligned} \mathbf{x}_k^T &= [-(\mathbf{y}_{k-1}^f)^T, -(\mathbf{y}_{k-2}^f)^T, \dots, -(\mathbf{y}_{k-n}^f)^T, \\ &(\Gamma_1^f(\mathbf{u}_{k-1}))^T, (\Gamma_1^f(\mathbf{u}_{k-2}))^T, \dots, (\Gamma_1^f(\mathbf{u}_{k-m}))^T, \\ &(\Gamma_2^f(\mathbf{u}_{k-1}))^T, (\Gamma_2^f(\mathbf{u}_{k-2}))^T, \dots, (\Gamma_2^f(\mathbf{u}_{k-m}))^T, \\ &(\Gamma_s^f(\mathbf{u}_{k-1}))^T, (\Gamma_s^f(\mathbf{u}_{k-2}))^T, \dots, (\Gamma_s^f(\mathbf{u}_{k-m}))^T] \end{aligned} \quad (31)$$

and the matrix of parameters

$$\begin{aligned} (\boldsymbol{\theta}^M)^T &= [\mathbf{F}_1, \mathbf{F}_2, \dots, \mathbf{F}_n, \mathbf{B}_1\mathbf{D}_1, \mathbf{B}_2\mathbf{D}_1, \dots, \\ &\mathbf{B}_m\mathbf{D}_1, \mathbf{B}_1\mathbf{D}_2, \mathbf{B}_2\mathbf{D}_2, \dots, \mathbf{B}_m\mathbf{D}_2, \dots, \mathbf{B}_1\mathbf{D}_s, \\ &\mathbf{B}_2\mathbf{D}_s, \dots, \mathbf{B}_m\mathbf{D}_s] \end{aligned} \quad (32)$$

From (26)-(32) it follows that

$$\mathbf{y}_k = (\boldsymbol{\theta}^M)^T \mathbf{x}_k^0 \quad (33)$$

Let us introduce the matrix

$$\boldsymbol{\Phi}_k = \begin{bmatrix} \mathbf{x}_k^T & \mathbf{0} \\ & \ddots \\ \mathbf{0} & \mathbf{x}_k^T \end{bmatrix} = \mathbf{I} \otimes \mathbf{x}_k^T \quad (34)$$

where the symbol  $\otimes$  denotes the Kronecker product.

Let us introduce

$$\boldsymbol{\theta} = \text{vect } \boldsymbol{\theta}^M \quad (35)$$

Finally we have

We now will find the vector form of relation (26).

Using relations (11), (26) and next fact that

$$q^{-l}\Gamma_i(\mathbf{u}_k) = \Gamma_i(\mathbf{u}_{k-l}), \quad l = 1, 2, \dots, m \quad (27)$$

we have

$$\mathbf{y}_k = \boldsymbol{\Phi}_k \boldsymbol{\theta} \quad (36)$$

Where in last relation, according to (35),  $\boldsymbol{\theta}$  is a vector.

The projection algorithm follows from the following optimization problem. Given estimate  $\boldsymbol{\theta}_{k-1}$  and  $\mathbf{y}_k$ . Determine  $\boldsymbol{\theta}_k$  so that criterion

$$J = \frac{1}{2} \|\boldsymbol{\theta}_k - \boldsymbol{\theta}_{k-1}\|^2 \quad (37)$$

is minimized subject to

$$\mathbf{y}_k = \boldsymbol{\Phi}_k \boldsymbol{\theta}_k \quad (38)$$

Using relations (37), (38) and introducing a Lagrange multiplier one can get next functional

$$J_c = \frac{1}{2} \|\boldsymbol{\theta}_k - \boldsymbol{\theta}_{k-1}\|^2 + \boldsymbol{\lambda} [\mathbf{y}_k - \boldsymbol{\Phi}_k \boldsymbol{\theta}_k] \quad (39)$$

The necessary conditions for a minimum are [19]-[20]

$$\frac{\partial J_c}{\partial \boldsymbol{\theta}_k} = 0 \quad (40)$$

$$\frac{\partial J_c}{\partial \boldsymbol{\lambda}} = 0 \quad (41)$$

Having in mind that

$$\boldsymbol{\Phi}_k = \boldsymbol{\Phi}_k^T \quad (42)$$

from (40) and (41) it follows that

$$\boldsymbol{\theta}_k - \boldsymbol{\theta}_{k-1} - \boldsymbol{\lambda} \boldsymbol{\Phi}_k = 0 \quad (43)$$

$$\mathbf{y}_k - \boldsymbol{\Phi}_k^T \boldsymbol{\theta}_k = 0 \quad (44)$$

From (43) and (44) it follows that

$$\boldsymbol{\lambda} = \frac{\mathbf{y}_k - \boldsymbol{\Phi}_k \boldsymbol{\theta}_{k-1}}{\boldsymbol{\Phi}_k^T \boldsymbol{\Phi}_k} \quad (45)$$

If (45) substitute to relation (43) one can get fundamental form of Kaczmarz algorithm

$$\theta_k = \theta_{k-1} + \frac{\varphi_k}{\|\varphi_k\|^2} (y_k - \varphi_k \theta_{k-1}) \quad (46)$$

Modification of (46) is given in [21]

$$\theta_k = \theta_{k-1} + \frac{a\varphi_k}{c + \|\varphi_k\|^2} (y_k - \varphi_k \theta_{k-1}), \exists c > 0, a \in (0, 2) \quad (47)$$

Geometrical interpretation is given in next figure

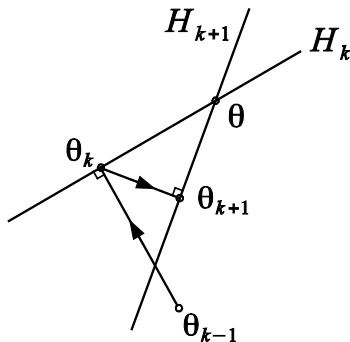


Figure 5: Geometric interpretation of recursive Kaczmarz algorithm

**Remark 2:** Further investigations of Kaczmarz algorithm is given in references [22]-[24].

### 5. CONCLUSION

The paper considers identification of MIMO Hammerstein models by using Kaczmarz algorithm. The algorithm is very simple and especially suitable for parameter estimation in the case of large data sets. It is considered very general MIMO models. The further investigations will be performed for next problems

- (i) Relaxation of condition (20) in the paper
- (ii) Design of adaptive invariant systems
- (iii) Design of robust stochastic recursive Kaczmarz algorithms.

Also, in the field of block-oriented methods, the potential application of iterative Kaczmarz algorithm is very important (especially randomized Kaczmarz algorithm).

### ACKNOWLEDGEMENTS

This paper is part of projects TR33026 and TR33027 at the University of Kragujevac, Faculty of Mechanical and Civil Engineering in Kraljevo, and it was supported by the Ministry of Education, Science and Technological Development of the Republic of Serbia.

### REFERENCES

[1] Y. Zhu, "Multivariable System Identification for Process Control", Elsevier Science, London (UK), (2000)

[2] E. Giri and E. Bai (Eds.), "Block-oriented Nonlinear System Identification", Springer, Berlin (Germany), (2010)

[3] L. Ljung, "System Identification: Theory for the User", Prentice Hall, New Jersey (USA), (1999)

[4] V. Filipovic, "Recursive Identification of Multivariable ARX Models in the Presence of A Priori Information: Robustness and Regularization", Signal Processing, Vol. 116, pp. 351-357, (2015)

[5] V. Filipovic, "A Global Convergent Outlier Robust Adaptive Predictor for MIMO Hammerstein Models", International Journal of Robust and Nonlinear Control, DOI: 10.1002/rnc.3705, (2016)

[6] R. Pearson, "Exploring Data in Engineering, the Sciences and Medicine", Oxford University Press, Oxford (UK), (2011)

[7] P. Huber, "Robust Estimation of a Location Parameters", Annals of Mathematical Statistics, Vol. 35, pp. 73-101, (1964)

[8] V. Filipovic, "Industrial Controllers", University of Kragujevac, Kraljevo, (2016), (in Serbian)

[9] C. Shannon, "Mathematical Theory of the Differential Analyzer", Journal of Mathematics and Physics, Vol. 20, pp. 337-352, (1941)

[10] V. Kulebakin, "On the Behaviour of the Continuously Distributed Automatic Linear Systems", Proceeding of the USSR Academy of Science, Vol. 68, pp. 73-79, (1949)

[11] Ya. Tsympkin, "Adaptive-Invariant Control Systems", Automatika i Telemekhanika, Vol. 55, pp. 96-124, (1991)

[12] Ya. Tsympkin, J. Manson and K. Warwick, "Identification of Linear Systems in the Presence of Piecewise Polynomial Disturbances", IEE Proceedings – Control Theory Application, Vol. 143, Issue 4, pp. 305-308, (1996), (in Russian)

[13] S. Kaczmarz, "Angenäherte Auflösung von Systemen Linearer Gleichungen", Bulletin International de l'Academie Polonaise des Sciences et des Lettres, Vol. 35, pp. 355-357, (1937)

[14] V. Filipovic, "Robust Stochastic Approximation Algorithm for Identification of MIMO Hammerstein OE Models", Nonlinear Dynamics, Accepted for Publication, (2017)

[15] P. Parks, "S. Kaczmarz (1895-1939)", International Journal of Control, Vol. 57, pp. 1263-1267, (1993)

[16] A. Galantal, "Projectors and Projection Methods", Koluwer, Boston (USA), (2004)

[17] R. Gordon, R. Bender and G. Herman, "Algebraic Reconstruction Technique (ART) for Three-dimensional Electron Microscopy and X-ray Photography", Journal of Theoretical Biology, Vol. 29, Issue 3, pp. 471-481, (1970)

[18] Y. Censor, "Row-Action Methods for Huge and Sparse Systems and Their Application", SIAM Review, Vol. 23, Issue 4 pp. 444-466, (1981)

- [19] G. Goodwin and K. Sin, "Adaptive Filtering, Prediction and Control", Prentice Hall, New Jersey (USA), (1984)
- [20] E. Aved'Yan, "Learning Systems", Springer, Berlin (Germany), (1996)
- [21] T. Strohmer and R. Vershynin, "A Randomized Kaczmarz Algorithm with Exponential Convergence", J. Fourier Anal. Appl. Vol. 15, pp. 266-278, (2009)
- [22] V. Filipovic and V. Djordjevic, "Kaczmarz Algorithm Based on Synergy of Fuzzy Identification and Machine Learning", (2017), to be Published
- [23] V. Filipovic, "Convergence Properties of Kaczmarz Algorithm for Identification of MIMO Hammerstein Models", (2017), to be published
- [24] V. Filipovic and V. Djordjevic, "Design of Multivariable PID controller for Boiler Plant Using Convex Analysis and Theory of Invariant Systems", (2017), to be published

# Philosophical Interpretation of Connection of Robust Statistics and Fuzzy Logic: The Robust Fuzzy Clustering

Vladimir Djordjevic<sup>1\*</sup>, Vojislav Filipovic<sup>1</sup>

<sup>1</sup>Department for Automatic Control, Robotics and Fluid Technique, Faculty of Mechanical and Civil Engineering, University of Kragujevac, Kraljevo (Serbia)

*Clustering methods have the key role in pattern recognition, computer vision, and control. In real applications, the data are corrupted with stochastic noise which often has outliers. It follows that clustering techniques need to be robust. It is observed that robust statistics and fuzzy set theory have much in common. Namely, the concept of weight functions in robust statistics can be related to the concept of membership function in fuzzy set theory. In the paper proposed the new objective function for cluster analysis. For the clustering the modified Gustafson-Kessel algorithm is used and the modification is based on possibility theory. The final goal is membership function determination. That is the important part of the Takagi–Sugeno models which represent the fuzzy model of nonlinear dynamic systems.*

**Keywords:** Robust statistics, IRLS, Possibility function, Robust clustering

## 1. INTRODUCTION

Robustness is a key attribute in engineering systems. It means that the performance of algorithm (in identification, estimation, and control) should not be affected significantly by small deviations from the assumed model. Also, it is important that it should not deteriorate drastically due to noise and outliers. In this paper, we consider clustering techniques which are used in different fields

- (i) Pattern recognition [1]
- (ii) Computer and robot vision [2]
- (iii) Control [3]

In real application data have outliers [4] and different procedures have to be robust. Two disciplines, robust statistics and fuzzy logic have developed independently. But, as we will see in this paper, they have much in common. That explains the claim of proponents of fuzzy set theory that a fuzzy approach is more tolerant to model variations and disturbances in comparison with the crisp approach.

In this paper, we first introduce some concept from robust statistics [5-6] (min-max property, infinite signal function and breakdown points). After that, we will describe, shortly, a few concepts from fuzzy logic. Finally, it will be established some philosophical connection between both areas.

The main goal of the paper is to find robust cluster procedure with small sensitivity to outliers. The unified view of the problem is presented in [7]. In this paper, we consider robust version of Gustafson-Kessel (GK) algorithm [8]. That algorithm is not considered in [7]. Also, we consider a possibilistic approach to clustering. A heuristic version of that theory is described in [10]. The main result is possibilistic Gustafson-Kessel algorithm (PGK). The primary objective of the possibilistic approach is to achieve membership value that is possibilistic, i.e. the membership value of a point in a class represents the possibility of the point belonging to the class.

For the robustness the number of clusters is also important. That problem is not considered in this paper but

attractive solution is given in [11]. Here is of interest cluster validity. Cluster validity measures the correctness of partition generated by a clustering algorithm. In [12] as a model validity test is used Kolmogorov-Smirnov test.

## 2. ROBUST STATISTICS

Robustness is a very important notion in modern science. In statistics, the robustness is low sensitivity to distribution changes of real processes. At present, in statistical sense, there are two key approaches to robustness

- (i) Quantitative robustness [13] known as a Huber's minmax approach
- (ii) Qualitative robustness [14] which is based on the concept of influence function.

We will first consider Huber's approach. Usually, the problem of parameter estimation is based on the assumption that the stochastic disturbance has a Gaussian distribution. Practical studies [4] show that in a population of observations there are rare large observations (outliers) and the result is that stochastic disturbance has a non-Gaussian disturbance. Such case is considered in [13] where class of distributions is modeled as

$$P_\varepsilon = \{P : P = (1 - \varepsilon)N + \varepsilon G, \quad G \text{ is symmetric}\} \quad (1)$$

where  $\varepsilon \in [0, 1)$  is the contamination degree and  $N(0, \sigma^2)$  denotes a zero-mean Gaussian distribution with a variance  $\sigma^2$ . Applying Huber's methodology [5] and [13] the least favorable probability density on a class (1) is obtained

$$p^*(e(k)) = \begin{cases} \frac{1 - \varepsilon}{\sqrt{2\pi}\sigma} \exp\left\{-\frac{(e(k))^2}{2\sigma^2}\right\}, & |e(k)| \leq k_\varepsilon \\ \frac{1 - \varepsilon}{\sqrt{2\pi}\sigma} \exp\left\{-\frac{k_\varepsilon}{\sigma^2} \left(|e(k)| - \frac{k_\varepsilon}{2}\right)\right\}, & |e(k)| > k_\varepsilon \end{cases} \quad (2)$$

where  $e(k)$  is a stochastic disturbance and where the relationship between the contamination degree  $\varepsilon$  and the Huber's parameter  $k_\varepsilon$  is given in the following relation

$$\frac{2\Phi_N(k_\varepsilon)}{k_\varepsilon} - 2\Phi_N(-k_\varepsilon) = \frac{\varepsilon}{1-\varepsilon}, \quad \Phi_N = \int_{-\infty}^{\infty} e^{-\frac{y^2}{2}} dy \quad (3)$$

The good performance of parameter estimation algorithm is provided for  $k_\varepsilon \in [2, 4]$ . The best performance is accomplished for  $k_\varepsilon = 3$  as is shown in [14-17]. In cited references, the robust recursive identification of MIMO (multiple-input multiple-output) is considered.

In what follows we will consider estimation of location and scale parameters.

**Remark 1.** It is possible to describe outliers with other probability distribution in comparison with (1). That is heavy-tailed (fat-tailed) distributions [18] whose density tails tend to zero more slowly than the normal density. An example is the Cauchy distribution with density

$$f(x) = \frac{1}{\pi(1+x^2)} \quad (4)$$

It is a particular case of the Student (or t) densities with  $\nu > 0$  degrees of freedom

$$f_\nu(x) = c_\nu \left(1 + \frac{x^2}{\nu}\right)^{-\frac{\nu+1}{2}} \quad (5)$$

where  $c_\nu$  is a constant

$$c_\nu = \frac{\Gamma\left(\frac{\nu+1}{2}\right)}{\sqrt{\nu\pi}\Gamma\left(\frac{\nu}{2}\right)} \quad (6)$$

and  $\Gamma(\cdot)$  is the gamma function. This family contains all degrees of heavy-tailedness. When  $\nu \rightarrow \infty$ ,  $f_\nu$  tends to the standard normal density. For  $\nu=1$  we have the Cauchy distribution.

We now consider M-estimate of location parameter. Using relation (2) we can define the function

$$\Phi(x) = -\log p^*(x) \quad (7)$$

or explicitly

$$\Phi(x) = \begin{cases} \frac{x^2}{2\sigma^2} + \ln \frac{\sqrt{2\pi}\sigma}{1-\varepsilon}, & |x| \leq k_\varepsilon \\ \frac{k_\varepsilon}{\sigma^2} \left(|x| - \frac{k_\varepsilon}{2}\right) + \ln \frac{\sqrt{2\pi}\sigma}{1-\varepsilon}, & |x| > k_\varepsilon \end{cases} \quad (8)$$

Let us define the model for location

$$y(k) = \theta + e(k) \quad (9)$$

where  $y(k)$  are the measurement,  $\theta$  is the location parameter and  $e(k)$  is the stochastic non-Gaussian process. According to maximum likelihood methodology criterion for parameter  $\theta$  estimation in (9) is

$$J(\theta) = E\{\Phi(y(k) - \theta)\} \quad (10)$$

where  $E\{\cdot\}$  is expectation operator. It is possible to approximate the last relation with empirical functional

$$J_k(\hat{\theta}) = \frac{1}{k} \sum_{i=1}^k \Phi(y(k) - \hat{\theta}(k)) \quad (11)$$

where

$$\hat{\theta}(k) = \arg \min_{\theta} \sum_{i=1}^k \Phi(y(k) - \theta) \quad (12)$$

If  $\Phi(\cdot)$  is differentiable, differentiating with respect to  $\theta$  yields

$$\sum_{i=1}^k \Psi(y(i) - \hat{\theta}(i)) = 0 \quad (13)$$

with  $\Psi(\cdot) = \Phi'(\cdot)$ . For probability distribution (1) the function  $\Psi(\cdot)$  is known as a Huber's function and has the analytical expression

$$\Psi(x) = \begin{cases} x, & |x| \leq k_\varepsilon \\ k_\varepsilon, & |x| > k_\varepsilon \end{cases} \quad (14)$$

and is showed in the next figure.

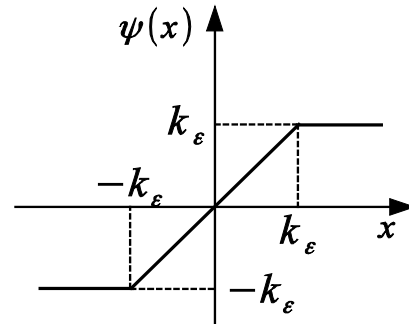


Figure 1: Huber's function

Let us notice that solution of equation (13) is estimated value of location parameter.

The same story is valid for estimation of scale parameter. In this case, the loss function is

$$\Phi\left(\frac{x}{\sigma}\right) \quad (15)$$

where  $\sigma$  is scale parameter.

The qualitative robustness is presented in [6] and has two concepts:

- (i) Influence function which is an infinitesimal approach (small deviations from the model assumptions should impair the performance of estimation only by a small amount). That concept has a local character;
- (ii) Breakdown point which means that larger deviations from the model assumptions have not catastrophic consequences. This concept has a global character.



The influence function can be defined using theory of a von Mises functionals [19].

**Definition 1.** [6] The influence function of a von Mises functional  $T$  on probability distribution  $F$  is given by

$$IF(x, T, F) = \lim_{\varepsilon \rightarrow 0} \frac{T[(1-\varepsilon)F + \varepsilon\Delta_x] - T(F)}{\varepsilon} \quad (16)$$

where  $\Delta_x$  is the probability measure which puts mass 1 at the point  $x$ .

The breakdown point is defined in [20]. Let us suppose that  $Z$  consist of  $N$  data points and  $T$  is estimator. Also,  $Z'$  is set which is given by replacing any  $M$  of the original data points by arbitrary values. Let us denote with  $bias(M, T, Z)$  the maximum bias in the estimate caused by such a contamination

$$bias(M, T, Z) = \sup_{Z'} \|T(Z') - T(Z)\| \quad (17)$$

If the bias is infinite, the  $M$  outliers have an arbitrary large effect on  $T$  and, thus, the estimator break down. The definition of breakdown point is

$$\varepsilon_{BP}^* = \min \left\{ \frac{M}{N} : bias(M, T, Z) \text{ is infinite} \right\} \quad (18)$$

Finally, we will consider important, from the computation point of view, concept known as the iteratively reweighted least square (IRLS) [21-23]. Let us consider relation (13) without index of estimate of location parameter  $\theta$ . That relation we can rewrite in the next form

$$\sum_{i=1}^k (y(i) - \theta) w(y(i) - \theta) = 0 \quad (19)$$

whereby  $w$  is weight coefficient

$$w(y(i) - \theta) = \frac{\Psi(y(i) - \theta)}{y(i) - \theta} \quad (20)$$

From relation (19) one can get

$$\theta = \frac{\sum_{i=1}^k w(y(i) - \theta) y(i)}{\sum_{i=1}^k w(y(i) - \theta)} \quad (21)$$

It follows that  $\theta$  is a weighted mean of the  $y(i)$  and can be solved iteratively.

It is important to note that for complex dynamic systems it is possible to approximate and relax computation by using principal component analysis [24].

The behaviour of weight  $w$  for probability distribution model (1) and Huber's function (14) is presented in the next figure.

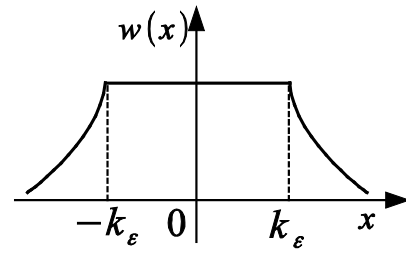


Figure 2: The weight function in location parameter estimation

### 3. FUZZY LOGIC

Fuzzy logic now has high theoretical level with applications in many fields. The key notation in fuzzy logic is the set membership function which is used for characterization of fuzzy sets [25].

A fuzzy set  $A$  on the universe set  $X$  is a set defined by a membership function  $\mu_A(x)$  represent a mapping

$$\mu_A(x) : X \rightarrow [0,1] \quad (22)$$

Here the value of  $\mu_A(x)$  for the fuzzy set  $A$  is called the membership value or the grade of membership of  $x \in X$ . The membership value means the degree of  $x$  belonging to the fuzzy set  $A$ .

Exist different form of set membership function and they presented in next figure.

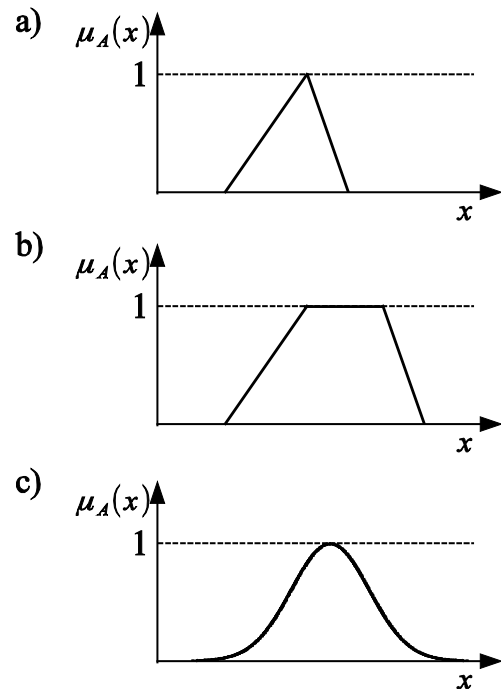


Figure 3: Different form of fuzzy sets: a) triangular, b) trapezoidal, c) exponential

Also, a very important concept in fuzzy logic is a possibility theory [26-27]. That is a complement theory to probability theory to deal with uncertainty. There are two approaches to possibility theory: (i) one, proposed in [26], was to introduce possibility theory as an extension of

fuzzy set theory; (ii) the other, described in [28], was to introduce possibility theory in the framework of Dempster-Schafer's theory of evidence. This approach puts possibility theory in an axiomatic manner.

The major topics in possibility theory are fuzzy arithmetic which is concerned with the operations and computations of fuzzy numbers. Fuzzy numbers are useful for computation in physical sciences and engineering when only imprecise or uncertain sensory data are available for computations. Important notion in the possibility theory is the possibility distribution.

Given fuzzy set  $A$  in  $U$  and the proposition "  $x$  is  $A$  " the possibility distribution associated with  $x$ , denoted by  $\pi_x$ , is defined to be numerically equal to the membership function of  $A$ , that is

$$\pi_x(u) = \mu_A(u) \quad (23)$$

One of the major difference between possibility and probability can be seen from the following

$$P(A) + P(\bar{A}) = 1 \quad (24)$$

$$\Pi(A) + \Pi(\bar{A}) \geq 1 \quad (25)$$

where  $P(\cdot)$  is probability and  $\Pi(\cdot)$  is possibility.

Possibility theory will be used for design of possibilistic cluster algorithm in the next paragraph.

#### 4. THE ROBUST CLUSTERING AND THE POSSIBILISTIC GUSTAFSON-KESSEL ALGORITHM

Clustering is fundamental part of identification of dynamic systems. Namely, the identification procedure consist of three parts:

- (i) Cluster analysis
- (ii) Determination of the membership function
- (iii) Identification parameters of set of models (off-line or recursive) where number of models equal to number of clusters.

In this paper we consider only of first two items. It is supposed that measurements include outliers which one unavoidable in practice. The clustering is based on optimization and in that sense criterion of clustering must be determined.

Let us denote with  $\mu_{*j}$  membership of point  $\mathbf{x}_j$  in the class of outliers [7]. The membership of point  $\mu_{*j}$  in the noise cluster is defined to be

$$\mu_{*j} = 1 - \sum_{i=1}^c \mu_{ij} \quad (26)$$

where  $c$  is the number of clusters and exists condition

$$\sum_{i=1}^c \mu_{ij} \leq 1 \quad (27)$$

Criterion for possibilistic cluster method (PCM) is introduced in [9]

$$J_{PC} = \sum_{i=1}^c \sum_{j=1}^N (\mu_{ij})^m d^2(\mathbf{x}_j, \boldsymbol{\beta}_i) + \sum_{i=1}^c r_i \sum_{j=1}^N (1 - \mu_{ij})^m \quad (28)$$

where  $N$  is the number of observations,  $r_i$  are positive numbers,  $\boldsymbol{\beta}_j$  is the prototype (center of clusters),  $m \in (1, \infty)$  (usually  $m = 2$ ) is a weighting exponent and  $d(\mathbf{x}_j, \boldsymbol{\beta}_i)$  suitable defined distance. For the Gustafson-Kessel algorithm the distance is Mehalanabis distance

$$d^2(\mathbf{x}_j, \boldsymbol{\beta}_i) = (\det \mathbf{F}_i)^{\frac{1}{n}} (\mathbf{x}_j - \mathbf{c}_i)^T \mathbf{F}_i^{-1} (\mathbf{x}_j - \mathbf{c}_i) \quad (29)$$

where  $\mathbf{F}_i$  is the fuzzy covariance matrix of cluster

$$\mathbf{F}_i = \frac{\sum_{j=1}^N (\mu_{ij})^m (\mathbf{x}_j - \mathbf{c}_i)(\mathbf{x}_j - \mathbf{c}_i)^T}{\sum_{j=1}^N (\mu_{ij})^m} \quad (30)$$

and  $\mathbf{c}_i$  centers of clusters ( $i = 1, 2, \dots, c$ ). The algorithm (28)-(30) is the Gustafson-Kessel possibilistic cluster algorithm.

From equation

$$\frac{dJ_{PC}}{d\mu_{ij}} = 0 \quad (31)$$

it follows that

$$\mu_{ij} = \frac{1}{1 + \left[ \frac{d^2(\mathbf{x}_j, \boldsymbol{\beta}_i)}{r_i} \right]^{\frac{1}{m-1}}} \quad (32)$$

From (28) and (32) it follows that [7]

$$J_{PC} = \sum_{i=1}^c \sum_{j=1}^N \left( \frac{1}{1 + \left[ \frac{d_{ij}^2}{r_i} \right]^{\frac{1}{m-1}}} \right)^{m-1} \cdot d_{ij}^2 = \sum_{i=1}^c \sum_{j=1}^N w_{ij} d_{ij}^2 \quad (33)$$

From (33) one can get center of cluster as

$$\mathbf{c}_i = \frac{\sum_{j=1}^N w_{ij} \mathbf{x}_j}{\sum_{j=1}^N w_{ij}} \quad (34)$$

Using last relation one can to see that the weights in IRLS technique has the role of membership. The quantitative relation between function  $\Phi(\cdot)$ ,  $\Psi(\cdot)$  and  $w$  and membership function is given in [7]. That is connection between robust statistics and fuzzy logic (relation (34) in [7]). Main differences between algorithms in this paper and reference [7] is in the form of distance  $d_{ij}$ .

In stochastic case good alternative for presented methodology are gradient algorithms. When the outliers are present in the measurements and when the membership function has a Gaussian form the gradient algorithm, based on Huber's approach in robust statistics, is presented in

[30]. The case of identification of complex dynamic systems, using Takagi-Sugeno models, is considered in [31].

## 5. CONCLUSION

In the paper is considered identification of nonlinear dynamic system. The nonlinear system is approximated with fuzzy system (finite collection of Takagi-Sugeno models). The local point in fuzzy identification is determination of membership function. Strategy of determination is based on, owing the outliers presence in measurements, robust clustering. The clustering is based on possibilistic Gustafson-Kessel algorithm. The robustness is based on criterion modification. Also, established the conceptual connection between robust statistic and fuzzy logic.

## ACKNOWLEDGEMENTS

This paper is part of projects TR33026 and TR33027 at the University of Kragujevac, Faculty of Mechanical and Civil engineering in Kraljevo, and it was supported by the Ministry of Education, Science and Technological Development of the Republic of Serbia.

## REFERENCES

- [1] C. M. Bishop, "Pattern Recognition and Machine Learning", Springer, Berlin (Germany), (2006)
- [2] R. M. Harlick and L.G. Shapiro, "Computer and Robust Vision", Addison-Wesley, New York (USA), (1992)
- [3] J. Espinosa, J. Vandewalle and V. Wertz, "Fuzzy logic, identification and predictive control", Springer, Berlin (Germany), (2005)
- [4] R. Pearson, "Exploring Data in Engineering, the Science and Medicine", Oxford University Press, Oxford (UK), (2011)
- [5] P. Huber and E. Ronchetti, "Robust Statistics", Wiley, New York (USA), (2009)
- [6] F. Hampel, P. Rousseenw, E. Ronchetti and W. Stahel, "Robust Statistics. The Approach Based on Influence Functions", Wiley, New York (USA), (1986)
- [7] R. Dave and R. Krishnapuram, "Robust Clustering Methods: A Unified View", IEEE Transactions on Fuzzy Systems, Vol. 5, pp. 270-293, (1997)
- [8] D. E. Gustafson and W. C. Kessel, "Fuzzy Clustering with a Fuzzy Covariance Matrix", Proceedings of IEEE Conference on Decision and Control including the 17<sup>th</sup> Symposium on Adaptive Processes, San Diego (USA), 10-12 January 1979, pp. 761-766, (1979)
- [9] R. Krishnapuram and J. Keller, "A Possibilistic Approach to Clustering", IEEE Transactions on Fuzzy Systems, Vol. 1, pp. 98-110, (1993)
- [10] D. A. Viattchenin, "A Heuristic Approach to Possibilistic Clustering", Springer, Berlin (Germany), (2013)
- [11] F. Lindsten, H. Ohlsson and L. Ljung, "Clustering using Sum-of-norms Regularization with Application to Particle Filter Output Computation", Technical Report: LiTH-ISY-R-2993, Linkoping University, Linkoping (Sweden), (2011)
- [12] V. Filipovic and V. Djordjevic, "Fuzzy Cluster Validity Method based on Kolmogorov-Smirnov test", to be published
- [13] P. Huber, "Robust Estimation of a Location Parameter", Annals of Mathematical Statistics, Vol. 35, pp. 73-110, (1964)
- [14] V. Filipovic, "Recursive Identification of Multivariable ARX Models in the Presence of a Priori Information: Robustness and Regularization", Signal Processing, Vol. 116, pp. 68-77, (2015)
- [15] V. Filipovic, "A Global Convergent Outlier Robust Adaptive Predictor for MIMO Hammerstein Models", International Journal of Robust and Nonlinear Control, DOI: 10.1002/rnc.3705, (2016)
- [16] V. Filipovic, "Outlier Robust Identification of MIMO ARMAX Models", Asian Journal of Control, Accepted for publication, (2017)
- [17] V. Filipovic, "Robust Stochastic Approximation Algorithm for Identification of MIMO Hammerstein OE Models", Nonlinear Dynamics, Accepted for publication, (2017)
- [18] B. Grigelouis, "Student's t-distribution and Related Stochastic Process", Springer, Berlin (Germany), (2013)
- [19] L. T. Fernholz, "Von Mises Calculus for Statistical Functionals", Springer, New York (USA), (1983)
- [20] F. R. Hampel, "Beyond Location Parameters: Robust Concepts and Methods", Bulletin of the International Statistical Institute, Vol. 46, No. 1, pp. 375-382, (1975)
- [21] P. W. Holland and R. E. Welsch, "Robust Regression Using Iteratively Reweighted Least Squares", Communication Statistics – Theory and Methods, Vol. A6, pp. 813-827, (1977)
- [22] D. P. O'Leary, "Robust Regression Computation Using Iteratively Reweighted Least Squares", SIAM Journal on Matrix Analysis and Applications, Vol. 11, pp. 466-480, (1990)
- [23] K. Chen, Q. Lu, Y. Lu and Y. Dou, "Robust Regularized Extreme Learning Machine for Regression Using Iteratively Reweighted Least Squares", Neurocomputing, Vol. 230, pp. 345-358, (2017)
- [24] V. Filipovic, "Robust Recursive Principal Component Analysis in Process Monitoring", to be published, (2017)
- [25] L. Zadeh, "Fuzzy set", Information and Control, Vol. 8, pp. 338-353, (1965)
- [26] L. Zadeh, "Fuzzy Sets as Basis for a Theory of Possibility", Fuzzy Sets and Systems, Vol. 1, pp. 3-28, (1978)
- [27] D. Dubois and H. Prade, "Possibility Theory: An Approach to Computerized Processing of Uncertainty", Plenum Press, New York (USA), (1988)

[28] G. Shafer, "Mathematical Theory of Evidence", Princeton University Press, Princeton (USA), (1979)

[29] J. Abonyi, "Fuzzy Model Identification for Control", Birkhauser, Boston (USA), (2003)

[30] V. Filipovic and V. Djordjevic, "Robust Identification of Fuzzy Models Using Gradient Methods", in preparation, (2017)

[31] V. Filipovic and V. Djordjevic, "Complexity Reduction in Fuzzy System Identification Using Robust Principal Component Analysis", to be published, (2017)

# Self-tuning PID Controller Based on Time Response Characteristics

Novak N. Nedić<sup>1\*</sup>, Saša Lj. Prodanović<sup>2</sup>

<sup>1</sup>Faculty of Mechanical and Civil Engineering in Kraljevo, University of Kragujevac, Kraljevo (Serbia)

<sup>2</sup> Faculty of Mechanical Engineering, University of East Sarajevo, East Sarajevo (Bosnia and Herzegovina)

There are various tuning methods for PID controller and its shorter variants. Simpler procedures are preferable due to less time consuming and reducing possibility of making mistakes. This aim is supported by approaches which contain some of the automated tuning options. Self-tuning PID controller based on characteristic parameters of the time response, has been tested and described in the present paper. The main idea was to make tuning algorithm which can set controller parameters depending on the state of the system time response during its functioning in changeable working conditions. Therefore, presented procedure requires involving of entire control algorithm into computer. This is in line with their current expansion as control units. Research was carried out using simulations. Effectiveness of defined way was proved on a few single-input single-output (SISO) systems.

**Keywords:** PID control, Self-tuning controller, SISO system

## 1. INTRODUCTION

System behaviour under different functional conditions is subject of many surveys. Ensuring stability and system performances are always actual tasks for engineers operators and therefore researchers. After passing through the dynamical area and reaching of steady (stationary) state, control system can be exposed to unpredictable and unmeasurable disturbance. Numerous methods for controller tuning were investigated and suggested with aim to obtain good transition area of response and efficient rejection (compensation) of disturbance. Because of their wide usage in industry PID controllers also occupy the main place in the scientific researches [1-5]. There are a lot of surveys which were focused on improving of control algorithm for particular objects [6-9]. Considering this kind of controllers involves all of their variants, i.e. combinations of proportional P, integral I and derivative D term. Surely, the most appropriate feasible type and values of controller gains should be chosen for controlled object. Computer-controlled systems due to their digital nature provide an opportunity for iterative approach in controller tuning. Some of these methods are presented in [10,11]. Authors [11] also use frequency response as a quality indicator in the tuning procedure. It is very important to have in mind that majority of control and monitoring systems have graphical display of controlled variable and more importantly that time response gives real representation of system behaviour.

Present paper contain attempt to use information about one parameter (characteristic) of time response, i.e. its changing in time, to design self-tuning controller.

## 2. PROBLEM DEFINITION AND CONTROLLER TUNING

PID controller expressed by Eq. (1) or its other shorter variants can be tuned using many methods.

$$G_c(s) = \frac{U(s)}{E(s)} = K_p \left( 1 + \frac{1}{T_i s} + T_d s \right) = K_p + \frac{K_i}{s} + K_d s \quad (1)$$

Where:  $K_p$ ,  $K_i$  and  $K_d$  are proportional, integral and derivative controller gains, respectively, while  $T_i$  and  $T_d$

are integral and derivative time constant, respectively.  $U(s)$  is manipulated variable and  $E(s)$  is error of controlled variable. Presented well known controller can enable appropriate system dynamic behaviour regarding dynamic and static part of time response and in the most circumstances appropriate disturbance rejection. However, problem appears in the case of higher disturbance intensity that can lead system into instability. Due to that, research of possibilities for designing of controller that can achieve a wider influence range regarding disturbance rejection, has led to idea of introducing additional controller and therefore design more efficient entire controller. It must satisfy two significant demands: activation in the moment of disturbance appearing and to be self-tuning. After carrying out of numerous simulations it is derived that parallel P additional controller gives the best results. Configuration for its introducing into control system is given in figure 1.

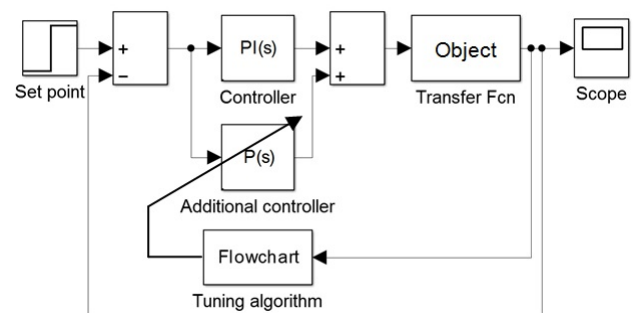


Figure 1: Configuration for self-tuning additional P controller application

Moment of tuning and activation of additional P controller is determined by monitoring of response overshoot  $P_0$ , while  $P_1$  is overshoot in the next iteration. It has to influence while overshoot caused by disturbance exists. Therefore  $P_0$  is overshoot without action of additional controller. In order to intensify that action, proportional gain  $K_p$  is incrementally rising in every sampling period while the overshoot drops under defined value  $P_{max}$ . Afterward  $K_p$  should be set to 0. Flowchart that describes steps in self-tuning of additional P controller is shown in figure 2. In this flowchart  $P_{inkr}$  is overshoot for

incrementally set  $K_p$ . Tuning has been performed by repeating of simulations. It has served to prove method efficiency, but in real system, estimation of tracked response characteristic (in this research overshoot) and adjusting of  $K_p$  should be carried out in every sampling period.

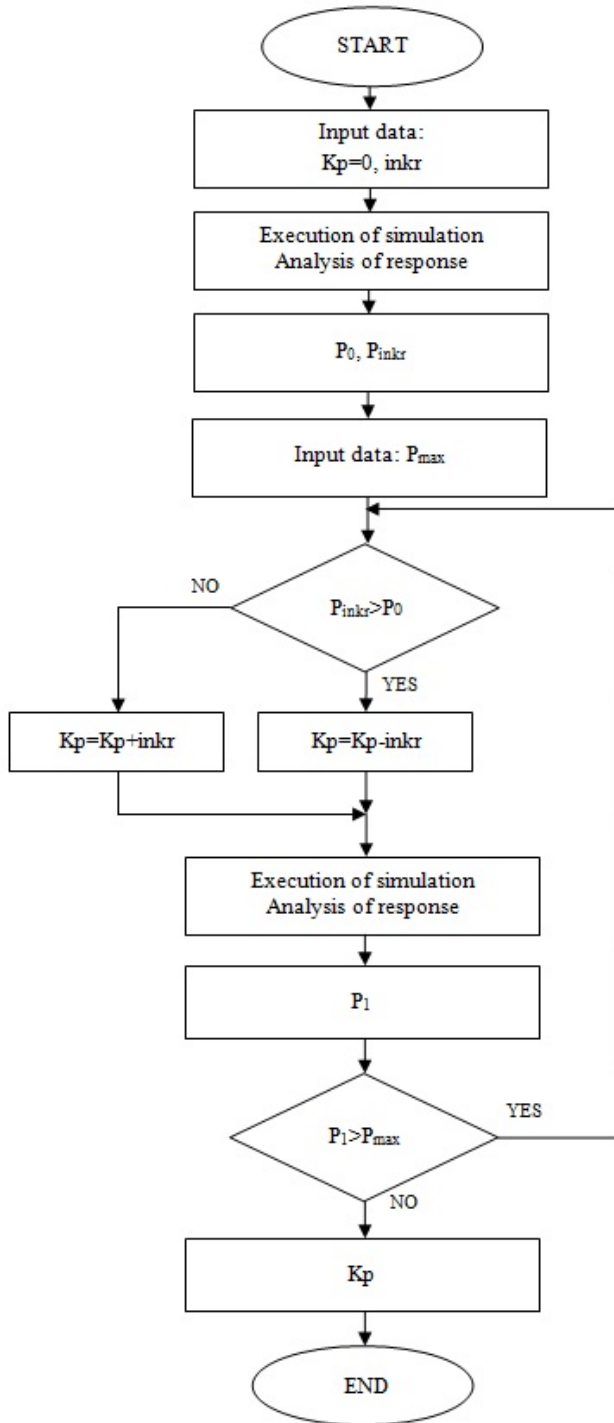


Figure 2: Flowchart for additional P controller self-tuning

3. EXAMPLES

Described control strategy and tuning procedure has been tested on three single-input single-output characteristic examples. For the simulation purpose disturbances were introduced sequentially with defined period and in rising order of their intensity [12], as it shown in figure 3. In this research following values have been chosen: time of introducing of the first disturbance

$t_0=500$  s, period between starts of the adjacent disturbances  $t_p=200$  s, disturbance duration  $\Delta t=10$  s, number of disturbance steps  $n=4$ . Other signs are:  $i$  – disturbance intensity,  $d_i$  – ordinal number of disturbance.

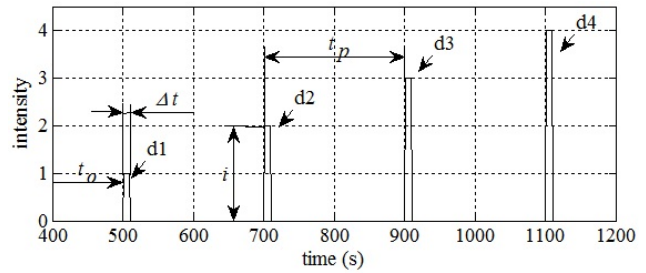


Figure 3: Array of square disturbances

In following examples disturbance intensity was increased 10 times. Actually, these values are not real, but they were used in simulation to test possibilities of suggested control algorithm. For all three examples PI controllers have been tuned using Matlab Toolbox. Simulation is performed for cases with and without additional P controller in order to show effects of the suggested approach. In all examples unit step function was taken as reference value.

3.1. Example 1

This example contain first-order object given by Eq. (2). Increment can takes different values. Higher values speed up simulation, i.e. increase of proportional gain  $K_p$  during disturbance compensation. Parameters of PI controller are  $K_p=10.248$ ,  $K_i=0.163$ . Maximum overshoot value is being taken such to satisfy operator’s demands. Here it is  $P_{max}=2\%$

$$G_{ex.1}(s) = \frac{1}{63s + 1} \tag{2}$$

Carrying out simulation gives value of  $K_p=2400$  that is very high, which obtain responses shown in figure 4 and its zoomed display in figure 5. These figures show effectiveness of control strategy that contain additional self-tuning P controller. The advantages are reflected in significantly reduced disturbance amplitude and time for its rejection. It means that there are large theoretical possibilities of proposed method, but its practical feasibility depends on limitations in the actuators.

3.2. Example 2

Controlled object presented by second-order transfer function (Eq. (3)) has been tested in this example.

$$G_{ex.2}(s) = \frac{9}{s^2 + 14.6s + 1} \tag{3}$$

Parameters of PI controller are  $K_p= 0.442$ ,  $K_i= 0.028$ . Maximum overshoot value is taken  $P_{max}=2\%$ . Simulations give responses in figure 6 and its enlarged view in figure 7. It is also noticeable significant improvement in disturbance rejection in the case with additional P controller, but its gain reaches also high value  $K_p=3400$ .

3.3. Example 3

Second-order object with one left half-plane zero has been simulated here. Its transfer function is given by Eq. (4).

$$G_{ex.3}(s) = \frac{9s + 1}{s^2 + 14.6s + 1} \tag{4}$$

Parameters of PI controller are  $K_p= 4.252$ ,  $K_i= 61.579$ . Maximum overshoot value is taken  $P_{max}=3\%$ . Responses in figure 8 and its enlarged view in figure 9 are obtain when gain of additional controller reach pretty high value  $K_p=2000$ . Disturbance amplitude is notably reduced, while

time for its rejection is a little extended. As it mentioned, disturbance amplitude values are purposely taken 10 to 40 times higher than reference value. The obtained responses show very large differences between control algorithm with and without additional P controller.

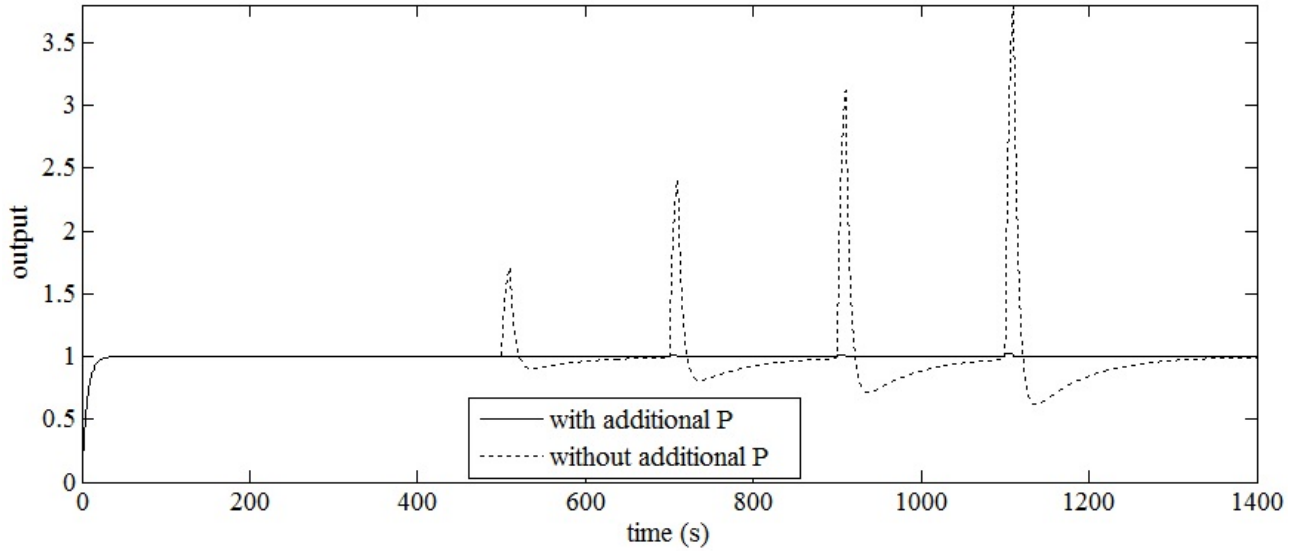


Figure 4: Disturbance rejection with and without additional self-tuning P controller (example 1)

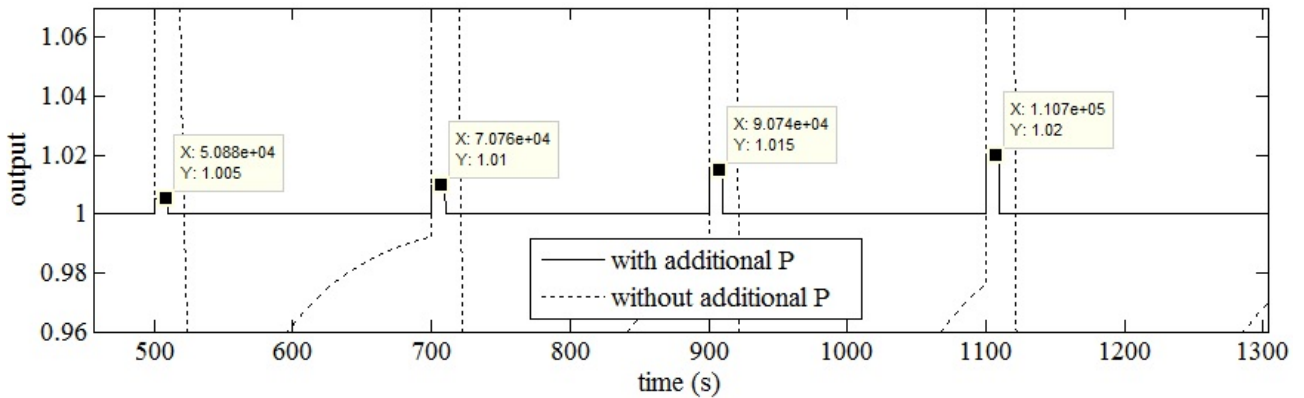


Figure 5: Enlarged display of figure 4

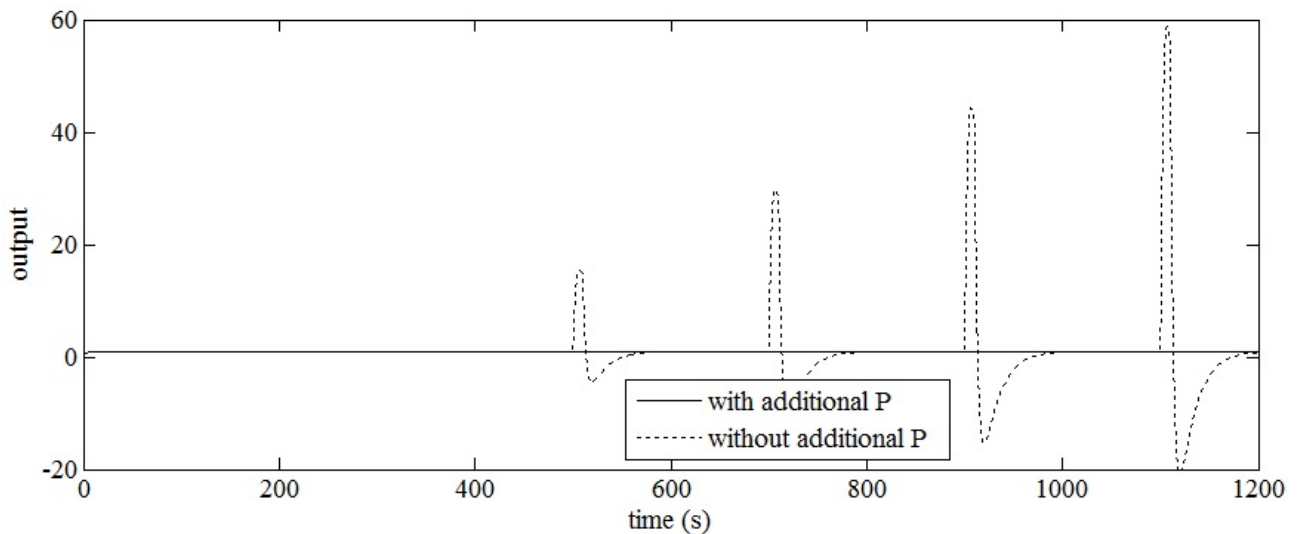


Figure 6: Disturbance rejection with and without additional self-tuning P controller (example 2)

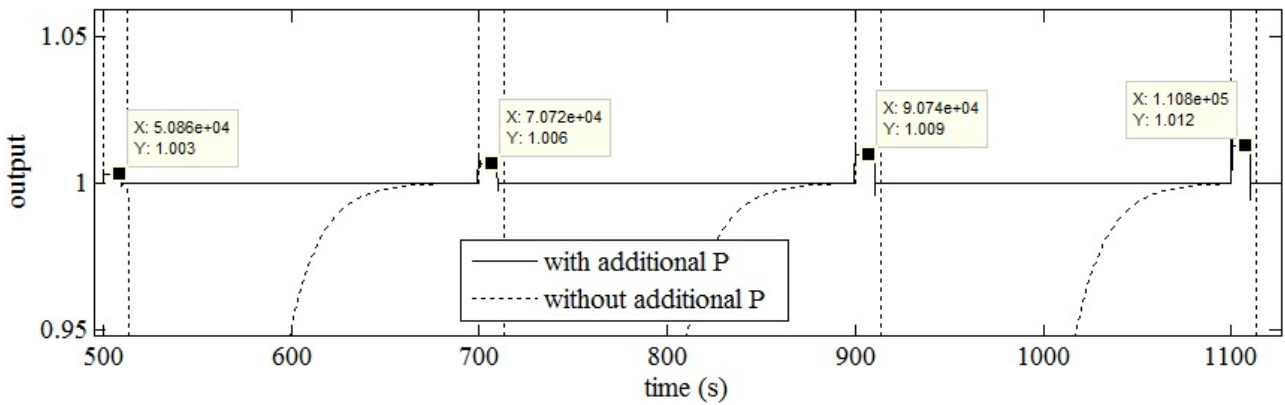


Figure 7: Enlarged display of figure 6

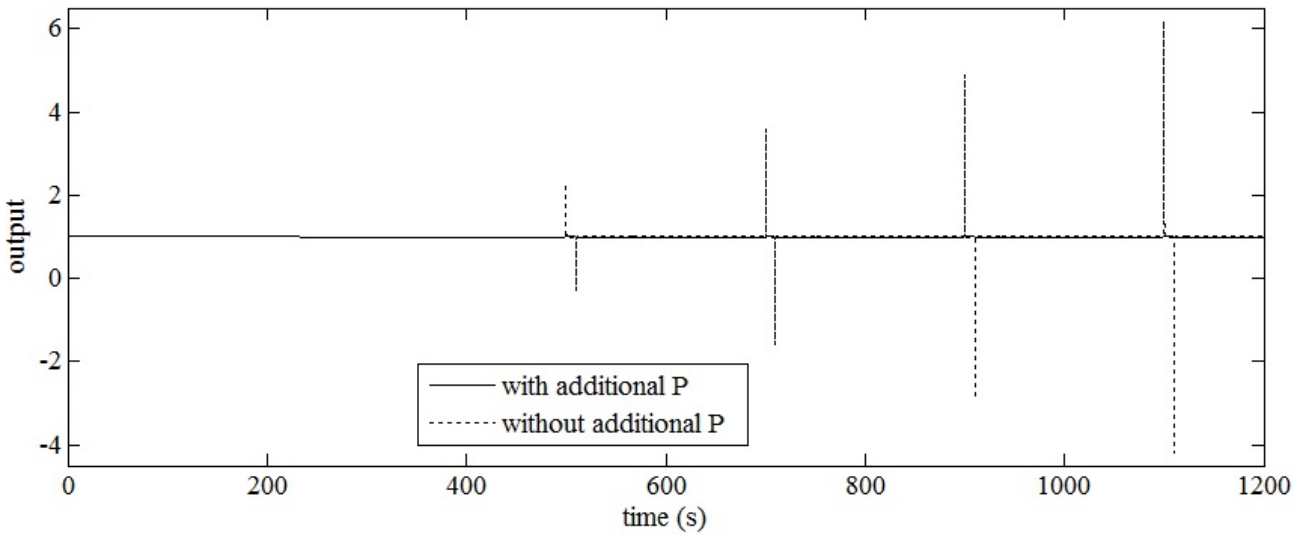


Figure 8: Disturbance rejection with and without additional self-tuning P controller (example 3)

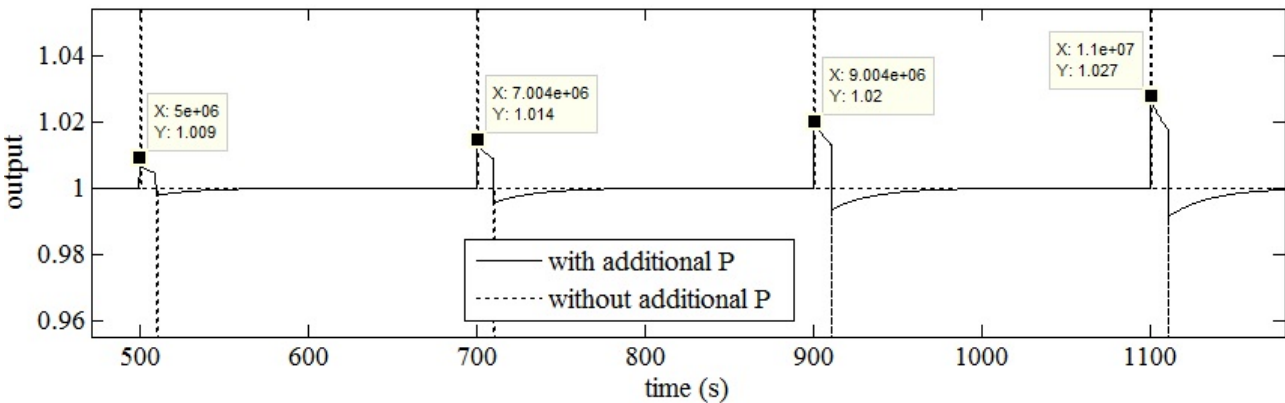


Figure 9: Enlarged display of figure 8

4. CONCLUSIONS

Complex controller consisted of its PI and P parts in parallel connection has been formed and tested. Its efficiency was proved on the some characteristic transfer function of objects. Timely reaction of P controller has been achieved through the its self-tuning using chosen characteristic of time response (overshoot). Any response characteristic can be estimated and limited for this purpose. Due to very high disturbance amplitudes introduced into object also large values of  $K_p$  has been obtained. Feasibility of such high proportional gains in real system is practically impossible because of actuators limitations regarding saturation. Even when computer generate that output signal there are great chance that physical nature of actuator cannot follow such very

rigorous request. But this study shows possible way and ideal case which should be followed. Striving towards theoretically obtained values of proportional gain  $K_p$  of additional controller has to be performed using various combinations of actuators and by improving of their characteristics. Namely, this research is the first step in the realisation of controller part that should operate periodically, i.e. only when object is disturbed. Here it was carried out based on iterative method, but in the industrial environment it should be incorporated into real time control system, where chosen response characteristic is estimated in every sampling period. That will be subject of future investigations.



## REFERENCES

- [1] K. J. Åström, T. Hägglund, "PID Controllers: Theory, Design and Tuning", Research Triangle Park, NC: Instrumental Society of America, (1995)
- [2] V. Ž. Filipović, N. N. Nedić, "PID Controllers", University of Kragujevac, Faculty of Mechanical Engineering, Kraljevo, (2008), (in Serbian).
- [3] C. C. Yu, "Autotuning of PID Controllers", Springer, London, (Great Britain), (2006)
- [4] I. Branlea, I. Petrovic and N. Peric, "Toolkit for PID dominant pole design", 9th International Conference on Electronics, Circuits and Systems, Vol. 3, pp. 1247-1250, (2002)
- [5] Q-G. Wang, Z. Zhang, K. J. Åström, L. S. Chek, "Guaranteed dominant pole placement with PID controllers", J. Process Control, Vol. 19, pp. 349-352, (2009)
- [6] S. Lj. Prodanović, N. N. Nedić, V. Ž. Filipović, "Improved auto-tuning PID controller of level in condenser of turbine in thermal power plant using saturation-relay feedback", Proceedings of the X Triennial International SAUM Conference on Systems, Automatic Control and Measurement, Niš (Serbia), pp. 68-71, (2010)
- [7] N. N. Nedić, S. Lj. Prodanović, "Some Modifications in the Process Identification and Tuning of Controller of Level in Condenser in Thermal Power Plant", Proceedings of the XI Triennial International SAUM Conference on Systems, Automatic Control and Measurement, Niš (Serbia), pp. 382-385, (2012)
- [8] N. N. Nedić, V. Ž. Filipović, S. Lj. Prodanović, "Energy saving in the power plants using automatic control", Proceedings of ECOS 2011 – The 24th International Conference on Efficiency, Cost, Optimization, Simulation and Environmental Impact of Energy Systems, Novi Sad (Serbia), pp. 1843-1855, (2011)
- [9] V. Ž. Filipović, N. N. Nedić, S. Lj. Prodanović, "Reduced energy cost through the furnace pressure control in power plants", Proceedings of ECOS 2012 – The 25th International Conference on Efficiency, Cost, Optimization, Simulation and Environmental Impact of Energy Systems, Perugia (Italy), pp. 367 1-9, (2012)
- [10] Q. G. Wang, B. Huang, X. Guo, "Auto-tuning of TITO decoupling controllers from step tests", ISA Transactions, Vol. 39, 407-418, (2000)
- [11] F. Vázquez, F. Morilla, S. Dormido, "An iterative method for tuning decentralized PID controllers", Proceedings of the 14th IFAC World Congress, Beijing, (China), (1999)
- [12] S.Lj. Prodanović, N. N. Nedić, Lj. S. Lukić, "Possibilities for disturbance rejection in the decoupled TITO process", Proceedings of the 12th international scientific conference, Novi Sad, (Serbia), pp. 71-74, (2015)



# Design of Fixed Order $H_\infty$ Controllers with Specified Settling Time using D-Decomposition

Ljubiša Dubonjić<sup>1\*</sup>, Vojislav Filipović<sup>1</sup>, Novak Nedić<sup>1</sup>, Vladimir Đorđević<sup>1</sup>

<sup>1</sup>Faculty of Mechanical and Civil Engineering in Kraljevo, Department for Automatic Control, Robotics and Fluid Technique, University of Kragujevac, (Serbia)

**Abstract:** The  $H_\infty$  control theory has the high level. But application in industry, owing the complexity of theory, is limited. Controller design is based on complex numerical procedure (Nevanlinna–Pick algorithm) and given parameters does not have physical meaning. Also, the order of the controller is high (at least as an order of system). Owing that facts in this paper we propose simple interactive procedure for  $H_\infty$  PI controller design. The procedure is simple and is based on D-decomposition. In comparison with original  $H_\infty$  controller here we introduce constraint in the form of specification of settling time. The program for procedure of  $H_\infty$  PI controller design is simple and based on MATLAB (Robust Control Tool Box). Given PI controller is applied for control of CSTR (continuous stirred–tank reactor). The process is described as linear model with time delay. In this paper the time-delay approximated with second order Pade approximation. Finally, designed controller provides nominal performance for control systems.

**Keywords:**  $H_\infty$  Controller, Settling time, D- Decomposition,  $H_\infty$  PI Controller

## 1. INTRODUCTION

Robust control theory based on the mathematical theory of infinite-dimensional Hardy space has reached a high level [1-2]. There are applications of this theory in different areas. However, there are quite serious difficulties in including this methodology in a wide application in the industry. First, the controller design procedure is very complicated and it is based on numerical procedures (Nevanlinna-Pick procedure [3-4]). Secondly, the controller is of high order (as a rule, it is higher order than the order of the model) and its parameters have no physical significance. Third, the dispersion of controller parameters is large (parameter values differ by many size orders). The result of this fragility is controller because the numerical implementation introduces errors in the implementation of digital controllers. For these reasons and the fact that staff in the industry is not able to understand  $H_\infty$  control theory there is a natural resistance to the application of this theory.

On the other hand, there is dominant application of PI (PID) controllers in the industry. Here, the regulator parameters have physical meaning, they are easy to set up and suitable, in complexity, for personnel which lead industrial processes. Therefore, the design procedure of robust PI controllers, which satisfy the optimization criterion  $H_\infty$ , is proposed in this paper. Also, it is introduced the restriction which the controller must satisfy, and it is the settling time. The design procedure of  $H_\infty$  PI controller is based on the application of D - decomposition and it is independent of the model order. A network of points for the stability area of the system is constructed, provided that it is a PI controller. At each point of the network, the PI controller is designed and using the MATLAB (Robust Control Toolbox), the minimum of  $H_\infty$

criteria is determined. Based on this, it is formed a catalog of a reference response, a catalog of a load disturbance response and minimum criteria on which basis the operator, through an interactive procedure, selects the controller that suits the best.

A simplified design procedure of the  $H_\infty$  controller based on the input-output model is proposed in reference [5]. The problem is reduced to solving two Diophantine equations. A similar procedure to this one presented in the paper is proposed in the reference [6]. The difference is that the approximation of the delay is not carried out. Reference [6] is dedicated to the design of  $H_\infty$  controller for communication computer networks. For the design methods of the  $H_\infty$  controller, a suitable model [8-9] is also needed. A new approach to machine learning – based identification is proposed in the reference [10].

This paper discusses the regulation of the CSTR (Continuous Stirred-Tank Reactor) using the  $H_\infty$  PI controller. The process is described as a linear process with a delay [7, 11-14]. The problem is, subject to a limitation on relative stability, considered in the reference [15]. When at the same time, there are limitations on the relative stability and the settling time, the design of standard PI controllers, is discussed in references [16-17]. In all of these cases, D-decomposition was used [18-20].

## 2. MATHEMATICAL MODEL OF A CSTR

Continuous stirred-tank reactors have widespread application in industry and embody many features of other types of reactors [21].

Consider a simple liquid-phase, irreversible chemical reaction where chemical species A reacts to form species B. The reaction can be written as

\*Corresponding author: Dositejeva 19, 36000 Kraljevo, dubonjic.lj@mfv.kg.ac.rs

$$A \longrightarrow B \tag{1}$$

It is supposed that the rate of reaction is first-order with respect to the component A

$$r = kc_A \tag{2}$$

where r is the rate of reaction A per unit volume, k is the reaction rate constant (with units of reciprocal time and c<sub>A</sub> is the molar concentration of species A. For single phase reactions, the constant k is given by the Arrhenius equation

$$k = k_0 \exp\left\{-\frac{E}{RT}\right\} \tag{3}$$

where k<sub>0</sub> is constant, E is the activation energy and R is the gas constant. The parameters k<sub>0</sub> and E are determined by fitting experimental data. The last two equations can be considered to be semi-empirical relations.

The schematic diagram of the CSTR is shown in Fig. 1.

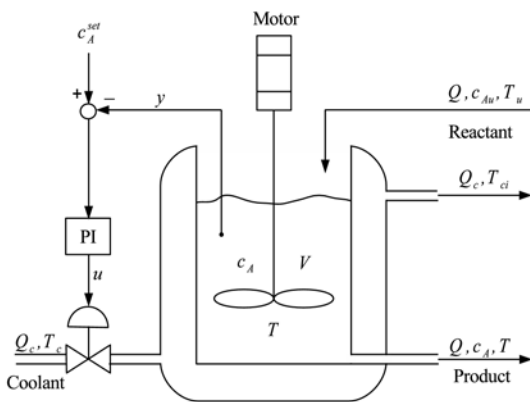


Figure 1. CSTR with cooling jacket

The designations in the figure have the following meanings:

c<sub>Au</sub> - concentration of the reactant in the feed CSTR [kg·mole/m<sup>3</sup>]

c<sub>A</sub> - concentration of the reactant in the feed CSTR [kg·mole/m<sup>3</sup>]

c<sub>A<sup>set</sup></sub> - set point for the concentration [kg·mole/m<sup>3</sup>]

T<sub>u</sub> - temperature of the feed [°C]

T<sub>c</sub> - temperature of the coolant [°C]

T<sub>ci</sub> - output temperature of the coolant [°C]

T - temperature in the CSTR [°C]

Q - flow of the reactant and product [m<sup>3</sup>/s]

Q<sub>c</sub> - flow of the coolant [m<sup>3</sup>/s]

y - measurement of the concentration [kg·mole/m<sup>3</sup>]

u - input signal

The CSTR model development [13-14] is based on three assumptions:

- (i) The CSTR is perfectly mixed
- (ii) the mass densities of the feed and product streams are equal and constant
- (iii) the liquid volume V in the CSTR is kept constant

The mathematical model of CSTR is taken from [11-12] and has the form

$$G(s) = \frac{Y(s)}{U(s)} \tag{4}$$

$$G(s) = \frac{1.308}{(13.515s + 1)(6.241s + 1)} e^{-4.896s}$$

The goal of the control systems is to control the CSTR composition (y) by manipulating the cool rate through the control signal (u). Different control strategies are presented in [13].

In this paper we shall approximate the element of delay by a second-order Padé approximation. The general form of Padé approximation, according to [22-23], is

$$e^{-T_d s} = \frac{\left(1 - \frac{sT_d}{2n} + \frac{1}{3}\left(\frac{sT_d}{2n}\right)^2\right)^n}{\left(1 + \frac{sT_d}{2n} + \frac{1}{3}\left(\frac{sT_d}{2n}\right)^2\right)^n}, T_d = -4.896 \tag{5}$$

In this paper, the approximation for n=2 is used and, in that case, the transfer function or the process is:

$$G(s) = \frac{1.308}{(13.515s + 1)(6.241s + 1)} = \frac{\left(1 - \frac{sT_d}{2n} + \frac{1}{3}\left(\frac{sT_d}{2n}\right)^2\right)^2}{\left(1 + \frac{sT_d}{2n} + \frac{1}{3}\left(\frac{sT_d}{2n}\right)^2\right)^2}, T_d = -4.896 \tag{6}$$

The application of Padé approximation for delay is widely used in chemical industry [20].

Note 1. Possible approximations for delay are:

A) Laguerre shift

$$e^{-T_d s} = \lim_{n \rightarrow \infty} \frac{\left(1 - \frac{sT_d}{2n}\right)^n}{\left(1 + \frac{sT_d}{2n}\right)^n} \tag{7}$$

This type of approximation is applied in robust control theory [19].

B) Kautz shift

$$e^{-T_d s} \cong \frac{\left(1 - \frac{sT_d}{2n} + \frac{1}{2}\left(\frac{sT_d}{2n}\right)^2\right)^n}{\left(1 + \frac{sT_d}{2n} + 2\left(\frac{sT_d}{2n}\right)^2\right)^n} \tag{8}$$

It was analytically shown that this type of approximation is more accurate than the Laguerre one [19].

### 3. DESIGN OF H<sub>∞</sub> PI CONTROLLERS BY APPLYING D-DECOMPOSITION

We will now expose the design procedure for the H<sub>∞</sub> PI controller that will be used for regulating the CSTR process. The purpose of the constraints is to specify an area, in z-plane, in which the complex-conjugate roots of the characteristic system equation are located.

For the system to possess the required settling time, it is necessary that all the real parts of the poles of the transfer function of the closed loop are located left to the real line σ<sub>m</sub> = const., from Figure 2. In this way, we map

the area from the "s" plane, left of the line  $\sigma_m = \text{const.}$ , (Fig. 2), in the area of the corresponding settling time  $\sigma_{\min} = \text{const.}$ , in the parameter plane of the adjustable controller parameters ( $K_p, K_i$ ). Here, it is necessary to find the minimum undamped frequency that will satisfy the condition:

$$|\sigma_{\min}| \geq |\sigma_m|; |\xi \cdot \omega_{n \min}| \geq |\sigma_m| \quad (9)$$

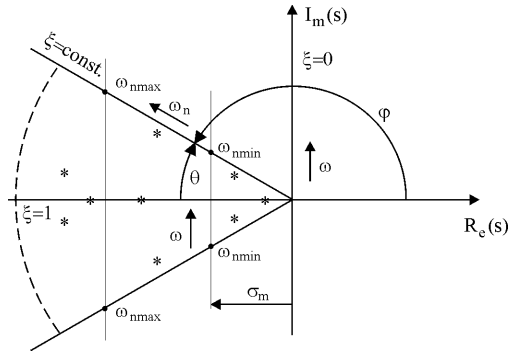


Figure 2. Area with the required settling time  $\sigma_m$

Having in mind the constraint given by the equation (9), the following criterion is minimized

$$J = \sup_{0 \leq \omega \leq \omega_1} \|S(j\omega)\| \quad (10)$$

Let us note that, instead of the constraint (9), a constraint that relates to the settling time may also be introduced. It is possible to introduce both criteria simultaneously [16].

The procedure of design of  $H_\infty$ PI controllers is as follows:

1. Select the area of settling time of the system in the s plane.
2. Choose the points on the curve  $\xi = \text{const.}$  and determine the parameters  $K_p$  and  $K_i$  PI of the controller for each point.
3. Based on the transfer function of the  $C(s)$  controller (obtained on the basis of the parameters  $K_p$  and  $K_i$ ) and the transfer function of the  $G(s)$  process, calculate the sensitivity of the system  $S(s)$ .
4. Compute the minimum of criterion  $J_{\min}$  based on the equation (10), by applying MATLAB (Robust Control Toolbox).
5. Create a catalogue which contains:
  - a) graphical presentation of the reference responses
  - b) graphical presentation of suppression of disturbances
  - c) minimum of the criterion  $J$
6. In accordance with engineering reasoning, choose the PI controller which provides nominal performances of the system.

The proposed procedure is an interactive graphical procedure which is simple and enables engineers in industry to use, in a comprehensible and easy way, the latest accomplishments in automatic control theory. In this case, it is  $H_\infty$  optimization.

The advantages of the proposed procedure are as follows:

- a) Simple structure of the controller (PI controller), which allows physical interpretation of its parameters.

b) Superiority of thus obtained controller in comparison with the original  $H_\infty$  controller (which has a high order), which was shown for the case when there are no constraints (9).

c) Elimination of the need to determine the weight function  $W(s)$ , which is a non-trivial problem.

The simulation results were done on the CSTR model.

Figure 3 shows the parameter plane with the limit values of the PI controller parameters for the required settling time.

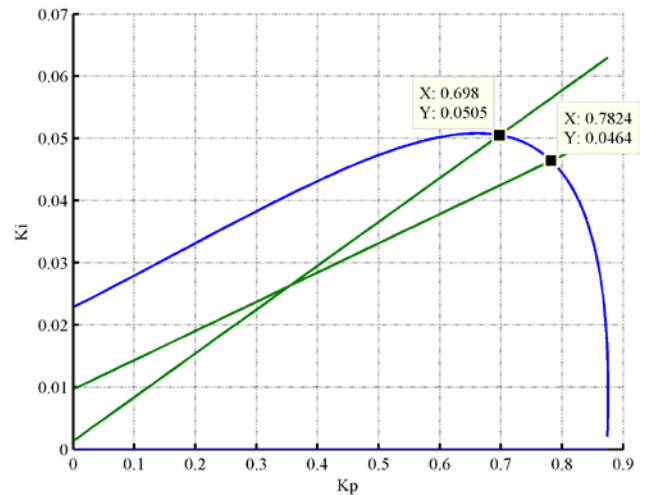


Figure 3. The parameter plane for the required settling time  $\sigma_m$

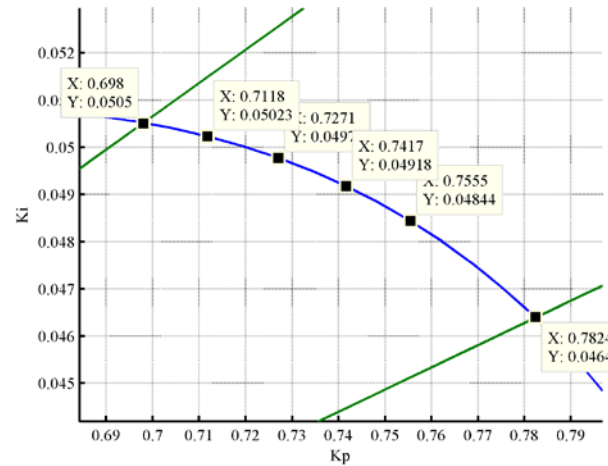


Figure 4. The parameter plane with catalog of PI controllers for the required settling time

From Figure 4 it can be seen, viewed from left to right, as it is formed a catalog of 6 (C1-C6) PI controllers with a corresponding step. For each of these controllers, the minimum of  $J$  criteria is calculated and it is established a catalog of a reference response, and a catalog of a load disturbance response.

For a formed response catalog of controllers C1 to C6, a minimum of  $J$  criteria is determined based on the corresponding program written in Matlab, and its result is:  $J = \min(\{J1, J2, J3, J4, J5, J6\}) = \min(\{0.9968, 0.9968, 0.9969, 0.9969, 0.9970, 0.9971\}) = (J1, J2) = 0.9968$ .

Based on this result, it can be seen that the two controllers, C1 and C2, meet the minimum of J criteria in the already defined interval of the parametric plane that meets the condition of the required settling time. Figures 5 and 6 show the reference system response and load disturbance response for the limit values of the C1 and C6 controllers as well as the C2 controller which fulfills the minimum of J criteria.

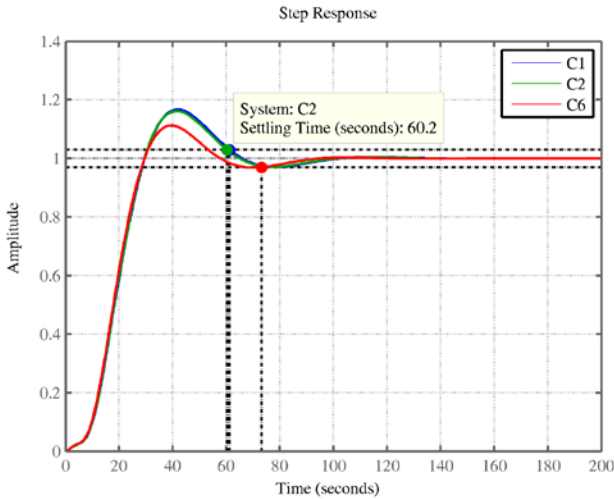


Figure 5. System response to reference for three controllers C1,C2 and C6

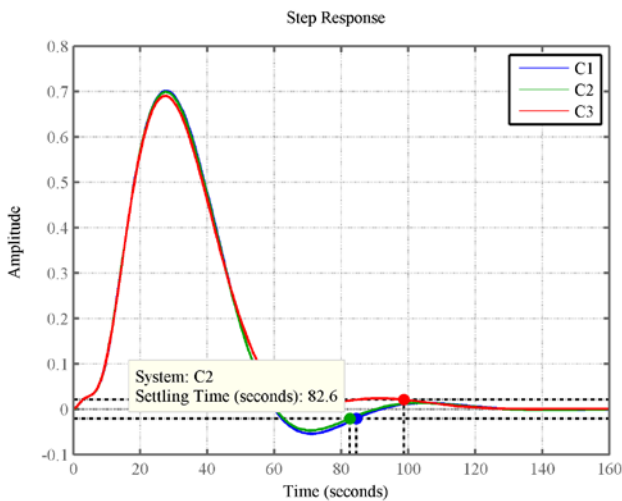


Figure 6. System response to load disturbance for three controllers C1,C2 and C6

On the basis of the results shown in Figures 5 and 6, it can be seen that C2 controller gives the best result from the aspect of the responses to the reference and to the load disturbance rejection.

Figure 7 shows Bode diagrams with system characteristics that are designed based on the values of the controller parameters C2. The picture shows that the system has the correct values of the phase margin and the gain margin.

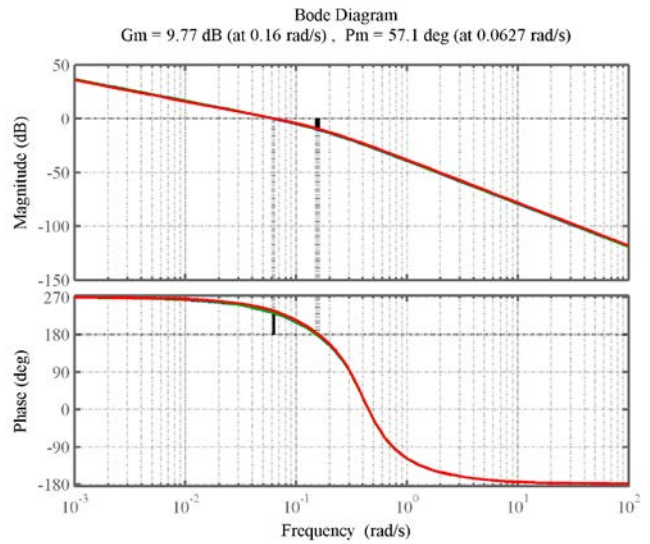


Figure 7. Bode diagrams for open loop designed with controller C2

CONCLUSIONS

In this paper, a simple interactive procedure, based on D-decomposition, is proposed for the design of the  $H_\infty$ PI controller. The design of the controller includes a limitation in the form of a given settling time. Through the simulation, it is formed a catalog of: response to reference, a response to suppression of load disturbance and minimum of  $H_\infty$  control criteria. Based on the catalog, a controller is considered to be most suitable for the given process. The resultant controller was of a much lower order than the original  $H_\infty$  controller that is obtained by using very complex numerical procedures. Also, the parameters of the  $H_\infty$  PI controller have a physical meaning.

ACKNOWLEDGEMENTS

This paper was supported by the Republic of Serbia, Ministry of Education, Science and Technological developments, through project no. 33026-TR.

REFERENCES

[1] Zhou K, Doyle JC, Glover K. *Robust and Optimal Control*. Prentice-Hall, New Jersey, 1996.  
 [2] Duren PL. *Theory of  $H_p$  Spaces*. New York, Academic Press, 1970.  
 [3] Pontryagin LS, Boltyanski VG, Gamkerelidze RV, Mischenko EF. *Mathematical Theory of Optimal Processes*. Nauka, Moskow, 1969. (in Russian)  
 [4] Pick G. Über Beschränkungen analytischer Funktionen, welche durch vorgegebenen Funktionswerte bewirkt sind. *Math. Ann.* 1916; 77: 7-23. (in German)

- [5] Filipovic V. Design of  $H_\infty$  controllers using delta operators and interpolation theory. *IFAC Low cost*, Peking, China, 1998.
- [6] Filipovic V, Đorđević V. Design of  $H_\infty$  PI controllers for AQM Routers Supporting TCP Flows. To be published, 2017.
- [7] Filipović V. *Industrial Controllers*, Kraljevo, University of Kragujevac, 2016. (in Serbian)
- [8] Filipovic V. Identification in  $H_\infty$  in the Presence to Deterministic and Stochastic Noise. *Third European Control Conference ECC 95*, Roma, Italy, 1995.
- [9] Filipovic V. Robust Identification in  $H_\infty$  of non-Gaussian Systems. *Symposium. of Identification IFAC*, Santa Barbara, USA, 2000.
- [10] Filipovic V.  $H_\infty$  Identification on Class of Distributions based on Robust Statistics and Machine Learning. To be published, 2017.
- [11] Henson MA, Seborg DE. Input-output line optimization of general nonlinear processes. *AIChE J.* 1990; 36: 1753-1757.
- [12] Huang CT, Chon CJ, Wang JL. Tuning of PID controllers based on the second-order model by calculation. *J. Chin. Inst. Chem. Eng.* 1996; 27: 107–120
- [13] Schmidt LD. *The Engineering of Chemical Reactions*. Oxford, Oxford University Press, 1998.
- [14] Bequette BW. *Process Dynamics Modeling, Analysis and Simulation*. New Jersey, Prentice-Hall, 1998.
- [15] Dubonjić LJ, Filipovic V, Nedić N, Đorđević V. Design of an  $H_\infty$  PI controller with given relative stability and its application to the CSTR problem. *Hem. Ind.* 2017; to be published.
- [16] Dubonjić LJ, Nedić N, Filipović V, Pršić D. Design of PI controllers for hydraulic control systems. *Math. Probl. Eng.* 2013; 2013: 1–10.
- [17] Prodanović S, Nedić N, Filipović V, Dubonjić LJ. Modified approach to distillation column control. *Hem. Ind.* 2016; In press
- [18] Neimark YI. (1948) Search for the parameter values that make automatic control system stable. *Automatica i Telemekhanika.* 1948; 9(3):190–203. (in Russian)
- [19] Mitrović D. Graphical analysis and synthesis of feedback control systems. I-Theory and analysis, II-Synthesis, III-Sampled-data feedback control systems, *AIEE Trans. (Appl. and Industry)*. 1959; 77: 476–496.
- [20] Šiljak D. Analysis and synthesis of feedback control systems in the parameter plane. I-Linear continuous systems, II-Sampled-data systems, *AIEE Trans. (Appl. and Industry)*. 1964; 83: 449–466.
- [21] Stephanopoulos G. *Chemical Process Control: An Introduction to Theory and Practice*. New Jersey, Prentice-Hall, 1984.





# Data Classification Using a Set of Neural Networks

Srdjan Ribar<sup>1\*</sup>

<sup>1</sup>Faculty of Mechanical engineering, University of Belgrade, Belgrade (Serbia)

*Neural networks are often used in data classification. Ordinary neural networks show inadequate accuracy solving such problem. Noticeable improvement in data classification is reaching using a set of ordinary neural networks. In this paper bioimpedance data classification using self-organizing mapping neural network is analysed.*

**Keywords:** bioimpedance, neural networks

## 1. INTRODUCTION

Artificial Neural Networks (NN) are widely applied as a classification tool in medical diagnosis [1], [2], [3]. Various types of NN can be used for classification. No matter of NN which is used, the procedure for its applying is always the same: based on measured given data of a known classes, NN is trained to perform the best classification which means: to get the same NN output for input of the same class. NN are generally divided into two classes according to training method. They could be trained supervised or unsupervised. During supervised training supervisor feeds NN with correct output. Unsupervised training is applied on NN which set its output in input space according input data distribution.

After training period NN is tested with new set of data presented to NN for the first time. If type and structure of NN is well chosen, training successfully completed the classification should be well performed.

According to a type of training NN are divided into two classes: supervised or unsupervised. Supervised training means that prior training is known for each input in which class it belongs. NN during training is adapting to perform correct input-output mapping. Unsupervised NN perform mapping with no information about the class of input element.

This paper is concerned with bioimpedance data classification using self-organizing mapping neural network (SOM). This type of NN is trained unsupervised. During training this NN tends to place its nodes in input space according to input data distribution. The number density of the nodes in input space is approximately proportional to the probability density of input data.

SOM has unique feature that for one input only one node is active while all others are inactive. It means that for each input only one single node is active while all others are inactive (only one node has value=1, all others=0). The active node is nearest to input presented to NN.

Bioimpedance – bioelectrical impedance analysis is a method widely applied in biomedical diagnostics [4], [5]. It is based on electrical properties of biological tissue measurements analysis. It is a noninvasive low cost method. Some research suggest that bioimpedance measurements depend on age [6], race [7] and gender [8]. In this paper it is analyzed if bioimpedance data could be divided into two classes according to gender: male and female. This classification is performed using SOM,

neural network which performs unsupervised training. The whole procedure is described in detail.

## 2. MATERIAL AND METHODS

In this paper are used the results of the in vivo bioimpedance measurements of human skin. The results are after measurement divided into two groups: elder and younger examinees. Each examinee is presented by its Coleplot [9], fig.1.

The Cole equation:

$$Z = R_{\infty} + \frac{R_0 - R_{\infty}}{1 + (j\omega\tau)^{\alpha}} = Z' + jZ'' \quad (1)$$

with:

$$(j\omega)^{\alpha} = \omega^{\alpha} [\cos(\alpha\pi/2) + j\sin(\alpha\pi/2)]$$

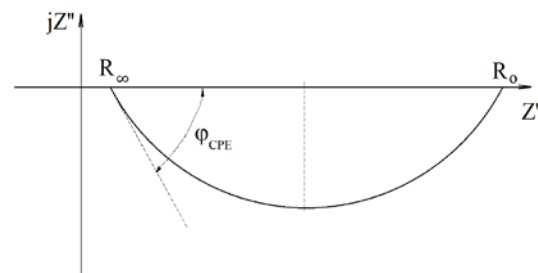


Figure 1: Cole plot

represents impedance distribution in complex plane.  $Z'$  and  $Z''$  are real and imaginary part of impedance. Cole plot is a part of a circle with centre above  $Z'$  axis. For ideal capacitor plot is a semicircle with a centre on  $Z'$  axis while pure resistor plot lies on  $Z'$  axis. Constant phase angle (CPE),  $\varphi_{CPE}$ , [10] is a tangent angle, fig.1 while parameter  $\alpha$  is defined as:

$$\varphi_{CPE} = (\alpha\pi)/2 \quad (2)$$

$\alpha \in (0,1)$ .  $\alpha=1$  describes an ideal capacitor while the case  $\alpha=0$  describes a pure resistor.

Four parameters are defined on this plot:  $R_0$ ,  $R_{\infty}$ ,  $\alpha$ ,  $\tau$ .

$R_0$  - resistance at low frequency,

$R_{\infty}$  - resistance at high frequency,

$\alpha$  - parameter

$\tau$  - time constant:

$$\tau = [(R_0 - R_{\infty})C]^{1/\alpha} \quad (3)$$

Time constant is calculated as:

$$\tau = \frac{1}{\omega^*} \tag{4}$$

Where  $\omega^*$  represents  $I_{min}=I(\omega^*)$ .

NN training of SOM contains few steps as follows:

- 1) Inputs are classified in predefined classes (male and female examinees)
- 2) Input data is presented to NN and it responds with its outputs
- 3) After training period follows testing. All nodes of NN which are active only for inputs from one input class perform good classification. If such node is active it suggests a class of input element. Furthermore activation of such node refers to a class of input element. Also for all input elements that activated such nodes is assumed that are well classified.
- 4) Classification of input data that are not well classified should be performed in other way (by other NN or other classification method).

### 3. INPUT DATA

NN input data consists of training set and test set data.

#### 3.1. Test data

As a test data bioimpedance measurements are assumed. Test data consists of bioimpedance measurements of 31 female and 33 male healthy examinee and they form two classes of data. Since Cole plot, fig.1 presents frequency response for a range of frequencies  $\omega \in (0, +\infty)$  it is impossible to perform a measurement to obtain the whole Cole plot. Bioimpedance measurements were performed on certain alternative current frequencies and some finite number dots of Cole plot were obtained. Since the Cole plot curve is a circle arc minimum three measurements are necessary. Based on these measurements (three dots) Cole plot is fitted through these dots fig.2.

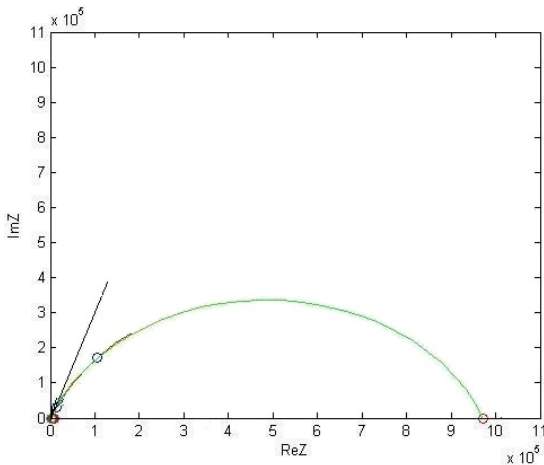


Figure 2: Cole plot fitting

On fig.2 small circles present bioimpedance measured values. Circle arc is fitted through these values. Interception of arc with abscissa define values:  $R_0$  and  $R_\infty$ . Tangent line is constructed defining angle  $\phi_{CPE}$ . Parameter  $\alpha$  obtained from eq. (2), and time constant  $\tau$  from eq. (3). During calculating time constant it is necessary to estimate the frequency where  $Z''$  - the imaginary part of impedance

reaches its minimum. In that way it is obtained that each test data consists of four Cole parameters:  $R_0$ ,  $R_\infty$ ,  $\alpha$ ,  $\tau$ .

#### 3.2. Training data

Training data set represents virtual data that is generated on the bioimpedance measurements data. There are two groups of bioimpedance measurements: male and female examinee. For each group average value and standard deviation is calculated. Based on these parameters, two groups, each comprising 500 elements with same statistic characteristics were generated.

### 4. NETWORK STRUCTURE

Number of NN nodes, its basic characteristic, is an arbitrarily chosen value. That number should be at least the same as number of classes of input data. Since number of input classes are two (male and female) and dimension of input vector is four, minimum of number of nodes is:  $2 \times 2 \times 2 \times 2 = 2^4$  (two classes on each axis). Generally, in order to improve classification, the number of nodes is chosen to be greater than calculated minimum (16) so in this case it is  $5 \times 5 \times 5 \times 3 = 375$ . It means that NN should have on three axis 5 subclasses on fourth axis 3 subclasses. This number is always much greater than number of classes of input data and depends on rate how input data of different classes are mutually mixed. In this case it is assumed that input data could be well classified with 375 nodes. This assumption will be tested during simulation.

#### 4.1. Network training

Each element of input data (1000 elements) is used to train the network during training period. Whole set of input data is repeatedly presented to NN. By each iteration nodes are slightly moving in input space tending to be positioned according to probability density of input data. Each training iteration implies using all 1000 input elements as NN input at random order.

Number of training iterations is experimental variable which depends on how input data of different classes are mutually mixed. In this case 500 iterations were performed. It was tested that increase of number of training iterations do not lead to better input-output mapping accuracy.

### 5. SIMULATION RESULTS

#### 5.1. NN testing to gender classification

##### 5.1.1. NN testing with whole set of input data

Testing NN occurred after network training is finished. Testing was performed with bioimpedance measurements of 31 female and 33 male examinees.

First bioimpedance measurements of 31 female and 33 male healthy examinees are set as input data of NN with 375 nodes. Simulation results are: some NN nodes were activated by 23 female examinees only and other NN nodes were activated by 17 male examinees only. It is concluded that these nodes were active only by input of the same class and it is assumed that further activation of these nodes implies known input class.

There are 8 female and 16 male examinees that activated the same nodes. Since same node was active for inputs of different class, classification of these data is unsatisfactory. Further activation of such node do not

determine the input class. For that reason these measurements are not well classified by this NN. Classification of these measurements should be performed in other way.

5.1.2. NN testing with 3 Cole parameters

In this paper is suggested classification of unclassified data in a special way: the use of combination of set of NN for further classification. These NN will use as input unclassified data only which in this case means: 8 female and 16 male examinees. The rest data is considered well classified in a first step.

Unclassified data (8 female and 16 male examinees) are presented to a new NN. New NN deals with a simplified input data: from four Cole parameters of input data, it chosen three of them. First combination of three Cole parameters that are chosen as NN input are:  $R_\infty$ ,  $\alpha$ ,  $\tau$ . Since input measurements are now three dimensional, structure of NN is simplified. Number of nodes are chosen as:  $5 \times 5 \times 5 = 125$ . It means 5 nodes on each axis which should be satisfactory for classification. Number of training iterations was set to 500. Results of such choice are: 3 female examinees 3 male are well classified (different nodes were activated by male and female inputs). Unclassified data remained: 5 female and 13 male examinees.

Next step is usage a NN with new combination of input Cole parameters:  $R_0$ ,  $\alpha$ ,  $\tau$ . NN structure and number of training iterations were the same for all kinds of three dimensional inputs:  $5 \times 5 \times 5$  and 500, respectively. With this combination of input Cole parameters unclassified data are: 4 female and 13 male examinees. Furthermore next combination of Cole parameters:  $R_0$ ,  $R_\infty$ ,  $\alpha$  gives as a result 4 female and 12 male unclassified examinees. The last fourth combination of three Cole parameters  $R_0$ ,  $R_\infty$ ,  $\tau$  as a result leaves 3 female and 11 male unclassified examinees.

5.1.3. NN testing with 2 Cole parameters

New combination of input data is a pair of Cole parameters. These pairs are:  $R_0, \alpha$ ;  $R_0, \tau$ ;  $R_0, R_\infty$ ;  $R_\infty, \alpha$ ;  $R_\infty, \tau$ ;  $\alpha, \tau$ . Number of nodes are chosen as:  $5 \times 5 = 25$ . Number of training iterations was set to 500. Applying a pair  $R_0, \alpha$  as an input gives as a result 3 female and 10 male unclassified examinees. All other combinations of inputs do not improve classification and at the end of the whole this group of parameters remain 3 female and 10 male unclassified examinees.

5.1.4. NN testing with single Cole parameter

On the group of still unclassified examinees is chosen only one Cole parameter and testing was performed on it as an only input:  $R_0$ ,  $R_\infty$ ,  $\alpha$ ,  $\tau$  respectively. Number of nodes is 10. Number of training iterations was set to 100. There is no changes applying  $R_0$ ,  $R_\infty$ , parameter as input. Applying  $\alpha$  as input remain 3 female and 9 male unclassified examinees.

5.1.5. NN testing with increased the number of nodes

Testing was performed to improve classification with single Cole parameter with NN with 50 nodes. Number of training iterations was set to 500. All other conditions were the same as in 5.1.4. Applying  $\alpha$  as input

parameter remain unclassified 3 female and 9 male unclassified examinees. Further on applying  $R_0$  as input parameter remain unclassified 3 female and 4 male unclassified examinees. Increasing the number of nodes to 100 NN with  $R_0$  as input parameter gave slightly improvement: 3 female and 3 male unclassified examinees. All other inputs  $R_\infty$ ,  $\alpha$ ,  $\tau$  gave no improvement.

5.1.6. NN with additional parameter gain

Since classification was not performed satisfactory by varying a number of Cole parameters as an NN input, their quantitative analysis was performed

The range of first Cole parameter  $R_0$ , resistance at low frequency, is  $M\Omega$  order of magnitude. The range of first Cole parameter  $R_\infty$ , resistance at high frequency, is  $k\Omega$  order of magnitude. Cole parameter with minimum order of magnitude is  $\alpha$ ,  $\alpha \in (0, 1)$ , table 1.

Table 1: the order of magnitude of Cole parameters

$R_0 [M\Omega]$	$R_\infty [k\Omega]$	$\alpha [ ]$	$\tau [ms]$
6	3	-1	1

From table 1 is obvious that significance of parameter  $\alpha$  is smallest. It is shown that it varies relating to gender [8]. It is very obvious to notice such characteristic on Cole plot: coefficient  $\alpha$  is proportional to tangent angle of Cole plot, eq.2, and change of  $\alpha$  values shifts the Cole plot. In this measurements is obtained that average value for male examinees is  $\alpha=0,67$  and for female examinees is  $\alpha=0,86$ . It means that Cole plot for female examinees is above male examinees.

NN was tested with all four Cole parameters whereby values of parameter  $\alpha$  were multiplied by  $10^6$ . This way its influence was approximately the same as parameter  $R_0$ . Number of training iterations was 100. Such inputs slightly improved testing result: 3 female and 2 male unclassified examinees. Further increasing a number of iterations gave no improvement since after 500 iterations the number of unclassified examinees was the same: 3 female and 2 male unclassified examinees.

Further testing was focused on NN with three Cole parameters as inputs:  $R_\infty$ ,  $\alpha$ ,  $\tau$ , where values of parameter  $\alpha$  were multiplied by  $10^6$ . In this case, according to table 1 the most significant Cole parameter is  $\alpha$  since its values are multiplied by  $10^6$ .

In this case the rest of unclassified measurements, 3 female and 2 male are precisely classified. This means that classification is performed with no error and all data are classified.

In each testing procedure where number of unclassified measurements was reduced certain number of NN nodes are labelled as active for input from certain class. Further activity of such a node implies a class in which such input belongs to. In that way all active nodes are labelled and its class is defined. Further input should activate one of these nodes suggesting a class to which it belongs.

Network prepared in this way should perform classification with no error. This is possible to expect only if measured data are representative for its class. This is

general characteristic of all NN no matter of its type. This means that certain errors are possible to appear. Such errors are correcting in ordinary way: all new input data are presented to NN as train data and NN is adapting to them. After training period NN should make no error with such data.

## 5.2. NN testing to age classification

Measurements of 31 female and 33 male examinees used in 5.1 are also used to age classification by NN. It means that measurements of these examinees are sorted into two groups according to age: younger examinees up to 25 years of age and older ones. Since it is assumed that bioimpedance measurements depends on age [8], classification on two groups: younger and older examinees was performed by NN. Bioimpedance measurements of 45 young examinees represent first group and 19 bioimpedance measurements of the rest second group with older ones.

The type NN is SOM, NN structure  $5 \times 5 \times 5 \times 3 = 375$ . Test data are bioimpedance measurements. Since measured values are inadequate for training, virtual data training set is generated: group of 500 young and 500 old examinees with same statistic parameters as measured ones: young and old respectively. Number of training iterations is 500.

### 5.2.1. NN testing with whole set of input data

Both groups, 19 old and 45 young examinees are presented by four Cole parameters. The result is 9 young and 10 old unclassified examinees.

### 5.2.2. NN testing with 3 Cole parameters

These NN will use as input unclassified data only which in this case means: 9 young and 10 old unclassified examinees. The rest data is considered well classified in a first step. Input measurements are now three dimensional, structure of NN is simplified. Number of nodes are chosen as:  $5 \times 5 \times 5 = 125$ . Number of training iterations was set to 500.

First combination of three Cole parameters that are chosen as NN input are:  $R_\infty$ ,  $\alpha$ ,  $\tau$ . Unclassified data remained: 2 old and 5 young examinees. It is significant improvement in classification process since NN with 4 Cole parameters remained unclassified 9 young and 10 old examinees.

Now is applied NN with new combination of 3 Cole parameters input:  $R_0$ ,  $\alpha$ ,  $\tau$ . Number of unclassified examinees is still the same: 2 young and 5 old as it is with NN with next combination of 3 Cole parameters input:  $R_0$ ,  $R_\infty$ ,  $\alpha$ . Improvement is seen with last combination of 3 Cole parameters  $R_0$ ,  $R_\infty$ ,  $\tau$ : unclassified are 2 young and 4 old examinees.

### 5.2.3. NN testing with 2 Cole parameters

These pairs are:  $R_0, \alpha$ ;  $R_0, \tau$ ;  $R_0, R_\infty$ ;  $R_\infty, \alpha$ ;  $R_\infty, \tau$ ;  $\alpha, \tau$ . Number of nodes are chosen as:  $5 \times 5 = 25$ . Number of training iterations was set to 500. Applying a pair  $R_0, \alpha$  as an input makes no classification improvement: still unclassified are 2 young and 4 old examinees. The same result is with next two input pairs:  $R_0, \tau$  and  $R_0, R_\infty$ . The same improvement is seen with next input pair:  $R_\infty, \alpha$  unclassified are 1 young and 3 old examinees. Applying the next Cole parameters pair:  $R_\infty, \tau$

left 1 young and 2 old examinees unclassified. The last combination of Cole parameters pair:  $\alpha, \tau$  left unclassified 1 young and 1 old examinees only.

### 5.2.4. NN testing with single Cole parameter

Testing was performed on still unclassified inputs: 1 young and 1 old examinee. Number of nodes is 50. Number of training iterations was set to 100. Input was Cole parameter:  $R_0$ ,  $R_\infty$ ,  $\alpha$ ,  $\tau$  respectively. With  $R_0$  as input parameter certain improvement was achieved: unclassified is only 1 old examinee. No further improvement was achieved in classification with other Cole parameters since after whole set of such inputs still remained left unclassified 1 old examinee.

## 6. DISCUSSION

In this paper classification of bioimpedance measurements of human healthy examinees was performed. Bioimpedance spectroscopy is a popular method for characterizing the electrical properties of biological tissues. Classification was performed by gender as well as by age. All bioimpedance measurements were simplified by taking into account its basic values: four Cole plot parameters. Each examinee was presented by these four parameters. The problem that was analysed in this paper was to classify input data into classes by: a) gender, b) age.

Problem of such classification is that no prior information about input data is available. Common classification method that uses hyperplane to separate input data may not be useful. Input data of different classes could be mixed with each other with no clear boundary between them.

Since the distribution of input data is unknown, a specific classification method using neural networks is applied. Classification using specific type of neural network, self organizing mapping NN (SOM) lies in its underlying property: such NN sets its nodes in input space according probability density of input data. Nodes are distributed into input space according to input data density. Another important property of such NN is that after training, nodes which are on fixed positions in input space, are active only for input in its closest neighborhood. This important feature is used as a classification tool. It means that activation of certain node in test mode by certain input implies that input is close to that node. This basic property of SOM is used to perform satisfactory classification. The curve which separates input data on classes could be of any shape. It can form unlimited number of separated subsets of the same class in the input space. There are no limits of the shape of separation line in the input space also. It could be very convenient separation tool.

All these SOM properties have led to chose SOM as a best choice for classification such intricate input data. Dealing with NN as a classification tool one has to take into account certain limitations which are not particularly relating to NN. Input solitary data which is located far from any other data group, »outlier«, is very hard to classify regardless of the classification method. Since SOM distributes its nodes according probability density of input data, it is expected that outliers should not be well classified. It is practically impossible to determine the

outliers in these four dimensional input data. The only measure of its grouping could be statistical dispersion. The dispersion values of input data are the same order of magnitude and no outliers were deleted from input set data. It means that all bioimpedance measurements were included in NN training and testing.

After a type of NN has been chosen its structure is determined. Certain experience dealing with NN is necessary to define NN structure. Enormous number of NN nodes were chosen, much greater than number of input measurements. The number of NN nodes is chosen according to virtual training data rather than measurements.

At the beginning gender classification was performed (5.1.). First part of NN performance on the whole set of input data has shown that significant part of input data is not classified: 8 female and 16 male examinees. Since not all of Cole parameters are gender sensitive in the same way, partial analysis was performed using various set of input data. All combinations of input data were made: four Cole parameters, all combinations of three, two and single Cole parameter as NN input. Significant improvement was achieved with this method: the number of 8 female and 16 male unclassified examinees is reduced to 3 female and 9 male unclassified examinees. Increasing the number of nodes and number of iterations with single Cole parameter NN led to 3 female and 3 male unclassified examinees. Further applying gain on parameter  $\alpha$  with whole set of input data has led to 3 female and 2 male unclassified examinees. Finally, NN testing with 3 Cole parameters:  $R_{\infty}$ ,  $\alpha$ ,  $\tau$  with additional gain on parameter  $\alpha$  enabled accurate classification of whole input set data.

The similar procedure was performed in age classification (5.2.). Classification with the whole set of input data has shown that significant part of input data is not classified: 9 older and 10 younger examinees. Further significant improvement was achieved using three Cole parameters  $R_{\infty}$ ,  $\alpha$ ,  $\tau$  as NN input: 2 older and 5 younger unclassified examinees. Other combinations of three Cole parameters as inputs led to slightly improvement: 2 older and 4 younger unclassified examinees. All other combinations of two Cole parameters reduced unclassified examinees to: 1 older and 1 younger. The rest combination of NN with single Cole parameter led unclassified 1 older examinee only. The error of classification of this NN set is 5% of older examinees or 1,5% of whole examinees population. In age classification no further classification analysis increasing the number of iterations nor the number of nodes was performed.

To improve age classification by this type of NN it is imposed to deeply analyze influence of increasing the number of iterations and additional gain set to Cole parameters in the same way that it was performed in gender classification.

Dealing with NN it should always bear in mind that its performance always depends on input training data. So it is necessary to perform NN training procedure each time when new measurement data are presented to NN.

General remark to a proposed classification method is that is missing an information that could be significant. Since bioimpedance measurements are insufficient for proper NN training virtual data set is created. NN should

be trained on this virtual data set first. Classification of such data would be helpful in a manner to get the information how virtual data are classified. Ratio of classified and unclassified virtual data should give an information of classification quality. Moreover, it is possible that NN trained on virtual data only, perform satisfactory classification of virtual data as well as bioimpedance measurements.

This is proposal for further research which would be fruitful.

#### ACKNOWLEDGEMENTS

All bioimpedance measurements were performed in Nanolab, Department of automatic control, Faculty of Mechanical Engineering, University of Belgrade. These measurements were performed during 2010. under the leadership of professor Djuro Koruga. I am very grateful that I was a part of a team that performed this research. A part of this research concerning bioimpedance measurements represents the essence of my PhD thesis.

#### REFERENCES

- [1] Filippo Amato, Alberto López, Eladia María Peña-Méndez, Petr Vaňhara, Aleš Hampl, Josef Havel, "Artificial neural networks in medical diagnosis", *J Appl Biomed.* 11, pp. 47–58, (2013)
- [2] Xinghu Yu, Chao Ye, Liangbi Xiang, "Application of artificial neural network in the diagnostic system of osteoporosis", *Neurocomputing*, Vol. 214, pp. 376-381, (2016)
- [3] E. A. Mohamed, "Artificial neural network based fault diagnostic system for electric power distribution feeders", *Elsevier*, Vol. 35, Issue 1, pp. 1-10, (1995)
- [4] Anotoni Ivorra, "Bioimpedance Monitoring for physicians: an overview", *Centre Nacional de Microelectronica, Biomedical Applications Group*, (2002)
- [5] Sami F. Khalil, Mas S. Mohktar, Fatimah Ibrahim, "The theory and fundamentals of bioimpedance analysis in clinical status monitoring and diagnosis of diseases", *Sensors (Basel, Switzerland)*. 2014; 14(6): pp 10895-10928.,(2014)
- [6] Fat-free and fat mass percentiles in 5225 healthy subjects aged 15 to 98 years. Kyle UG, Genton L, Slosman DO, Pichard C Kyle UG, Genton L, Slosman DO, Pichard C
- [7] Validity of total and segmental impedance measurements for prediction of body composition across ethnic population groups. Deurenberg P, Deurenberg-Yap M, Schouten FJ Eur J Clin Nutr. 2002 Mar; 56(3):214-220.
- [8] Dittmar M., Reliability and variability of bioimpedance measures in normal adults: effects of age, gender, and body mass. *Am. J. Phys. Anthropol.* 2003 Dec; 122(4): 361-70,
- [9] Cole, K. S., R. H. Cole, "Dispersion and absorption in dielectrics. I. Alternating current characteristics", *J. Chem. Phys.* 9, 341-351, (1941)

[10] G.J.Brug, A.L.G van den Eeden, M.Sluyters-Renbach, J.H.Sluyters, "The analysis of electrode impedances complicated by the presence of a constant phase element " J. of electroanalytical chemistry and interfacial electrochemistry, Vol. 176, issues 1-2, pp.275-295, (1984)

[11] Ribar, S. "Hybrid software system for biophysical skin condition diagnosis using expert system, neural networks, fuzzy logic and genetic algorithms", University of Belgrade, Serbia, PhD thesis, (2011)

# Kinematic and dynamic analysis of the path of movement of the robot

Ljiljana Pecić<sup>1\*</sup>, Zvonko Petrović<sup>1</sup>, Nikola Kostić<sup>1</sup>

<sup>1</sup>College of Applied Professional Mechanical Studies/ University of Kragujevac, Trstenik (Serbia)

Kinematic and dynamic control problems for a pedestal-mounted robot with a multilink arm are formulated. The robot is considered as a system of perfectly rigid bodies controlled by a combined actuating system. The mathematical model of robot dynamics accounts for the elastic properties of actuator components based on the formalism of Lagrange equations of the second kind. A robot with a two-link arm is considered as an example.

**Keywords:** robot manipulator, kinematic control, dynamic control

## 1. INTRODUCTION

In this paper the Lagrange equations of a second order are formed for the given robotic system assuming that no elastic deformation exist.

Firstly, a model of the kinematic chain is formed, which consists of four members: a first support pillar-member, revolving platform - the second member, the stick - the third member, the rod-the fourth member. Members of the adopted kinematic chain adopted of a given robotic system build kinematic pairs of the fifth class - the revolving joints with one freedom degree. Joint axes are the axes of members relative rotation, which build kinematic chain pairs.

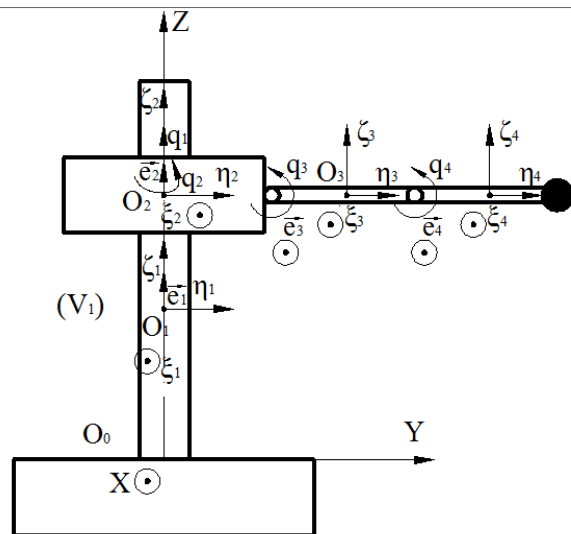


Figure 1. Robotic system model

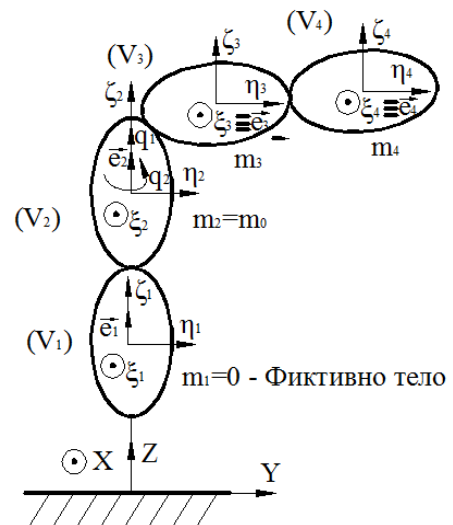


Figure 2. Open kinematic chain of adopted robotic system

As a first member a fictitious member body is introduced (a body whose mass is equal to zero), the second member is taking a translational movement and the third and fourth members are performing rotation. Local coordinate systems of a suitable orientation are dedicated to each member of a kinematic chain and their origins are settled in the mass centers of suitable members. The rotation angles around joint axes for each kinematic pair are also defined.

Rodrig transformation matrix equations are used for writing the equations for the angular velocity, angular acceleration, velocity and acceleration of the center of mass for each member of the kinematic chain. The governing equations are of the general type, that can be taken out for various combinations of movement of the members during their working process.

The whole procedure is done using a software package MatLab.

The robot structure includes spatially oriented multilink hinged-rod manipulator on a lift-and-turn platform that moves relative to a fixed post. A mathematical dynamic model of such a robot represented by a system of perfectly rigid bodies is constructed based on the formalism of Lagrange equations of the second kind.

It includes a system of interconnected nonlinear ordinary differential equations. Because the model takes the elastic properties of actuators into account, the order of

this system is twice as high as that in the model for a robot with rigid actuators. A robot with a two-link arm will be considered as an example.

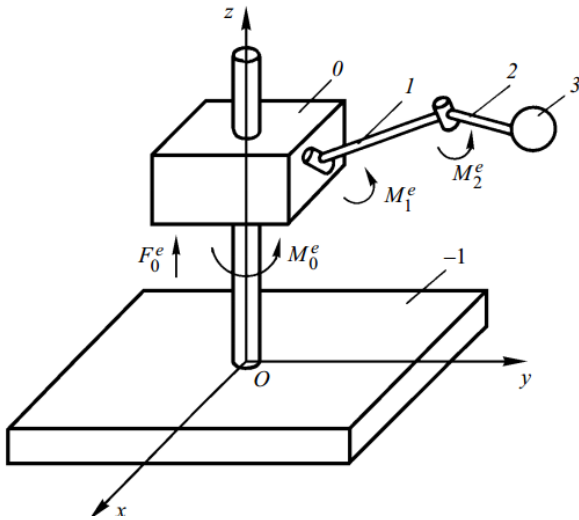


Figure 3. Industrial robot

2. FORMULATION OF CONTROL PROBLEM

Let us consider a pedestal-mounted industrial robot equipped with a hinged-rod arm (Fig. 1) to transport a finite-size weight to a prescribed location. The robot includes a vertical post on a fixed pedestal, a lift-and-turn platform moving along and rotating about the post, a multilink arm attached to the platform, and a weight rigidly attached to the last link of the arm. A mechanical model of this robot assumes all the above-mentioned bodies perfectly rigid and numbers them sequentially in the order they are connected (Fig. 1), the number -1 being assigned to the fixed pedestal. It is also assumed that the manipulator arm is a chain of  $N$  rectilinear rods connected to each other and to the platform by perfect cylindrical joints. Rectilinear motion is imparted to the platform by an actuating mechanism. It is mounted on the fixed pedestal and employs a tooth belt and a drum to transmit the rotary motion of the motor to the mobile platform. The actuators intended to rotate the platform and manipulator links are built directly into the joints of these units. Each of the above actuating mechanisms possesses elastic compliance and can control the corresponding unit, either in the angular acceleration of the motor shaft or in the shaft load moment generated by the motor. Let the actuator of rectilinear motion have the number -1 and each actuator of rotary motion have the number of the unit it drives. In order to construct a mathematical dynamic model of this mechanical system, let the platform be referred to a fixed coordinate system  $Oxyz$  with unit vectors  $\vec{i}, \vec{j}, \vec{k}$ , and the  $Oz$ -axis running along the post axis, as shown in Fig. 1. Let also each  $n$ th ( $n = \overline{0, N+1}$ ) mobile body be referred to a coordinate system  $C_n x_n y_n z_n$  with unit vectors  $\vec{i}_n, \vec{j}_n, \vec{k}_n$  the origin coinciding with the center of mass of the body, and the axes being the principal central axes of inertia. Further, we direct the coordinate axis  $C_n x_n$  along the axial line of the  $n$ th  $n = \overline{1, N}$  rod link of the manipulator and introduce an additional coordinate system  $O_n x_n y_n z_n$  with

the origin at the point  $O_n$  of the link and the axes parallel to those of the system  $C_n x_n y_n z_n$ . For the platform ( $n = 0$ ) and the body ( $n = N+1$ ) it carries, we orient the axes of the system  $C_n x_n y_n z_n$  so that the axes  $C_n x_n, C_n y_n$  and  $C_n z_n$  of all bodies in the mechanical system are parallel to the axes  $Ox, Oy,$  and  $Oz$  of the fixed coordinate system when the the robot kinematic chain is aligned in parallel to the  $Ox$ -axis.

Let the axis of each  $n$ th  $n = \overline{1, N}$  joint, which connects the ends of the  $(n - 1)$ th and  $n$ th bodies, with a unit vector  $\vec{e}_n$  coincide with one of the axes of the local coordinate system  $O_n x_n y_n z_n$  and, therefore, the equality  $\vec{e}_n = \vec{i}_n, \vec{e}_n = \vec{j}_n, \vec{e}_n = \vec{k}_n$  holds. With  $Z_0$  and  $\theta_0$  are denoted the coordinates of the platform's center of mass  $C_0$  in the fixed coordinate system  $Oxyz$  and the angle of rotation of the coordinate system  $C_0 x_0 y_0 z_0$  about the  $O_0 z_0$ -axis relative to the system  $Oxyz$  and by  $\varphi_n, \psi_n$  or  $\theta_n$  ( $n = \overline{1, N}$ ) are denoted the angles of rotation in the system  $C_0 x_0 y_0 z_0$  around one of the axes  $O_n x_n, O_n y_n,$  or  $O_n z_n$  relative to the system.  $O_{n-1} x_{n-1} y_{n-1} z_{n-1}$  (this angle is between the  $n$ th and  $(n - 1)$ th bodies of the mechanical system). Assume that the above angles of rotation are positive if rotations they describe go counterclockwise when viewed from the ends of the corresponding axes of rotation. Also assume that the platform is subjected in the joint  $C_0$  to an external force  $F_0^e$  and moment  $M_0^e$  ( $n = \overline{1, N}$ ) and the  $n$ th link is subjected in each  $n$ th ( $n = \overline{1, N}$ ) joint  $O_n$  to the external moment  $M_n^e$  transmitted from the corresponding actuator. The external force  $F_0^e$  is assumed positive if it tends to move the platform in the positive direction of the  $OZ$ -axis, and the external moment  $M_0^e$  ( $n = \overline{1, N}$ ) is positive if it tends to rotate the body in the positive direction.

Let us pose kinematic and dynamic control problems [10, 11]: carry out kinematic and dynamic control by specifying  $N + 2$  functions of angular accelerations  $\ddot{\alpha}_n = \ddot{\alpha}_n(t)$  ( $n = \overline{1, N}$ ) of the motor shafts and  $N + 2$  program laws of variation in the electromagnetic moments  $M_n = M_n(t)$  ( $n = \overline{1, N}$ ) developed by the motors. Assume that the time lag in the electric circuits of the motors can be neglected and that the electromagnetic moments are generated with a required accuracy. Hereafter, an overdot denotes a derivative with respect to time. The mechanical system with  $N + 2$  actuators that simulates the mechanical part of the robot has  $2(N + 2)$  degrees of freedom. For unique determination of its spatial configuration, we introduce a set of generalized coordinates  $q = q_n(t)$  ( $n = \overline{1, N}$ ) which are the coordinate of the center of mass of the 0th body and the angles of rotation of the  $n$ th ( $n = \overline{1, N}$ ) body about the  $(n - 1)$ th body, and  $q'_n = q'_n(t)$  ( $n = \overline{1, N}$ ) which are the angles



of rotation of the motor shafts. Then according to the notation adopted,  $q_{-1} = Z_0$  and  $q_0$  for the controlled bodies,  $q_n = \varphi_n$ ,  $q_n = \psi_n$  or  $q_n = Q_n$ , depending on the orientation of the  $n$ th ( $n = \overline{1, N}$ ) joint, and  $q'_{-1} = \alpha_{-1}$ ,  $q'_0 = \alpha_0$ ,  $q'_n = \alpha_n$  ( $n = \overline{1, N}$ ) for the actuator motors. To set up the equations of motion for the mechanical part of the robot, we take advantage of the Lagrange equations of the second kind:

$$\frac{d}{dt} \left( \frac{\partial L}{\partial \dot{q}_n} \right) - \frac{\partial L}{\partial q_n} = Q_n, \quad \frac{d}{dt} \left( \frac{\partial L}{\partial \dot{q}'_n} \right) - \frac{\partial L}{\partial q'_n} = Q'_n, \quad (n = \overline{-1, N}) \quad (1)$$

To evaluate the generalized forces  $Q_n$  ( $n = \overline{1, N}$ ) equal to the external actions  $F_0^e$  and  $M_n^e$  ( $n = \overline{0, N}$ ), let us reduce

the moments  $M_n$  ( $n = \overline{1, N}$ ) developed by the motors to the controlled bodies for each degree of freedom with allowance for the transmission ratios and design features of the transmission mechanisms. We will neglect lag effects in the transmission mechanisms and assume that the above-mentioned actions depend only on the elastic properties of reduction gears. Then

$$F_0^e = k_{-1} (q'_{-1} i_{-1}^{-1} - q_{-1} i_{-1}^{-1}) r_{-1}^{-1}, \quad M_n^e = k_n (q'_n i_n^{-1} - q_n i_n^{-1}) i_n^{-1} \quad (n = \overline{0, N}) \quad (2)$$

The generalized forces  $Q'_n$  are defined by

$$Q'_n = M_n \quad (n = \overline{-1, N}) \quad (3)$$

### 3. THE FORMING RODRIGO TRANSFORMATION MATRIX ANGULAR VELOCITY AND ANGULAR ACCELERATION OF ALL MEMBERS OF THE ROBOTIC SYSTEM

In the general case, the angel speed of  $i$ -th member of body  $V_i$  is:

$$\omega_i = \sum_{\alpha=1}^i \bar{\chi}_\alpha \dot{q}_\alpha \bar{e}_i = \sum_{\alpha=1}^i \bar{\Omega}_{\alpha(i)} \dot{q}_\alpha \quad (4)$$

where  $\bar{\Omega}_{\alpha(i)}$  is analogon of angular velocity of the generated coordinates and it is:

$$\bar{\Omega}_{\alpha(i)} = \begin{cases} \bar{\chi}_\alpha \bar{e}_\alpha, & \alpha \leq i \\ 0, & \alpha \geq i \end{cases} \dots \quad (5)$$

So, the angular speed in matrix form is:

$$\{\bar{\omega}_i^{(0)}\} = \sum_{\alpha=1}^i \bar{\chi}_\alpha [R_{0,\alpha}] \{\bar{e}_\alpha^\alpha\} \dot{q}_\alpha \dots \quad (6)$$

Whereby, the generated coordinates are the suitable angels:

$$\{q_1, q_2, q_3, q_4\} = \{\xi_1, \varphi_2, \varphi_3, \varphi_4\} \dots \quad (7)$$

The defined connections between members of kinematic chains are achieved across rotation joints, so joint type indicators take values:

$$\chi_1 = 1; \chi_2 = \chi_3 = \chi_4 = 0 \quad \text{и} \quad \bar{\chi}_1 = 0; \bar{\chi}_2 = \bar{\chi}_3 = \bar{\chi}_4 = 1. \quad (8)$$

Projections of adequate unit vectors  $\bar{e}_i^{(i)}$  on the axes of coordinate systems  $C_i \xi_i \eta_i \zeta_i$  are:

$$\begin{aligned} \bar{e}_1^{(1)} &= \begin{Bmatrix} 0 \\ 0 \\ 1 \end{Bmatrix} \\ \bar{e}_1^{(1)} &= \begin{Bmatrix} 1 \\ 0 \\ 0 \end{Bmatrix} \\ \bar{e}_1^{(1)} &= \begin{Bmatrix} 1 \\ 0 \\ 0 \end{Bmatrix} \\ \bar{e}_4^{(4)} &= \begin{Bmatrix} 1 \\ 0 \\ 0 \end{Bmatrix} \end{aligned} \quad (9)$$

Dual facilities  $[\tilde{e}_i^{(i)}]$  of adequate unit vectors  $\bar{e}_i^{(i)}$

are:

$$[\tilde{e}_1^{(1)}] = \begin{bmatrix} 0 & -e_{1\zeta_1}^{(1)} & e_{1\eta_1}^{(1)} \\ e_{1\zeta_1}^{(1)} & 0 & -e_{1\xi_1}^{(1)} \\ -e_{1\eta_1}^{(1)} & e_{1\xi_1}^{(1)} & 0 \end{bmatrix} \quad (10)$$

$$[\tilde{e}_1^{(1)}] = \begin{bmatrix} 0 & -1 & 0 \\ 1 & 0 & 0 \\ 0 & 0 & 0 \end{bmatrix}$$

$$[\tilde{e}_2^{(2)}] = \begin{bmatrix} 0 & -e_{2\zeta_2}^{(2)} & e_{2\eta_2}^{(2)} \\ e_{2\zeta_2}^{(2)} & 0 & -e_{2\xi_2}^{(2)} \\ -e_{2\eta_2}^{(2)} & e_{2\xi_2}^{(2)} & 0 \end{bmatrix} \quad (11)$$

$$[\tilde{e}_2^{(2)}] = \begin{bmatrix} 0 & -1 & 0 \\ 1 & 0 & 0 \\ 0 & 0 & 0 \end{bmatrix}$$

$$[\tilde{e}_3^{(3)}] = \begin{bmatrix} 0 & -e_{3\zeta_3}^{(3)} & e_{3\eta_3}^{(3)} \\ e_{3\zeta_3}^{(3)} & 0 & -e_{3\xi_3}^{(3)} \\ -e_{3\eta_3}^{(3)} & e_{3\xi_3}^{(3)} & 0 \end{bmatrix} \quad (12)$$

$$[\tilde{e}_3^{(3)}] = \begin{bmatrix} 0 & 0 & 0 \\ 0 & 0 & -1 \\ 0 & 1 & 0 \end{bmatrix}$$

$$[\tilde{e}_4^{(4)}] = \begin{bmatrix} 0 & -e_{4\zeta_4}^{(4)} & e_{4\eta_4}^{(4)} \\ e_{4\zeta_4}^{(4)} & 0 & -e_{4\xi_4}^{(4)} \\ -e_{4\eta_4}^{(4)} & e_{4\xi_4}^{(4)} & 0 \end{bmatrix} \quad (13)$$

$$[\tilde{e}_4^{(4)}] = \begin{bmatrix} 0 & 0 & 0 \\ 0 & 0 & -1 \\ 0 & 1 & 0 \end{bmatrix}$$

Rodrige transformation matrix is now:

$$[A_{r,i}] = [I] + \bar{\chi}_i \left[ (1 - \cos(q_i)) [\tilde{e}_i^{(i)}]^2 + [\tilde{e}_i^{(i)}] \cdot \sin(q_i) \right] \quad (14)$$

Differentiating relation  $(V_i)$  by time gives expression for the angular acceleration of the body,  $V_i$ , in

the form of:

$$\ddot{\bar{e}}_i = \frac{d\bar{\omega}_i}{dt} = \sum_{\alpha=1}^n \bar{\Omega}_{\alpha(i)} \ddot{q}_\alpha + \sum_{\alpha=1}^n \sum_{\beta=1}^n \bar{\Lambda}_{\alpha\beta(i)} \dot{q}_\alpha \dot{q}_\beta \quad (15)$$

where:

$$\begin{aligned} \bar{\Lambda}_{\alpha\beta(i)} &= \frac{\partial \bar{\Omega}_{\alpha(i)}}{\partial q_\beta} \\ \bar{\Lambda}_{\alpha\beta(i)} &= \begin{cases} \bar{\chi}_\beta \bar{e}_\beta \times \bar{\Omega}_{\alpha(i)} = \bar{\Omega}_{\alpha(i)} \times \bar{\chi}_\beta \bar{e}_\beta, \forall \beta \leq \alpha \\ \bar{0}, \quad \forall \beta > \alpha \text{ и } \forall \alpha > i \end{cases} \\ \bar{\Omega}_{\beta(\alpha)} &= \begin{cases} \bar{\chi}_\beta \bar{e}_\beta, \forall \beta \leq \alpha \\ \bar{0}, \quad \forall \beta > \alpha \end{cases} \end{aligned} \quad (16)$$

Using above mentioned relations, the equation for angular acceleration is:

$$\begin{aligned} \ddot{\bar{e}}_i &= \sum_{\alpha=1}^n \bar{\Omega}_{\alpha(i)} \ddot{q}_\alpha + \sum_{\alpha=1}^n \sum_{\beta=1}^n \bar{\Omega}_{\beta(\alpha)} \times \bar{\Omega}_{\alpha(i)} \dot{q}_\alpha \dot{q}_\beta \\ \ddot{\bar{e}}_i &= \sum_{\alpha=1}^i \bar{\chi}_\alpha \ddot{q}_\alpha \bar{e}_\alpha + \sum_{\alpha=1}^n \sum_{\beta=1}^n \bar{\chi}_\beta \bar{\chi}_\alpha \bar{e}_\beta \times \bar{e}_\alpha \dot{q}_\alpha \dot{q}_\beta \end{aligned} \quad (17)$$

The equation for body angular acceleration,  $V_i$ , in matrix form is:

$$\{\ddot{\bar{e}}_i^{(0)}\} = \sum_{\alpha=1}^i \bar{\chi}_\alpha [R_{0,\alpha}] \{\ddot{\bar{e}}_\alpha^{(a)}\} \dot{q}_\alpha + \sum_{\alpha=1}^i \sum_{\beta=1}^i \bar{\chi}_\beta \bar{\chi}_\alpha [R_{0,\beta}] [\bar{e}_\beta^{(b)}] [R_{\beta,\alpha}] \{\ddot{\bar{e}}_\alpha^{(a)}\} \dot{q}_\alpha \dot{q}_\beta \quad (18)$$

The mass center position vector  $c_i$  of a solid body in a relation to a fixed point is:

$$\overline{OC}_i = \bar{r}_{ci} = \sum_{k=1}^i (\bar{\rho}_k + \chi_k q_k \bar{e}_k) + \bar{\rho}_{ci} \quad (19)$$

Differentiating this relation per time, the expression for mass center velocity  $c_i$  of a solid body  $V_i$  is obtained:

$$\bar{V}_{Ci} = \frac{d\bar{r}_{ci}}{dt} \quad (20)$$

The mass center velocity of a solid body can be also defined through mass center position vector partial excerpt per generated coordinate:

$$\bar{V}_{Ci} = \sum_{\alpha=1}^i \frac{d\bar{r}_{ci}}{dq_\alpha} \dot{q}_\alpha = \sum_{\alpha=1}^i \bar{V}_{Ci,\alpha} \dot{q}_\alpha \quad (21)$$

Where by :

$$\bar{r}_{ci} = \bar{r}_{ci}(q_1, \dots, q_i) \text{ - Mass centers position vectors,}$$

$\bar{V}_{Ci,\alpha}$  - Velocity analogon for point  $c_i$  per generated coordinate  $q_\alpha$  .

Where by, for mass centers position vectors applies:

$$\begin{aligned} \frac{\partial \bar{\rho}_k}{\partial q_\alpha} &= \begin{cases} \chi_\alpha \bar{e}_\alpha q_k \times \bar{\rho}_k, \forall \alpha \leq k \\ \bar{0}; \forall \alpha > k \end{cases} \\ \frac{\partial \bar{e}_k}{\partial q_\alpha} &= \begin{cases} \bar{\chi}_\alpha \bar{e}_\alpha \times \bar{\rho}_k, \forall \alpha \leq k \\ \bar{0}; \forall \alpha > k \end{cases} \dots \dots (22) \\ \frac{\partial \bar{\rho}_{ci}}{\partial q_\alpha} &= \begin{cases} \chi_\alpha \bar{e}_\alpha \times \bar{\rho}_{ci}, \forall \alpha \leq k \\ \bar{0}; \forall \alpha > k \end{cases} \end{aligned}$$

Using this last expression, we got:

$$\begin{cases} \bar{V}_{ci,\alpha} = \bar{\chi}_\alpha \bar{e}_\alpha \times \left[ \sum_{k=1}^i (\bar{\rho}_k + \chi_k q_k \bar{e}_k) + \bar{\rho}_{ci} \right] + \chi_\alpha \bar{e}_\alpha; \quad \forall \alpha \leq i \\ \bar{V}_{ci,\alpha} = 0, \quad \forall \alpha > i \end{cases} \dots \dots (23)$$

Or in matrix form, the expression looks like:

$$\{\bar{V}_{ci}^{(0)}\} = \bar{\chi} [R_{0,\alpha}] \{\bar{e}_\alpha^{(a)}\} \left[ \sum_{k=1}^i [R_{s,k}] \{(\bar{\rho}_k^{(k)} + \chi_k q_k \bar{e}_k^{(k)})\} + [R_{s,\alpha}] \{\bar{\rho}_{ci}^{(a)}\} \right] + \chi_\alpha [R_{0,\alpha}] \{\bar{e}_\alpha^{(a)}\}, \quad \forall \alpha \leq i \quad (24)$$

Let we adopt that:

$$\overline{O_0 O_1} = l_1; \overline{O_1 O_2} = l_2; \overline{O_2 O_3} = l_3; \overline{O_3 O_4} = l_4 \quad (25)$$

So, this lengths in vector's form is:

$$\begin{aligned} \{\bar{\rho}_1^{(1)}\} &= \begin{Bmatrix} 0 \\ 0 \\ l_1 \end{Bmatrix} \\ \{\bar{\rho}_2^{(2)}\} &= \begin{Bmatrix} 0 \\ l_2 \\ 0 \end{Bmatrix} \\ \{\bar{\rho}_3^{(3)}\} &= \begin{Bmatrix} 0 \\ 0 \\ l_3 \end{Bmatrix} \\ \{\bar{\rho}_4^{(4)}\} &= \begin{Bmatrix} 0 \\ 0 \\ 0 \\ l_4 \end{Bmatrix} \end{aligned} \quad (26)$$

The mass centers position vectors in the ratio with the relative coordinate systems are:

$$\begin{aligned} \{\bar{\rho}_{c1}^{(1)}\} &= \begin{Bmatrix} 0 \\ 0 \\ l_{c1} \end{Bmatrix} \\ \{\bar{\rho}_{c2}^{(2)}\} &= \begin{Bmatrix} 0 \\ l_{c2} \\ 0 \end{Bmatrix} \\ \{\bar{\rho}_{c3}^{(3)}\} &= \begin{Bmatrix} 0 \\ 0 \\ l_{c3} \end{Bmatrix} \\ \{\bar{\rho}_{c4}^{(4)}\} &= \begin{Bmatrix} 0 \\ 0 \\ 0 \\ l_{c4} \end{Bmatrix} \end{aligned} \quad (27)$$

where:

$$\overline{O_0 C_1} = l_{c1}; \overline{O_1 C_2} = l_{c2}; \overline{O_2 C_3} = l_{c3}; \overline{O_3 C_4} = l_{c4} \dots \dots (29)$$

Differentiating per time the form for mass center velocity of a solid body of kinematic chain the form for mass center acceleration of solid body is received:

$$\begin{aligned} \bar{a}_{ci} &= \frac{d\bar{V}_{ci}}{dt} = \sum_{\alpha=1}^i \bar{V}_{ci,\alpha} \ddot{q}_\alpha + \sum_{\alpha=1}^i \frac{d\bar{V}_{ci,\alpha}}{dt} \dot{q}_\alpha; \text{ Where is: } \bar{V}_{ci,\alpha} = \bar{V}_{ci,\alpha}(q_1, \dots, q_i) \text{ so is: } \dots (30) \\ \frac{d\bar{V}_{ci,\alpha}}{dt} &= \sum_{\beta=1}^i \frac{d\bar{V}_{ci,\alpha}}{dq_\beta} \dot{q}_\beta = \sum_{\beta=1}^i \bar{\Gamma}_{ci,\alpha\beta} \dot{q}_\beta; \text{ where is: } \bar{\Gamma}_{ci,\alpha\beta} = \frac{\partial^2 \bar{r}_{ci}}{\partial q_\alpha \partial q_\beta} = \bar{\Gamma}_{ci,\beta\alpha} \end{aligned}$$

The expression is now:

$$\bar{a}_{ci} = \sum_{\alpha=1}^i \bar{V}_{ci,\alpha} \ddot{q}_\alpha + \sum_{\alpha=1}^i \sum_{\beta=1}^i \bar{\Gamma}_{ci,\alpha\beta} \dot{q}_\beta \dot{q}_\alpha \dots \dots (31)$$

For vector  $\bar{\Gamma}_{ci,\alpha\beta}$  now is applied:

$$\begin{aligned} \bar{\Gamma}_{ci,\alpha\beta} &= \bar{\chi}_\alpha \bar{e}_\alpha \times \bar{V}_{ci,\beta} = \bar{\chi}_\alpha \bar{e}_\alpha \times \frac{\partial}{\partial q_\beta} \left[ \sum_{k=1}^i (\bar{\rho}_k + \chi_k q_k \bar{e}_k + \bar{\rho}_{ci}) \right] = \bar{\chi}_\alpha \bar{e}_\alpha \times \frac{\partial \bar{r}_{ci}}{\partial q_\beta} = \bar{\chi}_\alpha \bar{e}_\alpha \times \bar{V}_{ci,\beta} \\ \left\{ \begin{aligned} \bar{\Gamma}_{ci,\alpha\beta} &= \bar{\chi}_\alpha \bar{e}_\alpha \times \bar{V}_{ci,\beta}, \forall \alpha \leq \beta \\ \bar{\Gamma}_{ci,\alpha\beta} &= \bar{\chi}_\beta \bar{e}_\beta \times \bar{V}_{ci,\alpha}, \forall \alpha > \beta \end{aligned} \right. \\ \text{so:} \\ \bar{\Gamma}_{ci,\alpha\beta} &= \bar{\chi}_\alpha \bar{e}_\alpha \times \bar{V}_{ci,\beta}; \text{ a} = \min(\alpha, \beta) \text{ и } \text{b} = \max(\alpha, \beta) \dots (33) \end{aligned}$$

In matrix form, the acceleration of mass center is:

$$\{\bar{a}_{ci}^{(0)}\} = \sum_{\alpha=1}^i \{\bar{V}_{ci,\alpha}^{(0)}\} \ddot{q}_\alpha + \sum_{\alpha=1}^i \sum_{\beta=1}^i \{\bar{\Gamma}_{ci,\alpha\beta}^{(0)}\} \dot{q}_\beta \dot{q}_\alpha; \quad \{\bar{\Gamma}_{ci,\alpha\beta}^{(0)}\} = \chi_\alpha [R_{0,\alpha}] [\bar{e}_\alpha^{(a)}] [R_{s,\beta}] \{\bar{V}_{ci,\beta}^{(b)}\} \quad (34)$$

4. SOFTWARE PACKAGE MATLAB APPLICATION FOR FORMING LAGRANGES EQUATIONS OF SECOND ORDER

The Lagranges equations of second order are formed in software package Matlab, using special part of Matlab dedicated for this kind of problems. The possibility to change initial data in this kind of defined mathematical model of robot's movement is the advantage.

The expressions for valocity and acceleration are obtained in next shape:

$$Vc1=(\chi_1 \cdot R01 \cdot e11 \cdot (R11 \cdot (\rho_1))) \cdot \phi_{1'} + R01 \cdot e1 \cdot \zeta_1'$$

$$\begin{pmatrix} 0 \\ 0 \\ \zeta_1' \end{pmatrix} \quad (35)$$

$$Vc2:=Vc21 \cdot \zeta_1' + Vc22 \cdot \phi_{2'} \quad (36)$$

$$\begin{pmatrix} 0 \\ 0 \\ \zeta_1' \end{pmatrix} \quad (37)$$

$$Vc4:=Vc41 \cdot \phi_{1'} + Vc42 \cdot \phi_{2'} + Vc43 \cdot \phi_{3'} + Vc44 \cdot \phi_{4'}$$

$$\begin{pmatrix} 0,5 \cdot \phi_3' \cdot \sin(\phi_2) \sin(\phi_3) - \phi_2' \cos(\phi_2) (0,5 \cdot \cos(\phi_3) + 0,7) \\ -\phi_2' \sin(\phi_2) (0,5 \cos(\phi_3) + 0,7) - 0,5 \cdot \phi_3' \cos(\phi_2) \sin(\phi_3) \\ \zeta_1' + 0,5 \phi_3' \cos(\phi_3) \end{pmatrix} \quad (38)$$

$$ac1:=Vc11 \cdot \zeta_1'' + Gc111 \cdot \phi_{1'} \cdot \phi_{1'}$$

$$\begin{pmatrix} 0 \\ 0 \\ \zeta_1'' \end{pmatrix} \quad (39)$$

$$\begin{pmatrix} 0 \\ 0 \\ \zeta_1'' \end{pmatrix} \quad (40)$$

$$ac2:=Vc21 \cdot \zeta_1'' + Vc22 \cdot \phi_{2'} + Gc211 \cdot \phi_{1'} \cdot \phi_{1'} + Gc212 \cdot \phi_{1'} \cdot \phi_{2'} + Gc221 \cdot \phi_{2'} \cdot \phi_{1'}$$

$$ac3:=Vc31 \cdot \phi_{1'} + Vc32 \cdot \phi_{2'} + Vc33 \cdot \phi_{3'} + Gc311 \cdot \phi_{1'} \cdot \phi_{1'} + Gc312 \cdot \phi_{1'} \cdot \phi_{2'} + Gc313 \cdot \phi_{1'} \cdot \phi_{3'} + Gc321 \cdot \phi_{2'} \cdot \phi_{1'} + Gc322 \cdot \phi_{2'} \cdot \phi_{2'} + Gc323 \cdot \phi_{2'} \cdot \phi_{3'}$$

$$\begin{pmatrix} \phi_2'^2 \sin(2 \phi_2) \sigma_1 + \phi_3'' \sin(\phi_2) \sin(\phi_3) 0,5 - \phi_2'' \cos(\phi_2) \sigma_1 + 0,5 \phi_2' \phi_3' \sin(\phi_3) (\cos(\phi_2) + 1) (\cos(\phi_2) + \cos(\phi_2) \cos(\phi_3) - 1) \\ \phi_2' \phi_3' \sin(\phi_2) \sin(\phi_3) (2,0 \cos(0,5 \phi_2)^2 \cos(0,5 \phi_3)^2 - 0,5) - \phi_2'' \sin(\phi_2) \sigma_1 - 1,0 \phi_2'^2 \cos(2 \phi_2) \sigma_1 - \phi_3'' \cos(\phi_2) \sin(\phi_3) 0,5 \\ 0,5 \cos(\phi_3) \phi_3'' \end{pmatrix} \quad (41)$$

$$ac4:=Vc41 \cdot \zeta_1'' + Vc42 \cdot \phi_{2'} + Vc43 \cdot \phi_{3'} + Vc44 \cdot \phi_{4'} + Gc411 \cdot \phi_{1'} \cdot \phi_{1'} + Gc412 \cdot \phi_{1'} \cdot \phi_{2'} + Gc413 \cdot \phi_{1'} \cdot \phi_{3'} + Gc414 \cdot \phi_{1'} \cdot \phi_{4'} + Gc421 \cdot \phi_{2'} \cdot \phi_{1'} + Gc422 \cdot \phi_{2'} \cdot \phi_{2'} + Gc423 \cdot \phi_{2'} \cdot \phi_{3'} + Gc424 \cdot \phi_{2'} \cdot \phi_{4'}$$

$$+ Gc431 \cdot \phi_{3'} \cdot \phi_{1'} + Gc432 \cdot \phi_{3'} \cdot \phi_{2'} + Gc433 \cdot \phi_{3'} \cdot \phi_{3'} + Gc434 \cdot \phi_{3'} \cdot \phi_{4'} + Gc441 \cdot \phi_{4'} \cdot \phi_{1'} + Gc442 \cdot \phi_{4'} \cdot \phi_{2'} + Gc443 \cdot \phi_{4'} \cdot \phi_{3'} + Gc444 \cdot \phi_{4'} \cdot \phi_{4'}$$

$$\begin{aligned} & \left[ \phi_3'^2 (\cos(\phi_3) \sin(\phi_2) (\sigma_8 + \cos(\phi_3)) - \cos(\phi_2) \sin(\phi_2) \sin(\phi_3) \sigma_7) - \phi_4'^2 \sin(\phi_2) \left( 0,45 \cos(\phi_2) - 0,9 \left( \frac{\cos(\phi_2)}{2} + \frac{1}{2} \right) \left( \frac{\cos(\phi_3)}{2} + \frac{1}{2} \right) \right) \right. \\ & \left. + \phi_4'' \sin(\phi_3 + \phi_4) \sin(\phi_2) 0,45 - \phi_2' \phi_3' \left( \sin(\phi_2)^2 (\sigma_9 + \sin(\phi_3)) - \cos(\phi_2) \sigma_5 \right) 2 + \phi_2' \phi_4' \sin(\phi_3 + \phi_4) \left( 0,45 \cos(\phi_3 + \phi_4) \cos(\phi_2)^2 + \right. \right. \\ & \left. \left. + 2 \phi_3' \phi_4' \sin(\phi_2) (0,9 \sigma_1 \sigma_2 - 0,9 \sigma_2 + 0,45) \right] \right. \\ & \left[ -\phi_3'^2 (\cos(\phi_2) \cos(\phi_3) (\sigma_8 + \cos(\phi_3)) - \cos(\phi_2)^2 \sin(\phi_3) \sigma_7) - \phi_4'^2 \left( 0,45 \cos(\phi_2)^2 (\sigma_1 - 1) + 0,45 \sigma_1 \cos(\phi_2) \right) + 2 \phi_2' \phi_3' (\sin(\phi_2) \right. \\ & \left. - \phi_2'^2 \cos(2 \phi_2) \sigma_6 - 0,45 \sin(\phi_3 + \phi_4) \cos(\phi_2) \phi_4'' - \sin(\phi_2) \phi_2'' \sigma_6 - \phi_3' \phi_4' (2 \sigma_4 - 1) \left( -0,45 \sigma_4 + 0,45 \sigma_1 + \cos\left(\phi_3 - \frac{\phi_2}{2} + \phi_4\right)^2 0,22 \right) \right. \\ & \left. + 2 \sin(\phi_3 + \phi_4) \phi_2' \phi_4' \sin(\phi_2) \left( 1,8 \sigma_2 \cos(0,5 \phi_3 + 0,5 \phi_4)^2 - 0,45 \right) \right] \quad (42) \end{aligned}$$

5. CONCLUSION

This paper presents the development of a model for anthropomorphic industrial robot, which can be

managed on the basis of knowledge of the equations for its peak motion. In this way, the process of forming the Lagrange's equations is simplified, so the robot control is easily and accurately.

According to high accuracy of this model, this method is suitable for the development, programming and testing simple and complex robot programs, which facilitates the process of programming, avoid unwanted bugs and damages on the very expensive industrial robots. In future, it is necessary to study the impact of robot load on positioning accuracy and movement valocity.

#### REFERENCES

- [1] P. D. Krut'ko, *Controlling Effector Systems of Robots* [in Russian], Nauka, Moscow (1991).
- [2] L. G. Loitsyanskii and A. I. Lur'e, *A Course of Theoretical Mechanics* [in Russian], Vol. 1, Nauka, Moscow (1982).
- [3] A. I. Lurie, *Analytical Mechanics* [in Russian], Fizmatgiz, Moscow (1961).
- [4] E. Nakano, *Introduction to Robotics* [Russian translation], Mir, Moscow (1988).
- [5] E. Hairer, S. P. Norsett, and G. Wanner, *Solving Ordinary Differential Equations 1. Nonstiff Problems*, 2nd ed., Springer-Verlag, New York (1993).
- [6] F. L. Chernous'ko, N. N. Bolotnik, and V. G. Gradetskii, *Robot Manipulator* [in Russian], Nauka, Moscow (1989).
- [7] W. Bernezen, B. Riege, and S. Hartmann, "Modelling and model fitting of flexible robots, a multibody system tool kit approach," *J. Intel. Rob. Syst.*, No. 5, 165-175 (1998).
- [8] M. S. DeQueiroz, S. Donepudi, T. Burg, and D. M. Dawson, "Model-based control of rigid-link flexible-joint robots: An experimental evaluation," *Robotica*, **16**, No. 1, 11-21 (1998).
- [9] V. B. Larin, "Attitude-determination problems for a rigid body," *Int. Appl. Mech.*, **37**, No. 7, 870-898 (2001).
- [10] L. G. Lobas, "The dynamics of finite-dimensional systems under nonconservative position forces," *Int. Appl. Mech.*, **37**, No. 1, 38-65 (2001).
- [11] N. P. Plakhtienko, "Onloads acting on a structure with a seismic damper," *Int. Appl. Mech.*, **37**, No. 3, 414-419 (2001).
- [12] M. Vukobratovic, V. Matijevic, and V. Potkonjak, "Control of robots with elastic joints interacting with dynamic environment," *J. Intel. Rob. Syst.*, **23**, No. 1, 87-100 (1998).

# Water Drain Emergency System

Nikola Terzić<sup>1</sup>, Dragan Pršić<sup>2\*</sup>

<sup>1</sup>Public Utility Company Waterworks and Sewerage, Kraljevo (Serbia)

<sup>2</sup> Faculty for Mechanical and Civil Engineering in Kraljevo, University of Kragujevac, Kraljevo (Serbia)

*Need for healthy drinkable water is growing from day to day, but available resources are limited. Accelerated development of information communication technologies opens the path for evolving upgrade of existing systems for production, distribution and consuming clear water on different levels. Internet of Things (IoT) technology is not suitable for real-time control and safety critical applications. Still, it makes possible that using public Internet networks we increase reliability of existing systems or develop application that are tolerant to time delay.*

*In this article we present a water drain emergency system which is using cheap network embedded system. On first level, it stops unwanted rise of water level in manholes of water network. On second level sends SMS alarm using GSM network. Data of alarm is keeping in database for further analyze.*

**Keywords: water level control, manhole, alarm service, Internet of Things, Arduino**

## 1. INTRODUCTION

Reserve of drinkable water in world and in our country are less by the day. It is expected that by 2025. year, about 2/3 of world's population feels serious missing of water. Water is becoming increasingly important strategic resource. Manufacturing and distributing sufficient amounts of water is becoming increasing technical challenge. Using modern information communication technologies in monitoring, management and maintenance may even a bit contribute in solving problems in this area.

Remarkable price drop for microprocessors and other electronic equipment opens possibility for wider application of network embedded systems (NESs) in different engineers disciplines and also in area of production and distribution of water. Different types of "smart" sensors and actuators are used more and more. They are containing microprocessor with additional processor power and network interfaces for remote communication. In addition to increased local possibilities (filtering, self-tuning, fault diagnostic, linearization, control) communication in real-time enables synchronization and optimal work on system level. Idea is to upgrade existing systems with not expensive NESs and with their synergy acquire new value. With that, system for distribution of water can easier implement in global system for providing services as distributing electric power, gas, heat, Internet, etc.

Embedded systems (ES) began to use during 70's years of past century. But for users, most visible presence of computers for general purpose are ES – which are having most wider use. For example, it is expected that Electricity Smart Grid Networks become 100 to 1000 times more ES than that is a case on whole Internet [1]. In the beginning, ES were watched only as small general-purpose computers with limited resources. Design of these systems are based to implementation some of optimization techniques. Recently, engineers realized that main

challenge in design this kind of systems arises in their interaction with physical processes and not from limited resources [2]. Interaction between ES and real world is changing continuously. It can be viewed from different levels. Depending of technology which is used in mutual communication, there are different names: Cyber-Physical System (CPSs), the Internet of Things (IoT), Industry 4.0, Machine-to-Machine (M2M), the Internet of Everything, etc.

It is often to in realization of one system, different technology are intertwined. For example, in production of pure water, we can use SCADA system for remote reading of consuming of water with use of IoT technology, GSM in maintenance, XML for exchanging of data, etc. Independent from technology which is used, NESs is backbone of networks. During the process of design NESs based system, it should be considered joint dynamics of physical processes, hardware, software and networks [2]. Happenings in real world have continuous character, while in virtual world changes are happening in discrete moments or they are event driven. With software for general purpose software it is important that time for execution of task be as shorter as possible, but it is not critical for functioning of system. With NESs based systems time could be crucial for acceptable functioning of system. "In the physical world, as opposed to the cyber world, the passage of time is inexorable" [2]. Besides, in real world many phenomena are happening parallel, with different speed. On the other hand, software processes in basic have sequential character [3]. Task is up to designer for using sequential semantics to solve parallel problems from the real world.

CPS technology is engaged in integration NESs system and physical processes on low-level layer. During designing question like software interrupts, memory architectures, assembly-level programming, device drivers are considered. They enables hard connections between two world and demand special access during design [2]. With IoT approach we are using Web technology for

\*Corresponding author: Dositejeva 19 Kraljevo, prsic.d@mfv.kg.ac.rs

communication. IoT is not suitable for real-time control and safety-critical applications, but it is simple and cheap for implementation. It is based on standard interfaces, open-source software and public communication networks. It is enabled for evolving development of system according to economical possibilities.

Many process in production and distributing of water are not time critical and tolerant to time delays. Those processes contains potential for further spread of IoT technology. In this paper, we will give example of water drain emergency system, who has a goal to prevent rise of water level in water manhole, above allowed value. With this kind of system, we are protecting equipment of damage and preventing unwanted water lost in network. It is used two levels of protection. On first level we have local feedback control loop which include submersible pumps for extracting water from manhole. On second level, if water level in manhole still rise, with public mobile network, SMS is sending to center for monitoring SMS. SMS server is writing arriving SMS to data base and send alarm to operator on duty. With help of saved data in database, we could execute additional reliable fault diagnosis and take various preventive measures.

## 2. SYSTEM DESCRIPTION

To secure sufficient water flow to all consumers/costumers, geographic distributive pumping stations are used in water network. Their assignment is to compensate energy losses which are show in some part of water pipelines. Pumps with measuring equipment and pumping equipment are placed into manholes which secure ambient conditions for their work. At a Figure 1, we have shown interior of manhole from water network of Kraljevo city.



Figure 1: Interior of one water network manhole from city of Kraljevo

Because of possibility of breaking pipes, entering outside atmospheric water or some other reason, there is possibility of rising water level above acceptable value. With this scenario, expensive equipment will be damaged (electric motors with invertors) and that will lead to

disruption in supply of water. In example of breaking pipe (Ø100) water will come to critical level in few minutes. Unfortunately, designer overlooked this possibility, so this system is needed to upgrade with system for protection of flood.

Water drain emergency (WDE) system which we are presenting in this paper uses NES with two levels of protection. Both levels of protection are based on Arduino microcontroller (Figure 2).



Figure 2: Single-board microcontroller Arduino

Arduino is a open program of several hardware and software companies surrounded around production of single-board microcontrollers and equipment for embedded system which are distributed as open source hardware and software (<https://www.arduino.cc/>). Products are licensed under GNU Lesser General Public License (LGPL) or GNU General Public License (GPL) which permitting the manufacture of Arduino boards and software distribution by anyone. Basic idea of project is building simple, low-cost development platform for embedded systems. First platform consisted of printed circuit board with ATmega168 microcontroller. We are using IDE (integrated development environment) for programming, based on Processing language project (<https://processing.org/>). Programs are written on one of C language dialects. Thanks to wealthy library of built-in functions, programming is simplified for users without a background in electronics and programming. Big popularity Arduino owe to different expansions boards (shields) which extends functionality of main board.

## 3. WDE - FIRST LEVEL

On first level for protection of flood we are using local feedback control loop with block diagram shown on Figure 3.

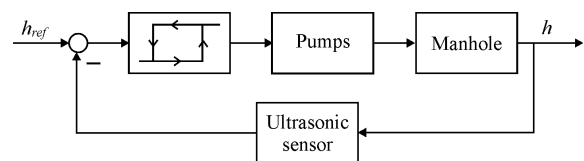


Figure 3: Local feedback control loop

For measuring water level in manhole, we are using ultrasonic module which is directly connected with Arduino board digital pins. Signal time chart for measuring is shown on Figure 4.

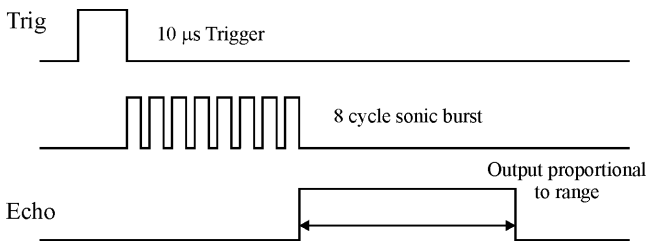


Figure 4: Ultrasonic sensor time chart

Arduino recipient is activated by setting on *High* digital port *Trig* in time span of  $10\mu s$ . After that, transmitter sends 8 pulses to obstacle by speed of sound, and returns to recipient. Echo port is going to state *High* by the time needed for ultrasound to go to obstacle and returns to sensor. Picture of ultrasonic module and mentioned pins are shown on Figure 5.



Figure 5: Ultrasonic sensor with pins

Example of program code for reading water level is shown on Figure 6.

```
// Sets the trigPort on HIGH state for 10 micro seconds
digitalWrite(trigPort, HIGH);
delayMicroseconds(10);
digitalWrite(trigPort, LOW);
// Reads the echoPort, returns the sound wave travel time in
//microseconds
T1 = pulseIn(echoPort, HIGH);
// Calculating the distance
WaterLevel= T1*0.034/2;
```

Figure 6: Reading water level by ultrasonic sensor

For turning on and off pumps, relay regulator is used with hysteresis, showed on Figure 7a. Size of hysteresis is adjusted by the noise gathered during measuring of water level. Software realization for Arduino is showed on Figure 7b.

Other than turning on drainage pump and turning off pump for supply when water level raise over acceptable value ( $WaterLevel > LevelHigh$ ) microcontroller sends SMS text message to Monitoring Centre. Goal is to turn attention of operator (dispatcher) to the point where he see thata system is gone into emergency regime. More on using SMS text messages will be in next section.

a) Characteristic
<pre>if (WaterLevel&gt;LevelHigh){     digitalWrite(relayPort, HIGH);     sms.beginSMS(remoteNumber);     sms.print("Alarm1 - Pump On");     sms.endSMS(); } else if (WaterLevel&lt;LevelLow){     digitalWrite(relayPort, LOW); }</pre>
b) Implementation by Arduino
Figure 7: Relay with hysteresis

Digital output of Arduino (*relayPort*) is connected to solid-state relays with normal open and normal closed contacts.

For securing independent work of microcontroller on longer time interval, we are using watchdog timer (WT). If it comes to failure of some kind in executing software, WT resets processor so microcontroller will continue with work (Figure 8).

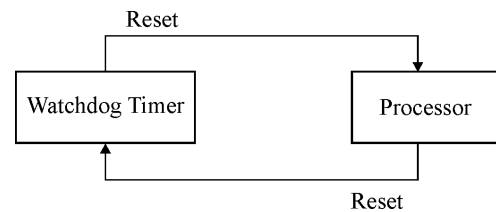


Figure 8: Watchdog mechanism

Essence is that processor must have periodical call to WT, so he will confirm work state. If after certain time WT don't have confirmation, WT assumes that software in processor is for some reason blocked, so WT restart processor. System starts startup procedure form the beginning. WT and processor are in same chip at Arduino microcontroller. Thanks to built-in library function WT can be implemented very easily. In Figure 9, it is shown procedure for processing WT mechanism by Arduino.

Inside of *setup()* function of main program, it is needed to make set up of WT. For example, it is needed to set time which WT counts down till reset of processor (*Treset*). By each parse through main loop, it is needed to answer to call of built-in function of WT – *wdt\_reset()*. If time between two calls of this function is greater than (*Treset*) it is assumed that there is mistake in process, so it restarts processor and calls bootloader again.

In main program we can write and procedure that can act upon WT interrupt. In previous example, function

*ISR(WDT\_vect)* can be used for sending alarm that will signal the creation of reset signal.

```

void setup() {
  //...
  watchdogSetup();
}
void loop() {
  //...
  wdt_reset();
  //...
}
ISR(WDT_vect) { // Watchdog timer interrupt.
  // Send alarm
}
    
```

Figure 9: Watchdog mechanism for Arduino

#### 4. WDE - SECOND LEVEL

On first layer of protection, we are trying to prevent raising level of unwanted water with local feedback control loop. However, if drainage pump don't have enough capacity or stops with work, amount of water will still raising. When water level goes over certain maximum permitted value, it will generate Alarm. Alarm signal on second level is formed by Arduino, with help of independent sensor of level ("red zone" alarm). Second level sensor is used to upgrade reliability of the system. Alarm is sent to center for monitoring (Figure 10).

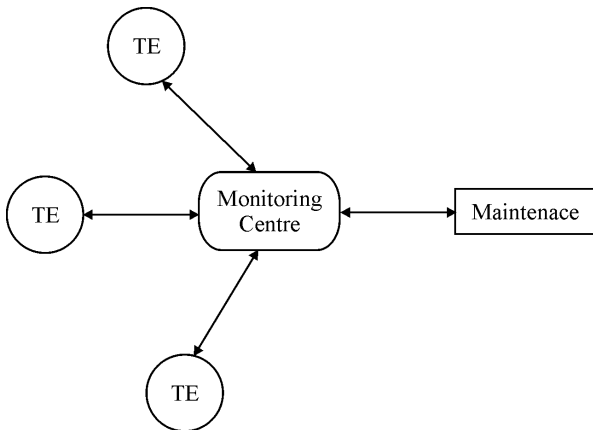


Figure 10: WDE Second level schematic View

As a terminal equipment (TE) we are using Arduino with GSM Shield (Figure 11). Arduino with GSM Shield (GSMS) is communicating over serial port using AT commands. From angle of Arduino, GSM shield is acting as modem, and from monitoring center angle is acting as mobile phone. GSMS enables to make phone calls, send and receive SMS messages and connect over Internet (over GPRS).

In this work, for communicating we are using SMS service with build-in GSM Library. Program code which sends SMS message about Alarms is shown on Figure 12 (<https://www.arduino.cc/>).



Figure 11: Arduino GSM Shield

```

// Include the GSM library
#include <GSM.h>

#define PinNum="..." // Number of SMS Server"
#define ServerNum="..." // Number of SMS Server"
void setup() {
  //...
  // Start GSM shield
  while (notConnected) {
    if (gsmAccess.begin(PinNum) == GSM_READY)
    {
      notConnected = false;
    } else {
      //...
    }
  }
}
void loop() {
  //...
  // send the message
  if (RedSensor) {
    sms.beginSMS(ServerNum);
    sms.print("Alarm 2 - Red Sensor On");
    sms.endSMS();
  }
  //...
}
    
```

Figure 12: Sending alarm SMS

After we import GSM library we insert PIN code of SIM card and number of SMS server. In *setup()* procedure Arduino makes connection with modem. In main loop, we constantly check state of *Red* sensor. If water level have raised to maximum value, it sends SMS text message to SMS server.

As before, SMS alarm could be send and by interrupt procedure of WT, which will be activated on the moment when signal comes from *Red* sensor.

As we could see from Figure 10, Monitoring Centre gets information's from terminal equipment located in different manholes. With that we can get reliable information of happening, because happenings from one manhole will reflect on other nearby. From internal database, by time table, SMS text sends to on call worker about need of his intervention on certain manhole.

All SMS messages are kept in database. In this case we are getting complete picture of happening in certain manholes in longer time period. With help of certain



software, we could make analysis and implement certain preventive measures.

In order to test system, we built experimental system (Figure13). Goal was to test functionality of system in laboratory condition before implement on real system.

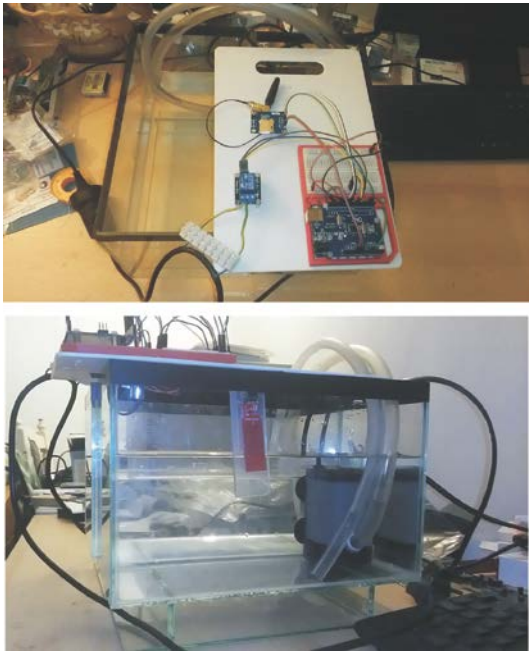


*Figure 13: Experimental test rig*

## 5. CONCLUSION

Reduced price of hardware and software open's door for wide application of NESs systems and certain Internet technologies on places where until now was unthinkable. Thanks to standard interfaces, it isn't obligatory large knowledge on software architecture. Even thou those technologies are still not in everyday use for strong real-time control and safety critical applications, there is still enough place to find their own spot. Managing production and distributing of water can reduce water loss, optimize spending, and enlarge energetic efficiency, synchronies production with changeable demands and so on. We used pretty low cost equipment and public (GSM) service to prevent damage that can be even larger. Application of this technology is at a beginning. There is still a large number of questions that must be solve , like reliability of this kind of systems.

## REFERENCES

- [1] S. Karnouskos, "Cyber-Physical Systems in the SmartGrid", IEEE Xplore Conference: Industrial Informatics (INDIN), 2011 9th IEEE International Conference on Industrial Informatics, Lisbon, Portugal, pp. 20-23, (2011)
- [2] E. A. Lee and S. A. Seshia, "Introduction to Embedded Systems - A Cyber-Physical Systems Approach", Second Edition, MIT Press, 2017.
- [3] E. A. Lee, "Cyber Physical Systems: Design Challenges", Technical Report No. UCB/EECS-2008-8, <http://www.eecs.berkeley.edu/Pubs/TechRpts/2008/EECS-2008-8.html>
- [4] <http://www.kth.se/en/sci/centra/railway>



**SESSION D**

**MACHINE DESIGN AND MECHANICS**



# Damping and Seismic Isolation Bearings Group, in Modular Design, for Bridges and Viaducts. Construction and Working Principle

Marian Dima <sup>1</sup>, Cătălin Frâncu <sup>1\*</sup>

<sup>1</sup> Faculty of Technological Equipment, Technical University of Civil Engineering, Bucharest (Romania)

*This paper presents the design and working principle and also the constructive solution for seismic isolation bearings group in modular design for bridges and viaducts.*

**Keywords:** Damping and seismic isolation bearings group, Bridges / viaducts, Seismic activity

## 1. INTRODUCTION

The isolation systems used for bridges are made up of isolation devices to improve the structure's response to seismic action. Typically, these devices are located between the superstructure and the bridges infrastructure on the top of the pile / abutments, in the usual placing positions and the usual bearing devices.

Improving structure behaviour consists in reducing internal forces (bending moments, shearing forces) on the cross-section of the infrastructure elements, reducing the displacements at the superstructure or at the top of the piles or in reducing both internal forces and displacements.

This favourable behaviour of the structure is obtained using the following dynamic tuning methods:

1. The increase of the fundamental period of the structure - which results in its removal from the motion amplification area, with large accelerations and the shift in an area of the response spectrum corresponding to lower acceleration values; as a consequence, the internal equilibrium forces on the sections of the piles and the abutments are reduced due to the reduction of the inertial forces induced in the structure, but also the displacements of the structure increase;
2. Increase in damping - which results in both the reduction of acceleration and displacements; this translates into a reduction of both the internal forces on the cross section of the piles / abutments and the reduction of the structural displacements.

The two methods can be combined to achieve the desired effect, both in terms of internal equilibrium forces on infrastructure elements, as well as structure displacements.

## 2. CONSTRUCTION AND WORKING PRINCIPLE

Damping and seismic isolation bearings group, in modular design, for bridges and viaducts carries out the functions of bearings used currently:

1. Takes over superstructure reactions as a result of external / internal actions that load the structure and at the same time allows displacements by the directions of the desired degrees of freedom in accordance with the displacement requirements for which they were designed;
2. Ensures the dissipation of part of the energy induced in the structure by the seismic motion; This can be done by using hysteretic isolation devices, viscous and dry friction isolators;
3. Ensures, by way of behaviour, the return of the structure close to the undeformed initial position in order to ensure the transmission of the vertical reactions from the superstructure to the infrastructure as in the absence of seismic action;
4. Ensures that the superstructure moves in relation to the infrastructure for the current actions in operation without reaching their limit of deformability, or without inducing significant internal equilibrium forces in the pile / abutment;
5. Ensure, through the constructive elements with which they are provided, the avoidance of the fall of the bridge superstructure from the pile / abutment during a seismic event

And additionally has the following features:

1. dampens all six components of motion of the bridge superstructure produced by seismic action (three translations and three rotations);
2. performs optimal dampening;
3. allows the return to the position of the superstructure after the seismic action ceases.

Damping and seismic isolation bearings group is composed of:

1. an HDRB or LRB elastomeric isolator;
2. FPS friction isolator or spherical bearing;
3. a system consisting of six hydraulic shock absorbers, arranged in a geometric configuration according to the kinematic diagram of the Stewart platforms;
4. Linking elements.

All components of the damping and seismic isolation bearings group are individual components in current manufacturing of experienced and field-proven companies with individually defined characteristics, commonly used and verified for the dynamic insulation of viaducts and bridges.

The damping and seismic isolation bearings group can be designed in two variants, each variant representing a systemic product from a conceptual, constructive and functional point of view. The functional schemes of the group for the two variants are shown in Figures 1 and 2. In the first embodiment of the damping and seismic isolation bearings group, the spherical bearing / friction isolator (1) is assembled in parallel with the hydraulic damping system arranged in Stewart configuration (3), and this subassembly is mounted in series with the HDRB / LRB elastomeric isolator (2). Further, this combination of devices will be referred to as the "series group".

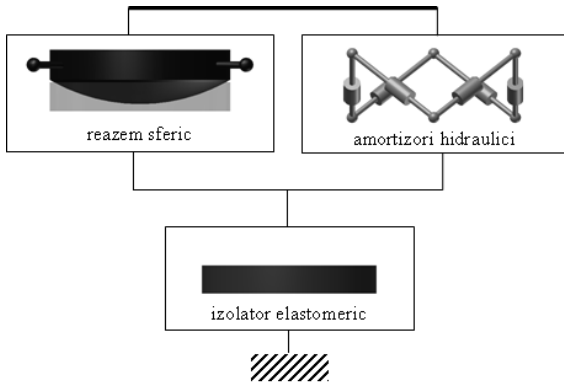


Figure 1. Series group

In the second embodiment, the spherical bearing / friction isolator (1) is assembled in series with the HDRB / LRB (2) elastomeric isolator, forming a subassembly which in turn is mounted in parallel with the hydraulic shock absorber system in Stewart configuration (3). This combination of devices will be referred to as the "parallel group".

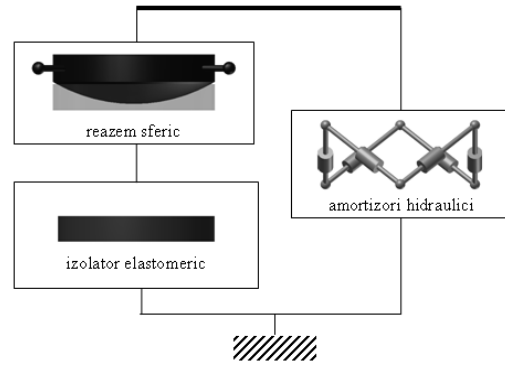


Figure 2. Parallel group

Based on the above-described functional schemes, the constructive solutions in Figure 3 are shown.

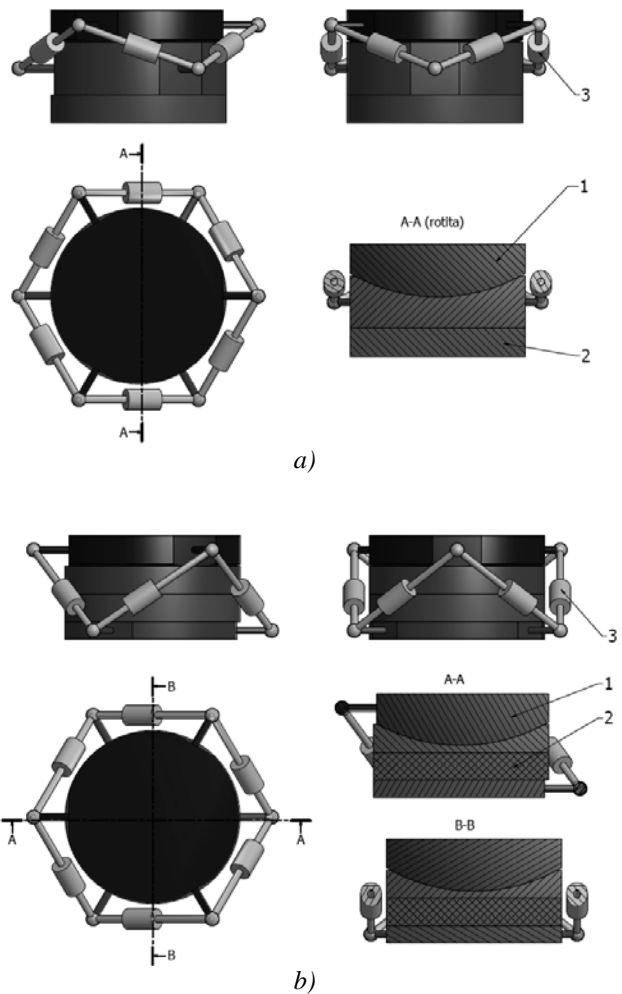


Figure 3. Constructive solutions of damping and seismic isolation bearings group; a) series group, b) parallel group

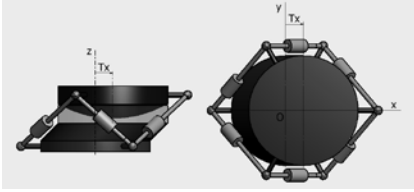
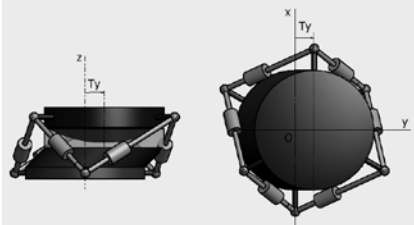
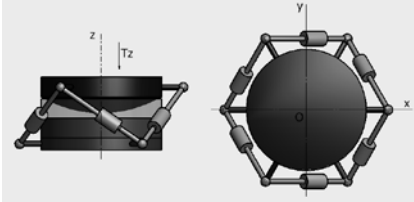
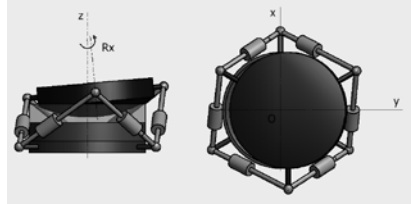
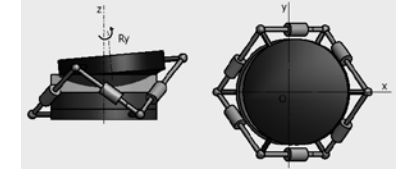
For the damping of the six components of the bridge superstructure, produced by the seismic action, the three elements that are part of the damping and seismic isolation bearings group participate differently. This mode is illustrated in Table 1 for a "parallel" group. Analysing this table shows that for each component of the absolute motion of the bridge superstructure, the group exhibits

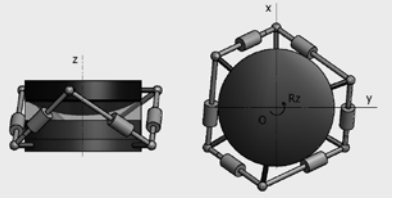
specific deformations that lead to relative motions of the group elements. It is found that:

1. the elastomeric isolator has a single relative translational movement relative to the reference system axes corresponding to the component of the absolute translation of the bridge superstructure;
2. the dry friction spherical bearing performs only one relative rotation relative to the axis of the reference system corresponding to the component of the absolute rotation of the bridge superstructure;
3. each of the six hydraulic dampers, in the Stewart configuration, have relative displacements for all six components of the absolute motion.

As a result, the elastomeric isolator participates in the damping of translational motions, the ball bearing participates in the damping of rotation motions, and the Stewart Hydraulic dampers system participates in the damping of all six components of the motion. It should be noted that for the elastomeric isolator and spherical bearing, the orientation of the axes in the horizontal plane relative to the longitudinal axis of the bridge does not influence the individual damping, but for the six Stewart hydraulic damper system, this orientation influences its own elongations and consequently its own damping.

Table 1. Analyse of a "parallel" group

	Absolute motion	Deformed state of the damping and seismic isolation bearings group	Relative motion of components / damping type		
			Spherical bearing	Elastomeric isolator	Hydraulic dampers
1	Translation Ox		$\varphi_x = ct$	$d_x = var$	$dl_{1...6} = var$
			$\varphi_y = ct$	$d_y = ct$	
			$\varphi_z = ct$	$d_z = ct$	viscous damping
2	Translation Oy		$\varphi_x = ct$	$d_x = ct$	$dl_{1...6} = var$
			$\varphi_y = ct$	$d_y = var$	
			$\varphi_z = ct$	$d_z = ct$	viscous damping
3	Translation Oz		$\varphi_x = ct$	$d_x = ct$	$dl_{1...6} = var$
			$\varphi_y = ct$	$d_y = ct$	
			$\varphi_z = ct$	$d_z = var$	viscous damping
4	Rotation Ox		$\varphi_x = var$	$d_x = ct$	$dl_{1...6} = var$
			$\varphi_y = ct$	$d_y = ct$	
			$\varphi_z = ct$	$d_z = ct$	viscous damping
5	Rotation Oy		$\varphi_x = ct$	$d_x = ct$	$dl_{1...6} = var$
			$\varphi_y = var$	$d_y = ct$	
			$\varphi_z = ct$	$d_z = ct$	viscous damping

6	Rotation Oz		$\varphi_x = ct$ $\varphi_y = ct$ $\varphi_z = var$	$d_x = ct$ $d_y = ct$ $d_z = ct$	$dl_{1...6} = var$
			dry friction damping	---	viscous damping

The optimal damping for the damping and seismic isolation bearings group will be achieved by combining the three types of devices in its composition by combining the three types of damping specific to each device, as well as by weighting the damping of each device in the total damping of the group. This weighting can be done in two ways: by choosing the appropriate type of device within the category to which it belongs (e.g. HDRB or LRB, with or without lead core for the elastomeric isolator, FPS or spherical bearing for the dry friction device), and also by appropriately choosing the characteristic parameters that affect damping for each device, i.e. equivalent viscous damping, dynamic friction coefficient and damping constant *c*.

3. CONSTRUCTIVE SOLUTION

The group, Figure 4, is made of a superior connection plate (1.1) to the bridge / viaduct superstructure, onto which the convex spherical bearing (1.3) of the dry friction sliding device is mounted, which is in permanent mechanical contact with the concave spherical bearing (2.1), on which the anti-seismic elastomeric isolator (4) is mounted, which is mechanically attached to the bottom plate for connection to the on the top of the pile / abutments of the bridge / viaduct (3.3). In parallel with the elastomeric isolator (4) and the spherical bearing (1.3, 2.1) between the upper plate (1.1) and the

lower plate (3.3), the hydraulic shock absorbers *Ah*<sub>1</sub>, *Ah*<sub>2</sub>, ..... *Ah*<sub>6</sub>, are connected by spherical joints *A*<sub>3</sub>, *B*<sub>3</sub>, *C*<sub>3</sub>, *D*<sub>3</sub>, *E*<sub>3</sub>, *F*<sub>3</sub> at the lower plate and spherical joints *A*<sub>1</sub>, *B*<sub>1</sub>, *C*<sub>1</sub>, *D*<sub>1</sub>, *E*<sub>1</sub>, *F*<sub>1</sub> at the upper plate. The six hydraulic shock absorbers *Ah*<sub>1</sub>, *Ah*<sub>2</sub>, ..... *Ah*<sub>6</sub> are mounted in the configuration of the Stewart platform.

Any relative displacement between the two plates(1.1, 3.3) produced by the seismic motion considered by its components in relation to a Cartesian reference system has the following effects: the relative translational components of the relative motion cause elastic displacement in the elastomeric isolator (4), between the surfaces (2.3, 3.1), predominantly in the horizontal plane and insignificant by the vertical axis, the rotation components of the relative motion between the plates produce rotation in the spherical bearing (1.3, 2.1) and at the same time all six components of the relative motion between the plates cause relative axial displacements in the six hydraulic dampers *Ah*<sub>1</sub>, *Ah*<sub>2</sub>, ..... *Ah*<sub>6</sub>.

The elastic bearing and lateral elastic displacement functions are provided by the elastomeric isolator (4), the progressive lateral displacement and the dry friction dissipation functions are performed by the convex spherical bearing (1.3) and the concave spherical half-shell (2.1). Viscous fluid dissipation is provided by the hydraulic shock absorbers *Ah*<sub>1</sub>, *Ah*<sub>2</sub>, ..... *Ah*<sub>6</sub>.

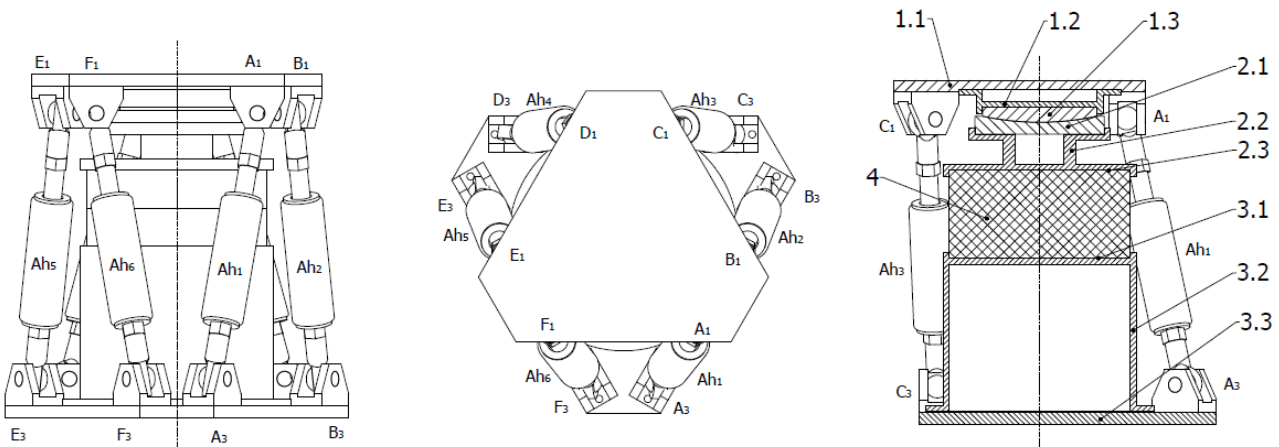


Figure 4. First embodiment of the damping and seismic isolation bearings group



A further embodiment is shown in Figure 5. In this embodiment, the spherical joints of the hydraulic shock absorbers are equidistantly arranged which results in a tilting of the hydraulic shock absorbers only in the axial plane which simplifies the constructive solution by the fact that the angular displacement in the damper joints is less

for the same relative displacement of the upper plate relative to the lower plate. Also in Figure 5 it is observed that the spherical bearing used in the bridges is replaced by two concentric spherical joints, one axial and the other radial which is specific to vehicles.

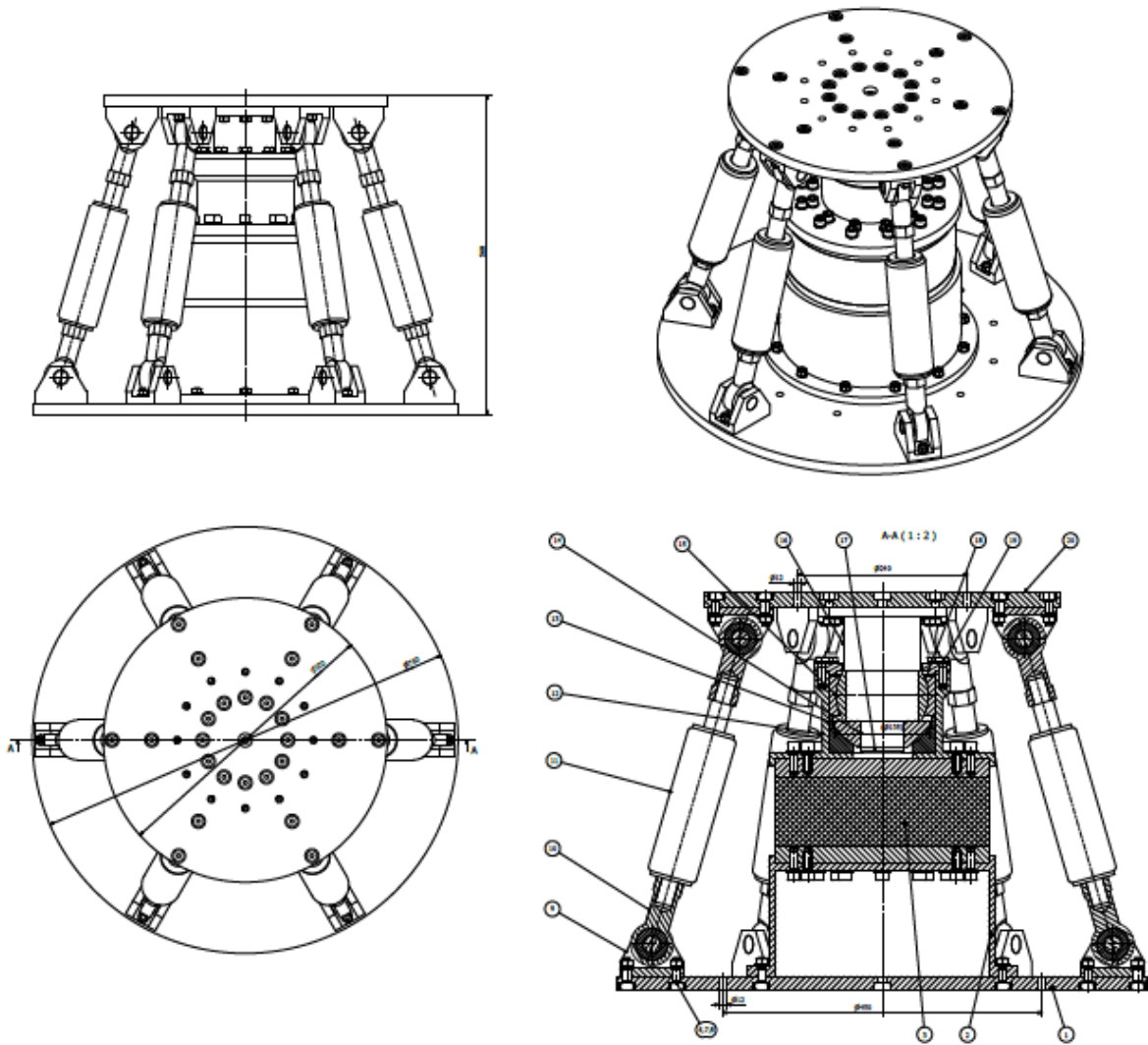


Figure 5. Second embodiment of the damping and seismic isolation bearings group

REFERENCES

[1] Dima M., Frâncu C, ș.a. - Damping and Seismic Isolation Bearings Group, in Modular Design, for Bridges and Viaducts. Contract PNII- Partnerships nr. 235/2014.  
 [2] Bratu P., Dima M. – Damping and Seismic Isolation Bearings Group, in Modular Design, for Bridges and Viaducts. Patent nr. 130978A0, BOPI nr. 3/2016.

[3] Brochures ALGA  
 [4] Brochures SOMMA.  
 [5] Brochures MAGEBA  
 [6] Brochures SKF.  
 [7] Brochures ACE.



# Dynamics of the Rotating Cantilever Beam

Aleksandar Nikolić<sup>1\*</sup>, Slaviša Šalinić<sup>1</sup>

<sup>1</sup>Faculty of Mechanical and Civil Engineering

University of Kragujevac, 36000 Kraljevo, Dositejeva 19 (Serbia)

*This paper presents the dynamic analysis of a rotating cantilever beam with a tip mass by using the rigid segment method. The elastic beam is discretized into the number of rigid segments which are interconnected by elastic joint elements with three degrees of freedom. The dynamic analysis is performed by using absolute coordinates in the frame of Euler-Bernoulli beam theory. The critical angular velocity at which instability of the proposed solution occurs is determined.*

**Keywords:** Rotating cantilever beam, rigid segment method, critical angular velocity

## 1. INTRODUCTION

Until now, the dynamic behavior of the flexible rotating beams has been investigated by many researches. The motive for this research lie in the fact that many engineering objects should be modelled as a rotating cantilever beam. Some of them are light robot arms, helicopter rotor blades, turbine blades, satellite linkages, etc. Modern industry has a need for machines of high-speed, increased accuracy and with the lowest possible weight. So, the rotational elements are lightweight and highly flexible. To ensure the accuracy of the motion of such elements, it is necessary to have an efficient control algorithm. Therefore, it is important to form a model of the flexible rotating beam that is simple and sufficiently accurate. The literature that deals with this problem is plenty (e.g. see [1-5]).

In this paper the rigid segment method will be used for the dynamic analysis of the flexible rotating cantilever beam with a tip mass. The basics about using this method in the free vibration analysis of the beams with variable axial parameters are described in [6] and [7] in detail. Here, this method will be adopted for the using in the analysis of the rotating flexible cantilever beam.

## 2. THE RIGID SEGMENT MODEL

Consider a hub beam system, shown in Fig 1. The hub is rigid and has the radius  $\overline{OA} = r$ . The flexible beam of a length  $L$  is rigidly connected to the hub at the point A. The beam material has the Young's modulus  $E$  and the mass density  $\rho$ . Also, the beam cross section area is  $A$ , and the beam cross section moment of inertia is  $I_z$ . A tip mass  $m_T$  is fixed at the free end B of the beam. Let's introduce the two coordinate systems that are necessary for the rotation analysis of the system considered. The first one is the inertial fixed coordinate system  $Oxyz$ , and the second one is the reference frame  $O\xi\eta\zeta$  whose axis  $\xi$  coincides with the direction of the undeformed beam. The angle  $\theta$  defines the rotation of the reference coordinate system  $O\xi\eta\zeta$  relative to the inertial coordinate system  $Oxyz$ .

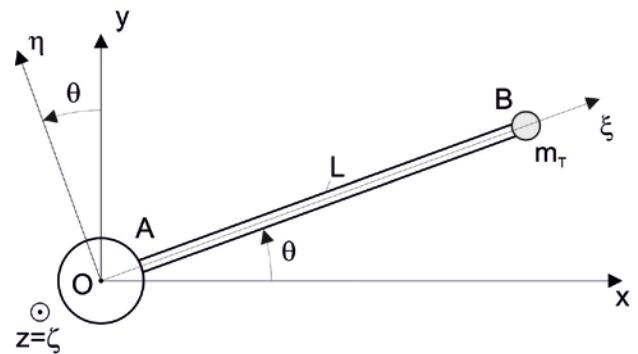


Figure 1: The rotating cantilever beam with a tip mass

Based on [5,6] the beam discretization is performed through two steps. At the first step, the beam is divided into  $n$  elastic segments which has the length  $L/n$  (see Fig 2(a)). After that, at the second step, all of the introduced elastic segments are replaced with two rigid segments of the length  $L/(2n)$  which are mutually connected by the elastic joint elements  $JE_i$  ( $i=1, \dots, n$ ) (see Fig 2(c)). The joint element  $JE_i$  allows three degrees of freedom, that are two relative translations in the axial and transverse direction,  $p_i$  and  $q_i$ , respectively, and one relative rotation  $r_i$  around the axis that is perpendicular to the motion plane. As mentioned above, the joint element  $JE_i$  is elastic, so the cylindrical and spiral springs are placed in the direction of the axial and rotational relative displacements, respectively (see Fig 2(d)). Based on [6], the stiffnesses of the introduced springs are:

$$c_{p_i} = n \frac{AE}{L}, \quad c_{q_i} = 12n^3 \frac{EI_z}{L^3}, \quad c_{r_i} = n \frac{EI_z}{L^3}. \quad (1)$$

Finally, the rigid segment model of the rotating flexible cantilever beam with the tip mass is formed as a system of  $n+1$  rigid segments which are mutually connected by  $n$  elastic joint elements  $JE_i$  (see Fig 2(b)).

For the purpose of further analysis, let's define the physical parameters of the introduced rigid segments. The length, mass and rotational inertia of the rigid segments should be defined as:

$$l_i = \begin{cases} R + L / (2n), & i = 0, \\ L / n, & 0 < i < n, \\ L / (2n), & i = n, \end{cases} \quad (2)$$

$$m_i = \begin{cases} m_h + \rho AL / (2n), & i = 0, \\ \rho AL / n, & 0 < i < n, \\ \rho AL / (2n) + m_T, & i = n, \end{cases} \quad (3)$$

$$J_{C_i \zeta} = \begin{cases} J_h + m_h \overline{O_0 C_0}^2 + \frac{1}{12} \rho A \left( \frac{L}{2n} \right)^3 & i = 0, \\ + \rho A \frac{L}{2n} \left( \overline{O_0 C_0} - \frac{L}{4n} \right)^2, & \\ \frac{1}{12} m_i l_i^2, & 0 < i < n, \\ \frac{1}{12} \rho A l_n^3 + \rho A l_n \left( \overline{O_n C_n} - \frac{L}{4n} \right)^2 & i = n, \\ + m_T \left( \frac{L}{2n} - \overline{O_n C_n} \right)^2, & \end{cases} \quad (4)$$

respectively, where

$$\overline{O_i C_i} = \begin{cases} \frac{\rho AL (R + L / (4n))}{2n \cdot m_h + \rho AL}, & i = 0, \\ l_i / 2, & 0 < i < n, \\ \frac{L (\rho AL + 4n \cdot m_T)}{4n (\rho AL + 2n \cdot m_T)}, & i = n, \end{cases} \quad (5)$$

is the distance of the mass center from the left side of the rigid segment ( $V_i$ ).

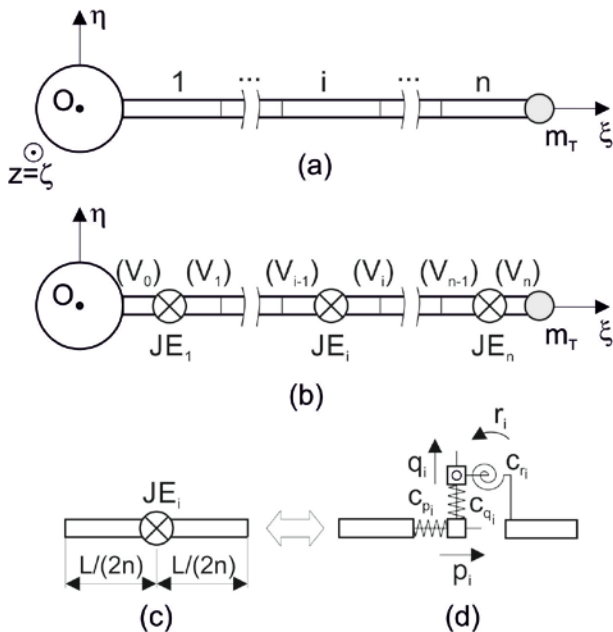


Figure 2: Discretization of the elastic beam into rigid segments and elastic joint elements

### 3. DIFFERENTIAL EQUATIONS OF MOTION

During the rotation, the flexible beam deforms. Therefore, the position of the rigid segment ( $V_i$ ) relative to the coordinate system  $O\xi\eta\zeta$  should be defined with axial and transversal coordinates of the rigid segment mass center,  $\xi_i$  and  $\eta_i$ , respectively, and with rotation angle  $\varphi_i$  of the rigid segment relative to the undeformed state of the beam.

The axial coordinate  $\xi_i$  can be defined as:

$$\xi_i = \xi_i(0) + \tilde{\xi}_i, \quad (6)$$

where

$$\xi_i(0) = \begin{cases} \overline{O_0 C_0}, & i = 0, \\ \sum_{k=0}^{i-1} l_k + \overline{O_i C_i}, & i > 0, \end{cases} \quad (7)$$

is the value of the axial coordinate in the undeformed state of the beam, and  $\tilde{\xi}_i$  represents the value of the axial deformation relative to the undeformed state of the beam. In the undeformed state, the values of the transversal coordinate  $\eta_i$  and rotation angle  $\varphi_i$  has zero values (see Fig 3).

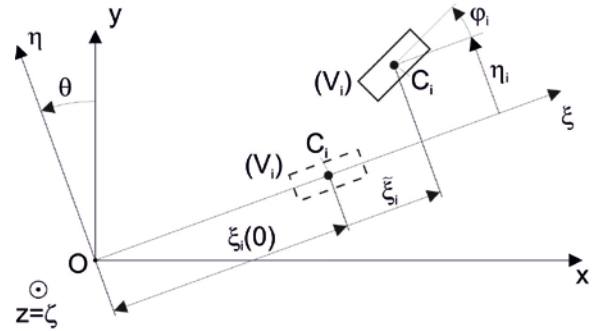


Figure 3: The motion of the rigid segment ( $V_i$ ) during rotation

The kinetic energy of the rigid segment model reads:

$$T = \frac{1}{2} \sum_{i=0}^n \left( m_i v_i^2 + J_{C_i \zeta} \omega_i^2 \right), \quad (8)$$

where  $v_i$  and  $\omega_i$  are the velocity of the mass center and the angular velocity of the rigid segment ( $V_i$ ), respectively. By using the above defined coordinates, the velocity  $v_i$  reads:

$$v_i^2 = \dot{x}_i^2 + \dot{y}_i^2, \quad (9)$$

where  $x_i$  and  $y_i$  are the coordinates of the mass center of the rigid segments ( $V_i$ ) relative to the inertial coordinate system  $Oxyz$  are given as:

$$x_i = \xi_i \cos \theta - \eta_i \sin \theta, \quad (10)$$

$$y_i = \xi_i \sin \theta + \eta_i \cos \theta. \quad (11)$$

Taking into account the expression (6), the time derivatives of the previously defined coordinates read:

$$\dot{x}_i = \dot{\xi}_i \cos \theta - \left( \xi_i(0) + \tilde{\xi}_i \right) \dot{\theta} \sin \theta - \dot{\eta}_i \sin \theta - \eta_i \dot{\theta} \cos \theta, \quad (12)$$

$$\dot{y}_i = \dot{\xi}_i \sin \theta + \left( \xi_i(0) + \tilde{\xi}_i \right) \dot{\theta} \cos \theta + \dot{\eta}_i \cos \theta - \eta_i \dot{\theta} \sin \theta. \quad (13)$$

Now, by using the expressions (6), (9), (12), and (13), the velocity of the rigid segment ( $V_i$ ) mass center takes the following form:

$$v_i^2 = \dot{\xi}_i^2 + \dot{\eta}_i^2 + 2\left(\left(\xi_i(0) + \tilde{\xi}_i\right)\dot{\eta}_i - \eta_i\dot{\xi}_i\right)\dot{\theta} + \left(\left(\xi_i(0) + \tilde{\xi}_i\right)^2 + \eta_i^2\right)\dot{\theta}^2, \quad (14)$$

The angular velocity of the rigid segment ( $V_i$ ) is given as:

$$\omega_i = \dot{\theta} + \dot{\varphi}_i. \quad (15)$$

By inserting the expressions (14) and (15) into the expression (8), the kinetic energy of the rigid segment model becomes:

$$T = \frac{1}{2} \sum_{i=0}^n \left( m_i \left( \dot{\xi}_i^2 + \dot{\eta}_i^2 + 2\left(\left(\xi_i(0) + \tilde{\xi}_i\right)\dot{\eta}_i - \eta_i\dot{\xi}_i\right)\dot{\theta} + \left(\left(\xi_i(0) + \tilde{\xi}_i\right)^2 + \eta_i^2\right)\dot{\theta}^2 \right) + J_{C_i\zeta} \left( \dot{\theta} + \dot{\varphi}_i \right)^2 \right), \quad (16)$$

The potential energy of the rigid segment model reads:

$$\Pi = \frac{1}{2} \sum_{i=1}^n \left( c_{p_i} p_i^2 + c_{q_i} q_i^2 + c_{r_i} r_i^2 \right), \quad (17)$$

where  $p_i$ ,  $q_i$ , and  $r_i$  represent the relative displacements in the elastic joint element  $JE_i$  (see Fig 2(d)).

By using the small deformation assumption, the relative displacements  $p_i$ ,  $q_i$ , and  $r_i$  should be obtained by using the rigid segments coordinates in the reference coordinate system  $O\xi\eta\zeta$  as:

$$p_i = -\tilde{\xi}_{i-1} + \tilde{\xi}_i, \quad (18)$$

$$q_i = -\eta_{i-1} + \eta_i - \frac{l_{i-1}}{2} \varphi_{i-1} - \frac{l_i}{2} \varphi_i, \quad (19)$$

$$r_i = -\varphi_{i-1} + \varphi_i. \quad (20)$$

Inserting the expressions (18)-(20) into the expression (17), the potential energy of the rigid segment model takes the following form:

$$\Pi = \frac{1}{2} \sum_{i=1}^n \left( c_{p_i} \left( -\tilde{\xi}_{i-1} + \tilde{\xi}_i \right)^2 + c_{q_i} \left( -\eta_{i-1} + \eta_i - \frac{l_{i-1}}{2} \varphi_{i-1} - \frac{l_i}{2} \varphi_i \right)^2 + c_{r_i} \left( -\varphi_{i-1} + \varphi_i \right)^2 \right). \quad (21)$$

Now, the differential equations of motion of the considered rigid segment model may be obtained by using the Lagrange equations of the second kind [8]:

$$\frac{d}{dt} \frac{\partial T}{\partial \dot{\xi}_i} - \frac{\partial T}{\partial \xi_i} = -\frac{\partial \Pi}{\partial \xi_i} + Q_{\tilde{\xi}_i}, \quad (22)$$

$$\frac{d}{dt} \frac{\partial T}{\partial \dot{\eta}_i} - \frac{\partial T}{\partial \eta_i} = -\frac{\partial \Pi}{\partial \eta_i} + Q_{\eta_i}, \quad (23)$$

$$\frac{d}{dt} \frac{\partial T}{\partial \dot{\varphi}_i} - \frac{\partial T}{\partial \varphi_i} = -\frac{\partial \Pi}{\partial \varphi_i} + Q_{\varphi_i}, \quad (24)$$

where  $i=1, \dots, n$ , and  $Q_{\tilde{\xi}_i} = Q_{\eta_i} = Q_{\varphi_i} = 0$ .

By using the expressions for the kinetic and potential energies, (16) and (17), the differential equations of motion (22)-(24) become:

$$m_i \ddot{\xi}_i - 2m_i \dot{\theta} \dot{\eta}_i - c_{p_i} \tilde{\xi}_{i-1} + \left( c_{p_i} + c_{p_{i+1}} - m_i \dot{\theta}^2 \right) \tilde{\xi}_i - c_{p_{i+1}} \tilde{\xi}_{i+1} = m_i \xi_i(0) \dot{\theta}^2 + m_i \eta_i \ddot{\theta}, \quad (25)$$

$$m_i \ddot{\eta}_i - 2m_i \dot{\theta} \dot{\xi}_i - c_{q_i} \eta_{i-1} - \frac{l_{i-1}}{2} c_{q_i} \varphi_{i-1} + \left( c_{q_i} + c_{q_{i+1}} - m_i \dot{\theta}^2 \right) \eta_i - \frac{l_i}{2} \left( c_{q_i} - c_{q_{i+1}} \right) \varphi_i - c_{q_{i+1}} \eta_{i+1} + \frac{l_{i+1}}{2} c_{q_{i+1}} \varphi_{i+1} = -m_i \left( \xi_i(0) + \tilde{\xi}_i \right) \ddot{\theta}, \quad (26)$$

$$J_{C_i\zeta} \ddot{\varphi}_i + \frac{l_i}{2} c_{q_i} \eta_{i-1} + \left( -c_{r_i} + \frac{l_i l_{i-1}}{4} c_{q_i} \right) \varphi_{i-1} + \frac{l_i}{2} \left( -c_{q_i} + c_{q_{i+1}} \right) \eta_i + \left( c_{r_i} + c_{r_{i+1}} + \frac{l_i^2}{4} \left( c_{q_i} + c_{q_{i+1}} \right) \right) \varphi_i - \frac{l_i}{2} c_{q_{i+1}} \eta_{i+1} + \left( \frac{l_i l_{i+1}}{4} c_{q_{i+1}} - c_{r_{i+1}} \right) \varphi_{i+1} = -J_{C_i\zeta} \ddot{\theta}, \quad (27)$$

where  $i=1, \dots, n$ ,  $\tilde{\xi}_0 = \tilde{\xi}_{n+1} = 0$ ,  $\eta_0 = \eta_{n+1} = 0$ , and  $\varphi_0 = \varphi_{n+1} = 0$ .

After summing, the above defined differential equations of motion (25)-(27) should be written in a matrix form as:

$$\mathbf{M}_v \ddot{\mathbf{v}} + \left( \mathbf{K} - \dot{\theta}^2 \mathbf{M}_m \right) \mathbf{v} - 2\mathbf{M}_{mv} \dot{\theta} = \mathbf{M}_{\theta v} \ddot{\theta} + \mathbf{M}_{m\zeta} \dot{\theta}^2, \quad (28)$$

where

$$\mathbf{v} = \left[ \tilde{\xi}_1, \eta_1, \varphi_1, \dots, \tilde{\xi}_i, \eta_i, \varphi_i, \dots, \tilde{\xi}_n, \eta_n, \varphi_n \right]^T, \quad (29)$$

$$\mathbf{M}_v = \text{diag} \left( \mathbf{M}_{v_1}, \dots, \mathbf{M}_{v_i}, \dots, \mathbf{M}_{v_n} \right) \in R^{3n \times 3n}, \quad (30)$$

$$\mathbf{M}_{v_i} = \text{diag} \left( m_i, m_i, J_{C_i\zeta} \right) \in R^{3 \times 3}, \quad (31)$$

$$\mathbf{K} = \begin{bmatrix} \mathbf{K}_{22}^{(1)} + \mathbf{K}_{11}^{(2)} & \mathbf{K}_{12}^{(2)} & \mathbf{0} & \mathbf{0} \\ \mathbf{K}_{21}^{(2)} & \mathbf{K}_{22}^{(2)} + \mathbf{K}_{11}^{(3)} & \mathbf{K}_{12}^{(3)} & \mathbf{0} \\ \mathbf{0} & \vdots & \ddots & \vdots \\ \vdots & \mathbf{0} & \mathbf{K}_{21}^{(i-1)} & \mathbf{K}_{22}^{(i-1)} + \mathbf{K}_{11}^{(i)} \\ \vdots & \vdots & \mathbf{0} & \vdots \\ \vdots & \vdots & \vdots & \mathbf{0} \\ \mathbf{0} & \mathbf{0} & \mathbf{0} & \mathbf{0} \\ \vdots & \vdots & \vdots & \vdots \\ \mathbf{0} & \vdots & \vdots & \vdots \\ \mathbf{K}_{12}^{(i)} & \mathbf{0} & \vdots & \vdots \\ \vdots & \vdots & \mathbf{0} & \vdots \\ \mathbf{K}_{21}^{(n-1)} & \mathbf{K}_{22}^{(n-1)} + \mathbf{K}_{11}^{(n)} & \mathbf{K}_{12}^{(n)} & \vdots \\ \mathbf{0} & \mathbf{K}_{21}^{(n)} & \mathbf{K}_{22}^{(n)} & \vdots \end{bmatrix} \in R^{3n \times 3n}, \quad (32)$$

$$\mathbf{K}_{11}^{(i)} = \begin{bmatrix} c_{p_i} & 0 & 0 \\ 0 & c_{q_i} & \frac{l_{i-1}}{2} c_{q_i} \\ 0 & \frac{l_{i-1}}{2} c_{q_i} & c_{r_i} + \frac{l_{i-1}^2}{4} c_{q_i} \end{bmatrix}, \quad (33)$$

$$\mathbf{K}_{12}^{(i)} = \begin{bmatrix} -c_{p_i} & 0 & 0 \\ 0 & -c_{q_i} & \frac{l_i}{2} c_{q_i} \\ 0 & -\frac{l_{i-1}}{2} c_{q_i} & \frac{l_{i-1} l_i}{4} c_{q_i} - c_{r_i} \end{bmatrix}, \quad (34)$$

$$\mathbf{K}_{12}^{(i)} = \left( \mathbf{K}_{21}^{(i)} \right)^T, \quad (35)$$

$$\mathbf{K}_{22}^{(i)} = \begin{bmatrix} c_{p_i} & 0 & 0 \\ 0 & c_{q_i} & -\frac{l_i}{2} c_{q_i} \\ 0 & -\frac{l_i}{2} c_{q_i} & \frac{l_i^2}{4} c_{q_i} + c_{r_i} \end{bmatrix}, \quad (36)$$

$$\mathbf{M}_m = \text{diag} \left( \mathbf{M}_{m_1}, \dots, \mathbf{M}_{m_i}, \dots, \mathbf{M}_{m_n} \right) \in R^{3n \times 3n}, \quad (37)$$

$$\mathbf{M}_{m_i} = \text{diag} \left( m_i, m_i, 0 \right), \quad (38)$$

$$\mathbf{M}_{mv} = \text{diag} \left( \mathbf{M}_{mv_1}, \dots, \mathbf{M}_{mv_i}, \dots, \mathbf{M}_{mv_n} \right) \in R^{3n \times 3n}, \quad (39)$$

$$\mathbf{M}_{mv_i} = \begin{bmatrix} 0 & m_i & 0 \\ m_i & 0 & 0 \\ 0 & 0 & 0 \end{bmatrix}, \quad (40)$$

$$\mathbf{M}_{\theta v} = \left[ \mathbf{M}_{\theta v_1}, \dots, \mathbf{M}_{\theta v_i}, \dots, \mathbf{M}_{\theta v_n} \right]^T \in R^{3n \times 1}, \quad (41)$$

$$\mathbf{M}_{\theta v_i} = \left[ m_i \eta_i, -m_i \left( \xi_i(0) + \tilde{\xi}_i \right), -J_{C_i \zeta} \right]^T, \quad (42)$$

$$\mathbf{M}_{m \xi} = \left[ \mathbf{M}_{m \xi_1}, \dots, \mathbf{M}_{m \xi_i}, \dots, \mathbf{M}_{m \xi_n} \right]^T \in R^{3n \times 1}, \quad (43)$$

$$\mathbf{M}_{m \xi_i} = \left[ m_i \xi_i(0), 0, 0 \right]^T. \quad (44)$$

#### 4. NUMERICAL SIMULATIONS AND RESULTS

The physical parameters of the beam which will be used here are follows:

- Length  $L=8$  [m],
- Mass density  $\rho=2.7667 \cdot 10^3$  [kg/m<sup>3</sup>],
- Cross-section area  $A=7.2968 \cdot 10^{-5}$  [m<sup>2</sup>],
- Young's modulus  $E=6.8952 \cdot 10^{10}$  [N/m<sup>2</sup>],
- Cross-section moment of inertia  $I_z=8.2189 \cdot 10^{-10}$  [m<sup>4</sup>],
- Hub moment of inertia  $J_h=200$  [kg·m<sup>2</sup>],
- Hub radius  $r=0.5$  [m],
- Tip mass  $m_T=(0.1-0.5)$  [kg].

It is also assumed that the angular velocity of the considered hub beam system is defined as a time function of the form:

$$\dot{\theta} = \begin{cases} \frac{w_f}{t_f} t - \frac{w_f}{2\pi} \sin\left(\frac{2\pi}{t_f} t\right), & 0 \leq t \leq t_f, \\ w_f, & t > t_f, \end{cases} \quad (45)$$

where  $w_f$  represents the stationary angular velocity of the hub beam system that will be achieved after time period  $t_f$ .

The Runge-Kutta method of the fourth order is used for the numerical integration of the differential equations of motion (28). Also, the elastic beam is discretized into 20 elastic segments, that is  $n=20$ .

Figure 4 shows the response of the beam tip along the transverse and the axial direction during the rotation. It is assumed that there is no tip mass, eg  $m_T=0$ ,  $t_f=15$  [s], and that the steady state angular velocity  $w_f$  has the values 1, 2 and 4 [rad/s]. In the case  $w_f=2$  [rad/s] our results for the transversal displacements shown in Fig 4(a) are the same as those ones from [4] obtained by the using zero order model (linear model).

It is obvious that by increasing  $w_f$  from 1 [rad/s] to 2 [rad/s], the maximum deflection in the both transverse and axial beam direction increases, too. For the  $w_f=4$  [rad/s], the results obtained by using the presented approach are divergent. The identically divergent result is obtained in [4] when the zero order model was used.

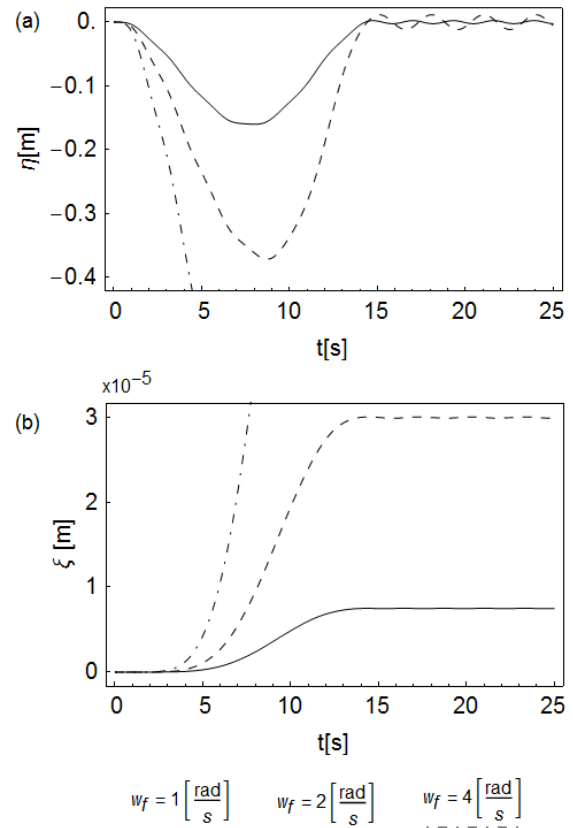


Figure 4: The beam tip response under the rotation:

(a) transversal direction, (b) axial direction.

The reason for the divergence of the results can be found by analyzing the differential equations of motion (28). Namely, the generalized stiffness matrix is defined by the matrix  $\mathbf{K} - \dot{\theta}^2 \mathbf{M}_m$ . As the angular velocity of the

hub-beam system  $\dot{\theta}$  increases, the same elements of the generalized stiffness matrix decrease. When the angular velocity  $\dot{\theta}$  reached some critical value, the generalized stiffness matrix is singular, and the solutions become divergent. So, the critical value of the angular velocity at which the presented rigid segment method failed to describe the dynamics of the rotating cantilever beam should be obtained by solving the following equation:

$$|\mathbf{K} - \dot{\theta}_{cr}^2 \mathbf{M}_m| = 0. \quad (33)$$

As the matrix  $\mathbf{M}_m$  depends on the masses of rigid segments (see (37) and (38)), the value of the critical angular velocity  $\dot{\theta}_{cr}$  decreases with the increasing of the tip mass  $m_T$ . The above statement is proved in Table 1. In the case when  $m_T=0$ , the critical angular velocity is  $\dot{\theta}_{cr} = 2.91[\text{rad/s}]$ . But, for  $m_T=1$  [kg], the value of the critical angular velocity significantly decreases to  $\dot{\theta}_{cr} = 1.55[\text{rad/s}]$ . Better insight into this dependance should be obtained by analyzing Figure 5.

Table 1: The values of the critical angular velocity corresponding to the different tip mass values

$m_T$ [kg]	0	0.1	0.3	0.5	0.7	0.9	1
$\dot{\theta}_{cr}$ [rad/s]	2.91	2.61	2.20	1.94	1.75	1.61	1.55

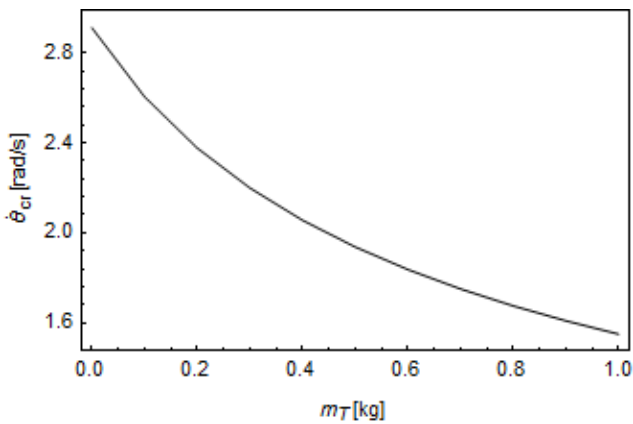


Figure 5: The impact of the tip mass to the critical angular velocity

Now, by analyzing the Table 1, we can determine the critical angular velocity at which divergence of the results occurs. Figure 6 shows the response of the beam tip in the transverse and axial direction during the rotation for  $m_T = 0.1$  [kg] and  $t_f = 30$  [s]. The value of the critical angular velocity for the given parameters is  $\dot{\theta}_{cr} = 2.61[\text{rad/s}]$ . When the steady state angular velocity is less than critical value  $w_f = 2$  [rad/s], the obtained results are correct. However, when the steady state angular velocity exceeds the critical value, eg when  $w_f = 2.7$  [rad/s], the obtained results become divergent. The situation is similar when the tip mass increases to  $m_T = 0.5$  [kg]. In this case, the critical angular velocity decreases to  $\dot{\theta}_{cr} = 1.94[\text{rad/s}]$  (see Table 1).

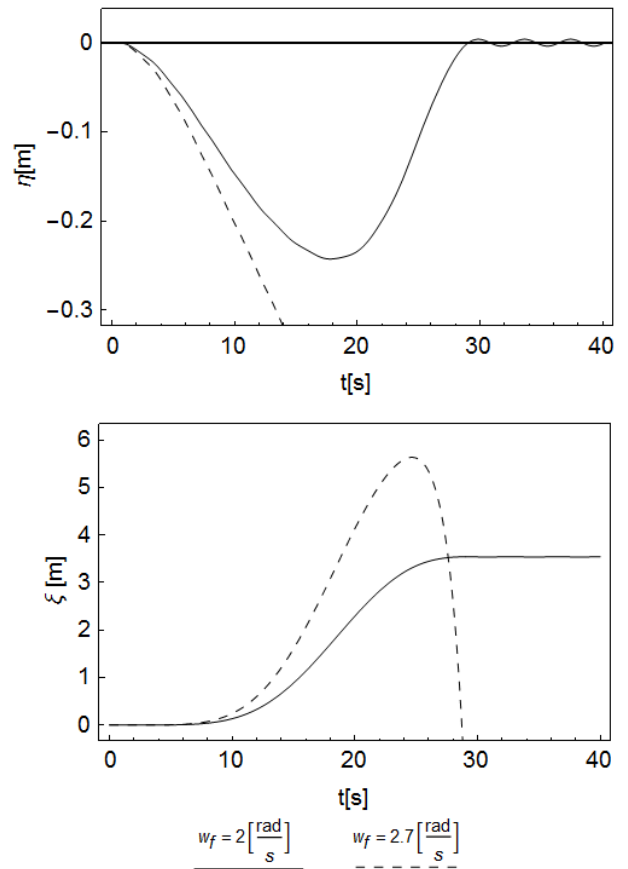


Figure 6: The beam tip response under the rotation at  $m_T = 0.1$  [kg]

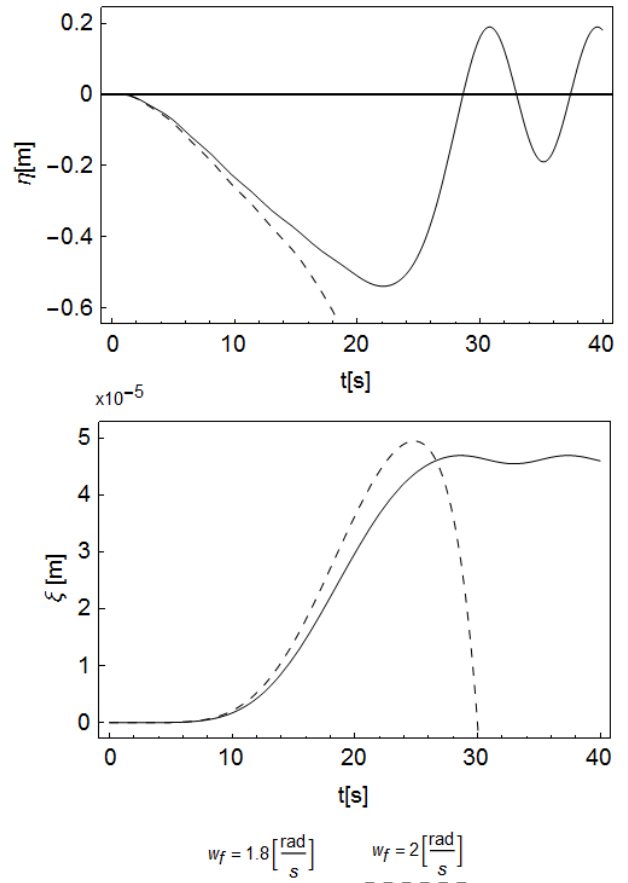


Figure 7: The beam tip response under the rotation at  $m_T = 0.5$  [kg]

When the steady state angular velocity is less than critical,  $w_f=1.8$  [rad/s], the obtained results are correct. As in the previous case, when the steady state angular velocity exceeds the critical value,  $w_f=2$  [rad/s], the results become divergent.

It is important to note that in both described cases (for  $m_T=0.1$  [kg] and for  $m_T=0.5$  [kg] ) the obtained results for the transversal displacement  $\eta(t)$  agrees very well with the results given in [1] obtained by using the traditional linear approximated model (TLAM). The values of the axial tip displacement  $\xi(t)$  are not presented in [1].

## 5. CONCLUSION

In this paper the dynamic analysis of the flexible rotating cantilever beam by using the rigid segment method has been performed. The rigid segment model considers the bending as well as the axial deformation of the beam during rotation. The obtained differential equations of motion in a matrix form (28) allow the efficient dynamic analysis of the considered rotating beam. Because the small deformation assumption has been used the considered method is linear.

As observed in [5], the use of the linear model leads to the conditionally stable results. Namely, if the angular velocity of the hub reaches the critical value of the angular velocity, the generalized stiffness matrix becomes singular and the results are divergent. So, before the proposed rigid segment method being used, it is necessary to determine the value of the critical angular velocity by using the expression (33). The precision of the presented method is demonstrated by numerical examples in which the good agreement with the results from [1] and [4] has been achieved.

In the further research, the presented method can be improved by taking into account the large deformation of the considered beam during the rotation. As a result of this assumption, the generalized stiffness matrix would be non-linear. It is expected that by using the above assumption the critical angular velocity of the rotating beam will be increased.

## ACKNOWLEDGEMENTS

This research was supported under grants no. ON174016 and no. TR35006 by the Ministry of Education, Science and Technological Development of the Republic of Serbia. This support is gratefully acknowledged.

## REFERENCES

- S. Bai, P. Ben-Tzvi, Q. Zhou, and X. Huang, "Dynamic modeling of a rotating beam having a tip mass", *Robotic and Sensors Environments- International Workshop (IEEE), ROSE*, October 2008 ,pp. 52-57, (2008)
- [1] Y. Wang, and R. L. Huston, "A lumped parameter method in the nonlinear analysis of flexible multibody systems", *Comput. Struct.*, Vol. 50(3), pp 421-432, (1994)
- [2] D.J. Zhang, R. L. Huston, "On dynamic stiffening of flexible bodies having high angular velocity", *Journal of Structural Mechanics*, Vol. 24(3), pp 313-329, (1996)
- [3] C. Li, X. Meng, and Z. Liu, "Dynamic modeling and simulation for the rigid flexible coupling system with a non-tip payload in non-inertial coordinate system", *J. Vib. Control*, Vol. 22(4), pp.1076-1094, (2016)
- [4] D. Garcia-Vallejo, H. Sugiyama, A. A. Shabana, "Finite element analysis of the geometric stiffening effect. Part 1: a correction in the floating frame of reference formulation", *P I Mech Eng K-J Mul*, Vol. 219(2), pp. 187-202, (2005)
- [5] A. Nikolić, S. Šalinić, "A rigid multibody method for free vibration analysis of beams with variable axial parameters", *J. Vib. Control*, Vol. 23(1), pp. 131 – 146, (2017)
- [6] A. Nikolić, "Free vibration analysis of a non-uniform axially functionally graded cantilever beam with a tip body", *Arch. Appl. Mech.*, doi:10.1007/s00419-017-1243-z, (2017)
- [7] A. I. Lurie, "Analytical Mechanics", Springer-Verlag, New York, 2002.



# Experimental Investigation of Tribological Behavior of Journal Bearing Coated by Babbitt Alloys Tegotenax V840

Amir Alsammarraie<sup>1\*</sup>, Dragan Milčić<sup>2</sup>, Milan Banić<sup>2</sup>, Goran Radenković<sup>2</sup>, Miodrag Milčić<sup>2</sup>

<sup>1</sup>Mechanical engineering faculty/ Department of Mechanics, University of Tikrit, Tikrit, Iraq

<sup>2</sup>Faculty of Mechanical Engineering, University of Niš, Serbia

*The present paper investigates the effect of sliding speed and normal load on temperature, coefficient of friction, roughness and wear property of tin base alloys- TEGOTENAX V840 coating experimentally. Special test rig was designed and fabricated. Experiments were performed under normal load 3000-4000 N, speed 2000 -3000 rpm and lubricant condition. Results show that the friction coefficient of sliding bearing slightly increase with the increase of sliding speed and significantly decrease in convergent with increase normal load, while the lubrication temperature of the bearing grows until reach a steady state operation vs sliding time. It is also found that the roughness in special positions change with sliding distance. It is also found that the wear rates increase with the increase of sliding speed and normal load.*

**Key word: Friction Coefficient, Normal Load, Sliding Speed, Wear, Sliding distance, Roughness**

## 1. INTRODUCTION

Study of mechanics of friction and the relationship between friction and wear dates back to the sixteenth century, almost instantly after the devise of Newton's law of motion. It was observed by several authors [1], [2], that the variation of friction and wear rate depends on interfacial conditions such as normal load, geometry, relative surface motion, sliding speed, surface roughness of the rubbing surfaces, type of material, system rigidity, temperature, stick slip, relative humidity, lubrication and vibration. through these factors sliding speed and normal load are the two main factors whose play significant role for the variation of friction and wear rate.

Changes in the sliding velocity result in a change in the shear rate which can influence the mechanical properties of the mating materials. The strength of many metals and nonmetals is greater at higher shear strain rates as stated by Bhushan and Jahnman [3, 4] which results in a lower real area of contact and a lower coefficient of friction in a dry contact.

Bearings are machine elements which are used to support a rotating part, namely a shaft. They transmit the load from the rotating part to a stationary part known as frame or housing. They permit relative motion of the two parts in one or two directions with minimum friction, and also prevent the motion in the direction of the applied load. The bearings are classified broadly into two categories based on the type of contact they have between the rotating and the stationary part:

- a. Sliding contact
- b. Rolling contact

Sliding contact bearings are classified in three ways

[5]:

- a) Based on type of load carried
- b) Based on type of lubrication
- c) Based on lubrication mechanism

High viscosity index lubricants were investigated in a low speed journal bearing by Kasai et al. [6] finding that high viscosity index VI lubricants lead to reduced bearing friction in some cases and higher maximum oil film pressure when compared to a polyalphaolefin base oil.

The test equipment was then modified by D W Childs et al. [7] to include dynamic testing capabilities using an arrangement of springs and hydraulic shakers, with a detailed analysis of the experimental uncertainties and parameter determination methods. In N M Franck et al. [8] the rig was used to compare the performance of several different hybrid bearing geometries. This study found that while each of the four geometries tested had specific advantages, the use of an inlet angled against the flow of rotation provided the most beneficial characteristics. A new developed bearing test rig [9] for measurement of hydrodynamic pressure and friction moment of plain journal bearing was presented by Mazdrakova et al. The stand is designed and constructed with exchangeable bearing bushes which are coated on the inner side with different finishes with a uniform thickness and various elastic characteristics. Static measurement capabilities include operating eccentricity and continuous circumferential pressure at multiple planes in axial direction.

The tribological behaviors of Babbitt alloy 16-16-2 sliding against aluminum bronze ZnCuAl9Mn2 lubricated by sea water were systematically investigated by Hairong Wu et al. [10]; the results indicated that the friction coefficient decreased as the load increased to 30N and then remained at a steady level at high loads, but decreased with increase in sliding speed. A. Zeren, E et al. [11] studied the tribological behavior of two different tin-based bearing materials in dry sliding conditions, one of these alloys with low Sb content (7%) is known as SAE 12 and is widely used in the automotive industry and the other with high Sb content (20%) is a Sn-Sb-Cu alloy. Search results have proved that WM-2 and WM-5 alloys can be used in dry sliding conditions, it is shown that performance of WM-5 under heavy service conditions is better than WM-2 due to its alloying elements.

In this paper, the journal bearings test rig [12] was modified specifically for this research to use in determining tribological properties of the bearings, and experimental research to study performance of the radial

\*Corresponding author: Mechanical engineering faculty/ Department of Mechanics, University of Tikrit, Tikrit, Iraq, amircraft.2011@yahoo.com

sliding bearing were coated with tin alloys- TEGOTENAX V840.

## 2. THEORETICAL ESTABLISHMENT OF THE WEAR AND FRICTIONAL HYDRODYNAMICALLY

Wear is related to interactions between surfaces and specifically the removal and deformation of material on a surface as a result of mechanical action of the opposite surface [13]. Wear can appear in many ways, depending on the material of the interacting contact surfaces, the operating environment, and the running conditions. The most common wear model is named Archard's Wear Law [14], although Holm [15] formulated the same model much earlier than Archard:

$$V = K \cdot \frac{F_N}{H} \cdot s, \quad (1)$$

where  $V$  is the wear volume,  $K$  is the dimensionless wear coefficient,  $F_N$  is the normal load,  $H$  is the hardness of the softer contact surface and  $s$  is the sliding distance. However, studies have found that wear coefficient is more suitable. The reason being that it takes the wear rate, the applied load, and the hardness of the wear material into account. Therefore, the wear coefficient  $K$  in the abrasive model is defined as:

$$K = \frac{H \cdot V}{F_N \cdot s} \quad (2)$$

As  $V$  can be estimated from weight loss  $W$  and the density  $\rho$ , the wear coefficient can also be expressed as:

$$K = \frac{H \cdot W}{F_N \cdot s \cdot \rho} \quad (3)$$

As shown in Figure 1 the coefficient of friction generated between journal bearing and lubricant can be determined by following equation.:

$$\mu = 2 \cdot \pi \cdot \frac{r^2 \cdot B}{c} \cdot \frac{\eta \cdot \omega}{F}, \quad (4)$$

where  $\mu$  is coefficient of friction [-],  $r$  is radius bearing [m],  $h=c$  is thickness of clearance [ $\mu\text{m}$ ],  $\eta$  is dynamic viscosity [ $\text{Ns/m}^2$ ],  $\omega$  is angular speed [1/sec],  $F$  is normal load [N] [13].

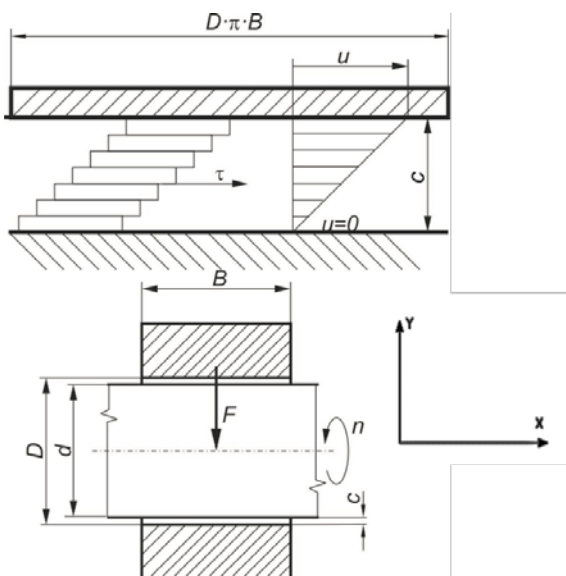


Figure 1: Loaded plain journal bearing

## 3. PREPARATION OF EXPERIMENTAL MATERIALS AND CONDITIONS

In this study, radial plain bearing specimens made of tin-based alloy -TEGOTENAX V840, these alloys are produced by casting and spray deposition method [16], were used as journal bearing and AISI 440C stainless steel was used as shaft. The chemical compositions of the journal and bearing materials used in the experiments were given in Table 1.

Dimensions of bearing specimens were as follows: inner diameter is  $40^{+0.05}$  mm, width 40 mm, outer diameter 60 mm, the relative bearing clearance 0.025 mm, the thickness of the white metal material 3 mm. The mechanical and physical properties of bearing are given in (Table 2).

The bearing was drilled with hole (dimension  $r = 1.5$  mm) in radial direction to ease lubrication oil flow into the contact zone. Circumferential groove was also made onto the outer surface of bush (width 2 mm, depth 0.5 mm) to include that lubrication oil arrives into the radial hole. as well, the spiral groove is made onto inner surface of sample (width 2 mm, average depth of  $30 \mu\text{m}$ ) to improve the lubrication process between the shaft and the bush as shown in Figure 2. The surface profiles of the plain journal bearing were determined prior the tests by using the Surface Roughness Tester "Surftest SJ-301".

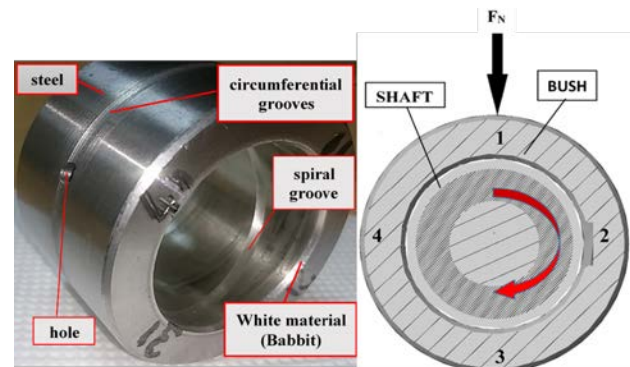


Figure 2: Tested plain journal bearing

Convection oven at  $60 \text{ }^\circ\text{C}$  for a period of half an hour to remove humidity, as the weight of the samples was measured using a digital balance and recording the values before and after the test for each test.

The specimens were tested by radial journal bearing wear test rig under lubricated condition. The tribological parameters were measured under lubricated conditions of (3000, 3500 and 4000) N average loads, (2000, 2500 and 3000) rpm sliding speed equals to 4.2, 5.25 and 6.3 m/s and every 1 h for change coefficient of friction, 5 h for wear losses each specimen. The lubrication was achieved by using ISO VG32 oil. Before and after testing, the specimens were cleaned by cleaner FLUXO S190 and dried using cotton and convection oven at  $60 \text{ }^\circ\text{C}$  for a period of half an hour to remove humidity, as the weight of the samples was measured using a digital balance and recording the values before and after the test for each test.

Table 1: Chemical composition of AISI440C wt- (%), and bearings materials wt- (%)

TEGOTENAX (V480) (big sticks), in TKL NOVA TVORNICA KLIZNIH LEZAJEVA (SLIDING BEARING MANUFACTURING), CROATIA											
WM	Sn	Sb	Cu	As	Bi	Ni	Pb	Cd	Fe	Al	Zn
Actual Value %	88.7	7.6	3.7	0.009	0.002	0.003	0.008	0.010	0.009	0.000	0.002
The alloy is free of lead and free of cadmium in compliance with RoHS Regulation (EU-Directive 2002/95/EC)											
AISI 440C	C	Si	Mn	Ni	Cr	Mo	P	S	-	-	-
	1.2	1	1	1	18	0.75	0.04	0.03	-	-	-
Mechanical Property Requirements For Material in the Annealed Condition to 1) AS2837 - 1986 440C and 2) ASTM A276-98b 440C											

Table 2: Mechanical and physical proprieties of bearing

White metal alloy TEGOTENAX			
Hardness	HB 10/250/180 (DIN ISO 4384 part 2)	20 [°C]	23
		50 [°C]	17
		100 [°C]	10
		150 [°C]	8
Young's modulus	$E$	56500 [N/mm <sup>2</sup> ]	
Density	$\rho$	7400 [kg/m <sup>3</sup> ]	
Lower melting point	$T_{lm}$	233 [°C]	
Poisson ratio	$\nu$	0.33	
Upper melting point	$T_{hm}$	360 [°C]	
Casting temperature	$T_c$	440 [°C]	

#### 4. RADIAL JOURNAL BEARING TEST RIG

Bearings materials in journal bearings are generally selected from materials, which have lower wear strength than the shaft material, that way dropping the wearing of the shaft safely. Therefore, journal bearing wear test apparatus are designed to examine the wearing of bearing materials. Therefore, it is possible to investigate different bearing and shaft materials and the effects of heat treatments on these materials. This test rig is divided into three main systems: Hydraulic Loading System, Rotation System, Lubrication system of the bush as shown in Figure 3.

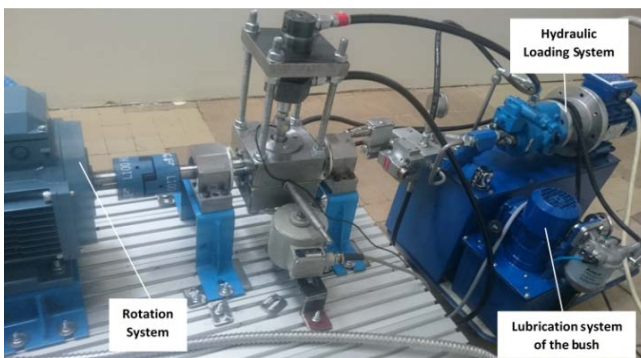


Figure 3: Illustration of journal bearing test rig

##### 4.1. Drive System

The drive system drove the shaft. The driving system test rig consists of an asynchronous induction motor (AIM) (ABB, 400 V, 50 Hz, 3 KW, 1460 rpm), which is attached by a flexible coupling to a shaft. The shaft is supported by two roller bearings and the test bearing is mounted between these two bearings (supporting the drive shaft). The motor was equipped for

the rotational speed measurement by incremental encoder. E720 - Wireless / Point laser was used to align shaft with the motor as shown in Figure 4.

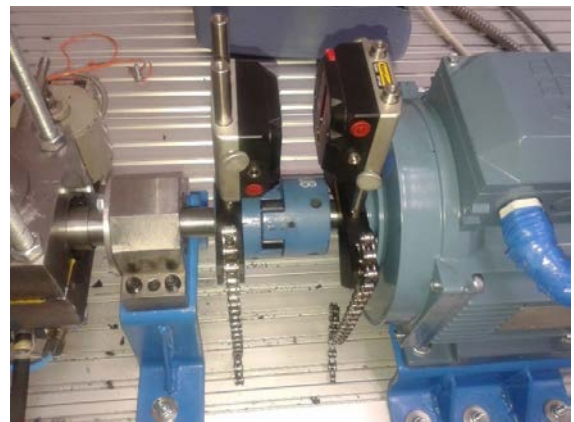


Figure 4: The reset shafts motor and housing bearing

##### 4.2. Hydraulic Loading System

The loading system generated the load on the bearing. Bearing loading system consists of electrical motor-pump assembly (HLS) (CEM motor - 0.75 KW, 380 V, 1420 rpm, 50Hz; EATON pump PVQ10) which is mounted on the 30 l tank and connected with high-pressure hydraulic flexible tubes which feed ISO VG 32 oil into the hydraulic cylinder through two holes (H and L) as shown in Figure 5. The hole H is inlet of high-pressure hydraulic feed from hydraulic pump and L is outlet hole of oil return to the tank. The hydraulic cylinder is in contact with radial force transducer (HBM U9C/10kN) which is located below it. The force transducer is threaded up the radial load supply that apply radial force directly into the bush.

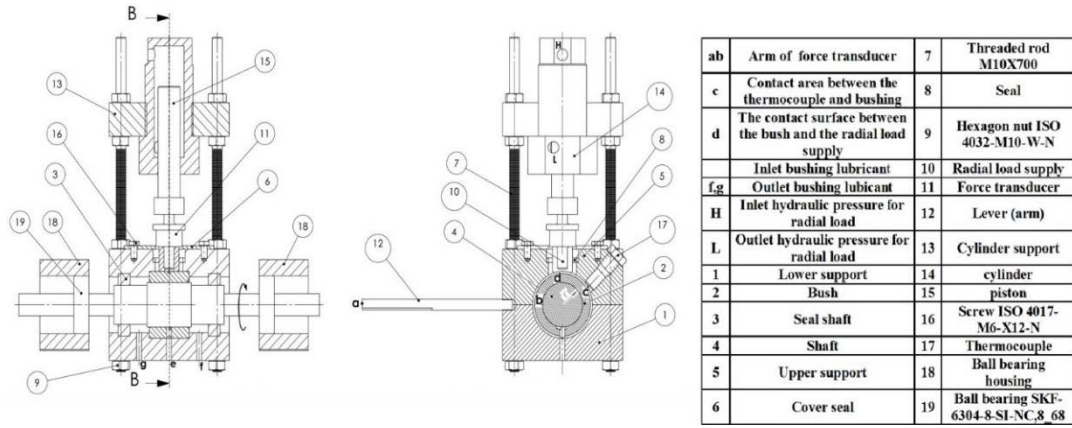


Figure 5: Schematic of the tool developed for testing of plain journal bearings of configurations

4.3. Lubrication system of the bush

The lubrication system supplied the lubricating oil for the bearing. Lubrication system contains of electric motor-pump assembly (ELP) (motor: 1450 rpm, 90 W, 220 V, 50 Hz; pump AMGP-03C) which was mounted on the 10 l hydraulic tank. The lubricant is supplied by the ELP to the bearing housing through two flexible tubes which are threaded up the housing through an assembly steel tube contacted into locations e, f, and g, as shown in Figure 5. The hole e is an inlet oil feed to housing, while holes f, g are an outlet oil feed into the lubrication oil tank. The lubrication system supplied oil pressure was monitored by pressure gauge mounted on the inlet oil supply. The same type of oil, ISO VG32, was used for bush lubrication.

4.4. Bearing Unit

Figure 5 shows that the sleeve of the shaft (4) is mounted on the plain bearing (2) which is radially and axially fixed by upper (5) and lower (1) parts of the support. Through the opening of the upper support (5) a force is induced by the hydraulic cylinder and transmitted to the bearing trough radial load supply (10). The magnitude of the force measured by the force sensor (11). The circumferential force, which represents the frictional force of the bearing, is measured by means of a lever (12), which is arranged perpendicularly to the axis of the bearing, and a force transducer Figure 5. The temperature of the bearing is measured by thermocouple (17). The sleeved thermocouples are placed inside fully drilled holes. The active part of the thermocouple is in contact (region c) with the outer surface of the bush. It was assumed that, under typical operating conditions, the point of maximum bearing temperature was close to the temperature measurement points.

Upper and lower supports are made of steel; there are also seals (3,8) to prevent oil leakage during the system operation. Upper and lower support were assembled and mounted by standard nuts and screws (7, 9, 16).

5. TEST RIG EXPERIMENTS

5.1. Determine of The Operating Procedure Test Rig

The tests were carried out for 5 hours' duration; the operating sequence was ELP, AIM than HLS, respectively. Pressure of the lubrication oil sent to the test bearing was 4 bar. Test was conducted out to determine time to fill

housing of bearing with oil by removing the upper support seal and switch on the lubricating pump. The time it takes to flooding housing is 15 seconds. The objective of this procedure, to ensure the flooding bushing during the test. The values were always kept under control throughout the tests. Each test was repeated less than three times to ensure the accuracy of results, the experiments were conducted at laboratory temperature i.e. 22 °C.

5.2. Determine of The Friction Coefficient of The Sliding Bearing

In the Figure.6 shown measurement procedure used in this research to determine coefficient of friction of the sliding bearing. The measurement method friction coefficient is based on the principle of torque balance resulting from the friction force and torque produced by the force of the sensor reaction.

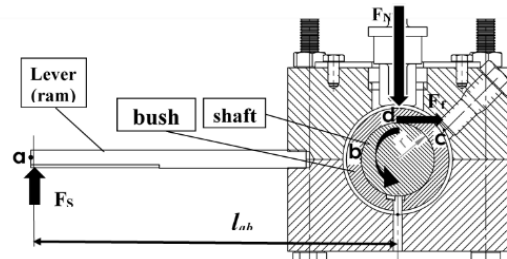


Figure 6: Scheme of the frictional force measurement

Coulomb equations associate load and friction coefficient as a function of time in the touch of two real bodies:

$$F_f(t) = \mu(t) \cdot F_N(t) \tag{5}$$

Moment of friction as a function of time was calculated as the product of the normal force of the sleeve (using reaction force transducer) and the distance on lever between the center of the bush and contact point of the force transducer

$$M_f(t) = F_s(t) \cdot l_{ab} = F_f(t) \cdot r \tag{6}$$

From (5), (6)

$$\mu(t) = \frac{M_f(t)}{r \cdot F_N(t)} = \frac{F_s(t) \cdot l_{ab}}{r \cdot F_N(t)} \tag{7}$$

6. RESULTS AND DISCUSSIONS

6.1. Frictional Behaviour

The variation in the coefficient of friction of Babbitt base alloys - TEGOTENAX V840 coatings for

radial sliding bearing is plotted in Figure 7 and 8, as a function of the bearing radial load in the range (3000, 3500 and 4000) N and sliding speed (2000, 2500 and 3000) rpm, respectively, for one hour sliding time.

The experimental test of the sliding bearing made of Babbitt metal has been observed that the coefficient of friction decreases when increasing the radial load of journal bearing for all average impact radial load and each sliding speed, the highest friction coefficients 0.04 occurred in average radial load 3000 N and 3000 rpm sliding speed, whereas the lowest friction coefficients 0.023 occurred in highest average radial load i.e. 4000 N and rotate shaft speed 2000 rpm. Change coefficient of friction values take the form of converging curves toward increasing the radial load at increasing rotate shaft speeds 2000, 2500 and 3000 rpm as shown in Figure 8.

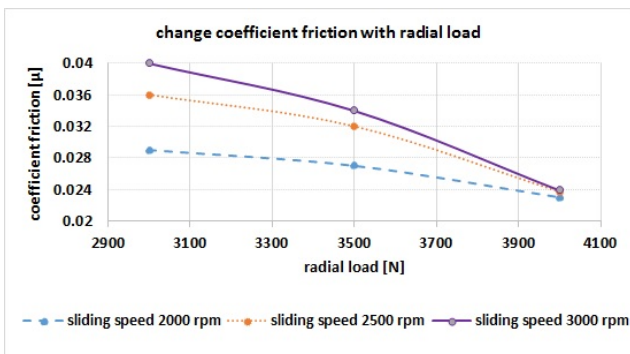


Figure 7: The figure shows the change in the coefficient of friction with the change in radial load

Figure explain in detail the relationship between friction coefficient and rotation speeds of shaft, friction coefficient increases with the increase of rotating shaft speed 2000 to 3000 rpm for average radial load 3000 and 3500 N, whereas remaining almost constant at radial load 4000 N. The friction between rotate shaft, bush and lubricant causes temperature growth of lubricant which results decrease in the shear stress of lubricant that lead to lowering viscosity of lubricant thus decrease coefficient of friction as shown in eq. 4

During this study, the oil film temperature, which was evaluated to be equal to the operating temperature, i.e. the temperature of the bearing under proven operating conditions. The temperature of the bearing was measured by using thermocouple placed on the bushing (see Figure. 6), The average maximum measured temperature in the bearing was used as the oil film temperature. At typical bearing loads, sliding speeds and direction of rotation (Counterclockwise), the maximum temperatures were measured at the temperature measurement point C (see Figure 6). It can be estimated that the error in the oil film temperature was about  $\pm 0.5$  °C.

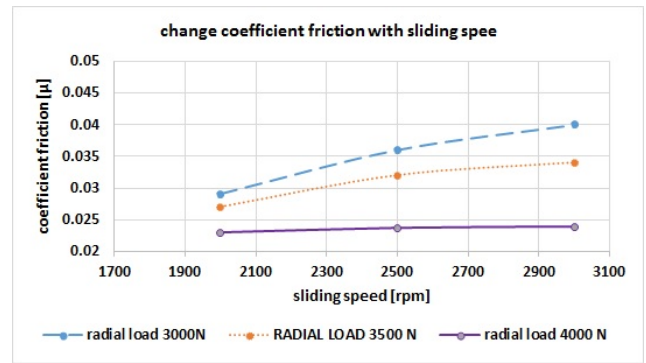


Figure 8: the change in the coefficient of friction with the change in sliding speed

Figure 10 shows the curves for 2000 N average load, 3000 rpm rotation speed and 18000 s sliding time as representing the effect of the lubrication temperature change on the coefficient of friction on the surfaces of the plain journal bearing. It can clearly be seen that the coefficient of friction decreased with the operated time, while the generated heat in the bearing causes increase of oil temperature. As mentioned earlier, the coefficient of friction is directly proportional to dynamic viscosity ( $\eta$ ), and the oil temperature rise leads to decrease of the dynamic viscosity which certainly leads up to decrease of the coefficient of friction. We can distinguish from the Figure 10 two zones, unsteady and steady state. In unsteady state the temperature within the system increase with time, is estimated unsteady state approximated (0-4000)s. Second zone is steady state zone in which temperature remains approximately constant, it's here about 50°C.

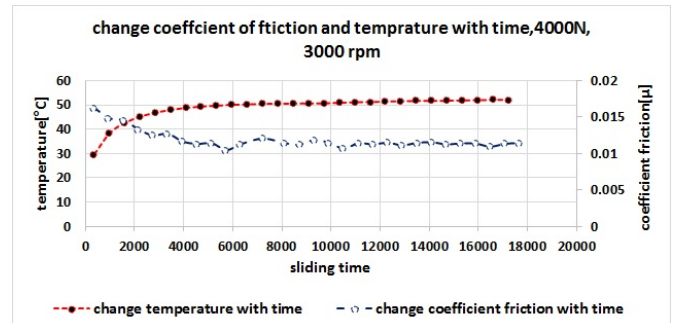


Figure 10: Change temperature and coefficient of friction with time rotating plain journal bearing under average load 4000 N, 3000 rpm, 5 hours

The duration of access to steady state decreases with increasing speed of rotation and load, this is due to the increase of the amount of lost power, although the value of the coefficient of friction is reduced. Increase in the friction power losses accelerates reaching steady state i.e., access to the thermal balance between bush, shaft and lubricant as shown in table 3.

Table 3: Effect of the sliding speed and radial load on the unsteady state process

Rotation speed [rpm]	Radial load [N]	Average coefficient of friction $\mu$ [-]	Loss power [W]	Duration of unstable state [s]
2000	3000	0.029	365.4	0-4850
	3500	0.02	294	0-5470
	4000	0.012	201.6	0-6100
2500	3000	0.032	504	0-4700
	3500	0.0237	435.4	0-4900
	4000	0.016	336	0-5050
3000	3000	0.04	756	0-3850
	3500	0.034	749.7	0-3800
	4000	0.0239	602.28	0-4000

6.2. Roughness surface behaviour

The surface profiles of the plain journal bearing were determined prior the tests by using the Surface Roughness Tester "Surftest SJ-301". Values of surface roughness before and after wearing process were shown in Figure 11. the profiles of plain journal bearing were investigated, it was found that total average roughness ( $R_z$ ) of inner surface of four specimens tested are 2.71, 2.1, 2.13 and 1.66  $\mu\text{m}$  respectively and average roughness ( $R_z$ ) of shaft is 1.15  $\mu\text{m}$ , it means that even the presumably smooth plain journal bearing has some in dents and protrusions.

Generally, at all the positions marked 1, 2, 3 and 4 roughness surface journal bearing material decreases with increasing sliding distance, perhaps because of the roughness of surfaces are still in the process of stability,

the roughened of shaft may be cause change inner surface roughness of bearings, surface roughness has been stabilized and the bearing surface has conformed to the shaft surface after about 30000-75000 m for all position as shown in Figure 11. Biggest drop in the roughness occurred in positions 1 than 3, while the decrease in the position 4, than 2 was a slight for load 4000 N, may be due to that position 1 in direct and continuous contact with the shaft rub. The continuing slide was causing increasing roughness for all positions, a significant degradation of the surface in position 1 followed by position 4, while slightly increase in average roughness  $R_z$  in position 2 and 3, which may be attributed to the direction of rotation speed of shaft and direction and region of impact of load, that drives debris toward the two positions 1 and 4.

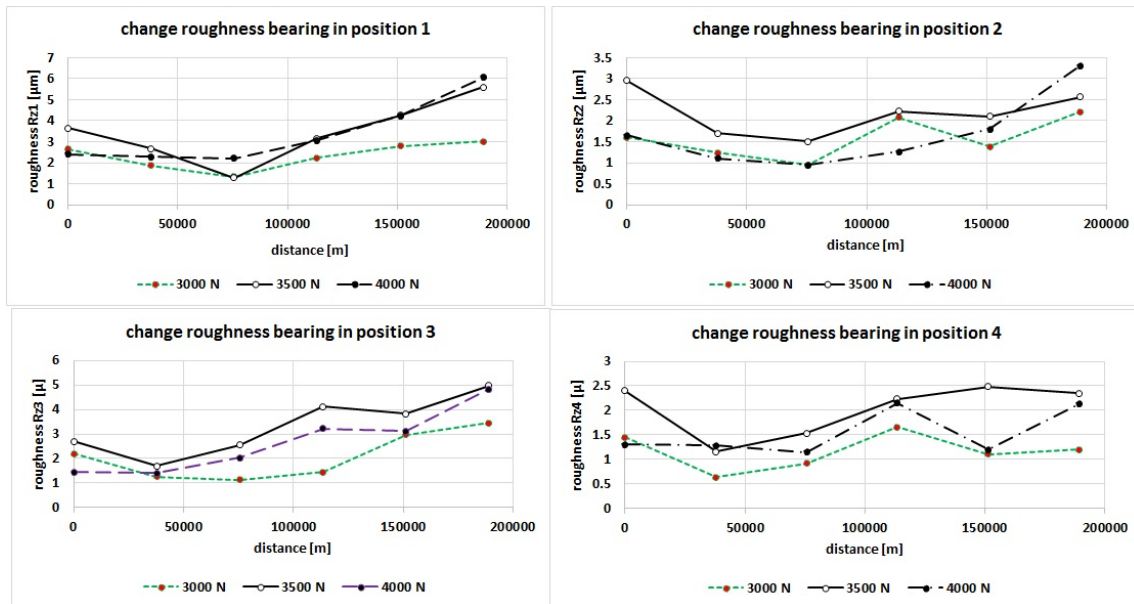


Figure 11: Change Roughness surface  $R_z$  with sliding distance

6.3. Wear Behaviour

The wear of materials has been described by weight loss, In Figure 12, were investigated of tin-based

TEGOTENAX (V480) bearing material in lubricant sliding at different average radial load 3000, 3500 and 4000 N and variation rotation speed of shaft 2000, 2500 and 3000 rpm vs sliding distance. In Figure 12 shows three

unsteady-state zones and three steady-state zones. First unsteady-state zone has Sharply wear increases vs sliding distance for all average radial load (3000-4000) N, value loss material 2.3, 2.75 and 3.2 mg respectively. At the beginning of sliding process until access first steady-state wear process at 75600 m sliding distance. Long distance of first steady-state zone is 226800 m, average loss material in first steady-state wear process was 2.3, 2.8 and 3.5 mg under 3000-4000 N radial load respectively, and rotation speed 2000 rpm. The cause of rapid loss of material at the beginning of operation i.e. first unsteady-state may be due to get to the case of compatibility between shaft and bush. At change rotation speed from 2000 to 2500 rpm lead to a second unsteady-state zone wear process for 94500 m sliding distance, value loss material about 3.4, 4.1 and 4.7 mg under (3000-4000) N average radial load respectively, followed by second steady-state wear process zone, long distance of second steady-state zone is 283500 m an average loss material in second steady-state wear process 3.4, 3.9 and 4.6 mg under (3000-4000) N average radial load respectively. Finally, third unsteady-state zone under which changes rotation speed of shaft from 2500 to 3000 rpm, where the amount of loss material 4.6, 5.35 and 5.8 mg under (3000-4000) N average radial load respectively, long distance unsteady-state zone 113400 m sliding distance, followed by third steady-state wear process zone which long distance 340200 m, average loss material in third steady-state wear process 4.5, 5.1 and 5.8 mg under (3000-4000) average radial load respectively as shown in Figure 12. It is clear that lost material increases as increase radial forces and sliding speeds vs increase sliding distance but effect sliding speed of shaft biggest than radial load.

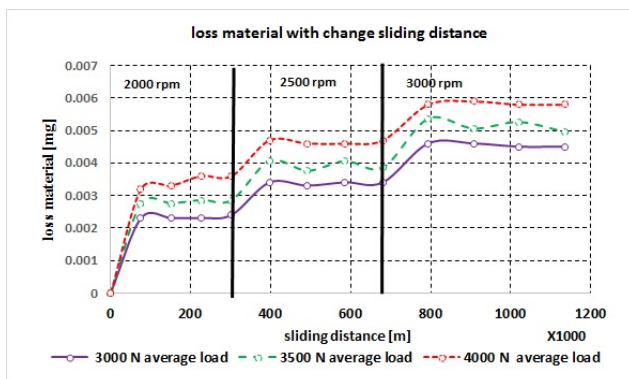


Figure 12: Loss material with change sliding distance

## 7. CONCLUSION

Tribological properties in conditions of sliding distance contact can vary over many orders of magnitude. In this study, the tribological behaviour of tin-based journal bearing material was evaluated and focusing on the effect of sliding distance in change of roughness, loss material and coefficient of friction surface contact of tin-based journal bearing. The following conclusions can be drawn:

- Friction coefficient with respect to radial load is lowest in highest radial load for each shaft rotational speed, it decreases extremely when increasing the radial load of journal bearing.

- Change coefficient of friction values take the form of converging curve toward increasing the radial load at increasing rotate shaft speeds.
- Coefficient of friction increases slightly with an increase of shaft rotational speed for same average radial load.
- The coefficient of friction at highest load and lowest rotation speed of shaft have been lowest values, Vice versa as regards lowest radial load and highest sliding speed coefficient of friction have highest values.
- at beginning of experimental test, contact surfaces roughness of samples decreases and is lower on the impact line of the vertical load i.e. at the two positions 1 and then 3.
- The continuing slide was causing increasing roughness for all positions, a significant degradation of the surface in position 1 followed by position 4, while slightly increase in average roughness  $R_z$  in position 2 and 3,
- Results wear tests is noted three unsteady-state zones and three steady-state zones, according to change in the speed of rotating shaft.
- The highest wear loss 5.8 mg in steady-state zones occurred in load 4000 N and rotation speed 3000 rpm at sliding distance 1134000 m, under similar tribological conditions.
- The highest wear loss 3.2 mg in unsteady-state zones occurred in load 4000 N and rotation speed 2000 rpm at sliding distance 75600 m i.e. at the beginning of the test.

## REFERENCES

- [1] E. J. Berger, C. M. Krousgrill, F. Sadeghi, October, "Stability of Sliding in a System Excited by a Rough Moving Surface", ASME, Vol. 119, pp. 672- 680, (1997)
- [2] B. Bhushan, "Principle and Applications of Tribology", John Wiley & Sons, Inc., New York, pp. 344-430, (1999)
- [3] B. Bhushan, W. E. Jahnman, "Propagation of Weak Waves in Elastic-Plastic and Elastic-viscoplastic Solids With interfaces", Int. J. Solids and Struc, Vol. 14, 39-51, (1978)
- [4] B. Bhushan, W. E. Jahnman, "Measurement of Dynamic Material Behavior under Nearly Uniaxial Strain Condition", Int. J. Solids and Struc., Vol. 14, pp. 739-753, (1978)
- [5] Gopinath, K., Mayuram, M., M., "Sliding contact bearings", Indian Institute of Technology Madras, Machine Design II
- [6] Kasai, M., Fillon, M., Bouyer, J., Jarny, S. "Influence of lubricants on plain bearing performance: Evaluation of bearing performance with polymer-containing oils", Journal of Tribology International, Volume 46, pp. 190-199, (2012)
- [7] Childs, D.W., Hale, K., "A test apparatus and facility to identify the rotor dynamic coefficients of high-speed

hydrostatic bearings", Journal of Tribology, Vol. 116, pp.337–343, (1994)

[8] Franchek, N.M., Childs, D.W., "Experimental test results for four highspeed, high-pressure, orifice-compensated hybrid bearings", Journal of Tribology, Vol. 116, pp.147-153, (1994)

[9] Mazdrakova, A., Javorova, J., Radulescu, A., Mirev, A., Rakanov, Y., "Hydrodynamic journal bearing test rig with pressure measurement at elastic deformations of contact surfaces capabilities", XV International Scientific Conference "RE&IT 2016", Bulgaria, pp.33-36, (2016)

[10] Hairong, W., Qinling, B., Shengyu, Z., Jun, Y., Weimin, L.m "Friction and wear properties of Babbitt alloy 16-16-2 under sea water environment", Journal of Tribology International, 44 (10), pp.1161–1167, (2011)

[11] Zeren, A., Feyzullahoglu, E., Zeren, M., "A study on tribological behaviour of tin-based bearing material in dry

sliding", Journal of Materials & Design, Vol. 28, Issue 1, pp. 318–323, (2007)

[12] Bojić, N. Milčić, D., Banić, M., Milčić, M., "Effect of coverage of graphite on self-lubricating plain bearings", 14th International Conference on Tribology SERBIATRIB'15, Belgrade, Serbia, May 13 – 15, 2015 pp. 309-313, (2015)

[13] Rabinowicz, E., "Friction and Wear of Materials", New York, John Wiley and Sons.(1995)

[14] Archard, J.F., "Wear theory and mechanisms", In: M.B. Peterson, W.O. Winer (eds.). Wear Control Handbook, ASME, (1980)

[15] Holm, R., "Electric Contacts", Almqvist & Wiksells Boktryckeri AB, Uppsala,(1946)

[16] D. Dowson, "History of Tribology", Professional Engineering Publishing, p.768, (1998)



# Surface Quality of Maraging Steel Parts Produced by DMLS

Nebojša Bogojević<sup>1</sup>, Aleksandar Vranić<sup>1</sup>, Nusret Muharemović<sup>2</sup>, Nenad Drvar<sup>3</sup>

<sup>1</sup> Faculty of Mechanical and Civil Engineering in Kraljevo, University of Kragujevac, Kraljevo, Serbia

<sup>2</sup> Plamingo, Gračanica, Bosnia and Herzegovina

<sup>3</sup> Topomatika, Zagreb, Croatia

*The main applications of the additive manufacturing are in rapid prototyping, for production of different types of prototypes and models. During the last decade, due to advances in fields of materials and technologies, the additive manufacturing has also become a competitive technology for production of tools. The competitive advantage of the additive manufacturing is the possibility to build, in a very short time, complex models with adequate precision. However, besides the precision and the speed of production, the parts produced by additive manufacturing need to satisfy a wide spectrum of requirements concerning their mechanical characteristics. One of the most demanding requests in the tooling production is high surface quality. During manufacturing process arise flaws within the material volume, such as porosities, inclusion, voids and micro-cracks. Later, during the post-processing of the manufactured tools by machining, grinding or polishing, these flaws are brought to the surface of the tool. In most cases, the appearance of the flaws on surface is an undesirable phenomenon in tooling industry, especially for the tools with high-gloss surface. The paper presents a comparison of the surface quality of parts produced by additive manufacturing and parts produced by a conventional technology. The surface quality has been estimated and by visual inspection of surfaces using the microscopy with the aim to study the surface porosity.*

**Keywords:** Additive manufacturing, surface quality, surface porosity

## 1. INTRODUCTION

Unlike subtractive manufacturing methods that start with a solid block of material and then cut away the excess to create a part, additive manufacturing builds up a part (or features onto parts) layer by layer from geometry described in a 3D design model. The 3D models are, usually, created by Computer-Aided Design (CAD) software package. After the process of the modelling, parts have been divided into a thin layers and prepared for additive manufacturing. The layer thickness depends on several different factors, such are a type of the technology, the type of the material, speed, etc.

Additive manufacturing it covers a several different technologies which can be divided on the basis of the method of layer manufacturing [1-3]. Major processes include material extrusion, material jetting, binder jetting, sheet lamination, vat photo-polymerization, powder bed fusion and directed energy deposition.

The technology of the additive manufacturing has been invented 1980's. In the beginning, the additive manufacturing has been focused on the Rapid Prototyping and on the visualisation of the final products. More recently, additive manufacturing is used for production of the end-user products, parts for the automotive, aerospace, dental industry, for production of the medical implants as well and for "printing" a human tissue. Each of this different technologies have its own advantages and drawbacks, therefore, depends on the industry requests, on the market we may found almost all types of the additive manufacturing technologies.

In the last years, beside the rapid prototyping, the additive manufacturing has significant role in the rapid production and digital fabrication.

The additive manufacturing has a lot advantages compared to subtractive manufacturing methods, such are

the speed, precision, building the parts without moulds, build the parts with complex geometry. Disadvantages of the additive manufacturing are slow building rate, high production costs, parts steel needs to be post-processed, relatively small building volume, poor mechanical properties.

In this paper, the surface quality of the parts produced by Direct Metal Laser Sintering (DMLS) are presented. The surfaces of the parts produced by DMLS are compared with surfaces of the parts produced by subtractive manufacturing methods.

## 2. DIRECT METAL LASER SINTERING

Direct metal laser sintering is an additive manufacturing technology which belongs to powder bed fusion and it is occasionally referred to as selective laser sintering (SLS) or selective laser melting (SLM). DMLS allows us to build a metal parts and tools directly from digital – CAD models using a variety of the metal alloys powders.

### 2.1. Building process

The DMLS process begins with a 3D CAD model, which is, in the next step, is sliced in z direction on thin layers. Using a laser, the metal powder has been melted in created layers, so we can say that whole process of the manufacturing is performed in one plane. When the melting in one plane is finished, the building platform is moved down, the recoater applying a new layer of the metal powder on the building plate, see Figure 1 and the melting in the new plane is again performed. The laser has enough power to transform powder to liquid state, and it is allowed to liquid metal solidify before a new layer is recoated and melted.

The process of metal sintering is performed in the highly controlled environment. The scanning speed of

laser beam, layer thickness, temperature, level of the oxygen and gas flow in the working chamber of the DLMS machine are highly controlled.

In the process of the laser sintering, besides that the level of the oxygen is very low (from 0,5% to 1%), a metal oxide called residuals, has been created, as it is shown in the Figure 2. A certain amount of the residuals has been removed by gas flow in the working chamber, see Figure 1, while one part of the residuals remains over and around the sintered parts, in the powder bed.

2.2. Porosities

The density of the parts produced by DMLS should be around 99% and mechanical properties of these parts

are very close to the parts produced by machining out of ingots or cast stock.

The latest research in the field of DMLS has shown that produced part have a certain voids or inclusions through the whole volume. These irregularities in the material composition of the parts are also called and porosities. According to some researchers [4,5,6] these porosities are connected to the process of the sintering and to the part orientation during building of the parts. On the other side, these inclusions can be result of the not melted powder, gasses or residuals which are trapped inside melted metal [7, 10-14], shown in Figure 3.

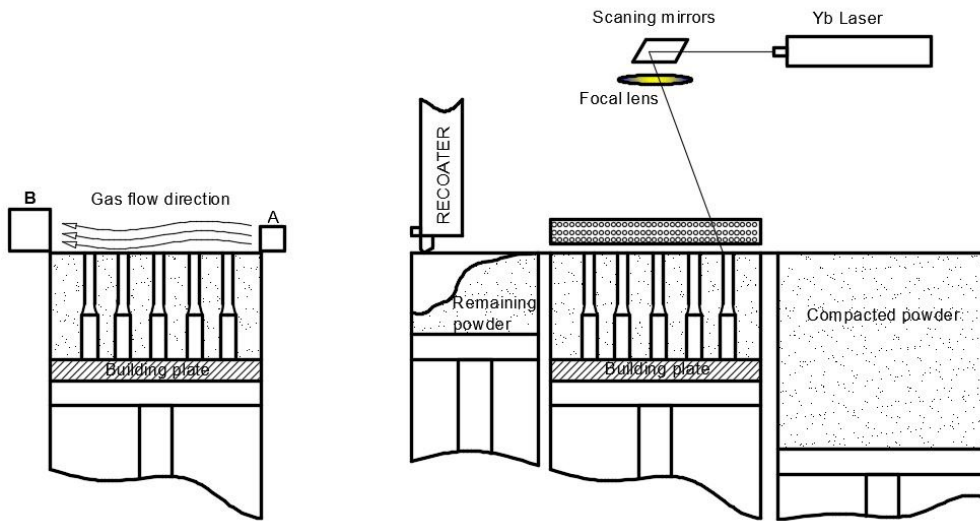


Figure 1. Schematic representation of the building volume and gas flow

Regarding that oxygen is not completely removed from working chamber, there is possibility and to some oxide be trapped into melted metal [15]. The trapped inclusions in the melted metal can be connected and to process parameters, such are layer thickness, scanning strategy, laser power, working atmosphere, etc.

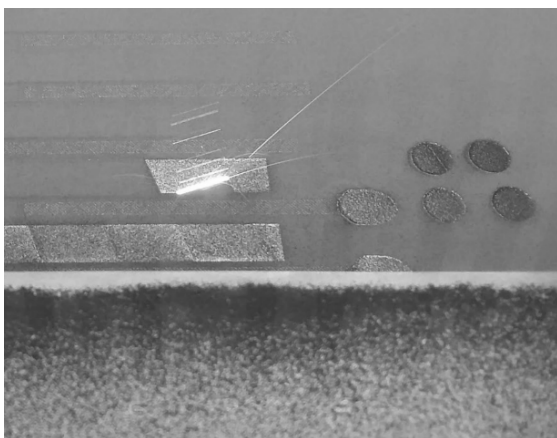


Figure 2. Residuals in the process of the DMLS

Those inclusions are present in all parts produced by DLMS, regardless of the type of metal which is used for parts production. Those imperfections are spread into whole volume of the part as well and on the part surface.

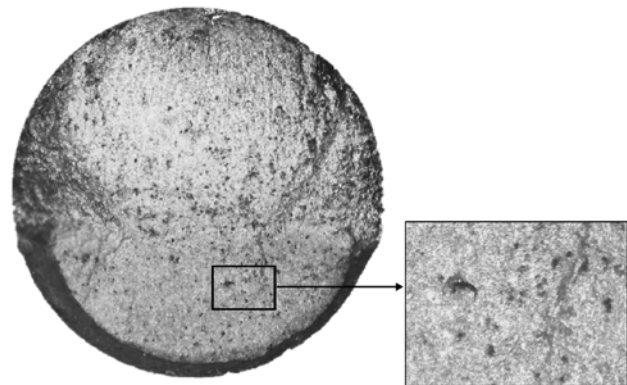


Figure 3. Voids inside part produced by DMLS from MS1 – marginig steel

The parts produced by DLMS has major applicability in the moulding industry for production of the moulds and inserts. Regarding to possibility to create very complex shapes in relatively short time, this type of the production starting to be competitive in the moulding industry.

In the tool production industry, especially for the cosmetics products, the surface quality is one of the main parameters which have a big influence on the final part quality.

In order to compare the quality, the surface of the parts produced by DMLS are compared to the surface of the part produced by subtractive methodology.

### 3. THE SAMPLES PREPARATION

In order to compare the surfaces of the parts produced by DMLS, the set of the samples has been produced on EOS M 280 machine, from maraging steel – MS1. The maraging steel - MS1 is a steel which has been optimized especially for processing on EOSINT M systems. The MS1 have a chemical composition corresponding to US classification 18% Ni Maraging 300, European 1.2709 and German X3NiCoMoTi 18-9-5 [17].

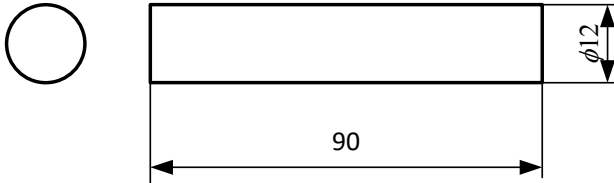


Figure 4. Test sample geometry

The bars 90 mm length and 12 mm of diameter has been chosen as test samples, shown in Figure 4.

Test samples by DMLS has been orientated in the vertical direction. The samples have been directly connected to the base plate, the support structure was not being used between samples and base plate. All samples were produced in one building volume in EOS M 280 machine, with same set of the parameters call "direct tool", with layer thickness of 0.4mm. This set of parameter has double exposition in the first 3 layers in order to provide better bonding of the samples to the base plate.

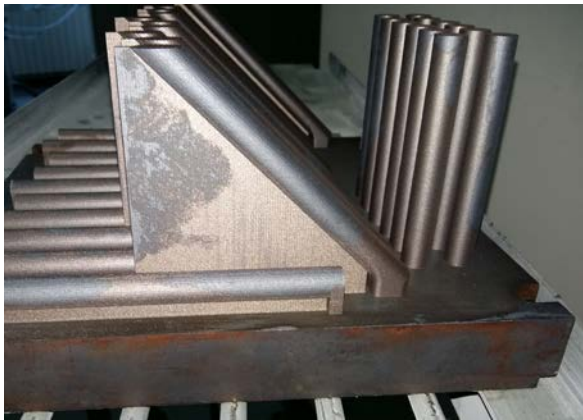


Figure 5. Samples position and orientation in working volume on EOS M 280

In order to create references for surface comparison, the set of the reference samples has been created from steel who has similar mechanical properties to the margining steel MS1 and it is a commonly used in tool production. The reference samples have created from tool steel and hard alloy with chemical composition according to European classification 1.2343 and German X37CrMoV5-1 [20].

The samples polished with diamond paste with particle size of  $9\mu\text{m}$  has noted as K2.1 and K2, while the samples polished with diamond paste with particle size of the  $0.25\mu\text{m}$  has been noted as K1.1 and K1. Samples K1 and K2 are made by subtractive methods – turning and polished from steel 1.2343. Samples noted K1.1 and K2.1

are manufactured by DMLS on EOS M280, heat treated according to the EOS recommendation, and finally polished.

All samples are polished with corresponding diamond paste, after production, in same manner – 3 hour on polishing machine.

Visual inspection of the surface was conducted with Olympus Bx51-P Polarizing Microscope, shown in Figure 6, with magnification of 50x and 100x.



Figure 6. Olympus Bx51-P Polarizing Microscope

Surface roughness was tested with Taylor-Hobson Surtronic 3P measuring device, shown in Figure 7. The surface roughness was tested on the surface length of 25mm. Each specimen is tested three times, where between tests specimen is rotated for  $90^\circ$ .



Figure 7. Taylor-Hobson Surtronic 3P for measurement of the surface roughness

### 4. RESULTS AND DISCUSSION

Results of the visual comparison of the parts produced by subtractive methods (K1 and K2) and parts produced by DMLS are shown on Figures 8 – 15. From the provided figures it is clear that parts produced by DMLS have more voids (inclusions) on the surface than the parts produced subtractive methods from 1.2343 steel. This surface condition and amount of the inclusion on it is best shown on the parts wich are polished with diamond paste with aprticle size of the  $0.25\mu\text{m}$ , which is presented on the Figures 12-15. The arithmetical mean roughness value -  $R_a$  and maximum roughness depth –  $R_{z\text{max}}$  are measured on the surface of the specimen.

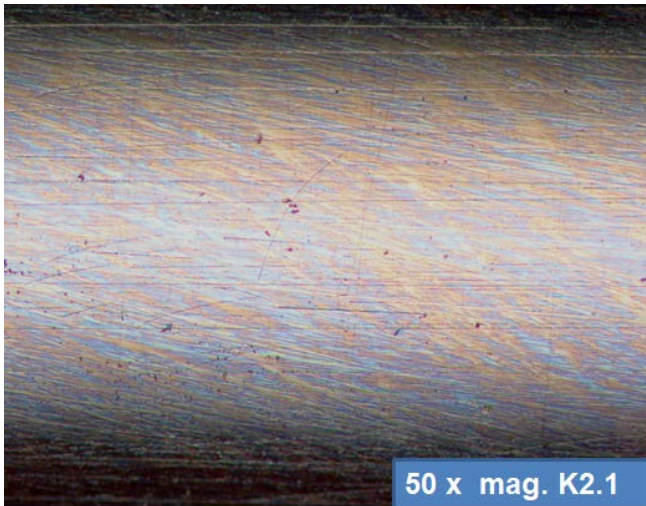


Figure 8. Test sample K2.1, material: steel 1.2709, polished with diamond paste 9  $\mu\text{m}$ , magnification 50x

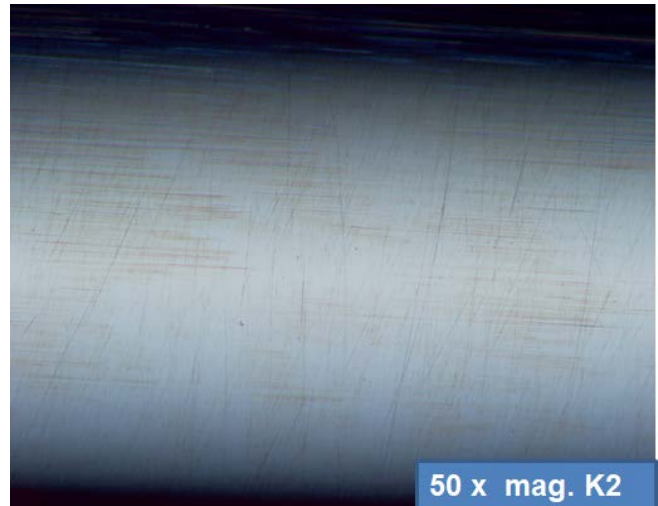


Figure 9. Test sample K2, material: steel 1.234, plished with diamond paste 9  $\mu\text{m}$ , magnification 50x

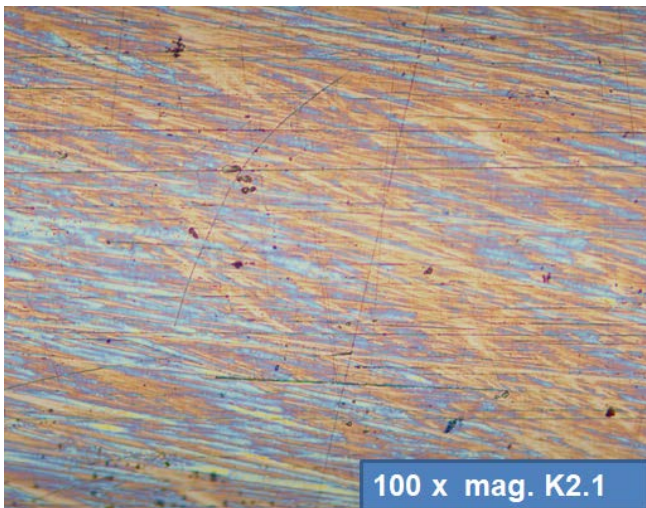


Figure 10. Test sample K2.1, material: steel 1.2709, polished with diamond paste 9  $\mu\text{m}$ , magnification 100x

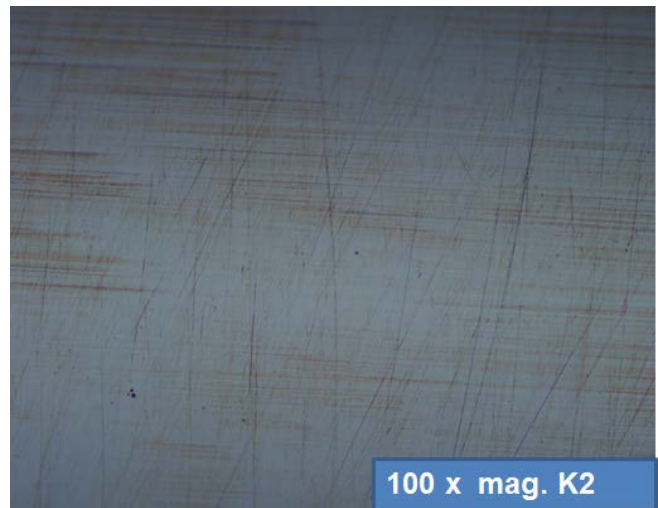


Figure 11. Test sample K2, material: steel 1.2343, plished with diamond paste 9  $\mu\text{m}$ , magnification 100x

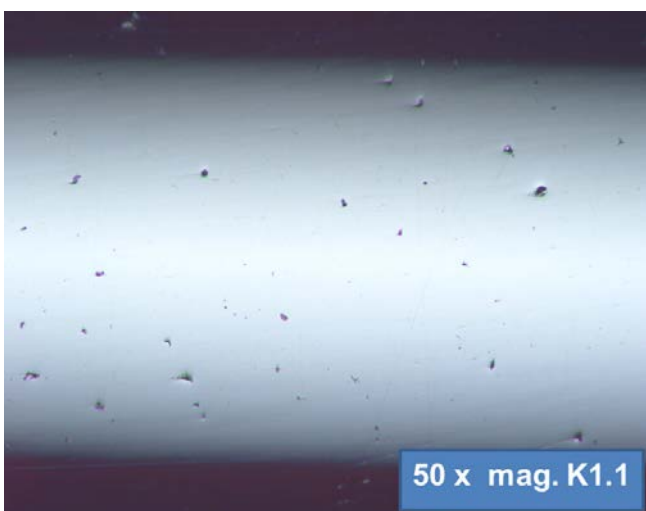


Figure 12. Test sample K1.1, material: steel 1.2709, polished with diamond paste 0.25  $\mu\text{m}$ , magnification 50x

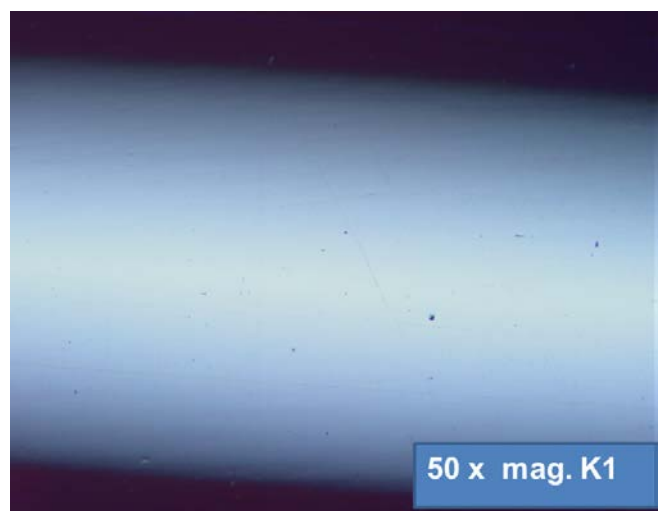


Figure 13. Test sample K1, material: steel 1.2343, plished with diamond paste 0.25  $\mu\text{m}$ , magnification 50x



Figure 14. Test sample K1.1, material: steel 1.2709, polished with diamond paste 0.25 μm, magnification 100x

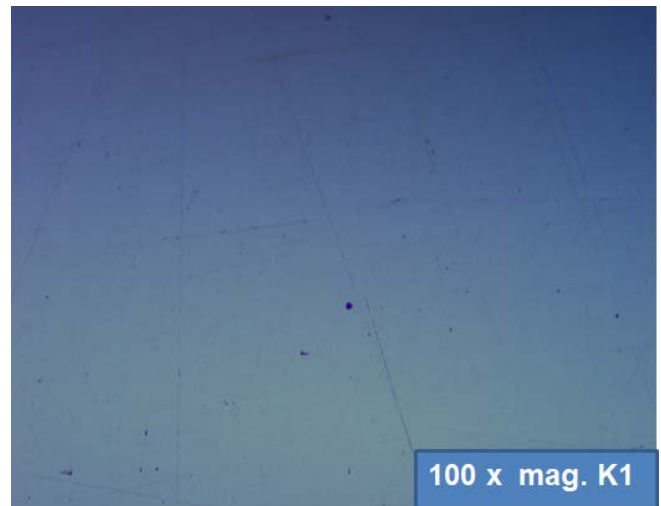


Figure 15. Test sample K1, material: steel 1.2343, polished with diamond paste 0.25 μm, magnification 100x

The results of measurement of the surface roughness are shown in the Table 1. From obtained results it can be seen that there are not significant differences in the surface roughness between specimens. This can be explained that inclusion – voids on the surface of the specimen are not an empty space. Each “black spot” on the surface is filled with metal oxide and during of the process of the polishing is levelled with the rest of the material. Because of this, the measurement of the surface roughness is not capable to distinct voids from metal surface.

Table 1. Masurement of the surface roughness

Samples	Ra (μm)	Rzmax (μm)
Surface polished with 0.25 μm polish paste		
<b>K 1</b>	0.05	0.32
	0.06	0.44
	0.04	0.35
<b>K 1.2</b>	0.05	0.38
	0.04	0.63
	0.07	0.78
Surface polished with 9 μm polish paste		
<b>K1</b>	0.08	1.12
	0.12	0.90
	0.1	1.10
<b>K2.1</b>	0.1	0.98
	0.12	1.1
	0.1	0.95

### 5. CONCLUSION

The surface comparison of the parts produced by DMLS from margining steel and parts produced by subtractive methods are presented in this paper.

From obtained results can be concluded that parts produced by DMLS has significant amount of the residues (inclusion, voids), on the surface. Those inclusions may have a big influence, in the tooling industry, on the quality of the injection molded parts, especially on the surface conditions.

Measurement of the surface roughness has not gave the clear distinction between parts produced by DMLS and parts produced conventional methods. From one side this is good, because, we may achieve on all parts same surface quality. On the other side, measurement of the roughness has not able to detect the existence of the inclusion on the part surface. The surface imperfections, in this case, may be detected only under the microscope.

In order to improve surface on the parts produced by DMLS, the micrography and metallography should be conducted. The influence of the parameters of the sintering process on the inclusion during part production should be considered.

Based on the presented results of the surface quality, the production of the tools and molds for the cosmetic parts by injection molding should be considered in the future.

### ACKNOWLEDGEMENTS

This research is part of a project that has received funding from the European Union’s Horizon 2020 research and innovation programme under the Marie Skłodowska-Curie grant agreement No 734455.

### REFERENCES

- [1] Bourell, D. L., et al. "A brief history of additive manufacturing and the 2009 roadmap for additive manufacturing: looking back and looking ahead." Proceedings of RapidTech (2009): 24-25.
- [2] Herderick, E. "Additive manufacturing of metals: A review." Materials Science & Technology (2011): 1413-1425.
- [3] Aliakbari, Mina. "Additive manufacturing: State-of-the-art, capabilities, and sample applications with cost analysis." (2012).
- [4] Adrián Bača, Radomila Konečná, Gianni Nicoletto, Ludvík Kunz, Influence of Build Direction on the Fatigue Behaviour of Ti6Al4V Alloy Produced by Direct Metal Laser Sintering, Materials Today: Proceedings, Volume 3, Issue 4, 2016, Pages 921-924, ISSN 2214-7853, <http://dx.doi.org/10.1016/j.matpr.2016.03.021>.

- [5] P. Edwards, M. Ramulu, Fatigue performance evaluation of selective laser melted Ti-6Al-4V, *Materials Science and Engineering: A*, Volume 598, 26 March 2014, Pages 327-337, ISSN 0921-5093, <http://dx.doi.org/10.1016/j.msea.2014.01.041>.
- [6] Yadollahi, Aref, et al. "Effects of building orientation and heat treatment on fatigue behavior of selective laser melted 17-4 PH stainless steel." *International Journal of Fatigue* (2016).
- [7] Sateesh, N. H., et al. "Microstructure and Mechanical Characterization of Laser Sintered Inconel-625 Superalloy." *Procedia Materials Science* 5 (2014): 772-779.
- [8] Kruth, Jean-Pierre, et al. "Part and material properties in selective laser melting of metals." *Proceedings of the 16th international symposium on electromachining*. 2010.
- [9] Leuders, S., et al. "On the mechanical behaviour of titanium alloy TiAl6V4 manufactured by selective laser melting: Fatigue resistance and crack growth performance." *International Journal of Fatigue* 48 (2013): 300-307.
- [10] Seifi, Mohsen, et al. "Process mapping, fracture and fatigue behavior of Ti-6Al-4V produced by EBM additive manufacturing." *Ti-2015: The 13th World Conference on Titanium*. 2016.
- [11] Ferreira, J. A. M., et al. "Assessment of the fatigue life on functional hybrid laser sintering steel components." *Procedia Structural Integrity* 1 (2016): 126-133.
- [12] Yasa, Evren, et al. "Microstructure and mechanical properties of maraging steel 300 after selective laser melting." *Solid Freeform Fabrication Symposium Proceedings*. 2010.
- [13] Kruth, Jean-Pierre, et al. "Binding mechanisms in selective laser sintering and selective laser melting." *Rapid prototyping journal* 11.1 (2005): 26-36.
- [14] Weingarten, Christian, et al. "Formation and reduction of hydrogen porosity during selective laser melting of AlSi10Mg." *Journal of Materials Processing Technology* 221 (2015): 112-120.
- [15] Simchi, A. "Direct laser sintering of metal powders: Mechanism, kinetics and microstructural features." *Materials Science and Engineering: A* 428.1 (2006): 148-158.
- [16] Brandl, Erhard, et al. "Additive manufactured AlSi10Mg samples using Selective Laser Melting (SLM): Microstructure, high cycle fatigue, and fracture behavior." *Materials & Design* 34 (2012): 159-169.
- [17] Zeng, Kai, Deepankar Pal, and Brent Stucker. "A review of thermal analysis methods in laser sintering and selective laser melting." *Proceedings of Solid Freeform Fabrication Symposium Austin, TX*. 2
- [18] Simonelli, Marco, et al. "A study on the laser spatter and the oxidation reactions during selective laser melting of 316L stainless steel, Al-Si10-Mg, and Ti-6Al-4V." *Metallurgical and Materials Transactions A* 46.9 (2015): 3842-3851.
- [19] Aboulkhair, Nesma T., et al. "On the formation of AlSi10Mg single tracks and layers in selective laser melting: Microstructure and nano-mechanical properties." *Journal of Materials Processing Technology* 230 (2016): 88-98

# Machining and Heat Treatment Effects on the Fatigue Properties of Maraging Steel Produced by DMLS

S. Ćirić-Kostić<sup>1</sup>, N. Bogojević<sup>1</sup>, A. Vranić<sup>1\*</sup>, D. Croccolo<sup>2</sup>, M. De Agostinis<sup>2</sup>, S. Fini<sup>2</sup>, G. Olmi<sup>2</sup>

<sup>1</sup>Faculty of Mechanical and Civil Engineering in Kraljevo, University of Kragujevac, Serbia

<sup>2</sup>Department of Industrial Engineering (DIN), University of Bologna, Bologna, Italy

*DMLS enables manufacturing of functional parts with complex shapes in a short time. This technology has some drawbacks: high manufacturing cost, residual stresses, and volume and surface imperfections. These problems can be solved by additional post processing (machining, heat treatment and shot peening), which increase manufacturing cost and time. There is an increasing interest towards the mechanical response of parts in the as-fabricated state. Being able to manage these parts, without the need for machining or heat treatment, would strongly increase the great potentials of this technology. The present study deals with the effect of machining and heat treatment (aging at the temperature of 490°C for 6 hours) on the fatigue response of DMLS Maraging steel parts, with vertical build orientation. Specimens have been manufactured according to ISO 1143 for fatigue tests under rotating four-point bending. The experimental campaign has been arranged as a 2-by-2 factorial plane, with a total amount of four treatment combinations. The first results, processed also by tools of analysis of variance, indicate that heat treatment has the greatest beneficial impact on the fatigue response and that even without machining a fatigue limit in the order of 25% of the ultimate tensile strength can be achieved.*

**Keywords: Fatigue strength, Maraging steel, Additive manufacturing, Direct Metal Laser Sintering, Aging heat treatment, Machining.**

## 1. INTRODUCTION

Additive Manufacturing (AM) process is based on layer manufacturing, without any additional tools or machining processes [1-4]. Direct Metal Laser Sintering (DMLS) and Selective Laser Melting are the two most important Additive Manufacturing technologies. Both of them are powder bed-based technologies.

Concept of layered built parts dates from more than one century. AM enables manufacturing without tools, using just one AM machine fed by a CAD model. CAD model is split into two-dimensional layers with constant thickness, by specific software. These layers can be regarded as areas that will be melted with thickness corresponding to the distance between layers (thickness of the layer). Every new layer is fused with the previous one during the AM process. Part is built, by repeating this process until the last layer is stacked.

There are several AM technologies that are divided, based on the type of material, how material is applied, fused etc. Powder Bed technology is based on material application on the entire building surface; afterwards, the laser or electron beam melts the area that corresponds to the sliced surface. The process is repeated, until part completion. Wire or powder feed technology is based on step-by-step material application and melting, forming the surface that correspond to the sliced layer. In this case, material is applied just to the surface that is being manufactured. A further classification of the AM techniques could be made, based on the principle of material melting (laser beam, electro beam, electro-arc etc.). In almost all the technologies for AM of metal parts, the material is completely melted and bonding between layers is achieved during solidification. DMLS and SLM are nowadays quite close technologies. Their different names mostly arise from different trademarks [5]. At the early stages of development of these technologies,

components after manufacturing were porous, density was not full due to partial fusion. The sintering process was different and material was based on Iron, Copper and Nickel alloy. Additional processing was needed to achieve better density and fusion [6,7].

AM technologies are used not only in industrial applications but also in the medical field. It is possible to use these technologies and material, to build custom implants. Using 3D CT scanners, it is possible to model implants that perfectly fit the person's need [8-10]. These materials have good bio-compatibility that gives them good potential for dental and medical purposes [11].

Since AM of metal parts is based on manufacturing of fully functional parts that can be built directly into machine, with minimal post processing, mechanical and physical characteristics of the built parts are of high importance. Layer based manufacturing provides characteristic microstructure of the built parts that is different than casted structure of the same material. In AM, material melting takes place on one plane (build plane), whereas the stacking direction is normal to this plane. Material melting and cooling rates are very high. Fast melting is the result of high energy concentration. Fast cooling arises from the small amount of melted material with low surrounding temperature. This high temperature gradient usually induces high residual stresses. Part building starts on thick steel plate (base-plate). Part can be built directly on the plate or with a support structure, generated between plate and part. Its purpose is part constraining, moreover it facilitates heat flow from the part during the scanning (melting) process. Support structure needs to be strong enough, to restrain any kind of deformation that residual stress can cause.

With casting technology, a much larger amount of material keeps heat accumulated for a longer period time. Melting and solidification of material is a slow process

\*Corresponding author: Faculty of the Mechanical and Civil Engineering, 36000 Kraljevo, Dositejeva 19, vranic.a@mfvk.kg.ac.rs

and involves the whole volume. For this reason, it is interesting to explore influence of layer manufactured structure on mechanical properties. Machine manufactures usually provide some data regarding the mechanical properties of AM built parts in the material datasheets [12]. However, these mainly deal with static properties, such as ultimate tensile strength, yield strength, hardness, mechanical characteristics after ageing etc.

Maraging steel is one of the most promising materials, for use in Additive Manufacturing [13]. Density of AM built parts are >90%. Hardness of AM built parts from maraging steel is similar to those made by conventional ways like casting. It has good mechanical characteristics and it can be a good candidate for high-carbon steel substitution. It is resistant to corrosion and crack initiation during tempering and it has good machinability [14-16]. It has a relatively high ultimate tensile strength (*UTS*) after the heat treatment, around 2000MPa. Thanks to its high *UTS*, it is a promising material to be used for complex structures exposed to high states of load. This becomes more attractive, considering that AM technologies gives the chance to build multi-part object as a single part [17]. Research contributions on the Fatigue limit (*FL*) and the fatigue strength (*FS*) of Maraging steel made by some of AM processes are quite limited, to the authors' best knowledge. This paper presents a follow-up of a previous research by the same authors [18].

Components produced by AM can have different orientation with respect to the stacking direction of the layers. The aim of the previous research was to explore the effect of build orientation on the fatigue strength of Maraging Steel samples built by DMLS EOS M280 machine. The obtained results indicate that part orientation did not have significant effect on *FS* and *FL*.

Literature studies dealing with orientation influence on the mechanical properties of the parts made by AM are few. Most of the research deals with the influence of orientation and additional post-processing on tensile strength [19-21]. Few papers are concerned with research on the part orientation effect on fatigue strength of Aluminium alloy [22-25], Inconel alloy [26] and Titanium alloy samples [27]. Review papers have been written, trying to collect all the technologies and all the available mechanical testing results [28]. However, a lack of consistency between the testing procedures and the obtained results can be noticed, when all these data are rounded together. Different technologies provide different results for same materials. This may be due to the lack of Standards in AM that define the parameters of the process, how building preparation of samples should be managed, etc.

There is an increasing interest in lowering down post-manufacturing expenses in AM, and in speeding up the process from design to installation. Sometimes, post processing is not possible, for instance, when treating lattice structures, cooling channels in injection moulds or in turbine blades. In particular, machining or shot-peening cannot be performed on internal surfaces. This was the main motivation that led to this study. This topic has been tackled experimentally: for this purpose, an experimental campaign has been arranged as a 2-by-2 factorial plane,

with a total amount of four treatment combinations as shown in Table 1, presenting four sample types, one for each of the treatment combinations.

Table 1: 2-by-2 research plan

<b>N</b> Not heat treated As Built	<b>M</b> Not heat treated Machined with 0.5mm allowance
<b>H</b> Heat treated As Built	<b>I</b> Heat treated Machined with 0.5mm allowance

As an extension of the previous research [18], this paper focuses on the effects of heat treatment and machining influence on *FS* and *FL*. Samples without machining, named "as built" underwent only shot peening as surface post processing.

## 2. MATERIALS AND METHODS

Testing procedure was based on ISO 1143 Standard for rotating bending fatigue testing [29]. Standard defines testing procedure, loads and specimen geometry. Specimens were designed with cylindrical smooth geometry with reduction at the gage cross section. Specimen geometry with uniform 6mm diameter at the gage the as smallest dimension purposed by the Standard, has been chosen as the best compromise, considering the high manufacturing costs. A drawing of the specimen is shown in Fig. 1. The specification regarding surface quality was not considered for the "as built" to properly account for the influence of machining.

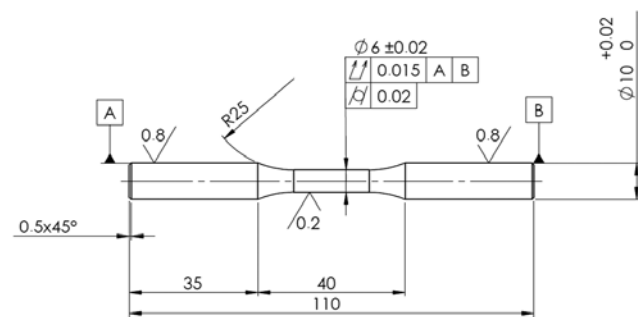


Figure 1: Specimen drawing with the 6mm diameter at gauge, according to the ISO 1143 standard

The specimens have been manufactured by M280 DMLS machine (EOS GmbH – Electro Optical Systems, Germany), equipped by Ytterbium fibre laser with 200W power and emitting 0.2032mm thickness and 1064nm wavelength infrared light beam [30]. Specimen material was MS1 maraging steel (EOS GmbH – Electro Optical Systems, Germany), equivalent to 1.2709 steel [31]. Chemical composition of the material is provided in Table 2. Specimen manufacturing was done in the processing chamber of the machine. The recoater applies material from the dispenser platform on building plate and takes excess material onto collector platform. Building starts on the base plate with working area of 250×250mm in horizontal plane and with maximum building height up to 325mm. Base plate was preheated to the temperature of 40°C.



Table 2: Chemical composition of MS1 Maraging Steel by EOS

	Fe	Ni	Co	Mo	Ti	Al	Cr	Cu	C	Mn	Si	P	S
%		17-19	8.5-9.5	4.5-5.2	0.6-0.8	0.05-0.15	≤0.5	≤0.5	≤0.03	≤0.1	≤0.1	≤0.01	≤0.01

Manufacturing process typically takes place in nitrogen inert atmosphere, generated from compressed air by nitrogen generator that is built inside machine. Process chamber consists of three platforms and recoater: The Dispenser platform, where material powder is contained, the Building platform, on which the base plate is set and building process is done, the Collector platform for the collection of excess material. Schematics of the building chamber is presented on Fig. 2

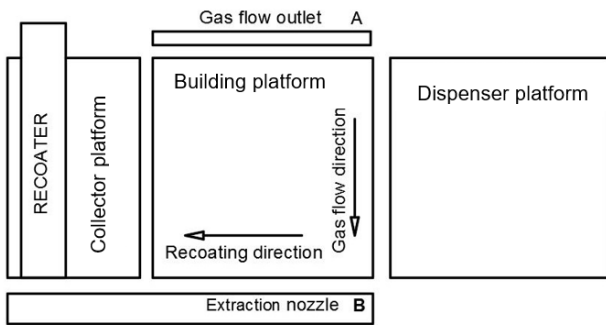


Figure 2. Process chamber schematics

Material is applied with 40µm thickness that corresponds to layer thickness for the MS1 Maraging Steel. Building parameters (laser speed, laser power, laser offset, layer thickness etc.) of the EOSINT M280 for MS1 sample manufacturing were kept constant. They were provided by the EOS as a predetermined set of parameters named "PERFORMANCE". This parameter set is a good compromise between good surface quality and manufacturing speed, for which EOS warrants mechanical characteristics of the built parts.

Scanning strategy was set in such way, where laser scans surface in parallel traces in one layer. For next layer, scanning strategy was rotated by an angle of 67°. For every layer, the contour of the scanned surface was finally rescanned, in order to get better surface quality. Example of the scanning process is shown in Fig. 3 a).

Specimens were built directly on the base plate, without using a support structure, Fig. 3 c). Proceeding this way, the surface quality of the as built specimens could keep unaffected by the support structure teeth traces on the surface. After building process, specimens were taken from the process chamber, cleaned from excessive powder by shot-peening, using stainless steel spherical shots with 400 µm diameter. Cutting off samples from the base plate was done by wire cutting with Electrical Discharge Machining (EDM).

Samples planned for heat treatment underwent age-hardening by heating in oven. Temperature was increased from room temperature to 490 °C in 1h, afterwards, they were kept at constant temperature for additional 5h (total 6h process). This heat treatment was particularly important for lowering or relaxing the residual stresses, which arise from AM process, thus enhancing fatigue response of the built specimens [32, 33]. Since these samples were built vertically, their geometry was not influenced by residual

stress. After heat treatment process, specimens were cooled to room temperature in fresh air. Shot-peening gave effect just in better surface quality and closing micro pores for as built samples. For heat treated samples surface hardening induced by plastic deformation was lost after ageing, due to relaxation of the compressive residual stresses induced by shot-peening. The effect of micro shot peening was also questionable for the machined samples, since allowance for machining was 0.5mm. There is large probability that the hardened surface following micro shot peening was removed upon machining. Finally, specimens planned for machining, underwent machining and refining by grinding with the aim of achieving the surface quality required by the ISO 1143 Standard and also to improve the fatigue performance [29].

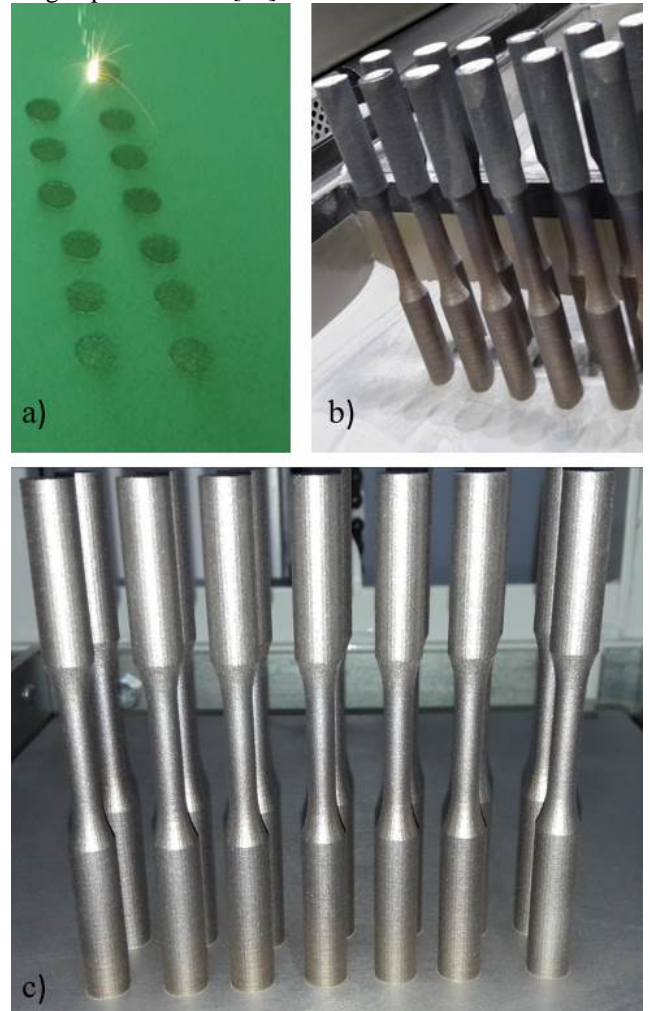


Figure 3. a) As Built specimens during scanning, b) Specimens cleaning from powder, c) Specimens after micro shot peening

For this research campaign, three sets of samples were built, all with vertical build orientation, with dog bone shape and shot peened. The first specimen set, type 1 (with additional age-hardening and machining with 0.5mm

allowance), was tested in the previous research campaign [18] and the related results were used here for comparisons. The second specimen set type M, for machined condition without age hardening, was built under the same conditions as the first one, with 0.5mm allowance for machining. The last two sets in the as built condition (one with age hardening, type H, the other without age hardening, type N) were built without any additional material allowance. Their surface roughness was lowered just by micro shot peening process.

Specimens were mounted on the testing rig, by tightening their heads into chuck collet, on both sides of the specimen Fig 4. Load was kept constant and bending moment was constant at gage during testing Fig. 5. The Testing rig, for four-point rotating bending was described in [18].

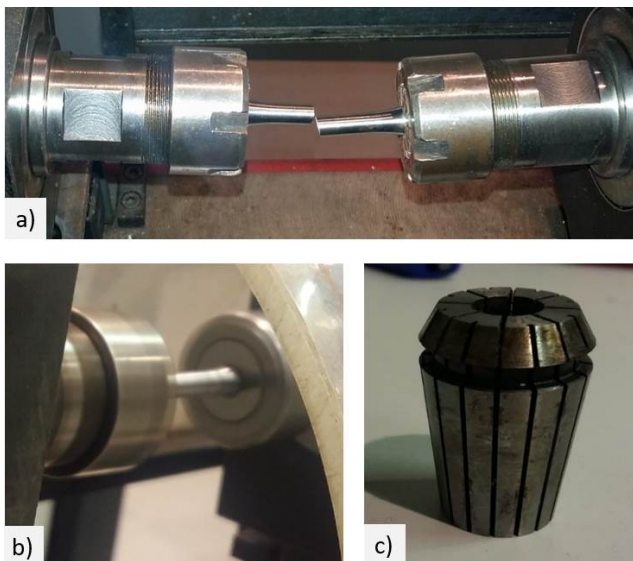


Figure 4. a) Clamped specimen after break,  
b) Specimen running,  
c) Chuck collet

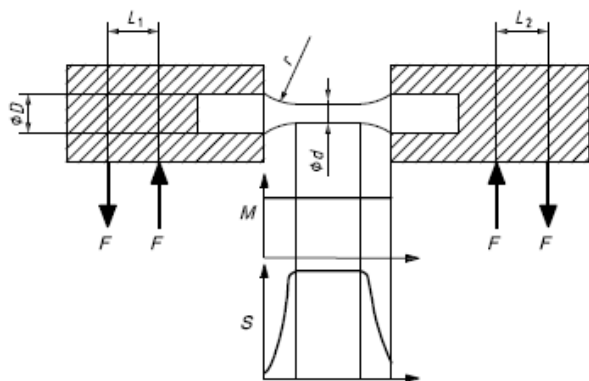


Figure 5. Load distribution

The specimens were tested until failure or until  $10^7$  cycles: in this case the specimen was marked as "RUN OUT". Each sample set consisted of 7 to 14 specimens. In the previous stage of the research, some samples were damaged during the manufacturing process, so they were not considered.

Using the aforementioned procedure, it was possible to obtain  $FL$  and the  $S-N$  curve for finite life domain. Fatigue limit was obtained by the Dixon stair-case method for small number of sample trials with failure or

non-failure outcomes [34]. Dixon method is a modified stair-case method that makes it possible to estimate  $FL$  even from small series of nominal trials (in this case four to seven). Standard deviation was estimated to estimate the uncertainty and to determine the confidence band for  $FL$ . ISO 12107 was used for processing data in finite life domain [35]. Data were linearly interpolated in logarithmic diagram. Upper and lower limits of the logarithmic curve were determined, based on the standard deviation of fatigue life, with the probability of failure of 90% for upper limit and 10% for lower limit and with the confidence level of 90%.

### 3. EXPERIMENTAL

All the samples have undergone geometry measurement, to check drawing requirements accomplishment. Diameter dimension and surface roughness have been measured at the head and gauge. For this purpose, a micrometre screw gauge, (with the resolution of 0.01mm) and a portable surface roughness tester (with the resolution of 0.01  $\mu\text{m}$ , Handysurf E-30A; Carl Zeiss AG, Oberkochen, Germany) have been used.

Diameter measurement checks have been done at two points at the heads, replicating measurement with  $90^\circ$  rotations at each point, for a total of eight replications, including both specimen heads. Diameter at the gauge was measured at three points, with two replications for each, by  $90^\circ$  rotation for an overall number of 6 replications.

Surface roughness on the both heads was measured at four points, with  $90^\circ$  angular spacing, with two replications, for a total number of eight replications per head. Surface roughness at the gauge was measured only after breakage, in same manner as at the heads, with eight replications per broken side. Specimens that survived testing, marked as run-out, were not measured for surface roughness at the gauge.

Average values of the diameter and surface roughness measurements are presented in Tables 3 to 6.

Table 3. Diameter and roughness measurement for sample type I

Specimen ID	Gauge diameter			Head diameter		
	Mean [mm]	ST. Dev. [mm]	Roughness [ $\mu\text{m}$ ]	Mean [mm]	ST. Dev. [mm]	Roughness [ $\mu\text{m}$ ]
1.1	6.00	0.004	0.248	9.93	0.004	0.26
1.2	6.00	0.004	0.470	9.93	0.000	0.21
1.3	6.00	0.000	0.447	9.93	0.000	0.29
1.4	6.01	0.000	0.395	9.93	0.000	0.20
1.5	6.00	0.004	/	9.92	0.000	0.31
1.6	6.01	0.000	/	9.93	0.000	0.22
1.7	6.00	0.000	/	9.93	0.007	0.27
1.8	6.00	0.004	0.697	9.93	0.000	0.30

Specimen types I and M are well consistent with the drawing requirements presented in Fig.1. Measurements indicate minor diameter deviations from the drawing specifications, according to ISO 1143, for specimen types H and N. Surface roughness values for the same specimen types were almost five times higher than specifications. It is reasonable, considering that these specimens were in as-built condition. Although these specimens did not satisfy surface roughness requirements, their testing was justified by the increasing demand for as-built parts and by the need for an estimation of their

fatigue response. After measurement procedure, fatigue tests were carried out, loading the samples under four-point rotary bending.

Table 4. Diameter and roughness measurement for sample type H

Specimen ID	Gauge diameter			Head diameter		
	Mean [mm]	ST. Dev. [mm]	Roughness [µm]	Mean [mm]	ST. Dev. [mm]	Roughness [µm]
H.1	6.05	0.004	4.063	10.09	0.017	4.90
H.2	6.06	0.015	4.700	10.10	0.012	4.95
H.3	6.06	0.008	4.055	10.07	0.010	5.02
H.4	6.06	0.011	3.738	10.10	0.015	4.55
H.5	6.05	0.004	3.769	10.09	0.004	4.13
H.6	6.06	0.008	/	10.08	0.010	5.50
H.7	6.06	0.008	/	10.09	0.017	4.78
H.8	6.05	0.003	/	10.09	0.013	4.30
H.9	6.05	0.006	4.000	10.08	0.014	4.70
H.10	6.08	0.005	4.195	10.11	0.019	4.67
H.11	6.04	0.012	5.614	10.09	0.006	6.38
H.12	6.05	0.014	3.714	10.07	0.014	4.55

Table 5. Diameter and roughness measurement for sample type N

Specimen ID	Gauge diameter			Head diameter		
	Mean [mm]	ST. Dev. [mm]	Roughness [µm]	Mean [mm]	ST. Dev. [mm]	Roughness [µm]
N.1	6.08	0.012	4.24	10.07	0.020	5.54
N.2	6.09	0.010	4.12	10.08	0.004	5.48
N.3	6.08	0.008	3.97	10.06	0.010	5.19
N.4	6.09	0.008	4.37	10.07	0.013	4.74
N.5	6.09	0.005	4.57	10.07	0.019	5.28
N.6	6.09	0.009	/	10.07	0.012	4.75
N.7	6.09	0.010	/	10.08	0.007	4.43
N.8	6.08	0.007	/	10.07	0.008	4.24
N.9	6.09	0.007	4.07	10.06	0.010	4.76
N.10	6.09	0.009	5.12	10.08	0.011	5.65
N.11	6.10	0.012	4.54	10.08	0.014	4.72
N.12	6.08	0.012	2.30	10.07	0.015	4.86
N.13	6.08	0.009	3.75	10.08	0.008	5.10
N.14	6.09	0.014	4.21	10.05	0.003	4.48

Table 6. Diameter and roughness measurement for sample type M

Specimen ID	Gauge diameter			Head diameter		
	Mean [mm]	ST. Dev. [mm]	Roughness [µm]	Mean [mm]	ST. Dev. [mm]	Roughness [µm]
M.1	5.99	0.006	0.753	10.01	0.003	0.24
M.2	5.99	0.009	0.544	10.02	0.002	0.94
M.3	5.99	0.007	0.701	10.02	0.001	0.29
M.4	5.99	0.005	0.694	10.04	0.058	0.95
M.5	5.99	0.008	0.748	10.01	0.002	0.94
M.6	5.99	0.006	/	10.02	0.002	0.30
M.7	5.99	0.007	0.765	10.00	0.005	0.29
M.8	6.00	0.004	/	10.02	0.002	0.36
M.9	6.02	0.005	/	10.01	0.002	0.94
M.10	5.99	0.005	0.714	10.02	0.002	1.03

Tightening was done in such a way that specimen heads could not revolve in any chance inside chuck collets. It was also important to avoid overtightening, otherwise superposition of the chuck collet pressure and load may have occurred, which is likely to result in some irregular results. After specimen was mounted, radial misalignment of the gage section was checked. Total misalignment

between spikes, was also checked for all samples during machining process. Testing was done under reversed bending load with stress ratio  $R=-1$  and with the frequency of 60Hz. Fractographic and micrographic analysis have been done as well for some samples, after the end of the testing campaign to examine fracture initiation and propagation areas.

4. RESULTS

The results of the testing campaign are collected in Tables 7 to 9. The Tables provide data regarding specimen ID, applied loads, nominal stress value at the gage, observed life and comment regarding the trial outcome. In particular, "Run-out" indicates that the specimen survived testing at given load after  $10^7$  cycles, whereas "Yes" indicates that failure occurred. In this case the number of cycle to failure is also reported.

Table 7. Test results for sample type I

Specimen ID	Load [N]	Stress [MPa]	Life [cycles]	Failure
1.1	211.9	699	2 277 295	Yes
1.2	201.6	665	3 374 203	Yes
1.3	180.5	596	6 090 458	Yes
1.4	158.9	524	-	Run-out
1.5	169.7	560	-	Run-out
1.6	169.7	560	-	Run-out
1.7	180.5	596	-	Run-out

Table 8. Test results for sample type H

Specimen ID	Load [N]	Stress [MPa]	Life [N]	Failure
H.1	211.8	699	85 768	Yes
H.2	184.9	610	120 572	Yes
H.3	157.4	520	127 820	Yes
H.4	103.0	340	-	Run-out
H.5	139.3	460	-	Run-out
H.6	148.6	490	-	Run-out
H.7	148.6	490	-	Run-out
H.8	157.4	520	-	Run-out
H.9	166.7	550	523 162	Yes
H.10	175.5	580	491 671	Yes
H.11	166.7	550	56 331	Yes
H.12	161.8	534	405 247	Yes

Table 8. Test results for sample type N

Specimen ID	Load [N]	Stress [MPa]	Life [N]	Failure
N.1	184.9	610	175 804	Yes
N.2	166.7	550	236 637	Yes
N.3	148.6	490	3 577 212	Yes
N.4	130.4	430	8 336 653	Yes
N.5	121.2	400	9 659 056	Yes
N.6	112.3	370	-	Run-out
N.7	121.2	400	-	Run-out
N.8	130.4	430	-	Run-out
N.9	139.3	460	8 069 582	Yes
N.10	130.4	430	-	Run-out
N.11	139.3	460	9 900 777	Yes
N.12	184.9	610	151 212	Yes
N.13	166.7	550	156 691	Yes
N.14	148.6	490	687 908	Yes

Table 9. Test results for sample type M

Specimen ID	Load [N]	Stress [MPa]	Life [N]	Failure
M.1	184.9	610	81 160	Yes
M.2	157.4	520	219 333	Yes

M.3	139.6	460	2 415 186	Yes
M.4	121.2	400	7 885 879	Yes
M.5	112.3	370	3 035 027	Yes
M.6	103.0	340	-	Run-out
M.7	112.3	370	7 879 073	Yes
M.8	103.0	340	-	Run-out
M.9	112.3	370	-	Run-out
M.10	121.2	400	5 662 050	Yes

Finally, each specimen was removed from the chuck collets and carefully examined for any irregularity.

5. DISCUSSION

The results of specimen testing presented in the previous Section were processed, to obtain the S-N curves in the finite life domain [35]. Curves trends with their upper and lower bounds for 90% confidence levels, obtained using linear regression method, are shown in Figures 6 to 9, using double logarithmic scale.

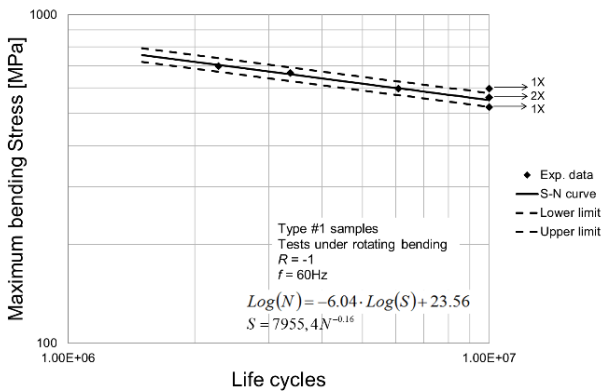


Figure 6. S-N Curve for sample type 1

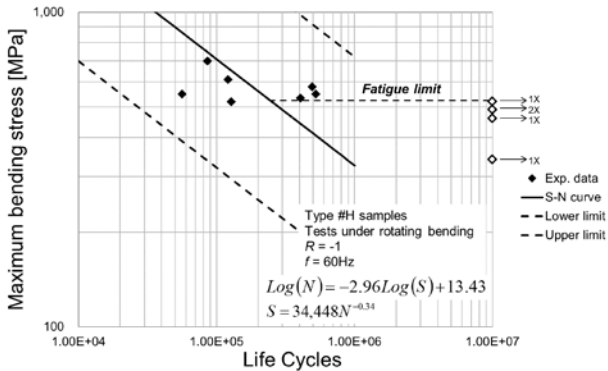


Figure 7. S-N Curve for type sample H

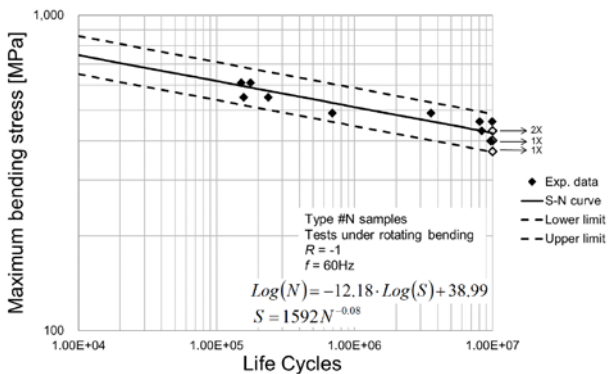


Figure 8. S-N Curve for sample type N

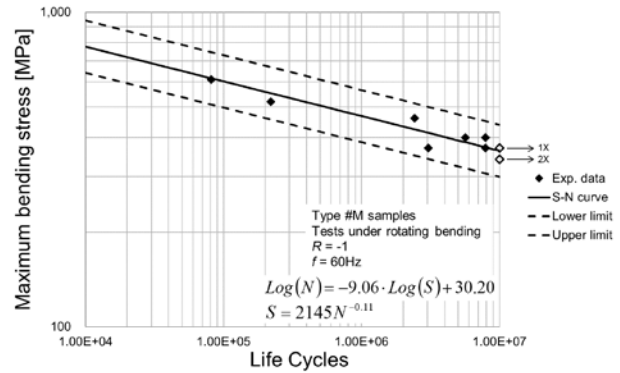


Figure 9. S-N Curve for sample type M

Details regarding specimen type, load ratio, testing frequency and the equation of the curve are also included in the same graphs. Run outs are marked with arrows on the graphs with indication of how many of them occurred at any load level. For all sample types, inclination angles between S-N curves and vertical axis were calculated. For sample type 1 the angle value it is 76°, for sample type H, it is 71°, for sample type N, 85° and for sample type M, 84°. Larger angle between the vertical axis and the S-N curve means that those sample types are more sensitive to load increase. For those sample types with smaller angle value, the number of cycles to failure decreases less with load increase. Change in load leads to smaller change in cycle number. Sample types N and M exhibit a higher sensitivity to load increase than sample types 1 and H. A reason for this can be influence of age hardening, their hardness should be increased from 33-37 HRC to 50-56 HRC [31]. Sample type H exhibited greater scattering of the results than the other three sample types, which can be seen in Fig. 7. Specimens experienced failures at the same or close load levels with considerable differences in life cycle numbers, which also affected the unusual S-N curve inclination. As an effect of these outcomes, the confidence band for this curve is particularly wide (much wider than the others), which will probably require to run further tests at the next stages of this research.

Fatigue limit for every sample type was obtained using Dixon stair case method, based on the retrieved series of failure, and not-failure outcomes.

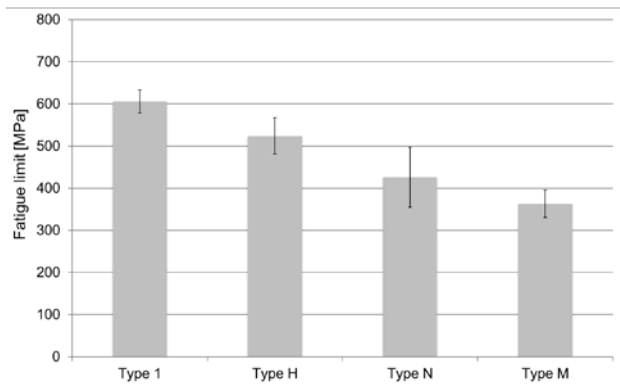


Figure 7. Fatigue limits with confidence bands

Fatigue limits for all sample types with their confidence band (95% confidence level) are presented in the bar graph in Fig. 7. The first two sample types underwent heat treatment, whereas the second two ones

were without heat treatment. The calculated value of *FL* for sample type 1 is 606MPa, for sample type H is 524MPa, for sample type N is 426MPa and for sample type M is 363MPa. These results indicate that heat treatment significantly enhances *FL*. *UTS* of MS1 maraging steel is 1100MPa in as the built condition, after hardening it is incremented up to 2050MPa, corresponding to almost 100% increase of *UTS*, following heat treatment [31]. Sample types 1 and H underwent hardening and their *FL* is respectively 29% and 25% of *UTS*. Sample types N and M were without hardening and their *FL* is indeed lower but respectively 39% and 33% of the corresponding *UTS* without heat treatment. These ratios are much lower than the commonly accepted ratios of *FL* over *UTS* of 50% for machined samples, but are in agreement with some literature research, when considering as built parts [38-39]. This is not surprising, due to the layered characteristic of specimens. Sample type N had greater *FL*, than machined sample type M. Both samples were without any heat treatment. First, it must be observed that the difference between type N and type M fatigue strengths is quite small: a statistical test, based on the Analysis of Variance and on the Fisher-test, indicated that these differences are not significant at the 5% significance level. Anyway, some possible reasons for unmachined samples having a better performance than machined ones is provided in the following. Sample types N had greater surface roughness than types M. This is possible outcome of shot peening which is known to have positive effect on *FL* [40].

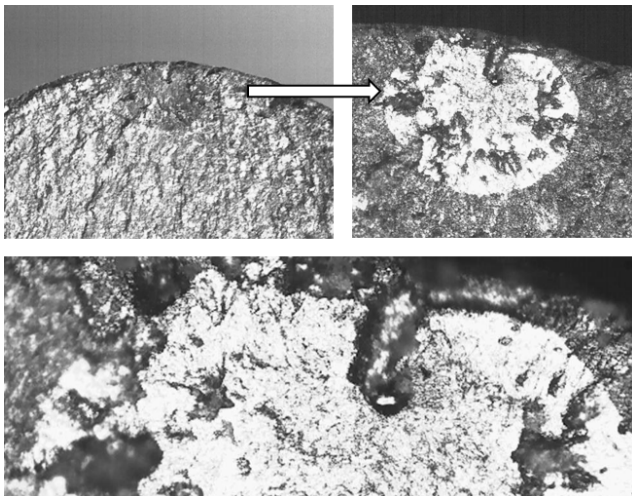


Figure 8. Pore in crack initiation zone, close to the surface for H.5 specimen

The surfaces of the sample types N were hardened by shot peening plastic deformation, and all micro pores were closed as a result of this process, conversely for sample type M, this effect is shadowed because of the machining. Machining also took possible irregularities and porosities inside material to surface, which are possible sources of premature crack initiations [27].

The previous statement can be confirmed by the many porosities and voids revealed during fractographic and micrographic analysis. During fractographic analysis of break surface of both sides of the broken sample, it was found that crack initiation and nucleation starts at one point on the surface or just beneath it, as shown in Fig. 8. Some amount of voids and inclusions were noticed on

fractured surface of all samples. It is indeed possible that voids or inclusions were responsible for crack initiation: most cracks seem to start from such defects. On all the samples, only one crack initiation point was noticed. There have been some doubts for as built samples, due to surface roughness influence (notch effect).

Fracture surface of as built samples without heat treatment showed coarse-grained structure.

Some specimens were cut, embedded into phenolic resin, and polished for micrographic analysis Fig.9.



Figure 9. Specimen preparation for micrography

Specimen surface was etched with combination of 150cc of water (H<sub>2</sub>O), 50cc of Chloridric Acid (HCl), 25cc of Nitric Acid (HNO<sub>3</sub>) and 1g of Calcium Chloride. Etching was done at room temperature for 70 seconds. It must be pointed out that laser scanning traces were visible both in longitudinal and in transverse sections, regardless of heat treatment execution.

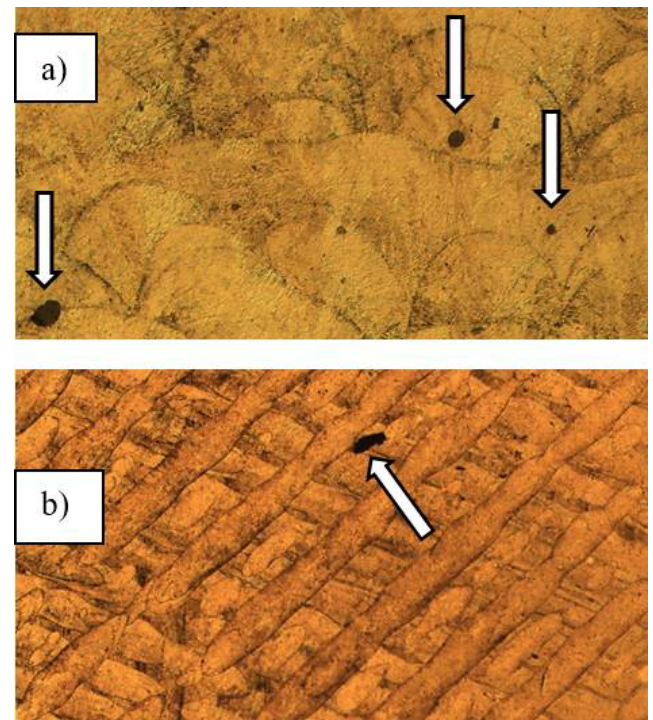


Figure 10. a) Longitudinal section of the N.2 specimen without heat treatment

b) Build plane section (normal to specimen axis)

Some inclusions were noticed and marked with arrows in Fig.10. Scanning pattern in build plane section Fig.10 b), shows some scanning traces underneath with rotation angles corresponding to the aforementioned angle of 67°. Specimens without heat treatment had more pronounced scanning traces than those that had undergone the heat treatment by age hardening (see Fig 11). This outcome indicates that heat treatment had some effect on

fusion of the laser traces but was not effective at completing deleting these traces. For all the four sample types a comparable amount of inclusion was observed. Heat treatment had no effect on the presence of porosities in material.

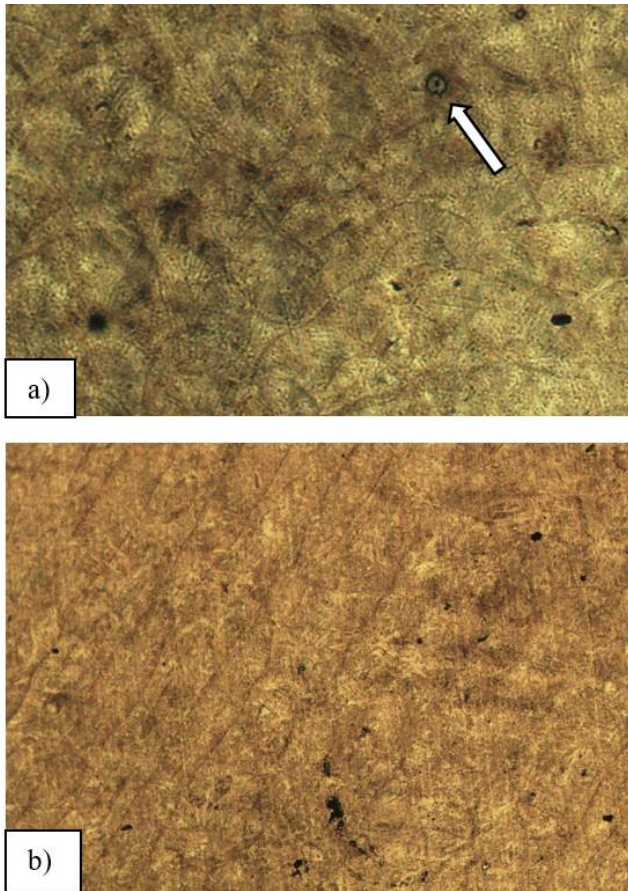


Figure 11. a) Longitudinal section of the specimen with heat treatment

b) Build plane section (normal to specimen axis)

## 6. CONCLUSION

This paper aims at a study on machining and heat treatment effects on fatigue limit and fatigue strength of Maraging Steel specimens manufactured by DMLS EOSINT M280 machine. Four sample sets were considered, all with vertical stacking direction during building. No deformation of the specimens as a result of residual stresses was observed. All the sets were shot peened as part of cleaning process. Two sets underwent machining procedure for 0.5mm allowance and two were left in the as built surface state. One machined and one as built set were heat treated by age hardening in oven. All sample sets were then tested under four point bending tested with  $R=-1$  load ratio at the frequency of 60Hz. All the experimental results were processed for the determination of  $S-N$  curves in the finite life domain and fatigue limits. The heat treated samples exhibited steeper  $S-N$  curve than the samples without heat treatment. Moreover, heat treated samples without machining exhibited a great result scattering that can be attributed to notch effect deriving from surface roughness. Anyway, this outcome will need further testing and investigations at the next stages of the research. Heat treated sample types had greater fatigue limits than samples without heat

treatment. Fatigue strength to ultimate tensile strength ratio for unmachined heat treated samples was around 25%, which is consistent with other research but lower than the corresponding ratios for the other two sample sets. In fact, when running comparative analysis, it must be noticed that the ultimate tensile strength for samples without heat treatment is almost one-half of the value for heat treated ones.

Machined samples without heat treatment had lowest ultimate tensile strength. A possible reason is that, following machining, pores, inclusions and micro cracks were brought to the surface and became source of micro stress concentration, thus inducing crack initiation and detrimentally affecting fatigue limit. In addition, the hardened surface obtained by plastic deformation (and the related compressive residual stress state) via shot peening was also taken away, which is not the case for as built sample without heat treatment, resulting in a greater fatigue limit.

in the future it could be possible to expand research with shot peening effect on machined samples after machining. In this way all the pores and microcracks brought to surface would be closed, the surface would be hardened by plastic deformation and a potentially beneficial compressive residual stress state could be induced.

## ACKNOWLEDGEMENTS

This paper represents a part of research performed within the project "Advanced design rules for optimal dynamic properties of additive manufacturing products - A\_MADAM", which received funding from the European Union's Horizon 2020 research and innovation programme under the Marie Skłodowska-Curie grant agreement No.734455.

Two of the authors (S. Ćirić-Kostić and A. Vranić) wish also to acknowledge the support of Ministry of Education, Science and Technology Development of Republic of Serbia through grants No.TR35006 and No.TR37020.

## REFERENCES

- [1] Bourell, D.L., Beaman, J.J., Leu, M.C. and Rosen, D.W., 2009. A brief history of additive manufacturing and the 2009 roadmap for additive manufacturing: looking back and looking ahead. *Proceedings of RapidTech*, pp.24-25.
- [2] Aliakbari, M. "Additive manufacturing: State-of-the-art, capabilities, and sample applications with cost analysis." (2012).
- [3] Pandey, P.M., 2010. Rapid prototyping technologies, applications and part deposition planning. Retrieved October, 15.
- [4] Herderick, E. "Additive manufacturing of metals: A review." *Materials Science & Technology* (2011): 1413-1425.
- [5] Shellabear, M., and O. Nyrhilä. "DMLS-Development history and state of the art." *Laser Assisted Netshape Engineering 4*, *Proceedings of the 4th LANE* (2004): pp. 21-24.

- [6] Campanelli, S.L., Contuzzi, N., Angelastro, A. and Ludovico, A.D., 2010. Capabilities and performances of the selective laser melting process. In *New Trends in Technologies: Devices, Computer, Communication and Industrial Systems*. InTech.
- [7] Naiju, C. D., M. Adithan, and P. Radhakrishnan. "An Investigation of Process Variables Influencing Fatigue Properties of Components Produced by Direct Metal Laser Sintering." *KMUTNB: International Journal of Applied Science and Technology* 4.1 (2011): pp. 63-69.
- [8] Parthasarathy, J., Starly, B. and Raman, S., 2011. A design for the additive manufacture of functionally graded porous structures with tailored mechanical properties for biomedical applications. *Journal of Manufacturing Processes*, 13(2), pp.160-170.
- [9] Jardini, A. L., M. A. Larosa, M. F. Macedo, L. F. Bernardes, C. S. Lambert, C. A. C. Zavaglia, R. Maciel Filho, D. R. Calderoni, E. Ghizoni, and P. Kharmandayan. "Improvement in Cranioplasty: Advanced Prosthesis Biomanufacturing." *Procedia CIRP* 49 (2016): pp. 203-208.
- [10] Jardini, A.L., Larosa, M.A., Maciel Filho, R., de Carvalho Zavaglia, C.A., Bernardes, L.F., Lambert, C.S., Calderoni, D.R. and Kharmandayan, P., 2014. Cranial reconstruction: 3D biomodel and custom-built implant created using additive manufacturing. *Journal of Cranio-Maxillofacial Surgery*, 42(8), pp.1877-1884.
- [11] Bertol, L.S., Júnior, W.K., da Silva, F.P. and Aumund-Kopp, C., 2010. Medical design: direct metal laser sintering of Ti-6Al-4V. *Materials & Design*, 31(8), pp.3982-3988.
- [12] <https://www.eos.info/material-m>
- [13] Brookes, K.J., 2016. Maraging steel for additive manufacturing—Philipp Stoll's paper at DDMC 2016. *Metal Powder Report*, 3(71), pp.149-152.
- [14] Yasa, E., Kempen, K., Kruth, J.P., Thijs, L. and Van Humbeeck, J., 2010, August. Microstructure and mechanical properties of maraging steel 300 after selective laser melting. In *Solid Freeform Fabrication Symposium Proceedings* (pp. 383-396).
- [15] Kempen, K., Yasa, E., Thijs, L., Kruth, J.P. and Van Humbeeck, J., 2011. Microstructure and mechanical properties of Selective Laser Melted 18Ni-300 steel. *Physics Procedia*, 12, pp.255-263.
- [16] Casalino, G., Campanelli, S.L., Contuzzi, N. and Ludovico, A.D., 2015. Experimental investigation and statistical optimisation of the selective laser melting process of a maraging steel. *Optics & Laser Technology*, 65, pp.151-158.
- [17] [https://www.eos.info/industries\\_markets/aerospace/engines](https://www.eos.info/industries_markets/aerospace/engines)
- [18] Crocchio, D., De Agostinis, M., Fini, S., Olmi, G., Vranic, A., Ciric-Kostic, S.: "Influence of the build orientation on the fatigue strength of EOS maraging steel produced by additive metal machine", *Fatigue and Fracture of Engineering Materials and Structures* 39 (5) (2016), pp. 637-647
- [19] Casati, R., Lemke, J.N., Tuissi, A. and Vedani, M., 2016. Aging Behaviour and Mechanical Performance of 18-Ni 300 Steel Processed by Selective Laser Melting. *Metals*, 6(9), p.218.
- [20] Gibson, I. and Shi, D., 1997. Material properties and fabrication parameters in selective laser sintering process. *Rapid Prototyping Journal*, 3(4), pp.129-136.
- [21] Baufeld, B., Van der Biest, O. and Gault, R., 2010. Additive manufacturing of Ti-6Al-4V components by shaped metal deposition: microstructure and mechanical properties. *Materials & Design*, 31, pp. S106-S111.
- [22] Edwards, P. and Ramulu, M., 2014. Fatigue performance evaluation of selective laser melted Ti-6Al-4V. *Materials Science and Engineering: A*, 598, pp.327-337.
- [23] Bača, A., Konečná, R., Nicoletto, G. and Kunz, L., 2016. Influence of build direction on the fatigue behaviour of Ti6Al4V alloy produced by direct metal laser sintering. *Materials Today: Proceedings*, 3(4), pp.921-924.
- [24] de Vree, W.K., 2016. On the influence of build orientation on the mechanical properties of direct metal laser sintered (DMLS) Ti-6Al-4V flexures.
- [25] Konečná, R., Kunz, L., Bača, A. and Nicoletto, G., 2016. Long fatigue crack growth in Ti6Al4V produced by direct metal laser sintering. *Procedia Engineering*, 160, pp.69-76.
- [26] Smith, D.H., Bicknell, J., Jorgensen, L., Patterson, B.M., Cordes, N.L., Tsukrov, I. and Knezevic, M., 2016. Microstructure and mechanical behavior of direct metal laser sintered Inconel alloy 718. *Materials Characterization*, 113, pp.1-9.
- [27] Brandl, E., Heckenberger, U., Holzinger, V. and Buchbinder, D., 2012. Additive manufactured AlSi10Mg samples using Selective Laser Melting (SLM): Microstructure, high cycle fatigue, and fracture behavior. *Materials & Design*, 34, pp.159-169.
- [28] Lewandowski, J.J. and Seifi, M., 2016. Metal additive manufacturing: a review of mechanical properties. *Annual Review of Materials Research*, 46, pp.151-186.
- [29] International Organization for Standardization ISO 1143:2010 (E) (2010) *Metallic Materials – Rotating Bar Bending Fatigue Testing*, International Organization for Standardization (ISO), Geneva, Switzerland.
- [30] [https://www.eos.info/systems\\_solutions/metal/system\\_s\\_equipment/eosint\\_m280](https://www.eos.info/systems_solutions/metal/system_s_equipment/eosint_m280)
- [31] [https://www.eos.info/material\\_m/werkstoffe/download/EOS\\_MaragingSteel\\_MS1.pdf](https://www.eos.info/material_m/werkstoffe/download/EOS_MaragingSteel_MS1.pdf)
- [32] Sanz, C. and Navas, V.G., 2013. Structural integrity of direct metal laser sintered parts subjected to thermal and finishing treatments. *Journal of Materials Processing Technology*, 213(12), pp.2126-2136.
- [33] Aboulkhair, N.T., Maskery, I., Tuck, C., Ashcroft, I. and Everitt, N.M., 2016. Improving the fatigue behaviour of a selectively laser melted aluminium alloy: Influence of heat treatment and surface quality. *Materials & Design*, 104, pp.174-182.

- [34] Dixon, W.J. and Massey, F.J., 1969. Introduction to statistical analysis (Vol. 344). New York: McGraw-Hill.
- [35] International Organization for Standardization ISO 12107:2003, "Metallic Materials – Fatigue Testing – Statistical Planning and Analysis of Data", International Organization for Standardization (ISO), Geneva, Switzerland, (2003)
- [36] Bunker, R. S. Innovative gas turbine cooling techniques. WIT Press, Southampton, UK, 2008.
- [37] Kasperovich, G. and Hausmann, J., 2015. Improvement of fatigue resistance and ductility of TiAl6V4 processed by selective laser melting. *Journal of Materials Processing Technology*, 220, pp.202-214.
- [38] Stoffregen, H.A., Butterweck, K. and Abele, E., 2014. Fatigue analysis in selective laser melting: review and investigation of thin-walled actuator housings. In *25th Solid Freeform Fabrication Symp.*
- [39] Niemann, G., Winter, H. and Hohn, B. R. (2005) *Maschinenelemente*, Springer-Verlag: Berlin Germany.
- [40] Olmi, G. and Freddi, A., 2013. A new method for modelling the support effect under rotating bending fatigue: application to Ti-6Al-4V alloy, with and without shot peening. *Fatigue & Fracture of Engineering Materials & Structures*, 36(10), pp.981-993.



# A Heuristic Approach to the Estimation of the Mass of the Waste Powder During Selective Laser Sintering of Polyamide PA2200

Zlatan Šoškić<sup>1\*</sup>, Simona Montanari<sup>2</sup>, Gian Luca Monti<sup>2</sup>, Michele Monti<sup>2</sup>

<sup>1</sup>Faculty of Mechanical and Civil Engineering in Kraljevo, University of Kragujevac, Kraljevo (Serbia)

<sup>2</sup>Studio Pedrini s.r.l, Bologna (Italy)

*Waste powder is part of the powder used during selective laser sintering that is not built into products and cannot be re-used. The amount of the waste powder influences the costs of the manufacturing. A part of the waste powder is the powder that remains attached to the products after their removal from the production chamber. The amount of the attached powder depends on many factors, and the estimation of the amount of the attached powder is a complex task.*

*This paper presents three methods for simple and fast, although not very accurate, estimation of the mass of the attached powder on the basis of calculation of mass of the products and the total mass of powder used during a production process. The results show that the methods may give a useful estimation of the mass of the waste powder in the long run if the products are not lightweight structures.*

**Keywords:** Additive manufacturing, Selective laser sintering, Manufacturing costs

## 1. INTRODUCTION

The topic of costs of the additive manufacturing (AM) technologies became of interest in late 1990s, after the AM technologies left laboratories and started becoming commercial manufacturing technologies. However, a common and comprehensive model of the manufacturing costs is not developed after two decades of the efforts made by expert teams, which usually consist of experts in economy and AM engineers and technicians as consultants. One of the important reasons for lack of the common cost model of AM technologies is variety of the AM technologies. Various AM technologies have different costs, so that limited experience of the consultants often translated to limited applicability of the cost models developed by the economic experts. An extensive overview of the cost models of the AM is recently given in [1].

The progress in the development of cost models consisted in expansion of the considered number of factors that influence the AM costs. The initial cost models [2] were based on experiences of injection moulding, and it considered only variable AM costs, including machine costs per part, labour costs per part and material costs per part. Such models neglected important aspects of AM technologies, such as ability for recycling of the used material and requirements for extensive post-processing. An important breakthrough in the development of cost models was separation of the AM costs to direct and indirect costs, which led to proper consideration of high overhead costs of the AM technologies [3]. Further step in the development of the cost models was extensive study of the energy consumption [4], which exposed importance of the proper treatment of the utilization of the capacity of the used machine [5]. Due to the complexity of the AM technology, the refinement of the AM cost model was performed by advance modelling of the AM technology process by the Event-driven Process Chains methodology. The model was first that considered post-processing as an important aspect of the AM technology and it was further used for activity based calculation of AM costs [6].

Further improvement of the cost model was development of an algorithm for calculation of the production time fraction for each of the parts in a single AM job [7]. The described study of the AM costs led to the state-of-the-art model of the selective laser sintering (SLS) technology costs [8], which considers recycling of the used powder. However, this model does not consider structure of the waste material costs in the SLS process.

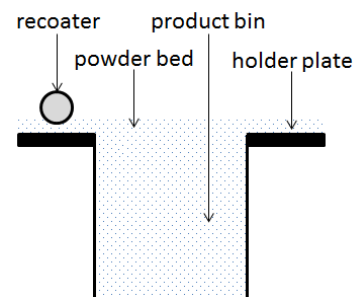


Figure 1: Part of a SLS production chamber where the powder resides

The waste powder represents a part of the powder that is not built into products, but still may not be used for recycling. There are two main sources of waste powder during SLS, the powder that remains in the production chamber after a production process, and the powder that remains attached to the products after they are taken out of the product bin.

The production process of AM technologies consists of sequence of processes of production of individual layers of the products. With the SLS technology, each of the layers is manufactured by melting of a thin layer of powder in the powder bed (Figure 1), which is closed inside the production chamber of a SLS machine. Before production of each of the layers, a small amount of the powder is brought to the production chamber, and the recoater of a SLS machine distributes uniformly the added powder over the top surface of the powder bed. After the production of a layer, a movable platform at the bottom of the product bin is lowered, and the manufactured layer is covered by the powder added for

manufacturing of the next layer. However, since the product bin is supported by a holder plate, the powder is also distributed over the surface of the plate. When the product bin is removed from the production chamber, the powder on the holder plate remains in the production chamber, and has to be removed by vacuum cleaner before a new production process is started. The amount of the powder that remains in the production chamber after a SLS production process is roughly constant, and represents a part of the fixed production costs.



Figure 2: Removal of waste powder by machines (left) [9] and hand tools (right) [10]

When a product of the SLS manufacturing is taken out of the production bin, an amount of the powder remains attached to it. Some of the attached powder is connected to the product by adhesion, but a part of the attached powder is closed in internal cavities, holes and openings within the products. The attached powder is removed by dusting and blasting using machines, but sometimes is required time-consuming removing by hand tools (Figure 2).

The amount of the attached powder is variable for each product and production process, and depends on many unpredictable factors. Some of the factors are of the objective nature, such as:

- shape, surface and volume of the product,
- quality and the composition of the powder,
- arrangement of products in the product bin,
- duration and regime of cooling of the product bin,
- quality of the manipulating equipment,

but some factors are of subjective nature, such as skill of the person who removes the powder and skill of the person who plans the spatial distribution of the products in the product bin. For that reason, even the processes that produce the same products, and with the same procedure, end up with different amounts of the waste powder.

The experience of research work (that will be presented later in the paper, see discussion of the results presented in the Figure 3) shows that the amount of the waste powder is in many cases even higher than the amount of the powder built in products and used for recycling, which inspired research presented in this paper.

## 2. MODELS

The total mass of the waste powder ( $W$ ) may be expressed as the sum of the mass of the powder that remains in the production chamber ( $C$ ) and the mass of the attached powder ( $A$ ):

$$W = C + A \quad (1)$$

Since the area of the holder plate ( $S$ ), the thickness of the powder bed ( $t$ ) and the density of the powder ( $d$ ) are known, the mass of the powder that remains in the production chamber may be calculated as:

$$C = S \cdot t \cdot d \quad (2)$$

On the other hand, as explained, the amount of the attached powder is almost impossible to calculate, and even very hard to estimate in general case. This conclusion calls for development of a methodology that may be "tuned" for specific cases, which may vary from SLS machine to SLS machine, from market to market, or even from company to company.

The nature of the problem calls for the *soft computing* techniques, which are applied to complex problems with many input variables that do not require high accuracy of solution. The soft computing techniques include fuzzy logic, evolutionary computation, machine learning and probabilistic reasoning. Since "tuning" of all of the aforementioned methodologies require substantial knowledge and understanding, in this paper we consider a simple heuristic approach that may be easily implemented in all cases.

Heuristic approach to problem, by Wikipedia, is "any approach to problem solving, learning, or discovery that employs a practical method not guaranteed to be optimal or perfect, but sufficient for the immediate goals. Where finding an optimal solution is impossible or impractical, heuristic methods can be used to speed up the process of finding a satisfactory solution. Heuristics can be mental shortcuts that ease the cognitive load of making a decision." While the most obvious examples of heuristics include using a rule of thumb, educated guesses, intuitive judgment, stereotyping, profiling and common sense, in the recent decades were discovered and studied many heuristic techniques [11][12] that humans use unconsciously, which shows the evolutionary importance of the techniques.

One of simple, but often used, heuristics is *one-reason-decision-making*, where a complex estimation is made by looking for *only one* "smart" predictor, and the estimation is based on that predictor. With the aim to select the "smart" predictor that will be used to estimate the mass of the attached powder, in this paper are studied various possible descriptors of SLS processes, which are based on masses of products and product bin after production.

The masses are selected as the "smart" predictors for two reasons. The first reason is practical, since masses are quantitative parameters that may be subjected to numerical methods of theoretical and experimental research. Furthermore, the masses may be calculated before the start of the production processes, and measured after the process. Therefore, selection of the masses as the predictor of the SLS process enables development of quantitative models and their application for prediction of the amount of the attached powder. The other reason for selection of the masses as the "smart" predictor is that mass of the products and the powder are connected to some parameters that affect the amount of the attached powder, such as the size of the products and, to a certain measure, even their shape and arrangement in the product bin. Of course, the masses are not connected to many of the remaining relevant parameters, and one cannot expect accurate predictions using one-reason-decision-making heuristic approach to such a complex problem. Based on the same input data (the masses of products and whole powder in the production bin), several different one-reason-decision-making methods may be proposed.

### 2.1. Absolute mass method

The first approach is to use raw input data, the calculated or measured mass of products ( $P$ ) and calculated or measured total mass of the product bin after production ( $T$ ), as the predictor variables. The mass of the products is calculated using the data about the volume of the products ( $V$ ), which may be taken from 3D modelling software, and the density of the products ( $w$ ).

$$P = V \cdot w. \quad (3)$$

The mass of the product bin after production consists of the mass of the empty bin ( $B$ ), the mass of products, and the mass of non-product powder ( $N$ ):

$$N = T - B - P. \quad (4)$$

The non-product powder consists of the attached powder and the powder that may be used for recycling, so that mass of the powder for recycling ( $R$ ) may be expressed as

$$R = N - A. \quad (5)$$

The simplest models based on the measured or calculated masses are based on the assumptions that the attached powder is proportional to the mass of products:

$$A = C_p \cdot P, \quad (6)$$

or to the mass of the mass of non-product powder

$$A = C_N \cdot N. \quad (7)$$

The heuristic approach here consists in translation of the common-sense statement CS1: "the more products you have, the more powder will be attached" to the sentence H1: "the higher mass of products, the higher mass of the attached powder is". The last sentence may be modelled by the differential equation:

$$dA = C_p \cdot dP, \quad (8)$$

which has the solution  $(A - A_0) = c_p(P - P_0)$ . Since without products ( $P_0 = 0$ ) there is no attached powder ( $A_0 = 0$ ), the common-sense statement CS1 is modelled by the equation (6). The critical step here, which introduces the heuristic error, is actually heuristic translation of the sentence CS1 to the sentence H1. While it is true that addition of another product to a production process always leads to increase of the amount of the attached powder, it is not always true that a production bin with higher mass of products will have higher amount of the attached powder in comparison with a production bin with smaller mass of products. In other words, various production bins with the same mass of products may have very different amounts of the attached powder. Hollow products, such as lightweight structures, contain substantially higher amounts of the attached powder than compact products.

A similar heuristics approach is applied to the derivation of the equation (7), where the common-sense statement CS2: "attached powder is a part of the non-product powder" is translated to the sentence H2: "the higher mass of the non-product powder, the higher mass of the attached powder is". The logical connection between the sentences is less obvious, and it has to be assessed from the aspect of comparison of two product bins that have similar products mass, but different non-product powder masses: in such a case, the higher non-product powder mass indicates larger volume of space within and between the products, which leads to higher amounts of the waste powder.

The heuristic constants  $C_p$  and  $C_N$  should account for the influence of numerous remaining factors that affect the amount of the attached powder. The constants should

be calculated using some exploitation data, and they may be applied for prediction of the attached powder if the other factors and exploitation conditions remain unchanged.

### 2.2. Relative mass method

The absolute mass method explicitly assumes proportionality between the masses of products and the attached powder, implying "scalability" of the model, which means that the model does not make differences in the prediction of the attached powder between small and large product volumes. In reality, the boundaries of the product bin and boundaries of the other products affect the amount of the powder that remains attached to a product. Therefore, it is possible to assume that the part of a product bin occupied by the products may be a valid predictor of the mass of the attached powder.

One way to estimate the part of a product bin occupied by the products is to calculate the ratio between the mass of the products and the total mass of the products and non-products, which is equal to the initial mass of powder ( $I$ )

$$I = P + N. \quad (9)$$

The ratio

$$p = P/I \quad (10)$$

represents the relative mass of the products ( $p$ ), and the ratio

$$n = N/I \quad (11)$$

represents the relative mass of the products ( $n$ ). Obviously, both  $p$  and  $n$  are positive and smaller than one, and it holds

$$p + n = 1. \quad (12)$$

If, using the heuristic approach, the common-sense sentence CS3: "The more space occupied by products, the more attached powder will be" is translated to the sentence H3: "The higher relative mass of products, the higher relative mass of the attached powder", then it may be modelled by the equation

$$a = c_p \cdot p, \quad (13)$$

where  $a$  stands for the relative mass of the attached powder,

$$a = A/I, \quad (14)$$

which serves as the estimator of the amount of the attached powder in this method.

By a similar heuristic approach the common-sense sentence CS4: "The more space occupied by non-product powder with the same space occupied by products, the more attached powder will be" is translated to the sentence H4: "The higher relative mass of products, the higher relative mass of the attached powder", then it may be modelled by the equation

$$a = c_n \cdot n, \quad (15)$$

The heuristic constants  $c_p$  and  $c_n$  may be also determined from the exploitation data, and used for prediction in the similar exploitation conditions.

### 2.3. Product-to-non-product ratio method

The previous methods reveal that the common-sense cases may be made both for the assertion that the mass of products increases the mass of the attached powder and the assertion that mass of non-products increases the mass of the attached powder. On the other

hand, considering one product bin, the increase of the mass of products means decrease of the mass of non-products and vice versa, so it is clear that one of the masses may hardly be the "smart" predictor that is looked for.

Another heuristic approach to the problem may be to characterize a production process (and a production bin) by the ratio between the mass of products and mass of non-product powder in the product bin ( $\Pi$ ):

$$\Pi = P/N = p/n. \quad (16)$$

The advantage of the approach is that it combines two input factors (masses of products and non-product powder) into a single predictor. The predictor is called *the product-to-non-product ratio* (abbreviated as PNPr) in this paper. The PNPr predictor may be connected to the characteristic arrangements that arise in practice: hollow and lightweight structures are characterized by small values of PNPr, and compact packaging of products are characterized by high values of PNPr. The problem with PNPr is that in both of its extreme cases (low and high values of PNPr) the amount of the attached powder is high, so it is clear that a simple linear dependence between the attached powder and PNPr may not be established.

Using an analogy (that is also a heuristic technique) to the methods of absolute and relative masses, an estimator of the amount of the attached powder may be introduced

$$\alpha = A/P = a/p, \quad (17)$$

which may be related to the PNPr. The indicator  $\alpha$  will be called in this paper *the attached-to-product ratio* (abbreviated as APr).

A heuristic approach applied in this method is more complex because the selected predictor is more complex. If the extreme cases of the lightweight structures and highly compact packaging are omitted, than the higher values of PNPr generally indicate products with smaller amounts of cavities and channels, therefore smaller amount of the powder attached to products of the same mass, which, in turn, means that the APr will decrease. Therefore, the previous reasoning may be expressed by the common-sense sentence CS5: "The products with less holes, cavities and channels have less attached powder", which may be, using heuristics, translated into the sentence H5: "Increase of the PNPr leads to the decrease of the APr". The sentence may be mathematically modelled in different ways, and here will be modelled by the equation:

$$\frac{d\alpha}{\alpha} = -n \cdot \frac{d\Pi}{\Pi}, \quad (18)$$

which means that the relative reduction of the attached powder is proportional to the relative increase of the attached powder. This model is selected because it was noted in the practice that, from the aspect of the amount of the attached powder, "more empty" production bins are more sensitive to addition of new products in comparison to "more full" production bins. The explanation is that a part of the powder that will be attached to a new product is in "more full" production bins already attached to other products. The solution of the equation (18) is

$$\alpha = \frac{\alpha_{PN}}{\Pi^n}, \quad (19)$$

where  $\alpha_{PN}$  represents the APr of the production processes with product mass equal to the non-product powder mass ( $P = N$ ), when  $\Pi = 1$ . As it was the case with the previous methods, the heuristic constants  $\alpha_{PN}$  and  $n$  should be determined using the existing exploitation data.

### 3. DATA

The proposed heuristic approaches are tested by the estimation of the waste powder in the "3D Impulse" SLS facility of the Faculty of Mechanical and Civil Engineering in Kraljevo of University of Kragujevac. The facility uses EOS Formiga P100 machine, and the dataset under study were the results of 186 production processes performed for various purposes, predominantly for the rapid prototyping applications. The selected processes were performed with the PA2200 polyamide powder, using the process parameters recommended by the manufacturer of the machine.

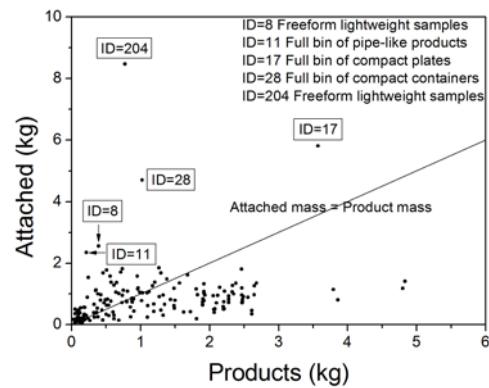


Figure 3: The masses of the products and the attached powder of the whole dataset

The mass of the powder that remains in the production chamber was calculated using the equation (2), and the obtained result was  $C = 580$  g. The weight of the empty product bin was measured to be  $B = (6450 \pm 5)$  g. The mass of the product bin after the production, the mass of the product bin after the removal of the parts with the attached powder, and the mass of the products were measured using an electronic stand with measurement error smaller than 5 g, and the obtained results were used for calculation of the non-product powder mass and the mass of the attached powder.

The mass of the attached powder was less than 2 kg in 181 of the production processes, and the relative mass of the attached powder was less than 30% in the 182 of the production processes. The masses of the products and the attached powder of the whole dataset are shown in the Figure 3, with the indicated data points that represent the production processes that had mass of the attached powder higher than 2 kg. In the inset are written explanations about the products manufactured in the five indicated processes. In two of the cases (production processes with ID numbers 8 and 204) the manufactured products were freeform lightweight structures that were manufactured for education and promotion purposes. In the three remaining indicated cases (production processes with ID numbers 11, 17 and 28), the manufactured products had the shapes that enabled compact arrangement of the products inside the product bin. An example of the compact arrangement of the manufactured products is given in the Figure 4, where

the products were containers with dimensions suitable for stacking. Therefore, all of the indicated cases did not satisfy the assumptions of the heuristic models, and they were excluded from further consideration.

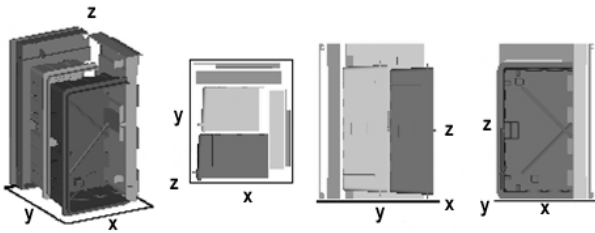


Figure 4: The arrangement of products in the product bin in a case of high mass of the attached powder due to the compact arrangement of products

The distribution of the mass of the attached powder versus the products and non-product powder masses for the remaining 181 production processes is shown in the contour diagram shown in the Figure 5.

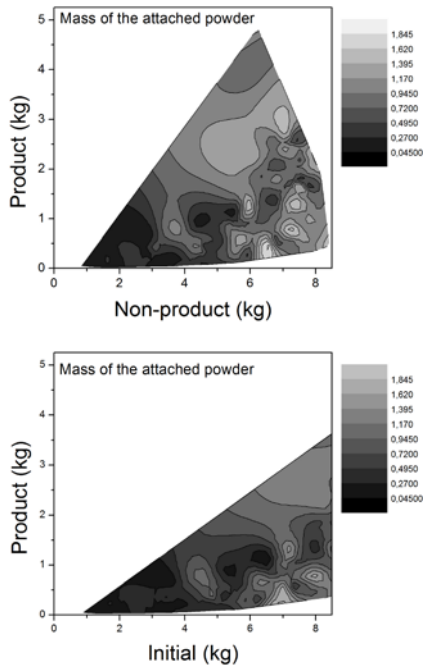


Figure 5: Contour plot of the masses of the attached powder vs. products and non-product powder masses (top diagram) and vs. products and initial powder masses (bottom diagram) of the dataset

Since the light colours in the used grey-scale scheme indicate higher amounts of the attached powder, the Figure 5 indicates that the lowest values of the attached powder mass occurs with small masses of products in small production volumes, while the largest masses of the attached powder are found in production processes with small masses of products and large masses of non-product powder.

#### 4. RESULTS

The presented data were tested against the models presented in the section "Models" of the paper.

##### 4.1. Absolute mass method

Figure 6 shows the exploitation data (points) presented according to the absolute mass methods, using

the products mass, in the top diagram, and non-product powder mass, in the bottom diagram.

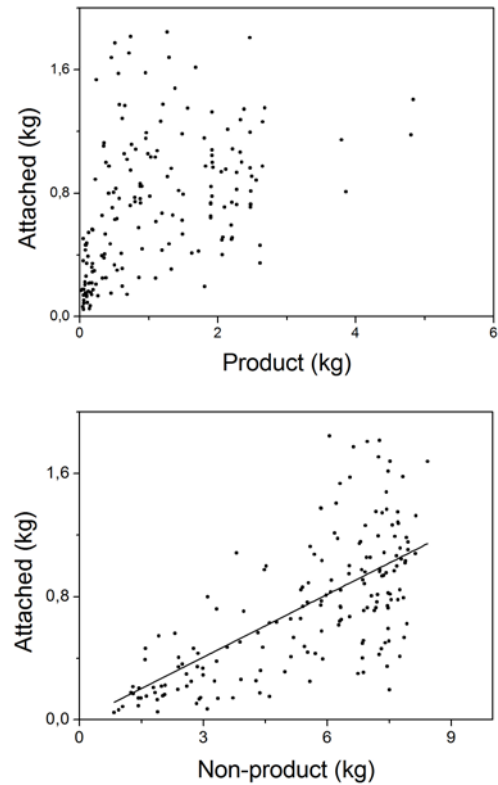


Figure 6: The results of the analysis of the exploitation data according to the absolute mass methods using the equation (6), at top, and (7), at bottom

Even the visual inspection of the diagrams in the Figure 6 suggests that products mass cannot be a predictor of the attached powder mass. The conclusion is confirmed by the calculation of the correlation coefficients between the considered quantities: the correlation coefficient between the products mass and the attached powder mass ( $r_{AP}$ ) is not strong,  $r_{AP} \approx +0.41$ , indicating positive weak correlation between the products mass and the attached powder mass. That means that, while in many cases higher products mass appears along higher mass of the attached powder, there are still many cases when higher products mass appears along lower mass of the attached powder. Therefore, the translation of the CS1 to H1 is often incorrect, and calculation of the attached powder mass using the equation (6) is not justified.

On the other hand, the correlation coefficient between the non-product powder mass and the attached powder mass ( $r_{AN}$ ) is substantially higher,  $r_{AN} \approx +0.69$ , indicating a stronger positive correlation between the products mass and the attached powder mass. That means that in a substantial number of cases higher non-product powder mass appears along higher mass of the attached powder, so there is evidential support for the CS2, and even, to some extent, to the translation of the CS2 to H2. By linear regression of the exploitation data to equation (7), the value  $C_N = 0.135 \pm 0.005$  is obtained, and the coefficient of determination (COD) of the regression is 0.86.

#### 4.2. Relative mass method

Figure 7 shows the exploitation data (points) presented according to the relative mass methods, using the relative products mass, in the top diagram, and the relative non-product powder mass, in the bottom diagram.

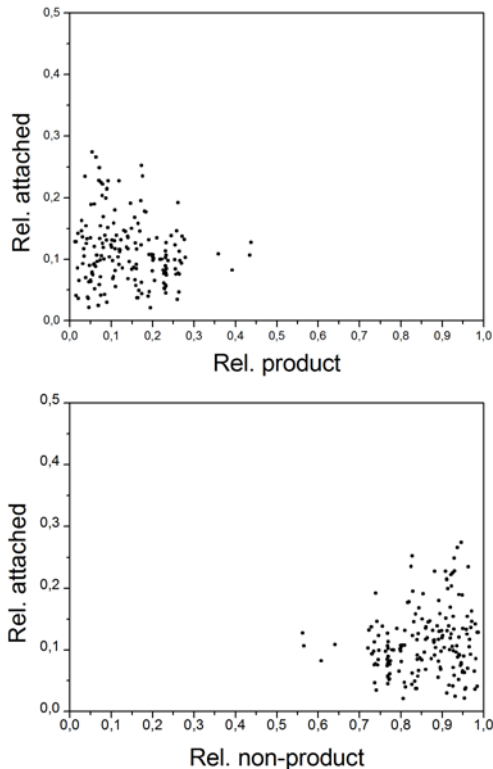


Figure 7: The results of the analysis of the exploitation data according to the absolute mass methods using the relative product mass (top), and relative non-product mass, (bottom)

The visual inspection of the diagrams in the Figure 7 clearly suggests that relative product mass, nor relative non-product mass, may be predictors of the relative attached powder mass. The conclusion is confirmed by the calculation of the correlation coefficients between the considered quantities.

The correlation coefficient between the relative product mass and the relative attached powder mass ( $r_{ap}$ ) is negative and small,  $r_{ap} \approx -0.18$ , indicating a very weak negative correlation between the relative products mass and the relative attached powder mass. That means that higher relative product mass appears a bit more often with lower than with higher relative masses of the attached powder.

Similar holds also for the correlation between the relative non-product mass and the relative attached powder mass, since the correlation coefficient ( $r_{an}$ ) is positive and small,  $r_{an} \approx +0.18$ , indicating a very weak positive correlation between the relative non-product mass and the relative attached powder mass. That means that higher relative non-product mass appears a bit more often with higher than with lower relative masses of the attached powder.

Therefore, the heuristic translations of both CS3 to H3 and CS4 to H4 are incorrect, so models proposed by the equations (13) and (14) are not valid.

#### 4.3. Product-to-non-product ratio method

As it was explained in the section „Models“, the connection between the PNPr and the amount of the attached powder is complex, and it is illustrated in the Figure 8, which shows exploitation data in the attached-to-the-non-product ratio vs. PNPr diagram (at top) and the relative product mass vs. PNPr diagram (at bottom).

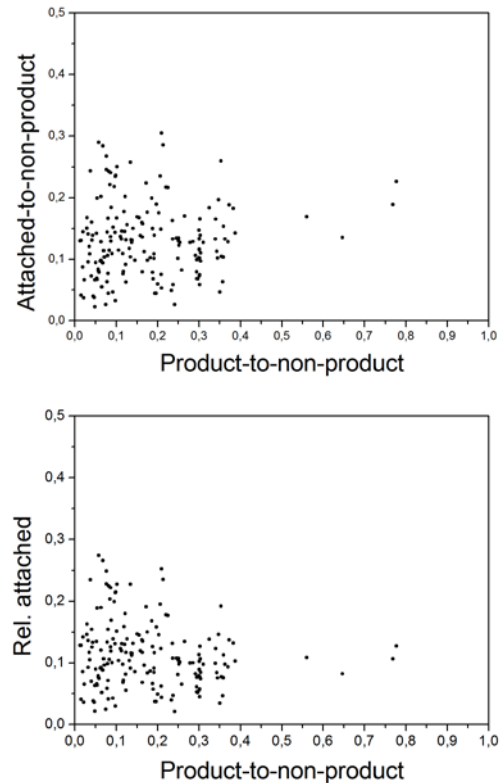


Figure 8: The exploitation data presented in the attached-to-the-non-product ratio vs. PNPr diagram (at top) and the relative product mass vs. PNPr diagram (at bottom)

The correlation between the attached-to-the-non-product ratio and PNPr is very weak and negative, with the coefficient of correlation being  $r_{81} \approx -0.17$ , and the correlation between the relative product mass and PNPr practically does not exist, with the coefficient of correlation being only  $r_{82} \approx +0.06$ .

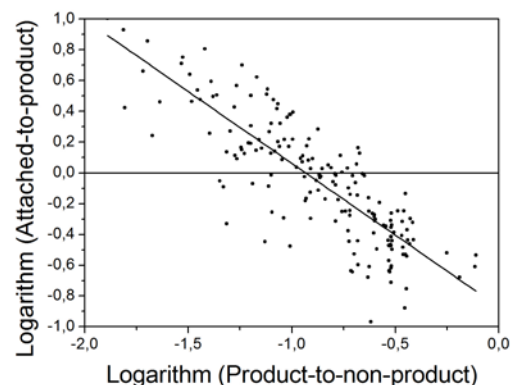


Figure 9: The exploitation data presented in the log-log diagram of APPr vs. PNPr ratio

For the analysis of the product-to-non-product ratio method, the exploitation data are presented in the form of log-log diagram of APPr vs. PNPr ratio in the Figure 9. The equation (19) may be re-written in the form

$$\log \alpha = \log \alpha_{PN} - n \log \Pi, \quad (20)$$

which shows that the heuristic model based on the PNPr predicts a linear form of the APr versus PNPr log-log diagram.

The coefficient of correlation between the quantities shown in the Figure 9 is  $r_9 = -0.86$ , which shows strong negative correlation between the two quantities, further supporting the heuristic translation of the CS5 to H5 and model represented by the equation (19). If the data in the APr versus PNPr log-log diagram are fitted to the equation (20), the values  $\log \alpha_{PN} = (-0.87 \pm 0.05)$  and  $n = (0.93 \pm 0.05)$  are obtained, with the coefficient of determination (COD) close to 0.70. Therefore, the fitting procedure predicts that the  $\alpha_{PN} \approx 0.135$ .

### 5. ANALYSIS

The results presented in the section "Results" of the paper, and summarized in the Table 1, show that two of the proposed models may explain correlation between the mass of the attached powder and the masses of products and non-products. The first model is the absolute mass model that predicts the attached mass on the basis of the mass of non-product powder using the equation (7) with value  $C_N = 0.135$ . The second model is the PNPr model that predicts the APr on the basis of the PNPr using the equation (19) with values  $\alpha_{PN} = 0.135$  and  $n = 0.93$ .

Table 1: Correlation between the predictors and estimators

Heuristic predictor	Attached powder estimator	Correlation coefficient
Product mass	Attached mass	+0.41
Non-product mass	Attached mass	+0.69
Rel. product mass	Rel. attached	-0.18
Rel. non-product	Rel. attached	+0.18
Product-to-non-product ratio	Rel. attached	-0.17
Product-to-non-product ratio	Attached-to-non-product	+0.06
Logarithm of product-to-non-product ratio	Logarithm of attached-to-non-product ratio	-0.84

It may be shown that the PNPr model reduces to the absolute mass model if it is assumed that  $n \approx 1$ . Actually, the identity  $\alpha_{PN} = C_N$  holds because of the definitions of the two quantities

$$\alpha_{PN} = \left( \frac{A}{P} \right)_{(P=N)} = \frac{A(P=N)}{P(P=N)} = \frac{A(P=N)}{N(P=N)} = C_N, \quad (21)$$

and if it is assumed the  $n \approx 1$ , then

$$\alpha = \frac{\alpha_{PN}}{\Pi^n} = \frac{\alpha_{PN}}{\Pi} \Rightarrow \frac{A}{P} = \frac{C_N}{\frac{P}{N}} \Rightarrow A = C_N \cdot N. \quad (22)$$

With the aim to estimate the difference between the two methods, the amounts of the attached powder predicted by the two methods are calculated using the equation (7) and the equation

$$A = C_N P \left( \frac{N}{P} \right)^n, \quad (23)$$

which may be derived from the equations (19) and (21). The obtained results are used to calculate two measures of the quality of prediction:

- the prediction of the amount of the attached powder in subsets of the initial dataset; the total amount of the attached powder is essentially the business relevant quantity, because it measures the overall quality of predictions;
- the average relative error of the prediction over the whole dataset, which measures the quality of individual predictions;

The results of the calculations are shown in the Table 2, and they show that the absolute mass method has better prediction of the overall waste.

Table 2: Relative error of prediction of the attached powder in the subsets of the dataset

Subset boundaries	Absolute mass method	PNPr method
1-30	18%	32%
31-60	19%	6%
61-90	2%	7%
91-120	6%	15%
121-150	4%	16%
151-181	10%	6%
Average	10%	14%

The average relative error of the individual predictions is 53% for of the absolute mass method, and 46% for the PNPr method.

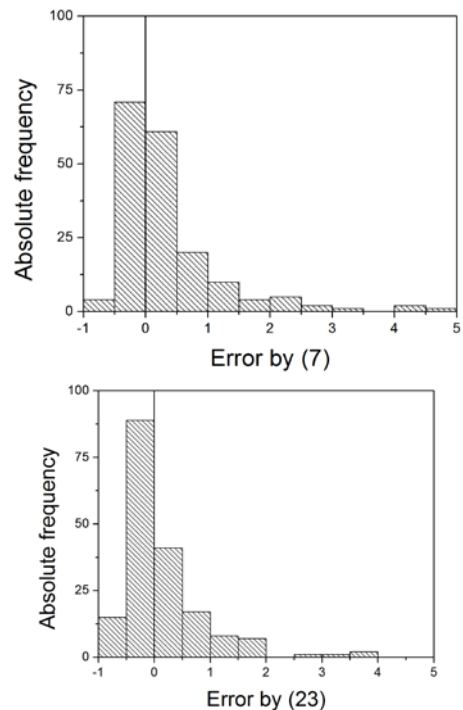


Figure 10: The distribution of errors of the absolute mass method (top) and the PNPr method (bottom)

The explanation for the apparent discrepancy in the estimation of the quality of the methods (although the PNPr method has better predictions for individual production processes, the absolute mass method has better overall prediction) is that the PNPr method mainly underestimates the amount of the attached powder, while the absolute mass method has better balance between the overestimation and underestimation of the estimated quantity. The distribution of errors of the absolute mass method and the PNPr method are presented in the Figure 10, which illustrates the much larger asymmetry of

the predictions of the PNPr method in the relative error range (-0.5, 0.5), where the majority of the errors belong.

## 6. CONCLUSION

The paper presented a study of possibilities to develop simple methods for estimation of the amount of powder that remains attached to products after manufacturing by SLS technology. The study analysed the data about 181 manufacturing process obtained during exploitation of the EOS Formiga P100 machine using the PA2200 powder in "3D Impulse" laboratory of the Faculty of Mechanical and Civil Engineering in Kraljevo.

Three groups of methods for prediction of the mass of the attached powder were developed. Using a heuristic approach "one characteristic of the production process may be sufficient to roughly estimate the mass of the attached powder", each of the methods uses just one predictor quantity that is calculated on the basis of masses of products and the non-product powder in a production process. On the basis of a heuristic reasoning, which used common-sense statements about the selected predictors, for each of the methods were developed mathematical models for prediction of the mass of the attached powder.

The models were tested against the exploitation data, and the results show that only two methods:

- an absolute mass method model, based on the proportionality of the non-product powder mass, as predictor, and the mass of the attached powder, as estimator, expressed by equation (7), and
- a PNPr method model, based on ratio between the masses of the products and non-product powder, as predictor, and the ratio between the attached powder and the product mass, as the estimator, expressed by the equation (19),

show significant correlation between respective predictor and estimator. The absolute mass method is simpler and has better prediction of the overall mass of the attached powder, but the PNPr has slightly better predictions of the mass of the attached powder of the individual production processes.

Due to the large errors of estimations of both methods, the conclusion of the research is that the heuristic approach to the calculation of the waste powder in SLS processes may be used in commercial purposes for long-term estimations of the waste powder, using the method described by the equations (1), (2) and (7). In the case of the PA2200 powder and EOS Formiga P100 machine, the long-term estimation of the waste powder of a production process is obtained by summing the fixed part of the waste powder, with mass 580 g, with the variable part of the waste powder, which is, with long-term accuracy of the order of 10%, estimated as 13.5% of the mass of the non-product powder of a production process.

Further research will be oriented toward extension of the analysis to wider set of input quantities, such as the surface of the products and the volumes occupied by products and non-product powder.

## ACKNOWLEDGEMENTS

This paper represents a part of research performed within the project "Advanced design rules for optimal

dynamic properties of additive manufacturing products – A\_MADAM", which received funding from the European Union's Horizon 2020 research and innovation programme under the Marie Skłodowska-Curie grant agreement No 734455. One of the authors (Z.Š.) wishes also to acknowledge the support of Ministry of Education, Science and Technology Development of Republic of Serbia through grant No. TR37020.

## REFERENCES

- [1] G. Costabile, M. Fera, F. Fruggiero, A. Lambiase, and D. Pham. "Cost models of additive manufacturing: A literature review." *International Journal of Industrial Engineering Computations* 8, no. 2, pp. 263-283 (2017)
- [2] Neil Hopkinson and P. Dicknes. "Analysis of rapid manufacturing—using layer manufacturing processes for production." *Proceedings of the Institution of Mechanical Engineers, Part C: Journal of Mechanical Engineering Science* 217, no. 1, pp.31-39, (2003)
- [3] M. Ruffo, C. Tuck & R. Hague, "Cost estimation for rapid manufacturing-laser sintering production for low to medium volumes". *Proceedings of the Institution of Mechanical Engineers, Part B: Journal of Engineering Manufacture*, 220(9), 1417–1427 (2006)
- [4] Martin Baumers, "Economic aspects of additive manufacturing: benefits, costs and energy consumption." PhD dissertation, Loughborough University (2012)
- [5] Ruffo, M., and Richard Hague. "Cost estimation for rapid manufacturing' simultaneous production of mixed components using laser sintering." *Proceedings of the Institution of Mechanical Engineers, Part B: Journal of Engineering Manufacture* 221, no. 11: pp. 1585-1591 (2007)
- [6] Christian Lindemann, Ulrich Jahnke, Matthias Moi, and Rainer Koch, "Analyzing product lifecycle costs for a better understanding of cost drivers in additive manufacturing", In 23th Annual International Solid Freeform Fabrication Symposium—An Additive Manufacturing Conference. Austin Texas USA 6th-8th August. 2012.
- [7] L. Rickenbacher, A. Spierings, K. Wegener, "An integrated cost-model for selective laser melting (SLM)", *Rapid Prototyping Journal*, Vol. 19 Issue: 3, pp.208-214 (2013)
- [8] Malte Schroeder, Bjoern Falk, Robert Schmitt, Evaluation of Cost Structures of Additive Manufacturing Processes Using a New Business Model, *Procedia CIRP*, Volume 30, pp. 311-316 (2015)
- [9] <http://ult3d.com/>
- [10] <http://varia3d.com/techonology/laser-sintering/>
- [11] Amos Tversky and Daniel Kahneman, "Judgment under uncertainty: Heuristics and biases", *Science* Vol. 185, Issue 4157, pp. 1124-1131 (1975)
- [12] Gerd Gigerenzer, and Wolfgang Gaissmaier, "Heuristic decision making", *Annual review of psychology* 62, pp.451-482 (2011)



# Practical Examples of Regeneration of the Damaged Heavy Machinery Parts

Dr Svetislav Lj. Marković<sup>1\*</sup>, Vladimir Stepanović<sup>2</sup>, Lazar Jovičić<sup>3</sup>, Milijan Ćirić<sup>4</sup>,  
Ivan Stanišić<sup>5</sup>, Miroslav Ćurčin<sup>6</sup>, Nemanja Petrović<sup>7</sup>

<sup>1</sup>Technical College, 32000 Čačak, Svetog Save 65, Serbia, e-mail: svetom@mts.rs

<sup>2</sup>Preduzeće za puteve „Beograd“, Dula Karaklajića 21 A, 11550 Lazarevac, e-mail: stvlada75@gmail.com

<sup>3</sup>Brajkovac, 11561 Dudovica, e-mail: joviciclazar805@yahoo.com

<sup>4</sup>JP Kolubara, Dula Karaklajić 41/6, 11550 Lazarevac, e-mail: milijanciric83@gmail.com

<sup>5</sup>JP Kolubara, Živojina Žujović 76, 11550 Lazarevac, e-mail: ivstanišic@gmail.com

<sup>6</sup>JP TENT Obrenovac, Kolubarski trg 147, 11550 Lazarevac, e-mail: miroslavui37@gmail.com

<sup>7</sup>Kolubara Usluge, Valandovska 67b, 11550 Lazarevac, e-mail: nemanja.petrovic1993@gmail.com

*Hard facing represents the process of applying additional material on a certain surface with the aim of achieving the desired characteristics or dimensions of a machinery part which is being regenerated. Today more than 50 per cent of worn out machinery parts is regenerated by hard facing. The applied material makes a whole with the basic material and is attached to it closely and reliably. This paper contains characteristic examples of damaged vital machinery parts which were successfully regenerated by hard facing, thus making the process most economical.*

**Keywords: machinery part, regeneration, reparatory hard facing**

## 1. INTRODUCTION

Regeneration of damaged machinery elements has a lot of advantages which account for its increasing application in industrial practice of most countries some of them are listed below [1]:

- More and more complex machinery parts are being exploited in all industrial branches, which creates the need of providing a great number of spare parts necessary for their maintenance. When it is impossible to provide new spare parts or to meet the delivery deadline, regeneration of damaged machinery parts considerably shortens the time which a failed machinery system spends in stoppage. It takes up to ten times more time to supply new parts than to regenerate the old ones.
- Regeneration completely eliminates great expenses of storing spare parts, which are sometimes up to 30 per cent of the price of a new part. Regeneration enables rapid overhaul of a machinery system without unnecessary storage of spare parts.
- The time necessary for regeneration is often considerably shorter than that needed for manufacturing new spare parts, which shortens the time necessary for overhaul and decreases the losses in the production cycle of the machinery system which has been subjected to overhaul.
- Refinement of surfaces at regeneration can considerably prolong the life-span of the regenerated machinery part which can be longer than that of the new spare part.
- There have been cases when the life-span of the regenerated parts was considerably longer than that

of the new, serially manufactured machinery parts, sometimes even 2-2.5 times longer.

- The cost of regeneration is considerably lower than that of the new machinery part, while the quality and life-span are similar.
- Regeneration accomplishes full employment of the capacities and technological possibilities of overhaul enterprises.

However, the predominant factors for introduction regeneration are completely different in industrially developed and undeveloped countries. In industrially undeveloped and underdeveloped countries great advantage is given to regeneration of damaged machinery elements due to their inability to invest largely in providing new equipment and spare parts by import. The spare parts for the outdated machinery systems, which are still in use in these countries, are not manufactured any more. Regeneration of the damaged parts of these systems enables their further exploitation. The high prices of the spare parts demand that the technical services in underdeveloped and undeveloped countries give advantage to regeneration of damaged machinery elements.

Taking into account the limited resources of certain chemical elements, which have enormous importance in mechanical engineering, regeneration of damaged machinery elements is given an important place in industry of many technologically developed countries. This especially applies to Ni, Co, Cr, W, Va, Mn, Mo and other chemical elements. Even superfluous analyses show great losses when a worn part of steel alloy is discarded and substituted by a new one. These parts retrieve the demanded exploitative characteristic by application of regenerative methods [2].

Economical effectiveness of regenerating machinery elements is accounted for by considerably lower losses in work and material than at manufacturing new spare parts. From the aspect of economy, not all machinery parts are suitable for regeneration. Purposefulness of regeneration must be appreciated for each machinery part individually.

The modern regenerative methods must provide the fastest, cheapest and most reliable possible regeneration of exploitative characteristics of mechanical, hydrodynamic, pneumatical, electronic and other parts. Correctly organized regeneration of damaged machinery parts decreases the costs of providing and storing spare parts, employs the production capacities of overhaul and other enterprises, reduces the cost of overhaul of machinery systems and fastens their return in exploitation, i. e. shortens the period of stoppage.

There is a great number of regeneration methods which are more or less practically applied. The most often used method is hard facing (manual arc hard facing before all), then overhaul measures, metallization and chromium plating. But, other methods as well have their fields of application in specific conditions when the most often applied methods do not give adequate results [3].

## 2. REPARATORY HARD FACING

Of all regeneration methods known today hard facing is the one which is the most often used. Greater number of advantages in comparison with the other regenerative methods accounts for the fact that this is the most often applied regeneration method [2]:

- Hard facing procedures allow obtaining a new layer of metal on the worn machinery part quickly.
- The hard faced layer can be of considerable thickness if necessary, which is especially important at worn machinery parts.
- This method of regeneration is often very economical.
- The hard faced surfaces have proved very reliable in exploitation.
- The process of hard facing can be highly productive.
- This regenerative method is relatively simple from the aspect of organization.
- Hard facing allows the possibility of changing chemical, physical, mechanical and metallurgical characteristics of the working surfaces of the regenerated machinery parts in relation to the basic material.
- Hard faced layers can have good antifrictional properties, they are resistant to wear, acids, high temperatures etc.
- It can be applied for regeneration of parts manufactured of various materials and with different types of damage.
- Hard facing with hard electrodes is a technological procedure which is most often more expensive than usual procedures of heat and chemical treatment (such as quenching, cementation, nitrate plating and others), but the working life of the hard faced parts

is several times longer, i. e. the hard faced working surfaces are stronger.

- For performing hard facing procedures simple and cheap equipment will suffice.
- Hard facing is also applied for regeneration of the most vital and complex machinery parts (gears, shafts, and other).
- Machinery parts regenerated by hard facing are several times cheaper than new ones with the same or better characteristics of working capacity.
- A great number of procedures for regenerating machinery parts by hard facing has been developed.

Due to everything above mentioned hard facing represents the most efficient way of regenerating damaged machinery elements.

Besides numerous advantages, regeneration of machinery elements by hard facing also has some disadvantages:

- The change in structure of materials due to great local warming.
- The occurrence of residual stresses and distortions, due to local heat input, which brings about deviation of geometrical measures, shapes and positions of the parts.
- The occurrence of local stresses in the seam and deformation of the part.
- The quality of the regenerated part depends largely on the applied technology, but also on the knowledge and carefulness of the task performer-a welder.

The electrodes used for hard facing are either the same as the ones used for welding or special electrodes for hard facing. The types of electrodes, wires and welding fluxes are chosen regarding the demands which a hard faced layer of material should meet. In order to make the working requirements accomplishable and the whole procedure technically and economically justified, it is necessary to choose the additional material and hard facing procedure correctly, taking into account the shape and chemical composition of the part.

Technological process of regeneration by hard facing is almost the same as in all methods of applying layers and consists of the following [3]:

- Washing and cleaning the parts which are to be regenerated,
- Hard facing process itself,
- Removal of the slag machine processing after hard facing,
- Eventual heat treatment and
- Final grinding.

The regime of hard facing of worn surfaces is determined by the following sequence of procedures: the thickness of the hard faced layer is determined first, then the type and diameter of the electrode is chosen regarding the demanded hardness and thickness of the hard faced layer, after which the optional parameters of hard facing are determined [4].

The hard faced surface is mostly rough, and therefore subsequent machine processing is imminent. The hard faced layers of the highest surface quality are obtained TIG by hard facing with the padded electrodes (MMA procedure). The hard faced surfaces of elements

the hardness of which goes up to HRC 45 can be subjected to machine processing by the tools with the plates of hard metals and grinding, and the surfaces of greater hardness only to preceding and final grinding.

### 3. THE EXAMPLES OF MACHINERY PARTS SUCCESSFULLY REGENERATED BY REPARATORY HARD FACING

There are numerous examples of the damaged machinery parts which have been successfully regenerated by reparatory hard facing. Some of them are listed below and they show the obvious economical justification of reparatory hard facing:

#### 1. The camshaft of the motorcycle HONDA

*Damage:* All teeth on the gear worn.



Figure 1: The damaged camshaft (the worn teeth of the gear in the middle)

*Regeneration method:* MMA hard facing of the whole toothed wreath with additional material (AM) EVB2 Cr Mo followed by manufacturing the teeth on the milling machine. Hard facing is performed longitudinally and crosswise in order to avoid distortion of the shaft. Cooling process must be gradual with careful prompting.

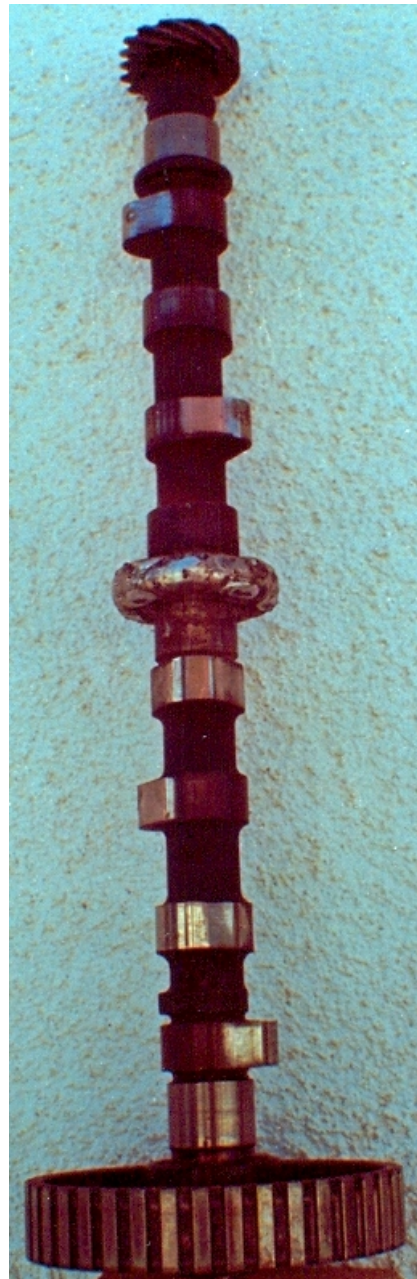


Figure 2: The appearance of the regenerated camshaft before machine processing

#### 2. The gear of a milling machine

*Damage:* Considerable abrasive wear in one sector of the gear.



Figure 3: The damaged gear of the milling machine

*Regeneration method:* MMA hard facing with AM UNIS 65 (the first layer) and UNIS 670 (the surface layer) with subsequent processing by Pfanter procedure. The surface hardness of the teeth is  $58 \pm 2$  HRC.



Figure 4: The appearance of the regenerated gear of the milling machine

### 3. The gear of the machine used for grinding stone in cement production

The gear has 1800 mm in diameter. The material: grey cast iron.

*Damage:* The breakdown damage of the teeth created by falling into the coupling of an alien body.



Figure 5: The damaged gear of the machine used for grinding stone in cement production

*Regeneration method:* MMA hard facing with a cast iron electrode (HRC<40) and subsequent processing on a milling machine.

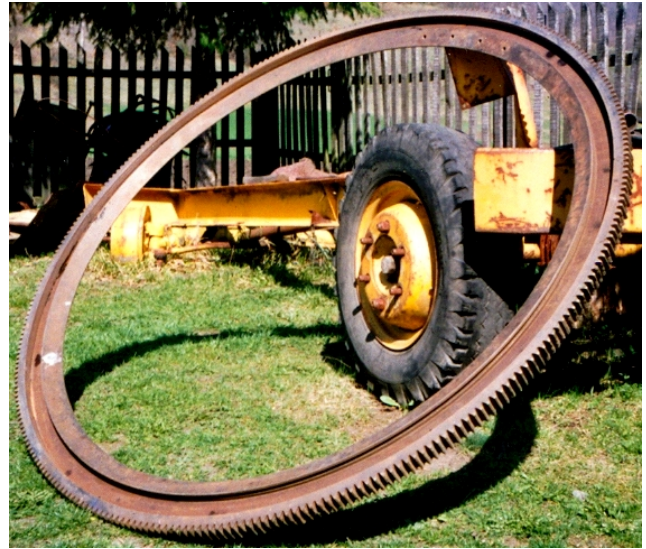


Figure 6: The appearance of the regenerated gear of the machine for grinding stone in cement production

### 4. The two-part gear of the paper processing machine

*Damage:* The damage on the working surfaces of the several teeth due to mistakes during casting.

*Regeneration method:* MMA hard facing with a cast iron electrode (the manufacturer Jasenice). The assembled gear is processed on the milling machine (the two parts joined together).



Figure 7: The appearance of the regenerated gear

**5. The crankshaft of the motor ARAN**

*Damage:* Worn wedge grooves.



*Figure 8: The damaged crankshaft of the motor ARAN*

*Regeneration method:* MMA hard facing of the grooves and processing on the lathe and milling machine.



*Figure 9: The appearance of the regenerated crankshaft of the motor ARAN*

**6. The crankshaft of the motor VOLKSWAGEN**

*Damage:* Excessive wear of a journal.

*Regeneration method:* hard facing by TIG procedure (longitudinally and with a turn). Prompting must be taken care of in order to avoid distortions at cooling.

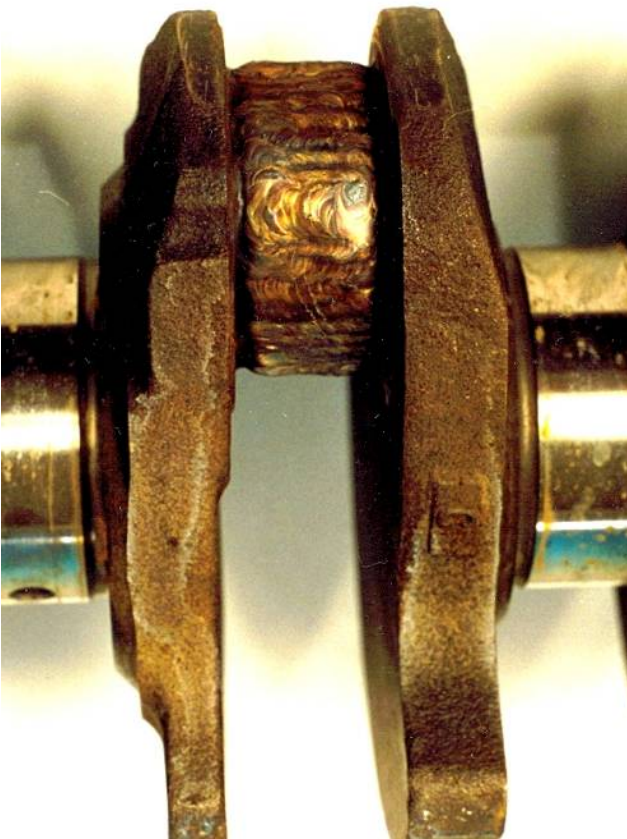


*Figure 10: The appearance of the regenerated crankshaft of the motor VOLKSWAGEN (the hard faced journal is zoomed)*

## 7. The crankshaft of the motor VOLKSWAGEN-GOLF

*Damage:* A worn seat on the journal.

*Regeneration method:* Hard facing by TIG procedure. Hard facing is to be performed in one layer with interruptions in order to avoid excessive warming and distortions.

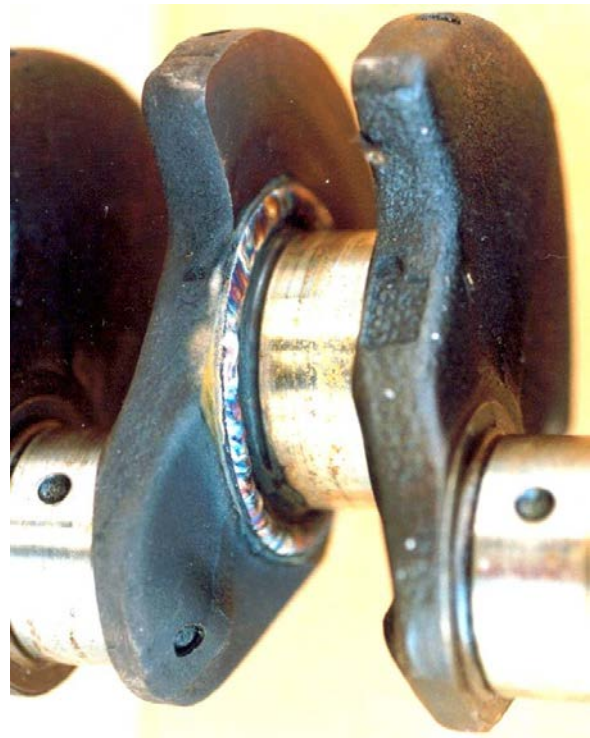
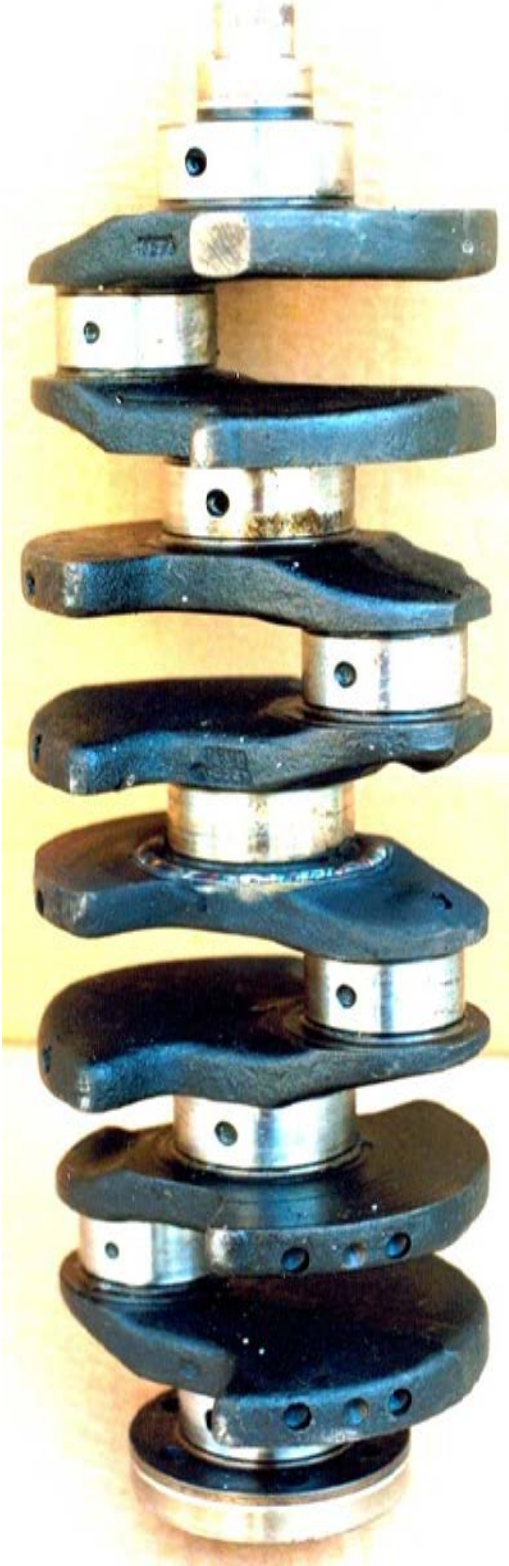


Figure 11: The appearance of the regenerated crankshaft of the motor VOLKSWAGEN-GOLF (the hard faced seat is zoomed)

## 4. CONCLUSION

Hard facing procedures have become widely applied in corrective maintenance of machinery systems because of their effectiveness. Due to its increasing application, hard facing has grown into a separate branch of welding technique although the same procedures and instruments are used for their performing. However, hard facing is not only one of the most often used regeneration technologies, but it is also a modern technological procedure which allows obtaining new parts with the required mechanical characteristics, applying anticorrosive covering (platinum plating, explosion plating) and additional processing of the new parts with a flaw.

## REFERENCES

- [1] Marković S., Josifović D.: *Regeneracija zupčanika*, monografija, Jugoslovensko društvo za tribologiju, Kragujevac (1998).
  - [2] Dr Rene Wasserman: *Wie spart man millionen durch abbau der ersatzteillager*, RTB Bor, Institut za bakar Bor, Indok centar (2003).
  - [3] Marković S.: *Technical and economical justification of applying tooth repair welding with regeneration of the heavy loaded gears*, Zbornik referata sa Međunarodne konferencije "Zavarivanje 2003", Beograd, 18÷19. septembar (2003).
- Marković S.: *Tribological characteristics of gears reparatorily hardfaced wit "hard" and "soft" additional materials*, Proceedings 11<sup>th</sup> International Research/Expert Conference "Trends in the Development of Machinery and Associated Technology" TMT 2007, Hammamet, Tunisia, 5÷9. September (2007).

# Analysis of Free Oscillation of 3D Frames Applying the Method of Consistent Masses

Rade Vasiljević<sup>1\*</sup>

<sup>1</sup>High Technical School of Vocational Studies, Belgrade (Serbia)

*In this paper presented the analysis of free oscillation of 3D frames applying approach continually distributed mass replacement consistent masses. The setting of the theoretical problem is numerically implemented in the example 3D frame. The theoretical results are verified simulation by Autodesk Inventor software.*

**Keywords:** 3D frames, Consistent mass, FEA, Free oscillation, Frequencies, Autodesk Inventor

## 1. INTRODUCTION

In structural engineering has great importance to the problem oscillation. Modal analysis of conceptual designs of structural design is the first and most essential element of dynamic analysis for estimation of their dynamic stability. The process of determining the eigenvalues in complex systems (systems with a large number of degrees of freedom) is the most expensive phase in the dynamic analysis [1].

Earlier studies determining the natural frequencies of complex structures have been based on the use of approximate expressions and methods [2]. Some examples of the approximate methods are shown in [3]. Accurate determination of natural frequencies was limited to simple structures (simple beams and brackets). In complex elastic bodies for a solution frequency equation was difficult because it contained trigonometric and hyperbolic functions. Today, mathematical software enables routine solving of complex oscillation frequency equations of elastic bodies. Accurate determination of natural frequencies is important in optimizing the structures.

However, applying analytical methods at complex structures is limited. In this case, for the determination of natural frequencies by the structures we opt for one of the numerical methods. The main advantage of numerical methods is that they very complex structures can be viewed as a reduced model, whose analysis the aspect of engineering accuracy is sufficient to evaluate the behavior of complex structures.

3D frames in realty are complex structures with continuously distributed mass. In other words, spatilal frames are systems with infinite number of freedom. Continually distributed masses of frames is replaced by consistent mass or consistent mass. In [4] shown that a approximation by consistent masses better than approximation direct lumped mass.

In this paper discusses the free oscillations of 3D frame. Pursuant to the aforesaid, the modal analysis discussed 3D frame is conducted numerically. The is represented by finite element approach to frequency analysis, ie the mathematical model with the consistent masses. The theoretical results of numerical analyzes are verified applying the simulation software (Autodesk<sup>®</sup> Inventor<sup>®</sup>).

## 2. ANALYSIS OF 3D BEAM ELEMENT

Spatial frame is presented via 3D beam finite elements with two nodal points. In the generale case (finite element of the type  $ik$ ), node have six degrees of freedom (Figure 1).

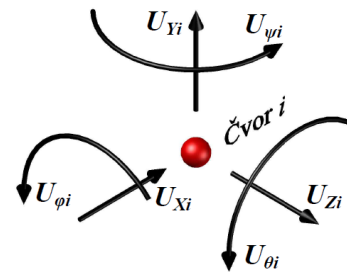


Figure 1: Nodal displacements

Vector of generalized displacements and vector of generalized forces of 3D of beam element read:

$$\mathbf{q}^T = \{u_i \ v_i \ w_i \ \theta_i \ \phi_i \ \psi_i \ u_k \ v_k \ w_k \ \theta_k \ \phi_k \ \psi_k\} \quad (1)$$

$$\mathbf{R}^T = \{N_i \ T_{yi} \ T_{zi} \ M_{xi} \ M_{yi} \ M_{zi} \ N_k \ T_{yk} \ T_{zk} \ M_{xk} \ M_{yk} \ M_{zk}\} \quad (2)$$

For both sides restrain beam element of constant cross-section vector interpolation function read [5]:

$$\mathbf{N}^T = \begin{bmatrix} 1-\xi & 0 & 0 & 0 & 0 & 0 \\ 0 & 1-3\xi^2+2\xi^3 & 0 & 0 & 0 & 0 \\ 0 & 0 & 1-3\xi^2+2\xi^3 & 0 & 0 & 0 \\ 0 & 0 & 0 & 0 & 1-\xi & 0 \\ 0 & x-2l\xi^2+l\xi^3 & 0 & 0 & 0 & 0 \\ 0 & 0 & -x+2l\xi^2-l\xi^3 & 0 & 0 & 0 \\ \xi & 0 & 0 & 0 & 0 & 0 \\ 0 & 3\xi^2-2\xi^3 & 0 & 0 & 0 & 0 \\ 0 & 0 & 3\xi^2-2\xi^3 & 0 & 0 & 0 \\ 0 & 0 & 0 & 0 & \xi & 0 \\ 0 & l\xi^2-l\xi^3 & 0 & 0 & 0 & 0 \\ 0 & 0 & l\xi^2-l\xi^3 & 0 & 0 & 0 \end{bmatrix} \quad (3)$$

where  $\xi=x/l$ .

The 3D rotation beam element in the generale case (complex rotation) is shows at Figure 2. Detailed analysis of complex 3D rotation beam element in the generale case is given in [5].

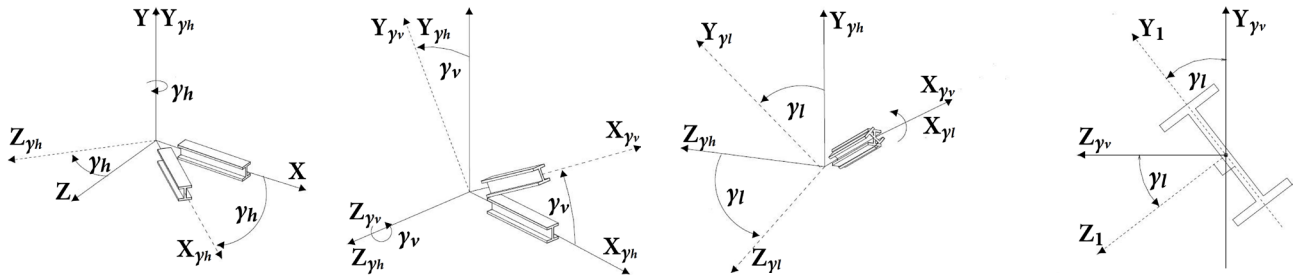


Figure 2: 3D rotation of the beam element in generale case

The transformation matrix of vector  $\mathbf{t}$  is equal to (Figure 2):

$$\mathbf{t} = \begin{bmatrix} \lambda & \mu & \nu \\ \frac{-\lambda\mu \cos \gamma_l - \nu \sin \gamma_l}{\sqrt{\lambda^2 + \nu^2}} & \sqrt{\lambda^2 + \nu^2} \cos \gamma_l & \frac{-\nu\mu \cos \gamma_l - \lambda \sin \gamma_l}{\sqrt{\lambda^2 + \nu^2}} \\ \frac{\lambda\mu \sin \gamma_l - \nu \cos \gamma_l}{\sqrt{\lambda^2 + \nu^2}} & -\sqrt{\lambda^2 + \nu^2} \sin \gamma_l & \frac{\nu\mu \sin \gamma_l + \lambda \cos \gamma_l}{\sqrt{\lambda^2 + \nu^2}} \end{bmatrix} \quad (4)$$

The transformation matrix element read:

$$\mathbf{T} = \begin{bmatrix} \mathbf{t} & \mathbf{0} & \mathbf{0} & \mathbf{0} \\ \mathbf{0} & \mathbf{t} & \mathbf{0} & \mathbf{0} \\ \mathbf{0} & \mathbf{0} & \mathbf{t} & \mathbf{0} \\ \mathbf{0} & \mathbf{0} & \mathbf{0} & \mathbf{t} \end{bmatrix} \quad (5)$$

### 2.1. Stiffness matrix of the 3D beam element

In determining the stiffness matrix of the starting from the connection between the vector of generalized forces  $\mathbf{F}$  and the vector of generalized displacements  $\mathbf{q}$ :

$$\mathbf{F} = \mathbf{k}\mathbf{q} \quad (6)$$

The corresponding stiffness matrix of the line element is defined based on interpolation functions (3):

$$\mathbf{k} = \int_V \mathbf{E}\mathbf{N}^T \mathbf{N} dV \quad (7)$$

The stiffness matrix elements can be determined by applying the principle of superposition, the separation of the spatial state of stress in the elements:

- Axial strain,
- Bending about  $z$  axis in the plane  $xy$ ,
- Bending about  $y$  axis in the plane  $xz$ , and
- Rotating about  $x$  axis (torsion).

Now, the relationship between the vector of generalized forces  $\mathbf{F}$  and the vector displacements  $\mathbf{q}$  can be presented in the form of:

$$\begin{Bmatrix} \mathbf{F}_a \\ \mathbf{F}_{sz} \\ \mathbf{F}_{sy} \\ \mathbf{F}_t \end{Bmatrix} = \begin{bmatrix} \mathbf{k}_a & \mathbf{0} & \mathbf{0} & \mathbf{0} \\ \mathbf{0} & \mathbf{k}_{sz} & \mathbf{0} & \mathbf{0} \\ \mathbf{0} & \mathbf{0} & \mathbf{k}_{sy} & \mathbf{0} \\ \mathbf{0} & \mathbf{0} & \mathbf{0} & \mathbf{k}_t \end{bmatrix} \begin{Bmatrix} \mathbf{q}_a \\ \mathbf{q}_{sz} \\ \mathbf{q}_{sy} \\ \mathbf{q}_t \end{Bmatrix} \quad (8)$$

where:

- $\mathbf{k}_a$  – stiffness matrix of axial oscillation of the element,
- $\mathbf{k}_{sz}$  – stiffness matrix of transverse oscillation of the element in the plane  $xz$ ,
- $\mathbf{k}_{sy}$  – stiffness matrix of transverse oscillation of the element in the plane  $xy$ , and

- $\mathbf{k}_t$  – stiffness matrix of torsional oscillation of the element.

The stiffness matrix of the axial oscillation of the beam finite element of the type  $ik$  in the local coordinate system, on the basis of expressions (3) and (7), read:

$$\mathbf{k}_a = \begin{bmatrix} 1 & -1 \\ -1 & 1 \end{bmatrix} \frac{EA}{l} \quad (9)$$

The stiffness matrices of the transverse oscillation in the plane  $xy$  of the beam finite element of the type  $ik$  in the local coordinate system, on the basis of expressions (3) and (7), read:

$$\mathbf{k}_{sz} = \begin{bmatrix} 12 & 6l & -12 & 6l \\ 6l & 4l^2 & -6l & 2l^2 \\ -12 & -6l & 12 & -6l \\ 6l & 2l^2 & -6l & 4l^2 \end{bmatrix} \frac{EI_z^3}{l^3} \quad (10)$$

The stiffness matrices of the transverse oscillation in the plane  $xz$  of the beam finite element of the type  $ik$  in the local coordinate system, on the basis of expressions (3) and (7), read:

$$\mathbf{k}_{sy} = \begin{bmatrix} 12 & 6l & -12 & -6l \\ 6l & 4l^2 & 6l & 2l^2 \\ -12 & 6l & 12 & 6l \\ -6l & 2l^2 & 6l & 4l^2 \end{bmatrix} \frac{EI_y^3}{l^3} \quad (11)$$

The stiffness matrix of the torsion oscillation of the beam finite element of the type  $ik$  in the local coordinate system, on the basis of expressions (3) and (7), read:

$$\mathbf{k}_t = \begin{bmatrix} 1 & -1 \\ -1 & 1 \end{bmatrix} \frac{GI_x}{l} \quad (12)$$

The stiffness matrix of the 3D (spatial) beam element is formed from the partial matrix to the stiffness,  $\mathbf{k}_a$ ,  $\mathbf{k}_{sz}$ ,  $\mathbf{k}_{sy}$  and  $\mathbf{k}_t$ , so their components are distributed in the appropriate position according to the appropriate sequence of generalized displacements and the generalized forces:



$$\mathbf{k} = \begin{bmatrix} \frac{EA}{l} & 0 & 0 & 0 & 0 & 0 & -\frac{EA}{l} & 0 & 0 & 0 & 0 & 0 \\ 0 & \frac{12EI_z}{l^3} & 0 & 0 & 0 & \frac{6EI_z}{l^2} & 0 & -\frac{12EI_z}{l^3} & 0 & 0 & 0 & \frac{6EI_z}{l^2} \\ 0 & 0 & \frac{12EI_y}{l^3} & 0 & -\frac{6EI_y}{l^2} & 0 & 0 & 0 & -\frac{12EI_y}{l^3} & 0 & -\frac{6EI_y}{l^2} & 0 \\ 0 & 0 & 0 & \frac{GI_x}{l} & 0 & 0 & 0 & 0 & 0 & -\frac{GI_x}{l} & 0 & 0 \\ 0 & 0 & -\frac{6EI_y}{l^2} & 0 & \frac{4EI_y}{l} & 0 & 0 & 0 & \frac{6EI_y}{l^2} & 0 & \frac{2EI_y}{l} & 0 \\ 0 & \frac{6EI_z}{l^2} & 0 & 0 & 0 & \frac{4EI_z}{l} & 0 & -\frac{6EI_z}{l^2} & 0 & 0 & 0 & \frac{2EI_z}{l} \\ -\frac{EA}{l} & 0 & 0 & 0 & 0 & 0 & \frac{EA}{l} & 0 & 0 & 0 & 0 & 0 \\ 0 & -\frac{12EI_z}{l^3} & 0 & 0 & 0 & -\frac{6EI_z}{l^2} & 0 & \frac{12EI_z}{l^3} & 0 & 0 & 0 & -\frac{6EI_z}{l^2} \\ 0 & 0 & -\frac{12EI_y}{l^3} & 0 & \frac{6EI_y}{l^2} & 0 & 0 & 0 & \frac{12EI_y}{l^3} & 0 & \frac{6EI_y}{l^2} & 0 \\ 0 & 0 & 0 & -\frac{GI_x}{l} & 0 & 0 & 0 & 0 & 0 & \frac{GI_x}{l} & 0 & 0 \\ 0 & 0 & -\frac{6EI_y}{l^2} & 0 & \frac{2EI_y}{l} & 0 & 0 & 0 & \frac{6EI_y}{l^2} & 0 & \frac{4EI_y}{l} & 0 \\ 0 & \frac{6EI_z}{l^2} & 0 & 0 & 0 & \frac{2EI_z}{l} & 0 & -\frac{6EI_z}{l^2} & 0 & 0 & 0 & \frac{4EI_z}{l} \end{bmatrix} \quad (13)$$

2.2. Mass matrix of the 3D beam element

In determining the stiffness matrix of the starting from the connection between the vector of generalized inertial forces  $\mathbf{F}_{in}$  and the vector of generalized accelerations  $\ddot{\mathbf{q}}$ :

$$\mathbf{F}_{in} = \mathbf{k}\ddot{\mathbf{q}} \quad (14)$$

The corresponding mass matrix of the line element is defined based on interpolation functions (3):

$$\mathbf{m} = \int_V \rho \mathbf{N}^T \mathbf{N} dV \quad (15)$$

The mass matrix elements can be determined by applying the principle of superposition, the separation of the spatial state of stress in the elements:

- Axial strain,
- Bending about  $z$  axis in the plane  $xy$ ,
- Bending about  $y$  axis in the plane  $xz$ , and
- Rotating about  $x$  axis (torsion).

Now, the relationship between the vector of generalized inertial forces  $\mathbf{F}_{in}$  and the vector accelerations  $\ddot{\mathbf{q}}$  can be presented in the form of:

$$\begin{Bmatrix} \mathbf{F}_a^{in} \\ \mathbf{F}_{sz}^{in} \\ \mathbf{F}_{sy}^{in} \\ \mathbf{F}_t^{in} \end{Bmatrix} = \begin{bmatrix} \mathbf{m}_a & \mathbf{0} & \mathbf{0} & \mathbf{0} \\ \mathbf{0} & \mathbf{m}_{sz} & \mathbf{0} & \mathbf{0} \\ \mathbf{0} & \mathbf{0} & \mathbf{m}_{sy} & \mathbf{0} \\ \mathbf{0} & \mathbf{0} & \mathbf{0} & \mathbf{m}_t \end{bmatrix} \begin{Bmatrix} \ddot{\mathbf{q}}_a \\ \ddot{\mathbf{q}}_{sz} \\ \ddot{\mathbf{q}}_{sy} \\ \ddot{\mathbf{q}}_t \end{Bmatrix} \quad (16)$$

where:

- $\mathbf{m}_a$  – mass matrix of axial oscillation of the element,
- $\mathbf{m}_{sz}$  - mass matrix of transverse oscillation of the element in the plane  $xz$ ,
- $\mathbf{m}_{sy}$  - mass matrix of transverse oscillation of the

element in the plane  $xy$ , and

- $\mathbf{m}_t$  - mass matrix of torsional oscillation of the element.

The consistent mass matrix of the axial oscillation of the beam finite element (type  $ik$ ) in the local coordinate system, on the basis of Eqs. (3) and (15), read:

$$\mathbf{m}_a = \begin{bmatrix} 2 & 1 \\ 1 & 2 \end{bmatrix} \frac{\rho Al}{6} \quad (17)$$

The consistent mass matrices of the transverse oscillation of the beam finite element (type  $ik$ ) in the local coordinate system, on the basis of Eqs. (3) and (15), read:

$$\mathbf{m}_{sz} = \begin{bmatrix} 156 & 22l & 54 & -13l \\ 22l & 4l^2 & 13l & -3l^2 \\ 54 & 13l & 156 & -22l \\ -13l & -3l^2 & -22l & 4l^2 \end{bmatrix} \frac{\rho Al}{420} \quad (18)$$

$$\mathbf{m}_{sy} = \begin{bmatrix} 156 & -22l & 54 & 13l \\ -22l & 4l^2 & -13l & -3l^2 \\ 54 & -13l & 156 & 22l \\ 13l & -3l^2 & 22l & 4l^2 \end{bmatrix} \frac{\rho Al}{420} \quad (19)$$

The consistent mass matrix of the torsion oscillation of the beam finite element (type  $ik$ ) in the local coordinate system, on the basis of Eqs. (3) and (15), read:

$$\mathbf{m}_t = \begin{bmatrix} 2 & 1 \\ 1 & 2 \end{bmatrix} \frac{\rho AL}{6} \quad (20)$$

The consistent mass matrix in the space of the beam element is formed from the partial matrix to the stiffness,  $\mathbf{m}_a$ ,  $\mathbf{m}_{sz}$ ,  $\mathbf{m}_{sy}$  and  $\mathbf{m}_t$ , so their components are distributed in the appropriate position according to the appropriate sequence of generalized accelerations and the generalized inertial forces:

$$\mathbf{m} = \begin{bmatrix} 140 & 0 & 0 & 0 & 0 & 0 & 70 & 0 & 0 & 0 & 0 & 0 \\ 0 & 156 & 0 & 0 & 0 & 22l & 0 & 54 & 0 & 0 & 0 & -13l \\ 0 & 0 & 156 & 0 & -22l & 0 & 0 & 0 & 54 & 0 & 13l & 0 \\ 0 & 0 & 0 & \frac{140I_x}{A} & 0 & 0 & 0 & 0 & 0 & \frac{70I_x}{A} & 0 & 0 \\ 0 & 0 & -22l & 0 & 4l^2 & 0 & 0 & 0 & -13l & 0 & -3l^2 & 0 \\ 0 & 22l & 0 & 0 & 0 & 4l^2 & 0 & 13l & 0 & 0 & 0 & -3l^2 \\ 70 & 0 & 0 & 0 & 0 & 0 & 140 & 0 & 0 & 0 & 0 & 0 \\ 0 & 54 & 0 & 0 & 0 & 13l & 0 & 156 & 0 & 0 & 0 & -22l \\ 0 & 0 & 54 & 0 & -13l & 0 & 0 & 0 & 156 & 0 & 22l & 0 \\ 0 & 0 & 0 & \frac{70I_x}{A} & 0 & 0 & 0 & 0 & 0 & \frac{140I_x}{A} & 0 & 0 \\ 0 & 0 & 13l & 0 & -3l^2 & 0 & 0 & 0 & 22l & 0 & 4l^2 & 0 \\ 0 & -13l & 0 & 0 & 0 & -3l^2 & 0 & -22l & 0 & 0 & 0 & 4l^2 \end{bmatrix} \frac{\rho Al}{420} \quad (21)$$

### 3. ANALYSIS OF THE SYSTEM

A paper should contain title, names and affiliations of authors, abstract, list of keywords, paper body, acknowledgement and references.

#### 3.1. Stiffness matrix of the system

Stiffness matrix of element  $n$  in the global coordinate system is equal to:

$$\mathbf{K}_n = \mathbf{T}_n^T \mathbf{k}_n \mathbf{T}_n \quad (22)$$

Stiffness matrix of the carrying structure:

$$\mathbf{K} = [\mathbf{K}]_{d \times d} = \sum_1^n \mathbf{K}_n \quad (23)$$

where  $d$  number displacements.

The stiffness matrix of the system in the direction of unknown displacements read:

$$\mathbf{K}_{uu} = [\mathbf{K}]_{d-k \times d-k} \quad (24)$$

where  $k$  number known displacements.

#### 3.2. Mass matrix of the system

Mass matrix of element  $n$  in the global coordinate system is equal to:

$$\mathbf{M}_n = \mathbf{T}_n^T \mathbf{m}_n \mathbf{T}_n \quad (25)$$

Mass matrix of the system read:

$$\mathbf{M} = [\mathbf{M}]_{d \times d} = \sum_1^n \mathbf{M}_n \quad (26)$$

Mass matrix of the system in the direction of unknown displacements read:

$$\mathbf{M}_{uu} = [\mathbf{M}]_{d-k \times d-k} = \sum_1^n \mathbf{M}_n \quad (27)$$

### 4. ANALYSIS OF FREE OSCILATIONS OF THE SYSTEM

The equation of the free undamped oscillation of the system read:

$$\mathbf{M}_{uu} \ddot{\mathbf{U}}_{uu} + \mathbf{K}_{uu} \mathbf{U}_{uu} = \mathbf{0} \quad (28)$$

where:

- $\ddot{\mathbf{U}}_{uu}$  - vector of unknown accelerations, and
- $\mathbf{U}_{uu}$  - vector of unknown displacements.

Eigenfrequencies of the carrying structure are obtained by solving algebraic equation:

$$\det(\mathbf{K}_{uu} - \omega^2 \mathbf{M}_{uu}) = 0 \quad (29)$$

Based on the circular natural frequencies obtained by the oscillation periods via expression:

$$T_i = \frac{2\pi}{\omega_i} \quad (30)$$

Frequencies of the carrying structure are obtained based on expression:

$$f_i = \frac{\omega_i}{2\pi} = \frac{1}{T_i} \quad (31)$$

### 5. NUMERICAL EXAMPLE

By applying the methods of consistent mass in the numerical example is carried out frequency analysis specific 3D frame (Figure 3). The results are compared to the results obtained applying the program Autodesk® Inventor®.

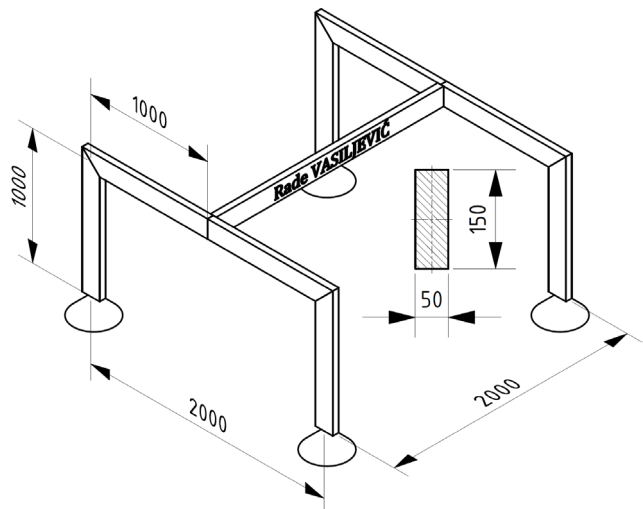


Figure 3: 3D frame

#### 5.1. Theoretical results obtained applying the method of consistent masses

The finite model of the 3D frame is shown at Figure 4.

The main mechanical characteristics of the 3D frame (Figure 3), i.e. of all finite elements of the formed FE model 3D frame (Figure 4) are equal:

- Module of elasticity,  $E=2.1 \times 10^{11}$  [N/m<sup>2</sup>];
- Slipping module,  $G=0.8 \times 10^{11}$  [N/m<sup>2</sup>]; and
- Density,  $\rho=7850$  [kg/m<sup>3</sup>].

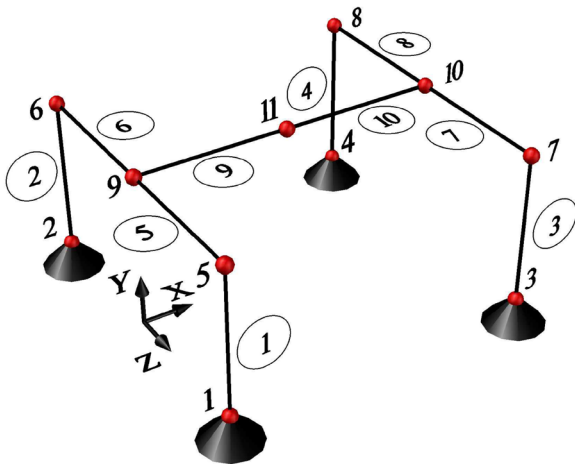


Figure 4: FE model 3D frame

Based on theoretical assumptions in the subtitle 2 and defined starting data in Mathematica® [6], was written computer code "RV-ModAnalysis" for calculating the oscillation period, circular frequencies, and the the frequency. Obtained are their value for all degrees of freedom ( $i= 54$ ), but are in Table 1 shows the values for the first 6 modes of oscillation.

Table 1: Periods, circular frequencies and frequencies

Mode No	Period $T$ [s]	Circular freq. $\omega$ [rad/s]	Frequency $f$ [Hz]
1	0.1353	46.45	7.392
2	0.0645	97.34	15.49
3	0.0523	120.12	19.12
4	0.0343	183.12	29.14
5	0.0325	193.31	30.77
6	0.0281	223.77	35.61

5.2. Verification of the theoretical results of simulation by Autodesk® Inventor® software

In order to verify the theoretical results, the software Autodesk Inventor is formed and solved finite element model of the 3D frame. The FE model of the 3D frame is shown in Figure 5.

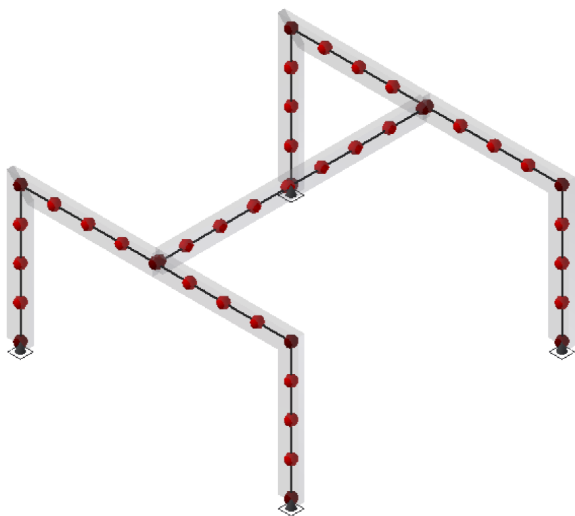


Figure 5: FE model 3D frame in Autodesk Inventor

Presented finite element model is a 3D model. By implementation the modal analysis in Autodesk Inventor, obtained the values frequencies and main mode shapes of considered 3D frame.

Table 2 shows the values of the first six frequency oscillating of 3D frame.

Table 2: Periods and frequencies – Autodesk Inventor

Mode No	Frequency $f$ [Hz]
1	7.409
2	15.48
3	19.08
4	28.98
5	30.69
6	35.55

The first two modes oscillation of 3D frame are shown in Figure 6 and 7.

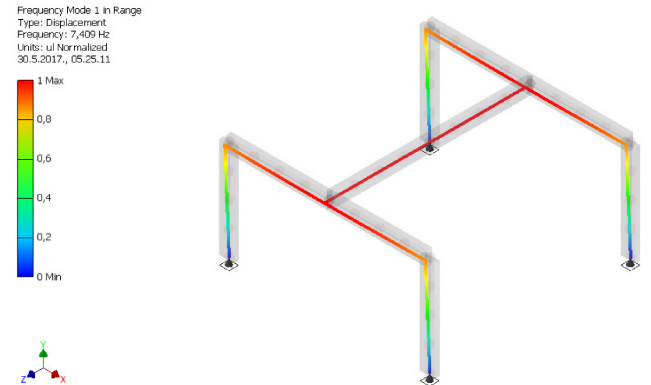


Figure 6: 1<sup>st</sup> mode shape

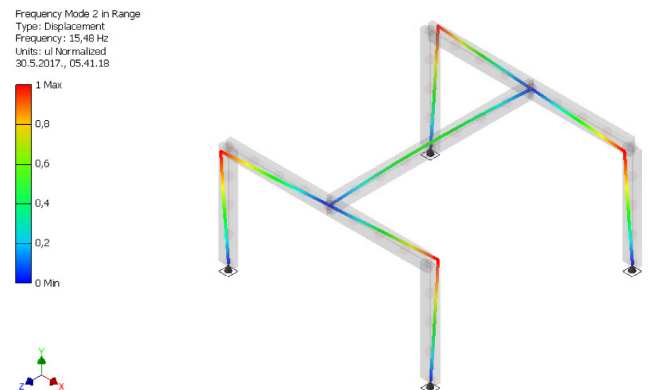


Figure 7: 2<sup>nd</sup> mode shape

Table 3 shows the comparative results for the first six circular frequencies.

Table 3: Frequencies – comparative results

Mode No	Frequency $f$ [Hz]		Difference $\Delta$ [%]
	Method of Consistent masses	Simulation by Inventor software	
1	7.392	7.409	0.23
2	15.49	15.48	0.06
3	19.12	19.08	0.21
4	29.14	28.98	0.55
5	30.77	30.69	0.26
6	35.61	35.55	0.17

By comparing the values of frequencies obtained through the mathematical model with the finite element approach and in a purely numerical way (FEA software Autodesk Inventor), excellent coinciding between the results of the first frequency and the relative difference

$\Delta=0.23$  [%] is noticed. Other frequencies coincide well, too. Thus, for example, for the next five frequencies the relative difference is up to 0.55 [%], which is very good for the 3D model.

## 6. CONCLUSION

The problem of oscillation in the space is present in mechanical and civil engineering.

In this paper discussed the frequency analysis of 3D frame. Has been applied approach to replace distributed mass consistently (equivalent) mass. In adopted accordance with the approach was formed in finite-element model considered spatial frame. To formed by the finite element model set is a mathematical formulation of free oscillations. On the theoretical basis presented in subtitles 2 and 3, the software package Mathematica written computer code for automated calculation of frequency and the oscillation period.

Validation of the theoretical results of frequency analysis applying the method of consistent masses was conducted simulation by software (Autodesk Inventor).

It has been proved that applying the method of consistent masses divide of the beam elements into finite elements may be coarser than that of the applying software Autodesk Inventor.

## REFERENCES

- [1] Ćorić B., Ranković S., Salatić R., "Dinamika konstrukcija", Univerzitet u Beogradu, Beograd (Srbija), (1998)
- [2] Filippov A. P., "Vibration of deformable systems", Moscow (Russian), (1970)
- [3] Maglaić Z., Simonović G., Hadžović R., Ademović N., "Određivanje osnovne forme i perioda oscilovanja građevina približnim metodama", Materijali i konstrukcije, Vol. 49(3-4), pp. 72-82, (2006)
- [4] Vasiljević R., Bulatović R., Savković M., "The Approaches to the Mathematical-Mechanical Modeling Supporting Construction", IMK-14 – Research & Development in Heavy Machinery, Vol. 19(1), pp. EN29-38, (2013)
- [5] Vasiljević R., "Uticajni parametri na dinamičko ponašanje noseće konstrukcije portalnih dizalica velikih nosivosti – Doktorska disertacija", Univerzitet u Kragujevcu, Kraljevo (2016)
- [6] Magrab E., "ENGINEERS GUIDE TO MATHEMATICA<sup>®</sup>", John Wiley and Sons, Chichester, (2014)

# Numerical Analysis of Tribomechanical System Brake Disc-pad for Heavy Duty Vehicles

Nadica Stojanovic<sup>1\*</sup>, Jasna Glisovic<sup>2</sup>, Blaza Stojanovic<sup>3</sup>, Ivan Grujic<sup>4</sup>

<sup>1</sup> University of Kragujevac, Faculty of Engineering/Department for Motor Vehicles and Motors, Kragujevac (Serbia)

<sup>2</sup> University of Kragujevac, Faculty of Engineering/Department for Motor Vehicles and Motors, Kragujevac (Serbia)

<sup>3</sup> University of Kragujevac, Faculty of Engineering/Department for Mechanical Constructions and Mechanization, Kragujevac (Serbia)

<sup>4</sup> University of Kragujevac, Faculty of Engineering/Department for Motor Vehicles and Motors, Kragujevac (Serbia)

*Brake system in addition to a steering system actively intervenes to help defuse critical driving situations and prevent accidents from happening come under the heading of active safety. The braking system is expected to be a reliable and durable under normal operating conditions of the vehicle, but also in extreme conditions. For an understanding of the nature of any problem, it is necessary first to realize where the problem originates and to analyze the influential factors. The problems of braking process are characterized by their tribological nature. This paper presents the application of contemporary - alternative materials for making the brake discs for heavy duty vehicles. Analysis was carried in the ANSYS software and the results of the analysis are shown, and also a comparison is made with the conventional discs. The obtained results point to problems that require more effort to develop the MMS materials whose cost and friction characteristics bring advantages over conventional material.*

**Keywords: Safety, Reliable, Steady, Alternative materials, MMS materials**

## 1. INTRODUCTION

All machines, assemblies and mechanisms consist, as a rule, of several basic movable machine elements [1]. There is relative motion of different surfaces in all these elements that are in direct or indirect contact.

Friction is in most cases, undesirable phenomenon, but not in the brake system. The negative side of friction in any system is heat generated due friction.

The main purpose of brakes is to stop or slow down the vehicle, by friction in the friction pair (brake disc and brake pads), and through contact between the tires and the road. They also need to adapt their effect to traffic conditions, and also to keep the vehicle in a steady state. The kinetic energy is transforming to heat that is generated on disc, and then is dissipated to environment [2]. The braking power in case of emergency braking is far greater than the engine power. The distribution of braking forces on each wheel, or more accurate on the front and rear axle, is very important, and it is essential to prevent traffic accidents.

Modern heavy duty vehicles are more and more equipped with disc brakes, and they use compressed air for transferring force to executive organs – brakes.

Disc brakes have numerous advantages in respect to drum brakes. Of course, they also have some disadvantages, but in most cases, advantages outweigh the disadvantages. One of the biggest advantages is that disc brakes can generate and dissipate a large amount of heat into the atmosphere. Friction occurs only on the surface contact between brake disc and pads. For this reason, the entire disc is not all exposed to friction, but only one part of the disc. The mechanism behind this phenomenon is such that part of the disc that has been exposed to friction and generates the heat in the next moment is no longer subjected to friction, but rotates freely and is exposed only to air, which also serves to release the generated heat due

to friction into the atmosphere. In this case, the advantage of these brakes is more efficient cooling that makes them better than other types of brakes. So, they are very suitable for use in heavy duty vehicles, and all this allows that these brakes maintain their characteristics and to be more efficient [3].

The brake discs are made of various kinds of high quality cast irons and rarely from steel. Cast irons are more suitable in respect to steel, because they are very easy for casting and for shaping in the desired form. Furthermore, they are easy for machining and have a high wear resistance. Surface contact that is achieved between cast iron and friction materials provides satisfactory friction coefficients, good properties at elevated temperatures; they are not deforming, and have very good thermal conductivity. In addition to all of this, they have low price.

Aluminum alloys have advanced application, due to the high strength, low density, durability, workability and availabilities. The composites of the aluminum metal matrix are combined with two or more additional ingredients, one of which is the matrix, while the other is the filler (reinforcing). Aluminum metal matrix may be a laminar, fibrous or in a particulate form. In general, the cast iron is used for the production of brake discs; however AMMC (Aluminum Metal Matrix Composite) is selected for several reasons in respect to the cast iron. The main purpose of the discs is to slow down or stop the vehicle or to maintain a constant speed, or to keep the vehicle stationary. Properties of these discs are defined by a suitable hardness, chemical composition, ultimate tensile strength and other necessary characteristics depending on the intended application. When preparing or mixing during the casting of the metal matrix with the composite, one must pay attention to the following factors:

- it is necessary to achieve a uniform distribution of the reinforcing material;
- it is necessary to achieve a good lubrication between the two main substances, and
- it is necessary to reduce porosity in the casting.

Aluminum alloys are increasingly used in the automotive industry, for reasons of achieving a weight reduction of vehicle and fuel consumption. It can be said that fuel consumption has a direct impact on carbon emissions. Application of composite materials has the potential to improve the braking performance thanks to its attractive properties compared to cast iron.

Joshi et al. [4] is performed a comparison of discs made of cast iron and MMC. Wear in case of cast iron increases with increasing load and sliding speed, while the friction coefficient is constant, but wear of the friction material is slightly higher compared with a cast iron. In the case of the MMC, this is not the case. Load and sliding speed have less influence on the wear. Brake pads have a higher degree of wear when the disc is made of the MMC, so it is necessary to develop new friction materials. The friction forces between the friction material and the MMS is 20% higher than in the case when the same friction material was in contact with the cast iron so that it directly affects the braking performance.

The main objective of Alnaqi et al. [5] was to replace conventional cast iron discs with discs made of aluminum alloys that are lighter. The main challenge is that costs are not high as well as to satisfy the basic requirements of modern vehicles. The influence of different parameters depending on the temperature is analyzed. The disc is made of wrought aluminum alloy coated with alumina in order to strengthen it. An alumina (dehydrated alumina) is coated using the plasma electrolytic oxidation process. The research showed that surface temperature of the disc reached 500°C, without any damage to the disc brake, except that the friction coefficient is decreased due to fade. In extreme brake conditions, the temperature of brake disc reached 550°C and at this temperature the disc was disintegrated. Authors came to the conclusion that it is not necessary to coat the entire disc because in this way, the heat dissipation from the disc to the environment is reduced; it is enough to coat the contact surfaces. It is also analyzed the effects of the coating thickness; which is the best, and they come to the conclusion that the optimum thickness is 30 µm, while the total disc thickness is 12.24 mm. This design of the disc could sustain two different and very extreme braking, if the vehicle's mass was 1400 kg.

During the studies that have been carried out by Adebisi et al. [6], the brake disc was made by the stir casting process. Weight of the disc in comparison with conventional discs is reduced for 50%. Compared to cast iron discs, the rate of heat dissipation into the environment has increased for 25% for pressure within the range of 1.5 - 2 MPa. In such conditions, there is no excessive heating, which negatively affects the braking process. Furthermore, the results obtained by numerical analysis have a good agreement with the experiment results. In the end, it was concluded that the cast iron disc can be replaced by alternative materials, and in addition they are very profitable.

Kumar et al. [7] have compared AIHMMC (Hybrid Aluminum Metal Matrix Composite) with Al6061. Hybrid alloy has a higher hardness compared to Al6061 for 45%. With a longer sliding distance, the wear resistance of AIHMMC is higher compared to AL6061 for 20-50%, depending on the effects of load and sliding speed. Ingredients that are added to the material during the manufacturing of the brake disc contribute to this. Stable mean friction coefficient is achieved for AIHMMC at a load of 20 N, sliding speed of 6.28 m/s and sliding distance of 2400 m, while for Al6061 can be achieved at 40 N, 4.18 m/s and 2400 m. By optimizing the parameters, it has been shown that at 20 N; 2.06 m/s and 800 m, AIHMMC has a smaller specific wear rate compared to Al6061. It can be said that the wear rate in the first place most affected by the load, then sliding speeds and eventually sliding distance. Based on the observed wear rates for both materials, it has been shown that the sliding speed for Al6061 has an influence of 39.57% and 42.51% for AIHMMC. Applied load for AIHMMC has a greater influence compared to the sliding speed.

The friction coefficient depends on the coating of the brake disc. The braking process is conducted on the dynamometer, and the values were in the range 0.28 - 0.34, that is acceptable for modern braking systems [8]. The coated discs were highly resistant to elevated temperatures, and it was found that at a temperature of about 500°C disc was not damaged. Disc made of aluminum alloy without the coating, as well as the disc of the MMC could not withstand such severe conditions. Furthermore, the experiment has shown that in the aluminum alloy coated, the surface was uniform and more resistant, unlike the aluminum metal matrix which was also coated. Discs of aluminum alloy coated had a very good performance. However, when reaching a temperature of 550°C it was disintegrated.

Manufacturers of brake discs for various categories of vehicles offer different solutions regarding use the aluminum in brake disc manufacturing. The application of aluminum brake discs, that are one of the most important vehicle assemblies, is primarily intended to reduce the mass of the rotating parts that are responsible for braking distance. Vehicle weight also has influence on fuel consumption, which is one of the prominent demands that are placed in front of each vehicle. Fuel consumption has a direct impact on the emission of carbon oxides from the vehicle, and the fuel consumption is direct related to the vehicle mass.

An example of the latest technologies in the field of braking is the American company Matrix, which not only made the motorcycle brakes, but brakes for NASA and also for the US Army Research Laboratory. Their patent is, in fact, a brake disc made from MMC that is still on pending. They are primarily focused on discs that are installed on the Harley-Davidson and Indian Motorcycles. The company claims that such a disc provides powerful performance and a good adjustment, and they are available for motorcycle manufacturers [9]. The brake disc of Matrix Company is shown in Figure 1. The price of such a disc is 399.00 dollars.

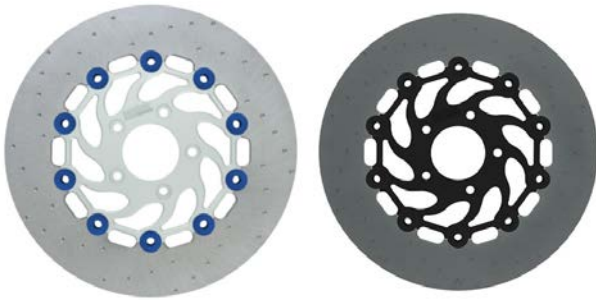


Figure 1: Matrix Company brake discs [10]

Composite brake discs are the latest innovation in braking. They are very light because they are manufactured from aluminum metal matrix which in addition offers a lifetime warranty, but only in cases when used with the appropriate brake pads recommended by the manufacturer. Advantages of such brake discs on motorcycles are the following:

- never corrode;
- generate less dust in the braking process;
- produce ten times less noise in the braking process, and
- five times faster cooling compared to discs of cast iron to a temperature of 750°C [10].

Tehter is a German company that manufactures brake discs and brake pads for road vehicles. The two-part brake discs of mentioned company consisting of a disc top hat (2) and friction ring (1), made of high carb cast iron, that are connected with rivets, are shown in Figure 2. The use of aluminum for disc brake head can decrease disc's weight for 15-20%, thereby reducing the so-called not suspension mass of a brake disc [11]. Two-piece discs with reduced weight do not affect only on improving the driving properties, but also reduce emissions. They are available in a large number of models of BMW Company. The advantages of two-piece discs are reflected in the following:

- Optimal driving properties by reducing a non suspension mass;
- Fuel consumption reduction;
- Quality improvement of the thermal conductivity, which leads to the reduced thermal stresses, and this reduces oscillations of a brake disc;
- Greater resistance on load that occurs during the braking process, thanks to the optimization of brakes dynamic;
- Better visual appearance of the disc;
- Resistance to corrosion;
- Lower noise level during braking process and
- Less time needed during the production of discs, thanks to the application of screws.



Figure 2: Two-piece brake discs 1-friction ring, 2-top hat [11]

Also, two-piece discs are used on trucks. One such brake disc made in Hendrickson Company is shown in Figure 3. These discs are also offered in the catalogs of other manufacturers such as Wabco and Knorr/Bendix [12]. The same as in the case of passenger vehicle brakes, trucks brake disc cover is made of aluminum, while the friction ring is made of cast iron (Figure 3). The reason for this is to reduce the non suspended mass [13, 14].



Figure 3: A two-part disc used on trucks [12]

Application of alternative solutions is now present in trains, too. The brake discs made of aluminum, are reinforced, and as already mentioned reduce the brake system's weight by 50% and also reduce the wear of the brake disc and the brake pads. It can be said that the wear of such a friction pair is much lower compared to the brake disc made of cast iron [15].

Depending on the speed the train can achieve, and also the transit type engaged (maximum permissible speed), a particular type of disc brakes is installed on trains, or more accurate disc brakes that are manufactured from specific materials, Figure 4. If one train can develop a speed greater than 400 km/h, allowed brake discs are discs made of ceramic or cast steel. If the train is moving at speeds up to 200 km/h, it does not need these discs, but can use discs made of aluminum or cast iron. Proper selection of the brake disc and the brake pads has a significant influence on the amount of costs and service life of such components [15].

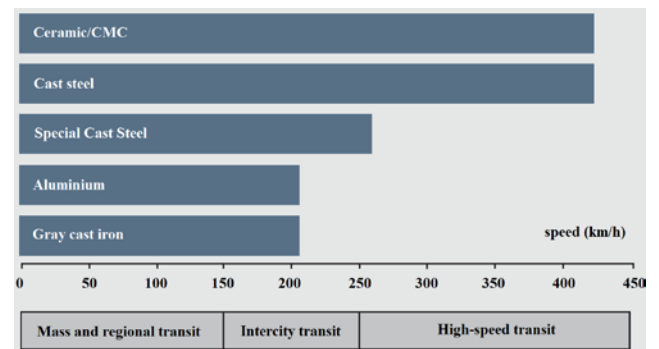


Figure 4: Typical application areas for brake disc's materials for rail vehicles [15]

## 2. TRIBOLOGICAL STUDY OF BRAKES

It is very difficult to perform an analysis of interaction between the disc and pads because of composition of brake pads, surface structure, and because of differences in mechanical properties of the brake pads' materials [16]. These differences existing among the elements create a barrier to consistency and reproducibility of results. Microscopic research has largest application in

terms of the contact geometry, the surface composition and the mechanical characteristics of the contact zone.

Overview of the dynamic contact that is made between the two contact surfaces, in this case, the disc and the brake pads, is very difficult to achieve, primarily because of type of two surfaces that are in contact. A particular problem is the fact that it is possible to see the topography of the area just before or after the braking process. Based on this, it is difficult to determine what happens during the contact, and we can only anticipate.

Surface contact between the brake pads and the disc does not represent two ideal flat surfaces. It can be said, for each of them, to have a plateau, as protrusions and recesses and contact are achieved between these peaks of uneven surfaces. There are two types of contact plateaus: primary and secondary (see Figure 5). The primary contact plateau is the result of the hard fibers of the brake pads that have a lower tendency to wear. These contact plateaus formed a map of channels on the disc, and also influence on the appearance of secondary contact plateaus [16]. Fibers scratch disc leaving channels behind, and the material removed from the disc in this way is collected on the brake pad. Through contact plateaus, the frictional force is achieved. All this has a great influence on the friction that is achieved between the contact surfaces.

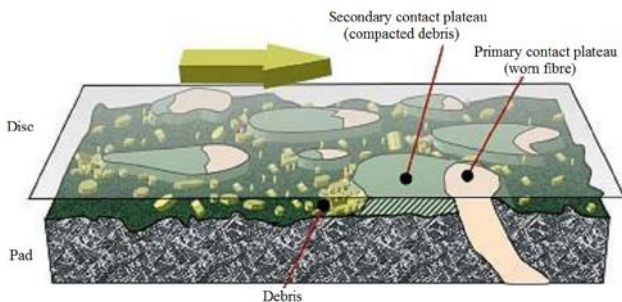


Figure 5: Systematic representation of contact plateaus [16]

It is believed that the wear debris accumulation depends on the wear intensity, the distance between the disc and the brake pads, friction and the normal loads. The formation and growth of secondary contact plateaus can be started in one moment, but only in the case when there are favorable conditions for the formation [16]. Within a thin layer that is formed on the upper layer of the secondary plateaus, the tribofilm has of high density and strength. It can be said that tribofilm has hardness close to fibers used to produce brake pads, while the rest of the film, under the secondary plateaus, is much softer, and this is shown in Figure 6.

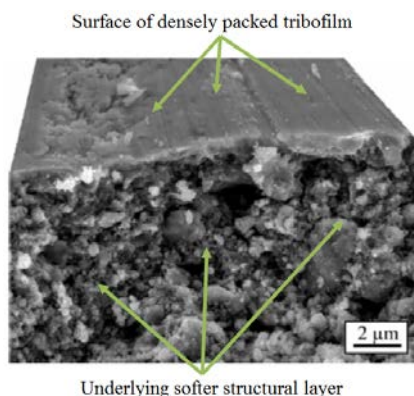


Figure 6: SEM cross-section of secondary plateaus [16]

The lower surface between plateaus is more prone to the accumulation of wear debris, or more accurate these are parts of the brake pad consisted of binders, fillers and friction modifiers. This represents a paradox because the topography remains in a stable condition. Lower areas are never in direct contact, but the stable state of topography indicates that there is a wear. The occurrence of the wear can be explained by the existence of a direct contact with a third body, such as the wear debris [16]. Wear due to wear debris are much higher in the space between the brake pads and disc because they cannot "escape" from the contact zone and comes to grinding. These particles become smaller and smaller until they succeed to "escape" from the contact zone or become a part of the secondary plateaus.

The study of contact surfaces i.e. the plateaus in contact showed that the extent of these irregularities depends on the brake pressure. At low brake pressures, the average size of plateaus that has been recorded is in the range of 50 to 500  $\mu\text{m}$ , and represents 10-30% of the nominal area of the brake pads [16]. Under the high pressures and temperatures, the plateaus can reach the size up to one millimeter.

### 3. NUMERICAL ANALYSIS

The performed analysis is dynamic analysis that depends on time. Analysis provided us with an answer regarding the behavior of structures depending on the time under load [17]. Analyzed assembly is shown in Figure 7.

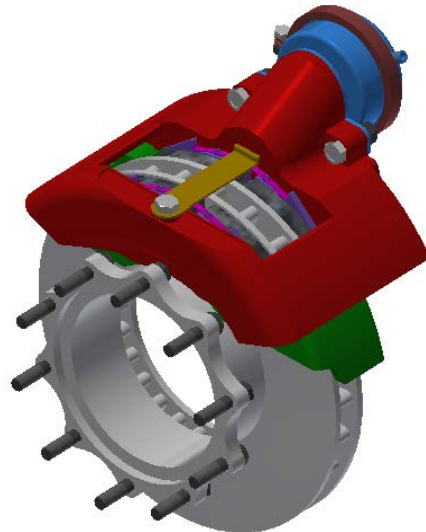


Figure 7: Air disc brakes for heavy duty commercial vehicle

However, as the subject of this paper is tribomechanical analysis of the system - the brake disc and brake pads, only they will be considered. The design of the considered assembly is shown in Figure 8.

#### 3.1. Defining material properties

The mechanical properties of materials used for the analysis of the friction pairs are shown in Table 1. It is necessary first to define the material properties. This was done because the applied software provides properties of general-standard materials. For the specific case, it is necessary to define the properties of the applied material.



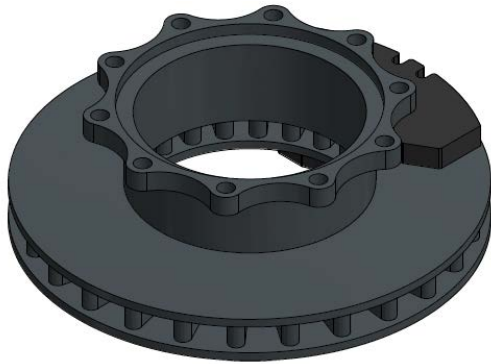


Figure 8: Ventilated disc brake and brake pads

Table 1. Mechanical properties of materials of brake disc and pads [18]

	Disc	Pad
Density [kg/m <sup>3</sup> ]	2903	2595
Young's modulus [GPa]	113	22
Poisson ratio [-]	0.24	0.25
Friction coefficient [-]	0.3 – 0.35	

3.2. Model creating

Various software packages, which have the main task to carry out the structural analysis of the parts and assemblies, are not suitable for the formation of complex models (CAD). They have the possibility of modeling parts, but this design phase is significantly more complicated to perform, in contrast to the software which has the main purpose of creating parts, specifically refers to the applied software package. ANSYS enables import of parts models that have already been created in a software package specifically designed for modeling.

3.3. Boundary conditions

The materials used for this specific case allow the friction coefficient within the range of 0.3 to 0.35 at the pressure of 1 - 2 MPa [18]. Adopted value of the friction coefficient is 0.336, while the value of the pressure is 1 MPa.

After defining the contacts, it is necessary to define the finite element mesh. Disc and pads are shown in Figure 9, in the form of finite elements mash.

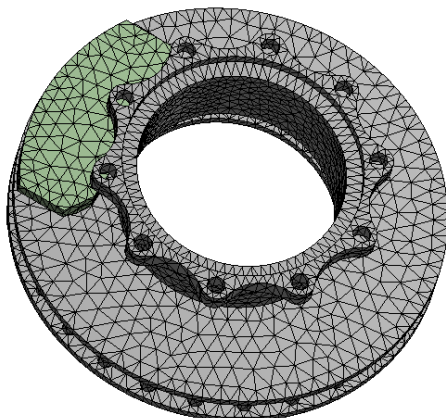


Figure 9: Disc and brake pads represented as the finite element mesh

To achieve a credible analysis that accurately represents what is happening in exploitation of brakes, it is

necessary to define the disc's speed at the moment of contact with pads, and the intensity of force pads acting on the disc. Adopted value of pressure pads acting on the disc is 1 MPa. However, it is necessary to specify the load in the form of force. The force the pads acting on the disc is 18340 N. The initial speed of the disc is 10 rad/s, which corresponds to the vehicle speed of 20 km/h.

4. RESULTS AND DISCUSSION

Obtained results in contact of the disc and both brake pads external and internal, are shown in Figures 10-15. Analysis is performed for the disc that is made of MMC materials, while the friction material has the organic origins because it is only possible to achieve a required friction coefficient between these two materials.

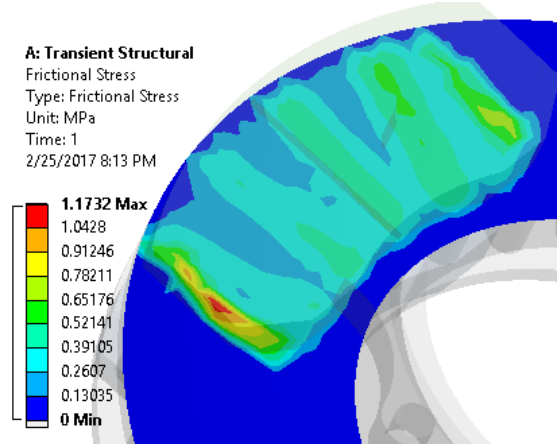


Figure 10: Contact frictional stress at the outside of the disc

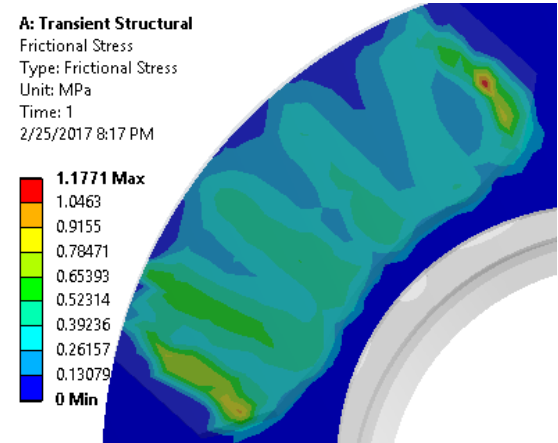


Figure 11: Contact frictional stress at the inside of the disc

Frictional stress that occurs in the contact pair is represented in Figures 10 and 11. The definition of the frictional stress is the stress that occurs between the two elements which slide onto one another, with condition that their contact surface is defined by friction [19]. First, it can be concluded that the higher values are obtained on the inner contact pairs. Observing Figure 10, where the disc rotates in mathematically positive direction, it can be concluded that the highest values of the frictional stress occur in the first part. This is a consequence of the impact load. Furthermore, the same can applies to the inner contact.

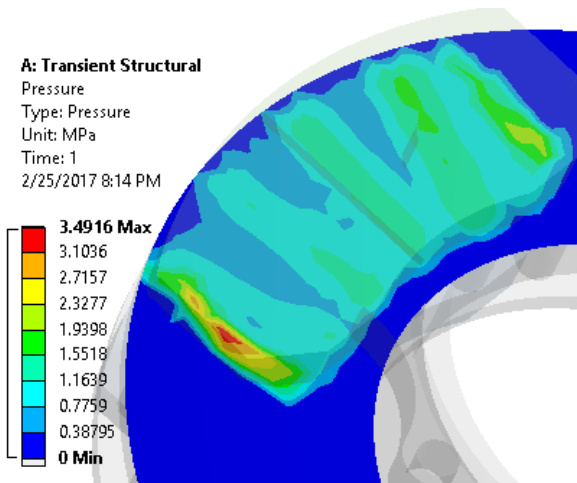


Figure 12: Contact pressure at the outside of the disc

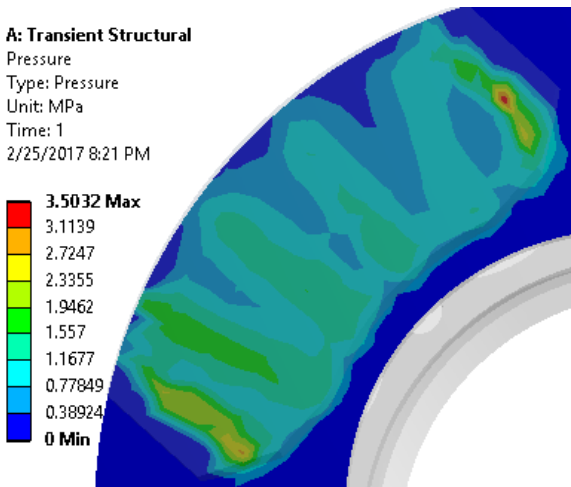


Figure 13: Contact pressure at the inside of the disc

Contact pressure that occurs at the inner and outer side of the disc, is shown in Figures 12 and 13. Furthermore, like in previous case, larger pressures are achieved at the inner side of the disc.

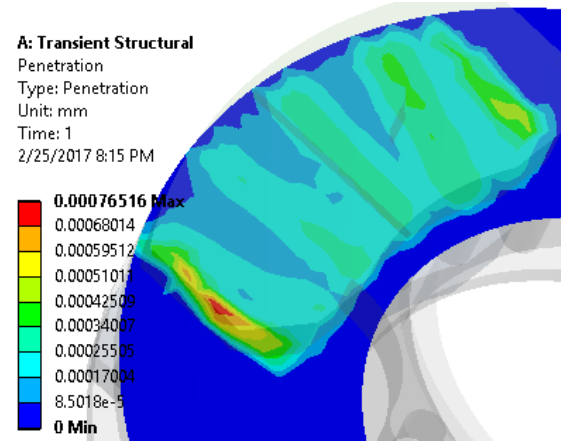


Figure 14: Contact penetration at the outside of the disc

Values of the contact penetration are shown in Figures 14 and 15. However, unlike the frictional stress and pressure, the greater penetration is achieved at the outside of the disc. The highest values of the penetration occur, the same as before, in places where the first contact occurs.

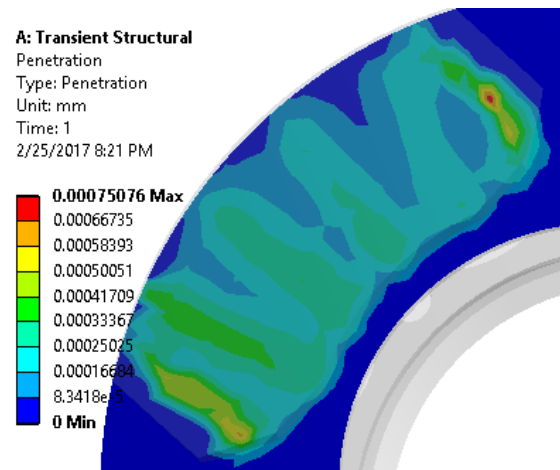


Figure 15: Contact penetration at inside of the disc

Most widely used materials for manufacturing brake discs are cast iron. It is very important to take into account the choice of materials used to produce brake pads. The reason for this lies in the fact that the required friction coefficient can not be achieved between any friction material and disc. The material properties for cast iron, as well as the friction material, which combines with the mentioned material is given in Table 2.

Table 2: Material properties of the MMC brake disc and brake pads [20]

	Disc	Pad
Density [kg/m <sup>3</sup> ]	7250	1400
Young's modulus [GPa]	138	1
Poisson ratio [-]	0.28	0.25
Friction coefficient [-]	0.336	

Below is a comparison of the frictional stress, pressure and penetration that is realized whether it is MMC brake discs or discs made of cast iron. Analysis is carried out under the same exploitation conditions.

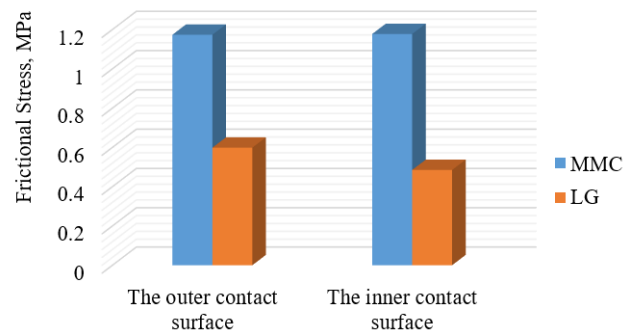


Figure 16: Frictional stress that occurs on the inner and external contact surface depending on the material properties of the friction pair

By observing the Figure 16, it can be noticed that the higher values of frictional stress are realized for discs made of MMC materials. The result of this is that the properties of materials used for the production of discs and brake pads. Comparing the properties of the material used for disc, as well as the materials used for the production of brake pads, it can be seen that they are different. First, the properties of the material used for disc made of MMC are observed, and it has smaller values for all properties compared to the cast iron. While the properties of material use for the brake pads that are combined with the MMC

disc, have greater density and Young's modulus of elasticity than the pads that go in combination with cast iron, while the Poisson's ratio is equal.

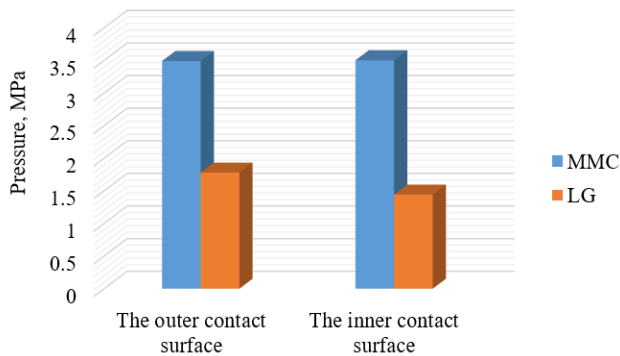


Figure 17: Contact pressure that occurs on the inner and external contact surface depending on the material properties of the friction pair

When it comes to the pressure, it is the same situation as with frictional stress (Figure 17). Higher values occur for discs made of MMC.

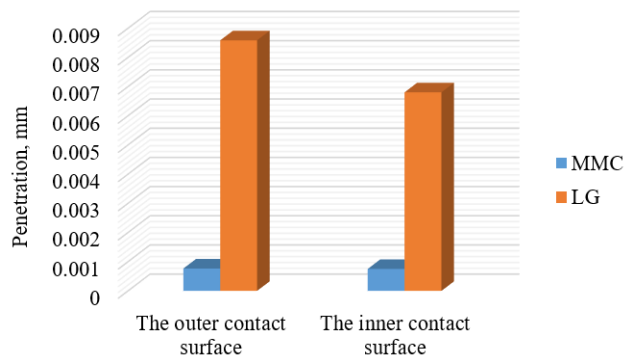


Figure 18: Penetration that occurs on the inner and external contact surface depending on the material properties of the friction pair

At the end, a comparison of penetration values between discs that are made of MMC and cast iron is performed. Unlike the two previous analyses, higher values occur for the discs that are made of cast iron. This means that the higher wear occurs on discs made of cast iron, as shown in Figure 18.

## 5. CONCLUSION

Obtained results showed that the higher frictional stresses and pressures occur on the inner side of the disc. This directly affects the bending of the friction ring to the outside, so-called „umbrella effect“. Higher values of penetration are achieved on the outside of the disc. This is precisely the result of higher values of pressure and stresses that are obtained on the inner side of the friction ring.

Furthermore, one more analysis that shows the comparison between discs made of MMC and of cast iron is performed. Obtained results show that greater pressures and stresses are obtained on discs that are made of MMC, while higher values of penetration occur on disc made of cast iron.

For further research because the emphasis is placed on the alternative materials, it is necessary to modify the materials applied for the analysis. The result would be less

value to be obtained for the pressure and stress. Achieved great stresses and pressures can have a major influence on fatigue and can result in catastrophic failure of the brake disc. Furthermore, performed a numerical analysis must be validating by the experiment. Of course, the goal of the research is to start applying MMC discs on the other classes of road vehicles, not just on motorcycles.

## ACKNOWLEDGEMENTS

This paper was realized within the researching project "The research of vehicle safety as part of a cybernetic system: Driver-Vehicle-Environment" ref. no. 35041, funded by Ministry of Education, Science and Technological Development of the Republic of Serbia.

## REFERENCES

- [1] [http://www.rgf.rs/predmet/RO/VII%20semestar/Eksploatacija%20i%20odrzavanje%20gasovodnih%20sistema/Pr edavanja/EiOGasS\\_12.pdf](http://www.rgf.rs/predmet/RO/VII%20semestar/Eksploatacija%20i%20odrzavanje%20gasovodnih%20sistema/Pr edavanja/EiOGasS_12.pdf)
- [2] B. J. Breuer and U. Dausend, "Advanced Brake Technology", Warrendale, Pa. SAE International, R-352, (2003).
- [3] <http://lincolntrial.integr8cms.net/index.php/27-disc-brakes/section-6/discbs/7-discbs-advantages-and-disadvantages-of-disc-brakes>
- [4] Y. G. Joshi, A. R. Gupta and R. U. Shingarwade, "Scrutinization of A356/25sic AMC and Gray Cast Iron as Brake Rotor Material", International Journal of Research in Advent Technology, Vol. 2 (2), pp. 1-6, (2014).
- [5] A. Alnaqi, S. Shrestha, D. Barton, and P. Brooks, "Optimisation of Alumina Coated Lightweight Brake Rotor", SAE Technical Paper 2014-01-2501, (2014).
- [6] A. A. Adebisi, A. Maleque and Q. H. Shah, "Performance assessment of aluminium composite material for automotive brake rotor", International Journal of Vehicle Systems Modelling and Testing, Vol. 9 (3/4), pp. 207-217, (2014).
- [7] M. Kumar, V. Baskaran and K.S. Hanumanth Ramji, "Effect of sliding distance on dry sliding tribological behaviour of Aluminium Hybrid Metal Matrix Composite (AlHMMC): An alternate for automobile brake rotor – A Grey Relational approach", Proceedings of the Institution of Mechanical Engineers, Part J: Journal of Engineering Tribology, Vol 230 (4), pp. 402-415, (2016).
- [8] A. Alnaqi, S. Kosarieh, D. Barton, P. Brooks and S. Shrestha, "Material characterisation of lightweight disc brake rotors", Proceedings of the Institution of Mechanical Engineers, Part L: Journal Materials: Design and Applications, (2016).
- [9] <https://www.ethz.ch/content/dam/ethz/special-interest/matl/departement/news/materialsday/materialsday-2001-beffort.pdf>
- [10] <https://www.matrixbrakes.com/about-us-a/263.htm>
- [11] <http://textar.com/composite-brake-discs/>
- [12] <http://www.hendrickson-intl.com/Trailer/Wheelend-Brakes/Air-Disc-Brakes#tabs>

- [13] <http://www.kenworth.com/news/news-releases/2013/december/bendix-air-disc-brakes/>
- [14] <http://www.foundationbrakes.com/media/documents/airdiscbrakes/overviewbrochure.pdf>
- [15] [http://www.knorr-bremse.com/media/documents/railvehicles/product\\_broschures/brake\\_systems/Brake\\_Disc\\_Pads\\_P\\_1264\\_EN.pdf](http://www.knorr-bremse.com/media/documents/railvehicles/product_broschures/brake_systems/Brake_Disc_Pads_P_1264_EN.pdf)
- [16] <http://www.ewp.rpi.edu/hartford/~ernesto/F2013/FWLM/StudProj/Feist/Feist-TPR.pdf>
- [17] C. Xiaolin and L. Yijun, "Finite Element Modeling and Simulation with Ansys Workbench", CRC Press, New York, (2014), ISBN 978-1-4398-7385-4.
- [18] A. A. Adebisi, M. A. Maleque and Q. H. Shah., "Surface temperature distribution in a composite brake rotor" International Journal of Mechanical and Materials Engineering, Vol 6(3), pp. 356-361, (2011).
- [19] G. Skeie, N. Sødahl and O. Steinkjer, "Efficient Fatigue Analysis of Helix Elements in Umbilicals and Flexible Risers: Theory and Applications", Journal of Applied Mathematics, Vol. 2012, pp.1-22, (2012).
- [20] A. Belhocine and M. Bouchhetara, "Thermomechanical Behaviour of Dry Contacts in Disc Brake Rotor with a Grey Cast Iron Composition", Trans Indian Inst Met, Vol 65(3), pp. 231-238, (2012).

# Analytical, Experimental and Numerical Study of Semi-rigid Beam-to-Column Connections in the Steel Structure of Pallet Racks

Rodoljub Vujanac<sup>1</sup>, Snezana Vulovic<sup>2</sup>, Nenad Miloradovic<sup>3</sup>, Aleksandar Disic<sup>4</sup>

<sup>1</sup>Faculty of Engineering/Mechanical Construction and Mechanization, University of Kragujevac, Kragujevac (Serbia)

<sup>2</sup>Faculty of Engineering/ Applied Mechanics and Automatic Control, University of Kragujevac, Kragujevac (Serbia)

<sup>3</sup>Faculty of Engineering/Mechanical Construction and Mechanization, University of Kragujevac, Kragujevac (Serbia)

<sup>4</sup>Faculty of Engineering/ Applied Mechanics and Automatic Control, University of Kragujevac, Kragujevac (Serbia)

*In practice, there are different types and designs of beam-to-column connections, which characterize the different racks manufacturers. In general classification and modelling of connections has been treated according to Eurocode 3. But, as it is impossible to develop a general analytical model for calculating of these connections, currently the only way to determine the properties of such connections is an experiment. In this paper are shown the test procedure and results of beam-to-column connections behavior according to the procedure defined in the FEM recommendations. In order to avoid a large number of expensive tests with aim to determine structural properties for different types of connection which in practice may be very much, in this paper are shown developed analytical procedure as well as numerical model which simulate the experiment. After verification of the numerical model to the available experimental results, it can be applied to various combinations of beam-to-column connections*

**Keywords:** Pallet racks, Moment-rotation curve, Stiffness, Beam-to-column connection, Finite element method

## 1. INTRODUCTION

Racking systems play a key role in achieving today's manufacturing and distribution needs determined by competitive markets. When choosing storage equipment, an engineer is faced with a wide array of options. Racking systems ranging from the conventional selective/adjustable rack, double-deep selective rack, push-back, drive-in or drive-through rack, to live pallet storage and mobile storage system are the most common pallet storage configurations, [1].

In this paper connections that are established between elements of the steel structure of conventional, i.e. selective pallet racks were analysed. In general classification and modelling of connections has been treated according to Eurocode 3. As it is impossible to develop a general analytical model for calculating these connections, currently the only way to determine the properties of such connections is an experiment. In this paper is analysed the test procedure and results of beam-to-column connections according to the procedure defined in the FEM recommendations in order to determine the moment-rotation curve ( $M-\Phi$  curve), [2]. Influence of connections to the global structural racks behavior introduced with  $M-\Phi$  curve and its structural properties: stiffness, bending strength and rotational capacity. In order to avoid a large number of expensive tests with aim to determine the  $M-\Phi$  curves for different types of connection which in practice may be very much, this paper presented developed numerical model which simulate the experiment using the finite element method. After verification of the model to the available experimental results, it can be applied to various combinations of beam-to-column connections. Reliable determination of

structural properties of the connection using the developed model can be made a global analysis of the structural behavior and the calculation of elements according to the procedures defined in the FEM recommendations, too.

The study on joint rigidity dates back to the beginning of the nineties both at experimental and analytical front. But the studies on joint for cold-formed steel particularly on pallet rack system are only few decade old.

## 2. CONFIGURATION OF PALLET RACKING SYSTEM

A typical selective pallet rack configuration is shown in figure 1, [1]. The vertical frames and horizontal beams, usually made of thin-walled cold-formed profiles form a spatial frame structure of pallet racking system. Upright frames lie in the vertical plane, in the cross aisle direction, normal to the main aisle of the rack. They consist of two perforated uprights linked together by a system of diagonal and/or horizontal bracing welded or bolted to the uprights. This bracing system provide rack stability in cross-aisle direction. Beams connecting adjacent frames and lying in the horizontal direction parallel to the main aisle. Beam-end connectors are welded to or otherwise formed as an integral part of the beams, which has special devices which engage in holes or slots in the upright. The down-aisle stability primary is provided by the stiffness of the joints between uprights and beams. In the current practice connections are characterized as rigid or elastic, i.e. traditional method of calculation based on the assumption of an ideal relationship between the structural elements, [3]. However, the practice and laboratory tests have shown that there are connections with

characteristics between the elastic and rigid. Therefore, the classification of connection was made as:

- simple or elastic joint,
- continuous or rigid and
- semi – rigid.

The beam end connector provides a semi-rigid connection between the beam and the upright. The semi-rigid behaviour is due to the distortion of upright-walls, tearing of upright perforation and distortion of beam end connector. In practice, there are different types and designs of these connections, which characterize the different racks manufacturers, [1]. The overall performance of a rack system depends on the efficiency of beam end connector.

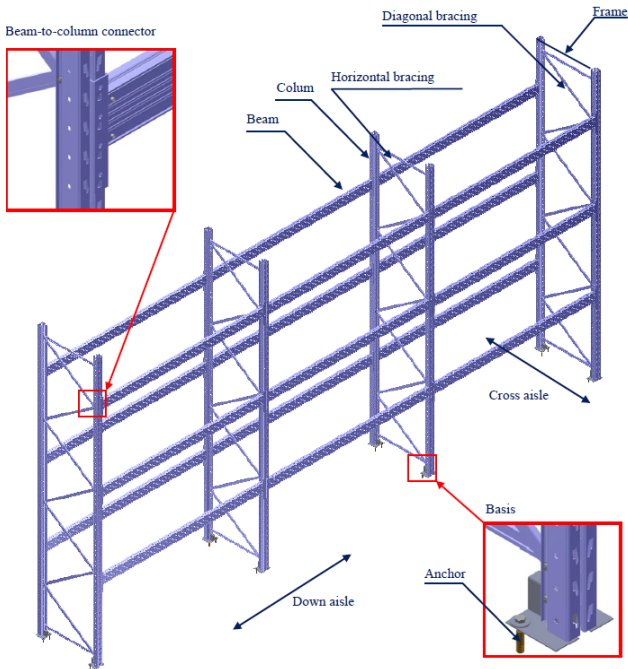


Figure 1: Main elements of the steel structure of pallet racks

### 3. ANALYSIS OF BEAM-TO-COLUMN CONNECTION

#### 3.1. Structural properties of the connection

Behaviour of connection is defined by the curve which shows the correlation between the bending moment in the connecting point  $M_{j,Ed}$  and relative rotation of the joint  $\Phi_{Ed}$ . This curve is known in literature as  $M-\Phi$  curve or  $M-\Phi$  characteristic as shown on figure 2 and can be determined experimentally, based on semi-empirical expressions given for various types of connection, applying some numeric methods, or based on the recommendations in the regulations that deal with this issue (Eurocodes, FEM regulations). In some cases, the real  $M-\Phi$  characteristic includes some rotation due to effects such as screw slippage, mistakes in execution, etc. This can result in significant initial rotations that should be included in the calculation  $M-\Phi$  curve.

Using  $M-\Phi$  curve can be determined three main structural properties of the connection:

- bending strength  $M_{j,Rd}$ ,
- rotational stiffness  $S_j$  and
- rotational capacity  $\Phi_{Cd}$ .

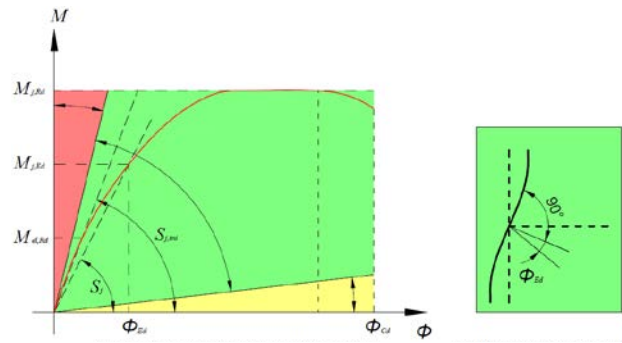


Figure 2:  $M-\Phi$  curve with structural properties

#### 3.2. Bending tests on beam end connectors

The purpose of the test is to determine the stiffness and the bending strength of the beam end connector, [2]. The structural behaviour of the upright and beam end connector assembly is critical to the behaviour of the complete structure. It is influenced by a large number of factors, particularly:

- the type of the upright;
- the thickness of the upright;
- the type of beam;
- the position of the beam on the connector;
- the method of connecting the beam to the connector;
- the bracket type;
- the properties of the materials used.

All combinations of these factors, which occur in the design of the structural system, shall be tested separately, unless it can be reasonably demonstrated that interpolation of results provides a conservative estimate of performance.

For each upright and connector assembly, a number of nominally identical tests shall be made so that the results may be interpreted statistically in accordance with [2] and [3].

##### 3.2.1. Test Arrangements

A short length of upright shall be connected to a relatively very stiff testing frame at two points with a clear distance,  $h$ , between them where:

$$h_c < \text{beam connector length} + 2 \times \text{column face width} \quad (1)$$

Over this distance there shall be no contact during the test between the upright and the testing frame. A short length of beam shall be connected to the upright by means of the connector to be tested, and beam locks shall be in place. Typical examples of suitable test arrangements are shown in figure 3.

Sideways movement and twisting of the beam end shall be prevented by a lateral restraint which, however, allows the beam component to move freely in the direction of the load. Alternatively, a pair of connectors may be tested in parallel.

The load shall be applied at 400 mm from the face of the upright by an actuator at least 750 mm long between pinned ends, as shown in figure 3. The rotation may be measured by:

- displacement transducers bearing onto a plate tack-welded to the beam close to the connector, but with enough clearance to allow for connector distortion (Gauges C1 and C2 in figure 3), or
- by an inclinometer connected to the beam close to the connector.

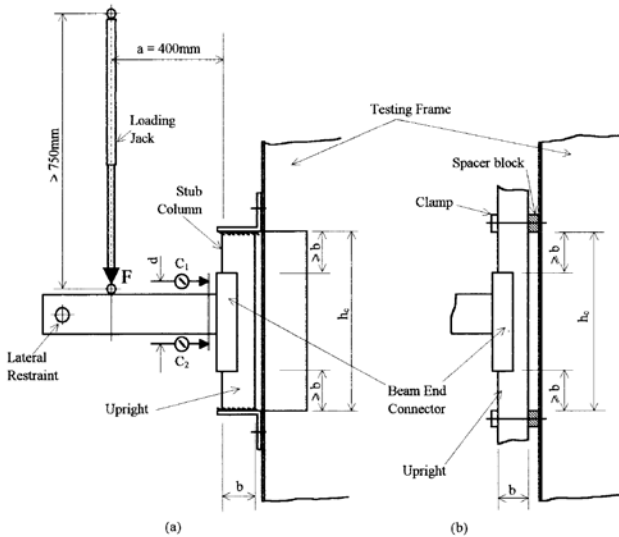


Figure 3: Arrangement for beam end connector bending test with alternative methods of supporting the upright

Figure 4 shows a photograph of the realized tests, fully in accordance with the above described scheme. A bending test on beam end connectors is carried out in accordance with norm UNI EN 15512, [2].

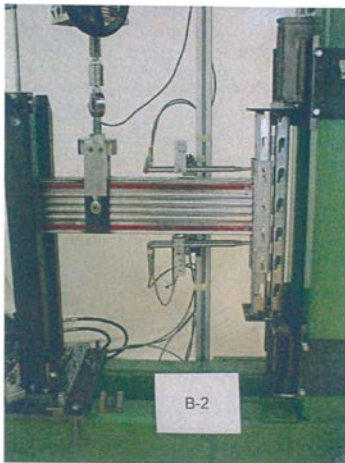


Figure 4: Photos of experiment settings

Referring to the experiments carried out on various connections, a bending test on beam end connectors are determined by measuring the size of all related to the dimensions and position of the elements of the sample in the testing equipment, and it is shown on figure 5 and given in table 1. Dimensions which determine the position of the device for measuring displacement are shown on figure 5 as well as given in table 2.

In this paper was analysed part of very large family of uprights marked alphanumeric as S80L and beams marked as R140L, both made by the same manufacturer. The symbols L, L, M, MH, and H in the columns respectively indicate the wall thickness of 1.25; 1.5; 2; 2.5 and 3 mm. The symbols L, M and H in the beams respectively denote the thickness of the beam wall of 1; 1.25 and 1.5 mm. Bending tests have been carried out on five samples as shown in tables. Each sample consists of a part of the column, beam which is connected to the column through beam end connector and secured from falling out by a safety pin. The first four samples were subjected to the load caused by normal operating conditions (bending moment is conventionally defined as

positive), while the fifth pattern is subjected to a stress in such a way that the load tends to separate the connection (bending moment is a negative value).

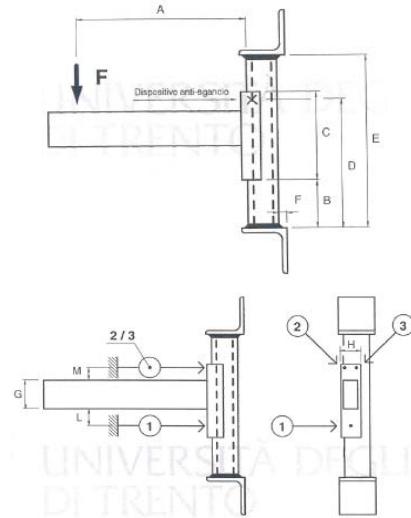


Figure 5: Disposition of dimensions which determine the position of a samples as well as device for measuring displacement under tests

Table 1: Dimensions which determine the position of a samples

Joint	Sample	A	B	C	D	E	F
S80ML-R100L	G-5	400	119	215	311	454	17.0
	G-6	400	120	215	312	454	19.1
	G-7	400	118	214	311	454	19.9
	G-8	400	118	214	311	454	19.3
	G-9	400	119	215	140	454	18.5
S80M-R120M	A-5	400	120	214	311	455	23.2
	A-6	400	120	215	311	454	23.0
	A-7	400	120	215	311	455	23.6
	A-8	400	120	215	311	455	23.9
	A-10	400	120	214	143	455	23.5
S80M-R140L	B-5	400	119	290	386	530	24.1
	B-6	400	119	290	385	530	23.7
	B-7	400	119	290	386	530	23.5
	B-8	400	119	289	386	530	23.6
	B-10	400	119	290	142	530	23.5

Table 2: Dimensions which determine the position of device for measuring displacement under tests

Joint	Sample	G [mm]	H [mm]	L [mm]	M [mm]
S80ML-R100L	G-5	99.5	69.2	47	12
	G-6	99.5	69.3	55	19
	G-7	99.5	69.3	56	18
	G-8	99.6	69.4	55	19
	G-9	99.6	69.4	49	33
S80M-R120M	A-5	119.9	69.5	35	18
	A-6	119.9	69.7	35	18
	A-7	119.9	69.3	27	19
	A-8	119.6	69.4	27	18
	A-10	119.9	69.5	30	30
S80M-R140L	B-5	139.8	69.1	43	17
	B-6	139.5	69.1	43	16
	B-7	139.1	69.3	42	17
	B-8	140.1	69.2	42	15
	B-10	139.00	69.2	42	29

### 3.2.2. Test Procedure

The tests described here load the connector vertically downwards in shear. If tests in the reverse direction show results for stiffness and strength which are less than 50% of the values measured in these tests, then the actual figures shall be measured for use in design.

Separate values for the stiffness and strength shall be obtained for both right and left hand connectors and the mean value used in design.

An initial load,  $F$ , equal to 10% of the anticipated failure load may be applied to the assembly and then removed as a preload in order to bed in the components. The gauges should then be reset. The load,  $F$ , shall then be increased gradually until the maximum load is reached and the connection fails. The rotation of the connection shall be observed and, for each test, a plot of the moment  $M$  and the rotation  $\Phi$  shall be made, in which:

$$M = a \cdot F \tag{2}$$

and

$$\Phi = \frac{\delta_2 - \delta_1}{d} \tag{3}$$

where:

- $a$  - lever arm for the load  $F$ ,
- $d$  - distance between the gauges  $C_1$  and  $C_2$ ,
- $\delta_1$  - deflection measured by gauge  $C_1$ ,
- $\delta_2$  - deflection measured by gauge  $C_2$ .

Based on tests realization connection rotation  $\Phi$  is determined from the equation:

$$\Phi = \frac{\delta_2 + \delta_3 - \delta_1}{L + G + M} \tag{4}$$

where:

- $\delta_k$  - deflection measured by gauge  $C_3$ ,
- $L$ ,  $G$  and  $M$  – dimensions shown in figure 5.

Bending tests on beam end connectors up to collapse under normal operating conditions (bending moment is conventionally defined positive) were performed on this rack structure. An initial loading-unloading cycles up to the maximum loading level  $F_0$  was performed, which is provided assembling and fitting of the elements in the connection, after which the load is increased incrementally until it reaches the value of the failure  $F_{ii}$ . In the table 3 are given the maximum measured values of the achieved load for each sample which corresponding to the moment calculated according to formula 2. In the table are also given duration of each probe as well as each sample.

Table 3: The measured values of the achieved load

Joint	Sample	$F_0$ kN	$F$ kN	$t$ s	$M_{ii}$ kNm
S80ML - R100L	G - 5	0.762	4.168	496	1.667
	G - 6	0.393	4.087	577	1.635
	G - 7	0.402	4.093	575	1.637
	G - 8	0.394	4.084	495	1.634
S80M - R120M	A - 5	0.581	5.678	340	2.271
	A - 6	0.578	5.458	381	2.183
	A - 7	0.563	5.708	407	2.283
	A - 8	0.554	5.741	436	2.296
S80M - R140L	B - 5	0.632	5.741	324	2.296
	B - 6	0.632	6.162	341	2.465
	B - 7	0.620	5.771	320	2.308
	B - 8	0.635	5.930	274	2.372
	B - 10	-0.590	-4.119	316	-1.647

### 3.2.3. Derivation of the Results

The failure moment,  $M_{ii}$ , shall be taken to be the maximum observed moment, as indicated in figure 7.

For each upright and connector assembly, the characteristic failure moment  $M_k$  shall be calculated in accordance with section 3.2.2. The design moment for the connection is then  $M_{Rd}$ , where:

$$M_{Rd} = \frac{M_k}{\gamma_M} \tag{5}$$

in which:

$\gamma_M$  - partial safety factor for connections, defined in [2] and [3].

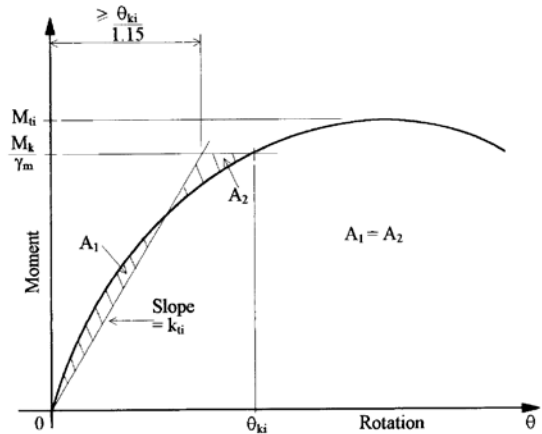


Figure 7: Derivation of connector stiffness

The rotational stiffness of the connector shall be obtained as the slope  $S_{ii}$  of a line through the origin which isolates equal areas between it and the experimental curve, below the design moment,  $M_{Rd}$ , as shown in figure 7, provided that:

$$S_{ii} \leq 1,15 \frac{M_k}{\Phi_{ki} \cdot \gamma_M} \tag{6}$$

The design value,  $S_d$ , of the connector stiffness shall be taken as the average value,  $S_m$  as shown in table 4, where:

$$S_m = \frac{1}{n} \sum_{i=1}^n S_{ni} \tag{7}$$

Table 4: Test results

Joint	Sample	$M_{ii}$ kNm	$M_m$ kNm	$M_k$ kNm	$M_{Rd}$ kNm	$S_{ii}$ kNm/rad	$S_m$ kNm/rad
S80ML -100L	G-5	1.667	1.643	1.601	1.455	32.65	37.20
	G-6	1.635				41.07	
	G-7	1.637				35.28	
	G-8	1.634				39.79	
S80M-120M	A-5	2.271	2.258	2.121	1.928	46.22	44.15
	A-6	2.183				43.05	
	A-7	2.283				43.43	
	A-8	2.296				43.90	
S80M-140L	B-5	2.296	2.360	2.153	1.957	92.06	94.54
	B-6	2.465				99.35	
	B-7	2.308				87.06	
	B-8	2.372				99.68	

### 3.3. Analytical polynomial model by the Frye-Morris method

The Frye-Morris method [4] proposes a non-dimensional polynomial model for determining the moment-rotation characteristic of a single connection, which is generated by replacing the size of its individual



parameters in a standardized connection. The size of the parameters used to determine the equation can be the thickness of the wall of the column  $t_u$ , the beam height  $d_b$  and the thickness of the wall of the beam profile  $t_b$ . The standardized link is then given by the equation:

$$\Phi_r = C_1(K \cdot M) + C_2(K \cdot M)^3 + C_3(K \cdot M)^5 \quad (8)$$

where is:

- $\Phi_r$  – relative rotation *rad*,
- $M$  – moment of rotation *kNmm*,
- $K$  – coefficient that escalates the ordinate of curves,
- $C_1, C_2, C_3$  – constants for fitting curves.

The factor  $K$  which scales the ordinates at the curve, taking into account the size of the individual connection parameters is calculated according to:

$$K = \prod_{j=1}^m q_j^{a_j} \quad (9)$$

Where is:

- $q_j$  - numerical value of  $j$  parameter *mm*,
- $a_j$  - exponent that shows the effect of the size of the  $j$  parameter on the moment-rotation relation,
- $m$  - number of parameters  $j$ ,

The determination of the exponent  $a_j$  in the equation (9) is performed on the basis of the pair of experimentally obtained curves moment-rotations for two joints which are identical, but in which they do not figure out the parameter  $q_j$  being considered.

The relationship between the moments  $M_1$  and  $M_2$  for connections 1 and 2 at rotation  $\Phi$  is assumed in the form:

$$\frac{M_1}{M_2} = \left( \frac{q_{j1}}{q_{j2}} \right)^{a_j} \quad (10)$$

where  $q_{j1}$  and  $q_{j2}$  are the values of the parameters  $q_j$  for connections 1 and 2 respectively.

From the relation (10) we can express the coefficient  $a_j$  according to:

$$a_j = \frac{\log(M_1 / M_2)}{\log(q_{j2} / q_{j1})} \quad (11)$$

The expression (11) is used to calculate the values of  $a_j$  corresponding to different rotations for each combination of experimental curves. When the mean value is calculated for all "m" exponents  $a_j$ , they are applied to a standardized moment-rotation diagram. Finally, the fitting procedure of curve is used to generate a standardized moment-rotation connection.

The mean value  $a_1$  for variable column thickness is  $-0.126$ , and  $a_2$  for variable heights of the beam is  $-2.981$  and  $a_3$  for the variable thickness of the beam is  $-0.121$ . Therefore, the standardized coefficient  $K$  follows that:

$$K = t_u^{-0,126} \cdot d_b^{-2,981} \cdot t_b^{-0,121} \quad (12)$$

Constants for fitting curves obtained for all connectors are shown in the Table 5, and the procedure developed in Microsoft Excel is used for their calculation.

The mean values of the coefficients are:

$$C_1= 4.3693e+1; C_2= 3.93e-2; C_3=4.35e-4$$

The Frye-Morris equation for the observed construction is:

$$\Phi_r = 4,36E+01(KM) + 3,93E-02(KM)^3 + 4,35E-4(KM)^5 \quad (13)$$

Table 5: Constants for fitting curves

Joint	Sample	$C_1$	$C_2$	$C_3$
S80ML-R100L	G-5	34.10479	2.00e-02	2.00e-04
	G-6	28.20721	2.01e-02	3.00e-04
	G-7	30.61559	7.01e-02	6.00e-04
	G-8	27.61125	1.44e-02	2.00e-04
S80M-R120M	A-5	44.65244	1.59e-02	1.00e-04
	A-6	46.20446	8.75e-02	5.00e-04
	A-7	47.30988	1.33e-02	8.00e-04
	A-8	47.27306	1.25e-02	6.00e-04
S80M-R140L	B-5	41.19487	2.25e-02	4.00e-04
	B-6	38.47692	3.26e-02	6.00e-04
	B-7	41.81794	8.47e-02	7.00e-04
	B-8	36.31579	2.23e-02	3.00e-04

### 3.4. Numerical Analysis

Numerical models for all joints are developed in the Femap with NX Nastaran [5] software based on the technical documentation of producer and the data given in tables 1 and 2. LS-Dyna software was used for numerical analysis [6]. The parts in the set are modelled with 3D 8-nodal finite elements and contain 263204 elements and 451489 nodes. The load transfer plate is modelled with the shell elements, too. In the figure 8, a mesh of finite elements model of cantilever test for analysis of the beam to column connection is shown.

The system for transfer loading is modelled with 1D finite elements, i.e. rods. The connection between the parts in the assembly are modelled by the surface-to-surface contact elements. Contact finite elements are used for modelling the following connections: column-beam end connector, beam end connector-beam, beam-parts for blocking lateral movement. The analysis used an elastoplastic material model with kinematic reinforcement, [6].

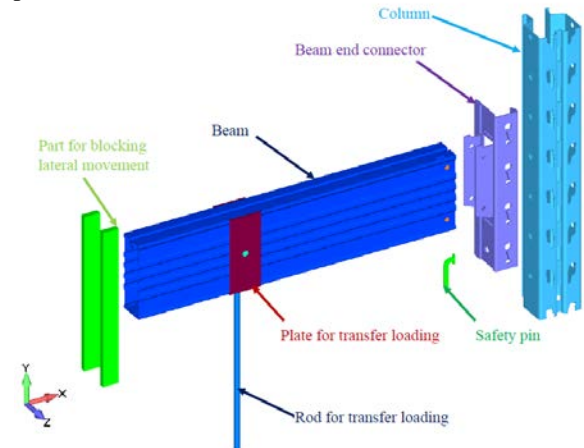


Figure 8: Model of cantilever test for beam to column connection of the joint S80M-R140L

The column and side plates are fixed at the ends. Figure 9 shows the boundary conditions as well as given load.

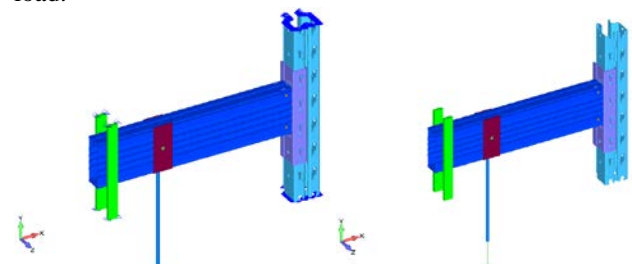


Figure 9: Boundary conditions and load

At the end of the rod, the movement in the negative direction of the y axis is set according to the diagram in figure 10. The value of the given displacement at the point of effect of the force is calculated according to the experimental data for the relation between the angle of rotation and the corresponding force value, i.e. moment of bending.

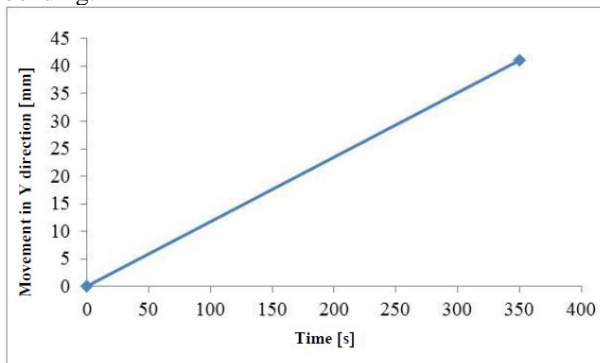


Figure 10: Diagram of the given displacement

Figure 11 shows the curves of the moment-rotation of the four samples of the joint S80M-R140L obtained experimentally, curves generated using the analytic polynomial model by the Frye-Morris method as well as the curves obtained by the numerical simulation of the experiment

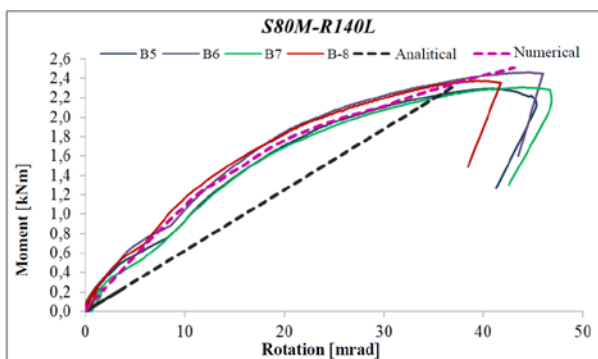


Figure 11: Moment-rotation curves for joint S80M-R140L

The moment-rotation curves for the joint S80M-R140M obtained only by numerical and analytical application of expression (13) are shown in figure 12. An analogy with the numerical results that was verified by experimental results can be seen from the diagram. Based on this, it can be concluded that the developed model of finite elements can be reliably applied to determine the construction properties of the considered connection.

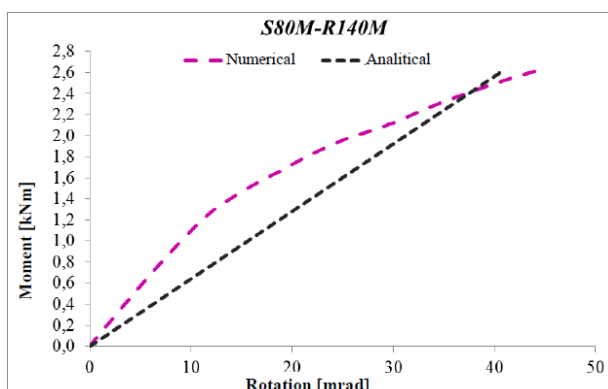


Figure 12: Moment-rotation curves for joint S80M-R140M

#### 4. CONCLUSIONS

Constructive design and derivation of connections between elements of the spacious steel structure of pallet racks is of great importance both for the load capacity and for the economy. Semi-rigid connections between the beams and columns of the frame pallet structure provide a reduction in the consumption of materials, as well as the costs of manufacturing and assembly, which is the main reason for their mass application. Determination of the structural properties of the beam-to-column connection and its structural properties on the basis of the moment-rotation curve is the basis for further analysis of the connection behaviour as well as its influence on global structure. In order to avoid expensive experimental analysis and determination of this characteristic, it is resorted to the development of analytical or numerical models. So far, analytical models did not give satisfactory results while numerical analysis and application of the finite element method in the simulation of the test conditions gave very good results. By simply changing the model of the experiment enabled by modern computer technology, it can be examined and determined by the characteristic of the connections of various combinations of elements in the joint. In this way, the rough approximations of real characteristics and their introduction into the calculation are avoided. Further research in the field of semi-rigid connections of the elements of the rack construction will certainly refer to the possibility of improving the connection, or increasing the load capacity, for example, by enabling an additional, multiple contact of the parts of the beam end connector and the column. Problems that would occur in this case, such as, for example, the weakening of the column due to multiple perforations, would simply be analyzed and solved using the developed model. Numerical analysis enables rapid and at the same time reliable optimization without the need of experimental testing.

#### ACKNOWLEDGEMENTS

The paper is a part of the research done within the project TR32036 supported by the Ministry of Education, Science and Technological Development of the Republic of Serbia.

#### REFERENCES

- [1] R. Vujanac, "The Influence of Semi – Rigid Connections of the Pallet racking Elements on the Global Analysis of the Structure", PhD Thesis, Faculty of Engineering University of Kragujevac, (2014)
- [2] FEM 10.2.02: RACKING DESIGN CODE, "The Design of Static Steel Pallet Racking", August, 2000.
- [3] EUROCODE 3: Design of steel structures, Part 1-3: General rules – Supplementary rules for cold formed thin gauge members and sheeting, Part 1-8: Design of joints
- [4] P. Prabha, V. Marimuthu, M. Saravanan, S. A. Jayachandran, "Evaluation of connection flexibility in cold formed steel racks", Journal of Constructional Steel Research, Vol. 66, p.p. 863 – 872, (2010)
- [5] FEMAP with NX Nastran - Finite element program
- [6] LS-DYNA - Finite element program

**SESSION E**

**RAILWAY ENGINEERING**



# The Purpose of Diagnostics of Pantographs Used in the Serbian Railways

Branislav Gavrilovic<sup>1\*</sup>, Zoran Bundalo<sup>1</sup>

<sup>1</sup>Railway College, Belgrade, Serbia

*The paper presents a method of modelling catenary construction elements especially continuous media (contact wire and messenger wire) using lumped conservative and dissipative elements. In order to determine the mathematical model of the line used in the Serbian Railways, the Lagrange's energy method was used. To model the contact wire and messenger wire, the authors propose to use a string of 8-node elements. The spatial arrangement of nodes provides a longitudinal and lateral stiffness of the wire. In the first approach, an assumption was made that the compliance of equivalent springs is the same in the model of the contact wire and the messenger wire. The same assumption was made with respect to the equivalent damper parameters. With this approach, the influence of wear of the contact wire to its dynamics can be mapped by adjusting the relative position of the nodes in the 8-node element string.*

**Keywords:** Electric traction, overhead catenary, mathematical modelling, Pantograph-Catenary System

## 1. INTRODUCTION

Railway traction model is a complex mix of electrical and mechanical parameters. The capability of a current collection system depends on an interaction between locomotive, pantograph and catenary system, see Figure 1. When developing such systems, it is important to have the ability to predict the dynamic performance of the system.

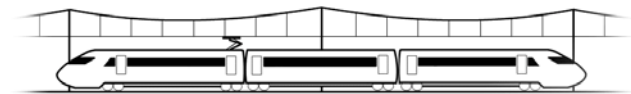


Figure 1: A train with its catenary-pantograph system

These types of systems have been analysed by several engineers during the last decades. Depending on factors such as the actual configuration of the systems, available information, desired accuracy of simulation results, simulation methods etc. different types of models are applicable.

The large variation in infrastructure characteristics in different countries and railway companies, different designs of pantographs, different types of traffic (types of vehicles, running speed etc.), makes it almost impossible to develop a final simulation model of the system. It is also difficult to recommend models for specific cases, since the relevant model depend on access to information, wanted accuracy of the results, accessible resources etc. Instead, it would be favourable to have a tool that has the ability to set up models of the system, choose relevant detail of the models, perform simulations and finally visualise the results. Then the user can validate the created model for the specific application.

To make the developed tool useful for engineers, design experts as well as simulation experts, the functionality of the computer tool must be worked out. For example, it would be favourable if the engineer does not need to have specific knowledge about the details in the different models and solution methods.

The work presents methodical aspects of modelling the critical components of a catenary construction, i.e. a

contact wire, a messenger wire and a dropper used in the Serbian Railways. In the future, the models of these components will form the basis for the construction of a line reference model, first, and then of a complete model of the strain section of the line that is needed to diagnose the current collectors. The paper also presents the issues of identifying the contact wire model parameters based on measurements. At the same time, the complexity of the dynamics of the wire vibration in 3D space has been shown.

## 2. MODELING OF PANTOGRAPH-CATENARY

Pantograph is an important link to transfer the electric energy from the power conductor to loco transformer. It is a mechanical system composed of an articulated frame, carrying a collector head on which the collector strips for current collection are mounted. Constant pressure is applied at the head of the pantograph through pneumatic control mechanism to ensure that it always remain in contact with the contact wire. When the electric train moves, a dynamic force is applied on the contact wire by the head of the pantograph. The contact wire after the passage of pantograph suddenly sags and starts vibrating due to the elasticity of the system. The quality of current collection by the pantograph depends upon the contact pressure between the pantograph head and speed of the train [1]. If the pressure is kept too low, it may lead to unsatisfactory current collection and sparking whereas very high pressure increases the wear and tear of the contact wire. For 25kV ac system, the pressure between 4-6 bars is considered optimum. The supply from catenary to the power conductor to loco transformer through pantograph form a dash pot mass spring system. Fig. 2 shows the contact description of the pantograph-catenary system [1].

The choice of a simple catenary for simulation is made because this system has the same behaviour under dynamic action effect like compound catenary. Catenary equivalent mechanical model is presented in Fig.3.

Pantograph equivalent mechanical model is presented in Fig.4 [2].

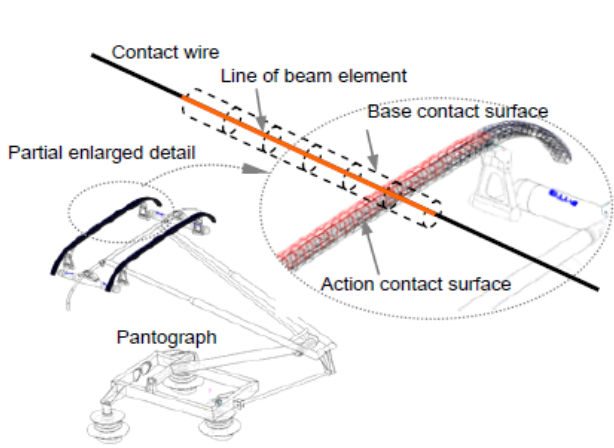


Figure 2: Contact description of the pantograph-catenary system

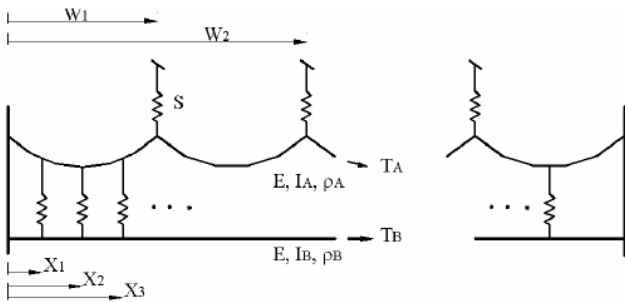


Figure 3: Catenary equivalent mechanical model  
 Where are: Tower stiffness-  $S$ ; Dropper stiffness-  $K$ ;  
 Distance to the  $j$ -th tower -  $W_j$ ; Distance to the  $i$ -th dropper -  $X_i$ ; Stiffness of the two wires-  $E, I_A, E, I_B$ ; Density of the two wires-  $\rho_A, \rho_B$ ; Tension in the two wires-  $T_A, T_B$

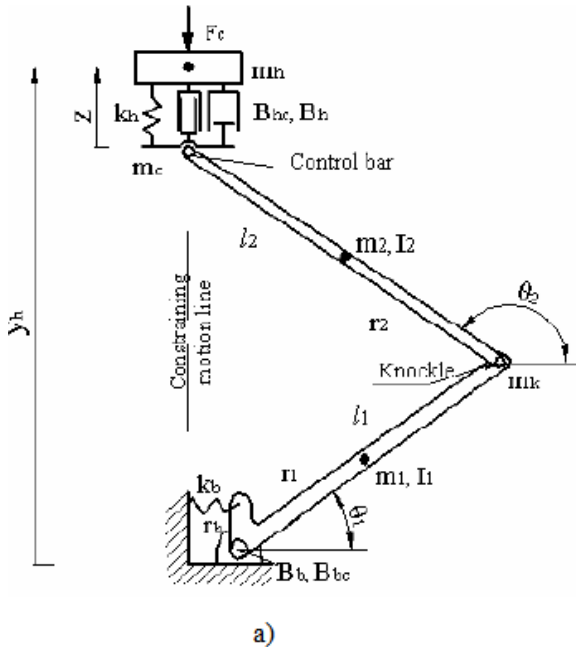


Figure 4a: Pantograph mechanical model

Physical description of a nonlinear analytical model is presented for the following mode (fig. 4a and 4b): Nonlinear pantograph model; Static model; Linear model.

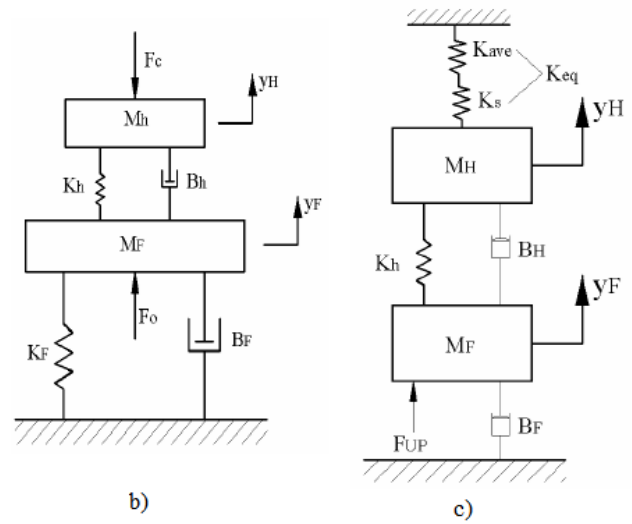


Figure 4: Pantograph equivalent mechanical model

The pantograph model used to control the design is the same for two-mass model [2]; but, the wire height,  $y_{cat}$ , cannot be realistically measured; catenary is modelled as a constant spring which value is the average catenary stiffness,  $k_{ave}$ . Fig. 4c shows this scheme.

The pantograph equivalent mechanical model used to control the design is the same for two-mass model. The upper mass represents the head mass while mass of frame is represented by lower mass. The contact between the head of the pantograph and the catenary is represented by a spring with a constant stiffness  $K_{ave}$ . The displacement of catenary is the function of force on the catenary due to pantograph.

The two models are coupled through the spring that represents the stiffness of the carbons on flexure of the head,  $K_s$  (Fig. 5).

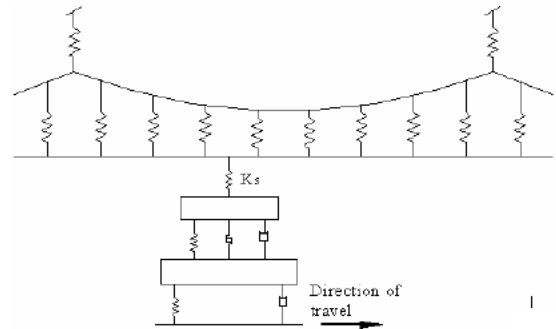


Figure 5: Coupling of the pantograph and catenary models

### 3. MATHEMATICAL MODELLING OF SELECTED ELEMENTS OF CONTACT LINE

#### 3.1 Assumptions

The modelling methodology adopted in this work is based on the Lagrangian energy method. The methodology has been applied only to those components that were included in the EN 50318 specification [3]. Specification of the reference model of the line according to EN 50318 defines only the geometrical arrangement, the set of input parameter values and the corresponding set of results for the impact at the collector-contact wire tangency point. It is therefore not a mathematical model, but a set of guidelines for its construction, which must be taken into

account. The reference model is not intended to represent the mechanical structure of a particular line. Its purpose is to validate any method of simulation, especially dynamic states in the contact line-current collectors system. If the test simulation method will be positively verified on the basis of the reference model, it may be approved for experimental verification.

The geometric system of the reference line [3] consists of a series of 10 identical sections along the length of tension. Each section (Fig. 6) represents the span length and its length is 60 m. The reference line includes: a single contact wire, a messenger wire and droppers. The messenger wire is fixed to stationary brackets and restrained at both ends of the tension segment. The current collector of the vehicle moving on the railway line is modelled as a discrete system: masses-springs-dampers (Fig. 7) [3].

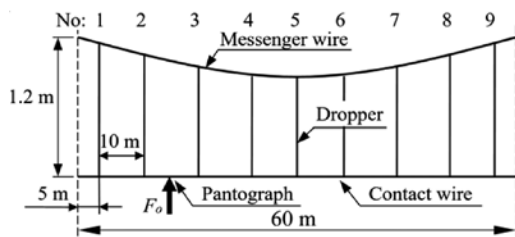


Figure 6: Geometry of the reference catenary single suspension section

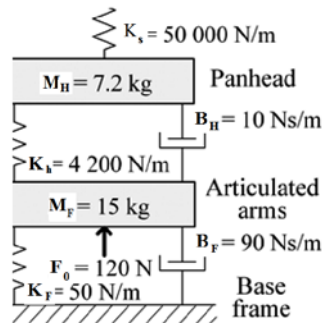


Figure 7: Pantograph model

### 3.2. Modelling methodology adopted for the analysis of the catenary construction

According to the adopted method, the contact wire, the messenger wire and the droppers were divided into lumped conservative (kinetic and potential) elements and dissipative elements (dampers). The concept of division of the contact wire and the messenger wire is shown in Fig. 8a, whereas the division of the dropper is shown in Fig. 8b. The contact wire and the messenger wire are represented by a string of 8-node elements. In the particular mechanical nodes, lumped mass elements are arranged. Adjacent nodes are connected by lumped equivalent springs and dampers. This arrangement provides a longitudinal (axial) and lateral stiffness, and the distribution of nodes in a cross-section of the wire allows to simulate the effect of wear of the contact wire. The dropper is represented by two inertial elements placed in the nodes of the contact wire and the messenger wire, joined with an equivalent damper and spring with nonlinear characteristics.

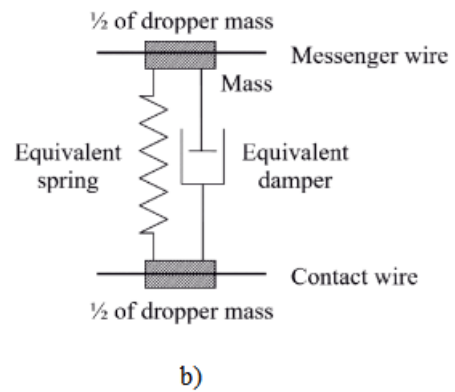
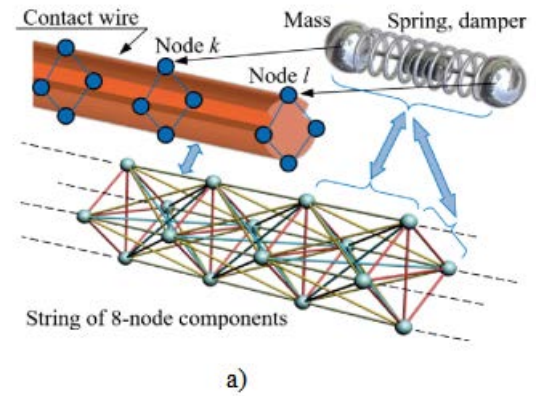


Figure 8: The concept of dividing the elements of the catenary construction into a group of conservative and dissipative lumped elements: a) contact wire or messenger wire, b) dropper

The mathematical model is based on the Lagrangian formalism. This formalism requires defining: coenergy of kinetic inertial elements, energy of the potential elements and Rayleigh dissipation function for dissipative components. Kinetic coenergy of the inertial element  $a$  in translational motion expressed in coordinates associated with the element  $a$  is:

$$E_{k,a}' \left( \frac{dx_a}{dt}, \frac{dy_a}{dt}, \frac{dz_a}{dt} \right) = \frac{1}{2} m_a \left[ \left( \frac{dx_a}{dt} \right)^2 + \left( \frac{dy_a}{dt} \right)^2 + \left( \frac{dz_a}{dt} \right)^2 \right] \quad (1)$$

where:

$m_a$  – the mass of the element  $a$ ,

$\frac{dx_a}{dt}, \frac{dy_a}{dt}, \frac{dz_a}{dt}$  – the components of its velocity, respectively in the  $x, y$  and  $z$  directions.

The potential energy of a linear elastic element  $b$  in translational motion expressed in the coordinates associated with the  $b$  element is:

$$E_{p,b} = \left[ \frac{(x_b + X_b)^2 + (y_b + Y_b)^2 + (z_b + Z_b)^2}{-2R_b \sqrt{((x_b + X_b)^2 + (y_b + Y_b)^2) + (x_b + X_b)^2}} + R_b^2 \right] \cdot \frac{1}{2 \cdot K_b} m_a \quad (2)$$

where:

$K_b$  – the compliance of the spring  $b$ ,

$x_b, y_b, z_b$  – components of the relative spring terminals displacement respectively in the  $x, y$  and  $z$  directions,

$X_b, Y_b, Z_b$  – the dimensions of the spring in a state of zero potential energy, respectively in the  $x, y$  and  $z$  directions,  
 $R_p$  – the length of the spring.

Rayleigh dissipation function of the linear viscous dissipative element  $c$  in translational motion expressed in the coordinates associated with the element  $c$  is:

$$E_{m,c} \left( \frac{dx_c}{dt}, \frac{dy_c}{dt}, \frac{dz_c}{dt} \right) = \frac{1}{2} D_c \cdot \left( \left( \frac{dx_a}{dt} \right)^2 + \left( \frac{dy_a}{dt} \right)^2 + \left( \frac{dz_a}{dt} \right)^2 \right) \quad (3)$$

where:

$D_c$  – the damping coefficient of kinetic component  $c$ ,

$\frac{dx_c}{dt}, \frac{dy_c}{dt}, \frac{dz_c}{dt}$  – relative components of the damper terminals velocity, respectively in the  $x, y$  and  $z$  directions.

In the next step, a constraint equation is set, which defines the relationship between the coordinates of individual lumped elements with generalised coordinates (degrees of freedom of the system). On this basis, the Lagrangian was formulated:  $L\left(\frac{d\xi}{dt}, \xi\right)$ , and its general form with generalised coordinates is as follows:

$$L\left(\frac{d\xi}{dt}, \xi\right) = E_k\left(\frac{d\xi}{dt}, \xi\right) - E_p(\xi) \frac{d\xi}{dt} = \begin{bmatrix} \frac{dx_1}{dt} \\ \frac{dy_1}{dt} \\ \frac{dz_1}{dt} \\ \dots \\ \frac{dx_n}{dt} \\ \frac{dy_n}{dt} \\ \frac{dz_n}{dt} \end{bmatrix}, \xi = \begin{bmatrix} x_1 \\ y_1 \\ z_1 \\ \dots \\ x_n \\ y_n \\ z_n \end{bmatrix} \quad (4)$$

where:

$E_k\left(\frac{d\xi}{dt}, \xi\right)$  – the resultant coenergy of the kinetic system,

$E_p(\xi)$  – the resultant potential energy of the system,

$\frac{d\xi}{dt}$  – the generalised velocity vector,

where in:

$\frac{dx_k}{dt}, \frac{dy_k}{dt}, \frac{dz_k}{dt}$  – the components of the velocity of the node  $k$ ,

$\xi$  – the vector of generalised displacement,

where in:

$x_k, y_k, z_k$  – components of displacement of the node  $k$ .

Then, an Euler-Lagrange equation was set, that, for the free node  $k$ , can be succinctly expressed by the formula:

$$\frac{d}{dt} \left[ \frac{\partial L\left(\frac{d\xi}{dt}, \xi, t\right)}{\partial \left(\frac{d\xi_k}{dt}\right)} \right] - \frac{\partial L\left(\frac{d\xi}{dt}, \xi, t\right)}{\partial \xi_k} + \frac{\partial P\left(\frac{d\xi}{dt}\right)}{\partial \left(\frac{d\xi_k}{dt}\right)} = Q_k(t) \quad (5)$$

where:

$P\left(\frac{d\xi}{dt}\right)$  – a Rayleigh dissipation function of the system,

$Q_k(t)$  – a generalised force – the external force acting on the free node  $k$  of the system.

#### 4. IDENTIFICATION OF THE MECHANICAL PARAMETERS OF THE CONTACT WIRE

An important element of the overhead line is the contact wire. Its irregular cross-section results in the need for detailed exploration of the selected mechanical parameters. For this purpose, it was necessary to measure the deflection and vibration for typical trolley wires used in the Serbian Railways, Inc., i.e. Djp 100. The tests were performed on a simple experimental setup shown schematically in Fig. 9.

The wire is mounted rigidly on one side. In case of static measurements, different values of the force  $F$  were applied at the end of the wire, and by means of a laser rangefinder, the deflection  $y$  in the consecutive points spaced along the length  $l$  of the wire was measured.

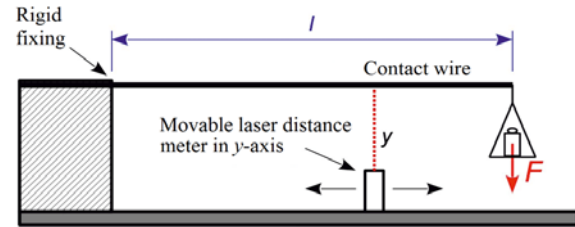


Figure 9: The scheme of the experimental setup for testing mechanical parameters of contact wires, where:  $l$  – wire length (800 mm)  $F$  – force function;  $y$  – deflection of the wire

The wire is mounted rigidly on one side. In case of static measurements, different values of the force  $F$  were applied at the end of the wire, and by means of a laser rangefinder, the deflection  $y$  in the consecutive points spaced along the length  $l$  of the wire was measured.

On the basis of measurements and catalogue data of the contact wires, mechanical parameters of the concentrated elements were identified, i.e. inertial mass of the nodal elements, compliance of the substitute elastic elements and damping coefficients of kinetic equivalent dampers. In determining the susceptibility of equivalent springs in the contact wire, it was established at the outset that the characteristics of these springs are the same. It is also assumed that the characteristics of the equivalent dampers in the contact wire are the same. Similar assumptions were adopted for the springs and dampers representing the catenary construction.

The measurement results, which show the trajectory of the end of the wire, are shown in Fig. 10. When the axis of symmetry of the wire lies in the axis of force function  $F$  or is perpendicular to that surface, then the vibration occurring in the one axis (movements similar to those shown in Fig. 10a were obtained for wires rotated by 90 and  $-90^\circ$ ). If the axis of symmetry is not in the axis of the force function, we observe a complex vibration in the  $x$  and  $y$  axes (see Fig. 10b and 10c).

The resulting registrations of trajectory indicate that the simple models based on the reference model, which describes the movement of the system only in the vertical



direction, may not fully reflect the complex nature of the phenomena for network sections with a special structure.

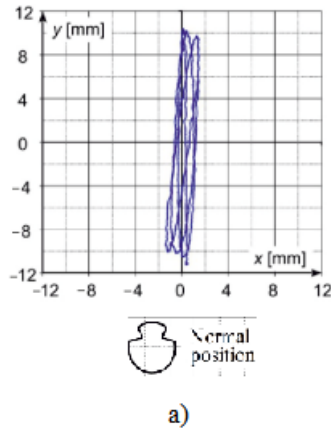


Figure 10a: The trajectory of vibrations at the end of the wire at step reduction of the loading force: wire Djp100 respectively in normal position

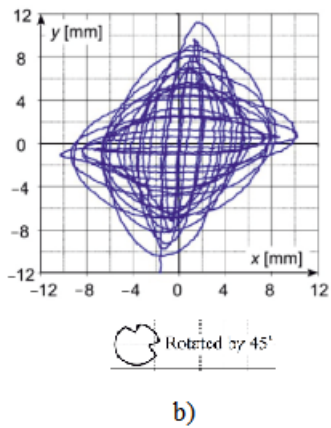


Figure 10b: The trajectory of vibrations at the end of the wire at step reduction of the loading force: wire Djp100 respectively rotated by 45° (b)

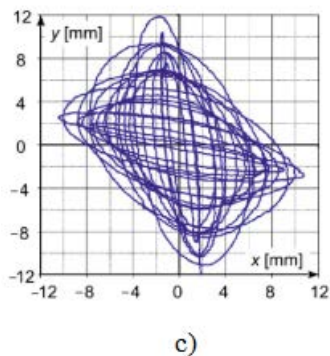


Figure 10c: The trajectory of vibrations at the end of the wire at step reduction of the loading force: wire Djp100 respectively) rotated by -45° (c);

### 5. EXAMPLES OF SIMULATION RESULTS

Comparison of the results of simulations and measurements of the deformation of the section of unilaterally fixed wire Djp 100 is shown in Fig. 11. These results relate to a new wire in a normal position. The parameters of the lumped elements of the wire model are as follows: the mass of the inertial element in the node is

$m = 0.032$  kg, the compliance of the equivalent spring is  $K = 3.5 \times 10^{-5}$  m/N, the kinetic damping coefficient is  $D = 0.038$  Ns/m (Fig.8b). The  $K$  value is the same for all the springs in the wire model (Fig.8b). The value of  $D$  is also constant for all dampers in the wire model.

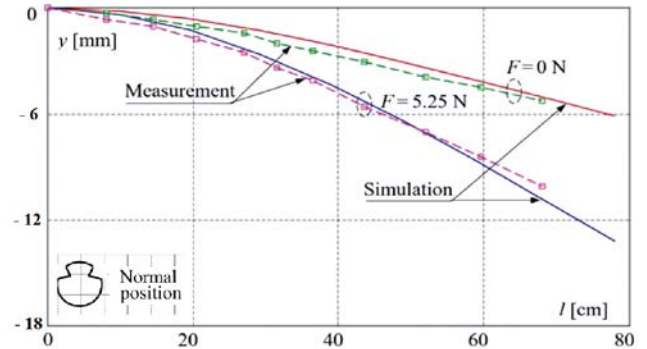


Figure 11: Comparison of the results of simulations and measurements of deformation of a section of the wire Djp 100 in normal position, fixed unilaterally

Simulation of the dynamic state of the same section of the wire is shown in Fig. 12. The graph shows the dynamic deformation of the end of the wire Djp 100 in conditions similar to the conditions of measurement. In the model developed for the purposes of this work, the so-called viscous dampers were used. In further research, dry friction will also be analysed. As was demonstrated by a preliminary analysis of the envelope, dry friction may be a part of the dissipation of mechanical energy in the structure of the wire.

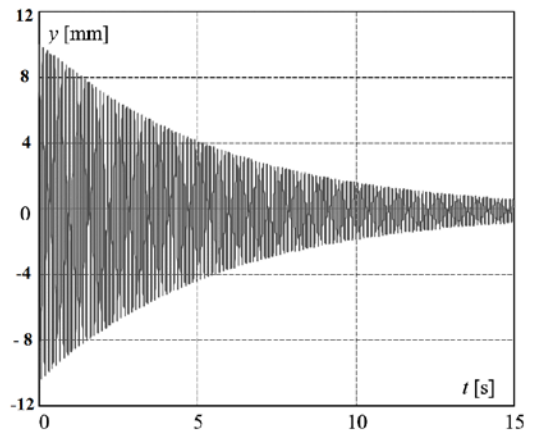


Figure 12: The simulation result of the dynamic state of the section end free deformation for the wire Djp 100 in normal position, fixed unilaterally

From the comparison of simulation and measurements, a conclusion can be drawn that the proposed model of the division of wire into lumped elements, relatively correctly reproduces static and dynamic states. It also turned out that the use of equivalent elastic elements having the same characteristics in the structure of the contact wire and messenger is justified. This also applies the same characteristics of dissipative elements. This approach greatly facilitates the appointment of equivalent elastic and damping elements.

## 6. CONCLUSIONS

The overhead contact line is the most effective way for supplying railway electric vehicles. The increase of the speed of vehicles increases power consumption and requires ensuring proper cooperation of pantographs with overhead contact line. The paper describes the novel mathematical model of the overhead contact line used in the Serbian Railways and the simulation results.

The primary objective is a more accurate analysis to increase the reliability of the evaluation of monitoring and diagnostics. The model was based on the Lagrange energy method. The paper presents the structure of the model and equations describing it, as well as the results of some laboratory tests that were performed to determine the model parameters. The selected results of simulations concerning the effects of force impact on the contact wire were carried out using the created model. The prepared program can be used for creating computer tools, which will support designers of overhead contact line used in the Serbian Railways.

The conducted experimental studies were used to determine the parameters of the concentrated elements of the model. They demonstrated the rather complicated dynamics of the vibration of the contact wire, especially at its different angular position.

Comparison of the results of the experiment and the simulation showed the validity of the approach for modelling the overhead line elements, especially the contact wire. Despite the linear characteristics of equivalent springs and equivalent dampers, a relatively good coherence of simulation results and measurements was achieved.

Currently, a software is developed that will be able to simulate the entire overhead contact line used in the Serbian Railways taking into account elements that bring irregularities, for example, connectors, insulators, as well as heterogeneity of the cross-section of the wire, etc.

Adding a software module for the calculation of electrical quantities, e.g. a simulation of useful voltage based on the distribution of substations with regard to vehicle motion, will develop useful tools for designing overhead lines.

## ACKNOWLEDGEMENTS

This work was supported by the Serbian Railways, Railway College in Belgrade and Dobrinka Atmadzhova.

The authors would like to thank for this support.

## REFERENCES

- [1] S.D. Eppinger, et al, "Modeling and Experimental Evaluation of Asymmetric pantograph Dynamics", *Journal of Dynamic System, Measurement and Control*, June 1988, Vol. 110/169, pp 168-174, (1988)
- [2] D. O'Connor, "Modeling and simulation of pantograph-catenary systems", PhD Thesis, University of Massachusetts, (USA), (1988)
- [3] A. Alberto, J. Benet, E. Arias, D. Cebrian, T. Rojo, F. Cuartero., "A high performance tool for the simulation of the dynamic pantograph-catenary interaction" *Mathematics and Computers in Simulation*, Vol. 3(79), Elsevier, pp. 652-667, (2008)
- [4] Y. H. Cho, "Numerical simulation of the dynamic responses of railway overhead contact lines to a moving pantograph, considering a nonlinear dropper", *Journal of Sound and Vibration*, Vol. 315 (3), pp. 433-454, (2008)
- [5] R.H. Huan, G. F. Pan, W. Q. Zhu, "Dynamics of Pantograph-Catenary System Considering Local Singularities of Contact Wire with Critical Wavelengths", *Proceedings of the 1st IWHIR*, Vol. 1, LNEE 147, Springer - Verlag Berlin Heidelberg 2012, pp. 319-333, (2012)
- [6] W. Koc, A. Wilk, "Investigations of methods to measure longitudinal forces in continuous welded rail tracks using the tamping machine, Proceedings of the Institution of Mechanical Engineers, Part F, *Journal of Rail and Rapid Transit*, Vol. 223, No. F1, pp. 61-73, (2009)
- [7] Emil M. Mihaylov, Dobrinka Atmadzhova: "Reasons for early demolition of safety element in the construction of a tram current collector Пф-80", *International Symposium SRMA 2015, Kraljevo, Serbia*, (2015)
- [8] Atmadzhova D., M. Mihalev, "Analysis of the reliability of bogie electric locomotives, *International Symposium SRMA 2014, Kraljevo, Serbia*, 2014, pp.116-119, (2014).

## Processes and Dependencies Related to Nadal's Formula

Dobrinka Atmadzhova<sup>1</sup>

<sup>1</sup>Machinery and Construction Technologies in Transport/Transport Equipment, Todor Kableshkov University of Transport, Sofia (Bulgaria)

**Abstract** - The paper presents a force analysis of Nadal's formula representing the admissible boundary state with regard to derailment of railway vehicles. A number of important universal features and dependencies of this process (derailment) as interaction between two groups of forces or force functions are revealed. The argument of functions (independent variable) is the so-called criterion against derailment  $Y/Q$  (the ratio of horizontal to vertical forces at the contact point of rail and attacking wheel). The proposed graphic interpretations of force functions contribute to visualizing the derailment process and create additional conveniences and opportunities of future research.

**Keywords** – Railway vehicles, derailment, Nadal's formula.

### 1. INTRODUCTION

Although the problems of providing safety against rolling stock derailment had existed since the appearance of railway transport (i.e. for nearly two centuries), the first theoretical dependencies were presented by engineer Poshe in 1882. Later these dependencies were further developed by G. Marje, M. J. Nadal, etc. and became fundamentals of the modern theory of reliability against railway derailment. The contribution of M. J. Nadal is very substantial because in 1908 he suggested the following working formula, which is topical even nowadays [1, 2, 3, 4, 5, 6]:

$$\frac{Y}{Q} < \frac{tg\beta - \mu}{1 + \mu \cdot tg\beta} = tg(\beta - \rho) \quad (1)$$

where:

$Y$  and  $Q$  are the horizontal transverse force and vertical load transmitted from the attacking wheel to the rail at the contact point;

$\beta$  – the angle of slope of the flange forming in its straight part or in its inflection point if it does not have a straight part;

$\mu$  and  $\rho$  - the coefficient of friction and angle of friction between the flange and rail respectively.

Although not very precise, this formula reflects the effect of the main force and geometrical factors to prevent derailment quite completely. At that it shows these factors clearly and briefly. This formula will be paid special attention to in further analysis.

In 1930s G. Marje put some corrections in Nadal's formula considering the friction force of non-attacking wheel  $Q'$  and it took the kind of:

$$\frac{Y}{Q} < \frac{tg\beta - \mu}{1 + \mu \cdot tg\beta} - \frac{Q'}{Q} \cdot \mu' \quad (2)$$

where:  $Q'$  and  $\mu'$  are the vertical load on the rail and the coefficient of friction with it of the non-attacking wheel respectively (the other symbols are given in the previous formula).

It should be pointed out that the experimental determination of horizontal and vertical forces ( $Y$ ,  $Q$  and

$Q'$ ) in the formulas mentioned above under operational conditions was not possible at the time of their creation and even long years after.

During the period right after the World War II, thanks to the great improvement of measurement equipment explained by fast development and wide abilities of tensometrics, it became possible to measure forces in the axle box and axle of the wheel axle.

That grounded a new trend in development of the theory of safety against derailment characterized with examination on the entire wheel axle (together with the axle box unit and all forces applied to and transmitted from it) as well as with using other criteria based on the axle unit and axle of wheel axle. The contributions to the theoretical fundamentals of safety against derailment that belong to this group were first developed in [9, 10, 11, 12, 13]. Some of them are summarized in this paper emphasizing mainly on the basic results.

The author of [11] from 1948 examined the entire wheel axle and worked out a new criterion for derailment, which is a ratio between horizontal cross-wise force  $F$  to vertical force  $P_1$  applied to the axle neck from the side of attacking wheel; this criterion depends on the wheel axle parameters and bandage profile as well as on the ratio between vertical loads  $P_2$  and  $P_1$  on the two axle necks. In [12, 13, 14] works are presented general notes of safety against derailment in graphical or analytical method by the methods ERRI [1], UIC 518 [5] and EN 14363 [6].

A number of studies have been carried out in recent years and implementations for methods and means for measuring forces  $Y$  and  $Q$  in the contact point and the creation of a tensometric wheel and a calibration bench [5, 6, 7, 8].

The dependence of Nadal's formula is not limited with the formula itself because the clear, short and simple dependencies connected with it are not less important. Thanks to their clarity and briefness the latter ones are used to discover and explain the complex processes of derailment [14, 15]. It is why the paper presents the very way of working-out the formula, which despite its popularity is justifiable due to the necessity to focus

attention on some significant intermediate results to be used later.

Here also, while working-out this formula, one begins from the state of lifted-up attacking wheel so that it contacts the rail through the flange in its conic zone and from the condition that it is capable to return to its normal state on the rail under the effect of forces applied to it, and these are resultant forces  $Q$  and  $Y$  (Fig. 1) – in vertical and horizontal transverse directions respectively – designed on the tangent  $t_A$  to the tangential area at contact point  $A$  as well as friction force  $\mu N$  along the direction of tangent  $t_A$  and with direction „up“, i.e. opposite to the direction of pre-set movement (Fig.1).

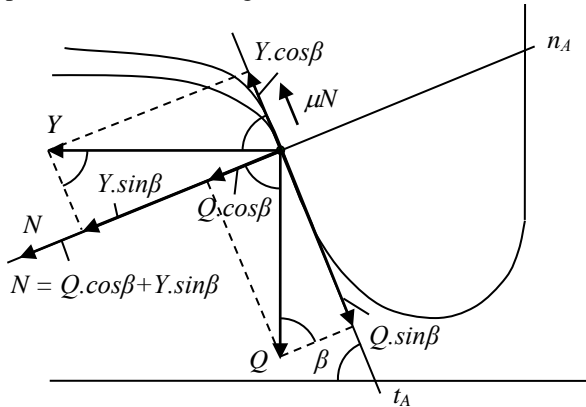


Figure 1: Towards working out formula (4)

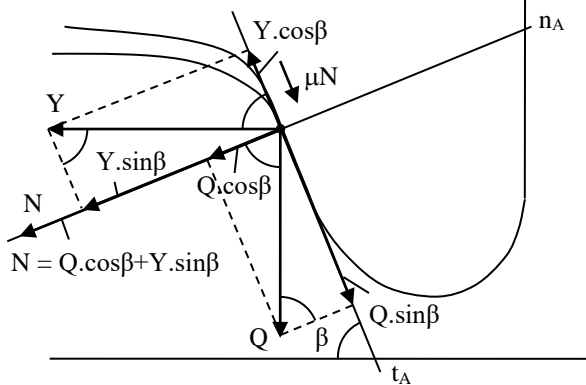


Figure 2: Towards working out formula (7)

Taking into account the preconditions mentioned above and the symbols given in Fig. 1, the requirement of the attacking wheel return, i.e. of movement “downwards”, it is possible to write the following inequality:

$$Q \cdot \sin \beta > Y \cdot \cos \beta + \mu \cdot N \tag{3}$$

and because normal force  $N$  consists of projections on normal  $n_A$  of active forces  $Q$  and  $Y$ , namely:

$$N = Q \cdot \cos \beta + Y \cdot \sin \beta$$

Inequality (1) takes the kind of:

$$Q \cdot \sin \beta > Y \cdot \cos \beta + \mu \cdot (Q \cdot \cos \beta + Y \cdot \sin \beta) \tag{4}$$

or

$$Q \cdot \sin \beta - Y \cdot \cos \beta > \mu \cdot (Q \cdot \cos \beta + Y \cdot \sin \beta) \tag{5}$$

$$Q \cdot (\sin \beta - \mu \cdot \cos \beta) > Y \cdot (\cos \beta + \mu \cdot \sin \beta)$$

$$\frac{Y}{Q} < \frac{\sin \beta - \mu \cdot \cos \beta}{\cos \beta + \mu \cdot \sin \beta}$$

and finally

$$\frac{Y}{Q} < \frac{\operatorname{tg} \beta - \mu}{1 + \mu \cdot \operatorname{tg} \beta} \tag{6}$$

or

$$\frac{Y}{Q} < \operatorname{tg}(\beta - \rho), \text{ where } \rho = \operatorname{arctg} \mu.$$

If in inequality obtained (6), which presents Nadal’s formula, the sign of inequality is replaced with the sign of equality, it radically changes its contents because this replacement expresses the boundary state (the so-called “boundary state”) – there is not an area of values but only one value of ratio  $Y/Q$ , namely:

$$\frac{Y}{Q} = \frac{\operatorname{tg} \beta - \mu}{1 + \mu \cdot \operatorname{tg} \beta} = \left( \frac{Y}{Q} \right)_{S-F} \equiv \left( \frac{Y}{Q} \right)_I \tag{7}$$

which is completely determined by the values of parameters  $\beta$  and  $\mu$  and which, by its nature, is a boundary value, the so-called *I-st* boundary value defining the border between the zones of safety (S) and friction (F) (deadlock).

With the smallest increase of ratio  $Y/Q$  in regard to its boundary value  $(Y/Q)_{S-F} \equiv (Y/Q)_I$ , the system enters the “friction” zone (or “deadlock”, “indifferent equilibrium”), which continues (together with the further increase of  $Y/Q$ ) to reach the next (*II-nd*) boundary state – between the zones of friction and derailment. The calculation scheme for this boundary state (Fig.2) differs from the previous one (Fig.1) only by the direction of friction force  $\mu \cdot N$  – here it is directed downwards because the moment (minute) when the attacking wheel flange begins to slide along the rail edge in upward direction is examined. In this case the following inequality is in force:

$$Y \cdot \cos \beta > Q \cdot \sin \beta + \mu \cdot N$$

and since

$$N = Q \cdot \cos \beta + Y \cdot \sin \beta$$

it is obtained that

$$Y \cdot \cos \beta > Q \cdot \sin \beta + \mu \cdot (Q \cdot \cos \beta + Y \cdot \sin \beta)$$

or

$$Y \cdot (\cos \beta - \mu \cdot \sin \beta) > Q \cdot (\sin \beta + \mu \cdot \cos \beta) \cdot \cos \beta^{-1}$$

and finally

$$\frac{Y}{Q} > \frac{\operatorname{tg} \beta + \mu}{1 - \mu \cdot \operatorname{tg} \beta} \text{ or } \frac{Y}{Q} > \operatorname{tg}(\beta + \rho), \text{ where } \rho = \operatorname{arctg} \mu \tag{8}$$

The resulting inequality (6) defines a whole area of  $Y/Q$  ratio values with which the attacking wheel flange is pushed on the rail, i. e. derailment occurs.

The boundary state between the friction and derailment zones (F-D) will be expressed naturally, analogous to the previous boundary state as follows:

$$\frac{Y}{Q} = \frac{\operatorname{tg} \beta + \mu}{1 - \mu \cdot \operatorname{tg} \beta} = \left( \frac{Y}{Q} \right)_{F-D} \equiv \left( \frac{Y}{Q} \right)_{II} \tag{9}$$

as it is characterized by a single value of ratio  $Y/Q = (Y/Q)_{S-F} \equiv (Y/Q)_I$  ratio defined by parameters  $\beta$  and  $\mu$  according to the formula.

Depending on the value of  $Y/Q$  ratio, different states of “wheel (flange) – rail” system are given in Table 1.

Table 1: Condition of "wheel (flange) – rail" system depending on  $Y/Q$  ratio

№	Value of $Y/Q$	Characteristics of the state
1.	$Y/Q < (Y/Q)_{S-F}$	Area (zone) "safety against derailment"
2.	$Y/Q = (Y/Q)_{S-F}$	Boundary equilibrium state – between "derailment" and "friction" zones
3.	$(Y/Q)_{S-F} < (Y/Q) < (Y/Q)_{F-D}$	"Friction" (or "deadlock") area (zone)
4.	$Y/Q = (Y/Q)_{F-D}$	Boundary equilibrium state – between "friction" and "derailment" zones
5.	$Y/Q > (Y/Q)_{F-D}$	"Derailment" area (zone)

## 2. MECHANISM OF PROCESSES DEPENDING ON $Y/Q$ CRITERION

To analyse the processes involved in derailment and particularly to reveal their connections with the main factor –  $Y/Q$  criterion, a number of intermediate dependencies will be used to work it out. For instance, dependency (4) and Fig. 1

$$Q \cdot \sin \beta > Y \cdot \cos \beta + \mu \cdot (Q \cdot \cos \beta + Y \cdot \sin \beta) \quad (10)$$

which gives an illustration of equilibrium (balance) or unbalance between acting forces: active force  $Q \cdot \sin \beta$ , which strives to return the attacking wheel to its normal position on the one hand, and on the other hand – force of dry friction  $\mu \cdot (Q \cdot \cos \beta + Y \cdot \sin \beta)$ , which strives to keep the wheel in a critical state of its flange on the edge of the rail, plus active force  $Y \cdot \cos \beta$ , which strives to push the wheel out (i.e. to derail the wheel).

With these studies, the dependency in modification will be mainly used

$$Q \cdot \sin \beta - Y \cdot \cos \beta \geq \mu \cdot (Q \cdot \cos \beta + Y \cdot \sin \beta) \quad (11)$$

which is not essentially different from (4). What is characteristic here, it is that acting forces are differentiated into two groups:

- the group of active forces in the left part of (5), denoted with A:

$$A = Q \cdot \sin \beta - Y \cdot \cos \beta \quad (12)$$

- the group of dry friction forces on the right side of (5) denoted with T:  
or (11)

$$T = \mu \cdot Q(\cos \beta + \frac{Y}{Q} \cdot \sin \beta) \quad (13)$$

Then (3) obtains the kind of:

$$Q \cdot (\sin \beta - \frac{Y}{Q} \cdot \cos \beta) \geq \mu \cdot Q \cdot (\cos \beta + \frac{Y}{Q} \cdot \sin \beta) \quad (14).$$

Strength groups A and T are radically different in nature and there is an extremely complex interaction between them that determines the nature of ongoing processes. In order to facilitate their study as well as to universalise the dependencies and the results obtained, it will be accepted to work with dimensionless (non-dimensional) magnitudes and mathematical expressions. For this purpose the

equation/ inequality (14) is shortened with  $Q$  and the same is obtained in a dimensionless form.

$$\sin \beta - \frac{Y}{Q} \cdot \cos \beta \geq \mu \cdot (\cos \beta + \frac{Y}{Q} \cdot \sin \beta) \quad (15)$$

where the left part of (15) is

$$\frac{A}{Q} = \sin \beta - \frac{Y}{Q} \cdot \cos \beta = A_c \quad (16)$$

and the right part of the same is

$$\frac{T}{Q} = \mu \cdot (\cos \beta + \frac{Y}{Q} \cdot \sin \beta) = T_c \quad (17)$$

as dimensionless quantities  $A_c$  and  $T_c$  express force and it is expedient to call them "specific active force" and "specific friction force" or "specific force  $A_c$ " and "specific force  $T_c$ " where the definition of "specific" (or "relative") is justified insofar as  $A_c$  and  $T_c$  actually represent the relative share of real force (force group respectively)  $A$  or  $T$  in regard to vertical force  $Q$  (because as it can be seen in (17) and (16)  $A_c = A/Q$  and  $T_c = T/Q$ ).

Since the specific forces  $A_c$  and  $T_c$  are linear functions of the  $Y/Q$  criterion, to build the scheme or diagram of the processes connected with derailment, the coordinates of the 2 or 3 points are required but the coordinates of 4 or 5 node points for ongoing processes are known (or can be determined), namely (Fig.3):

- for force  $A_c$  – points NN  $A_{c0}$ ,  $p_b$ ,  $O_{Ac}$ ,  $p_{II}$  are according to Fig. 3;

- for force  $T_c$  – points NN  $T_{c0}$ ,  $p_b$ ,  $d_1$ ,  $d_2$ ,

as abscissas  $Y/Q$  and ordinates  $A_c$  or  $T_c$  are defined as follows:

For Force  $A_c$  :

1. For the starting point  $A_{c0}$  at  $Y/Q = 0$  we define the

ordinate from (12) with  $Y/Q = 0$  -  $A_{c0} = \sin \beta$ ;

2. For point  $P_I$  of the I-st equilibrium state: the abscissa is

$$\left(\frac{Y}{Q}\right)_I = \frac{\text{tg}\beta - \mu}{1 + \mu \cdot \text{tg}\beta},$$

and the ordinate (defined by (12)) is:

$$A_c = \sin \beta - \left(\frac{Y}{Q}\right)_I \cdot \cos \beta$$

3. For point  $O_{Ac} = 0$ , with  $A_c = 0$  the abscissa (determined by (12) with  $A_c = 0$ ) is

$$\frac{Y}{Q} = \text{tg}\beta$$

4. For point  $P_{II}$  of the II equilibrium state: the abscissa is

$$\frac{Y}{Q} = \left(\frac{Y}{Q}\right)_{II} = \frac{\text{tg}\beta + \mu}{1 - \mu \cdot \text{tg}\beta}$$

and the ordinate (determined by (12)) –

$$A_c = \sin \beta - \left(\frac{Y}{Q}\right)_{II} \cdot \cos \beta$$

For force  $T_c$

1. For starting point  $T_{c0}$  with  $Y/Q = 0$  the ordinate is determined from (13) –  $T_c = \mu \cdot \cos \beta$

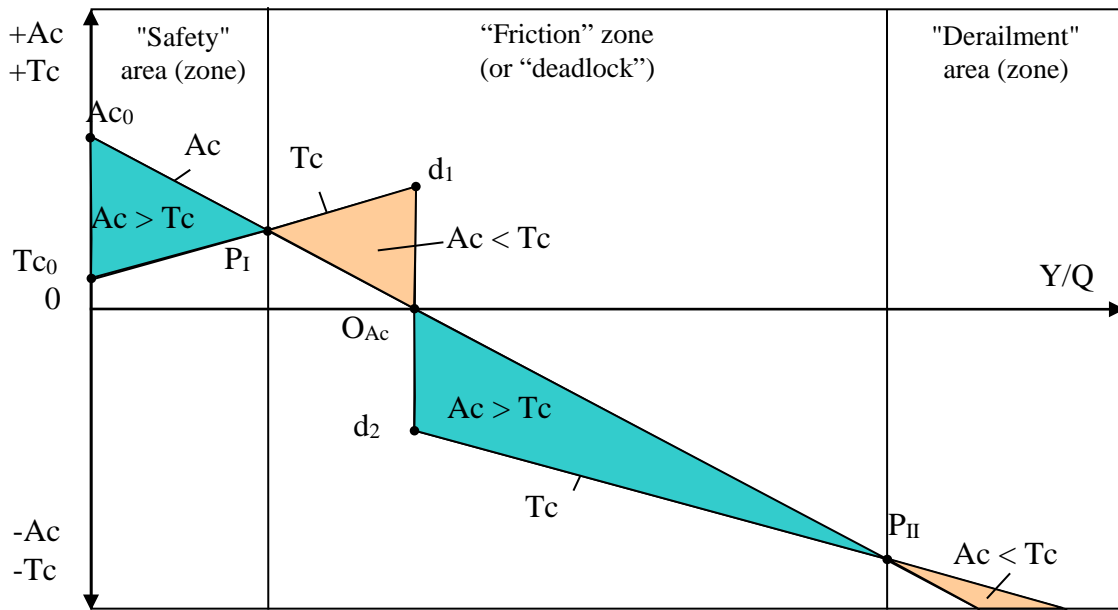


Figure 3: Scheme of the linear graph of processes occurring with derailment.

2. For point  $P_I$  (because it is a point of intersection between  $A_c$  and  $T_c$ ) the coordinates have been already determined with examining force  $A_c$  but it is advisable (for checking) to determine them for force  $T_c$  in the same way (where the difference is only in the use of expression (13) for force  $T_c$  instead of that for  $A_c$ ).

3. For points  $d_1$  and  $d_2$  the abscissa is the same and ordinate is with mutually opposite signs „ $\pm$ “ and equal absolute values; a jump change of the sign of force  $T_c$  is characteristic for  $A_c$  in direct dependence on the sign of active force  $A_c$ ; hence the abscissa of points  $d_1$  and  $d_2$  is the same as those already determined for point  $O_{Ac}$ , i.e:  $Y/Q = tg\beta$ , and the ordinate is obtained by substituting abscissa  $Y/Q$  with  $tg\beta$  in (13) according to the above dependency, i.e:

$$T_c = \mu \cdot (\cos \beta + tg\beta \cdot \sin \beta) = \mu \cdot (\cos \beta + tg\beta \cdot \sin \beta) = \mu \cdot \left( \frac{\cos^2 \beta + \sin^2 \beta}{\cos \beta} \right)$$

and finally:

$$T_c = \frac{\mu}{\cos \beta} \text{ - for point } d_1, T_c = -\frac{\mu}{\cos \beta} \text{ - for point } d_2,$$

4. The abscissa for point  $P_{II}$  is:

$$\frac{Y}{Q} = \left( \frac{Y}{Q} \right)_{II} = \frac{tg\beta + \mu}{1 - \mu \cdot tg\beta}$$

and the ordinate is determined by (13) for force  $T_c$  but taken with sign „-“, i.e.:

$$T_c = -\mu \left[ \cos \beta + \left( \frac{Y}{Q} \right)_{II} \cdot \sin \beta \right]$$

Based on the above-presented approach for determining the node points in the diagram of processes, the latter can be built with specific values of parameters  $\beta$  and  $\mu$ , for instance, applying the above-presented approach for  $\beta = 60^\circ$  and  $\mu = 0.30$ , first the solution for the coordinates of nodal points is given as follows:

$$A_{c0}(0; 0.866); P_I(0.942); O_{Ac}(1.732; 0); P_{II}(-4.230; 1.249); T_{c0}(0; 0.15); P_I(0.942); d_1(1.732; 0,6); d_2(1.732; -0,6); P_{II}(4.230; 1.249);$$

The diagram is shown in Fig. 4 where the coordinates with their numerical values are written after indicating the points in brackets.

Fig. 5 presents the diagram of processes related to derailment with parameter values  $\beta = 70^\circ$  and  $\mu = 0.25$ .

Solution: the coordinates of points.

$$A_{c0}(0; 0.94); P_I(1.48; 0.43); O_{Ac}(2.75; 0); P_{II}(-9.57; -2.33); T_{c0}(0; 0.085); P_I(1.48; 0.43); d_1(2.75; 0.73); d_2(2.75; -0.73); P_{II}(9.57; -2.33).$$

The examples shown here and some others give an impression that the duration of the zone "deadlock", i.e. the difference between the first and second boundary state changes within wide limits. To find the theoretical dependence, answering this question, it is logical to find the difference between  $(Y/Q)_{II}$  and  $(Y/Q)_I$  or

$$\frac{tg\beta + \mu}{1 - \mu \cdot tg\beta} - \frac{tg\beta - \mu}{1 + \mu \cdot tg\beta}$$

The final result of this solution is:

$$\left( \frac{Y}{Q} \right)_{II} - \left( \frac{Y}{Q} \right)_I = \frac{tg\beta + \mu}{1 - \mu \cdot tg\beta} - \frac{tg\beta - \mu}{1 + \mu \cdot tg\beta} = 2 \cdot \mu \cdot \frac{1 + tg^2 \beta}{1 - \mu^2 \cdot tg^2 \beta} \tag{14}$$

i.e. it shows that the difference between the two boundary states (or the forming deadlock zone strongly depends on the slope of the flange  $\beta$ -forming and friction coefficient  $\mu$ . By substituting the data of the above given example in (14), i.e. with  $\beta = 60^\circ$  and  $\mu = 0.30$  the difference is 3.288 as it is in the linear diagram (Fig. 4) obtained in another way. It is where the dual role of friction can be seen from: in the derailment zone friction is cutting and in the "safety" on it is harmful.

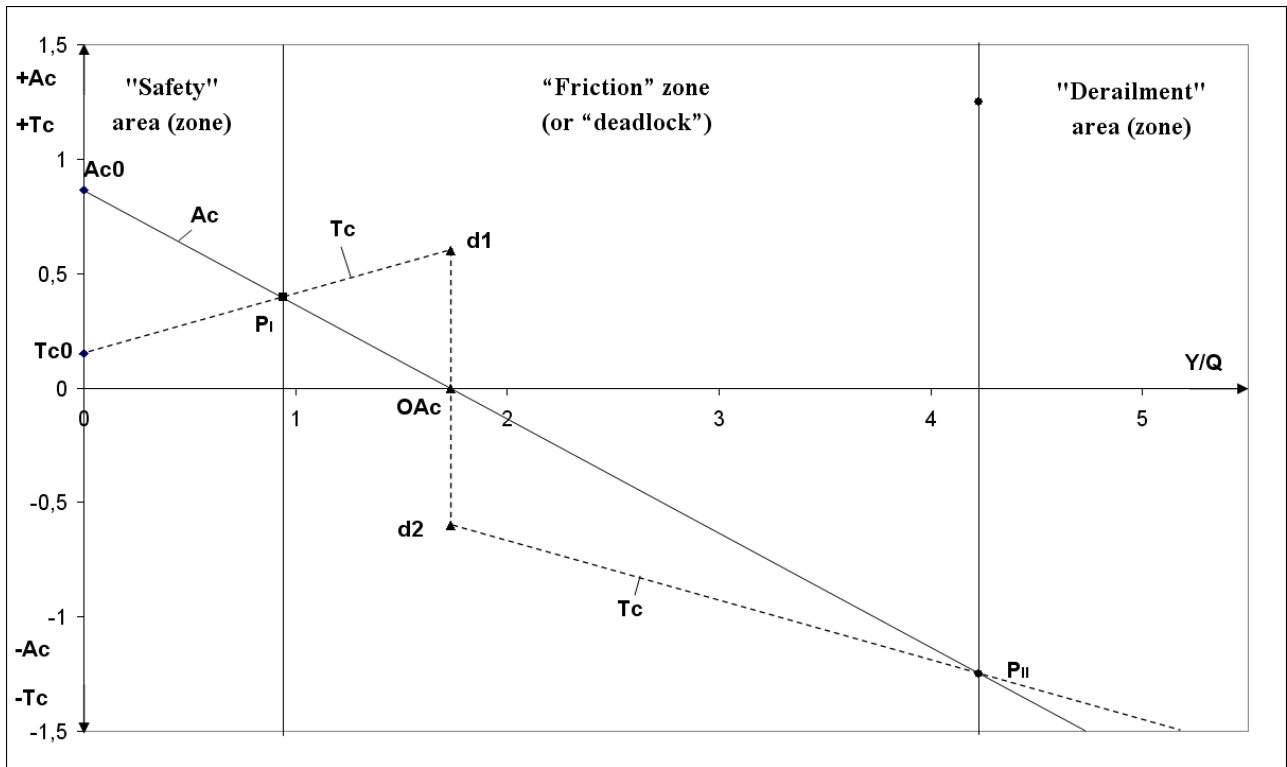


Figure 4: Linear graph of the processes related to derailment with  $\beta = 60^\circ$  and  $\mu = 0.3$ .

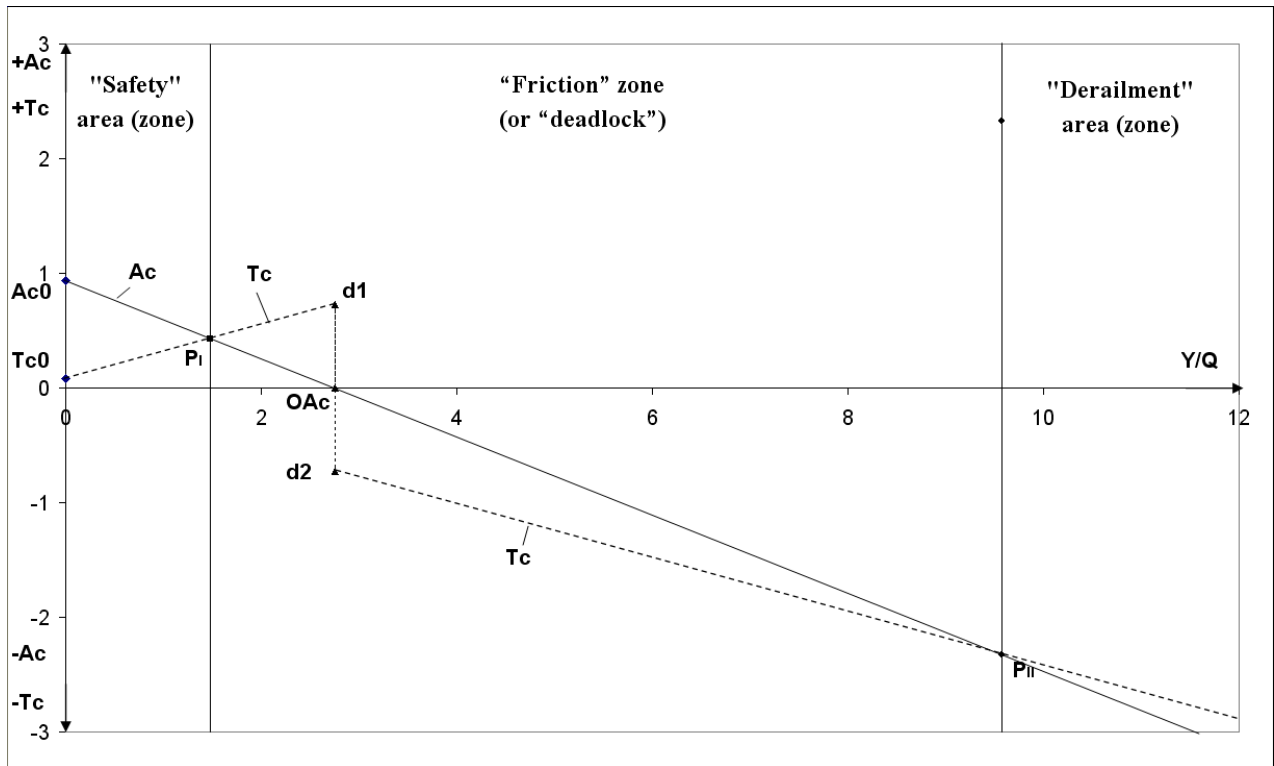


Figure 5: Linear graph of the processes related to derailment with  $\beta = 70^\circ$  and  $\mu = 0.25$ .

In some cases, the specific forces  $A_c$  and  $T_c$  is more convenient to define them as the ratio of  $A$  or  $T$  to  $Q \cdot \sin \beta$ .

$$A_c = \frac{A}{Q \cdot \sin \beta} = 1 - \frac{Y}{Q} \cdot \cot g \beta \quad (12a)$$

$$T_c = \frac{T}{Q \cdot \sin \beta} = \mu \cdot (\cot g \beta + \frac{Y}{Q}) \quad (13a)$$

Then the equation/inequality (10) is:

$$1 - \cot g \beta \cdot \frac{Y}{Q} \geq \mu \cdot \frac{Y}{Q} + \mu \cdot \cot g \beta \quad (10 a)$$

or

$$1 - p \cdot \frac{Y}{Q} \geq q \cdot \frac{Y}{Q} + r \quad (10b)$$

where:  $p = \cot g \beta$ ,  $q = \mu$ , and  $r = \mu \cdot \cot g \beta$ .

Obviously, all members of equations (10a) and (10b) represent projections of horizontal transverse forces, referred to (or separated by)  $Q \cdot \sin \beta$ , but by origin and mode of action are characterized as follows:

The first member is an active force with a return to normal wheel position and a value of 1 (or 100%);

The second member is an active force with an outward-pushing (i.e. derailing) action;

The third and fourth members are friction forces with retentive action, the first one being a variable dependent on the  $Y/Q$  argument.

In Fig. 6 is a detailed linear schedule based on dependence (3) with parameters  $\beta = 60^\circ$ ,  $\mu = 0,3$ , therefore coefficients in (10b) are  $p = \cot g \beta = \cot g 60^\circ = 0.577$ ;  $q = \mu = 0.3$ ,  $r = \mu \cot g \beta = 0.3 \cdot 0.577 = 0.173$  and the type of forces functions  $A_c$  and  $T_c$  are  $A_c = 1 - 0.577 \cdot Y/Q$ ;  $T_c = 0.3 \cdot Y/Q + 0.173$ .

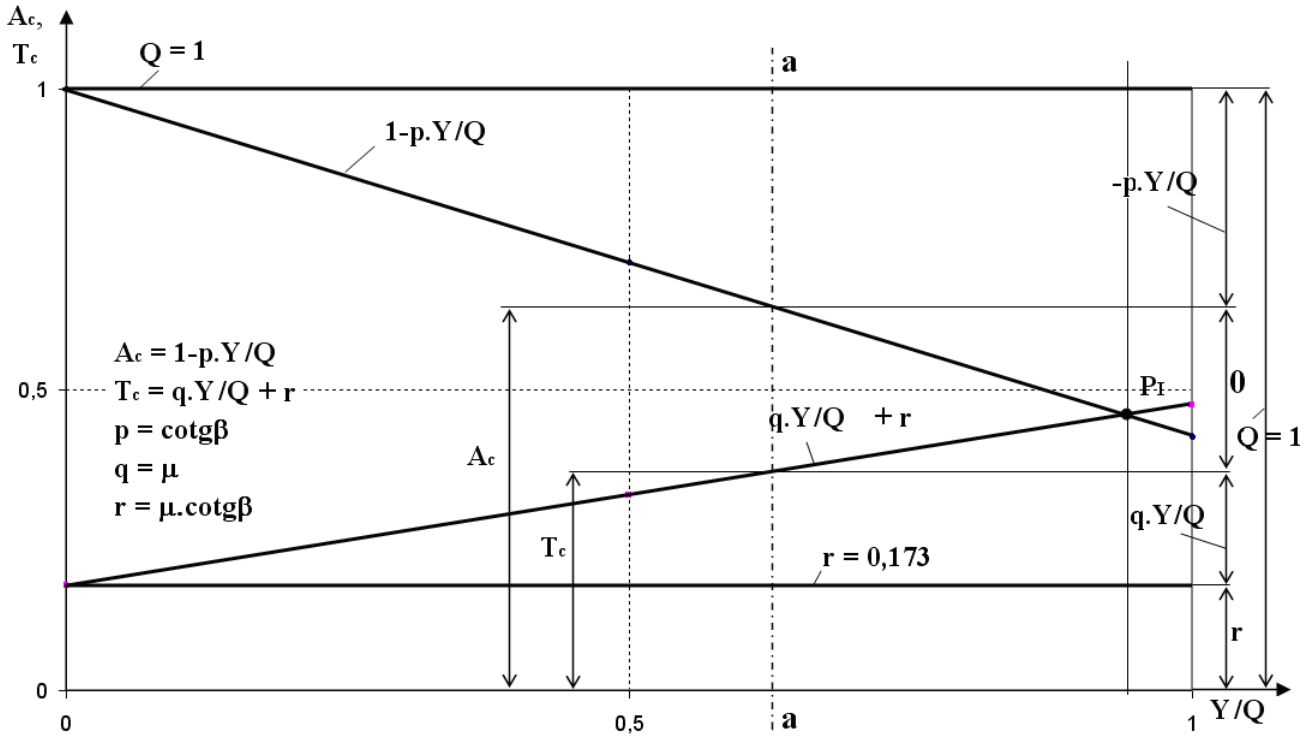


Figure 6: Detailed linear schedule based on dependence (3) with parameters  $\beta = 60^\circ$ ,  $\mu = 0.3$ .

### 3. CIRCULAR DIAGRAM OF "DERAILMENT" PROCESS

It turns out that there is an extremely comfortable geometrical interpretation of Nadal's criterion and the related dependencies. This is immediately apparent from Fig. 7, where in the Cartesian coordinate system there is in-built ¼ part ( $0^\circ \div 90^\circ$ ) of a circular coordinate system with the same central point  $O$  with considering angles in counter clockwise direction and beginning from the abscissa of  $Q$  – vertical force. Horizontal force  $Y$  is recorded (or applied) along the ordinate axis, which corresponds to an angle of  $90^\circ$  of the circular coordinate system.

Using Nadal's formula in the kind of

$$\frac{Y}{Q} = \left( \frac{Y}{Q} \right)_I = \operatorname{tg}(\beta - \rho) \tag{15}$$

(where  $\beta$  is the angle of flange forming in the conical part, and  $\rho$  - the angle of friction between the flange and rail), from Fig. 6 it can be seen that point  $P_i$  of  $OM$  beam making angle  $(\beta - \rho)$  with the abscissa, satisfies dependency (15), i.e. the relationship between its ordinate  $Y_i$  and abscissa  $Q_i$  is actual  $\operatorname{tg}(\beta - \rho)$ .

This finding – that coordinates of point  $P_i$  satisfy the dependence (15) - it obviously refers to all points of  $OM$  beam, hence it is the geometric place of points with equal ratio between the ordinate and abscissa, i.e. with the same value of  $\operatorname{tg}(\beta - \rho)$ , representing the value of angle coefficient of  $OM$  beam, which in turn expresses the I-st boundary equilibrium between the zones of safety zone and deadlock (friction).

With an arbitrary, although very small, change in the value of ratio  $(Y/Q)_I$ , it will satisfy dependency (15) no longer because its right part (defined by angle  $(\beta - \rho)$ ) of  $OM$  beam does not change. For example, assuming that the change in  $Y/Q$  ratio represents a decrease in its value due to the decreasing ordinate (relative to that of  $P_i$ , it will correspond to point  $B$  for which dependency is valid:

$$\frac{Y}{Q} < \operatorname{tg}(\beta - \rho) \tag{16}$$

characterising "safety" area, which in turn refers to all points – for the whole area (zone) of points being under  $OM$  beam.

Conversely, if the value of  $Y/Q$  ratio is increased regarding to  $(Y/Q)_I$ , then there is dependence  $Y/Q > \operatorname{tg}(\beta - \rho)$  characterizing the zone of deadlock (or friction), which is located under  $OM$  beam being limited on the other side



by *OS* beam on the next (II-nd) boundary equilibrium relationship we will rely on here.

Reasoning analogously to what has been said about *OM* beam so far, that has been applied for *OS* beam (Fig. 6); each point of the *OS* beam with current coordinates  $Q_{II}$  and  $Y_{II}$  satisfies the dependency:

$$\frac{Y}{Q} = \left( \frac{Y}{Q} \right)_{II} = \text{tg}(\beta + \rho) \quad (17)$$

Therefore, *OS* beam is a geometric place of points with "ordinate/abscissa" ratio equal to  $\text{tg}(\beta + \rho)$  and representing the beam angular factor.

According to its functional purpose, *OS* beam

represents *II-nd* state of boundary equilibrium between the "deadlock" (or "friction") and "derailment" zones. Any deviation of the  $Y/Q$  ratio from the value of  $\text{tg}(\beta + \rho)$  means a collapse of the equilibrium boundary state and falling into one of the adjacent zones:

- or derailment zone if

$$\frac{Y}{Q} > \text{tg}(\beta + \rho) \quad (18),$$

- or deadlock (or friction) zone if

$$\frac{Y}{Q} < \text{tg}(\beta + \rho)$$

E.7 (19)

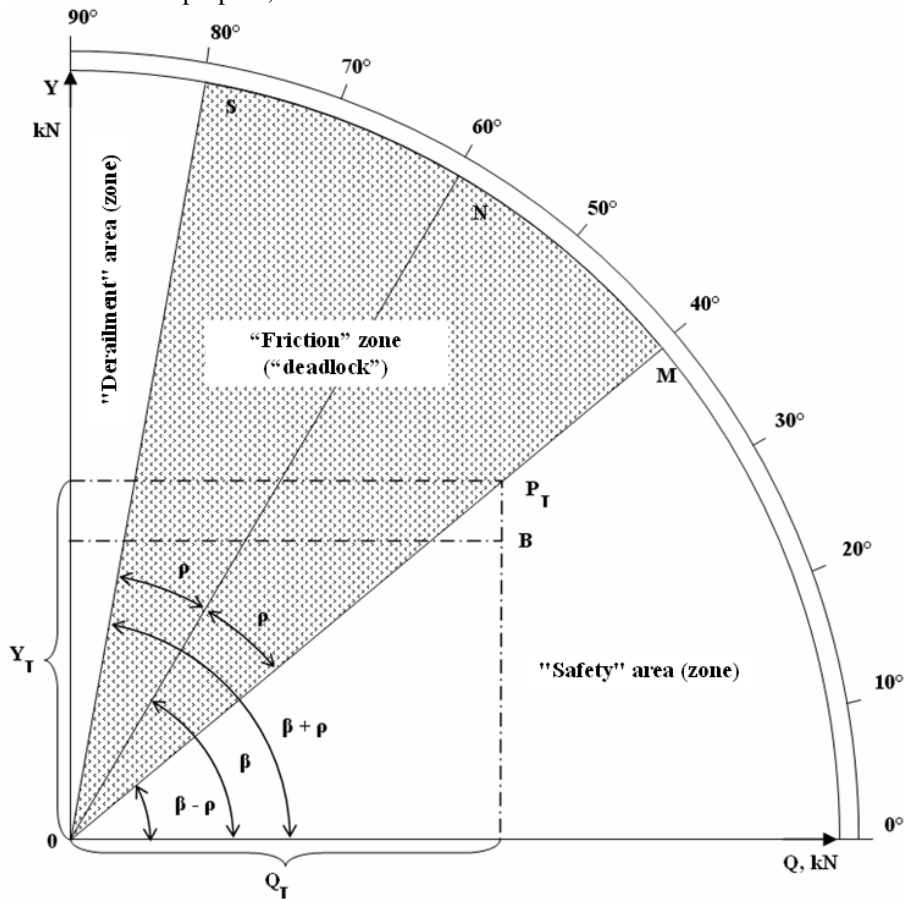


Figure 7: Circular diagram of "derailment" process – explanation scheme.

but since it has been found above that the zone of deadlock is limited by the other side, i. e. "under", from the *I* state of boundary equilibrium where (15) is in force, the condition of "deadlock" zone can be defined as follows:

$$\text{tg}(\beta - \rho) < \frac{Y}{Q} < \text{tg}(\beta + \rho) \quad (20)$$

$$\text{or } \left( \frac{Y}{Q} \right)_I < \frac{Y}{Q} < \left( \frac{Y}{Q} \right)_{II}$$

*ON* beam on the diagram corresponds to the angle of the flange forming  $\beta$  and expresses an idealized state of boundary equilibrium - directly between the "safety" and "derailment" zones according to the dependency

$$\frac{Y}{Q} = \text{tg}\beta \quad (21),$$

which would be in force at zero friction angle  $\rho$  and friction coefficient  $\mu$ , a condition where "deadlock" (or "friction") zone gets narrower to a complete cancellation.

As it can be seen from the above analytical dependencies and geometrical interpretation of the diagram, **the width of "deadlock" (or "friction") zone in the circle diagram** is equal to  $2\rho$ . However, attention should be paid that it refers to the width of "deadlock" zone in the circle diagram itself. With examining the linear schedule of force interaction in previous point 2, this problem (of the width of "deadlock" zone was discussed but in another aspect – in a force aspect and more exactly as a difference between the force ratios for the *II* and *I* state of the boundary equilibrium, i.e.

$$\begin{aligned} \left( \frac{Y}{Q} \right)_{II} - \left( \frac{Y}{Q} \right)_I &= \frac{\text{tg}\beta + \mu}{1 - \mu \cdot \text{tg}\beta} - \frac{\text{tg}\beta - \mu}{1 + \mu \cdot \text{tg}\beta} = \\ &= 2 \cdot \mu \cdot \frac{1 + \text{tg}^2\beta}{1 - \mu^2 \cdot \text{tg}^2\beta} \end{aligned} \quad (22),$$

hence the width of "deadlock" zone in the linear schedule unlike in the circular diagram has very specific real

content – it shows the difference in the values of strength ratio  $Y/Q$  between the II and I boundary equilibrium.

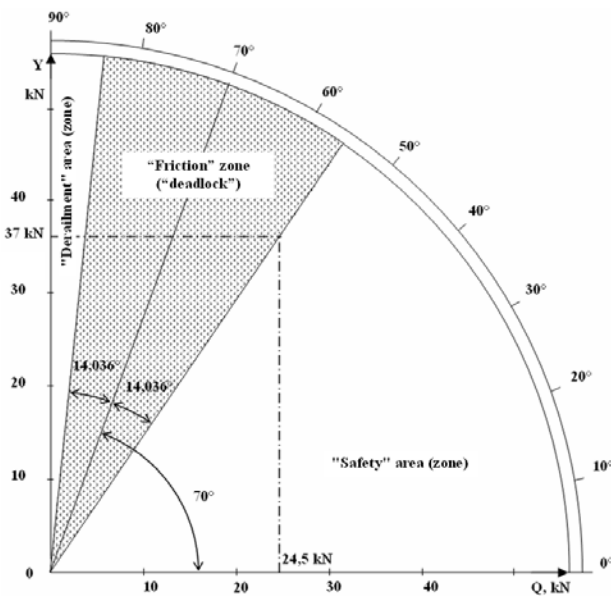


Figure 8: Circular diagram of "derailment" process with  $\beta = 70^\circ$  and  $\mu = 0.25$ .

The circular diagram of "derailment" process is given in Fig. 8 for  $\beta = 70^\circ$  and  $\mu = 0.25$  ( $\rho = 14.0$ ) and in Fig. 9 for  $\beta = 60^\circ$  and  $\mu = 0.3$  ( $\rho = 16.7$ ).

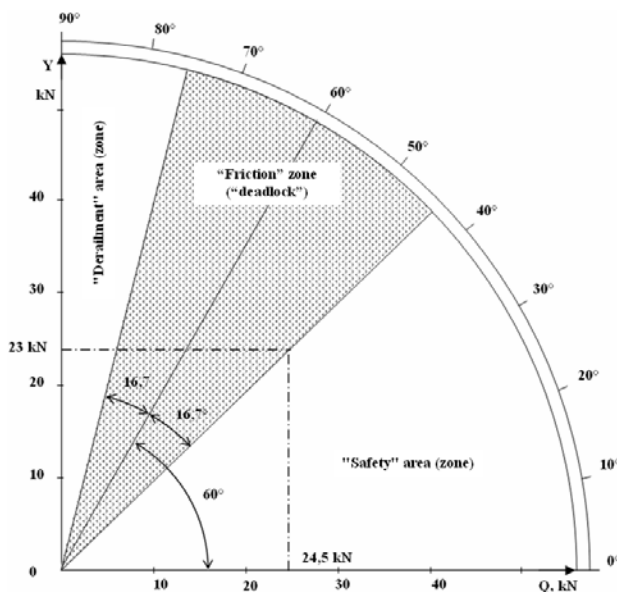


Figure 9: Circular diagram of "derailment" process with  $\beta = 60^\circ$  and  $\mu = 0.3$ .

### CONCLUSION

The first theoretical dependencies to assess safety against rolling sock derailment were introduced by Poshe as early as in 1882 and were further developed by Marje, Nadal, etc. The contribution of Nadal is exceptionally substantial because in 1908 he suggested a formula, which is still in use. Marje made correction in Nadal's formula considering the non-attacking wheel force of friction.

Galeev examined the whole wheel axle and worked out a new criterion for derailment that is the ratio between the horizontal transversal force and vertical one applied to the axle neck by the attacking wheel.

Despite the wide popularity of Nadal's formula of the criterion against derailment, it is justifiable to analyse this formula once again focusing on some significant processes and dependencies related to it.

The paper presents the analysis of two groups of forces and strength functions where the argument (independent variable) is the so-called criterion against derailment.

A graphical presentation of the zones of "safety", "friction" and "derailment" is suggested. The circular diagrams of derailment process are built with different values of the angles of flange forming in its conical part and the coefficient of "flange-rail" friction. The graphical interpretations of strength factors contribute to illustrate the process of derailment and create additional convenience and possibilities for further research.

### REFERENCES

- [1] ORE/ERRI B55: „Entgleisungssicherheit von Guterwagen in Ggleisverwindungen“. Arbeitsergebnis NN 1-8, Utrecht, 1962-1982
- [2] Heumann H., GRUNDZUGE DER FUHRUNG DER SCHIENEN-FAHRZEUGE-SONDERDRUCK AUS ELEKTRISCHE BAHNEN VERLAG R. OLDENBOURG MUNCHEN, 1954
- [3] Драган Д. Милковић, Утицај параметара додира точак-шина на динамичко понашање шинских возила Докторска дисертација, Универзитет у Београду, Машински факултет, Београд 2012
- [4] Bizic M. ИСТРАЖИВАЊЕ УТИЦАЈНИХ ПАРАМЕТАРА У ИНТЕРАКЦИЈИ ТОЧАК-ШИНА НА СТАБИЛНОСТ КРЕТАЊА ЖЕЛЕЗНИЧКИХ ВОЗИЛА, Докторска дисертација, Краљево, 2015 година
- [5] UIC Code 518: Testing and approval of railway vehicles from the point of view of their dynamic behaviour – Safety – Track safety – Running behaviour, International Union of Railways (UIC), 4th edition, Paris, September 2009
- [6] EN 14363: Railway applications - Testing for the acceptance of running characteristics of railway vehicles - Testing of running behaviour and stationary tests, June 2005
- [7] Bromberg, E. M. Interaction of the track and rolling stock / E. M. Bromberg, M. F. Verigo, V. N. Danilov, M. A. Frishman; Under the Society. Ed. M.A. Frishman. - Moscow: Gostranzheldorizdat, 1956. - 280 p.
- [8] Verigo, M. F. Interaction of the track and rolling stock / MF Verigo, A. Ya. Kogan. - Moscow: Transport, 1986. - 559 p.
- [9] Verigo, M. F. Questions of the interaction of the track and the rolling stock and the problems of calculating

the path / MF Verigo // Proceedings of the Central Research Institute of the Ministry of Railways. - 1963. - Issue. 268. - 125 p.

[10] Verigo, MF. Modernization of spring suspension of MT-50 trucks / MF Verigo, LO Gracheva, PS Anisimov / Proceedings of VNIIZhT. - 1968. - Vol. 372. - 112 p.

[11] Galeev, AU To the problem of the theory of derailment of wheels from rails / AU Galeev / Proceedings of MIIT. - 1948. - No. 55. - P. 179-191.

[12] Luisa-Izabel DUNGAN NOȚIUNI GENERALE PRIVIND SIGURANȚA CONTRA DERAIERII, Universitatea „Politehnica” din Timișoara, Buletinul AGIR nr. 1-2/2009, aprilie-septembrie p.117-122

[13] Ș. Sebeșan, Siguranța contra deraierii la vehicule de cale ferată, Revista Căilor ferate, 7, 1961.

[14] Klimenko I. V. Development of theoretical foundations and methods for assessing and improving the safety of rolling stock. DNUZHT, Ukraine, Dnepropetrovsk, 2015.

[15] Milan Bizic, Milos Tomic, Zoran Djinovic, Dragan Petrovic, *Test stand for calibration of measurement railway wheelsets*, Proceedings of the 7th International Conference Research and Development of Mechanical Elements and Systems – IRMES, Zlatibor, Serbia, pp. 419-424, 2011.

[16] Zlatan Soskic, Dragan Petrovic, Nebojsa Bogojevic, Ranko Rakanovic, Suggestions for Development of Sensors for Measurement of Forces at Wheel-Rail Contact 2007 art. ID:82 Academic journal, Mechanics, Transport, Communications, 2007

[17] Milan BIŽIĆ, Dragan PETROVIĆ, METHODOLOGIES OF EXPERIMENTAL DETERMINATION OF WHEEL-RAIL CONTACT FORCES The XVI Conference RAILCON '14 Faculty of Mechanical Engineering, Niš, Serbia

[18] Milan Bižić, Dragan Petrović, Dušan Stamenković BASICS OF EXPERIMENTAL DETERMINATION OF WHEEL-RAIL CONTACT FORCES USING INSTRUMENTED WHEELSETS, FACTA UNIVERSITATIS SERIES: Mechanical Engineering Vol. 1, N° 10, 2003, PP. 9 - 2

[19] Lysyuk V. S. Causes and mechanism of wheel derailment from the rail. The problem of wear of wheels and rails, 2 nd ed., Pererab. And additional-M.: Transport, 2002-215 p.

[20] Guangxiong, Ch. A New Method for Evaluation of Wheel Climb Derailment/ Chen Guangxiong, Jin Xincan. – 2000 ASME/IEEE Joint Railroad Conference, April 4-6, 2000, P. 9-13.



# Oscillation of Reservoir of Tank-wagon in Dynamic Longitudinal Load

Dragan Petrović\*, Milan Bižić

Faculty of Mechanical and Civil Engineering in Kraljevo, University of Kragujevac, Kraljevo (Serbia)

*Tank-wagons are typically designed to satisfy the static forces as well as their enlargement which is caused by the dynamic loads. However, sudden longitudinal impacts may cause a very rapid deformations of structural elements which can lead to the very complex physical phenomena. Apart from the oscillations of structural elements, changes of rheological properties of material, temperature changes, chemical changes, etc., may arise. During these occurrences, the behaviour of the structure can be completely different from the behaviour at the static load. Construction fails to obtain displacements that correspond to rapid changes in load, which can lead to sudden deformation of the structure. The sudden action of longitudinal load causes radial oscillations of reservoir. Thereby, if the load  $p_x$  is less than a certain value  $p_{x,kr}$ , these oscillations will have no increase in the amplitude of deflection around the equilibrium position. On the contrary, if the load  $p_x$  is higher than the value  $p_{x,kr}$ , amplitude of deflection increases with time and the reservoir loses stability. Besides, these oscillations may adversely affect the quality of running and safety of the train. Accordingly, this paper shows an example of tank-wagon and provides a method of determining the critical load from which an unlimited increase in the amplitude of deflection of the tank arises.*

**Keywords:** Oscillation, Reservoir, Tank-wagon, Dynamic longitudinal load

## 1. INTRODUCTION

The study of behavior of elastic bodies at impact loads is very interesting both from the theoretical and practical aspects. In that case, the most expressed dynamic process of deformation is appeared, which may be characterized by a minimal number of variable parameters. Knowledge of the impact and values of dynamic parameters provides better design of the structure. In addition, the study of the behavior of structure at the dynamic load is necessary for the proper planning, execution and analysis of experimental research.

The reservoir of the wagon is made in the form of a circular cylinder of radius  $R$ , of constant thickness  $h$ , and length  $l$  (Fig. 1). The reservoir is over the edges supported on the underframe, so the supports on one of the ends usually have freedom of movement in the direction of the longitudinal axis. In this way, it is partially protected from the effects of horizontal axial forces that comes from the buffers at the wagons impact.

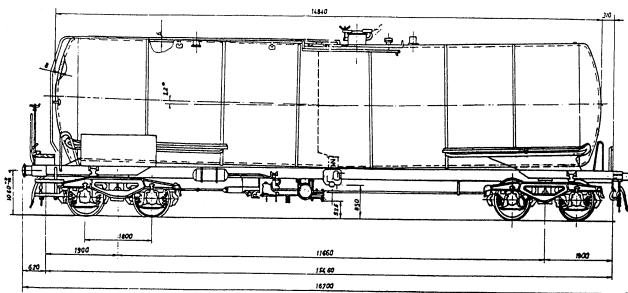


Figure 1: The tank-wagon

During maneuvering and changing of the running regime (acceleration, braking), or impacts caused by the track geometry, significant loads may arise at impact of fluid on the bottom of the reservoir. These loads can cause stresses and strains which can be a threat for the structure of the tank-wagon (Fig. 2).



Figure 2: The deformed tank-wagon

## 2. BEHAVIOR OF ELASTIC BODIES AT IMPACT

The behavior of an elastic body loaded by the forces that do not change over time belongs to the field of statics. Besides, this includes quasi-static cases where the load changes over time is slow. If the load changes over time are fast, as in the case of impact loads, then it belongs to the field of dynamics. In this case, equations of static equilibrium of elastic body should be replaced with the equations of motion. In this case, the effect of dynamic (impulse) load are not transferred immediately in all points of the body. In loaded area there are waves of stresses and strains that have a finite speed of propagation. As in the famous case of propagation of sound in the air, a certain point will be excited only when the wave reaches it. In elastic body there is not one but several types of waves and they have different speeds of propagation. Rapid changes in strains and stresses caused by the impact cannot be precisely determined without considering the wave processes. Therefore, where possible, in the theoretical study of behavior of the elastic body in impact the wave character of propagation of deformation is analyzed.

However, for railway vehicles, where the complex geometry of the supporting structure is present and speeds

\*Corresponding author: Dositejeva 19, 36000 Kraljevo, Serbia, petrovic.d@mfkv.kg.ac.rs

of impact are not so large, the model of elastic body which is insensitive to the speed of deformation can be formed. In this way, the local effects related to the triaxial stress state can be avoided. Thereby, the impact is defined with a certain speed of one of the cross-sections of the rod or shell and a mass ratio of the observed element and the load.

Consideration of the impact phenomena in this manner is different from the case where the change of several physical factors is present and wherein the material structure changes are dominant. So, most of the structures subjected to the effects of impact can be treated in this way.

### 3. DIFFERENTIAL EQUATIONS OF MOTION OF RESERVOIR

Today's constructions of railway vehicles have a supporting structure that is part of the polygonal shell which is combined with elements of beams and plate. Design of these structures requires a detailed study of their behavior. In that sense, the considerations of dynamic problems of railway vehicles can be found in the works of Timoshenko [1, 2].

The reservoir of tank-wagon is loaded as shown in Fig. 3.

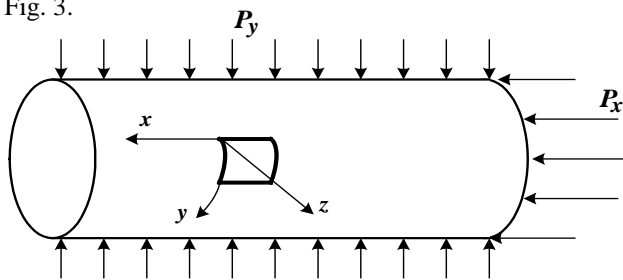


Figure 3: The loads of reservoir of the tank-wagon

The general equations of motion of the cylindrical shell given by the following expressions are used for analysis [3]:

$$\frac{D}{h} \nabla^4 (w - w_0) = L(w, \Phi) + \nabla_k^2 \Phi + \frac{q}{h} - \frac{\gamma}{g} \frac{\partial^2 w}{\partial t^2} \quad (1)$$

$$\frac{1}{E} \nabla^4 \Phi = -\frac{1}{2} [L(w, w) - L(w_0, w_0)] - \frac{1}{R} \frac{\partial^2}{\partial x^2} (w - w_0) \quad (2)$$

where:

- $h$  – thickness of reservoir,
- $D$  – cylindrical rigidity of shell,
- $\nabla^4$  – double Laplace operator,
- $w$  – deflection of reservoir,
- $w_0$  – initial deflection of reservoir,
- $\Phi$  – function of stress,
- $\gamma$  – specific gravity of material,
- $g$  – gravity acceleration,
- $t$  – time,
- $q$  – cross load of shell,
- $E$  – modulus of elasticity,
- $R$  – radius of cylinder.

By its structure the previously given system of equations describing the propagation of waves of tension-compression and bending-slipping. Given that the exact method of integrating of given equations have not yet been developed, their approximate solutions are found in the

form of order. So, the solution of deflection of reservoir can be assumed as the following order:

$$w = f(t) \cdot \left( \sin \frac{m\pi x}{l} \cdot \sin \frac{ny}{R} \right) \quad (3)$$

where:

- $f(t)$  – amplitude of deflection,
- $l$  – length of cylinder,
- $R$  – radius of cylinder,
- $m$  – number of half-waves per length of cylinder,
- $n$  – number of waves per radius.

Experimental tests have shown that deflections of reservoir towards the center of curvature and from the center of curvature are not the same. Deflections directed towards the center of curvature are greater than the deflections directed from the center of curvature. Therefore, for assumed displacements  $w$ , equation (3) is amended with member which takes into account the asymmetry of amplitude of deflection:

$$w = f(t) \cdot \left( \sin \frac{m\pi x}{l} \cdot \sin \frac{ny}{R} + \psi \cdot \sin^2 \frac{m\pi x}{l} \right) \quad (4)$$

where:

- $\psi$  – time function of correction of amplitude.

Additionally it is assumed that the reservoir has an initial deflections  $w_0$ , amplitudes of deflection  $f_0(t)$ , or the irregularities of the same character as well as the total deflection  $w$ :

$$w_0 = f_0(t) \cdot \left( \sin \frac{m\pi x}{l} \cdot \sin \frac{ny}{R} + \psi \cdot \sin^2 \frac{m\pi x}{l} \right) \quad (5)$$

Assumption that  $\alpha = m\pi/l$  and  $\beta = n/R$  leads to the following assumed total and initial deflections:

$$w = f(t) \cdot (\sin \alpha x \cdot \sin \beta y + \psi \cdot \sin^2 \alpha x) \quad (6)$$

$$w_0 = f_0(t) \cdot (\sin \alpha x \cdot \sin \beta y + \psi \cdot \sin^2 \alpha x)$$

The operators  $L(w, \Phi)$ ,  $L(w, w)$ ,  $L(w_0, w_0)$ ,  $\nabla^4$  i  $\nabla_k^2$  have the following shape:

$$L(w, \Phi) = \frac{\partial^2 w}{\partial x^2} \frac{\partial^2 \Phi}{\partial y^2} + \frac{\partial^2 w}{\partial y^2} \frac{\partial^2 \Phi}{\partial x^2} - 2 \frac{\partial^2 w}{\partial x \partial y} \frac{\partial^2 \Phi}{\partial x \partial y}$$

$$L(w, w) = 2 \left[ \frac{\partial^2 w}{\partial x^2} \frac{\partial^2 w}{\partial y^2} - \left( \frac{\partial^2 w}{\partial x \partial y} \right)^2 \right]$$

$$L(w_0, w_0) = 2 \left[ \frac{\partial^2 w_0}{\partial x^2} \frac{\partial^2 w_0}{\partial y^2} - \left( \frac{\partial^2 w_0}{\partial x \partial y} \right)^2 \right] \quad (7)$$

$$\nabla^4 = \nabla^2 \nabla^2 = \frac{\partial^4}{\partial x^4} + 2 \frac{\partial^4}{\partial x^2 \partial y^2} + \frac{\partial^4}{\partial y^4}$$

$$\nabla_k^2 = k_y \frac{\partial^2}{\partial x^2} + k_x \frac{\partial^2}{\partial y^2}$$

Depending on the oscillation form of the reservoir, the parameters  $m$  and  $n$  are changing (Fig. 4). These two parameters can be influenced by structural modifications or installation of rings on the reservoir (Fig. 5).

From the previous considerations, it can be concluded that in the case of plates and shells there is

mixed stress state or there are stresses from bending and forces (Figs. 6 and 7). Thereby, two extreme cases can be distinguished:

- no-moment stress state, when the bending stresses are negligible in comparison to the stresses induced by the forces (Fig. 6),
- pure moment condition, when the stresses induced by the forces are negligible in comparison to the bending stresses (Fig. 7).

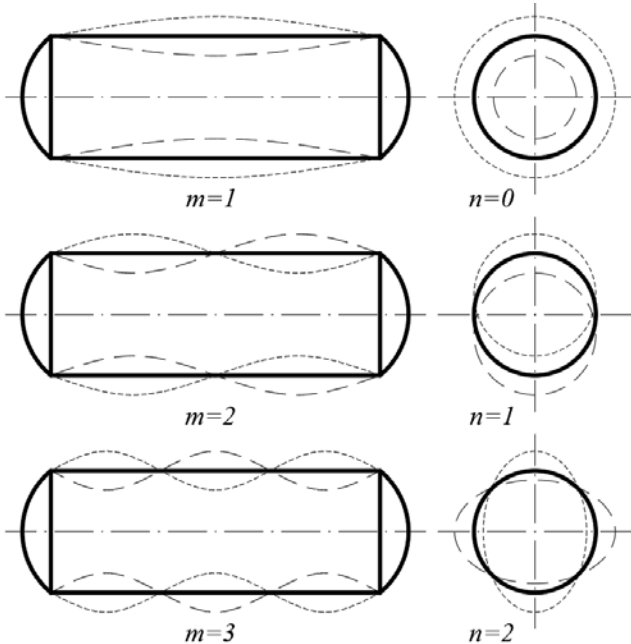


Figure 4: The different forms of oscillations of reservoir



Figure 5: The rings on reservoir of tank-wagon

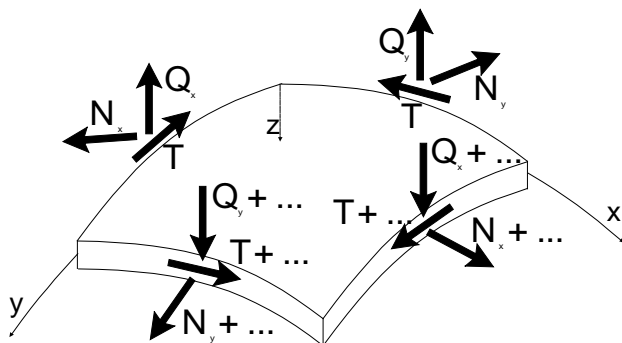


Figure 6: The normal forces  $N$ , lateral forces  $Q$  and tangential forces  $T$  on the element of shell

If the radii of curvature along the  $x$  and  $y$  directions are denoted with  $\rho_x$  and  $\rho_y$ , the curvature of the corresponding surfaces will be  $k_x=1/\rho_x$  and  $k_y=1/\rho_y$ .

Given in mind that their thickness is smaller in comparison to the other two dimensions, plates and shells are sensitive to the bending where there are large stresses and deflections. Such condition is very dangerous in practice, so it is natural that it should be avoided. The no-

moment condition is much more convenient, where plates and shells are uniformly loaded over the entire thickness while the external load is the most rationally transferred on the supports.

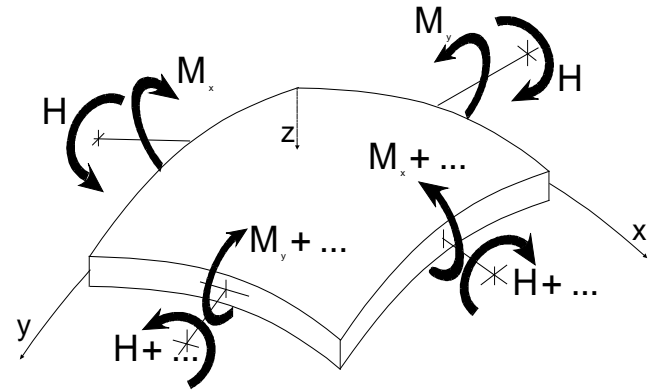


Figure 7: The bending moments  $M_x$  and  $M_y$ , and torque moment  $H$  on the element of shell

In cases where no-moment condition cannot be realized it is possible to find alternative solutions. The stress state of a mixed type is localized at the ends of plates and shells (eg. on the bottom of the reservoir), while elsewhere there is no-moment stress state which significantly simplifies the mathematical operations.

This is in connection with the term "edge effect" in which at moving away from the edge of shell or plate the stress state of mixed type significantly decreases. It is important to note that the source of "edge effect" can be not only the edge of plate and shell but also any line of middle surface with radical change of curve or thickness of plate and shell.

#### 4. STRESS FUNCTION

The shell of constant thickness  $h$  with a coordinate system in the central plane of the shell is considered in this chapter (Figs. 6, 7 and 8). In order to transformation of three-dimensional into two-dimensional problem, the hypothesis of undeformed normals (Kirchhoff–Love hypothesis) is applied [3].

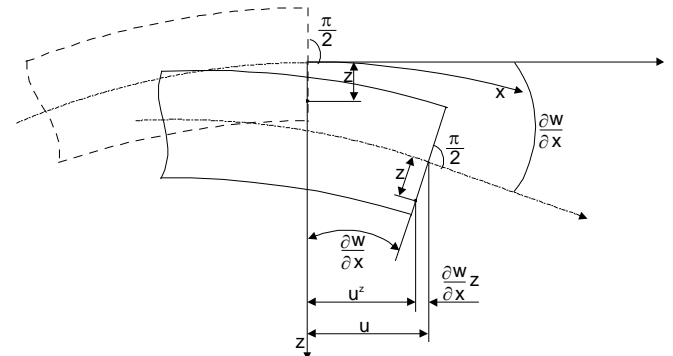


Figure 8: The deformation of shell element according to the Kirchhoff–Love hypothesis

The basis of this hypothesis is assumption that each fiber which is perpendicular to the middle plane after deforming remains right and normal to the median plane, which causing that the length of the fiber along the length of the shell remains unchanged. Therefore, the normal stresses in direction of normal on the median plane can be neglected in comparison with the basic stresses. In the theory of the shell, the basic stresses are related to the

normal and tangential stresses in the central plane and in layers which are parallel to the central plane. This hypothesis is considered as the model of the first approximation. It is very suitable for solving of many static and dynamic problems while the obtained results are suitable for the practical use.

In order to simplification of writing and solving the equations of motion of shell (1) and (2), the stress function  $\Phi$  is introduced in the central plane of the shell. It is assumed that the stresses acting on the unit length of the shell. The relations of normal stresses ( $\sigma_x$ ,  $\sigma_y$ ), tangential stresses ( $\tau$ ), normal forces ( $N_x$ ,  $N_y$ ), tangential forces ( $T$ ) and thickness of the shell  $h$ , with stress function  $\Phi$  are given with the following expressions [3]:

$$\sigma_x = \frac{N_x}{h} = \frac{\partial^2 \Phi}{\partial y^2} \quad (8)$$

$$\sigma_y = \frac{N_y}{h} = \frac{\partial^2 \Phi}{\partial x^2} \quad (9)$$

$$\tau = \frac{T}{h} = -\frac{\partial^2 \Phi}{\partial x \partial y} \quad (10)$$

#### 5. STABILITY OF RESERVOIR OF TANK-WAGON IN DYNAMIC LONGITUDINAL LOAD

The theoretical considerations from the previous chapters are applied on concrete example of the tank-wagon (Fig. 1) with the following characteristics:

$E=21 \cdot 10^{10} \text{ N/m}^2$  – elastic modulus of material of reservoir,

$\nu=0,3$  – Poisson's ratio,

$h=6 \text{ mm}$  – thickness of reservoir,

$R=1450 \text{ mm}$  – radius of cylinder,

$l=14200 \text{ mm}$  – length of reservoir.

For solution of equations (1) and (2), the method of Bubnov–Galerkin is applied [4]. In general case, the loads of the reservoir along the directions  $x$ ,  $y$  and  $z$  are as follows:

$q$  – lateral load which is normal to the medium surface,

$p_x$  – pressure or tension load which is acting along the  $x$  direction,

$p_y$  – pressure or tension load which is acting along the  $y$  direction.

External loads for the reservoir of tank-wagon along the directions  $x$  and  $y$  are as follows:

$$\begin{aligned} \bar{p}_x &= p_x \cdot R / 2h \\ \bar{p}_y &= p_y \cdot R / h \end{aligned} \quad (11)$$

Solving the equations (1) and (2) is performed by applying the Bubnov–Galerkin method [4], wherein  $X$  is the following function:

$$X = \frac{D}{h} \nabla^4 (w - w_0) - L(w, \Phi) - \frac{1}{R} \frac{\partial^2 \Phi}{\partial x^2} - \frac{q}{h} + \frac{\gamma}{g} \frac{\partial^2 w}{\partial t^2} \quad (12)$$

Function  $X$  must be equal to zero for all points of the reservoir and must satisfy the following equations:

$$\int_0^{2\pi R} \int_0^0 X \sin \alpha x \cdot \sin \beta y dx dy = 0 \quad (13)$$

$$\int_0^{2\pi R} \int_0^0 X \sin^2 \alpha x dx dy = 0 \quad (14)$$

By using the boundary and initial conditions, the equation (12) is solved, wherein is obtained the following square of frequency of natural oscillations of the reservoir:

$$\omega_0^2 = c^2 \left[ \frac{\alpha^4}{R^2 (\alpha^2 + \beta^2)^2} + \frac{h^2 (\alpha^2 + \beta^2)^2}{12(1-\nu^2)} \right] \quad (15)$$

The speed of propagation of elastic waves is:

$$c = \sqrt{\frac{E}{\rho}} = \sqrt{\frac{Eg}{\gamma}} \quad (16)$$

As is known, the reservoir has an infinite number of degrees of freedom. This means that the number of natural frequencies is infinitely large, while each frequency has its own form of oscillation.

Solution of the equation (15) will be periodic if  $\omega_0^2 < 0$ , or periodic if  $\omega_0^2 > 0$ , wherein the amplitudes of the deflection will increasing with time, which leads to the losing of stability of the reservoir.

The diagrams of changes of the natural oscillations  $\omega_0$  [Hz] of the reservoir of tank-wagon in dependence of change of number of waves per radius  $n$  and in dependence of number of half-waves per length of cylinder  $m$ , as well as the diagram of change of  $\omega_0$  in function of change of parameters  $m$  and  $n$  are shown in Fig. 9.

Considering that  $\bar{p}_y = 0$ , from the condition

$$\omega_0^2 - \frac{\alpha^2}{\rho} \bar{p}_{kr} = 0, \text{ the critical load is determined as:}$$

$$\bar{p}_{kr} = E \left[ \frac{\alpha^2}{R^2 (\alpha^2 + \beta^2)^2} + \frac{h^2 (\alpha^2 + \beta^2)^2}{12(1-\nu^2)\alpha^2} \right] \quad (17)$$

In order of analytical determining of the minimum of function  $\bar{p}_{kr}$ , the first derivative of the function should be equated with zero:

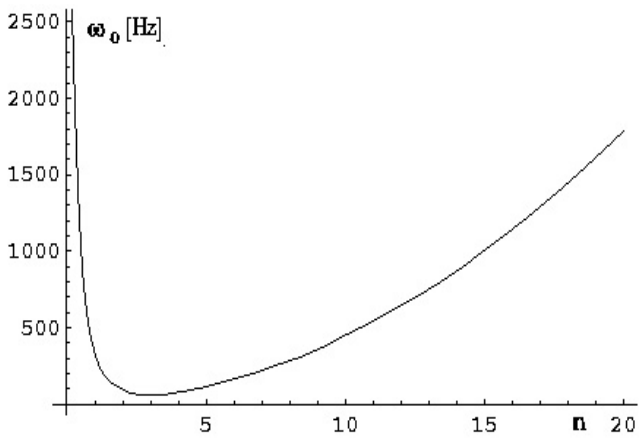
$$\bar{p}_{kr}^{min} = E \frac{h}{R} \frac{1}{\sqrt{3(1-\nu^2)}} \quad (18)$$

For the observed reservoir of the tank-wagon is  $\bar{p}_{kr}^{min} = 5,259 \cdot 10^8 \text{ N/m}^2$ , wherein minimal value of stress in the direction  $x$  caused by the external load is determined from the expression (11), as follows:

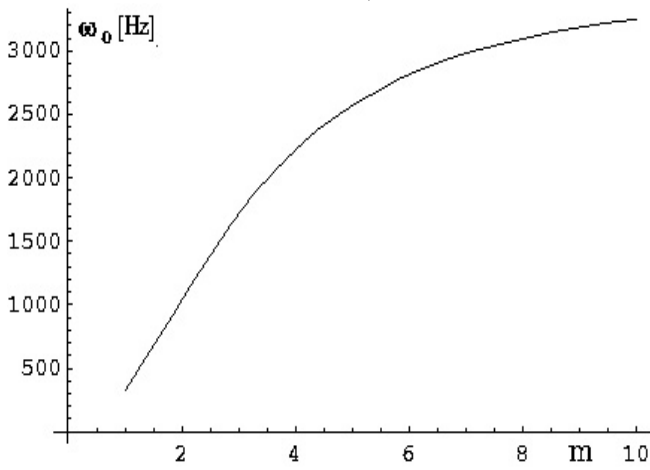
$$p_{x,kr}^{min} = \bar{p}_{kr}^{min} \cdot \frac{2h}{R} = 43,52 \cdot 10^5 \frac{\text{N}}{\text{m}^2} \quad (19)$$

The diagram of change of the critical load in function of change of parameters  $m$  and  $n$  is shown in Fig. 10, where the minimum of function  $\bar{p}_{kr}$  is marked with dart.

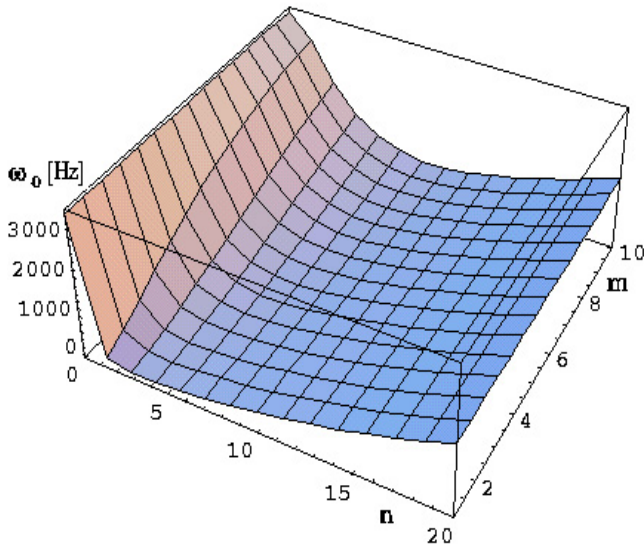




a)



b)



c)

Figure 9: The change of frequency of natural oscillations of reservoir of tank-wagon in function of change of parameter  $n$  (a), parameter  $m$  (b) and parameters  $m$  and  $n$  (c)

In the case of a longitudinal impact load  $p_x(t)$  reservoir will lose stability when active load reaches a value  $p_{x,kr} = p_{x,kr}^{min}$ . Thereby, from a set of possible types of losses of stability, reservoir will be distorted with forming of  $m$  and  $n$  half-waves, which are given in the above diagram. If any external cause excites the distortion in some another form, the critical value of load  $p_{x,kr}$  will be

greater from the minimal critical load  $p_{x,kr}^{min}$  along the direction  $x$ .

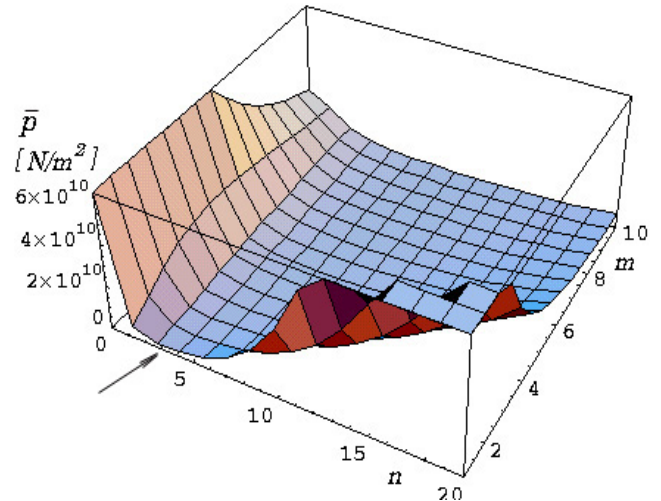


Figure 10: The change of critical load  $\bar{p}_{kr}$  in function of parameters  $m$  and  $n$

At impact dynamic loading, the analysis of influences of shapes of oscillation on the occurrence of lost of stability has also been made, and the results are shown in Fig. 11. From the diagram it can be concluded that at dynamic action of load that arises at the impact of wagons at the speed of 19.5 m/s, critical load obtains at the number of semi-waves  $m=1$  and  $n=4$ . In addition to that, the value of minimum critical load which the tank can stand is for higher at dynamic load in relation to static load.

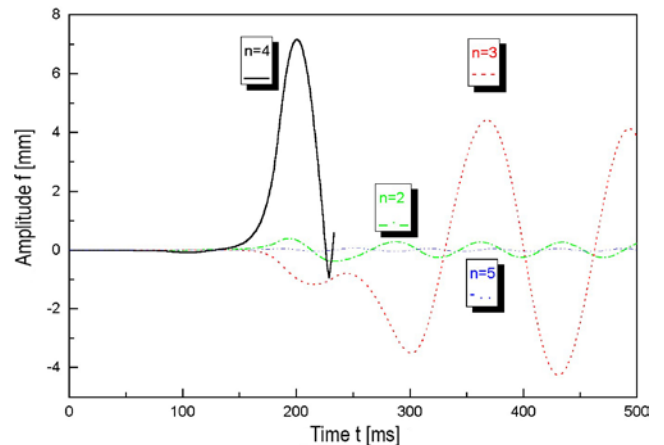


Figure 11: Influence of shapes of oscillation on amplitude of deflection of the tank for  $m=1$

## 6. CONCLUSION

The aim of the research presented in this paper is related to the stability of the reservoir of tank-wagon at action of impulse loads. In forming the mathematical model, the theoretical assumptions of the nonlinear dynamics of plates and shells are used. Established mathematical model is described via the coupled partial differential equations which are solved by using the Runge-Kutta method of fourth order. The convergence of the obtained solutions is checked and realistic picture of the physical phenomena is obtained. The minimal critical load at which amplitude of deflection suddenly increase or

when the reservoir losing stability at the dynamic longitudinal load, is defined.

In forming the mathematical model, the influence of initial deflection and oscillation forms on the stability of the reservoir is taken into account. If there is a possibility of adjusting the number of half-waves  $m$  and  $n$ , then it is possible to enlarge the dynamic load that can withstand a reservoir, without loss of the stability.

The developed model of oscillation of the reservoir of tank-wagon with appropriate initial and boundary conditions can be applied to all types of reservoirs exposed to the dynamic loads.

#### ACKNOWLEDGEMENTS

The authors wish to express their gratitude to Serbian Ministry of Education, Science and Technology for supporting this paper through project TR35038.

#### REFERENCES

- [1] S.P. Timošenko, "Teorija elasticne stabilnosti", Naučna knjiga, Beograd, (1952), (in Serbian).
- [2] S.P. Timošenko, "Staticske i dinamičke probleme teorije uprugosti", Izdatelstvo «Naukova dumka», Kiev, (1975), (In Russian).
- [3] D. Petrovic, "Dynamic of impact of waggons", Zaduzbina Andrejevic, Beograd, (2001), (in Serbian).
- [4] A. С. Волмир, "Нелинейная динамика пластинок и оболочек", Издательство «Наука», Москва, (1972), (In Russian).
- [5] D. Petrović, M. Bižić, "Stability of reservoir of tank-wagon at longitudinal impact", IMK-14 – Research and development, Volume 18, Number 1, pp. EN19-23, (2012).
- [6] W. Goldsmith, "Impact, The theory and Physical behaviour of colliding solids", E. Arnold, London, (1965).
- [7] N. Parezanović, D. Kolar, "Fortran 77", Naučna knjiga, Beograd, (1989), (in Serbian).
- [8] D. Petrovic, M. Bizic, M. Djelosevic, "Determination of Dynamic Sizes During the Process of Impact of Railway Wagons", Archive of Applied Mechanics, Volume 82, Number 2, (2012), 205-213, ISSN 0939-1533, doi: 10.1007/s00419-011-0549-5.
- [9] Atmadzhova D., An Electronic System for Measuring the Attack Angle of Railway Wheelsets at a Running in Curves, First International Conference on Road and Rail Infrastructure CETRA Opatija, Croatia, 2010.
- [10] Dragan Petrović, Dobrinka Atmadzhova, Milan Bižić, Advantages of installation of rubber-metal elements in suspension of railway vehicles, Proceedings of the Third International Conference on Road and Rail Infrastructure – "CETRA 2014", pp. 491-497, Split, Croatia, (2014), ISSN 1848-9842.

# Reliability Indicators of the Brake Distributors KE 1 for Rolling Stock in Operation

Vasko Nikolov\*

Department Transport Equipment, Todor Kableshkov Transport University, Sofia, Bulgaria

**Abstract:** This paper presents a methodology for quantitative assessment of reliability of brake distributors of KE type for freight cars in Bulgaria. The dependencies for determining reliability indicators for brake distributors are derived. Defined are the most important indicators that are evaluated using the methodology.

**Keywords:** Reliability, Brake distributor, Rolling stock, Freight cars.

## 1. INTRODUCTION

The brake distributor is an element of the braking system of the freight car and the train as a whole. Its reliability in service significantly affects traffic safety and rail crossing capacity. The KE family brake distributors are designed and built by Knorr Bremse, they meet the international requirements for modern braking systems and are used extensively in the rolling stock deployed in Bulgaria. They have an important principle in which the distribution valve can be upgraded and supplemented with details according to the operational requirements of the vehicle in question, i.e. a composite design principle is applied.

## 2. OVERVIEW

Rolling stock for freight transport uses distributors KE 1 type.



Figure 1: Distributor valve KE 1

Brake distributors of this type are sophisticated apparatus built of many elements to ensure their normal operation. They consist of three basic building blocks:

- Three-pressure device (command part);

- Four-piston attachment (executive part);
- R-charger.

The executive and control blocks except the A camera are formed in the valve carrier which connects to the frame of the vehicle and engages the other parts. Air pipes are connected to the carrier. These brake distributors can perform the following processes:

- Charging;
- Graduated application;
- Ceasing application;
- Full application;
- Emergency application;
- Graduated release;
- Ceasing release;
- Full release;
- Automatically supplementing the brake cylinder losses.

The assessment of the reliability indicators of the brake distributors shall be carried out taking into account the particulars in service as well as the system of maintenance and repair of the freight cars. On this basis, tests are carried out on the quantitative assessment of the reliability of the brake distributor valves used in Bulgaria.

To test the reliability of this important for the proper functioning of the braking system of the freight cars and their overall operation it is necessary to specify and refine the reliability indicators on which it will be assessed, the assessment criteria and the elements of their structure that should follow be subjected to a study to obtain quantitative characteristics giving a clear picture of the level of reliability of these devices as a whole.

## 3. DEFINING THE INDICATORS OF RELIABILITY

The reliability of products is their ability to perform set functions by preserving over time the values of certain metrics corresponding to set modes and conditions of use, maintenance, repairs, storage and transportation. Rail safety vehicles should also include "ensuring traffic safety under complex operating conditions".

Reliability is a complex property of the research object which, depending on its purpose and the conditions of its operation, is determined by the following basic properties:

- **Faultlessness** – feature of the object continuously maintains its working capacity for a certain time

or work. Under the notion of *continuously* for rolling stock is understood – without forced interruptions for the elimination of failures in the periods between scheduled technical servicing and repairs. Two groups of uniform objects observed under the same operating conditions have higher flammability rates than those who have received a lower number of failures in the same continuous period of continuous work.

- **Durability** – feature of the object to preserve its working capacity until a borderline condition occurs under a certain system of maintenance and repair. From two groups of the same type of surveyed objects under the same operating conditions and maintenance and repair systems, a greater durability has the one at which the boundary state of the subjects occurs later.
- **Repairability** – feature of the object, expressed in adaptability to prevent and detect the causes of failures and damages and to eliminate their consequences by performing repairs and maintenance. It can be divided into two parts:
  - Ability to alert and detect failures;
  - Ability to remove failures;
- **Storability** – feature of the object to constantly preserve the proper condition for work during and after the storage or transport under specified conditions.

The reliability and durability are taken into account as quality characteristics of the brake distributors in the braking performance of the train. The properties of repairability and storage are of no interest in terms of the operation of the functional valves of the rolling stock. The quantitative indicators of reliability measured during the research are:

- For non-recoverable details:
  - Probability of fail-safe operation, respectively the probability of failure:

$$\bar{P}(t) = \frac{N - n(t)}{N}$$

where:

$N$  – Number of items at the start of the observation;

$n(t)$  – Number of failures at the time  $t$ .

$$\bar{Q}(t) = \frac{n(t)}{N}$$

$$P(t) + Q(t) = 1$$

- Frequency of failures - probability of occurrence of failure per unit time;

$$\bar{f}(t) = \frac{\Delta n(t)}{N \Delta t}$$

- Intensity of failures - conditional density of the probability of rejection immediately after the moment  $t$ , provided that no withdrawal has occurred so far;

$$\bar{\lambda}(t) = \frac{\Delta n(t)}{N(t) \Delta t}$$

- Average work-up to refusal:

$$\bar{T}_o = \frac{\sum_{i=1}^N t_i}{N}$$

- For the distributor as a whole operating as a recoverable item:

- Average workout between failures:

$$\bar{T} = \frac{\sum_{i=1}^N \sum_{j=1}^{m_i} t_{ij}}{\sum_{i=1}^N n_i}$$

where:

$t_{ij}$  – Time (work) between  $(j - i)$ -th и  $j$ -th failures of the  $i$ -th element;

$n_i$  – Total number of received failures in the  $i$ -th element;

$N$  – Total number of elements under observation.

- Fault flow parameter:

$$\bar{\omega}(t) = \frac{n(t + \Delta t) - n(t)}{N \Delta t} = \frac{\Delta n(t)}{N \Delta t}$$

where:

$\Delta n(t)$  – number of all failures in the range  $\Delta t$ .

Quantitative indicators for durability are measured only for the distributor valve as a whole because it acts as a recoverable product, while most of its components are details of the first failure, i.e. non-recoverable, and the features of faultlessness and durability coincide at them.

The durability indicators are:

- Resource  $T_p$  – work-up of the object from the start of operation or from its restoration to reaching its border condition;
- Operating period  $T_e$  – calendar duration of the operation of the object from the beginning of its operation or the restoration after major overhaul until its border condition;
- Gamma Percentage Resource  $T_{p\gamma}$  – work-up, during which the object will not reach its border condition with the probability  $\gamma$  %.

Failure of the distributor valve means the loss of ability to carry out to the required extent the normal operation of the brake and the negative impact of these processes on the train, such as:

- Lack of application;
- Lack of release;
- Self-application;
- Self-release;
- Unable to perform graduated release;
- Delayed application;
- Delayed release;
- Inability to supplement the brake system failures.

The failures of the distributors in service, taking into account the specificities of operating and servicing the brakes, can be conventionally divided into visible and hidden. The first ones result in the brake failure of the entire car and are determined in the operating conditions when performing the braking tests, in most cases visually (for example, in the position of the piston rod piston rod). These include Lack of application, Lack of release, Self-application, Self-release and so on. In these cases, as a rule, the distributors shall be removed from the car and replaced with other ones that are in working condition or the brake of the car shall be isolated. If these signs are missing, in the absence of faults on the other parts of the car braking system, the distributor is considered to be upright, i.e. provides the required braking pressure on the wheel.

Hidden failures refer to different deviations from the characteristics of the distributors from the established norms that cannot be determined in the operating conditions without a special check. For this reason, assessing the reliability of the distributors for such failures can only be practical in qualitative terms.

A quantification of the faultlessness of distributors in operation can be given on the basis of statistics on apparent failures, which is also the basis of the methodology for gathering information on the condition of these apparatuses.

The observing and inspection of the work of the distributors are carried out on cars in the trains of the freight trains located in the starting stations, when carrying out complete braking tests carried out according to the requirements of the normative documents. Inspection data is placed on work cards, and then downloaded. Consider the types and modes of operation of the distributors, the number of apparatuses switch on and in good condition ones, the failures in their work.

In order to specify the information received, the method provides for the stroke of the piston rod and for the preliminary work on the removal of the compressed air passages in the connection of the distributor valve with them so as not to affect the evaluation of the operation of the apparatus. The methodology provides for an observation of the cars from the end of the train to the it's beginning. This is caused by the fact that in this part of the train, due to faults from the main air pipe, the distributors are in the most unfavourable conditions in terms of their operation. In addition, when checking the front of the train, the performance of the compressed air may influence the performance of the distributor (non-uniform air consumption at loosening the brake under different conditions).

At the same time, such an approach makes it difficult to detect the brake's lack of application at the end of the train, since, depending on the length of the composition and the density of its braking system, delayed release may qualify as lack of release. Practice shows that the distributor's lack of release occurs much less frequently than other malfunctions. Additionally, removing the flaws prior to the test of distributor valve allows the lack of release due to undershooting or losing the apparatus's density to be excluded. Therefore, the release characteristic is marked according to the method as normal or apparently delayed compared to adjoining devices checked.

To obtain confidence values of the reliability, the volume of the sample should be large enough:

$$n > \frac{PQx^2}{\epsilon^2} 10^4$$

where:

$P$  – Probability of occurrence of a separate event;

$Q$  – Probability of non-occurrence of a separate event;

$\epsilon$  – Permissible error, %.

The dimension  $x^2$  is given by a table for values of the integral of the probability at the determined (confidence level) probability on the assumption  $Q$ . In this case it is accepted  $P=Q=0,5$ . The value of  $x$  at  $Q=0,99$  is  $x=1,5758$ ; at  $Q=0,95$   $x=1,96$ . For the indicated values of

$P$ ,  $Q$  and  $x$  a plot of the dependencies of the number of investigated apparatuses  $n$  of the permissible error  $\epsilon$  in confidence probabilities is 0,99 (1) and 0,95 (2) (Figure 2). It is evident from the figure that in order to obtain the result whose average value would be different from the real one with a probability of  $Q = 0,99$  with no more than 3%, it is necessary to study about 1850 distributor valves, at  $\epsilon = 5\%$  to be tested at least 660.

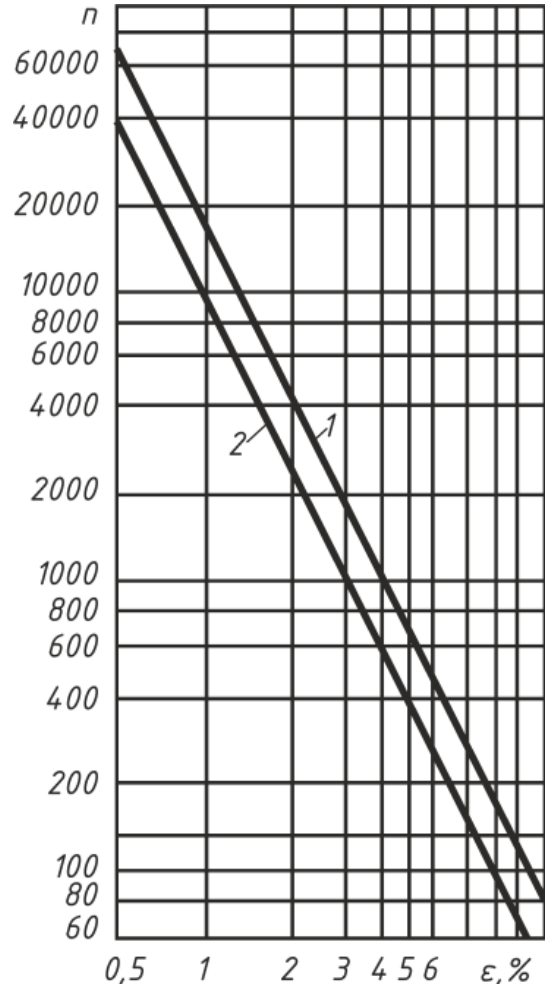


Figure 2: Dependence of requirement quantity tests  $n$  on tolerable error with a confidence probability of observations

A tolerable error is assumed in determining the reliability of the distributor valves as a whole for each study period of no more than 2% at a confidence level of 0.99 and with a relative number in use of not more than 5%. According to that and also taking into account the number of supposed observation points, the methodology envisaged to examine at each point a total of 500 distributors for the entire study period.

The study of the condition and work of the distributor valves is carried out at train stations.

It is necessary to specify how many distributors work in the freight train mode – G and how many in the passenger train mode – P.

The received distributor status data in use is used to determine the reliability indicators that are considered probability  $P_i$  or absence  $Q_i$  of a particular sign:

$$P_i = \frac{n_i}{N_i}$$

$$Q_i = 1 - P_i$$

where:

$N_i$  – Total number of PVs examined, considering the presence or absence of the  $i^{\text{th}}$  sign;

$n_i$  – Number of distributors with the  $i^{\text{th}}$  sign.

In the present case, the aforementioned conditions of distributor valve leading to deviations from its normal functioning are considered to be signs. The probabilities  $P_i$  and  $Q_i$  are determined as follows:

- The probability of distributor being in one or other state is determined by the total number of distributors tested;
- The probability of failure or lack of failure – by the total number of distributors included;
- The probability of normal or delayed release, as well as the impossibility or delay of completing the leakage – by the number of distributors with normal release.

The probability of a faultlessness operation of the distributor is considered as the main reliability indicator, i.e. loyalty to the lack of obvious failures. The probability of a failure (self-release, lack of application, partially delayed release, etc.) is used to analyze the performance of the distributor at different periods of observation and comparison with other types of distributors.

As the trains have been tested in the process or before their departure, the traceability indicators generally characterize the performance of the distributors during the freight train operation.

#### 4. CONCLUSIONS

The methodology makes it possible to assess the reliability and durability of brake distributors as one of the most important elements of the freight wagon braking system. The resource estimation and the probability of faultless operation of the instrument as a whole and its individual elements can be made through the quantitative evaluation of the reliability indicators.

#### REFERENCES

- [1] Василев, С. и др. Влакови спирачки, С. Техника, 1985.
- [2] Димитров, Ж. Надеждност на железопътната техника, С. 1989.
- [3] Крылов, В. В., Кузмина, Е. И. Показатели надежности воздухораспределителей грузового подвижного состава в эксплуатации, Исследование автотормозов железнодорожного подвижного состава, М., Транспорт, 1984.
- [4] Цанков, А. Автоматична влакова спирачка със съгъстен въздух КЕ – устройство, действие и поддържане, С., Техника, 1966.

# The Importance of the Railway Infrastructure in the Operational Program "Transport and Transport Infrastructure"

Mira Zafirova<sup>1</sup>

Faculty of Machinery and Construction Technologies in Transport  
Department of Transport Construction and Equipment / University of Transport "T.Kableshkov", Sofia (Bulgaria)

## Abstract

*Operational Program "Transport and Transport Infrastructure" (OP "TTI") 2014-2020 is continuation of OP "Transport" 2007-2013 and it is developed and based on a series of relevant documents in line with the applicable community and national strategies and policies. It was prepared and based on the needs defined in the analysis of the current state of the transport sector in Bulgaria, made for the purposes of the program.*

*The strategy of OP "TTI" 2014-2020 foresees the completion of major national and European transport routes in the country.*

*The main part of the railway infrastructure in Bulgaria was built in XX century. With the changes after 1989 there is almost full advantage of road transport.*

*In the developed report is analyzed one of the national priorities of the Operational Program "Transport and Transport Infrastructure" (OP "TTI") from 2014 to 2020 - to improve and enhance the competitiveness of rail transport in the country.*

**Keywords: Operational programs "Transport" and OP "Transport and Transport Infrastructure", railway infrastructure, priorities**

## 1. INTRODUCTION

The first railway line in Bulgaria is the Rousse - Varna line, built in 1866.

Main railway lines were built at the end of the 19th and early 20th centuries. Particularly intense is their development after World War II until 1990. During this period industrial and civil construction intensively unfolds. In order to absorb the fast growing passenger and freight transport, a number of measures are being taken to increase the throughput and transport capacity of the railway lines. The main railway lines are doubled: Sofia - Gorna Oryahovitsa - Varna, Sofia - Plovdiv and part of the Plovdiv - Burgas line. Much of the rail network is electrified. All the nodal, passenger, freight and distribution stations have been reconstructed and modernized. Route-relay, stationary, dispatching centralizations and many other facilities have been put into operation. More than 1500 passenger and several freight wagons have been produced in the country's railway plants.

After the socio-economic changes in the country after 1990 there is a reverse trend in the development of the railway transport in Bulgaria. Both the number of trains carrying passengers and the number of wagons in one line were reduced. For example, From 6 to 10 wagons on a fast train until 1990, only 3-4 wagons now a day. Trains run only with 1 wagon. Passenger traffic has decreased for a number of reasons: a small number of

large-scale trains between them, a long journey, a poor state of comfort. The journey does not include bedrooms, couch wagons and buffets. At the result the lowered passenger traffic has sharply reduced revenue. The State contributions to compensate for reduced revenue from ticket travellers a "reduced tariff" for students, retirees and railway employees are insufficient and non-regular.

The situation with international trains is same. International trains from Sofia to Belgrade, Bucharest and Istanbul run only 2 wagons and the three Thessaloniki trains are cancelled. With a number of regulations an almost complete advantage of road transport is provided, the formation of unfair competition by the road carriers.

The share of passenger travel by rail for 2011 is 11.9% of all journeys, and the share of freight transported by railway transport is 9.3% [2].

One of the indicators characterizing passenger transport is the number of far trains carrying passengers departing from Sofia for the different directions [3].

Figure 1 shows the number of long distance passenger trains departing from Sofia Station for the period from 1935 to 2015.

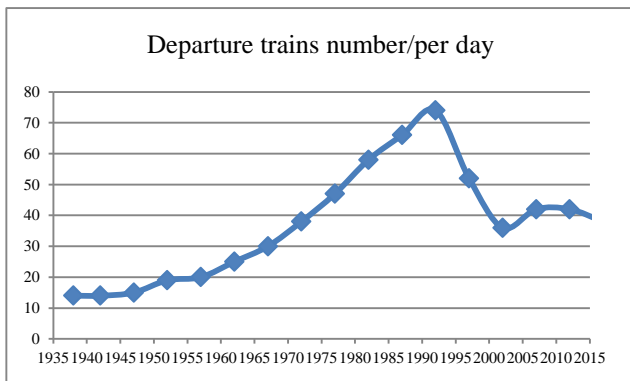


Figure 1: Far passenger trains departing from Sofia station

The volume of freight traffic is an indicator of the activity of the railways.

Figure 2 shows the volume of loads transported by railway during the period from 1935 to 2015

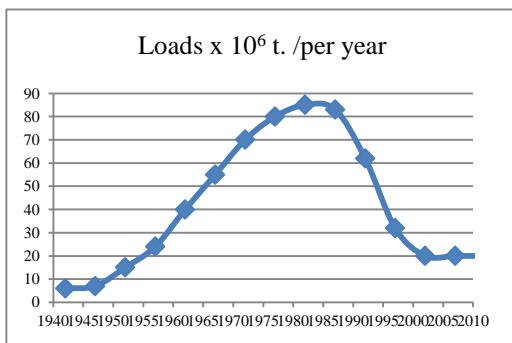


Fig.2. Loads transported by rail

Bulgaria's accession to the European Union reinforces the need to use territorial factors for growth and sustainable development. These objective realities require Bulgaria to pursue a regional policy aimed at reducing inter-regional disparities in employment and incomes of the population and, above all, in implementing regional and cross-border cooperation.

For the first programming period 2007 to 2013 seven operational programs were funded with EU funds through the three Funds: European Regional Development Fund (ERDF), European Social Fund (ESF), Cohesion Fund (CF). Operational Program "Transport" 2007-2013 has been developed following an analysis of the current state of the transport sector in Bulgaria.

Operational Program "Transport and Transport Infrastructure" OP (TTI) 2014-2020, is a continuation of OP "Transport". Its strategy is to complete the main national and pan-European transport routes on the territory of the country.

The elaborated report analyzes one of the national priority areas for the Transport and Transport Infrastructure Operational Program (TTI) 2014-2020 - improving and increasing the competitiveness of the railway transport in the country.

## 2. OPERATIONAL PROGRAMS AND PRIORITIES:

Rail transport is the main mode of transport in all industrialized countries in the world. Its advantages over other modes of transport are:

- Proposes environmentally cleaner transport
- Transport of larger volumes of cargo
- Much safer transportation
- Less expensive transport
- Higher energy efficiency
- Railways use 2-3 times less land for its activities.

In the OP "Transport" 2007-2013 and the Operational Program "Transport and Transport Infrastructure" (TTI) 2014-2020 a number of measures have been identified in the railway sector of the transport infrastructure. The aim of these measures is to overcome the decline in its development over the past few decades.

The main directions in the development of this area are dictated by the following factors:

- The main railway infrastructure in Bulgaria is built;
- High degree of electrification and the density of railway lines;
- Cross-country location of the country, enabling the development of transit traffic in the direction of the Pan-European transport corridors;
- Available strategy for development of intermodal transport;
- High professional staffing potential;
- European policy supporting development;
- High degree of harmonization of transport legislation related to rail transport with that of the EU;
- More environmentally friendly and safe than other modes of transport;



Fig. 3. Map of Europe

The weak places in the available infrastructure are:

- Unsatisfactory technical condition and level of maintenance of the existing railway infrastructure, obsolete technologies incompatible with those of the European Union;
- Too low traffic, which does not provide funds for the standard maintenance of the built infrastructure;



- Lack of railway lines allowing speeds of 160 km/ h for passenger transport and 120 km/ h for freight;
- Morally and physically outdated transport park;
- Low degree of market development of rail compared to other modes of transport;
- Failure to reach the design speed in much of the railway infrastructure;
- There are limitation gauge restrictions associated with tunnels, bridges, etc. when an appropriate rolling stock have been used.
- Rail-to-road inequality.

The strategy of OP "TTI" 2014-2020 envisages the completion of major national and pan-European transport directions on the territory of the country. The main investments are directed towards the infrastructure projects with an advanced degree of implementation, mainly funded under OPT 2007-2013, aiming at the maximum completion of their modernization or their completion.

The priorities of OP (TTI) 2014-2020 related to the development of the railway sector are:

A) Development of the railway infrastructure on the "core" Trans-European Transport Network, development of cross-border relations with neighbouring countries;

B) Development of the infrastructure needed for intermodal transport. Reconstruction of key station complexes along the main railway lines;

C) Innovation in management and services - implementation of modernized infrastructure for traffic management, improvement of safety and Transport security";

D) Developing environmentally friendly, EU-compliant, rail freight and passenger transport modes and technologies, reducing the negative impact of transport on the environment and human health. Creating the right conditions for sustainable transport growth with increased energy efficiency.

*Pr.1. Development of railway infrastructure on the "main" Trans-European Transport Network, development of cross-border relations with neighbouring countries.*



Fig. 4. Map of the railway lines in Bulgaria

The main directions under OPTI 2014-2020 are:

- Dragoman (Serbian border) – Sofia – Plovdiv – Burgas/ Svilengrad (Turkish /Greek border); Within the framework of the OPT 2007-2013 were financed and are in the process of Completion of investment projects on part of sections of the railway lines. The other part is provided for funding From the Connecting Europe Facility.
- Vidin (Rumanian border); – Sofia – Kulata (Greek border); ;
- Sofia – Radomir – Gyueshevo (Macedonian border);
- Sofia – Mezdra – Gorna Oryahovitsa;
- Russe – Stara Zagora – Dimitrovgrad

It is necessary to build rail links with the neighbouring countries with the same exploitation characteristics, which ensure fast and safe travel for longer distances from and through Bulgaria. During the programming period 2007 - 2013, a large part of the route "Eastern/Mediterranean" corridor from the main TEN-T network to Turkey is completed, which ensures greater reliability and quality of the transport services on the route Sofia - Plovdiv - Istanbul. During the period 2014-2020 the activities for complete completion of this part of the corridor will be continued through the modernization of the sections on the Sofia-September railway line.

Cross-border links to Romania are expected to be significantly improved with the construction of the Danube Bridge 2 (Vidin-Calafat). The next steps are the planned modernization in the period 2014 - 2020 of the first part of Vidin - Medkovets from the Vidin - Sofia railway line.

Contributing to improving the cross - border relationship with Serbia is the realization of Project "Modernization of the railway line Sofia - Dragoman" for which they are carried out feasibility studies. Conceptual designs have been developed and prepared cost - benefit analysis (CBA). The preparation have been done with funds from OPT 2007-2013 and at the end of 2015 complete design readiness is achieved.

By realizing the modernization projects of the Sofia - Kulata railway line (in the regions Sofia - Pernik - Radomir and Radomir - Kulata), cross-border relations with Greece will be significantly improved.

The Radomir-Gyueshevo railway line is part of a major link to Macedonia. It is planned to prepare the project "Modernization of Radomir - Gyueshevo Railway Line" in the period 2014 - 2020, including updating of the conceptual design, elaboration of detailed development plans.

*Pr.2. Development of the infrastructure needed to implement intermodal transport (in transport cargo and for passengers). Reconstruction of key station complexes along the main railway lines*

The analysis of OP "Transport" in this sector outlines the following:

Several Trans-European Transport Corridors (IV, VII, VIII, IX and X) pass through the territory of Bulgaria. The main routes for domestic and international intermodal

transport coincide with the directions of the Bulgarian sections and the directions of the main and extended trans-European transport network. There is a need for the potential for the organization of a combined transport sector. However, all existing intermodal terminals are inadequately used. Intermodal operators are poorly equipped as regards intermodal rail wagons.

The existing park of freight wagons is primarily adapted for transporting ISO containers. There is a lack of road equipment that can be operated by a TEU carrier (containers, carrier-carriers) for Ro-La and Ro-Ro techniques. Typically, the combined traffic flow (containers and cell phones) amounts to less than 0.5% of total traffic, which is extremely low compared to about 4% in Western European countries.



Fig. 3. Map of Europe with major transport corridors

At present, the combined transport services market on the territory of Bulgaria is not well developed. Most containers are loaded and unloaded at the port of Varna and are not transported further on the territory of the country as container shipments. There is a limited flow of road transit containers and also a limited number of containers by rail. There is only one single train / regular train for containers or combined transport, Sofia-Thessaloniki / which was put into operation in 2003. Another stream of containers exists between Plovdiv and Burgas, Varna and Maritsa East.

To increase the use of intermodal transport it is necessary [2]:

- Development of the network of terminals meeting the requirements for modern freight services to ensure better coordination between the different modes of transport in the direction of the development of intermodal services, establishment of reliable and fast rail connections between the terminals. Needs assessment points to the necessity of building terminals in Sofia as well as in Southeastern, North-East and North-West planning regions,

- Development of intermodal connections between ports and the rail network in order to promote the potential growth of trade and transit traffic,

- Expansion and development are the storage areas of many freight terminals.

- Improved access to passenger transport at key stations.

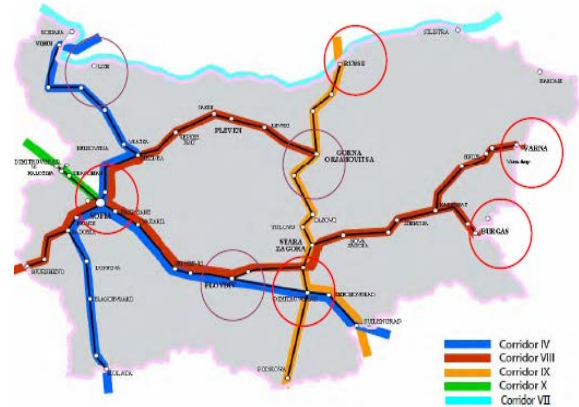


Fig. 4. Map of intermodal terminals in Bulgaria

The objective of this investment priority is:

- Via the construction of intermodal freight terminals, conditions are created for the integration of different modes of transport and efficient use of the specific advantages of individual species in a single multimodal transport chain.

- Reconstruction of key station complexes This is necessary for:

- improvement of the functional requirements for carrying out the main activities related to train movement management,
- creating conditions for providing higher quality of service to customers - passengers and carriers.

The reconstruction of the station complexes helps to improve the intermodality of the passengers by linking the station complexes with the other types of transport - metro / bus / air, as well as through a communication solution for the transport and pedestrian connections of the station complex.

At the same time, the station is brought in line with the requirements of the normative framework for building an accessible environment in the urbanized territories. Measures are being taken to increase the energy efficiency of public spaces, to introduce intelligent modern systems for passive and active systems of heating, air conditioning, lighting, information, etc.

The advantages of the railway infrastructure, the infrastructure and the analysis of the Operational programs "Transport" 2007-2013 and "Transport and transport infrastructure" 2014-2020 show the potential of today's generation to work towards the preservation and further development of the railway sector.

The fall in demand for rail transport services is partly due to external factors such as the demographic and financial crisis.

The need to develop passenger and freight rail transport in the future is essential for the following reasons:

- overload of road infrastructure;
- from high prices of automotive fuels,;
- the national policy for environmental protection;

- Increasing traffic safety.

On the other hand, by improving the technical and operational state of the main railway infrastructure, the transport infrastructure will also have a significant impact on the efficiency of the search for passenger trips and freight transport by rail within Bulgaria. Demand for the service will contribute to the accumulation of funds for its maintenance.

The good infrastructure is the basis for the successful integration of the Bulgarian transport system into the European one and for the change in the distribution of the international flows passing through the country by volume and by type of transport.

The benefits of the OP "TTI" (in particular development of intermodal transport for passenger and reconstruction of key stations) interventions will have the following effect:

- At the Operational Program "Human Resources Development" and Operational Program "Rural Development" will contribute to the development of the economy and to raising the living standards of the population in accordance with the objectives of the "Europe 2020" Strategy.
- Reducing rural poverty in rural areas.
- Growth by improving the connectivity of the regions and opening new jobs, especially in the more lagging regions of the country. (In the first half of the programming period 2007-2013 the main challenges in creating and preserving the administrative capacity are associated with a shortage of human resource with the necessary level of competence, high level of staff turnover, lack of training, incentives and incentives material and technical conditions for the work of the employees whose functions are directly related to the preparation, implementation and control of OPT 2007-2013 projects).

*Pr.3. Innovation in management and services - implementation of modernized infrastructure for traffic management, improvement of safety and Transport security*

Operational Program Transport is aimed at developing the transport infrastructure in Bulgaria and adapting it to the European one. But once built, it is necessary to lay down measures to preserve the newly built and modernized railway infrastructure throughout the lifetime. To this end, the maintenance and operation system should be improved.

There are necessary to input some measurement to increase efficiency in the operation and maintenance of the railway infrastructure, incl. built with Structural and Cohesion Funds The EU.

- the formation and implementation of the new tariff policy and the elaboration of a market-oriented methodology for the formation of the fees for access and use of the services in the railway infrastructure.
- the completion of the project "Design and Implementation of a Resource Planning and Management System in the National Company "Railway Infrastructure", which concerns the basic business processes, related to resource management and planning,

incl. The management of railway infrastructure maintenance.

Under OPTTI 2014-2020, the financing of investments in the input intelligent traffic management systems, improve safety and security of transport. The Activities aiming at the deployment of Intelligent Management Systems Traffic, improving the safety and security of rail transport is based on two key strategic documents:

- "Strategy for Implementation of the Technical Specifications for Interoperability for the Conventional Railway System in the Republic of Bulgaria 2013 - 2030", Which contains 11 strategies for the individual subsystems, as well as a common strategy;
- "The Strategy for the Implementation of the European Governance System Railway Traffic (ERTMS) in the Republic of Bulgaria "and" The National Plan for the implementation of the European rail management system Traffic (ERTMS) "

*Pr.4. Developing environmentally friendly, EU-compliant, rail freight and passenger transport modes and technologies, reducing the negative impact of transport on the environment and human health. Creating the right conditions for sustainable transport growth with increased energy efficiency.*

Operational program "Transport and Transport Infrastructural" will have a specific contribution and impact on national aims at the climate change policy. The main sources of greenhouse emissions are:

- The privatization of road transport;
- The significant reduction of subsidies for rail transport;
- The closing down of railway routes;

That leading to a change in the structure of transport - from rail to road.

The most significant contribution is made to the increase in greenhouse gas emissions by private cars, followed by heavy goods vehicles. In 2009, passenger and heavy goods vehicles are the source of 60% and 21%, respectively emissions in the sector.

OP "TTI" envisages as a concrete direct effect contributing to the achievement of national climate change targets - increasing the share of rail transport and construction of intermodal terminals for combined transport.

## CONCLUSION

The development of the railway infrastructure is a responsible task for modern Bulgarian society. On the one hand, it is an essential part of the integration of national and European transport, increasing the competitiveness of the Bulgarian economy. On the other hand, it is a duty to preserve the efforts and resources of the previous generations - the main part of railway infrastructure has built early 20th centuries.

Its efficient use will help solve the increasing problems of traffic safety, congestion and environmental protection.

Successful investments by the nowadays generation are a pledge for the future development of the country.

#### REFERENCE:

- [1]. Operational program „Transport“ 2007-2013
- [2]. Operational program „Transport and Transport Infrastructure“ 2014-2020
- [3]. Tasev Y., M. Lepoev, "Role of the state for the development of Bulgarian Railways" academic journal „Mechanics, Transport, Communications“, t. 11, N 3,

# Study of the Interaction "Wheelset-track" of the Attacking Wheelset of Tram Bogie Type T81 in Exploitation in Sofia

Dobrinka Atmadzhova<sup>1</sup>, Emil M. Mihaylov<sup>1\*</sup>, Emil Iontchev<sup>2</sup>

<sup>1</sup>Department of Transport Equipment, University of Transport, Sofia, Bulgaria.

<sup>2</sup>Department of Telecommunications and Safety Equipment and Systems, University of Transport, Sofia, Bulgaria.

In this material the interaction during the process of derailment of the attacking tram wheelset from tram bogie T81 and a track with gauge 1009 mm build with grooved rails in a curved section of the road has been examined. Various variants of "wheelset-track" interaction occurring under real operating conditions have been modelled. The contact points between the wheels and the rails have been determined when the wheelset enters in the curve, as well as the contact points during the process of derailment have also been determined. The experiments were carried out in operating conditions at the deflection wheel in the neighbourhood of Iliyantsi, Sofia. It has been found that in a track gauge with the size of 1025 mm in a curve with a radius of 24 m the directing force is implemented at the point of contact of the non-operative side of the flange of the inner wheel with the inner rail. This is a possible explanation for the lack of cases of derailment in a particular curve despite the borderline wear on the rails.

**Keywords:** tram, wheelset, railway track, wheelset entry, derailment

## 1. INTRODUCTION

Derailment has a particular place in railway accidents. In the analysis of the dynamic behaviour of railway vehicles, two groups of problems are the most important: the wheel-rail interaction in the straight stretches of road and problems experienced in curved sections. In the movement of wheelsets there are very intense vibrations and forces of interaction at the contact points, which has a very negative impact on comfort, at certain speeds they can lead to instability of the movement and also cause wear on the wheels and rails. When moving in a curved section of the road the forces of interaction in the contact "wheel-rail" and the present angle of attack between the wheel and rails may reach such values in which very intense wear appears, appearance of defects and breakdowns on the chassis of the vehicles and the track is also possible, as well as violating the safety of movement with the appearance of derailment. [1, 2, 3].

It has been proven that a number of factors affect the derailment process - forces, geometric characteristics and road and wheel condition [1, 2, 3, 4, 5, 6]. At the same time, all cases of derailment are unique in their course. When changing some of the factors during the process, it may slow down or even cease. Observations show that in the case of grooved rails, the derailment process may be interrupted by turning the wheelset back into the track or by repeating the stage of the first climbing the flange on the rail several times.

The studies of the mutual influence between the chassis and the rail track in Sofia show that there are no derailments in the presence of large wear on the rails.

## 2. GENERAL

To track the contact between the rail track in the curve and the attacking wheelset of tram bogie T 81 three distinct cases have been chosen.

- Track with new grooved rails Ri60N in a curve with radius  $R = 20$  m (figure 1.) and wheelset with nominal dimensions and wheel tyre profile T81 (figure 2.);
- Actual track (figure 3.) – deflection wheel in the neighbourhood Iliyantsi, curve with radius  $R = 24$  m with marginal worn grooved rails and wheelset with nominal dimensions and wheel tyre profile T81;
- Actual track – deflection wheel in the neighbourhood Iliyantsi, curve with radius  $R = 24$  m with marginal worn grooved rails and wheelset with characteristic wear on the wheel tyre of the trams operating primarily in this direction (figure 4.).

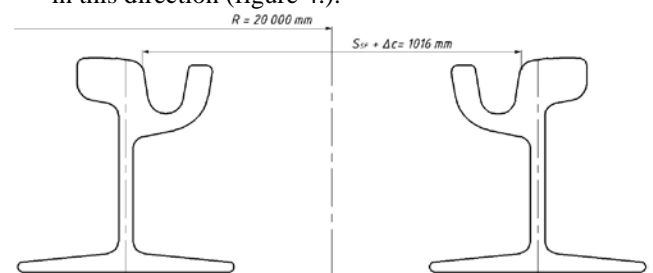


Figure 1: Track – variant A.

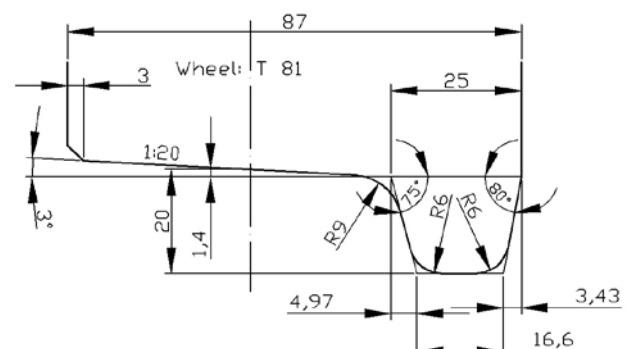


Figure 2: Wheel tyre profile T 81.

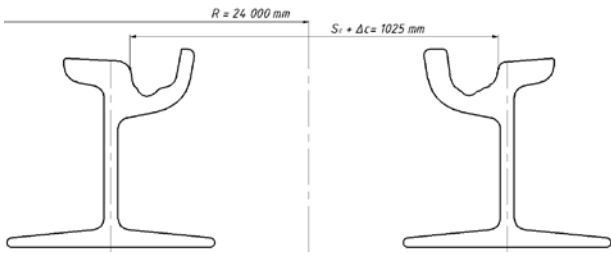


Figure 3: Track – Deflection wheel of trams in Iliyantsi, Sofia.

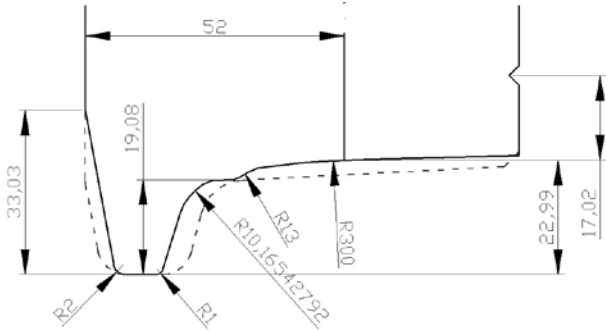


Figure 4: Wheel tyre profile of improperly worn wheels.

It is assumed that the wheelset is in the left-hand curve on half of the bogie base - 800 mm from the axis of the curve in "entry" position with a three-point contact (figure 5.). The following positions simulate the climbing of the wheel flanges on the head or flange of the rails. The wheel set moves with a 1 mm step forward along the axle until the points of contact of the two wheel flanges cross the tops of the curves of the rails in transverse direction. At the same time in all subsequent situation the wheelset rotates at an angle  $\varphi = 0,155^\circ$ , which defines an arc on the top of the flange which is 1mm long. The entry position of the wheelset is considered to be zero, and each subsequent position has a sequential number. In the beginning of the derailment process from the point where the driving force is realized  $K_{Rf}$  to the point which is the first from the process of climbing on the rail  $K_{Rf1}$ , it is assumed that the wheelset rotates around a single contact point and it's axle is positioned over point  $K_{Rf1}$ .

Determined are the contact points between the wheelset and track for each position of the wheelset moved in the direction of travel. Determined are the values of the tilt angle of the wheelset  $\gamma$  relative to the axis  $n$  as a result of the climbing of the wheels on the head and flange of the rails for each position.

The coordinate system for the track  $O_1xyz$  (figure 5.) starts at the crossing point of the axis of the track in a plane of control points of the track gauge for each of the test positions. The starting point of the coordinate system of the wheelset  $O_2mnk$  (figure 6.) is it's geometrical center.

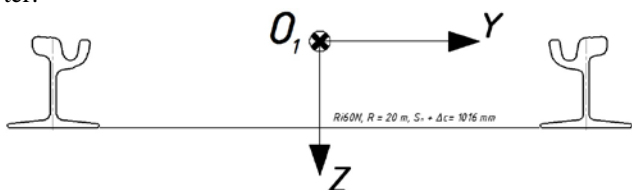


Figure 5: Coordinate system of the track.

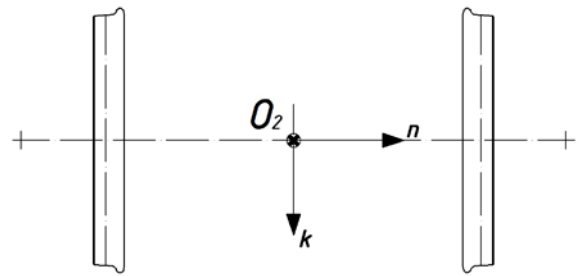


Figure 6: Coordinate system of the wheelset.

The track gauge of the Sofia railroad is  $S_{sf} = 1009 \text{ mm}$ , the examined curves are with an added standard widening  $\Delta c$ . The elevation of the outer rails is not taken into consideration.

Based on the obtained coordinates of the contact points on axes  $y$  и  $z$  for track  $n$  and  $k$  for the wheelset in the process of derailment graphs have been built for the trajectory of which the contact points are positioned. Determined are the equations of the obtained graphs with their respective coefficients of determination.

### 3. VARIANT A.

Track with new grooved rails Ri60N in a curve with radius along the track axis  $R = 20 \text{ m}$  and wheelset with nominal dimension and wheel tyre profile T81. Track gauge  $S_{sf+\Delta c} = 1016 \text{ mm}$ .

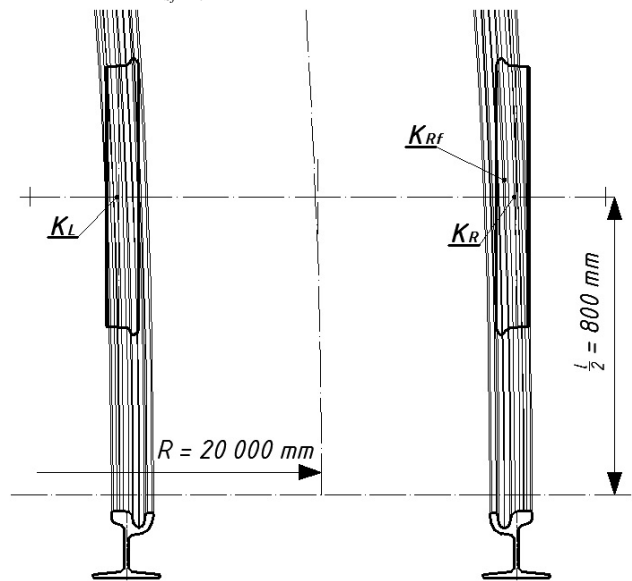


Figure 7: Position of an attacking wheelset T81 when entering in a curve with  $R = 20 \text{ m}$ .

When entering the curve (figure 7), the wheelset contacts the track at 3 points. The left wheel at point  $K_L$  on the conical surface of the wheel tyre. The right wheel has two contact points –  $K_R$  on the conical surface of the wheel tyre and  $K_{Rf}$  on the flange. Table 1 shows the coordinates of the points in the two coordinate systems and the tilt of the wheelset in the "entry" position.

The derailment process of this variant is carried out in two stages. The first step (Figure 8.) is to climb the outer wheel on the rail head while the inner wheel starts to contact the inner rail flange.

Table 1: Coordinates of the contact points in the "entry" position for variant A.

coordinate system $O_1xyz$							
Left rail				Right rail			
Point	$x$	$y$	$z$	Point	$x$	$y$	$z$
$K_L$	0,00000000	-531,36901484	-8,55778172	$K_R$	0,00000000	531,0395776	-8,54051096
				$K_{Rf}$	45,67454723	506,6582166	3,96013227
coordinate system $O_2mnk$							
Left wheel			Right wheel		Wheelset		
Point	$n$	$k$	Point	$n$	$k$	$\varphi$	$\gamma$
$K_L$	-535,14420841	349,78281124	$K_R$	527,2643039	350,1957795		0,02134000
			$K_{Rf}$	500,21935700	365,5488853	7,17774419	

In the first stage of derailment, the curves of the contact point describe a graph with equations (1) for the left wheel and (2) for the right on axes  $y$  and  $z$ . In the coordinate system of the wheelset on axes  $n$  и  $k$  the graph is described with (3) for the left wheel and (4) for the right one.

$$z = 0,0056y^3 + 8,985y^2 + 4787y + 850125; \quad (1)$$

$$R^2 = 0,9997$$

$$z = -3,1305y^3 + 4763,1y^2 - 2.10^6y + 4.10^8; \quad (2)$$

$$R^2 = 1$$

$$k = 9.10^{-9}n^3 + 10^{-5}n^2 + 0,06n + 379,2; \quad (3)$$

$$R^2 = 1$$

$$k = -1,7789n^3 + 2666,6n^2 + 10^6n + 2.10^8; \quad (4)$$

$$R^2 = 1$$

In the second stage of the derailment, an ascent of the inner wheel flange on the rail flange starts.

For the second stage the curves of the contact point describe a graph with equations (5) for the left wheel and (6) for the right wheel on axes  $y$  and  $z$ . Accordingly the curves of the contact points on axes  $n$  и  $k$  describe the graph with equation (7) for the left wheel and (8) for the right wheel.

$$z = 0,001y^3 + 0,01y^2 + 0,26y + 1,57; \quad (5)$$

$$R^2 = 1$$

$$z = -0,006y^3 + 9,2193y^2 - 4756,8y + 81815; \quad (6)$$

$$R^2 = 1$$

$$k = -0,5688n^3 - 823,76n^2 - 397655n - 6.10^7; \quad (7)$$

$$R^2 = 0,9998$$

$$k = -0,0274n^3 - 40,833n^2 - 20255n - 3.10^6; \quad (8)$$

$$R^2 = 1$$

Diagram 1. shows the graph of the change of the contact points of the wheelset and the track. The curve is constructed according to the coordinates of the points on the  $x$  and  $z$  axes.

Diagram 2. shows the graph of the change of contact points on the wheelset and track. The curve is constructed according to the coordinates of the points on the axes  $m$  and  $k$ .

Figure 8. shows the contact points of the left-hand wheel with the inner rail and in Figure 9. the right-hand contact points of the outer rail.

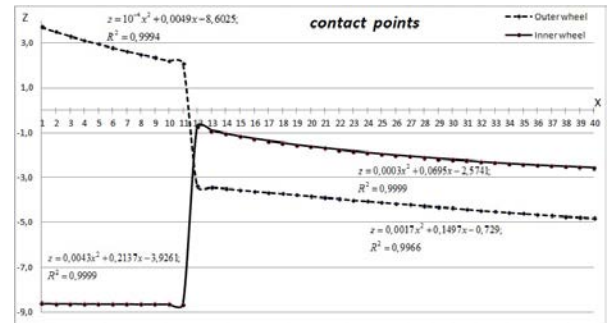


Diagram 1: Graph of the change of contact points in relation to the track.

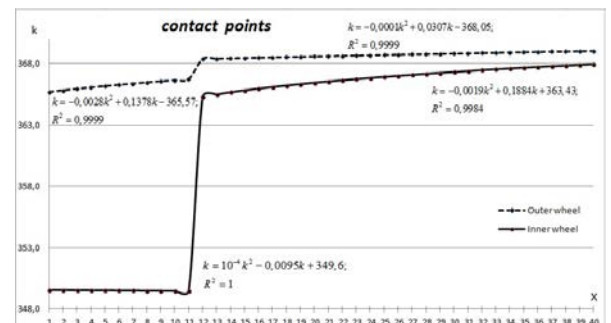


Diagram 2: Graph of the change of contact points in relation to the wheelset.

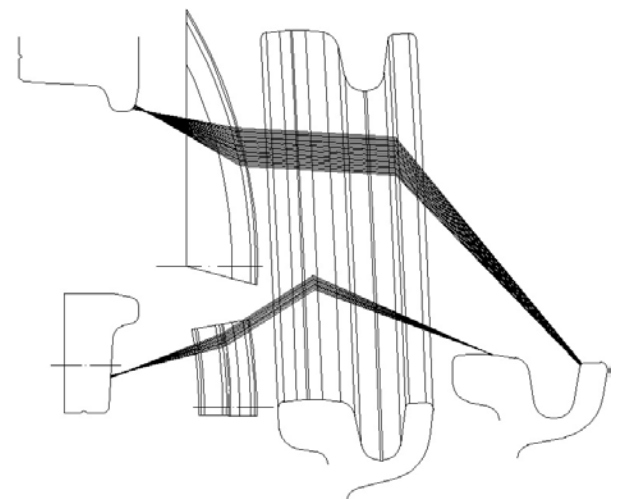


Figure 8: Contact points of the left-hand wheel with the inner rail.

The tilt of the wheelset during the process changes is shown in Diagram 3.

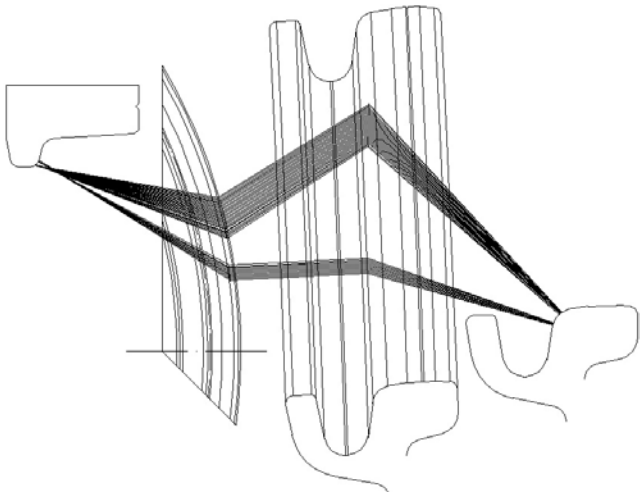


Figure 9: Contact points of the right-hand wheel with the outer rail.

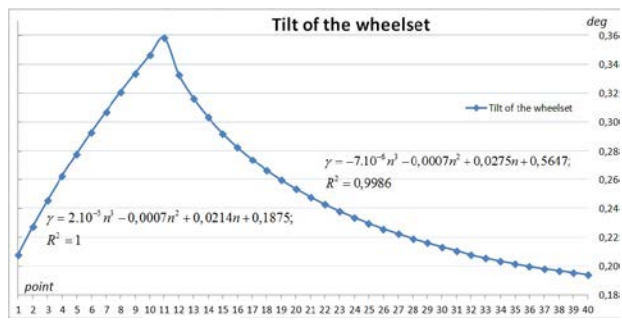


Diagram 3: Tilt of the wheelset.

The graph of the change of angle  $\gamma$  is described by equations (9) for the first stage and (10) for the second one.

$$\gamma = 2.10^{-5} n^3 - 0,0007n^2 + 0,0214n + 0,1875; \tag{9}$$

$$R^2 = 1$$

$$\gamma = -7.10^{-6} n^3 - 0,0007n^2 + 0,0275n + 0,5647; \tag{10}$$

$$R^2 = 0,9986$$

Observations show that it is entirely possible to terminate the process after the first stage and to return the wheelset to the "entry" position. This can happen when changing some of the parameters of the vehicle movement, for example the driver reduces the thrust. Also, with a suitable combination of factors, the first step may be repeated more than once, and only then the process continues or the wheelset returns to the "entry" position.

4. VARIANT B.

Actual track – the deflection wheel in the neighborhood Iliyantsi in Sofia. The track is with worn out grooved rails Ri60N (picture 1.) in a curve with radius on the axis of the track  $R = 24$  m, track gouge (picture 2.)  $S_{Sf+\Delta c} = 1025$  mm. Wheelset with nominal dimensions and wheel tyre profile T81.

When entering the curve (figure 10.), the wheelset contacts the track at 3 points. The left wheel has two contact points –  $K_L$  on the conical surface of the wheel tyre and  $K_{Lf}$  on the flange. The right wheel has a contact point  $K_R$  on the conical surface of the wheel tyre.



Picture 1: Track – Deflection wheel of trams in Iliyantsi, Sofia



Picture 2: Track - measurement of track gauge.

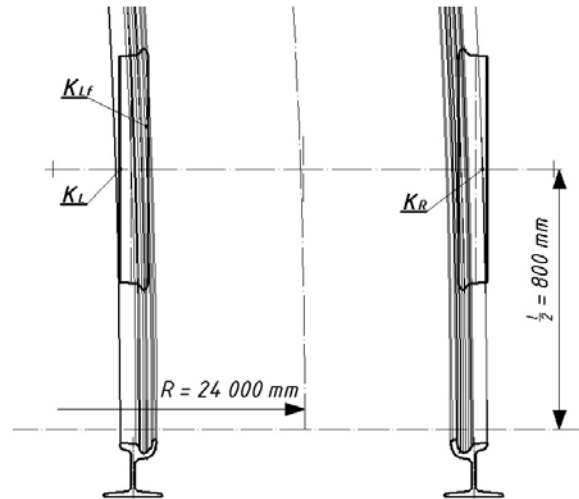


Figure 10: Position of attacking wheelset T81 when entering a curve - at deflection wheel in Iliyantsi.

Table 2 shows the coordinates of the points in the two coordinate systems and the tilt of the wheelset in the "entry" position.

In this case, the steering force is realized by the inner wheel at the contact point of the non-working side of the flange with the flange of the inner rail (picture 3.).



Picture 3: Contact of the non-working side of the flange with the flange of the inner rail.



Table 2: Coordinates of the contact points in the entry position of variant B.

coordinate system $O_1xyz$							
Left rail				Right rail			
Point	$x$	$y$	$z$	Point	$x$	$y$	$z$
$K_L$	0,00000000	-554,2179474	-8,24591697	$K_R$	0,00000000	559,7626494	9,00131516
$K_{Lf}$	131,80380140	-467,88923339	-17,02314099				
coordinate system $O_2mnk$							
Left wheel			Right wheel			Wheelset	
Point	$n$	$k$	Point	$n$	$k$	$\varphi$	$\gamma$
$K_L$	-563,00000000	348,32295106	$K_R$	550,98067466	348,95285721		-0,07124293
$K_{Lf}$	-481,52430430	465,98810495				21,16279939	

However, when the climbing of the wheel flange on the rail flange starts, the ascent of the outer wheel flange also starts on the head of the outer rail.

Typical for this track is that the flange of the inner rail has lost its roundness, however a sharp edge has been formed due to the constant friction from the wheel flange. Then the contact points of the rail are at this edge, and the change is in the contact on the roundness of the flange (Figure 11).

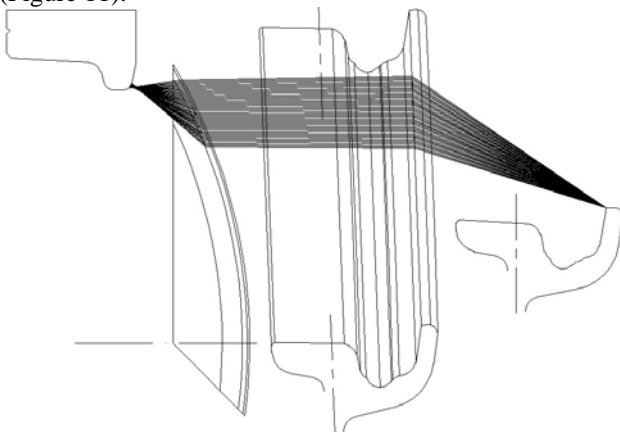


Figure 11: Contact the left wheel with the flange of the inner rail.

At the same time, the contact points of the right wheel with the head of the outer rails change their height until they reach the top of the curve (Figure 12.).

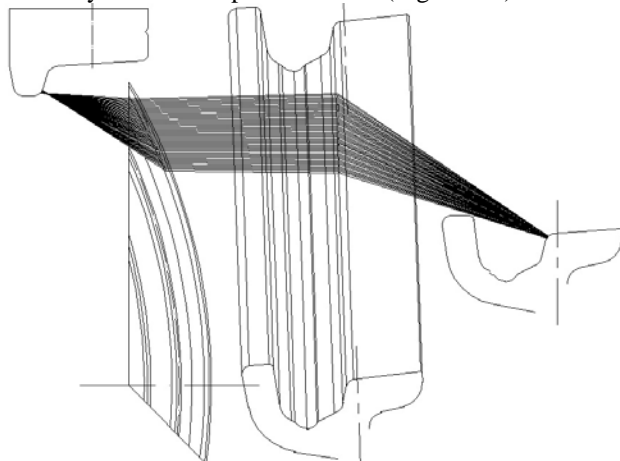


Figure 12: Contact the right-hand wheel with the outer rail.

Thus, the process does not interrupt and flows quickly due to the changes of the rail caused by the wear. Diagram 4. shows the graph of the change of contact points on the wheelset and track. The curve is built on the coordinates of the right wheel of the points on the  $y$  and  $z$  axes. In this case the left wheel is in constant contact with the edge of the flange of the inner rail.

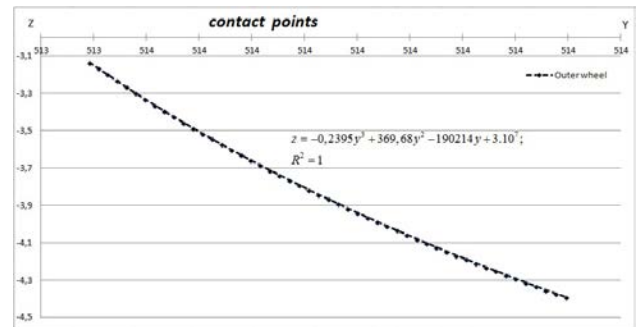


Diagram 4: Graph of the change of contact points in relation to the track.

The curve of the contact points describe the graph with equation (11) for the right wheel on axes  $y$  и  $z$ .

$$z = -0,2395y^3 + 369,68y^2 - 190214y + 3.10^7; \quad (11)$$

$$R^2 = 1$$

Diagram 5. shows the graph of the change of the contact points of the wheelset and the track. The curve is constructed according to the coordinates of the points on the axes  $m$  and  $k$ .

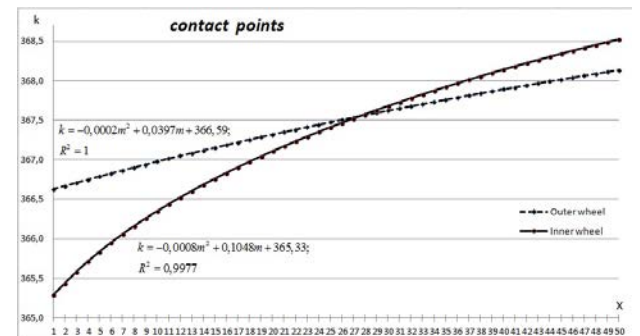


Diagram 5: Graph of the change of contact points in relation to the wheelset.

The contact point curves describe the graph with equations (12) for the left wheel and (13) for the right one on axes  $n$  and  $k$ .

$$k = -0,3103n^3 - 449,81n^2 - 217322n - 3.10^7; \quad (12)$$

$$R^2 = 0,9996$$

$$k = -0,1871n^3 + 279,81n^2 - 139517n + 2.10^7; \quad (13)$$

$$R^2 = 1$$

The tilt of the wheelset during the process changes as shown in Diagram 6.

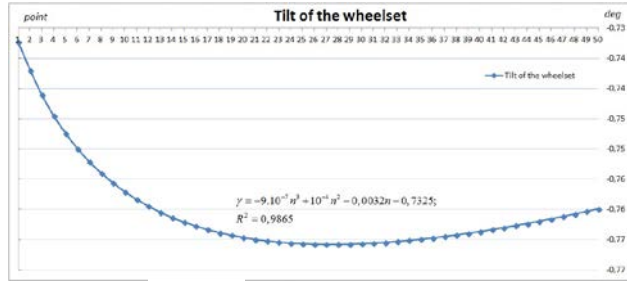


Diagram 6: Tilt of the wheelset.

The graph of the change of angle  $\gamma$  is described by equations (14):

$$\gamma = -9.10^{-7}n^3 + 10^{-4}n^2 - 0,0032n - 0,7325; \quad (14)$$

$$R^2 = 0,9865$$

5. VARIANT C.

Actual track – the deflection wheel in the neighborhood Iliyantsi in Sofia (figure 13.). Wheelset with initial wheel tyre T81 and characteristic wear on the wheel tyre (figure 18). The example wear of the wheel tyres used for this study is characteristic for the trams operating to the deflection wheel. Symmetrical wear of the wheel tyres which is very rare has been accepted. In most cases, the two wheels are worn in different sections of the profile. From the various wear patterns for this study have been taken into account the double ("lying") flange and high wear on the non-working side of the flange [7], which is characteristic of the movement on the highly worn gauge rails.

When entering the curve (figure 13.) the wheelset contacts the track at 3 points. The left wheel has two contact points –  $K_L$  on the conical surface of the wheel tyre and  $K_{Lf}$  on the flange. The right wheel has a contact point  $K_R$  on the conical surface of the wheel tyre.

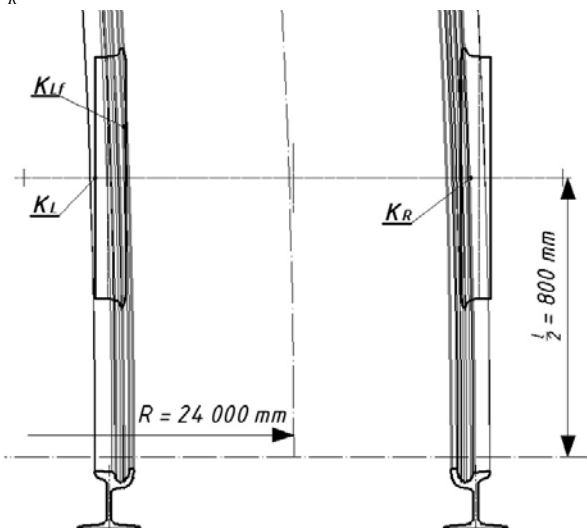


Figure 13: Position of an attacking wheelset with improper wear at the turning wheel entry in Iliyantsi.

Table 3 shows the coordinates of the points in the two coordinate systems and the tilt of the wheelset in the "entry" position.

In this case, the drive force is realized by the inner wheel in the contact point of the non-working side of the flange with the flange of the inner rail. However, despite climbing of the wheel flange on the flange of the inner rail, the outer wheel flange contacts only with a series of points with the same height on the wall of the outer rail head.

Figure 14. shows the contact points of the left-hand wheel with the inner rail and in Figure 15. the contact points of the right-hand wheel with the outer rail.

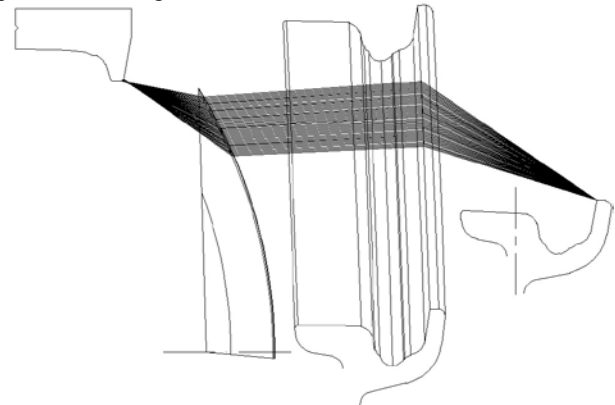


Figure 14: Contact the left wheel with the flange of the inner rail.

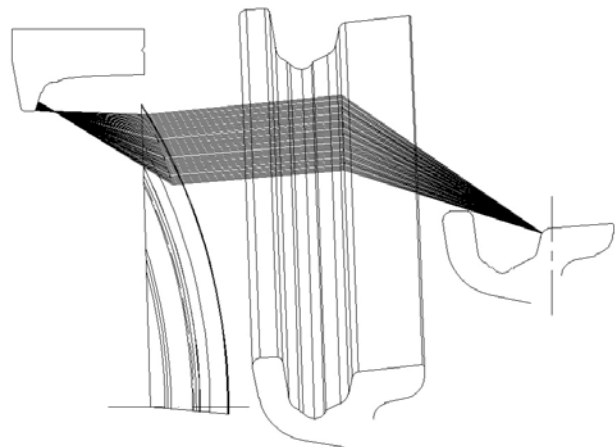


Figure 15: Contact of the right-hand wheel with the outer rail.

Diagram 7. shows the graph of the change of contact points on the wheelset and track. The curve is built on the coordinates of the points on the y and z axes.

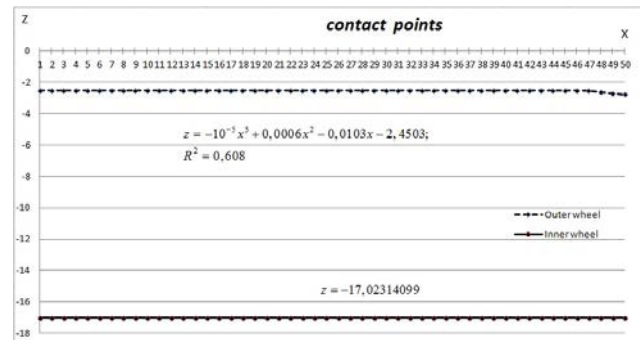


Diagram 7: Graph of the change of contact points in regards to the track.

Table 3: Coordinates of the contact points in the "entry" position for variant C.

coordinate system $O_1xyz$							
Left rail				Right rail			
Point	$x$	$y$	$z$	Point	$x$	$y$	$z$
$K_L$	0,00000000	-554,21794738	-8,24591697	$K_R$	0,00000000	520,06622614	-6,05970818
$K_{Lf}$	146,22479061	-467,88923339	-17,02314099				
coordinate system $O_2mnk$							
Left wheel			Right wheel		Wheelset		
Point	$n$	$k$	Point	$n$	$k$	$\varphi$	$\gamma$
$K_L$	-566,00000000	346,10357943	$K_R$	508,5701898	350,9228531		-1,14567263
$K_{Lf}$	-484,78998850	494,16893668				23,38805218	

Diagram 8. shows the graph of the change of the contact points of the wheelset and track. The curve is constructed according to the coordinates of the points on the axes  $n$  and  $k$ .

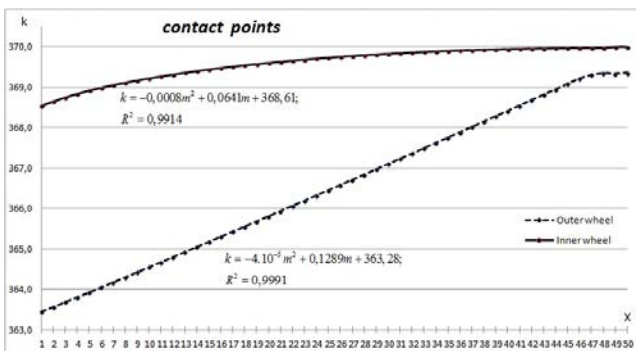


Diagram 8: Graph of the change of contact points in regards to the wheelset.

The contact point curves describe the graph with equations (15) for the left wheel and (16) for the right one on axes  $y$  and  $z$ .

$$z = -7.10^{-12}y^2 - 7.10^{-9}y + 17,023; \quad (15)$$

$$R^2 = 0,0391$$

$$z = -8,5775y^3 + 13208y^2 - 7.10^6y + 10^9; \quad (16)$$

$$R^2 = 1$$

The contact point curves describe the graph with equations (12) for the left wheel and (13) for the right one on axes  $n$  and  $k$ .

$$k = -0,2367n^3 - 345,47n^2 - 168061n - 3.10^7; \quad (17)$$

$$R^2 = 0,9982$$

$$k = 0,0029n^3 - 4,3595n^2 + 2156,9n - 354830; \quad (18)$$

$$R^2 = 1$$

The tilt of the wheelset during the process changes as shown in Figure 9.

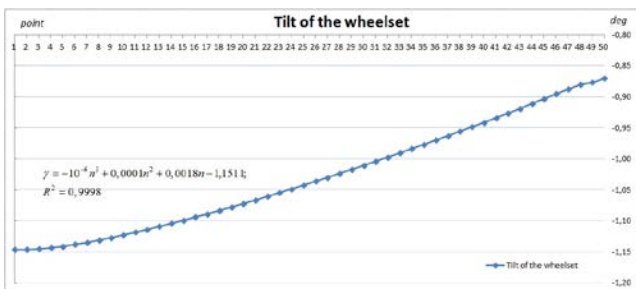


Diagram 9: Tilt of the wheelset.

The graph of the change of angle  $\gamma$  is described by equations (19):

$$\gamma = -10^{-6}n^3 + 0,0001n^2 + 0,0018n - 1,1511; \quad (19)$$

$$R^2 = 0,9998$$

The fact that during the climb of the left wheel flange on the flange of the inner rail, the right wheel contacts the outer rails in a series of points on one level or with minor deviations from it obstructs the development of the derailment process.

6. IMPACT OF THE WEAR OF THE RAILS.

When looking at the locations of the contact points of the wheelset and the track in the "entry" position, it will be seen that the point of the flange in contact with the rail at each subsequent variant moves forward. This also increases the angle between the horizontal plane at the point of contact on the rail and the tangent to the circumference of the wheel on which the contact point lies (Figure 16). Ie. It is becoming increasingly difficult to begin the process of climbing of the attacking flange on the rail.

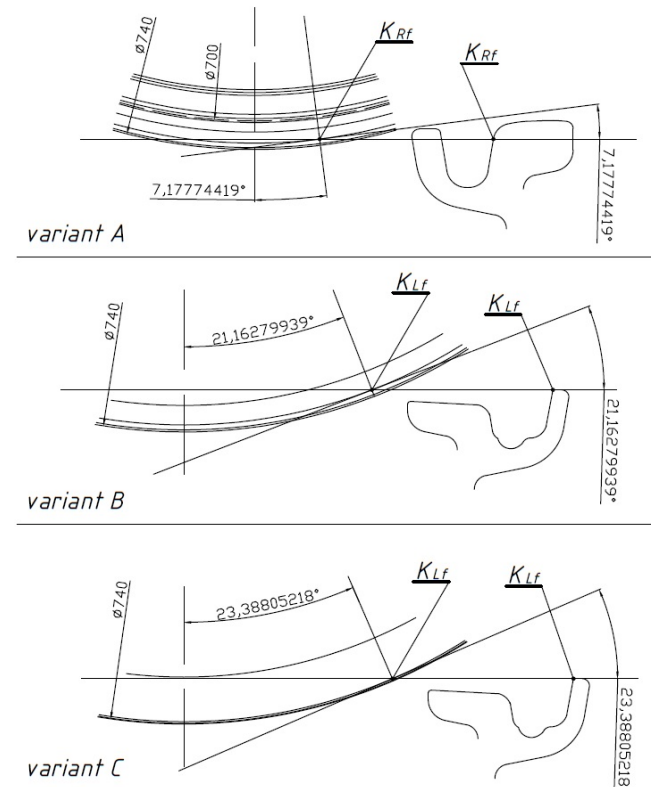


Figure 16: Angle between the horizontal plane and the tangent of the circle of the contact point.

In variants B and C due to the wear of the rails, the wheels fall low relative to the flange of the rail. This means that the chute is shallow and increases the possibility of the influence from foreign bodies in it.

### 7. CONCLUSION

The conclusions based on the examined variants of contact between the attacking tram wheelset and a track made out of grooved rails in a curve, to a great extent, explain the lack of cases of derailment of trams in curved sections with high amounts of wear on the rails [8].

The study of the "wheelset-track" interaction of the attaching wheelset of tram bogie T81 and track with 1009 mm track gauge, built with grooved rails in a curved section of the road, is realized in three variants:

- A wheelset with new wheels in the curve of a track with new rails;
- A wheelset with new wheels and specific actual track with marginal worn grooved rails;
- A wheelset with typical wear wheel tyres and specific actual track with marginal worn grooved rails.

As a result of the three modelled variants of the interaction "wheelset-track" the contact points of the wheels and rails when the wheelset enters the curve have been determined, as well as the contact points in the derailment have also been determined. It has been found that in a track gauge with the size of 1025 mm in a curve with a radius of 24 m the directing force is implemented at the point of contact of the non-operative side of the flange of the inner wheel with the inner rail. This is a possible explanation for the lack of cases of derailment in a particular curve despite the borderline wear on the rails.

The experiments were carried out in actual operating conditions at the deflection wheel in the neighbourhood Iliyantsi in Sofia. The results of the experiments confirm the results of the modelling.

[1] Atmadzhova D., „Определяне критерия за дерайлиране на железопътна колоос. Квази-статичен анализ на колоос.”, XX International Scientific Conference „Transport 2011”, Т. Kableshkov University of Transport, Sofia, 2011.

[2] Atmadzhova D., „Анализ на математически изрази за определяне критерия за дерайлиране на железопътна колоос”, XX International Scientific Conference „Transport 2011”, Т. Kableshkov University of Transport, Sofia, 2011.

[3] Atmadzhova D., Penchev C., „Influence of Track Subsidence on Rolling Stock Derailment Risk”, VIII International Scientific Conference HEAVY MACHINERY 2014, Kraljevo, Serbia, 2014

[4] Овечников Е., Сосянц В., „Рельсовые пути трамваев и внутризаводских железных дорог”, Издательство МКХ РСФСР, Москва 1959 г.

[5] Atmadzhova D., Mihaylov E., „Tram vehicle movement safety”, Regional workshop „Transport research and business cooperation in SEE”, Т. Kableshkov University of Transport, Sofia, 2010 г.,

[6] Atmadzhova D., Mihaylov E., „Model for quasi-static entry of a tram bogie in a curved stretch of road”, XXII International Scientific Conference „Transport 2015”, Т. Kableshkov University of Transport, Borovec, 2015.

[7] Mihaylov E., „Wear of the non-operative side of the rim of tramwheels when passing through tracks built with grooved rails”, XXII International Scientific Conference „Transport 2015”, Т. Kableshkov University of Transport, Borovec, 2015.

[8] Mihaylov E., „Comparison of the standards of tram wheelsets and track gauge 1009 mm, powered grooved rails”, XXII International Scientific Conference „Transport 2015”, Т. Kableshkov University of Transport, Borovec, 2015.

# Overview of Wheel-rail Rolling Contact Theories

Milan Bižić\*, Dragan Petrović

<sup>1</sup>Faculty of Mechanical and Civil Engineering in Kraljevo, University of Kragujevac, Serbia

*In the contact area between wheel and rail there are intensive action and reaction forces that have a key influence on the dynamic behaviour of railway vehicles and track. These forces play a key role in supporting, guiding, traction and braking of railway vehicles. Bearing in mind that the wheel-rail contact problem is in fact the problem of rolling of two nonlinear profiles which occurs under the influence of many parameters, its solution and exact determination of wheel-rail contact forces belongs to the most complex tasks in railway engineering. Basically, solving the wheel-rail contact problem is reduced on solution of two types of contact problems - normal and tangential. These mutually coupled problems are solved from many researchers and today there are several different theories. Simpler theories are based on the assumptions under which the normal and tangential contact problem are solved completely separately. This results in a significantly simpler and faster calculation, but with greater error. On the other hand, more complex theories are based on coupled or iterative solving of given problems. As a result, they are characterized by greater accuracy, but also with more complicated calculation that requires significantly more computing time. In that sense, the aim of this paper is to analyse the wheel-rail rolling contact theories for solving the normal and tangential contact problems, with especial emphasize on determination of wheel-rail contact forces. Established conclusions are of particular importance for research of dynamic behaviour of railway vehicles.*

**Keywords:** Wheel-rail contact, Rolling contact theories, Wheel-rail contact forces.

## 1. INTRODUCTION

Accurate determination of the wheel-rail contact forces is one of the most important tasks in the analysis of the dynamic behavior of railway vehicles. These forces are directly connected to the key functions of realization of railway traffic such as supporting, guiding, traction and braking of railway vehicles. Accordingly, the wheel-rail contact forces are the key influential parameters and indicators of the quality of the dynamic behavior of railway vehicles. Their values are the basis for evaluation of safety against the derailment which is obligatory in the phase of certification of all types of newly designed or modified railway vehicles. The international standards prescribe exclusively experimental tests as the way for determination of the wheel-rail contact forces in the certification process [1, 2]. Given in mind that these experimental tests are very expensive, certain simulations of dynamic behavior of railway vehicles must be performed, especially in the phase of development of railway vehicles. In such simulations, the wheel-rail contact forces and other parameters of dynamic behavior of railway vehicles must be determined on analytical or numerical way. Considering the complexity and stochasticity of geometry of the wheel-rail contact [3], analytical determination of forces in that contact is very complex task which is solved from many researchers over the past years. The task is related to the solving the problem of rolling of one nonlinear profile (wheel profile) via another nonlinear profile (rail profile). At the same time, the intensity of pressure between these profiles is changeable (under the influence of wear), the shapes of these profiles are changeable and mutual position between these profiles is changeable. During such dynamic process, in the contact surface between mentioned profiles of wheel and rail there are normal and tangential contact forces that depend on large number of influential parameters and that have a key influence on the dynamic behavior of railway

vehicles. In contemporary analysis of dynamic behavior of railway vehicles, the analytical determination of these forces is based on solving of two types of mutually coupled problems – normal and tangential contact problem [4–6]. The different ways of solution of these problems are basis for numerical determination of wheel-rail contact forces and other parameters of dynamic behavior of railway vehicles. They are incorporated in all software tools for simulation of dynamic behavior of railway vehicles. Some of the most useful and most powerful software in this area of are Adams, Simpack, Vampire, Gensys, Nucars, etc. Thus, the aim of this paper is to give the main postulates and to analyze the wheel-rail rolling contact theories, with especial accent on their reliability in simulations of dynamic behavior of railway vehicles.

## 2. NORMAL CONTACT PROBLEM

Normal contact problem is related to determination of shape and size of contact surface, normal stress or contact pressure and its distribution in the contact surface which is caused by the action of normal force. The solution of normal contact problem between wheel and rail is usually based on application of Hertz static theory of contact of elastic bodies [7, 8]. This theory can be applied to the wheel-rail contact under the following assumptions: displacements and strains are small; contact surface is small in comparison to the dimensions of wheel and rail or rolling radius of the wheel (semi-space assumption); area in vicinity of contact surface is described with constant curve; surfaces of contact of wheel and rail are smooth (roughness is neglected); there are only elastic deformations; materials of wheel and rail are homogenous and isotropic [4]. Therefore, a key assumption implies that the bodies in contact (wheel and rail) are geometrically and elastically the same or quasi-identical. This assumption enables that normal and tangential contact problem can be solved separately.

\*Corresponding author: Dositejeva 19, 36000 Kraljevo, bizic.m@mfkv.kg.ac.rs

According to the Hertz theory the contact surface between wheel and rail compressed with normal force  $N$  has an elliptical shape with semi-axis  $a_e$  in direction of movement and semi-axis  $b_e$  in lateral direction (Fig. 1).

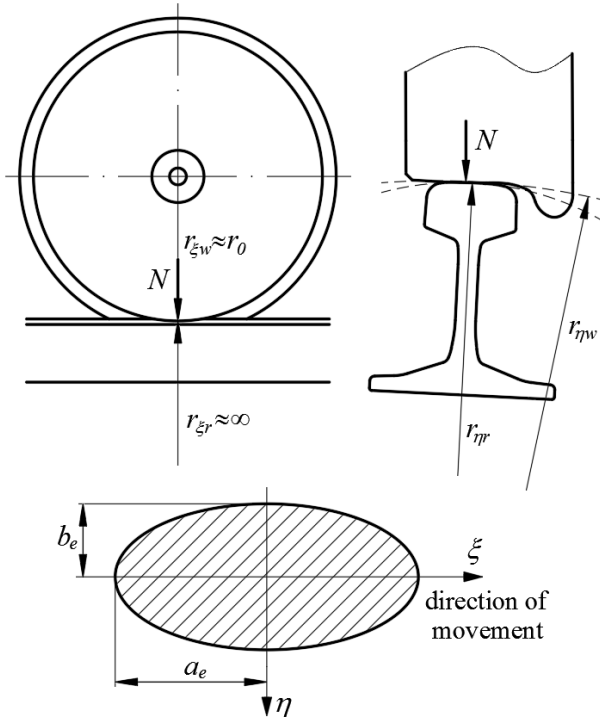


Figure 1: The contact surface between wheel and rail according to the Hertz theory

Semi-axes of elliptical contact surface can be calculated from the following expressions:

$$a_e = m \cdot \sqrt[3]{\frac{3}{2} \cdot \frac{N(1-\nu_p^2)}{E(A+B)}} \quad (1)$$

$$b_e = n \cdot \sqrt[3]{\frac{3}{2} \cdot \frac{N(1-\nu_p^2)}{E(A+B)}}$$

where:

$E$  – modulus of elasticity,

$\nu_p$  – Poisson's ratio,

$N$  – normal force between wheel and rail,

$m, n$  – constants,

$A, B$  – functions that are dependent on the radii of wheel and rail curvatures.

Functions  $A$  and  $B$  are defined with the following expressions:

$$A = \frac{1}{2} \left( \frac{1}{r_{\eta r}} - \frac{1}{r_{\eta w}} \right) \quad (2)$$

$$B = \frac{1}{2} \left( \frac{1}{r_{\xi r}} + \frac{1}{r_{\xi w}} \right) \approx \frac{1}{2r_{\xi w}} \approx \frac{1}{2r_0}$$

where:

$r_{\xi w}$  – radius of the wheel curvature in longitudinal direction (direction of movement),

$r_0$  – rolling radius of the wheel,

$r_{\eta w}$  – radius of the wheel curvature in lateral direction,

$r_{\xi r}$  – radius of the rail curvature in longitudinal direction,

$r_{\eta r}$  – radius of the rail curvature in lateral direction.

The constants  $m$  and  $n$  are determined from the appropriate tables, on the basis of value of the following function:

$$\theta = \arccos \left( \frac{A-B}{A+B} \right) \quad (3)$$

The surface of the ellipse or the contact area between wheel and rail is:

$$A_e = \pi \cdot a_e \cdot b_e \quad (4)$$

The distribution of contact pressure or normal stress in contact surface has the shape of semi-ellipsoid (Fig. 2), and it is defined with the following expression:

$$\sigma_\zeta(\xi, \eta) = \frac{3}{2} \cdot \frac{N}{A_e} \cdot \sqrt{1 - \left( \frac{\xi}{a_e} \right)^2 - \left( \frac{\eta}{b_e} \right)^2} \quad (5)$$

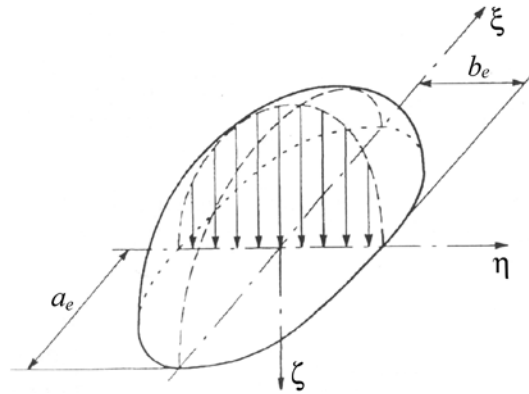


Figure 2: The distribution of contact pressure in wheel-rail contact surface according to the Hertz theory [4]

The numerical example of application of previously exposed Hertz theory for solution of normal wheel-rail contact problem in case of 4-axled freight waggon is given in the Table 1.

Table 1: The solution of normal contact problem between wheel profile UIC-ERRI S1002 and rail profile 60E1

Modulus of elasticity	$E=21000 \text{ kN/cm}^2$	
Poisson's ratio	$\nu_p=0.3$	
Radius of the wheel curvature in longitudinal direction	$r_{\xi w}=r_0=46 \text{ cm}$	
Radius of the wheel curvature in lateral direction	$r_{\eta w}=32 \text{ cm}$	
Radius of the rail curvature in longitudinal direction	$r_{\xi r}=\infty$	
Radius of the rail curvature in lateral direction	$r_{\eta r}=30 \text{ cm}$	
Function	$A=0.104$	
Function	$B=1.087$	
Function	$\theta=145^\circ$	
Constant	$m=0.53$	
Constant	$n=2.4$	
Normal force	$N=40 \text{ kN}$	$N=110 \text{ kN}$
Semi-axis	$a_e=0.32 \text{ cm}$	$a_e=0.45 \text{ cm}$
Semi-axis	$b_e=1.45 \text{ cm}$	$b_e=2.02 \text{ cm}$
Surface	$A_e=1.46 \text{ cm}^2$	$A_e=2.85 \text{ cm}^2$
Normal stress	$\sigma_{\zeta \max}=41.1 \text{ kN/cm}^2$	$\sigma_{\zeta \max}=57.9 \text{ kN/cm}^2$

It is important to emphasize that Hertz theory can be applied only on the cases of non-conformal contact between wheel and rail.

### 3. CREEP AND PARAMETERES IN WHEEL-RAIL CONTACT SURFACE

Due to the elasticity of the material, during the rolling along the rail, there is very small difference between the tangential velocity and the transnational velocity or velocity of the wheel progression (Fig. 3). This phenomenon is called creep and it has very significant influence on the dynamic behavior of railway vehicles which was first discovered from Carter [9, 10]. The proper analysis of creep is crucial for solution of tangential contact problem between wheel and rail.

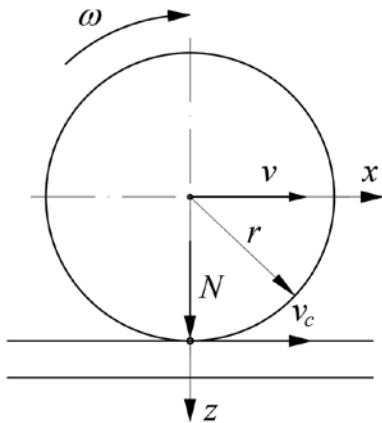


Figure 3: The rolling of the wheel along the rail and creep velocity

The creep velocity  $v_c$  represents a difference between tangential velocity of wheel with radius  $r$  which is revolving with angular velocity  $\omega$ , and transnational velocity of wheel  $v$ :

$$v_c = r \cdot \omega - v \tag{6}$$

Due to a large number of influential parameters, ideal rolling of wheelset is very rare in practice, especially at running through the curves. Therefore, ideal radial steering of wheelset is extremely rare. During the running in the curves, wheelset is usually positioned in some under-radial position when guiding wheel under certain angle  $\psi$  is attacking outer rail (Fig. 4).

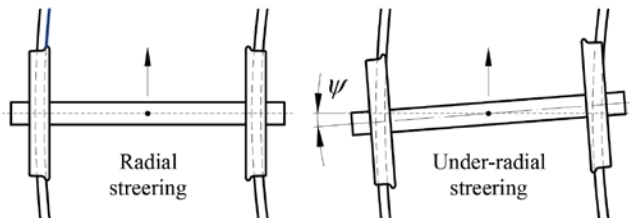


Figure 4: The radial and under-radial steering of wheelset in the curves

As a consequence of the previous considerations it can be observed that there is not only creep in running direction as shown in Fig. 3, but there is some resulting creep that can have an arbitrary direction and which, in addition to transnational, contains certain rotational component. These two components cause the occurrence of tangential force and moment in the contact surface between the wheel and rail. Therefore, parameters in wheel-rail contact surface are shown in Fig. 5.

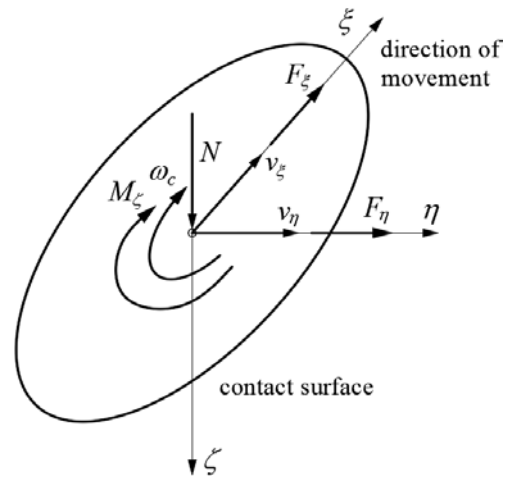


Figure 5: The parameters in wheel-rail contact surface

In Fig. 5 are:

- $N$  – normal force,
- $v_\xi$  – velocity of longitudinal creep,
- $v_\eta$  – velocity of lateral creep,
- $\omega_c$  – angular velocity of rotational creep,
- $F_\xi$  – tangential force of longitudinal creep,
- $F_\eta$  – tangential force of lateral creep,
- $M_\xi$  – moment of rotational creep.

The determination of given tangential forces and moment is based on reduced creepages which are obtained when the velocities of the longitudinal and lateral creep and angular velocity of the rotational creep are reduced to velocity of wheel progression  $v$ :

$$\begin{aligned} v_\xi &= \frac{v_\xi}{v} \\ v_\eta &= \frac{v_\eta}{v} \\ \phi &= \frac{\omega_c}{v} \end{aligned} \tag{7}$$

Thus, total translational reduced creep is:

$$v = \sqrt{v_\xi^2 + v_\eta^2} \tag{8}$$

The components of reduced creepages play a key role in all methodologies that dealing with solving of the tangential contact problem.

### 4. TANGENTIAL CONTACT PROBLEM

The tangential contact problem is related to the determination of tangential forces and stresses which are generated in wheel-rail contact surface due to the presence of friction and creepage. For solving the tangential contact problem, there are various methodologies such as: simplified theory, exact theory, dynamical theory, quasi-static theory, three-dimensional theory, two-dimensional theory, etc. One of the most important reviews of these theories is made from Kalker in his research [11, 12].

Key problems in solving of the tangential contact problem are the existence of creep between wheel and rail, as well as the nonlinear character of the change of tangential force which is shown in Fig. 6. Consequently, the exact determination of tangential forces in wheel-rail contact must be based on the nonlinear theory. However, at smaller values of creep the change of tangential force

has almost linear character and under such assumption its calculation can be performed with application of linear theory. This fact had a great impact on the development of the theories for solving the tangential contact problem. The most important theories are given below.

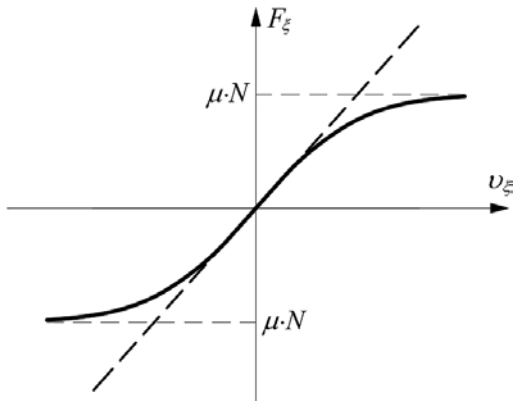


Figure 6: The change of tangential force in function of creep

4.1. Carter's theory

In 1926 Carter is developed a theory for solving the problems of rolling with friction which is applied in solution of the tangential contact problem [9, 10]. This theory is especially important because establishes analytical relation between longitudinal creep and tangential force. The wheel is considered as a cylinder and rail as thin plate, under assumption that radius of the wheel is much higher in comparison with the dimensions of the contact surface. In this way, the problem is solved under the assumption of half-space, wherein in the contact surface, in addition to normal stress, there is tangential stress in the longitudinal direction. The distribution of tangential stress and change of tangential force in contact surface according to Carter's theory are shown in Fig. 7.

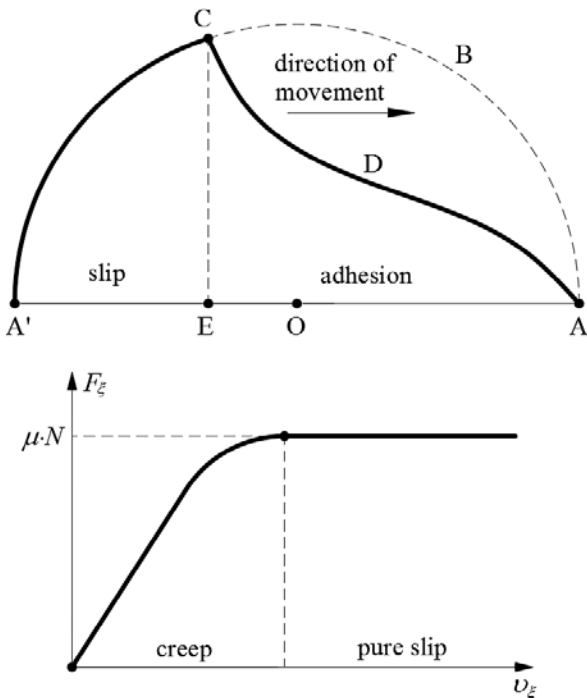


Figure 7: The distribution of tangential stress and change of tangential force in contact surface according to Carter's theory [13]

In wheel-rail contact surface according to Carter's theory there are two areas – adhesion area and slip area. A'EOA line in Fig. 7 represents the contact surface during the rolling of wheel over the rail in the longitudinal direction. In the point A observed piece of material comes in contact with the rail, while its contact with the rail ceases in the point A'. Curve ABCA' defines the distribution of limit value of tangential stress in the cross section of the contact surface. Curve ADCA' defines the real distribution of tangential stress in the cross section of the contact surface or in adhesion area and slip area. In the adhesion area (area below curve ADC) there are absolutely adhesion and no mutual displacement of material particles of the wheel and rail. Thereby, the value of the tangential force is less than the limit value which is determined with the force of Coulomb friction in which there is completely sliding of the wheel along the rail ( $F_{\xi} < \mu N$ ). Analogously, the tangential stress is less than the limit stress which is determined with the curve ABCA'. In slip area (area below the curve A'C) there is mutual displacement of pieces of material of the wheel and rail. At the same time, the value of the tangential force reaches limit value where is  $F_{\xi} = \mu N$ , and tangential stresses are equal to the limit stresses. In the case of the complete sliding of the wheel along the rail, the tangential force in the whole contact surface reaches a limit value at which the tangential stresses are equal to the limit tangential stresses (line ABCA'). This situation usually occurs in cases of traction or braking of railway vehicles or in cases of blocking of wheels for other reasons.

The main disadvantage of Carter's theory is related to the neglecting of lateral and rotational creep. That is why application of this theory in analysis of dynamic behavior of railway vehicles is very limited. Nevertheless, this theory is of a great importance in the study of phenomena related to the wheel-rail contact and forms the basis for the development of advanced theories for solving the tangential contact problem.

4.2. Theory of Johnson and Vermeulen

In 1985 Johnson is expanded Carter's theory on the case of contact of two spheres that roll on one another, wherein in addition to the longitudinal, lateral creep is taken into account [14]. After that he in 1964, together with Vermeulen, defined the theory which establishes analytical relation between creep in longitudinal and lateral direction and appropriate tangential forces [15]. The theory is based on the assumption that between wheel and rail there is only translational creep, while rotational creep is neglected. In contact surface there are two areas – slip area and adhesion area. The adhesion area has an elliptical form which touches the ellipse of contact surface in its headmost point (Fig. 8).

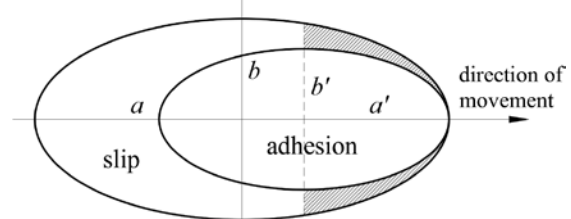


Figure 8: The areas in contact surface according to the theory of Johnson and Vermeulen [11]



The experimental tests have shown that error in calculation of the resulting tangential force according to the theory of Johnson and Vermeulen is less than 25%. This is certainly consequence of assumption that adhesion area has an elliptical shape. This theory is limited to the cases where there are only longitudinal and lateral creep, while rotational creep does not exist. This is the main disadvantage because this theory has limited application in analysis of dynamic behavior of railway vehicles.

4.3. Theory of strips of Halling, Haines and Ollerton

In 1963 Halling, Haines and Ollerton are developed an approximate theory for solving the tangential contact problem in case of the elliptical contact surface and pure longitudinal creep [16, 17]. In accordance with this theory, area of contact is divided on a certain number of strips which are parallel to the direction of movement (Fig. 9). Every strip is analyzed by using Carter's theory while mutual interaction between strips is neglected.

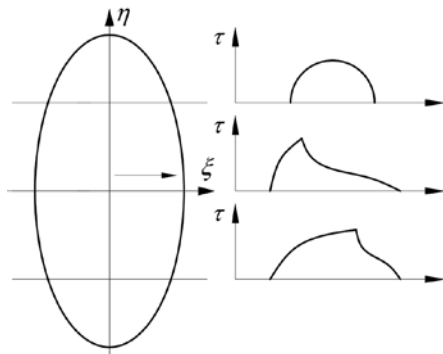


Figure 9: The contact surface according to the theory of strips of Halling, Haines and Ollerton [11]

The correctness of the theory of Halling, Haines and Ollerton has been confirmed by experimental tests using the method of photo-elasticity. The results of tests have shown that shape of the adhesion area is very similar to the shape which is assumed with the theory. The main drawback of this theory is limitation on the case of pure longitudinal creep. That is why its using in rail vehicles dynamics is very rare.

4.4. Kalker's extended theory of strips

In 1967 Kalker is expanded the theory of strips of Halling, Haines and Ollerton, whereby, in addition to the longitudinal, lateral and small rotational creep are taken into account [18]. The areas of adhesion and slip according to this theory are shown in Fig. 10.

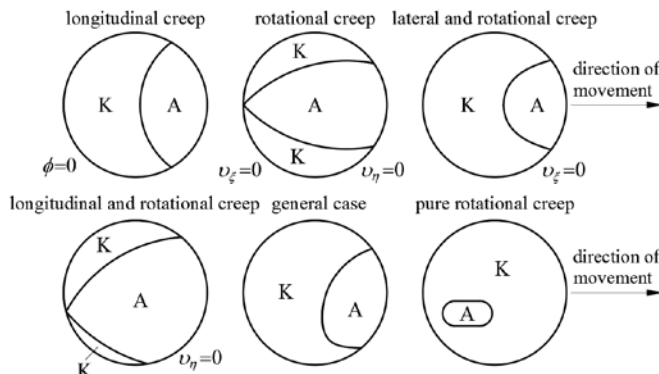


Figure 10: The areas in contact surface according to the extended theory of strips [11]

The main drawback of extended theory of strips is limitation on cases with small values of rotational creep and cases in which the longer axis of contact surface is directed in lateral direction regard to the direction of movement. These are the reasons why this theory, despite a relatively accurate determination of the shape and size of the areas of adhesion and slip, are rarely used in analyzing the dynamic behavior of railway vehicles.

4.5. Kalker's linear theory

In 1967 Kalker is developed linear theory of rolling of two elastic bodies in conditions of dry friction [19]. This theory is based on assumption of DePater that for small values of creepages slip area in the contact surface is so small that its influence can be completely neglected [20]. The consequence of this assumption is that in the whole contact surface there is the state of adhesion. The research has shown that Kalker's linear theory gives satisfactory results if the following condition is fulfilled [4]:

$$|v| + |\phi / 1000| \leq 0,002 \tag{9}$$

In accordance with the Kalker's linear theory, longitudinal and lateral tangential forces and moment of creep are determined from the following expressions:

$$\begin{aligned} F_{\xi} &= -\kappa_{33} \cdot v_{\xi} \\ F_{\eta} &= -\kappa_{11} \cdot v_{\eta} - \kappa_{12} \cdot \phi \\ M_{\zeta} &= \kappa_{12} \cdot v_{\eta} - \kappa_{22} \cdot \phi \end{aligned} \tag{10}$$

The previous expression show that, according to Kalker, longitudinal tangential force does not depend on the lateral and rotational creep, while the lateral tangential force and moment do not depend on the longitudinal creep. The coefficients of creep  $\kappa_{11}$ ,  $\kappa_{12}$ ,  $\kappa_{22}$ , and  $\kappa_{33}$  are determined on the basis of values of semi-axis of ellipse of contact surface  $a$  and  $b$ , determined on the basis of Hertz's contact theory and Kalker's coefficients  $C_{11}$ ,  $C_{22}$ ,  $C_{23}$  and  $C_{33}$ :

$$\begin{aligned} \kappa_{11} &= (a \cdot b) \cdot G \cdot C_{22} \\ \kappa_{12} &= (a \cdot b)^{3/2} \cdot G \cdot C_{23} \\ \kappa_{22} &= (a/b)^2 \cdot G \cdot C_{33} \\ \kappa_{33} &= (a \cdot b) \cdot G \cdot C_{11} \end{aligned} \tag{11}$$

The coefficients  $C_{11}$ ,  $C_{22}$ ,  $C_{23}$  and  $C_{33}$  are determined from Kalker's table on the basis of Poisson's ratio  $\nu_p$  and ratio of semi-axis of ellipse of contact surface  $a$  and  $b$  [13]. It is very important to emphasize that Kalker's coefficients mean the existence of dry friction between wheel and rail whereby the coefficient of friction is  $\mu \approx 0,6$  [4]. However, the practical experiences have shown that there are not always the conditions of dry friction between wheel and rail, or the conditions under which Kalker's linear theory is formulated are not always fulfilled. On a certain sections of the track, due to presence of various impurities such as oil, dirt, dust, moisture, ice, snow, etc., there is reduction of coefficient of friction or reduction of value of limit tangential force at which pure slipping of the wheel along the rail occurs. Taking into account this stochastic change of friction coefficient, this influence is very complex for analytical describing. It is usually taken into account through corrections of creep

coefficient in Kalker's linear theory with certain correction factors. Despite of significant approximations under which is defined, Kalker's linear theory has very large application in rail vehicles dynamics, especially in analysis of lateral dynamic stability of railway vehicles at their running on the tangent track.

#### 4.6. Kalker's nonlinear exact numerical theory

All the previously discussed theories have certain limitations and do not provide a complete solution of the tangential contact problem. From this reason Kalker is developed a nonlinear exact numerical theory which is based on numerical solution of the problem by using computers [11, 12]. This theory is based on the condition that real total tangential stress in the contact surface must meet the Coulomb's inequality  $\tau \leq \mu \sigma$ . Based on the Kalker's nonlinear theory, in 1967 has been developed a computer program CONTACT which allows universal numerical solution of all types of half-space contact problems. After that, in 1978 has been developed a computer program DUVOROL which is based on the assumption of equal constants of elasticity of bodies in contact [21]. The results of experimental tests conducted on British railways have confirmed that, in conditions without presence of impurities on contact surfaces of wheels and rails, the program DUVOROL gives very reliable results in solution of the tangential contact problem. The main disadvantage of computer programs CONTACT and DUVOROL is very large computing time. That is why these programs are not suitable for usage in analysis of dynamic behavior of railway vehicles.

#### 4.7. Kalker's empirical theory

Kalker is developed empirical theory which establishes relationship between longitudinal and lateral creep and total tangential force in contact surface between wheel and rail [22]. Somewhat simpler empirical expression with reduced accuracy in relation to the Kalker's are defined by Johnson and Vermeulen [15]. In empirical theory, at solving the tangential contact problem, the total normalized creep  $\nu_n$  is used. It is determined on the basis of components of creepages  $\nu_\xi$  and  $\nu_\eta$ , semi-axis of ellipse of contact surface  $a$  and  $b$ , shear modulus  $G$ , coefficient of friction between wheel and rail  $\mu$ , normal force  $N$  and coefficients of normalization  $c_1$  and  $c_2$ . Coefficients of normalization are read from tables on the basis of ratio of semi-axes of ellipse of contact surface  $a$  and  $b$ , combined Poisson's ratio for materials of wheel and rail  $\nu$ , and elliptical integrals defined in theory of Johnson and Vermeulen [13]. Kalker's empirical theory gives very good results for all eccentricities of ellipse of contact surface and can be used in solving the contact problems in cases when materials of wheel and rail have different constants of elasticity. However, due to the neglecting of rotational creep this theory has very limited application in analysis of dynamic behavior of railway vehicles.

#### 4.8. Approximate nonlinear theory (heuristic nonlinear model)

Researches in area of theory of wheel-rail contact have shown that is necessary to form considerably complex models in order to obtain more accurate results [23]. In this sense, Shen, Hedrick and Elkins are formed an

approximate nonlinear theory which is based on heuristic nonlinear model [24]. The theory is based on calculation of tangential forces by using Kalker's linear theory and determination of their limit values by using the theory of Johnson and Vermeulen, wherein the rotational creep is neglected. Input data in the model are ratio of semi-axis of ellipse of contact surface  $a$  and  $b$ , and normalized creepages  $\nu_{\xi n}$ ,  $\nu_{\eta n}$  and  $\phi_n$ . The ratio of semi-axis of ellipse of contact surface is function of radii of curves of elastic bodies which are in contact which is calculated with Hertz's theory, while normalized creepages are functions of normal force in contact surface between wheel and rail. The researches have shown that heuristic nonlinear model enables accurate description of nonlinear relations in wheel-rail contact in cases when two from three creepages are equal to zero [13]. Despite the fact that neglects the influence of rotational creep to the tangential forces in wheel-rail contact, approximate nonlinear theory is often used in analysis of dynamic behavior of railway vehicles.

#### 4.9. Kalker's simplified theory and computer programs

The main motivation for development of Kalker's approximated theory was very long computer time for numerical solution of the tangential contact problem by using the exact numerical theory. Consequently, Kalker is defined simplified theory on the basis of which a few computer programs for determination of tangential forces and moment in wheel-rail contact are developed. The most famous are SIMROL, ROLCON and FASTSIM [25, 26]. The main version of program SIMROL has been written from the Kalker in ALGOL-60 programming language. Later, it is translated on the programming language FORTRAN-IV by Goree [27]. The program ROLCON has been written in 1978 by the Knothe and colleagues in programming language FORTRAN-IV [28]. Its speed of calculation is five times larger in relation to the program SIMROL. The program FASTSIM also has been written from the Kalker in 1980. It is very simple and its speed of calculation is 25 times larger in regard to the program SIMROL. The main advantage of Kalker's simplified theory is in fact that it enables satisfactory accurate description and solution of the tangential contact problem, while the time of computer's calculations is significantly shorter in regard to the exact numerical theory. Therefore, this theory has by far the greatest application in modeling the wheel-rail contact and analysis of the dynamic behavior of railway vehicles.

## 5. CONCLUSION

Condition in the contact surface or wheel-rail contact forces during the running of railway vehicles along the track are affected by large number of influential parameters. In addition to the geometries of profiles of the contact surfaces, the significant influence has the friction coefficient between wheel and rail or behavior of adhesion and slip. The important influence have the characteristics of material of the wheel and rail, roughness of contact surfaces, wear, as well as presence of water, oil, dirt, dust, mud, snow, ice and other environmental factors. All these influential parameters during the running along the track have stochastic character which is not possible to describe by analytical procedures in a reliable way. Consequently, the theory of wheel-rail contact is based on large number

of approximations which are necessary for analytical formulation and numerical solution of the problem by using some of the previously analyzed methodology. The solving the contact problem and determination of the wheel-rail contact forces by using all mentioned methodology is based on the previous knowledge of creepages in the contact surface. Due to the nonlinearity of the wheel-rail contact geometry and stochasticity of change of parameters which determining the track geometry, accurate determination of creepages in contacts of wheels and rails and its change during the running along the track is very hard and complex. In the analytical models wheelset is usually considered as rigid body with six degrees of freedom. Forming of analytical expressions for determination of longitudinal, lateral and rotational creep in such models is based on a large number of assumptions and approximations without which it is not possible to provide mathematical description and solution of the problem. The most of analysis of dynamic behavior of railway vehicles is based on numerical calculation of creepages on basis of formed analytical models and recorded data about track geometry, after which the theory of contact is used for solution of normal and tangential contact problem and calculation of wheel-rail contact forces. This approach is applied in all modern software packages for simulation of dynamic behavior of railway vehicles. These software packages enable analyzing of dynamic behavior for certain operating conditions still under development phase of new or modification of existing railway vehicles. In this way very expensive experimental tests can be avoided. The simulations are very useful in analysis of certain phenomena, especially in quasi-static conditions of moving. However, due to the large number of simplifications and approximations their results are not enough reliable for derivation of final conclusion about quality of dynamic behavior of railway vehicles. These facts are very important and must be taken into account in any analysis of dynamic behavior or railway vehicles. It can be concluded that the best and the most reliable way for determination of parameters of dynamic behavior of railway vehicles, especially those most important such as wheel-rail contact forces, is experimental testing in exploitation conditions [29]. This fact is confirmed from relevant standards UIC 518 and EN 14363 which prescribe experimental tests in the certification of railway vehicles, while simulations are allowed only in certain cases when validity of developed models is experimentally confirmed.

#### ACKNOWLEDGEMENTS

The authors wish to express their gratitude to Serbian Ministry of Education, Science and Technology for supporting this paper through project TR35038.

#### REFERENCES

- [1] UIC CODE 518 OR, Testing and approval of railway vehicles from the point of view of their dynamic behavior – Safety – Track fatigue – Running behavior, 4th edition, International Union of Railways – UIC, (2009)
- [2] EN 14363, Railway applications – Testing for the acceptance of running characteristics of railway vehicles – Testing of running behavior and stationary tests, European Committee for Standardization – CEN, (2005)
- [3] M. Bižić, D. Petrović, I. Pančić, Functions of wheel-rail contact geometry, Proceedings of the Eighth Triennial International Conference HEAVY MACHINERY – "HM 2014", pp. F77-F84, Zlatibor, Serbia, (2014)
- [4] E. Andersson, M. Berg, S. Stichel, Rail Vehicle Dynamics, Railway Group KTH, Stockholm, (2007)
- [5] S.D. Iwnicki, Handbook of Railway Vehicle Dynamics, CRC Press, Taylor & Francis Group, Boca Raton, (2006)
- [6] N. Bosso, M. Spiriyagin, A. Gugliotta, A. Somà, Mechatronic Modeling of Real-Time Wheel-Rail Contact, Springer-Verlag Berlin Heidelberg, (2013)
- [7] H. Hertz, Über die Berührung fester elastischer Körper, Journal für die reine und angewandte Mathematik, vol. 92, pp. 156-171, (1881)
- [8] H. Hertz, Gesammelte Werke, Vol. 1, Leipzig, (1895)
- [9] F.W. Carter, Railway Electric Traction, Arnold, London, (1922)
- [10] F.W. Carter, On the action of locomotive driving wheel, Proceedings of the Royal Society, A, London, vol. 112, no. 760, pp. 151-157, (1926)
- [11] J.J. Kalker, Review of wheel-rail rolling contact theories, The general problem of rolling contact, ASME, Applied Mechanics Division, vol. 40, pp. 77-92, (1980)
- [12] J.J. Kalker, Survey of wheel-rail rolling contact theory, Vehicle System Dynamics, 8, pp. 317-358, (1979)
- [13] V.K. Garg, R.V. Dukkipati, Dynamics of Railway Vehicle Systems, Academic Press, Toronto, (1984)
- [14] K.L. Johnson, The effect of a tangential force upon the rolling motion of an elastic sphere upon a plane, Journal of Applied Mechanics, 25, pp. 339-346, (1958)
- [15] K.L. Johnson, P.J. Vermeulen, Contact of non-spherical bodies transmitting tangential forces, Journal of Applied Mechanics, 31, pp. 338-340, (1964)
- [16] J. Hailing, Microslip between a rolling element and its track arising from geometric conformity, Journal of Mechanical Engineering Science, 6, pp. 64-73, (1964)
- [17] D.J. Haines, E. Ollerton, Contact stress distributions on elliptical contact surfaces subjected to radial and tangential forces, Proceedings of the Institution of Mechanical Engineers, 177, pp. 95-144, (1963)
- [18] J.J. Kalker, A strip theory for rolling with slip and spin, Proceedings of the Koninklijke Nederlandse Akademie van Wetenschappen, Series B, 70, pp. 10-62, (1967).
- [19] J.J. Kalker, On the Rolling Contact of Two Elastic Bodies in the Presence of Dry Friction, PhD dissertation, Delft University of Technology, Delft, Netherlands, (1967)
- [20] A.D. DePater, On the reciprocal pressure between two bodies, Proc. Symp. Rolling Contact Phen., pp. 29-75. Elsevier, Amsterdam, (1962)
- [21] A.S.K. Tjoeng, J.J. Kalker, User's Manual for the Program DUVOROL in ALGOL-60 and FORTRAN for the Computation of Three-Dimensional Contact with Dry

Friction, Delft University of Technology, Delft, Netherlands, (1980)

[22] J.J. Kalker, The tangential force transmitted by two elastic bodies rolling over each other with pure creepage, *Wear*, 2, pp. 421-430, (1968)

[23] R.C. White, D.A. Limbert, J.K. Hedrick, Cooperrider N.K., Guideway-Suspension Tradeoffs in Rail Vehicle Systems, Report DOT-OS-50107, U.S. Department of Transportation, Washington, (1978)

[24] Z. Shen, J. Hedrick, J. Elkins, A Comparison of Alternative Creep Force Models for Rail Vehicle Dynamic Analysis, Proceeding of the 8th IAVSD Symposium on Dynamics of Vehicles on Roads and on Tracks, Cambridge, Boston, pp. 591-605, (1983)

[25] J.J. Kalker, A fast algorithm for the simplified theory of rolling contact, Internal Report, Department of Mathematics, Delft University of Technology, Delft, Netherlands, (1980)

[26] J.J. Kalker, Three dimensional elastic bodies in rolling contact, Kluwer Academic Publishers, Dordrecht, Netherlands, (1990)

[27] J.G. Goree, User's Manual for Kalker's Exact Non-linear Creep Theory, Report FRA/ORD-78/50, National Technical Information Service, Springfield, Virginia, (1978)

[28] K. Knothe, D. Moelle, H. Steinborn, ROLCON, Ein Schnelles vielseitiges Digitprogramm zum rollenden Kontakt, *ILR Mitt.* 55, TU, Berlin, (1978)

[29] M. Bizic, Research of influential parameters in wheel-rail interaction on running stability of railway vehicles Doctoral Dissertation, University of Kragujevac, Faculty of Mechanica and Civil Engineering in Kraljevo, Serbia (in Serbian), (2015)

# Study of the Movement of the Attacking Tram Wheelset on Track with Gauge 1009 mm

Emil M. Mihaylov<sup>1\*</sup>, Emil Iontchev<sup>2</sup>, Vladimir Zhekov<sup>3</sup>, Zornitsa Evlogieva<sup>3</sup>, Metodi Atanasov<sup>3</sup>

<sup>1</sup>Department of Transport Equipment, University of Transport, Sofia, Bulgaria.

<sup>2</sup>Department of Telecommunications and Safety Equipment and Systems, University of Transport, Sofia, Bulgaria.

<sup>3</sup>Department of Transport Construction and Equipment, University of Transport, Sofia, Bulgaria.

*The paper describes the methodology of exploring the movement of an attacking wheelset bogie of a tram. The methodology includes both monitoring and recording the movement of the wheelset via an audio and video recording and reporting of accelerations in axle box caused by railway traffic. Tram bogie T 81 is selected due to its technical characteristics. The aim of the study is to make a connection between the positioning of the wheelset relative to the track and the different types of wear on the wheel rim, as well as binding the wheel relative to the rail and the squeal noise produced by the wheel in curved as well as straight segments together. The other part of the study's aim is by using the values of accelerations in the wheelset to assess the condition of the track and its influence on the bogies of the trams. All of the above is achieved by a simultaneous and synchronized reading of the monitored parameters. The chosen route must contain segments of the railroad with different design and in different state. The established methodology is preceded by separate measurements of accelerations and sound with a different purpose. Examples of measurements and their results are shown in this paper.*

**Keywords:** tramway, wheelset, track, acceleration, squeal noise, noise

## 1. INTRODUCTION

The dynamic interaction between the "wheel-rail" creates noise and vibrations, which are transmitted to the surrounding rail-road environment - buildings, facilities and people in the area of their distribution [1]. Research has shown that the most harmful to the environment are the low-frequency oscillations that occur when the wheel interacts with the rail. Other contributors to the noise and vibration are also the engine vibrations and other systems from the interior of the rolling stock, as well as the air friction when travelling at high speeds.

The main sources of vibrations are the irregularities on the rails and the wheels [2, 3], which induce additional inertial forces on the unmolded masses, creating vibrations in the rails transmitted to their adjacent environments [4]. It has been found that the vibrational effect is perceived directly by the human body whereas the receptors respond to oscillations of frequency of about 30Hz. In addition to the unpleasant experiences they bring to people, the vibrations also cause purely technical consequences, which are due to the accelerated accumulation of residual deformations, the more intense loosening of the bolt connections in the intermediate fasteners, the reduction of the longitudinal resistances when the rails are moving.

In the analysis of the dynamic behaviour of railway vehicles the most important are two groups of problems: the "wheel-rail" interaction when moving into a straight section of the railroad with emphasis on "stability of the movement" [2, 5] and problems while travelling in curved sections of the road [6]. During the movement of the wheelsets in a straight section of the road the oscillations and the interaction forces in the contact points are very intense, which has a very negative effect on the comfort, and at certain speeds may lead to instabilities in the movement [4], which is also one of the causes of wear on the wheels and the rails [2]. When moving in curved sec-

tions, the forces of interaction in the contact "wheel-rail" and the presence of an angle of attack between the wheels and the rails can reach such values that they cause very intensive wear, defects and breakdowns of the transmission of the vehicles and the railroad tracks, as well as violation of the traffic safety through the emerging risk of derailment [6, 7]. A number of rail administrations have explored the "wheel-rail" interaction at the design stage, testing of test specimens and operational tests. A monitoring system for safety and control of the traffic management on the railway infrastructure has been introduced [8, 9].

The problems mentioned above describe the need to further investigate the impact of the attack angle on the parameters defining the criterion of derailment of the attacking wheel in its travel through a curved section [10] and measurements during operating conditions.

In the last years, in Sofia have been carried out a number of studies concerning the movement of trams in different technical condition. The measurements performed on different occasions and through different activities, were executed through different types of bogies. Only one measurement parameter has been recorded.

The previously performed data analysis showed that a study is needed, whereas the data across all studies to be synchronized and also the data from all receiving devices to be analyzed.

## 2. DESCRIPTION OF THE METHODOLOGY

Research of the movement of the attacking wheelset of tram bogie T81 involves simultaneous recording of:

- the accelerations in the axle box
- the sound of the wheel movement
- video feed of the wheel position, relative to the rail.

The T 81 tram bogie (Figure 1) was developed in the 1970s to equip trams with a new concept of chassis

and power transmission. The T81 has two wheelsets, with a two-stage spring suspension, guide of the axle box, with

a base of 1600 mm. The bulkhead line consists of a single set of cylindrical screw springs.

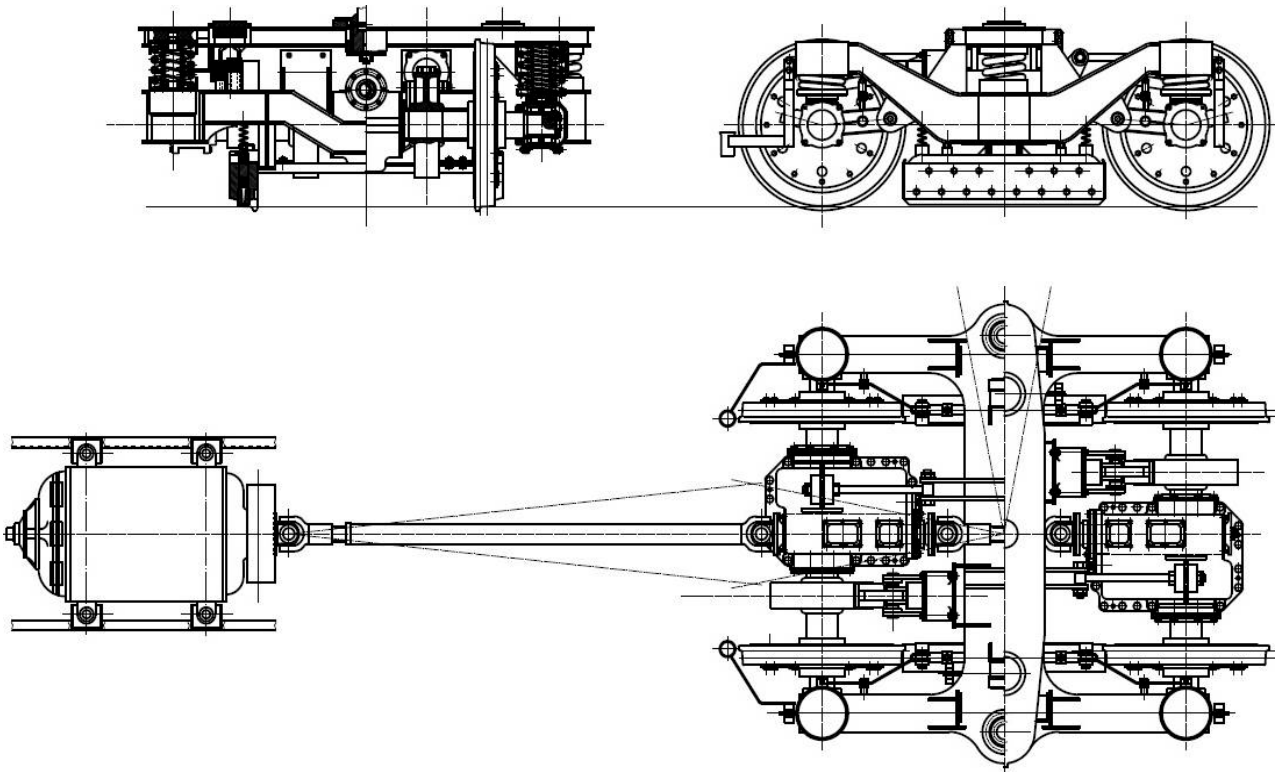


Figure 1: General view tram bogie type T81.

The wheels are type "Bochum 54" (Figure 2), the elastic elements (4) are rubber pads between the hub (1) and the band (2), laterally secured by the hoop (3). The wheel tyre profile T81 (Figure 3) is standardized for Sofia City.

- from Metro station "Khan Kubrat" to the Iliyantsi district;
- from Metro Station "Khan Kubrat" next to the Obelya district.

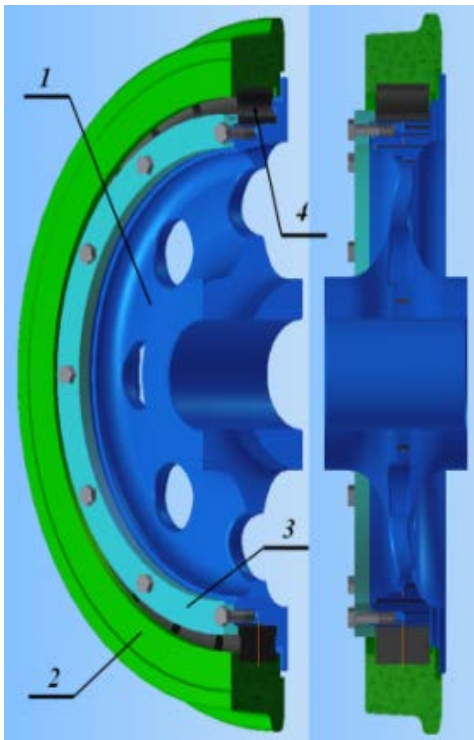


Figure 2: Wheel type „Bochum 54”.

The measurement will be made during the day with tram (TM) type T6M 700 using two routes:

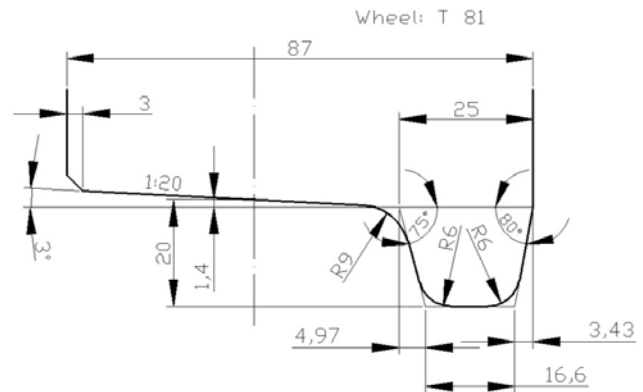


Figure 3: Wheel tyre profile of T 81.

Research routes include sections with different types of tramway construction – ballasted track and embedded track, as well as different tram track conditions – new, varying degrees of rail wear and track in satisfactory condition. The measurement will be taken with bogie with wear on the wheel tyre, suitable for the needs of the experiment.

The sensors will be mounted on axel box on the first wheelset. The recording equipment will be in the passenger compartment.

It is possible to include other parameters measured on other routes at the request of the test tram owner "Sofia public Electric Transport" EAD.

### 3. TECHNICAL IMPLEMENTATION

The devices will be mounted via stands which will be attached to the axle box of the first wheelset (figure 4).

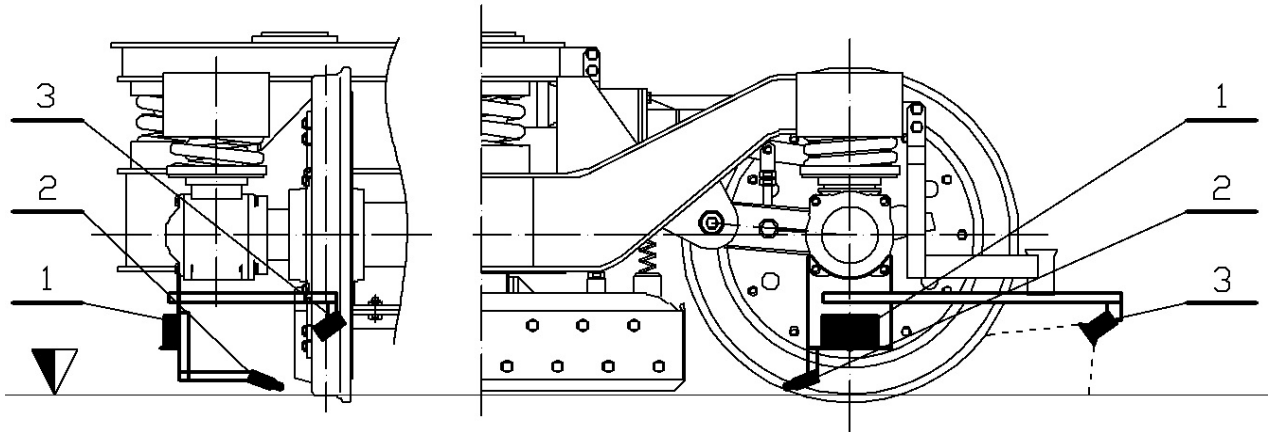


Figure 4: Mounts for the equipment.

Figure 4 shows the location of the measuring devices. Accelerometers (1) are fastened on the stand just below the axle box. The microphone (2) is fastened to a stand, positioned on the side of the right wheel. The video cameras (3) are placed in front of the attacking wheels so that they are right in front of the working side of the flange.

Recording and control devices will be located in the passenger compartment.

### 4. DESCRIPTION OF THE METHODS OF ANALYSIS

Title of the paper, the abstract and the keywords list are written in a text section with one column, while the body of text, acknowledgements and references are written in a section with two columns. The width of the columns in the second section is 8.35 cm, with spacing 0.8 cm between them. The columns at the last page should have equal length.

#### 4.1. Sound analysis

The measurement will be performed using a calibrated microphone, sound card and personal computer (Figure 5). The results obtained will be processed using a software product analyzing the noise parameters generated by the sound sources.

The measurement stage includes the following devices:

- USB Sound Card "LEXICON I-O 22".
- Measuring microphone "DBX RTA-M"
- Microphone cable - to connect the measuring microphone to the sound card.
- Software product for analysis of noise parameters.

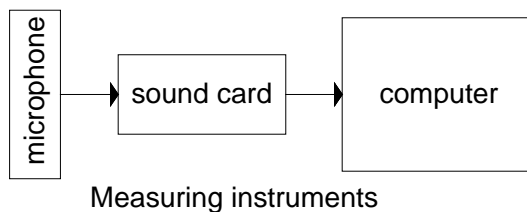


Figure 5: Diagram of the measuring system

The microphone is selected to be of Class 1, thus meeting the requirements of IEC 61672-1: 2013 [11]. In order to record only the noise of the tram and in particular the noise emitted by rolling the wheel along the rail and minimizing the side noise. The microphone will be positioned on a stand opposite to the right wheel (Figure 4).

The sound card is high-end class, providing better recording quality. The use of +48V phantom power for the microphone ensures low attenuation and parasite noise.

The processing of the recorded data will be done with NoiseLAB, performing SPL or octave analysis.

#### 4.2. Acceleration analysis

In numerous scientific articles, devoted to the assessment of the state of the railway track, are used parameters of the dynamic response, which is caused by the interaction of the systems vehicle-road. These are: the dynamic forces in the wheels of the rolling stock; the induced noise; the linear and angular accelerations. A method for assessing the railway track condition is proposed in [12] using the measured vertical accelerations in the axle box of wheelset of tram. In the upcoming measurements, apart from the vertical accelerations, the lateral accelerations of the wheelset are also evaluated using a measuring system whose block diagram is shown on figure 6.

The mounting place of the measuring system, Figure 4, is chosen from the requirement to provide a proportional, frequency independent wheel-road connection. The three axes linear accelerometer produced by MEMS technology is used to measure linear accelerations. The built-in satellite navigation receiver works with the signals from the GPS system. The working algorithm of the system provides for each sample of the geographical coordinates to record the accelerations in the given point, also, the number of recorded samples of acceleration is dependent on the programmed clock sampling frequency. This frequency can be 40 or 160 Hz. Data is recorded on a SD card with a maximum capacity of 2 GB, which is sufficient for continuous recording for about 40 days. The satellite navigation receiver not only delivers geographic coordinates, but also coordinated universal time (UTC), which is convenient for combining data from different sources, recorded at time synchronized with the UTC one.

This is used in the algorithms to process data from measuring the noise and video measurement of motion of the

wheelset and their synchronization with the accelerations.

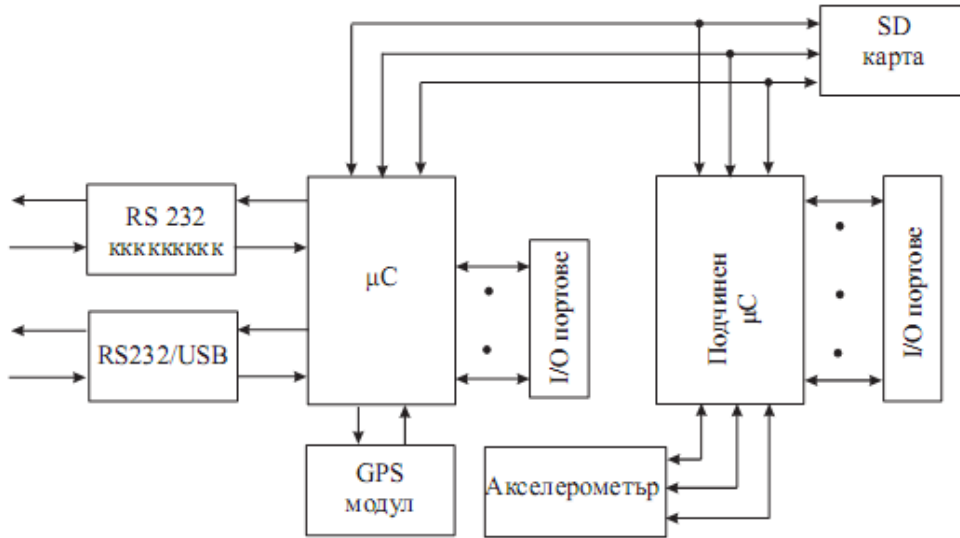


Figure 6: Block diagram of the measuring system

The measurement system was extended by adding a gyroscope mounted to the accelerometer to measure the angular speeds of the wheelset in three directions. This provide additional information about the attacking wheelset behaviour while motion.

Measured data is processed in Matlab. Statistical data processing according to [12] is applied in the time domain, and peak and effective values of inertial data are determined. Data is additionally processed in the frequency domain for their filtering and determination of their spectral characteristics.

Due to lack of recommended threshold values for the accelerations in tram wheelsets, ensuring its safe movement, threshold values are borrowed from the railroad transport [13]. The evaluation of the lateral accelerations in the wheelset is made using the derailment risk assessment. These are the peak lateral acceleration, which should not exceed  $12 - \left(\frac{M_b}{5}\right)$  and the effective value,

which should not be greater than  $6 - \left(\frac{M_b}{10}\right)$  in the frequency band  $f_0 \mp 2Hz$ .

Where  $M_b$  is the mass of the wheelset,  $f_0$  is its resonance frequency. The developed algorithm depicts locations with poor track geometry on map and places where whistling occurs and there is a risk of derailment.

4.3. Analysis of the video footage

The monitoring of the position of the wheelset during motion is necessary to determine the relationship between all remaining recorded parameters. The visual tracking will make it easier to synchronize data from other sensors. Of particular interest is the position of the wheelset in relation to the rails during squeal.

5. RESULTS OF STUDIES CONDUCTED TO DATE

The method of analysis by measuring the accelerations generated in the chassis of railway vehicles as a consequence of road misalignment can be applied in both directions. Originally the method was developed to assess

the condition of the tram track, but in several successive measurements was made an assessment of the impact of the rail on the vehicles.

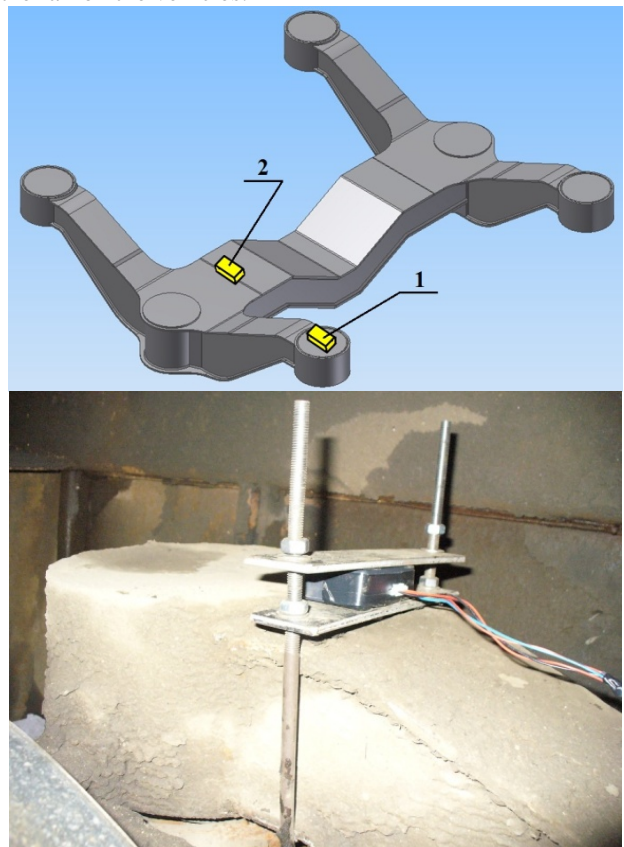


Figure 7: Place of installation of meters on the bogie frame.

In 2014, the acceleration was measured in the T81 tram carriage frame above the BRC [14] in search of the causes for the occurrence and development of cracks in the transom beam of the frame. Measurements were made at two points of the frame (Figure 7), the measurement being made along the route shown in Figure 8.



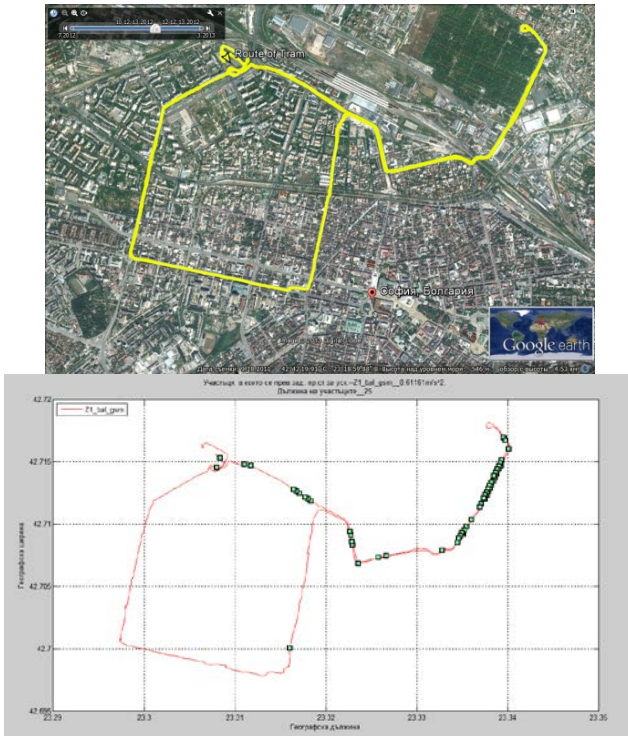


Figure 8: Route measurement.

Part of the results are shown in Figure 9 – average acceleration values and Fig. 10 - maximum values.

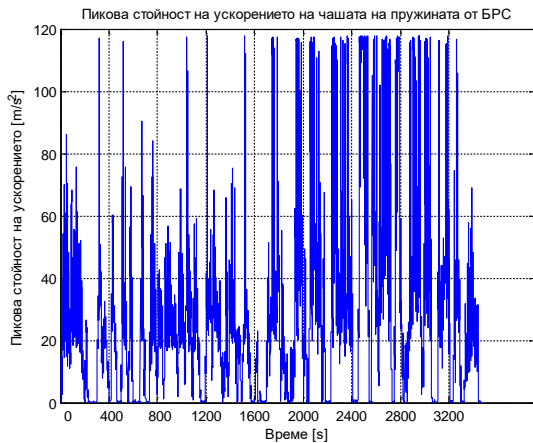


Figure 9: The peak value of the acceleration of the chateaux spring from BRS

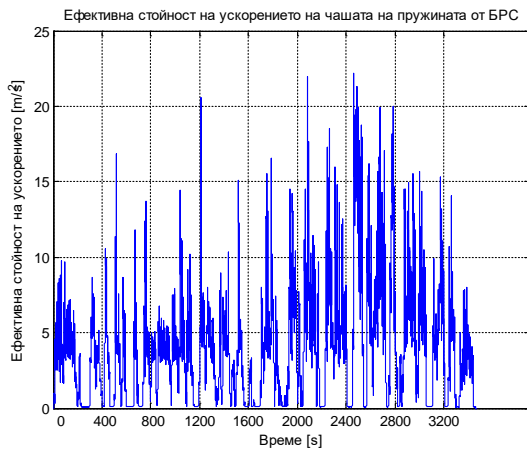


Figure 10: Effective acceleration of the cup spring from BRS

On the basis of these values was performed analysis by finite element method and was made Stress Analysis of the chassis frame (Figures 11 and 12)

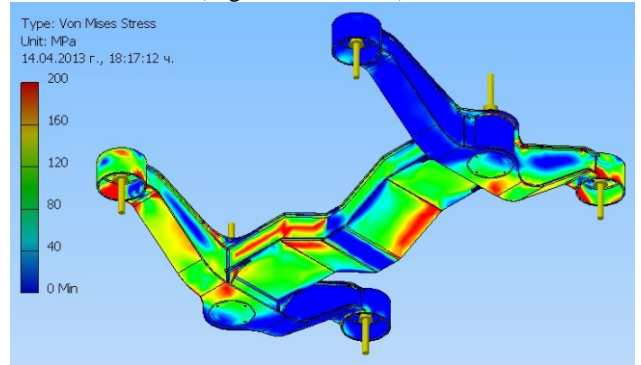


Figure 11: Tensions in bogie frame, with an average acceleration.

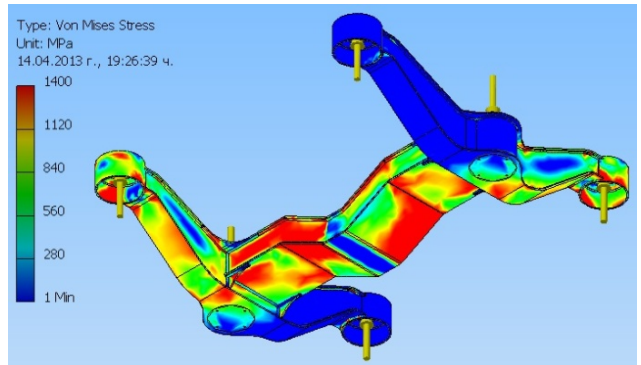


Figure 12: Tensions in bogie frame at maximum acceleration.

Also in 2014 "Sofia public Electric Transport" EAD ordered a comparative analysis between the two types of elastic wheels [15]. By measuring the accelerations near the bearing block (figure 13), the properties of the various elastic elements in the tram wheels had to be assessed.

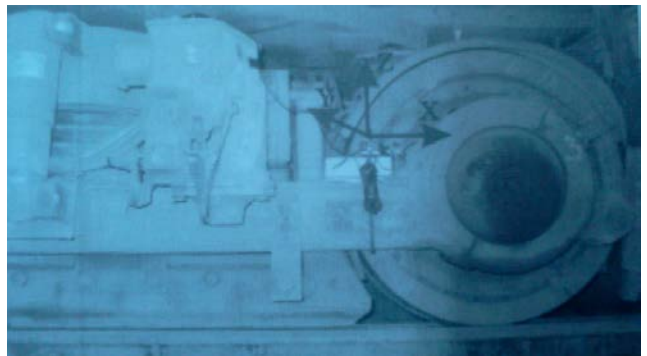


Figure 13: Installation of the measuring instruments.

Figure 14 shows some of the measurement results. On the basis of these results, it was concluded that the wheels "Tatra" could be replaced by wheels "Bochum 54" without altering the quality of the tram ride.

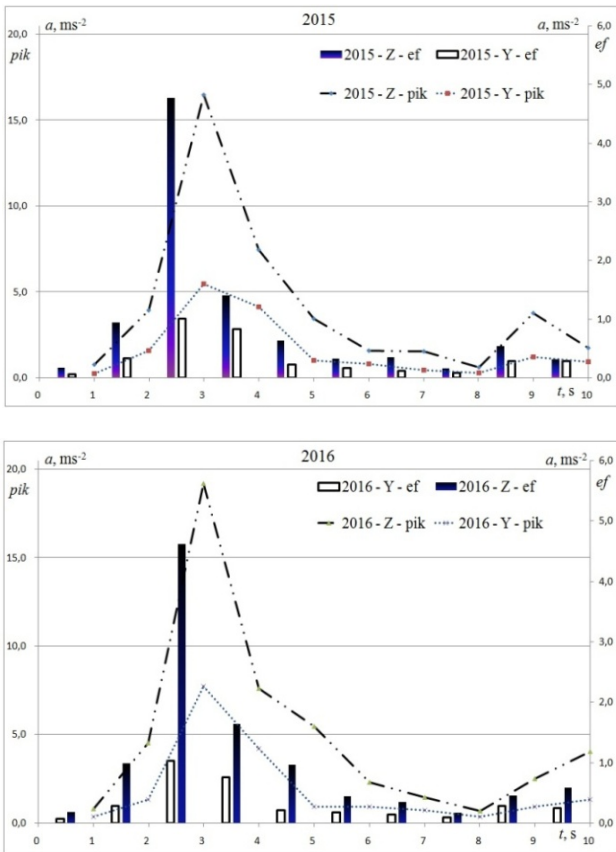


Figure 14: Accelerations in overcoming crossings.

In the same year, the method was applied by an experimental calculation of the own frequency of the tram bogie T81 [16]. Part of the results are shown in Figures 15 and 16. The theoretical calculation of the own bogie frame frequency was confirmed by the test results.



Figure 15: Spectral composition of accelerometer and gyroscope signals

In 2015 a measurement of the condition of the tram tracks has been conducted in Sofia [17]. Used is a method for evaluating the condition of the track using the measured accelerations in the three axes, in the axle box of the tram. The sensors were mounted on a T8A2-BG Tatra CKM tramcar, undergone major overhaul.

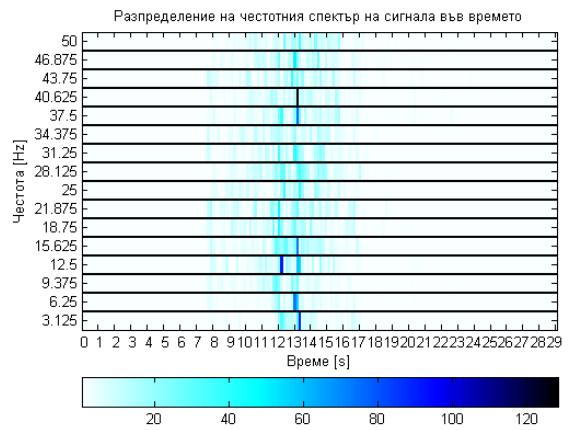


Figure 16: Spectral composition of signals obtained by wavelet conversion

The area where the study was conducted is shown in Fig. 17.



Figure 17: Route of the measurements.

The study route was chosen by two evaluation criteria:

- type of construction – ballasted track, track on concrete base, panels construction;
- service years.

The objective is to assess the condition of the track with different types of construction, according to the year of commissioning.

The assessment method is based on determining a threshold value, to which the received accelerations are compared. As such, it is chosen to be the median value of the data obtained from the particular measurement. This choice avoids single maximum acceleration values. For a measure of scattering, the standard deviation  $\sigma$  is chosen. The threshold values in the different sections of the surveyed route were calculated, on the basis of which analysis and conclusions were drawn on the state of the track in the different sections [17].

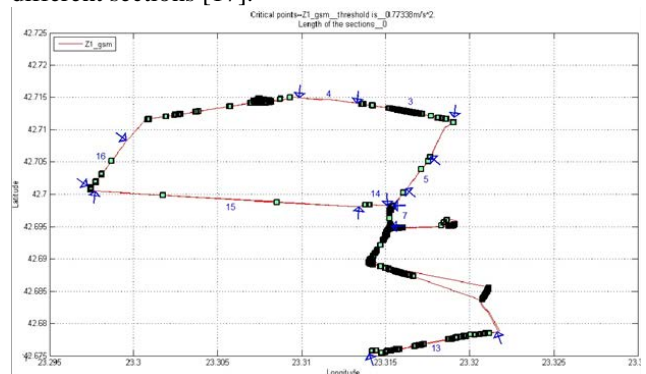


Fig. 18: Route marked where the effective acceleration values exceed the specified threshold value

Fig. 18. shows the route of the tramway where the effective acceleration values exceed the specified threshold (determined from the data of the whole route section) by  $3\sigma$ .

The analysis of the results shows that the rail sections with panels have several times higher accelerations compared to those with a concrete base and short service life. Increases in acceleration values are seen as a result of tram track operation during the time.

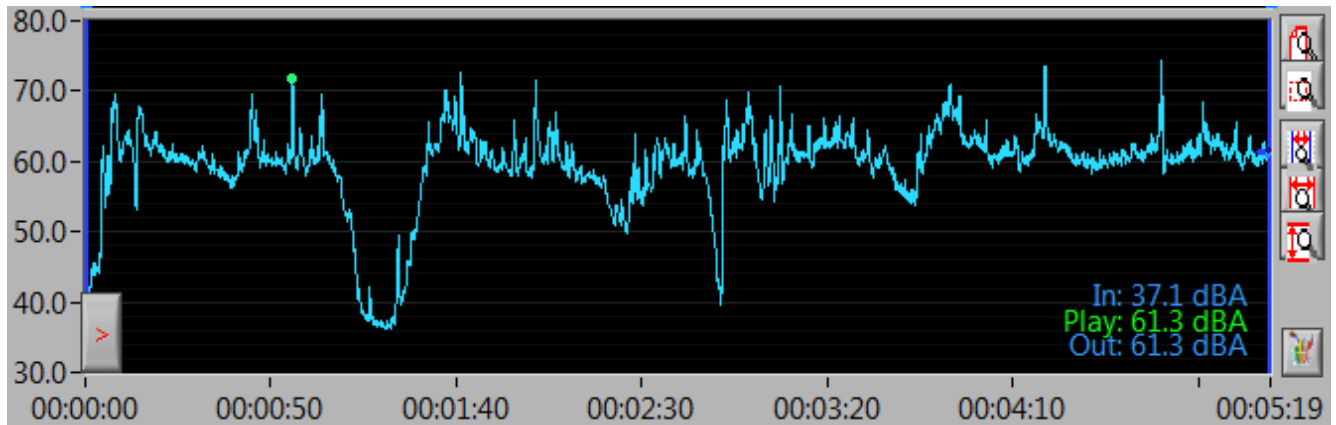


Figure 19: Recording of the noise of one of the wheels.

The analysis of the record showed that the noise levels generated by the wheel contacting the track have an average value of 60dB. Jointed track have peak values of about 70dB in the joints.

The squeal noise in curves is unpleasant and quite irritating, but as values it also does not exceed 70 dB.

## 6. EXPECTED RESULTS

### 6.1. Noise

Squeal from the wheels and rails contact is a noise that is not constant and is addition to the overall noise of the running of the rail vehicles. This effect is extremely irritating and is the main cause of protests by people living along tram routes. The purpose of the study is to locate the causes of its occurrence. To find the relationship between squeal and the state of the tracks: type and degree of rail wear, tram speed, curve position, curve radius, and so on.

It is also necessary to assess the effect of the noise reduction systems used to date, such as mounting of lubricants, the application of different types of noise protection elements, and others

### 6.2. Condition of the track

An analysis of the state of the track in the individual sections will be made, using the acceleration measurements and the methodology shown in V.V. The additional noise measurement data generated by the wheel - rail interaction will make it possible to determine the difference in noise levels at sections with different road conditions as well as in curves of different radius. As said before, the causes of squeal will be analyzed in terms of track parameters, state and type of rail construction, and curve entry.

The acceleration and noise data will be supplemented by camera footage, which will allow viewing of images in sections with acceleration near the thresholds, curve fitting, etc. This information will provide an oppor-

Along with the acceleration, a noise level measurement was also made at the axle box.

In order to isolate ambient noise as much as possible, the measurements were made at night, between 0.30 and 4.00 am. At this time there is no traffic in the main city arteries, the running speed may be more even, and stops are significantly less.

The microphone was mounted on a stand by positioning it on the side of the right wheel. Part of the resulting record is shown in Figure 19.

tunity for a broader analysis of the investigated sections and particularities of the wheel - rail interaction

### 6.3. Wear of the wheel tyre – types and degrees of wear

Conclusions made so far about the different ways of wearing wheel tyres are based on a comparison of various factors that are supposed to be influential. Such are: road state information on the various sections, data on the operation of the units, ie. constant movement over one single route, data on chassis repairs, and more. The upcoming study will clarify the links between the different types of wheel tyre wear and the ways in which the wheel-set contacts with the track.

The position of the wheelset with respect to the track and its contact with the rails will provide an explanation for the different types of wheel tyre and rail wear. There are virtually simultaneous defects on the road - with a long collapse of one rail there is a short collapse of the other, staggered long collapse of the two rails with overlapping, long sections with extreme wear on the rails and others. Such factors influence the wheels at the same time and result in a combination of two or more types of wear.

Interest is the so-called. high wear on the non-working side of the beads, which greatly reduces the wheel tyre resource. It is assumed that the reason for this wear is the moving on a track with extremely worn grooved rails. In a straight section, the winding of the bogie in combination with a modified track gauge in the positive tolerance or with the continuous failure of one rail leading to constant contact of the other wheel with the rail flange. In a curve with a small radius and worn rails, the guiding force is likely to be realized in the contact point of the inner rail with the forehead of the rib

## 7. CONCLUSION

The team, which developed the described methodology, expects the results of this study to prove or reject

the suggestions made so far about the reasons for wheel and rail wear and serve as a choice of methods and technical solutions to combat noise. The methodology described above can be expanded and used as a basis for the equipping of a measuring tram for railway control.

#### REFERENCES

- [1] D. Atmadzhova, „Воздействие транспортного комплекса на окружающую среду”, International scientific-expert conference, МГАКХиС, Moscow, Russia, 1-4 April 2009.
- [2] Atmadzhova D. „Wheel-rail contact wear, work and lateral force”, International Railway Symposium 2006 Ankara and Istanbul, TURKEY, 13-15 December 2006
- [3] Atmadzhova D., „Influence of wheel and rail profiles on railway vehicle dynamics”, First International Conference on Road and Rail Infrastructure CETRA 2010, 17-18 May, Opatija, Croatia, 2010
- [4] D. Atmadzhova, „Динамичен анализ на железопътен вагон. Многостепенни системи и бифуркационен анализ.”, Proceedings, International scientific conference „BulTrans-2010”, TU – Sofia, Sozopol, Bulgaria, 24-26 September 2010
- [5] Atmadzhova D. A method for determination of the wheel rail contact. Nis, XII Scientific-expert conference on railways RAILCON '06, Serbia and Montenegro, Faculty of Mechanical Engineering University of Nis, 2006.
- [6] Atmadzhova D., „A Methodology for Determining the Causes of Rolling Stock Derailment”, XVII International scientific-expert conference RAILCON '16 Niš, Serbia, at the Faculty of Mechanical Engineering 13-14 October, 2016, 41-44 p.
- [7] Atmadzhova D., „Изследване влиянието на ъгъла на атака върху безопасността на движение на железопътна талига”, Academic journal „Mechanics, Transport, Communications” 2016 art. ID:1339, 2016
- [8] Atmadzhova D., Dimitrov E., Nenov N., Control System for Trains in Movement, Int International Conference on Road and Rail Infrastructure CETRA 2012, 7- 9 May, Dubrovnik, Croatia, 2012
- [9] Nenov N., Skrobanski B., „Моделиране на система за мониторинг и контрол на ПЖПС в движение по железопътната мрежа на Р. България”, International scientific conference „BulTrans-2016”, TU – Sofia, 14 – 16.09.2016, Sozopol, Bulgaria, с. 185-190.
- [10] Atmadzhova D., „An Electronic System for Measuring the Attack Angle of Railway Wheelsets at a Running in Curves.”, ISSE 2010 WARSAW May 12 – 16 2010 Poland
- [11] IEC 61672-1:2013 Electroacoustics - Sound level meters - Part 1: Specifications
- [12] Iontchev E., Simeonov Iv., Miletiev R., „GSM/GPS/INS system for urban railway monitoring based on MEMS inertial sensors”, Proceedings of the 22nd Micromechanics and Microsystems Technology Europe Workshop, Tonsberg, Norway, 19-22 June 2011, pp. D81.
- [13] International union of railways, UIC 518: Test and approval of railway vehicles from the points of view of dynamic behaviour, safety, track fatigue, and ride quality, Leaflet, Paris, France, 1995
- [14] E. M. Mihaylov, E. Iontchev, D. Atmadzhova, „Measuring accelerations frame tram bogies T 81 in order to establish the reasons for the emergence and development of cracks”, XVI International Scientific-expert Conference on Railways, RAILCON'14, Serbia, Niš, October 09-10, 2014.
- [15] E. M. Mihaylov, D. Atmadzhova, „Comparative analysis of accelerations of type T6A2 tram bogie frames with different types of elastic wheels”, VI International symposium for students, Kraljevo, Serbia, November 06 - 08, 2014.
- [16] R. Miletiev, E. Iontchev, E. M. Mihaylov, R. Yordanov, „Measurement of the fundamental frequency of the tram cart by quad sensor inertial system”, 24<sup>th</sup> National Scientific symposium „Metrology and metrology assurance 2014”, Sozopol, Bulgaria, September 7 – 11, 2014.
- [17] V. Zhekov, E. Iontchev, „Assessment of the urban rail network based on the accelerations in the axle box of the tram”, The 5th Multidisciplinary Academic Conference in Prague 2015, Czech Republic, October 16 – 17, 2015.

# The Impact of the Characteristics of Train on the Train Braking Distance at Critical Sections of the Belgrade – Bar Railway Line

Dušan Vujović<sup>1\*</sup>

<sup>1</sup>Railway College of Vocational Studies, Belgrade (Serbia)

*This paper analyzes impact of the individual characteristics of the railway vehicles and the whole train composition to achieve a certain braking distance under different conditions. This paper also discusses the impact of the characteristics of critical sections of Belgrade - Bar railway line to train braking distance. As the empirical equation for train braking distance established, the modified equation established too, taking into consideration basic and periodical resistance of the train together. At the same, the newly established values are compared to values of previously length of train braking distance. On the basis of the obtained results the appropriate conclusions are given.*

**Keywords:** train braking distance, train characteristics, resistance of train

## 1. INTRODUCTION

The basic requirement for the safety of railway traffic is that the train can be stopped at any time, in any place and on the length of the prescribed stopping distance. During the last decades at railway traffic around the world the movement speed of passenger and freight trains are increasing. One of the basic conditions for introduction of higher speeds is using effective and safe brakes, which are able to react at any time when need arises and to stop the vehicle or train at the prescribed length of stopping distance.

Braking of traction vehicle and whole train composition is performed by brakes which have to slow down or stop the train that has a certain mass and length, by specified deceleration, at the prescribed length of the braking distance and at all conditions of exploitation.

In order to achieve this it is necessary that all the mentioned values are set to each other in such addition that assigning of one size provides determining the necessary values of other sizes.

## 2. TRAIN BRAKING DISTANCE

The entire braking distance of the train can be viewed as the sum of two distances. The first distance is bound for the time period between moment when became necessary apply braking to the moment when engine driver started braking process. Other distance is related to the process of train braking.

Train braking distance directly depends on the deceleration that is achieved during braking and movement speed at the starting process of braking. Deceleration directly depends of the mass of braked train and the interplay between the train braking force and resistance force which appears at braking distance of the train.

### 2.1. Train braking distance depending on deceleration

Train deceleration depends on the forces that affect movement of train during braking. If the train braking distance expressed by decelerating then it is possible to show braking distance value through addition to mentioned forces.

In order to express braking distance using deceleration it's need to start from general expressions for deceleration (i.e. acceleration) and distance:

$$a = \frac{\Delta V}{\Delta t} \quad \text{and} \quad S = V_{sr} \cdot \Delta t \quad (1)$$

Where:

$V_{sr}$  – average speed during observed time interval  $\Delta t$  (hereinafter  $\Delta t = t$ );

Because of:

$$V_{sr} = \frac{V_1 + V_2}{2} \quad (2)$$

Then:

$$S = V_1 \cdot t - \frac{a \cdot t^2}{2} \quad (3)$$

If, in this expression, time „t“ writes as:

$$t = \frac{\Delta V}{a} \quad (4)$$

Then expression for distance becomes:

$$S = \frac{V_1^2 - V_2^2}{2a} \quad (5)$$

Knowing the principle of train brakes functioning, expression (5) thus written cannot be used for precise determination of train braking distance. When starting the process of train braking, train brake force gradually increases until reaching its set value. Depending on the type of applied brakes, braking mode, moving speed and other factors the time, required to achieve maximum brake force, varies. The train basic resistances also depend on the movement speed. Considering that train deceleration depends on the forces that affect the train movement, it's understandable that, during train braking, deceleration is variable size. By increasing the brake force deceleration is also growing. Deceleration is proportional to brake force, but inversely proportional to train basic resistances. Observing the train extra resistances, then it's seen that the deceleration is in very complex dependency with all forces that affect the movement of the train during deceleration. As deceleration can be changeable at any moment in time, it's most precise taking value of deceleration for each little interval of movement speed changing and time change.

By mathematical notation of using expression (5), train braking distance can be calculated using the formula:

$$S = V_1 \cdot t_r + \frac{V_1^2 - V_2^2}{2 \cdot a_1} + \dots + \frac{V_{n-1}^2 - V_n^2}{2 \cdot a_{n-1}} + \frac{V_n^2}{2 \cdot a_n} \quad (6)$$

$$S = V_1 \cdot t_r + \sum_{i=1}^n \frac{V_i^2 - V_{i+1}^2}{2 \cdot a_i} \quad (7)$$

$$\forall i = 1, 2, \dots, n \quad n \rightarrow \infty$$

$$V_{n+1} = 0 \quad \Delta V = V_i - V_{i+1} \rightarrow \infty$$

Where:

$t_r$  – train driver reaction time.

$$a_1 < a_2 < \dots < a_{n-1} < a_n \quad (8)$$

$$\Rightarrow a_i < a_{i+1} \quad \forall i = 1, 2, \dots, n-1$$

When establishing train braking process there is rising pressure in brake cylinders until reaching its maximum value. Brake force follows rise of pressure and train deceleration, at unchanged movement resistance, follows the braking force and is rising consequently. The train resistances are dependent on train speed and in case of reduction movement speed their value decreases. Deceleration value, in terms of dependence on the movement resistance, should be decreases, but during trains braking, total train brake force has to be such value to prevents deceleration reduction at low speeds. When it's valid, expression (8) is written correctly. When the pressure in brake cylinders reached the largest value, then it's the largest value of brake force and the greatest value of deceleration is achieved:

$$a_n = a_{max} = a \quad (9)$$

2.2. Ratio of deceleration, brake force and movement resistance

Train braking force and train movement resistances together affect the deceleration of train. As the force depending on the mass that slows, also the deceleration depending on the mass when the value of the force is known. Based on this, can be written:

$$F_k + \sum W = Q_v \cdot a \quad (10)$$

i.e:

$$a = \frac{F_k + \sum W}{Q_v} \quad (11)$$

The values in the expression:

$F_k$  – braking force of entire train,

$\sum W$  – sum of train movement resistances during braking,

$Q_v$  – mass of entire train and

$a$  – train deceleration.

2.3. Train movement resistances

There are several different partitions of train movement resistances. They can be classified into the train basic resistances and train occasional resistances. The train basic resistances include basic resistances of traction vehicles (locomotives) and basic resistances of towed vehicles (wagons). By movement speed increasing the

value of these resistances increasing too. The occasional train resistances include slope resistances, curve resistances, wind resistances, tunnel resistances and others. Among them, only tunnel resistances are dependent on movement speed. All resistance dependencies of speed are squared, which means that resistances does not vary linearly at speed changes, but dependence is in the form of parabola. It is obvious that some of these resistances affect on train acceleration, and some affect on train deceleration. Basic movement resistances, curve resistances and tunnel resistances slowing train. Slope resistances, depending on whether it is positive or negative slope value, they can accelerating or decelerating the train. Wind resistances, depending on the wind direction, also affected movement of trains.

Total train brake force value has to be so high that train can unconditionally stops at the prescribed length of braking distance. This means that brake force value must be greater than all resistances that enhance movement. This is especially important during train braking on the decline, considering that slope resistance values may have a very great value.

### 3. TRAIN BRAKE FORCE

In order to obtain value of brake force for the entire train must be known brake forces of all train vehicles. Sum of braking forces of all train vehicles represents a braking force of the whole train (12).

$$F_k = \sum F_{km} \quad (12)$$

$$\forall m = 1, 2, \dots, \text{number of vehicles}$$

Value of brake force of individual vehicles depends on the type of applied brakes on the vehicle and of the characteristics of this brake. At all railway vehicles, except certain vehicles for repair, inspection and tracks maintenance, must exist the indirect automatic brake. These are pneumatic brakes in which braking depending on air pressure in the train main air conduit. They are called automatic because they automatically take effect due to falling air pressure in the main air duct. Indirectly, because the air in brake cylinders, for these brakes, comes from auxiliary reservoir, but not as direct, where air comes in brake cylinder from main reservoir. From the fall of air pressure value in the main air conduit depends how much would be value of air pressure increase in the brake cylinder, and therefore value of achieved brake force. When train break occurs a sudden drop in pressure of main air conduit occurs too and then achieves the maximum value of brake force in the shortest time.

#### 3.1. Determining train brake force

In order to determine brake power or examine the ability of braking individual railway vehicles, experimental braking performing. In these experiments vehicles are accelerated to a certain movement speed, and then start braking vehicles at maximum braking force. Towed vehicles achieved maximal value of the brake force by breaking of train, or uncoupling these vehicles at movement of certain speed. Vehicles rapidly reach maximum brake force value and then, by approximately constant deceleration, moving to a stop. These experiments are carried out mostly on horizontally part of

railway route without curves, because the slope and curve resistances would complicate collecting results process. After stopping the vehicle the distance travelled during rapid braking is measured and determines the braking mass of the vehicle. In order to determine maximum value of vehicle braking force experiment can be repeated several times. Then, the achieved average length of stopping distance and average elapsed time get the value of the average vehicle deceleration.

It is clear that in each experiment mass of the vehicle is same. Value of the vehicle basic resistances in each experiment has approximately the same value. Follows these experimental conditions the approximate value of vehicle braking force can be determined.

Based on (7) and (11) expression for calculation of approximate length of achieved stopping distance in the experiment can be written:

$$S_{exp} = \frac{t_{rko} \cdot V_1}{2} + \frac{Q_{km} \cdot V_1^2}{2 \cdot (F_{km} + W_{okm})} \quad (13)$$

$\forall m = 1, 2, \dots, \text{number of vehicles}$

Where:

$t_{rko}$  – brake equipment response time, from moment of seduction process of rapid braking to moment when the maximum pressure in vehicles brake cylinder established,

$V_1$  – initial speed of braking process,

$Q_{km}$  – vehicle mass,

$F_{km}$  – vehicle braking force and

$W_{okm}$  – basic vehicles movement resistances.

At the first part of the product expression time and speed is divided by two, which is made an approximation of expression (7). This is done because of expression simplification, but considering that braking, at one time, performed by the maximum braking force, which is very quickly established at process of fast braking. This factor is representing a part of distance corresponding to time required for establishing value of maximum braking force. It further, follows from expression (13) leads to the expression for calculation individual vehicle braking force:

$$F_{km} = \frac{Q_{km} \cdot V_1^2}{2 \cdot S_{exp} - t_{rko} \cdot V_1} - W_{okm} \quad (14)$$

It is known that vehicles main movement resistances are equal to product of the vehicle mass and the vehicle basic, specific, movement resistances:

$$W_{okm} = \omega_{okm} \cdot Q_{km} \quad (15)$$

$\omega_{okm}$  – vehicle basic, specific, movement resistances (vehicle movement resistances value expressed per unit of mass of the vehicle).

According to expression (15), vehicle braking force (14) becomes:

$$F_{km} = Q_{km} \cdot \left( \frac{V_1^2}{2 \cdot S_{exp} - t_{rko} \cdot V_1} - \omega_{okm} \right) \quad (16)$$

The proof of accuracy of this expression is reduced to a simple mutual correspondence between units of specified physical quantities in this expression. Value of the vehicle braking force, determined in this way, is correct under the condition:

$$F_{kmmax} = F_{athmmax} = Q_{km} \cdot \varphi_{\alpha} \cdot g \quad (17)$$

$$\text{if } F_{km} > F_{kmmax} \text{ then } F_{km} = F_{kmmax}$$

Where:

$F_{kmmax}$  – maximum achieved vehicle braking force value,

$F_{athmmax}$  – maximum vehicle adhesion force,

$\varphi_{\alpha}$  – adhesion coefficient,

$g$  – gravitational force acceleration.

The maximum value of vehicle braking force must not exceed the maximum vehicle adhesion force. When exceeding occurs then vehicle axles become blockaded and vehicle wheels started to sliding on rails instead of rolling on. The sliding of two metal surfaces, one on another, friction that occurs between this two surfaces depends on the material properties of these surfaces. The sliding force depends on friction of contact surfaces. Rolling force and braking force contribute to deceleration of the vehicle. In the routine of railway vehicles is often the case that the value of the sliding force is less than the braking force. Therefore, deceleration of the vehicle which slips is less than in the case of the vehicle with wheels which normally rotate during braking. This results an increase in the length of braking distance of vehicle with blocked axles. In order not to bring into question the safety of rail traffic, wheels sliding on rails must not be allowed. Modern railway vehicles are equipped with some braking devices which prevent axles blocking. These devices respond to first occurrence of wheel slip and reduce value of braking forces acting on axis wheels which slip. In this way it is possible to maintain braking force value along the border of adhesion force. In this way during braking the maximum brake force value is achieved and it's approximately constant and consequently approximately constant value of vehicle deceleration.

The maximum value of vehicle adhesion forces depends on the vehicle mass and adhesion coefficient. As the adhesion coefficient is variabed size, value of adhesion force changes depending on it. The adhesion coefficient depends on many factors and determining its value is a very complex process. It is known that its value decreases with worsening of conditions at contact point of wheels and rails (humidity, ice, grease, leaves and grass) and also decreases with increasing of vehicle speed. Declining of adhesion value is much more pronounced at higher speeds. For purposes of this paper vehicle speed will not exceed 100 km/h and until this speed there is no significantly changes of adhesion coefficient values. Furthermore deeply into issues of adhesion will not be subject of this paper.

### 3.2. Ratio of train braking force and other parameters of train movement

Once it is determined the braking force value of each train composition vehicle then it's possible to determine the brake force of the whole train. The sum of all vehicle braking forces gives a total train brake force. Train brake force is directly related to train deceleration. Using expression (7) train maximum deceleration can be written as follows:

$$\alpha_n = \frac{V_n^2}{2 \cdot \left( S - V_1 \cdot t_{rko} - \sum_{i=1}^{n-1} \frac{V_i^2 - V_{i+1}^2}{2\alpha_i} \right)} \quad (18)$$

If a braking distance for some speed is known value, then can be determined required train deceleration that would satisfy this length of braking distance. The value of obtained deceleration defines the minimum value of train brake force. If the value of brake force is greater than or equal to the minimum necessary braking force value, then the train certainly be stopped at the prescribed length of braking distance. It is clear that sum of all braking forces of individual train vehicles must be greater than or equal to the minimum necessary braking force value.

$$\text{if } \sum F_{km} \geq F_{kmin} \text{ then } S \leq S_{max} \quad (19)$$

Where:

$$F_{kmin} \geq \frac{Q_v \cdot V_n^2}{2 \cdot (S_{max} - V_1 \cdot t_{rko} - \sum_{i=1}^{n-1} \frac{V_i^2 - V_{i+1}^2}{2 \cdot a_i})} - \sum W \quad (20)$$

The proof of accuracy of this expression is reduced to a simple mutual correspondence between units of specified physical quantities in this expression. Inequality (20) can be used to finding the minimum train brake force value, which is necessary to unconditionally stopped the train at the prescribed length of braking distance, at some speed of movement and at a certain section on the railway line.

At movement speed  $V_n$  train has achieved maximum brake force value and braking at maximum deceleration. During braking, without releasing brakes to a stop, this deceleration remains unchanged until the moment of stopping.

#### 4. REQUIRED TRAIN BRAKE FORCE AT CRITICAL SECTIONS OF BELGRADE – BAR RAILWAY LINE

Route of railway line from Belgrade to Bar is one of the most complicated and the most demanding, as for maintenance as well exploitation. This railway line abounds high bridges, long tunnels, deep clefts, high embankments and small radius curves. The major part of the route is situated in hilly and mountainous terrain.

Considering that it is a mostly hilly route, overcoming height difference at a short distance achieved by the construction of big gradient values. Often the big gradients are places where trains, because of traffic or other reasons, stop. The most common example of such places are station home signals.

Prescribed stopping distance also depends on the maximum permitted speed of some railway line section. For speeds from 80 km/h to 100 km/h prescribed stopping distance is 700 m. If trains braking on the part of the route where gradient has negative value, i.e. the negative resistance value of gradient, then it is normal to increase stopping distance. For that reason, the most railway lines have extended necessary length of stopping distance, if the braking sections have a negative gradient. For the mentioned speeds, the length of stopping distance for negative gradient sections, be longer than 700 m.

Specifically for this railway line is uniform length of stopping distance, regardless of the movement speed and gradient of sections where trains braking to a stop. Prescribed length of stopping distance on the Belgrade - Bar railway line is approximately 1000 m. The reason for

$F_{kmin}$  – minimum necessary train brake force value and  $S_{max}$  – maximum prescribed length of train braking distance.

Such written requirement for necessary train brake force value can be used for comparing train brake force depending to preset train movement parameters for certain train composition, at the specific railway line and the specific place of train braking. It is possible to write this by inequality using some of the previous expressions (10) and (18).

this is planned installation of automatic block system, i.e. block signals. Each distant signal, is shifted from station home signal at about 1000m. This is usually distance between them. Automatic block system on this railway line is never done, but distant signals remain in places for future installation of block signals, at a distance of 1000 m in front of home signals.

Length of stopping distance 1000 m under normal conditions, speeds up to 100 km/h, at parts of the railway line in a small negative gradient and for normal braked train is enough. Problem represent parts of the route which are largely represented by large negative gradients. Under the term "small negative gradient" are considered default gradients usually represented on the lines, in the range between the horizontal and gradient of about ten promiles. Each gradient greater than about ten promiles in this paper is discussed under the term "greater negative gradient".

##### 4.1. Critical sections of the Belgrade – Bar railway line where trains stop

As at on a large part of the Belgrade – Bar route are gradients greater than ten, it is clear that there are sections of route where it is difficult to stop trains. When looking parts between distance and home station signals, track sections in gradients from 15 ‰ to 20 ‰ are, for example:

- Valjevski Gradac – Lastra,
- Užice – Stapani,
- Stapani – Sušica,
- Sušica – Branešci,
- Bijelo Polje – Kruševo,
- Kruševo – Mijatovo Kolo,
- Mijatovo Kolo – Mojkovac,
- Mojkovac – Trebaljevo,
- Trebaljevo – Kolašin,
- Kolašin – Mateševo,
- Mateševo – Kos and
- Kos – Trebešica.

Considering that there are many sections with a gradient greater than 10 ‰ and 15 ‰, critical sections, in this paper, shall be considered the ones between distance signals and station home signals which have gradients greater than 20 ‰. There are three such sections:

- Trebešica – Lutovo,
- Lutovo – Bratonožići and
- Bratonožići – Bioče.



In case of any need to stop trains at home signals some of the above stations (home signals of Lutovo, Bratonožići and Bioče, because the railway line on that part have negative gradient in direction to Podgorica) train braking is performed on negative gradient of 25 ‰. Distances between distance and home signals have one parts without curves and other parts with curves. Radius of these curves are in the range from 300 m to 500 m.

For purposes of simplified calculations in this paper is considered a curve radius of 400 m and length of 300 m. Maximum permitted speed of trains on these three sections is 60 km/h. On each of these sections there are tunnels of different lengths.

#### 4.2. Values of resistances force at the critical sections of the Belgrade – Bar railway line

Total force of resistances that occur on the line is equal to the sum of all individual resistance forces (hereinafter referred as resistance). For the present case there are locomotive basic resistances, vehicle basic resistances, resistance of gradients, curve resistances and tunnel resistances.

Locomotive basic resistances (21) depend on constructive characteristics of locomotives and in some cases their value given by locomotive manufacturer, in some cases are determined experimentally, but it is possible to adopt a certain value, as in the case of this paper. Values for locomotive basic resistances for different speeds of movement amounts:

$$\begin{aligned} W_{o160} &= 350 \text{ daN}; W_{o150} = 300 \text{ daN}; \\ W_{o140} &= 250 \text{ daN}; W_{o130} = 200 \text{ daN}; \\ W_{o120} &= 150 \text{ daN}; W_{o110} = W_{o10} = 100 \text{ daN}; \end{aligned} \quad (21)$$

During train braking different locomotive basic resistances act on the train at any moment. With adequate precision it could be taken a unique value obtained as average of the values at different speeds from the range of speeds during braking. Then the locomotive basic resistances are equal:

$$W_{o1} = 200 \text{ daN} \quad (22)$$

Vehicle basic specific resistances depend on movement speed and total vehicle basic resistances are equal to product of their specific values and total mass of all vehicles. Specific values can be found using the known forms which are applicable on railway.

$$\omega_{ok} = 2.2 - \frac{80}{V + 38} + (k + 0.007) \cdot \left(\frac{V}{10}\right)^2 \quad (23)$$

Coefficient „k“ depends on the type of train composition. In the case of mixed freight train composition  $k = 0,057$ , if it is a freight train homogeneous composition  $k = 0,032$  and in the case of a passenger train of four-axled passenger vehicles then  $k = 0,025$ . The calculated values of vehicle basic specific resistances are shown in tables.

Table 1: Basic specific vehicle resistances of mixed freight train composition

V km/h	60	50	40	30	20	10
k	0.057	0.057	0.057	0.057	0.057	0.057
$\omega_{ok1}$ daN/t	3.69	2.89	2.20	1.60	1.08	0.60

Table 2: Basic specific vehicle resistances of freight train homogeneous composition

V km/h	60	50	40	30	20	10	0
k	0.032	0.032	0.032	0.032	0.032	0.032	0.032
$\omega_{ok2}$ daN/t	2.79	2.27	1.80	1.37	0.98	0.57	0.09

Table 3. Basic specific vehicle resistances of passenger train

V km/h	60	50	40	30	20	10	0
k	0.025	0.025	0.025	0.025	0.025	0.025	0.025
$\omega_{ok3}$ daN/t	2.54	2.09	1.69	1.31	0.95	0.57	0.09

During train braking different vehicle basic resistances act on the train at any moment. With sufficient accuracy can be taken a unique value obtained as the average of values at different movement speeds from the range of speeds during braking.

Masses of trains for purpose of this case amount:

- 880 t for all freight train vehicles,
- 120 t for locomotive and
- 120 t for three passenger coaches.

Accordingly mass of observed freight train is 1000 t and mass of observed passenger train is 240 t.

Using the values of previously set masses, vehicle basic resistances are:

$$W_{oktm} = \omega_{ok1} \cdot Q_k = 1.74 \frac{\text{daN}}{\text{t}} \cdot 880 \text{ t} = 1531 \text{ daN} \quad (24)$$

$$W_{okth} = \omega_{ok2} \cdot Q_k = 1.41 \frac{\text{daN}}{\text{t}} \cdot 880 \text{ t} = 1241 \text{ daN} \quad (25)$$

$$W_{okp} = \omega_{ok3} \cdot Q_k = 1.32 \frac{\text{daN}}{\text{t}} \cdot 120 \text{ t} = 158,4 \text{ daN} \quad (26)$$

Where:

$W_{oktm}$  – vehicle basic resistances of mixed freight train composition,

$W_{okth}$  – vehicle basic resistances of freight train homogeneous composition and

$W_{okp}$  – vehicle basic resistances of passenger train.

Gradient resistances depend on mass of the train and specific gradient resistances. Specific gradient resistances numerically are equal to gradient values expressed in promiles. For the observed part of the railway line which is located on a constant negative gradient of 25 ‰, gradient resistances values are:

$$W_{it} = \omega_i \cdot Q_{vt} = -25 \frac{daN}{t} \cdot 1000 t = -25000 daN \quad (27)$$

$$W_{ip} = \omega_i \cdot Q_{vp} = -25 \frac{daN}{t} \cdot 240 t = -6000 daN \quad (28)$$

Where:

$W_{it}$  – gradient resistances of freight train,

$W_{ip}$  – gradient resistances of passenger train,

$\omega_i$  – specific gradient resistances,

$Q_{vt}$  – mass of freight train and

$Q_{vp}$  – mass of passenger train.

Curve resistances depend on specific values of curve resistances, mass and train length. Dependence of these resistances on the length of train exists only if the length of train is longer than length of curve. For the purposes of this calculation the length of each train is shorter than the length of the curve. Specific values of curve resistances depend on curve radius values. Specific values is possible to find using the known forms that apply to the railway. For analyzed example curve resistance values are:

$$W_{kt} = \omega_k \cdot Q_{vt} = \frac{650}{R_k - 55} \cdot Q_{vt} = 1884 daN \quad (29)$$

$$W_{kp} = \omega_k \cdot Q_{vp} = \frac{650}{R_k - 55} \cdot Q_{vp} = 452 daN \quad (30)$$

Where:

$W_{kt}$  – curve resistance of freight train,

$W_{kp}$  – curve resistance of passenger train,

$\omega_k$  – specific curve resistance and

$R_k$  – curve radius.

Considering that the three observed sections include short rail tunnels, resistance value of the tunnel is ignored. Sum of all resistances makes resistances force and it is equal to the sum of the previously calculated resistances:

$$\sum W = W_{ot} + W_{ok} + W_i + W_k \quad (31)$$

Table 4: Sum of all resistances of three different train compositions

Type of train composition	Mixed freight train composition	Freight train homogeneous composition	Passenger train
$\sum W$	-21385 daN	- 21675 daN	- 5190 daN

#### 4.3. Brake force of three different train compositions

In order to determine train brake force, using expression (20), next to known and by now calculated values it remains to determine the values of individual decelerations and speeds which figuring in this expression. Train deceleration can be found using expression (7). When train is braked by maximum braking force, then at the calculation of stopping distance it is enough to use three speed ranges and three different deceleration values. Thus calculated value will have acceptable accuracy. The

proof for this claim is the value of one train deceleration in the range up to 4. second since the initiation of braking, when established pressure value in brake cylinder corresponding to initial stage of braking, then the value of deceleration in the range from 4. second to the moment of establishing half of the maximum pressure value in brake cylinder and the final value of deceleration (maximum achievable train deceleration) at the last time interval, corresponds to maximum achievable pressure in brake cylinder and which remains unchanged to a stop. Each time interval corresponds to certain change of movement speed. Length of stopping distance of such braked train is:

$$S = V_1 \cdot t_{rko} + \frac{V_1^2 - V_2^2}{2 \cdot a_1} + \frac{V_2^2 - V_3^2}{2 \cdot a_2} + \frac{V_3^2 - V_4^2}{2 \cdot a_3} \quad (32)$$

Diagram of train braking distance for the present case is shown in Figure 1.

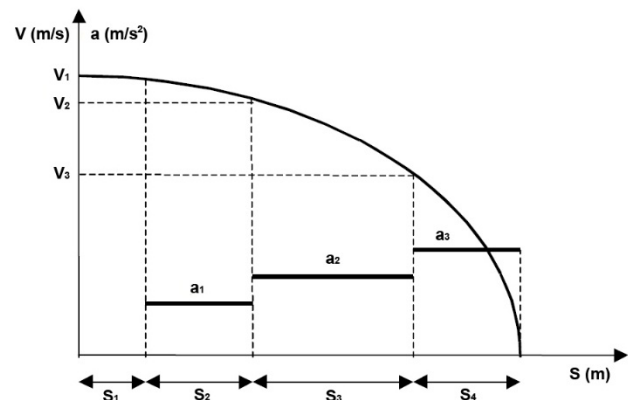


Figure 1. Train braking diagram

By replacing the appropriate values into expression (32) the required deceleration values are obtained. During the first interval of the observed braking in brake cylinder pressure increase is established and it takes approximately 4 seconds. In the second interval pressure in the brake cylinder increases to a certain value corresponding to approximately one quarter of maximum pressure which will be achieved in the shown braking, without brake release or reduction of pressure. In the third interval pressure in the brake cylinder continues to increase and the increase lasts until it reaches maximum pressure corresponding to given loss of air pressure in the main train air conduit. During the entire fourth interval the maximum air pressure in the brake cylinder is presented and then the train has approximately constant value of deceleration. According to previously written, and follows expression (32) it is possible to find train maximum deceleration value.

$$a = \frac{4 \cdot V_1^2 - 2 \cdot V_2^2 - V_3^2 - V_4^2}{2 \cdot S - 2 \cdot V_1 \cdot t_{rko}} \quad (33)$$

Maximum required train deceleration, for the length of stopping distance of 1000 m, initial speed  $V_1 = 60 \text{ km/h}$ , end speed  $V_4 = 0 \text{ km/h}$  and for the values  $V_2 = 55 \text{ km/h}$  and  $V_3 = 40 \text{ km/h}$  from the braking diagram is:  $a = 0.279 \frac{m}{s^2}$

The minimum required train brake force, that would enable previously calculated value of the maximum deceleration is obtained based on expression (10) and its

values, for the three discussed types of train, are given in the table 5.

Table 5: The minimum required train brake force value

Type of train composition	Mixed freight train composition	Freight train homogeneous composition	Passenger train
$F_{kmin}$	49285 daN	49575 daN	11886 daN

The same value of of the minimum required braking force are obtained by replacing the same values the speeds and decelerations into expression (20).

## 5. CONCLUSION

In train traffic planning it is often necessary to introduce into traffic some new train or to modify existing train composition. Also, at the railway is common introduction of new rolling stock, special traction vehicles. Each railway vehicle must fulfil conditions of certain standards that it would be able to operates on some railway network. Each railway line on the same network has its own characteristics, which is different from other. For example such is the Belgrade – Bar railway line which has route characteristics significantly different from other railway lines in the region.

When arises need for homologation or testing of new vehicle then special attention is paid to the braking characteristics of the vehicle. For existing fleet some parameters of vehicles braking characteristics are already fortified. Follows from vehicle braking characteristics values of maximum vehicles braking force is known. In case of need, this value can be used for finding some other important parameters during braking. Same is true in the opposite, when the values of some parameters of braking must be fulfilled, then by using the values of braking forces is checking if vehicles satisfy these parameters. Parameters of individual vehicles, into sum of all vehicles together, may provide significant parameters of the entire train compositions.

This paper presents a few ways to compare each other parameters values of the train and individual vehicles

during their braking to a stop. Relation between the braking force, distance, deceleration, resistance force, movement speed and elapsed time is considered. To make it easier to comprehend the full story related to problems of train braking at the critical sections of some railway line, example of three different train braking is made for critical sections of the Belgrade – Bar railway line.

## REFERENCES

- [1] A. Hougardy, A. Chiappini, P. Guido, "Introduction to ETCS Braking curves", European Railway Agency, Ertms Unit, (France), (2016)
- [2] M. Vukšić, "Effect of Response Time on Stopping Distance", Institute "Kirilo Savić", Belgrade, Research accessory, Vol. 32(1), (Serbia), (2014)
- [3] P. Presciani, M. Malvezzi, G. L. Bonacci and M. Balli, "Development of a Braking Model for Speed Supervision Systems", FS – Trenitalia, University of Florence, (Italy), (2012)
- [4] RSSB, "Braking System and Performance for Freight Trains", Torrens Street, London, (England), (2011)
- [5] C. Cruceanu, "Train Braking", University Politehnica of Bucharest, (Romania), (2012)
- [6] UIC CODE 544-1, "Brakes – Braking power", 4<sup>th</sup> edition, Paris, (France), (2014)
- [7] D. Barney, D. Haley and G. Nikandros, "Calculating Train Braking Distance", Queensland Rail, Brisbane, (Australia), (2002)
- [8] D. Vujović, "Princip funkcionisanja kočnja i kočnica voza i neke neregularnosti u radu kočnica", Saobraćajni fakultet, Univerzitet u Beogradu, Završni rad, (Serbia), (2014)
- [9] D. Vujović, "Princip rada kočnica na železničkim vozilima i faktori koji utiču na dužinu zaustavnog puta", Saobraćajni fakultet, Univerzitet u Beogradu, Master Thesis, (Serbia), (2015)



# Methods for Carrying Out Track Maintenance and Optimization Opportunities

Metodi Atanasov

<sup>1</sup>Faculty of Machinery and Construction Technologies in Transport, University of Transport "Todor Kableshkov", Sofia (Bulgaria)

The report examines the present system for detecting irregularities and the methodology to fulfil repairs on the railway network in Bulgaria. There is a review made of the different defects and deviations from the geometry which required maintenance work on railway track. In the report is made an analysis of the problems in infrastructure maintenance work. Based on the analysis are described possibilities of applying methods to predict the deterioration of the railroad and optimization of track maintenance. The report aims to establish the workability of methods for optimizing maintenance and cost effectiveness of the Bulgarian railway track maintenance in presence of limited funds for maintenance. Based on this analysis the report presents recommendations for opportunities to integrate the optimized track maintenance systems.

**Keywords: Railway, Track, Deterioration, Maintenance**

## 1. INTRODUCTION

The railway network in Bulgaria is 4071 km long with a standard track gauge of 1435 mm, of which 24% is double-track and 67% electrified. The maintenance and the repair works of the railway lines are integrated into a complex system of activities which are carried out according to the technological processes for a certain type of repair. The main section for exploitation and maintenance of the railway infrastructure in the country is the "Railway infrastructure and equipment". This unit performs monitoring of the good railway condition. As a result of the system reorganization it is necessary to implement methods to improve the availability of the track in order to reduce the maintenance costs, to achieve better track conditions and safety of the railway traffic. The construction of the strategic railway infrastructure in Republic of Bulgaria along the main directions which are part of the Trans-European corridors will be accompanied by an increased operational traffic and need of optimization of the maintenance system.

## 2. DEFECTS AND DEVIATIONS IN RAILWAY SYSTEM

### 2.1. Rails

The rails are the main element of the superstructure which takes over the train load. On the other hand the rails support and guide the wheels of the train vehicles. Taking over train loads generates greater intensity of deformation in the track.

The determination of the wear depends on the axle load, the maximum speed and the distance between the sleepers. The largest contact stresses are concentrated in the area of the railhead where plastic deformation are also created.

There are two types of the rail wear – vertical and lateral. Vertical wear reduces the rail section and consequently the rail resistance. The maximum permissible vertical wear of the rail is a function of the maximum train speed and of traffic load. Lateral wear reduces the rail section and consequently the rail resistance

and affect to the gauge of the track too. As in case of vertical wear, the maximum permissible lateral wear of the rail is a function of the maximum train speed and of traffic load.

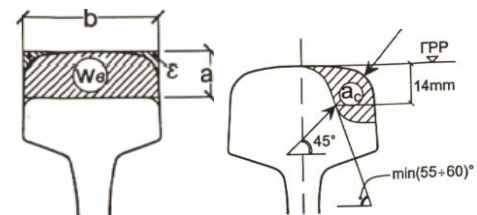


Figure 1: Vertical and lateral wear of the rail [1]

$b$  – the width of the railhead;

$a$  – vertical wear in the middle of the railhead;

$W_e$  – area of the worn profile ;

$\varepsilon$  - the area that is in the corners of the profile;

$a_c$  – lateral wear measured 14 mm from the top edge of the rail at an angle of 45°.

The side wearing of the rails has different meaning from train traffic safety point of view and from protection of derailment point of view.

The total admissible wear is obtained as a sum of the vertical and the lateral wear. It is used to determine the time which is needed in order for the rails to be changed.

The maximum admissible vertical wear of the UIC60 (60E1) rail is  $a=22$  mm and the maximum admissible lateral wear is  $a_c=11$  mm. The total admissible wear is 12 mm at speeds of 120 km/h and more, regardless of the track classification. In case the web of the rail is thinner than 10 mm, regardless of its type, the rail is removed from the railroad. [2]

It is essential for the normal exploitation of the railway track to have detection, classification and study of the rail defects on time. Defects are catalogued according to their position, appearance and cause in the UIC leaflet 712. The current classification contains 55 different types of rail defects. The most common defects are shown in table 1.

The stress is so high that it can lead to plastic deformation of the wheel and the rail, particularly when tangent forces (slip, braking and acceleration forces) occur together with the vertical forces. [3]

Those stresses gradually decrease the mechanical strength of the rail due to repeated loading. That is called fatigue. Once the fatigue limit is reached, the rail is brought to failure.

Table 1: Most frequent rail defects in long welded tracks [3]

Numbering	Short designation of the rail defect
111 /211	Tache ovale
2222	Shelling
2223	Head Checks
not contained in the UIC leaflet	Belgrospis
227	Squats
301	Indentations
125/225	Skid marks
2201	Corrugation
2202	Waves
411/421/431	Cross-cracks (welding)

Corrugation is one of the most common defects in the rails. There are various attempts to explain the development of corrugation. It only seems to be certain that corrugation is caused by friction, slipping and oscillation processes between wheel and rail. Corrugation increases the vibration and dynamic stresses of the track, reduces durability of the rails and other elements from superstructure. The typical wavelength is 3-6 cm, depth is 0.1-0.4 mm. They occur mainly in places where the vehicles move in sinusoidal form, as, e. g. on straight track or in curves with large radius. [4]. Corrugations are removed by rail planning, rail milling or rail grinding machines.

## 2.2. Rail fastening

The purpose of the rail fastenings is to maintain track gauge and transmit forces acting on and in the rails to the sleepers. They contribute to the spatial consolidation and ensuring the necessary elasticity of the track. Another function of the fastening system used on concrete sleepers is to electrically insulate the sleeper against the remaining track grid. [3] The rail fastenings perform their function normally when they are sufficiently tightened. A moment of torsion of  $250 \pm 10\%$  Nm has to be applied to the elastic fastenings SKL-14. When a moment of torsion is less than 160 Nm, they have to be retightened under an operating condition. The track section performs control measurements using torque wrench to determine the moment.

## 2.3. Elastic rail pads

Rail pads serve as an elastic damping element which decouple vibration. Only elastic rail pads which are able to absorb the torque of the sleepers can absorb the forces acting in a longitudinal track direction (acceleration, braking and temperature forces). This means that the rail pad also has a load distributing effect. The rail fastenings

must withstand the creeping movement. Creep is eliminated by using fastening with a sufficient clamping force and ballast with an adequate shearing form.

## 2.4. Sleepers

The Bulgarian Railway Administration uses wooden and reinforced concrete sleepers. Replacement of wooden sleepers with concrete sleepers is obligatory for the construction of a welded track with rails (60E1). The main function of the sleepers is to transmit the forces from the rails to the ballast bed and to provide stability of the track.

The life cycle of wooden sleepers is 25-45 years - depending on the quality and sort of wood used, as well as on the methods of impregnation. The wooden sleeper may bend or twist due to the drying and impregnation process of the wood. Defects of wooden sleepers occur due to base plates pressed into the sleeper, widening of the fastening holes and occurrence of longitudinal cracks and defects due to rusty water coming from the fastenings. [5]



Figure 2: Decay and defects due to rusty water coming from the fastenings

There are two basic types of concrete sleeper. The first one consists of two blocks of reinforced concrete connected by a coupling rod or pipe. The second one is a monoblock sleeper which is based on the shape of a beam.

Concrete sleepers are loaded and tested statically in accordance with the expected operational loads. It is accepted that the monoblock concrete sleepers with "K" type rail clip are to be laid in curves with a minimum radius of 300 m for jointed track and radius of 500 m for welded track.

When a sleeper is loaded by a wheelset, it is advantageous to know which part of the load the individual sleeper has to take. Due to the elasticity of the permanent way the rail sags and acts therefore as a load distributor. The optimum settlement of the rail under a 22.5-ton axle is about 1.5 mm.

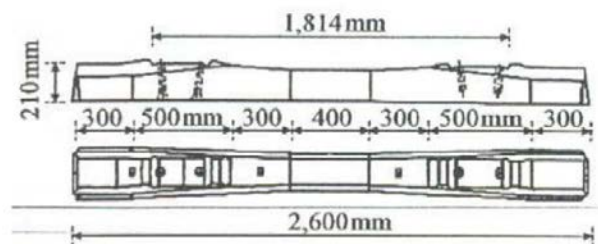


Figure 3: Monoblock concrete sleepers

Disadvantages of the concrete sleepers are sagging of the sleepers during handling, manual tamping or tamping with heavy-duty tamping machines. Defects due

to corrosion or fatigue of the steel beam and related track gauge defects.

### 2.5. Ballast bed

The ballast bed's task is to transmit the sleeper pressure to the subsoil, to ensure good air condition and water permeability in order to maintain the bearing capacity of the subsoil, and also to ensure the track elasticity in order to minimize dynamic forces and to provide high resistance towards longitudinal and lateral sleeper displacement.

The construction of a ballast bed is using crushed ballast with grain size of 22 mm to 60 mm. The shape of ballast grains should be close to the cubic form with sharp edges according to BDS EN 13450:2003/AC:2005.

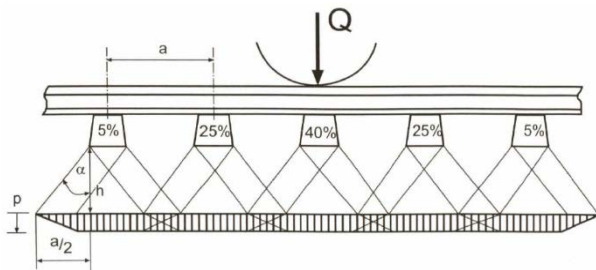


Figure 4: Load distribution on sleepers [3]

The optimum ballast thickness is the thickness where ballast exerts constant pressure on the formation.

The reasons for the deterioration of the ballast are: operational load of the dynamic forces which may overstress the ballast and lead to shelling, grain shifting and abrasion. Maintenance work - wear by tamping or cleaning. Material rising from the subsoil, if there are no formation protection layers or if they are defective. Ballast contamination by lost cargo, remainders of vegetation and other environmental influences. [3]

If the bed of a heavily contaminated track is not cleaned, but if the track is only tamped in these areas, it will return to a poor geometric position within a short time.

After ballast cleaning, it is necessary to move the track into its design position, restore the ballast bed cross section, consolidate the ballast properly and stabilise the track. The track position is restored and the track is stabilised in one operation with the help of a group of machines like as ballast regulating machine and a Dynamic Track Stabiliser (DTS).

The state of the art to achieve spatial consolidation together with restoration of the resistance to lateral displacement, is the dynamic stabilisation of the track after tamping and sleeper end consolidation. [6] As unconsolidated material may be consolidated best by horizontal vibration, this fact was used for the Dynamic Track Stabiliser (DTS).

### 3. IDENTITY FAULTS AND TRACK MAINTENANCE WORK PROCESSES

Track gauge and superelevation are controlled by a measuring device for measuring the track gauge and superelevation. It is for track gauge 1435 mm -10 mm to +40 mm and superelevation -35 mm to +195 mm. The construction is equipped with measuring bolt for flat bottom rails (14 mm).



Figure 5: Control of the track gauge and superelevation

Track measuring laboratory "PLASSER & THEURER" EM-120, which is intended for measuring of geometrical parameters of the railway track in Bulgaria. The movement of the track measuring laboratory EM-120 is self-propelled with measuring speed of 120 km/h in both directions. The record of the measured values of the railway track parameters is made every 250 mm simultaneously and in synchronized manner on magnetic type and on PC's hard-disk in a uniform format. With the help of the measuring-analyzing computer system the data is processed and printed out on paper in real time.



Figure 6: Measuring laboratory EM - 120[7]

The track measuring laboratory has an analyzing system that compares the values measured with the set-up in advance limiting values in accordance with the category and the class of the measured track section. This analytical report, indicating the values (the defects) that exceed the admissible limits for the relevant class and category of the railway track are indicated by a separate printing device in real time during the measuring of the track.

The overall assessment of railway track is determined based on the measurements made by the laboratory. The above mentioned assessment defines the overall condition of the track. It is obtained as a sum of the penalty units for each kilometre and after that an average value for each section of the railway network.

Unfortunately, the track measuring laboratory is not equipped with a video recording camera which is a major disadvantage. Possibilities should be further explored in order to implement laser railway scanning which will help to detect defects and to assess the condition of the railroad.

Researches primarily use the laser setup described for high precision gage detection. Along with this setup, researchers have also developed a second setup consisting of high-speed line scan cameras. This setup helps obtain high-resolution images without any motion blur. [8]

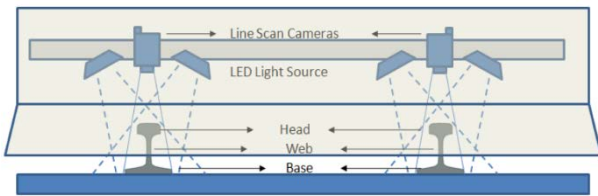


Figure 7: Graphical illustration of the proposed setup for image acquisition [8]

The main goal for using images of the track is to eliminate, or reduce as much as possible, the visual inspection done by workers walking along the track to detect any fault, missing components, etc. The state of the art of these instruments does not yet allow a complete and safe elimination of the inspection done by humans, but helps a lot and, also, allows detecting a number of risky situation difficult to detect by the human eye.

The restoration of the ballast geometry is performed by the "ballast profiling machine" which is a special train which can pull, move or replace the ballast by its mechanical blades, and give the ballast the adequate cross section profile. [9]

The ballast becomes dirty as a result of the splitting and abrasion of the ballast particles under traffic loading, materials falling from wagons and weed growth. Dirty ballast results in reduced carrying capacity so that the ballast is unable to fulfil its function. A critical level of fouling is reached when 40% of the total consist of fine material – at this level surface water is prevented from draining away properly. [10]

The ballast cleaning machines are able to reach around 25 cm below the sleepers and grab stones smaller than 25 mm in order to replace them. The different ballast machines can work together, in an only "tramping train", which increases the performance of all of them.

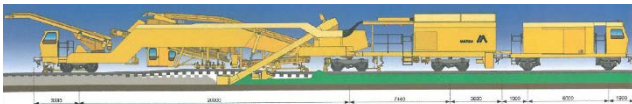


Figure 8: The ballast-cleaning machine from Matisa [11]

The tamping operation restores the track to the desired geometrical position. Conventional tamping machines operate in cycles: to advance from one sleeper to the next the entire machine has to accelerate from standstill. A dynamic track stabilizer (DTS) is incorporated in the machine and gives a stable, safe and long-lasting track condition. This combination incorporates improvements in its levelling system, enabling it to compensate for greater sinking resulting from stabilization through a predefined amount of lift during tamping, thereby producing optimum longitudinal elevation.

Table 2: Tamping machines in National railway infrastructure company (NRIC), Bulgaria

Type of the heavy-duty tamping machine	Factory number	Register number in NRIC	Company
Tamping machine 08 327	2822	9952 9423008 – 2	„Plasser & Theurer” Austria
Tamping	2267	9952 9423	„Plasser &

machine 08 323		009 – 0	Theurer” Austria
Tamping machine 07 325	1807	9952 9423 007 - 4	„Plasser & Theurer” Austria
Tamping machine B45L - 1	4504	99529423 002-5	„Matisa” - Switzerland
Tamping machine B 45L - 2	4505	9952 9423003 – 3	„Matisa” - Switzerland
Dynamic track stabilizer DGS62N-2	434	9952 9420 002 - 8	„Plasser & Theurer” Austria
Ballast profile machine SSP203 - 2	642	9952 9425 004 - 9	„Plasser & Theurer” Austria

Heavy-duty tamping machines in section Vratza are shown in table 2. What is specific in their construction and equipment are the performed operations related to the repair and maintenance of the railway infrastructure.

It is necessary to purchase new heavy-duty machines which should be more functional and productive. NRIC needs to explore new technologies and possibilities to combine several working operations in one machine. This is very important because among the advantages of the machines are the cost efficient utilization of track possession and the planning maintenance.

#### 4. MATHEMATICAL MODELS FOR FORECAST OF THE DETERIORATION

The following models deal with the problem of defining the strategic maintenance concept for single elements of the infrastructure based on long-term deterioration or degradation models.

##### 4.1. ORE model

This model is developed by Office for Research and Experiments (ORE) of International Union of Railways (UIC). The deterioration is divided into two parts describes the deterioration directly after tamping  $e_0$ , and the second part describes the deterioration depending on traffic volume  $T$ , dynamic axle load  $2Q$  and the speed  $v$ . The condition of the railway track is determined by the following formula:

$$e = e_0 + h.T^\alpha (2.Q)^\beta .v^\gamma = m \cdot a \quad (1)$$

, where  $h$  is a constant and the parameters  $\alpha$ ,  $\beta$  и  $\gamma$  have to be estimated from experimental data. UIC suggests these values when the data doesn't exist  $\alpha = 1$ ,  $\beta = 3$ . Further, it is assumed that the influence of the speed can be neglected, implying that  $v^\gamma$  need not be treated separately, but may be included in the proportionality factor  $h$ . [12]

##### 4.2. The German study

Experiments under well controlled laboratory conditions at the Technical University of Munich representative of vehicles passing a dipped joint have been used to establish equations to calculate rate of settlement.

$$S = a.p.\ln \Delta N + b.p^{1.21}.\ln N \quad (2)$$

The first term represents the fast settlement just after a maintenance action.  $\Delta N$  expresses a pre-loading



period comprising the first passing axles.  $\Delta N$  should be  $\leq 10000$  and  $N$  in the second part should express the total number of passing axles. The ballast pressure ( $p$ ) should be calculated with the Zimmermann method. The parameters are constant suggested to be in the value range 1.57-2.33 for (a) and 3.04-15.2 for (b). [12]

4.3. Sato model

Sato studied the track degradation from track superstructural perspective. The degradation model developed by Sato is based on the growth of track superstructures conditions. The expression given for the deterioration is related to the passed tonnage, average velocity, structure factor, jointed or type CWR (Continuously Welded Rail) and quality of subgrade.

$$S = 2.04 \cdot 10^{-3} \cdot T^{0.31} \cdot V^{0.98} \cdot M^{1.10} \cdot L^{0.21} \cdot p^{0.26} \quad (3)$$

Where  $S$  is the average growth in section (mm/100days) as the main criterion of the track super structure condition,  $T$  is the passed tonnage (million tons/year),  $V$  is the average running speed (Km/h),  $M$  is the structure factor,  $L$  is the influence factor for jointed rail or CWR (1 for CWR and 10 for jointed) and  $P$  is the influence factor for subgrade (1 for good and 10 for bad). [13]

4.4. Shenton model

Shenton considered track settlement as the main controlling factor of track degradation from the sub structural aspect. The causal parameters which influence this settlement are sleeper type and size, ballast type, ballast and subgrade condition, the lift given by the tamping machine, equivalent axle load, and load cycles. The general equation which quantifies the track settlement is as follows:

$$S = K_s \cdot \frac{A_e}{20} \cdot ((0.64 + 0.028 \cdot L) \cdot N^{0.2} + 2.7 \cdot 10^{-6} \cdot N) \quad (4)$$

Where  $A_e$  is the equivalent axle load,  $N$  is the total number of passed axles,  $L$  is the lift given by the tamping machine and  $K_s$  is a factor which is a function of sleeper type and size, ballast type and of the subgrade. [13]

4.5. Bing and Gross model

Bing and Gross report on US model based on 460 observations from a test track, are estimated. An overall track geometrical quality index (TQI) is used as the main track degradation criterion from the geometry aspect. The final model includes the current geometry conditions of the track, speed, age of rails, ballast index, and the time since the last maintenance activity.

$$\frac{TQI_2}{TQI_1} = 1.25 \cdot \left(\frac{TQI_1}{TQI_1^*}\right)^{-0.58} \cdot \left(\frac{V_E}{V_E^*}\right)^{-0.18} \cdot \left(\frac{R_A}{R_A^*}\right)^{-0.11} \cdot \left(\frac{BI}{BI^*}\right)^{1.04} \cdot (1 + FS)^{-0.44} \quad (5)$$

In which  $TQI_1$  is the initial track quality index for the time period,  $TQI_2$  is the final track quality index for the time period,  $V_E$  is the equivalent train speed,  $R_A$  is the rail age,  $BI$  is the ballast index,  $FS$  is the fraction of segment surfaced.  $V_E^*$  and  $R_A^*$  are arbitrary fixed reference values of each parameter.

Ballast index  $BI$  is given by following formula:

$$BI = AI(BC + 1)^{1/3} + DF \quad (6)$$

, where  $AI$  is the aggregate index,  $BC$  is the ballast condition on a scale of zero for excellent to 3 for poor conditions,  $DF$  is the drainage factor (10 for good and 20 for bad conditions). Ballast index values range from 40 for excellent to 120 for very poor. [13]

4.6. Zhang model

Zhang has developed the Integrated Track Degradation Model (ITDM) model, which is a mechanistic model of track degradation. The mechanistic nature of ITDM means the model is railway system independent. The model does not require detailed historical track condition data to operate. This makes ITDM an ideal candidate track degradation model to use with Track Maintenance Planning Model (TPM) as it fits well with the stated objective that the model operates with a minimum of track condition and activity monitoring data. [14]

5. DETERIORATION OF THE RAILWAY TRACK

5.1. Influence of the speed

We will use calculations from the Sato model to illustrate the influence of the speed. The value of the deterioration at speed 160km/h is 37% higher than at speed 100 km/h at 24 mgt per year. At 6 mgt per year the difference in values is again 37% at lower relative values. This shows significantly higher rate of deterioration at high speeds.

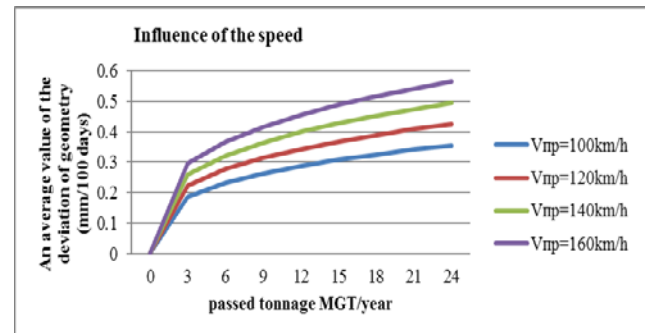


Figure 9: Influence of the speed [15]

5.2. Influence of the type of the track - jointed or welded track

The influence will be determined using the Sato model where the  $L$  parameter in formula is 1 for jointed track and 10 for welded track. Operational load of 24 mgt per year, the deterioration in jointed track is 45% higher than in welded track.

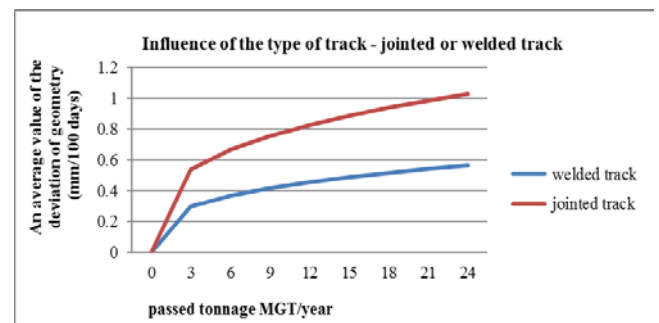


Figure 10: Influence of the type of the track – jointed or welded track [15]

### 5.3. Influence of the subgrade

The Sato model determines the influence of the subgrade on a scale from 1 to 10. Figure 11 shows the total deterioration of the track at a different condition of subgrade. Values at a very poor subgrade are 38% higher than a very good subgrade. This shows a great influence on the condition of the subgrade in the railway infrastructure.

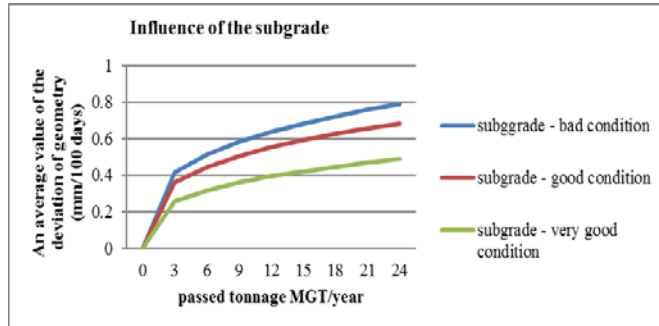


Figure 11: Influence of the subgrade [15]

### 5.4. Influence of the axle load

Using the Shenton model, we determined the depth of the settlement. It is obtained at different axle load values and different vehicle passing cycles. The total deterioration of the railroad is 29% higher at an axle load of 22.5 t compared to 16 t (at 10 000 cycles).

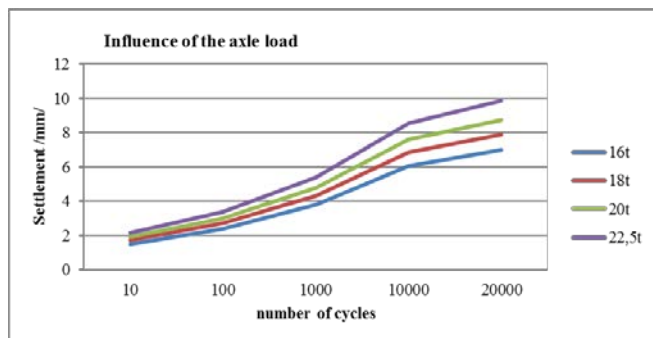


Figure 12: Influence of the axle load [15]

## CONCLUSION

The examined mathematical models allow to establish the relationship between the various track parameters and their impact on the deterioration of the track in result of exploitation. On the basis of the presented results there is an opportunity to make a combination of jointed and welded track with a permissible axle load. The application of modern maintenance technology enhances the value of modern railway operation and enables the track system to be kept in top condition. The possibility of integrated predictive deterioration models in the NRIC should be further

explored as it will help optimizing the maintenance and reduction the total cost of repairs in the railway infrastructure.

## REFERENCES

- [1] Z. Dencheva, "Superstructure and maintenance of the railway", Bulgaria (Sofia), (2014)
- [2] "Instruction for the structure and maintenance of the superstructure of the track and the railway switches", Sofia, (2010)
- [3] B. Lichtberger, "Track Compendium", Eurailpress Germany (Hamburg), (2005),
- [4] R. Clark, "Rail Corrugation - recent theories", Research & Development Division, British Railways Board, p. 899
- [5] R. Ahlf, "Matching M/W practice to require use of track - Part II: ties and ballast", RT&S Railway Track & Structures, (1979)
- [6] K. Klugar, "Überlegungen zur Stabilisierung des Gleises", TU-Graz, Vortrag in Budapest, Juni, (1977)
- [7] <http://tinsabg.com>
- [8] M. Shah, "Automated visual Inspection/Detection of railroad track", July, (2010)
- [9] N. Jimenez, A. Barragan, P. Cembrero, F. Benitez, N. Caceres, F. Schubert, A. Simroth, C. Santanera "Automated and cost effective railway infrastructure maintenance", (2011)
- [10] B. Lichtberger, "The track system and its maintenance" RTR Special, July, (2007)
- [11] K. Riebold "Heavy-duty track machines – an overview – RTR Special, July, (2007)
- [12] I. Misra, B. Krishna, "Handbook of Performability Engineering", Springer Science & Business Media, (2008)
- [13] J. Sadeghi, and H. Akarinejad, "Influences of track structure, geometry and traffic parameters on railway deterioration", November, (2007)
- [14] S. Simson, L. Ferreira, M. Murray, "Modelling rail track maintenance planning using simulation", (1999)
- [15] V. Zhekov, M. Atanasov, "Optimization of the railroad maintenance through calculation models used for forecast of the deterioration during exploitation", Mechanics Transport Communications Vol. 3, pp. 72-77, (2015)

# Measurements of Noise Levels of Freight Train on Serbian Railways

Jelena Tomić<sup>1\*</sup>, Nebojša Bogojević<sup>2</sup>

<sup>1</sup> School of Electrical Engineering, University of Belgrade, Serbia, tomic.j@mfv.kg.ac.rs

<sup>2</sup> Faculty of Mechanical and Civil Engineering in Kraljevo, University of Kragujevac, Serbia

*During the last few years Serbian Railways introduced several new types of rail vehicles for passenger transport, but for the freight transportation, the main type of the locomotive remains diesel unit of class JŽ 661. The freight composition usually consists of a large number of loaded vehicles pulled up by a locomotive. The freight trains operate day and night on commercial tracks and, therefore, represent a significant source of noise in the urban areas. This paper describes the measurement procedure for the assessment of the noise levels of the freight trains on Serbian railways. The equivalent noise level and one-third octave spectrum of the diesel unit are measured in stationary condition and during freight composition running at constant speed. All measurements are conducted according to the ISO 3095:2013 standard.*

**Keywords:** noise, railway, measurement

## 1. INTRODUCTION

Environmental noise is frequently described as undesirable sound caused by transport, industrial and recreational activities [1]. According to the World Health Organization noise can significantly affect human health and productivity, causing stress, sleep disturbance, cardiovascular problems, etc., as it has been shown in many medical studies [2-4]. Moreover, the environmental noise pollution has a great impact on real estate prices [5] (since it causes a 5 % drop in real estate prices). Therefore, during past decades, numerous studies focused on traffic noise issue are conducted by many researchers from all around the world [6-11].

During the last fifteen years European Union has been implementing the strategy for combating noise according to the Environmental Noise Directive (2002/49/EC) [12], which was passed by the European Parliament in June of 2002. Under this directive, Member States are obliged to produce noise maps every five years for all agglomerations and for all major roads and major railways within their territories. Furthermore, the competent authorities, based on results of noise mapping, have to draw up action plans in order to manage noise issues and effects, including noise reduction if necessary. As Serbia is in accession process to the European Union, Serbian legislation related to noise protection is in accordance with Environmental Noise Directive. The latest data obtained from the strategic noise mapping for the EU agglomerations and major roads, indicate that more than 89 million people are exposed to daytime noise levels above the excess exposure threshold, fixed by the EU at 55 dB(A) [13].

The major sources of noise pollution in the living environment are transportation systems [14]. As significant part of the railway transport is performed within urban areas, this form of transport is an important source of urban noise. European authorities are trying to increase the transport of passengers and goods by rail transport systems due to economic aspects, but also in order to reduce GHG emissions. Increase of the volume of the rail transport will lead to increase of the railway noise pollution.

In April 2011 the European Union Agency for Railways published guidelines for the noise measurement and assessment, as well as emission limits of railway vehicles noise, in the technical specification for interoperability – TSI [15]. In 2015 this requirement became mandatory for all vehicles running on commercial trucks in all EU member states.

This paper presents results of measuring the equivalent A-weighted levels of noise generated by locomotive type 661 in stationary conditions, as well as pass-by noise level of freight composition running at constant speed. The measurements are conducted according to the TSI recommendations and ISO 3095:2013 standard [16].

## 2. RAIL VEHICLE AS THE NOISE SOURCE

Rail vehicles are complex mechanical systems with multiple noise sources which emit sound waves due to [17]:

- interaction between contact surfaces in wagon circuits,
- interaction between the outer surface of locomotives and wagons with air during movement,
- interaction between the track and the substrate,
- interaction between wheel and break,
- running of basic and additional equipment in locomotives and wagons.

Based on type of interaction, the noise of rail vehicles may be classified in following categories [18]:

- rolling noise,
- curve squeal,
- aerodynamic noise,
- bridge noise,
- ground noise and vibration,
- internal noise and vibration,
- traction noise.

The wheel – rail contact represents dominant noise source of rail vehicles for speeds within the range of 40 km/h to 140 km/h. Rolling noise, which is caused by the interaction between the wheel and the track, increases with train speed  $v$  at a rate of about  $30\log(v)$  [18].

\*Corresponding author: Dositejeva 19, 36000 Kraljevo, Serbia and bogojevic.n@mfv.kg.ac.rs

Traction motors, engines and rails vehicle equipment are main sources of traction noise, which is dominant at lower speeds.

The aerodynamic noise, caused by air motion around vehicle and pantograph system, is dominant at higher speeds (speeds over 140 km/h), as it is shown in Figure 1.

Further, rail vehicles in the curves produce a squeal noise due to sliding of the wheel over the top of the rails. The various infrastructure objects, such as bridges and tunnels, also have great influence on railway noise generation.

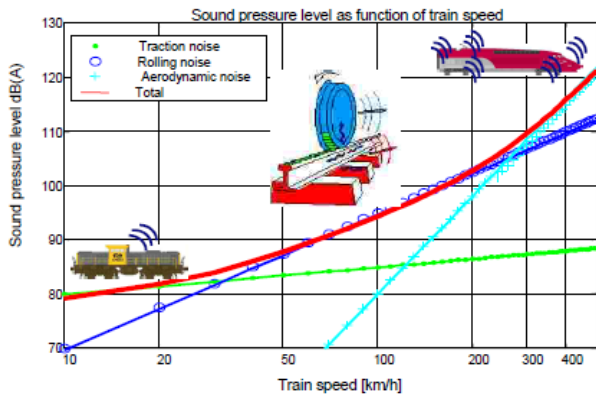


Figure 1: Relative strength and speed dependence of sources of railway noise [19]

Frequency ranges for different types of railway noise are shown in Table 1.

Table 1: Frequency range for different types of railway noise

Noise type	Frequency range [Hz]
Rolling	250 - 5000
Flat spots	50 - 250 (function of speed)
Ground borne vibrations	4 - 80
Engine	50 - 250
Top of rail squeal	1000 - 5000
Flanging noise	5000 - 10000

### 3. MEASUREMENTS

Diesel-electric locomotives of series 661, shown in Figure 2, were produced in the American factory "GM EMD". This type of locomotive was introduced on Serbian railways in 1960, and, until today, the locomotives of series 661 are intended for hauling heavy freight and passenger trains on the rail lines of Serbia. Basic technical data of diesel-electric locomotive type 661 are given in Table 2.

According to the TSI specification a series of measurements should be performed in order to determine stationary noise, as well as the noise emitted by the train unit running at a constant speed.

For locomotives, multiple units, beside stationary and pass-by-noise, locomotive starting noise and interior noise in the driver cabin should be measured, too [15].



Figure 2: Diesel-electric locomotive type 661-162

Table 2: Basic technical data of locomotive type 661

Manufacturer	General Motors CO
Max pull-up power	1342 kW (1800 KS)
Diesel motor power	1454 kW (1950 KS)
Maximal speed	124 km/h
No of cylinders	16
Motor type	"V", 45° between cylinders
Diameter of the cylinder	216 mm
Piston stroke	254 mm
Compression	16:1
Maximum RPM	835 o/min
Weight of the loco	110 t
Numbers of the wheelset	6
Unit length	19 m

This paper presents measurements of the stationary noise of the locomotive type 661-162 and pass-by-noise of the freight train. Measurement positions were located at distance 7.5 m from the track centerline, at a height of 1.2 m above the rail upper surface. The area within radius three times larger than the distance between the measurement point and the track centerline was free of large reflecting objects. Further, the area between the track and the microphone position was free of natural and artificial obstacles to sound propagation, sound absorbing matters and reflective coverings. All measurements were performed according to the TSI recommendations and ISO 3095:2013 standard.

#### 3.1. Stationary test

The noise emitted by a stationary locomotive was measured using Bruel&Kjaer hand-held analyser type 2270. The car was divided into areas with identical horizontal length of 4.5 m, and four measurement positions were located at middle of the corresponding areas. An additional measurement position was located at 30° from the track centreline, on a circle having a radius of 7.5 m and centre in the midpoint of the unit end, as it is shown in the Figure 3. The measurements were performed only on one side of the unit, since both sides of the unit are acoustically identical. Ground surface was in level with the top of the rail surface.

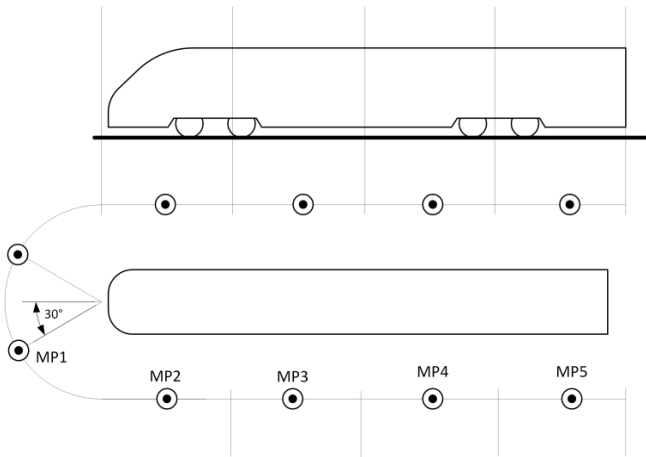


Figure 3: Measurement points for stationary test

3.2. Constant speed test

Bruel&Kjaer PULSE analyser was used for measuring the noise produced by freight train which ran at a steady speed. Free-field microphones and a suitable microphone windscreen were used. The vehicle moved at a speed of 45 km/h along the track whose curvature has the radius larger than 1000 m.

The location of the measurement point relative to the rail track is shown in Figure 4. Ground surface level was in the range of -1.5 m to 0 m relative to the top of the rail. The acoustic rail roughness has not been taken into account.

The total length of the freight train was 461 m and it has been composed of different types of the freight wagons. At the measurement location, the terrain between the railway track and the microphone was covered with grass, while, as shown in Figure 5, the other side of the track was covered with trees. During the measurement time interval, the traffic on a nearby road has been stopped.

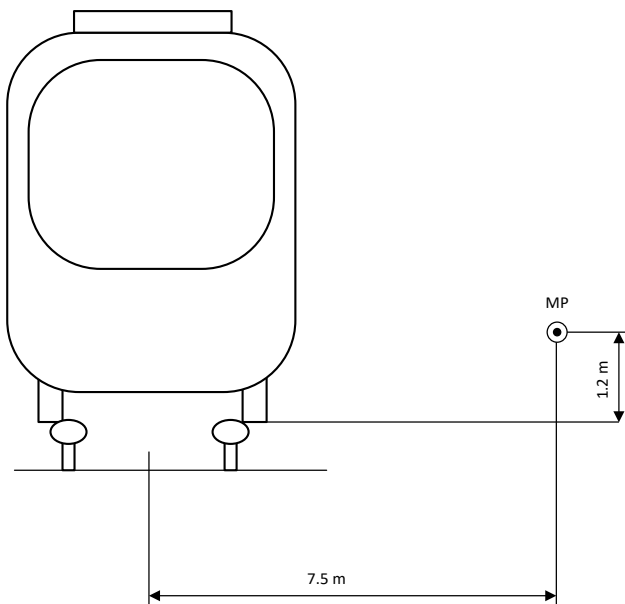


Figure 4: Measurement point for constant speed test



Figure 5: Measurement site for constant speed test

4. RESULTS

Equivalent A-weighted noise level and one-third octave spectrum of the stationary locomotive of series 661 were measured during 20 s time interval. The obtained noise levels at each measurement positions are given in Table 3.

According to ISO 3095 standard, noise emission level of the unit should be calculated by energy averaging  $L_{pAeq,T}^i$  measured noise levels at all positions  $i$  according to following equation:

$$\langle L_{pAeq,T} \rangle_{unit} = 10 \log \left( \sum_{i=1}^n \frac{l_i}{l_{tot}} 10^{L_{pAeq,T}^i / 10} \right), \quad (1)$$

where  $n$  is the number of measurement positions,  $l_i$  length associated with measurement position  $i$ , while  $l_{tot}$  represents the sum of all  $n$  lengths. Calculated noise emission level of the stationary locomotive type 661 – 162 has a value of 73.58 dBA, and, therefore, satisfies the acoustic requirements of the Technical Specifications for Interoperability. TSI defines noise level of 75 dBA as the limiting value for the stationary noise of this type of locomotive.

Figure 6 shows one-third octave noise spectrum at measurement position with the highest measured equivalent A-weighted noise level.

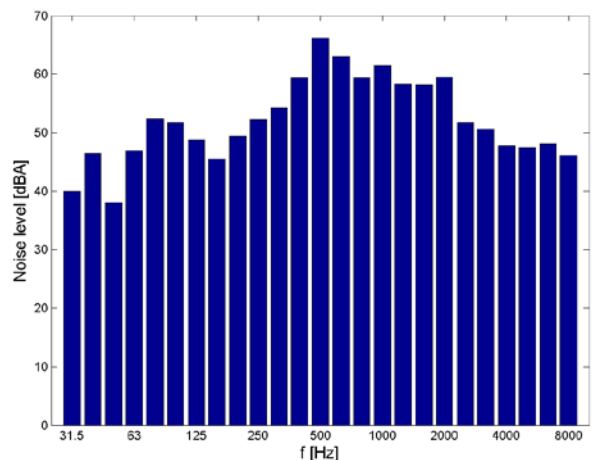


Figure 6: One-third octave noise spectrum of stationary unit

Table 3: Stationary unit noise levels

	MP1	MP2	MP3	MP4	MP5
L <sub>Aeq</sub>	71.12	73.69	75.13	74.32	72.03
31.5 Hz	39.96	41.22	34.86	40.67	38.68
40 Hz	46.48	47.92	39.16	51.14	48.87
50 Hz	38.3	42.9	46.9	46.03	43.46
63 Hz	46.98	49.42	52.2	51.12	45.52
80 Hz	52.38	57.06	61.66	57.58	49.48
100 Hz	51.74	52.93	52.11	52.17	50.77
125 Hz	48.77	49.32	49.3	50.69	47.34
160 Hz	45.51	50.79	52.64	49.67	50.67
200 Hz	49.38	55.98	54.35	54.56	52.3
250 Hz	52.27	54.75	60.2	56.48	56.06
315 Hz	54.19	58.33	60.74	58.76	58.13
400 Hz	59.34	64.01	66.87	64.83	62.59
500 Hz	66.09	68.06	69.72	70.2	68.34
630 Hz	62.95	64.54	65.06	64.99	62.28
800 Hz	59.39	62.92	65.08	61.44	59.21
1 kHz	61.42	62.44	62.88	63.02	59.77
1.25 kHz	58.28	60.74	61.35	60.42	58.18
1.6 kHz	58.17	60.9	61.77	60.78	57.2
2 kHz	59.44	63.23	62.75	61.25	57.66
2.5 kHz	51.69	56.79	56.16	55.07	52.26
3.15 kHz	50.54	52.85	54.11	53.03	50.7
4 kHz	47.83	50.22	51.88	50.72	47.67
5 kHz	47.37	47.73	48.76	48.27	45.85
6.3 kHz	48.5	46.53	47.22	46	42.26
8 kHz	46.5	42.57	43.67	42.36	38.21

For the constant speed test, equivalent A-weighted noise level and one-third octave noise spectrum were measured during freight composition pass-by. Experimentally obtained equivalent A-weighted noise level L<sub>Aeq</sub> and statistical noise levels L<sub>10</sub>, L<sub>50</sub> and L<sub>90</sub> are given in table 4, while the sound pressure levels in one-third octave bands are shown in Table 5. By definition the statistical noise level L<sub>n</sub> represents the noise level which is exceeded during n % of the time.

Table 4: Freight composition pass-by noise levels

L <sub>Aeq</sub> [dBA]	86.86
L <sub>10</sub> [dBA]	89.75
L <sub>50</sub> [dBA]	85.2
L <sub>90</sub> [dBA]	82.17

Table 5: Freight composition one-third octave noise spectrum

	Rail noise [dBA]
31.5 Hz	44.939
40 Hz	48.386
50 Hz	52.94
63 Hz	52.602
80 Hz	64.677
100 Hz	68.012
125 Hz	61.912
160 Hz	65.962
200 Hz	68.832
250 Hz	69.988
315 Hz	71.496
400 Hz	73.434
500 Hz	76.693
630 Hz	76.93
800 Hz	78.34
1 kHz	76.9
1.25 kHz	75.112
1.6 kHz	77.046
2 kHz	75.373
2.5 kHz	74.346
3.15 kHz	73.701
4 kHz	73.157
5 kHz	71.571
6.3 kHz	67.911
8 kHz	65.217

Changes in equivalent A-weighted sound pressure level during freight train pass-by are shown in Figure 7, while the Figure 8 shows corresponding one-third octave noise spectrum. Since the traction noise is dominant at lower speeds, the highest noise level of approximately 96 dBA was measured during locomotive pass-by, as shown in Figure 7.

## 5. CONCLUSION

The measurements of the noise generated by locomotive type 661 – 162 in stationary conditions, as well as pass-by noise of freight composition running at constant speed, have been presented in this paper. The obtained A-weighted levels of the equivalent noise are very close to the limit values requested by TSI specifications.

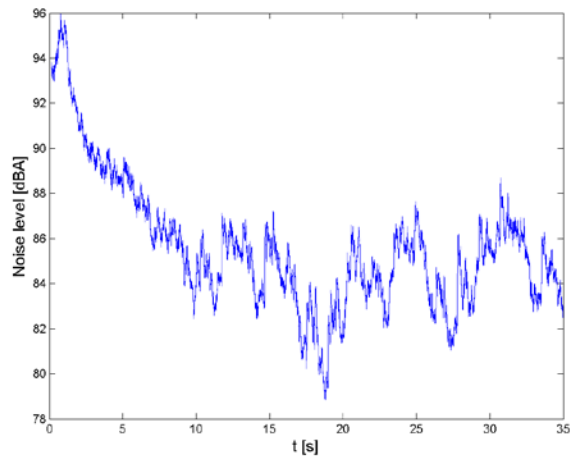


Figure 7: Freight composition pass-by noise

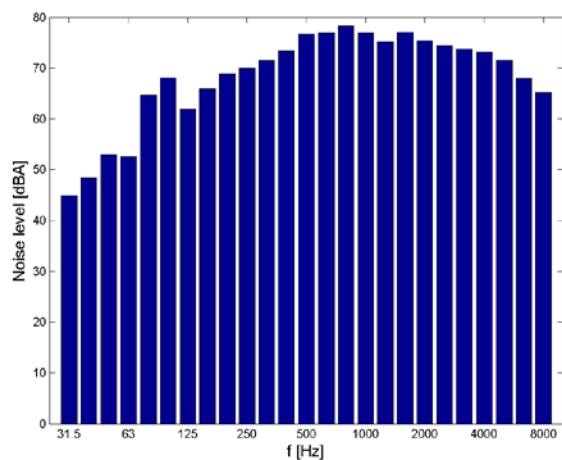


Figure 8: One-third octave spectrum of freight composition pass-by noise

The average stationary noise of this type of locomotive satisfies the acoustic requirement of TSI specification, while the equivalent noise level of the freight train running at constant speed of 45 km/h exceeds the limit value of 85 dBA, which is defined for pass-by noise of the freight composition at speed of 80 km/h.

Considering that rail acoustical roughness has not been taken into account, the emitted noise level of this type of vehicle may deviate significantly from presented results at different railway sections.

#### ACKNOWLEDGEMENTS

The authors wish to express their gratitude to Serbian Ministry of Education and Science for support through Project No. TR37020.

#### REFERENCES

- [1] Department of Environment Heritage and Local Government, Ireland, 2006. Statutory Instrument Number 140 of 2006, Environmental Noise Regulations.
- [2] Ohrstrom, E.; Rylander, R. "Sleep disturbance by road traffic noise - A laboratory study on number of noise events". *Journal of Sound and Vibration*, vol. 143, no. 1, pp. 93–101, 1990.

- [3] Fyhri, A.; Klboe, R. "Road traffic noise, sensitivity, annoyance and self-reported health - A structural equation model exercise". *Environment International*, vol. 35, no. 1, pp. 91–97, 2009.
- [4] Pirreera, S.; Valck, E. D.; Cluydts, R. "Nocturnal road traffic noise: A review on its assessment and consequences on sleep and health". *Environment International*, vol. 36, no. 5, pp. 492–498, 2010.
- [5] Theebe, M. A. "Planes, trains, and automobiles: The impact of traffic noise on house prices". *Journal of Real Estate Finance and Economics*, vol. 28, no. 2, pp. 209–234, 2004.
- [6] Pandya, G. H. (2001). Urban noise - a need for acoustic planning. *Environmental Monitoring and Assessment*, 67, 379–388.
- [7] Korfali, S. I., & Massoud, M. (2003). Assessment of community noise problem in greater Beirut area, Lebanon. *Environmental Monitoring and Assessment*, 84, 203–218.
- [8] Georgiadou, E., Kourtidis, K., & Ziomas, I. (2004). Exploratory traffic noise measurements at five main streets of Thessaloniki, Greece. *Global Nest the International Journal*, 6(1), 53–61.
- [9] Jamrah, A., Al-Omari, A., & Sharabi, R. (2006). Evaluation of traffic noise pollution in Amman, Jordan. *Environmental Monitoring and Assessment*, 120, 499–525.
- [10] Omokhodion, F. O., Ekanem, S. U., & Uchendu, O. C. (2008). Noise levels and hearing impairment in an urban community in Ibadan, Southwest Nigeria. *Journal of Public Health*, 16, 399–402.
- [11] Doygum, H., & Gurun, D. K. (2008). Analysing and mapping spatial and temporal dynamics of urban traffic noise pollution: a case study in Kahramanmaraş, Turkey. *Environmental Monitoring and Assessment*, 142, 65–72.
- [12] Directive 2002/49/EC of the European Parliament and the Council of June 2002, Official Journal of the European Communities, 2002.
- [13] De Vos, P.; Licitra, G. "Noise maps in the European Union: An overview". In Licitra, G. (Ed.), *Noise mapping in EU: Models and Procedures*, pp. 285–310, USA: CRC Press, 2013.
- [14] Stansfeld S., Haines M, Brown B., Noise and health in the urban environment, *Rev Environ Health*. 2000 Jan-Jun;15(1-2):43-82. PMID: 10939085
- [15] TSI Noise, 2011-04-13. Commission Decision of 4 April 2011 concerning the technical specifications of interoperability relating to the subsystem 'rolling

- stock – noise' of the trans-European conventional rail system (2011/229/EU).
- [16]BS EN ISO 3095:2013 – Acoustics – Railway application – Measurement of noise emitted by railbound vehicles (ISO 3095:2013)
- [17]Predrag Petrović, Živojin Petrović, Stanislav Glumac, Railway noise resources, key environmental problem in the European union, Noise and Vibration, Niš, Serbia, 2014.
- [18]Thompson, D., Railway noise and vibration – Mechanisms, modeling and means of control, Elsevier Ltd, UK, 2009.
- [19]van Beek A, Beuving M, Dittrich M, Beier, Zhang X, Jonasson H, et al. HARMONOISE. Work package 1.2. Rail sources. Task 1.2.1. State of the art (Technical report No. HAR12TR-020118-SNCF10). Paris, France: Research and Technology Department, Physics of the Railway System and Comfort; 2002.



# **SESSION F**

## **THERMAL TECHNIQUE AND ENVIRONMENT PROTECTION**



# Modelling of Technological Equipment and Technological Transportation Flows of the Industries Binder Using Mathematical Methods

PhD. Assist. Eng. Sescu Gal Cristina <sup>1\*</sup>

<sup>1</sup>Faculty of Technological Equipment, Bucharest, (Romania)

*The modelling of technological flows and equipment in the binder industry, especially the cement industry, requires consideration of all factors involved in the manufacturing circuit. Regardless of the approach, considering the connections between the components of the installation, the type of modelling applied must encompass the whole system. Used primarily for efficiency and reduce energy costs, analysis of the movement, and processing the mixture of materials in the cement manufacturing process can be used to estimate the emission amount of a gas discharge chimneys. Thus, the mathematical modelling method with the help of the circulation matrices built in the present paper offers the possibility to know the quantities of materials or gases passing through the analysed installation / equipment.*

**Keywords: modelling, systems theory, matrices of movement, emissions**

## 1. INTRODUCTION

The manufacture of binders for the building materials industry, especially cement, requires complex thermo-technological processes through which the raw material reaches the finished product. Following these processes occur transformations physicochemical the raw materials and the study on how to place these changes is quite complex and take into account the influences and interdependencies that occur in the raw material at all stages of manufacturing. The current technological processes used for the production of cement are processes that are carried out in a continuous, high-energy and electric energy-consuming process necessary to obtain the temperatures at which the chemical reactions occur, especially for clinkering the raw mixture. According to the literature and research in the field, optimization of the environmental management of the emissions generated by cement production requires, first and foremost, the optimization of the technological process. Therefore, any method used to optimize the technological process - the selection of raw materials, the modernization and control of equipment operation, the use of unconventional fuels - can be considered as a method of optimizing environmental management to reduce emissions.

## 2. ENVIRONMENTAL POLLUTION MODES IN CEMENT MANUFACTURING

The emissions from the manufacture of cement contribute to the pollution of the environment directly and indirectly. Most harmful elements are released into the atmosphere and come from the processes of raw material combustion. All biosphere systems are subject to both direct pollution by the release of harmful substances directly to the exhaust gas coils, as well as indirect pollution by the circulation of matter in nature. At present, in Romania as well as in other countries, environmental issues are acutely raised, especially as a result of intense local pollution, as well as the existence of cross-border pollution, which has led in some areas to ecosystem

deregulation and deterioration Environmental quality. The current challenge, targeting all industrial areas, is to achieve environmental goals and ensure sustainable economic growth in a sustainable manner.

### 2.1. Direct pollution and indirect pollution of the environment

Generally, when we talk about environmental pollution, we mainly refer to atmospheric pollution, which is the most "polluted" component of the biosphere. But the pollution of a biosphere element leads directly to the degradation of the other components, which are in constant communication and interconnection. The mode of environmental damage by the cement manufacturing process is synthesized in Figure 1.

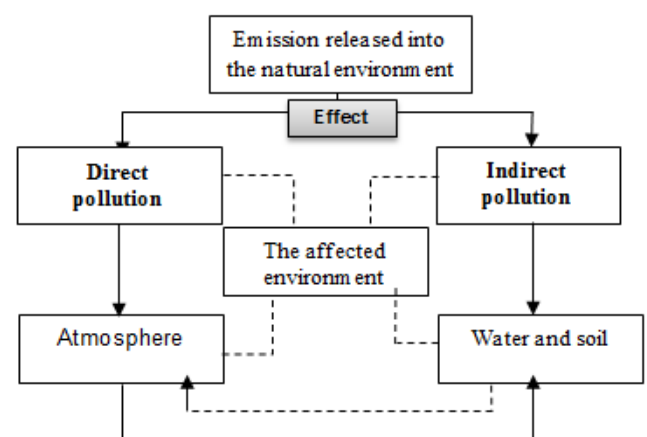


Figure 1. - Types of pollution specific to cement factories

Sources of emissions from a cement plant are given by the technological equipment used in the production stream and the necessary materials: raw materials, additives and fuels. Direct pollution of the atmosphere is achieved by releasing emission at the exhaust chimney and illustrates the most significant and visible pollution. Direct water and soil

pollution in cement production is reduced compared to atmospheric pollution. Direct soil pollution is achieved through the inappropriate exploitation of raw materials (soil degradation) and the discharging of the soil of fuels and lubricants into the quarries and transport operations, and direct pollution of water is achieved by the use of water in the technological process. The mechanism through which the direct and indirect pollution, occurs is as follows: at the gas exhaust chimney within the plant, emissions whose content varies depending on the technological equipment of the exhaust chimney are

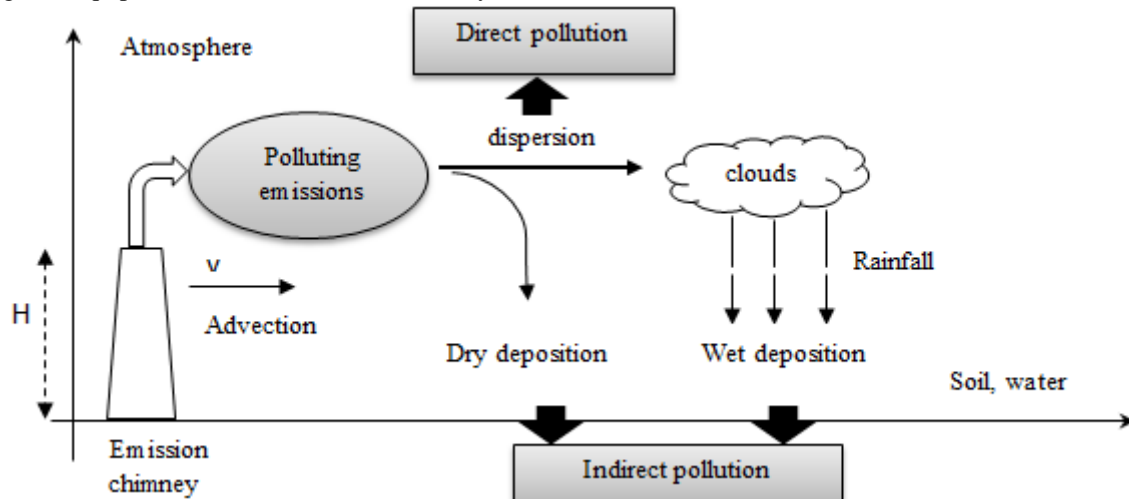


Figure 2. - Mechanism of direct and indirect pollution

## 2.2. The concept of the dispersion of emissions

The dispersion of atmospheric emissions characterizes the evolution in time and space, of an ensemble of particles (aerosols, gases, dust) into the atmosphere. In case of release of pollutant gases at the level of the evacuation chimneys, the concentration of pollutants at the soil level must be determined and the maximum value is established by the legislative acts of the EU Environmental Policy and represents the immission of the pollutants. The dispersion of a cloud of pollutants depends on several factors, of which:

- physical characteristics of the source (gas velocity and temperature, chimney height and diameter, emission duration);
- the chemical characteristics of the emission (concentration of the pollutant cloud and its chemical composition);
- natural factors - meteorological parameters: wind speed and duration, air humidity, atmospheric precipitation, air pressure; Relief factors: valleys corridors, depression areas, orographic barriers; the

$$\tilde{C}(x, y, z) = \frac{Q}{2\pi\sigma_y\sigma_z u} \exp\left(-\frac{y^2}{2\sigma_y^2}\right) \cdot \left\{ \exp\left[-\frac{(z-H)^2}{2\sigma_z^2}\right] + \exp\left[-\frac{(z+H)^2}{2\sigma_z^2}\right] \right\} \quad (2)$$

in that was taken of the relationship:

$$\int_0^t \int_0^t \delta \cdot \left[ \frac{x}{u} - (t-t') \right] dt' dt = 1 \quad (3)$$

eliminated in the atmosphere: dust, NO<sub>x</sub>, SO<sub>x</sub>, CO, CO<sub>2</sub>, TOC, dioxins and furans, HCl, HF, heavy metals. On entering the atmosphere the dispersion of the emissions cloud occurs part of which reaches the ground (dust) with the indirect pollution of the soil and on the water meshes, resulting in the indirect pollution of the water, figure 2. The term immission according to [1], defines the transfer of pollutants in the air to a receiver, and the amount of immission flowing into the hydrosphere and lithosphere natural material moving in the biosphere.

presence of woodland areas capable of retaining particles and neutralizing some gases.

The dispersion mode evaluation is based on models, and in the case of fixed-point emissions, the exhaust chimney, the Gaussian model is used to determine the statistical properties (averages, overflow frequencies, etc.) of the field of concentrations. The concentration of pollutant, after [2], can be calculated with the relation (1) valid for certain calculation assumptions:

$$\tilde{C}(x, y, z) = \int_0^t \int_0^t \frac{C(x, y, z, t-t')}{q} \cdot Q(t') dt' dt \quad (1)$$

where:  $C(x, y, z, t-t')/q$  - dispersion factor;

$\tilde{C}(x, y, z)$  - concentration of pollutant.

Emissions at the chimney in cement manufacturing are identified with continuous emission sources whose full equation of the Gaussian dispersion model, considering the emission rate  $Q(t') = Q$  independent over time is given by relation (2) [2]:

For low wind speeds (<1 m / s) or zero (atmospheric calm) the Gaussian model is not recommended to be applied due to the fact that diffusion along the wind direction becomes important.

### 3. GLOBAL MODELING OF A CEMENT PLANT

Using new computing facilities provided by computer software and increases their computing power constructive and functional changes have been made to the installations in the cement factories that have led to their performance improvement. In this moment, these increases are limited by the cost of the necessary investments, so that by overcoming a cost threshold, the investments made will considerably influence the final price of the cement. In view of the need to respect the pollutant emission values, especially in the EU, it is necessary optimal design, operation and control of processes to increase efficiency, in full compliance with the technological requirements for the final product, is required. To solve the multiple problems posed by the design and exploitation of cement plants, the use of mathematical models has become a common practice, being regarded as a tool that allows partial or total replacement of experimental investigations. The analysed installations are thermo technological installations, so that for the mathematical modelling it is necessary to perform the thermal balances sheet and materials balance. It is therefore necessary to identify the types of material flows entering /going into / from different components of the installation, fluxes that can be identified through the traffic matrix of the material.

According to the principle of conservation of mass, the sum of all materials entered into a system within a given time interval and those existing at the initial time must be equal to the sum of the materials ejected in the same time interval and those remaining in the system.

Material balance concepts are used for closed and isolated systems, in which case inputs are equal to outputs, for systems where there are accumulations, or for systems where there are time-dependent processes. The relationship for conservation of mass and expressed by the balance equation of the respective size has the following general form (4):

$$\frac{Q_s}{\Delta t} = \frac{Q_i}{\Delta t} - \frac{Q_e}{\Delta t} + \frac{Q_p}{\Delta t} - \frac{C_s}{\Delta t} \quad (4)$$

Where:

$Q_s$  - accumulation of material in the system;

$Q_i$  - inputs of material into the system;

$Q_e$  - material exits from the system;

$Q_p$  - materials produced in the system;

$C_s$  - consumption of materials in the system;

$\Delta t$  - unit of time.

The material balance relationship for a plant / system which comprises both solid state materials entering / leaving the system as well as those in the gaseous state defined in matrix form is [3]:

$$A \cdot M + D \cdot (G+S) + F + B + V = 0 \quad (5)$$

Where:

$A$  - the traffic matrix of material circulation in the considered installation / system;

$M$  - flows of material leaving the installation / system and containing elements;

$D$  - the traffic matrix of gas circulation in the considered installation / system;

$G$  - mass flow rate of exhaust gas from the considered installation / system;

$S$  - flow rate of dust that is entrained the exhaust gas from the considered installation / system;

$F$  - the flow of material entering the considered installation / system;

$B$  - the fuel flow introduced into the installation / system considered without considering ash;

$V$  - the flow of air introduced into the considered installation / system.

The major difficulty in designing, management and optimization of facility stems from the fact that in most cases input and / or environmental parameter values record strong disturbances within a short time in relation to the values taken into account.

### 4. ANALYSIS OF MATERIAL FLOWS IN CEMENT MANUFACTURING PLANTS

Knowledge of displacement mode, transforming and mixing materials in the manufacture of cement is studying with the purpose to increase efficiency of operation which involves reducing energy costs, as well as to determine the possibility to reduce stack emissions. The process of manufacturing cement involves, in addition to heat transfer thermo-technological processes, mixing, melting, cooling, shredding, material transfer processes that take place inside the technological installations. Following these processes occur physicochemical changes in the raw material, resulting in a finished product, cement, or a blank with pre-established characteristics clinker.

#### 4.1. The systemic approach to a cement manufacturing plant

The mathematical modelling of cement plants, complex installations characterized by a large number of process parameters in interdependence, cannot be achieved by using all methods of industrial process modelling, economics, etc. In order to achieve a more rigorous mathematical approach to a cement plant, system concepts, systemic approach, or system theory apply. The first step in the study of a system or process is the realization of a model, which may be physical to other dimensions or a mathematical formalization of the system behaviour to be studied. Analysis of systems assumes defining and knowing as accurately as possible the behaviour of a system with a given structure, so that subsystems can be defined quantitatively by expressions of type (6).

$$Y_j = \Psi_j \cdot (X_i, D_k), j = 1, 2, \dots, n \quad (6)$$

Where:

-  $Y_j$  is the vector of the variables at the exit of the subsystem; it depends on the input variables  $X_i$  and the vector of the control quantities  $D_j$ ;

-  $X_i$  is the vector of the input variables;

-  $D_k$  is vector of control quantities, that is, sizes that condition the transformations  $X_i - Y_j$ .

Applying the method of analysis of general systems theory, it is considered the entire installation of a cement factories, which is made up of three subsystems main whose definition can specify the area of the border by which detaches from the environment and / or system and how are interactions between them.

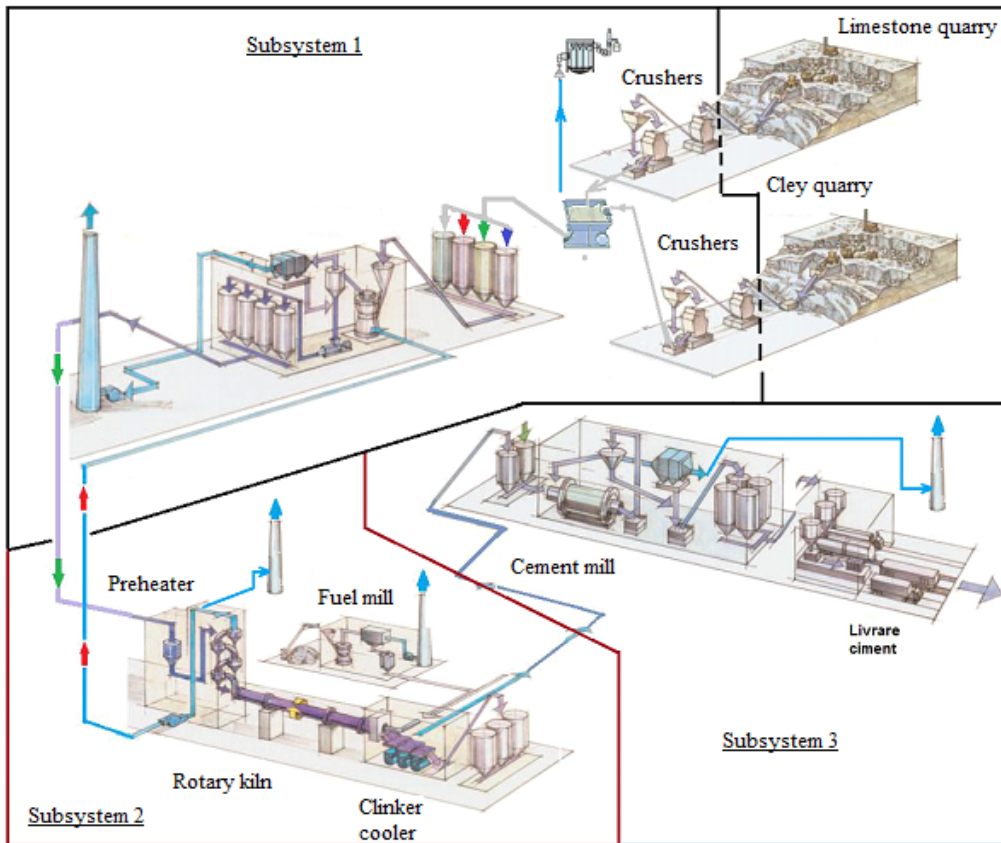


Figure 3 - Cement manufacturing system: → hot gas flow in admixture with particulate material collected from the cyclone tower; → material flow

For a cement manufacturing plant on a dry process, the systematization of the equipment and its decomposition in three subsystems is shown in Figure 3, in which the three subsystems were delimited as follows:

- the subsystem 1 comprises the process of making the crude mixture which includes its storage and mixing equipment;
- the subsystem 2 includes the combustion process of the homogenised mixture and the clinker cooling; From the clinker storage system there is the possibility that a part of

it is shipped from the plant as a raw material for separate cement milling installations;

- the subsystem 3 represents the cement grinding plant with the additives specified in the manufacturing recipe.

4.2. Modelling the plant by graph theory

Having defined the subsystems of the installation in Figure 3, modelling of the whole plant is performed using the matrix approach based on the graphs corresponding to the three subsystems shown in Figure 4, which underlie the defining of the traffic matrices.

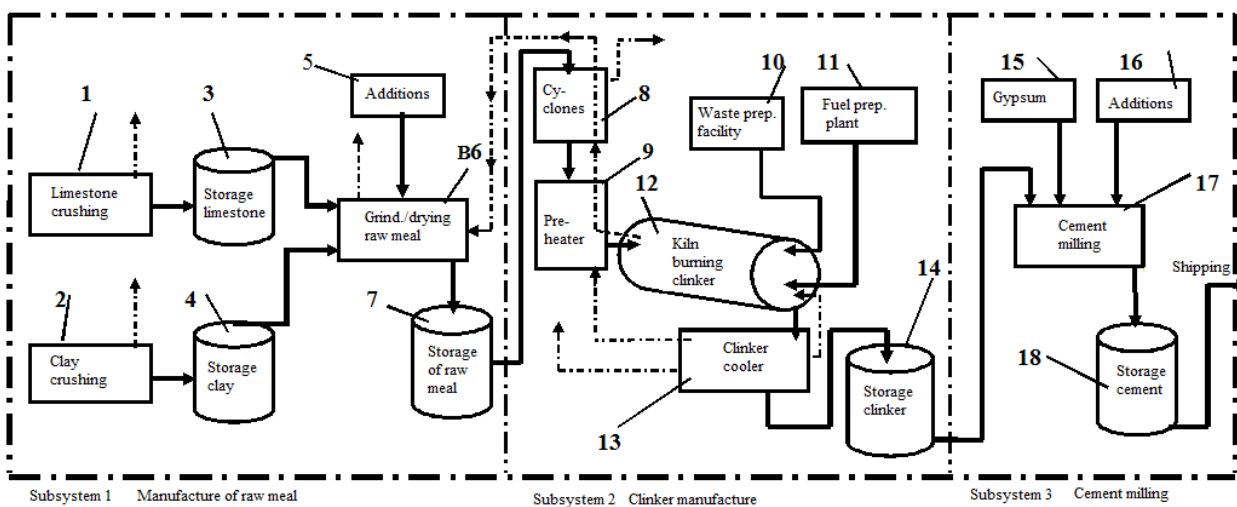


Figure 4. - The scheme of the cement manufacturing plant - Material flow; → Material flow; - - - → material fraction entered the gas flow

4.3. Matrix modelling of subsystem 1. Define traffic matrix material

The processes that take place in this subsystem are given by preparing the raw mixture, storing, pre-homogenizing, grinding and drying the raw materials with the formation of a powder called cement flour. For the installation adopted in this analysis and shown in Figure 4, the drying of the raw materials takes place in the fine grinding plant. The process uses the hot air from the clinker cooling system, passed through the calciner and the cyclone tower. In this way, an important energy saving is achieved, which also leads to the reduction of the harmful emissions corresponding to this process. In the case of relatively high humidity raw materials, an auxiliary

combustion chamber is required to initiate the process to provide the additional heat required for the raw material drying process, thereby achieving a saving in heat consumption.

The technological equipments in the installation are represented by the nodes of the graph and the way of moving the material by arrows, oriented in the direction of their circulation. This method offers the possibility to use the advantages of matrix computation by analysing each graph with a matrix, determining the quantities of materials and gases passing through the system / subsystem / equipment analysed. Figure 5 shows the matrix modelling of the subsystem 1 by means of graphs in which the material movement can easily be identified.

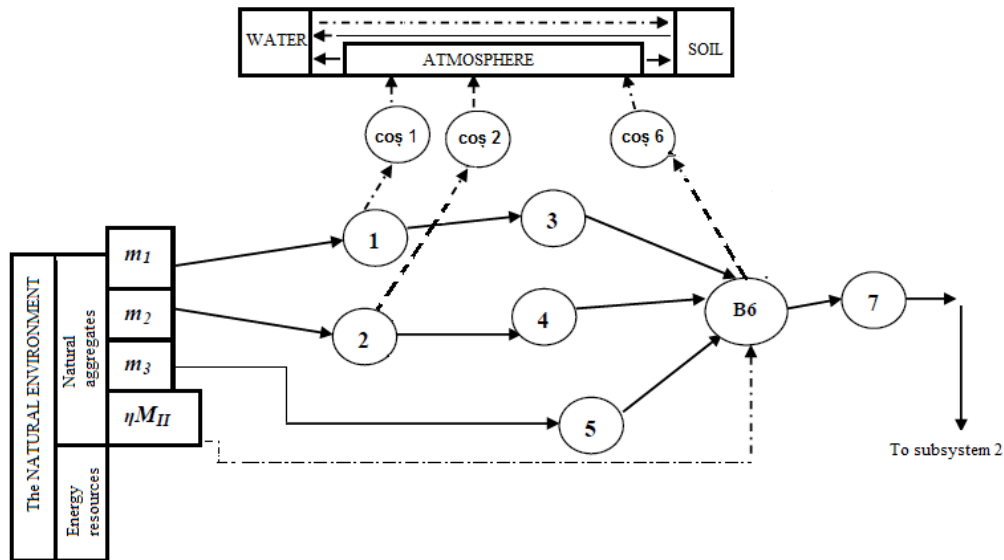


Figure 5. – Modelling subsystem 1 using graph theory - Manufacture of raw meal

Parameters that occur in the graph defining subsystem 1 are:

- $m_1$  - limestone, raw material for the manufacture of cement having a granulation resulting from the coarse crushing normally taking place in the quarry;
- $m_2$  - clay, raw material for the manufacture of cement having a grain resulting from the rough coarse mining normally taking place in the quarry;
- $m_3$  - admixtures for the gross mixture: ash of pyrite, iron ore or slag from the non-ferrous metallurgical industry, high in iron oxides or even metallic iron to correct  $Fe_2O_3$  content in cement; Are introduced into the manufacturing stream in the grinding step of the crude mixture;
- $\eta M_{II}$  - fraction of the material conveyed by the hot gases from the cooler and from the clinker process, consisting of tertiary air, secondary air and primary air; The tertiary and the secondary air are recovered from the clinker cooling plant from which it exits with a temperature of approximately 900-1000°C; the primary air is the one introduced to achieve the combustion conditions of the fuels; the hot gas flow contains particles collected from the furnace system, from fuels, from the calcining system and from the cyclone tower;

The representation of the traffic matrix corresponding to the graph in figure 5 is given in Table 1. When constructing this matrix, it was taken into account that of matrix element  $a_{ij}$  shows the gravimetric fraction of material in the equipment  $i$  passing through  $j$ . Within this traffic matrix, the elements  $a_{ij}$  coming out of equipment get a negative value, which means that the exit is considered a negative input. In this way, the sum of the elements on the column indicates the fraction of the material leaving the stage  $i$  leaving the subsystem. The assumptions underlying the matrix development:

- a) It is considered that the fractions of material leaving the system from the crushing phase by means of dust emissions are identical for the two types of raw materials, namely limestone and clay: it is noted with  $c_u (1-\delta) m_i$ ;
- b) The amount of material remaining inside the equipment / plant and on the interphase transport routes is neglected.

The specification of the notations in the material matrix in subsystem 1 is as follows:

- $(1-\delta) m_1$  - Fraction of limestone leaving the subsystem entrained by the air circulation in the fine crushing operation;
- $(1-\delta) m_2$  - Fraction of clay leaving the subsystem entrained by the air circulation in the fine crushing operation;

- $\delta m_1$  - Limestone remaining from the total amount considered after fraction removal  $(1-\delta) m_1$ ;
- $\delta m_2$  - Clay remaining from the total amount considered after fraction removal  $(1-\delta) m_2$ ;
- $m_6$  - The total quantity considered as consisting of the elements entering the apparatus B6;

- $(1-\varepsilon) m_6$  - Fraction of the  $m_6$  material leaving the subsystem driven by the gas stream through the exhaust chimney; Also contains water vapour which evaporate from the solid material entering the mill;
- $\varepsilon m_6$  - Material remaining in apparatus B6 and consisting of raw meal which is stored in silos in the dry state.

Table 1: The material matrix corresponding to the graph for subsystem 1

i\j	I	1	coş 1	2	coş 2	3	4	5	B6	coş 6	7	$\Sigma a_{ij}$
I	0	$m_1$	0	$m_2$	0	0	0	$m_3$	$\eta M_{II}$	0	0	$m_1+m_2+m_3+\eta M_{II}$
1	$-m_1$	0	$(1-\delta) m_1$	0	0	$\delta m_1$	0	0	0	0	0	0
1'	0	$-(1-\delta) m_1$	0	0	0	0	0	0	0	0	0	$-(1-\delta) m_1$
2	$-m_2$	0	0	0	$(1-\delta) m_2$	0	$\delta m_2$	0	0	0	0	0
2'	0	0	0	$-(1-\delta) m_2$	0	0	0	0	0	0	0	$-(1-\delta) m_2$
3	0	$-\delta m_1$	0	0	0	0	0	0	$\delta m_1$	0	0	0
4	0	0	0	$-\delta m_2$	0	0	0	0	$\delta m_2$	0	0	0
5	$-m_3$	0	0	0	0	0	0	0	$m_3$	0	0	0
B6	$-\eta M_{II}$	0	0	0	0	$-\delta m_1$	$-\delta m_2$	$-m_3$	0	$(1-\varepsilon) m_6$	$\varepsilon m_6$	$-\eta M_{II}-\delta(m_1+m_2)-m_3+m_6$
6'	0	0	0	0	0	0	0	0	$-(1-\varepsilon) m_6$	0	0	$-(1-\varepsilon) m_6$
7	0	0	0	0	0	0	0	0	$-\varepsilon m_6$	0	0	$-\varepsilon m_6$
$\Sigma a_{ii}$	$-(m_1+m_2+m_3)-\eta M_{II}$	0	$(1-\delta) m_1$	0	$(1-\delta) m_2$	0	0	0	$\eta M_{II}+\delta(m_1+m_2)+m_3-m_6$	$(1-\varepsilon) m_6$	$\varepsilon m_6$	0
	I	1	coş 1	2	coş 2	3	4	5	6	coş 6	7	$\Sigma a_{ij}$

The construction of traffic matrices for gas streams passing through a plant / equipment is the basis of modelling for knowing, yet from the stage of study, the amount of gas to be Which will be evacuated at the chimney. Conventional representation of the circulation matrix for subsystem 1 is given in Table 2.

Table 2: Circulation matrix for subsystem 1

i\j	I	1	coş 1	2	coş 2	3	4	5	B6	coş 6	7
I	0	1	0	1	0	0	0	1	1	0	0
1	-1	0	1	0	0	1	0	0	0	0	0
coş 1	0	-1	0	0	0	0	0	0	0	0	0
2	-1	0	0	0	1	0	0	0	0	0	0
coş 2	0	0	0	-1	0	0	0	0	0	0	0
3	0	-1	0	0	0	0	0	0	1	0	0
4	0	0	0	-1	0	0	0	0	1	0	0
5	-1	0	0	0	0	0	0	0	1	0	0
B6	-1	0	0	0	0	-1	-1	-1	0	1	1
coş 6	0	0	0	0	0	0	0	0	-1	0	0
7	0	0	0	0	0	0	0	0	-1	0	0

### 5. CONCLUSION

The precise calculation of the processes taking place within each subsystem, equipment or plant, as well as the determination of optimal operating parameters, is an intensely researched objective. The proposed goal is more difficult to achieve due to the peculiarities of the clinking process, in which all the researches and studies carried out at the present time have phenomena that can not be controlled.

The modeling of the cement manufacturing plant was carried out using system theory, by following the following steps:

- The cement manufacturing plant was divided into three main subsystems that were individually modeled;



- The method of modeling subsystems has been applied through graphs and matrices for the movement of materials and gases within the subsystem;
- Simplified assumptions have been used for internal processes that cannot be controlled.

Circulation matrices have been developed in a new, approach that actually uses the quantities that transit through the equipment, subsystem, or technology system in a time unit. This analysis can be used to establish as close as possible to the real level of material flows in installations. Using the same method, the raw material grinding plant was modeled, and the gas traffic matrix in the plant was realized.

The continuation of the studies also involves the application of other mathematical methods to identify the influences of some parameters or factors on the amount of pollutant emissions at the exhaust chimneys.

## REFERENCES

- [1] <http://ro.wikipedia.org/wiki/>.
- [2] G. Cuculeanu, "Approach Eulerian of the diffusion of pollutants into the atmosphere," Economy Magazine, Management Series, year IX, no. 1, pp. 98-102, (2006);
- [3] Z. D. Ghizdăveț, "Mathematical modelling of some plants in the cement industry," PhD Thesis, Polytechnic University of Bucharest (2006);
- [4] C Sescu Gal, "Contributions to the improvement of the environmental management of technological equipment and processes in the cement plants", PhD Thesis, Technical University of Civil Engineering of Bucharest (2015);
- [5] I. Teoreanu, ș.a, "Thermo technical installations - binders, glass, ceramics", Technical Publishing House, Bucharest, (1979).



# Ensuring Phonic Comfort in the Urban Environment

Vasile Bacria<sup>1</sup>, Nicolae Herisanu<sup>1,\*</sup>

<sup>1</sup>Faculty of Mechanical Engineering, University Politehnica Timisoara, Timisoara (Romania)

*Within the urban environment, a continuous interest is addressed to the phonic pollution generated by heavy and light transportation means, industrial activities, construction sites, commercial areas, open door restaurants, stadiums, playing spaces for children. This phonic pollution is detrimental for inhabitants, affecting their health. In this paper we dealt with an investigation of phonic pollution in the urban environment with application to the city of Timisoara. In this respect, we have identified the main sources of noise from the urban environment, the degree of discomfort generated by these sources, its time evolution, and we have established some possible actions directed to realize the phonic comfort. The efficiency of such measures is also assessed.*

**Keywords:** Urban environment, phonic comfort

## 1. INTRODUCTION

It is reality that recent and increased development of society leads to a potential phonic pollution. This makes human being, especially in urban environment, to live nowadays in a continuous sonorous ambience, being permanently surrounded by noise and vibration which could affect his comfort and health.

Due to its noxious character and its presence in real life, the phonic pollution represents a major problem for local authorities in European countries. This preoccupation to fight against phonic pollution should be continuously increased since the areas affected by noise are found in a continuous extension. On this line is directed our paper concerned with investigation of noise pollution and realization of acoustic comfort in the urban environment, with application to the area of Timisoara city.

In this respect, we have identified the main noise sources from the urban environment, we have evaluated the degree of discomfort produced and its evolution in time and we have established some measures intended to realize the phonic comfort, after that we have evaluate their efficiency.

## 2. SOURCES OF NOISE IN THE URBAN ENVIRONMENT

2.1. Modern urban environment is characterized by an intense activity and people inside the cities are interested to a faster displacement in this environment. As a consequence, urban roads are crossed by more and more cars, trams, buses, trolleybuses, trucks, tractors, motorcycles, etc. Moreover, some cities benefit by metro or are traversed by railways on which are present trains, and also some cities have in their vicinity airports with an intense air traffic producing significant noise.

All these noisy activities are developing in parallel with industrial activities, construction sites activities, functioning of market places, restaurants, stadiums, and other marks of civilization which become important noise sources in the urban environment.

Noise generated by urban road traffic is characterized by their frequency spectra, acoustic pressure levels and a specific variation of these parameters in time. In general, the noise sources from the urban traffic are

characterized by low frequencies and partly middle frequencies.

Noise and vibration produced by transportation means are generated by the functioning of the engine, transmission system, braking system, air resistance and rolling on the way. Moreover, an increased noise is produced by malfunctioning of various systems of the vehicles, such as the gas exhausting system and the braking system.

The overall noise produced by the urban traffic depends on the intensity and composition, on the speed of displacement, as well as on the distance from the source.

The noise produced by rolling on the way depends on the type of the vehicle, speed of displacement and the nature of the superstructure of the road.

Railway transportation means generate noise and vibration due to the variation of their speed of displacement, distance between non-welded rails, unevenness, curves, the elasticity of the rails, eccentricity and deviation of the shape of the wheels, braking and acceleration.

In general, for a displacement of a train on rails mounted on reinforced concrete sleepers, the noise level at the axle reaches 125-130 dB(A), which is very close to the threshold of pain.

The main sources of noise and vibration for airplanes are represented by the engine, the propeller, or in the case of modern ones, the turboprops.

Taking into account the noise produced by airplanes, this represent an important issue for the personnel of the airport as well as for the residential areas in neighbourhood.

As regards ships, the noise and vibration are produced by the main and auxiliary engines, the propulsion propeller, cooling or oil and fuel pumps [1].

Industrial noise specific to urban environment is due to the equipment and machines employed in production operations, as well as in auxiliary installations, such as warming, ventilation, compressed air or steam installations. From the point of view of the spectral composition, it is to remark that the industrial noise covers the whole spectrum of frequencies.

On the construction sites, the noise is generated by pneumatic hammers, mobile compressors, roller

compactors, levellers, excavators. The characteristic level of these ranges between 85-110 dB(A) and the frequency spectrum between 30-300 Hz.

Supplementary, one cannot neglect in the urban environment the noise produced by restaurants, stadiums, outdoor concerts and so on. These activities generate noise which ranges between 70-75 dB(A) and produce phonic discomfort for inhabitants living in the neighbourhood.

### 3. NOXIOUS EFFECTS OF PHONIC DISCOMFORT

Noise generated by the sources from the urban environment creates a phonic discomfort which is extremely detrimental for the life and health of people.

It was shown [4] that in the presence of an equivalent noise level of 75 dB(A), 80% of the population is disturbed.

Acting on the human body, the noise affects the auditory system, and also internal organs, reducing the work productivity and the intelligibility of speech.

The action of the noise on the auditory organ is more dangerous and intense when this is discontinuous and it appears suddenly, has a large spectrum of frequencies and is accompanied by mechanical vibration.

Various organs and systems of the human body are affected by noise which exceeds 40 dB(A). The phonic discomfort produces variations of the arterial pressure, the blood pulse accelerates, intracranial vascular tension increases even three times, the acuity of vision decreases, the breathing rhythm changes, the fatigue process is accentuated, attention and mental reactions weaken, asthenia or even nerve diseases could appear.

It was proved that phonic discomfort could influence the contractions of the stomach walls increasing them and making them irregular, while the blood pressure within the stomach walls is increased.

The phonic discomfort affects the nervous system of people, producing psychophysiological modifications, blood circulation modifications, sleep disturbances, and possibly the visual function and the activity of the endocrine glands are adversely influenced, producing biochemical disturbances.

In the same time, phonic discomfort produces a general fatigue of the body, affecting physical work which requests concentration and especially intellectual work.

Any activity developed in the presence of phonic discomfort leads to increasing the risk of accidents mainly because it reduces the possibility to acoustic signaling, to orient upon some characteristic noises and reduces the intelligibility of the speech at the working place [2].

### 4. REGULATIONS ON SOUND COMFORT

Having in view detrimental effects of the phonic discomfort, in order to ensure some normal conditions of life and activity, there were established admissible limits for noise levels, which should not be exceeded.

Starting from the reality that for different working places are imposed different norms, there were established separate norms for industrial noise, residential noise, and urban noise or for the noise produced by transportation means.

At the basis of Romanian standards issued for noise limitation stand the curves I.S.O., which are curves of equal level, known also as noise curves ( $C_z$ ), which define

the relation between the characteristic frequency of a sound and corresponding level of acoustic pressure in the conditions of an equivalent subjective sensation. Other elements used for noise limitation are the continuous equivalent noise level ( $L_{ech}$ ) and the peak level ( $L_{10}$ ).

In this respect, in Romania, according to STAS 10009-88, "Urban Acoustics", there were established admissible limits for the noise in urban environment, differentiated by zones and technical categories of streets, based on specific technical regulations in force regarding environmental protection. In the same time, the location of residential buildings on streets of different categories or at the limit of some zones, as well as the organization of the road traffic will be made so that to ensure the value of 50 dB(A) of the exterior noise level measured at 2 meters from the building's wall, and the noise curve  $C_z=45$  [6]. Moreover, STAS 6156-86 establish the admissible limits for the interior noise level in residential and socio-cultural buildings.

Romania's accession to the European Union determined the adoption of European regulations related to environmental protection. In this respect, the European Parliament and the Council adopted the Directive 2002/49/EC in 25.06.2002, which was adopted in Romanian law by H.G. 321/14.04.2005, whose main aim is to create a common base for evaluation and management of the noise.

The main point here is the request to create strategic acoustic maps for roads, railways, airports, and industrial areas, by using as noise indicators  $L_{den}$ ,  $L_n$ , after that informing and consulting the people about the exposure to noise, its effects and measures which could be taken to fight against noise pollution. Moreover, action plans are foreseen to be established, but the Directive does not establish the measures which should be taken, which will be a task to be undertaken by the local authorities [9].

### 5. EVALUATION OF PHONIC DISCOMFORT

Knowing the extremely dangerous effects of the phonic discomfort generated by noise sources from urban environment, we proceeded to investigation and evaluation of the noise. The study was conducted on the city of Timisoara, which is known for the fact that on its roads circulate a large number of transportation means (the second place in Romania after the capital - Bucharest - in what concerns the number of vehicles), it has a large number of industrial units and construction sites, it is crossed from East to West by a railway and has an airport in the North-West part of the city. Moreover, within the town are present many markets, restaurants and open doors cinemas, stadiums, etc. In this respect, there were performed systematic investigations of the phonic pollution since 1996, based on some scientific research contracts financed by the local authority and developed by the University Politehnica Timisoara, Department of Mechanics and Vibration.

The main results consisted in the identification of the main sources of noise and vibration from the urban traffic of the city, their effects on the life and activity of people, characteristic values, which are obtained by measurements. Some methods intended to reduce the noise pollution were established and their effectiveness was evaluated.

There were performed measurements for the noise level generated by the road traffic in the main crossings, as well as measurements of the rail noise and noise of the airport located near the city.

These measurements were performed using equipment such as statistical distribution analyser B&K 4426 and the noise investigator B&K 2237, noise level meter NL-20, and the analyser RC324.

The results of these measurements allowed establishing the first noise map of Timisoara city, depicted in fig.1.

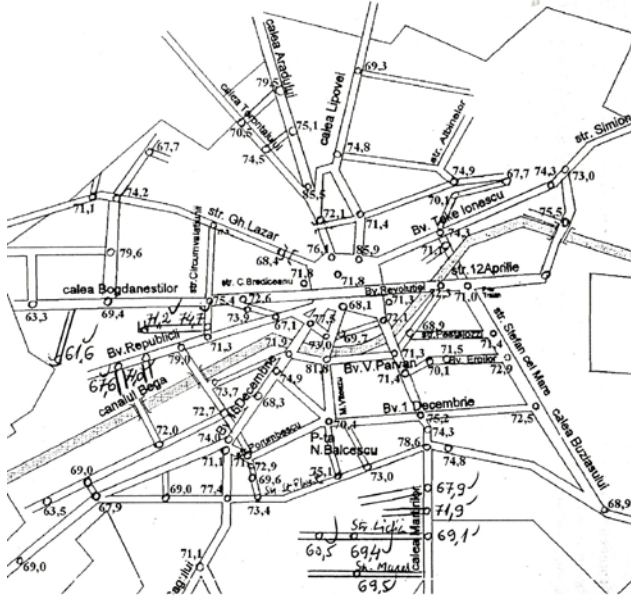


Figure 1: The first noise map of Timisoara, 1996

The utilized equipment allows the determination of the main noise indicators such as Lech, MaxP, Lmax, L0.1, L5, L10, L50, L90, L95. The primary investigations of the noise indicators have been made in the years 1996, 2000, 2001, 2002, 2003, 2004 and 2005, measurements being taken during 8 hours, usually between hours 7.30-15.30.

Simultaneously with noise measurements, the intensity and composition of the traffic were determined, and the speed of displacement of transportation means, as well.

For each of the measurements were made detailed measurement reports, and following the values obtained after measurements, it was concluded that from 119 investigated crossings, in 95 of them (79,83%) the equivalent noise level exceeded the limit admitted by STAS 10009-88 concerning Urban Acoustics. The exceeding ranged between 0.1 and 16.1 dB, while the traffic intensity ranged between 9 and 2681 vehicles/hour at a speed of displacement of 50-60 km/h. In these conditions, the admissible limit noise level measured at 2 m distance from the buildings, which is 50 dB(A), was exceeded with 1.3-32.9 dB(A).

In what concerns the noise produced by the railway traffic, the admissible value of 70 dB(A) at the limit of railway zone was exceeded along the entire length of the urban rail, the exceeding being of 2.2-12.7 dB(A).

Last but not least, the noise level generated by the air traffic measured according to [8] on the Timisoara Airport exceeded the admitted limit with 7 dB(A).

## 6. MEASURES TO ACHIEVE PHONIC COMFORT

Based on the above mentioned results of measurements, one can conclude that the noise generated by the transportation means participating to road, rail and air traffic in Timisoara city, exceeds the admitted limits and produce phonic discomfort.

Consequently, there was a need to identify some measures to be implemented in order to re-establish the phonic comfort.

In order to reduce the noise there were indicated some measures related to the organization and systematization of the urban traffic, improvement or changing of the superstructure of the rolling way, limiting the speed of displacement in some areas, replacing old trams with new ones, improvement of technical condition of vehicles, mounting a layer of rubber between the rails and the sleepers, constructing a ring road to bypass encircling the town, creating protection zones, absorbing screens or green areas between the roads, rails and airport and the residential areas [10].

After implementing these measures, there were performed new measurements in order to evaluate their effects. These measurements were performed in 46 points chosen near the most important crossings from Timisoara.

From the obtained data resulted that in these 46 measurement points, the equivalent noise level has been reduced with 0.1-12.4 dB(A) and in 32 of them (69.56%), the noise level does not exceed any more the admitted value.

In 10 points located at the limit of the railway zone, the equivalent noise level has been reduced with 0.1-9.3 dB(A) and in 6 of them (60%), the admitted value is not exceeded anymore.

The mean equivalent level in these 46 measurement points was 71.8 dB(A) for a mean traffic intensity of 1260 veh/h before applying the reduction measures and respectively 67.3 dB(A) for a mean traffic intensity of 1429 aut/h after the application of noise reduction measures.

In these circumstances, it is obvious that the applied measures contributed to a significant reduction of the noise pollution, leading consequently to a reduction of the percentage of people disturbed by noise.

## 7. ACOUSTIC MAPPING

Once with the accession of Romania in the EU, it was adopted the norm H.G. 321/2005, which implement the EU noise Directive, whose task is to create a common base for evaluation and management of the environmental noise. In this respect, after the elaboration in 2006 of a study concerned with the opportunity of elaboration of a noise map for Timisoara city, in 2007 started the working on the map, taking into account road, rail, air and industrial noise.

Based on the requirements of EU noise Directive, noise mapping activities start with 3D modelling of the whole town, by considering all buildings, collecting real and statistical data about traffic intensity, determination of the acoustic power emission of the industrial zone, which are useful for building up a noise map by simulations using specialized software. This simulation should be after that validated by real measurements in evaluation points. Based on the results obtained by acoustic mapping, action

plans were established with the aim to reduce the noise level in the city of Timisoara. Measures were foreseen concerning improving road traffic and the street network, landscaping, improvement of the technical state of roads, achieving a more silent functioning of noise sources, enhancement of the bicycle road network, achieving the ring road so that heavy traffic will avoid the city, active and passive protection measures against the rail and industrial noise.

These measures were gradually implemented. A real situation is depicted in fig.2-5, where can be seen the noise maps for road traffic taking into account the parameters  $L_{den}$  and  $L_n$  [11].

Starting from these data, in order to analyse the existing situation with the aim to identify reduction methods where needed, one were taken into account the limit values in force, imposed by OM MMDD no.152/13.02.2008.

In these circumstances, the situation was as follows: one were emphasized 21 roads with significant impact of the noise on the population, 24294 persons exposed to a noise level above 65 dB, according to the indicator  $L_{den}$  and 45562 persons exposed to a noise level above 50 dB according to the indicator  $L_n$  due to the road traffic, 51 persons exposed to a noise level above 65 dB for the indicator  $L_{den}$  and 535 persons exposed to a noise level above 50 dB for the indicator  $L_n$  due to the rail traffic, and concerning the industrial noise, one were identified 10 persons exposed to a noise level above 60 dB for the indicator  $L_{den}$  and 99 persons exposed to a noise level above 50 dB for the indicator  $L_n$ .

The action plans issued in this situation incorporated some measures such as modernization of certain sensitive crossings, construction of some protecting screens between some roads and residential areas, construction of the ring road in the southern part of the city, replacing the regular asphalt with rubberized asphalt on some sensitive roads, establishing of some green protection areas, development of a program concerning acoustical treatment of some buildings, construction of protecting screens along the urban railway.

It was estimated the number of people benefiting of these measures: for the road traffic noise, 14300 persons in terms of  $L_{den}$  and 18920 in terms of  $L_n$ ; for the rail traffic - 149 persons in terms of  $L_{den}$  and 508 persons in terms of  $L_n$ ; for the industrial noise - 94 persons in term of  $L_n$ . Supplementary, the action plans foreseen delimitation of quiet zones within the city. The efficiency of these measures foreseen in the action plans will be assessed with the occasion of achieving the new acoustic maps of the city by the end of 2017.

Moreover, a long-term strategy was settled, mentioning some future project such as: completing the ring road of the city - 2020; constructing some modern crossings with modern passages - 2019; construction of 5 new bridges over Bega river, in order to fluidize the road traffic - 2020; application of a layer of rubberized asphalt on a significant number of roads - 2025; construction of protecting acoustic screens for schools, hospitals, universities - 2020; conservation and extension of green protection areas - 2025; replacing a part of surface transport with subway trains (subway lines) - 2030.

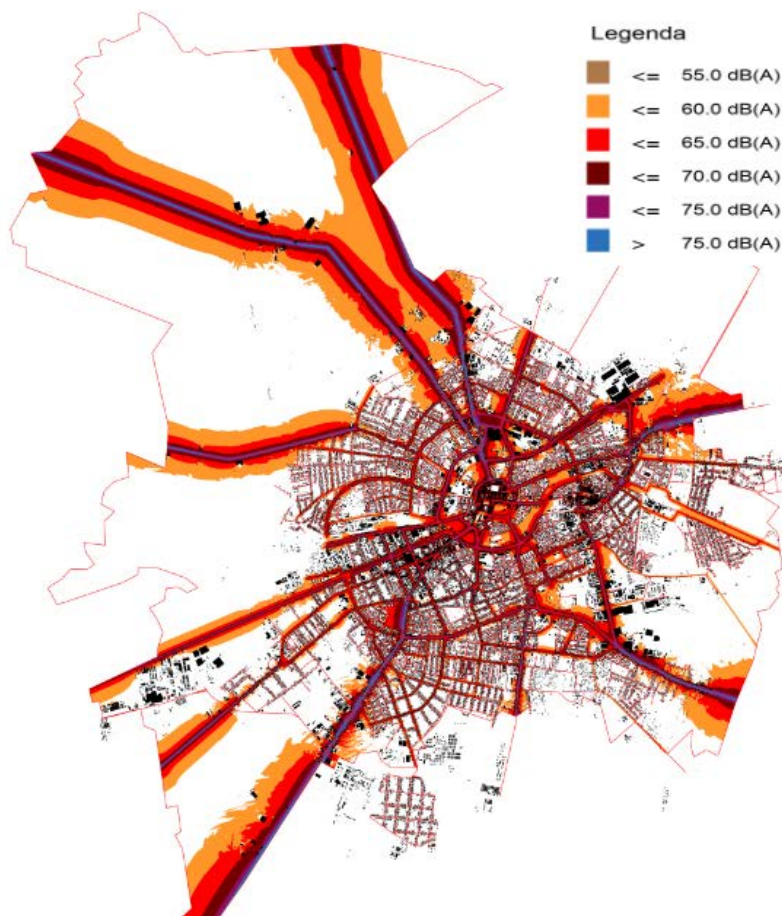


Figure 1: Road traffic noise map -  $L_{den}$

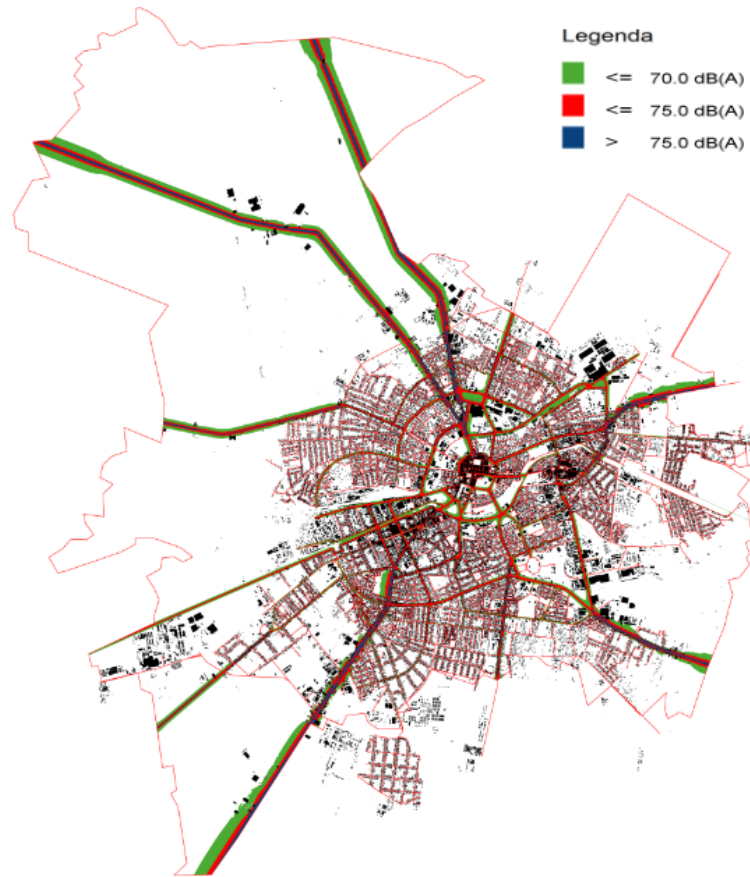


Figure 2: Conflict map for road traffic noise -  $L_{den}$

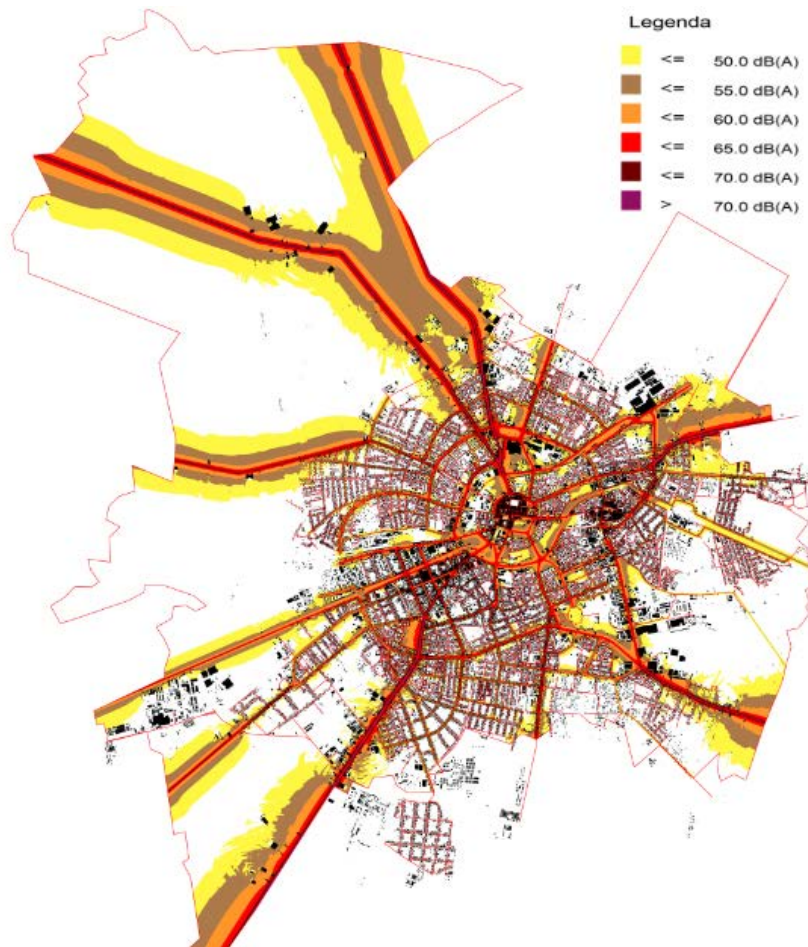


Figure 3: Road traffic noise map -  $L_n$



Figure 4: Conflict map for road traffic noise -  $L_n$

## 8. CONCLUSIONS

Achieving phonic comfort is an important and complex task, not very easy to be accomplished. In this respect it should be identified the noise sources, it should be determined the generated noise levels which should be compared with the admitted limits in force. When a exceeding is identified, reduction measures should be established and implemented. The effectiveness of these measures could be evaluated by new measurements. The identification of the presence of noise may be made by achieving noise maps by simulations with the help of specialized software. In this respect, we anticipated this facility of mapping the noise in the urban environment even from 2007 by achieving not digital maps, but analogic noise maps emphasizing the distribution of the noise in the city of Timisoara. In this respect, we anticipated this facility of mapping the noise even from 2007 by achieving not digital maps, but analogic noise maps emphasizing the distribution of the noise in the city, built up by real measurements in the crossings and along the roads of the city.

## REFERENCES

- [1] A. Darabont and D. Vaiteanu, "Combaterea poluarii sonore si a vibratiilor" Ed. Tehnica Bucuresti (Romania), (1975)
- [2] M. Grumazescu, A. Stan, N. Wegener, "Combaterea zgomotului si vibratiilor", Ed. Tehnica Bucuresti (Romania), (1964)
- [3] E.Ia Iudin, "Izolarea impotriva zgomotului", Ed. Tehnica Bucuresti (Romania), (1968)
- [4] \*\*\* Larmbekamfung in Wien, Entwicklung Stand Tendenzen, Magistratsabteilung, 22, Umweltschutz
- [5] \*\*\* Standtebaulike Larmfibel, Hinweise fur die Bauleitplanung Baden Wurtenberg Innenministerium, 1991
- [6] \*\*\* STAS 10009-88 Acustica urbana. Limite admisibile ale nivelului de zgomot
- [7] \*\*\* STAS 6161/3-82 Metode de determinare a nivelului de zgomotin localitatile urbane
- [8] \*\*\* STAS 10183/1,2,3,4-75 Supravegherea zgomotelor produse de aeronave pe aeroporturi si in vecinatatea acestora
- [9] \*\*\* Directive 2002/49/EC of European Parliament and European Commission
- [10] N. Herisanu, V. Bacria, M. Toader, S. Popa Radovan, "Investigation of noise pollution in urban area", WSEAS Trans. Syst., vol.7, p.1648, (2007)
- [11] <http://www.primariatm.ro>
- [12] V. Bacria, N. Herisanu, "Action plans for noise prevention and reduction in the city of Timisoara", Facta Universitatis, Series Working and living environmental protection , vol.12, p. 139, (2015)



## Optimization of the Flow Schemes in Radiant Recuperators

Rade Karamarković<sup>1,\*</sup>, Vladan Karamarković<sup>1</sup>, Miloš Nikolić<sup>1</sup>, Nenad Stojić<sup>1</sup>, Miljan Marašević<sup>1</sup>

<sup>1</sup>Faculty of Mechanical and Civil Engineering in Kraljevo/Department for Thermal Technique and Environment Protection, University of Kragujevac, Kraljevo (Serbia)

*In glass production and metallurgical processes, radiant recuperators are used to preheat combustion air by heat exchange with high temperature flue gases. For these recuperators, the most popular is concurrent flow arrangement, which compared to other solutions has the lowest interface temperature and the longest lifetime. Compared with concurrent, radiant countercurrent recuperators have only one drawback: the interface temperature is higher at the flue gas entrance. Their comparative advantages are: lower average interface temperature, higher efficiency and smaller pressure drop. Compared with pure concurrent and countercurrent radiant recuperators, designs with double air annulus are slightly more efficient and have a bit smaller interface temperatures, whereas cost and pressure drop are their disadvantages. In the paper, all these four flow configurations are combined by the division of airflow and by the use of different airflow schemes. The improved design is a combination of a countercurrent and a concurrent radiant recuperators. Depending on the geometry, there is an optimal airflow division in the combined recuperator. For the analysis, a cell modeling method validated on a 15 m high, concurrent radiant recuperator used in a glass fiber production process is used. Different solutions are analyzed comparing their effectiveness, energy and exergy efficiencies, and interface temperatures.*

**Keywords:** Radiant recuperator, Heat transfer, Cell modelling method, Effectiveness, Double annulus, Flow division

### 1. INTRODUCTION

Flue gases leaving metallurgical and glass production furnaces contain highly valuable sensible heat. In glass fiber production, flue gas exit temperatures higher than 1200 °C are usual [1]. Thermodynamically, the preferable use of high temperature waste heat is for power production, but in these industries, it is economically justified to use this heat to maintain high temperatures of technological processes. This is achieved by recuperators, in which combustion air is preheated by heat exchange with hot flue gases. The use of preheated air increases combustion temperature and the process efficiency [2].

Recuperators are classified according to [3]: (i) their material: metallic or ceramic, (ii) dominant mode of heat transfer: convective, radiant, and combined (convection and radiation) recuperators etc. Two types of radiant recuperators are frequently used [3]: pipe-in-pipe, depicted in Figs. 1 and 2, and tubular of cage type recuperator. In this field the ongoing research spreads in [3,4]: (i) developing new materials and coatings, (ii) developing new designs, (iii) modification and optimization of the existing designs, and (iv) mathematical modelling.

Compared with concurrent, radiant countercurrent recuperators have only one drawback: the interface temperature is higher at the flue gas entrance. Their comparative advantages are: lower average interface temperature, higher efficiency and smaller pressure drop [4]. The lowest interface temperature produces the longest useful, life-time for a recuperator, and is the main reason why concurrent arrangement is the most popular for recuperators [5]. Compared with pure concurrent and countercurrent radiant recuperators, designs with two air annuluses (see Fig. 2 (e), and (f)) are slightly more efficient and have a bit smaller interface temperatures, whereas cost and pressure drop are their disadvantages. Table 1 shows the recommendations for air and flue gas velocities depending on the design of pipe-in-pipe radiant recuperator [4,6].

*Table 1. Recommended velocities of flue gas and air depending on the design of radiant recuperators. The designs are depicted in Fig.2 (c) – (f).*

	Pipe-in-pipe	Double pipe-in-pipe
Flue gas [m/s]	3-5 [6]	3-5 [4]
Air [m/s]	20-30 [6]	in the outer annulus <2 [4] in the inner annulus 25-30 [4]

The purpose of the paper is to solve the problem of high interface temperatures in countercurrent radiant recuperators without a noticeable decrease of its efficiency by the division of air flow or by the use of different air flow arrangements. Figure 3 shows the examined arrangements. Figure 3 (a) depicts a combined recuperator obtained by the division of air flow. This design distinguishes two different sections and presents combination of a countercurrent and a concurrent heat exchanger. The aim is to unite positive features of both designs. At the flue gas entrance into the recuperator, one air stream flows concurrently to the gas. On the opposite end, the other air stream flows countercurrently to the flue gas. Figure 3. (b) depicts a double pipe-in-pipe (double annulus) configuration, which is similar to the one shown in Fig. 3 (a). The difference is that the air firstly flows through outer and then through the inner annulus. Fig. 3 (c) shows the air flow arrangement without the separation of the air flow. This arrangement also has two different sections. At the entrance of the flue gas, there is a double annulus with a concurrent air flow to the flue gas that flows through the central pipe and a countercurrent flow of the air in the outer annulus to the air in the inner annulus. The air leaving this part of the recuperator than enters into the other part, which has opposite flow configuration. The proposed designs are not a novelty. They have been reported in [5,7] but they have not been thermodynamically analyzed and compared.

\*Corresponding author: Dositejeva 19, 36000 Kraljevo, Serbia, karamarkovic.r@mfv.kg.ac.rs

The basis for the analyses is a 15 m high recuperator used downstream of a glass fiber kiln, which is shown in Figs. 1 and 2. It is a concurrent pipe-in-pipe radiant heat exchanger in which both fluids: flue gas and combustion air, enter from the bottom and exit at the top. Flue gas flows through the central pipe and combustion air flows through the annulus, which is shown in Fig. 2 a) and b). The annulus has fins over the perimeter of the outer surface of the inner cylinder. These fins are placed over the entire annulus length. They influence the heat transfer but are placed primarily to facilitate assemblage, secure the distance

between the cylinders, and prevent buckling and bulging of the innermost cylinder. The structure hangs supported from the above, which means that the maximum load on the material is at the top of the recuperator. To secure material strength in this zone a cooling air is introduced just above the combustion air exit, as can be seen in Fig. 1. The examined recuperator is built from high temperature resistant chrome nickel steel.

The tool for the analysis is a cell modelling method described and validated in [4]. Four different cells enable modelling of all examined flow configurations.

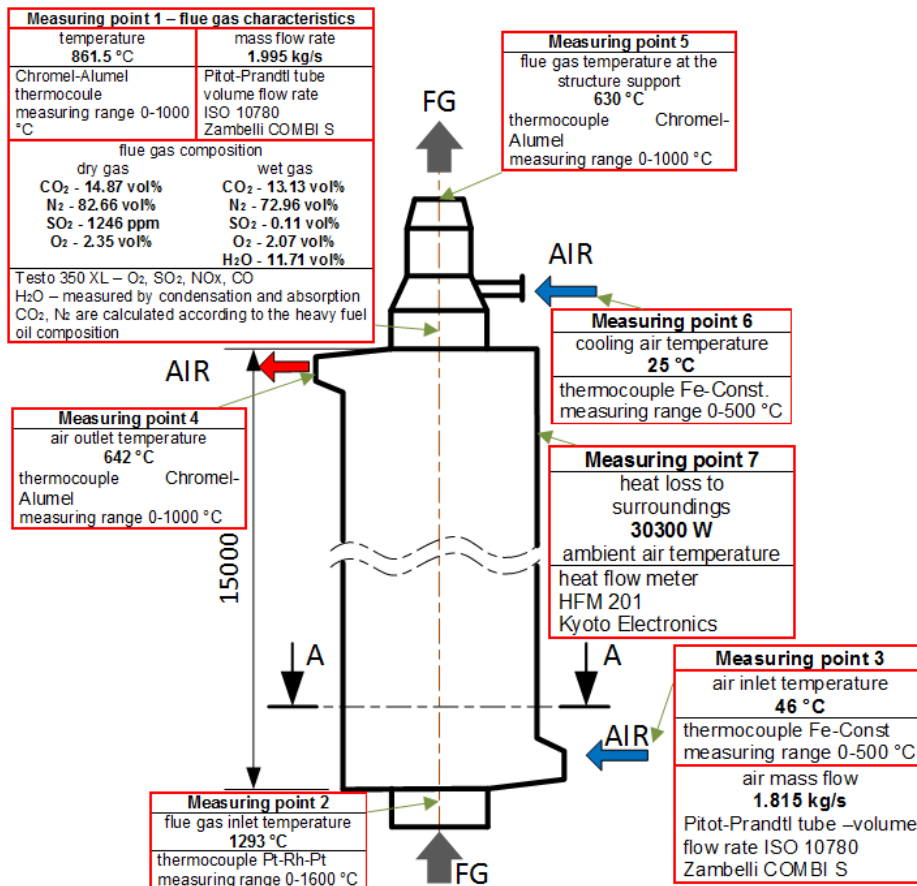


Figure 1: Measuring points, instruments, and results for the examined radiant recuperator.

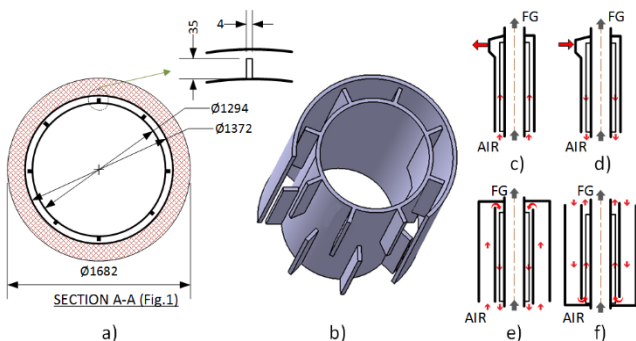


Figure 2: (a) cross section A-A from Fig. 1 of the examined recuperator with the detail of fins, (b) annular air passage, (c) pipe-in-pipe concurrent, (d) pipe-in-pipe countercurrent, (e) double pipe-in-pipe countercurrent, (f) double pipe-in-pipe concurrent recuperator.

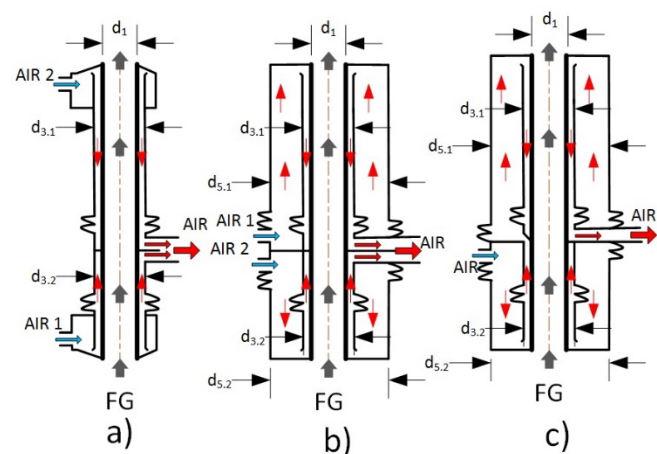


Figure 3: Examined recuperators: (a) combined pipe-in-pipe recuperator, (b) combined double pipe-in-pipe recuperator, (c) combined flow arrangement.

## 2. MASS AND ENERGY BALANCE OF THE EXAMINED RECUPERATOR

Figure 1 shows the mass and energy balances of the examined recuperator. The balances are obtained after 12 hours of examination by combining average measurement values and calculations.

The recuperator is used to preheat air, here at 642°C, for the combustion of heavy fuel oil in a continuous glass furnace. The recuperative furnace produces 669.12 kg/h of glass fiber by the use of 970.03 kg/h or raw material. The temperatures in the furnace are kept in the range from 1298 to 1580 °C by the use of side burners. The flue gas, whose composition is given in Fig. 1, leaves the furnace at 1293 °C. Gravity drives molten glass out of the furnace.

In the figure, the measuring devices are given, too. The relative errors of the measured quantities are: for O<sub>2</sub> ±0.8%, SO<sub>2</sub> ±5%, H<sub>2</sub>O ±3%, volume flow rates ±3%, and for temperatures less than ±0.5%. The presented values are in agreement with [1].

## 3. MODEL

The applied model is explained and validated in [4]. Figure 4 shows the structure of the applied heat transfer model. The heat exchanger is divided into a finite number of area elements over which the two fluid streams flow. In this, so-called cell modelling method, a heat exchanger is represented by a system of interconnected but not overlapping cells. The application of this concept gives insight into the interior of a heat exchanger. The concept also allows representation of a stream with a single cell. There are three types of cells in the model, for: flue gas, air, and insulation. Additionally, there are two types of air cells: with and without fins.

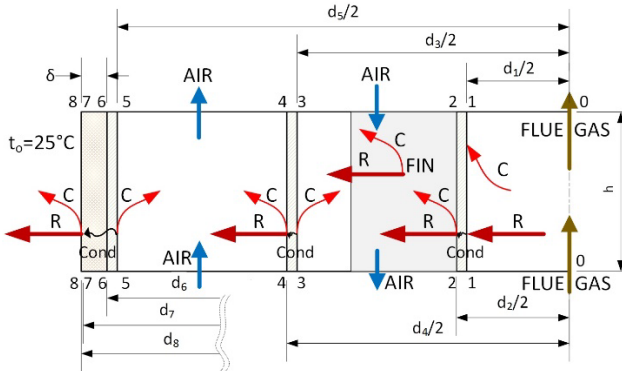


Figure 4: The structure and the principle of the applied cell modeling method.

The first assumptions made in developing the model is that the problem of fluid flow and heat transfer is symmetrical to the central axis of the innermost pipe through which flue gas flows. In Fig. 4, the flue gas cell is limited by the rectangle 0-0-2-2. High temperature flue gas flowing through a pipe is cooled down by convection and radiation. The energy balance for the flue gas in the *i*-th cell is

$$\dot{m}_{FG} c_{pFG} \Big|_{T_{in,FG_i}}^{T_{out,FG_i}} (T_{in,FG_i} - T_{out,FG_i}) = \dot{Q}_{con,FG_i} + \dot{Q}_{rad,FG_i}, \quad (1)$$

where,  $\dot{m}_{FG} = 1.995$  kg/s is the mass flow rate,  $c_p$  in J/kg is the average heat capacity between the inlet  $T_{in,FG}$  and the

outlet  $T_{out,FG}$  temperature of the flue gas in the *i*-th cell. The first term on the right side of Eq. (1) is the convective heat flow rate  $\dot{Q}_{con,FG}$  in W from the flue gas to the pipe wall in the *i*-th cell and is calculated by the model presented in [8]. The second term on the right side of Eq. (1),  $\dot{Q}_{rad,FG}$  in W represents the radiative heat transfer rate from the flue gas mixture onto the circumference of the enclosing pipe. The radiative heat transfer is calculated by the model presented in [9]. The heat transfer rate, which the inner wall of the pipe (1-1 in Fig. 4) obtains by the convective and radiative heat transfer rate from the flue gas is transmitted to the outer side of the innermost pipe (2-2 in Fig. 4) by the conduction heat flow rate  $\dot{Q}_{cond,FG}$ :

$$\dot{Q}_{cond,FG_i} = \dot{Q}_{con,FG_i} + \dot{Q}_{rad,FG_i} = \frac{T_{w1_i} - T_{w2_i}}{2\pi\lambda_{steel} \frac{1}{d_1} \ln \frac{d_1}{d_2}}, \quad (2)$$

where  $\lambda_{steel} = 31$  W/mK is the thermal conductivity for the pipe [10]. The diameters in Eq. (2) are shown in Fig. 4.

The rectangle 2-2-4-4 in Fig. 4 limits the air cell. The air flowing through the concentric annular duct is heated by convective heat transfer rates from the inner (2-2) and the outer cylinder (4-4 in Fig. 3). The energy rate balance for the air flow in the *i*-th cell is:

$$\dot{m}_a c_{pa} \Big|_{T_{in,a_i}}^{T_{out,a_i}} (T_{out,a_i} - T_{in,a_i}) = \dot{Q}_{con,in_i} + \dot{Q}_{con,out_i}, \quad (3)$$

where  $\dot{m}_a = 1.815$  kg/s is the mass flow rate of air (see Fig. 1),  $c_p$  in J/kg is the average heat capacity between the inlet  $T_{in,a}$  and the outlet  $T_{out,a}$  temperature of the air in the *i*-th cell.  $\dot{Q}_{con,in}$  in W and  $\dot{Q}_{con,out}$  in W are the convective heat transfer rates from the inner and outer surface of the annulus, respectively. A model given in [11] that calculates the heat transfer in concentric annular ducts for fully developed turbulent flow is used to calculate the heat transfer coefficient, which is used to calculate heat transfer rate in each air cell.

In addition to the air flow energy rate balance Eq. (3), the energy rate balances in W for the outer surface of the inner cylinder Eq. (4) and the inner surface of the outer cylinder Eq. (5) are used (surfaces 2-2 and 3-3 in Fig. 4):

$$\dot{Q}_{cond,FG_i} = \dot{Q}_{con,in_i} + \dot{Q}_{rad,in_i}, \quad (4)$$

$$\dot{Q}_{rad,in_i} = \dot{Q}_{con,out_i} + \dot{Q}_{cond,out_i}. \quad (5)$$

The heat flow rate from the corresponding flue gas cell  $\dot{Q}_{cond,FG}$  is partly transferred by heat convection to the air  $\dot{Q}_{con,in}$  and partly radiated to the outer surface of the annulus  $\dot{Q}_{rad,in}$ . The radiated heat is then transferred by heat convection to the air  $\dot{Q}_{con,out}$  and partly transferred to the surroundings or the outer air cell  $\dot{Q}_{cond,out}$  depending on the examined construction.

The radiative heat transfer rate  $\dot{Q}_{rad,in}$  consists of two components, which are calculated by the model presented in [12]. The first component of the radiative heat transfer is from the outer surface of the inner cylinder (surface 2-2 in Fig. 4) to the inner surface of the outer cylinder (3-3) [12]. The other component is from the fins to the inner surface of the outer cylinder (3-3).

The term  $\dot{Q}_{\text{cond,out}}$  in Eq. (5) is the heat transfer rate through the outer surface of the air cell, which is calculated in each cell as in Eq. (2)

$$\dot{Q}_{\text{cond,out}_i} = \frac{T_{\text{out}_i} - T_{4_i}}{\frac{1}{2\pi\lambda_{\text{steel}} \ln \frac{d_4}{d_3}}} \quad (6)$$

The heat transfer rate defined by Eq. (6) from all outer air flowing cells is transferred by heat conduction through an insulating layer and then by natural convection  $\dot{Q}_{\text{con,loss}}$  and radiation  $\dot{Q}_{\text{rad,loss}}$  to the surroundings. These two components define the heat loss  $\dot{Q}_{\text{loss}} = \dot{Q}_{\text{con,loss}} + \dot{Q}_{\text{rad,loss}}$ . The heat flow rate towards the surroundings by convection is calculated by [13], whereas the radiative heat loss is calculated by [12]. As there are several air cells that are connected to an insulation cell, the temperature at the outer surface of the outermost air-flowing cylinder is determined as the arithmetic mean of the corresponding temperatures for all air cells connected to the insulation cell.

The physical properties of all the quantities in the model are referred to the mean air temperature in the cell. Densities, thermal conductivities, thermal diffusivities, dynamic viscosities, Prandtl numbers and air specific heat capacities and enthalpies are calculated by [14-16]. Specific heat capacities and enthalpies of gas species in the flue gas are calculated by [17].

Each cell is 2.5 m high, except the insulation cell which is 15 m high. The disadvantage of the developed model is the negligence of the radiative heat transfer between cells of the same type. This impact is very small between air cells due to tiny view factors. Oppositely, the view factor between two adjacent flue gas cells is not negligible.

### 3.1. The effectiveness and exergy efficiency of recuperators

The determination of the outlet temperatures of flue gas and combustion air for a recuperator enables calculating its effectiveness  $\xi$ , which is the dimensionless ratio between the actual heat transfer and the maximal possible one in a heat exchanger [18]:

$$\xi = \frac{T_{a,\text{out}} - T_{a,\text{in}}}{T_{FG,\text{in}} - T_{a,\text{in}}} \quad (7)$$

It allows comparison of the analyzed designs. Additionally, exergy efficiency enables the comparison between the analyzed designs. It is defined as the ration between all the exergy flow rates that leave the system (flue gas, heat loss, air) to the exergy flow rates that enters the system (flue gas and air):

$$\psi = \frac{\sum_{\text{out}} \dot{E}x}{\sum_{\text{in}} \dot{E}x} \quad (8)$$

In Eq. (8) all exergy flow rates are calculated as in [19].

### 3.2. Flow ratio

The all analyses are performed with the constant air flow of 1.815 kg/s. In designs presented in Fig. 3 a) and b) the flow is divided. The measure of the division is the flow ratio  $m$  [-], which is the mass flow rate of air through the

countercurrent section  $\dot{m}_{cc}$  relative to the total air mass flow  $\dot{m}$

$$m = \frac{\dot{m}_{cc}}{\dot{m}} \quad (9)$$

## 4. RESULTS

The data presented in this section relate to the examined recuperator and its input data (flow rates and inlet temperatures as in Fig. 1). Figure 5 shows what has been stressed in the introduction section, compared with the pure concurrent radiant recuperator, the countercurrent has a higher interface temperature at the flue gas entrance.

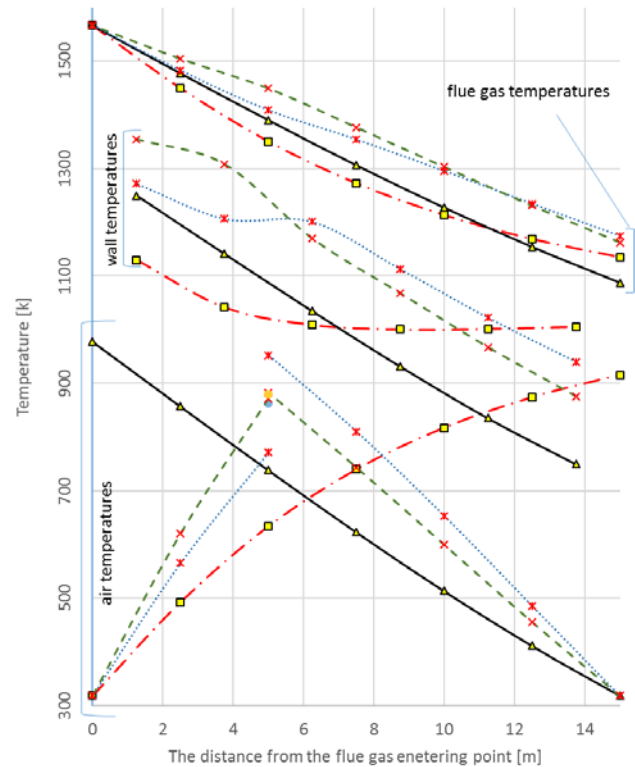


Figure 5: The temperature profiles of flue gas, air and inner surface of the innermost cylinder along the recuperator for different designs that have the same geometry as the experimental recuperator (solid line – countercurrent (Fig. 2 d)), long dash dot line – experimental concurrent (Fig. 2 c)), dash line – combined  $m=0.7$  (Fig. 3 a)  $d_1=1284$  mm,  $d_{3,1}=d_{3,2}=1372$  mm), dotted line – combined  $m=0.5$ ).

If the air flow is divided to obtain a combined recuperator, which consists of a concurrent section at the flue gas entrance and a countercurrent section at the flue gas exit, the exit temperature of air is obtained as a mixture of two streams (see Fig. 3. a)). The effectiveness, exit temperatures and interface temperatures depend on the flow ratio  $m$  if the combined recuperator has the existing dimensions (diameters and fins), which are shown in Figs. 1 and 2, and if the air flow is divided so as the the concurrent and the countercurrent sections are 5 and 10 m long, respectively. The division of the recuperator onto two unequal sections is made based on the interface temperatures for pure concurrent and countercurrent radiant recuperator. These temperatures are shown in Fig. 5. If the existing dimensions are kept, the effectiveness of the combined recuperator is substantially lower than for the existing concurrent recuperator (see Fig. 6). Additionally, maximal interface temperatures are extremely high for

$m=0.5$  and  $m=0.7$ , as it is shown in Fig. 5. The reason for this behavior are the air velocities in the both sections. If the same dimensions are retained as in the existing concurrent recuperator, the temperatures and mass flow rates of air through the sections of the combined recuperator are smaller. Although there are high temperature differences (see Fig. 5) and equal surface areas for the convective heat transfer, the heat flow rate from the flue gas to the air is smaller. Compared to its dependence on temperature difference, the heat transfer coefficient in these annular ducts depends more on air velocity.

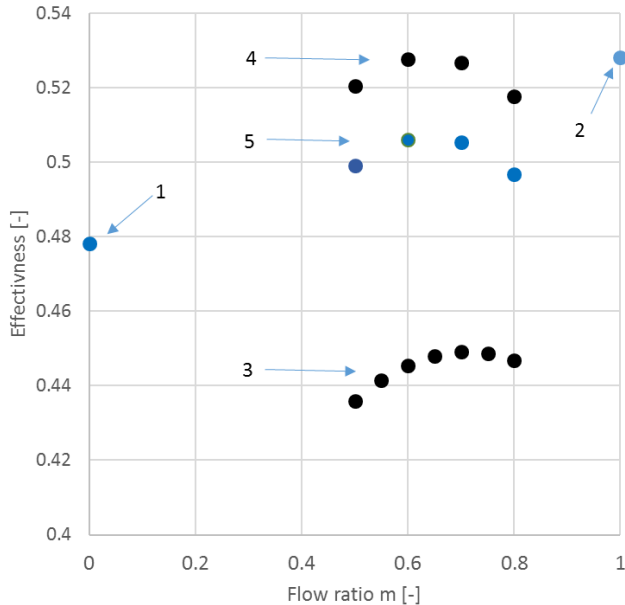


Figure 6: The effectiveness for different radiant recuperator designs; 1 – the existing concurrent recuperator, 2 – the existing countercurrent, 3 – combined ( $d_1=1284$  mm,  $d_{3,1}=d_{3,2}=1372$ mm), 4 – combined ( $d_1=1284$  mm,  $d_{3,1}=1338$  (fins  $18 \times 4 \times 500$ mm),  $d_{3,2}=1330$  (fins  $15 \times 4 \times 500$  mm)), 5 – combined ( $d_1=1284$  mm,  $d_{3,1}=1354$  (fins  $25 \times 4 \times 500$ mm),  $d_{3,2}=1334$  (fins  $15 \times 4 \times 500$  mm))

The effectiveness increases if the cross sections of the annuluses decrease (see Fig. 6). This influences the rise of the velocities in both sections of the combined recuperator as can be seen in Fig. 8. However, the cross section of the annulus cannot decrease substantially as it can produce a large pressure drop. Figure 6 shows that for the examined dimensions of combined radiant recuperators, there is an optimal flow ratio. For the recuperator with the existing dimensions the optimal ratio  $m$  is around 0.7, whereas for smaller annuluses the optimal ratio is around 0.6.

The combined radiant recuperators, which have an approximately isothermal mixing of two air streams, have the maximal effectiveness. This is shown in Fig. 9, which also depicts the flue gas, wall (interface), and air temperatures across the examined recuperators. For the applied dimensions of air annuluses, the interface temperatures for flow ratio of 0.6 are substantially lower than for the pure countercurrent radiant heat exchanger (see Fig 5.). The reason is a larger temperature difference between the flue gas and the air.

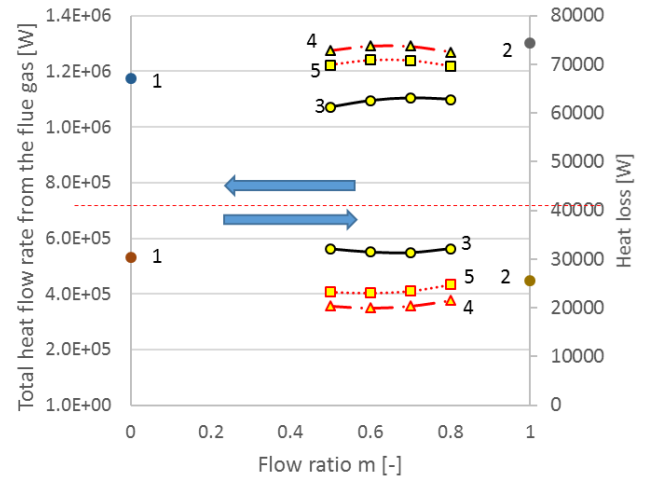


Figure 7: The total heat flow rate from the flue gas and the heat loss depending on the flow ratio  $m$ , for different designs: 1 – existing concurrent recuperator, 2 – existing countercurrent, 3 – combined ( $d_1=1284$  mm,  $d_{3,1}=d_{3,2}=1372$ mm (fins  $35 \times 4 \times 500$ )), 4 – combined ( $d_1=1284$  mm,  $d_{3,1}=1338$  (fins  $18 \times 4 \times 500$ mm),  $d_{3,2}=1330$  (fins  $15 \times 4 \times 500$  mm)), 5 – combined ( $d_1=1284$  mm,  $d_{3,1}=1354$  (fins  $25 \times 4 \times 500$ mm),  $d_{3,2}=1334$  (fins  $15 \times 4 \times 500$  mm))

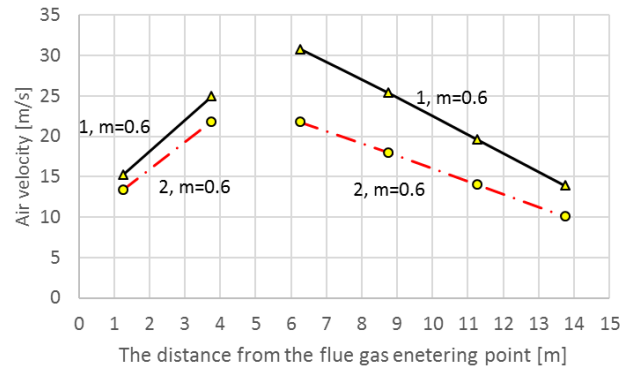


Figure 8: The average air velocities in different sections of the combined recuperator, 1 -  $d_1=1284$  mm,  $d_{3,1}=1338$  (fins  $18 \times 4 \times 500$ mm),  $d_{3,2}=1330$  (fins  $15 \times 4 \times 500$  mm), 2 –  $d_1=1284$  mm,  $d_{3,1}=1354$  (fins  $25 \times 4 \times 500$ mm),  $d_{3,2}=1334$  (fins  $15 \times 4 \times 500$  mm)

The combined recuperator with tighter annuluses has larger velocities (see Fig. 8) and consequently a larger average heat transfer coefficient. The temperature profiles along these recuperators are shown in Fig. 9. The figure shows that the most suitable interface temperature have the designs with the largest effectiveness (see Figs. 6 and 7), which have approximately isothermal mixing of two streams.

Figure 7 shows that a lot of different designs of combined recuperator could perform better than the existing concurrent one. Figure 7 also shows the heat losses to the surroundings for the same thickness of insulation applied over the examined designs: 20 cm of mineral wool covered with an aluminum sheet. The differences in heat losses are due to the different air temperatures in air annuluses (the smaller the air temperature the smaller the outer wall temperature) and different outer diameters (the larger the diameter the larger the heat loss).

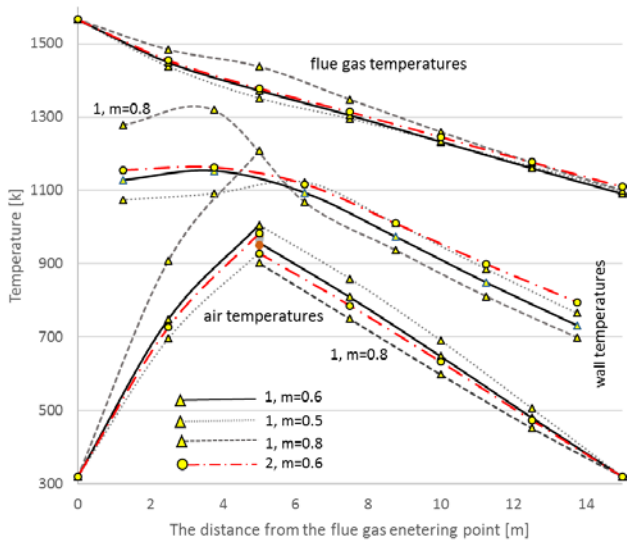


Figure 9: The temperature profiles of flue gas, air and inner surface of the innermost cylinder along the recuperator for different designs of combined recuperator and different flow ratios; 1 and 2 marks the same designs as in Fig. 8.

The application of the second outer annulus over the combined recuperator (double pipe-in-pipe combined design (DC)), with the dimension of the inner annulus as in the existing recuperator, substantially decreases the interface temperature and increases its effectiveness (see Fig. 10 and Tab. 2). Of course, the outer annulus increases the total surface area for the heat transfer. By the variation of all the diameters in this design an improved effectiveness could be obtained.

The smaller interface temperatures could be obtained with a different flow arrangement too. Figure 10 shows this as well. The drawback of the presented CFA design is the pressure drop, which depends on air velocities that are shown in Fig. 11.

Table 2. Properties of the combined double pipe-in-pipe recuperator DC (Fig. 3 b),  $d_1=1284$  mm,  $d_{3,1}=1338$  (fins  $18 \times 4 \times 500$  mm),  $d_{3,2}=1330$  (fins  $15 \times 4 \times 500$  mm),  $d_{5,1}=1650$ ,  $d_{5,2}=1450$ , material thickness 5 mm,  $m=0.61$ ) and for the combined flow arrangement CFA shown in Fig. 3 c) ( $d_1=1284$  mm,  $d_{3,1}=d_{3,2}=1372$  (fins as in Fig. 2),  $d_{5,1}=d_{5,2}=1550$ , material thickness 5 mm)

	DC (Fig 3 b))	CFA (Fig 3 c))
Total heat flow rate [MW]	1.30	1.24
Heat loss [W]	20800	19500
Effectiveness	0.529	0.507

The exergy efficiency is not suitable for the application on the examined designs, because it is primarily influenced by the flue gas exergy. Compare with the air exergy, the exergy of the flue gas is substantially larger and influences small variations between exergy efficiencies of the examined designs. Nevertheless, for the examined designs the change in exergy is proportional to the change in effectiveness.

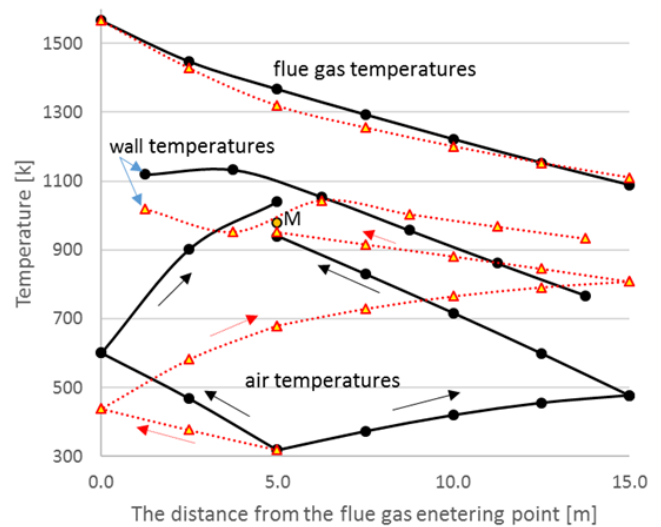


Figure 10: The temperature profiles of flue gas, air and inner surface of the innermost cylinder along the recuperator; solid line – DC recuperator ((Fig 3. b)  $d_1=1284$  mm,  $d_{3,1}=1338$  (fins  $18 \times 4 \times 500$  mm),  $d_{3,2}=1330$  (fins  $15 \times 4 \times 500$  mm),  $d_{5,1}=1650$ ,  $d_{5,2}=1450$ , material thickness 5 mm,  $m=0.61$ ), dotted line – CFA ((Fig. 3 c)  $d_1=1284$  mm,  $d_{3,1}=d_{3,2}=1372$  (fins as in Fig. 2),  $d_{5,1}=d_{5,2}=1550$ , material thickness 5 mm)

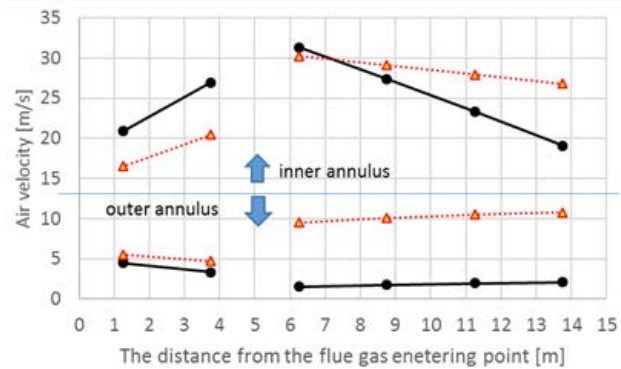


Figure 11: The average air velocities along the DC and CFA recuperators (dimensions are given in Fig. 10)

### 5. CONCLUSIONS

From the applied analysis, it can be concluded that the effectiveness of a radiant recuperator could be increased and the interface temperature could be decreased by the implementation of the combined radiant recuperator, double combined recuperator and combined air flow arrangements. The presented solutions sum up comparative advantages of concurrent, countercurrent and double-pipe-in-pipe radiant recuperators.

Depending on the applied geometry, there is an optimal airflow division to concurrent and countercurrent sections of a combined radiant recuperator. For the examined designs, the optimal dimensions should be obtained by an economic analysis. Certainly, designs that are more complex are more expensive. Also, smaller cross section areas of air flow annuluses influence larger heat transfer coefficients and oppositely larger pressure drops.

For all presented solutions (see Fig. 3), the optimal design should have the variable diameters of annuluses along the recuperator.

## REFERENCES

- [1] [http://www.lehigh.edu/imi/teched/GlassProcess/Lectures/Lecture03\\_Hubert\\_industglassmeltingfurnaces.pdf](http://www.lehigh.edu/imi/teched/GlassProcess/Lectures/Lecture03_Hubert_industglassmeltingfurnaces.pdf)
- [2] Dolianitis, I., *et al.*, "Waste heat recovery at the glass industry with the intervention of batch and cullet preheating," *Thermal Science*, Vol 20 (4), pp. 1245-1258, (2016)
- [3] Sharma, H., *et al.*, "A review of metallic radiation recuperators for thermal exhaust heat recovery", *Journal of Mechanical Science and Technology*, Vol 28 (3), pp. 1099-1111, (2014)
- [4] S. Knežević, R. Karamarković, V. Karamarković, N. Stojić, "Radiant recuperator: modeling and design", *Thermal Science*, Vol 21 (2), pp. 1119-1134, (2017)
- [5] Marnell, C.J., "Development of the radiant recuperator", *Proceedings of The first industrial energy technology conference*, Houston, TX, April 1979, pp. 607-619, (1979)
- [6] Mitov, I., "Comparative analysis of the energy efficiency of metal recuperators with a different design", *Journal of the University of Chemical Technology and Metallurgy*, Vol. 46 (4), pp. 427-432, (2011)
- [7] Meder S.R., White A. J., "Air-cooled radiation recuperator", US Patent No. 3446279 A, (1969)
- [8] Gnielinski, V., "Heat Transfer in Pipe Flow", in: VDI Gesellschaft, VDI Heat Atlas, second ed., Springer, Heidelberg (Germany), pp. 693-699, (2010)
- [9] Vortmeyer, D., Kabelac, S., "Gas Radiation: Radiation from Gas Mixtures", in: VDI Gesellschaft, VDI Heat Atlas, second ed., Springer, Heidelberg (Germany), pp. 979-989, (2010)
- [10] Kozić, Dj., *et al.*, "Handbook for Thermodynamics (Priručnik za termodinamiku)", Faculty of Mechanical Engineering, Belgrade (Serbia), (1995)
- [11] Gnielinski, V., "Heat transfer in concentric annular and parallel plate ducts", in: VDI Gesellschaft, VDI Heat Atlas, second ed., Springer, Heidelberg (Germany), pp. 947-959, (2010)
- [12] Kablec, S., Vortmeyer, D., "Radiation of surfaces", in: VDI Gesellschaft, VDI Heat Atlas, second ed., Springer, Heidelberg (Germany), pp. 947-959, (2010)
- [13] W. Kast, H. Klan, "Heat Transfer by Free Convection: External Flows", in: VDI Gesellschaft, VDI Heat Atlas, second ed., Springer, Heidelberg (Germany), pp. 667-671, (2010)
- [14] Kleiber, M., Joh, R., "Calculation methods for thermophysical properties", in: VDI Gesellschaft, VDI Heat Atlas, second ed., Springer, Heidelberg (Germany), pp. 121-152, (2010)
- [15] Kleiber, M., Joh, R., "Properties of selected important pure substances", in: VDI Gesellschaft, VDI Heat Atlas, second ed., Springer, Heidelberg (Germany), pp. 153-299, (2010)
- [16] Kleiber, M., Joh, R., "Properties of pure fluid substances", in: VDI Gesellschaft, VDI Heat Atlas, second ed., Springer, Heidelberg (Germany), pp. 301-417, (2010)
- [17] Balmer, R.T., "*Thermodynamics*", West Publishing Company, ST. Paul, New York, Los Angeles, San Francisco, (USA), (1990)
- [18] <http://www-unix.ecs.umass.edu/~rlaurenc/Courses/che333/lectures/Heat%20Transfer/Lecture21.pdf>
- [19] V. Karamarković, M. Marašević, R. Karamarković, M. Karamarković, "Recuperator for waste heat recovery from rotary kilns", *Appl. Therm. Eng.*, Vol. 54 (2), pp. 470-480, (2013).





## Acoustic Properties of Recycled Rubber at Normal Incidence

Milan Kolarević<sup>1\*</sup>, Branko Radičević<sup>1</sup>, Nicolae Herisanu<sup>2</sup>, Miloje Rajović<sup>1</sup>, Vladan Grković<sup>1</sup>

<sup>1</sup>University of Kragujevac, Faculty of Mechanical and Civil Engineering, Kraljevo, Serbia

<sup>2</sup>"Politehnica" University of Timisoara, Faculty of Mechanical Engineering, Timisoara, Romania

*This paper presents the results of testing acoustic properties of samples formed of recycled rubber granules and a binding agent made of polyurethane resins. The testing was performed in an impedance tube with the diameter of 100mm by using the transfer function method between two microphones defined by the standard SRPS EN ISO 10534-2. The samples with the thickness between 10mm and 50mm were tested. The results show that recycled rubber has excellent absorption properties and that the increase in thickness of the material leads to the increase in the values of the sound absorption coefficient at lower frequencies.*

**Keywords:** recycled rubber, absorption coefficient, passive noise protection

### 1. INTRODUCTION

The consequence of constant increase in human population and development of engineering is big environmental problems which are particularly pronounced in the increased level of noise in urban environments and the need for storing different types of industrial waste. Storing and recycling of used car tyres have become, in the last decades, one of the biggest problems related to the environment. The solution of the problem is being searched for in the possibility of recycling rubber waste.

Until several years ago, waste tyres in Serbia were deposited in legal and illegal waste dumps. They were used as a fuel in technically inadequate furnaces and uncontrolled burning processes (brick yards/fields, lime pits...) thus being a serious ecological problem. Since 2009, these problems have been coordinated with the EU legal regulations and today, in compliance with the Rulebook on Methods and Procedures for Waste Tyre Disposal Management (The Official Gazette of RS number 104/2009), more and more waste tyres are being recycled into various rubber raw materials and products [1].

Acoustic properties of rubber have been the subject of a lot of research [2÷14] in order to test the possibility of using rubber for passive noise protection. It has been shown that the preliminary results of the absorption coefficient of these tyre samples, under normal incidence conditions, are rather high.

This paper presents the initial results of the research organised for the purpose of finding possibilities for mastering new products on the basis of recycled rubber granules. The research was realised within the project TR

37020 "Development of Methodologies and Means for Noise Protection in Urban Environments" financed by the Ministry of Education, Science and Technological Development of the Republic of Serbia [15].

### 2. EXAMINATION OF ABSORPTION PROPERTIES OF RECYCLED RUBBER

#### 2.1. Research plan

The research plan foresaw testing of acoustic properties of recycled rubber granules in the frequency range 125Hz-1600Hz as well as the dependence of the sound absorption coefficient on the material thickness. The factors tested and the intervals of their change are presented in Table 1.

*Table 1. Factors for response surface study*

Factor	Name	Mark	Units	Low	High
				Level (-1)	Level (+1)
<b>A</b>	frequency	$f$	Hz	125	1600
<b>B</b>	thickness	$d$	m	0.01	0.05

#### 2.2. Material and preparation of samples

The testing samples were made of recycled rubber granules (granule dimensions from 3 to 5mm) and a binding agent made of polyurethane resins. They were cast in moulds whose diameter was 100mm and thickness 10mm, 20mm, 30mm, 40mm and 50mm (Figure 1) without pressing in order to provide the porosity of samples. Porosity is necessary because it provides the loss (dispersion) of sound energy in interconnected pores of the material.



*Figure 1. Samples made of recycled rubber*

The physical properties of the material made of recycled rubber were taken from the catalogue of the manufacturer "Tigar – Technical Rubber" a.d. – Pirot [16], and they are shown in Table 2.

Table 2. Physical properties of the material made of recycled rubber [16]

Hardness	[ShA]	70±10
Density	[kg/m <sup>3</sup> ]	750 - 900
Tensile strength	[MPa]	0.4
Abrasion resistance	[mm <sup>3</sup> ]	200
Elongation	[%]	50
Compression	[%]	4.3

### 2.3. Method and equipment

The measurement of absorption was done in the impedance tube by using the transfer function method between two microphones, described in the SRPS EN ISO 10534-2 standard [17]. This method is based on the decomposition of the standing wave which is formed in the tube by recording signals from two microphones and calculating their transfer function. The reflection

coefficient is calculated from the transfer function, and then the absorption coefficient is calculated. This method results in obtaining the values of the absorption coefficient at normal incidence, in the frequency range defined by the physical dimensions of the tube and the distance between the microphones. By using this method, it is possible to obtain fast measurements for normal incidence, using small samples.

$$\alpha = 1 - |R|^2 \quad (1)$$

where R is the reflection coefficient calculated according to the expression:

$$R = \frac{H - e^{-jks}}{e^{jks} - H} e^{j2k(l+s)} \quad (2)$$

Where:

- $H$  – the corrected transfer function,
- $s$  – the distance between the microphones,
- $l$  – the distance between the closer microphone and the sample, and
- $k$  – the wave number.

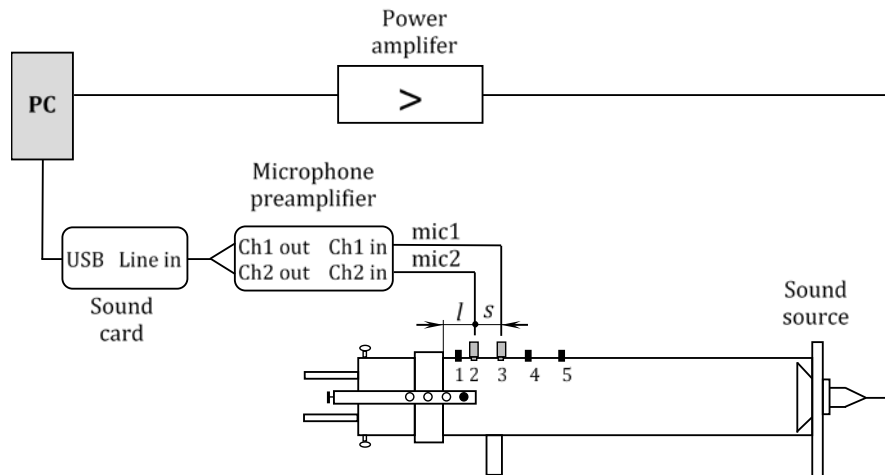


Figure 2. System for measuring absorption according to the standard SRPS EN ISO 10534-2 [17]

The method of impedance of the tube has numerous advantages, which are described in the literature [17], the most important of them being:

- the measuring device is of small dimensions, so that it is very practical for use,
- the samples themselves have small dimensions, which facilitates their preparation for measurement,
- small costs of the experiment.

The disadvantages of this method:

- only normal incidence of waves are measured, although it is possible to apply correction to obtain a value of the absorption coefficient with random incidence,
- different diameters of tubes and samples are necessary in order to cover a wider frequency range.

## 3. RESULTS AND DISCUSSION

### 3.1. Experimental results

Experimental values of the absorption coefficient per 1/3 octave bands for different material thicknesses obtained by measuring in the impedance tube are shown in Table 3.

Table 3. Values of the absorption coefficient for recycled rubber

$f$ (Hz)	$d$ (cm)				
	1	2	3	4	5
125	0.062079	0.061709	0.074983	0.079582	0.078801
160	0.046224	0.048147	0.061382	0.072933	0.082575
200	0.050688	0.064102	0.071529	0.088792	0.093929
250	0.033774	0.043948	0.060364	0.095229	0.10363
315	0.047438	0.051707	0.078651	0.11827	0.13687
400	0.052127	0.067505	0.08809	0.17284	0.20107
500	0.051058	0.069412	0.11152	0.23979	0.28714
630	0.057375	0.086028	0.14524	0.36262	0.44561
800	0.068572	0.111380	0.20821	0.5924	0.72293
1000	0.077245	0.146640	0.31118	0.85416	0.95535
1250	0.10620	0.245290	0.54574	0.91899	0.87541
1600	0.14311	0.410970	0.85543	0.72432	0.65755

From Table 3 and Figure 3 the following can be noted:

- At low frequencies up to 400Hz, recycled rubber does not have pronounced absorption properties and the absorption coefficient ranges in the interval from 0.03 for the thickness of 10mm to 0.2 for the material thickness of 50mm.

- The absorption coefficient increases with the increase in the material thickness. For the material thicknesses from 10mm to 30mm, the maximum value of the absorption coefficient is at the frequency of 1600Hz, as follows: for d=10mm it is  $\alpha=0.14$ , for d=20mm it is  $\alpha=0.42$  and for d=30mm it is  $\alpha=0.86$ .
- For the rubber thickness of d=40mm, the maximum value of the absorption coefficient is  $\alpha=0.92$  for the frequency f=1250Hz, while this value decreases at higher and lower frequencies. Rubber accomplishes the highest efficiency regarding absorption in the

range from 800Hz to 1600Hz, where the absorption coefficient ranges in the interval from 0.6 to 0.92.

- For the rubber thickness d=50mm, the maximum value of the absorption coefficient is  $\alpha=0.96$  for the frequency f=1000Hz, while this value decreases at higher and lower frequencies. Rubber accomplishes the highest efficiency regarding absorption in the range from 700Hz to 1600Hz, where the absorption coefficient ranges in the interval from 0.6 to 0.96.

It can be concluded that the absorption coefficient of recycled rubber increases with the increase in the material thickness, but at the same time its maximum moves toward relatively lower frequencies up to 1000Hz.

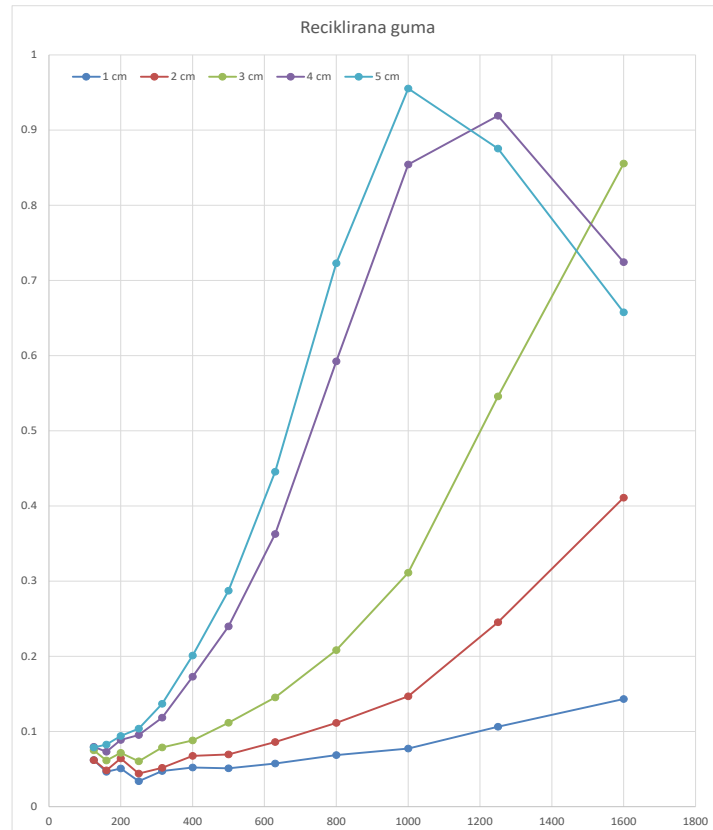


Figure 3. Values of the absorption coefficient for recycled rubber

### 3.2. Procession and analysis of the experimental results

In order to carry out the procedure of regression analysis and perform the selection of an adequate regression model after the selection of the experimental plan and performed experimental measurements, it is necessary to carry out the following phases [18, 19]:

- Entering experimental data
- Summary statistics of possible mathematical models
- Selection of the stochastic model
- ANOVA analysis – evaluation of the significance of the model
- Evaluation of the model adequacy
- Interval evaluation of the model parameters
- Diagnostics of the model and, if necessary, transformation of the model
- Interval evaluation of the regression function
- Graphical interpretation and interpretation of the model.

The data procession was performed in the software package Design Expert v.9.0.6.2. [20, 21]. Out of the available mathematical models, the models proposed have the form of third and fourth degree polynomials (Table 4).

Table 4. Summary statistics of possible mathematical models

Source	Std. Dev.	R-Squared	Adjusted R-Squared	Predicted R-Squared	PRESS
Linear	0.37	0.8620	0.8571	0.8418	8.71
2FI	0.32	0.8933	0.8875	0.8514	8.18
Quadratic	0.30	0.9140	0.9060	0.8680	7.27
Cubic	0.14	0.9812	0.9779	0.9681	1.76 Suggested
Quartic	0.12	0.9876	0.9837	0.9473	2.90 Suggested
Fifth	0.10	0.9922	0.9885	0.9369	3.47 Aliased

The cubic model was adopted. In order to improve the results of the analysis, it was necessary to perform the transformation of the response function by means of the natural logarithm (Natural Log,  $k=0, \lambda=0$ ). After reduction

of nonsignificant members from the proposed model, the analysis of variance (ANOVA) for the transformed cubic model was performed.

Table 5. ANOVA report for recycled rubber

ANOVA for Response Surface Cubic model					
Source	Sum of Squares	df	Mean Square	F Value	p-value Prob > F
Model	54.02	9	6.00	290.60	< 0.0001 significant
A-f	5.89	1	5.89	285.21	< 0.0001
B-d	6.56	1	6.56	317.81	< 0.0001
AB	0.72	1	0.72	34.69	< 0.0001
A^2	1.03	1	1.03	49.83	< 0.0001
B^2	0.69	1	0.69	33.37	< 0.0001
A^2B	2.51	1	2.51	121.63	< 0.0001
AB^2	0.65	1	0.65	31.65	< 0.0001
A^3	0.25	1	0.25	12.26	0.0010
B^3	0.28	1	0.28	13.68	0.0005
Residual	1.03	50	0.021		
Cor Total	55.05	59			

The high F value of the model (F=290.60) and the low value of probability (p<0.0001) indicate that the model is significant. The coefficient of determination (R-Squared) and other statistics (Table 6) have good values, which justifies the selection of the adopted mathematical model.

Table 6. Calculation values of the statistics for the evaluation of the mathematical model

Std. Dev.	0.14
Mean	-1.99
C.V. %	7.22
PRESS	1.76
R-Squared	0.9812
Adj R-Squared	0.9779
Pred R-Squared	0.9681
Adeq Precision	53.276

The value of regression coefficients of the mathematical model, the standard error, 95% confidence intervals and the Variance inflation factor (VIF) of regression coefficients are presented in Table 7.

Table 7. Values of coefficients of the mathematical model and confidence intervals

Factor	Coefficient Estimate	df	Standard Error	95% CI		VIF
				Low	High	
Intercept	-1.25	1	0.042	-1.33	-1.17	
A-f	1.58	1	0.093	1.39	1.77	9.55
B-d	1.55	1	0.087	1.38	1.73	11.02
AB	0.26	1	0.044	0.17	0.35	1.43
A^2	-0.38	1	0.054	-0.49	-0.27	1.10
B^2	-0.30	1	0.051	-0.40	-0.19	1.33
A^2B	-0.84	1	0.076	-0.99	-0.68	3.17
AB^2	-0.41	1	0.072	-0.55	-0.26	2.76
A^3	-0.36	1	0.100	-0.57	-0.15	8.30
B^3	-0.32	1	0.087	-0.50	-0.15	9.03

The final equation of the mathematical model which adequately describes the dependence of the sound absorption coefficient of recycled rubber on the frequency and the material thickness is:

$$\ln(\alpha) = - 1.69947 - 4.40877E-003*f - 131.00232*d + 0.23296*f*d + 3.93762E-006*f^2 + 4089.88397*d^2 - 7.68280E-005*f^2*d - 1.37867*f*d^2 - 9.03081E-010*f^3 - 40439.17333*d^3 \quad (3)$$

The diagnostics of statistical characteristics of the model (diagram of normal distribution of residuals, Box-Cox diagram, etc.) show that residuals are normally distributed and that the model has satisfactory statistical characteristics (Figures 4 and 5).

The graphical presentation of the mathematical model described by Eq. (1) is shown in Figures 6 and 7.

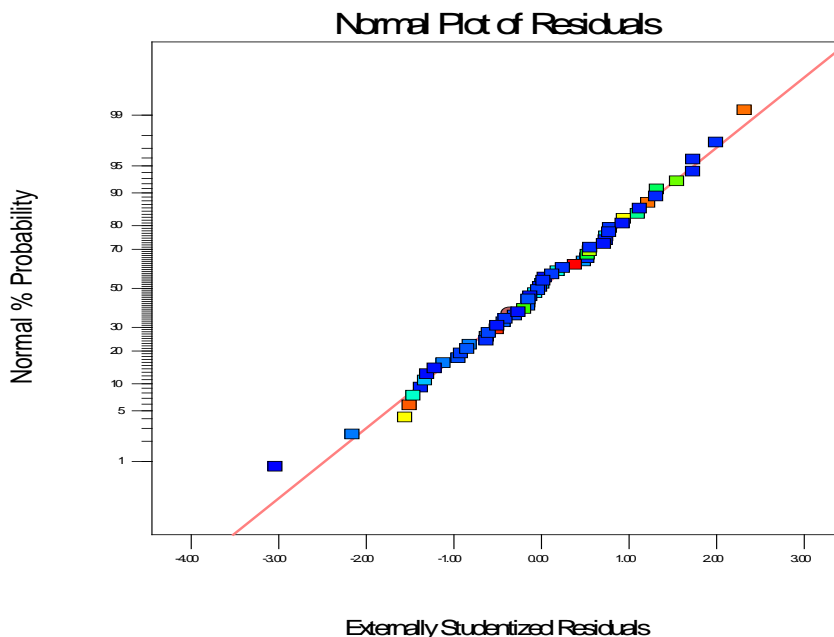


Figure 4. Diagram of the normal distribution of residuals

Design-Expert® Software  
 Ln(Alfa (GUMA))  
 Lambda  
 Current = 0  
 Best = -0.1  
 Low C.I. = -0.24  
 High C.I. = 0.04  
 Recommend transform:  
 Log  
 (Lambda = 0)

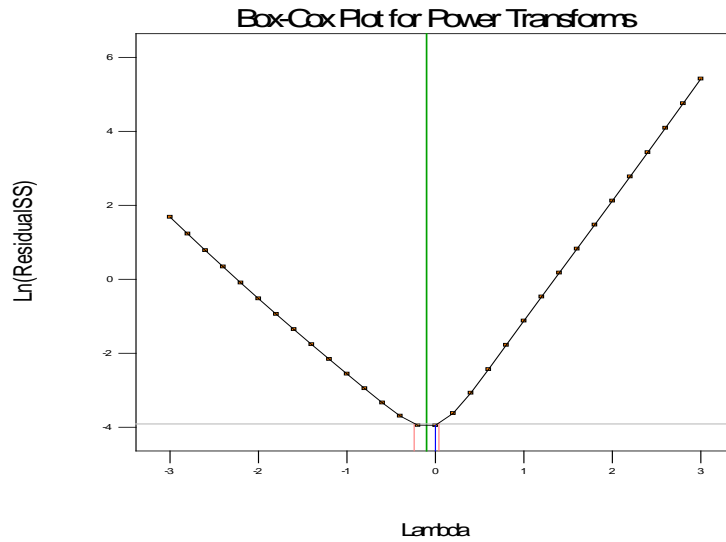


Figure 5. Box-Cox diagram for the corrected model for recycled rubber

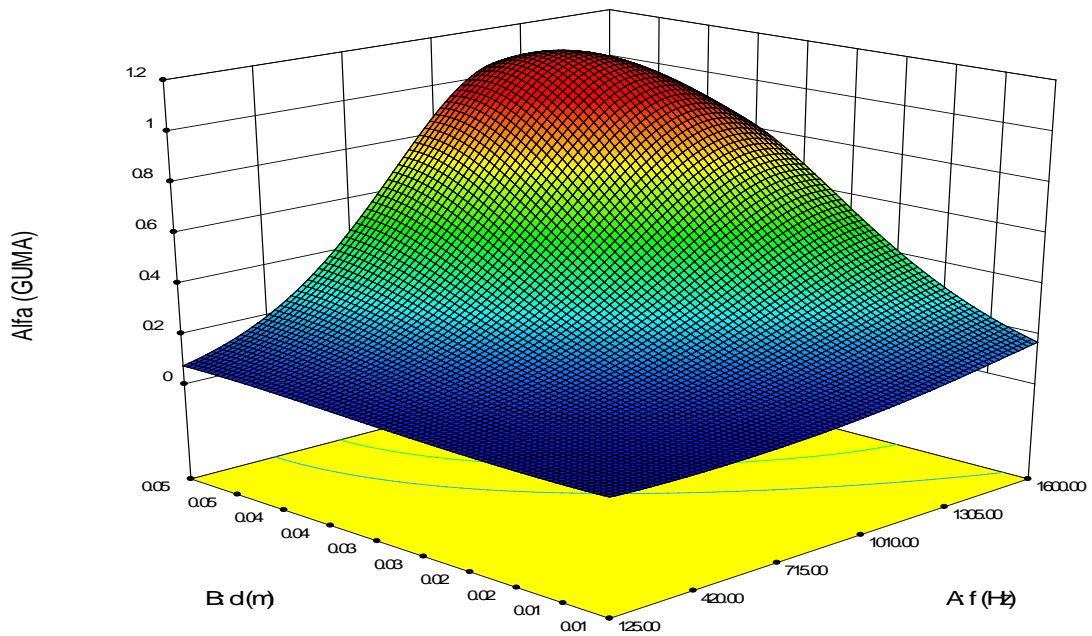


Figure 6. 3D graphical presentation of the dependence of the absorption coefficient on the material thickness in the examined frequency range

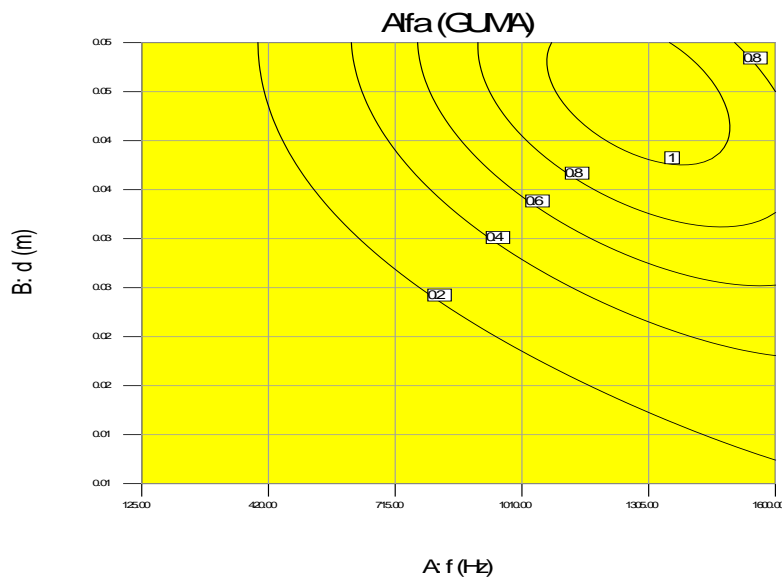


Figure 7. Contour 2D presentation of the mathematical model for recycled rubber

#### 4. CONCLUSION

Experimental results show that the absorption coefficient of recycled rubber increases with the increase in frequency up to the value of 1300Hz, and after that it decreases. The best values are obtained in the interval from 800Hz to 1600Hz, which justifies the application of recycled rubber as the absorption material for noise protection.

As for the influence of material thickness, it can be stated that the increase in thickness has its purpose up to 45mm, and after that the absorption coefficient decreases. It also confirms why the examination was carried out on the samples up to 50mm thick.

Further work will imply new examinations with samples with varying dimensions of rubber granules, pressing forces while forming the samples, parameters of installation, etc., as well as examination of mechanical properties, fire resistance, thermal conductivity, etc.

#### ACKNOWLEDGEMENTS

The authors express their gratitude to the Ministry of Education, Science and Technological Development of the Republic of Serbia for the support to this research through the project TR37020.

The authors owe special gratitude to the Laboratory for Acoustics of the Faculty of Electrical Engineering in Belgrade, where part of the measurements presented in this paper was performed.

#### REFERENCES

- [1] D. Stanojević, M. Rajković, D. Tošković, „Upravljanje korišćenim gumama u svetu i stanje u Srbiji“, Hemijska industrija, Vol. 65(6), pp. 727-738, (2011).
- [2] A. Chettah, S. Chedly, M. Ichehou, “Acoustic absorption of granular multi-layers made from fire rubber”, International Congress on Sound and Vibration, Krakow (Poland), 5-9 July 2009, (2009).
- [3] Arenas J., Crocker M., “Recent Trends in Porous Sound-Absorbing Materials”, www.SandV.com
- [4] G. Pispola, K.V. Horoshenkov, “Consolidated granular media for sound insulation: Performance evolution through different methods”, International Congress on Sound and Vibration, Lisbon (Portugal) (2005).
- [5] F. Asdrubali, F. D’Alessandro, S. Schiavoni, “Sound absorbing properties of materials made of rubber crumbs”, Proceedings of Euronoise acoustic’08, Paris (France), (2008).
- [6] C. Aciu, “Possibilities of the Recycling Rubber Waste in the Composition of Martars”, ProEnvironment, Vol. 6, pp. 479-483, (2013).
- [7] R. Maderuelo-Sauz, J.M.B. Morillas, M. Martin-Castizo, V.G. Escobar, G.R. Gazalo, “Acoustical performance of porous absorber made from recycled rubber and polyurethane resin, Lat. Am. j. solids struct., Vol.10(3), (2013).
- [8] H. Zhu, D.D. Carlos, “A spray based crumb rubber technology in highway noise reduction application”, Journal of solid waste technology and management, Vol. 27(1), pp. 27-33, (2001).
- [9] M.J. Swift, P. Bris, K.V. Horoshenkov, “Acoustic absorption in re-cycled rubber granulates”, Applied Acoustics, Vol. 57, pp. 203-212, (1999).
- [10] K.V. Horoshenkov, M.J. Swift, “The effect of consolidation on the acoustic properties of loose rubber granulates”, Applied Acoustics, Vol. 62, pp. 665-690, (2001).
- [11] J. Pfretzschner, R.M. Rodriguez, “Acoustic properties of rubber crumbs” Polymer testing, Vol. 18, pp. 81-92, (1999).
- [12] J. Pfretzschner, “Rubber crumb as granular absorptive acoustic material”, Proceedings of the Forum Acusticum Sevilla 2002, Sevilla (Spain), 16-20 Sep 2002, pp. 43.50.Rq, 43.55.Ev, (2002).
- [13] G. Iannace, L. Maffei, M. Fasullo, “Proprietà acustiche di materiali granulari ottenuti dalla triturazione di pneumatici fuori uso”, Proceedings of the 33rd National Congress of the Italian Association of Acoustics (AIA), Ischia, 10-12 May 2006, pp. 635-638, (2006).
- [14] M. Sobral, A.J.B. Samagaio, J.M.F. Ferreira, J.A. Labrincha, “Mechanical and acoustical characteristics of bound rubber granulate”, Journal of Materials Processing Technology, Vol. 142, pp. 427–433, (2003).
- [15] M. Kolarević, Z. Šoškić, Z. Petrović, B. Radičević: “Noise Protection In Urban Environment”, Description of a Project, Mechanics, Transport, Communications, Academic journal, Todor Kableskov University of Transport, Sofia, ISSN 1312-3823, issue 3, pp.IV-69-IV-78, (2011).
- [16] Tigar, proizvodi od reciklirane gume, <http://www.internet-prodaja.tigar.com/Sajt/katalozi/Proizvodi%20od%20reciklirane%20gume.pdf>
- [17] SRPS EN ISO 354:2008, Akustika - Merenje zvučne apsorpcije u reverberacionoj komori.
- [18] D. Montgomery, “Design and Analysis of Experiments”, 5th edition, John Wiley&Sons, INC, New York, (2001).
- [19] M. Kolarević, M. Vukičević, B. Radičević, M. Bjelić, V. Grković, “A Methodology for Forming the Regression Model of Ternary System”, Proceedings of VII International Conference “Heavy Machinery HM 2011”, Vrnjačka Banja (Serbia), 29 June-2 July 2011, pp. E 1-6, (2011).
- [20] Design Expert v.8 User`s Guide, Stat-Ease, [http://www.statease.com/dx8\\_man.html](http://www.statease.com/dx8_man.html)
- [21] Stat-Ease. Handbook for Experimenters version 09.01.03, Stat-Ease, Inc. 2014, [www.statease.com/pubs/handbk\\_for\\_exp\\_sv.pdf](http://www.statease.com/pubs/handbk_for_exp_sv.pdf)

# Designing Recuperator on a Rotary Kiln Supplied with Enriched Air During the Calcination of Dolomite

Miljan Marasevic<sup>1</sup>, Vladan Karamarkovic<sup>1</sup>, Nenad Stojic<sup>1</sup>, Milos Nikolic<sup>1</sup>, Djordje Novcic<sup>1</sup>

<sup>1</sup>Faculty of Mechanical and Civil Engineering in Kraljevo, University of Kragujevac, Kraljevo (Serbia)

*The paper analyzes the possibility of using a recuperator on a rotary kiln in the case where the heat for calcination of dolomite is obtained by the combustion of heavy fuel oil (HFO) with enriched air. The combustion air is enriched with oxygen up to 23%. The recuperator uses both the convective and radiant heat loss from the mantle, prevents overheating and could be implemented over rotary kilns with similar surface temperature distribution. A mathematical model that determines the diameter of the recuperator is developed and presented. The use of the suggested recuperator is impossible when air enriched with oxygen over 23% is used for the combustion of HFO in the kiln. It is necessary to consider other possibilities for the use of waste heat from the mantle of a rotary kiln.*

**Keywords:** rotary kiln, waste heat, recuperator, enriched air.

## 1. INTRODUCTION

The increased efficiency in non-ferrous metallurgy has a very great potential in the process of dolomite calcination, which is carried out in rotary kilns. The thermal efficiency of energy transformation is relatively low in the process of dolomite calcination in rotary kilns, and range between 55% and 60% (usable heat means the heat of decarbonisation and physical heat of produced calciner) [1].

The most prominent heat losses are:

- Loss due to external cooling through the mantle of a rotary kiln (up to 30% of the energy input),
- Loss contained in the physical heat of combustion products (20% of the energy input).

In addition to these losses, the problems of more efficient operation of rotary kilns represent and the lower actual combustion temperature in the calcination zone. Lower actual temperatures have a negative effect on the quality of produced calciner and in further production, lead to increased specific energy consumption in electrical kilns.

Enrichment of combustion air is one of the ways to increase the efficiency of rotary kilns and before all, their capacity. The enrichment procedure results in a reduced amount of nitrogen, decreased volume and reduced loss of physical heat in exhaust gases. On the other hand, enrichment of air with oxygen causes an increase in the burning rate, temperature, composition and aerodynamic properties of the flame. Higher temperatures of fuel combustion cause the improved of calciner quality and intensify heat radiation in the calcination zone.

However, there are negative effects that accompany the use of enriched air. With the increase in combustion temperatures, the heat loss due to external cooling increases, too. The increased temperature in the calcination zone results in a higher temperature at the mantle of the rotary kiln, which increases heat loss.

## 2. OXYGEN IN THE COMBUSTION PROCESS

The well-known properties of oxygen are that it is colourless, odorless; in liquid stage, oxygen has a distinctive light blue color and it is slightly heavier than water. Compared with air combustion, combustion with enriched air is more intense and followed by higher combustion temperatures.

Table 1.1 Physical properties of oxygen [1]

Dimensions	Tags	Value	Unit
Molecular mass	M	32	kg/k mol
Gas constant	R	259.9	J/kg K
Density (at 0° C and 1 bar)	$\rho_0$	1.429	kg/m <sup>3</sup>
Boiling temperature (at 1 bar)	$t_s$	-182.98	°C
Liquid density (at the boiling temperature)	$\rho$	1140	kg/m <sup>3</sup>
Specific heat capacity (at 0° C and 1 bar)	$c_p$	913	J/kg K
Specific heat capacity (at 0° C and 1 bar)	$c_v$	653	J/kg K
Adiabatic exponent	$\kappa$	1.4	-
The heat of vaporization (1bar)	r	213	kJ/kg
Critical temperature	$t_k$	-118.82	°C
Critical pressure	$p_k$	50.37	bar
Thermal conductivity (at 0° C and 1 bar)	l	0.024	W/m K

### 2.1. Methods of enriching the air with oxygen

The use of oxygen has led to the fact that two different basic methods of enriching the air with oxygen are:

- equivalent enrichment,
- additional enrichment.

In equivalent air enrichment, the amount of air is reduced while a certain amount of oxygen is added and the total amount of oxygen for combustion is not changed.

In additional air enrichment, the amount of air is not changed, but desired amount of oxygen is added to the air.

## 2.2. Extraction methods of oxygen

There are several methods for extraction of oxygen from air [2]:

- cryogenic distillation,
- molecular sieves and
- absorption process.

The selection of method for separation of air into its components is applied depends on various factors, including the requirements of the technological process, economic, i.e. financial conditions and security of the entire systems. Atmospheric air is separated into its main components: nitrogen and oxygen, while argon and some other inert gas are sometimes extracted. The adsorption process in the literature, is called Pressure Swing Adsorption (PSA), or adsorption process with alternating change of the pressure (adsorption and desorption).

## 2.3. Methods for oxygen introduction

There are three methods for introducing oxygen in a rotary kiln:

- Direct, in air canal,
- Direct, using nozzles and
- Using a special burner,

The direct method is the oldest and most famous method for oxygen introduction. The low investment cost and simplicity are the main advantages of this method. The positive sides of this method are obvious even for the small quantities of enrichment (1-2% of oxygen). The direct method of introduction of oxygen into the canal is used in this paper.

## 3. ROTARY KILN

At the magnesium production company "Bela Stena" in Baljevac on the river Ibar, the "magnetherm" process is used for the production of magnesium. Figure 3.1 shows the main parts of the line for production of dolomite calciner [2]:

- Supply system,
- Driving unit,
- Receiving storage for calcined material,
- Cooler for gases,
- A bag filter for purification of exhaust gases,
- Dust transportation system,
- Fan,
- Chimney.

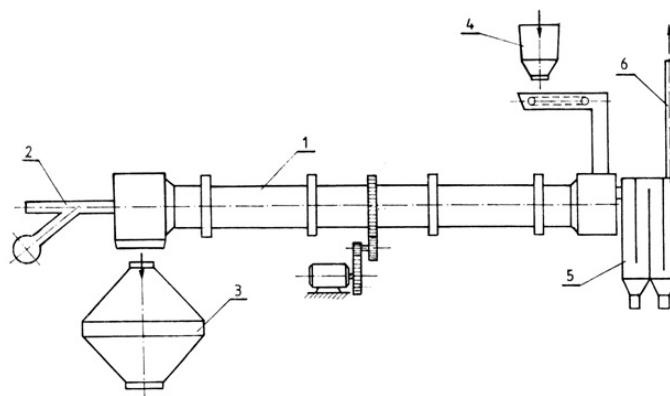


Figure 3.1. Calciner production line. 1. Rotary kiln. 2. Burner. 3. Calciner storage. 4. Dolomite storage. 5. Electrostatic precipitator. 6. Chimney.

Table 3.1 Characteristics of the rotary kiln

Manufacture	FIVES CAIL - BABCOCK - FRANCUSKA
External diameter of kiln	2800 mm
Length of kiln	80m
Kiln inclination	3 %
Rotation per minute (Rpm)	0.75 - 0.95 min <sup>-1</sup>
Nominal capacity	135t of calciner per day
Kiln capacity	9150 kg/h
Fuel	Heavy oil

Raw dolomite is double carbonate ( $\text{CaMg}(\text{CO}_3)_2$ ) with a slight admixture of manganese and iron. The transportation system transports raw dolomite from reception bunker to the crusher. After crushing, dolomite goes to washing where mechanical impurities are removed. The purified dolomite passes through the sieves, resulting in a dolomite grain size of 3 to 30mm. The belt conveyer transports grained dolomite to the bunker located above the rotary kiln. The mechanical feeders continuously feed the rotary kiln with dolomite. Due to the rotation and inclination of the kiln, dolomite is slightly moves with stirring through kiln, lifts up by the rotation wall a the certain height and then drops through the stream of hot gases. Dolomite passes several temperature zones on its way through the rotary kiln.

The mantle of a rotary kiln can be divided into few temperature zones or areas.

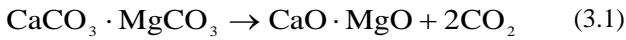
At about 20m of kiln length, temperature values are in the range between 100 and 400°C and that part of the kiln is made of refractory concrete (3m of length) and the second part is coated with refractory bricks (17m of length) and this is the preparation zone. In this zone of the rotary kiln, fins or buckets are used to lift up dolomite.

At the next 40m, the temperature value is around 700°C and for this part of the rotary kiln improved materials are used for the kiln wall. This is the drying zone.

At the last 20m, the temperature is around 1300°C, and the quality of refractory bricks is best in this part of the kiln. This is the calcination zone. In this zone,



calcination of dolomite takes place according to the chemical reaction:



#### 4. RECUPERATOR

In order to increase energy efficiency of the current production line, it is very important to reduce heat loss from the mantle of the rotary kiln. In cement industry, this loss is 8-15% of the total heat input [2], while in the magnesium production process it is higher. Chakrabarti [3] obtained even larger losses, 24.8% of the total heat input for the rotary kiln located in the hall and 34.7% of the total heat input for the rotary kiln located in the open air.

Among the factors that affect this heat loss are: technological characteristics of inside process of the kiln, temperature distribution, thermal stability and resistance of refractory lining inside the kiln, ambient conditions at the kiln location, kiln dimensions, thermal properties of the outer insulating layer and rotational speed.

The heat loss of the rotary kiln to the surroundings is either reduced by the use of the heat exchangers or by the use of stationary insulation screens around the kiln [7, 8]. The heat exchangers are also a part of external shell [4, 5], and they are usually used to preheat the water for district heating systems.

As mentioned in the previous sections, an examination rotary kiln is used for calcination of dolomite in the magnesium production company. The requirement to utilize the total heat loss by radiation and convection was the reason to utilize waste heat to preheat the air used for the combustion of fuel.

Figure 4.1 shows the basic idea of the proposed solution. In the first part of the rotary kiln (calcination zone), where the surface temperatures are highest, the recuperator is set to preheat air. The amount of the heat that would be waste to the surroundings, in case that the recuperator does not exist, is used to preheat air.

After passing through the concentric annular, the preheated air is transported by the blower to the burner.

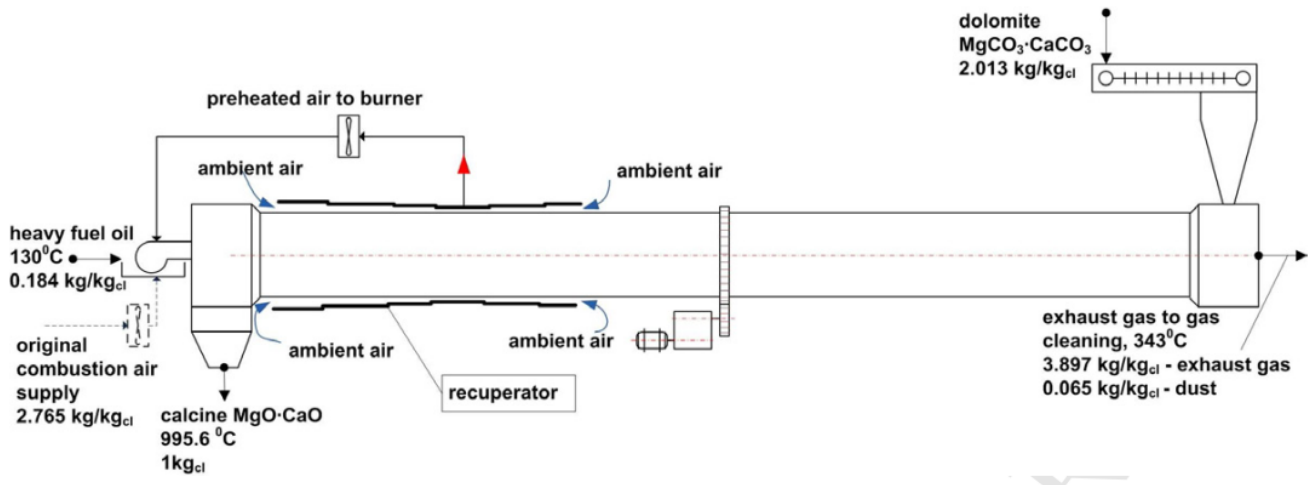


Figure 4.1 Schematic view of a rotary kiln and recuperator

#### 5. MATHEMATICAL MODEL

A mathematical model that gives the geometry of the recuperator is developed. The model is based on the requirement that heat loss, due to external cooling of the kiln, is used to preheat the air [1].

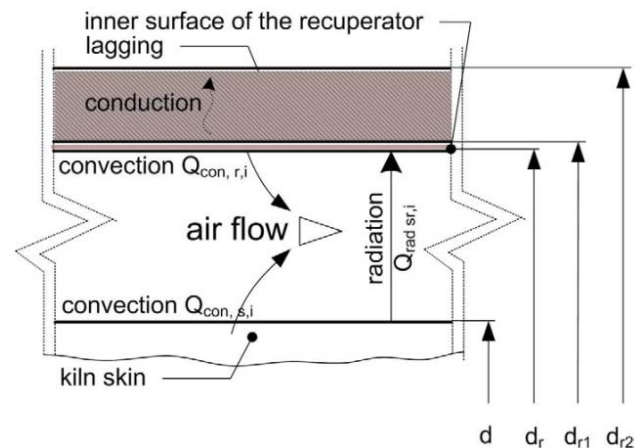


Figure 5.1 Mathematical model of the recuperator

Figure 4.1 shows changes of the recuperator diameter by sections. The preheated air is extracted approximately in the middle of the recuperator. Actually, preheated air is extracted over the section of the rotary kiln with the highest temperature.

As the surface temperature of the rotary kiln changes along it, and equal amount of air flows along each section to extract the heat from each section of the kiln equal to the heat loss from the bare kiln; the recuperator diameter changes in each section. Figure 5.1 shows the principle of the model used for diameter calculation and the temperature of preheated air. Two energy balance equations (5.1) and (5.2) are used:

$$\dot{Q}_{conv,s,i} + \dot{Q}_{conv,r,i} = \frac{\dot{m}_a}{2} C_{p,a} (t_{aout,i} - t_{ain,i}), \quad (5.1)$$

$$\dot{Q}_{rad,sr,i} = \dot{Q}_{conv,r,i} + 0.03 \dot{Q}_{s,i}. \quad (5.2)$$

Equation (5.1) represents the energy balance of the air that flowing through  $i$ -th section of the recuperator, where:

- $\dot{Q}_{conv,s,i}$  - the heat flow rate exchanged between the kiln and the air by convection,  $\dot{Q}_{conv,r,i}$  the heat flow rate exchanged between the air and the recuperator by convection.

- $\dot{m}_a / 2$  - is a half of the mass flow used for the heavy oil combustion in the rotary kiln. The airflow is divided into two equal streams flowing from both ends of the recuperator,

- $t_{aout,i}, t_{ain,i}$  - are the temperatures of air at the inlet and at the outlet of the  $i$ -th section of the recuperator.

Equation (5.2) is energy balance per unit of time for the inner surface of the recuperator and states that one part of the radiant heat flow received from the outer surface of the kiln is transferred by convection to the air while the other is transferred to the surroundings by conduction through insulation of the recuperator. The thickness of the insulation and the outer diameter of the recuperator are determined from the adopted fact that 3% of the initial heat loss of the kiln is lost through the insulation of the recuperator ( $0.03 \dot{Q}_{s,i}$  in Equation (5.2)).

The total heat loss ( $\dot{Q}_{s,i}$ ) from the  $i$ -th section of the recuperator is equal to the initial heat loss from the  $i$ -th section of the bare kiln, obtained by

$$\dot{Q}_{s,i} = \dot{Q}_{conv,s,i} + \dot{Q}_{rad,sr,i} \quad (5.3)$$

where:

- $\dot{Q}_{conv,s,i}$  - the heat flow rate of the  $i$ -th section of the kiln transferred by convection to the air flowing through the concentric annular,

- $\dot{Q}_{rad,sr,i}$  - the heat flow rate of the  $i$ -th section of the kiln transferred by radiation from the outer surface of the kiln to inner surface of the recuperator.

The heat flow rate  $\dot{Q}_{rad,sr,i}$  is obtained for the case of two concentric tubes [13] by

$$\dot{Q}_{rad,sr,i} = \frac{\sigma}{\frac{1}{\varepsilon_{s,i}} + \frac{A_{s,i}}{A_{r,i}} \left( \frac{1}{\varepsilon_{r,i}} - 1 \right)} A_{s,i} (T_{s,i}^4 - T_{r,i}^4), \quad (5.4)$$

where:

- $\varepsilon_{s,i} = \varepsilon_{r,i} = 0.8$  - the degrees of emissivity of the kiln surface and recuperator [8, 9],

- $T_{s,i}, T_{r,i}$  - the temperatures on  $i$ -th section of the kiln and recuperator,

- $A_{s,i}, A_{r,i}$  - the areas on  $i$ -th section of the kiln and recuperator.

The model given in [10] that calculates the heat transfer in the concentric annular ducts for fully developed turbulent flow is used to obtain the heat flow rate by convection on the  $i$ -th sections of the kiln  $\dot{Q}_{conv,s,i}$  and the recuperator  $\dot{Q}_{conv,r,i}$ . In the model, dimensionless numbers for  $i$ -th section of the recuperator  $Nu_i = \frac{\alpha_i d_{h,i}}{\lambda}, Re_i = \frac{w_i d_{h,i}}{\nu}$  are determined by the use of the hydraulic diameter given by

$$d_{h,i} = d_{r,i} - d, \quad (5.5)$$

where:

- $d_{r,i}$  - the inner diameter of the  $i$ -th section of the recuperator,

- $d$  - the outer diameter of the rotary kiln.

It is important to note that the physical properties relate to the mean temperatures of the air.

$$t_{a,m} = (t_0 + t_p) / 2, \quad (5.6)$$

where:

- $t_0$  - the temperature of ambient air,

- $t_p$  - the temperature of preheated air.

For fully developed turbulent flow  $Re > 10^4$  in the concentric annular duct, the modified equation of Petukhov and Kirilov [11], is used [11]:

$$Nu_{ann,i} = \frac{(k_{ann,i})_{s,r,i}}{k_{s,r,i} + 0.027 \sqrt{k_{ann,i} (k_{s,r,i}^2 - k_{s,i}^2)}} \cdot \left[ 1 + \left( \frac{k_{s,i}}{k_{s,r,i}} \right)^{1/4} \right] \cdot F_{ann,i}, \quad (5.7)$$

where:

$$k_{1,i} = 1.07 + \frac{900}{Re_{s,i}} - \frac{0.63}{(1+10 \cdot Pr_{r,i})} \quad (5.8)$$

The friction factor  $\xi_{ann}$  depends on the ratio  $\alpha_i = d/d_{r,i}$  and is obtained by [10]

$$\xi_{ann,i} = (1.8 \cdot \log_{10}(Re_{s,i}) - 1.5)^{-2} \quad (5.9)$$

where:

$$Re_{s,i}^* = Re_{s,i} \cdot \frac{[1+\alpha_i^2] \cdot \ln \alpha_i + [1-\alpha_i^2]}{[1-\alpha_i^2] \cdot \ln \alpha_i} \quad (5.10)$$

For the boundary condition "heat transfer to the inner wall, the outer wall is insulated", which is valid for the examined recuperator,  $F_{ann,i}$  in Equation (5.7), is obtained from [10] by

$$F_{ann,i} = 0,75 \cdot \alpha_i^{-0,17} \tag{5.11}$$

Equation (5.7) which calculates the Nusselt number is modified by the use of the correction factor that includes the variation of fluid properties with temperature [10]:

$$K_i = \left( \frac{T_{a,m,i}}{T_{r,i}} \right)^{0,45}, \tag{5.12}$$

The presented model enables determination of the preheated air temperature, the temperature of the inner wall and the diameter in each section of the recuperator. The temperature at the outer surface of the  $i$ -th section of the recuperator is obtained by

$$0,03 \dot{Q}_{s,i} = \frac{T_{r2,i} - T_0}{\frac{1}{2\pi\lambda_{steel} \ln \frac{d_{r1,i}}{d_{r,i}} + \frac{1}{2\pi\lambda_{insulation} \ln \frac{d_{r2,i}}{d_{r1,i}}}} \tag{5.13}$$

Equation 5.13 is a well-known equation for one-dimensional steady state heat conduction through the tube wall, in which  $\lambda_{steel} = 48 \text{ W/mK}$  and  $\lambda_{insulation} = 0,041 \text{ W/mK}$  are thermal conductivities of the steel mantle and thermal insulation (mineral wool) over the annular duct. Equation 5.13 uses the already mentioned fact that the 3% of the initial heat loss from the bare kiln is transferred to the surroundings through the recuperator insulation.

### 6. MODEL FOR DETERMINATION OF THE INNER DIMENSIONS OF THE RECUPERATOR

Based on the examined model and determination of mass and heat balance of the rotary kiln, the temperatures of the inner and outer surface, dimensions and other parameters for each section of the recuperator are obtained. The calculations for these models are very complex because the mathematical model includes a large number of interactions.

For the simple resolving of exact mathematical model, the special program is developed for determination of the recuperator dimensions and temperatures at the inner and outer surface. The program obtains the curve of change of the recuperator diameter where the mantle of the recuperator is divided into smaller and equal sections. With this, the basic calculation model is improved and other parameters can be tested. Based on the improved calculation, the recuperator parameters are determined in the case when enriched air is used for the combustion in the kiln.

The use of the developed model is not limited only to this kiln and it can be used for other cylindrical surfaces.

### 7. MASS AND ENERGY BALANCE OF THE KILN SUPPLIED WITH ENRICHED AIR

At the kiln for dolomite calcination, measurements are carried in case where enriched air is used for combustion. The equivalent or additional enrichment is used for the air enriching. In this case, equivalent enrichment is used in the range of 21.5% to 23%, with the step of 0.5%. The determined results are shown in the tables below.

Table 7.1 Mass balance of the kiln with different percentages of enriched air.

	Mass flows	O <sub>2</sub> (%)				
		21	21.5	22	22.5	23
Input	Raw material	2,013	2,013	2,013	2,013	2,013
	Fuel	0,184	0,184	0,184	0,184	0,184
	Air	2,765	2,654	2,593	2,536	2,481
	Total	4,962	4,851	4,790	4,733	4,678
Output	Calcliner	1	1	1	1	1
	Exhaust products	3,897	3,786	3,725	3,668	3,613
	Dust	0,065	0,065	0,065	0,065	0,065
	Total	4,962	4,851	4,790	4,733	4,678

Table 7.2 Energy balance of the kiln with different percentages of enriched air.

Heat inputs	O <sub>2</sub> (%)	21	21,5	22	22,5	23
		<u>kJ/kgcal</u> %	<u>kJ/kgcal</u> %	<u>kJ/kgcal</u> %	<u>kJ/kgcal</u> %	<u>kJ/kgcal</u> %
Combustion of fuel (Q <sub>1</sub> ) - LHV		7435,44 98,96	7435,44 98,97	7435,44 98,98	7435,44 98,98	7435,44 98,99
Sensible heat of fuel (Q <sub>2</sub> )		41,07 0,55	41,07 0,55	41,07 0,55	41,07 0,55	41,07 0,55
Sensible heat of air (Q <sub>3</sub> )		22,25 0,30	21,36 0,28	20,87 0,28	20,41 0,27	19,96 0,27
Sensible heat of the feed (Q <sub>4</sub> )		14,82 0,20	14,82 0,20	14,82 0,20	14,82 0,20	14,82 0,20
Total:		7513,58 100,00	7512,68 100,00	7512,20 100,00	7511,73 100,00	7511,29 100,00
Heat outputs	O <sub>2</sub> (%)	21	21,5	22	22,5	23
		<u>kJ/kgcal</u> %	<u>kJ/kgcal</u> %	<u>kJ/kgcal</u> %	<u>kJ/kgcal</u> %	<u>kJ/kgcal</u> %
Sensible heat of exhaust gas (Q <sub>5</sub> )		1423,01 18,94	1348,11 17,94	1303,85 17,36	1258,70 16,76	1221,06 16,26
Sensible heat of calcine (Q <sub>6</sub> )		1003,56 13,36	1003,565 13,36	1003,565 13,36	1003,5648 13,36	1003,565 13,36
Heat of formation of calcine (Q <sub>7</sub> )		3023,35 40,24	3023,352 40,24	3023,352 40,25	3023,352 40,25	3023,352 40,25
Sensible heat of dust (Q <sub>8</sub> )		19,66 0,26	19,66 0,26	19,66 0,26	19,66 0,26	19,66 0,26
Heat of decarbonization of dust (Q <sub>9</sub> )		15,12 0,20	15,12 0,20	15,12 0,20	15,12 0,20	15,12 0,20
Moisture associated with feed (Q <sub>10</sub> )		48,01 0,64	48,01 0,64	48,01 0,64	48,01 0,64	48,01 0,64
Total heat loss to surroundings (Q <sub>11</sub> )		1980,87 26,36	2054,88 27,35	2098,65 27,94	2143,34 28,53	2180,53 29,03
Total:		7513,58 100,00	7512,68 100,00	7512,20 100,00	7511,73 100,00	7511,29 100,00

Table 7.3 Fuel saves by the use of the recuperator with different percentages of enriched air

O <sub>2</sub> (%)	21		21.5		22	
	<u>kJ/kgcal</u>		<u>kJ/kgcal</u>		<u>kJ/kgcal</u>	
Total input energy	7513,58		7512,68		7512,20	
Temperature of the heated air	299,60	C	313,50	C	322,10	C
Specific heat capacity of the heated air	1,0453	<u>kJ/kgK</u>	1,0484	<u>kJ/kgK</u>	1,0504	<u>kJ/kgK</u>
Physical heat of the heated air	865,91	<u>kJ/kgcal</u>	872,18	<u>kJ/kgcal</u>	877,37	<u>kJ/kgcal</u>
Fuel consumption with use of the recuperator	0,1632	<u>kg/kgcal</u>	0,1631	<u>kg/kgcal</u>	0,1629	<u>kg/kgcal</u>
Fuel saves	0,0208	<u>kg/kgcal</u>	0,0209	<u>kg/kgcal</u>	0,0211	<u>kg/kgcal</u>
Saves percentage	11,28	%	11,38	%	11,46	%
Amount of fuel saves	2192,06	<u>kg/day</u>	2210,66	<u>kg/day</u>	2225,42	<u>kg/day</u>
O <sub>2</sub> (%)	22.5		23			
	<u>kJ/kgcal</u>		<u>kJ/kgcal</u>			
Total input energy	7511,73		7511,29			
Temperature of the heated air	333,20	C	341,90	C		
Specific heat capacity of the heated air	1,0529	<u>kJ/kgK</u>	1,0549	<u>kJ/kgK</u>		
Physical heat of the heated air	889,59	<u>kJ/kgcal</u>	894,69	<u>kJ/kgcal</u>		
Fuel consumption with use of the recuperator	0,1626	<u>kg/kgcal</u>	0,1625	<u>kg/kgcal</u>		
Fuel saves	0,0214	<u>kg/kgcal</u>	0,0215	<u>kg/kgcal</u>		
Saves percentage	11,63	%	11,70	%		
Amount of fuel saves	2258,38	<u>kg/day</u>	2272,77	<u>kg/day</u>		

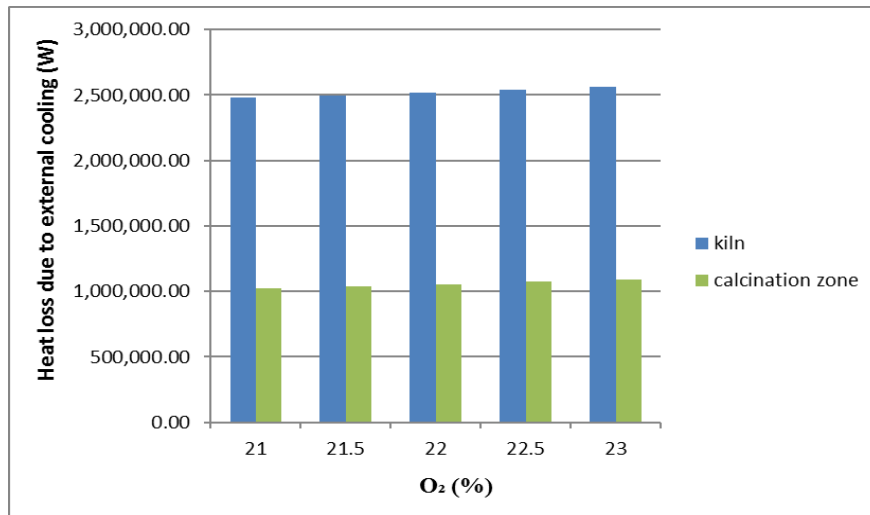


Figure 7.1 Heat balance of the entire kiln and calcination zone with different percentages of oxygen

8. RESULTS

The measured values of the temperature on the mantle of the kiln at various percentages of oxygen are approximated with the polynomial function of the fifth degree:

$$t = B_0 + B_1 \cdot l + B_2 \cdot l^2 + B_3 \cdot l^3 + B_4 \cdot l^4 + B_5 \cdot l^5 \quad (8.1)$$

Table 8.1 Polynomial functions of temperature.

O <sub>2</sub> (%)	B <sub>0</sub>	B <sub>1</sub>	B <sub>2</sub>	B <sub>3</sub>	B <sub>4</sub>	B <sub>5</sub>
21	321,997726	7,18033	-6,71522	1,84127	-0,17576	0,005250
21.5	325,875640	7,21080	-6,69770	1,83900	-0,17570	0,005250
22	329,597560	7,23120	-6,70552	1,84050	-0,17580	0,005251
22.5	332,287569	7,18947	-6,69980	1,83940	-0,17572	0,005250
23	336,589742	7,27050	-6,71860	1,83899	-0,17570	0,005252

Table 8.2. The mass flow rate of air entering the recuperator at various percentages of oxygen (half of the total mass flow rate)

O <sub>2</sub> (%)	21	21.5	22	22.5	23
$\frac{m_{air}}{2}$ (kg/s)	1.6894	1.6213	1.5844	1.5492	1.5155

Figure 8.1 shows the recuperator diameters at various percentages of enrichment.

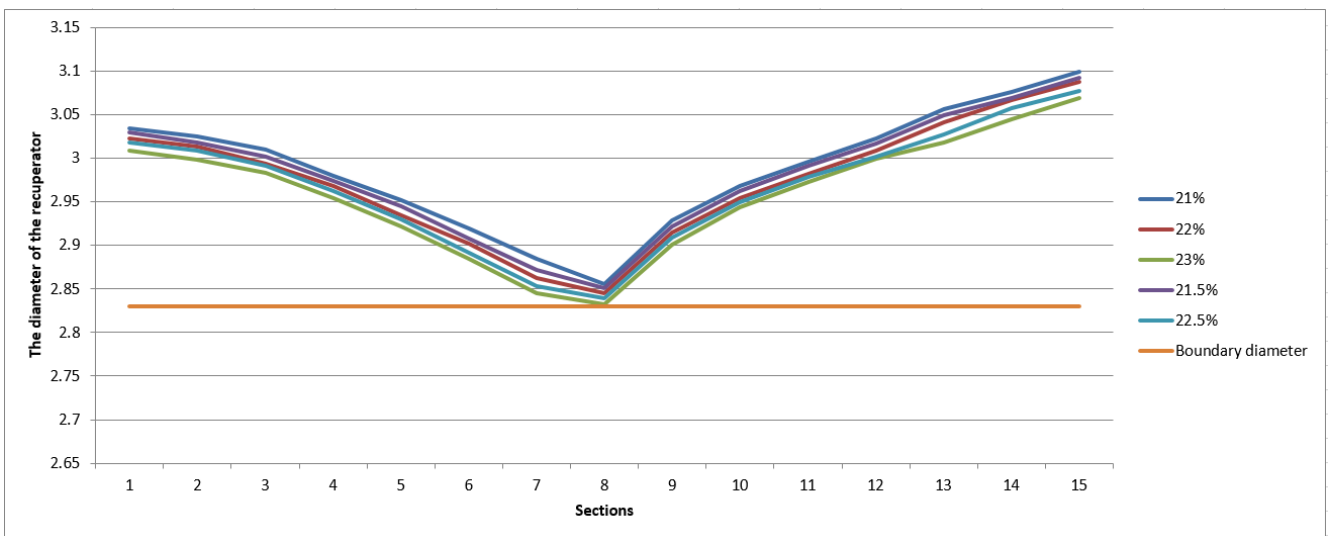


Figure 8.1. The diameters of the recuperator with different percentages of oxygen in the air

## 9. CONCLUSION

With the increase of oxygen in the air for combustion, the temperatures at the mantle of the kiln and the heat loss due to external cooling increase. This loss of heat is recycled through the recuperator, which changes dimensions according to the different enrichment of the air. The heat recuperation is carried in the calcination zone where the temperatures are highest.

The diameter of the recuperator decreases with the increase of oxygen in the air. Figure 8.1 shows that the mathematical model cannot be applied for further enrichment (over 23% of oxygen). In the case that enriched air has 23% of oxygen, the diameter of the recuperator, per value, is very close to the diameter of the kiln. The diameter of the kiln is 2.8m, but for the smooth functioning the smallest diameter of the recuperator is 2.83m.

For the enrichment of over 23% of oxygen, the recuperator cannot be applied and it is necessary to consider different ways of using heat from the mantle of the kiln. The developed mathematical model for dimension determination, presented in this paper, can be applied to other smaller or larger kilns.

## REFERENCES

- [1] V. Karamarković, M. Marašević, R. Karamarković, M. Karamarković, „Recuperator for waste heat recovery from rotary kilns“, *Applied Thermal Engineering*, Volume 54, Issue 2, 30 May 2013, Pages 470–480, DOI: 10.1016/j.applthermaleng.2013.02.027.
- [2] M. Marašević, „Ексергијска оптимизација рада ротационе пећи за калцинацију доломита, докторска дисертација Миљана Maraševićа, Факултет за машинство и грађевинарство у Краљеву, 2013. год.
- [3] B.K.Chakrabati, Investigations on heat loss through the kiln shell in magnesite dead burning process: a case study, *Appl. Therm. Eng.* 22 (2002) 1339-1345.
- [4] A.C. Caputo, Antonio, P.M. Pelagagge, P. Salini, Performance modeling of radiant heat recovery exchangers for rotary kilns, *Appl. Therm. Eng.* 31 (2011) 2578-2589.
- [5] Z. Söğüt, Z. Oktay, H. Karakoç, Mathematical modeling of heat recovery from a rotary kiln, *Appl. Therm. Eng.* 30 (2010) 817-825.
- [6] T. Engin, V. Ari, Energy auditing and recovery for dry type cement rotary kiln systems-A case study, *Energy Convers. Manage.* 46 (2005) 551-562.
- [7] M.J. Prins, K.J. Ptasinski, F.J.J.G. Janssen, Energy and exergy analysis of the oxidation and gasification of carbon, *Energy* 30 (2005) 981-1002.
- [8] Thermal properties of liquid fuels, [http://ottp.fme.vutbr.cz/vyuka/thermomechanics/therm\\_op\\_Liq.pdf](http://ottp.fme.vutbr.cz/vyuka/thermomechanics/therm_op_Liq.pdf). (accessed 21.6.12).
- [9] R. Span, Properties of dry air, in: VDI Gesellschaft, VDI Heat Atlas, second ed., Springer, Heidelberg, 2010, pp. 172-191.
- [10] A.S. Gutiérrez, J.B.C. Martínez, C. Vandecasteele, Energy and exergy assessments of a lime shaft kiln, *Appl. Therm. Eng.* 51 (2013) 273-280. [26] V.Gnielinski, Heat transfer in concentric annular and parallel plate ducts, in: VDI Gesellschaft, VDI Heat Atlas, second ed., Springer, Heidelberg, 2010, pp. 947-959.
- [11] B.S. Petukhov, V.V. Kirilov, On heat exchange at turbulent flow of liquids in pipes, *Teploenergetika* 4 (1958) 63-68 (in Russian).

## Dynamic Pinch Analysis

Aleksandar Vičovac<sup>1\*</sup>, Rade Karamarković<sup>1</sup>, Dragan Pršić<sup>2</sup>

<sup>1</sup>Faculty of Mechanical and Civil Engineering in Kraljevo, (Serbia) Department of Energy and Environmental Protection,

<sup>2</sup>Faculty of Mechanical and Civil Engineering in Kraljevo, (Serbia) Department of Energetic and Automatic Control,

*Needs for heating and cooling in Serbia is growing up. Existing systems in buildings and industrial processes are increasingly using renewable energy. To improve the competitiveness of the domestic economy, a great character given to improving energy efficiency. The paper analyzes the possibility of integrating technological processes with heating and cooling systems at the plant for production of mineral water. The aim is to improve the energy efficiency of the system both considered by mutual integration into a single system with the use of locally available renewable energy. Integrating is analyzed using a "pinch" analysis (methods of minimum temperature difference). The aim of this work is to improve the model by means of the acquisition of physical parameters and influence the process of exchanging heat of warm and cold currents were optimal energy-saving energy. The first part represents the composite and the cumulative curve in the case of an industrial process, and determines the state of the necessary energy in the summer and winter period and of the technological HVAC systems. The second part shows the variable pinch point in the summer and winter periods on the basis of changes in ambient temperature and technological process. Possibility of year-long use of geothermal heat pumps and geothermal energy.*

**Keywords:** Heat Exchanger Networks, Methods of minimum temperature difference, Pinch

### 1. INTRODUCTION

Reducing production costs is one way of improving the competitiveness of the product (or company). In the sphere of energy, reducing production costs is reflected in the reduction of energy costs. These costs reduced by improving the energy efficiency of the production process. As a rule, improving energy efficiency was followed by a decrease in the emission of pollutants into the environment.

The company, whose manufacturing processes followed a large number of technological flows which can heat and cool, at the same time to improve energy efficiency flows associated heat exchangers. The goal is to maximize heat dissipation, which is subtracted from the streams that are cooled from streams which are heated. Maximizing heat exchange within the company as a result has a minimum consumption of energy for heating and cooling.

Pinch analysis of 80s [1,2] of the last century are used for optimal connection of production streams, which are at the same time heated and cooled. This method was the first applied in the petrochemical industry. According to this method, all flows in the company, all of streams who are heated, are seen as the cold streams and contrary, all the streams that are cooled are seen as warm streams.

The problem boils down to maximizing the exchange of heat between these two streams. This method is applied liberally and prosper so that it begins used for optimum energy mutual connectivity and more companies [3]. Papers [4,5] provide an overview of the latest developments in the field of integration of production processes. Into the Serbia there is great potential for thermal integration of production processes to improve energy efficiency in the food industry, in dairies, manufacturer of alcoholic and non-alcoholic beverages and food products. On the other hand, relatively large variations in ambient temperature requires heating and

cooling of the administrative area of the companies as well as some production facilities to fulfill the prescribed conditions employee benefits.

The aim of this paper is that in the case of one company replied that it is possible to improve energy efficiency:

- better integration of the production process,
- integration of production processes of heating and cooling production and administrative space,
- integration of the production process and space for heating and cooling with geothermal heat resource available at the location of the test company.

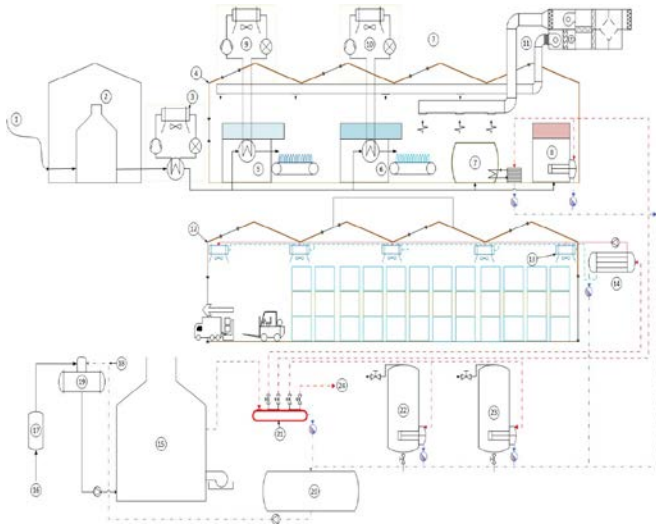
Renewable energy should be a link that connects manufacturing and process of the heating and cooling into factory space and for providing: heat for heating, heat sink for cooling and heat accumulators.

By integrating all three links optimizes not the only the manufacturing process but he links in unbreakable whole with the natural environment in which it is located.

In this paper, are integrated production process, a process of heating and air-conditioning systems and geothermal energy in company "Knjaz Miloš" in Arandelovac.

The aim is the creation of optimal energy system at the plant, which will operate efficiently throughout the year.

Therefore, it is tracked the changes of critical point (pinch) per annum and the paper defines a new concept: the dynamic (variable in time) pinch.



Simplified process diagram of the investigated "Knjaz Miloš" company, where: 1 is 7 km long uninsulated underground piping that connects a mineral water spring and the company, 2 – reverse osmosis with the mineral water accumulation tank, 3 – 1<sup>st</sup> stage of the mineral water cooling, 4 – PET hall (production hall), 5 – production line for PET bottles filling with the mineral water, 6 – production line for glass bottles filling with the mineral water, 7 – energy drink production, 8 – molasses and juice production, 9 – 2<sup>nd</sup> stage of mineral water cooling (immediately before CO<sub>2</sub> absorption), 10 – 2<sup>nd</sup> stage of mineral water cooling, 11 – Air handling unit of the air conditioning system for the PET hall, 12 – warehouse, 13 – hot water fan coil system for the heating of warehouse, 14 – heat exchanger (steam/hot water), 15 – 3 steam natural-gas-fired boilers in the boiler room, 16 – make up water, 17 – base exchange softening, 18 – condensate return, 19 – boiler feed tank, 20 – condensate tank, 21 – steam header, 22 – CIP washing, 23 – domestic hot water, 24 – branch towards the part of the company that is excluded from the analysis.

## 2. MODELING

Composite curve shows which is the minimum amount of energy necessary to take from the streams to be cooled and supplied to the flows that are heated, as well as the minimum temperatures heated fluid necessary in order to achieve the given heating and cooling of technological process. In the analysis of Pinch-a had been used assumption that is minimum temperature difference in the heat exchangers  $\Delta t_{min} = 4^{\circ}\text{C}$ . The analysis shows that is: The critical temperature of the process at ambient temperature in the summer 36°C. This means that if there is a heat exchange with heat pump, streams that is simultaneously cooled and heated in the industry, heat pump (or heat pump system) has to take the heat below and above the critical temperature surrender.

As can be seen from the diagram composite blame a lot of power, which is below the Pinch-a - it is necessary to cool, while a small part of above of Pinch and need to be heated to the high temperatures. So, the problem is where to

submit this excess heat. Project solutions, with acquisition of variable Pinch-in a given time points and influencing exchange process heat and cooling energy, it is possible to make a "stream networks" with as more even distribution of energy. When we say "stream networks" primarily refers to the optimal power flow heat exchanger and appropriate automatization of streams that flows. temperature and fluid flow participating in the heat exchange. There are two conditions in an industrial plant that must comply with the following:

- Technological process
- Specify conditions in HVAC (internal design conditions HVAC)

Any change of Pinch and the impact on the process of heat exchange, must meet the above two conditions, and to there by achieve energy saving with constantly monitoring theory Pinch and that:

*Do not use cold side above the Pinch*

*Do not use hot side below the Pinch*

*Do not use heat transfer through the point Pinch*

For stacking flows, there are the following two rules: In the section above the Pinch, the number of warm streams (including their branches) should be smaller or equal to cold flow (including their branches), such that:

$$N_h \leq N_c \text{ (above Pinch)}$$

Otherwise, the flow separation is necessary to provide full given condition.

Similarly, the area under the Pinch-a is an inverse inequality

$$N_h \geq N_c \text{ (under Pinch)}$$

For the part above the Pinch-a warm stream (or branch of warm streams) should be less than or at least equal to that cold streams (or branch cold flow) should correspond, so that:

$$(\dot{M}c_p)_h \leq (\dot{M}c_p)_c \text{ ( under Pinch)}$$

For part of the area under the Pinch, reign inverted inequality,

$$(\dot{M}c_p)_h \geq (\dot{M}c_p)_c \text{ ( under Pinch)}$$

### 2.1. The basis for defining dynamical Pinch

The input data for the algorithm:

- Initial (supply) temperatures,
- Final (target) temperatures,
- Heat capacity flow rates,
- Minimum temperature difference

Value of output sizes are:

- Temperature,



- Heat flow at pinch.

The following shows an algorithm for the determination of dynamic Pinch.

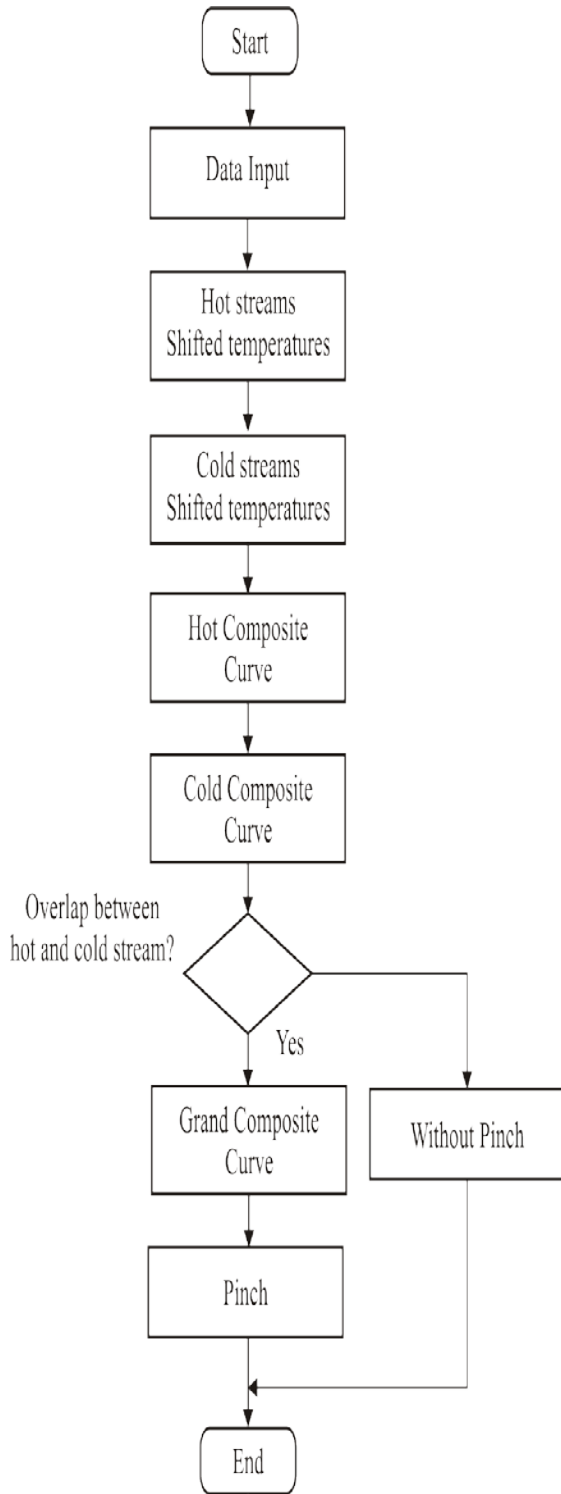


Figure 1: Algorithm Dynamic Pinch

## 2.2. Composite curve and Grand composite curve summer

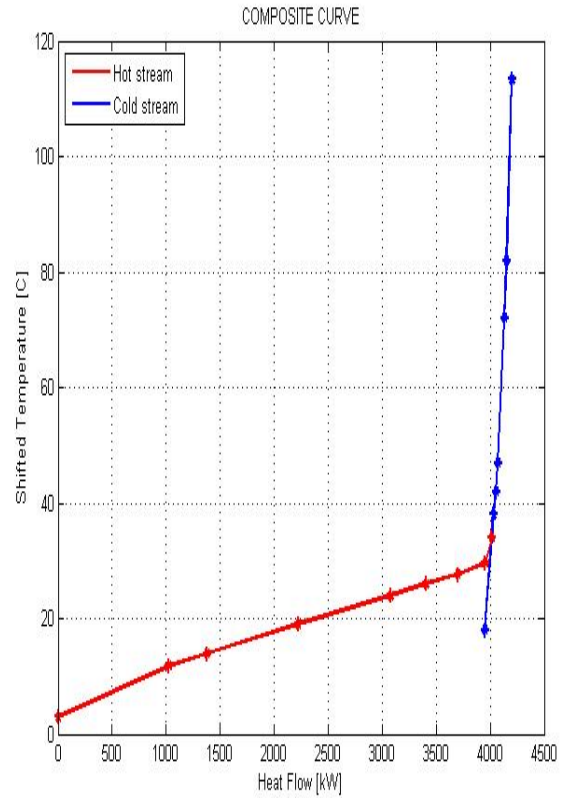


Figure 2: Composite curve (summer period)

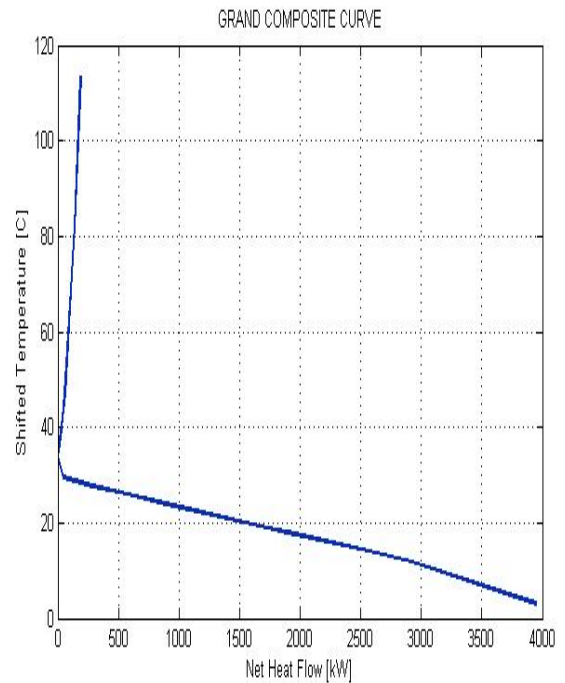


Figure 3: Grand Composite curve (summer period)

Figure 4. Grand Composite curve. Changing the air temperature in the Company data into the function:

$$Tts(1,1)=29.63+6.9\cdot\sin(2\cdot\pi\cdot T(k1)/Tk)$$

Watching the air condition part into the part off Company, the production hall has largest dissipation of heat from the production process. Also, had to had taken into consideration the heat gain in the summer. The sum of two sources is the total energy cooling balancing in the summer. The internal temperature and humidity in the room must not exceed the values that disrupts the basic environmental conditions for people. However, if it is simulating temperature changes, and thus the consumption of the cooling capacity of the constant value of the heat capacity of the stream gives the following parameters and the cumulative composite curve.

Changing of the temperature of air in Company may be simulated with a sinus function:

$$Tts(1,1)=29.63+6.9\cdot\sin(2\cdot\pi\cdot T(k1)/Tk)$$

$$Tts=[29.63\ 13.8; 31.6\ 5; 36\ 28; 26\ 16; 36\ 21]$$

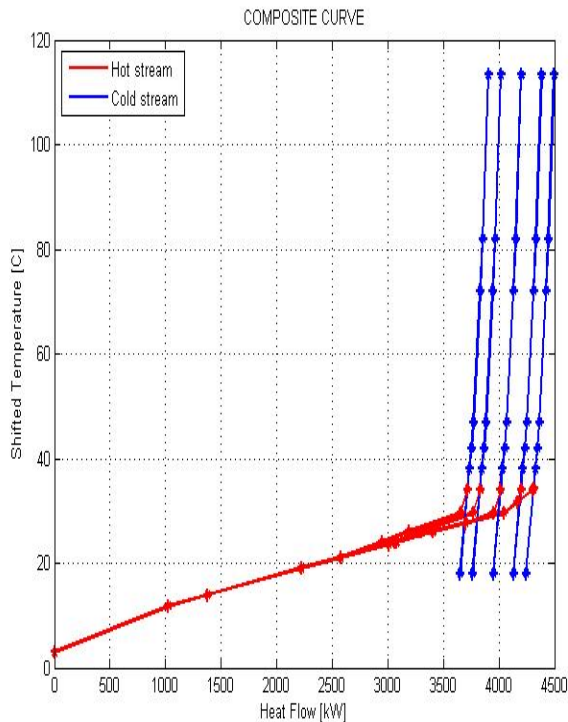


Figure 5. Composite curve. Temperature changes in HVAC area:  $Tts(1,1)=29.63+6.9\cdot\sin(2\cdot\pi\cdot T(k1)/Tk)$

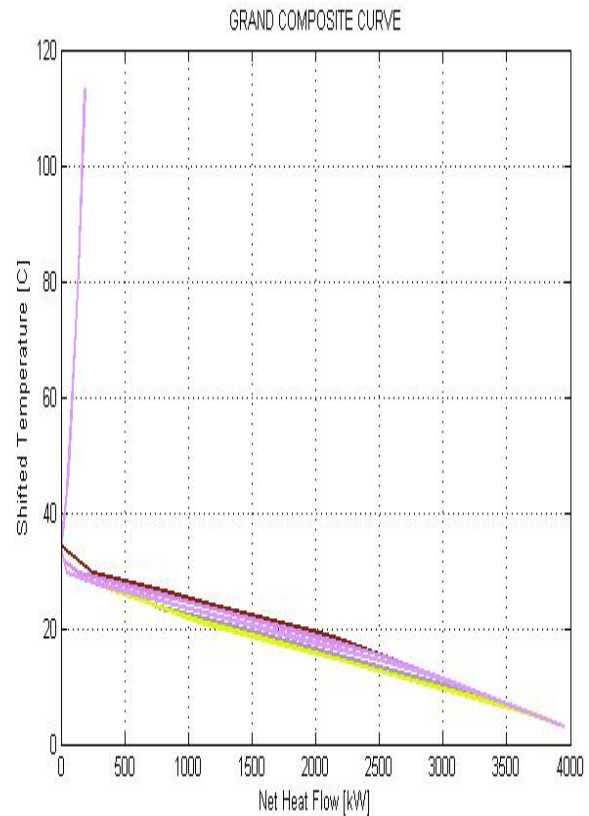


Figure 6. Grand Composite curve. Start point - and point temperature changes in HVAC area :

$$Tts(1,1)=29.63+6.9\cdot\sin(2\cdot\pi\cdot T(k1)/Tk)$$

$$Tts(1,2)=13.8+6.9\cdot\sin(2\cdot\pi\cdot T(k1)/Tk)$$

Regardless of the change in start points, and end points temperature of air in the installation of air conditioning, Pinch point is not moved. Its scroll occurred only when the air temperature is higher than the ambient temperature.

From the cumulative curves can be seen requisite for cooling capacity below Pinch.

Refrigeration consumption decreases and increases with temperature differential. The daily temperature fluctuations depends on two factors:

- External temperature in the summer during 24h and,
- dissipating heat heating machines in the plant.

In any case, the temperature changes are visible, except concerning individual monitoring does not lead to crucial changes. This is important for the HVAC system precisely, flow manage of cooling energy as an option for the volumetric flow of fresh air and circulating air in the cooling unit through a closed system of automatic control.

On further analysis, we can determine whether HVAC affects the overall energy picture into Company. Which model can be turned to the optimum distribution of cooling and thermal energy. Perceive coupling HVAC and technological processes.

It is particularly interesting to see changes into slope of cumulative and composite curves, by the change of fluid flow into the Company.

Daily fluctuations in energy and energy state of the productions of mineral water (to market products related industries, changes in climate on a daily basis, seasonal and annual, of discomfort that does not include a variety of design solutions, and enter the sum of energy, etc.).

By measuring accurately predicted parameters of temperature and flow measurement of all fluids, which are the main carriers of energy at any time we can gain picture in a realistic time where and when changes occur Pinch.

When it identifies changes of the Pinch and changes in the slope of composite and cumulative guilty in the industry, it can be promptly affect onto the streams flows and redirect energy exchange in a way that requires a theory Pinch-a.

Furthermore, it is interesting to observe the mathematical parameters of a real change of current flows of technological processes. It is noteworthy that the flow of heat capacity in certain areas of technological processes may be changing for several reasons.

The first reason of the changes of the masses flow of water from the water resources of the ground, as well as the temperature that is at the beginning of the process and at the end of the process is in the fact that during the process of manufacturing a need for production capacity is changing. This can be justified by market needs during the production cycle. The second component, the temperature, changes throughout the day and seasons depending on the time of year. Transporting fluid in the piping may be exposed to natural (weather conditions, etc.). Chillers, active cooling in the industry, not stationary process. Unsteadiness cause various disorders in the work. Each disorder leads to temperature changes in the fluid.

This is a prelude to further analysis which will show changes in the energy state of working fluid, which mainly affects the overall thermal and cooling consumption.

According to the parameters given in practice and samples of the particular case, we can say with certainty that in the installation can be applied višestepni transfer of heat and cooling energy, all depending on the current energy situation of the Company.

Here are primarily think on the optimization of the cooling towers, air - water heat pumps , water-water geothermal heat pumps, gas-turbine power-plants, solar collectors, etc..

Now let's introduce changes in the equation initial and final temperature of mineral water, but leave out change the temperature in HVAC.

$$T_s = [29.63 \ 13.8; \ 31.6 \ 5; \ 36 \ 28; \ 26 \ 16; \ 36 \ 21];$$

$$\%T_s(1,1) = 29.63 + 6.9 \cdot \sin(2 \cdot \pi \cdot T(k1)/Tk)$$

$$\%T_s(1,2) = 13.8 + 6.9 \cdot \sin(2 \cdot \pi \cdot T(k1)/Tk)$$

$$T_s(2,1) = 31.6 + 10 \cdot \sin(2 \cdot \pi \cdot T(k1)/Tk)$$

$$T_s(2,2) = 7 + 2 \cdot \sin(2 \cdot \pi \cdot T(k1)/Tk)$$

Here we show only a change Pinch-and without changes in temperature due to the volume of data.

It is easy with a particular programming language to get the value of addressing the above equations to the appropriate place.

From this we can conclude that the value of the Pinch-a changed when the temperature of mineral water has reached a value greater than ambient temperature. This means that for the installation of the factory, now the temperature of the Pinch-not determined ambient temperature (outside air temperature at a given time). This can be attributed to exposures of the sunrays to the energy pipelines, directly. Indirect exchange of solar energy radiated on the outer piping, leads to increase in temperatures mineral water above the critical temperature of the environment, ie. its daily peak.

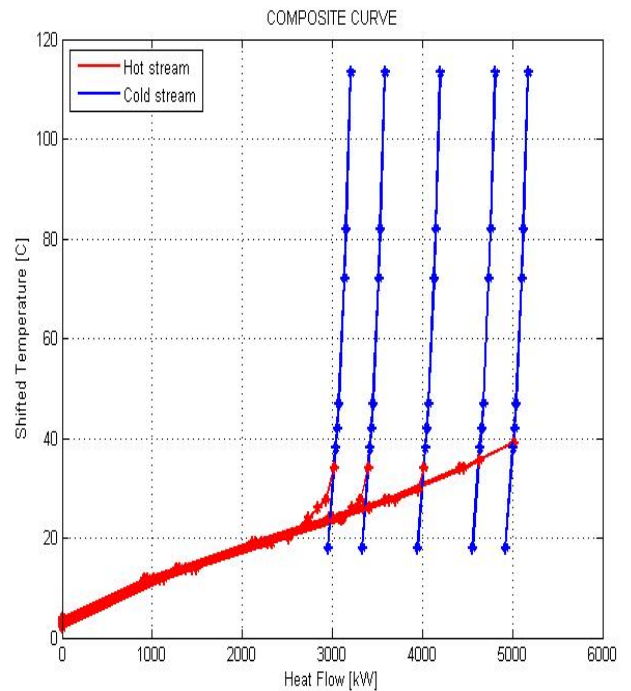


Figure 7. Composite curve. Temperature changes in mineral water process:

$$T_s(2,1) = 31.6 + 10 \cdot \sin(2 \cdot \pi \cdot T(k1)/Tk)$$

$$T_s(2,2) = 7 + 2 \cdot \sin(2 \cdot \pi \cdot T(k1)/Tk)$$

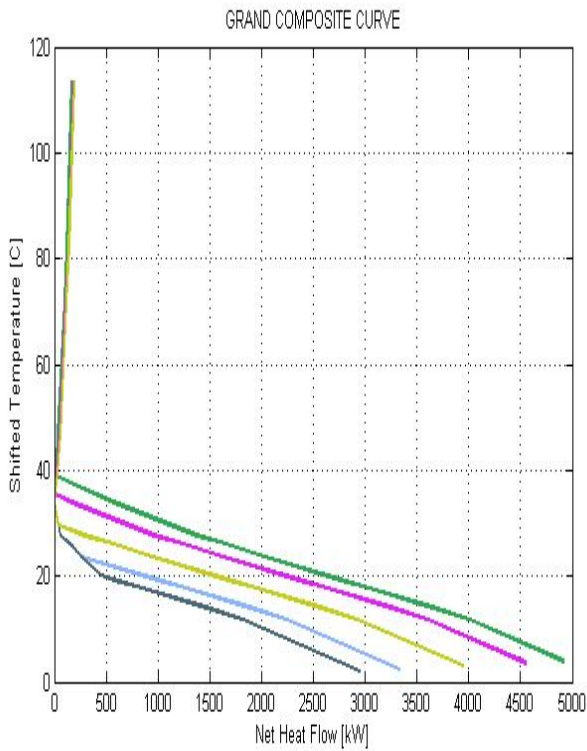


Figure 8. Grand Composite curve. Temperature changes in mineral water process:

$$Tts(2,1)=31.6+10\cdot\sin(2\cdot\pi\cdot T(k1)/Tk)$$

$$Tts(2,2)=7+2\cdot\sin(2\cdot\pi\cdot T(k1)/Tk)$$

$$Tts=[29.63 \ 13.8; \ 31.6 \ 5; \ 36 \ 28; \ 26 \ 16; \ 36 \ 21];$$

$$Tts(1,1)=29.63+6.9\cdot\sin(2\cdot\pi\cdot T(k1)/Tk)$$

$$Tts(1,2)=13.8+6.9\cdot\sin(2\cdot\pi\cdot T(k1)/Tk)$$

$$Tts(2,1)=31.6+10\cdot\sin(2\cdot\pi\cdot T(k1)/Tk)$$

$$Tts(2,2)=7+2\cdot\sin(2\cdot\pi\cdot T(k1)/Tk)$$

### 3. DYNAMIC WINTER PINCH

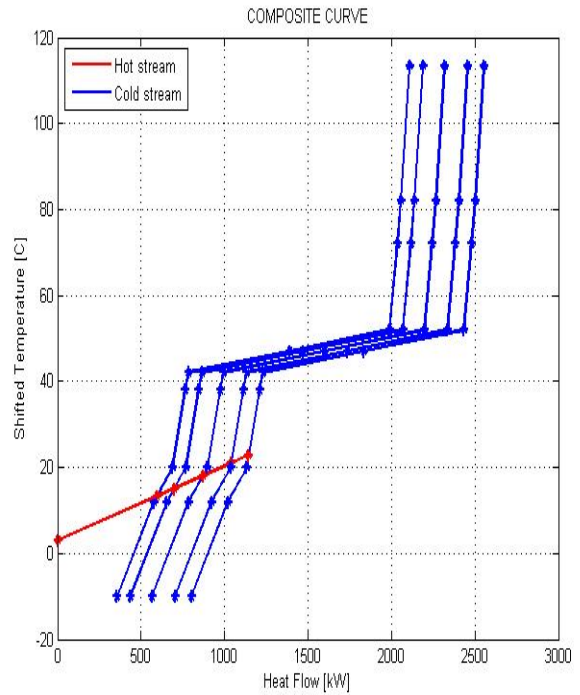


Figure 10. Composite curve winter.

$$Tts(1,1)=20+5\cdot\sin(2\cdot\pi\cdot T(k1)/Tk)$$

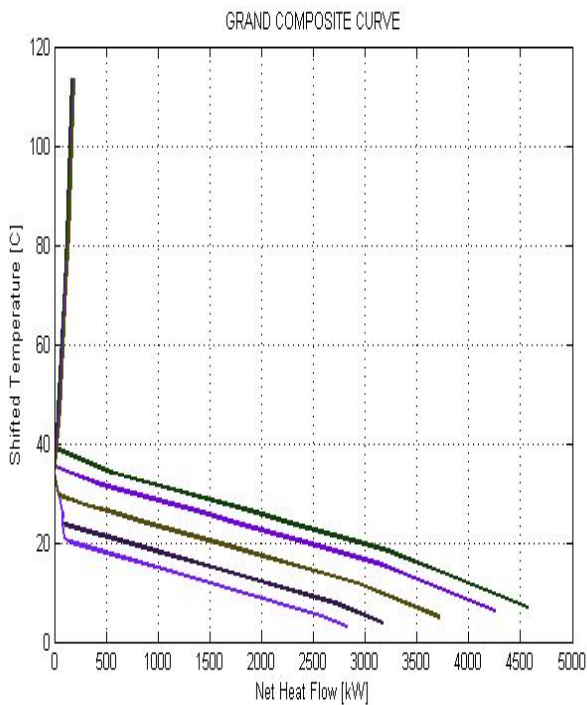


Figure 9. Grand Composite curve. Temperature changes in mineral water process and HVAC area:

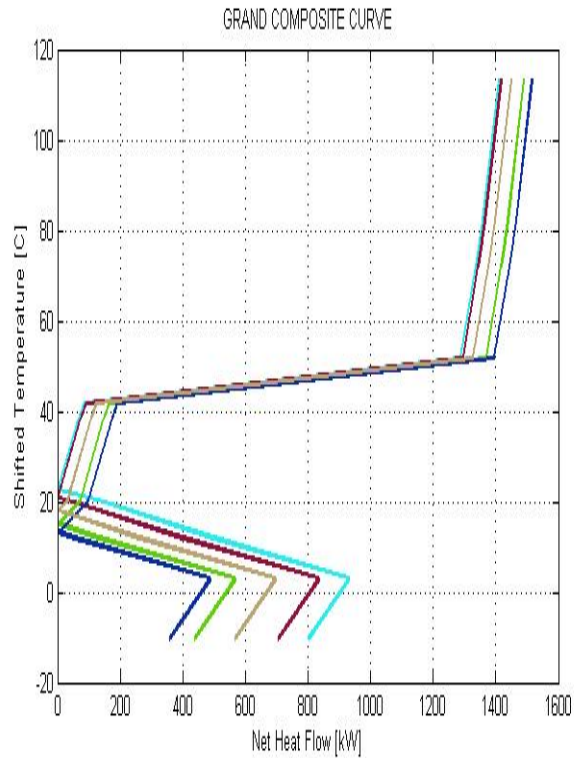


Figure 11. Grand Composite curve winter.

$$Tts(1,1)=20+5\cdot\sin(2\cdot\pi\cdot T(k1)/Tk)$$

Temperature changes in the technological process significantly affects the temperature change Pinch-a. Flows which are cooled, with warm stream in the winter significantly affect on change Pinch.

From the diagram of the composite curve ratio of heat and cooling consumption is far better that is not a huge difference between the flows that are heated and cooled by. The diagram shows that the percentage of energy that is required to be deducted by the cold currents and to surrender to the other side of the warm stream is more evenly distributed.

Naturally, needs for heating in winter is greater, especially when it cools and warms at the same time.

Here we see that at lower temperatures from 3°C to 52°C needs for cooling and heating is 1.395,00kW, of the total heat capacity 1,515.00 kW at a temperature of 113,4°C.

Therefore, the need for heating at low temperatures (which corresponds to the temperatures of the heat pump water/water), indicates that it may be fulfilled with ~ 92% share of the heat consumption.

However, it is important to look variables temperature Pinch-a that match active compressor cooling or passive evaporative cooling system - use of energy of the environment in the process of cooling in the winter.

Here the question is, when and how much is needed to activate the passive cooling system in relation to the active system cooling of the compressor and activating another energy source for heating plant and production process.

The most important thing is to determine the system and take the control to him that would not arise inverse processes above or below the pinch-and during work process.

It should show slope of the composite and cumulative curve for different load cases.

Make mathematical dependence and optimize process.

Further analysis will show all the possible variables in the process.

With the given mathematical model is necessary to determine the energy situation in the system which would be a starting point for possible monitoring and automatisisation cycle in operation, with a greater energy savings.

In addition, the technological process during the production process changes the mass flow of the filling line. Flows that are cooled (cold current). The data changes can be summarized by the following equations:

$$dT_{min}=4;$$

*Flows that heat (cold stream)*

$$T_{hs}=[10 \ 111.38; 36 \ 111.38; 10 \ 40; 10 \ 70; 10 \ 45; 10 \ 80; 40 \ 50; -12.1 \ 18; ];$$

$$C_{PHs}=[0.64 \ 0.992 \ 1.617 \ 0.24 \ 1.16 \ 0.509 \ 117.43 \ 9.95 \ ];$$

*%Heat Capacity flowrate [kW/K]*

*Flows that are cooled (thermals):*

$$T_{ts}=[20 \ 5;];$$

$$T_{ts(1,1)}=20+5 \cdot \sin(2 \cdot \pi \cdot T(k1)/T_k);$$

$$\%T_{ts(1,2)}=8+3 \cdot \sin(2 \cdot \pi \cdot T(k1)/T_k)$$

$$C_{PTs}=[58]; \ %Heat \ Capacity \ flowrate \ [kW/K]$$

$$C_{PTs(1)}=58+35 \cdot \sin(2 \cdot \pi \cdot T(k1)/T_k)$$

Move of phase in heating and cooling technological process and the external temperature:

$$T_{ts(1,1)}=20+5 \cdot \sin(2 \cdot \pi \cdot T(k1)/T_k - 2);$$

$$T_{ts(1,2)}=8+3 \cdot \sin(2 \cdot \pi \cdot T(k1)/T_k - 2);$$

$$T_{hs(8,1)}=-5+7.1 \cdot \sin(2 \cdot \pi \cdot T(k1)/T_k + 3)$$

Diagrams of the phase shifted in heating and cooling:

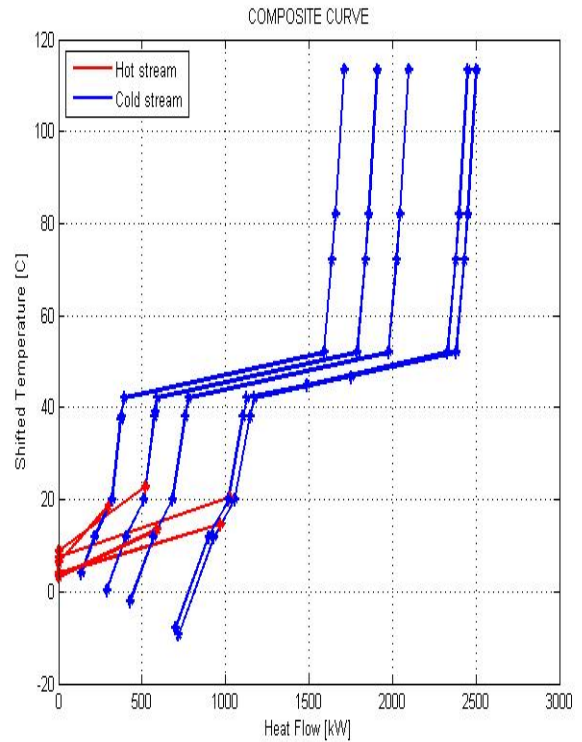


Figure 12. Composite curve with phase change winter.

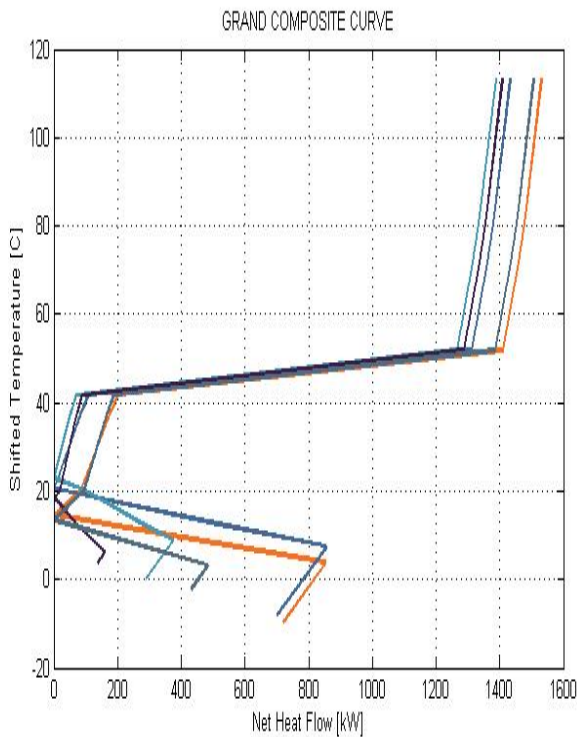


Figure 13. Grand Composite curve with phase change winter.

$$\theta_A = \theta_{Am} \cdot \sin\left(2 \cdot \pi \cdot \frac{\tau}{\tau_0}\right) \text{ Where was given:}$$

$\theta_A$  - temperature changes;

$\theta_{Am}$  - the amplitude of the temperature changes;

$\tau$  - time;

$\tau_0$  - time temperature periods;

#### 4. CONCLUSIONS

To determine the critical temperature for the use of different heating and cooling in the winter, so continuous monitoring of the temperature of the Pinch, of the environment (air and water), then the value of the heat and refrigerant of consumption through the tangens of the angle of inclination of hot and cold currents, and its absolute value.

Let consider a given data point Pinch-a.

The range in this case is 13,45°C - 22.9°C. That are physical size which are shown earlier in the winter period represented cumulative and composite curve. When using a heat pump water-water, with a constant temperature water source out of the ground (considered to be a very small change in the temperature of the groundwater as compared to temperature changes) can be taken following relation:

$T_{pinch,critical} = T_I = T_W = T_{environment} - \Delta T_{min}$  - energy used for first degree of cooling (energy groundwater in an open system heat pump water to water).

$T_{pinch,critical} \leq T_W$  i  $T_{II} < T_{environment} - (\Delta T_{min} + \epsilon)$  uses the energy of the second degree of cooling (energy from the air "passive cooling" air system - glycol). The coefficient depends on the characteristics of the air exchangers - glycol and the setpoint temperature  $T_t$  extreme temperature processes. If the ambient temperature equalizing with  $T_{II}$ , the process should be stop and moves on I level cooling.

It is important to note that from Figure 13 shows that for lower temperature of the Pinch temperature of groundwater ~ 15 °C, needs for cooling process is minimal, precisely between 200kW and 300kW, a heating demand is much greater than 1200kW to 1400kW at lower temperatures up to 52°C.

Using the second degree of cooling is favorable because it reduces the power consumption of the compressor. For the practical needs of small cooling capacity better uses passive cooling, while for heating and other conventional heat, use such as gas.

Pinch point tracking paving the way for redirecting of the stream fluid, their measuring, switching on and off of the energy systems and monitoring energy consumption at any given time.

#### REFERENCES

- [1] Linnhoff B, Mason DR, Wardle I (1979) Understanding heat exchanger networks. *Comp Chem Eng* 3:295-302
- [2] Kemp I C, Pinch Analysis and Process Integration, 2<sup>nd</sup> edition, Elsevier, Amsterdam, London, New York, 2007, 415 p.
- [3] C.L. Chang, X.L. Chen, Y.F. Wang, X. Feng, An efficient optimization algorithm for waste heat integration using a heat recovery loop between two plants, *Appl. Therm. Eng.* 105 (2016), pp. 799-821
- [4] Editorial board, New developments in Heat Integration and intensification, including Total Site, waste-to-energy, supply chains and fundamental concepts, *Applied Thermal Engineering* 61 (2013), pp. 1-6
- [5] Editorial, board, Recent developments in applied thermal engineering: Process integration, heat exchangers, enhanced heat transfer, solar thermal energy, combustion and high temperature processes and thermal process modelling, *Applied Thermal Engineering* 105 (2016), pp. 755-762

# Selection of the Optimal Route of Transportation – a Case Study of Transport of Municipal Waste in the Municipality of Trstenik

Nikola Kostić<sup>1\*</sup>, Milomir Mijatović<sup>1</sup>, Saša Babić<sup>1</sup>, Branimir Milosavljević<sup>1</sup>, Zvonko Petrović<sup>1</sup>  
<sup>1</sup>College of Applied Professional Mechanical Studies/ University of Kragujevac, Trstenik (Serbia)

*In the last 20 years with the help of information technology and changes in transport contributed to more dynamic life of people and became the most important link in the logistics chain. Collection of municipal waste is one of the most complex operational problems in all cities of the world. For economic reasons, the municipal transport WASTE should have the optimum route of transportation.*

*Using appropriate methods and mathematical models in the work of the selected optimum route for transporting municipal waste Trstenik municipality. First defined input data transmission problems ie. mathematical model of the transport problem. A couple of methods for obtaining optimal alignment TRANSPORT a method of Chinese postman obtained optimal route of transportation.*

**Keywords: Optimal transport, Chinese postman, Routing vehicles**

## 1. INTRODUCTION

In the EU countries each year creates about 4 tons of waste per citizen, while a third of all the resources ends up as waste and emissions. Due to the large quantity and the harmfulness to the environment, waste is considered to be one of the most important environmental problems of the modern world. Under municipal waste we consider wastes from household (domestic waste), as well as other waste which, because of their nature and composition is similar to household waste (commercial waste), and waste that is collected from a certain territorial unit, usually of the municipality. The largest part of municipal waste in the EU is still disposed of in landfills, but are increasingly recycled or incinerated with energy production [1].

Within the framework of regulations and planning documents of the EU, waste reduction is more and more promote, which would result in the reduction of waste at the source. There is, however, a significant difference in the application of this principle in EU member states. The percentage of recycling wastes is of from 10 to 65%, and the percentage of disposal of municipal waste from 10% to 90%. The principle of reducing the amount of waste includes initiatives for the introduction of cleaner technology and comprehensive campaign to raise public awareness among the population. The EU policy on waste emphasizes the development of measures such as:

- promoting cleaner production;
- removal of hazardous waste characteristics treatment;
- establish technical standards to limit the content of certain hazardous substances in products;
- promoting reuse and recycling of waste;
- application of the economic instruments;
- analysis of the product life cycle;
- developing a system of eco-labeling [2].

The waste management hierarchy Figure 1 is a strategy that ranks management options in accordance with its environmental advantages, and in accordance with the framework directive on waste (Directive 2008/98/EC)

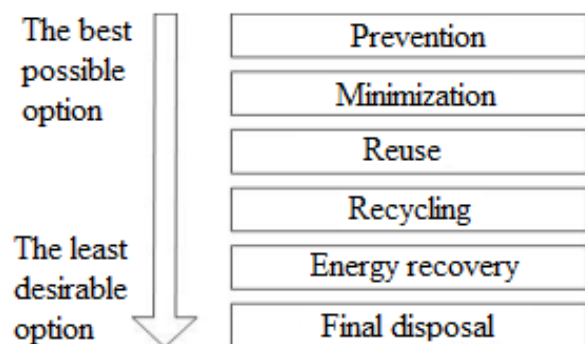


Figure 1. The hierarchy of waste management [3]

Collection and removal of waste is a difficult and complex task. Waste occurs in every household, shopping center and industrial plants, as well as on the street, the park, even on free surfaces. It is a known fact that the process of collection and waste disposal is an expensive operation in the whole system of handling waste, and if we take into account the fact that the total amount of waste increases, the logistics of collecting is becoming increasingly complex. Although these problems existed before, they are now becoming more critical due to the high cost of fuel and labor. This fact is very important because only small improvements in the collection operation may result in significant savings in total costs.

## 2. VEHICLE ROUTING PROBLEM (CLASS OF PROBLEMS)

Vehicle Routing Problem (VRP) is the name for a whole class of problems that require optimum trajectory to the vehicle circled the given number of cities starting from the central warehouse. Under optimal path is the one that has the lowest cost of transport between cities. The concept vehicle routing problem occurs at the end of the 50s of the 20th century as a central problem in the transportation, distribution and logistics companies. In some industries, a large percentage of the product price goes to transportation costs, and optimizing their total cost of the product can be reduced from 5% to 20% [4].

Generalized definition of the problem of routing of the vehicle (PRV) is restricted in practice additional requirements such that the PRV can be classified in several classes [4]:

- The vehicles have a limited capacity (eng. Capacitated VRP - CVPR)
- Clients should be served in a given time period (eng. VRP with Time Windows - VRPTW)
- The vehicle can be used to supply several warehouses (eng. Multiple Depot VRP - MDVRP)
- The customer can return a certain amount of goods in the warehouse (eng. VRP with Pick-Up and Delivering - VRPPD)
- The client can be provided by a number of vehicles (eng. Split Delivery VRP - SDVRP)
- Some of the values (the number of customer requirements, the time of supply) are random variables (eng. Stochastic VRP - GORD)
- Delivery can take a few days (eng. Periodic VRP - PVRP)

The above-mentioned models have a vehicle routing application in the collection of goods at each node of the graph, but not along the branch. Since the collection of municipal waste is carried along each branch is necessary to apply other models, including the simplest solution as "Chinese postman problem".

### 3. TRANSPORTATION OF MUNICIPAL WASTE

The collection of municipal waste is one of the most complex operational problems encountered by local authorities in all cities of the world. One of the most important segment of the collection process in which can be made a significant improvement is the transport. The approach to the analysis and the importance of transport in logistical support, it is necessary to examine some of its essential elements: transport network, transport capacity, transport costs etc. In the transport process, the most important item of each company are the costs ie. lower costs with the involvement of a small number of vehicles and people. Due to its stochastic character, routes optimization process and scheduling of vehicles is one of the most complex problems of transport municipal waste.

In order to perform routing of waste collection vehicles, it is necessary to know the incoming data on the amount of waste to be collected by branches of the transport network, and the number and capacity of vehicles that the company has at its disposal. Today there are a number of models for solving problems routing vehicle depending on the complexity of the transport process. As vehicles for garbage collection must go to all branches of the transport network, the problem boils down to the "Chinese postman problem" as the simplest case of vehicle routing problem.

### 4. CHINESE POSTMAN PROBLEM

*Chinese postman problem and Euler graph* were created in the first half of the 18th century, when the question arose: "How to pass all seven bridges that connect the shores of two rivers in Keninzberg so that each bridge passes exactly once, and then to return to home point. The original problem is shown in Figure 2. Euler route is a route that passes from each branch of the graph

G, which means that every field contains exactly one, and it was closed. Graph G has Euler graph if there is existing routes Euler [5].

The case of "Seven Keninzberg bridges" can not be resolved because there is no closed Euler route. Related Euler graph is one in which all nodes are even degrees. The level of the node is determined by the number of branches that connect it with other nodes of the graph. Connected graph is one in which, for each of the two nodes in the graph, there is a path from one node to another. Suppose a postman delivering mail in one part of the city (area). Postman has the task to visit all streets in the area at least once. Visiting all the streets can happen in several ways. This raises the problem of optimization, which way postman use to deliver the letter, and be as successful as possible. In other words, which route should postman use to visit the area and to visit every street at least once and to exceeds the less distance and return to the same place where he started. Chinese postman problem may relate to various field of work such as routing vehicles for street cleaning, waste collection and other municipal services, such as services for snow removal, etc...

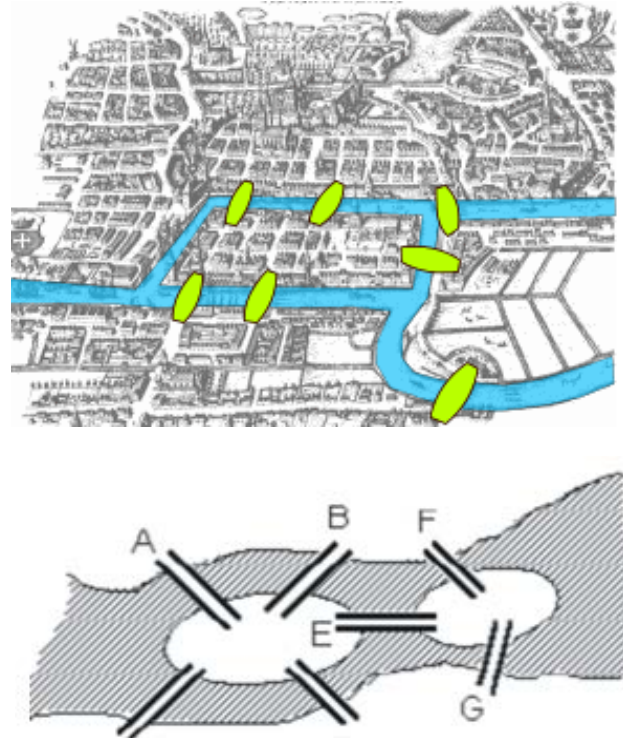


Figure 2. The problem of seven Keninzberg bridges

For the undirected graph  $G=(N, A)$  where the length of the branch are  $d(i, j) > 0$ ,  $(i, j, A)$  problem of the Chinese postman can be defined as follows:

$$\sum s_{ij} * d(i, j) \rightarrow \min, (i, j) \in A, \quad (1)$$

where the  $s_{ij}$  - the number of branch passage.

If the Euler graph solves the Chinese postman problem, it can be concluded that the solution is trivial because it represents Euler route. The sum of length of arcs is the length of path that the postman should be transferred because he will visit all arcs only once and return to the initial node. If the graph is not Euler's then postman should visit some of the branches several times.



Optimization problem consists in determining which branches postman has to visit more than once, to ends his route with a minimum distance traveled.

There are three different graph shown in Figure 3. Finding Euler routes can be identified with the attempt of drawing a graph in one stroke without lifting the pen from the paper. For the first graph in Figure 3 (labeled 1) can not find the order of drawing of branches in a single stroke without lifting the pen from the paper. It can be concluded that this graph is not Euler's graph.

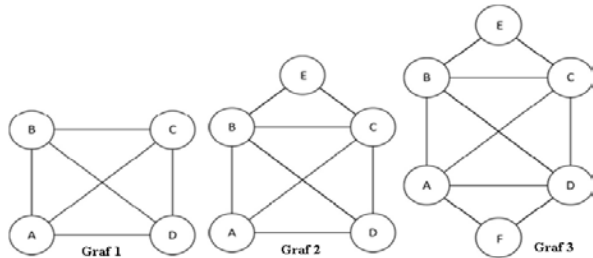


Figure 3. Three test graph Euler route

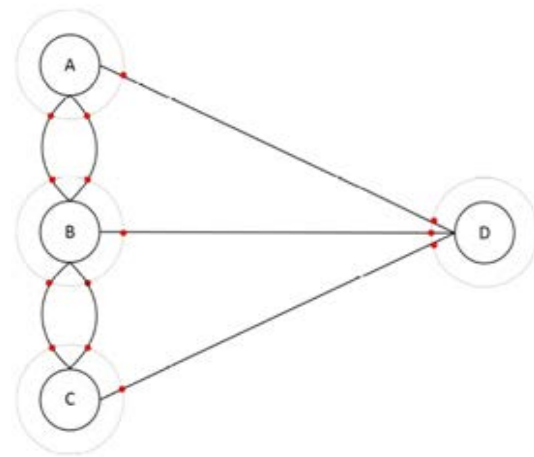
For the second graph in Figure 3, it is possible to draw all branches in a single stroke without lifting the pen from the paper, but the beginning and end of the drawing are never the same point, so this graph is not Euler's graph neither.

For the third graph of Figure 3, it is possible to draw all the branches in a single stroke without lifting the pen from the paper, so it is an Euler's graph. From Table 1 we can see that all nodes of the third graph are even level degrees, so it is possible to find an Euler route [5].

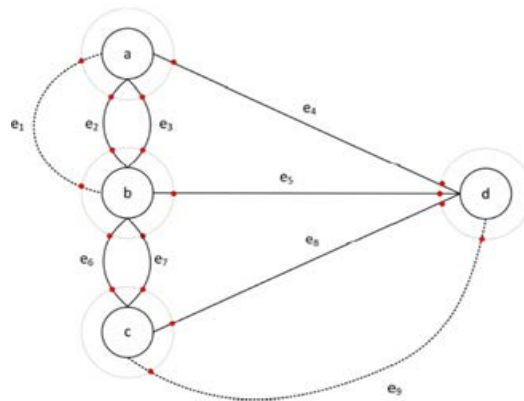
Table 1. Degrees of nodes from graphs in Figure 8

Degrees of graf 1	Node degree e	Degrees of graf 2	Node degree e	Degrees of graf 3	Node degree
A	3	A	3	A	4
B	3	B	4	B	4
C	3	C	4	C	4
D	3	D	3	D	4
		E	2	E	2
				F	2

In graph 2, Figure 3, it is possible to make a Euler path, but not the route. The difference between the route and the track is that the track have different start and finish node. To solve the problem of Chinese postman adding branches, we assume that the graph where the postman should distribute mail is shown in Figure 4a. The branch corresponds to the street where the mail is distributed in mailboxes and the node is a place where the postman can change direction and move in a new street that is linked to the previous one. The postman has to go through every street with the least possible distance traveled. Some streets must pass multiple times because the graph is not Euler's.



a)



b)

Figure 4. Adding artificial branches in order to form the Euler graph

To determine the shortest route it should be taken into account the parameters (length or time required to pass the streets) and thus we obtain a weighted graph. A weighted graph is a pair  $(G, \omega)$ , where  $G$  is - graph, and  $\omega$  - a function that each branch  $e$  from the  $G$  joins the non-negative number  $\omega(s)$ . The value of  $\omega(e)$  is called the weight of the branches  $e$ . To solve the problem of Chinese postman on a graph that is not Euler's, it is necessary to expand the existing graph by adding new branches. The objective of adding these new, artificial branches, is that the degree of each node leads to an even number. Thus, the graph of Figure 4a. was transformed into a new graph of Figure 4b. which Euler's and which has Euler trail.

If the postman use path on the graph that is not Euler's and wants to returned to the starting node from which the journey began, it is necessary to insert new branches between individual nodes. Number of newly installed branch between two nodes corresponding to the number of repeated passes through the original branch between the two nodes. Each new inserted branch is used for counting passes through the original branch, and this branch is called "artificial". Artificial branches connecting the nodes of odd degree. If we have two such nodes in the graph, it is possible to connect only one way. Figure 5 shows the various possible ways of pairing nodes of odd degree in order to obtain the graph Euler

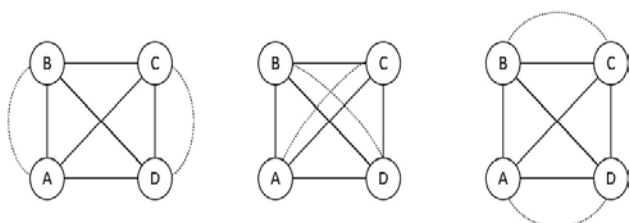


Figure 5. The possible pairing of graph with the 4 odd node

For six nodes ABCDEF odd degree, node A can be linked to the other five, and the remaining four can be connected in three ways. So, for six nodes of odd degree can be 5 x 3 x 1 connection methods. Similar considerations can be carried out for eight or more nodes of an odd degree, Table 2.

Table 2. Template of connecting nodes of odd degree

The number of nodes of odd degree	The number of connecting pairs of nodes
2	1
4	3 x 1
6	5 x 3 x 1
8	7 x 5 x 3 x 1
10	9 x 7 x 5 x 3 x 1
n	(n-1) x (n-3) x (n-5) x ... x 1

To find the routes with minimum total length it is necessary to use an algorithm which, in the case that the graph is not Euler's, will insert artificial branches in the best possible way. The steps required to solve the problem of Chinese postman at no deflection graph are shown in the algorithm.

Algorithm: An algorithm for solving the problem Chinese postman:

- Count all nodes of odd degree
- Count all possible pairs of nodes connecting an odd degree
- Find connect nodes with the lowest weight of artificial branches
- In the original graph add connectivity with minimum weight

The total weight of the route is the sum of the weights of all the branches of the graph.

### 5. EXAMPLE OF ROUTING VEHICLES FOR THE COLLECTION OF MUNICIPAL WASTE IN THE CITY OF TRSTENIK SLOVING THE PROBLEM CHINESE POSTMAN

Public communal company JKSP "Komstan" Trstenik holds 5 waste collection vehicles with the following capacity:

- Trash truck FAP 26-28, with a capacity of 10,6 t
- Trash truck FAP 19-21, with a capacity of 8,6 t
- Trash truck SKANIA VABIS-G-820, with a capacity of 4,8 t
- Trash truck FAP 12-13, load of 4,1 t
- Trash truck FAP 14-18, capacity 3,5 t

All vehicles are engaged in collection and removal of waste from the territory of the city. Figure 6 shows the network of streets which the waste collection vehicles pass, and Figure 7 shows a simplified view, with distances between network nodes.



Figure 6. The network of streets in the Trstenik town

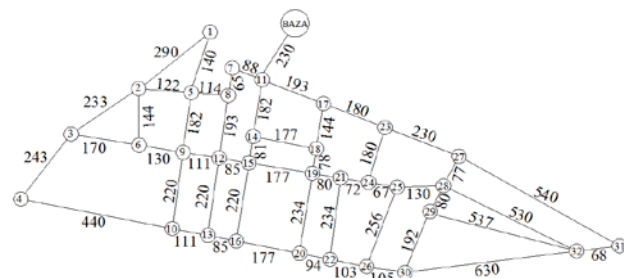


Figure 7. The transport network of the city Trstenika

All nodes are counted and their values of vertex degrees are given in Table 3. Based on the foregoing table the Euler's graph can be formed.

Table 3. The levels of the nodes of the transport network

Node	Node degree	Node	Node degree	Node	Node degree	Node	Node degree
1	2	9	4	17	3	25	3
2	4	10	3	18	3	26	3
3	3	11	4	19	4	27	3
4	2	12	4	20	3	28	4
5	4	13	3	21	3	29	3
6	3	14	3	22	3	30	3
7	2	15	4	23	3	31	2
8	3	16	3	24	3	32	4

Because the base can be considered as a block, there are 20 nodes with an odd degree, which can be connected to 654,729,075 ways. Due to the very large number of possible pairing a simple algorithm has been applying for pairing nodes with odd degree:

**Step 1.** Start from the first network node, which has odd degree, and match it with the next closest adjacent node, which has an odd degree. In other words, connecting to the neighboring nodes that are closest to one another, starting from the first network node with an odd degree.

**Step 2.** Repeat step 1 until there are odd nodes on the network.

The described algorithm may not provide optimal pairing, but it will give enough good solution for a reasonable time and in a simple way. Adding branches, in the form of arcs, is shown in Figure 8. This gives a transport network, having a Euler's route, and the route for waste collection vehicles can be designed. The lengths of branches are given in meters.

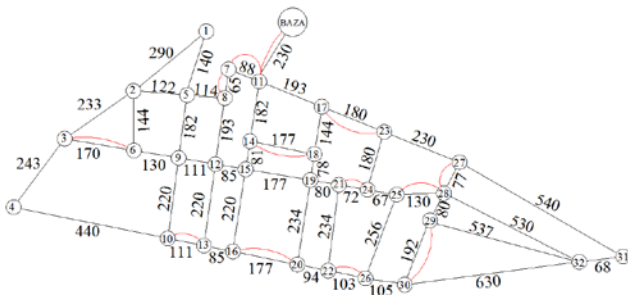


Figure 8. The transport network of the city of Trstenik, which has Euler route

The amount of waste, in tons, which is necessary to pick up is shown in the Figure 9. This information is adopted in accordance with the average amount of waste which is necessary to pick up on the network branches.

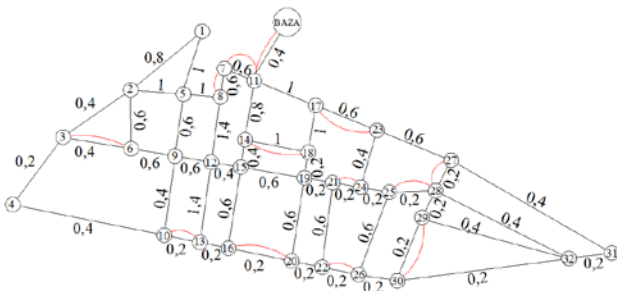


Figure 9. The amount of waste that needs to pick up at the branches of the transport network

Total amount of waste that need to be picked up on the transport network amounts to 26 t. The company has enough capacity in the form of trucks for waste collection. This ensures that practically there is no empty kilometers during transport.

Distribution of vehicles on work assignments, were obtained following routes Figure 10:

**Route 1: Base-11-7-8-5-1-2-3-4-10-9-6-3-6-2-5-9-12-8-7-11-Base**

Route 1 used trash truck FAP 26-28, with a capacity of 10,6 t. On this route, vehicle pick up a total of 10,6 t of waste, making this vehicle utilized 100%. On this route, the vehicle does not collect garbage on the branch Base - 11.

**Route 2: Base-11-14-15-12-13-10-13-16-15-19-18-14-18-17-11-Base**

Route 2 used trash truck -FAP 19-21, with a capacity of 8,6 t. On this route, vehicle pick up a total of 8,2 t of waste, making this vehicle utilized 95%. On this route, vehicle collect garbage at every branch of the transport network, including branch Base – 11.

**Route 3: Base-11-17-23-24-21-19-20-16-20-22-21-24-25-28-27-23-17-11-Base**

Route 3, used trash truck SKANIA VABIS-G-820, with a capacity of 4,8 t. On this route vehicle collected a total of 4,2 t of waste, and the efficiency of the vehicles is 87%. On this route, the vehicle does not collect garbage on the branches Base - 11 - 17.

**Route 4: Base-11-17-23-27-31-32-28-29-32-30-29-30-26-22-26-25-28-27-23-17-11-Base**

Route 4 used trash vehicle FAP-14-18, with a capacity of 3,5 t. On this route, vehicle pick up a total of 3 t of waste, but the efficiency of the vehicles is 86%. On this route, the vehicle does not collect garbage on the branches Base – 11 – 17 – 23 – 27.

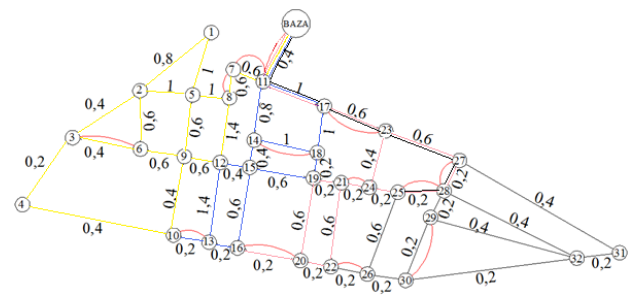


Figure 10. Routes for transportation of municipal waste

Solving the Chinese postman problem the shortest routes for the collection and transportation of municipal waste are identified, which have achieved significant cost savings for the company. Based on the obtained solutions, company took four of five vehicles at its disposal, thus reducing the number of workers to collect waste.

## 6. CONCLUSION

Due to the large quantity and the harmfulness to the environment, waste is considered to be one of the most important environmental problems of the modern world. Waste generation is the result of the overall economic activity of each country. Continuous growth of urban settlements and changes in the structure of the needs of citizens are increasingly exacerbating the problem of waste. Increasing the amount of packaged goods and packaging, increases the amount of waste. The amount of twaste is growing, because it increases the demand for food and goods for prolonged use.

The collection of municipal waste is one of the most complex operational problems encountered by local authorities in all cities of the world. In order for companies to operate economically with maximum cost reduction it is necessary to make the proper deployment of vehicles and choose the optimal route. The case of the city Trstenik shows an example of cost saving with optimal routes, troubleshooting Chinese postman.

JKSP "Komstan" Trstenik has five waste collection vehicles of different capacities that were engaged in the collection and removal of waste from the territory of the city. By using appropriate algorithms a significant savings has been achived in the number of vehicles and number of workers. Using four of five vehicles the amount of exhaust gas, fuel consumption, as well as the maintenance costs of the vehicle is reducing with achieving the maximum effect.

The work of facilities for the collection and removal of municipal waste is of great importance, because municipal waste belongs to the group of hazardous materials and could have a major impact on the ecology. In the transport process, the most important item of each company are the costs ie. expenses as low as possible with the involvement of a small number of vehicles and people.

## REFERENCES

- [1] Cvetanović B, Jovanovic M, A Milošević, Ristic M., "Modern means for the collection and transportation of solid waste", 5th Symposium "Recycling Technologies and Sustainable Development," Hotel "Zdravljak" Soko Banja 12.- 15. September, 2010.

[2] "Waste Management Strategy" for the period 2010 - 2019 (Figure Gazette no. 29/10) Basic text effective as of 15/04/2010, effective from 15/04/2010

[3] Dragana Neskovic Markić, "Modeling and optimization of municipal waste management by applying the analysis of material flows and life cycle assessment", doctoral dissertation, Faculty of Environmental Protection, Sremska Kamenica 2016.

[4] [Dr. Bernabé Dorronsoro Díaz, The VRP Web] - <http://neo.lcc.uma.es/radi-aeb/WebVRP>

[5] Tonči Carić "TRAFFIC OPTIMIZATION PROCESS", Faculty of Traffic Engineering, University of Zagreb, 2014.

# Design improvement of a side water intake on a small hydropower plant

Miloš Nikolić<sup>1\*</sup>, Vladan Karamarković<sup>1</sup>, Rade Karamarković<sup>1</sup>, Miljan Marašević<sup>1</sup>

<sup>1</sup>Faculty of Mechanical and Civil Engineering in Kraljevo, University of Kragujevac, Kraljevo (Serbia)

*This paper deals with the problem of flow distribution at the water intake of a small hydropower plant (SHPP). The plant, with the capacity of 1.25 MW, has been in operation since the end of 2013. At the side intake of the SHPP an uneven distribution of water flow in three parallel chambers of a settling basin has been observed. This anomaly has been noticed during the rinse of different chambers of the settling basin. Each chamber precipitated different amounts of sand. In this paper, water intake is simulated using computational fluid dynamics (CFD) and a technical solution for equalizing flow in three chambers of the settling basin is recommended. The solution should be characterized by: minimal price, simplicity and the lowest possible pressure drop.*

**Keywords: Small hydro, Water intake, CFD modelling**

## 1. INTRODUCTION

Hydropower plants have a global installed capacity of 1064 GW in 2015 with overall productivity of the electric power of 3940 TWh, which represents about 16.6% of the total electricity production [1], [2]. On that basis, hydropower represents the largest source for the production of electricity from renewable energy sources.

Hydropower plants are usually classified based on the size or installed capacity (Table 1.).

Table 1. Classification of Hydropower by Size

Classification	Size
Micro hydropower	Up to 100 kW
Mini hydropower	Between 100 kW and 1000 kW
Small hydropower	Between 1 MW and 10 MW
Medium hydropower	Between 10 MW and 100 MW
Large hydropower	Larger than 100 MW

In Serbia, the energy potential of renewable energy sources is estimated at 4.8 Mtoe per year, of which 0.6 Mtoe is potential for hydropower [3], [4]. The Serbian hydropower potential for producing electricity is 17000 GWh, of which 10000 GWh was used, so that the remaining potential for use is 7000 GWh [5]. The potential of small hydro power plants (up to 10 MW) at 856 locations on rivers in Serbia, including small rivers, with installed capacity of 450 MW is 1,590 GWh per year [6], [7].

There are two basic types of hydro power plants: run of river and storage. Small hydro power plants are being built as a run of river power plant, in which the available flow of water diverted from rivers in the forebay, and the penstock leading to mechanical plant, which is located downstream.

Different types of water intake used in hydropower plants to divert water from the river. Run of river type of small hydro used three main types of water intake:

1) Side intake: The intake is located at the side of the river along one of the banks,

2) Frontal intake: The intake faces the river flow sometimes even perpendicular to the flow,

3) Bottom intake: The intake withdraws water from the riverbed and conveys it directly into the penstock.

In this paper is observed a small run of the river hydropower plant with a lateral water intake. The installed capacity of this power plant is 1.25 MW. In the exploitation conditions, it was observed that the abstraction of the water over the side water intake comes to uneven distribution of water flow in three parallel chambers of the settling basin, which leads to uneven distribution of sediment and create resistance that leads to a reduction of net head. The aim of this paper is to propose a technical solution for equalizing flow (velocity) of water in the chambers of the settling basin. The solution should be characterized by simplicity, minimum price and the lowest possible pressure drop. For the simulation and analysis of the proposed constructional changes at the water intake was used computational fluid dynamics (CFD). A two-dimensional CFD model of the side water intake of small hydropower plant has been presented in this paper for the simulation and analysis of the various structural changes in order to equalize the speed in the chambers of the settling basin. Results of a CFD model of the current situation are compared with different construction solutions in order to find the optimal solution of the perceived problem.

Similar CFD models are used in hydro Engineering for simulation of fluid flow and optimize the various structures for the abstraction or discharge of water. The two CFD models from [8] and [9] are interesting for the problem which is considered in this paper. In this study was used the commercially available CFD software package to simulate the flow of water in the water intake. The advantage of using the software packages (STAR-CD, FLUENT, CFX, or Flow3D) is that the codes are extensively tested and verified.

## 2. WATER INTAKE STRUCTURE

Planar structure model of the side water intake with the lake is shown in Figure 1. Maximum installed capacity of water intake amounts to 5.65 m<sup>3</sup>/s. A project is defined biologically required minimum flow rate of 740 l/s. The dam built across the width of the river is 14 m long.

\*Corresponding author: Faculty of Mechanical and Civil Engineering, University of Kragujevac, 36000 Kraljevo, Dositejeva 19 (Serbia), milosqw@gmail.com

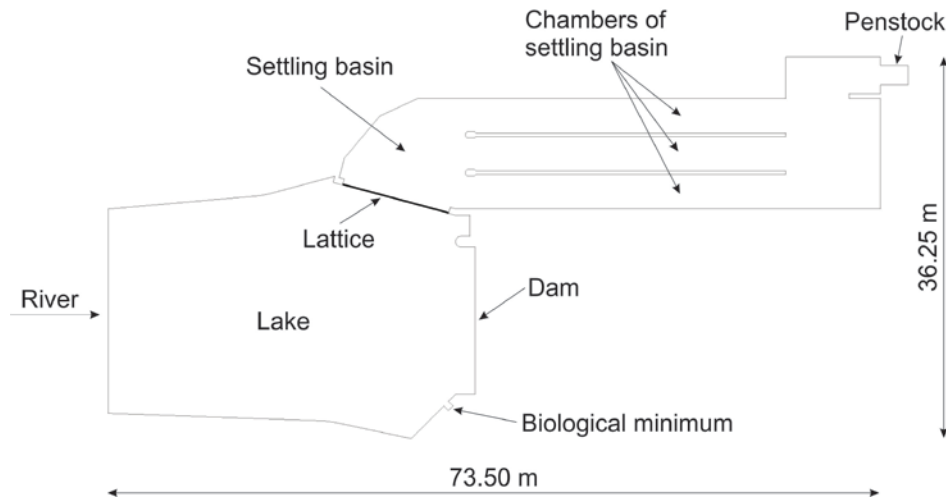


Figure 1: Water intake structure

In this type of hydropower plant and water intake has a role to ensure the projected water level. At the entrance to the settling basin is located lattice, 10.50 m wide and 1.20 m high which has a role to prevent large sediment or other elements that the river carries to enter to the settling basin. The width of the openings in the lattice is 25 mm, while the width of the solid material is 8 mm.

Sedimentation tank is 52.67 m long and 15.50 m wide, and consist of three parallel chambers which are 30.47 m long and 3.30 m wide. The chambers are divided by a concrete wall thickness of 0.30 m. The role of the settling basin in the water intake that directs water from the lake to the pipeline, ensuring the flow of pressure to mechanical plant, based on the projected level of water that held in the settling basin and the lake. The second function of the settling basin is to stop the smaller sediments that have passed through the lattice to avoid the pipeline and then to mechanical installations. For this reason settling basin consists of three chambers, of which is for rinse sediments in one chamber other two chambers closed by slide gate, and the total flow is directed to a chamber which is rinsing. In this way the velocity of the water increases significantly and water together with sediments get out from the settling basin into the river.

### 3. COMPUTATIONAL DOMAIN

#### 3.1. Computational grid

One of the most important steps in the use of commercial CFD software to the problem of fluid flow is to develop a computer grid with adequate resolution. In defining a grid, the essential is to find the optimal number of elements so that the model is credible in presenting the real state, and on the other side higher resolution form a larger number of elements and therefore these extend simulation time and achieving convergence [10].

Computational grid of the 2D water intake model which is observed in this paper consist of 217979 elements and 227339 nodes. In generating the grid using module Mesh in Ansys software, physical preferences are defined as CFD, solver preferences as Fluent, with relevance 100. In defining the size of the grid elements, it was selected a curvature size function with fine relevance. Curvature Normal Angle is set to 12.0 degrees. Minimum element size is 8.4 mm, while the maximum size of the area and max tet size are limited to 100 mm.

Because of the lattice which is relatively dense in relation to the defined grid, it is necessary in the field of lattice define local finer grid. Edge Sizing was used as a function with defined geometry of lattice edge. The parameter for generating local grid is the element size of a maximum of 5 mm.

#### 3.2. Boundary conditions

The boundary conditions defined on the two-dimensional CFD model of side water intake considered in the paper and shown in Figure 2. are: Fluid\_inlet, Fluid\_outlet, and Biological\_minimum.

Boundary condition at the entrance to forebay represent the Fluid\_inlet with the defined volumetric flow of water with a value of 6.39 m<sup>3</sup>/s. Velocity field of water at the entrance is normally distributed with respect to the boundary surface.

The model is defined that the output of the settling basin has set as a boundary condition "Outlet", Fluid\_outlet with the volumetric flow of water than 5.65 m<sup>3</sup>/s, which is the maximum installed flow of the small hydropower plant.

Biological minimum which is necessary to provide for the fish's path, is defined as a boundary condition "Outlet", with a water flow rate of 0.74 m<sup>3</sup>/s.

#### 3.3. Solving procedures

The parameter for comparison of the proposed technical solutions is the velocity of water flow in the chambers of the settling basin. To describe the fluid velocity and turbulence in the river or hydraulic systems, such as a water reservoir, water discharge structure, or water intake structure of small hydropower plants, are used Navier-Stokes equations. For turbulent flow are commonly used version of the Reynolds averaged Navier-Stokes equations (RANS). In this paper was used Pressure-Based RANS model, with absolutely defined speeds. It was suggested the planar, no gravity, and a stationary velocity field. RANS model defined in the [11] is used in this study for modeling fluid flow in the structure of water intake:

$$\frac{\partial U_i}{\partial t} + U_j \frac{\partial U_i}{\partial x_j} = \frac{1}{\rho} \frac{\partial}{\partial x_j} (-P \delta_{ij} - \overline{\rho u_i u_j}) \quad (1)$$

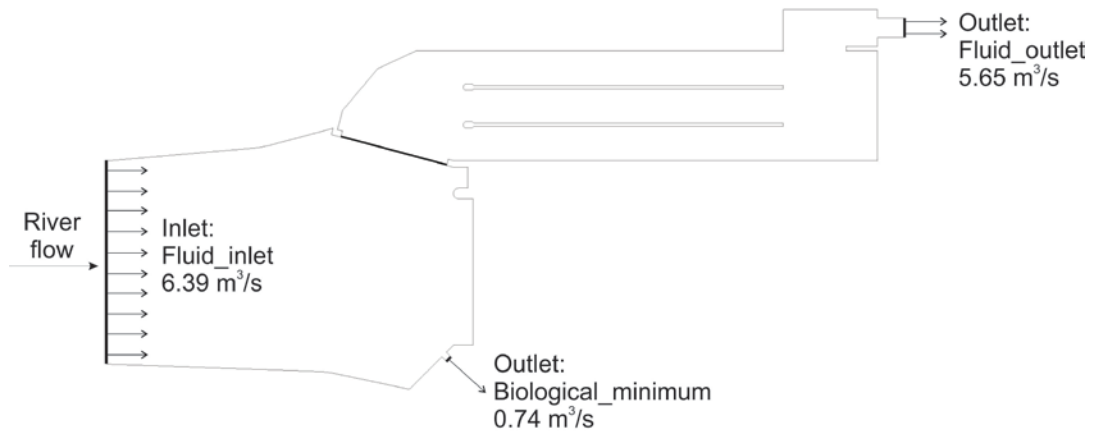


Figure 2: Boundary conditions

Where  $U$  is the average value of the velocity,  $u$  is fluctuating value of the velocity,  $P$  is pressure,  $\rho$  is density, and  $\delta_{ij}$  is Kronecker delta, with a value of 1 if  $i=j$  or 0 in other cases. A Reynolds stress term from the equation (1) is modeled by approximating Boussinesq’:

$$-\overline{\rho u_i u_j} = \rho v_T \left( \frac{\partial U_i}{\partial x_j} + \frac{\partial U_j}{\partial x_i} \right) - \frac{2}{3} \rho k \delta_{ij} \quad (2)$$

Where the variable  $k$  is turbulent kinetic energy, and  $v_T$  is turbulent eddy viscosity. By inserting equation (2) into the (1) is obtained the final form of equation:

$$\frac{\partial U_i}{\partial t} + U_j \frac{\partial U_i}{\partial x_j} = \frac{1}{\rho} \frac{\partial}{\partial x_j} \left[ - \left( P + \frac{2}{3} k \right) \delta_{ij} + v_T \frac{\partial U_i}{\partial x_j} + v_T \frac{\partial U_j}{\partial x_i} \right] \quad (3)$$

The first member of the equation on the left of the previous equation is a non-stationary member, which is set in the model is zero, because the velocity of the water in the water intake is defined as stationary. For calculation of the turbulent eddy viscosity, in equation (2) the  $k-\epsilon$  model from [11] was used:

$$v_T = c_\mu \frac{k}{\epsilon} \quad (4)$$

Where the turbulent kinetic energy  $k$  modelled as:

$$\frac{\partial k}{\partial t} + U_j \frac{\partial k}{\partial x_j} = \frac{\partial}{\partial x_j} \left( \frac{v_T}{\sigma_k} \frac{\partial k}{\partial x_j} \right) + P_k - \epsilon \quad (5)$$

Where:

$$P_k = v_T \frac{\partial U_j}{\partial x_i} \left( \frac{\partial U_j}{\partial x_i} + \frac{\partial U_i}{\partial x_j} \right) \quad (6)$$

Dissipation of turbulent kinetic energy  $k$  is denoted by  $\epsilon$ , and modeled as:

$$\frac{\partial \epsilon}{\partial t} + U_j \frac{\partial \epsilon}{\partial x_j} = \frac{\partial}{\partial x_j} \left( \frac{v_T}{\sigma_\epsilon} \frac{\partial \epsilon}{\partial x_j} \right) + C_{\epsilon 1} \frac{\epsilon}{k} P_k + C_{\epsilon 2} \frac{\epsilon^2}{k} \quad (7)$$

Where constants in the  $k-\epsilon$  model have the following standard values:  $c_\mu = 0.09$ ;  $C_{\epsilon 1} = 1.44$ ;  $C_{\epsilon 2} = 1.92$ ;  $\sigma_k = 1.0$ ;  $\sigma_\epsilon = 1.3$ ;

Semi – Implicit Method for Pressure – Linked (SIMPLE) is used for solving described a model of the water intake.

#### 4. RESULTS

For simulating the results of the side water intake in the paper, the commercial computational fluid dynamics (CFD) software package Ansys is used. This software package is able to use two modules to simulate fluid flow: Ansys Fluent and Ansys CFX. In the case of 3D flow, it is possible to use both modules, CFX and Fluent. When the 2D flow model is set, as is the case in this study, it is possible to use only module Fluent.

Ansys Fluent, like other CFD software packages, solves the fundamental equations of fluid flow [12], conservation of mass and momentum, known as Reynolds-averaged Navier-Stokes (RANS) equations. The Software solves additional equations that represent the turbulent characteristics ( $k-\epsilon$ ) to determine eddy viscosity and mixing coefficients. Ansys Fluent discretized partial differential equations using finite volume method, and solve the resulting algebraic equations by implicit methods [13], [14], and [15].

##### 4.1. Existing state

The result of the simulation of the current state of the water intake of small hydropower plant is shown in Figure 3. Shown is a planar velocity field of the flow of water in the range from 0 to 1.35 m/s. It may be noted that the water velocity in the chambers of the settling basin drastically different. Top speed, i.e. the flow is realized in the third chamber of settling basin. In the secondary chamber is achieved somewhat lower speed, while in the first chamber, the water is almost not moving, and the flow rate is approximately zero, except for a few local fields of velocity different than zero (see Figure 3).

##### 4.2. Proposed technical solutions

To overcome the problem of uneven flow in the three chambers of the settling basin, 12 technical solutions are proposed and shown in Figures from 4 to 15. The Settlement provides for a change in a part of settling basin between the lattice and the chambers of the settling basin. The proposed technical solutions are characterized by simplicity, the minimum price and the lowest possible pressure drop. The aim of the presented results that are based on established criteria is to determine the best technical solution to reduce the difference in speed and flow in the chambers of the settling basin.

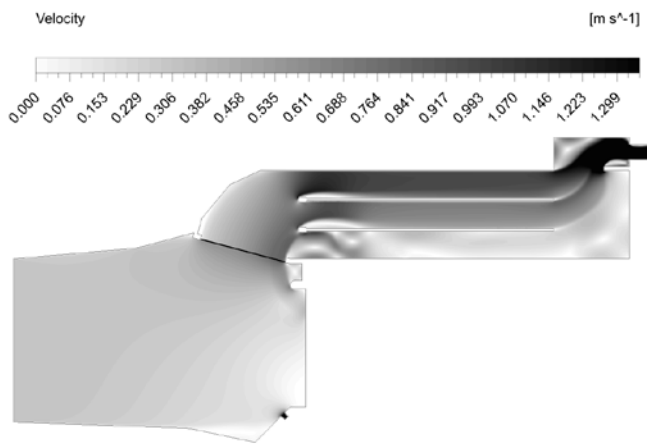


Figure 3: Existing state

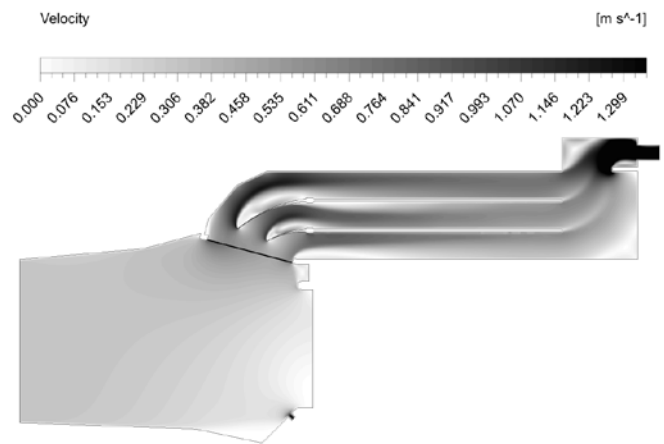


Figure 7: Solution 4

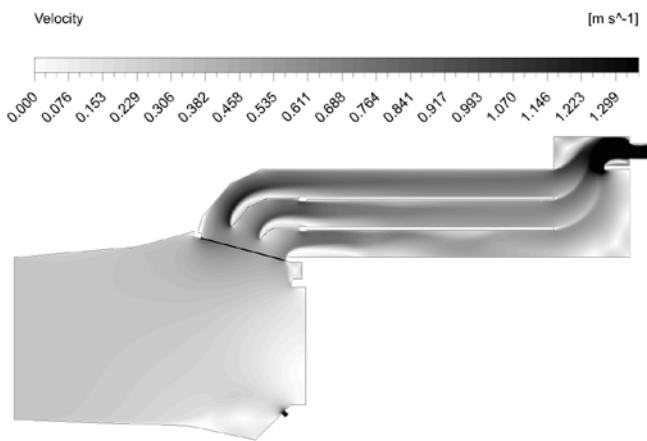


Figure 4: Solution 1

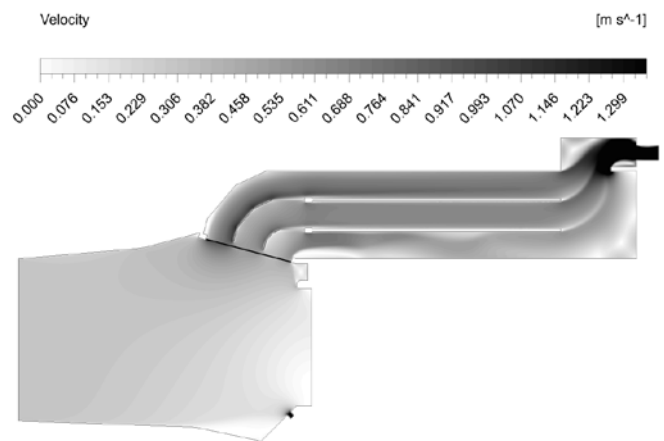


Figure 8: Solution 5

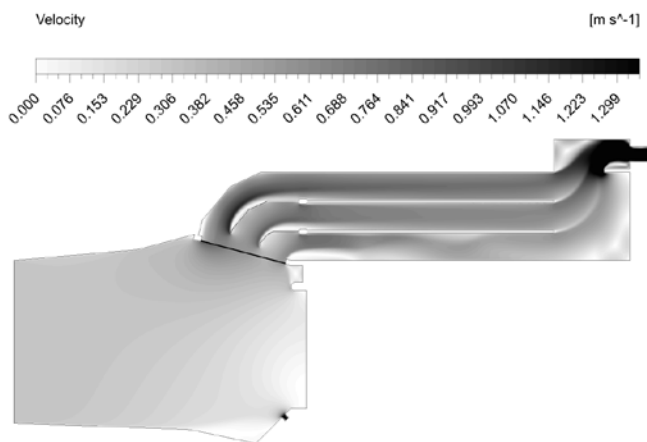


Figure 5: Solution 2

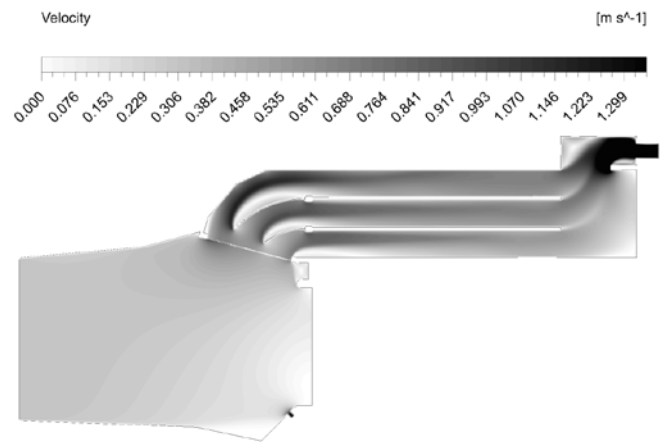


Figure 9: Solution 6

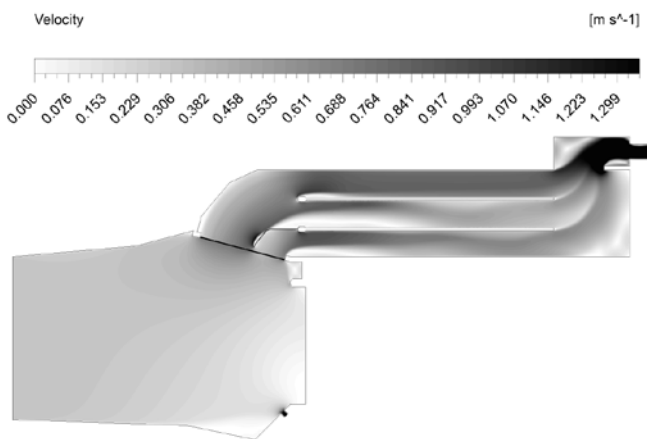


Figure 6: Solution 3

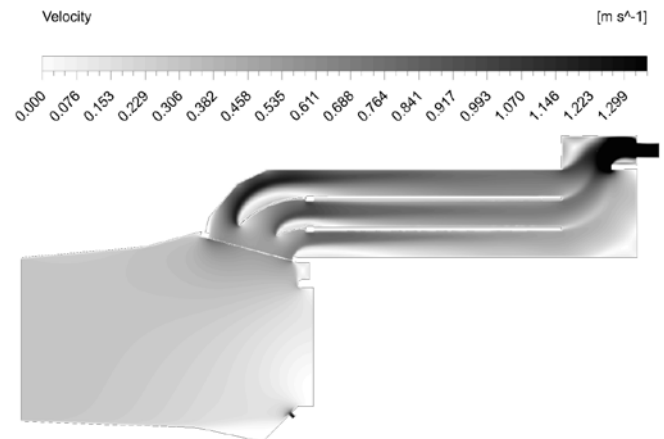


Figure 10: Solution 7



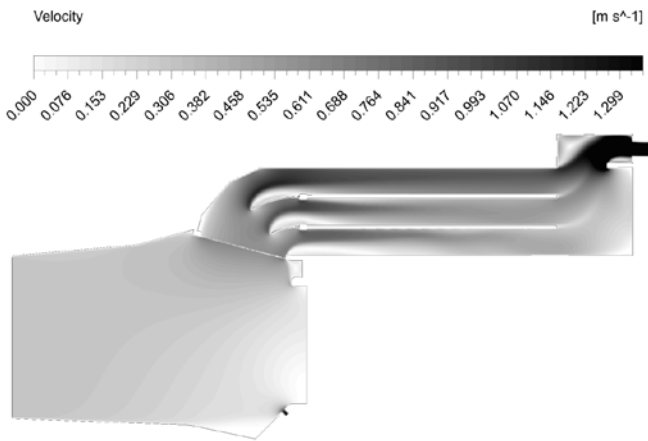


Figure 11: Solution 8

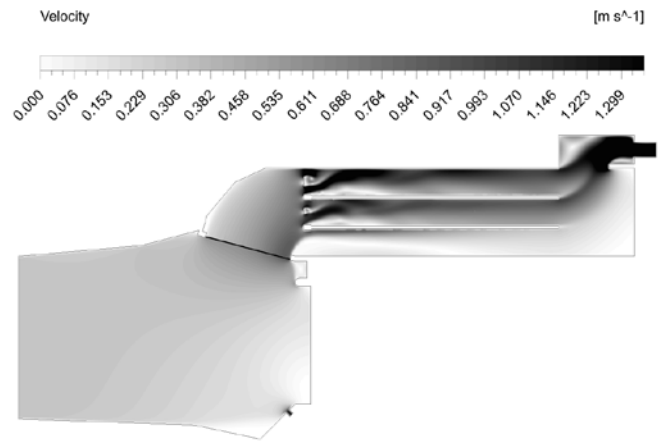


Figure 15: Solution 12

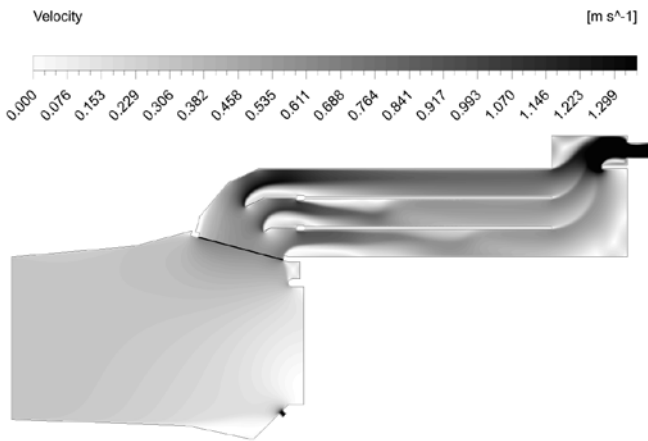


Figure 12: Solution 9

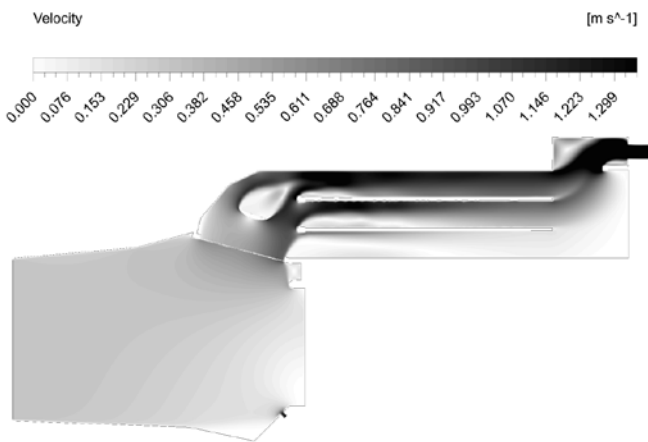


Figure 13: Solution 10

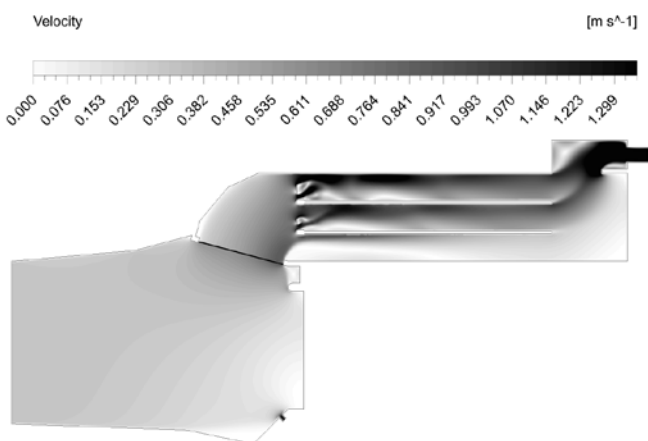


Figure 14: Solution 11

If one looks at the current state of the side water intake (Figure 3) it can be seen that the velocity in the area of the lattice approximately evenly distributed. The problem arises because of the intensity of the speed that is on average between 0.611 and 0.688 m/s at the entrance. Based on these facts were proposed technical solutions for adding a router and a barrier in the area between the lattice and the chambers of the settling basin. The idea is to determine the optimal shape and length of the router of water in order to achieve the desired effect, equalizing the water speed in the chambers of the settling basin.

In the figures 13, 14, and 15 are shown the results of simulation of the proposed technical solutions with the increase of the resistance in the first and second chamber (see Figures 14 and 15), wherein the partition wall is greater in the first chamber in the relative to the wall in the second chamber, for the reason that in the analysis of the current state (see Figure 3.) first chamber has the highest speed. The difference between solutions 11 and 12 is in the position of placing a barrier in relation to the chambers of the settling basin. The solution 10 (in Figure 13.) represent the reconstruction in order to create a resistance to the central part of the settling basin, between the lattice and the chambers, where is the main direction of flow of the water towards the first chamber, and a smaller portion to the second chamber. This three solutions would cause a deterioration compared to the current situation, so it are rejected.

The solution 3 (Figure 6) provides for the installation of a router between the second and the third chamber. This solution increases the velocity in the third chamber, but significantly reduced in the second chamber. The Solution 4 (Figure 7.) provides for the installation of special shape router, but this solution increases the speed in the first chamber.

Solutions 1, 2, 5, and 9 are shown in Figures 4, 5, 8, and 12, respectively. This group of solutions represents the installation of the flow router with the criterion that the width of new chambers be equal. The differences between these four solutions are in lengths of dividers. Here can be seen that for a solution is beneficial that the routers as long as possible. Solutions 1, 2, and 5 provide approximately the same result, because the differences between the lengths of the flow deflector are very small. These three solutions, which essentially boils down to one solution with different router lengths, represent a potential solution to the observed problem.

The remaining solutions 6, 7, and 8, are presented in Figures 9, 10, and 11. These three solutions provide for the installation of the router in the form of an arc, wherein the different lengths between the three solutions. These three solutions have led to substantial improvements compared to the current situation, but speeds continue to vary, so that the speed is higher in the first chamber, and in a third smaller, relative to the rate flow of the water in the second chamber of settling basin, wherein is exception is the solution 6 (Figure 9) where the speed in the chambers quite balanced.

Based on the analysis of all the proposed solutions, the best results in the equalization of speed in the chambers of settling basin can be achieved by installing a router as provided by solutions 1 (Figure 4.) and 6 (Figure 9.).

## 5. CONCLUSION

The small hydropower plant with installed capacity of 1.25 MW, which is in operation since the end of 2013 was observed in this study. This hydropower plant is run of the river type with lateral water intake. In the exploitation conditions, it has been observed that the flow of water in the three chambers of the side intake settling basin differs drastically, so that a single chamber is almost no flow.

The aim of this study has been to propose a technical solution for the reconstruction of water intake so as to equalize the speed and flow in the chambers of the settling basin. Criteria for selection of the optimal solution are: minimum price, simplicity, and the lowest possible pressure drop. To solve this problem a two-dimensional CFD model was formed, that is generated by a grid with 217979 elements and 227339 nodes, and by defined boundary conditions.

In order to solve the defined model is used the Ansys Fluent software package, on the basis of equations of a turbulent flow of the fluid (RANS) and additional equations which describe the turbulent characteristic ( $k-\epsilon$ ). The Semi-Implicit Method for Pressure-Linked (SIMPLE) algorithm was used for solving the model in a Fluent module of Ansys software package. As a result, showing the 12 simulations of the proposed technical solutions. Based on the results, several technical solutions lead to a reduction in the difference in the speeds of which are the best results achieved with solutions 1 and 6.

Continued research should consist of drafting and 3D simulation model of the side water intake, and the inclusion of sediments in the fluid flow.

## ACKNOWLEDGEMENTS

This work was conducted within the project TR 33027 supported by the Ministry of Education, Science and Technological Development of the Republic of Serbia.

## REFERENCES

[1] Pandey, Bikash, and Ajoy Karki. *Hydroelectric Energy: Renewable Energy and the Environment*. CRC Press, 2016.

[2] REN21, Renewables 2016 Global Status Report. REN21 Secretariat, Paris, 2016.

[3] Jovančić, P. D., Kolonja, B., Ignjatović, D., Tanasijević, M., Madžarević, A., & Krstić, V. (2016). Energy resources in the Republic of Serbia: Development policy. *Energy Sources, Part B: Economics, Planning, and Policy*, 11(11), 1020-1026.

[4] <http://www.srbijavode.rs/sr-latin/home/Aktuelno/mhe.html> (in Serbian)

[5] Pekez, J., Radovanovc, L., Desnica, E., & Lambic, M. (2016). The increase of exploitability of renewable energy sources. *Energy Sources, Part B: Economics, Planning, and Policy*, 11(1), 51-57.

[6] <https://energija.wordpress.com/2009/01/05/katastar-malih-hidro-elektrana/> (in Serbian)

[7] <http://www.elektrosrbija.rs/me/images/dokumenti/Katastar%20MHE%20u%20Srbiji.pdf> (in Serbian)

[8] Lai, Y. G., Weber, L. J., & Patel, V. C. (2003). Nonhydrostatic three-dimensional model for hydraulic flow simulation. I: Formulation and verification. *Journal of Hydraulic Engineering*, 129(3), 196-205.

[9] Khan, L. A., Wicklein, E. A., Rashid, M., Ebner, L. L., & Richards, N. A. (2004). Computational fluid dynamics modeling of turbine intake hydraulics at a hydropower plant. *Journal of Hydraulic Research*, 42(1), 61-69.

[10] Thompson, Joe F., B. K. Soni, and N. P. Weatherill. "Handbook of Grid Generation CRC Press." Boca Raton, Florida (1999).

[11] Olsen, Nils Reidar B. "Hydroinformatics, fluvial hydraulics and limnology." *Norwegian University of Science and Technology. Trondheim, Noruega* (2004).

[12] Khan, Liaqat A., Edward A. Wicklein, and Mizan Rashid. "A 3D CFD model analysis of the hydraulics of an outfall structure at a power plant." *Journal of Hydroinformatics* 7.4 (2005): 283-290.

[13] Olsen, Nils Reidar B. "Computational fluid dynamics in hydraulic and sedimentation engineering." *The Norwegian University of Science and Technology, Trondheim* (1999).

[14] Rodi, W. "Turbulence Models and Their Applications in Hydraulics, International Associate for Hydraulic Research, Delft, The Netherlands." (1980).

[15] Lomax, Harvard, Thomas H. Pulliam, and David W. Zingg. *Fundamentals of computational fluid dynamics*. Springer Science & Business Media, 2013.

# Measurement and Analysis of Changes in Total Quantity of Injection Depending on the Changes in Value of Pressure in Common Rail System

Nikola Kostić<sup>1\*</sup>, Božidar Krstić<sup>2</sup>, Milomir Mijatović<sup>1</sup>, Saša Babić<sup>1</sup>, Branimir Milosavljević<sup>1</sup>  
<sup>1</sup>College of Applied Professional Mechanical Studies/ University of Kragujevac, Trstenik (Serbia)  
<sup>2</sup>Faculty of engineering/University of Kragujevac, Kragujevac (Serbia)

*The paper describes the process of measuring and analyzing of the set and actual pressure value and the total quantity of injection in common rail system with continuous and sudden acceleration. The measurements were carried out on the vehicle Citroen Berlingo 1.6 Hdi using universal diagnostic device Bosch KTS 540. The conducted analysis shows the relation between changes in set and actual pressure value and the total amount of injection which has an impact on fuel consumption and vehicle emission.*

**Keywords:** pressure changes, the total amount of fuel injection, fuel consumption, exhaust emissions

## 1. INTRODUCTION

Technical diagnostics is a technical discipline that deals with monitoring the state of the vehicle and machine. By diagnostic devices it is possible to determine the condition of parts and assemblies without dismantling and disrupting the initial feedback, and with knowledge of the conditions and maintenance of vehicles in the past, it is possible to predict their behavior in the future and thus prevent the occurrence of sudden cancellation [1].

Diagnostics has a very large and important role in the prevention of malfunction of motor vehicles [3] where it is necessary to analyze the symptoms and diagnostic parameters and their functional connection with the state of the system structure and establish the diagnostic norms and criteria on which they are determined. Application rules "six steps" [2] is an indispensable prerequisite for the successful diagnosis and successful of any defects on the transport device. By applying suitable diagnostic devices and software tools [4], it is possible to signal acquisition with electronic control systems on vehicles that provide the possibility of further processing. The main goal is to create a useful database for preventive and corrective maintenance of vehicles.



Figure 1. Diagnostics of motor vehicles

In addition to determining the occurrence of cancellation of the vehicle, advanced diagnostic devices and monitoring parameters enable the operation of certain systems on the vehicle:

- engine,
- transmission,
- steering,
- ABS,
- central electronics ...

Knowing the limit values of these parameters, it is possible to predict the occurrence of failure and thereby reduce costly repairs and parts replacement.

This paper describes the measurement and analysis of change in the total quantity of injection depending on the change in value of the pressure in the common rail system.

## 2. MATERIAL AND WORKING METHODS

For the purposes of measurement it was used a universal diagnostic tool Bosch KTS 540 (Figure 1) which is connected (via USB cable or Bluetooth connection) to the PC on which is installed the ESI[tronic] 2.0 software.



Figure 1. Bosch KTS 540 universal diagnostic tool

The measurements were carried out on the vehicle Citroen Berlingo 1.6 HDi with Bosch common rail injection system (Figure 2).



Figure 2. The test vehicle and equipment

Manufacturer in this model fitted aluminium engine capacity of 1,560 cm<sup>3</sup> (Tab. 1), the maximum power 69 kW at 4000 [rpm]. and maximum torque 215 Nm at 1750 [rpm].

For fuel injection it is used the second generation of Bosch's common rail system (Figure 3), with pressure ranges from 250 [bar] to 1600 [bar] when the engine is under full load.

Table1. Technical characteristics of the test vehicle

TECHNICAL CHARACTERISTICS	
<b>CITROEN BERLINGO</b>	<b>Hdi 92 Multispace</b>
<b>Version</b>	<b>Hdi 92 Multispace</b>
ENGINE	
Type	Turbo diesel with direct injection High pressure 16 valve
Cylinders No.	4
Displacement [cm <sup>3</sup> ]	1560
Diameter x piston stroke[mm]	75 x 88,3
Maximum power [kw/rpm]	69(92)/4000
Maximum torque /rpm	215/1750
Engine standard	EURO IV

On figure 3 is presented schematic of the Bosch common-rail system that is fitted in test vehicle.

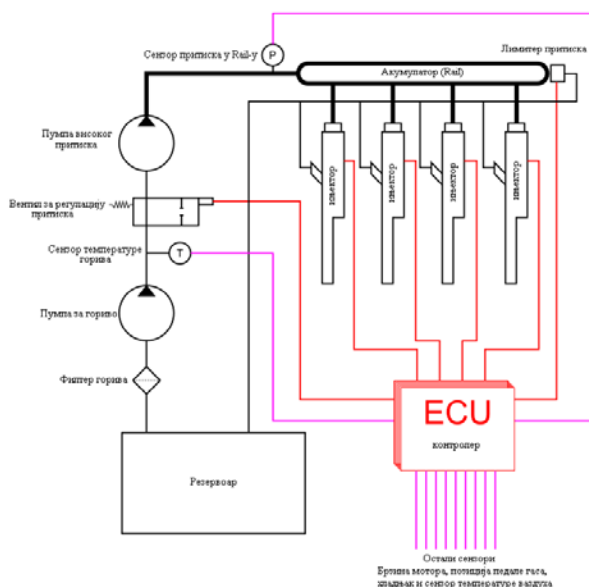


Figure 3. Schematic representation of the common rail system of test vehicle

After connecting vehicle with diagnostic device it is necessary to identify the test vehicle, entering the basic information (country of origin, type of vehicle, type of operation, engine code, etc.) (Figure4). The software provides the ability to identify the vehicle and through the VIN number (chassis number).



Figure 4. Information of the identified vehicle

By clicking the "Diagnosis" type, the diagnostic device communicate with all systems present in the vehicle and reports if there are errors present (Figure5).

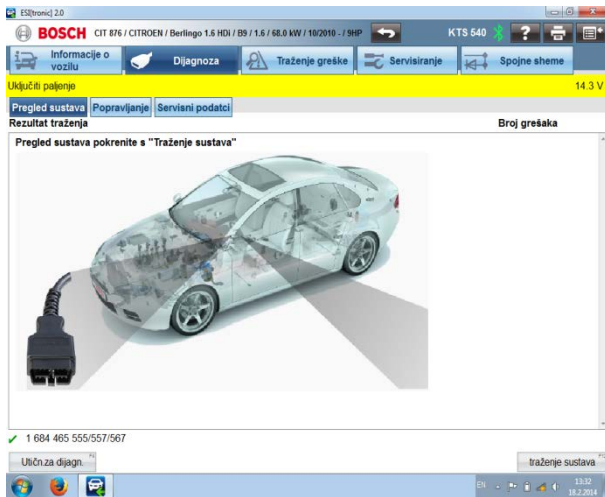


Figure 5. Search for systems that are present on the vehicle and detecting errors

If errors are identified, diagnostic device present a list of the operations that could be carried out in order to eliminate errors. Since the errors were not found on tested vehicle, it can be concluded that all systems are functioning correctly and that there are no problems in operation.

Besides identifying errors Bosch KTS 540 enables monitoring of specific operating parameters of the system to the vehicle by reading the current (actual) value, with the ability to change certain parameters if the system allows it.

The following paper presents a method of measurement and analysis of set and actual values of pressure in the common rail system, as well as the change in the amount of injection depending on the regime of engine operation.

### 3. SELECTION OF MEASUREMENT PARAMETERS

After identifying the systems that are present on the vehicle (engine management, ABS, central electronics ...), choose the option "Engine management". This option displays a submenu that offers the possibility of reading errors, erase error memory, monitoring actual values and change the settings of certain parameters (Figure 6).

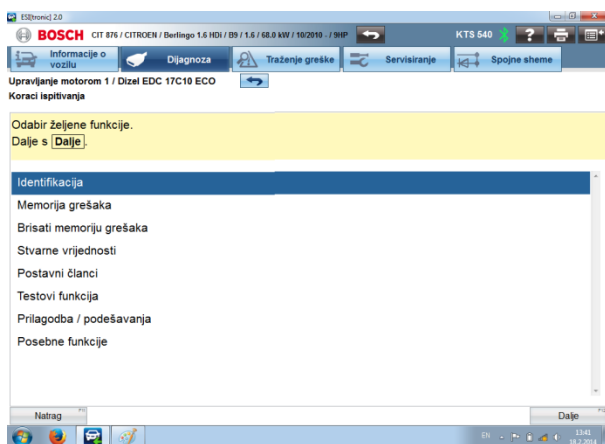


Figure 6. The operations which can be performed in the engine submenu

By entering the option " actual values " we select parameters, from a list of options, which want to monitor (Figure 7). For our measurements we were elected engine

speed, the actual pressure value in Rail, the setpoint pressure in the Rail and the total amount of injection.

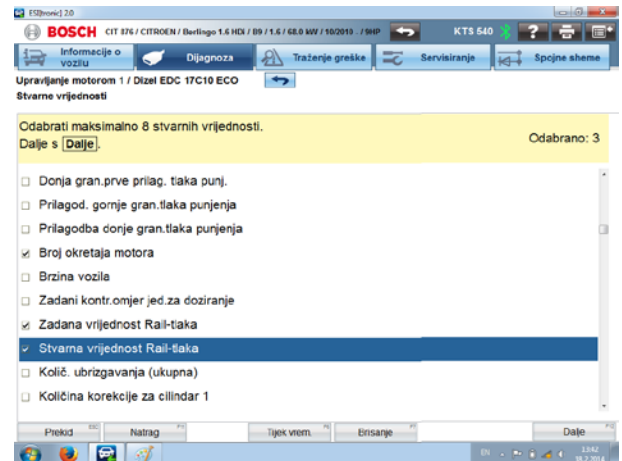


Figure 7. The parameters that can be monitored

The system offers a choice of up to 8 parameters that can be simultaneously monitored.

### 4. THE MEASUREMENT PROCESS OF PRESSURE VALUE AND THE TOTAL AMOUNT INJECTION IN COMMON RAIL SYSTEM

The measurement process consists of two parts. In the first part was performed measurement of set and actual pressure value and the total amount of fuel injection during the continuous acceleration (Figure 8), while in the second part was performed measurement of set and actual pressure value and the total amount of fuel injection during sudden acceleration (Figure 9).



Figure 8. Diagram of set and actual values of pressure in the common rail system with continuous acceleration

The figure shows that the engine in the first 2 [s] is idling which also reveals the same set and actual pressure value. Then in the next 6.5 [s] it was accelerated gradually until 4300 [rpm] where the set and actual pressure value grow continuously.

After that engine were decelerated gradually in the next 10 [s] until 700 [rpm] where the set and actual pressure value decreases evenly. It is also possible to notice that the total amount of injection uniformly changes with pressure. This completes the first part of the measurement.

After completing the first part of the measurement engine is idling 4 [s] to stabilize the system, and then came the second part of the measurements for 15 [s] with sudden engine acceleration.

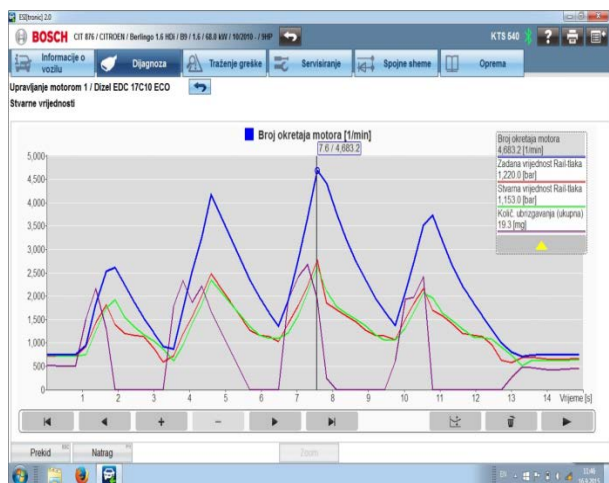


Figure 9. Diagram of set and actual values of pressure in the common rail system with sudden acceleration

During this measurement we notice sudden changes in engine speed, which resulted in the sudden change in the value of pressure in the common rail system and the overall amount of injection. This completes the second part of the measurement.

### 5. RESULTS AND DISCUSSION

One of the common errors of the vehicle is increased dressing nozzles. By checking the parameters it can be seen that the actual pressure cannot follow specify, ie. there is too much negative deviation.

After completion of the measurement, data processing was carried out separately for continuous and sudden engine acceleration to determine whether there are large deviations between actual and setpoint pressure and how it impact the change of total amount of injection.

The diagram (Figure 10) showing the relationship of changes in actual and setpoint pressure in the common rail system with a continuous change of the engine speed.

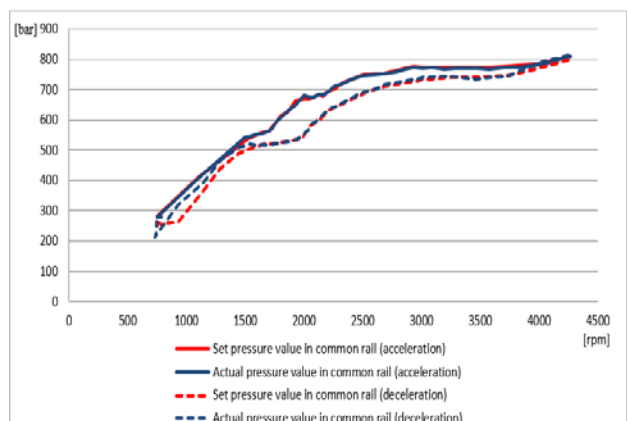


Figure 10. The change of set and actual pressure values during the continuous engine acceleration and deceleration

This clearly shows that with the gradual acceleration from 700 [rpm] to 4300 [rpm] both the set and actual pressure value have continuous growth with a nearly identical pressure values. After that the engine was

decelerated to 700 [rpm] where we also notice the continuous change of set and actual pressure values.

To determine if there is large deviations between actual and setpoint pressure we performed statistical analysis of the measurement results. In Tab. 2 is presented the correlation and determination coefficient, as well as measurement error.

Table 2. Statistical analysis of measurement results during the continuous engine acceleration and deceleration

R	0.998
R <sup>2</sup>	0.996
Mean error	0.708
Mean absolute error	6.250
Mean absolute relative error	0.015

Based on the Tab. 2 it can be seen that between the actual and the setpoint pressure is a high degree of correlation 0,998, as well as the mean absolute relative error is 0.015. This clearly shows that there are no major differences in the change of the pressure value so we can conclude that the system is correct. After the analysis of continuously engine acceleration and deceleration, follows the result presentation of the second measurement, ie. changes in the value of pressure during sudden engine acceleration and deceleration.

The Figure 11 shows a diagram of the change in the set and actual values of pressure in the common rail system with a sudden engine acceleration and deceleration while the vehicle is idling. During this measurement engine in a short period of time suddenly change speed, where can be observe more pronounced differences between actual and setpoint pressure.

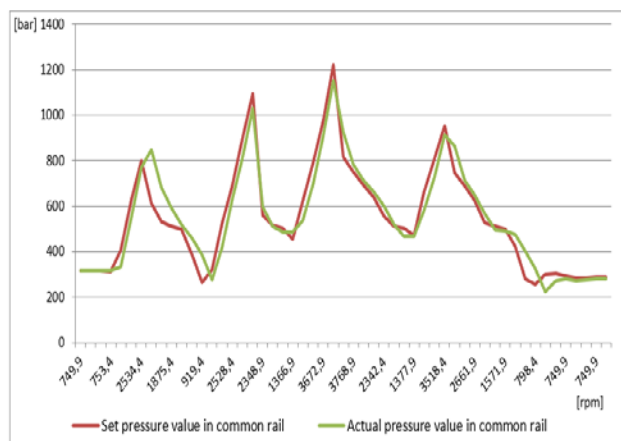


Figure 11. The change of set and actual values of pressure during sudden engine acceleration and deceleration

On the basis of the displayed diagrams it can be noted that the maximum deviation between actual and set value of pressure occurs in 2600 [rpm] where the actual pressure value is 846 [bar] and the set pressure value is 614 [bar], which is 232 [bar] more.

In Tab. 3 is presented the correlation and determination coefficient, as well as measurement error.

Table 3. Statistical analysis of measurement results during the sudden engine acceleration and deceleration

R	0.953
R <sup>2</sup>	0.908
Mean error	2.226
Mean absolute error	51.811
Mean absolute relative error	0.097

From the table it can be seen that there is a high degree of correlation of 0.953 between the set and actual pressure values as well as mean absolute relative error of the measurement is 0.097. It can therefore be concluded that the system is correct, and that the appearance of significant deviations on certain engine speeds can be attributed to the delay in the communication between ECU and PC.

After analyzing the change between set and actual values of pressure in the common rail system in further work will be shown the change of total amount of fuel injection during the continuous and sudden changes in engine speed. The aim of this measurement is to demonstrate what impact has the driving style (continuous and sudden acceleration) on fuel consumption.

In Figure 12 is shown the total amount of fuel injection during the continuous changes in engine speed.

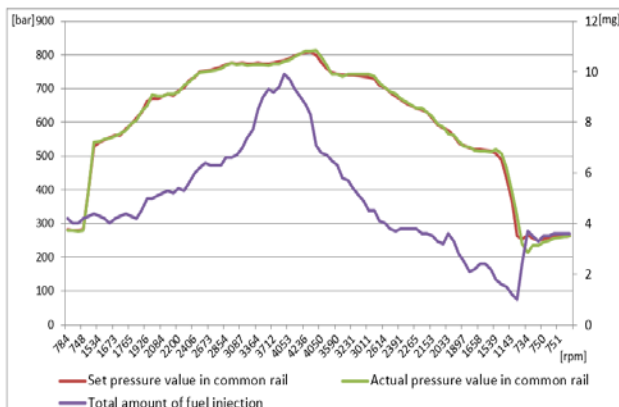


Figure 12. Change in the total amount of fuel injection during the continuous changes of engine speed

From the presented it is evident that with continuous changes of engine speed, set and actual pressure value and the total quantity of fuel injection have a continuous change, which is manifested in lower fuel consumption. During sudden changes of engine speed (Figure 13) there is large deviations between set and actual values of pressure, and therefore the larger is deviations in the total amount of fuel injection, which is manifested in higher fuel consumption.

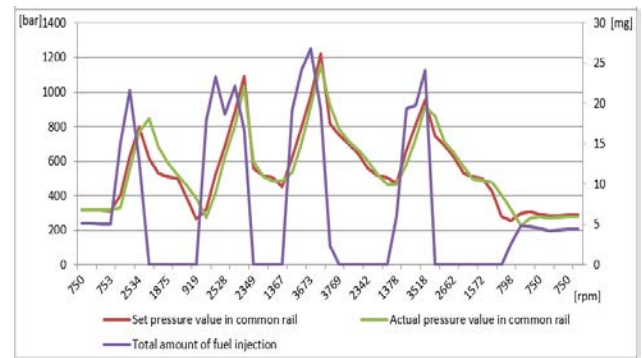


Figure 13. Change in the total amount of fuel injection during the sudden changes of engine speed.

The highest value of the total amount of fuel injection during sudden changes of engine speed is 26 [mg] at 3600 [rpm], while during the continuous changes of engine speed, at the same rpm, this value is 10 [mg].

Based on the above analysis it can be concluded that the continual changes in driving mode has a number of advantages that are reflected in lower fuel consumption, exhaust emissions and noise generated by motor vehicles.

## 6. CONCLUSION

The paper describes the process of measuring and analysis of pressure in the common rail system with continuous and sudden engine acceleration. The aim of this measurement is to show how the monitoring of actual operating parameters of a system can spot irregularities. Therefore it is possible to perform preventive maintenance or replacement of parts in order to avoid the failures. This significantly affect the extension of the life cycle of vehicles, and also significantly facilitates the work of repairers.

ECU determines the setpoint pressure under which its inject fuel into the cylinder. If the difference between the set and actual pressure values is higher the higher is the fuel consumption. From this we can conclude that during continuous engine acceleration fuel consumption is economical, while sudden engine acceleration caused uneconomical fuel consumption and therefore higher emissions (CO, NOx ...).

This demonstrates that the technique of driving have significant impact on fuel consumption. Driving with sudden acceleration reflect the deterioration in fuel economy as compared to driving with continuous acceleration that takes place at considerably more consistent speeds. This type of measurement is important from the aspect of driver training in objective of pointing at consequences of the violent ride that most reflected in fuel consumption.

## REFERENCES

- [1] Krstić, B.(2009). Technical exploitation of motor vehicles and engines, Faculty of Mechanical Engineering, Kragujevac.
- [2] Papić, V, Mijailović, R, Momčilović, V. (2007). Transport equipment and maintenance, Faculty of Transportation, Belgrade.
- [3] Klinar, I, Torović, T, Nikolić, N, Antonić, Ž. (2003). Some aspects of IC engine exploitation and maintenance system, Agricultural Engineering, Vol.8, No3. pp.36-43

- [4] Dunderski, I, Vukić, D, Matijević, D, Petrović, V. (2013). Methods for improving the teaching in the field of technical diagnostics of vehicles using computers, YU INFO 2013, Kopaonik, No.19, pp.232-236.



## Determination of Transfer Function of Photoacoustic System by Acquisition Cards with Non-synchronized Input and Output

Slobodan Todosijević<sup>1,2\*</sup>, Nenad Drvar<sup>3</sup>, Zlatan Šoškić<sup>2</sup>

<sup>1</sup>School of Electrical Engineering, University of Belgrade, Belgrade (Serbia)

<sup>2</sup>Faculty of Mechanical and Civil Engineering in Kraljevo, University of Kragujevac, Kraljevo (Serbia)

<sup>3</sup>Topomatika d.o.o, Zagreb (Croatia)

*Determination of transfer function of the photoacoustic system provides the possibility to eliminate influences of the system components with later digital signal processing. Components which influence the transfer function are microphone, photoacoustic cell, amplifier and acquisition card. The transfer functions are obtained with the use of swept sine signal as excitation and five different microphones are tested as a part of detection side. Measurements are performed in an anechoic chamber. One acquisition card was used for generation and the other for the recording of the signal. The cards were not synchronized. The paper shows five transfer functions and their analysis.*

**Keywords:** Photoacoustic measuring system, microphone frequency response, acquisition card

### 1. INTRODUCTION

When a sample is exposed to electromagnetic radiation, a part of the excitation energy is absorbed and transformed into heat. The process is called photothermal (PT) effect [1, 2]. Due to the PT effect occur various phenomena, such as infrared emission, refractive index variation, surface displacement, emission of acoustic waves and thermal waves (Figure 1).

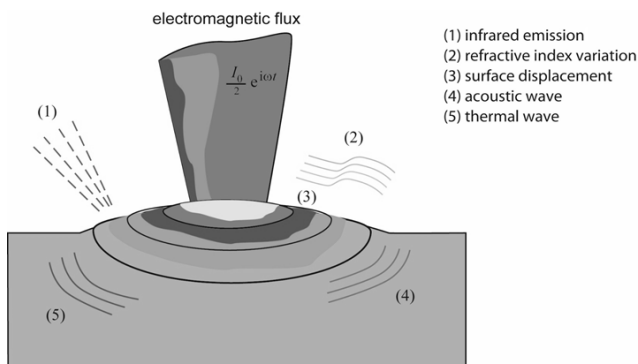


Figure 1: Phenomena occurred due to photothermal effect

The formation of the acoustic wave in the sample and in the surrounding gas due to radiation from the light source is called photoacoustic (PA) effect. Figure 2 shows sequence of the steps in PA effect, from light source excitation to acoustic wave detection. The frequency of the detected acoustic wave is equal to the frequency of modulation of the light. The PA effect is used for various material characterization techniques. One example is PA spectral analysis, where the modulation frequency is constant, but the wavelengths of the light source are varied with the aim to study the optical properties of samples [3, 4].

The PA technique that is studied in this paper is frequency PA technique [5-7]. The concept of the technique is variation of the modulation frequency, and analysis of the variations of the amplitude and the phase delay of the detected acoustic signal. Both the amplitude and the phase delay of the detected signal monotonously decrease with increase of the modulation frequency. Fitting of the experimental data to theoretical models

enables calculation of thermal parameters of samples such as thermal diffusivity, heat capacity, thermal conductivity and thermal effusivity [8-10].

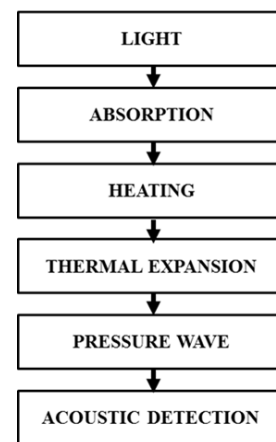


Figure 2: Generation of PA effect

The most used model for thermal characterization of materials using the frequency PA technique is Rosencwaig – Gersho PA model [11], also called the classical PA model, but there are other models that consider some additional phenomena [12-16]. A recent study of theoretical models has shown [17] that the modulation frequency range used in a frequency PA measurement should have bandwidth of least three decades in order to enable thermal characterization of thin samples with sufficient accuracy.

Figure 3 shows block – diagram with amplitude ratio and phase difference between two signals as the outputs of frequency PA measurement system. The two detected signals are outputs of the microphone and photo-detector.

The PA measurement system may be divided into excitation and detection part. The excitation part comprises the light source with modulator, and the detection part comprises the sample, PA cell, microphone, amplifier, lock-in amplifier and acquisition card. Each of the mentioned components on the detection side affects the

amplitude and phase characteristics of the PA measurement system by their frequency responses.

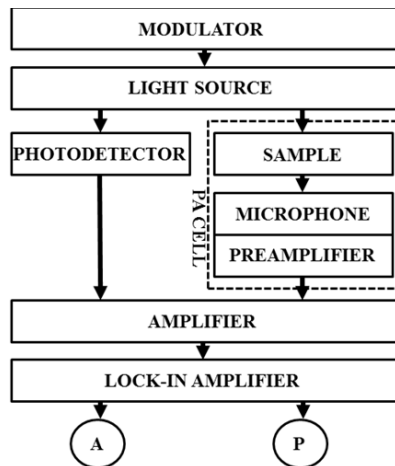


Figure 3: Scheme of PA measuring system

Measurement systems are usually applied in the bandwidths where their amplitude and phase characteristics may be considered fairly constant, but the acoustics detection systems do not have such "flat characteristics" in wide frequency ranges required for thermal characterization by PA techniques. Therefore, the knowledge of the amplitude and phase frequency characteristics of the used PA measurement system in a wide range is precondition for thermal characterization by frequency PA technique.

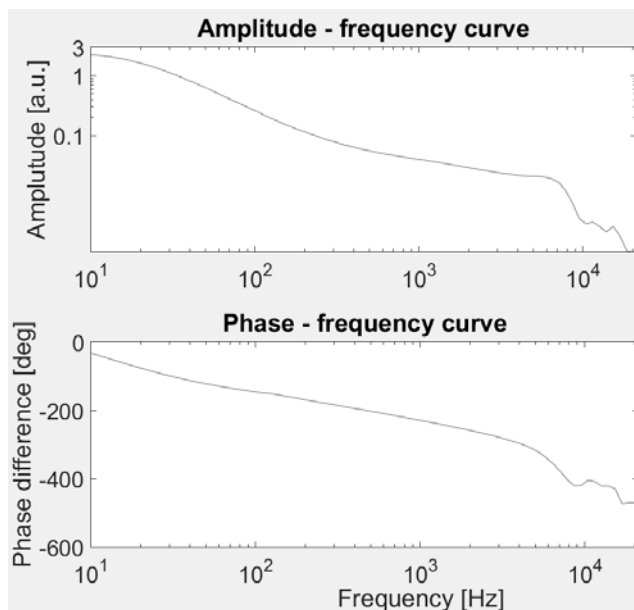


Figure 4: Amplitude and phase frequency dependence curves of the 290  $\mu\text{m}$  thick aluminium sample

During PA measurement system design, the intention is to select components that have "flat" response (without resonances) in the range of interest (audio range – 20 Hz to 20 kHz). The component that is most difficult to select is the acoustic detector, usually a microphone. Figure 4 shows the microphone influence on the amplitude-frequency characteristics obtained in frequency PA technique. An aluminum sample of 290  $\mu\text{m}$  thickness is tested, and the upper diagram shows the amplitude-frequency characteristic while the lower

diagram shows the phase-frequency characteristic. The PA response decreases monotonously, and the influence of the microphone frequency response is visible in the region above the frequency of 6 kHz.

A correction procedure may be used to calculate the PA response of the sample,

$$P_{PA}(f) = \frac{S(f)}{G(f)} \quad (1)$$

where  $P_{PA}$  represents the PA response,  $S$  is the signal obtained from the PA measurement system and  $G$  is the transfer function of the detection part of the PA measurement system.

This paper presents the results of studies of transfer characteristics of five microphones for PA measurements. The transfer functions of detection part were obtained using the sound excitation signal generated by one acquisition board and detected by another acquisition board. The non-synchronized acquisition card input and output enables more accurate determination of a transfer function than application of synchronized input and output acquisition boards [19].

## 2. EXPERIMENT

The experiments were performed at anechoic chamber of the Laboratory of Acoustics of the Faculty of Electronic Engineering of University of Niš. Inner dimensions of the chamber are 7m x 7m x 7m, and the low cut-off frequency is 50 Hz.

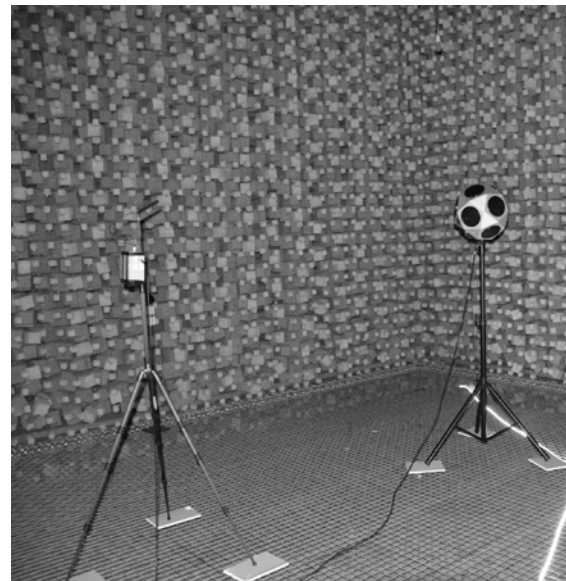


Figure 5: Experimental setup in the anechoic chamber [19] (the picture shows a sound source that was not used in the measurements, but the used sound source had the same position as the sound source in the picture)

The experimental setup is shown in Figure 5. At the left side of the picture is the stand with microphones and at the right side is the sound source. The distance between the sound source and microphone was more than 3 m, and the distances between the parts of the experimental setup and walls of the anechoic chamber were more than 1.5 m. The position of the microphone stand was the same for all the tested microphones, including the reference microphone.

The dodecahedral omnidirectional sound source, which generated the excitation sound signal, uses a commercial Sony TA-FE510R amplifier.



Figure 6: Microphones from the left to the right: 1) POM-5238L-R microphone from PROJECTS UNLIMITED and the other microphones from Kingstate Electronics Corp. 2) two KEEG1538WB-100LB and 3) two KECG2742TBL-A microphones

The microphones selected for the study are commercial electret condenser microphones. They are selected because they are commercially available, inexpensive and may be easily adjusted for the PA applications. Namely, if the dust cover is removed from the top of such a microphone, the small vent that remains may be used as a PA cell. The obtained PA cell has small dimensions, which is advantageous because of the weak power of a PA signal. Besides, due to the small dimensions, frequencies of the standing waves inside the PA cell do not belong to the audio range.

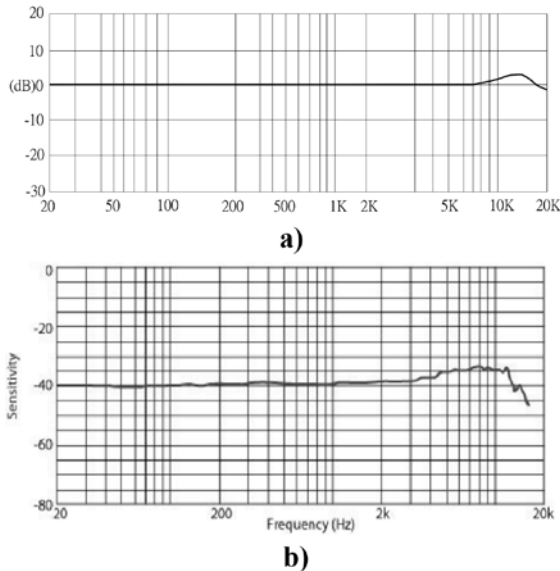


Figure 7: The microphone frequency responses for a) the microphones manufactured by Kingstate Electronics Corp. and b) POM-5238L-R microphone manufactured by PROJECTS UNLIMITED

The following microphones were used: 1) two KECG2742TBL-A microphones, manufactured by Kingstate Electronics Corp. [20], 2) two KEEG1538WB-100LB microphones manufactured also by Kingstate Electronics Corp. [21] and 3) one POM-5238L-R microphone manufactured by PROJECTS UNLIMITED [22]. Figure 6 shows the microphones, Figure 7 shows the

frequency responses of the microphones as provided by the manufacturers, while the other characteristics of the studied microphones, also as provided by the manufacturers, are shown in Table 1.

Table 1: Microphones' characteristics

Microphone	KECG274 2TBL-A	KEEG1538 WB-100LB	POM- 5238L-R
Operating voltage	2 V	2 V	2 V
Maximum supply current	0.5 mA	0.5 mA	0.5 mA
Output impedance	2.2 kΩ	2.2 kΩ	2.2 kΩ
Diameter	6 mm	4 mm	6 mm
Signal/noise	60 dB	58 dB	60 dB
Sensitivity 1kHz, 1Pa 0dB=1V/Pa	-42±3 dB	-38±3 dB	-38±3 dB

The amplifier that is used for the microphone signal amplification, located in the box on the stand visible in Figure 5, may have amplifications 2, 4.9, 7.8, 11, 19, 48, 69 and 101. Figure 8 shows schematic diagrams which represent the amplifier. In Figure 8a is shown microphone power supply, which uses voltage regulator LM78L. Figure 8b shows the operational amplifier supply that uses voltage regulators LM7805 and LM7905 for voltage supply of ± 5 V. The operational amplifier is OP07 CP and is shown in Figure 8c. The most important characteristic of the operational amplifier, which influenced the transfer function, is the bandwidth of 500 kHz. At the non-inverting input of the operational amplifier is high-pass filter with a cut-off frequency of 5.3 Hz, made by the series connection of capacitors C9 and C10 and the resistor R2. At the operational amplifier output is a high-pass filter with a cut-off frequency of 1.42 Hz, made by the parallel connection of electrolytic capacitors C11 and C12 and the resistor R12. Both of the filters do not influence the transfer function characteristic in the audio range of the microphone.

For acquisition of the recorded data were used acquisition boards National Instruments (NI) USB-6351 [23] and NI PCI-6014 [24]. Both acquisition boards have 16 bits resolution.

The reference measuring system consists of the B&K microphone Type 4188-021-A and data acquisition system B&K 3560-B driven by Time Data Recorder, a part of the Pulse software package. The system has a built-in high-pass filter with cutoff frequency at 22.4 Hz. Figure 9 shows the frequency response of the B&K reference microphone, which is "flat" in the range of 10 Hz – 10 kHz.

### 2.1. Experimental procedure

The excitation of the system was exponential sweep sine signal in frequency range 20 Hz – 22050 Hz. The stepwise increase of the amplitude of the signal (so-called fade-in) and the stepwise decrease of the amplitude of the signal at the end of signal (so-called fade-out), with the aim to avoid pre-ringing, is shown in Figure 10 [25].

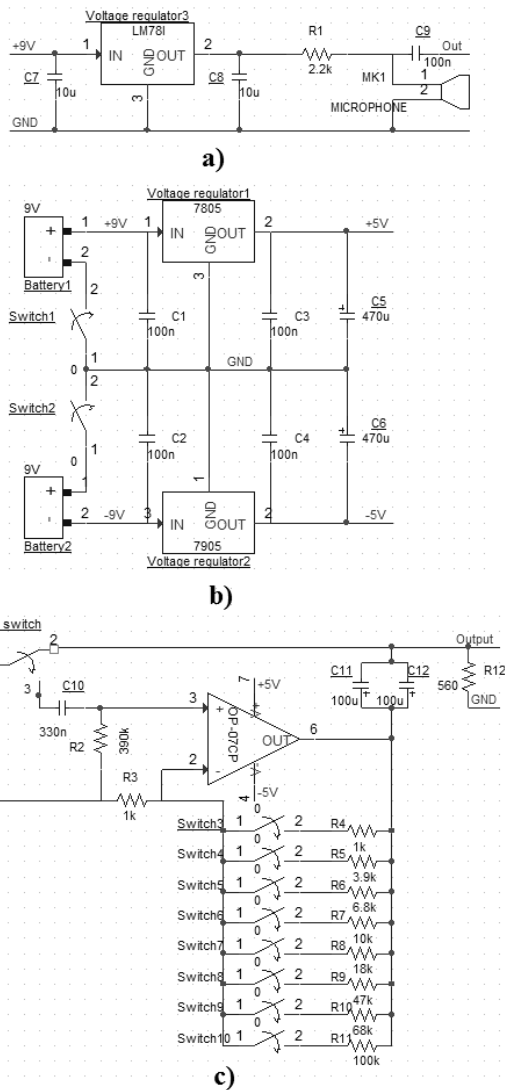


Figure 8: a) Microphone power supply, b) power supply of operational amplifier OP07 CP and c) amplifier with an operational amplifier.

The excitation consisted of the signal with duration of 16 s and a pause of 3 s. It was generated using an analogue output of NI USB – 6531 acquisition board with 65536 Hz sampling rate and the amplifier of the sound source. The acoustic signal generated by the sound source was detected using a microphone and then amplified 69 times. The same amplification was used for all measurements. The amplified signal was led to an analogue input of the NI PCI - 6014 acquisition board using also the sampling rate of 65536 Hz, and then recorded at PC as a digital signal. The clocks of acquisition cards were not synchronized.

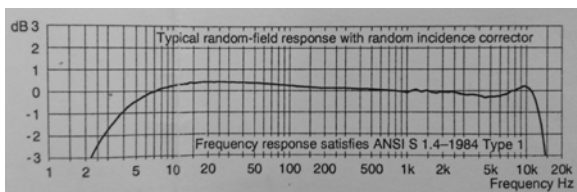


Figure 9: The frequency characteristic of microphone used in the reference measuring system.

Digital signal processing was performed using the "inverse filter of the sweep sine" signal. The inverse filter was generated as a WAV file on the PC with the sampling

rate of 65536 Hz and it also had duration of 16 s as the excitation signal. The time variation of the inverse filter signal is shown in Figure 11. If the transfer function inverse filter is denoted by  $X_s(f)$ , and the Fourier transform of the measured response is denoted by  $Y(f)$ , then the impulse response of the measurement system  $h(t)$  can be calculated as [26]:

$$H(f) = X_s(f) \cdot Y(f) \tag{2}$$

$$h(t) = \text{real}\{iFFT[H(f)]\}$$

The transfer function of the PA measurement system can be obtained as the Laplace transform of the calculated impulse response:

$$G(s) = L[h(t)] \tag{3}$$

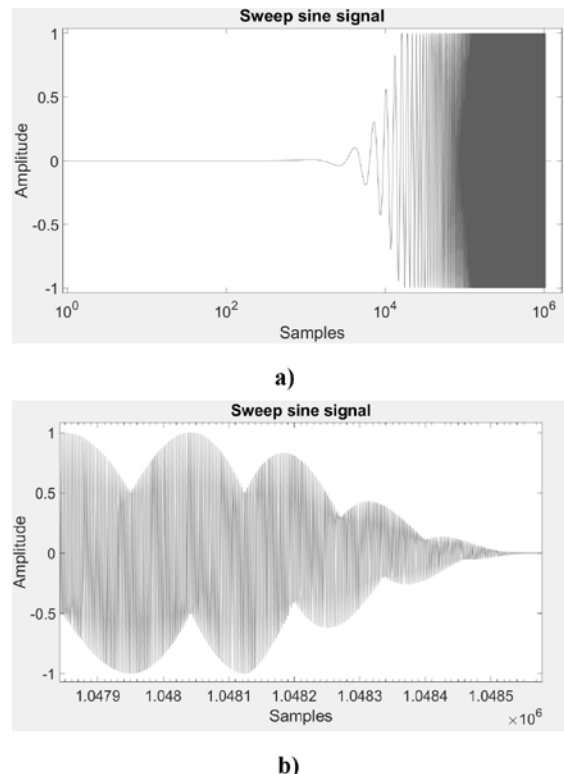


Figure 10: Sweep sine signal a) fade – in and b) fade - out (both with logarithmic x-axis representation)

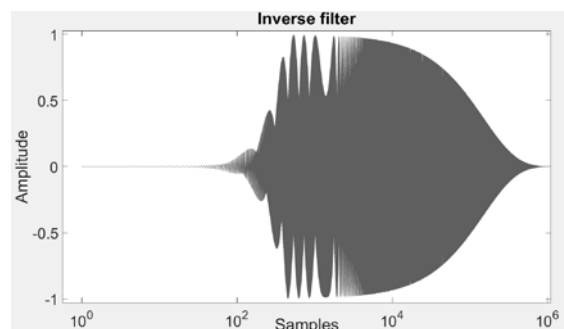


Figure 11: Inverse filter (with logarithmic x-axis representation)

Measurements for each of the tested microphones and the reference microphone were performed five times, and the obtained frequency spectra were averaged during the digital signal processing. The transfer functions of the microphones were calculated by subtracting the reference

system spectrum from the spectra of the tested microphones.

For the control of the measurements and data processing was used software package Matlab with Data Acquisition Toolbox.

### 3. RESULTS

The obtained transfer functions of the five microphones are shown in Figure 12. The amplitude characteristics consist of a slightly increasing part in the range 20 Hz - 100 Hz, a fairly flat part in the range 100 Hz - 6 kHz and the part with significant decrease in amplitude at frequencies higher than 6 kHz. The oscillatory variations may be observed at frequencies lower than 80 Hz and in the range 2 kHz – 2.6 kHz.

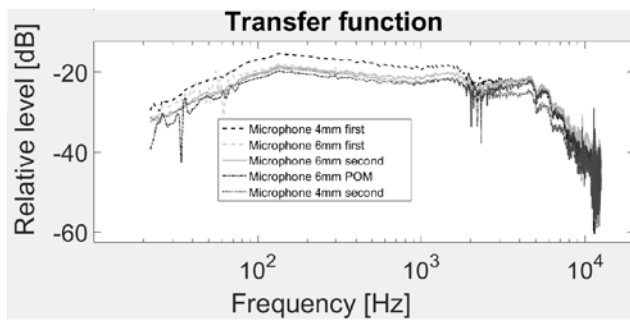


Figure 12: The transfer function characteristics of the five measured microphones

Figure 13 shows the signal recorded with the microphone KECG2742TBL-A (denoted in Figure 12 as "Microphone 6 mm first"). If the region where the signal amplitude is the weakest at the upper left picture in the Figure 13 is zoomed, the upper right picture of Figure 13 is obtained. The zoomed region corresponds to the excitation signal range where the sweep frequency is around 2 kHz. The upper right picture of Figure 13 shows four antinodes, and if the fourth antinode is further zoomed, the lower left picture of Figure 13 is obtained. The lower right picture of Figure 13 presents background noise sample during the measurements, and the dashed lines in the lower pictures represent the amplitude of background noise, and one may conclude that the amplitude of the excitation signal is comparable to noise when the excitation frequency is close to 2 kHz.

### 4. DISCUSSION AND CONCLUSION

This paper presents a continuation of research efforts presented in papers [19] and [27]. The obtained transfer functions are bent compared to those obtained in [27]. The transfer functions presented in [27] are obtained with the acquisition card with synchronized analogue input and output, which is not the case with the transfer functions presented in this paper. Non-synchronization of the NI USB – 6351 and NI PCI - 6014 acquisition boards' inputs and outputs reveals the bending of the amplitude characteristics of the transfer functions. A part of the bending may be attributed also to the differences between the A/D and D/A converters of the two acquisition boards. The amount of the contribution may be determined with synchronization of the acquisition boards, which is the topic for a future research.

The appearance of the oscillatory variations in the range 2 kHz – 2.6 kHz and below the frequency of 80 Hz

is attributed to the insufficient signal-to-noise ratio in those ranges.

The decrease of the amplitude characteristic above a frequency in the range 6 kHz – 7 kHz occurs due to limitations of the amplifier. The used operational amplifier had 500 kHz bandwidth and the gain used in measurements was 69, which means that a cut-off frequency close to 7.25 kHz should be expected.

With the exception of the oscillatory variations in the range 2 kHz – 2.6 kHz, the determined transfer function of the microphones should be considered reliable in the range 80 Hz – 6 kHz.

For the determination of reliable transfer function's characteristics in a wider range, some additional measurements need to be performed. First, the amplifier has to use an operational amplifier with wider frequency bandwidth. It is in the plan to use NE5532 or TL071/72 operational amplifiers. Further, a sound source with "flat" characteristic in the region of 2 kHz – 2.6 kHz could be used to avoid insufficient signal to noise ratio, or amplification of a sound source could be set with higher sound level. Finally, synchronization of the analogue input and output needs to be performed.

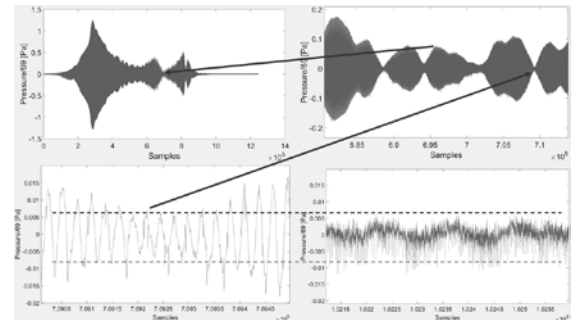


Figure 13: Amplitude of the signal measured with the microphone KECG2742TBL-A. On the upper images are shown the sound source characteristic and the region with the lowest amplitude (the region with four nodes). On the lower images is shown the comparison of the signal from the fourth node and the noise.

### ACKNOWLEDGEMENTS

The authors would like to acknowledge the support of European Commission through the project "Advanced design rules for optimal dynamic properties of additive manufacturing products – A\_MADAM", which has received funding from the European Union's Horizon 2020 research and innovation programme under the Marie Skłodowska-Curie grant agreement No 734455. The author S. Todosijević would also like to acknowledge the support of Technological Development Program of the Republic of Serbia through the grant with contract number TR37020.

### REFERENCES

- [1] H. Vargas and L. C. M. Miranda. "Photoacoustic and related photothermal techniques." *Physics Reports* 161, no. 2 (1988): 43-101.
- [2] Skvortsov Leonid. "Light-induced absorption in materials studied by photothermal methods." *Recent Patents on Engineering* 3, no. 2 (2009): 129-145.
- [3] Allan Rosenzweig. "Photoacoustic spectroscopy of solids." *Optics Communications* 7, no. 4 (1973): 305-308.

- [4] David W Ball. "Photoacoustic spectroscopy." SPECTROSCOPY-SPRINGFIELD THEN EUGENE THEN DULUTH- 21, no. 9 (2006): 14.
- [5] A. C. Tam, "Applications of photoacoustic sensing techniques." *Reviews of Modern Physics*, vol. 58, no. 2, pp. 381, 1986.
- [6] M. D Rabasovic, M. G Nikolic, M. D Dramicanin, M. Franko and D. D Markushev, "Low-cost, portable photoacoustic setup for solid samples," *Measurement Science and Technology*, vol. 20, no. 9, pp. 095902, 2009.
- [7] S. Todosijević, Z. Šoškić, Z. Stojanović and S. Galović. "Analysis of the Measurement System and Optimization of the Measurement Procedure for Detection of Thermal Memory Effects by Photoacoustic Experiments." *International Journal of Thermophysics* 38, no. 5 (2017): 72.
- [8] H. K. Park, C. P. Grigoropoulos and A. C. Tam. "Optical measurements of thermal diffusivity of a material." *International journal of thermophysics* 16, no. 4 (1995): 973-995.
- [9] Nibu A. George, C. P. G. Vallabhan V. P. N. Nampoori, A. K. George, and P. Radhakrishnan. "Use of an open photoacoustic cell for the thermal characterisation of liquid crystals." *Applied Physics B: Lasers and Optics* 73, no. 2 (2001): 145-149.
- [10] Christ Glorieux, Jan Fizez and Jan Thoen. "Photoacoustic investigation of the thermal properties of layered materials: Calculation of the forward signal and numerical inversion procedure." *Journal of applied physics* 73, no. 2 (1993): 684-690.
- [11] A. Rosencwaig, *Photoacoustics and Photoacoustic Spectroscopy*, Malabar, Florida, USA: R. E. Krieger Publishing Company, 1980.
- [12] F. Alan McDonald and Grover C. Wetsel Jr. "Generalized theory of the photoacoustic effect." *Journal of Applied Physics* 49, no. 4 (1978): 2313-2322.
- [13] F. Alan McDonald. "Photoacoustic determination of small optical absorption coefficients: extended theory." *Applied optics* 18, no. 9 (1979): 1363-1367.
- [14] Herbert S. Bennett and Richard A. Forman. "Frequency dependence of photoacoustic spectroscopy: Surface-and bulk-absorption coefficients." *Journal of Applied Physics* 48, no. 4 (1977): 1432-1436.
- [15] C. L. Cesar, H. Vargas, J. A. Meyer and L. C. M. Miranda. "Photoacoustic effect in solids." *Physical Review Letters* 42, no. 23 (1979): 1570.
- [16] R. S. Quimby and W. M. Yen. "Photoacoustic theory including energy migration." *Journal of Applied Physics* 51, no. 9 (1980): 4985-4989.
- [17] Zlatan Šoškić, Snežana Ćirić-Kostić and Slobodanka Galović. "An extension to the methodology for characterization of thermal properties of thin solid samples by photoacoustic techniques." *International Journal of Thermal Sciences* 109 (2016): 217-230.
- [18] P. R. Barja, A. M. Mansanares and PLCA ALVES. "Photosynthesis induction in eucalyptus urograndis seedlings and cuttings measured by open photoacoustics." In *Analytical Sciences/Supplements Proceedings of 11th International Conference of Photoacoustic and Photothermal Phenomena*, pp. s555-s558. The Japan Society for Analytical Chemistry, 2002.
- [19] S. Todosijević, D. Ćirić, B. Radičević and Z. Šoškić. "Experimental characterization of a photo-acoustic measurement system", *Proceedings of 25th International Conference "Noise and Vibration"*, Tara pp. 23-26, 2016.
- [20] <http://store.comet.rs/CatalogueFarnell/Product/494293/>
- [21] <http://store.comet.rs/CatalogueFarnell/Product/1403956/>
- [22] <http://store.comet.rs/CatalogueFarnell/Product/1015601/>
- [23] <http://www.ni.com/en-rs/support/model.usb-6351.html>
- [24] <http://sine.ni.com/nips/cds/view/p/lang/en/nid/11442>
- [25] Angelo Farina. "Advancements in impulse response measurements by sine sweeps." In *Audio Engineering Society Convention 122*. Audio Engineering Society, 2007.
- [26] S. Müller, " Measuring transfer-functions and impulse responses, " in Finn Jacobsen (Ed), Part I: Acoustic Signals and Systems, in D. Havelock, S. Kuwano, M. Vorländer (Eds.), *Handbook of Signal Processing in Acoustics*, Volume 1, New York, USA: Springer Science, 2008, pp. 65–86.
- [27] Slobodan Todosijević, Dejan Ćirić and Branko Radičević. "Analysis of Experimentally Determined Transfer Function of Photoacoustic System Detection Part", *Proceedings of 4th IcETran*, Kladovo, Serbia, June 5 – 8, 2017, TO BE PUBLISHED.

# Prototype System for Gas Tanks Cleaning

Zoran Petrović<sup>1\*</sup>, Uglješa Bugarić<sup>2</sup>, Dušan Petrović<sup>2</sup>, Mirosljub Babić<sup>3</sup>

<sup>1</sup>Tecon Sistem d.o.o, Belgrade (Serbia)

<sup>2</sup>Faculty of Mechanical Engineering/Department of Industrial engineering, University of Belgrade, Belgrade (Serbia)

<sup>3</sup>Makpetrol d.o.o, Belgrade (Serbia)

**Keywords:** Conveyor, Gas tank cleaning, Siner's circle of wash

## 1. INTRODUCTION

Contemporary usage of LPG in Serbia and Macedonia, in the house holds, or in process of food preparation, in food industry is mainly focused on usage of the gas in the steel tanks. Capacity of the tanks that are most common in use are: 2 kg, 3 kg, 5 kg and 10 kg. Gas tanks with capacity of 2 and 3 kg are usually used for mobile applications (usually for camping, outdoor food preparation, etc.), while 5 and 10 kg gas tanks are usually used in households and food preparation in food industry sector.

Refilling of the gas tanks is one of the main business activities in gas sales process.

Information provided by investor is that 90% of the refilling is covering gas tanks weighted 5 kg and 10 kgs. One of the main problems in refilling of the gas tanks is that they are in time covered by dust, or organic and/or nonorganic dirt which is causing two main problems.

First one is covering safety issues, since residual dust and dirt on gas tanks can, in contact with elements of conveying system, cause sparks, which can then cause explosion, since environment in the filling facility is considered as potentially very explosive.

Second problem is with retention of the gas tanks, since customers are avoiding to buy dirty tanks and they are staying in the warehouse for indefinite time, making additional cost for keeping them on stock.

In order to solve this problem, prototype of conveyor which is driving gas tanks through washing and drying modules is made.

Gas tanks washing process has two main aspects that were considered.

First one is referring to quality of the wash, which depends on the Siner's circle. [1]

Second problem was the design of conveyer which was conveying gas tanks through washing and drying modules.

## 2. SINERS CIRCLE OF WASH

For quality wash there are 4 interconnecting factors, known as „Siner Circle“ – simple formula for cleaning cycle of any cleaning operation (Figure 1).

### 2.1. Mechanical action

First factor is mechanical action, which is removing dirt by application of mechanical force. Mechanical force that can be used in washing cycle has its limit, since excessive use of the force can produce damage to the washed surface as result of excessive wear and potentially

explosion since system is working in hazardous environment.

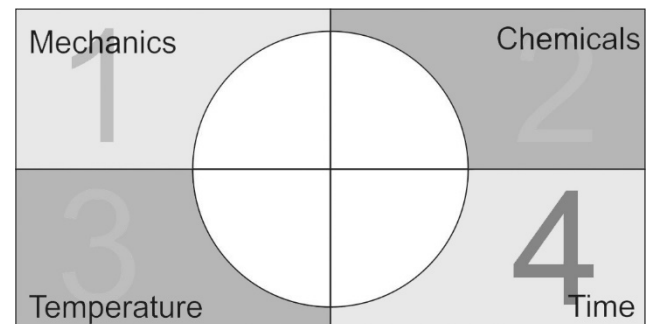


Figure 1: Siner's Circle of wash

### 2.2. Chemical action

Chemical action is defined as usage of cleaning agents in the cleaning cycle. Choice of right cleaning agent is essential for wash quality, along with economics of washing process. Use of chemical agent with optimal dosage of chemicals is only way to obtain optimum results without damaging surfaces, or influencing environmental pollution.

### 2.3. Temperature

Depending of the type of washing circle, temperature has different influence. For any kind of wash in which surfaces are covered with grease or oil, washing temperatures have significant influence. Like with all other cleaning factors, excessive usage of high temperatures can damage washing surface and also damage equipment.

### 2.4. Time

Time is one of the crucial factors, since longer washing cycles are giving better results. Washing time depends on the surface type to be cleaned, the dirt which has built-up and the chemical agents used.

## 3. DESIGN OF THE SYSTEM

Investor demand was that complete system for gas tanks cleaning, should be added to existing gas filling line. Gas tanks that should be washed should include standard tanks net weight 10 kg and 5 kg. Capacity of the system should be 400-500 gas tanks per hour. Extension should be with the same elements as existing one in order to provide complete unification of spare parts. System should be modular and consist of 3 washing and drying modules.

3.1. First module – spraying of the chemicals

First module should provide distribution and spraying of dissolved chemical agent with hot water in order to better penetrate into the dirt on the surface of gas tanks. Chemicals should provide strong adhesion of the molecules of chemical agent to form layer on the surface of gas tanks, in order to move residual dirt on top of the layer (Figure 2). Regarding Siner's circle, in the first module, temperature of the water along with right choice of chemicals are providing optimal results in moving residual dirt above layer of chemicals.

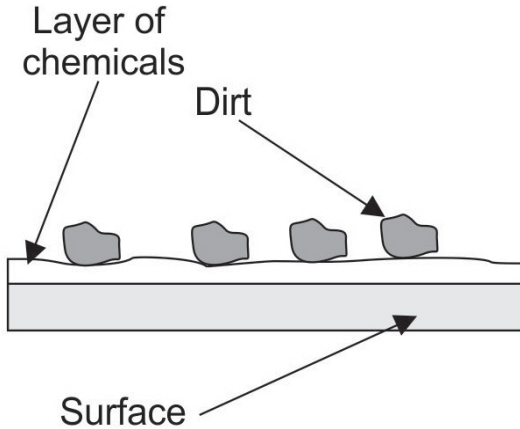


Figure 2: Chemical adhesion to the surface of gas tanks

3.2. Second module – rinsing and applying drying agent

Second module should provide rinsing of the gas tanks, with hot and cold water in order to remove chemicals along with dirt from cylinder surface.

Two systems for rinsing will be used.

First one is with hot water with temperature up to 60°C on high pressure of 150 bar in order to provide enough mechanical action to clean residual dirt.

Second one is with cold water, sprayed in low pressure up to 10 bar in order to remove residual chemicals and cool down gas tanks before conveying them to filling station.

On the exit side of the module, there is chemical drying agent spraying system. Chemical drying agent has similar role as chemicals in the washing process. Since chemical agent has the form of anion, when applied, water drops are pushed to the top of the surface layer, which makes easier to remove them with air blow system. Second role of drying agent is levelling surface of the tanks which have micro abrasions (Figure 3).

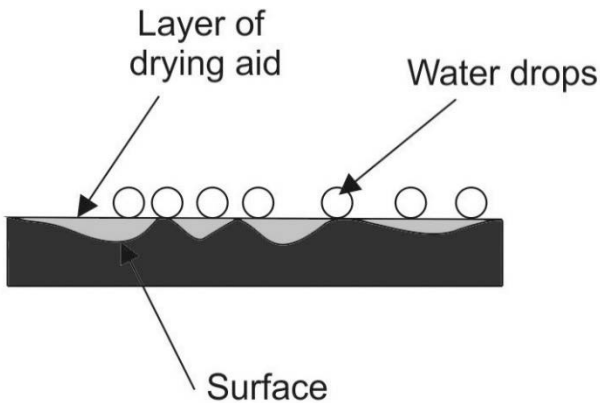


Figure 3: Chemical adhesion to the surface of gas tanks

This way air stream is flowing with less turbulences which effects quality of drying. Also, layer of drying agent resides on the surface of the gas tanks, which has the role of protective film against corrosion and protects gas tanks of excessive dirt while in usage. When gas tanks come to refilling, they are cleaned much easier then first time. Picture of drying agent moving water drops above the layer is given of Figure 4.



Figure 4: Drying agent moving water drops on top of the layer

3.3. Third module – drying of the gas tanks

Third module should provide removing of the water from gas cylinder surface with side and top air blowers. One explosion proof motor of 3 kW power and 1200m<sup>3</sup>/h of air flow is used in order to blow water drops from surface of gas cylinders.

4. CONVEYOR FOR GAS TANKS

Conveyer is designed in order to provide maximum capacity for filling up to 500 gas tanks per hour.

Speed of conveyer:

$$v_{con} = \frac{500}{60} = 8,33 \frac{m}{min} \tag{1}$$

Diameter of 10 kg tank is 300 mm, so there are 3 gas tanks in 1 meter conveyer length.

In order to provide flexible speed of conveyer, frequency regulator is chosen for regulating speed of the conveyer.

In order to provide optimum cleaning and drying results, technological parameters that must be followed are:

- minimum elapsed time from applying washing chemicals to rinsing: 1 min.
- minimum elapsed time from applying drying aid chemicals to air drying: 1 min.

When putting those two restrictive conditions together, minimal length of conveyer should be 16,66 m.

In order to follow up complete process of taking empty gas tanks from outside storage, length of conveyer must be prolonged.

With entry and connection point defined, one more technical aspect of the system was important for complete defining of the conveyer track and that is minimal radius of the curve of the conveyer.

According to information provided by chain producer, minimal radius of the curve has to be 1000 mm in order that chain doesn't stuck on the curve section.

Also, entry point of the conveyer is defined by investor in order to provide enough space on the outside storage.



Since one of the main aims of the conveyor is to connect outside storage with existing conveyor, length after last, third module (drying) is enlarged in order to provide connection for existing conveyor.

Disposition of the complete conveyor is given on the Figure 5.

#### 4.1. Calculation of chain tension force

Calculation of chain tension force (empty conveyor)

[2]:

$$F_o = 1,05 \cdot [F_{min} + g \cdot (\omega \cdot q_M \cdot L_h^{RO} + 2\omega q_{tr} L_h \pm q_M \cdot H) + W_o + W_{PL}] = 12275 \text{ N} \quad (2)$$

Calculation of chain tension force:

$$F_o^e = 1,05 \cdot [F_{min} + g \cdot (2\omega q_{tr} L_h \pm q_M \cdot H) + W_o + W_{PL}] = 6521,7 \text{ N} \quad (3)$$

$\omega$  – friction coefficient of chain,  $\omega = 0,55$ . Coefficient is increased 50% from one stated in the table (0,3-0,35), since conveyor is working on outside temperatures with possibility of frost in the driving channel of conveyor.

$q_M$  – weight of the transported material,  $q_M = 42 \text{ kg/m}$

$L_h^{RO}$  - length of horizontal projection of pulling section of chain conveyor,  $L_h^{RO} = 38 \text{ m}$

$q_{tr}$  - weight of driving mechanism of conveyor (weight of the chain),  $q_{tr} = 16 \text{ kg/m}$

$L_h$  - length of horizontal projection of conveyor,  $L_h = 38 \text{ m}$

H – lifting height of conveyor

$W_o$  - friction force on the side of driving conveyor channel,  
 $W_o = 10^{-3} \cdot \mu h^2 \rho g l_b \quad (4)$

$W_o = 0$ , gas tanks are not touching side channels

$\mu = 0,5-0,8$  – friction coefficient cast iron on steel

$W_{PL} = 0$  - friction force of plowing mechanism on the conveyor end.

Minimal driving force is calculated: as [3]:

$$F_{min} = 6000B + 40L = 6000 \cdot 0,086 + 40 \cdot 38 = 2036 \text{ N} \quad (5)$$

B – width of driving plate surface, or in this case double width of the chain

L – length of the conveyor,  $L = 38 \text{ m}$

$$B = 2 \cdot 0,043 = 0,086 \text{ m} \quad (6)$$

Maximal number of gas tanks on the conveyor: 126 tanks.

Weight of the empty gas tank = 12,7 kg

Total weight on the conveyor

$$q_M = \frac{126 \cdot 12,7}{38} = 42,11 \frac{\text{kg}}{\text{m}} \quad (7)$$

Needed power on the shaft of chain sprocket:

$$P_o = \frac{F_o \cdot v}{10^3 \eta_v} = \frac{11705 \cdot \frac{8,33}{60}}{10^3 \cdot 0,95} = 1,71 \text{ kW} \quad (8)$$

$\eta_v$  – coefficient of efficiency on sprocket shaft.

Power of electro motor (minimal):

$$P_o = \frac{P_o}{\eta_{meh}} = \frac{1,71}{0,94} = 1,82 \text{ kW} \quad (9)$$

$\eta_{meh}$  - coefficient of efficiency of gearbox.

Torque on the chain sprocket (empty conveyor):

$$T^e = \frac{D}{2} \cdot F_o^e = 978,25 \text{ Nm} \quad (10)$$

Where diameter of the sprocket is:

$D = 300 \text{ mm}$

Motor chosen for this application has following characteristics: Nominal power: 3 kW Emerson, gearbox with transmission ratio  $i=103$ , with nominal torque  $M=1900 \text{ Nm}$ .

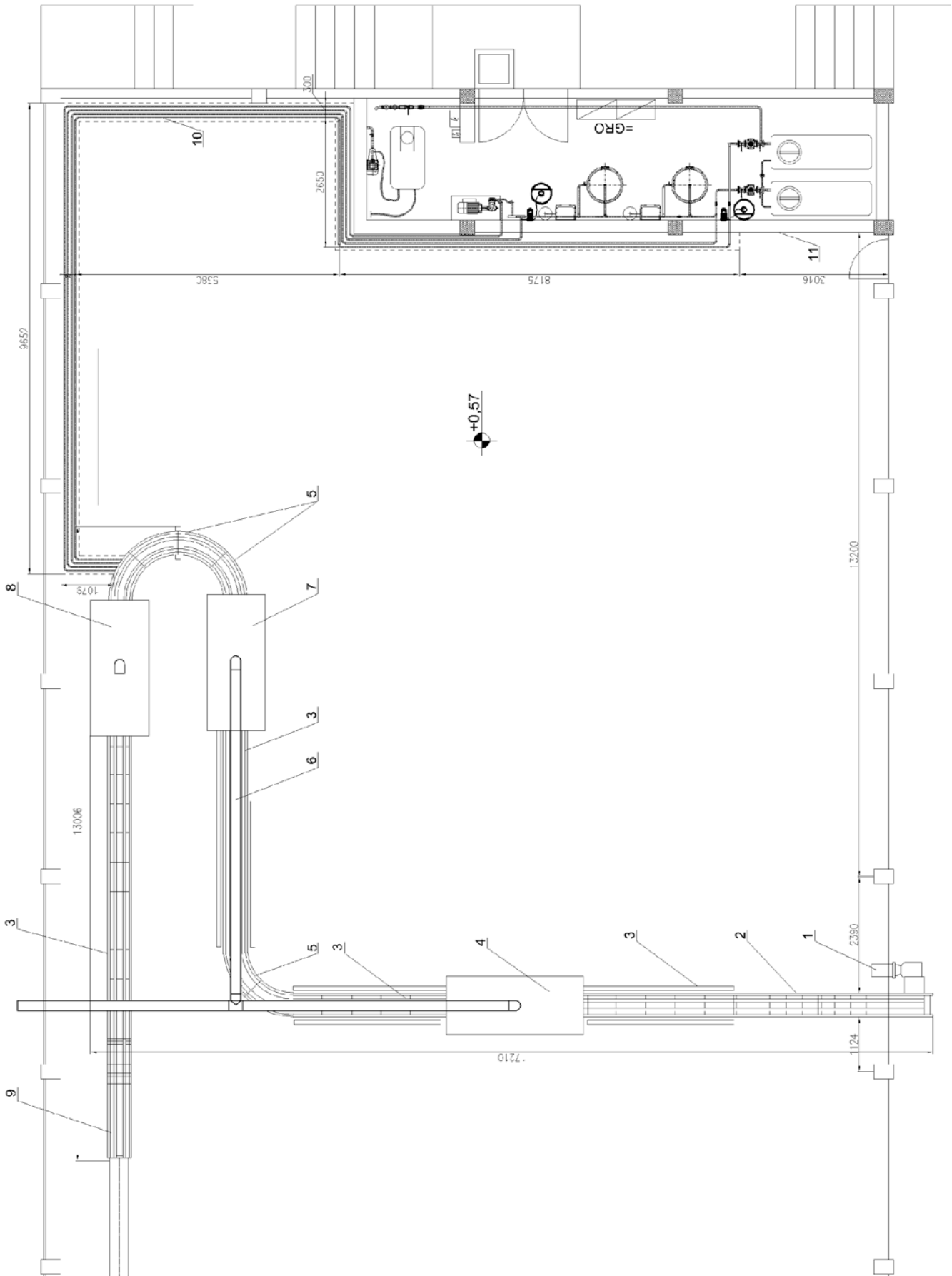


Figure 5: Disposition of the system in the hall

Elements of the system (Figure 5):

1. Motor for conveyor
2. Input conveyor module
3. Standard conveyor module
4. Module for chemical spraying
5. Curved module
6. Adjustment module
7. Module for rinsing and drying aid spraying
8. Module for drying
9. Connecting module
10. Channel for connection hoses
11. Technical room for equipment

Connection of the motor and sprocket can be seen on the Figure 6.



Figure 6: Connection of the motor and sprocket

Calculated torque was verified during the testing phase, with empty conveyer. Since motor of the conveyer is connected to the frequency inverter, torque can be read in real time on the display as percentage of the motor maximum torque.

Measured torque was going from the 67% at the start of the motor, to 49,99% in nominal working regime (Figure 7).



Figure 7: Generated torque on the motor

Calculated relation between torque on chain sprocket on empty conveyer and maximum torque can be measured by frequency inverter:

$$e = \frac{T^e}{T_{mot}^{max}} = \frac{978,25}{1900} = 0,51 \quad (11)$$

## 5. CONCLUSION

Prototype design is always heavy task, specially when it includes different research fields.

In this case, first field that was explored was filed of industrial cleaning.

This field, from methodology point of view in in lack of published articles for different industrial applications. For that reason, general approach, which is given through Siner's circle was used. This approach doesn't give quantitative analyses for washing quality, it rather gives recommendations of most important factors for satisfying cleaning results.

Relation between Mechanical work, Chemicals – agents and consumptions, Temperature of wash and Time elapsed for washing are giving optimal washing results. For mentioned application, some factors were limited due to the technical, , safety, and/or environmental issues.

Mechanical force used in this application was focused on the water flow and pressure through nozzles in order to follow restriction on usage of friction in hazardous areas.

Chemical action was limited on usage and dosage of the chemicals used in the washing process.

Temperature used is limited to the maximum operating temperature of the both centrifugal and piston pumps. For centrifugal pumps this temperature is rather low, while temperatures on the high pressure piston pumps can go up to 60°C.

Last factor – time is also limited by defined capacity of the system. Since demanded capacity of the conveyer was 500 gas tanks/hour, speed of the conveyer is at least 8,33 m/min. This means that gas tanks must have satisfactory cleaning results conveying through the system with mentioned speed.

With all mentioned restrictions, mechanical force is limited to pressure wash, temperature with maximum temperature that equipment can bare, time with demanding capacity, only type of chemicals and dosage can be changed in the cleaning process. This leads to much more simple choice in the design of the system, having really only one variable.

All mentioned above and washing technology, determined design of the washing system with 3 modules, which includes: module for chemical spraying, module for rinsing of chemicals along with residual dirt and drying module.

Calculation of the conveyor was based on some assumptions for the straight line conveyor with some coefficient enlarged. Calculation was made based on the assumption that system is working on outside temperatures, with high friction coefficient. After measuring torque on the frequency inverter results were very close to calculated ones.

Obviously, high friction coefficients for the low temperatures of the surrounding in which conveyer is working, covered fraction of the curved elements of the conveyor, but this can be the problem for complex conveyor paths, with curves. In order to closer describe mentioned problem, further research will be done. There are some papers on this subject written by Sumpf, Bankwitz and Nendel and Rasch [4], but they covered only special plastic multiflex chains in their work.

Further research of the authors will be in this field, in order to get more accurate calculation of the reaction forces of complex conveyors.

#### REFERENCES

- [1] H. Sinner „Über das Waschen mit Haushaltwaschmaschinen“, Haus&Heim, Verlag, (1960)
- [2] S.B. Tošić „Transportni uređaji, mehanizacija transporta“, Mašinski fakultet, Beograd, (1989)
- [3] A.A. Вайнсон А.А. “Подъемно-транспортное оборудование в легкой промышленности”, Легпромбытиздат, Москва, (1985)
- [4] J. Sumpf J, H. Bankwitz , K. Nendel, K, Rasch “Novel calculation method for chain conveyor systems”. Logistics Journal, Vol. 2014,p 1-12,(2014)

**SESSION G**

**CIVIL ENGINEERING AND MATERIALS**



# Machine for Impact Testing of Plastic Pipes - IMPACT 2000 Design, Development and Prototyping

Ivan Milićević<sup>1\*</sup>, Miloš Božić<sup>1</sup>, Vojislav Vujičić<sup>1</sup>, Radomir Slavković<sup>1</sup>, Zvonimir Jugović<sup>1</sup>  
<sup>1</sup>Faculty of Technical Science, University of Kragujevac, Čačak (Serbia)

*At the Faculty of Technical Sciences in Čačak, in 2016 was realized a machine prototype for impact testing of plastic pipes "Impact 2000", the project of direct cooperation with industry. It is a complex mechatronic system for testing of plastic pipes with impact of falling weight, according to the requirements defined by the standards SRPS EN 744: 2008 and EN 1411: 2008 standard.*

*This paper presents the implementation of an integrated approach to the design of complex technical systems, from conceptual design to industrial prototype. Based on the set technical requirements we made a necessary analysis, the analytical and experimental, and we made synthesis of the relevant data to make the system best. Were carried out some experimental measurements, as a verification of the obtained analytical results. Modeling, simulating and analyzing, are defined by the particular parameters of the process and the particular solutions for the individual segments of the system. We solved a number of practical problems and realized an industrial prototype. In this paper, it's provided an overview of representing solutions on the world market. Based on a comparison of our machine with machines of renowned manufacturers, in terms of technical characteristics and economic aspects, as well as experience obtained from users after nine months of exploitation in production, results and conclusions of an appropriate were summarized.*

**Keywords:** Impact tester, falling weight, plastic pipe

## 1. INTRODUCTION

Machine for impact plastic pipe testing is designed for continuous quality control immediately after the production process.

There is a huge range of these machines in the world, but there is not such a machine that is made in Serbia. These machines can be manual and semi-automatic.

In manual machines test procedure is performed using human power of workers and these machines are very difficult to use because it may be necessary to lift the weight up to 16kg at a height of two meters.

With most semi-automatic machines lifting of weight at given height is made automatically, thus the physical effort of workers is reduced to minimum. Worker just have to put the particular weights on machine. Placing the sample pipe in position for testing in some machines are done manually, while the more expensive solution is performed automatically, using a motor drive.

These machines have generally similar work, but the essential difference is reflected in the type of drive that is used to lift weight (electric or pneumatic drive). Also the big difference is in the human-machine interaction.

An example of a machine that has a pneumatic lift system is a machine of American manufacturer Qualitest, Model 300C (Figure 1).

The machines that use an electric motor for lifting weight up are presented, as an example. Model no.1713 (Figure 2) company IPT (Germany), Universal Falling Weight Impact Tester company Ray-Ran (Great Britain) DIT302 company Vance (China), GT-7037-DA company GOTECH (Taiwan), etc.

One of the best (and the most expensive) machine that can be found on the market, with probably the best user interface (Figure 3b) is Model B50 Danish manufacturer SCITEQ (Figure 3a). It has a pneumatic lift system (also-called Vacuum method).



Figure 1: Qualitest Falling Weight Impact Tester Model300C [1]



Figure 2: IPT Falling Weight Impact Tester Model no.1713 [2]



Figure 3: a) SCITEQ B50 Impact Tester; b) Interface of B50 [3]

## 2. DEFINING THE PROJECT TASK

### 2.1. Technical requirements

Basic technical requirements that each device for impact testing of plastic pipes must meet are defined in standards:

- SRPS EN 744: 2008 (identical to European standard EN 744: 2008: 1996) - Plastics piping and ducting systems - Thermoplastics pipes - Test method for resistance to external blows by the round-the-clock method. [4]

- SRPS EN 1411: 2008 (identical to European standard EN 1411: 1996) - Plastics piping and ducting systems - Thermoplastics pipes - Determination of resistance to external blows by the staircase method. [5]

These standards define the basic structure of testing machines, with its basic elements (Figure 4).

According to these standards, operator takes from the production line a prescribed number of samples of the pipe length  $200 \pm 10$  mm. Prepared in this way samples were placed on a stable steel base (i.e. V-block, Figure 4E). Then weight that has defined mass and shape is free falling from the prescribed height. (Figure 5). That weight strikes the pipe sample placed in the V-block with its head. At the moment of impact, speed must be at least 95% of the theoretical speed of free fall.

According to EN 744 (round-the-clock method) weight is always released from a height of 2 m. Standards prescribed number of shots, depending on the diameter of the test pipes. After each impact, pipe must be rotated for a certain angle, which is equal to  $360^\circ/n$ , where  $n$  - is the prescribed number of strikes. Masses of weight, depending on the diameter of the pipe, ranging from 0.25-3,2 kg. The shape of weight head can be of type d25 and d90 type (Figure 5).

According to EN 1411 (Staircase Method) each sample is stroke only once, with a weight significantly

greater than the weight of the round-the-clock methods (up to 12.5 kg depending on the diameter and the tube material). The height from which the weight is free falling is in the range of 0.5-2 m. The shape of the weight head can be of type d25 and d90 type (Figure 5).

For most plastic materials used in the manufacture of pipes, the samples that are going to be tested must be previously cooled to a temperature  $0^\circ\text{C}$  (for round-the-clock method) or  $-10^\circ\text{C}$  (for Staircase method). Therefore, the standards defined the maximum duration of the test. For *Staircase method*, the time that elapses from the moment of taking the sample from the cooling chamber to the impact of weight, should not exceed 10s. For *round-the-clock method*, the maximum time duration of the test depends on the diameter of the tube, is defined by the standard EN 744, and depending on the nominal diameter of the pipe ( $D_n$ ) is: 10 s for  $D_n \leq 110$  mm; 30 s for  $110 < D_n \leq 200$  mm; 60 s for  $D_n > 200$  mm.

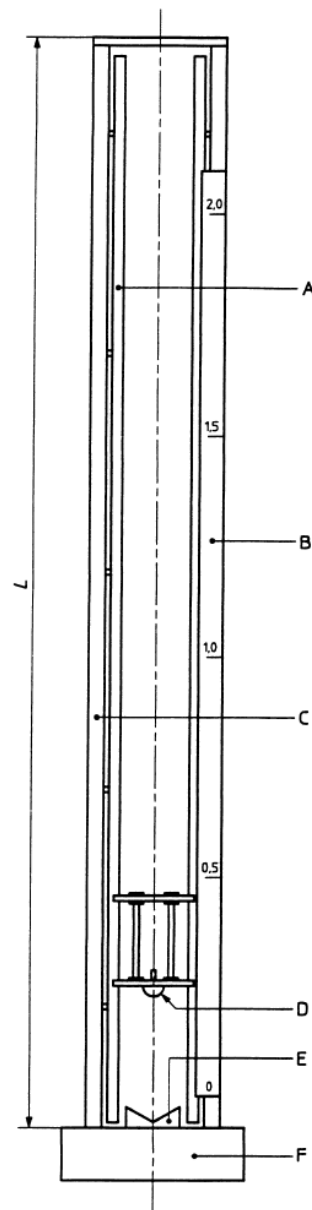


Figure 4: Typical impact testing machine  
A - Guide; B - Graduated scale, vertically adjustable for different sizes of pipe; C - Main frame; D - Striker; E - Steel block  $120^\circ$ , V-shaped; F - Solid base; L - Sufficient to give a clear height from striker to pipe of at least 2 m.



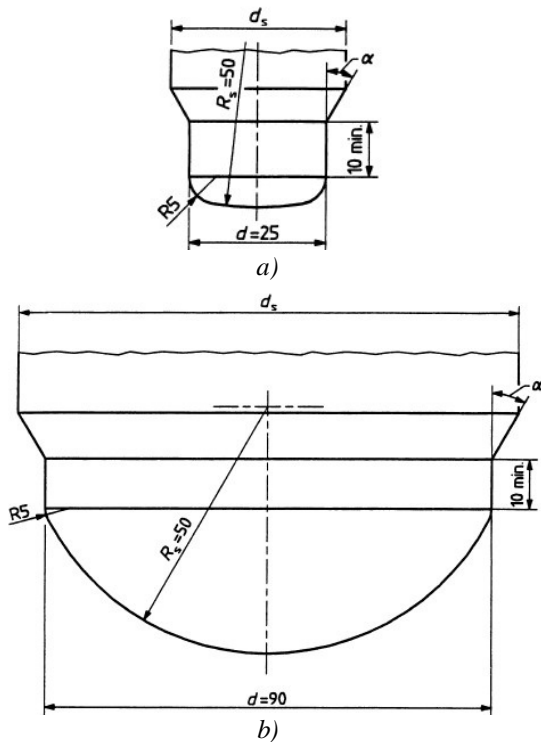


Figure 4: Dimensions of strikers, two basic types  
a) Type d25; b) Type d90

2.2. Conceptual solution making

Based on technical requirements and analysis of available information on existing technical solutions adopted methodology for designing is in accordance to the algorithm shown in Figure 6.



Figure 6: The methodology conceiving conceptual design

According to the adopted methodology parameters of the process was defined. Also, functions which are necessary for the execution of tasks was defined. Partial functions are divided into three phases, according to the manner of execution.

**Phase I - realized by the operator:**

- Placing the pipe samples on the V block;
- Selection of a standard, from database, which will be used for testing;
- Set up the required weight.

**Phase II – realized by machine:**

- Positioning the sample in position for testing;
- Positioning of weight in height for testing;
- Releasing the weight;

**Phase III - realized by the operator:**

- Checking sample condition and proceed or stop testing;
- Removal of a sample.

Define possible modes of realization of the individual partial functions, i.e. performed the formation of variation solutions. Based on the technical requirements the necessary analysis, analytical and experimental and

synthesis of the relevant information, the best structure was defined.

Table 1: Variant solutions and selection of optimal variant

Function	Possible types of realization		
	1	2	3
Sample support	V-block	Flat steel block	
Wight catching	Gripper system	Electro-magnet	
Sample platform movement	Trapezoidal screws and nuts	Rack and pinion	Lead screw with ballnut
Weight movement	Pipe limiters	Linear rail shaft	Profiled guide rails
Wight catcher movement	Cylindrical guides and slider	Profiled guide rail and slider	
Platform movement drive	AC motor	DC motor	Servo motor
Weight catcher movement drive	AC motor	DC motor	Servo motor
Platform transmission system	Gear transmission	Timing belts transmission	Chain transmission
Weight catcher transmission system	Gear transmission	Timing belts transmission	Chain transmission
Control unit	Relays	Microcontroller	PLC
Supporting structure	Rigid	Modular	

3. STRUCTURAL ELABORATION

This phase of the design process refers to the concretization of the concept of variant solutions adopted. It comes down to finding the most appropriate structural solutions, based on the information specified in the list of demands. This leads to the main dimensions of the machine, according to which can be made a general conceptual design of machines, for several parallel versions. This is followed by elaboration of each variant, the performance of calculations and kinematic analysis of movement necessary for the realization of the testing cycle. Modeling, simulating and analyzing, are defined by the particular parameters of the process and the optimal solutions for the individual segments of the system was determined. For building the 3D model, simulation of movements and for the structural analysis (FEM) software package SolidWorks was used. When testing virtual models [6-9] yielded satisfactory results, the technical solution was finally adopted, the technical documentation was made - drawings of individual elements, sub-assemblies and assemblies.

3.1. Experimental testing

For testing of critical demands the laboratory setup was made (Figure 7). On this setup, velocity and acceleration during the free fall of trolley along guides was measured. This setup provides experimentally confirmation the speed at the moment of impact is larger of 95% of the theoretical velocity of free fall given in standard. The procedure consisted of measuring the time

required for the weight travel a predefined path - in this case path of 2 m. The sensor system is composed of a permanent magnet attached to the moving trolley and stationary Hall sensor.

Detecting the position of the weight is done by two sensors based on the Hall-effect, installed at the end positions at a distance equal to the length of 2 m, i.e. the path that the weight needs to move. The primary output parameter is the time of the fall of the weight. Sensors detect the effect of a permanent magnet mounted on the weight that are moving down the cylindrical guides. Accurate measurement of time is performed using a digital oscilloscope (Fig. 8). Processing of the results, i.e. calculation of acceleration and speed of the weight on the basis of the measured time is described in detail in [10].

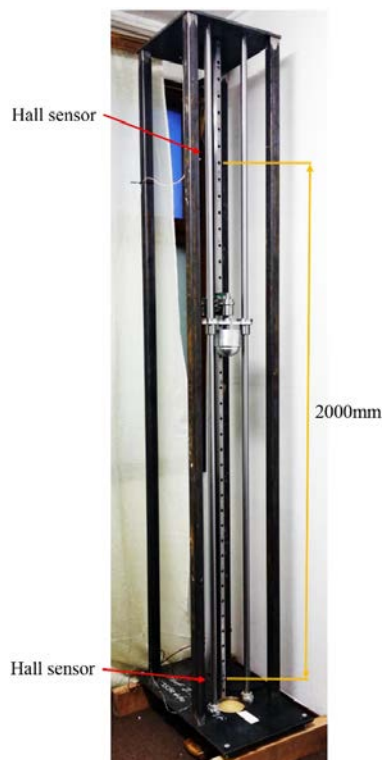


Figure 7: Laboratory setup for pipe impact testing

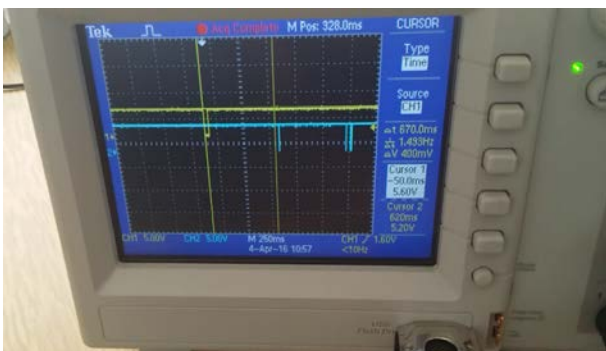


Figure 8: Speed of free fall measurement on a digital oscilloscope

On the same laboratory setup, numerous experiments and testing the control and measuring system, were also carried out. After analyzing the results and drawing conclusions the creation of the machine began.

## 4. DESCRIPTION OF REALIZED TECHNICAL SOLUTION

### 4.1. Construction

The final appearance of the 3D model of the adopted technical solution is shown in Figure 9.

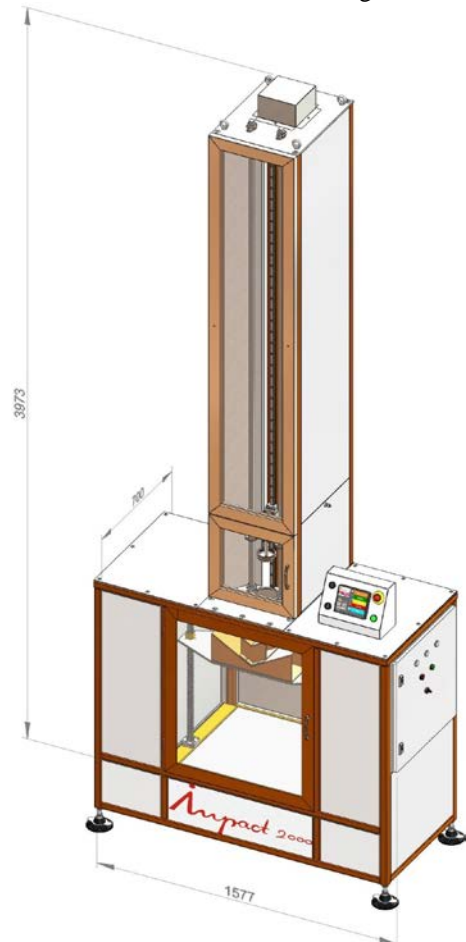


Figure 9: 3D model with projected dimensions [11]

As the machine has a great height (4 m), for easy transportation and assembly, the machine consists of two assemblies, the upper and bottom sub-assembly.

1) The bottom sub-assembly – represents a protected chamber in which will be placed the pipe for testing. The chamber is protected with a transparent door and lighted from the inside. During testing it is very easy to see the condition of the pipe sample. During the testing phase, the door is locked. Inductive proximity sensor [12] detects when the door is open and triggers the alarm. The chamber has a possibility of automatic height positioning of the pipe sample. Maximum sample diameter is 630 mm. The sample holder is V shape prism which is defined by the standard. The lifting mechanism of the V shape consists of a ball and screw spindle which drives an asynchronous motor controlled by a frequency converter.

2) The upper sub-assembly – Represents a module for weight lifting, positioning and releasing. Maximum weight lifting is 12kg and maximum lifting height is 2m. Lifting and positioning was implemented using a servo motor drive technology. Catching of weight sets is realized using electromagnets. After the electromagnet catch the weights, trolley on linear guides are raised to the required height. After reaching the required height weights are

released and fall free. The linear movement of the trolley is realized by using a timing belt and linear guides. This module is also implemented in the form of a chamber which has a door for easy access for change the weight sets. The front of the module is transparent and illuminated. Transparent front allows observation of the rising and falling of the weight sets. Lighting provides information about the current state of the machine.

4.2. Human machine interface and control

Machine control is based on PLC technology [13], [14] and interaction with machine is implemented through color HMI display (Figure 10). Control of machine is very simple and intuitive. It is realized in such a way that guides the operator through the process of testing. Machine has in its memory all the standards relating to pipe testing. There is also possibility of implementation of the internal standard on customer's request. There are three levels of access to machine: the operator, controller and service.

Immediately after the starting the machine performs initialization. Initialization brings all moving parts of the machine in home position (Figure 10b). After successful initialization, the operator must choose standard for pipe testing (Figure 10c). Human machine interface leads operator through the procedure, so in this way there is small possibility for errors. In bottom part of HMI screens there is status line through which operator has information about current machine state. Next step is choosing the desired test method (Figure 10d) and the relevant pipe diameter (Figure 10e). Based on the selection of these parameters, the HMI receive all the data required for testing so, the necessary mass of weight sets, the shape of impact head and the height from which the weight will fall (Figure 10f).

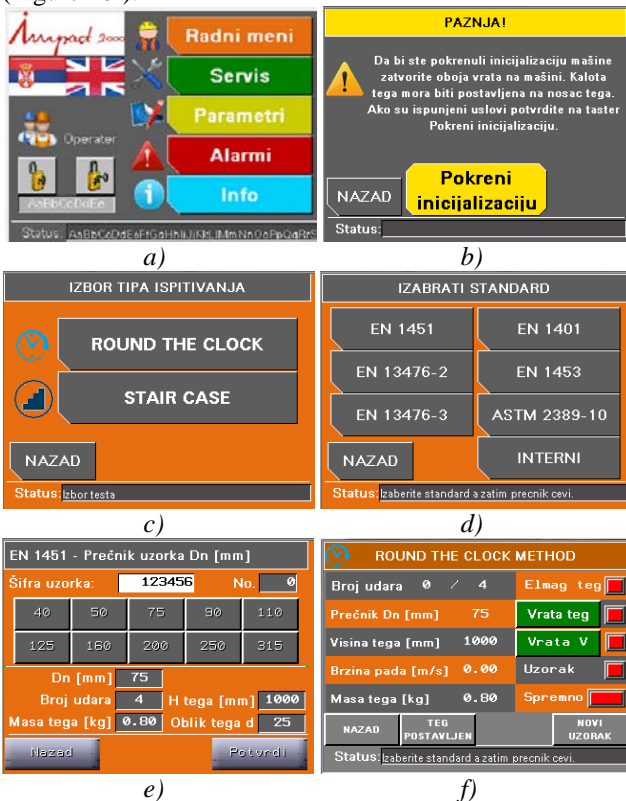


Figure 10: The screens of HMI from start to test point

4.3. Safety functions

During designing the machine, special attention was paid to safety functions. The request was to implement protective system that will eliminate the human factor. Testing cannot start if the doors are not closed. Both doors are equipped with electromagnetic locks which automatically lock the doors and cannot be opened manually when the testing procedure is in progress. Built-in light signaling provides information on the current state of the machine. If the front panel shines red this means that the door is locked, it is potentially dangerous to open the door because of the moving parts. If the front panel shines green this means that the door is unlocked and it is safety to open door to rotate sample, change weight set etc (Figure 11). Operation is implemented in such a way that it cannot enter the next step if all necessary conditions are not met. After completion of the testing of each sample, test data are automatically saved to the USB memory.



Figure 11: Falling Weight Impact Tester - IMPACT 2000

#### 4.4. Machine technical specifications

- Automatic positioning of the height of the weight release
- Motor lifting and automatic positioning of the V-block
- Speed measurement
- Safety functions
- Operator panel with color touch screen
- Simple and intuitive interface
- Guiding through testing procedure
- Implemented standard base
- Three level of access control
- Saving data to USB stick
- Test samples diameter range Ø 32 - 650 mm
- Speed of impact is not less than 95% of free fall
- Maximal weight height is 2000mm
- Weights: Up to 12.5 kg
- Power supply: 230V/400V, 50 Hz
- Dimensions machine: 1540x700x4000 mm

#### 5. CONCLUSION

The development of mechatronic systems burdened by a series of insufficiently explored segments. Existing knowledge and reference literature does not explain and do not give sufficiently recommendations in a way that would allow an efficient and generally applicable concept of solving complex technical problems and design of complex production systems.

Mechatronic approach to engineering design of complex technical systems based on the integration of various scientific disciplines to be applied at each stage of design, to achieve optimal solutions. Such a solution cannot be achieved by conventional method, individual examination of system components belonging to different scientific fields, but requires a comprehensive analysis of the entire system.

In this paper, theoretical and experimental study of the design of complex technical system was performed. Practical example of implementation and embodiments of the mechatronic systems was shown on machine for testing plastic pipes IMPACT 2000. A complex concept of equipment that is enabled to indicate the complexity of the design of the mechatronic system, perform the necessary analysis, the analytical and experimental character, and the synthesis of the relevant data structure defines the best system.

The machine meets all the necessary criteria, both in terms of functionality and design, and from the standpoint of safety at work and technical characteristics are not inferior to machines from renowned European and world producers. This technical solution, from concept to implementation, is fully implemented by the project team of the Faculty of Technical Sciences in Čačak and represents a contribution to the domestic industry. In the domestic market, there is no such machines...

Future research can be carried out in the direction of constructing machines that would have the ability to automatically rotate the pipe test samples. According to the conducted research, the machine with such opportunities do not currently exist on the world market.

#### ACKNOWLEDGEMENTS

Machine for plastic pipes impact testing - IMPACT 2000 was realized as a cooperation project with the industry. The project investor and user is the company Peštan d.o.o Arandjelovac.

#### REFERENCES

- [1] <http://www.worldoftest.com/drop-weight-impact-tester>
- [2] <https://www.iptnet.de/en/products/mechanical-tests/falling-weight-tester.html>
- [3] <http://www.sciteq.com/products/pipe-and-fitting-testing/sciteq-impact-tester-b50/>
- [4] BS EN 744:1996 - Plastics piping and ducting systems - Thermoplastics pipes - Test method for resistance to external blows by the round-the-clock method
- [5] BS EN 1411:1996 - Plastics piping and ducting systems - Thermoplastics pipes - Determination of resistance to external blows by the staircase method
- [6] Mandić, V., *Virtuelni inženjering*, Mašinski fakultet, Kragujevac, 2007.
- [7] Mandić, V., Erić, D., Adamović, D., Janjić, M., Jurković, Z., Babić, Ž., Čosić, P.: *Concurrent engineering based on virtual manufacturing*, Technical Gazette, ISSN 1330-3651, Vol.19, No4, pp.885-892, 2012.
- [8] Milicevic, I., Slavkovic, R., Mandic, V., Jugovic, Z., Popovic, M., *Virtual Models Application for the Analysis of Strain-Deformation States in the Process of Metals Processing by Plastic Deformation*, IMK-14 – Research & Development in Heavy Machinery 19(2013)3, EN 89-96, 2013.
- [9] Milićević, I., Savković, S., Šekarić, M., Slavković, R., Dučić, N., Popović, M.: *The use of virtual models in the design of mechanisms*, The Eighth Triennial International Conference Heavy Machinery HM 2014, ISBN 978-86-82631-74-3, Proceedings, Session E: Mechanical design and mechanics, pp.29-34, Zlatibor, Serbia, 25-28 June, 2014.
- [10] Savković, S., Vujičić, V., Milićević, I., Marjanović, M., Slavković, R., Dučić, N.: *Determination of velocity and acceleration of the object in motion moving down along vertical cylindrical rails*, 6th International Conference, Technics and Informatics in Education – TIO 2016, Proceedings, ISBN 978-86-7776-192-9, pp. 463-469, Faculty of Technical Sciences, Čačak, 28-29th May, 2016.
- [11] Savković, S., *Projektovanje mehatroničkog sistema za ispitivanje otpornosti plastičnih cevi na mehanički udar*, Master thesis, Faculty of Technical Sciences, Čačak, 2016.
- [12] Paul P.L. Regtien, *Sensors for Mechatronics*, ISBN 978-0-123-94409-2, Elsevier Science, 2012.
- [13] Bolton, W.: *Programmable Logic Controllers*, Elsevier Newnes, Oxford, UK, 2006.
- [14] J.R. Hackworth, F.D. Hackworth: *Programmable Logic Controllers: Programming Methods and Applications*, Pearson/Prentice Hall, 2004.

# Multi-criteria Selection of Optimal Mechanization for Road construction

Vladimir Mandić<sup>1\*</sup>, Saša Marinković<sup>1</sup>, Jovana Bojković<sup>1</sup>

<sup>1</sup>Faculty of mechanical and civil engineering in Kraljevo, University of Kragujevac, Kraljevo (Serbia)

*The selection of optimal solution for road construction mechanization has been presented on the example of access road construction. For selection between possible alternatives the Promethee method of multi-criteria decision analysis has been used. The alternatives were evaluated through the several criteria (number of mashinery, total cost, time, machinery reserve, practice effect, number of people, price of effective working hour) and the impact of each criteria on the final ranking of alternatives has been analyzed. The optimal solution was determined by comparing the two differend scenarios (with different relative weights for criterias) in the multicriteria decision analysis model. Conclusions on each criteria influence on final ranking were presented in this paper.*

**Keywords: Multicriteria decision analysis (MCDA), Promethee, relative weights**

## 1. INTRODUCTION

In this paper, attention was given on solving the multicriteria problems wich primarily requires the definition of a system of criteria, and then defining relative importance of criteria before the final ranking. The selection process of the systems optimal concept is multidisciplinary and requires a comprehensive approach [1]. Determination of the optimal solution is a decision-making problem, when selection of one of the possible alternatives was evaluated through many different criteria. For good decision making, reliable basic data are not enough, adequate and a scientifically based methodological support are required [2,7].

Having in consideration the large number of influences through several criteria evaluation of alternatives, leads to the selection of the best or the optimal alternative [3,8]. The optimal solution is an alternative that provides maximum value of criterion function according to all criteria, while satisfying all given limitations [4,6].

## 2. METHODS AND MATERIALS

The optimal solution of the considered problem was determined using a multi-criteria analysis method called PROMETHEE. Method PROMETHEE (eng. Preference Ranging Organization Methods of Evaluation Enrichment) solves the problem of multiple criteria ranging of possible alternatives using the predefined functions of criteria evaluation [9, 10].

Based on the specified alternatives and defined criteria functions for each criterion, the method PROMETHEE, determines the preference function for each pair of alternatives. The inclusion of weight

coefficient in this model allows the assignment of importance (or the relative weight) of certain evaluation criteria in comparison to another criteria. This is a very important characteristic of this method because it allows to analyze the same alternatives using the same criteria but with different importance (relative weights) of these criteria [11]. Based on the determined values of the preference index for each pair of alternatives, the PROMETHEE method determines the value of positive (output) and negative (input) preference index flow for each alternative. Using the positive and negative preference index flow for each alternative, it is possible to make a partial ranking of alternatives, and it is possible to determine which alternatives are mutually comparable, and which are not [13,14]. With PROMETHEE method it is possible to do the final ranking of considered alternatives using the function of "pure" or the netto preference index flow [12]. The multi-criteria model is offering the optimal solution according to the parameters entered into the model of multi-criteria analysis to the decision maker[5,6].

Materials for all analysis in this paper were taken from experts work (Božović Ž.) [15] and project documentation (Saobraćajni institut CIP, 2010).

## 3. MDCA MODEL

Multicriteria optimization model has been used to determine the optimal variant of the road construction mehanization for building final pavement layers on the road building "Severna tangenta - LOT 5 ". The PROMETHEE multi-criteria optimization method has been used to determine the optimal variant of the road construction mehanization for construction works on the described road route. The created model was used to choose among three available variants of the road construction mehanization for road building.

The following table shows the possible variants of the road construction mechanization:

Table 1: Possible alternatives of road construction mechanization

Var.	Road construction mechanization	No.
V1	1. Asphalt base MARINI 200t	1
	2. Dumper truck Man DFK	16
	3. Asphalt paver VOLVO ABG 5820	1
	4. Vibro roller DYNAPAC CC122	2
	5. Vibro roller BOMAG 190 AD-4 HF	1
	6. Vibro roller BOMAG BW 284 AD	1
V2	1. Asphalt base MARINI 200t	1
	2. Dumper truck Man DFK	16
	3. Asphalt paver VOGELE SUPER 1800	1
	4. Asphalt paver VOGELE SUPER 2100	1
	5. Vibro roller DYNAPAC CC122	2
	6. Vibro roller BOMAG 190 AD-4 HF	1
	7. Vibro roller BOMAG BW 284 AD	1
V3	1. Asphalt base MARINI 200t	1
	2. Dumper truck Man DFK	5
	3. Bagger Takeuchi TB145	1
	4. Asphalt paver VOGELE SUPER 800-3i	1
	5. Vibro roller BOMAG BW 900-50	3

The evaluation of possible alternative solutions was performed by forming a multi-criteria optimization model according to Promethee method. According to available

data seven criteria has been created for evaluating the alternative solutions. In the Table 1 are shown the adopted criteria for evaluation of alternative solutions, with the values of criteria for each parameter, whether the criterion maximizes or minimizes and the measurement units for the values of the each criterion parameters.

Criterion "C1. Number of machines" was determined by counting the total number of engaged machines by variant solutions. Criterion "C2. Number of people" was determined as the counted number of people required for operating and servicing the selected machines.

Criterion "C3. Practicle effects of work" is defined as the minimum practical effect of certain types of machines for each variant of the machinery selection. While the criteria "C4. Price of effective working hours" was specified for each variant solutions as the sum of costs divided with practical effect.

Criterion "C5. Machinery reserve" was determined as the ratio of the maximum and minimum practical effect, and shows how much, in theory, the efficiency could be increased, or how big machinery reseve was. Criteria "C6. Time for finishing the project" evaluated the time required to complete a given project. Criterion "C7. Total cost" weighted overall cost of all works on building the specified road route.

Table 2: Input data for multiple criteria optimization

Valuation of variants			Variants		
Criteria	Units	max/min	V1	V2	V3
C1. Number of machines	number	max	22	23	11
C2. Number of people	number	min	29	32	19
C3. Practicle effect of work	m <sup>3</sup> /h	max	54.19	55.20	25.20
C4. Price of effective working hour	eur/h	min	2669.83	2814.29	2379.87
C5. Machinery reserve	/	max	9.810	10.130	4.865
C6. Time for finishing project	days	min	527	509	568
C7. Total cost	mil.euro	min	16.884	17.189	16.221

Figure 1 shows a model for multi-criteria analysis created in the Visual Promethee 1.4. software.

On this way formed multi-criteria optimization model, for each of the three alternative solutions it was considered which of the criteria may influence the values of the positive (output) preference index flow, and which of the criteria may influence the values of the negative (input) preference index flow.

Figure 2 shows a diagram of individual criteria impact on the value of preference index current for all three alternative solutions.

In Figure 2, on the upper side of the axis "0-0" are listed the names of the criteria that form the value of the positive (output) preference index flow, and on the lower side of the axis "0-0" are listed the names of the criteria which give the value of the negative (input) preference index flow for all three alternative solutions.

Figure 1: MCDA model in Visula Promethee 1.4. software

Scenario1	Num.Mash.	Numb.Peop.	Prac.Effect	Price EWH	Mach.Reserve	Time	Total Cost	
Unit	Number	Number	m3/h	eur/h	/	Days	mil. e	
Cluster/Group	◆	◆	◆	◆	◆	◆	◆	
<b>Preferences</b>								
Min/Max	max	min	max	min	max	min	min	
Weight	1,00	1,00	1,00	1,00	1,00	1,00	1,00	
Preference Fn.	V-shape	V-shape	Linear	V-shape	Linear	V-shape	V-shape	
Thresholds	percentage	percentage	percentage	percentage	absolute	absolute	percentage	
- Q: Indifference	n/a	n/a	0,03	n/a	2,259	n/a	n/a	
- P: Preference	13	13	0,25	0,25	5,769	0	0,25	
- S: Gaussian	n/a	n/a	n/a	n/a	n/a	n/a	n/a	
<b>Statistics</b>								
Minimum	11	19	25,20	2379,87	4,865	509	16,221 mil. €	
Maximum	23	32	55,20	2814,29	10,130	568	17,189 mil. €	
Average	19	27	44,86	2621,33	8,268	535	16,765 mil. €	
Standard Dev.	5	6	13,91	180,64	2,410	25	0,404 mil. €	
<b>Evaluations</b>								
<input checked="" type="checkbox"/>	V1	22	29	54,19	2669,83	9,810	527	16,884 mil. €
<input checked="" type="checkbox"/>	V2	23	32	55,20	2814,29	10,130	509	17,189 mil. €
<input checked="" type="checkbox"/>	V3	11	19	25,20	2379,87	4,865	568	16,221 mil. €

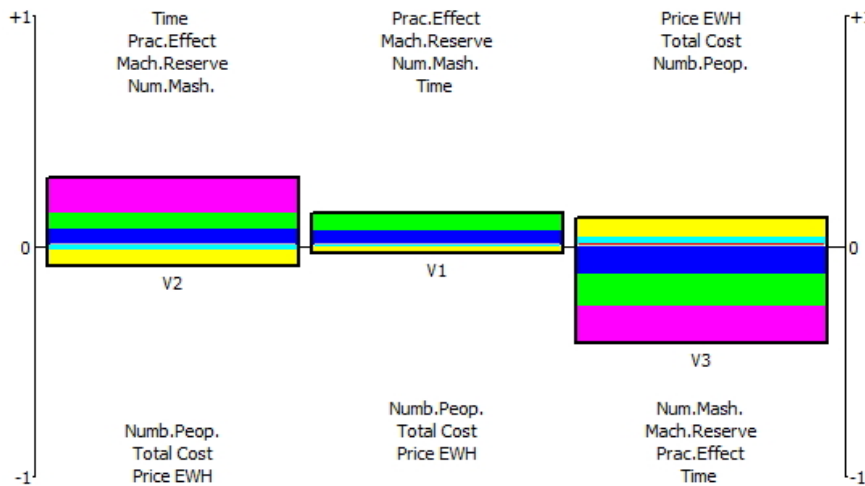
As shown on Figure 2, for a variant solution V1, positive (output) value of preference index flow provides criteria: "C3. Practicle effect of work", "C5. Machinery reserve", "C1. Number of machines" and "C6. Time for finishing project", and the negative (output) values of preference index flow for this variant solution provides criteria: "C2. Number of people", "C7. Total cost" and "C4. Price of effective working hour".

flow for this variant solution provides criteria: "C2. Number of people", "C7. Total cost" and "C4. Price of effective working hour".

For a variant solution V2, positive (output) value of preference index flow provides criteria: "C6. Time for finishing project", "C3. Practicle effect of work", "C5. Machinery reserve" and "C1. Number of machines", while the negative (output) values of preference index

For a variant solution V3, positive (output) value of preference index flow provides criteria: "C4. Price of effective working hour", "C3. Practicle effect of work", "C7. Total cost" and "C2. Number of people", while the negative (output) values of preference index flow for this variant solution provides criteria: "C1. Number of machines", "C5. Machinery reserve", "C3. Practicle effect of work" and "C6. Time for finishing project".

Figure 2: Criteria impact on preference function value



4. RESULTS

Based on the sensitivity analysis of criteria impact on the optimization model, two scenarios for the calculation of the optimal solution were formed:

**Scenario S1 - all criteria have the same relative weights**

According to this scenario all criteria have equal relative importance (weight) for the selection of optimal solution. Based on the model established this way, for the scenario S1 obtained results are shown in Figure 3.

The upper part of Figure 3 shows diagram of comparison alternative solutions with PROMETHEE II method for scenario S1, in terms of function of pure or net flow, while the lower part of Figure 3 shows that all the criteria for scenario S1 have the same coefficients of relative weights.

**Scenario S2 – the different relative weights of the criteria**

This scenario shows what solution will be obtained if the relative weight of some criterias increase the value. Based on the a sensitivity analysis, the relative weight values of these criterias were increased: "C4. Price of effective working hour" and "C7. Total cost".

Based on the model established this way, for the scenario S2 obtained results are shown in Figure 4. The upper part of the figure 4 shows the comparison diagram of alternative solutions according to function of pure or net flow for scenario S2 with PROMETHEE II method, while on the lower part of Figure 4 shows the distribution of the weight coefficients by the criteria, where can be seen that the criteria: „C4. Price of effective working hour" and „C7. Total cost", participates with 27% each, while the other criteria participate with 9% share in the total value of criteria weight sum.

Figure 3: Scenario S1 results

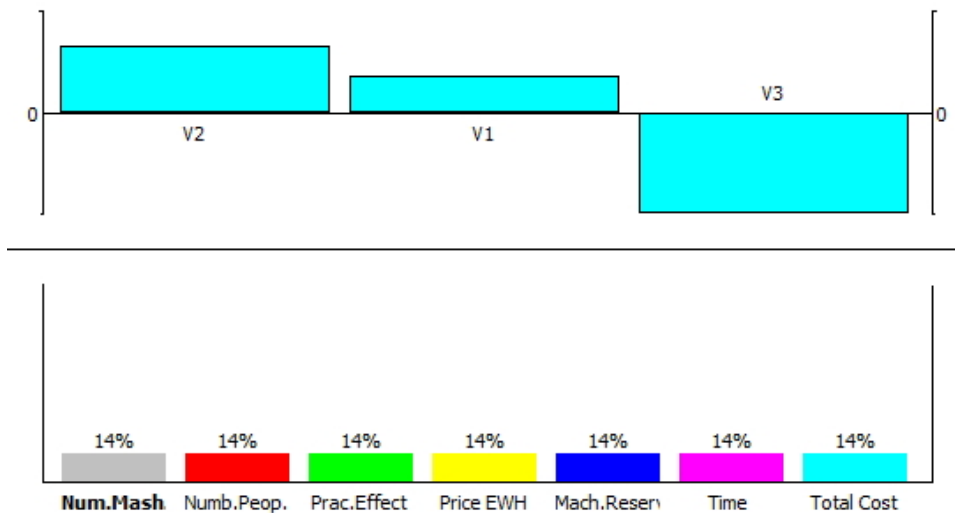
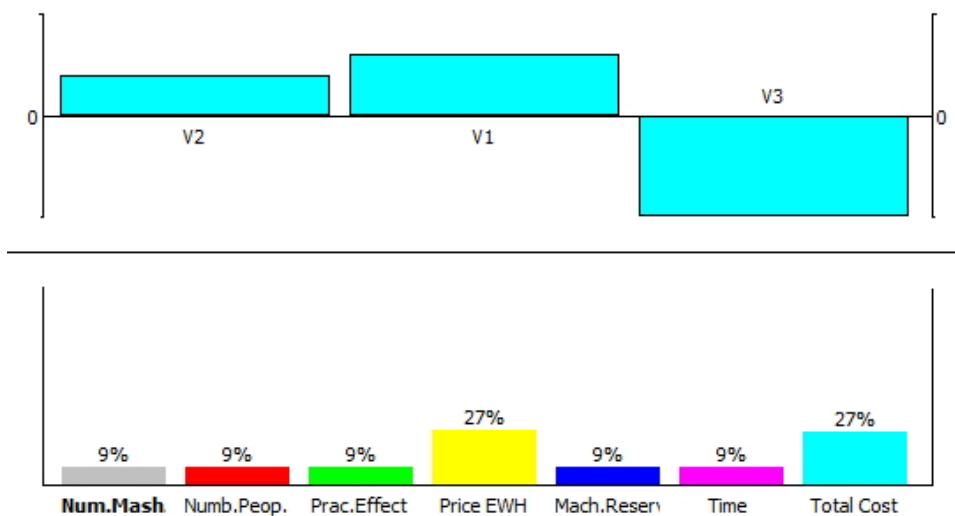


Figure 4: Scenario S2 results





From the the previous figure 3 can be seen that the scenario S1, according to which all the criteria have the same values of relative weights, obtained variant V2 as the optimal solution of the considered problem.

For the scenario S2, according to which criterias "C4. Price of effective working hour" and "C7. Total cost" have higher values of relative weight in comparison to other evaluation criterias, as the optimal solution of the considered problem obtained variant V1 of road construction machinery.

The question arises: "What solution should be adopted?"

5. DISCUSSION OF THE OBTAINED RESULTS

Although the multi-criteria optimization method Promethee II give the final ranking of considered alternatives based on the preference index function of the net flow, necessary is to apply the multi-criteria optimization method Promethee I, which gives a partial ranking of considered alternatives and opportunity for inter-comparability analysis of the alternatives.

For the scenario S1 graphical representation of the results of Promethee I method has been given in the figure 5.

Figure 5: Results of Promethee I method for scenario S1

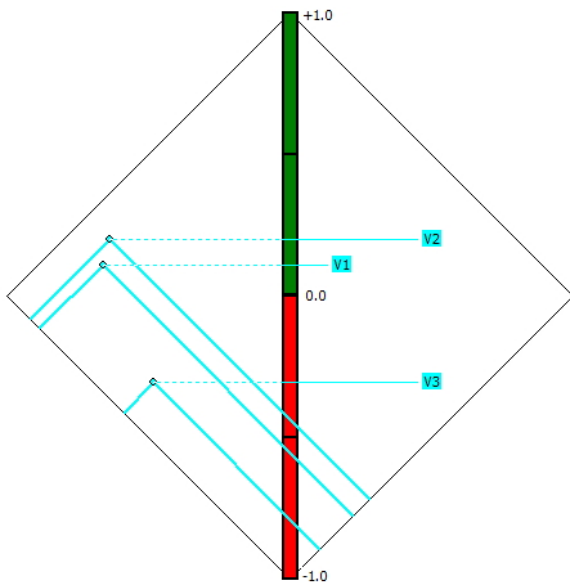


Figure 5 shows on the angular axis specified values of positive and negative preference flow, and the intersection points correspond to the functions of net flow.

The figure 5 shows that the values of of a positive and a negative flow for all three alternative solutions are not mutually intersect, from which it may be concluded that all three alternative solutions are mutually comparable.

For the scenario S2, graphical representation of the results of Promethee I method are shown in Figure 6.

Figure 6 shows that the values of of a positive and a negative flow for all three alternative solutions intersects mutually, resulting in the conclusion that these alternative solutions are mutually incomparable.

For understanding the obtained results it is necessary to get back to the model stability analysis and to check why the increase of the relative weights for these two criteria results that alternative solutions becomes mutually incomparable for the scenario S2.

Figure 7 shows the changes in the values of positive and negative preference flow for all three alternative solutions in comparison with the change of the relative weight of criteria "C4. Price of effective working hour". On figure 7, the value of the relative weight of 27% is marked for the scenario S2.

Figure 6: Results of Promethee I method for scenario S2

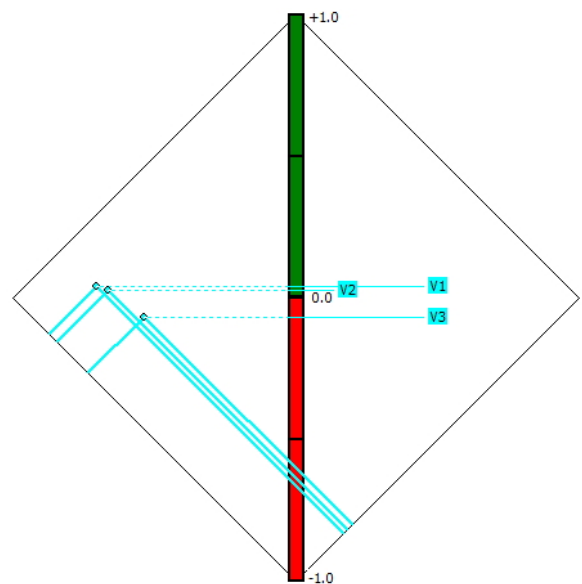


Figure 8 shows the changes in the values of positive and negative preference flow for all three alternative solutions in comparison with the change of the relative weight of criteria "C7. Total cost". On figure 8, the value of the relative weight of 27% is marked for the scenario S2.

The sensitivity analysis of the criteria "C4. Price of effective working hour" and "C7. Total cost" sets these criterias as the criterias that can increase the value of the net preference flow for the variant V1 and reduce the value of the net preference flow for the variant V2.

Figures 7 and 8 shows that the adopted values of weight coefficients, of criteria: "C4. Price of effective working hour" and "C7. Total cost", of the 27% causes the that alternative solutions becomes mutually incomparable.

Figure 7: Impact of relative weight of C4. criteria

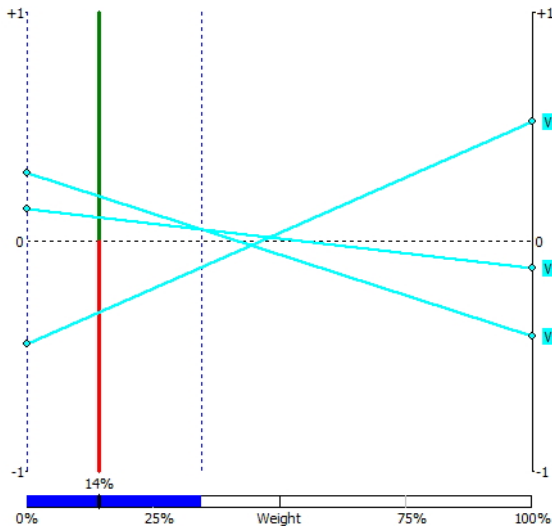
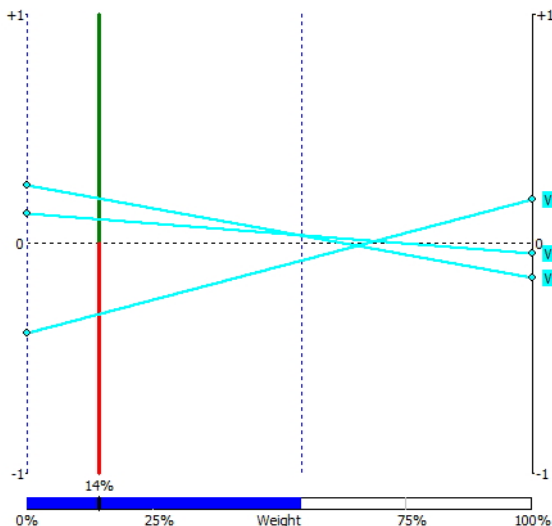


Figure 8: Impact of relative weight of C7. criteria



## 6. CONCLUSION

In this paper was analyzed what impact on the model's stability will have increase of criterias relative weight for: "C4. Price of effective working hour" and "C7. Total cost" criterias, according to the scenario S2. It has been shown that this model, for the scenario S2, does not provides good results, because the alternative solutions are mutually incomparable. For consider problem the optimal solution is the selection of road construction mechanization V2, according to the scenario S1, with equal weight coefficient values for all the criteria.

The biggest problem of multi-criteria optimization methods is a large quantity of subjective decisions, form the stage of the criteria and variant selection as well as in the stage of the relative weights of the criteria determination.

The increase in the relative weights of the criteria in multi-criteria analysis could result the mutually incomparable alternative solutions, as shown in the example scenario S2.

When there is a need for the increasing the relative weights of the certain criteria, it is necessary to perform a

sensitivity analysis of relative weights increasing, and also the application of Promethee I method to show whether the alternative solutions are mutually comparable.

Removing the impact of subjective decisions in the multi-criteria optimization process, by forming a algorithms and analysis to determine the relative weights of the individual criteria, remains a topic for further research.

## REFERENCES

- [1] G. Marković, "Model regionalne logistike transportnim sistemima", Doktorska disertacija, Univerzitet u Kragujevcu, Fakultet za mašinstvo i građevinarstvo u Kraljevu (2014.)
- [2] I. Hot, "Upravljanje izradom generalnih projekata u oblasti infrastrukture primenom višekriterijumske analiza", Doktorska disertacija, Univerzitet u Novom Sadu Fakultet tehničkih nauka, (2014.)
- [3] S. Opricović, "Višekriterijumska optimizacija sistema u građevinarstvu", Građevinski fakultet Univerziteta u Beogradu, Beograd, (1998.)
- [4] G. Miodragović, et al., "Primena biološki inspirisanih algoritama za optimizaciju parametara obrade", IMK-14, Vol.21(3), (2015.)
- [5] Z. Bogičević, et al., "Izbor opreme za rukovanje materijalom primenom integrisanog Fuzzy AHP i VIKOR metoda", IMK-14, Vol.21(3), (2015.)
- [6] V. Tomić, et al., "Primena TOPSIS metode kod rešavanja lokacijskih problema, slučaj zapadna Srbija", IMK-14, Vol.20(3), (2014.)
- [7] M. Popović, et al., "Procena vrednosti mehanizacije primenom komparativnog pristupa", IMK-14, Vol.20(3), (2014.)
- [8] V. Grković, et al., "Modifikovani algoritam kolonije mrava za rešavanje inženjerskih optimizacionih problema", IMK-14, Vol.18(4), (2012.)
- [9] Brans, J.P., Mareschal, B., PROMETHEE: A new family of outranking methods in multicriteria analysis, Operational Research IFORS 84, (1984.)
- [10] Brans, J.P., Mareschal, B., PROMETHEE: A new family of outranking methods in multicriteria analysis, Operational Research IFORS 84, (1984.)
- [11] Brans, J. P.; Vincke, P. H. A preference ranking organization method: The PROMETHEE Method for Multiple Criteria Decision Making. Management Science. 31, 6 (1985.)
- [12] Brans J.-P., Mareschal B., Chapter V: Promethee Methods, Book: Multiple Criteria Decision Analysis: State of the Art Surveys, Book Part III, pp 163-186, (2005.)
- [13] VPSolutions Ltd., Visual PROMETHEE 1.4 Manual
- [14] URL: <http://www.prometheegaia.net/files/VPManual.pdf>
- [15] Ž.Božović, "Stručni rad", Inženjerska Komora Srbije, (2016.)

# Prediction of Acoustic Properties of Porous Building Materials

Jovana Bojković<sup>1\*</sup>, Branko Radičević<sup>1</sup>, Nedeljko Manojlović<sup>2</sup>, Mišo Bjelić<sup>1</sup>, Vladimir Mandić<sup>1</sup>,  
Saša Marinković<sup>1</sup>

<sup>1</sup> University of Kragujevac, Faculty of Mechanical and Civil Engineering Kraljevo (Serbia)

<sup>2</sup> University of Kragujevac, Faculty of Medical Sciences (Serbia)

*This article presents an empirical model for predicting acoustic properties of a composite material which is a mixture of sand and polyurethane resin as the binder. The parameters of the model were determined based on the experimental testing of samples with the thickness from 10mm to 50mm. Measurements of the sound absorption coefficient were performed in the impedance tube using the transfer function method (SRPS EN ISO 10534-2: 2008). The same samples were used for measurement of the air flow resistance in order to form an empirical model. The measurements were made according to the method defined by SRPS ISO 9053:1994. It was concluded that the proposed model can be used in order to predict the absorption properties of sand as well as of other building materials whose grain structure is air permeable.*

**Keywords: Empirical model, Sound absorption, Sand, Material structure**

## 1. INTRODUCTION

Today, noise has become a serious problem. In order to reduce its negative impacts in the form of hearing loss or a sleep disorder, people are looking for better acoustic solutions that will improve their living conditions. A lot of research is based on the development of materials that are suitable for sound absorption and noise reduction. Therefore, there is an increasing demand for materials with a high coefficient of sound absorption. As noise is a growing problem in the world, the research in the sound absorption of materials gains importance. Sound-absorbing materials are used to improve indoor acoustic comfort, and in recent years their application in the open has been increased in the form of absorption barriers. Among other things, protection against noise is one of the segments where natural materials, such as granular and fibrous, has a prominent place. Therefore, these materials are the subject of numerous studies.

Composite materials are increasingly used for sound insulation. Particularly important are the so-called organic compositions, such as rubber, plastics and the materials that represent a waste of industrial processes. Zainulabidin et al. [1] studied the acoustic properties of two materials: rubber sponges and fiber glass wool.

The prediction of acoustic properties of materials from recycled rubber and polyurethane resin was performed using the model Allard & Champoux [2]. New innovative sound absorbers based on organic materials have great potential in the future because they are cheaper compared to other available materials [3].

Soleimani [4] and others examined the acoustic properties of a mixture of wood fibers and recycled plastics. Our results show that the addition of nano-clays in composite resin decreases water absorption and that plastics have a negligible water uptake. Perna [5] and others studied the absorption coefficient of materials which results from the mixing of sand and geopolymers. Geopolymers were used as a substitute for epoxy resin.

Mahzan S. et al. [6] investigated combinations of materials in which coconut is used as the main raw material and recycled rubber as a raw material with the use

of polyurethane as the binder. Tests have shown that the absorption of this mixture is suitable for medium and high frequencies. The samples with 25% recycled rubber gave absorbance values greater than those that had 35% recycled rubber.

Semiha Yilmazer and Mesut B. Ozdeniz [7] analyzed the effect of moisture content on the acoustic properties of panels made of expanded perlite. The best results in terms of sound absorption in a moist environment were produced by silicate coated perlite.

Perna Ivana et al. [8] tests were performed based on the determination of the absorption coefficient of the material formed as a mixture of sand and geopolymers. The results showed that geopolymer-sand mixtures have good absorption properties and can be used as a substitute for epoxy resin. The mixing of two different fractions of sand results in a higher absorption coefficient. Another result of improving the sound absorption of this type of material is the possibility of its installation between other types of composite materials.

## 2. MATERIAL

By their nature, materials can be classified into two main groups: natural and artificial. Natural materials are those that can be installed in buildings without processing, such as wood, stone, sand, gravel, grain, materials of vegetable origin, while artificial materials, e.g. cement, gypsum, bricks or concrete are not found in nature - they are obtained through special technological procedures. Sand is a natural granular material. It is obtained by natural crushing and disintegration of rocks, where the level of fragmentation of the rock material is quite large. Sand can be described as an unconsolidated sediment with the size of grains of up to 4mm. In order to trace the grain size distribution, two methods are used: the method of sieving and the sedimentation method. With regard to the grain size of aggregates used in construction, the grain size distribution of these materials is most commonly defined by the sieving method [9].

Therefore, both of these experimental studies performed on circular patterns were made of sifted sand

\*Corresponding author: Dositejeva 19, 36000 Kraljevo, Serbia and kalicanin.j@mfkv.kg.ac.rs

and a binder. The structure of the sample was formed by using granules of sand, gravel, and 10% of polyurethane resin as the binder. The binder has the same percentage share in all samples. The maximum size of granules was determined by the size of the mesh openings of 3mm. The samples were poured into moulds with the diameter of 100mm and a thickness of 10mm, 20mm, 30mm, 40mm and 50mm.



Figure 1: A sample of the mixture of sand and polyurethane resin

### 3. METHODS

The measurement of absorption was carried out in an impedance tube, by applying the transfer function method between two microphones, described by the standard EN ISO 10534-2 [10]. This method is based on the decomposition of a standing wave formed in the tube, by recording signals from the two microphones and calculating their transfer function. The reflection coefficient is calculated from the transfer function, and then the absorption coefficient is found in the conditions of normal incidence.

$$\alpha = 1 - |R|^2 \quad (1)$$

where:  $R$  is the reflection coefficient which is calculated according to the expression:

$$R = \frac{H - e^{-jks}}{e^{jks} - H} e^{j2k(l+s)} \quad (2)$$

where:  $H$  – the corrected transfer function,  $s$  – the distance between the microphones,  $l$  – the distance of the microphone which is closer to the sample,  $k$  – the wave number.

The method with a constant air flow was used for measuring airflow resistance, according to the standard ISO 9053:1991 [11]. The practical realization of the system for measuring airflow resistance is presented in paper [12]. The measuring cell has the form of a circular cylinder; it is made of plexiglass so that placing of the sample could be visually monitored. The inner diameter of the measuring cell is 100 mm. The vacuum pump ZAMBELLI, type ZB1 is used as a device for creation of airflow. The airflow is measured by means of a ball rotametre. The measuring range of the rotametre is 2÷30 l/min. A differential pressure meter TESTO 512 is used for measuring the pressure drop through the sample. This gauge has a measuring range of 0-200 Pa with the

resolution of 0.1 Pa. The error of the measurement equipment is smaller than required by the standard [11].



Figure 2: A view of the realized measurement system for determination of airflow resistance

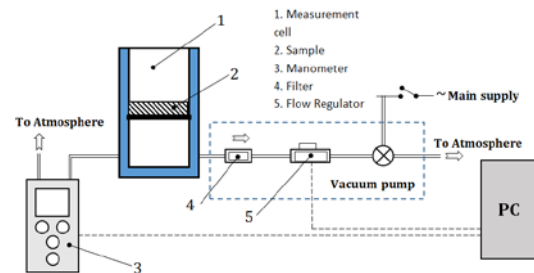


Figure 3: Block diagram of the steady-state airflow system

### 4. PROPOSAL OF A NEW EMPIRICAL MODEL FOR DETERMINATION OF ACOUSTIC PROPERTIES OF GRAIN MATERIALS

Theoretical models require five input parameters, which cannot often be simply and reliably determined. This is the main weakness of the so-called phenomenological or micro models for determination of acoustic properties of porous materials. Therefore, an experimental macro model for prediction of acoustic properties of composite materials made of sand, gravel and polyurethane resin is developed in this paper. The main advantage of such models is in their having one input parameter – longitudinal airflow resistance.

Sound propagation in an isotropic homogeneous material can be represented by the characteristic impedance ( $Z_c$ ) and the constant of sound propagation in the absorption material.

$$Z_c = R + jX \quad (3)$$

$$\gamma = \alpha + j\beta \quad (4)$$

Starting from the well-known Delany & Bazley relations:

$$R = \rho_0 c_0 \left[ 1 + C_1 \left( \frac{\rho_0 f}{r} \right)^{-C_2} \right] \quad (5)$$

$$X = -\rho_0 c_0 \left[ C_3 \left( \frac{\rho_0 f}{r} \right)^{-C_4} \right] \quad (6)$$

$$\alpha = \left( \frac{2\pi f}{c_0} \right) \left[ C_5 \left( \frac{\rho_0 f}{r} \right)^{-C_6} \right] \quad (7)$$

$$\beta = \left( \frac{2\pi f}{c_0} \right) \left[ 1 + C_7 \left( \frac{\rho_0 f}{r} \right)^{-C_8} \right] \quad (8)$$

where R and X are the real and imaginary parts of the characteristic acoustic impedance  $Z_c$ , and  $\alpha$  and  $\beta$  the real and imaginary parts of the constant of propagation ( $\gamma$ ) of sound in the absorption material,  $\rho_0$  – the air density,  $f$  – the frequency, and  $r$  – the longitudinal airflow resistance.

Starting from the equations (9) through (13) and the recommendations of the European standard EN 12354-6:2003, the diffusion coefficient of sound absorption of porous materials can be calculated. For a diffuse acoustic field, the absorption coefficient  $\alpha_s$  can be defined as:

$$\alpha_s = \int_0^{\pi/2} \alpha_\varphi \sin 2\varphi d\varphi \quad (9)$$

$$\alpha_\varphi = 1 - |r_\varphi|^2 \quad (10)$$

$$r_\varphi = \frac{Z' \cos\varphi - 1}{Z' \cos\varphi + 1} \quad (11)$$

$$Z'_c = \frac{Z_c}{\rho_0 c_0} \quad (12)$$

$$Z' = Z'_c \coth \gamma d \quad (13)$$

where:

- $\varphi$  - the angle of incidence, in radians,
- $\alpha_\varphi$  - the absorption coefficient for the plane sound wave, related to the angle  $\varphi$ ,
- $r_\varphi$  - the reflection coefficient for the plane sound wave, related to the angle  $\varphi$ ,
- $Z'$  - the normalized surface impedance of the layer
- $Z'_c$  - the normalized characteristic impedance of the absorption material,
- $d$  - the layer thickness, in meters.

The empirical macroscopic model for determination of acoustic properties of composites made of sand, gravel and polyurethane resin are rarely available in the scientific literature. The new model for prediction of acoustic properties of the mentioned composite was developed by applying the method of least squares. The calculation of coefficients C1, ..., C8, was done in such a way that the deviations of the absorption coefficient should be minimum in relation to the values obtained by the measurements in the impedance tube.

The accuracy of prediction of the absorption coefficient was evaluated on the basis of the value of absolute and relative errors in relation to the measurement values in the impedance tube. The comparative analysis showed that new models for determination of the absorption coefficient give the values of absolute and relative error within the allowed limits, defined for this type of empirical models.

Table 1: Empirical model for determination of acoustic properties of sand

Material	Sand
Longitudinal airflow resistance, $r$ [Pas/m <sup>2</sup> ]	72032
Characteristic impedance, $Z_c$	$Z_c = \rho_0 c_0 \left[ (1 + 0.010 \cdot C^{1.107}) - i(0.492 \cdot C^{0.700}) \right]$
Propagation coefficient, $\gamma$	$\gamma = \frac{2\pi f}{c_0} \left[ (0.840 \cdot C^{0.007}) + i(1 + 0.477 \cdot C^{1.030}) \right]$
Absorption coefficient EN123546:2003	$\alpha_s = \int_0^{\pi/2} \alpha_\varphi \sin 2\varphi d\varphi$
Mean absolute error, $\Delta\bar{\alpha}$	0.0383
Mean relative error, $\bar{\varepsilon}$ [%]	30.69

### 5. MEASUREMENT RESULTS

The measurement results for the absorption coefficient of different patterns of sand on the diagram.

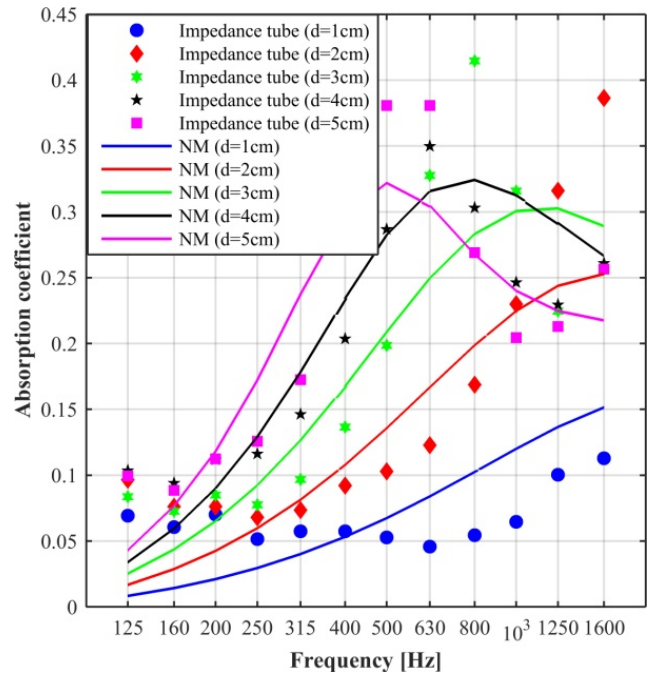


Figure 4: Empirical and experimental values of the absorption coefficient of sand

The following can be concluded for sand:

- the absorption coefficient of sand has considerably lower values than the absorption coefficient of recycled rubber and recycled plastics within the whole frequency range,
- the absorption coefficient of sand also increases with the increase in frequency up to a certain value, and then it decreases and has a maximum at considerably lower frequencies in relation to rubber and plastics,
- the material thickness also influences the increase of the absorption coefficient, but it behaves differently at low and high frequencies. At higher frequencies, over 1000 Hz, there is no point in using materials thicker than 20 mm because they

cause an opposite effect, i.e. they decrease the absorption coefficient. At lower frequencies, e.g. about 400 Hz, the effect of absorption coefficient is evident up to the thickness of 45 mm,

- in comparison with recycled rubber and plastics, sand has considerably worse absorption properties at the frequencies above 630 Hz, but it has considerably better properties at the frequencies from 400 to 630 Hz.

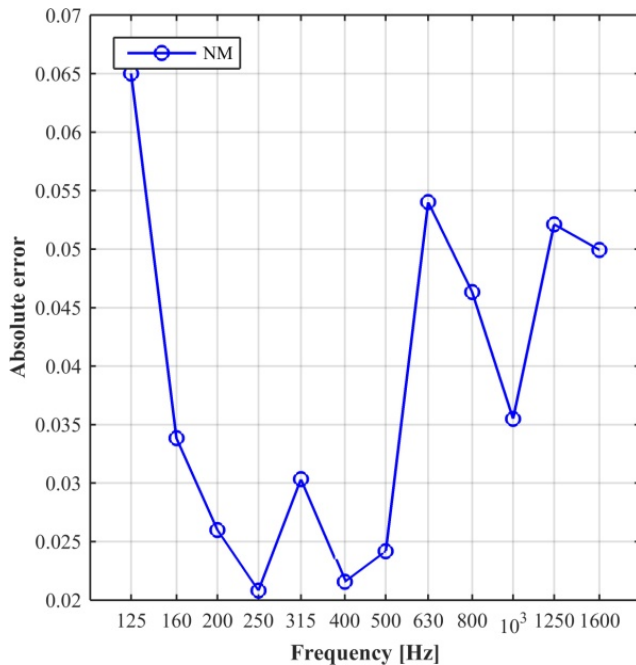


Figure 5: Absolute and relative error model

## 6. CONCLUSION

This paper presents the methodology of forming a macroscopic empirical model to predict acoustic properties of composite sand and polyurethane resins. The measured longitudinal airflow resistance for five different sample thicknesses was used as an input parameter for the model. The new model was confirmed by good absorption properties of composites in relation to recycled rubber and recycled plastic. The mean absolute error of the new model is 3.83% compared to the measured values of sound absorption coefficient in the impedance tube. Based on this, the new model can be considered to be a good estimate of the acoustic properties of sand with the maximum grit size of up to 3 mm, applying a binding agent of polyurethane resin. With the increasing number of materials that can be applied to the new model, one can expect its improvement in terms of predicting acoustic properties. Given that the analyzed material has a granular structure, it is realistic to expect that this model can be applied to predict the acoustic properties of other porous materials with a granular structure.

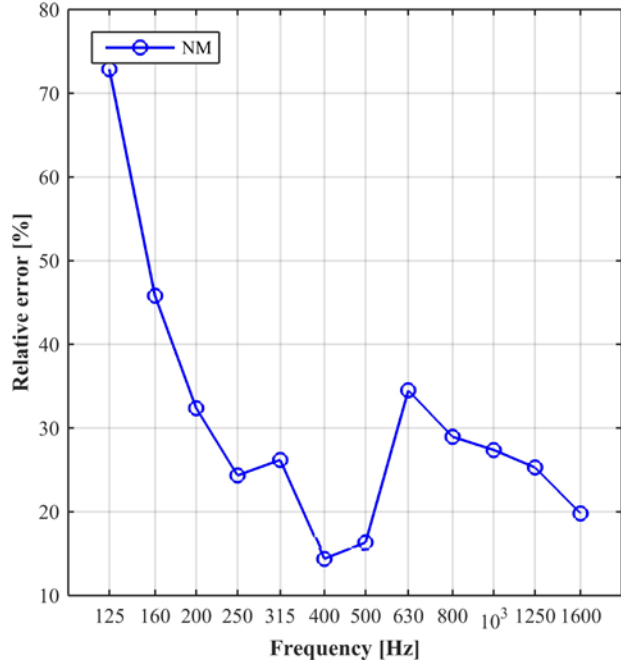
## ACKNOWLEDGEMENTS

The authors express their gratitude to the Ministry of Education, Science and Technological Development of the Republic of Serbia for the support to this research through the project TR37020.

The authors owe special gratitude to the Laboratory for Acoustics of the Faculty of Electrical Engineering in

Belgrade, where part of the measurements presented in this paper was performed.

The deviation of the absorption coefficient obtained by the application of the newly proposed model in relation to the measurements in the impedance tube is 3.83%, [13] which is very good in comparison with the most frequently used limit value of 10% from the available scientific literature. The mean relative error has a slightly higher value of 35%, but it is primarily the consequence of deviations at greater thicknesses of samples and higher frequencies.



Belgrade, where part of the measurements presented in this paper was performed.

## REFERENCES

- [1] M. H. Zainulabidin, M. H. Abdul Rani, N. Nezero, and A. L. Mohd Tobi, "Optimum Sound Absorption by Materials Fraction Combination," *Int. J. Mech. Mechatronics Eng.*, vol. 14, no. 02, pp. 118–121, (2014)
- [2] J. F. Allard and Y. Champoux, "New empirical equations for sound propagation in rigid frame fibrous materials," *J. Acoust. Soc. Am.*, vol. 91, no. 6, pp. 3346–3353, (1992)
- [3] R. Maderuelo-Sanz, J. M. B. Morillas, M. Martín-Castizo, V. G. Escobar, and G. R. Gozalo, "Acoustical performance of porous absorber made from recycled rubber and polyurethane resin," *Lat. Am. J. Solids Struct.*, vol. 10, no. 3, pp. 585–600, (2013)
- [4] H. Soleimani, B. Kord, M. M. Pourpasha, and S. Pourabbasi, "The Relationship Between Plastic Virginity and Engineering Properties of Wood Plastic Composites," *World Appl. Sci. J.*, vol. 19, no. 3, pp. 395–398, (2012)
- [5] H. Soleimani, B. Kord, M. M. Pourpasha, and S. Pourabbasi, "The Relationship Between Plastic Virginity and Engineering Properties of Wood Plastic Composites," *World Appl. Sci. J.*, vol. 19, no. 3, pp. 395–398, (2012)
- [6] S. Mahzan, M. A. Zaidi, N. Arsat, M. N. M. Hatta, M. I. Ghazali, S. R. Mohideen, "Study on Sound Absorption Properties of Coconut Coir Fibre Reinforced Composite

with Added Recycled Rubber" Integrated Engineering, (Mechanical, Materials and Manufacturing), 1–6, (2009)

[7] S. Yilmazer, M. B. Ozdeniz, "The effect of moisture content on sound absorption of expanded perlite plates", Building and Environment, vol. 40, no. 3, pp. 311–318, (2005)

[8] I. Perná, T. Hanzlíček, P. Straka, M. Steinerová, "Acoustic absorption of geopolymer/sand mixture", Ceramics - Silikaty, vol. 53, no. 1, pp. 48–51, (2009)

[9] M. Muravljov (2000) "Građevinski materijali," (IV, vol. 3.2), pp. 179-188

[10] Determination of sound absorption coefficient and impedance in impedance tubes - Part 2: Transfer - function method, EN ISO 10534-2:2001

[11] Acoustics - Materials for acoustical applications - Determination of airflow resistance, ISO 9053:1991

[12] M. Kolarević, B. Radičević, V. Grković, and Z. Petrović, "A Realization of the System for Measuring Airflow Resistance," FACTA Univ. Work. Living Environ. Prot., vol. 12, no. 1, pp. 83–94, (2015)

[13] B. Radičević, "Razvoj modela odlučivanja za izbor optimalne smeše zvučno apsorpcionih materijala," Doktorska disertacija, Fakultet za mašinstvo i građevinarstvo u Kraljevu, Univerzitet u Kragujevcu, Srbija, (2016)





# Flotation Tailings from Copper Mining and Smelting Plant as Mineral Additives for SCC

Saša Marinković<sup>1\*</sup>, Vladimir Mandić<sup>1</sup>, Jovana Bojković<sup>1</sup>, Stefan Mihajlović<sup>2</sup>

<sup>1</sup>Faculty of Mechanical and Civil Engineering/Civil Engineering, University of Kragujevac, Kraljevo (Serbia)

<sup>2</sup>Faculty of Technical Sciences/Civil Engineering, University of Novi Sad, Novi Sad (Serbia)

*Flotation tailings from copper mining and smelting plants are industrial waste and their disposal presents ecological problem. We have investigated usage of two different types of flotation tailings as mineral additives for production of self-compacted concrete (SCC). First tailing is mainly derived from flotation of the mining ore and second is derived from flotation of secondary raw material in copper smelting plant. Mechanical characteristics (compressive, flexural and tensile splitting strength) were tested on specimens of SCC with flotation tailings and compared with mechanical characteristics of commonly used self-compacted concrete with limestone powder as mineral additive. In all concrete mixtures were maintained same water-cement ratio of 0.5 and same water-powder ratio of 0.385.*

**Keywords: Self-compacting concrete, Mechanical characteristics of concrete, Flotation tailing, Limestone powder**

## 1. INTRODUCTION

In the last few decades increasing attention has been directed towards the ecological problems following the fast industrial progress, and one of the most important of these problems is the disposal and recycling of waste materials and industrial by-products. On the other hand, concrete is used very often as the construction material, and since it is possible to add various materials to the mixture, even the industrial waste products, addition of these materials in concrete can contribute to solving the problem of their disposal. However, in order to achieve this goal, it is necessary to find out how these materials affect the characteristics of concrete and in which proportions they can be added to the mixture in order not to disturb the desirable characteristics that make concrete such a useful building material. The aim of this paper is the analysis of influence of flotation tailings, which occurs in the copper production process, used as the mineral additive for concrete, on the compressive, flexural and tensile splitting strength, that in the authors' opinion represents a solid basis for further investigation of the wider use of these, "eco-friendly" concretes in everyday construction practice.

Self-compacting concrete (SCC), according to many authors "the most revolutionary discovery of concrete industry of the 20<sup>th</sup> century", does not need vibrating when placing and compacting. Under the influence of its own weight, it completely fills all parts of the formwork, even in the presence of dense reinforcement. Its advantages are fast construction, a reduced number of required workers, better final surface, easier placement, and increased durability, greater freedom in designing elements, noise reduction, vibration absence, and therefore healthier work environment. It is estimated that when using self-compacting concrete instead of vibrated concrete, the need for workers is reduced by about 10%; when using prefabricated elements, construction time is shorter by about 5%, and demand for workers decreased by about 20%; when applying sandwich elements (steel - concrete) time saving is 20%, and savings in the labour force 50%. The main

disadvantages of the use of self-compacting concrete are higher material prices, stricter quality requirements and increasing pressure on the formwork compared to vibrated concrete. With self-compacting concrete, its most important characteristics are in its fresh state. When designing mixtures, emphasis is placed on the ability of concrete to be levelled out only under the influence of its own weight and to fully fill the formwork of any shape and dimensions without leaving voids, to pass through dense reinforcement without blocking, to retain a homogenous structure without separating aggregate from paste or water from the solid phase, as well as without the tendency of coarse aggregates to "fall" through the concrete mass under the influence of gravity (segregation). Therefore, the key characteristics of fresh SCC are floating, viscosity (expressed by floating rate), passing ability and resistance to segregation [1]. Concrete mixture will be classified as SCC only if all the above properties are fully achieved, wherein each of them can be tested in a number of ways. The basic components of the mixtures in vibrated and self-compacting concrete are the same, but ratios differ, so that SCC contains more fine aggregate and fine particles, as well as additives of the latest generation (modifiers of viscosity and high capacity water reduction) compared to vibrated concrete. Properly designed and placed, SCC is characterized by a greater compactness and homogeneity compared with the vibrated concrete, wherein the properties of the hardened self-compacting concrete are tested in the same way as the corresponding properties of the vibrated concrete.

As the SCC is used more and more widely, pushing the conventional, vibrated concrete out of usage, in this paper we limited ourselves to investigating the influence of the flotation tailings on the characteristics of SCC [2].

During copper production process large amounts of waste material are created that must be disposed. Storage of this material is a major environmental problem. Flotation tailing (FT), as one of the copper production process by-products, is rich in iron oxides and silicates, thus it is suitable for concrete and mortar production. According to its chemical composition, it can be used as a

\*Corresponding author: Faculty of Mechanical and Civil Engineering, Dositejeva 19, 36000 Kraljevo, marinkovic.s@mfkv.kg.ac.rs

supplement to Portland cement or as a substitute for smaller aggregate fractions. In this way it is possible to solve large metallurgical environmental problem with economic benefit, while at the same time reducing greenhouse gas emissions and energy required to produce the same amount of material with preserving natural resources [3]. Onuaguluchi and Eren showed that the concrete with addition of FT has improved mechanical properties compared to the reference concrete. SCC with FT as a mineral additive increased compressive, flexural and tensile splitting strengths. Moreover, increased resistance to abrasion and smaller depth of chloride penetration were observed. These enhanced properties were more notable when using 5% FT and higher water-cement ratio (increased water absorption when using FT) [4]. They also tested chemical effects on concrete with FT and showed that increase presence of FT in the concrete increased the resistance to acid attack, and reduced the resistance to destructive sulfate expansion at the same time [5].

Limestone powder (LS) is more widely used as a cement additive than a concrete additive. SRPS EN197-1:2013 [6] provides two classes of Portland cement with limestone powder whose labels are CEM II/L (or L-L instead of A-L) and CEM II/BL (or L-L instead of B-L). The former contains between 6 and 20% of LS and the latter 21- 35%. Requirements that limestone powder for cement should meet are the following: CaCO<sub>3</sub> content should be greater than 75%, clay content, determined by methylene blue test, must not exceed 1.20g/100g, the total content of organic carbon must not exceed 0.20% for LL limestone powder and 0.50% for L limestone powder. The presence of LS causes the acceleration of the hydration process and hydration shrinkage of concrete in the first few hours, because the particles of LS are used as additional cores for hydration [1].

## 2. EXPERIMENT

For the purposes of the experimental work, three three-fraction concrete mixtures were produced of the self-compacted concrete with different mineral additives: limestone powder and two different types of flotation tailings. SCC mixtures were marked according to used mineral additives: M-LS, M-FT1 and M-FT2, respectively.

The mixtures were produced with Portland cement CEM I 52,5R from the manufacturer: "Holcim" Popovac, which meets all the quality requirements designated with SRPS EN 197-1 standard. Three fractions (0/4 mm, 4/8 mm, 8/16 mm) of natural aggregate from South Morava River were used for production of mixtures from the separation: "Vodogradnja" Ltd. Pukovac. Used aggregate meets all the quality requirements designated with SRPS EN 206-1:2011 [7] and SRPS EN 12620:2010 standards [8]. In all SCC mixtures superplasticizer "TKK Srpenica Cementol Hiperplast 463" was used. Limestone powder as mineral additive was obtained from the "Jelen Do" Ltd. Požega. Both types of flotation tailing were obtained from the "Copper Mining and Smelting Company Bor". In mixture M-FT1 was used first type of flotation tailing (FT1) which is mainly derived from the mining ore and in mixture M-FT2 second type of flotation tailing (FT2) which was obtained from flotation of the secondary raw material in copper smelting plant.

Chemical composition of portland cement (PC) and flotation tailings used in experiment are given in Table 1. which shows that the most silicon dioxide (SiO<sub>2</sub>) was contained in FT1 and that FT2 had higher content of ferro oxides (Fe<sub>2</sub>O<sub>3</sub>). Both types of flotation tailings had high percentage of compounds with pozzolanic properties (SiO<sub>2</sub>, Fe<sub>2</sub>O<sub>3</sub>, Al<sub>2</sub>O<sub>3</sub>), around 70%. Table 1. shows that FT1 had higher presence of undesired aggressive components (S, K<sub>2</sub>O). Limestone powder was mostly comprised of calcium oxide (CaO), around 53%, and because of that LS is more often used as cement additive then a concrete additive. Used LS had content of Ca translated to CaCO<sub>3</sub> around 94%. The presence of other oxides in mineral additives for concrete mixtures was negligible. Chemical analysis of flotation tailings were conducted at the Mining and Metallurgy Institute Bor and composition of LS was provided by manufacturer.

Table 1: Chemical composition of Portland cement and flotation tailings in concrete mixtures

Component [%]	PC	FT1	FT2
SiO <sub>2</sub>	21.62	40.8	33.24
CaO	60.16	7.36	3.61
MgO	2.34	0.86	0.96
Al <sub>2</sub> O <sub>3</sub>	7.0	5.9	5.04
Fe <sub>2</sub> O <sub>3</sub>	2.6	21.72	30.26
K <sub>2</sub> O	0.66	1.2	0.96
Na <sub>2</sub> O	0.33	0.35	0.96
SO <sub>3</sub>	2.55	-	-
S	-	2.35	0.47

Appearance of the LS and FT used in concrete mixtures is shown in Figure 1. and Figure 2, respectively.



Figure 1: Appearance of limestone powder



Figure 2: Appearance of copper flotation tailing

Composition of concrete mixtures is shown in Table 2. The criterion in the designing of mixtures was to achieve the same consistency of concrete, or approximately similar results by slump-flow test. Water-cement ( $w_c$ ) and water-powder ( $w_p$ ) ratios were kept constant in all mixtures, 0.5 and 0.385, respectively. Mass of superplasticizer was modified in all mixtures in order to

fulfill a requirement of roughly the same spreading of fresh mixtures of self-compacted concrete. Specifications, recommendations and possible tolerances for the results of spreading in Slump-flow test were used according to the SRPS EN 12350-8:2012 standard [9] and EFNARC guidelines [10].

Table 2: Composition of concrete mixtures

Mixture ID	Aggregate [kg]			PC [kg]	Water [kg]	Mineral additives [kg]			Superplasticizer [kg]	$w_c$	$w_p$
	0-4 mm	4-8 mm	8-16 mm			LS	FT1	FT2			
M-LS	763	286	541	400	200	120	-	-	7.36	0.5	0.385
M-FT1	763	286	541	400	200	-	120	-	2.8	0.5	0.385
M-FT2	763	286	541	400	200	-	-	120	3.0	0.5	0.385

### 3. TEST RESULTS

For the purpose of the experiment twelve specimens with dimensions 15x15x15cm were created for each mixture in order to test compressive strength and three specimens with dimensions 10x10x40cm for testing of flexural and splitting tensile strength, hence the total number of tested specimens was forty-five. The tests were performed in the Laboratory for construction materials at the Faculty of Civil Engineering and Architecture in Niš.

The fresh concrete tests were done for density, temperature, fluidity - slump-flow test according to SRPS EN 12350-8:2012 [9], viscosity -  $T_{500}$  test according to SRPS EN 12350-8:2012 [9], the ability of passing between the reinforcement - L box test according to SRPS EN 12350-10:2012 [11], segregation resistance - Sieve segregation test according to SRPS EN 12350-11:2012 [12]. The test results for concrete mixtures in a fresh state are shown in Table 3.

All concrete samples matured in the water chamber until the day of testing according to SRPS EN 196-3:2010 standard [13].

Table 3: Properties of fresh concrete mixtures

Mixture ID	M-LS	M-FT1	M-FT2
Temperature [°C]	23.1	21.4	22.2
Slump-flow test [mm]	650	655	660
$T_{500}$ test [s]	3.5	6.0	6.5
L-box test $H_2/H_1$ [mm/mm]	0.94	0.91	0.92
Sieve stability test [%]	14.0	6.75	6.0
Density [kg/m <sup>3</sup> ]	2375	2398	2405

The compressive strength of concrete was measured on the specimens after aging of 2, 7, 28 and 90 days and was determined according to SRPS EN 12390-3:2010 standard [14]. Average values on three specimens of compressive strength are shown in Table 4. Testing of compressive strength was performed on hydraulic press as shown in Figure 3 (left).



Figure 3: Testing of compressive strength (left); Testing of flexural strength (right)

The change of the measured compressive strength over time for specimens of all concrete mixtures is shown in Figure 4. The correlation coefficients are in the range of

$R^2=0.9794$  (for mixture M-FT1) to  $R^2=0.9977$  (for mixture M-LS) which indicates good approximation of functions for the change of compressive strength over time.

Table 4: Compressive strength test results

Mixture ID	Compressive strength [Mpa]			
	2 days	7 days	28 days	90 days
M-LS	39.6	49.1	57.3	65.1
M-FT1	35.8	44.8	59.3	64.2
M-FT2	36.6	46.2	59.7	64.7

Flexural strength was determined according to SRPS EN 12390-5:2010 standard [15] on concrete specimens after aging of 28 days. Testing of flexural strength was performed on hydraulic presse as shown in Figure 3 (right). Test results are shown on chart at Figure 5.

Tensile splitting strength was also tested on concrete specimens after aging of 28 days according to SRPS EN 12390-6:2012 standard [16]. Test results are shown on chart at Figure 6.

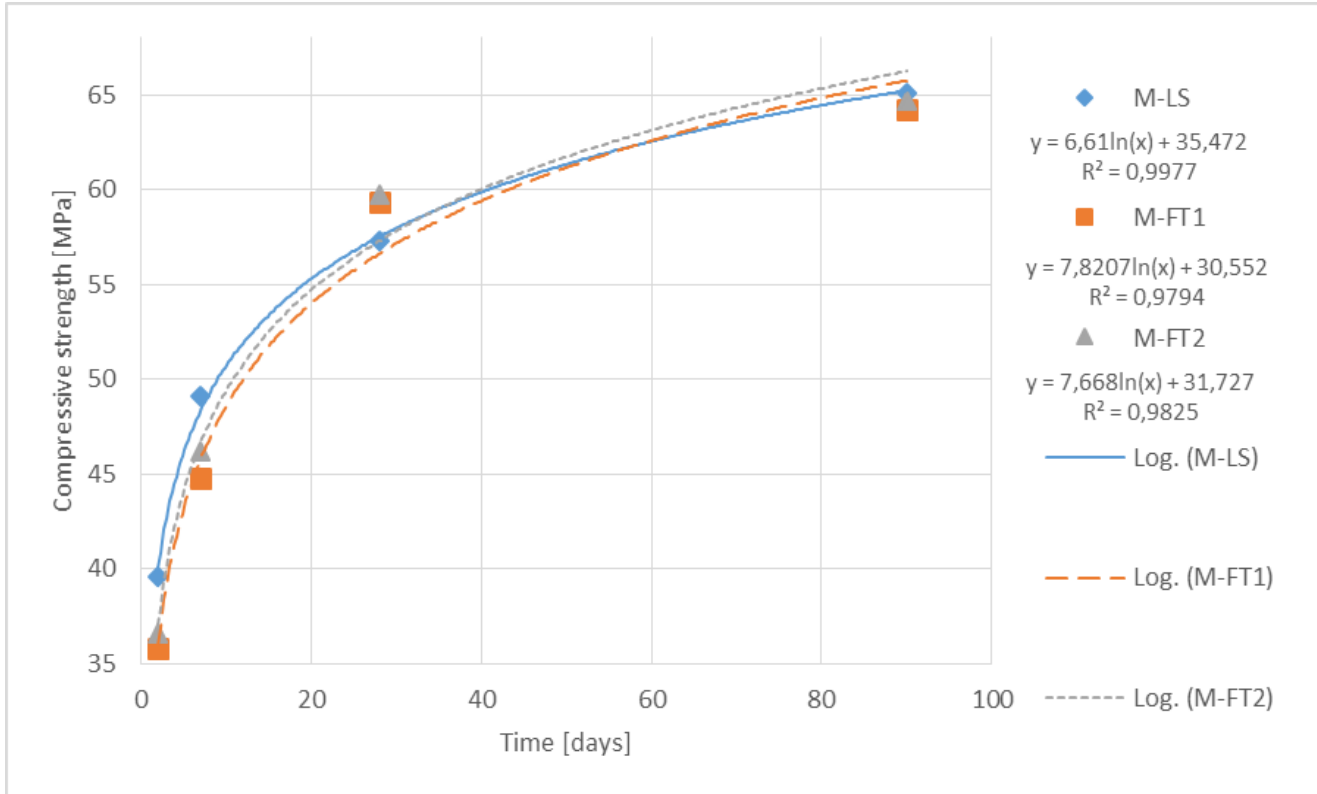


Figure 4: Change of compressive strength over time on tested specimens

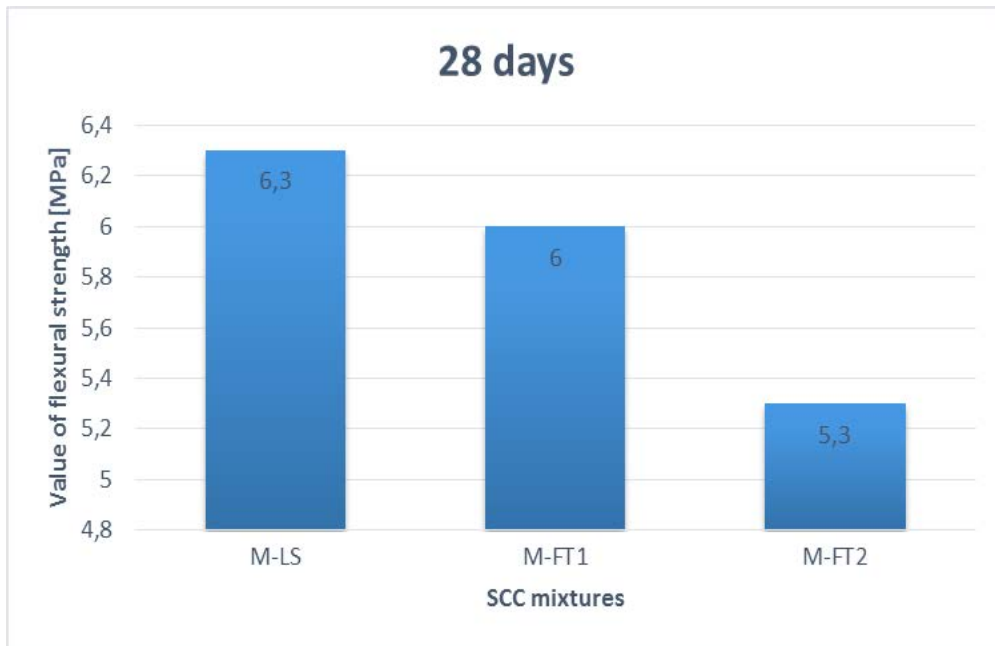


Figure 5: Flexural strength of SCC mixtures after 28 days of aging

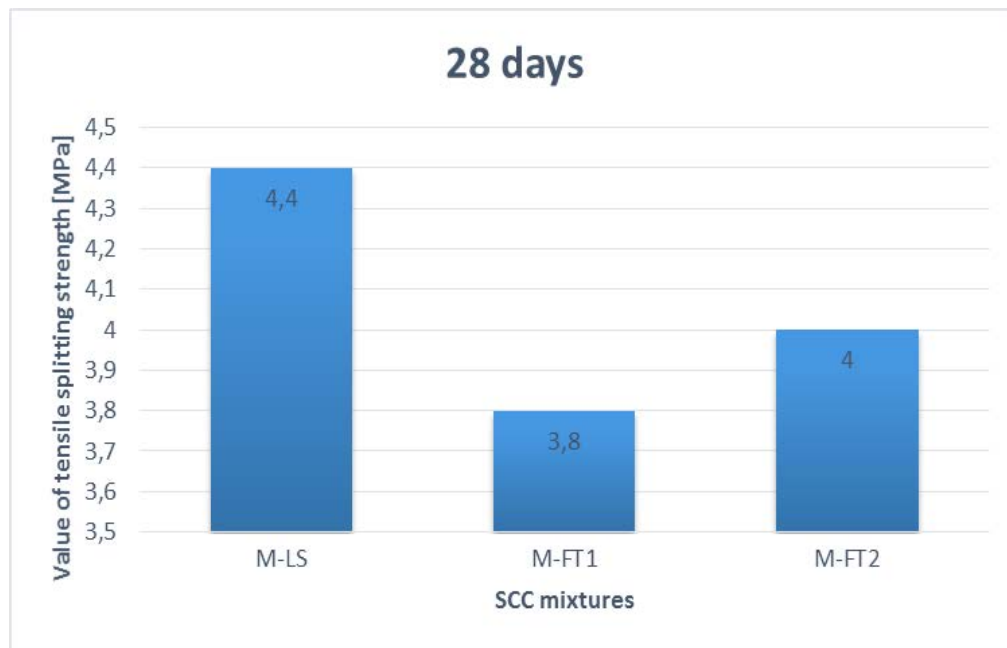


Figure 6: Tensile splitting strength of SCC mixtures after 28 days of aging

#### 4. DISCUSSION OF THE RESULTS

##### 4.1. Properties of fresh concrete mixtures

Spreading or flowability of mixtures was measured using Slump-flow and  $T_{500}$  tests. Slump-flow showed spreading of mixtures in range of 650 to 660 mm. Difference of only 1cm was good indicator that objective of creating mixtures with similar consistencies was achieved. M-LS showed the lowest, while M-FT2 showed the highest flowability. Only M-FT2 belong to class SF2 (660-750 mm) while SCC mixtures with flotation tailings can be classified into class SF1 (550-650 mm).

$T_{500}$  test shows time in which concrete reaches 500 mm diameter of spreading.  $T_{500}$  time is a measure of the speed of flow and hence the viscosity. Results obtained by this test were in range of 3.5 to 6.5 seconds. Mixtures with flotation tailings were less flowable than mixture with limestone powder. M-FT2 had time that deviated from recommended values (3.5-6s), but still showed good viscosity. Time longer than 2 seconds classifies all mixtures as VS2. No segregation was observed, nor water separation.

The L-box test was used to determine passing ability of SCC mixtures through reinforced area. Passing ability is calculated as the ratio of height of concrete remaining at the leading edge in the horizontal section to that in the vertical section. Test was conducted with 3 reinforcement bars and the obtained results were between 0.91 and 0.94 showing good passing ability for all mixtures and classifying them into PL2 class ( $>0.8$ ). The highest passing ability had M-LS.

Segregation resistance of fresh SCC was tested with the sieve stability test. The highest percentage of cement paste passing through sieve had M-LS (14%) which was over 100% higher than passing through sieve of mixtures with flotation tailings (6.75% for M-FT1 and 6% for M-FT2). Results showed good segregation resistance for all mixtures and passing percentage lower than 15% classifies them into SR2 class.

All tests on fresh concrete showed good and similar consistency of all mixtures. Best properties of self-compacting were achieved by using limestone powder. M-LS had the best fluidity and viscosity, after passing through reinforcement concrete was almost horizontal, but it had minimum segregation resistance. Tests confirmed that concrete containing flotation tailings is more cohesive and less prone to segregation and therefore less workable mixtures. M-FT2 had better ratio of diameter of spreading (fluidity) and segregation resistance and smaller difference at the ends of L-bo than M-FT1.

All SCC mixtures had similar densities. M-LS had the lowest density in the fresh state and among mixtures with flotation tailings M-FT2 had the highest density (0.3% higher than M-FT1 and 1.3% higher than M-LS). Higher density of mixtures with flotation tailings can be explained by lower participation percentage of superplasticizer in order to satisfy the desired flow properties, meaning that aggregate, cement and the mineral additive have greater share in 1 m<sup>3</sup> of concrete. In the same way, the lowest density of M-LS can be explained by the highest participation percentage of superplasticizer, and thus the lower percentage share of aggregate, cement and mineral additives compared to the other mixtures.

##### 4.2. Compressive strength

The highest value of the compressive strength after 2 days was recorded in M-LS and it was 10.6% higher than of M-FT1 and 8.2% higher than of M-FT2. M-LS had the highest compressive strength after 7 days, which was 9.6% higher than compressive strength of M-FT1 and 6.3% higher than strength of M-FT2. After 28 days M-FT2 had the highest compressive strength and it was 0.7% higher than the strength of M-FT1 and 4.2% higher than the strength of M-LS. On specimens after 90 days of aging again was recorded the highest compressive strength in M-LS which was 0.6% higher than strength of M-FT2 and 1.4% higher than strength of M-FT1. Order of strength

among SCC mixtures had changed only at 28 days when M-LS had the lowest result.

The presence of limestone powder in concrete accelerate the reactions of hydration, thus giving M-LS higher early strengths in comparison with mixtures with flotation tailings. Among mixtures with flotation tailings M-FT2 had higher compressive strength in each time period of testing. Slower early strengths of concrete with flotation tailings prevent their application where high early strength is expected, which can be solved by using accelerator. Differences in compressive strength between concrete with limestone powder and concrete with flotation tailings did not exceeded 10.6% at the same quantities of cement. Concrete with LS had better performances in the fresh state, what should be borne in mind, particularly if the economic factor is included, but concrete with tailings have greater ecological value because they solve the problem of depositing huge quantities of waste material.

#### 4.3. Flexural strength

Among SCC mixtures, M-LS had the highest flexural strength after 28 days which was 18.9% higher than the flexural strength of M-FT2 and 5% higher than the strength of M-FT1. M-FT1 had 13.2% higher flexural strength than M-FT2. Replacement of the certain amount of the filler in the mixtures with mineral additives reduces the porosity, and fine particles become additional hydration centers, which leads to better hardening of the cement paste, and increased flexural and tensile splitting strengths compared to concrete without mineral additives.

#### 4.4. Tensile splitting strength

When SCC mixtures were compared among themselves, M-LS had the highest tensile splitting strength after 28 days, which was 15.8% higher than the lowest strength of M-FT1 and 10% higher than the strength of M-FT2. M-FT2 had 5.3% higher tensile strength than M-FT1. Different mineral additives have different effects on increase of tensile strengths which originates from the differences in microstructure of these materials, and at the same time there is not a direct link between tensile strength and compressive strength.

### 5. CONCLUSION

The primary objective of this study was to evaluate influences on mechanical properties of SCC with two different types of flotation tailings as mineral additives and compare results with properties of SCC with limestone powder (LS) as mineral additive. First type of used flotation tailing was derived from mining ore (FT1) and second type was derived from secondary raw material in copper smelting plant (FT2). Results from the study indicate the following:

- The mixtures with flotation tailings had higher density than mixture with LS.
- The mixture with LS had the highest workability among SCC mixtures and mixture with FT2 had better workability than mixture with FT1.
- The mixture with LS had the highest compressive strength and mixture with FT2 had higher compressive strength than mixture with FT1.

- The mixture with LS had the highest flexural strength after 28 days among SCC mixtures and mixture with FT1 had higher flexural strength than mixture with FT2.

- The mixture with LS had the highest splitting tensile strength after 28 days among SCC mixtures and mixture with FT2 had higher tensile strength than mixture with FT1.

This research has proved that it is possible to use considered flotation tailings as mineral additives in self-compacting concretes, which would help solving the environmental problem of disposing this waste materials, and would obtain concrete with similar mechanical properties compared to SCC with limestone powder as mineral additive. SCC mixture with FT2 as mineral additive proved to be more favorable in comparison to other SCC mixture with FT1 as mineral additive.

### REFERENCES

- [1] I. Despotović, "Influence of different mineral additives on properties of self-compacted concrete", PhD Thesis, University of Niš (Serbia), (2014)
- [2] N. Stirmer, I. Banjad Pecur, "Mix design for self-compacting concrete," *Gradjevinar*, Vol. 4, pp. 321–329, (2009)
- [3] C. Shi, C. Mayer, A. Behnood, "Utilization of copper slag in cement and concrete," *Conservation and Recycling*, Vol. 52, pp. 1115-1120, (2008)
- [4] O. Onuaguluchi, O. Eren, "Copper tailings as a potential additive in concrete: Consistency, strength, and toxic metal immobilizer," *Indian Journal of Engineering & Materials Sciences*, Vol. 19, pp. 79-86, (2012)
- [5] O. Onuaguluchi, O. Eren, "Cement mixtures containing copper tailings as an additive: durability properties," *Materials Research*, Vol. 15, pp. 1029-1036, (2012)
- [6] SRPS EN197-1:2013 Cement - Part 1: Composition, specifications and conformity criteria for common cements, The Institute for Standardization of Serbia, (2013)
- [7] SRPS EN 206-1:2011 Concrete - Part 1: Specification performance, production and conformity, The Institute for Standardization of Serbia, (2011)
- [8] SRPS EN 12620:2010 Aggregates for concrete, The Institute for Standardization of Serbia, (2010)
- [9] SRPS EN 12350-8:2012 Testing fresh concrete - Part 8: Self-compacting concrete - Slump-flow test, The Institute for Standardization of Serbia, (2012)
- [10] EFNARC: Specification and Guidelines for Self-Compacting Concrete, European Federation of National Associations Representing for Concrete, (2002)
- [11] SRPS EN 12350-10:2012 Testing fresh concrete - Part 10: Self-compacting concrete - L box test, The Institute for Standardization of Serbia, (2012)
- [12] SRPS EN 12350-11:2012 Testing fresh concrete - Part 11: Self-compacting concrete - Sieve segregation test, The Institute for Standardization of Serbia, (2012)

- [13] SRPS EN 196-3:2010 Methods of testing cement - Part 3: Determination of setting times and soundness, The Institute for Standardization of Serbia, (2010)
- [14] SRPS EN 12390-3:2010 Testing hardened concrete - Part 3: Compressive strength of test specimens, The Institute for Standardization of Serbia, (2010)
- [15] SRPS EN 12390-5:2010 Testing hardened concrete - Part 5: Flexural strength of test specimens, The Institute for Standardization of Serbia, (2010)
- [16] SRPS EN 12390-6:2012 Testing hardened concrete - Part 6: Tensile splitting strength of test specimens, The Institute for Standardization of Serbia, (2012)





# Research of Shear Strength and Compatibility by Heat Conditioning of Sheets for Waterproofing used in Concrete Bridge Decks

Eng. Nikolina Porozhanova  
VTU "Todor Kableshkov", 158 Geo Milev str., Sofia, Bulgaria

*This report views the basic characteristics of the already applied over the bridge bitumen waterproofing membranes and the significance of these characteristics for the facility durability. Examined are two of these characteristics of the already applied over the bridge bitumen sheets for waterproofing and the significance of these characteristics for the durability of the equipment. The methods for testing these characteristics are presented and the shear strength and compatibility in terms of heating of the different types of bituminous waterproofing are examined.*

**Keywords: waterproofing sheets, shear strength, compatibility by heat conditioning**

## 1. INTRODUCTION

Bridges are one of the most responsible transport facilities. Proper protection from the harmful effects of surface and ground water, and icing agents used in winter road maintenance are the basis for the provision of transport's operating performance and their bearing capacity.

Concrete road bridges are among the most important transportation facilities of our daily life. They are found frequently not only outside, but very often inside residential places. Their proper protection and resistance to water, moisture and corrosion is of key importance, in order to be safe for exploitation by people.

The main goal of bridges waterproofing is to protect their construction against impact by water, moisture, and their corrosive action.

The modern development of the chemical industry, especially in the building and building materials industry, has also contributed to the development of new waterproofing systems with faster, easier and safer application. Products with features that allow a shorter period of time to produce a sufficiently robust, ready-to-use layer, on which construction works can continue without problems, are increasingly emerging.

The bridges waterproofing has to prevent water penetration to the construction. The waterproofing is used between the concrete bridge desk and the asphalt concrete overlay. It is laid directly under the road surface, which is most exposed to weather events and impacts. The materials used for concrete bridge surfaces waterproofing are the following:

- mastic asphalt;
- liquid rubber compositions – they are a two-component polymer-bitumen mixture, in which two components are mixed immediately prior to application and form a thin film adhered to the base;
- resins/polyurethane – this is also a modern system for waterproofing which is stored in liquid form and is applied as a spray on the concrete surface. The resulting layer is

continuous - without seams and splices, with high elasticity and resistance to joints;

- plastic and rubber sheets;
- bitumen-polymer membranes.

The bitumen-polymer membranes are quite recently applied and their share in comparison to the other waterproofing materials types is growing. The road surface asphalt is laid directly above waterproofing membranes. Bitumen is modified with SBS (styrene-butadiene-styrene rubber) elastomer or APP (atactic polypropylene polymer) plastomer. The use of different modifiers is to achieve varying degrees of better physical and mechanical properties of waterproofing.

The bitumen sheets, modified with APP can be used at much higher temperatures - from 130 to 150 ° C, in comparison to the materials of oxidized bitumen, which tolerate only up to 70 - 80 ° C. Thanks to this property, they age 3 to 4 times slower than waterproofing bitumen, as cracks begin to appear only after 10 to 15 years. Increased heat resistance allows this type of waterproofing to be used to treat vertical and sloping surfaces without softening. Most applications are used to protect flat, open surfaces at high summer temperatures, which, combined with the ability to run without a protective layer, makes them ideal for waterproofing bridges.

The styrene-butadiene-styrene (SBS) modified bitumen waterproofing also has increased heat resistance compared to oxidized bitumen to 120 ° C, but it is lower than that of the APP modified bitumen. Due to this fact, the latter are best suited for the processing of flat, open surfaces at high atmospheric temperatures. The advantage of SBS modified waterproofing lies in the increased resistance to low temperatures. This kind of materials has high elasto-plastic properties, which are retained even at low temperature of application - to -35°C. Very good adhesion to bituminous pre-treated concrete surfaces is achieved, which is extremely important in bridge constructions. Among them are the qualities and durability, and slow aging.

Polyester nonwoven fabric is used as reinforcing basis. It gives significantly better physical and mechanical

properties, very high tensile strength and low deflection at break. Thus waterproofing membranes achieve high mechanic performance.

## 2. WATERPROOFING SYSTEM

A bridges waterproofing system presents layers between the bridge concrete slab and the surface covering (Figure 1). Usually this system consists of a bitumen primer, one or more bitumen membrane layers and a protective layer, if it is specified by the manufacturer.

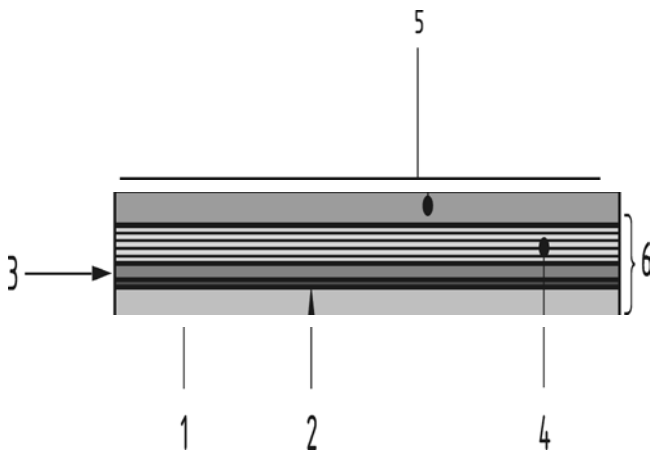


Figure 1: Components of a Bridge Waterproofing System

### Legend:

1. Bridge concrete slab;
2. Primer;
3. Reinforced bitumen sheet(s)
4. Protective layer;
5. Surface covering;
6. Bridge waterproofing system (2 + 3 and 4, if specified).

Bitumen sheets which are part of waterproofing systems have the following basic characteristics:

- visual defects – the product should not have any visible defects;
- mass per unit area;
- thickness;
- tensile properties;
- water tightness;
- cold flexibility - this test did not gives results that directly meet the requirements of practical application;
- flow resistance at elevated temperature;
- water absorption;
- size stability at high temperature.

The following characteristics are specific only for bitumen waterproofing sheets for application of concrete bridges:

- initial amount of protective mineral coating on the membrane surface mainly with the grain size of more than 0,125 mm. It is important to be determined, as too high surface protection may cause sliding between the membrane and the layer above it;
- size stability of bitumen waterproofing

membranes for concrete bridges to be specified according to [EN 1107-1], but at the temperature of 160°C. This test simulates the effect of the cast asphalt application above the membrane.

- thermal aging performance is estimated during exposure to the temperatures from -15°C to +100°C – to check the behavior on thermal aging product characteristics, which should be determined before and after testing in accordance with [EN 1296] for a period of 12 weeks. The relevant characteristics are cold flexibility and flow resistance at elevated temperatures. The purpose of the test in accordance with [EN 1296] is to characterize the thermal stability of bitumen in terms of durability.

The waterproofing must have a certain mechanical resistance to be able to handle the specific loads and impacts to which the bridge is exposed. The waterproofing is subject to the same effects: i.e. shock, temperature and weather impacts, mechanization load during the asphalt laying and compaction, continuous dynamic loads caused by the passing vehicles, etc. The characteristics of the already applied waterproofing are therefore as important as described in the standard – [EN 14695] – “Flexible sheets for waterproofing. Reinforced bitumen sheets for waterproofing of concrete bridge decks and other trafficked areas of concrete. Definitions and characteristics”. They are to be considered during concrete applications. They are:

- bond strength /adhesion/ to concrete base – a basic requirement to ensure the waterproofing system durability is to strictly follow the application technology. Very good adhesion to surfaces, especially to the concrete ones is necessary to be ensured to keep the insulation from damages in case of the bridge construction deformation;
- shear strength - determines the shear resistance of the waterproofing system laid above a concrete surface, covered with an asphalt layer;
- crack bridging ability – ability of reinforced bitumen membranes to withstand movements of the crack of the concrete base without deterioration their quality;
- compatibility by heat conditioning – characterizes the ability of waterproofing to keep their properties for a long period of time;
- resistance to compaction of an asphalt layer – determines the ability of waterproofing systems to resist damage from compaction of an asphalt layer;
- resistance to dynamic water pressure after damage by pre-treatment – determines the water tightness of the applied waterproofing system;

- behavior of bitumen sheets during application of mastic asphalt – determines their resistance to the bitumen component increase when laying mastic asphalt. The report explores two of these essential characteristics: shear strength and compatibility by heat conditioning;

### 3. DETERMINATION OF SHEAR STRENGTH

The purpose of the test is to determine the shear strength properties of the waterproofing system.

This test simulates action of dynamic forces, e.g. braking. Shear strength – shear stress at maximum force, when testing the shear resistance in a waterproofing system. The principle of the test is according to [EN 13653]: a force is induced in the waterproofing system laid between base specimen and asphalt layer to determine the shear strength of waterproofing. Testing is carried out in compression at constant displacement rate. The force is applied at an angle of 15° to the plane of shearing. The loading is applied through the center of the waterproofing by loading device capable of producing a maximum load of 10 kN at a displacement rate relative to the supports of (10 ± 1) mm/min.

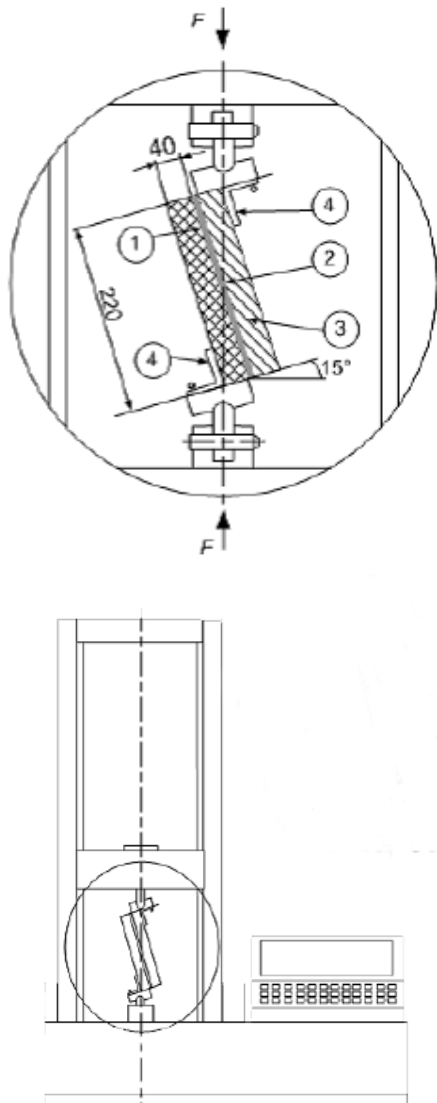


Figure 2: Example of loading device

#### Key:

- base specimen
- waterproofing
- asphalt layer
- adjustable support

Four different waterproofing sheets of the same type were subjected to the test. These are called: sample 1, sample 2, sample 3 and sample 4. The main characteristics of these sheets are given in Table 1:

Table 1: Main characteristics of sheets

Characteristics	Sample 1	Sample 2	Sample 3	Sample 4
Carrier	Polyester nonwoven	Polyester nonwoven	Polyester nonwoven	Polyester nonwoven
Thickness	4,5 mm	4,5 mm	4,5 mm	4,5 mm
Mass per unit area	5,2 kg/m <sup>2</sup>	5,4 kg/m <sup>2</sup>	5,6 kg/m <sup>2</sup>	5,2 kg/m <sup>2</sup>
Tensile properties, N/50 mm				
- longitudinal	830	950	1050	900
- transverse	720	800	970	780
Watertightness	200 kPa	200 kPa	200 kPa	200 kPa
Water absorption	0,3%	0,4%	0,2%	0,25%
Cold flexibility	-10°C	-10°C	-10°C	-10°C
Flow resistance at elevated temperature	120°C	120°C	120°C	120°C

All these waterproofing sheets have no visual defects – no blisters, cracks, holes and bare surfaces.

Four test pieces of each of the waterproofing sheets under test were prepared to perform the test. The test specimens prepared in accordance with [EN 13375]. Pre-prepared concrete slabs with a thickness of 40 mm and dimensions 220 mm x 110 mm. The surface shall be clean and dry and free of all dust or laitance, and have a surface texture of 0,5 mm to 1,0 mm. The waterproofing system is applied on to the thus prepared slab – bitumen primer and after its drying – waterproofing sheet by torch-on-welding. After cooling to room temperature, the waterproofing is cut along the edges of the concrete slabs and an asphalt layer is applied. The asphalt layer is a bituminous mixture of the following composition:

- aggregates: < 0,063 mm: 8 ± 0,5 % by mass  
0,63/2 mm: 32 ± 2 % by mass  
2/6 mm: 25 ± 2 % by mass  
6/10 mm: 35 ± 2 % by mass
- binder type: 40/60 according to EN 12591;
- binder content: (5,9 ± 0,5) % by mass;
- laying temperature: (160 ± 10) °C;

- thickness:  $(40 \pm 5)$  mm,  
The asphalt layer was sealed to obtain the content of voids between 5% and 9%.

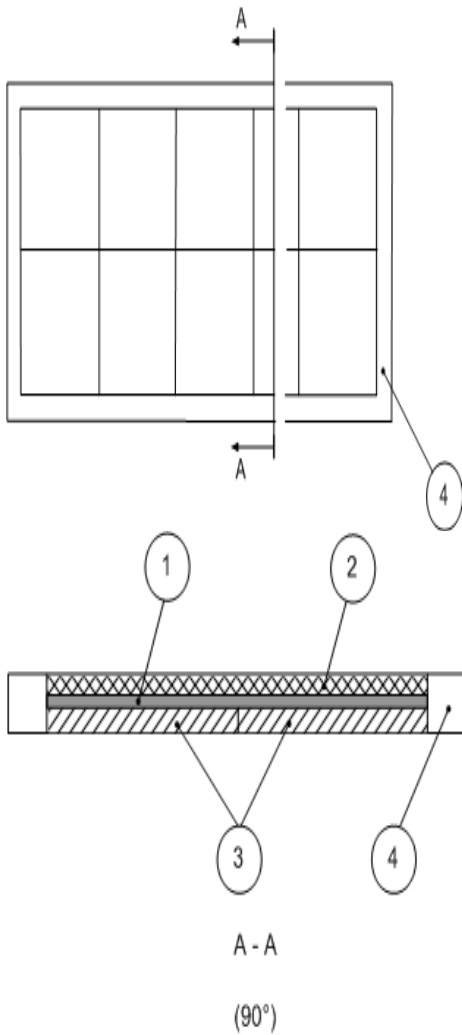


Figure 3: Application system for the test specimens (example)

**Key:**

1. waterproofing system
2. asphalt layer
3. base specimen
4. steel frame

Prior to testing the test specimens are conditioning at a test temperature 23°C for 24 hours. The longer dimension of the test specimen is in longitudinal direction of the flexible sheet.

The test specimen is placed in a material testing machine – a dynamometer fitted with an adapter for attaching the sample at an angle of 15°.



Figure 4: Test specimen before loading

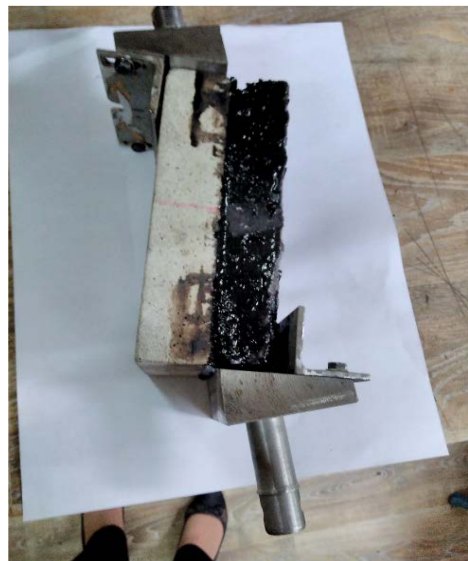


Figure 5: Test specimen before loading

A constant displacement is applied at a rate of 10 mm/min.



Figure 6: Test specimen after loading



Figure 7: Test specimen after loading

In the test the shearing occurs at the surface of the waterproofing system and the base.

The shear strength in N/mm<sup>2</sup> is calculated using the equation:

$$\tau_{\max} = (F_{\max} / A) \times \cos 15^\circ \quad (1)$$

where

$\tau_{\max}$  is the shear strength, in N/mm<sup>2</sup>

$F_{\max}$  is the recorded maximum force, in N

A is the test area of the test specimen, in mm<sup>2</sup>

The results are given in Table 2:

Table 2: Shear strength

	Sample 1	Sample 2	Sample 3	Sample 4
$\tau_{\max}$	15	20	24	22

#### 4. COMPATIBILITY BY HEAT CONDITIONING

Waterproofing systems are required to maintain performance over extended periods of time once installed on a concrete structure. Many flexible sheets used in the waterproofing of concrete bridge decks are based on materials that are subject to oxidation, migration, diffusion, and absorption of components within the system itself and/or those to which the system is adhered. These physicochemical effects occur over time, however, increased temperature will accelerate these effects.

The use of an accelerated heat-conditioning test will allow the evaluation of the change in a specific mechanical property, shear strength, over a significantly shorter time period than allowing the waterproofing system to age under normal ambient conditions. The use of the shear resistance test will allow the determination of any change in properties together with an indication of any migrational or interfacial long term incompatibility between the adherents.

The purpose of the test is to determine the compatibility of the waterproofing system in the installed condition by determination of the shear strength properties before and after accelerated heat conditioning. Heat conditioning is a process whereby the test specimen is held at an elevated temperature for a specified period of time.

By changing the shear resistance shifts in the properties of test specimens can be detected, when they are subjected to accelerated heat conditioning.

Eight test pieces of each of the waterproofing sheets under test were prepared. The type and dimensions of the test specimens are the same as those for testing the shear strength. Four test specimens are used for the heat conditioning, and four reference test specimens are used for comparison.

The four reference test specimens are conditioned at 23°C for 24 h prior to them being tested in accordance with [EN 13653] for shear strength. The other test specimens are placed horizontally in air-circulating oven in such a way as to allow free movement of air over and around the test specimen the temperature in the oven is (50 ± 2) °C. They stay in the dryer for 91 days, then they are removed, allowed to stand at a temperature (23 ± 2) °C for 24 hours and tested for shear strength. Before and after the test for shear strength, the test specimens were viewed visually for evidence of migration and separation of component layers. Such were not noticed.



Figure 8: Test specimen after conditioning



Figure 9: Test specimen after conditioning

Compatibility C (%) is expressed by:

$$C = \left( 1 - \frac{\tau_{\max 0} - \tau_{\max C}}{\tau_{\max 0}} \right) \times 100 \quad (2)$$

where

$\tau_{\max 0}$  = mean value of shear strength of reference test specimens;

$\tau_{\max C}$  = mean value of shear strength of conditioned specimens.

The results are given in Table 3:

Table 3: Compatibility by heat conditioning

	Sample 1	Sample 2	Sample 3	Sample 4
C %	81	85	84	80

### 5. CONCLUSION

Testing of basic characteristics related to the laying of waterproofing of bridges has been done for the first time in Bulgaria.

The tested waterproofing sheets show good results and good bond between the asphalt coating and the waterproofing system, which suggests that these materials retain their durability (permanence).

The basic requirement to ensure the durability of the waterproofing system has to be followed strictly, technology application must provide very good adhesion to surfaces in order to avoid compromising insulation deformations in bridge construction. Secure and properly laid waterproofing is a must for maintaining the reliability and trouble-free operation of bridge facilities. The examinations will continue with the characteristic – crack bridging ability.

### ACKNOWLEDGEMENTS

Thanks to the BUILDING RESEARCH INSTITUTE – NISI for the opportunity to carry out these tests using their laboratory and appliances.

Special thanks to the company "IZOLA-PETROV" Ltd., without whose assistance and support it would not have been possible to carry out this study.

### REFERENCES

- [1] EN 14695
- [2] EN 13596
- [3] EN 13653
- [4] EN 13375
- [5] EN 14691
- [6] EN 1296
- [7] EN 1107-1

# Welding of the Reservoirs for Oil Derivatives Storage with Self-shielded Cored Wire

Radomir Jovičić<sup>1\*</sup>, Olivera Erić Cekić<sup>2</sup>, Aleksandar Sedmak<sup>1</sup>, Sanja Petronić<sup>1</sup>, Vukić Lazić<sup>3</sup>

<sup>1</sup>University of Belgrade, Innovation Center of Faculty of Mechanical Engineering, Belgrade, Serbia

<sup>2</sup>University of Kragujevac, Faculty of Mechanical and Civil Engineering, Kraljevo, Serbia

<sup>3</sup>University of Kragujevac, Faculty of Engineering University of Kragujevac, Serbia

## Abstract

Until recently, *E* procedure (welding with coated electrodes) had been used for welding of oil derivative storage tank shell with volume up to 10.000m<sup>3</sup>. This procedure led to shell deflection due to a low welding speed and large number of extensions. Recent constructions of oil derivative storage tanks are improved with installed floating membrane. By floating on the surface of the working fluids, membrane substantially reduce evaporation. Given the fact that the pressure in the tank has to be equal to atmospheric pressure, the membrane significantly reduces the losses of the working fluid and the environmental pollution. In order to ensure free movement of the membrane and that the sealing between the membrane and shell is good enough, the storage tank shell must be strictly cylindrical and more accurately developed than in the case with previously made storage tanks. This is achieved with self-shielded core wire welding of oil derivative storage tanks.

**Keywords:** welding, strain, reconstruction, the reservoirs for oil derivatives storage, self-shielded wire

## 1. INTRODUCTION

Oil derivatives are flammable materials and big polluters. They are stored in a vertical cylindrical, above ground tanks. The construction of storage tanks is constantly improving in order to reduce a risk of fire, pollution of the environment and to minimize evaporation losses of derivatives in the atmosphere.

### 1.1. Storage tanks description

Figure 1 shows a storage tank with a volume of 5000 m<sup>3</sup>, a diameter of 25.1 m and a height of 13.7 m, which is made of low-carbon structural steel S235JRG2 [1]. Bottom of the tank is made of steel panel, which are interconnected by a foldable weld. The casing of the tank is composed with six frontally welded ring segments. The thickness of the first segment is 14 mm. The thickness of remaining segments is gradually reduced, so thickness of the sixth segment is 8 mm. The tank shell have inlet and pipe connectors for loading and unloading the tank. The tank roof is made of a supporting grid structure and cladding that includes the connector for measuring the level of the working medium and connector for equalizing the pressure in the tank to atmospheric pressure. In addition to pipeline filling and discharging, the tank have also a piping fire-extinguishing system and pipelines for cooling the water tank. Since they are flammable petroleum products and major polluters, the tanks are placed in concrete pools "bund", whose role is to prevent spilling of the working medium in the case of a leaking tank or in the case of fire.



Figure 1. Storage tank for oil derivatives

## 3. PRESSURE CHANGES IN THE STORAGE TANK

Due to the large cross-sectional area of the storage tank, even small changes in pressure can cause the emergence of great powers in the construction of tanks [2]. Changes in the storage tank pressure occurs when the level of working medium change, tank filling and tank discharging and changes in ambient temperature. With increasing ambient temperature the pressure in the tank increases due to the expansion of the working medium and increased evaporation. The problem is particularly acute when the working medium is gas. In the case of the fall of the ambient temperature the pressure in the reservoir decreases due to reduction of the volume of the working medium, and due to reduction of the volume of the gaseous phase above the working medium.

Described pressure changes are large enough that can lead to failure of the storage tank.

Therefore, so-called respiratory valve is installed on the storage tank, whose role is to continuously equalizes the pressure in the tank to atmospheric pressure. The result of

releasing steam of working medium by the the respiratory valve into the atmosphere cause environment polluting and material losses. The size of these losses is proportional to the surface of the working medium, ie. the size of the storage tank. In large tank volume of 60,000 to 80,000 m<sup>3</sup>, which are currently being built, the losses due to release steam of the working medium into the atmosphere are very large. This problem is so far, to a lesser extent, solved by cooling water tank.

#### 4. STORAGE TANKS STRUCTURE IMPROVING

New constructive solution which reduce losses due to evaporation of the working medium are floating membrane [1]. These membranes swim on the surface of the working medium and must well sealed the space within the shell of the tank. They are made of a thin aluminum sheet that is placed on floats. In order to perform its function, membranes must be free to move around the height of the tank, which means that the tank shell can't have any deformation that would hinder this movement. Picture 2 show the installation of a floating membrane.



Picture 2. Installation of aluminum floating membrane in the storage tank

#### 5. WELDING OF TANK SHELL WITH ATTACHED FLOATING MEMBRANE

The construction of oil products storage tanks are characterized by large diameters, relatively small thickness of the walls and the tread of great length welds in coatings. These structures are prone to deformations in welding [3]. The E process was used earlier for welding storage tank shells. This process is characterized by small welding speed and a relatively high heat input [4]. Under these conditions deformation occurs whose size in the tank with float membranes is not acceptable. In order to ensure the free movement of membrane and that the sealing between membrane and the shell is good enough, reservoir layer must be strictly cylindrical and made much more precisely than was in the case of an older construction of tanks. The required precision of craftsmanship tread is explained in Figure 3, which shows that joints overshoot the inside of the tread buffed up to the height of the base material.

Such precision in tank shell manufacturing can not be achieved in E welding process even if steps are taken to reduce deformation, such as reducing heat input, preheating, welding back step and welding with several

welders simultaneously. Therefore, the welding process had to be changed. Considering the fact that the welding is carried out in the open tank, the procedure of welding with self-shielded cored wire has been selected as best choice.



Figure 3. Overshoot of the compounds of the layer to the height of the base material on the inner side of the tank

#### 6. SELF-SHIELDED CORED WIRE AND IMPACT OF WELDING PARAMETERS ON WELDS

The use of self-shielded cored wire is increasing around the globe. The reason for this is their features that include good properties of electrodes and solid wires [5]. Self-shielded cored wire consists of a metal shield and non-metal charge. Shares of metal and non-metal part depends on the technology of wire. The functions of the metal coating are: creation of metal deposit of weld, shape formation, wire dimensions and transfer of electricity. Non-metallic filling have characteristics similar to the characteristics of electrode coating, and has the following features: ionization component enables ignition and maintenance of port, protects the metal drops and weld pool from the influence of air, generates slug which perform deoxidization and purified weld, which slows down the cooling and alloyed weld.

Most self-shielded cored wires has a charging base type. Main ingredients include calcium carbonate, calcium fluoride, titanium dioxide, and metals such as Al. The most important component of the charge is calcium carbonate, which, during welding dissolute on CaO and CO<sub>2</sub>. Carbon dioxide protects the zone arc and melted metal from the air impact, while CaO binds impurities and have composition of slag. Aluminum binds the nitrogen from the air that penetrates into the zone of the electric arch. Therefore, AlN particles are formed, which in the form of non-metallic inclusions remain weld.

In relation to the welding wire, full self-shielded cored welding wire is characterized by greater length of the wire, greater width of arch, less sensitive to the presence of impurities on the surface and a greater amount of flue gas. Increasing the length of the free end of wire (20 - 30 mm) has resulted in increased heating and performed melting more quickly, which has the effect to increase welding productivity. Increasing the width of the arch is due to the melting of the wire sheald. The components of non-metallic filling which have a role to purify all metal also reduce the sensitivity of these wires to the presence of coating and corrosion on the surfaces of the parts to be welded.



The basic parameters of welding with flux-cored wires are: arch voltage, wire feed speed (control of welding current), welding speed and length of free end of wire [6]. Increasing the voltage increases the arch length, which leads to formation of a wider and flatter weld surface. If the voltage is too high due to the excessive length of the arch, it can lead to deteriorating of gas protection which could have resulted in the occurrence of porosity in the weld. Increasing the speed of the wire feed increases the strength of the welding current which results in an increase in depth of welding penetration, increase in the wire melting speed and increase in the amount of deposited metal. Excessive speed of wire leads to formation of convex surface joint, which affects and impairs its appearance. In order to maintain the proper shape of the weld, voltage must be increased. Too small wire feed speed leads the welding wire to be welded to contact tip. Excessive welding speed increases swelling and roughness of surface joints. If welding is carried out too slowly it leads to intensive mixing of slag and metal which leads that appearance of slag inclusions and coarse are uneven on the surface of weld. Increasing the length of the free end of the wire reduces the welding current.



Figure 4. The visual appearance of self-shielded cored wire surface weld in a horizontal position

## 7. WELDING JOINT TESTS WITH SELF-SHIELDED CORED WIRE AND TEST RESULTS

We performed numerous welding tests under various conditions in order to conquer the challenge of welding technology with self-shielded cored wire.

Hereinafter, test results of a sample which was evaluated as the best, and on the basis of which welding technology is made [7], is applied to the welding of described tank shell.

### 7.1. Welding joint test

The test joint was performed by welding two plates of steel S235JRG2 with dimensions 500x200x14mm. Chemical composition and mechanical properties of this steel are given in the tables 1 and 2 [8]. Self-shielded cored wire was used as additional material E71T-8 (Innershield NR 232) diameter 1,7 mm, manufactured by Lincoln Electric. Chemical composition and mechanical properties of additional material are summarized in tables 3 and 4 [9].

Table 1. The chemical composition of steel S235JRG2

C	Si	Mn	P	S
≤ 0,17	-	≤ 1,40	≤ 0,045	≤ 0,045

Table 2 The mechanical properties of steel S235JRG2

Yield strength R <sub>p</sub> 0,2 MPa	Ultimate tensile strength R <sub>m</sub> MPa	Elongation A %	Impact toughness KV J at + 20°C
> 235	340 – 470	> 24	27

Table 3 The chemical composition of filler material E71T-8

C	Si	Mn	P	S	Al
0,17	0,27	0,65	0,006	0,004	0,55

Table 4 The mechanical properties of filler material E71T-8

Yield strength R <sub>p</sub> 0,2 MPa	Ultimate tensile strength R <sub>m</sub> MPa	Elongation A %	Impact toughness KV J at - 30°C
> 460	590	> 26	> 35

The joint test is welded in horizontal position in V baffle, whose dimensions are given in figure 5. The joint is welded by five welds. The weld number 5 is welded to the reverse side of the root after its sanding. Welding parameters are given in figure 5.

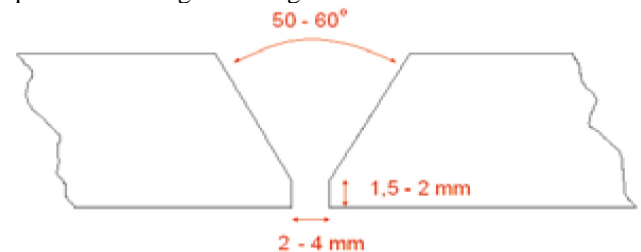


Figure 5 Shape and dimensions of baffle used for joint test welding

Table 5 The welding parameters of joint test \* for the process  $\eta = 0,8$

Specimen designation	Current I A	Voltage U V	Welding speed V <sub>z</sub> cm/min	Welding speed V <sub>z</sub> mm/sec	Heat input Q KJ/mm *	Remarks
1	126	20	6,5	1,08	1,87	
2	200	25	12,9	2,15	1,86	
3	235	26	16,0	2,67	1,83	
4	238	26	22,1	3,68	1,35	
5	228	26	17,8	2,97	1,60	

**7.2. Results of test methods without destruction**

Figure 6. lists the visual appearance of joint test surface. Visual inspection has concluded that joint surface have equal width and height and error-free in forming seam.

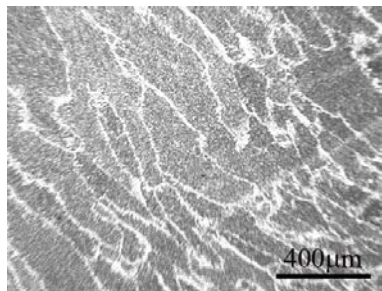
Joint surface shows partially poorly cleaned remains of slag. Weld, with the root side of the joint, has an equal width and height and show no mistakes in formation of the seam. Radiographs of joints didn't detected cracks or other defects in formation of the seam.



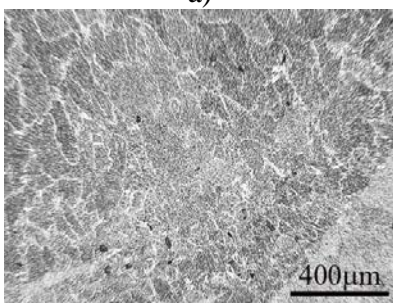
Figure 6. Surface appearance of joint test, welded with self-shielded cored wire, E71T-8 (Innershild NR 232)

**7.3. Results of destruction tests**

Figure 8 shows the macrostructure of joint test. Macrostructural examination detect no defects in forming.



a)



b)

Figure 7a-b). Ferrite - pearlite microstructure of weld

The hardness of joint test and core material are obtained on the sample that was used for testing the macrostructure.

Schedule of measuring points is specified in Figure 8, and results of the measurements are given in Table 6.

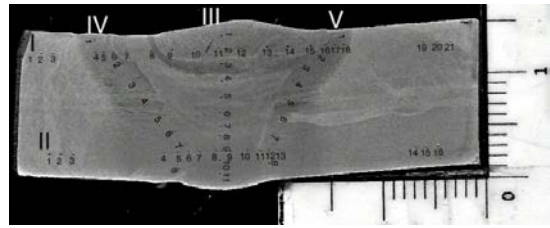


Figure 8. Schedule of spots for hardness measuring of joint test

Line No.	Measurement location, BM, hardness	Measurement location, HAZ, hardness	Measurement location, WM, hardness	Measurement location, HAZ, hardness	Measurement location, BM, hardness
I	1-3/172-186	4-6/212-227	7-15/216-246	16-16/210-240	19-21/175-181
II	1-3/184	4-6/227-236	7-10/215-226	11-13/208-240	14-16/178-188
III	-	-	1-11/219-231	-	-
IV	-	1-8/230-251	-	-	-
V	-	-	-	1-8/228-254	-

Table 6. Hardness of joint test and base material (HV 10)

Tensile properties of joint as a whole are determined by using flat tubes with the parallel flanks of the cut perpendicular to the axis of the joint. The test results are given in table 7. Tensile properties of weld were determined by examining round tube (Ø6mm). The test results are given in table 8.

Table 7. Test results of weld tensile characteristics as a whole

Specimen No.	Ultimate tensile strength R <sub>m</sub> MPa individually average	Place of fracture	Remarks
1	422	OM	
2	452		
3	452		

**Table 8.** Test results of weld tensile properties

Sample No	Yield strength $R_{p0.2}$ MPa		Ultimate tensile strength $R_m$ MPa		Elongation A %	
	individually	average	individually	average	individually	average
4	461	466	612	625	22	22
5	468		626		21	
6	466		636		22	

Bending test tube with joint as a whole has been done on specimens with parallel flanks. The test results are given in table 9.

**Table 9** Test results of joint by bending

Sample No	Tensile strength of base material	Bending angle °	Defects	Satisfactory/unsatisfactory
7	root	180	no	+
8	root	180	no	+
9	The face	180	no	+
10	The face	180	no	+

The weld toughness was examined on to standard Charpy V - notch incised vertically through the thickness of the weld. The test results are given in table 10. while figure 9. shows the fracture surface of the tube. Figure 9 shows that the weld fracture on all three tubes was tough.

**Table 10** Test results of weld toughness

Sample No.	Impact energy J	Testing of temperature °C
11	47	- 20
12	55	- 20
13	42	- 20



Figure 9. Appearance of the tubes fracture surface used in testing the toughness of weld

**7.4. Analysis of test results**

The results of visual inspection shows that surface of the seam is smooth, equal height and width, and with a gentle transition to the base material. No errors were detected on the surface of the weld. Radiographic examination also didn't detected any unacceptable errors in weld formation and its surroundings.

Table 7 shows that fracture occurred in the base material in all three tubes with whole joint. The tensile specimens of these plastic deformation begins in the basic material of which the yield stress is the lowest and is around 235 MPa, table 4. In case of further tightening of the tube, ie. during increased of voltage, the plastic deformation is carried out in base material, and elastic deformation occurs in seam. When reaching tensile strength of base material (422 MPa, table 7.) the refraction begins, while in the seam is still running only elastic deformation, because its higher yield stress (466 MPa, Table 8) of base material tensile strength. Fracture occurs in section of tube which has a lower tensile strength, and it is in this case the base material.

The test results on bending and macrostructure test shows that this welding technology does not lead to appearance of cracks and other defects of weld formation. Tube bending angle of 180 ° without cracking, and sides of surface and side roots circuit, table 9 shows that the material in welding formation and in HAZ is sufficiently plastic and joint did not show brittle microstructural component.

Relatively high levels of impact toughness and ductile fracture of Charpy tube guarantee that in case where errors occurs in joint, a risk of breakage is minimal.

**8. WELDING OF STORAGE TANK**

In order to obtain a satisfactory accuracy of tank dimensions without deformation, next to the corresponding welding process it is necessary to apply a proper order in assembling and welding of storage tank.

The shell tank is mounted on a steel bottom. By increasing a height of the tank shell increases its weight. It causes a deformation of the bottom. If there is a welded joint between the bottom and the shell, deformation of the bottom will be transferred to the shell. For this reason, a connection between the bottom and a shell should be welded only in case when bottom of the shell is "stabilized" ie. when it ceases to deform due to increasing weight of the shell. In the present case, the connection between the bottom and a shell of the tank is welded after setting three segments of the shell.

First, on each segment is welded vertical joints between the parts of the segments, and then is welded the circular joints between individual segments. Welding the two types of joints must be performed with several welders simultaneously (minimum four), because in this way the deformation caused by welding are symmetrically distributed in volume of the tank, figure 10 and 11. Only this deformation layout guarante circular form of the tank shell.

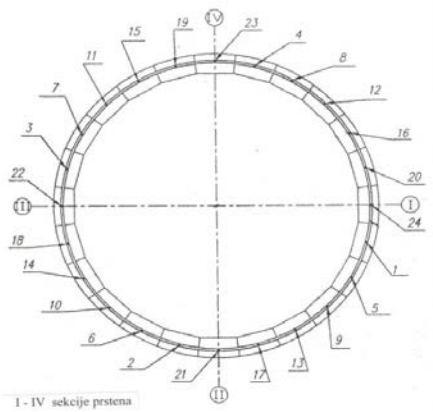


Figure 10. Welding layout of vertical joints in tank shell segments

All joints are welded with a “step back” technique, figure 11. It is defined that a length of the step back has to be 500 - 600 mm.

Given that the size of deformation is proportional to the heating layer of base material in the vicinity of the joint, it is clear that welding processes performed with higher speeds and less heat input generate less deformation of a shell. Earlier used E procedure caused a great amount of generated heat into the joints due to low welding speed and a large number of extensions (bits are practically heated two times because replacement of electrodes). With introduction of welding with self-shielded cored wire, an amount of heat input is reduced, because performed welding time is 3 times faster, at the expense of increasing the welding speed and at the expense of reducing the number of bits. This reduces deformation of the tank shell. Figure 12. generating displays of tank shell in the areas of joints between segments. The figure shows that walls are leveled and without deformation.

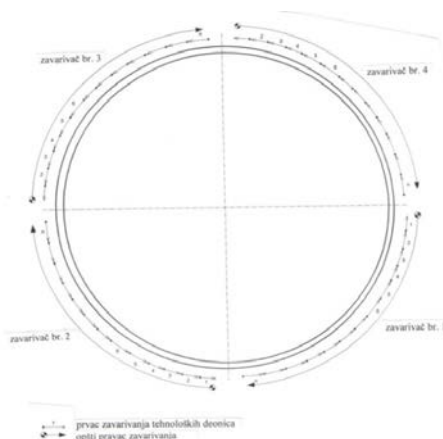


Figure 11. Welding joints of the shell between segments with a step back technique



Figure 12. Generating layer of the storage tank in the zones of joints between segments of a shell

9. CONCLUSIONS

Displayed welding technology enables development of coatings for storage tanks for oil products practically without deformation. This is possible primarily through the use of welding procedure with a self-shielded cored wire. The process is characterized by high speed welding which causes small heating of base material next to the joint and low level of deformation. In addition to welding procedure to reduce tank shell deformation, the big importance is a layout of assambeling, layout of welding and a back step technique performed in welding of individual joints.

Manufacturers of storage tanks have used E process so far for welding this tank shells, particularly for those with a volume of less than 10,000 m<sup>3</sup>. This process is characterized by ability to work in adverse weather conditions, which increases the number of working days in a year and a small welding speed. With application of welding with self-shielded cored wire, the work in adverse weather conditions is still possible while welding speed is considerably increased. In this way a welding productivity is increased and deadlines for the development of the tank is shorten.

Displayed welding technology has enable improvement of construction of storage tanks for oil products with an installation of floating membrane. Membrane significantly reduces the evaporation by floating on the working fluid. Given that a pressure in the tank needs to be constantly equal to atmospheric pressure, a membrane significantly reduces the losses of a working fluid to an atmosphere and thus pollution of the environment.

Compared to E procedure, device prices and additional materials for self-shielded cored wire are significantly higher. However, high productivity guarantee an economic viability of the method in a reasonable time.

ACKNOWLEDGEMENTS

The authors gratefully acknowledge research funding from The Ministry of Education, Science and Technological Development of The Republic of Serbia under grant number TR35024.

**REFERENCES**

- [1] Glavni mašinski projekat "Sanacija skladišta naftnih derivata", knjiga 3. Proces projekt inženjering, Beograd, mart 2012.
- [2] SRPS M.Z3.054/1981 – Skladištenje nafte i naftnih derivata, vertikalni cilindrični nadzemni rezervoari, zavareni, sa ravnim dnom i nepomičnim ili plivajućim krovom .
- [3] C. Hase, W. Reitze: Elektrolučno zavarivanje, priručnik, IRO Građevinska knjiga, Beograd, 1982.
- [4] M. Jovanović, D. Adamović, V. Lazić, N. Ratković: REL zavarivanje, Univerzitet u Kragujevcu, Mašinski fakultet, Kragujevac, 2006.
- [5] Nastavni materijal za kurs za Međunarodne inženjere i tehnologe zavarivanja, Institut Goša, Beograd, 2015.
- [6] Innershield Wire FCAW-S Welding Guide, The Lincoln Electric Company, Cleveland, Ohio, USA, 2015.
- [7] R. Jovičić: Tehnologija zavarivanja rezervoara za skladištenje derivata nafte, Inovacioni centar Mašinskog fakulteta u Beogradu, Beograd, 2012.
- [8] SRPS EN 10025-1/2011; Toplovaljani proizvodi od konstrukcionih čelika - Opšti tehnički zahtevi za isporuku
- [9] Product catalogue, The Lincoln Electric Company, Cleveland, Ohio, USA, 2011.



## Detailed Geotechnical Investigations of the Landslide Bocke

Mitar Đogo<sup>1\*</sup>, Milinko Vasić<sup>1</sup>

<sup>1</sup>Faculty of Technical Sciences/Department of Civil Engineering, University of Novi Sad, Novi Sad (Serbia)

*The landslide Bocke is located in the region of Sremska Kamenica, on the territory of the city of Novi Sad. The unstable area comprises an exceptionally large area, namely about 1.5 km<sup>2</sup>. The deepest sliding planes, which were previously active, are at a depth of 20-30 m. The landslide begins at the bottom of the Danube. Intensive surveys of the landslide began 18 years ago as a result of the problems arising from the inability to connect about 1000 buildings built on the landslide to the main water and sewage network. The survey took a long time and it was therefore conducted in several stages. Each new stage represented a continuation of the previous surveys. This yielded increasingly detailed and reliable data on the landslide. This approach to the surveys meant that it has only now become possible to begin planning the countermeasures.*

**Keywords: Landslide, Geotechnical engineering, Site investigation**

### 1. INTRODUCTION

The village of Bocke was built on the landslide, initially as an area with about 1000 holiday homes, which was later legalized and is now part of the city of Novi Sad. Bocke is located on the northern slope of the Fruška Gora, directly along the right-hand valley bank of the Danube. In the morphogenetic sense, this area is pronouncedly wavy and characteristic of areas affected by landslides along the Danube. The unstable area comprises an exceptionally large area, namely about 1.5 km<sup>2</sup>. The deepest sliding planes, which were previously active, are at a depth of 20-30 m, and this variable depth is caused by the present morphology of the terrain surface, which is a reflection of movements during the exceptionally long time period that the unstable slope has existed. Along the circumference of the unstable area, and especially in certain zones, are the regions of the main scars of the landslide with steep, almost vertical stretches that are 10-15 m high. The width of the landslide is the greatest in the Danube area and it is about 1.5 km. The width of the landslide decreases gradually up the slope and encompasses a length of about 1 km. To date, several stages of detailed geotechnical investigations of this landslide have been carried out, and numerous data have been collected. This paper will present only data relevant from the aspect of the projecting of the geotechnical investigations.

The dynamics of the movements of such a large landslide is definitely very complex, namely, such a large sliding mass moves partially in sections, that is in smaller landslides. All the geotechnical investigations and explorations of the dynamics of the movements must determine the following: geological and other prerequisites for reactivating landslides that have moved already, prerequisites for the sliding process to move up the slope, the directions in which the landslide is moving, the depth and intensity of the movements.

All of the above needs to be dealt with reliably during the planning process of the geotechnical investigations work and during its realization. As a rule, and according to our practical guidelines, in this and similar landslides, this was solved by a several-year-long process of planning exploratory work and its realization

through a number of stages, which is what is presented in this paper.

In the zone of the landslide, from the Danube to the top front scar, there are several distinct morphological sections that essentially represent the scars of certain main sliding stages. In the morphometric sense, the landslide area practically begins from the bottom of the Danube at an elevation of about 62 m and continues up the slope to an elevation of about 220 m.

Along the circumference of the landslide, there are loess sediments which are slightly tilted towards the Danube from the highest saddle areas.

### 2. INVESTIGATIONS OF LARGE LANDSLIDES OF THE DANUBE

The aim of the research is to provide conditions for the optimal choice of technical solutions to repair the landslide, which depend on the properties of the geological environment and are as follows: dividing the area into zones according to stability, predicting the future development of the sliding process as a result of constructing linear structures and urbanizing the area, recommending necessary countermeasures to improve the overall stability of the entire slope, determining the necessary geotechnical parameters and foundations for carrying out the main construction project of repairing the now active landslide, conditions for connecting buildings to the water and sewage networks in Bocke.

The task of the research is to define the following through the application of complex research methodology: lithogenic types of rocky masses, boundaries between them, spatial location, unstable areas with active and dormant landslides, tentatively stable areas and stable areas, the depth of sliding using inclinometers, the shape of the Danube riverbed through sonar scanning, hydrogeological properties of rocky masses and terrains, the physical and mechanical properties of samples and predictions of terrain behavior based on them, mathematical stability models, countermeasures that will be fully elaborated in the Main Countermeasure Project.

On the right-hand valley bank of the Danube, there is a large number of active landslides that create large unstable slopes [1, 2, 3]. Landslides particularly prominent

\*Corresponding author: Faculty of Technical Sciences, Trg Dositaja Obradovića 6, 21000 Novi Sad, Serbia, e-mail: mitar@uns.ac.rs

in this sense are in the following areas: Čerević, Novi Sad, Sremski Karlovci, Čortanovci, Inđija and Smederevo. All these unstable areas and the large number of landslides making them unstable have been studied in a particularly detailed manner during the past 60 years. The scope of the exploration and the survey can be followed in a large number of geotechnical studies, reports, and published scientific papers. Countermeasures were carried out on some landslides and certain experience was gained. The aim of this paper is not to quote these numerous materials and published papers, but to emphasize the necessity of being well acquainted with all those results in order to begin carrying out the project of geotechnical investigations on some of the landslides. Such an approach is important because sufficient quantitative and qualitative data has been gathered to classify landslides formed on the right-hand valley bank of the Danube as Danube-type landslides. Landslides of this type have certain specific features but also identical ones that can classify them as similar. The comprehensive geotechnical investigations carried out to date on Danube-type landslides, especially in the zone of the Sloboda bridge, the Beška bridge and Bocke, the landslides at Čortanovci, the landslides at Čerević and to a lesser extent landslides at Karlovci, confirm the following:

- unstable slopes comprise areas from the Danube to loess slopes
- unstable slopes are made up of a large number of smaller landslides
- the deepest sliding planes are exceptionally deep,
- the movements of the deep landslides are very slow
- repairing such landslides is exceptionally difficult and expensive
- the directions of the movements are both upriver and downriver towards the Danube

### 3. GEOTECHNICAL INVESTIGATIONS OF THE LANDSLIDE AT BOCKE

The first significant explorations and surveys of the landslide at Bocke were carried out during the period of compiling the basic geological mapping (BGM) and the basic engineering geological mapping (EGM). These surveys possess a general character and are based on methodological procedures regulated by the set of instructions for compiling these types of maps. Basically, these procedures serve to map the terrain, and only exceptionally were individual boreholes located in unstable areas. The reason for such procedures lies in the fact that for the purpose of compiling these maps, it is more important to define the lithogenic composition of the surveyed area than the relevant facts that define: the composition of the landslide, the dimensions of the landslide, the genesis of the sliding process and significant parameters of rock mass resistance within the body of the landslide, and especially in the sliding planes.

On the BGM, published in the Novi Sad map and the EGM, the Novi Sad map, in draft version, the landslide at Bocke is sufficiently precisely marked. In the period following the compiling of these maps and for the purpose of the Novi Sad – Beočin road, comprehensive and detailed geotechnical investigations were carried out in the zone of the landslide, including the precise survey of the landslide at Bocke along the road.

The 1<sup>st</sup> stage in 1998 was significant in the process of geotechnical investigations planning. At that time, a project carried out according to the adopted survey concept at the Faculty of Technical Sciences was supposed to determine the stability of the landslide, the dimensions of the landslide, the spatial distribution of rocky masses in the stable part of the terrain as well as the unstable region, the genesis of the sliding process and the dynamics of the movements, in accordance with the planned survey activities.

This stage of the survey involved the planning of exploratory fieldwork located both in the stable and unstable parts of the terrain (Fig. 1). All the planned exploratory fieldwork was carried out and the results were presented in the appropriate report by the Institute for Roads.

The first stage of the surveys and the plan for exploratory work within that stage were based mainly on exploratory boreholes and related data. A relatively large number of core samples was taken and detailed laboratory investigations were performed. Only one borehole had an inclinometer structure installed. No surveys were carried out in the Danube riverbed.

The survey yielded valuable data which permits us for the first time to say with certainty what the dimensions of the landslide at Bocke area. Still, these explorations were not sufficient in scope to allow us to commence a rational planning of countermeasures through construction projects. Namely, the landslide at Bocke comprises an exceptionally large area and previous exploration was carried out to solve the issue of the general stability of the slope. For those reasons, the surveys did not include the influence of the Danube on the sliding process and no boreholes were made in the Danube riverbed. In addition, only one inclinometer was installed, which is definitely insufficient for such a large landslide as the one at Bocke.

The process of the geotechnical planning of exploratory work at the Bocke landslide to be carried out in stages was resumed in 2011. At that time the project regarding the 2<sup>nd</sup> stage of exploratory work was conceived at the Faculty of Technical Sciences. The project was detailed and contained all the legal and usual parts. Basically, the project contains, along with the usual parts, the specially highlighted most important results of all the surveys until now, all the important dilemmas and unsolved problems.

All the planned exploratory work (Fig. 1) was carried out from 2011 to 2012 to a high standard and was presented in the geotechnical report by the Institute of Water Resources DTD.

Conceptually taken, the second stage of the geotechnical investigations project is based on the following:

- All exploratory field work is at the landslide,
- The depth of the boreholes is such as to penetrate only up to 5 m into the stable rocky mass,
- The boreholes are designed in such a way as to increase their density compared to the previous planning and exploratory stage,
- Three boreholes are in the Danube riverbed, where no such work was carried out previously,
- Each borehole contains an inclinometer structure (9) or a piezometer structure (4),



- Inclinomeric measurements are carried out until the completion of the geotechnical report (3 measurements) and afterwards (3 measurements),
- After the completion of the second stage, the landslide at Bocke must continue to be monitored.

Only after the completion of the report on the second stage were the necessary prerequisites met for commencing the construction projects. With regard to that, a preliminary construction plan will be produced of the repairs to the landslide at Bocke. Due to the urgency of constructing a water and sewage network for the village of

Bocke, in the opinion of this paper's authors, it is possible to carry out the main construction project of draining surface water from the entire area possibly with shallow drainage as well as the main construction project of the water and sewage networks. Both these projects must be in accordance with the preliminary project of repairing the landslide in question.

Figure 2 shows the landslide at Bocke and shows differently area of stability.

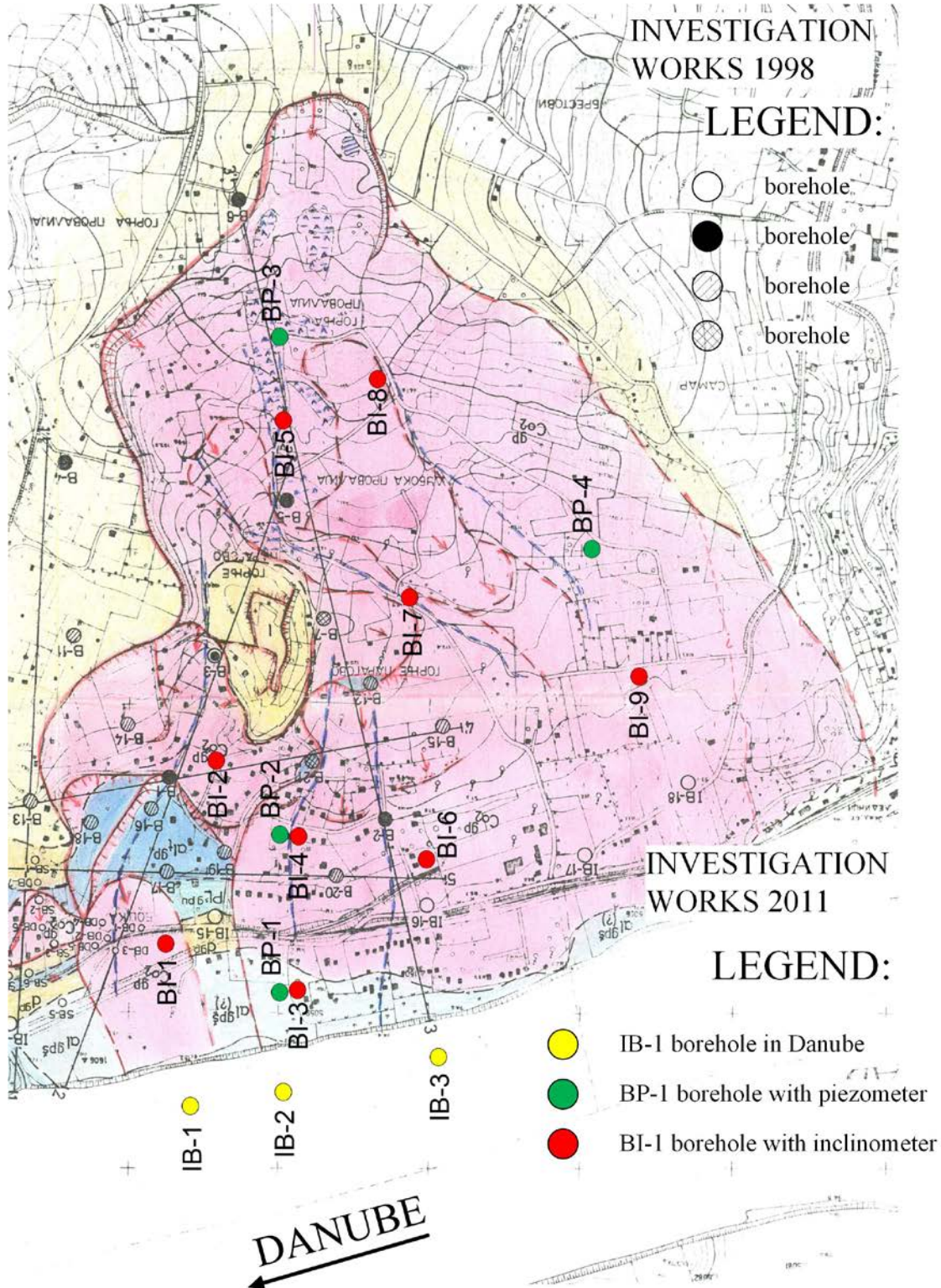


Figure 1: Investigation works in 1998 and 2011

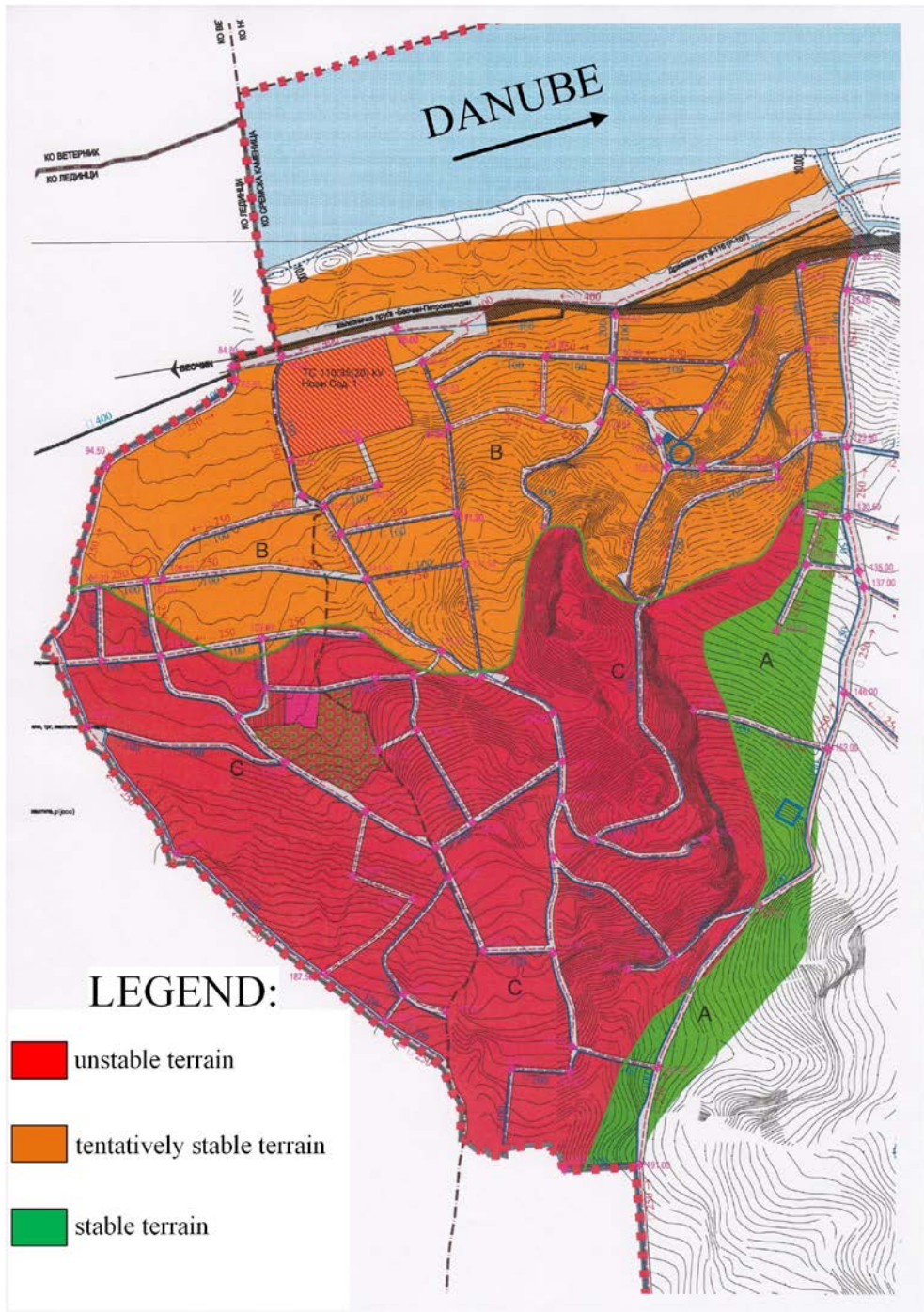


Figure 2: General classification of terrain according to stability

4. CONCLUSION

Surveying large Danube-type landslides must be carried out in stages. Two stages of detailed surveys have been carried out at the landslide at Bocke and appropriate equipment for the long-term monitoring of the landslide was installed. In the stage of planning the countermeasures and during their implementation it will be necessary to carry out additional as well as control surveys.

ACKNOWLEDGEMENT

This work was financially supported by research grant TR37017 of the Serbian Ministry of Science and Technological Development.

REFERENCES

- [1] Djogo M, and Vasić M. "Landslide in the area of the bridge on the Danube in Novi Sad" Proceedings of the ICE - Geotechnical Engineering 164 (1), pp. 3-10, (2011)
- [2] Lokin P, Sunarić D, Cvetković T, "Landslide in Neogene sediments on the right Danube bank, Yugoslavia" Proceedings of the 5th International Symposium on Landslide, Lausanne, Switzerland, pp. 202-208, (1988)
- [3] Lokin P, Vasić M, Saković S, Petričević M, "Landslide along the Danube bank at Novi Sad, Yugoslavia" Proceedings of the 7th International Symposium on Landslide, Trondheim, Norway, pp. 803-808, (1996)



CIP - Katalogizacija u publikaciji -  
Narodna biblioteka Srbije, Beograd

INTERNATIONAL Triennial Conference Heavy  
Machinery (9 ; 2017 ; Zlatibor)  
Proceedings [Elektronski izvor] / The Ninth International  
Triennial Conference Heavy Machinery HM 2017,  
Zlatibor, June 28 - July 1 2017 ; [editor Milomir Gašić].  
- Kraljevo : Faculty of Mechanical and Civil Engineering,  
2017 (Vrnjačka Banja : SaTCIP), 628 str. : ilustr; 29 cm

Sistemske zahteve: Nisu navedeni. - Naslov sa naslovne  
strane dokumenta. -Tiraž 100. -Bibliografija uz svaki rad.

ISBN 978-86-82631-89-7

621(082)(0.034.2)

621.86/.87(082)(0.034.2)

629.3/.4(082)(0.034.2)

622.6(082)(0.034.2)

681.5(082)(0.034.2)

COBISS.SR-ID 239679756